Coastal Engineering Practice





Edited by

Orville T. Magoon
Ronald M. Noble
Donald D. Treadwell
Young C. Kim

ASCE

COPRI

COASTS, OCEANS, PORTS AND RIVERS INSTITUTE

COASTAL ENGINEERING PRACTICE

PROCEEDINGS OF THE 2011 CONFERENCE ON COASTAL ENGINEERING PRACTICE

August 21–24, 2011
San Diego, California

SPONSORED BY
The Coasts, Oceans, Ports, and Rivers Institute (COPRI)
of the American Society of Civil Engineers

EDITED BY
Orville T. Magoon
Ronald M. Noble
Donald D. Treadwell
Young C. Kim

Published by the American Society of Civil Engineers

Copyright and Disclaimer

ISBN: 978-0-7844-1190-2

Any statements expressed in these materials are those of the individual authors and do not necessarily represent the views of ASCE, which takes no responsibility for any statement made herein. No reference made in this publication to any specific method, product, process or service constitutes or implies an endorsement, recommendation, or warranty thereof by ASCE. The materials are for general information only and do not represent a standard of ASCE, nor are they intended as a reference in purchase specifications, contracts, regulations, statutes, or any other legal document.

ASCE makes no representation or warranty of any kind, whether express or implied, concerning the accuracy, completeness, suitability, or utility of any information, apparatus, product, or process discussed in this publication, and assumes no liability therefore. This information should not be used without first securing competent advice with respect to its suitability for any general or specific application. Anyone utilizing this information assumes all liability arising from such use, including but not limited to infringement of any patent or patents.

Copyright © 2011 by the American Society of Civil Engineers.
All Rights Reserved.

ASCE and American Society of Civil Engineers—Registered in U.S. Patent and Trademark Office.

American Society of Civil Engineers
ASCE International Headquarters
1801 Alexander Bell Drive
Reston, VA 20191-4400 USA

Call Toll-Free in the U.S.: 1-800-548-2723 (ASCE)
Call from anywhere in the world: 1-703-295-6300
Internet: http://www.pubs.asce.org

Preface

The 2011 Conference on Coastal Engineering Practice was organized under the auspices of the Coasts, Oceans, Ports and Rivers Institute (COPRI) of the American Society of Civil Engineers. The conference was held at the Sheraton San Diego Hotel & Marina in San Diego, California on August 21-24, 2011.

The 2011 Conference on Coastal Engineering Practice focused on practical approaches in developing solution for coastal engineering problems as well as ensuring sustainable coastal development. An additional goal was to promote the exchange of experiences between practicing coastal engineers. Emphasis was placed on practical experience and actual projects rather than specific technical and scientific aspects of coastal engineering.

The 2011 Conference on Coastal Engineering Practice had the following eight themes:

A. Case Histories of Coastal Projects
B. Sustainable Coastal Development
C. Erosion and Shoreline Protection
D. Coastal Environment, Water Quality and Wetlands Restoration
E. Coastal Hazards and Risk Management
F. Coastal Sediment Processes
G. Ports, Harbors, and Marine Transportation
H. Local, State and Federal involvement in Planning, Design and Construction of Coastal Projects

The Conference Organizing Committee acknowledges the support received from the following cooperative organizations:

Association of Coastal Engineers (ACE)
Permanent International Association of Navigation Congresses (PIANC)
Coastal Zone Foundation

The Committee also recognizes the contributions of the following individuals from ASCE: Tom Chase, Director of COPRI, Barbara Hickman, Manager, Conferences & Meeting Services, Sean Scully, Manager, Sponsorship and Exhibit Sales, Donna Dickert, Publications, and Angie Lander, COPRI Coordinator.

Orville T. Magoon, Chair, Coastal Zone Foundation
Ronald M. Noble, Co-Chair, Noble Consultants, Inc.
Donald D. Treadwell, Co-Chair, Consulting Engineer
Young C. Kim, Technical Chair, California State University, Los Angeles

Acknowledgments

Organizing Committee

Orville T. Magoon, Chair, Coastal Zone Foundation
Ronald M. Noble, Co-Chair, Noble Consultants, Inc.
Donald D. Treadwell, Co-Chair, Consulting Engineer
Young C. Kim, Technical Chair, California State University, Los Angeles
Dan Muslin, Local Planning Chair, TEC Inc.
Water F. Crampton, Marketing Chair, TerraCosta Consulting

Technical Committee

Neal Gruber, Black & Veatch Corporation
Steve Hughes, U.S. Army Engineer Research and Development Center
Kathy Ketteridge, Anchor QEA
Ruben Kosyan, P.P. Shirshov Institute of Oceanology, Russian Academy of Sciences
Andrew T. Metzger, University of Alaska Fairbanks
Charles Shabica, Shabica & Associates, Inc.
Nels Sultan, PND Engineers, Inc.

Local Planning Committee

Tomas T. Jimenez, Fyfe Co. LLC
Robert Walker, Anchor QEA

Marketing Committee

Nabil Ismail, Maritime Academy for Science & Technology, Alexandria, Egypt
Alessio Mariani, The University of New South Wales
Thomas Richardson, Jackson State University
Tracy Stofferahn, Anchor QEA

Table of Contents

Plenary

Sea Level Trends and Accelerations Based on U.S. and Global Tide Gauges **1**
R. G. Dean and J. R. Houston

Case Histories of Coastal Projects

A Case Study on the Use of Advanced Fiber Wrap Composites for Timber Pile Repair and Protection of a Pier Structure **10**
T. Jiménez, D. Kost, and J. Percival

Design and Construction of Kaumalapau Harbor Breakwater Island of Lanai, Hawaii **15**
Scott P. Sullivan

Stabilization of the Tutong River Entrance, Brunei: A Comprehensive Coastal Engineering Project **29**
A. Mariani, J. T. Carley, D. Rayner, B. M. Miller, R. J. Cox, and Kok Kong Chin

The Forecast of Anapa Bay-Bar Coast Evolution and Sand Body Thickness Change **42**
R. D. Kosyan, B. V. Divinskiy, A. R. Kosyan, V. V. Krylenko, M. V. Krylenko, and S. B. Kuklev

Jet Grouting for the Re-Support of Pier 11A in San Diego, CA **56**
S. Arora and J. Kinley

Over Twenty-Five Years of Applied Coastal Engineering in Alaska **64**
Harvey N. Smith and Ruth A. Carter

Corrosion Protection for Concrete Structures in Marine Environments **78**
D. B. McDonald

Development of Inner Harbor Navigation Canal Hurricane Surge Barrier Project Hydrodynamics through Deterministic Methods, Physical Modeling, and Numerical Modeling **89**
Jena F. Gilman, Peter Grant, Jake San Antonio, and Mizan Rashid

Sediment Nourishment at Orchard Beach, the Bronx, New York **103**
Diane Rahoy, David Yang, Lynn Bocamazo, Shewen Bian, Frank Verga, Anthony Ciorra, and Bill Tai

Design and Construction of the Lake Borgne Surge Barrier in Response to Hurricane Katrina **117**
Scott R. Huntsman

Long-Term Monitoring and Effectiveness of Sediment Cap, Former Campbell Shipyard, San Diego, California **131**
Rolf Schottle, Larry McCauley, and Bill Hays

Indian River County—Sector 3 Beach and Dune Restoration Project **145**
Michael Walther and Tem Fontaine

Sediment Transport Modeling and Application for Ocean Beach and San Francisco Bight, CA **158**
H. Li, L. Lin, F. Wu, L. C. Andes, and J. G. Zoulas

Regional Beach Restoration and Monitoring in San Diego County: A 10-Year Retrospective **170**
Greg Hearon, Brady Richmond, and Shelby Tucker

Sustainable Concrete Mix Designs for 100-Year Service Life for Bridges in San Diego County Coastal Environments **184**
B. G. Smith, M. Creveling, and J. W. Teig

Maintenance of Navigable Depths at the Hawaii Kai Marina and Entrance Channel: Oahu, Hawaii **198**
Michael Whelan, Rob Walker, and Tracy Stofferahn

The Life and Death of North America's First Man-Made Surfing Reef **212**
Craig B. Leidersdorf, Brady Richmond, and Chad E. Nelsen

Capacity Enhancement at Coastal Disposal Sites **226**
R. David Espinoza and Michael F. Houlihan

Operation, Maintenance, and Repair of Coastal Wastewater Outfalls: San Francisco, Boston, Los Angeles County, and San Diego **235**
Brian J. Van Weele and Donald D. Treadwell

Coastal Environment, Water Quality, and Wetlands Restoration

Numerical Modeling Studies of San Elijo Lagoon Restoration Project **248**
Weixia Jin, Xiuying Xing, Chris Webb, and Doug Gibson

Modeling Study of Bacterial Dispersion for Marine-Coastal Waters, According to the European Directives **262**
L. Scroccaro, L. Colugnati, G. Umgiesser, and G. Mattassi

Masonville Dredged Material Containment Facility: Mitigation Design Including Shore Protection, Reef Creation, and Wetlands Restoration **274**
Peter W. Kotulak and Kristen Piggott

Influence of Small Rivers' Runoff on the Hydrochemical Structure of Coastal Waters of the North-Eastern Black Sea **286**
A. V. Kostyleva, O. I. Podymov, P. N. Makkaveev, and A. A. Polukhin

Restoring Malibu Lagoon: A Case Study in Collaborative Coastal Restoration **298**
Marc Beyeler, Steve Seville, and Mark Abramson

Water Quality Study for a Coastal Development at the Bahia de lost Sueños, Baja California, Mexico **312**

Wenkai Qin and Ronald M. Noble

Hydraulic Effects of Proposed Knik Arm Crossing **326**
J. Colonell, P. Mineart, and J. Gambino

Coastal Hazards and Risk Management

A Joint Hydraulic/Structural Methodology for the Rehabilitation of the Crescent City Marina **340**
J. O. Toilliez and M. P. Jorgensen

Operational Oceanographic System for the Southern Coastal Waters of Korea **351**
Hak Soo Lim, Chang S. Kim, Kwang Soon Park, and Jae Seol Shim

Application of Coastal Engineering Principles in Response to the Deepwater Horizon Disaster: Lessons Learned in Coastal Alabama **359**
Bret M. Webb, Scott L. Douglass, Caren R. Dixon, and Beau Buhring

Sea Level Rise Impact Assessment and Mitigation Alternatives Development for Balboa Island and Little Balboa Island, City of Newport Beach, California **373**
Ying Poon, Brett Sanders, Randy Mason, and Robert Stein

Comparison of Two Severe Storms in Terms of Wave Characteristics Based on Recorded Field Data **384**
Alireza Jafari, Nick Cartwright, and Peter Nielsen

Estimation of Storm Surge Inundation and Hazard Mapping **396**
Jae Seol Shim and Jong Joo Yoon

Coastal Engineering for Veterans Drive Improvements **410**
Manish Aggarwal and Jerald Ramsden

Vulnerability Assessment of Climate Change Impact on Groundwater Salinity in the Nile Delta Coastal Region—Egypt **422**
I. A. Elshinnawy and H. O. Abayazid

Seawall-Waves Interaction and Impact on Sediment Morphology **436**
Nabil M. Ismail and Walid El-Sayed

Coastal Structures and Sea Level Rise: Adaptive Management Approach **449**
John R. Headland, Dilip Trivedi, and Russell H. Boudreau

Coastal Sediment Processes

Subaqueous Cohesive Sediment Gravity Flows from Open Water Pipeline Dredge Disposal: Laboratory Experiments and Mathematical Modeling **460**
M. R. Chowdhury and F. Y. Testik

Modeling Regional Sediment Transport and Barrier Elongation on Long Island Coast, United States **473**
Le Xuan Hoan, Hans Hanson, Magnus Larson, Shigeru Kato, and Shin-ichi Aoki

Prediction of the Siltation in the Intake of Nuclear Power Plant Using the Water Depth Monitoring and Coupled Model 487
Bum-shick Shin and Kyu-han Kim

Analysis of Morphological Changes in the Gold Coast Seaway 495
M. Sedigh, R. Tomlinson, A. Golshani, and Nick Cartwright

Influence of JONSWAP Wave Spectra Form on Frequency Spectrum of Suspended Sediment Transport Values 509
I. S. Podymov, J. Grüne, R. D. Kos'yan, and T. M. Podymova

Cohesive Sediment Transport Modeling: Application to the Madura Strait, Indonesia 522
Nita Yuanita, Muhammad Ali Rini, and Undang Heriawan

Numerical Modeling of Wind-Waves and Its Effect on Sediment Transport—An Investigation of Spectral Terms 537
S. K. Khatri and I. R. Young

Enhancement of Cross-Shore Profile Evolution Models for Sustainable Coastal Design 548
Mohamed A. K. Elsayed and Nabil M. Ismail

Erosion and Shoreline Protection

In the Wet Placement of Articulated Concrete Block Mat by Divers 561
Eric Thorkildsen

Analytic Solution Shoreline at Jetty under Varying Wave Climate 566
Todd L. Walton, Jr. and Robert G. Dean

Event Ranking Methods for Calculation of 100-Year Wave Runup on Levees at Oakland International Airport, California 580
Jeremy Bricker, Philip Mineart, Sathish Murugaiah, John Paxton, Rajendram Arulnathan, Samuel Won, and Frank Lobedan

Surfability: A Proposed Scale for Surfable Waves 594
Chuck Mesa

Landslide Repair and Severe Erosion Mitigation Case Studies in Sensitive Coastal Areas 605
James Chinchiolo and Colby Barrett

Wave Effects on Bathymetric Depressions 616
Luce Bassetti and Sean O'Neil

Propeller Wash on a Slope 627
Ayşe Yüksel Ozan, Kubilay Cihan, and Yalçın Yüksel

Geotextile Tube Solution for Dos Bocas PEMEX Marine Facilities Beach Erosion Problem in Tabasco, Mexico 640
Felix Tseng, Zoe Lin, Alfonso Solis, and Marco Sánchez

The Hub Effect on a Propeller Scour around a Pile **650**
Kubilay Cihan, Ayşe Yüksel Ozan, and Yalçın Yüksel

Rockefeller Refuge Gulf Shoreline Protection Demonstration **658**
Brett L. Geesey, Daniel J. Heilman, and Ronald L. McPherson

The 2012 San Diego Regional Beach Sand Project **672**
Chris Webb and Shelby Tucker

Determination of Wave Transmission Coefficients for Oyster Shell Bag Breakwaters **684**
Richard J. Allen and Bret M. Webb

Shore Protective Revetment Crowned with Pedestrian Walkway at Strand Beach, California **698**
Chia-Chi Lu, Thomas J. Fischetti, and Ronald M. Noble

Extreme Total Water Levels for Twin Lakes Beach, Santa Cruz, CA **707**
C. Fassardi, L. Bassetti, and J. Davies

Determination of Shoreline Evolution: A Case Study **721**
H. Anıl Arı Güner, Yalçın Yüksel, and Esin Özkan Çevik

Efficacy of Stone Filled Marine Mattresses for Cable Protection in a Nearshore Mixed Sediment Environment **732**
M. Dalon, R. Muñoz, D. Gaffney, and J. Fiske

Monitoring Shore Protection Projects along the Florida Panhandle Using Three-Dimensional Spatial Data **742**
Lauren M. Dunkin and John McCormick

Myrtle Beach (2001-2010)—Another Decade of Beach Monitoring Surveys after the 1997 Federal Shore-Protection Project **753**
Timothy W. Kana, Haiqing Liu Kaczkowski, and Philip A. McKee

What's Left of the Malibu Coastline and a Method to Replenish the Beaches **766**
Reinard T. Knur

Behavior of Shore Protection Structures in Alexandria, Egypt, during the Storm of December 2010 **780**
B. El-Sharnouby and A. Soliman

Predictability of Beach Nourishment Project Performance in Florida **793**
Robert G. Dean and Luciano Absalonsen

Local, State, and Federal Involvement in Planning, Design, and Construction of Coastal Projects

Applying the Design/Build Project Delivery Method to Shore Protection and Other Coastal Works Projects **807**
James E. Spady

The Challenges of Permitting Coastal Projects in the 21st Century 820
Walter F. Crampton

Ports, Harbors, and Marine Transportation

Skagway Small Boat Harbor—Vertical Wave Barrier 831
Nels Sultan, Steve Spencer, Todd Nottingham, and Lisa Dale

Passing Vessel Hydrodynamic Model Validations in Complex Waterways 846
S. Fenical and F. Salcedo

Cruise Ship Maneuvering and Berthing at Pier 27 Cruise Terminal, San Francisco, CA 855
K. Von Blohn, J. Davey, M. Tirindelli, and S. Fenical

Elastic Buckling Capacities of Piles Subject to Partial Section Loss 868
Breanna Bailey, Prashant Deopurkar, L. U. Sankar Samudrala, and Lakshmana Rao Upputuri

Field Observations and Numerical Modeling of Infragravity Waves 878
Yang Zhang, Hemming Schäffer, Chris Carr, and Sean O'Neil

Coastal Engineering for Renovation of San Francisco Marina West Yacht Harbor 892
M. Hobson, F. Filice, S. Fenical, and M. Tirindelli

Floating Breakwater Modeling and Design for Oyster Point Marina 903
David Dykstra, Xiuying Xing, and Christopher Devick

Final Monitoring Results for Kaumalapau Harbor Breakwater, Lanai, Hawaii 917
Jessica H. Podoski, Thomas D. Smith, and Lyndell Hales

Modeling Support of the St. Johns River Project, Jacksonville, FL 931
Dennis W. Webb and Philip T. Sylvester

Wave Amplification at Harbor Entrance Due to Submerged Shoal 945
Hyung Seok Yoo, Byung Guk Min, Kyu Han Kim, and Sungwon Shin

Utilizing Vessel Based Mobile Laser and Bathymetry Survey Techniques for Survey of Four Southern California Breakwaters 957
T. J. Mitchell and M. N. Chang

Site Planning and Hydraulic Design of a Cargo Seaport Exposed to Typhoons and Tsunamis—A Project Case in the Philippines 970
E. C. Cruz

Measurement of Structure Response to Ferry Berthing Loads 984
Jonathan Hutchinson and Andrew T. Metzger

Port of Long Beach Sustainable Design and Construction Guidelines 1020
Renée Yarmy and Doug Sereno

Boat-Wake Observations at Jensen Beach, Florida 1034

A. Sheremet, U. Gravois, M. Tian, and T. K. Blankenship

Sustainable Coastal Development

Sustainable Coastal Development in Response to Natural and Anthropogenic Impacts As Well As to Climate Change **1043**
I. Brøker and K. Mangor

Renewable Ocean Energy **1057**
Billy L. Edge and Nancy M. White

Defining Engineering Guidance for Living Shoreline Projects **1064**
Rob Walker, Bonnie Bendell, and Louise Wallendorf

Demand Forecasting for Yacht Tourism Planning in Turkey **1078**
A. Karanci, I. Guler, A. Ergin, and A. C. Yalciner

Current Challenges in Coastal Management in the Netherlands: Examples of Pilot Projects **1088**
J. P. M. Mulder and J. A. van Dalfsen

Vacuum Sewers—A Viable Alternative for Wastewater Collection and Transport in Coastal Areas **1102**
Soma Bhadra and Denny Moss

Sustaining Port Development through Impact Mitigation **1113**
Michael Ludwig and Douglas Clarke

This page intentionally left blank

Sea Level Trends and Accelerations Based on U. S. and Global Tide Gauges

R. G. Dean[1] and J. R. Houston[2]

Abstract

Rising sea level represents a persistent coastal hazard due to the concentration of infrastructure and population along the World's shorelines. Methods of shoreline stabilization are limited and if sea level accelerates in the early 21st Century as many suggest, strategies will need to be developed and implemented on an expedited time frame. Here, to lay a foundation for improved understanding of sea level change, we address the question of whether sea level has accelerated over the approximate 20th Century. Two data groups from 57 U. S. tide gauges with monthly records were selected for analysis by two methods resulting in four combinations of data groups and analysis methods. The criterion for inclusion of individual tide records was a maximum of 5% missing data. One of the data groups extended from 1930 to 2010 and the other from 1910 to 2010. Analysis Method 1 (AM1) comprised a monthly running analysis of the average record of a data group to determine the sea level trend and acceleration, thereby allowing the effect of record length to be examined. AM2 conducted the same analysis on individual records followed by averaging the trends and accelerations. The sea level trend stabilized after approximately 55 years; however, the acceleration continued to oscillate over a small range of the full period analyzed. Overall, the accelerations appear to be very small and negative such that their contribution to sea level rise over a century would be about 1 cm. The results obtained from the two analysis methods and two data groups were consistent, thereby lending credence to the results. Finally, a recent study by Houston and Dean (2011) of global accelerations over the 20th Century found similar results.

Introduction

Climate models predict future increases in the rate of global sea level rise, yet the literature is divided on whether an acceleration is now detectable. We adopt the definition given by Douglas (1992) that acceleration is "… the deviation of sea level from a linear trend over the data span in question that is modeled by an algebraic term of the second degree in time."

A limited number of studies have focused on the acceleration of sea level rise. Woodworth (1990) analyzed long records from European tide gauges and found overall a slightly negative acceleration of mean sea level from 1870 to 1990, although he found positive accelerations in individual gauge records. He also analyzed the four oldest European gauge records from Brest, Sheerness, Amsterdam, and Stockholm starting in 1807, 1834, 1799, and 1774 respectively and found a small positive acceleration on the order of 0.004 mm /yr^2 that he indicated appeared typical of European Atlantic coast and Baltic mean sea level acceleration over the last few centuries. He noted that this small

[1] University of Florida, Gainesville, FL. USA
[2] US Army Corps of Engineers, Vicksburg, MS. USA

apparent acceleration was an order of magnitude less than anticipated from global warming. Jevrejeva et al (2008) perform a similar analysis based on the long-term tide gauge recordings at Amsterdam, Liverpool, and Stockholm, concluding that sea level rise has accelerated an average of about 0.01 mm/yr^2 over the past 300 years with the fastest rise between 1920 and 1950. Douglas (1992) analyzed 23 tide records of 75 years or greater from around the world and determined an apparent global deceleration of -0.011 ± 0.012 mm/yr^2 for the 80-year period from 1905 to 1985. He further analyzed 37 records that were less uniform but had an average length of 92 years and determined that from 1850 to 1991 the acceleration was 0.001 ± 0.008 mm/yr^2. Noting that global warming models forecast acceleration over the next five to six decades in the range of 0.1-0.2 mm/yr^2, he concluded there was no evidence of acceleration in sea level rise in the past 100 or more years that was significant statistically or consistent with values predicted by global warming models. Holgate and Woodworth (2004) analyzed 177 tide gauge records from 1948 to 2002 and compared global mean sea level trends for 10-year overlapping periods. This gave them a 45-year record that they split in half and obtained a trend of 1.3 mm/yr for the first half of the record and 2.2 mm/yr for the second. However, in a subsequent study that considered a longer period Holgate (2007) obtained the opposite result. He analyzed nine long and representative gauge records and found that the rate of sea level rise was greater from 1904 to 1953 (2.03 ± 0.35 mm/yr^2) than from 1954 to 2003 (1.45 ± 0.34 mm/yr^2). He observed that these results were consistent with "… a general deceleration of sea level rise during the 20th century" that he noted were suggested in analyses by Woodworth (1990), Douglas (1992), and Jevrejeva et al (2006). Church et al (2004) used TOPEX/Poseidon satellite altimeter data to estimate global empirical orthogonal functions (EOF) that were then combined with historical tide gauge data to estimate global sea level rise from 1950-2000. They concluded that "… there is no detectable secular increase in the rate of sea level rise over the period 1950-2000." Church and White (2006) used the same EOF method but extended the analysis back to 1870. They concluded that from January 1870 to December 2004 there was a sea-level rise acceleration of 0.013 ± 0.006 mm/yr^2 and a smaller acceleration of 0.008 ± 0.008 mm/yr^2 in the 20th century. The acceleration estimate of 0.013 ± 0.006 mm/yr^2 appears in the 2007 IPCC (Bindhoff, et al).

Data Selection

The monthly average tide gauge data available from the NOAA web site: (http://co-ops.nos.noaa.gov/station_retrieve.shtml?type=Tide+Data) provided the basis for the analysis herein. Data selection criteria included records of substantial length and a reasonably low percentage of missing data. The records were not corrected for ground motion reasoning that the associated trend would be constant over the period of record and thus would not affect accelerations.

A total of 59 U. S. tide gauge records exceed 60 years in duration. Of these, 2 Alaskan gauges have been removed (Seward, AK and Kodiak Island, AK) due to effects evident from the 1964 earthquake leaving a total of 57 records for potential analysis. The locations of the remaining 57 gauges are shown in Figure 1.



Figure 1. Locations of 57 U. S. gauges with record lengths exceeding 60 years.

Figure 2 presents the availability of monthly data from the 57 gauges over the period 1900 to 2010. The number of gauges contributing to a particular month reflects both the number of gauges in service and the missing data for any particular gauge and month. The maximum percentage of missing data (23.6%) occurred in July 1969. Due to the possible effects of missing data on trend and acceleration, data selection was constrained to those individual gages with a maximum of 5% missing data. Two data groups were selected for analysis. Data Group 1 (DG1) is for the period 1930 to 2010 and comprises records from all 18 U. S. qualifying (<5% missing data) gages and DG3 comprises the 6 long-term qualifying gages extending from 1910 to 2010.

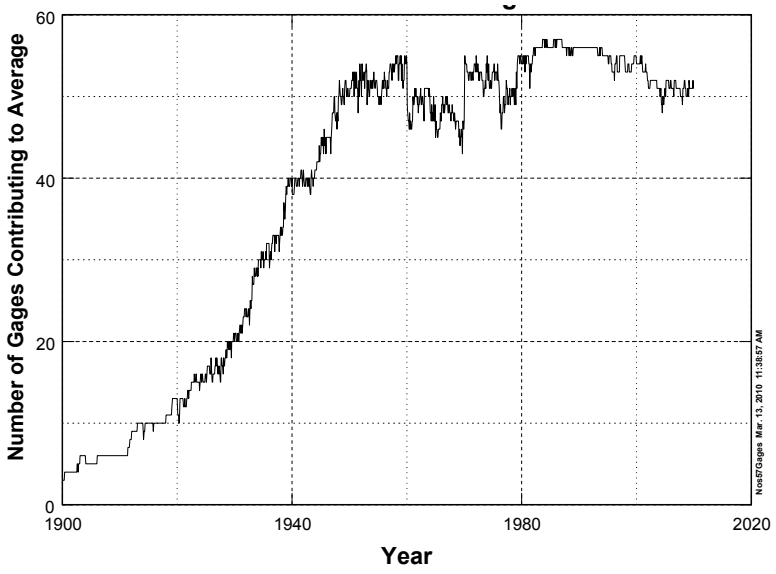


Figure 2. Number of monthly available tide measurements. All 57 U. S. gauges with record lengths exceeding 60 years.

Analysis Methods and Results

Although a number of analysis methods were examined preliminarily, only the two methods considered to be the most effective in quantifying a weak signal (the acceleration) in a noisy tidal signal are presented below.

For both analysis methods, a straightforward least squares procedure was applied to determine a_0, a_1 and a_2 in the equation

$$y(t) = a_0 + a_1 t + \frac{a_2}{2} t^2 \qquad (1)$$

where $y(t)$ is sea level at time t, a_0 is a record offset, a_1 is the trend of sea level rise and a_2 is the acceleration of the record. Although the focus is on acceleration, the trend results will be presented also.

Analysis Method 1 (AM1) consisted of a running monthly analysis of the average record for the data group such that the first results were for the period extending from the first available date for a period of 10 years, the second results extending from the first date for a period of 10 years and one month and so on such that that last result is for the full record thereby showing explicitly the effect of record length analyzed on trend and acceleration values. For AM 2, the individual records were analyzed for trend and acceleration and then the results were averaged. The purpose of applying these two methods was to identify any differences in the methods in extracting the trends and accelerations.

Detailed results will be presented for DG1 and AM1 followed by a summary for all data groups and analysis methods. The characteristics of DG1 are presented in Figure 3. The upper plot presents the average of the 18 gages and includes an 11 month running average. The oscillations evident are the seasonal variations primarily due to steric effects. The lower panel quantifies the monthly number of contributing gages. The maximum percentage of missing data (14.1%) occurred from June 1976 through September 1976. Although the maximum missing data criterion for individual records was 5%, the average of missing data was 2.9% for all 18 records.

AM 1 results for DG1 are presented in Figure 4 with the trend, a_1 and acceleration, a_2 determined from 1930 to increasing record lengths plotted at the end point of each monthly analysis. As expected, the trend and acceleration are quite dependent on record length and the "noisiness" of the results decreases with record length. The trend is reasonably well established at approximately 1.3 to 1.4 mm/yr by the year 2005; however, the acceleration is much weaker and continues to oscillate for the full 80 year record length. This figure demonstrates the dependence of calculated trend and acceleration on record length. The inset of Figure 4 presents the acceleration results over the longer period of analysis extending from 1930 to 1990 through 2010 with an expanded vertical scale.

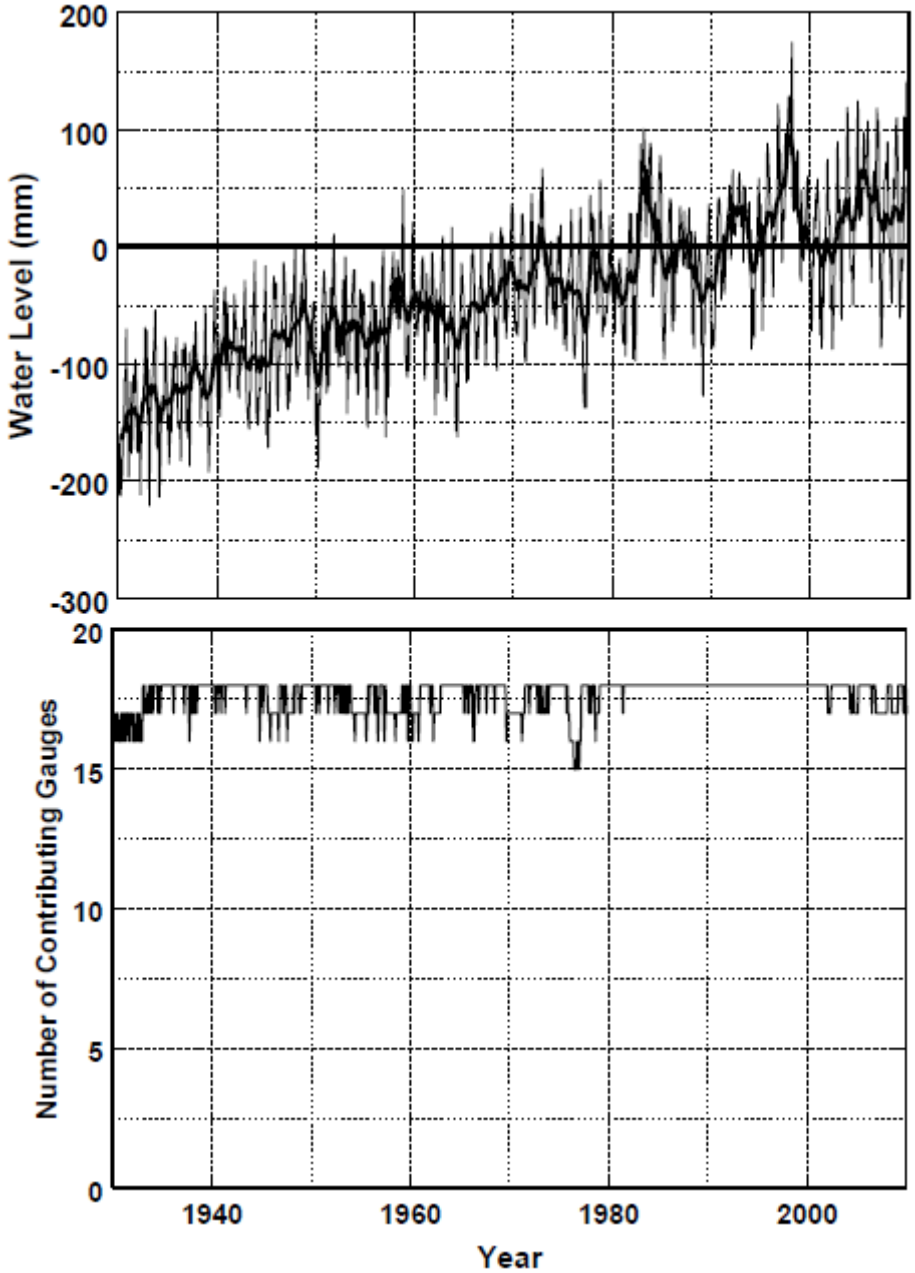


Figure 3. Characteristics of all 18 U. S. tide gauge records meeting maximum < 5% missing data criterion and in service before 1930. Upper panel: Average water level for 18 qualifying gauges and 11 month running average. Lower panel: Numbers of tide gauges contributing to each monthly average.

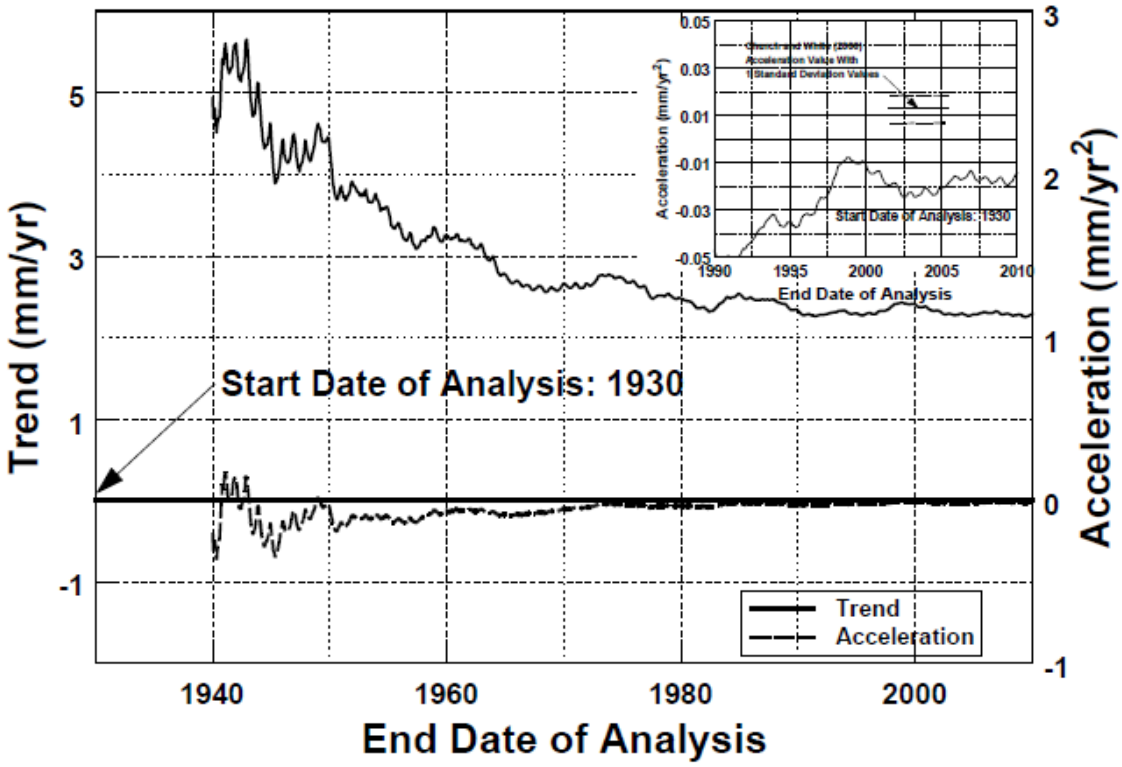


Figure 4. Data Group 1, Analysis Method 1. Sea level trend and acceleration based on analysis of average of 18 U. S. qualifying gauges. Inset is an expanded view of the acceleration results from 1990 to 2010 with the Church and White (2006) recommended acceleration of 0.013 ± 0.006 mm/yr^2 shown for comparison.

The acceleration of 0.013 ± 0.006 mm/yr^2 as recommended in Church and White (2006) is shown for reference. Based on this inset, it appears that the acceleration is approaching a small negative value.

An objective and reproducible method of extracting trend and acceleration estimates and associated errors from the two analysis methods and two data groups was applied as follows. Because the estimates improve with record length analyzed, the last maximum and minimum from data as available in Figure 4 were selected. The estimated value was taken as the average of the maximum and minimum and a measure of the error was defined as the deviation of this average from one of the extremes. Although this error measure has no formal significance, it is related to the uncertainty due to record length and not intended as a representation for the standard deviation. As an example of this method, the last maximum and minimum for the trend for DG1 and AM1 are 1.4410 mm/yr and 1.3877 mm/yr, respectively resulting in estimates for the trend and error of 1.414 ± 0.0267 mm/yr. Similarly, the last maximum and minimum for acceleration are + 0.005 mm/yr^2 and – 0.008 mm/yr^2, respectively resulting in estimates for the acceleration of -0.0015 ± 0.065 mm/yr^2. The trend and acceleration results for all combinations of

data groups and analysis methods are presented in Table 1. The results from the two analysis methods for each data group are in reasonable agreement. All of the accelerations are small and negative.

Table 1*
Results for both data groups and analysis methods

Data Group	Analysis Method			
	1		2	
	Trend (mm/yr)	Acceleration (mm/yr^2)	Trend (mm/yr)	Acceleration (mm/yr^2)
1 (1930-2010, 18 Gauges)	1.415 ± 0.0262	$- 0.0020 \pm 0.0068$	1.383 ± 0.0257	$+ 0.0016 \pm 0.0262$
2 (1910-2010, 6 Gauges))	1.968 ± 0.0305	$- 0.0044 \pm 0.0092$	1.969 ± 0.0386	$- 0.0050 \pm 0.0061$

* Note: Trends and accelerations are approximate and obtained from the values in figures of the type of Figure 4 as discussed earlier.

A sensitivity test was conducted to investigate the effect of the starting time of the analyses. The length of the record analyzed was maintained constant at 40 years and the starting time was increased monthly from 1950 to 1970 while the end time was increased from 1990 to 2010. The trends and accelerations at the ends of the 40 years analysis were found to oscillate with values determined as described previously of 1.43 ± 0.20 mm/yr and -0.0052 ± 0.0497 mm/yr^2 compared to the values in Table 1 for DG1 and AM1 of 1.415 ± 0.0262 mm/yr and $- 0.0020 \pm 0.0068$ mm/yr^2, respectively. The relatively short record length (40 years) is the reason that the error terms are so large.

Examining Figure 4 further, the longer period oscillations are due to the decadal fluctuations evident in Figure 3 (especially the 11 month average) and the shorter period oscillations are a consequence of the annual fluctuations in the average record. Recognizing the presence of the decadal oscillations, it is useful to consider their effect on the trend and acceleration values obtained. We consider a measured tide,

$$y_m(t) = b_0 + b_1 t + \frac{b_2}{2} t^2 + B\cos(\sigma t - \varepsilon) \qquad (2)$$

in which $B\cos(\sigma t - \varepsilon)$ represents the "noise" associated with the decadal oscillations, σ is the angular frequency associated with these oscillations ($\sigma = 2\pi / T_D$) where T_D is the decadal period and ε is a phase angle relating the phase of the decadal oscillations relative to the initial time of the analysis. Additionally, the coefficients determined in the analysis, a_n are expressed as the sum of the true coefficient $\tilde{a}_n$ and an error due to the contamination by the decadal oscillations, $\hat{a}_n$ ($a_n = \tilde{a}_n + \hat{a}_n$) and $\tilde{a}_n = b_n$. Following this analysis further, two informative results follow. The errors determined in the analysis approach zero as the record length increases and the rate depends on the individual coefficients. In particular, it can be shown that

$$\hat{a}_n = \frac{B}{T^n}\sum_{k=1}^{3}\frac{\alpha_{n,k}}{(\sigma T)^k} \qquad (3)$$

In which T is the record length analyzed and the α_k represent coefficients associated with the least squares solution not detailed here. Although it is somewhat surprising that the acceleration error decreases faster that the trend error, this general relationship has been tested from data as shown in Figure 4 and found to be correct. It is that the acceleration is so small that the oscillations are so critical in determination of an appropriate value.

Global Accelerations

Houston and Dean (2011) analyzed different sets of U. S. tide gages than those here and three global tide gauge data sets, including those of Church and White (2006) and a more recent set that they posted on the Permanent Service for Mean Sea Level (PSMSL) at *http://www.psmsl.org./data/*. Additionally, an extended analysis of the gauges selected by Douglas (1992) to represent global sea level were analyzed. All three of these global analyses yielded small negative accelerations reasonably consistent with those reported here for the U. S. gauges.

Summary and Conclusions

Two data groups were selected from the 59 U. S. gauge records of 60 years or greater in length. Specification of a maximum 5% missing data resulted in identification of qualifying gauges. Two analysis methods were selected based on their capability to quantify a weak acceleration signal in noisy tide gauge data and to illustrate the effects of record length.

AM 1 consisted of averaging the tide record in the data group and analyzing the averaged record for trend and acceleration. For AM2, all gages in the data group were analyzed individually for trend and acceleration and then the results analyzed to present results in the form of Figure 4.

With the reservation that the results presented in detail herein are limited to U. S. gauges and therefore not necessarily representative of global characteristics, it is of interest that the results agree qualitatively with those of several investigators of global sea level acceleration. Holgate (2007) analyzed nine long tide gauge records and found that the trend from 1904 to 1953 was 2.03 ± 0.35 mm/yr compared to the rate 1.45 ± 0.34 mm/yr for the period 1954 to 2003. Considering a quadratic representation for sea level variation, this is equivalent to an acceleration of – 0.0116 mm/yr^2, an order of magnitude greater than (but of the same sign) suggested by the results obtained herein. In a study of four long-term gages in Australia and New Zealand, Watson (2011) found small negative accelerations over the 20th Century. Church and White (2006) applied an EOF methodology and found an acceleration of + 0.013 ± 0.006 mm/yr^2 for the period 1870 to 2004 such that the midpoint of this period is 1937. For the "20th Century" with a mid-

point at 1950, they determined an acceleration of 0.008 ± 0.008 mm/yr^2. In a later study, Church and White (2011) determined an acceleration of 0.009 ± 0.004 mm/yr^2.
As an overall conclusion, our results do not support a positive acceleration in the U. S. tide gauge records as suggested by IPCC and some investigators. Rather, we find a very small deceleration. The results based on two data groups and two analysis methods are reasonably consistent internally consistent and with a recent reported analysis by Houston and Dean of three global data sets.

Acknowledgements. We appreciate the user-friendly accessibility of the NOAA tide gauge data and reviews provided by David Divoky, Mark Crowell and Bruce Douglas.

References

Bindoff, N.L., and Coauthors, 2007, Observations: Oceanic climate change and sea level, *Climate Change 2007: The Physical Science Basis,* S. Solomon et al, eds, Intergovernmental Panel on Climate Change, Cambridge University Press, 385-432

Church, J.A. White, N.J., Coleman, R., Lambeck, K., and Mitrovica, J.X. 2004, Estimates of the regional distribution of sea-level rise over the 1950 to 2000 period. Journal of Climate, 17 (13), 2609-2625.

Church, J.A. White, N.J. 2006 "20th century acceleration in global sea-level rise," Geophysical Research letters, 33 (1), L01602.

Church, J.A. and White, N.J., 2011. Sea-level rise from the late 19th century to the early 21st century, Survey Geophysics, doi:10.1007/s10712-011-9119-1.

Douglas, B.C. 1992, Global Sea Level Acceleration, Journal of Geophysical Research, 97 (C8), 12699-12,706

Holgate, J.R. and Woodworth, P.L., 2004, Evidence for enhanced coastal sea level rise during the 1990's, Geophysical Research Letters, 31, L07305, doi:10, 1029/2004GL019626

Holgate, S.J., 2007, On the decadal rates of sea level change during the twentieth century, Geophysical Research Letters, 34, L01602, doi:1029/2006GL028492

Houston, J. R. and R. G. Dean, 2011Sea-level acceleration based on U. S. tide gauges and extensions of previous global gauge analyses, Journal of Coastal Research, Vol. 27, No. 3, p. 409-417.

Jevrejeva, S., Grinsted, A.. Moore, J.C., and Holgate, S., 2006, Nonlinear trends and multiyear cycles in sea level records, Journal of Geophysical Research, 111, C09012, doi:10.1029/2005JC003229

Jevrejeva, S., Moore, J.C., Grinsted, A., and Woodworth, P.L., 2008, Recent global sea level acceleration started over 200 years ago?, Geophysical Research Letters, 35, L08715, doi:10, 1029, 2008GL033611.

Watson, P.J., 2011. Is there evidence yet of acceleration in mean sea level rise around mainland Australia?, Journal of Coastal Research, 27, 368-377.

Woodworth, P.L., 1990, A search for accelerations in records of European mean sea level, International Journal of Climatology, 10, 129-143.

A Case Study on the use of Advanced Fiber Wrap Composites for Timber Pile Repair and Protection of a Pier Structure

T. Jiménez, LEED AP[1] , D. Kost[2], and J. Percival[3]

[1] Fyfe Company LLC, Engineering Department, Project Engineer, 8380 Miralani Drive, San Diego, CA 92126; PH: 858-642-0694; FAX 858-444-2980; email: tommy@fyfeco.com
[2] Fyfe Company LLC, Engineering Department, Project Engineer, 8380 Miralani Drive, San Diego, CA 92126; PH: 858-642-0694; FAX 858-444-2980; email: dane@fyfeco.com
[3] Fibrwrap Construction Canada Limited, Vice President, Unit 31 – 15531 24th Ave, Surrey, British Columbia, Canada. V4A2J4 PH:604-542-5429; FAX:604-542-5439; email: john@fclp.com

ABSTRACT

The use of Advanced Fiber Wrap Composite systems has been widely used in buildings and bridges during the past two decades. As the global structural engineering community has adopted this technology, so has the coastal infrastructure community. This paper will cover in detail the use of this relatively novel technology in the repair and protection of timber piles. The pier structure, which is used for commercial purposes, was severely deteriorated due to the aggressive environmental conditions and the age of the structure. Advanced Fiber Wrap Composite Systems were being utilized to supplement confinement, and to provide protection to selected timber pile elements. Also, the use of special epoxy resins and proven repair methods which were implemented as part of the retrofit will be discussed. The aim of this paper will be to discuss the Advanced Fiber Wrap Composite Systems method of repair and to compare with the current alternative conventional methods of repair. The benefits and deterrents for the different repair methods which were discussed by the engineer of record and owner alike will be discussed both from the construction, structural, and from the financial standpoint.

The project that will be discussed is on the Halifax, Nova Scotia, Canada waterfront. Part of the scope for this project consisted of working from floating platforms to execute the repair of the piles. Underwater divers were also brought on to apply the Fiber Wrap System under water in the tidal zone. The FRP applicator successfully completed the project within schedule and on budget.

INTRODUCTION

For the past decade, the Department of Fisheries and Oceans Canada has worked with different provincial and municipal jurisdictions in rehabilitating the public and industrial waterfronts. Public Works and Government Services Canada Small Crafts and Harbors have been tasked with updating their aging wharves and piers in small fishing towns. The project at hand was directed by the City of Halifax's Waterfront Development Corporations Limited. The City of Halifax waterfront, like other Atlantic Canada cities, is in the midst of undergoing a comprehensive rehabilitation. The Cable Wharf, one of the city's most notable waterfront landmarks, has been receiving annual timber pile repair and preservation on the substructure.

Since the work is done through the City of Halifax's procurement department, the project goes out to public tender annually and the Tyfo® Fibrwrap® Systems have been installed on their timber piles for the last two years. The long term maintenance program is to continue until all of the piles are rehabilitated. The maintenance program has budgeted to fund work for about 50 piles per annum. The repair and preventative maintenance program started with the most compromised piles and will end with the more sound timber pile elements.

BACKGROUND

The owner retained ADI O'Halloran Campbell Consultants Ltd., a structural engineering firm with offices in Halifax, Nova Scotia to review all available as-built drawings and documentation, write an investigation report summarizing the condition assessment of the structure, provide repair methods, and construction drawings for the wharf repair. Fyfe Company worked closely with the engineer of record to provide a cost efficient solution that protects the timber structure.

An interesting note being that Halifax harbor has become a very clean waterfront due to recent environmental remediation measures. No longer being a dumping ground for sewage and ship bilges, most aquatic life has returned. One of these marine species being the wood boring Toredo worm. These marine worms can have a detrimental effect on timber structures. Acknowledging a wharf is a platform parallel to the waterfront at a harbor or navigable river for docking, loading, and unloading ships; a pier is a platform extending perpendicular from shore over water and supported by piles, used to secure, protect, and provide access to ships. The Cable Wharf is a timber structure consisting of a pier supported by wooden piles driven into the bay floor. Several of the timber piles had suffered major weathering/decay due to the severe marine environment and marine borers. The wharf supports a host of tourist shops and restaurants that rely on the soundness of the substructure.



Figure 1: Halifax Cable Wharf

Some new wooden bracing has been used for the regular upkeep of the timber structure however that did not address the issue of the piles with varying degrees of decay. Prior to the repair of the pier, the overall condition of the deck was found to be in fair condition. Portions of the substructure (piles), however, were in poor to very poor condition. The prevalent damage was in the form of decaying cross-

sections of the timber piles due to marine life degradation, and extreme freeze thaw cycles. See figures 2 and 3 for the before condition of the piles.





Figures 2 and 3: Timber piles with significant deterioration

REPAIR OPTIONS

When facing an aging marine timber structure, owners are faced with a few solutions. One option for dealing with deficient piles is the removal and replacement of the individual piles. This method would require large pile driving equipment, and adequate shutdown time for construction. With a structure like the Cable Wharf this is not feasible from a construction standpoint due to the existing businesses that are currently on the wharf. There simply is not enough access for this type of construction to occur.

Another option is the replacement of the entire pier structure itself. Although this might be the most attractive option from a durability and aesthetics standpoint, this solution is not cost effective for the owner, or the business owners that are on the timber structure.

For protection only, stay in place flexible fabric forms can be applied to the pile and backfilled with grout. This similar but more simple solution than fiber wrapping would be lower cost initially, however due to durability concerns this means of repair was not pursued. Fiber wrap was the chosen repair method because it allows the timber piles to be repaired with a rigid FRP jacket. Using fiber wrap allowed the businesses to remain in operation throughout the project. The life cycle cost of this method was the most ideal to the client. Also, the increase in structural capacity of the repair was attractive.

DESIGN AND INSTALLATION

Prior to the project start, a full review of the products and the methodology of application were undertaken by the owner. The specified GFRP system exceeded all required standards and was fully approved for use. Before the application of the FRP composites for protection/strengthening, the piles had to be thoroughly cleaned and all sea organisms removed. Upon completion of cleaning and determination of sectional loss of wood piles, the wrapping process could begin. All the piles that were considered to be deficient were to be repaired with one of two FRP solutions. The first being a pre-formed FRP jacket that gets backfilled with underwater curing grout. The grout fills the annular space between the FRP jacket as well as any voids in the timber piles where unsound material was removed. This solution was chosen for the piles that suffered the most loss of cross-section. The pre-cured jacket consisted of multiple layers of the Tyfo® SEH-51A System in both the horizontal and vertical direction.



Figure 4: Tyfo® PR-Jacket



Figure 5: Installed Tyfo® PR-Jackets

The second solution was to use "wet layup" of FRP applied to the piles that needed protection, but still had most of their original cross-sectional area. The fiber is saturated with a special underwater epoxy (hydrophilic) Tyfo® SW-1S ensures that the composite will cure in moist conditions. The Tyfo® SW-1S is easily recognizable by its grey color. See figures 6 and 7 for pictures showing the application of the underwater composite. All the piles were wrapped from the underside of beams to a minimum of twenty four inches below the tidal zone. The wet layup wrapping solution was performed by certified applicator divers to allow the piles to be protected below the water line.



Figure 6: Tyfo® SW-1S Saturation



Figure 7: Divers working below the water

Both of these systems were installed to extend the service life of the timber piles per the engineer of record. However these systems can be designed to provide additional shear strength, confinement, and bending strength to existing piles. Even though the project did not call for structural strengthening, the pre-cured FRP jackets provide nominal localized axial strength, and the wet lay-up provides a nominal increase in shear capacity and confinement.

CONCLUSIONS



The use of advanced composites for the rejuvenation, and environmental protection is a proven methodology. Not only does the system save in capital costs to the owners and operators of these marine terminals, but also in maintenance costs. By having a system that allows for the rehabilitation of piers, wharfs, and other waterfront structures, while maintaining full operation during construction process, ensures minimal disruption to business activities. In any business down time costs money, regardless if the project is public or private. Extending the service life of marine structures using advanced composites such as GFRP and CFRP fibrwrap systems can be summed up as being faster, cheaper, and better than any other conventional methodology.

REFERENCES

ACI 318-05 Building Code Requirements for Structural Concrete, American Concrete Institure, ACI, [2005].
IBC 2006, International Building Code, IBC, International Code Council, ICC [2006].
ICC ES ESR 2103, Concrete and Masonry Strengthening Using the Tyfo® Fibrwrap® Fiber-Reinforced Composite Systems, International Code Council, ICC [June 2008].
ICC AC125 Acceptance Criteria for Concrete and Reinforced and Unreinforced Masonry Strengthening Using Externally Bonded Fiber-Reinforced Polymer (FRP) Composite Systems, [October 2006].
Fyfe Co. LLC, Design Manual for the Tyfo® Fibrwrap® Systems, Rev. 8.
ACI 440.2R-08 Guide for the Design and Construction of Externally Bonded FRP Systems for Strengthening Concrete Structures, ACI Committee 440, American Concrete Institute

Design and Construction of Kaumalapau Harbor Breakwater Island of Lanai, Hawaii

Scott P. Sullivan[1]

[1]Sea Engineering, Inc., Makai Research Pier, Waimanalo, Hawaii 96795;
PH (808) 259-7966; FAX (808) 259-8143; email: ssullivan@seaengineering.com

Abstract

Kaumalapau Harbor is a small barge harbor located on the southwest coast of the island of Lanai in the State of Hawaii, U.S.A. The harbor was protected by an old, deteriorated, rock rubblemound breakwater, originally constructed in 1925. The breakwater was recently completely rebuilt by the U.S. Army Corps of Engineers, Honolulu District, in association with the State of Hawaii. Oceanographic design considerations included a water depth of about 21 m (70 ft) and direct exposure to possible 10.7 m (35 ft) hurricane strength storm waves. The repairs utilized an armor layer of 31.8 tonne (35 ton) Core-Loc™ concrete armor units, the largest units of this type used to-date. The use of Core-Loc units, a relatively new armor unit type, presented both design and construction challenges to insure that their performance capability was maximized. Particular attention was placed on developing a Core-Loc placement plan to achieve the required unit packing density, and utilizing rigorous construction techniques to achieve the specified armor layer placement. This project contributed significantly toward furthering design and construction guidelines for Core-Loc use. Construction was completed in 2007, and the project won the ASCE, Hawaii Section, 2008 Outstanding Civil Engineering Achievement Award.

Introduction and General Description

Kaumalapau Harbor is a small barge harbor located on the southwest coast of the island of Lanai in the State of Hawaii, USA (Figure 1). The harbor was constructed in 1925 by the Hawaiian Pineapple Company (Dole Company) for the export of pineapple, the island's primary product and business up until the early 1990s. The harbor is located in a small embayment providing a 4 hectare (10 acre) berthing area with water depths of 6.1 to 18.3 m (20 to 60 ft). A breakwater was constructed extending toward the south from the northwest headland of the embayment. The original length of the breakwater was about 107 m (350 ft), with a crest elevation of about +3 m (+10 ft) mean lower low water (MLLW). The breakwater was constructed of quarried stone and field stone from the island. Shoreside facilities on the north side of the embayment in the lee of the breakwater include a 122 meter (400 ft) long wharf, sheds, and barge loading and unloading equipment.

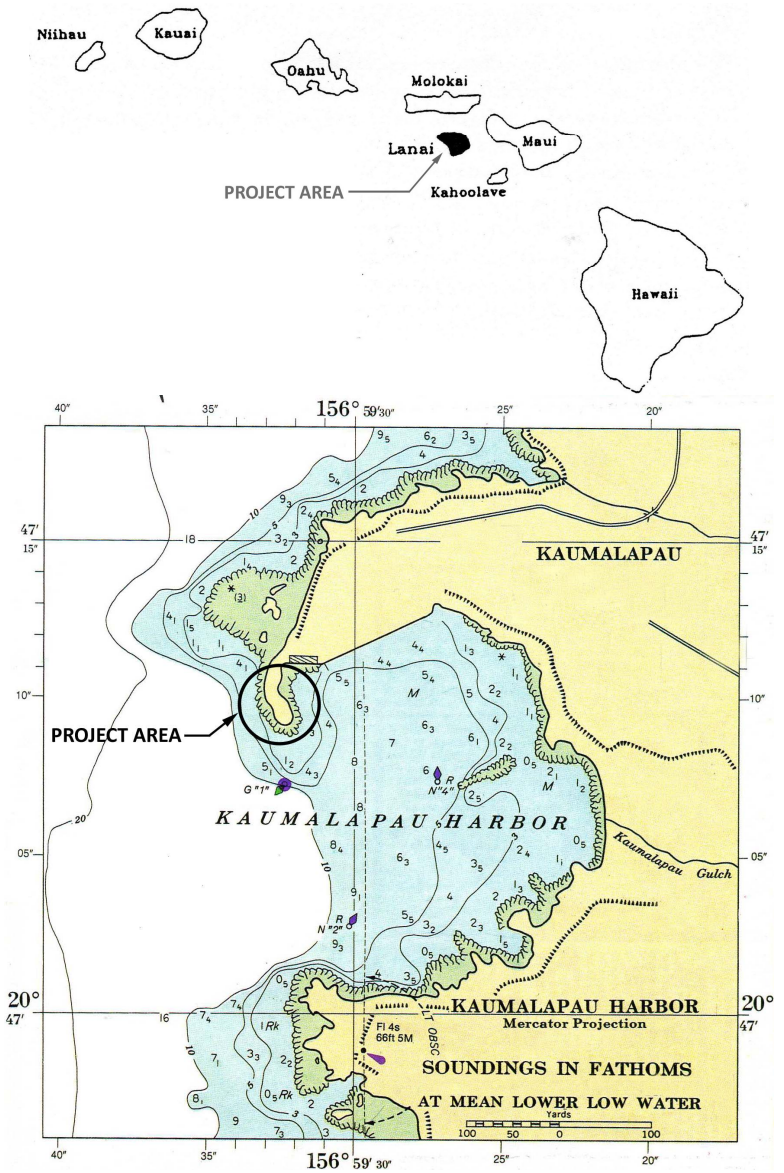


Figure 1. Kaumalapau Harbor location and vicinity

It is not known whether the original breakwater structure was an "engineered" design, or simply a rubblemound constructed of a random mix of available stone. Even if it was an engineered structure, it would not have met the criteria required by modern breakwater design practice, nor would sufficient information regarding oceanographic design conditions have been available to the designer. The breakwater suffered extensive damage over the years, and was repaired numerous times. Maintenance of the breakwater was done using rock, concrete rubble, concrete filled pineapple wagons, and even several concrete filled school buses. Repairs following Hurricane Iwa in 1982 were made using dolos concrete armor units, however the armor unit size using existing forms available in Hawaii was too small for the design conditions and the units were quickly broken and reduced to rubble. In 1992 Hurricane Iniki badly

damaged the breakwater, and only a portion of the structure remained above water level.

The project was designed and constructed by the U.S. Army Corps of Engineers, Honolulu District, for the State of Hawaii. Detailed project design and construction plans and specifications were completed by Sea Engineering, Inc. (SEI) under contract with the Honolulu District. The repairs utilized an armor layer of CORE-LOC™ (Core-Loc) concrete armor units, recently developed by the U.S. Army Engineer Research and Development Center, Coastal and Hydraulics Laboratory (ERDC/CHL). Core-Loc design assistance was provided by W.F. Baird & Associates, Ltd., licensed Core-Loc design engineers. Construction was completed in June 2007 at a final construction cost of $21,229,000. In 2008 the project won the American Society of Civil Engineers (ASCE), Hawaii Section, Outstanding Civil Engineering Achievement Award.

Oceanographic Design Parameters

The bottom slope directly seaward of the breakwater is about 1V:10H, with the toe of the old rubblemound breakwater in 21 m (70 ft) of water. A multibeam sonar system was used to accurately map the ocean bottom, the shoreline, and the existing rubblemound topography at the start of detailed design engineering.

The project site has direct exposure to long period southern swell, westerly waves generated by winter season low pressure systems passing through Hawaii, and partial exposure to winter season north swell refracting and diffracting around the islands. The site is completely sheltered from the prevailing northeast tradewind waves by the island of Lanai itself.

Although hurricanes occur very infrequently in Hawaiian waters, Kaumalapau is potentially directly exposed to hurricane strength storm waves approaching from the southeast to southwest. Hurricane Iwa (1982) and Hurricane Iniki (1992) are the only two hurricanes to strike the Hawaiian Islands in the past 50 years, and both passed west of Kaumalapau and struck the island of Kauai. Wave hindcasts for these two storms showed deepwater wave heights offshore of Kaumalapau of 6.7 and 6.1 m (22 and 20 ft) for hurricanes Iwa and Iniki, respectively. Predicted scenario hurricane parameters were used to determine extreme design waves for Kaumalapau. Numerical model generated deepwater wave heights of 10.7 m (35 ft) are estimated to result from a direct hurricane strike on the project site. In general, wave conditions at the project site are moderate, and an incident wave height of about 4.6 m (15 ft) was considered reasonable as an upper limit for harbor operating conditions, after which surge conditions at the dock would preclude vessel berthing and cargo handling. A hurricane event, with deepwater wave heights of 10.7 m (35 ft), was selected for structural design of the new breakwater.

The tide range in Hawaii is low, 0.7 m (2.2 ft) between mean lower low and mean higher high water at the site. (Note – all elevations are referenced to the mean lower low water datum.) A stillwater level rise of +1.5 m (+5 ft) is estimated during

hurricane conditions, including a mean high water tide, a rise due a drop in atmospheric pressure and storm surge due to wind stress. In Hawaii, with deepwater extending very close to shore, the effects of wind stress surge are almost negligible. And, because the seaward toe of the breakwater is in deepwater and the waves are non-breaking, there is no appreciable wave setup.

Breakwater Design

Initial planning and design for the repair project was accomplished by the Honolulu District, and included numerical and physical modeling to aid in selecting the general plan of improvement. Detailed design by Sea Engineering, Inc. was initiated in 1998, and went through several iterations, including value engineering and additional two-dimensional breakwater stability physical modeling. Kaumalapau Harbor breakwater repair utilized the largest Core-Loc armor units constructed to date (31.8 tonne), and the deepest Core-Loc toe (-13.7 m) and longest overall slope length (approximately 34 m) of any Core-Loc armored structure.

Final Design Elements

General Breakwater Configuration: The project site was topographically complicated, with a shallow nearshore rock bench at the seaward toe of the breakwater, and then a very steep drop to the sea floor. Thus the design required a complex three-dimensional approach. The breakwater alignment was designed for a best-fit position on the existing rubblemound, which was excavated and shaped to form the core of the new breakwater. Excavated material was used as core material for the breakwater head, and as stone for a harbor side toe berm. The selected crest cap elevation is +4.4 m (+14.5 ft), and provides for no overtopping during all prevailing wave conditions when the harbor can reasonably be expected to be operating, and only minor overtopping during typically occurring storm wave conditions. Portions of the Core-Loc units randomly extend about 1.5 m (5 ft) above the crest cap. The crest width is 12.2 m (40 ft) at the top of the underlayer stone (+2.9 m [+9.5 ft] elevation), which would permit use of a ringer crane for construction. A horizontal row of Core-Loc units was placed on the ocean side of the crest to improve armor stability and energy dissipation during wave overtopping conditions. It was not considered practical to construct a non-overtopping structure for the very infrequent extreme storm wave conditions to which the breakwater could possibly be subject. The sheer size of such a structure would not fit the physical confines of the project site, and the cost would have been prohibitive. In addition, there are limited harbor facilities which would be damaged by wave overtopping. Instead, the breakwater has been designed to be stable under possible significant wave overtopping conditions. The ocean side and harbor side breakwater slope is 1V to 1.5H.

Toe Depth and Configuration:

Ocean Side**:** The landward end of the breakwater toe was placed in a 1.2 m (4 ft) deep toe trench excavated into hard rock, and then secured by filling the trench with tremie concrete. This extends for approximately 30 m (100 ft), at which point the toe transitions down the existing bottom slope to a toe trench excavated into the existing

rubblemound at the -13.7 m (-45 ft) depth. The Core-Loc was placed over underlayer stone in the toe trench, and buttressed by a 4.6 m (15 ft) wide stone berm, with an elevation of -12.6 m (-41.5 ft). The toe berm also aids in stabilizing the structure during possible seismic (earthquake) loading conditions.

Harbor Side**:** The harbor side toe extends to a toe trench excavated into the existing rubblemound at a depth of -6.1 m (-20 ft), and is buttressed by a 9.1 m (30 ft) wide stone berm, with a crest elevation at -4.6 m (-15 ft).

Armor Layer: The armor layer consists of 31.8 tonne (35 ton) Core-Loc concrete armor units, placed in a random (non-uniform) matrix and oriented to achieve maximum interlocking. A detailed Core-Loc placement grid pattern was developed and specified in order to ensure that the desired packing density was maintained. A 0.58 packing density was initially considered to be the tightest placement that could realistically be achieved with such large units. This was revised to 0.62 during construction after a change was made in the Core-Loc shape and additional placement testing was accomplished. The placement grid specifies a precise x,y,z coordinate (position) for each Core-Loc unit. The placement pattern also considers the physical reality of placing 31.8 tonne (35 ton), nearly 4 m (13 ft) long armor units, and makes minor adjustments to the toe trench elevation to permit proper unit placement around the head. The placement pattern is based both on the hydraulic considerations of stable toe depth (as determined in the 2-D model tests), and achieving a uniform top surface and Core-Loc termination at the crest to maximize stability during design wave overtopping conditions.

Concrete Crest Cap: The final design utilized a solid mass non-reinforced concrete crest cap to contact and buttress the Core-Locs, and to contain the underlayer stone on the crest. On the ocean side, the crest is positioned such that the front edge has minimal exposure to wave uprush and pressure within the stone underlayer, and a horizontal row of Core-Loc units is placed on the underlayer stone crest fronting the concrete crest cap to help further dissipate overtopping wave energy. The crest cap is then completely formed around the Core-Loc crest units. The 1.5 m (5 ft) thick, nominal 7.6 m (25 ft) wide, crest cap was cast in 4.6 m (15 ft) sections, with shear keys between each section and a continuous key into the breakwater crest along the axis of the breakwater. The cap weighs about 8.2 tonnes (9 tons) per linear foot, and 122 tonnes (135 tons) per section.

Breakwater Section: Figure 2 shows the breakwater typical section, and a summary of final design parameters is shown on Table 1.

Table 1 Design summary

Crest	Elevation:	+4.4 m (+14.5 ft) MLLW (top of concrete cap)	
	Width:	Approx. 7.6 m (25 ft) clear width across concrete cap between ocean and harbor side Core-Locs. 12.2 m (40 ft) wide across top of underlayer and core stone at the +2.9 m (+9.5 ft) elevation.	
	Type:	Solid mass concrete cap, 1.5 m (5 ft) thick, unreinforced, formed around top row of Core-Loc units.	
Armor Layer Toe	Ocean Side: Sta. 0+00 to (-)1+00:	Elevation	1.2 m (4 ft) below existing hard bottom
		Buttress	Toe Trench with Tremie Concrete
	Sta. 0+00 to 2+20:	Elevation	-13.7 m (-45 ft)
		Buttress	4.6 m (15-ft) wide stone berm
	Harbor Side:	Elevation	-6.1 m (-20 ft)
		Buttress	9.1 m (30 ft) wide stone berm
Armor Layer	Type	Concrete Core-Loc	
	Weight	31.8 tonnes (35 tons)	
	Placement	Single layer, random orientation, individual unit position specified by a x,y,z coordinate placement grid to achieve a 0.62 packing density	
Underlayer	Material	Stone (Quarried and Salvaged)	
	Weight	2.3 to 4.1 tonnes (2.5 to 4.5 tons)	
	Placement	Layer thickness of 2.1 m (7 ft)	
Core	Material	Salvaged stone and concrete rubble	

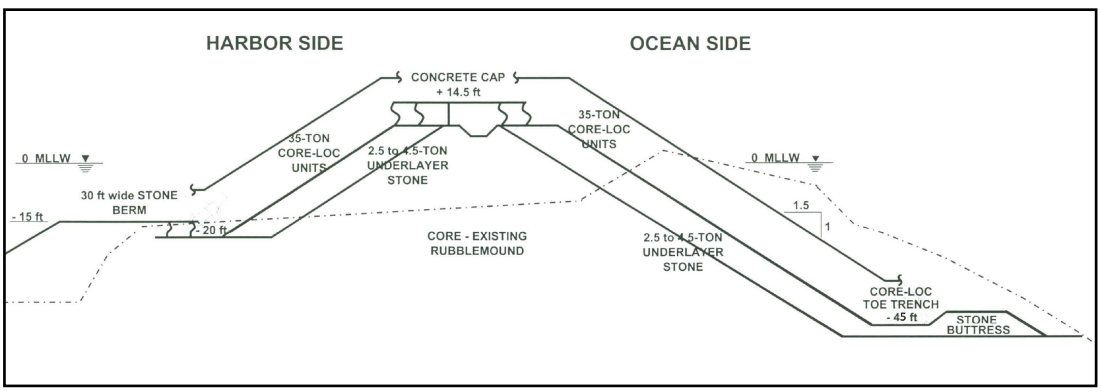


Figure 2. Typical breakwater section

Core-Loc Design Considerations

During initial planning and design studies for the project, a decision was made by the Honolulu District to use the newly developed Core-Loc concrete armor unit, created by ERDC/CHL. The Core-Loc shape is patented by the U.S. Army Corps of Engineers, and there are licensing requirements for both Core-Loc design and use. The Core-Loc unit has very good interlocking and thus a relatively high design stability coefficient (recommended K_D = 13 and 16 for breakwater head and trunk, respectively), and a robust shape which reduces the possibility of breakage of the unreinforced units. The units are also designed to be placed in a single layer, which reduces the volume of concrete required over typical two layer systems, and thus reduces cost. The units were so new that at the time of their selection for use at Kaumalapau Harbor there had not yet been a completed project built with Core-Loc units anywhere.

Core-Loc Shape

The Kaumalapau project used the largest Core-Loc units constructed to-date, and, because of the deep toe depth, the armor slope would be about 34 m (110 ft) long. The combination of large Core-Loc size and long slope length, which can result in unit movement as the armor layer consolidates over time, was considered to introduce a greater potential for failure of the Core-Locs due to static loads than existed on other previous Core-Loc projects. ERDC/CHL accomplished further study of the Core-Loc strength in order to define the structural response of the large Kaumalapau units. The study included physical model and numerical model studies. Study results indicated a maximum flexural stress in the toe row of Core-Locs of 3,450 kPa (500 psi). Based on these results, a Core-Loc concrete flexural strength of 4,825 kPa (700 psi) was recommended by ERDC/CHL and was required in the construction specifications. Small radius fillets were suggested to help relieve stress magnification in the chamfer areas.

As design for Kaumalapau Harbor proceeded, other projects began utilizing Core-Loc units and provided prototype experience suggesting ways to improve the units. One result of this experience was a recommendation to modify the original shape of the Core-Loc unit in an effort to further reduce stress concentration areas and improve fabrication techniques to maximize concrete strength. The shape changes were principally made to add larger radius fillets in the chamfer regions at the intersection of the Core-Loc legs, and thicken the center section to accommodate the fillet. The new Core-Loc shape is more “compact”, and thus heavier for the same given characteristic length (“C” dimension, or controlling height of the unit).

Packing Density and Placement

In order to provide adequate and uniform coverage on the breakwater slope and maintain unit-to-unit interlocking and contact, a sufficient packing density must be achieved. This is particularly critical for concrete armor units in a single layer configuration. Packing density is defined as the number of individual units required to cover a given area of slope, and is defined as a coefficient related to the volume of the unit. In general, the larger the unit becomes the lower the practicable achievable

packing density. Larger units become more difficult to handle, which limits the ability to pack them together, and the concrete crushes where they contact, increasing friction and making them "sticky" so they do not slip together as easily as lighter units. Initial testing of Core-Loc by ERDC/CHL showed stable structures built with packing densities ranging from 0.54 up to 0.64, with 0.60 generally recommended. A packing density coefficient of 0.62 was ultimately used for preparation of the Kaumalapau placement plan. This is a high coefficient for units weighing 31.8 tonnes (35 tons), however the Contractor was able to achieve it during construction of the Kaumalapau project.

Core-Loc was designed to be placed in a single layer thickness in a random orientation with a fixed packing density. The specified packing density must be strictly maintained during construction to assure proper interlocking between units in order to achieve the desired hydraulic stability. For the Kaumalapau project a Core-Loc placement plan was specified, with each unit being assigned a specific x,y,z coordinate for its location on the structure. Although Core-Loc units can be placed randomly along the toe, a uniform pattern placement has been shown to be more stable if it can be achieved in the field. The Kaumalapau construction plans specified that the Core-Loc toe units be placed in the toe trench in a "cannon style" pattern placement. The first course was set with the central fluke pointing seaward at a 45-degree angle like a cannon barrel, and were placed side-by-side with a minimal space between adjacent units. The second course was placed such that they straddled the first course toe units. Subsequent armor units moving up the slope to the crest were placed in a random matrix and oriented to achieve maximum interlocking. The typically very clear water at the project site greatly facilitated placement of the toe units in a uniform pattern, and permitted camera and diver placement verification prior to the placement of subsequent units.

Core-Loc Construction Specifications

Concrete for Core-Loc Units: The specified flexural strength of the Core-Loc concrete was 4,830 kPa (700 psi) at 28 days. The maximum allowable water/cement ratio was 0.40 by weight, and the total air content could not exceed 5%. Particular attention was given to the concrete temperature during curing. At no time could the temperature of the concrete exceed 74° C (165° F), and the maximum temperature differential between the interior and exterior concrete could not exceed 20° C (36° F). Portland Type II low alkali cement was specified. Pozzolan, if used, had to be fly ash conforming to the requirements of ASTM C 618, Class F. (Pozzolan is not commonly used in Hawaii, and was not used for this project.) Fiber reinforced concrete was specified, in accordance with ASTM C 1116, Type III, synthetic reinforced concrete, with 7.5 pounds of structural fibers per cubic yard of concrete used (forta fiber or equal). The concrete-placing temperature was not permitted to exceed 30° C (85° F), which basically necessitated that the Contractor cast the Core-Loc at night. In addition, in order to meet the concrete curing temperature requirements, the Contractor used a significant amount of water in the form of ice in the mix. The concrete mix resulted in a concrete unit weight of 2,400 kg/m^3 (150 pounds/cubic foot).

Placing Core-Loc Armor Units: The toe units (first and second rows) were placed in the "cannon" style of uniform placement. Placement of Core-Loc units on the slope was based on the following parameters.

i. Maintain the specified packing density by insuring that each unit is placed at its specified location according to the placement plan, with the centroid of each unit being within 0.38 m (15 inches) of the specified location. Care must be taken to avoid small error "creep" in the placement of individual units which may be additive, eventually resulting in being unable to place the units at their specified location.
ii. Moving up the slope, successively higher units should be "keyed" into and between two units below (i.e. fit the higher Core-Loc into the "pocket" between two adjacent lower units). Keying into the lower units should result in contact with at least one, and usually both, of the lower units. The keying into and between the lower units also results in units on the same horizontal row not being in contact.
iii. Every Core-Loc unit must rest on and contact the underlayer stone.
iv. The units shall be placed with a random orientation, and with different attitudes so as to interlock with and contact adjacent units to the maximum extent practicable. Every reasonable effort should be made to rotate and adjust the individual unit orientation so as to achieve the best interlocking and contact possible. However, it is recognized that interlocking and contact will vary, and that every unit may not have direct contact between all adjacent units.
v. Effort should be made to not place units with an H-member parallel to the slope, and less than one-third of the units shall be oriented this way, and they should be scattered throughout the structure and not placed in groups.

The specification for Core-Loc placement also included requirements for a physical scale model of the breakwater repair plan to be built by the Contractor, for building a test section of the Core-Loc placement on land, and for the Contractor to retain a Core-Loc Specialist to assist with construction. The purpose of the scale model was to give the Contractor an opportunity to see how the various component parts fit together, and thus aid in working out solutions to construction questions before actual construction takes place. Constructing with 31.8 tonne (35 ton) armor units is not easy, and errors in prototype construction can be costly and time consuming. This is also why a test section of the Core-Loc placement on land was required prior to starting work on the actual breakwater. This gave the Contractor a chance to practice slinging units and an understanding of unit attitude variation to facilitate interlocking, and practice adhering to a precise placement plan prior to placing units underwater. The requirement for the Contractor to retain a Core-Loc Specialist (CLS) was to insure that the Contractor had access to an experienced Core-Loc design and construction specialist. The CLS advised on the preparation of the Contractor's required Construction Execution Proposal, provided Core-Loc construction training, supervised Test Section practice, prepared modifications to the Placement Plan, and

assisted with Quality Control. This turned out to be an important requirement, and greatly facilitated construction of the breakwater.

Core-Loc Related Construction Highlights

Traylor Brothers (Pacific), Inc. (Traylor), headquartered in Irvine, California, was the successful construction bidder, and did the site preparation and all the on-site breakwater construction work. GPRM Prestress, LLC was the pre-cast fabricator for the Core-Loc armor units, which were made at their Campbell Industrial Park, Oahu, pre-cast facility and shipped by barge to Lanai. The Kaumalapau Core-Loc units won the 2008 Precast/Prestressed Concrete Institute award for "Best Custom Solution". The CLS was W.F. Baird & Associates Ltd.

Contractor's General Methodology

On-site construction was accomplished primarily by one piece of heavy equipment, a Manitowoc 2250 crane that was used to shape the existing rubblemound to form the core, place all the stone, and place the Core-Loc units. Ancillary equipment included a smaller Manitowac 999 crane for handling of the Core-Loc units on the barge, and low boy trailers used for moving Core-Locs to and from the inland stockpile area. Underlayer stone was obtained from a quarry site on the island of Molokai and barged to Lanai. Suitable stone salvaged from on-site, as approved by the Honolulu District, was also utilized in the construction. Positioning for survey of the lines and grades of the core and underlayer and precise positioning of the Core-Loc units was accomplished by using a Novatel Propak L1L2 RTK DGPS Base Station OEM4, and a Rover OEM4 Receiver with an antenna mounted on the crane boom head, outputting to Winops Positioning Software. The construction site and nearly completed breakwater are shown on Figure 3.



Figure 3. Kaumalapau breakwater construction site

Core-Loc Handling and Placement

The Core-Loc units were transported to the construction site on low boy trailers, and could be placed on the trailers in two different orientations (Figure 4). A sling from the crane was placed around the unit for lifting, and the sling had three ways of wrapping around the unit. Thus, six different Core-Loc orientations could be achieved during the lifting operation. Traylor developed a lifting frame for the Core-Loc units to which the sling attaches, and for which the rotation can be controlled with tugger winches from the crane. The combination of different unit sling orientations and the ability to rotate the unit permitted a good range of Core-Loc orientations to be achieved and maintained underwater. For the cannon style toe unit placement, two slings were used to maintain the proper uniform Core-Loc orientation. The slings were connected around the unit using a quick release hook.



Figure 4. Core-Loc rigged for offloading from trailer

It is extremely important that the Core-Loc units are placed at the correct grid locations. The use of a pre-determined placement plan with each unit assigned an x,y,z coordinate location assures that the units are placed at the right packing density on the slope, and that there are no voids or gaps between units. The placement grid is tied to the project coordinate system so that each unit can be presented to the slope at the correct x,y location. Correct underlayer stone lines and grades insures that the z (elevation) coordinate will be met at the respective x,y (horizontal) locations. The control is provided by the GPS positioning system that reports the precise location of the headworks of the crane. The GPS x,y location is fed into a computer at the crane controls, and with positioning software is overlayed onto the placement plan. Using a targeting feature in the software, the crane operator can locate the headworks of the crane, and thus the center of mass of the Core-Loc unit hanging directly below it, to the correct x,y location. It should be noted that this system was not perfect, as wind, waves (particularly long period swell) and currents will cause the Core-Loc to move slightly around the position reported by the GPS antenna. In general, however, the

system worked very well and resulted in very accurate placement with regard to the "ideal" pre-determined placement plan.

As units approach the waterline at the breakwater head the curvature becomes more pronounced. The spacing of the placement plan grid pattern is based on the centroid location of the units, not the slope contact point. As the curvature becomes more severe, the lower edges of the units touching the slope begin to interfere with each other, causing difficulties in placement. The placing pattern grid becomes slightly rotated around the head, and although the density is maintained, placement difficulty increases because gravity is not necessarily working to advantage in assisting with interlocking of the units. In some areas the tightest unit to unit interlock may be horizontal, and the crane has limited ability to interlock a unit horizontally, especially while gravity is trying to force the unit downhill. In addition, once out of the water, the cushioning effects of the water in slowing the swing of the unit, and the weight reduction due to buoyancy and resultant friction reduction, is lost. One Core-Loc unit on the head was broken during placement, through no apparent fault of Traylor. Because of these factors, the CLS recommended that the Core-Loc placement around the head above the waterline be revised to require that each unit be carefully placed in an optimal manner relative to the previously placed adjacent units following a random placement with random orientation protocol. Each unit was placed and oriented for its best fit into the structure, and its position recorded. Care was taken to achieve the greatest possible packing density, while minimizing the risk of breaking units during placement.

Visual observation for Core-Loc placement was obtained three ways:

i. The Core-Loc lifting frame had provision for up to four cameras to be mounted in protected locations at the outside corners of the frame. Typically two, and sometimes three, frame cameras were used.
ii. In shallow water, less than about 6 m (20 ft), a camera was mounted on an extendable pole and deployed by personnel from a small work boat. This was used primarily in shallow water when it was too rough for divers to work.
iii. A diver with helmet camera was used for final verification of correct Core-Loc placement before it was released from the sling. The diver was particularly important for placement of the cannon style toe units and the second row above them. Traylor also used diver placement and verification assistance for almost all the below water Core-Loc placement. The remote cameras worked well, and reduced the reliance on divers as well as providing visual observation as the units were being moved into position when it would have been too dangerous for a diver to be close. However the mobility of a diver and the ability to see close up was very important to be sure the unit interlocking was optimized and that the required contact between adjacent units and the underlayer stone was maintained for every unit placed.

The camera views were all fed into a split screen monitor for the crane operator to see what was going on from several angles simultaneously (Figure 5). This greatly aided

him in achieving correct and optimal unit placement. It should be noted that the very clear water and excellent underwater visibility greatly facilitated the visual observations.



Figure 5. Positioning display in crane cab

(Note: TV monitor shows camera views, top left and right and bottom right are lifting frame cameras, bottom left is diving helmet camera. The computer screen on the left displays the placement plan overlain by the GPS positioning/targeting software. Also note small model units at bottom center of the figure, used to help the crane operator visualize how the units are fitting together.)

Concrete Crest Cap Construction

The concrete crest cap was constructed in segments, beginning from the breakwater head and proceeding landward. The segments were initially to be 3 m (10 ft) long, however Traylor requested approval to pour them in 4.6 m (15 ft) lengths in order to optimize use of the batch plant production capability. Figure 6 shows a crest cap segment being prepared. Note the shear key female halves cast in the end of the previous segment, and the 1 m (3 ft) deep key trench excavated into the crest core material. Heavy wire mesh fencing material lined with geotextile filter fabric was used as the flexible formwork around the Core-Loc crest units, between the crest units and the cap. This worked very well, it could easily be made to conform to the varying contours of the Core-Locs, and it could be made to project into gaps between units. The mesh was held in place by a steel cable system until the concrete cured, and then any mesh and cables projecting above the concrete were cut off. The completed cap is illustrated on Figure 7.



Figure 6. Crest preparation for pouring concrete cap



Figure 7. Completed crest cap

Stabilization of the Tutong River Entrance, Brunei
A Comprehensive Coastal Engineering Project

A Mariani[1], J T Carley[1], D Rayner[1], B M Miller[1], R J Cox[1], Kok Kong Chin[2]

[1]Water Research Laboratory, School of Civil and Environmental Engineering, University of New South Wales, Sydney Australia; e-mail: a.mariani@wrl.unsw.edu.au

[2]Ove Arup Dan Rakan-Rakan Brunei

ABSTRACT

The Tutong River entrance on the Brunei coastline, presents navigational problems due to a sandbar obstructing the majority of the channel. While the existing western training wall is damaged, the eastern training wall is filled to capacity by the predominant westward littoral drift of sand. The Water Research Laboratory (WRL) of the University of New South Wales has provided specialist advice in the engineering design of the Tutong River training works for the stabilisation of the river mouth.

In this paper, we present the different studies undertaken including:

1. the field data collection undertaken on the Tutong River estuary;
2. the sediment transport assessment and littoral drift modelling;
3. the hydrodynamic modelling of the lower Tutong River estuary;
4. the physical modelling of the proposed training walls for armour stability and wave penetration.

INTRODUCTION

The Tutong River is one of Brunei's main rivers with its estuary centrally located on Brunei coastline and south-west of the Sultanate capital city Bandar Seri Begawan (Figure 1). Access to the Tutong River entrance is significantly affected by a sandbar obstructing the majority of the channel.

Wave breaking occurs on the sandbar causing navigational hazards to the boats accessing the channel. The existing western training wall is damaged, while the eastern training wall is filled to capacity by the predominant westward littoral drift of sand. Sand now bypasses the eastern training wall causing further growth of the sandbar formation while the area down-drift of the river entrance has suffered erosion in the past. The erosion is due to the interruption of sediment supply from the eastern area up-drift of the entrance.

The Water Research Laboratory (WRL) undertook specialist coastal engineering design of the Tutong River training works for the stabilisation of the river mouth. The main design issues were established as:

- the sediment transport processes on the Brunei coast in particular the littoral drift at the Tutong River entrance location;

- the hydraulic efficiency and structural stability of the proposed training works;
- the navigability and accessibility of the entrance.

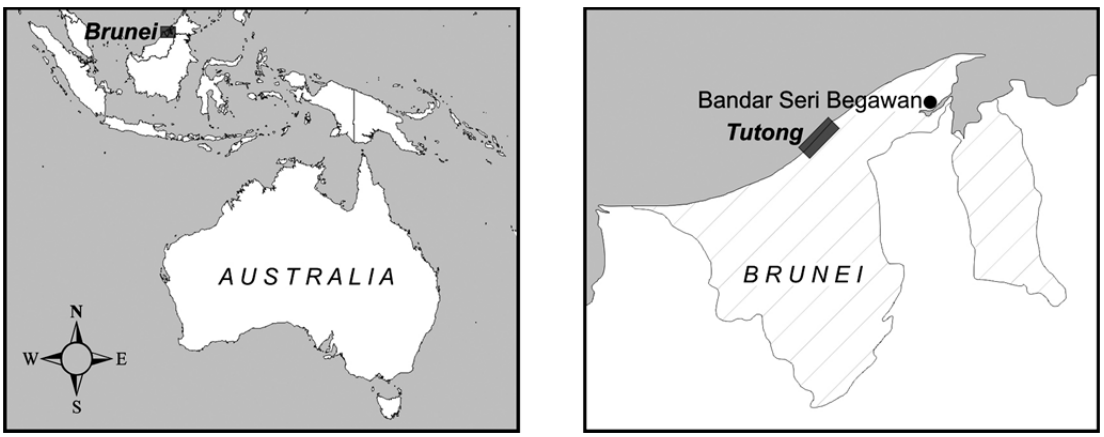


Figure 1. Tutong River location

These design issues were addressed through a series of complementary investigations in which state-of-the-art physical modelling and numerical modelling techniques were applied. In particular, the hydraulic stability of the training wall head and trunk armour was investigated under oblique wave attack using quasi three-dimensional model testing while the layout of the training walls was studied using full three-dimensional physical modelling.

DATA COLLECTION

An intensive fieldwork investigation was undertaken on the Tutong River during the inter-monsoonal period in April/May characterized by milder wave and wind conditions. The lower estuary and nearshore coastal waters were surveyed to collect the site specific data necessary for the subsequent modelling. The main physical parameters investigated were:

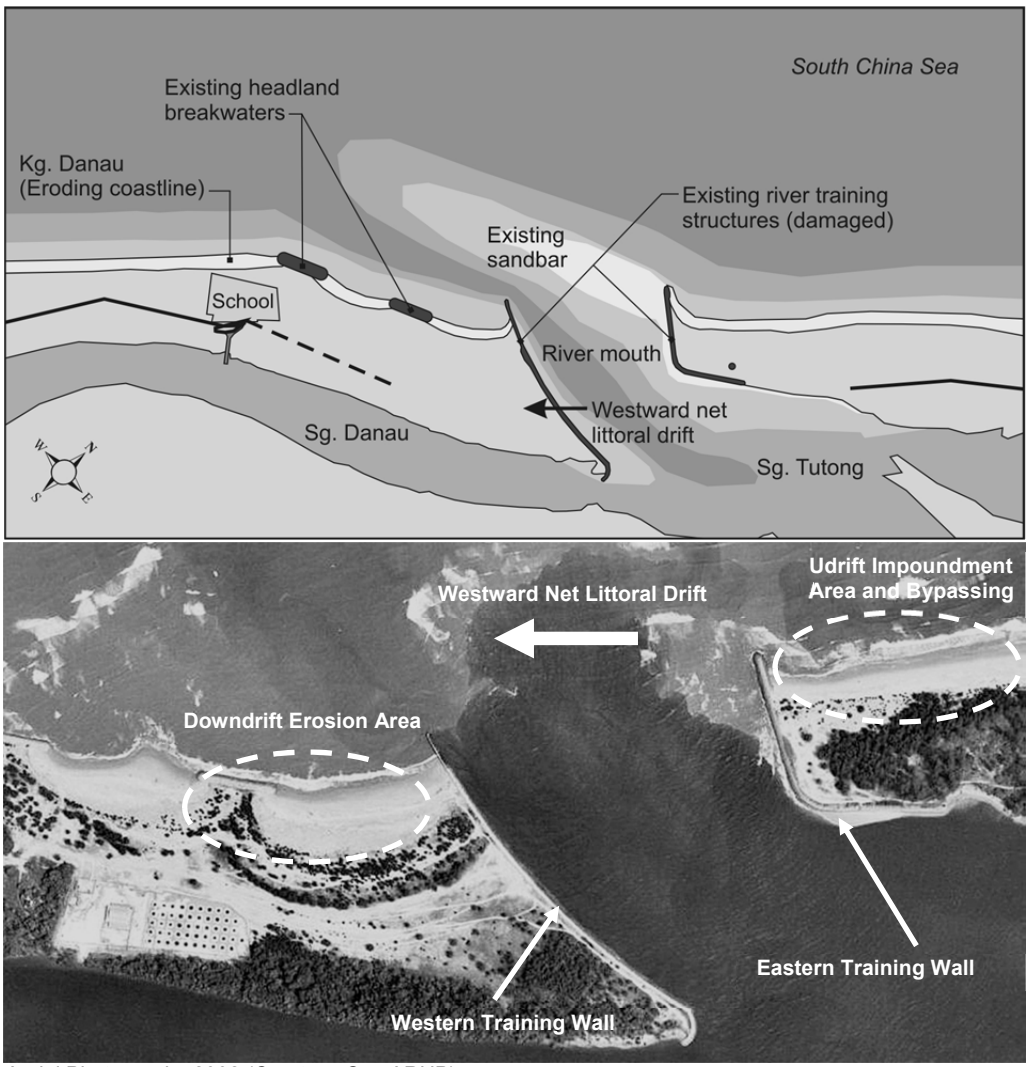
- estuary and offshore bathymetry;
- entrance and upstream water levels;
- currents and flow during various stages of the tidal cycle;
- bed sediment composition throughout the estuary and the immediate offshore seabed.

The bathymetric hydrosurvey was undertaken using RTK-GPS (Real Time Kinematic) echo sounding, while an ADCP (Acoustic Doppler Current Profiler) was employed for the estuary flow and current profiling.

Several water level followers were installed at key locations at the entrance and along the river and bed sediment was also collected and characterised through laboratory testing.

SEDIMENT TRANSPORT PROCESSES

The Tutong River entrance is located in a stretch of coastline dominated by westward sediment transport. This predominant westward drift is the cause of the infill of sand on the existing eastern training wall and the subsequent sand bypassing and sandbar formation across the channel. Subsequently, the down-drift beaches are eroding due to the interruption of sediment supply caused by the training walls (Figure 2).



Aerial Photography 2002 (Courtesy Ove ARUP)

Figure 2. Aerial photo and schematic representation of Tutong River Entrance

In order to determine the seaward extent and sand bypassing of the proposed training walls, accurate knowledge of the sediment transport processes was necessary. A best practice methodology was applied to estimate the littoral drift and sand bypassing in the absence of dredging records and sand impoundment measurements. The methodology implemented (i) wave modelling, (ii) littoral drift modelling and (iii) a sand bypassing model.

Wave Transformation Modelling

A 12 years dataset of offshore WW3 (WAVEWATCH by the National Oceanic and Atmospheric Administration of National Weather System) hindcast wave model output was obtained and analysed by WRL. The data consisted of a time series of significant wave height, peak spectral wave period and mean wave direction at 3 hour intervals. The offshore wave climate was then propagated nearshore using SWAN (Simulating Waves Nearshore by Delft Hydraulics, Netherlands).

The deepwater WW3 model predictions were checked against the ERA 40 (by the European Centre for Medium-Range Weather Forecasts) hindcast data set while the nearshore SWAN predictions were validated using wave measurements collected in several locations. The wave modelling allowed characterisation of the nearshore wave climate in the coastal waters fronting the Tutong River mouth. Wave roses were generated for the offshore and nearshore significant wave heights and are shown in Figure 3.

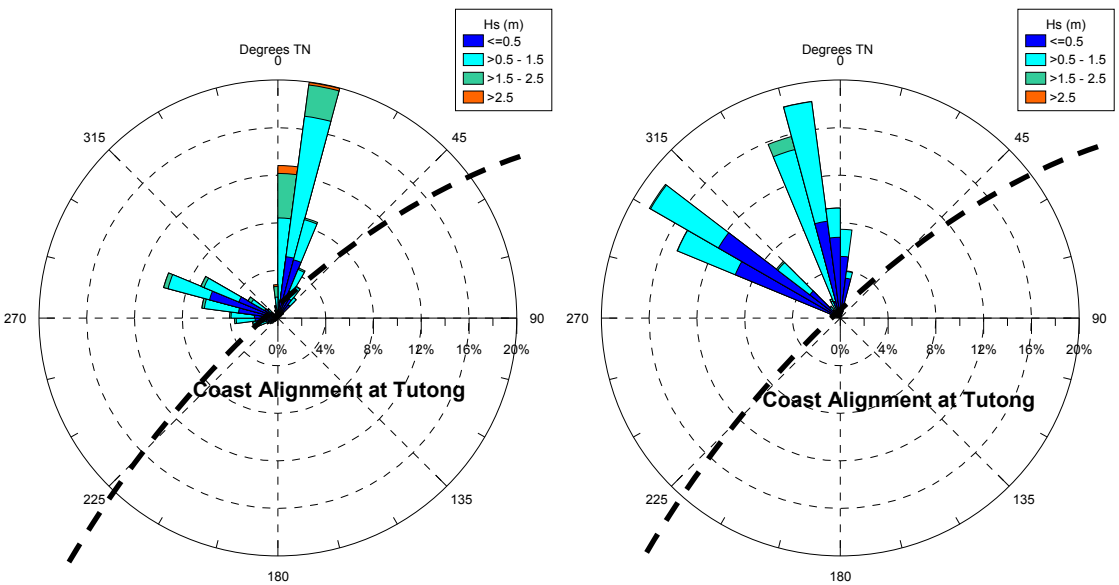


Figure 3. Offshore and nearshore wave roses – Significant wave height

Nearshore waves underwent reduction in heights and a general realignment parallel to the shore normal direction (approximately 310 deg TN) with waves from the north generally resulting in a greater angle of approach to the coast.

Littoral Sediment Transport

The wave transformation modelling output was used as the input for the Kamphuis formula (Kamphuis et al. 1986). The wave transformation modelling results consisted of a 12 year (from January 1997 to March 2009) time series at 3 hour intervals of wave height, period and direction in the nearshore coastal waters of

Tutong River entrance. For every 3 hour time step, an estimated transport rate (in m^3/s) was calculated and annual transport rates were then derived.

A mean net sediment transport towards the west of approximately 49,000 m^3/yr was estimated with 75,000 m^3/yr of sand being transported towards the west and 26,000 m^3/yr towards the east. Moreover, the annual variability shows that the net littoral drift varied from approximately 27,000 to 66,000 m^3/yr owing to the annual variability in wave climate, but was always westward. Previous studies based on field measurements estimated net littoral drift at the Tutong River entrance to be 30,000 to 50,000 m^3/yr westward which confirmed the findings of this study.

Sand Bypassing Curves

The Kamphuis/Queens formula estimates the total sediment transport rate over the entire surfzone. However, the sediment transport rates are not constant across the surfzone depending on the combined effect of wave breaking and longshore currents. The cross-shore distribution of the sediment transport rate is necessary to optimise the length of the training walls in order to reduce the sand bypassing and the subsequent entrance shoal formation.

Bijker's sand transport model (Bijker, 1971) was used to obtain the cross-shore distribution of the sediment transport based on the total transport rates previously calculated using Kamphuis/Queens. The Bijker formula was implemented at every 3 hour time step over the 12 years dataset and bypass rates were calculated for water depths from 0.5 to 3.5 m with 0.5 m increments.

Annual tide levels were generated (from constituents based on tidal analysis) for the 12 years period (January 1997 to December 2008) and coupled with the bypass rate estimates at every 3 hour time step. Actual sand bypassing rates were estimated at the isobaths from + 2 m BSD (Brunei State Datum approximately MSL) to -3 m BSD with 0.5 m increments. Mean (averaged over the 12 years period) annual bypassing rates towards the east and west of the Tutong entrance are presented in Figure 4.

The curves presented in Figure 4 show that by extending the eastern training wall beyond the -2 m BSD (Brunei State Datum) contour and the western training wall beyond the -1 m BSD, the annual sediment bypassing rates would be reduced to below 5,000 m^3/yr. If the eastern and the western training walls were to be extended to -3 and -2 m BSD respectively then minimal sand would bypass the river entrance. The above analyses represent best current engineering practice but do not consider sediment transport and bypassing which may result from rips which form along the training walls.

With nearly 100% of the sediment bypassing interrupted by the proposed training walls, an artificial sand-bypassing system will also have to be implemented at the Tutong River entrance to prevent further erosion of the beaches down-drift the estuary.

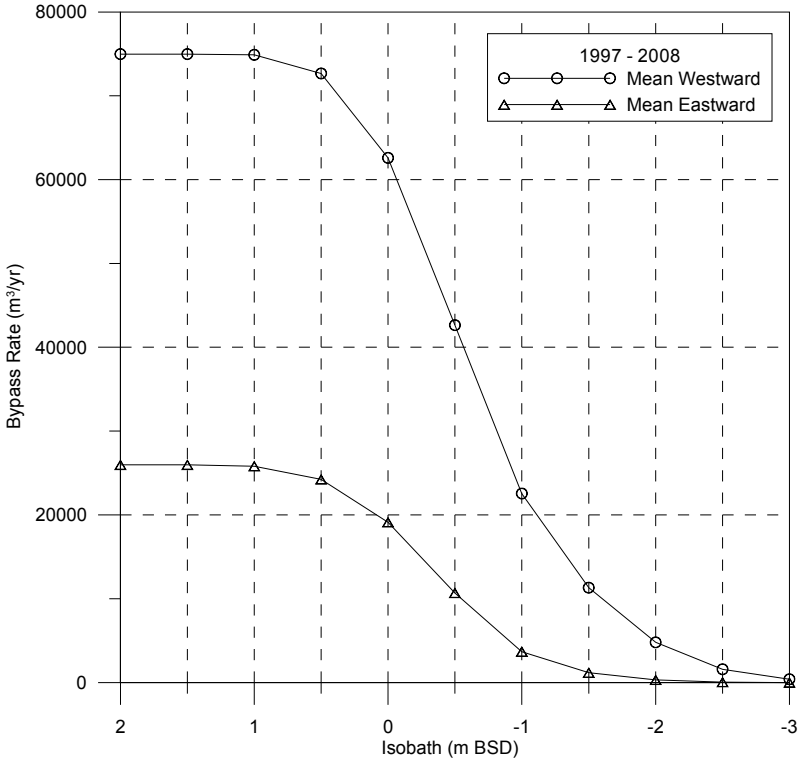


Figure 4. Sand bypassing rates mean from 1997-2008

HYDRODYNAMIC MODELLING

To develop the conceptual design of the training works, a hydrodynamic numerical model was then established to assess the potential impact on scour, sedimentation and water levels. The finite element RMA (King, 2002) modelling suite was utilized to undertake the investigation. The model was constructed and calibrated using the site specific data collected during the fieldwork campaign and several entrance configurations and dredging scenarios were tested.

Several entrance configurations and dredging scenarios were tested using the calibrated model. The entrance configuration characterised by training walls perpendicular to the coastline was chosen (Figure 5) as it minimised the training walls lengths and optimised the entrance navigability in relation to the prevailing winds, waves and currents.

The hydrodynamic model results allowed the assessment of potential scour and sedimentation of the proposed conceptual design. The entrance channel was predicted to consistently scour during ebb-tide thus ensuring the channel accessibility and minimization of dredging maintenance operations. Figure 5 presents an example of two-dimensional entrance flow paths during ebb and flood tide. Potential impacts of the training works at the entrance on upstream water levels were also assessed. The proposed training of the entrance was found to have negligible impacts on the water levels upstream under the tested wet and dry weather conditions.



Figure 5. Entrance flow paths during ebbing and flooding tide

PHYSICAL MODELLING

The physical modelling study objectives were:

- Sizing and configuration of the rock and concrete armour of the training walls;
- Optimisation of the training wall layout in terms of wave penetration and navigability.

Rock and concrete armoured structures were investigated using quasi three-dimensional (Q3D) physical modelling. The hydraulic stability of the training wall head and trunk revetments was investigated under oblique wave attack for the 1 in 100 year average recurrence interval (ARI) design event. The layout of the training walls was studied using full three-dimensional (3D) physical modelling. The wave climate within the river entrance channel was defined under different offshore wave conditions.

Quasi Three-Dimensional Testing

A total of 13 irregular wave tests were undertaken in WRL's "three metre" wave flume to optimize the training walls head and trunk armouring. The use of concrete armour units as primary armour was investigated in terms of hydraulic stability for the design event i.e. for the 1 in 100 year ARI storm. The choice of concrete units instead of rocks as the primary revetment was due to the scarcity on site of rocks of a suitable size. Several head sections were tested using both antifer cube and hanbar options. The testing program included the design event (1 in 100 year ARI event), overload testing, sea level rise scenarios and lower water level tests for toe stability.

Model Setup

Testing was undertaken in the "three metre" wave flume at WRL. This flume measures approximately 32 m in length, 3 m in width and 1.3 m in depth. Figure 6 shows the wave flume setup and a sketch of the tested cross section. Model scaling was based on geometric similarity with an undistorted scale of 1:32.9 being used for all the tests. The scaling relationship between length and time was determined by Froudian similitude. Test durations were equivalent to or greater than 1,000 waves (corresponding to 25 to 35 minutes in the model). Irregular (random) waves based on the JONSWAP spectrum were used. Measured wave heights during testing are presented in Table 1.

Table 1 Measured Wave Climates during Structural Testing

ARI	WL	Measured Waves -26 m BSD contour				Measured Waves -6 m BSD contour			
(yr)	(m BSD)	H_{sig} (m)	H_{max} (m)	$H_{10\%}$ (m)	T_p (s)	H_{sig} (m)	H_{max} (m)	$H_{10\%}$ (m)	T_p (s)
1	1.0	2.5	4.7	3.2	8	2.4	3.6	2.9	8
100	1.7	3.6	6..1	4.5	12	3.2	4.5	3.7	12
100SLR*	2.2	3.7	6.3	4.6	12	3.5	4.8	3.9	12

*water level includes sea level rise projection of 0.5 m

Results

The first structure tested in the wave flume was armoured with 5.0 tonne (t) antifer cubes. The revetment was not stable during the design event with up to 10% damage (i.e. 10% of the armour units displaced by wave attack) at the head and 4% damage on the trunk. Therefore, the antifer cubes size was increased to 7.6 t. Testing showed that the second structure tested met the design criteria (less than 5% damage).

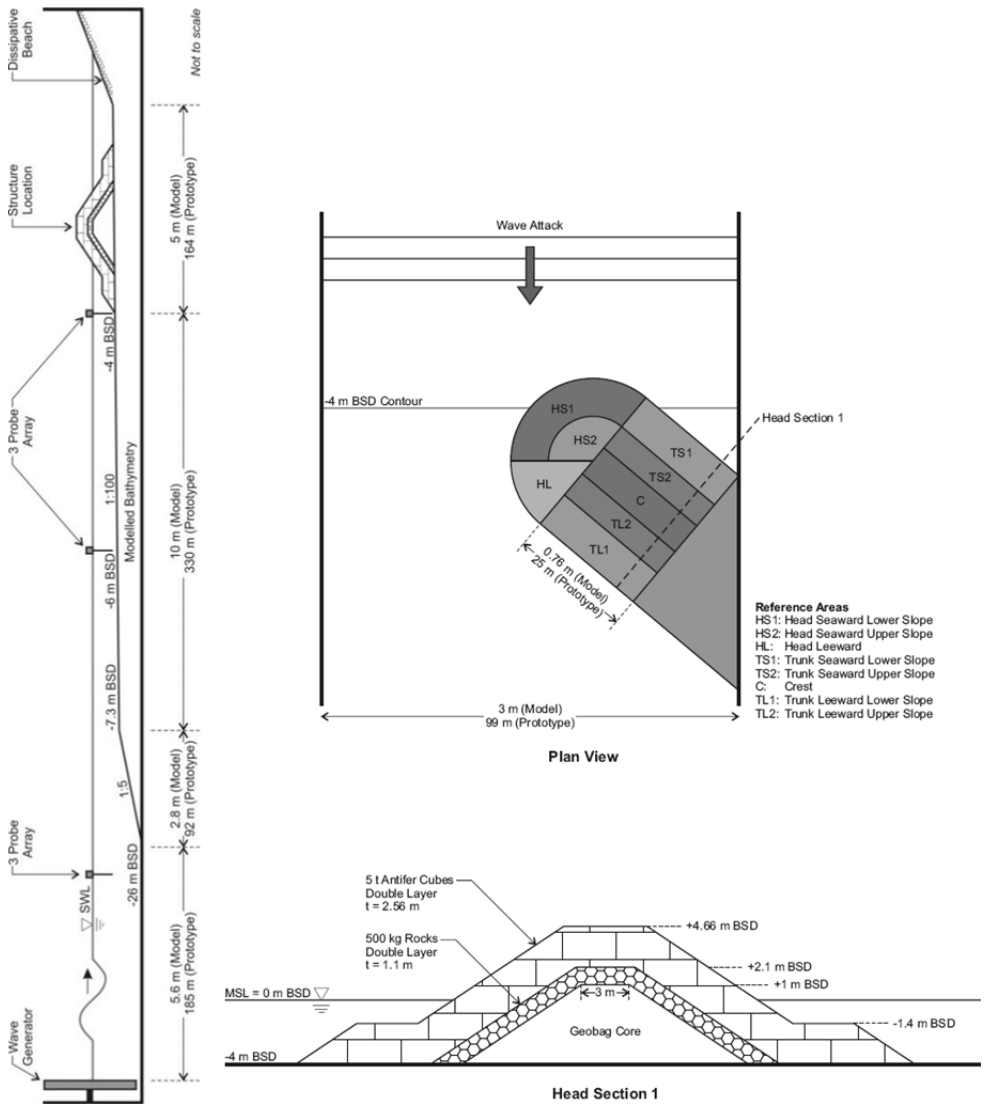


Figure 6. Wave Flume Setup

The third structure tested was armoured using 5.5 (t) hanbar units. Hanbar precast concrete units are widely used on Australian breakwaters (Figure 7), they are less bulky than the cubes and have higher interlocking capacity. In terms of percentage damage, the tested section met the design criteria. However, excessive rocking motion of the hanbar units was observed during testing. The rocking of the units would potentially cause breakage of individual units and overall loss of stability of the primary armour layer. The hanbar solution was not recommended without the implementation of a more rigorous maintenance program for the training walls.

In summary, initial desktop assessment (using CEM 2007) indicated that the eastern training wall head should be armoured with 11 t antifer cubes in order to meet the design criteria of less than 5% damage during the 1 in 100 year ARI event. Physical model testing allowed the reduction of the armour unit size to 7.6 t.



Figure 7. Hanbar units being placed on Australian breakwaters.

Three-Dimensional Testing

The focus of the three-dimensional testing was the characterisation of the wave climate within the proposed entrance. Photos of the built model are shown in Figure 8. All testing carried out for this study was undertaken in the three-dimensional wave basin at WRL. This basin measures approximately 29 m in length, 16 m in width and 0.7 m in depth. Model scaling was based on geometric similarity between model and prototype, with an undistorted length scale of 37.6 being used for all tests. Wave height measurements were recorded at 11 locations offshore and within the entrance channel as shown in Figure 9.

The entrance training walls were built protruding seaward perpendicularly to the shoreline with the eastern and western training walls 600 and 230 m long respectively and an entrance width of 280 m (real world measurements). Both irregular and regular wave testing was undertaken for the conservative scenario of shore normal wave direction.

The irregular testing results provided the expected wave climate within the entrance channel during the 10% exceedance event equaled or exceeded approximately 36.5 days per year. For this event, predicted wave conditions at the – 4 m BSD contour were: H_s = 1.0 m, T_p = 9 s and WL = 1.4 m BSD. Measured significant wave height at the end of the entrance channel was less than 0.5 m along the eastern training wall and approximately 1 m along the middle axis of the channel. Results are plotted in terms of wave height coefficient at each measurement location in Figure 9.

The regular wave testing provided estimates of wave height coefficients for operational conditions during which the processes of wave refraction, diffraction and shoaling dominate the wave penetration dynamics. Reductions in wave height of 70 to 90% were obtained at the end of the eastern half of the entrance channel.

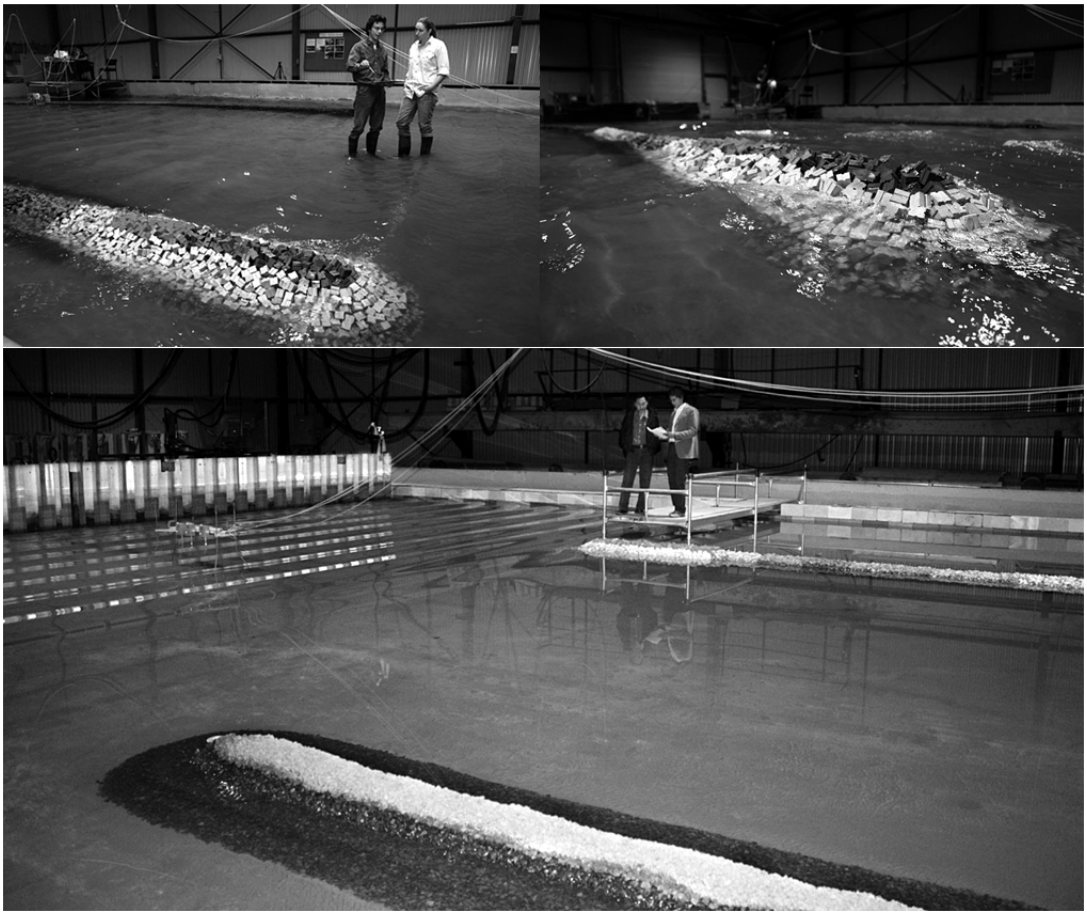
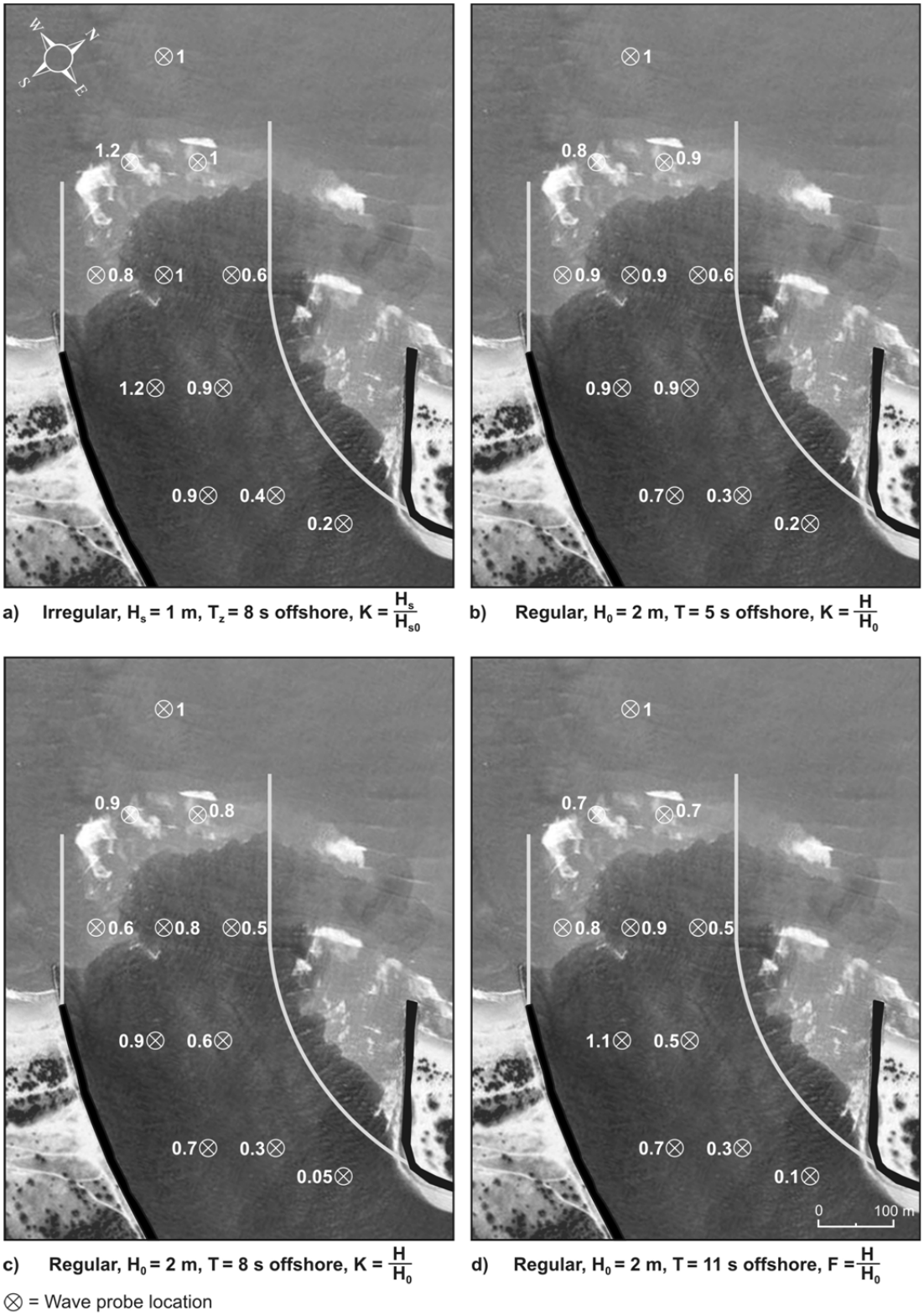


Figure 8. Three-dimensional testing of the Tutong training walls

Along the western half of the channel, reductions in wave height were less and in the range of 10% to 20%. Wave height attenuation is expected to be more important for wave directions that are not perpendicular to the shoreline. Results of the regular tests are plotted in terms of wave coefficients in Figure 9.

The proposed training wall alignment was considered optimised in terms of rubble mound structure lengths and navigability with prevailing winds, currents and waves. In summary, wave penetration testing showed that wave conditions inside the channel will remain mild during most of the operational conditions.



a) Irregular, H_s = 1 m, T_z = 8 s offshore, $K = \frac{H_s}{H_{s0}}$

b) Regular, H_0 = 2 m, T = 5 s offshore, $K = \frac{H}{H_0}$

c) Regular, H_0 = 2 m, T = 8 s offshore, $K = \frac{H}{H_0}$

d) Regular, H_0 = 2 m, T = 11 s offshore, $F = \frac{H}{H_0}$

⊗ = Wave probe location

Figure 9. Wave height coefficients

CONCLUSIONS

A comprehensive coastal engineering study was undertaken for the conceptual design of the Tutong River entrance training walls. Using state-of-the-art coastal engineering methods that involved field data collection, numerical and physical modelling, the training walls design was optimised in terms of:

- Minimisation of training wall lengths;
- Littoral sediment transport processes;
- Entrance accessibility and navigability by boats;
- Flow conditions within the entrance.

ACKNOWLEDGEMENTS

The authors would like to acknowledge the Department of Drainage and Sewerage, Public Works Department, Ministry of Development Negara Brunei Darussalam for the opportunity to work on this project and for their valuable comments and inputs. The authors would also like to acknowledge the precious input of the Ove Arup Brunei team, in particular Mr Siew Yong Lim and Mr Lee Sing Ding.

REFERENCES

Bijker, E. W., 1971. "Longshore Transport Computations." *Journal of Waterways, Harbors, and Coastal Engineering Division*, ASCE Vol. 97, No WW4, November 1971.

CEM 2007, "*Coastal Engineering Manual.*" Coastal Engineering Research Center, Waterways Experiment Station, US Army Corps of Engineer, Vicksburg, USA.

Kamphuis, J. W., Davies, M. H., Nairn, R. B. and Sayao, O. J., 1986. "Calculation of Littoral Sand Transport Rate." *Coastal Engineering*, 10, pp. 1-21.

King, I. P., 2002, "*A Two Dimensional Finite Element Model for Flow in Estuaries and Streams*". Version 7.0a RMA User Manual, October 2002.

The Forecast of Anapa Bay-Bar Coast Evolution and Sand Body Thickness Change

R.D. Kosyan[1], B.V. Divinskiy[2], A.R. Kosyan[3],
V.V. Krylenko[4], M.V. Krylenko[5], S.B. Kuklev[6]

[1]Prof., Dr., Southern branch of the P.P.Shirshov Institute of Oceanology (SBSIO), RAS, Gelendzhik, Russia, 353467, rkosyan@hotmail.com; +7(86141) 28281
[2]Dr., SBSIO, RAS, Gelendzhik, Russia, 353467,divin@coastdyn.ru; +7(86141) 28281
[3]Dr, A.N. Severtsov Institute of Ecology and Evolution, RAS, Leninsky pr. 33, Moscow, Russia, 119071, kosalisa@rambler.ru; +7(499)1351878
[4]Reseacher, SBSIO, RAS, Gelendzhik, Russia, 353467,krylenko@mail.ru; +7(86141) 28069
[5]Dr., SBSIO, RAS, Gelendzhik, Russia, 353467,krylenko@mail.ru; +7(86141) 28281
[6]Dr., SBSIO, RAS, Gelendzhik, Russia, 353467; +7(86141) 28069

ABSTRACT

Sandy beaches of the Russian Black Sea coast, Anapa bay-bar, represent the huge value as a recreational zone and as a unique natural complex. In this paper, the results of field researches in southern part of Anapa bay-bar are presented. The quantitative characteristics of lithodynamic processes are received, the estimation of possible influence of anthropogenous and natural factors on flows of a sandy material is given. Based on the received data the mathematical modeling with the purpose of the coast evolution and the bay-bar sandy body thickness change forecast is performed. Potential danger of degradation of the investigated area ecosystem is revealed.

INTRODUCTION

Anapa bay-bar is an extensive accumulative sandy body with the length almost 50 km, which is the unique natural formation. Anapa bay-bar is also referred to as Bugaz-Vitjazevo, Kiziltash-Vitjazevo, Anapa-Taman. Anapa bay-bar lies as a narrow strip from the cape of Anapa up to the Soljonoye lake. It separates the system of estuaries and lakes from the Black sea (Figure 1). Anapa bay-bar is subdivided into some characteristic sections: Soljonoye lake short bay-bar, accumulative terrace between Soljonoye lake and Bugaz estuary, Bugaz bay-bar, the section along the fossil cliff between Bugaz and the Vitjazevo estuaries, typical Vitjazevo bay-bar, the section between Vitjazevo estuary and Anapa city (Izmaylov, 2005).

Black Sea Anapa bay-bar sandy beaches represent a great value for Russia as the recreational zone and the unique natural complex. Recently, because of the

increased anthropogenous stress on coastal biocenosis on the one hand and intensive construction in the coastal zone and destructions of dunes on the other hand, their safety is under threat.

Rather complex modern hydro-lithodynamic and geomorphologic processes, taking place in the bay-bar area, are also defined by a lot of operating factors. They include fluctuations of climate, change of sediments granulometric composition, interaction between the eolian flow of sand and the sea coastal line migration processes, influence of the earth's crust immersing on coastal processes and many other things. The majority of authors consider that modern slow degradation of Anapa bay-bar occurs as a result of both natural and anthropogenous factors interaction (Artjukhin, Fedorova, 2010; Peshkov, 2000; Zenkovich, 1962).



Figure 1. Black Sea coast section from Taman peninsula to Anapa city (Google Earth).

However, necessary studying of Anapa bay-bar dynamics stopped in 60th of the last century. In the scientific literature there are very few data on modern coastal processes, as well as about processes of coastal dynamics on this section. Data on incoming volumes of shell detritus did not exist. Thus, at the moment there is no sufficient actual data for creating, modeling and authentic forecast of evolution of coast between the Anapka river mouth and Vitjazevo settlement.

In autumn 2010, employees of the Southern branch of Russian Academy of Science P.P.Shirshov Institute of oceanology have carried out the complex coastal researches of Anapa bay-bar southern part. Scientific researches represented in this

paper are devoted to southern part of Anapa bay-bar having the length of 10 km, from Vitjazevo settlement up to the Anapka river mouth (Figure 1).

HISTORY OF ANAPA BAY-BAR GENERATION

Anapa bay-bar was formed during the Black Sea transgression. In the beginning late Holocene, when the sea level achieved the level close to the modern one, three ingression water areas came up between Caucasian plunge and Taman elevations: Bugaz, Vitjazevo and Anapa gulfs. The similar situation usually leads to formation of blocking accumulative bodies.

With achievement of the modern sea level, the Kuban river alluvium accumulation place relocated to the gulfs on the place of modern Bugaz, Kiziltash, and Vitjazevo estuaries which were then the uniform hydrological object (Mikhailov, Magritsky, Ivanov, 2010).

The further formation of the bay-bar northwest part took place mainly due to the coarse-grained part of the Zhelezny Rog (Taman peninsula) paleo-cape abrasion material, combined by loose deposits. The destruction products were involved in the alongshore flow of sediments and moved to the southeast, forming the bar with the base in the area of Taman peninsula southern end, gradually blocking the entrance in the Bugaz gulf. After the joint of the bar with Blagoveshchensk residual outcrop, the Bugaz bay-bar was formed. The Kuban river alluvium accumulated during its confluence in the Black Sea and products of Blagoveshchensk paleo-cape destruction were shifted to the southeast where they formed the thickest southeast part of bay-bar. Vitjazevo bay-bar was formed from the Blagoveshchensk cape side, first in the form of bar which was transformed subsequently in the bay-bar. At last stage, the joint of Vitjazevo bay-bar with the southeast part happened. Now it is the most lowered strip of bay-bar which is partially flooded during storms.

After the connection of northern and southern parts, there was formed the uniform lithodynamic system of Anapa bay-bar with sediments movement prevailing direction from the north to the south. The fact that the iron-ore pebble which source is the cape Zhelezny Rog, was collected even at the most southern edge of the bay-bar, tells us about the intensity of the alongshore flow. Presence of breaks in the bay-bar surface part did not interfere the alongshore movement of sediments because the most part of the material moved along the bar line below the sea level.

The important feature of coastal zone development in the late holocene (5.2-5.3 thousand years ago), was the clockwise turn of the coast at Blagoveshchensk residual outcrop (Figure 2). The maximum size of this turn at extreme points (southern Taman and Anapa city) has made 1,1-1,5 km (according to some information up to 2 km) (Zenkovich, 1958). The analysis of the coastal line scheduled displacement in the late holocene shows, that in Vitjazevo bay-bar southern part of the coast receded with the speed of 0,1-0,2 m/years, and within the limits of Anapa holocene terrace (Vitjazevo - Anapa) it was moving forward with the speed of 0.2-0.4 m/year. All this has significantly affected on the subsequent transformations of Anapa bay-bar (Izmailov et.al, 1989).

Now Anapa bay-bar is the accumulative natural formation and represents sandy bar, leaned against the strong residual outcrops of cretaceous and tertiary age, which separates estuaries from the sea.

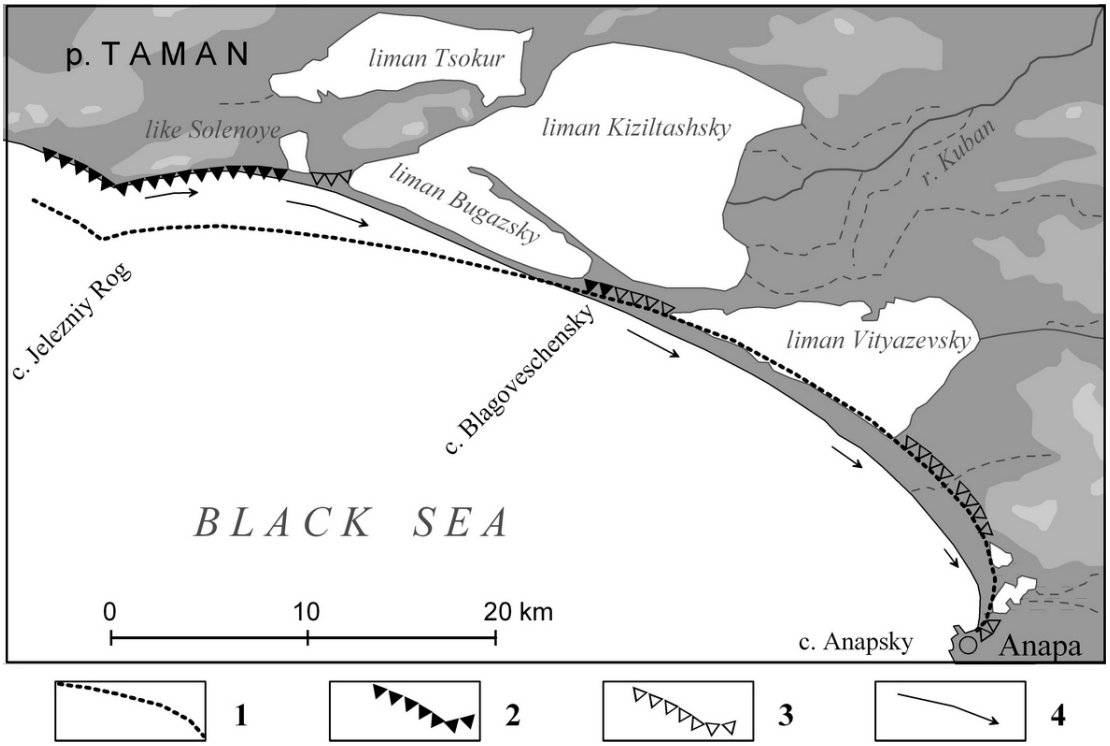


Figure 2. The scheme of coast development from Zhelezny Rog cape up to Anapa. 1 - coastal line former position; 2 - active cliff; 3 - fossil cliff; 4 - position of the coastal line in XX century (Zenkovich, 1958).

THE COASTAL LINE AND SAND STOCKS MODERN DYNAMICS

Anapa bay-bar had always been extremely dynamical object quickly changing under the external influence. The most essential factors influencing on the Anapa bay-bar modern dynamics are the change of a hydrodynamical regime (rise of a sea level and connected with it change of a wave regime, the mode of coastal currents), changes of sediments balance (transverse and alongshore flow of sediments, abrasion, shelly ground receipt, eolian (wind-born) processes), the increasing anthropogenous loading.

Formation **of a hydrodynamic regime** on the investigated area is caused by bathymetry features and by the configuration of the coastal line. Spatial features of the coastal part bathymetry are connected with an arrangement of underwater bars (Figure 3). In the southern part of the investigated section profiles of the underwater slope are rather even with implicitly expressed underwater bars at depth of 2 m and at the distance of 150-200 m of water's edge. In the central part the underwater bars are obviously expressed, with removal from the edge up to 200 m. The second underwater bar (distance from the edge 370 m) is formed northward. In the area of

Vitjazevo settlement, except for the described two underwater bars, one more bar in near-the-edge zone is shown. The growth of quantity and thickness of underwater bars in the direction from the south to the north is the bathymetric feature of the investigated section.

The hydrodynamic regime of water area was investigated using the model DHI Mike21/3 FM (www.ghigroup.com) uniting directly hydrodynamic and wave modules. The approach realized in Mike21/3, allows to realize dynamic interaction between sea currents and wind-induced waves, and also to consider major factors of hydrodynamic regime development: bottom friction, wind and radiation pressure, nonlinear intrawave interactions, dissipation of wave energy.

In area of Anapa currents of reversive type with prevalence of currents of two opposite directions - the northwest and the southeast ones are observed. In the coastal part the formation of currents structure is influenced by the radial pressure connected with local destruction of waves.

The most typical for Anapa area are currents with a speed from 1 up to 10 cm/s. Repeatability of currents with a speed more than 20 cm/s reaches 10 %. Such currents are observed during severe storms of northeast, southern and southwest directions.

The performed calculations have allowed tracking some features of the hydrodynamic regime:

- For the specified storm of the southern direction, on the sea border of the section the averaged speeds of currents make 8-12 cm/s (in a surface layer - 12-16 cm/s, in the near-bottom layer - 2-4 cm/s). In the coastal part strengthening speeds of the currents connected with influence of wind-and-wave motion of water (average speeds - 24-28 cm/s, in a surface layer - 28-32 cm/s, in the near-bottom one - 16-18 cm/s) are observed.
- The regularities of spatial distribution are kept at storms of the western direction. Thus, the higher values of currents speeds in a surface layer (in the coastal part reaching 36-40 cm/c) are observed. It is explained by the fact that the accepted for the calculations Western storm wind speeds are greater than the speeds of the Southern wind.
- Detailed elaboration of calculations has allowed revealing areas with local increase in speeds of currents: up to 80 cm/s in a surface layer and up to 50 cm/s in the near-bottom layer at the western storm. The strengthening of current speeds falls to the acme of underwater bars. In hollows between bars the speed of currents falls down to 55 cm/s in the surface layer and to 35 cm/s in the near-bottom one (Figure 4).
- The wave regime of considered area was investigated at specified storms of general directions (southern, southwest, western) which are possible once in 25 years. As calculations have shown (Table 1), the southern section of the investigated coast is exposed to the least active wave influence. The wave influence on the coastal zone increases in the north direction. Besides, the direction of waves in the southern part of the section is defined by the wave field refraction effects on details of local bathymetry and diffractions behind the cape and practically does not depend on the direction of an acting storm.

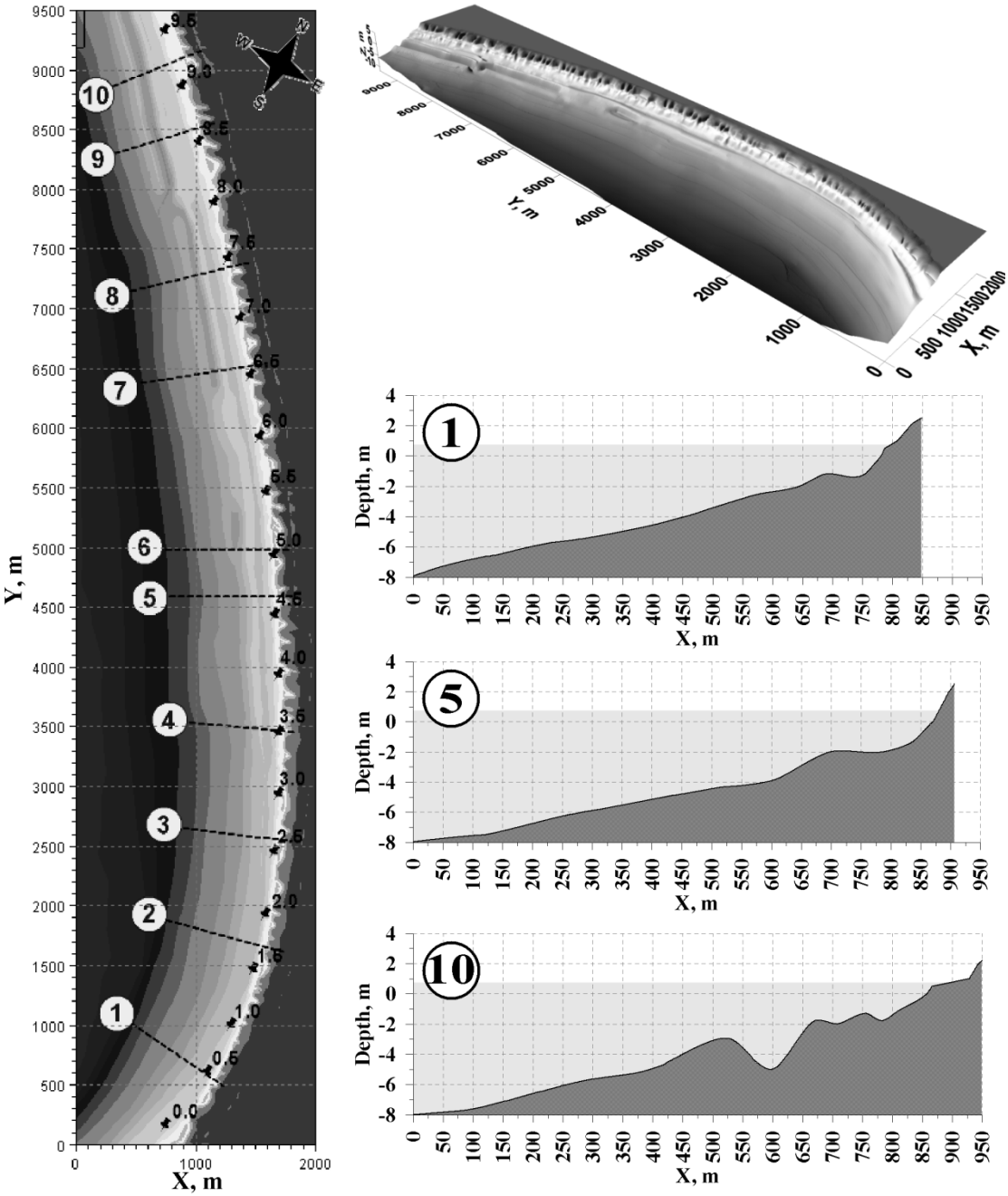
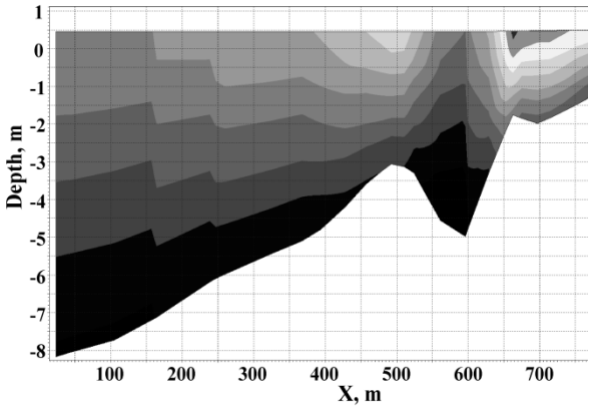


Figure 3. The bathymetry features and characteristic bottom profiles.

a



b

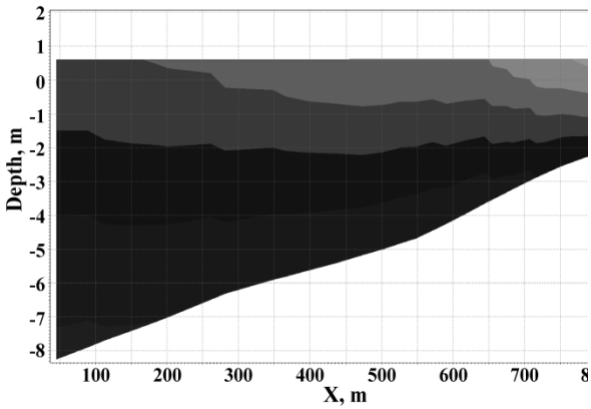


Figure 4. The module of horizontal current speed (m/s). Characteristic cuts on sections with underwater bars (a) and with rather slightly sloping bottom (b).

Table 1. Results of modeling in control points (h_m, h_s - the maximal and significant heights of waves, t_p - the period of the spectrum peak)

Storm	Points	h_m, m	h_s, m	t_p, s	Waves direction, degrees.
S	1	3.11	1.60	9.3	202
	2	3.02	1.59		211
	3	2.05	1.07		255
SW	1	3.42	1.83	9.4	220
	2	3.53	1.86		227
	3	3.40	1.83		260
W	1	3.38	1.75	9.3	238
	2	3.53	1.87		243
	3	3.46	1.84		267

Hydrodynamic regime research results have been used as input parameters **at calculations of sediment flows and dynamics of the underwater slope**. Researches were executed using the complex of programs for the calculation of transport of inconsistent sediments DHI LITPACK, considering angles of the

currents approach and waves, waves destruction, type of the underlying surface (smooth or riffled bottom), granulometric composition of deposits.

The performed calculations have shown that transverse storm flows of sediments have negative values, i.e. the flow is directed from the water edge deeper into the sea (Figure 5).

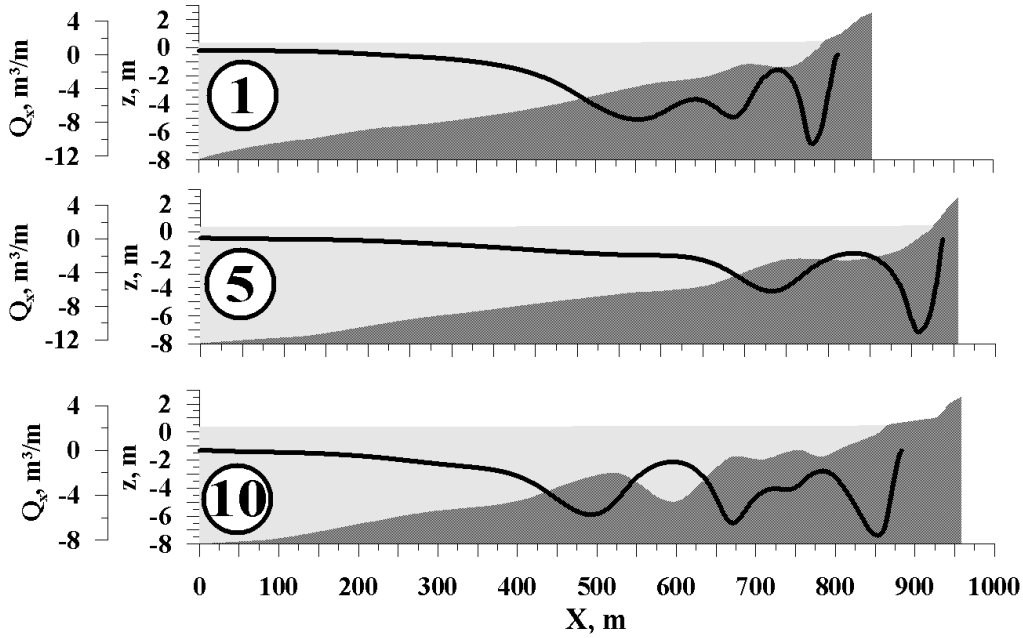


Figure 5. Transverse transport of sediments calculation example. Storm of SW direction.

It witnesses that during the storm there is a unidirectional process of removing of the beach-forming material to the deep-water part of the investigated water area. The granulometric analysis of the moved material shows, that sediments removal occurs due to fine-grained part of sand (fraction smaller than 0.1 mm).

In storm dynamics of the beach, the cellular structure is shown. In a southern part (0.0-2.0 km length), the accumulation is observed at all storms (Figure 6).

At the change of the storms direction in central and northern part of the investigated section the accumulation processes will be replaced by the processes of washout. The central part of the investigated section is exposed to the most active washout.

During the storm period the alongshore redistribution of sediments occurs extremely non-uniformly, thus zones of an underwater slope alluviaton are replaced by zones of washout with characteristic scales of the order 200 m. This regularity is shown in the near-the-edge zone. Results of modeling are proved to be true by the data of natural experiments (Report of BSE SRS, 1952, 1955): by results of diving inspection after storms the coastal underwater bars represent not uniform structure, but the system of separate alternating bars with the longitudinal sizes of 150-200 m.

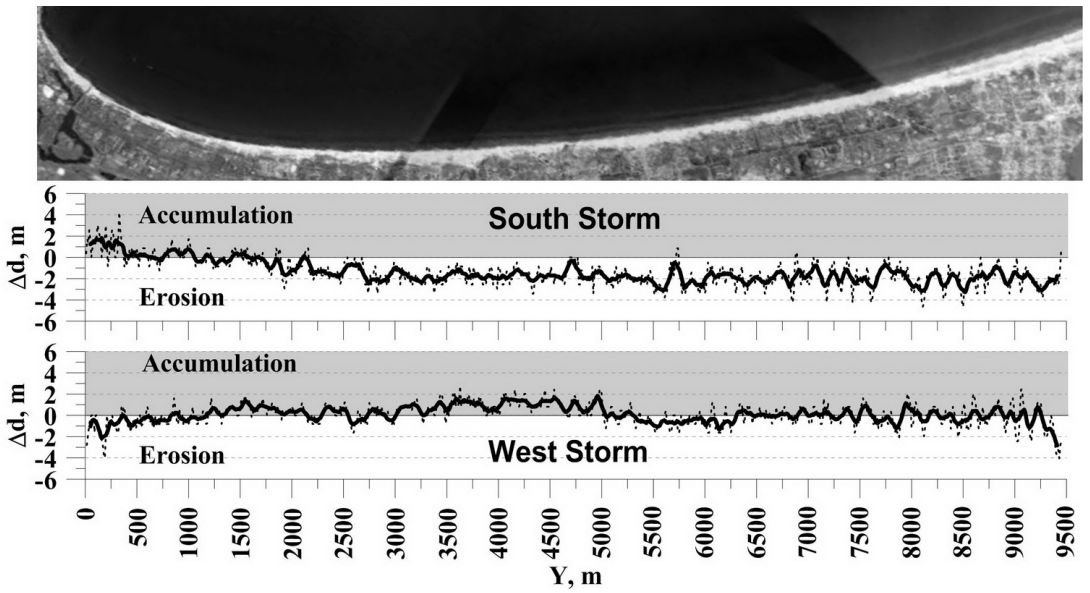


Figure 6. Relative change of the coastal line profile under the influence of southern and western storms.

In the annual cycle the alongshore flow of sediments has migratory character: at various storms the general flow of sediments is directed or from NW to SE, or from SE to NW. Prevailing transport occurs in the direction from NW to SE (45 thousands m^3/year). The transport from SE to the NW makes 35 thousands m^3/year (Figure 7).

Wind-induced processes. In a long-term mode winds of coastal directions (E, NE, N) – 48.9 % prevail in Anapa. Value of winds of southern compass points is essential – 35.1 %; these winds carry out sand transport deep into the land. The share of winds with velocities capable to translocate sediments during the whole year is rather high (not less than 50 %). Velocities higher than 10 m/s are registered in 9 % of cases, thus allocation of such winds between coastal and sea compass points is approximately equal. Winds of all directions can reach velocities higher than 20 m/s (the Russian sea register …, 2006).

The strong winds (velocities> 10 km/s) possess the greatest sediment moving forces (Vykhovanets, 2003). Significant eolian flows of sediments in explored territory are formed at winds with velocities not less than 4 m/s. During activity of coastal winds, the source of sediments for windy sand flow is the eolian zone and the sea beach. At alongshore winds, the eolian movements of sand very feebly influence on the eolian balance of sediment at surface of the Anapa bay-bar. They only redistribute already existing sediments. Fractions of fine-grained sand (0.1-0.25 mm) are involved in the transport first of all.

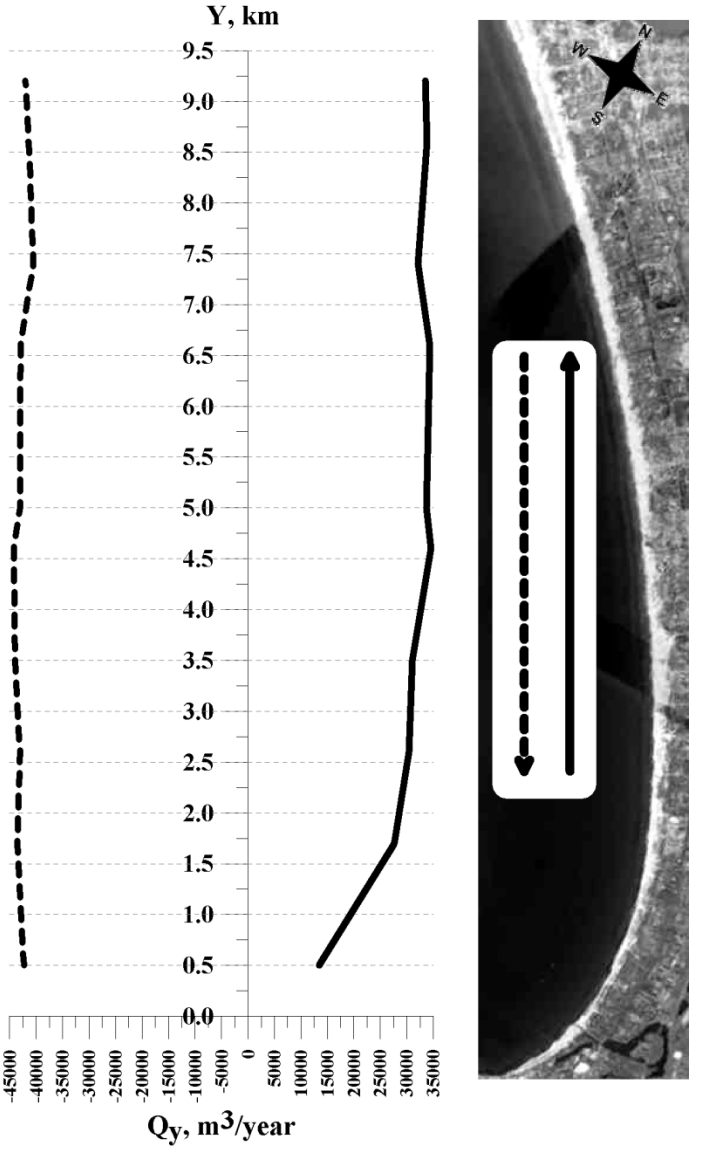


Figure 7. Resulting alongshore streams of sediments.

The analysis of grain-size composition. The analysis of alongshore granulometric composition variability shows the reduction of large particles share in the composition of beach and bottom deposits from the north to the south. As it was specified above, one of the sources feeding the bay-bar earlier was the material of Taman peninsula coast abrasion. While moving to the south under the influence of wave currents, the sand particles are gradually abraded and the average diameters of particles of the deposits, composing the beach and the underwater slope, decrease. The smallest particles leave the coastal zone for the major depths. The particles having the size of 0.063-0.1 mm accumulate on depths more than 7 m, and particles having the size less than 0.063 mm leave for depths more than 10 m, leaving the coastal zone forever.

Comparison of the grain-size analysis data 1949 (Zenkovich, 1962), 1973 (Antsyferov, Kosyan 1977) and 2010 (Figure 8) has shown that with time, the reduction of the mean particles sizes is also observed. It specifies the insufficiency of the lithodynamic bay-bar system of up-to-date nourishment by the coarse-grained sediments.

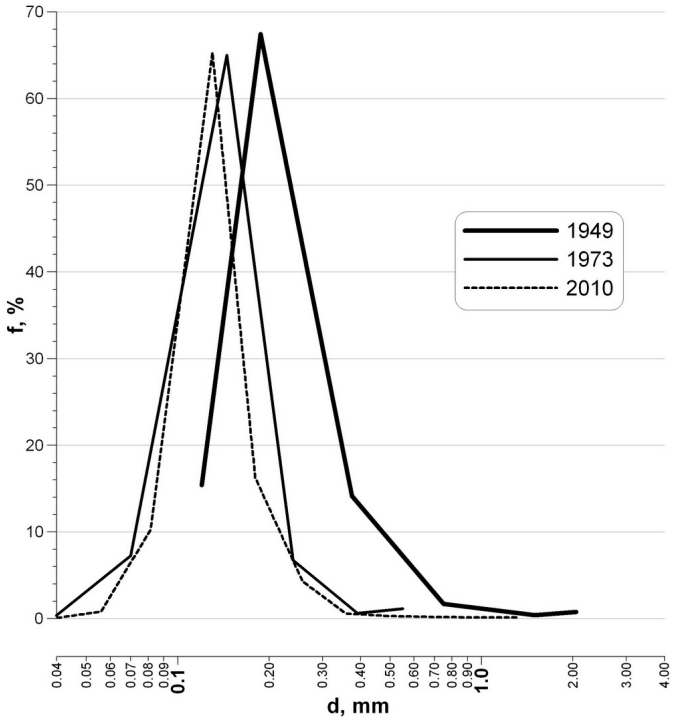


Figure 8. Comparison of bottom sediments granulometric composition distribution curves for years 1949, 1973, 2010

Biogene source of the material is rather variable. Interannual and seasonal fluctuations of distribution and biomass of mollusks are reflected in volumes of shell accumulation in the coastal zone. The major feature of shell component of sediments in the coastal zone is, on the one hand, continuous renewal of the biogene part in connection with annual benthos reproduction, and on the other hand, shells crushing and abrasion in the course of moving. Our researches have shown that emission of shell material from adjoining sea-bottom spaces is now one of the major sources of beach material for the Anapa bay-bar.

The dominating species on average biomass of shell carbonate and specimen number per square meter of the bottom is the hard clam *Chamelea gallina* (Table 2*)*. The next species is rapa whelk *Rapana venosa* though its number is minimal. On the third place in the stock of a "live" carbonate is *Donax trunculus*, while the biomass and number of *Nassarius reticulatus* is absolutely insignificant. Shell congestions are inclined to the coastal strip and zones with depths from 5 to 10 m where the average biomass makes 450 g/m2. Annual production of an organic carbonate on 1 running meter of the coast makes up to 200 kg (Kosyan, 2011).

Table 2. Average number (specimen/m^2) and biomass (g/m^2) of mollusks

Type of mollusks	Average number	Average biomass
Chamelea gallina	550,3	349,9
Donax trunculus	88,1	15,6
Rapana venosa	2,0	38,2
Nassarius reticulatus	3,1	2,0

The investigations **of the up-to-date morphology** of the coast under consideration carried by us, the comparison of the obtained data with the results of similar works in the past, the attraction of air photography materials, and space pictures, have allowed to gain a series of important results:

The shelf around the Anapa bay-bar represents low-angle flat land with a bias to the southwest, here and there complicated by exposures of indigenous rocks and the separate isolated bar-like bodies. Near to coast the bottom is shallow (slopes 0.015-0.020) and is combined preferentially by sand. Further on depths of 8-10 m (in northern part near 7-8 m) the sand slightly silts and becomes denser.

Three zones are traced in the structure of the bay-bar southern part: the beach, the zone of dunes, the zone of hilly sand. Almost flat surface of the beach having breadth from 10 up to 200 m occupies the space from water edge to front-dune. Behind the back part of the beach stretches the wide strip (50-170 m) of dunes. Dunes form some rows; their height reaches 15 m. Behind dunes ther are the dry hilly sands, strongly changed by processes of soil formation (Izmailov, 2005). Now practically just behind the strip of dunes, and here and there directly on artificially leveled or cut off dunes are located buildings of recreational objects (Figure 9).

On the section from the mouth of the Anapka river up to settlement Vitjazevo there are at least 60 annually updated artificial gashes of dune belt, made for passage on the beach. This leads to degradation of the natural relief and vegetation on the adjacent coast areas.



Figure 9. The beach and front dunes on the area.

According to the field measurements made from 1948 till 2010 (Artukhin, Fedorova, 2010; Zenkovich, 1962; Peshkov, 2000), the gradual reduction of the

breadth of Anapa bay-bar beach is observed. At average breadth of beaches of 50 m the up-to-date velocity of beaches washaway reaches 1.2 m/year.

The recession of water edge occurs on many sections; for last 20 years somewhere it has made 30-50 m. Yet, there are sites where recession of water edge does not occur and the coast line as a whole is stable. Against long-term dynamics of coast line on separate sections there are local changes of water edge line position. As a rule these oscillations are caused by the hydrodynamic causes.

CONCLUSION

Thus, it is found that there is a gradual exhaustion of Anapa bay-bar sand stocks. Our field researches and results of modeling have shown that at the moment the balance of beach forming material on the investigated section is negative. Annual losses of sand on the investigated area make, approximately, 28000 m^3.

There is a constant natural crushing of sand on the beach and in the underwater part of the coastal zone. Small-grained sand is easily made turbid by waves and in active storm is transferred by wind and wave currents to a deep-water part. Moving of beach forming material with the alongshore flow of sediments from the neighboring sections of the coast to Anapa beaches due to prevailing NW alongshore flow of sediments is not enough, supply of the material from biogene and eolian sources is not enough for the completion of sand losses. Local coast protecting actions such as artificial beach backfilling and construction of seawalls, will be ineffective.

Reduction of Anapa beaches width is also connected with a number of reasons of anthropogenous character: withdrawal of sand from the beach zone for needs of construction, placing of recreational complex objects in the zone of dunes, water area pollution.

Potential danger of the investigated area geosystem degradation is revealed. For prevention of the further washout of Anapa beaches and dune blocks destruction it is necessary making compensatory backfill of coarse-grained sand. The volume of single backfill should make 300-400 thousand m^3. Also it is necessary to restore the artificially broken sections of the dune deposit zone and bring to order the resort accomplishment and construction in the zone of dunes and the back part of the beach.

REFERENCES

Antsyferov S.M., Kosyan R. D (1977). Research of suspended fragmentary material movement in the top part of a shelf, seaward of bars zones. *Moscow, "Nauka", Oceanology*, V. 22, № 3, 497-505.

Artjuhin J.V., Fedorova S.I. (2010). Morpho-lithodynamic processes in a coastal zone of the Anapa bay-bar. *Moscow, "Nauka", Oceanology*, v.50, №4, 627-635.

Vyhovanets G. V (2003). Eolian process on the sea coast. *Odessa, Publishing house "Astroprint"*, 368.

Zenkovich V. P (1958). Coasts of the Black Sea and the Sea of Azov. *Moscow, Geograficheskaya Literatura*, 374.

Zenkovich V. P (1962). Doctrine bases about the development of sea coasts. *AS publication. USSR. Moscow*, 710.

Izmajlov J.A. (2005). Evolutionary geography of coasts of the Azov and Black seas. *The book 1. Anapa bay-bar. Sochi*, 174.

Izmajlov J.A., Arslanov H.A., Tertichnaja T.V., Chernov S.B. (1989). Reconstruction and dating of holocene coastal lines in delta of river Kuban. *Vestnik Leningr. Un-ta*.

Kosyan A.R. (2011). Role of sea shells in sediments balance of Anapa bay-bar. *Oceanology, in press*. [In Russian]

Mihajlov V. N, Magritskij D.V., Ivanov A.A. (2010). The hydrology of delta and mouth beach of river Kuban. *M. GEOS*, 728.

The report of CHE NIS of USSR AS Institute of oceanology. (1955). Dynamics of beachy accumulative coast and sandy deposits. Archive SBSIO RAS.

The report of CHE NIS of USSR AS Institute of oceanology. (1952). Researches of the coastal deposits dynamics using the luminophore. Archive SBSIO RAS.

Peshkov V. M (2000). Sea coasts. *Krasnodar: "Kubansky uchebnik*", 148.

The Russian seas register of navigation. (2006). The reference data on the wind and waves regime of Baltic, Northern, Black, Azov and Mediterranean seas. S.-Peterburg.

Jet Grouting for the Re-support of Pier 11A in San Diego, CA

S. Arora[1], J. Kinley[2]

1. Hayward Baker Inc., 301 Enterprise Street, Suite 3, Escondido, CA 92029; PH (760)-839-2870; FAX (760)-839-2245; email:sarora@haywardbaker.com
2. Hayward Baker Inc., 301 Enterprise Street, Suite 3, Escondido, CA 92029; PH (760)-839-2870; FAX (760)-839-2245; email:jjkinley@haywardbaker.com

ABSTRACT

Pavement failures occurred behind the retaining Wall at Pier 11A (former Navy Pier) in San Diego, California. The pavement failures were caused by a loss of soil directly beneath the pavement. It was presumed that the soil in the retaining wall was leaking through the tongue-and-groove joints between the concrete sheet piles located beneath the retaining wall footing, allowing water in, as well as marine borers that ate away the exposed portions of the timber piles, resulting in loss of timber pile support to the retaining walls. Inspection of the front of the retaining wall below the wharf deck revealed a regular pattern of cracks in the pile cap beams extending from the retaining wall to the pile-supported wharf. Jet grouting was successfully used to re-establish the structural support of the footing to the competent timber piles, and to fill the existing void spaces directly under the pile cap. This paper covers the test section, design, construction, and quality control measures on this challenging project.

INTRODUCTION

Pavement subsidence behind the retaining wall at Pier 11A in San Diego, California was caused by a loss of soil directly beneath the pavement.

The pier, originally built for the U.S. Navy, is over 60 years old, with a history of asphalt pavement failure at locations directly behind the retaining wall. It was presumed that the soil in the retaining wall was leaking through the tongue-and-groove joints between the concrete sheet piles located beneath the retaining wall footing, allowing water in, as well as marine borers that ate away the exposed portions of the timber piles, resulting in loss of timber pile support to the retaining walls.

Assumptions were validated by digging two test pits. Voids were discovered beneath the retaining wall, and the exposed timber piles were indeed eaten away by marine borers. Acceptable piling timber was found just below the mudline.

During inspection of the front of the retaining wall below the wharf deck, a regular pattern of cracks in the pile cap beams extending from the retaining wall to the pile-supported wharf was noted.

A jet grouting program was designed to re-establish the structural support of the footing to the competent timber piles, and to fill the existing void spaces directly under the pile cap. Soil conditions consisted of sand with some cobbles.

JET GROUTING

Jet grouting is a grouting technique that creates in situ geometries of soilcrete, using a grouting monitor attached to the end of a drill stem. The grouting monitor is advanced to the maximum treatment depth. High-velocity fluid jets are then initiated from ports in the side of the monitor. The jets erode and mix the in situ soil as the drill stem and grouting monitor are rotated and raised. Excess soilcrete rises to the surface through the borehole annulus where it is contained and disposed of. Depending on the application and soils to be treated, one of three variations is used: the single-fluid system (slurry grout jet), the double-fluid system (slurry grout jet surrounded by an air jet) or the triple-fluid system (water jet surrounded by an air jet, with a lower grout jet). The process constructs soilcrete panels or columns with designed strength and permeability. The technique has been used to underpin existing foundations, construct excavation support walls, and construct slabs to seal the bottom of planned excavations.

The jet grouting contractor had performed jet grouting on two similar projects.

The first project was in a combined residential/commercial development called Battery Park City, in New York City. The development was built on paced fill from nearby building excavations. As part of the overall development, a 21.3 m wide relieving platform was construction to support several feet of sol and to provide more useful land space. The front of the platform was construction as a timber retaining wall to support up to six feet of soil. Over the years, this timber retaining wall had been attacked by the Teredo Navalis mollusk. The borer activity would eventually destroy the existing bulkhead. The subsurface soils consisted of sand backfill placed against the bulkhead. This sand was underlain by filter stone placed over the quarry stone which contained cobles up to 23 cm in diameter. The double-fluid jet grouting system was used to construct a 1 m thick wall along the 244 and 153m long stretches of the bulkhead to a depth of 6m (Boehm, 2004).

The second project was in Milwaukee, Wisconsin. Excavation for an elevator pit as part of renovation of a warehouse into condominiums exposed four of the existing quarried limestone pile caps, sitting on a raft mat of wood and supported by untreated timber piles. The upper portion of the piles and the raft of wood timbers were in an advanced state of deterioration. Subsequent inspection at other interior columns, and at the perimeter foundation system supporting the masonry walls, revealed a similar condition. Jet grouting was used to underpin the pile cap and re-establish a competent connection in the upper eight feet of pile support directly below the quarried limestone floor (Hayward Baker, 1999).

For the Navy Pier 11A project, an enhanced double-fluid jet grouting system (SuperJet) was used to construct the large-diameter soilcrete columns (5 ft and 10 ft) to a depth of

6.5 ft below the foundation (Figure 1). A concrete vibrator was used to ensure a good bonding between the jet grout and existing footing.

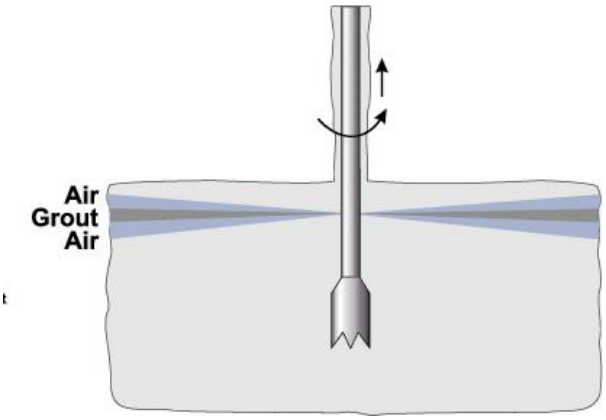


Figure 1. Enhanced double-fluid jet grouting (SuperJet) for large-diameter soilcrete column construction.

JET GROUTING DESIGN

Test Sections

Two test sections were constructed to determine the effectiveness of the design. Test section 2 is shown in Figure 2. The design of each test section was based on the orientation of piles and pilasters, and was incorporated into the production design. Eight-inch-diameter cores showed good bonding between the existing concrete and jet grouted soilcrete (Figures 3 & 4). Both test areas were successful in that the soilcrete bonded well with the existing concrete, and the soilcrete exceeded the specified strength requirement of 500 psi at 28 days of age.

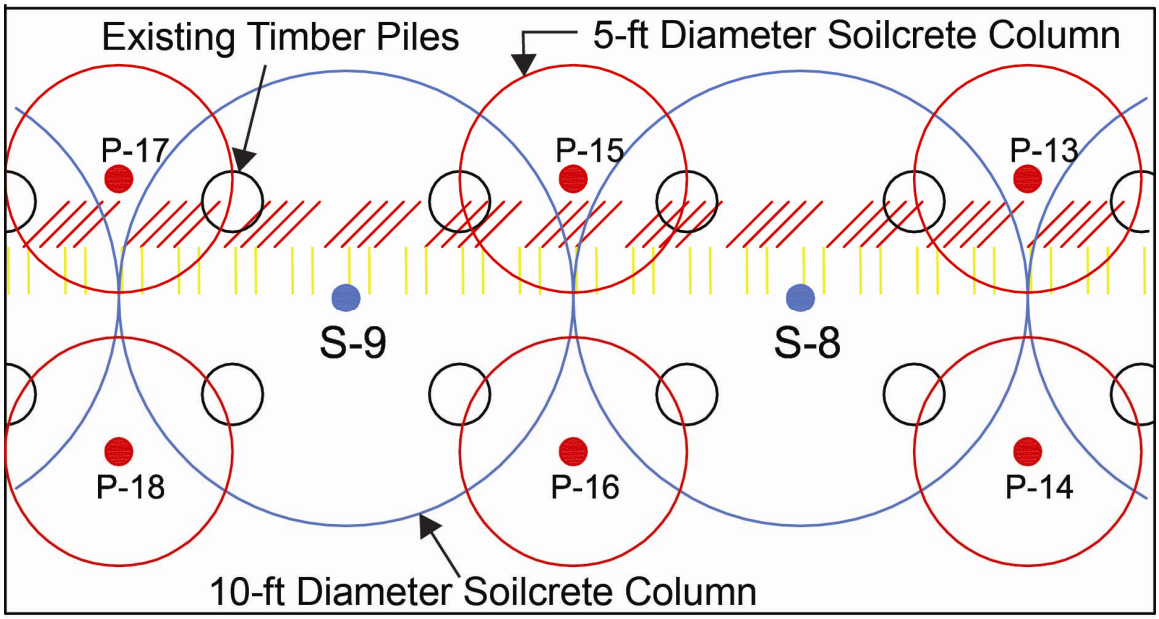


Figure 2. Test section 2.



Figure 3. Test section coring operation.



Figure 4. 8-inch-diameter core sample showing the effectiveness of the jet grouting.

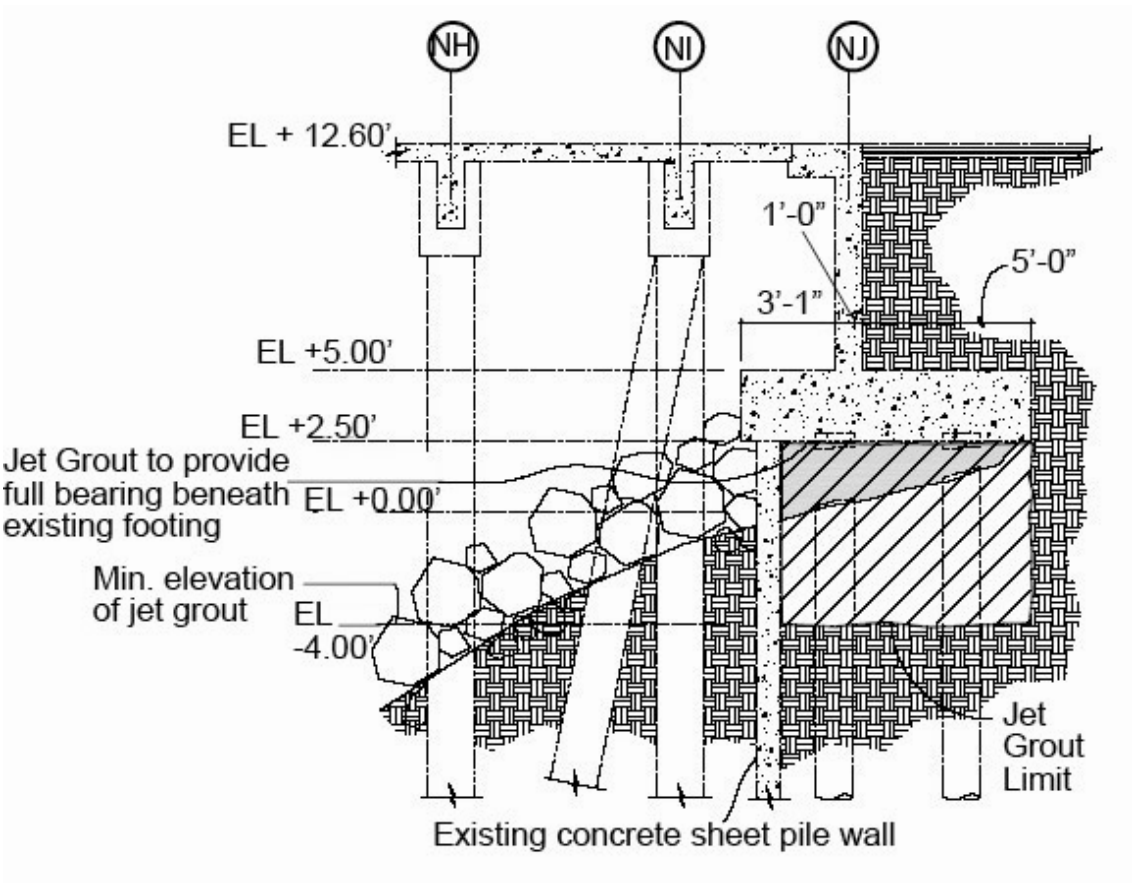


Figure 5. Jet grouting section view.

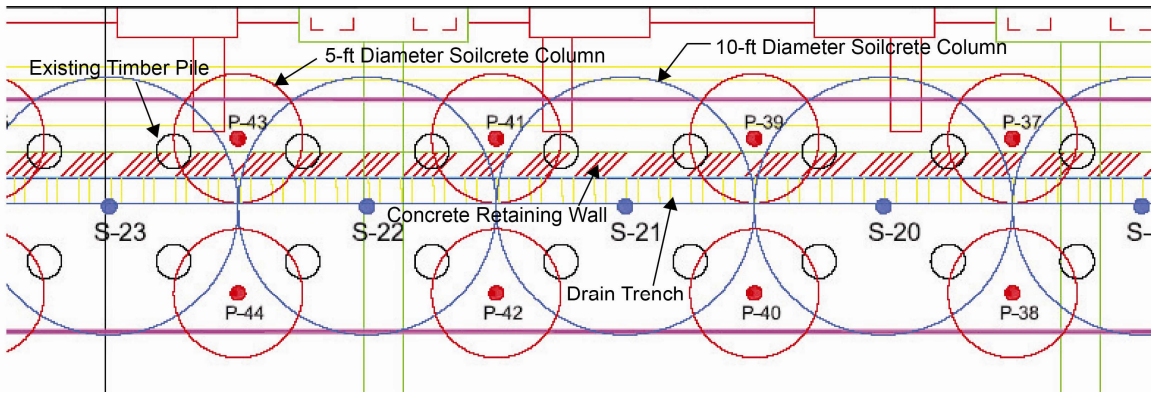


Figure 6. Partial jet grouted soilcrete column plan view.

CONSTRUCTION

The specified sectional area of treatment with jet grouting was specified as shown in Figure 5. It was possible that timber piles below the footing of the retaining wall could cause "shadows" during the jet grouting operation. This was a design challenge and was overcome by strategically placing jet grout columns of different diameters on both sides of the piles. Figure 6 shows the design layout of 5 ft and 10 ft diameter jet grout columns. This design as submitted to Owner's Engineer for approval and implemented for construction work after two test sections.

Trenches, 4 ft wide by 7 ft deep, were constructed on the inboard side of the retaining wall to allow the drill and crew to access to the top of the inboard footing. A total of 140 lineal feet of trench was required weekly to coincide with the jet grouting production. The trenches were later used to store excess soilcrete for about 24 hours while it reached initial set. In addition, lateral trenches, spaced 30 ft apart, were dug to allow excess soilcrete to travel farther inboard to a 20 ft by 20 ft by 5 ft-deep excavated pit to temporarily store the bulk of the excess.

Initially, all boreholes in a given reach were drilled with down-the-hole (DTH) hammers and then casing was installed. Jet grouting then commenced by installing every fifth column. Excess soilcrete traveled up through the borehole casing annulus and into the containment pits via the trenches. After a minimum of 24 hours, a second set of boreholes were drilled adjacent to the first set and jet grouted. This process continued until the pattern was complete.

A total of 402 primary (5-ft-diameter) and 123 secondary (10-ft-diameter) soilcrete columns were installed to a depth of 6.5 ft.

Construction challenges included keeping sufficient distance between all operations to ensure safety and avoid grout slurry from spilling into the bay. Changes in the traffic control plans, the trenching method, and tidal fluctuations also presented escalating difficulties to the project. Water side column locations were drilled (10" diameter) at the deck by a rock drill. The bottom of the footing was drilled (10" diameter) by DTH

method and then PVC (8”diameter) casings were installed. The footing on the water side could only be drilled when the jet grouting contractor was able to install PVC pipe at low tide, and to avoid any grout spill into the bay. Initially, a 6 ft wide and 8.5 ft deep trench was dug by the general contractor for the excess soilcrete. As the sand was hydraulically placed, the trench kept widening. This resulted in wider steel plates being needed for moving the drills. A 4 ft wide and 4-5 ft deep trench was dug to avoid unsafe conditions. Holes were drilled utilizing a down-hammer rig by going through 4-5 ft of sand. PVC casings were installed immediately after each hole was drilled.

QUALITY CONTROL

In addition to the test sections and coring, during construction jet grouting parameters such as rotation speed, lift rate, grout flow rate, injection pressure, and specific gravity of grout were automated and recorded.

Unconfined compressive strength (UCS) testing performed on soilcrete samples taken during production work demonstrated that the UCS of the soilcrete exceeded the 28-day specified strength of 500 psi (Figure 7).

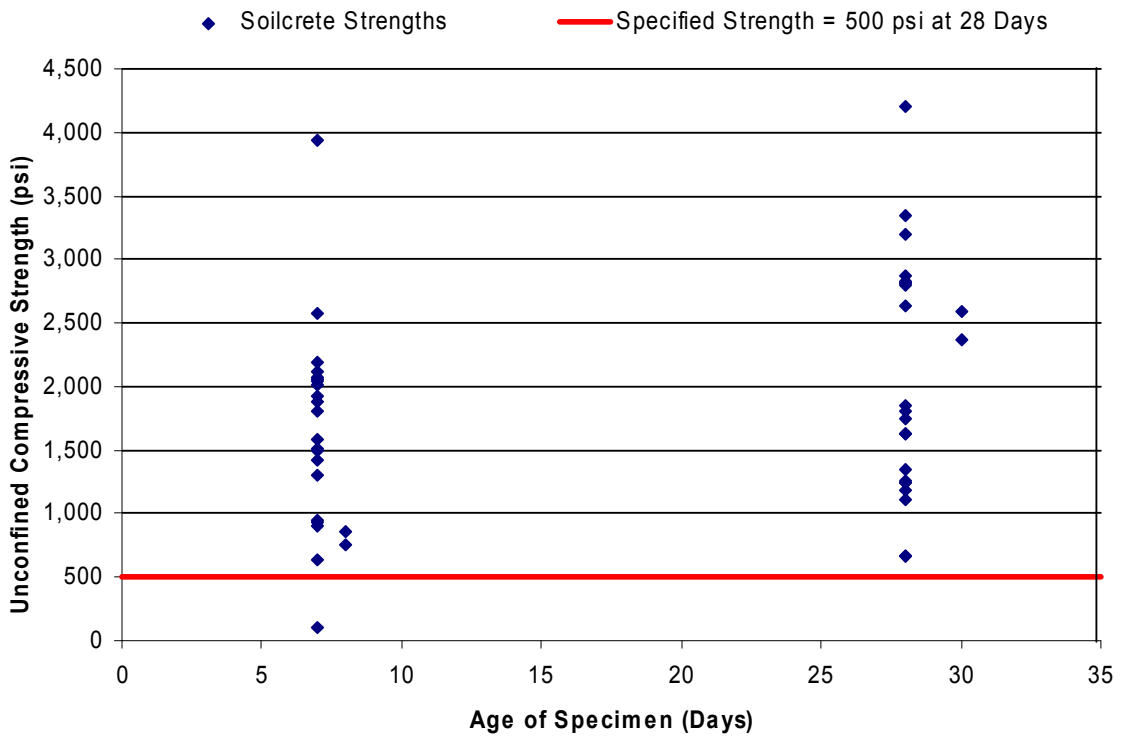


Figure 7. Soilcrete UCS test results.

CONCLUSIONS

Jet grouting successfully re-established the structural support of the footing to the timber piles to acceptable limits, and filled the existing void spaces directly under the pile caps. Effective construction planning allowed the project to be completed within budget and on schedule, with no negative impact on the bay.

REFERENCES

Boehm, Dennis W., 2004. *The Utilization of Jet Grouting and Soil Mixing Methods to Repair and Support Bulkhead Structures*. Proceedings of the Ports 2004 Conference, May 23-26, Houston, Texas, ASCE.

Hayward Baker Publication: "Project Summary: River Front Renovation, Water Street, Milwaukee, Wisconsin, 1999."

Over Twenty-Five Years of Applied Coastal Engineering in Alaska

Harvey N. Smith[1] and Ruth A. Carter[2]

[1] Alaska Department of Transportation and Public Facilities, Coastal Engineering Section, 5800 East Tudor Road, Anchorage, AK 99507-1286; PH (907) 269-6239; FAX (907) 269-6231; Harvey.Smith@alaska.gov
[2] Alaska Department of Transportation and Public Facilities, Coastal Engineering Section, 5800 East Tudor Road, Anchorage, AK 99507-1286; PH (907) 269-6241; FAX (907) 269-6231; RuthA.Carter@alaska.gov

ABSTRACT

Alaska Department of Transportation and Public Facilities, Coastal Engineering Section has developed numerous innovative designs for Alaska's arctic conditions and exposed shorelines. Case studies of ten challenging projects designed and constructed over the past 25 years will be presented; including a heliport at Little Diomede; buried cutoff wall for an airport at Gambell; 10 miles of shore protection for Seward Highway exposed to tidal bores and ice; energy absorbing pile guides for extreme wave conditions; and a dynamically stable beach at Unalakleet. Due to increasingly high costs for large armor, recent projects have relied more heavily on dynamic stability and softer designs. Most of these projects were constructed in remote areas of Alaska with little data available. Each case study will discuss challenges, technical design elements, and specific arctic coastal considerations. Designing in concert with site-specific conditions allows structures to survive and natural coastal processes to continue.

INTRODUCTION

The Coastal Engineering Section developed numerous innovative designs for Alaska's arctic conditions and exposed shorelines over the past 25 years. The projects have evolved from traditional rock revetments to softer, dynamically stable designs or alternatives such as retreating from the coast. In earlier years, as Alaska's infrastructure expanded, more work was done on harbor projects; as the state has divested itself of harbor ownership; coastal engineering work has been increasingly oriented toward airports and highways. Figure 1 shows a statewide distribution of projects and their modality. Due to increasingly high costs for large armor, recent projects have relied more heavily on dynamic stability and softer designs. Case studies of some of the more challenging projects constructed are presented herein.

Most of these projects were constructed in remote areas of Alaska with little data available. Each case study presents a problem, challenges and the solution along with technical design elements and specific arctic coastal considerations.

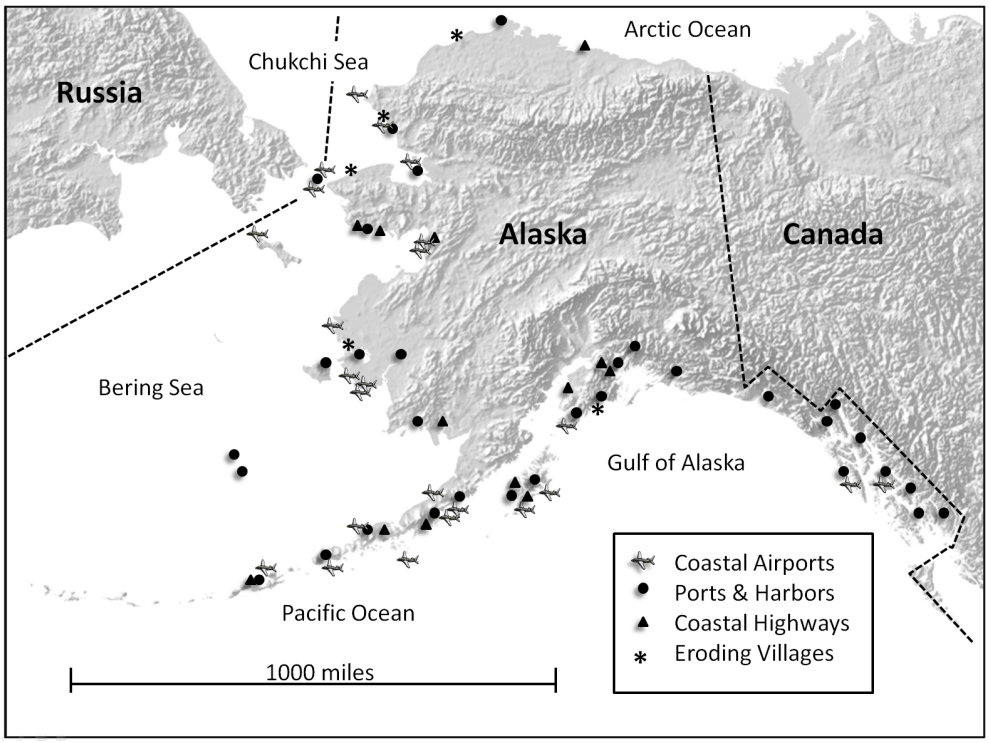


Figure 1 – Project locations (annotated base map © National Park Service)

CASE STUDY 1 – Little Diomede Heliport – Depth Limited Waves (1992)

In 1992, the State of Alaska determined that a heliport was needed for Little Diomede (Figure 2). The remote residents of Little Diomede Island can look over the Bering Straits and view the Russian Island of Big Diomede 2.5 miles away. The topography on and offshore near the village is steep and formidable; and, there was no flat area onshore large enough to land a helicopter. The community had used a grounded barge as a landing pad until it corroded to the point that it would no longer support the helicopters. There are deep water significant wave heights of over 35-feet. Plus the area is subjected to sheets of ice over 6-feet thick.

To deal with the large waves, the heliport was moved shoreward until the design wave was reduced to a 12-foot refracted, depth-limited wave; allowing the rock size to be reduced to a W50 of 6 tons. A circular design with a compound slope was used to accommodate winter ice conditions and reduce wave run up; the lower portion was constructed at a 4:1 slope with random placement that transitioned to special placement on a 1.5:1 on the upper reaches of the structure. The Kd value for the special placement allowed use of 6 ton armor stone on both slopes. Schematics of the heliport cross-section and plan view are shown in Figure 2.

High permeability was retained throughout the entire core of the structure to dissipate wave energy and minimize overtopping, further reducing the required armor size. High uplift forces from surging waves also required development of a special connection for the concrete planks that form the helicopter landing pad; the connection also improved the ease of handing and placement during construction.

Since its completion, the helipad landing lights have been periodically destroyed due to overtopping waves, but the structure has remained intact.

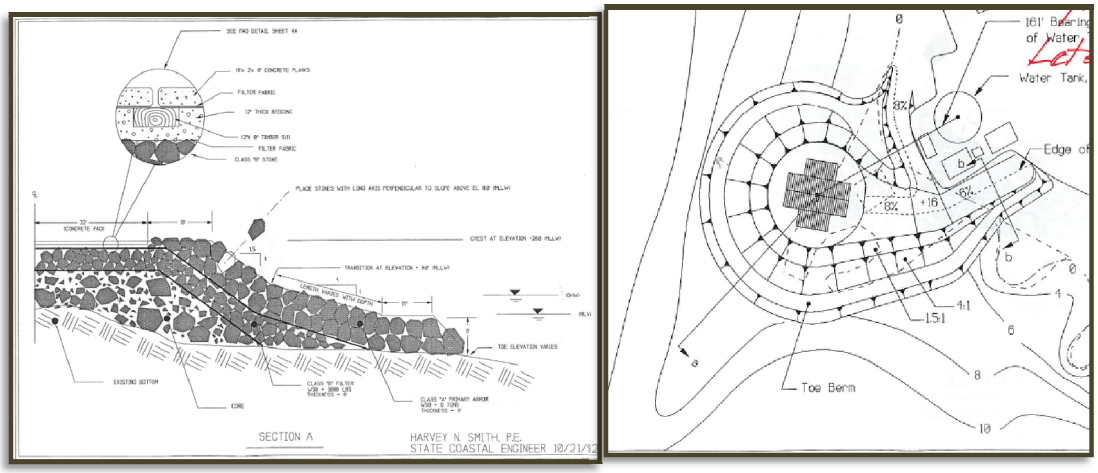


Figure 2 - Section showing composite slope, special placement and landing pad detail; right Plan View, Little Diomede Heliport (© Harvey Smith, 1992)

There is currently a proposal to construct a 3000 foot runway for the island. This project would preserve the heliport, provide a small boat basin and protected barge landing in addition to improving aviation safety. Figure 3 shows the completed heliport and a rendering of the proposed runway.



Figure 3 – Left Little Diomede (photograph by Jim Richardson, Anchorage, AK); Right proposed 3000-foot runway and small boat harbor (rendering by Harvey Smith, ADOT&PF, image by J. Richardson, Anchorage, AK)

CASE STUDY 2 – Seward Highway, Turnagain Arm – Ice Picking (1993)

The Seward Highway provides a vital link between Anchorage and the Kenai Peninsula. The pioneer highway alignment was along a steep slope where it would be closed several times each year due to avalanches. Consequently, beginning in 1993, sections of the Seward Highway were relocated onto the mudflats of Turnagain Arm in the upper reaches of Cook Inlet. The upper Turnagain Arm runs dry during lower tides except for residual drainage of saltwater tidal prism and influence of multiple

freshwater rivers. Low tide drainage channels change constantly. During winter months fast ice may form throughout the entire tidal range.

Shore protection for these eight miles of roadway are exposed to 5-foot waves, a 4-foot tidal bore, 35-foot tides and 6-foot ice floes (Figure 4). Tidal currents can reach six knots or more on ebb tides. Wind and tidal data was collected for three years at several locations along the arm; a complex statistical analysis of the data was used to determine phase and height relationships between this section of Turnagain Arm and the nearest established National Oceanic and Atmospheric (NOAA) tidal reference station at Anchorage. In addition to the phase and height variations, predicted tidal elevations along the project are effected by channel alignment, winds and ice. All coastal processes were combined to determine design conditions and evaluate risk of overtopping. Additionally an iterative analysis was used to evaluate incremental costs of each foot of roadway elevation in establishing the optimum elevation and balancing it with long term maintenance.



Figure 4 – Seward Highway near Girdwood with Harvey Smith in lower left for scale (photograph by Ruth Carter, Anchorage, AK, April 2011)

The revetment was designed with several unique features. Based on field observations of existing rockwork along the highway and railroad, the slope was flattened from a 1.5 to 2.0 horizontal to 1.0 vertical to reduce ice picking that was caused when cantilevered ice would topple carrying large armor stone down the slope. The top section used larger stone that was designed for waves using Hudson's formula; whereas the bottom was designed for currents using boundary shear stress. The rock sizes were modified to allow use of local rock adjacent to the project for the armor; these quarries created turnouts at Bird Creek (Figure 5) among others and reduced the cost from over $30 to about $11 per cubic yard. Additional rock was placed at the toe to create a launching section when undercut by migrating drainage channels.

The Turnagain Arm revetment project began in 1993 and has continued in phases; the next phase, closer to Anchorage, will be exposed to larger waves. The

design rock section presented herein has been adopted by the Alaska Railroad and department for use along Turnagain Arm with appropriate design modifications made to accommodate varying coastal exposure.



Figure 5 – Seward Highway turnout developed from project quarry (image by Harvey Smith, Anchorage, AK)

CASE STUDY 3 – Gambell – Last Defense (c. 1994)

Gambell, a Yup'ik community on St. Lawrence Island, is isolated except by air transport. The community is on a cuspate bar. Large storms from the south and southwest would periodically erode the beach and cause large waves to overtop Gambell runway and spilling into the lake on the lee side (Figure 6). During these events large segments of asphalt would be undermined and broken out. The lighting system would also be washed out. The runway could be shut down for several days stranding the villagers while repairs were made.



Figure 6 – Gambell, AK (oblique view to south; image © Google Earth)

Little data was available for this remote island community. The project was challenged by shallow permafrost and very dynamic coastal processes. The analysis was based on observations of historical overtopping events. The overtopping wave reportedly "*would probably wash away a pickup truck, but not a road grader*." The beach is exposed directly to 50-foot waves, which would erode the beach over one hundred feet in a single event. Net long shore transport is to the north from eroding bluffs. The beach is composed of rounded, four to six mm pebbles (pea gravel) on the natural angle of repose (2.5:1 slope). Figure 7 shows the beach with a close up of the material including a six inch ruler from our field measurement kit.

The solution was to design a system of last defense as near to the runway as the Federal Aviation Administration allowed and with the lowest impact to natural beach processes. The sheet pile is only exposed during storm recurrence intervals of five years or greater. The contractor had the option of installing a rock revetment or sheet pile wall. As seen in Figure 8, sheet pile was driven adjacent to the runway. Material in front of the wall was excavated for placement of a rock scour blanket. Beach material was re-graded in front of the wall and asphalt was used to form a seal along the top of the wall. Large storms still erode the beach and sand is thrown onto the runway, but there is no longer damage to the asphalt or lighting system. Nor has the airport been shut down for runway repairs.

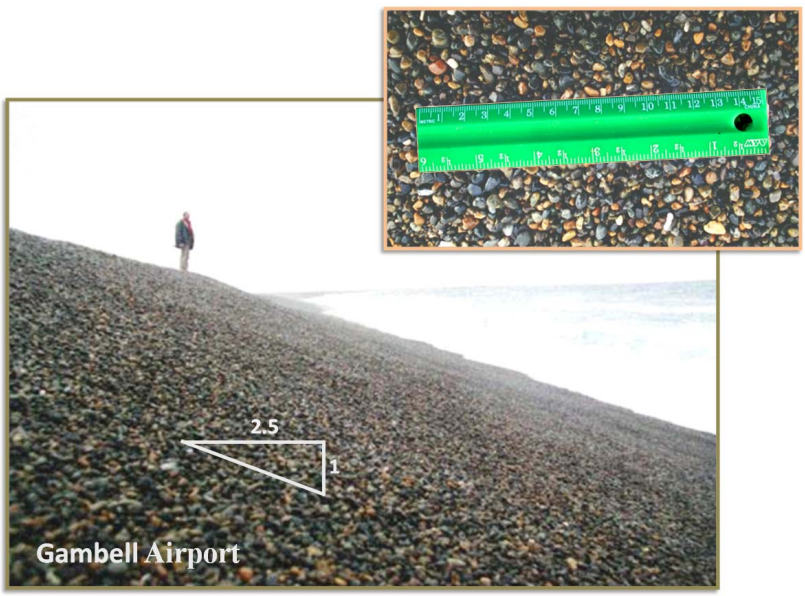


Figure 7 – Beach by Gambell Airport (@ Harvey Smith, ADOT&PF)



Figure 8 – Construction of wall along Gambell Airport (©ADOT&PF July 1999)

CASE STUDY 4 – Unalakleet – Dynamically Stable Beach/Soft Design (2008)

Unalakleet is on Norton Sound, 148 miles southeast of Nome. The road to the airport, which is the only link to the outside world, was washed out in a storm consisting of about a 10-foot surge and 7-foot breaking waves. Federal Emergency Management Administration funded only a portion of what was damaged.

There was no local quarry that could produce the size, quality and volume of rock needed to complete repairs using a traditional revetment design based on the

Hudson formula. Importing rock was not economical due to shallow water depths offshore, which were not sufficient for deep draft barges.

A survey of local material sites near the project disclosed a rock source that would produce a high yield of durable rock ranging from about 3 inches up to 12 inches with an average size of about 8 inches. This material size appeared to be well suited to take on the shape of a natural beach berm according to research done by Van der Meer and others. We plotted a natural beach slope using the 8 inch rock and compared it to a standard 2:1 slope. The volume for the smaller rock was only slightly greater; however, the benefits associated with availability of rock and ease of placement far outweighed the cost of the larger rock. Figure 9 shows construction of the revetment and the process of reshaping.

The section has survived a couple major storms over the past several years. After two years 17 of the original 20-foot crest width remains; the equilibrium crest width is about 10-feet. The rock is adjusting to the design slope and appears that it will conform to the theoretical shape. The project cost roughly one fifth of what a traditional revetment would have cost; the average weight of the rock in this dynamic system is only 1/100 that of a conventional design.



Figure 9 – Construction and shaping of dynamically stable beach at Unalakleet, Alaska (© ADOT&PF, 2008-2010)

This is the third dynamically stable beach engineered by the department to protect state infrastructure. The first was in response to maintenance concerns at Unalaska/Dutch Harbor Airport, where we recommended dumping 8 to 12-inch cobbles and boulders adjacent to 8-ton concrete Core-Loc armor units. Later, the

lagoon entrance and adjacent beaches to a popular fishing spot on Homer Spit were stabilized using terminal groins and beach nourishment; the lagoon is exposed to an 8-foot design wave; 2 to 3-inch cobbles have become stable on a 6:1 slope. Material sizes were based on equilibrium beach profile formula (Dean 2002; Figure 10).



Figure 10 – Dynamically stable beaches at Unalaska (left, 1995) and Homer (right, 1998), Alaska (Images © Ruth Carter, ADOT&PF)

CASE STUDY 5 – Chenega Small Boat Harbor (c. 1986) and Whittier Passenger Dock (c. 1995) – Energy Absorbing Fenders

The small village of Chenega, including harbor and dock (Figure 11), was constructed in the early 1980's in its current location; the original village was destroyed during Alaska's 1964 Good Friday earthquake and tsunami. Moorage requirement for the new harbor was for roughly 12 to 15 permanent vessels ranging from thirty feet to sixty feet plus additional moorage for transient vessels. The design wave for the site is 5-feet with a 3.5-second period.

Due to limited funds and relatively deep water a rubble mound breakwater was not an economical solution. The cost of a traditional pre-stressed or post tensioned floating breakwater was also about twice the available funds.



Figure 11 – Chenega Bay (© Alaska Division of Community and Regional Affairs, 2006)

Standard low cost float modules that were limited to use in protected basins were modeled using Boeings Computer Services, then modified to handle the five foot design wave and provide protection to the moored vessels. This was accomplished in several ways.

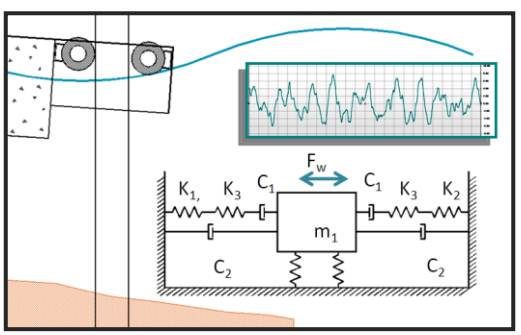
1. The standard 10-foot float was widened to 16 feet to attenuate the wave to acceptable ASCE criteria
2. A 12 by ¾-inch steel plate was sandwiched between two outside timber wales along the full 300-foot length of the float
3. A double row of 0.75-inch thru rods were added to the float system
4. The finger or stall floats were aligned into the incident wave
5. Piling were tied at top to stiffen the system and disallow resonance with the wave
6. Heavy marine fenders were incorporated into the pile guides to distribute the load more uniformly between mooring piles and also absorb much of the wave energy that is transferred into the float

The float has performed well for over thirty years and has experienced the design wave a number of times. Due to an error in construction, repairs were made to the system in 1992; including replacement of a small wedge section by a tire breakwater. Repairs incorporated use of a fiber reinforced plastic Chemgrate® for ramp surfaces. Access gangway was reinforced for use by small trucks and ATV's. During the cleanup of the Exxon Valdez oil spill, the float system was used as Exxon's center of operation.

A similar fender system was developed for a float outside the Whittier small boat harbor (Figure 12). The float, a refurbished concrete floating breakwater, was designed using principles of Naval Architecture. It is exposed to 7-foot waves in Portage Canal. The structure was designed using a "pushover" analysis forced by a random sea state (Figure 13). It features high energy absorbing cylindrical fenders and a permeable walking surface to allow waves to surge through the deck.



Figure 12 – Whittier Passenger Loading Dock left with high energy absorbing pile fenders with 16" steel pile shown on right (© Harvey Smith, ADOT&PF)



K_1, K_2 = Spring Constant for Piles
K_3 = Spring Constant for Fenders
C_1 = Damping from Fenders
C_2 = Damping due to Turbulence

Figure 13 – High energy absorbing fender system (© Harvey Smith, ADOT&PF)

CASE STUDY 6 – Kivalina – Move or Expand?

Kivalina is a small, Inupiat Eskimo village located on a barrier island in the Chukchi Sea. It has a population of roughly 400 people. The community has existed since before 1847; and the population has grown and fills all the available space, so that the village now encroaches on the natural shoreline. There have been assumptions that the island will be inundated due to climate change and sea-level rise. The community is slated for relocation; the residents are divided on whether to relocate or remain in place.

Large storms in 2004 and 2005, roughly 30 year events back to back, eroded areas of the shoreline adjacent to the city. Emergency responders constructed a non-engineered, gabion wall mining the beach to fill sand bags for the project. Needless to say, the gabions failed. Subsequently the beach has been rebuilding; however, a rock revetment has been constructed that further encroaches in the active littoral zone and the toe is laid directly on the beach, not keyed through the dynamic layer.

There is very little data from the remote community site; consequently, many assumptions are made by relying on data from an ore export facility located 13 miles south. To date, the only solution that has been considered is relocation; however there has not been an engineering erosion study and long term stability of the barrier island is not known. Historic photographs suggest the island, prior to man's intervention, was generally stable. There have been numerous conflicting planning studies. Since the community has been convinced that they need to relocate, most erosion control structures have been temporary.

More recently, we conceived the idea of looking at migration and adaptation by expanding the village landward onto a shallow fill in an adjacent lagoon. This would resolve the most immediate problems of population density and evacuation route, via a road across the lagoon away from the coast, in the case of a high storm surge. The road would provide access to inland material sites as well. The village could continue to migrate landward providing a greater natural buffer to the sea (Figure 14).



Figure 14 – Kivalina, AK, left panel shows oblique view to northeast; right includes a conceptual drawing of a village expansion and small boat harbor with an evacuation center near the mouth of the Wulik River (rendering by Harvey Smith, ADOT&PF; image source Google 2009)

CASE STUDY 7 – Unalaska/Dutch Harbor Airport – Overtopping (1995-2002)

Unalaska is located on the Aleutian Chain about 800 air miles southwest of Anchorage. The community, built on two islands connected by a bridge, is ideally situated for the commercial fishing industry; and is on the Great Circle shipping route for the Pacific Rim. Unalaska Airport was periodically overtopped from wave run-up, which posed a threat to airplanes landing during high wave conditions. The overtopping would also lift the asphalt and roll large boulders underneath.

The wave causing the damage was transitioned through 180 degrees before impacting the runway. Although modeled extensively for refraction, diffraction, and reflection, the observed wave could not be reproduced numerically. A video camera was provided to airport maintenance personnel with instructions to document conditions where waves would run onto the airport surface. The video tape was analyzed to select the 12-foot design wave.

We used 8-ton concrete armor units to solve this problem. “Core-Loc” units were selected due to their low profile, which had an acceptable FAA ‘roughness,’ and because their increased energy dissipation reduced run-up 40%. The size was selected due to availability of molds. Units were placed on a 5:1 slope; use of Core-Loc had not been tested on such a flat slope and required approval by the USACE. Figure 15 shows the shore protection along the runway; the Core-Loc units are exposed to 12 foot waves, which transition to 8-feet at the dynamically stable beach section.



Figure 15 – Left to right -- Core-Loc (2002), transition to Armor Stone, and finally a dynamically stable beach (1995) sections, Unalaska, AK (© ADOT&PF)

At the same time Core-Loc units were being placed, the Unalaska Beach Road was being improved. Construction personnel noted areas of erosion. A quick sediment analysis demonstrated that modifications to the runway were disrupting littoral processes; a revetment was designed during construction assuming a 5-foot design wave and has performed well. Figure 16 shows the revetment construction using filter stone (W50=90 lb), armor rock (W50=1800 lb) and finally the first storm.



Figure 16 – Left to right – Placement of Filter Stone, Armor Stone, and first storm impacting section along Unalaska Beach Road (© ADOT&PF)

CASE STUDY 8 – Pasagshak Road – Retreat

The road to a missile launch site on the west coast of Kodiak Island was constructed around a headland that was frequently battered by storms. Most of the "non-engineered" armor rock was displaced and the road became vulnerable to being completely cut off in the event of another high tide and storm. The road was of high priority since it is the only route for transporting missiles to the launch site.

The Coastal Engineering Section was tasked with designing a revetment to protect the road. The first step in the design was to find a suitable source of rock. The adjacent headland was not of the high quality normally specified for armor rock and yield for properly sized rock was small; however, its convenient location and relatively low cost made it an attractive source. We finally decided to write a specification to use this local rock source.

As the rock next to the road was quarried, it became evident that the volume required to produce armor would move the headland back over sixty feet. It soon became clear that the most logical and low risk solution was to realign the road through the quarry. The roadway protection became natural bedrock. Armor rock produced by the quarry was used on other projects. This significantly lowered the cost of protecting the road. The old road alignment became a convenient turnout that acts as a natural storm buffer.



Figure 17 – Left shows original alignment; right, improved Pasagshak Road, Kodiak Island, AK (© Harvey Smith, ADOT&PF)

Although this was a relatively small project, it clearly demonstrates the need for engineers to look at the overall project and not become too focused on one detail of a design.

CASE STUDY 9 – Homer Harbor –Rising Rock Costs (2010)

Homer is a typical Alaska small boat harbor with 920 reserved stalls and over 6000 linear feet of transient moorage. It is located in Kachemak Bay near the mouth of Cook Inlet south of Anchorage. It is exposed to about an eight-foot significant wave with a six-second period. The City entered an agreement with the US Army Corps of Engineers (USACE) and with the State of Alaska to evaluate the need for additional moorage to accommodate the local commercial fishing fleet. There is also

a high interest in moving a local 225-foot Coast Guard buoy tender and other Federal vessels into a harbor area with secure access.

The ADOT&PF provided technical assistance to the City of Homer, and contributed funding for the study. Among tasks completed by the Coastal Engineering Section was development of conceptual alternatives to meet engineering criteria, and economic needs for the study. The small boat harbor is at the end of a spit. It is subjected to visible sediment waves that wrap around the end of the spit and into the existing USACE entrance channel. Several times each year ice from Kachemak Bay is scooped into the entrance as well. For this reason, we also looked at circulation and flushing within the basins. Examples of harbor layouts are shown in Figure 18; the existing configuration is in the upper left-hand corner.



Figure 18 – Conceptual Harbor Layouts for Homer, AK (© Harvey Smith, ADOT&PF; image source Google 2007)

Due to escalating rock costs the estimated cost of construction rose to over $100 million. Consequently, none of the alternatives had positive benefit-cost ratios, and the study was put on hold prior to evaluating these concepts against the design criteria. This may be revisited if additional benefits or lower cost materials can be found.

SUMMARY

Each of the case studies presented herein was designed and constructed with little data. The designs relied heavily on evaluating existing coastal features and anecdotal lore from elders within the native communities.

Alaska has the longest and most variable coastline in the United States. There are more than 100 coastal communities scattered over 40,000 miles of coastline. Each has its own unique relationship with the sea. Many have learned to adapt and live in harmony, while others try to resist with brute force. Due to the increased cost of coastal construction, the state's position is to learn from those that adapt.

Consequently the trend of the Alaska DOT&PF Coastal Engineering Section is to increasingly use soft design so that we "Don't fight the sea with brute force but with soft persuasion. (Bijker 1996)"

REFERENCES

Bijker, W.E., (2007) "Dikes and Dams, Thick with Politics," ISIS, 98 109-123.

Cox, J., Smith, H.N., et al, PIANC WG 98 (2008) *Protecting Water Quality in Marinas.*

Dean, R.G., Kriebel, D.L. and Walton, T.L.. (2002). *Cross-shore sediment transport processes.* Chapter 3 of Part III of the Coastal Engineering Manual, EM 1110-2-1100.

Smith, H.N., Carter, R.A., Jones, D. (2002) *Achieving and Maintaining Water Quality in Small Boat Harbors.* Coastal Engineering Section, Alaska Department of Transportation and Public Facilities, Anchorage, Alaska.

Smith, H.N. and Carter, R.A. (2004). *Coastal and Harbor Design Procedures Manual.* Coastal Engineering Section, Alaska Department of Transportation and Public Facilities, Anchorage, Alaska, revised September 3, 2004.

Smith, H.N., Carter, R.A., Jones, D. (2008) "*Harbor Aquatic Vegetation Study*" (in review) Coastal Engineering Section, Alaska Department of Transportation and Public Facilities, Anchorage, Alaska.

Smith, H.N. and Carter, R. (1993). *Tidal Report for Seward Highway: Bird Point to Girdwood.* (1993) Coastal Engineering Section, Alaska Department of Transportation and Public Facilities, Anchorage, Alaska, September 22, 1993.

Van der Meer, J.W. (1988). *Rock Slopes and Gravel Beaches under Wave Attack.* Doctorial thesis, Delft University of Technology. Also, Delft Hydraulics Communication, Publication No. 396. 26 April 1988.

Corrosion Protection for Concrete Structures in Marine Environments

D.B.McDonald, Ph.D., P.E, FACI[1]

[1]Epoxy Interest Group of CRSI, 933 N Plum Grove Rd, Schaumburg, IL 60025;
PH (630) 380-5845; FAX (847) 517-1206; dmcdonald@epoxy.crsi.org

ABSTRACT
The deterioration of concrete structures in marine environments due to corrosion may result in costly and inconvenient maintenance. This paper presents information on corrosion mechanisms of steel in concrete and factors affecting corrosion performance. Information is also presented on concrete modification and other systems that increase the durability of concrete structures in corrosive environments. These include pozzolans and galvanized, epoxy-coated, and stainless steel (SS) reinforcing. Finally, the paper discusses other factors, such as sustainability, cost and availability of the various commonly used products.

INTRODUCTION
An analysis by the Federal Highway Administration (FHWA) in 2001 concluded that the annual cost of corrosion in the public port authority sector of the ports and waterways can be estimated at $182.3 billion (Koch, Brongers et al. 2001). Additionally, in 2006, it was estimated that the U.S. Department of Defense (DoD) that $10 billion was spent on facilities maintenance and that approximately $1.8 billion was spent on issues relating to corrosion of facilities and infrastructure (Herzber 2009). Corrosion of reinforcing in concrete structures in a marine environment without appropriate protection may occur very soon after construction. For example; Costa and Appleton report on marine structures in Portugal that exhibited corrosion within 5 to 10 years after construction (Costa and Appleton 2001).

Protection against corrosion in concrete structures requires an understanding of corrosion mechanisms and material selection. Within this paper, the types of corrosion protection systems and selection of these materials will be discussed.

CORROSION BASICS
The American Concrete Institute (ACI) defines corrosion as “destruction of metal by chemical, electrochemical, or electrolytic reaction within its environment." In concrete, it is generally recognized that corrosion occurs due to the formation of an electrochemical cell, where iron in the steel converts to iron ions.

For corrosion to proceed, four factors must be present:

- Anode – where iron metal is converted to iron ions
- Cathode – where electrons released from the anode react with oxygen and water
- Electrical path – a path that enables ready passage of electrons between the anode and cathode
- Ionic path – a path between the anode and cathode that enables the cell to maintain ionic balance.

Corrosion may be lessened by reducing or preventing any one of the four factors described above. These factors and preventative methods for marine structures are presented in Table 1.

Table 1. Methods to reduce corrosion

Anode	Cathode
• Reduce concrete permeability o w/cm o pozzolans o chemical additions • Increase chloride threshold o inhibitor o change reinforcing bar material • Force opposite reaction o cathodic protection	• Reduce area of reactive surface o coatings • Reduce oxygen o concrete permeability • Reduce cathode effectiveness o inhibitors
Electrical Path	**Ionic Path**
• Disconnect anode and cathode o coatings o physical separation	• Make pathway between anode and cathode more difficult o high resistivity concrete

When steel is placed into the high pH of concrete, it develops a passive film that protects it from future corrosion. This passive film may be interrupted by the presence of sufficient chloride or other halide ions, or by the reduction of the concrete pH, which may occur when carbon-dioxide in the environment reacts with the calcium hydroxide in the cement paste.

Once the iron ions are released from the anode, they may react with oxygen to form iron oxides that occupy a larger volume than the initial metal. When sufficient expansion has occurred, cracking and spalling of the concrete is likely. It has been found that as little as 25 μm of corrosion may cause cracking; however this value is dependent on the amount of concrete cover over the reinforcing (Pfeifer 2000).

Carbonation – Carbonation of concrete occurs when carbon-dioxide in the atmosphere reacts with the calcium hydroxide in the hydrated cement paste. The rate of carbonation is generally assumed to be governed by the following equation:

Depth of Carbonation = $C.t^{0.5}$

Where
t = time and C = coefficient dependent on concrete quality

Collepardi et al. (Collepardi, Collepardi et al. 2004) found that the value of C was highly dependent on the water-cement ratio (Table 1). Using data from this research, the time for concrete using straight Portland cement to carbonate 50 mm (2 in.) at a w/cm ratio of 0.7 would be 39 years, compared with 2,500 years for a concrete with a w/cm of 0.40. Thus, the effect of carbonation is clearly mitigated through use of appropriate w/cm ratios.

Table 2: Effect of water-cementitious ratio on carbonation coefficient for concrete containing Portland cement (mm·year^{½}) (Collepardi, Collepardi et al. 2004).

w/cm	Portland Cement Concrete (mm·year^{½})
0.70	8
0.60	4.9
0.50	4.0
0.40	1.0

Chloride ions - In concrete marine structures, corrosion is principally caused by the reinforcing steel reacting with chloride ions that penetrate the concrete pore water and through cracks. The exact mechanism of corrosion due to chloride in concrete is not well understood, but Sagoe-Crentsil and Glasser suggest that the chloride ions enhance the iron dissolution through the formation of a soluble iron chloro-complex with green rust as the main solubility-limiting phase (Sagoe-Crentsil and Glasser 1993). Once released, the iron ions react with oxygen and hydroxide, forming expansive oxides.

When the chloride ion concentrations reach a threshold level, then corrosion may proceed. This level is termed the *"corrosion threshold"* and depends on the steel and cement chemistry. Typical values range from 0.7 to 1.2 kg/m^3 (1.2 to 2 lb/yd^3) for uncoated steel reinforcing.

The ingress of chloride into sound concrete is normally assumed to follow Fick's 2nd Law of diffusion, which depends largely on the diffusion coefficient for the particular concrete. It is generally expressed as shown below.

$$C(x,t) = C_s - C_s.erf\left[\frac{x}{2\sqrt{D_{eff}.t}}\right]$$

Where
C_s = surface concentration of chloride
D_{eff} = effective diffusion coefficient
x = concrete cover
t = time
C(x,t) = concentration at depth (x) and time (t)

To increase the time until the critical chloride threshold is reached, the effective diffusion coefficient (D_{eff}) may be decreased or the cover (x) increased. In practice, increasing the cover for horizontal surface above 75 mm (3 in.) or for vertical surfaces above 100 mm (4 in.) is impractical and may lead to substantial additional cracking.

When the critical corrosion threshold has been reached, the corrosion propagates until expansive forces from the oxides crack or delaminate the concrete covering the bars. The time for this process to occur is termed the propagation period and is highly dependent on the cathodic area, as well as the moisture, air and water contents of the concrete.

CORROSION PROTECTION

There are many methods of providing corrosion protection to concrete. This includes modifications to the concrete and/or reinforcing bars, as discussed below.

Concrete Modification

Permeability – Reducing concrete permeability results in additional time prior to reaching the chloride threshold for a particular system. Reducing the permeability of the concrete also reduces the ionic flow, slowing the corrosion current and extending the propagation period.

The principal method used to reduce the permeability of the concrete is through reduction of the concrete water-cementitious ratio, or through the addition of pozzolans, such as silica fume, fly ash and slag cement (ASTM C1240, C618, C989). Permeability reducing admixtures may also be used. It is possible to reduce the concrete permeability by an order of magnitude or more; substantially delaying the onset of corrosion.

Methods used to reduce concrete permeability may also result in a greater elastic modulus and reduced creep of the concrete. These factors may substantially increase the risk of cracking, providing a ready pathway to allow marine waters to penetrate directly to the reinforcing.

Corrosion Inhibitors – Corrosion inhibitors may be specified using ASTM C1582. The amount of protection provided by these admixtures is largely dependent on the admixture dosage. The most commonly used corrosion inhibitor is calcium nitrite; however, three other classes of admixture are identified by a report recently published by ACI Committee 212 report, titled "Report on Chemical Admixtures for Concrete." As some of these inhibitors are water-soluble, concern has been raised as to whether they will leach from the concrete during long-term exposure to marine waters. Further, the performance of these inhibitors in cracked concrete may be poor.

Reinforcing Bars

Galvanized Reinforcing – Galvanized bars are specified according to ASTM A767 and have been frequently used to improve the performance of reinforced concrete in marine environments. Bars may be coated prior to or after coating. Andrade and Alonso found that the corrosion resistance of the galvanized bars depended highly on the chemistry of the cement and the zinc layers and that differences in coating microstructure may result in significant differences in performance (Andrade and Alonso 2004). Care is also required if galvanized bars are connected

to uncoated bars, as the zinc coating will galvanically corrode and the protective may be depleted prior to the arrival of the chloride ions (Safiuddin 2005).

Epoxy-coated Reinforcing - Epoxy-coated reinforcing bars are generally specified according to either ASTM A775 or A934 and the use of this product for marine structures has increased over the past 20 years. Bars meeting ASTM A775 are the most commonly used and these bars are able to be fabricated after coating. In Japan, epoxy-coated reinforcing bars are required for bridge structures within 1 km (0.6 mile) of the coastline and the material is more commonly used for marine structures, such as wharfs and piers in the Middle East, Korea, China and India.

Fusion-bonded epoxy on the steel surface substantially reduces the amount of area that is exposed to the ingress of chloride. The coating effectively reduces the anode and cathode areas and makes electrical pathways between different bars more resistive. As corrosion reactions are frequently governed by the cathode, this factor substantially reduces the corrosion rate once corrosion is initiated. In tests conducted for the FHWA, corrosion rates of less than 2 percent of the uncoated bars were observed, even when bars with substantial damage were used (Lee and Krauss 2004). Several researchers have also found that epoxy-coated bars performed well in cracked concrete (McDonald, Pfeifer et al. 1998; Draper, Darwin et al. 2009). Long-term tests conducted in Canada have found effective performance of epoxy-coated reinforcing bars exposed in a marine environment compared with other materials (Kondratova, Bremner et al. 1999).

In a number of studies, the chloride threshold for epoxy-coated bars appears to be greater than for uncoated bars (Cui, Lawler et al. 2007; Lawler, Krauss et al. 2011). While some have suggested that this factor is related to the location of the defects compared with the clear cover over the bars, calculations by the author found that this factor only accounts for a small portion of the observed threshold increase. Further research to understand this apparent increase in threshold is required.

Some highly cited instances of poor behavior of epoxy-coated bars have been documented (Powers 1987), but generally these relate to poor bar manufacture, improper handling and inadequate concrete conditions. Since 1991, substantial improvements have been made to the manufacture of epoxy-coated reinforcing bars in North America through a voluntary plant coating certification program run by the Concrete Reinforcing Steel Institute (CRSI).

In 2010, a paper was published on the performance of the nearly 300 structures containing epoxy-coated bars in Florida (Sagues, Lau et al. 2010). Of these, only 4 percent showed distress after 30 years of service and the majority was predicted to provide 100 year design lives.

Side-by-side comparisons of the performance of epoxy-coated and uncoated bars are rare; however, the author found excellent performance of piers constructed with epoxy-coated bars compared with an identical adjacent bridge in Melbourne, Florida.

Stainless Steel Reinforcing - Stainless steel reinforcing bars are specified according to ASTM A955. The performance largely depends on the chemistry of the particular stainless steel (Bower, Friedersdorf et al. 2000).

Progreso Pier, in Mexico, is frequently cited as an example of excellent performance of stainless steel reinforcing. This structure, built in 1940, is considered to be the oldest concrete structure containing stainless steel reinforcing (RAMBOL 1999). While generally good performance was observed, the report states that at several locations there was: "*serious laminated corrosion on the visible reinforcement and the reinforcement area was reduced to approximately 60 – 70%."*

A report from the Naval Facilities Engineering Command raised a significant issue regarding the need for oxygen to maintain passivity of stainless in a marine environment (Burke and Drake 2002), as follows:

> *"Stainless steel requires oxygen to maintain passivity, stainless steel is known to corrode rapidly when it is totally and continuously submerged in contact with seawater. Oxygen content is always of concern when using SS, since it influences the stability of the passive film governing corrosion resistance. With direct submersion, pits commonly initiate under crevices that limit access of oxygen. These crevices may be formed in a number of ways including metal-to metal contact, biofouling, etc. The situation is exacerbated by any situation that generates differences in O_2 content along the surface. When used as reinforcement, it is these differences and the influence of chloride content and pH, as well as the water O_2 content that will dictate corrosion activity…"*

During evaluation of cracking of the concrete curb at the Magnetic Silencing Facility, Point Loma, losses of stainless steel cross-section exceeded 50 percent (Polly, Burke et al. 2008). This report concluded that *"the reinforcement is inadequate for its environment despite being of stainless steel composition, which has generally been considered superior in marine concrete."*

OTHER METHODS

Bars - Other reinforcing bar coatings and materials, such as nickel or copper claddings have been suggested (McDonald, Pfeifer et al. 1998). Recent tests have shown that bars meeting ASTM A1035 corrode readily in salt spray and have poor performance in tests that are used to evaluate stainless steel reinforcing and for this reason are not recommended (Cui and Krauss 2006; Surgeon, O'Reilly et al. 2010). This performance is further dependent on whether the bars are provided in an as-received or pickled condition.

Glass and Basalt fiber bars have been suggested for structures; however, these are largely considered experimental.

Cathodic Protection - Impressed or passive cathodic protection may be provided to protect the concrete against corrosion damage (Sohanghpurwala 2009); however, it is typically used as a repair technique rather than as a method to suppress initial corrosion. Cathodic protection provides an external current that reverses reactions at the anode.

OTHER FACTORS

When selecting methods to protect marine structures against corrosion, factors such performance, cracking, sustainability, initial and life cycle cost, and availability should be evaluated.

Performance - Protection for marine structures is largely provided by the concrete. Concrete with an appropriate low water-cement ratio and appropriate cover is the most cost effective method for adding additional service life. However, poor mixture design and placement practices may result in less than expected performance.

When selecting reinforcing bar strategies, the expected design life of the structure should be considered. Epoxy-coated bars have been predicted to last at least 100 years in marine environments (Sagues, Lau et al. 2010).

Cracking – Care should be taken to ensure that appropriate methods are used to minimize concrete cracking. Individual mixtures may be evaluated using ASTM C1581. Additional consideration of thermal and early age cracking should also be made.

Sustainability - Materials and their sustainability may be considered, particularly when government funding is required. In general, use of pozzolans is considered a good strategy. Epoxy-coated and galvanized bars are generally manufactured using over 95 percent of recycled materials; compared with only 75 percent for specialty steels, such as stainless steel. Further, processing energy for stainless steel may be significantly greater than for epoxy-coated or galvanized bars.

Cost – Moderate modifications to the concrete are generally less expensive than modifications to other factors, such as the reinforcing. Some pozzolans are approximately the same cost as the cement they replace, thus adding durability with essentially no cost penalty. Corrosion-inhibiting admixtures may add an additional 15 percent or more to the concrete costs.

Epoxy-coated reinforcing bars have proven cost effective in life-cycle analyses and have a relatively low initial cost while galvanized reinforcing bars are generally more expensive than the epoxy-coated bars. Stainless steel bars may have costs 5 – 10 times that of epoxy-coated bars, limiting their use.

Availability - Pozzolans are more readily available east of the Mississippi river; primarily due to the location of coal deposits and corrosion inhibitors are widely found and available from a number of companies.

While galvanizing operations are found throughout the country, very few have experience with reinforcing bars. Many are unable to coat bar lengths greater than 40 ft and most do not have facilities for the required chromate treatment.

Epoxy-coated reinforcing bars are widely available in North America from over 35 suppliers in North America. Since 1991, most of these plants have been certified by CRSI as part of a program that evaluates a plant's capacity to produce and handle high-quality product. The majority of bars may be fabricated and on jobsites within a week of ordering.

Stainless steel reinforcing is only produced by three manufacturers in the U.S. and substantial lead times may be required. Further, fabrication of these products requires additional care to

ensure that the stainless reinforcing is not contaminated by foreign materials and is appropriately pickled.

Bars meeting ASTM A1035 are generally not readily available and are only produced by mills using a patent license. These patents are held by a single corporation that does not own steel rolling facilities.

SUMMARY AND CONCLUSIONS

Owner of marine structures faces a wide choice in the selection of materials for corrosion protection. Generally, concrete with a low water-cement ratio and pozzolans should be used. Based upon performance and cost, epoxy-coated bars are appropriate for 100 year design lives; however for greater design lives other materials may be considered.

Overall performance is not the only criteria that should used to select products for marine environments and consideration of sustainability, costs and availability should be made.

Using methods outlined in this paper, concrete marine structures with long design lives may be constructed.

REFERENCES

Andrade, C. and C. Alonso (2004). Electrochemical Aspects of Galvanized Reinforcement Corrosion. San Diego, Elsevier Inc.

Bower, J., L. Friedersdorf, et al. (2000). Application of Stainless Steel and Stainless-Clad Reinforcing Bars in Highway Construction. University Park, PA, Pennsylvania Department of Transportation. HWA-PA-2000-011.

Burke, D. and Drake, JE (2002). Durable Lightweight Concrete for the Modular Hybrid Pier. Port Hueneme, California, Naval Facilities Engineering Service Center. TR-2205-SH.

Collepardi, M., S. Collepardi, et al. (2004). The Influence of Slag and Fly Ash on the Carbonation of Concretes. CANMET/ACI International Conference on Fly Ash, Silica Fume, Slag and Natural Pozzolans in Concrete.

Costa, A. and J. Appleton (2001). "Concrete carbonation and chloride penetration in a marine environment." Concrete Science and Engineering 3(12): 242-249.

Cui, F. and P. D. Krauss (2006). Corrosion Resistance of Alternative Reinforcing Bars: An Accelerated Test. Northbrook IL, Wiss, Janney, Elstner Associates/Concrete Reinforcing Steel Institute.

Cui, F., J. Lawler, et al. (2007). Corrosion Performance of Epoxy-Coated Reinforcing Bars in a Bridge Substructure in a Marine Environment. Corrosion 2007. Nashville TN, NACE.

Draper, J., D. Darwin, et al. (2009). Evaluation of Multiple Corrosion Protection Systems for Reinforced Concrete Bridge Deck. F. H. Administration. Lawrence Kansas, University of Kansas. DTFH61-03-C-00131.

Herzber, E. (2009). The Annual Cost of Corrosion For DoD. 2009 DoD Corrosion Conference. Washington DC, Department of Defence.

Koch, G. H., M. P. H. Brongers, et al. (2001). Corrosion Cost and Preventive Strategies in the United States. Washington DC. FHWA-RD-01-156.

Kondratova, I., T. W. Bremner, et al. (1999). Long Term Testing of Concrete Slabs containg epoxy-coated steel in a marine environment. Durability and Protection of Constructions from Corrosion, Construction, Reconstruction, International Congress MOSCOW: 548-554.

Lawler, J. S., P. D. Krauss, et al. (2011). Condition Survey of Older West Virginia Bridge Decks Constructed with Epoxy-Coated Reinforcing Bar. TRB 2011. Washington DC.

Lee, S. and P. Krauss (2004). Long-Term Performance of Epoxy-Coated Reinforcing Steel in Heavy Salt-Contaminated Concrete. McLean VA, Federal Highway Adminstration. FHWA-HRT-04-090.

McDonald, D. B., D. W. Pfeifer, et al. (1998). Corrosion Evaluation of Epoxy-coated, Metallic-Clad and Solid metallic Reinforcing bars in Concrete, Federal Highway Administration. FHWA-RD-98-176: 137 p.

Pfeifer, D. (2000). "High performance concrete and reinforcing steel with a 100-year service life." PCI journal 45(3): 46-54.

Polly, D., D. Burke, et al. (2008). Corrosion of Stainless Steel Reinforcement in the Concrete Deperming Pier at Point Loma Port Hueneme, California 93043-4370, Naval Facilities Engineering Service Center. TR-2305-SHR

Powers, R. G. (1987). Corrosion Evaluation of Substructure - Long Key Bridge. Interim Report. Gainesville, FL, Florida Department of Transportation. Corrosion Rept 87-9A: 34.

RAMBOL (1999). Pier in Progreso Mexico, Inspection Report; Evaluation of Stainless Steel Reinforcement, RAMBOL.

Safiuddin, M. (2005). "Performance of galvanized steel reinforcing bars against corrosion in concrete." BRAC University, BU Journal 2(2).

Sagoe-Crentsil, K. and F. Glasser (1993). "Constitution of green rust and its significance to the corrosion of steel in portland cement." Corrosion 49(06).

Sagues, A. A., K. Lau, et al. (2010). "Corrosion of Epoxy-Coated Rebar in Marine Bridges---Part 1: A 30-Year Perspective." Corrosion 66(6).

Sohanghpurwala, A. A. (2009). Cathodic Protection for Life Extension of Existing Reinforced Concrete Bridge Elements. Washington DC, NCHRP. Synthesis 398.

Surgeon, W. J., M. O'Reilly, et al. (2010). Rapid Macrocell Tests of ASTM A775, A615 and A1035 Reinforcing Bars Structural Engineering and Engineering Materials. Lawrence Kansas, University of Kansas Center for Research Inc. SL Report 10-4.

Development of Inner Harbor Navigation Canal Hurricane Surge Barrier Project Hydrodynamics Through Deterministic Methods, Physical Modeling and Numerical Modeling

Jena F. Gilman[1], Peter Grant[2], Jake San Antonio[3] and Mizan Rashid[4]

[1]AECOM, 710 2nd Avenue, Ste 1000, Seattle, WA 98134 USA. PH (206) 403-4218; email: jena.gilman@aecom.com

[2]AECOM, 9521 Willows Rd. NE, Redmond, WA, 98052 USA. PH (206) 403-4274; email: peter.grant@aecom.com

[3]AECOM, 2 Technology Park Dr, Westford, MA 01886 USA. PH (978) 589-3308; email: jake.sanantonio@aecom.com

[4]AECOM, 9521 Willows Rd. NE, Redmond, WA, 98052 USA. PH (425) 202-2378; email: mizan.rashid@aecom.com

ABSTRACT

The Inner Harbor Navigation (IHNC) Surge Barrier project will provide 1.0% chance exceedance (or 100-year) storm risk reduction to eastern New Orleans from powerful hurricane storm surges and waves from the Gulf of Mexico. Two navigation gates along the 2.7 km surge barrier can be closed to prevent water surging up the IHNC into the heart of the city. This paper discusses the methodology to derive the hydraulic boundary conditions for design, including the deterministic methods and physical and numerical modeling used for verification and investigation of other specific design purposes. Probabilistic synthetic storms were used to provide initial storm surge and wave climate characteristics. Deterministic calculations were then used to shoal waves and calculated wave loads and overtopping. 2-D and 3-D 1:20 Froude scaled physical models were employed to verify hydrodynamic loading and stability, while also allowing investigation of characteristic overtopping and scour. Additionally, depth averaged RMA2 modeling was utilized for investigation of localized affects to navigation through the gates.

INTRODUCTION

The Inner Harbor Navigation (IHNC) Surge Barrier project will provide 1.0% chance exceedance storm risk reduction to eastern New Orleans from powerful storm surges and waves generated by hurricanes in the Gulf of Mexico. The site is located at the western edge of the Golden Triangle marshlands approximately 10 miles east of downtown New Orleans, near the confluence of the Gulf Intracoastal Waterway

(GIWW) and the Mississippi River Gulf Outlet (MRGO), and between Lake Borgne and Lake Pontchartrain. This area, like most of the Louisiana Coastal Zone, is geometrically and hydrodynamically complex. The region is covered by interconnected estuaries, bays, marshes, rivers, and channels, while the major relief is defined by features such as river banks and an extensive system of levees and raised roads. The low-lying topography, extensive water bodies, and the intricate system of raised features make the region very susceptible to flooding from hurricane storm surge. Hurricane surges can propagate rapidly across the floodplain, can come from many directions, and can experience dramatic localized amplification due to the topography and raised features (IPET, 2007).

Two navigation gates along the 2.7 km surge barrier can be closed to prevent water surging up the IHNC into the heart of the city (see Figure 1). The barrier is one component of the new Hurricane and Storm Damage Risk Reduction System (HSDRRS) that was authorized after Hurricane Katrina in 2005. The much needed IHNC barrier will greatly reduce the risk of flooding for hundreds of thousands of residents in the greater New Orleans area.

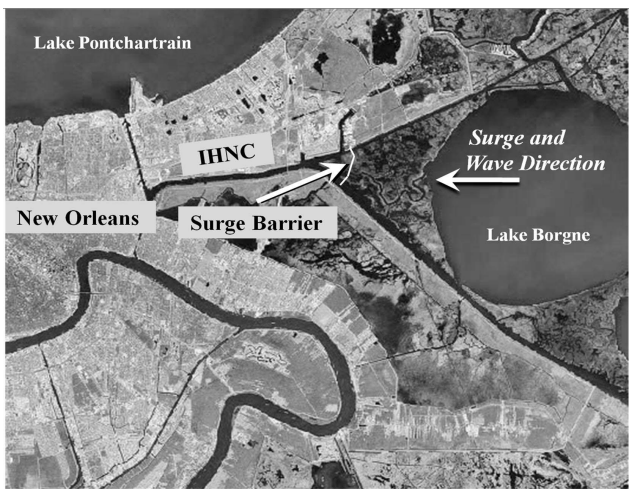


Figure 1. Overview of storm surge barrier outside New Orleans

The objective of this paper is to discuss the methodology to derive the hydraulic boundary conditions for the IHNC storm surge barrier, including the deterministic methods and physical and numerical modeling used for verification and other specific design purposes.

METHODOLOGY

PROBABILISTIC SYNTHETIC HURRICANE STORMS

A set of 152 synthetic hurricane storms were developed under FEMA/USACE (2008) by combining the "probable" combinations of central pressure, radius to maximum winds, forward speed, angle of track relative to coastline, and track.

Tracks

Tracks were defined by five primary tracks and four secondary tracks. The set of tracks, (nicknamed "RICK-fan") was treated by the interpolation of storm tracks of Hurricanes Rita, Ivan, Camille, and Katrina. Figure 2 shows the RICK-fan track set (FEMA/USACE, 2008).

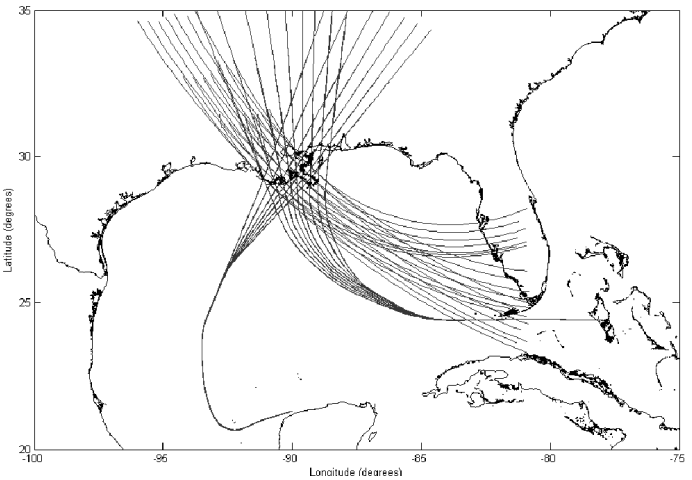


Figure 2. Set of Probable Hurricane Paths

Wind

Synthetic storm wind fields were generated for each storm in the set utilizing the Planetary Boundary Layer (PBL) model, developed by Ocean Weather, Inc. (OWI). These wind fields are required input into storm surge and wave models (FEMA/USACE, 2008).

Surge

The surge water level (SWL) was generated using the ADCIRC model, which solves the generalized wave-continuity equation on linear triangular elements. The grid developed for the analysis effort is known as the SL15 Grid and encompasses an area from the Sabine River, Texas, to Mobile Bay, Alabama. The grid is being used for all coastal analysis for Louisiana and Mississippi to ensure consistency and matching solutions at state line/regional boundaries.

Waves

Waves were computed using STWAVE, a nearshore wave model developed by the USACE Coastal and Hydraulics Laboratory. STWAVE numerically solves the steady-state conservation of spectral action balance along backward-traced wave rays.

The input for the grid includes the bathymetry (interpolated from the ADCIRC domain), surge fields (interpolated from ADCIRC surge fields), and wind (interpolated from the ADCIRC wind fields, which apply land effects to the OWI wind fields). The wind and surge applied in STWAVE is spatially and temporally variable for all domains. The grid covers the coastal areas, including the IHNC Surge Barrier project site, at a resolution of 200 meters (656 ft).

Initial Hydraulic Boundary Conditions

A statistical analysis based on the Joint Probability Method (JPM) was utilized to develop stage frequency relationships for the numerical model results of the storm events. This has been termed the Joint Probability Method-Optimal Sampling (JPM-OS) technique. Of these 152 storms, ten were selected to represent the variability in hydrographs exhibited by historical storms approaching New Orleans. The average of mean values of representative 1% chance exceedance storms were used to normalize storm hydrographs. Additionally, 1.5 ft was added to SWL under guidance of the Hurricane Protection Office (HPO) to account for sea level rise and non-linear effects of sea level rise on surge level for the 50-year design life condition (the year 2057) (AECOM, 2009a). Table 1 lists the initial hydraulic boundary conditions for the present and future (50-year) conditions provided by the ADCIRC/STWAVE output.

Table 1. 1-Percent Chance Exceedance Initial Hydraulic Boundary Conditions.

Scenario	Significant Wave Height (m)	Spectral Peak Wave Period (s)	Surge Elevation (m)	Standard Deviations		
Yr	H_s	T_p	SWL	σH_s	σT_p	σSWL
Present Day	2.13	7.70	5.73	0.21	1.54	0.30
50-Year	2.36	8.10	6.19	0.24	1.62	0.30

The wave parameters in the initial hydraulic boundary conditions where then used to develop a Texel, Marsen, and Arsloe (TMA) spectrum and subsequently an irregular wave time series used in physical modeling for verification of wave loads and scour. Additionaly, these wave parameters were used in deterministic wave transformations performed prior to calculating anticipated wave loads and overtopping at the surge barrier.

DETERMINISTIC WAVE TRANSFORMATIONS

The output surge and wave parameters (H_s and T_p) provided by the ADCIRC/STWAVE output were located over the Golden Triangle Marsh, which is approximately 1.6 km from the surge barrier for which deterministic wave loads and overtopping were calculated. Because waves shoal (i.e. increase or decrease in height) as they enter different water depths, the IHNC surge barrier project site presented several cases (such as when waves leave the marsh and enter either the GIWW or MRGO channels) where the STWAVE output was modified to best simulate likely prototype conditions; i.e. during design storm conditions. The

following calculation steps were included in the calculations of wave loads and wave overtopping volumes.

Initial Wavelength Calculation

Initial wave conditions were provided in the form of significant wave height (H_s) and peak wave period (T_p). Estimating the wavelength for the initial wave characteristics was accomplished by applying Pade approximate expansions as described by Hunt (1979). The linear frequency dispersion equation, given by $k_oh = kh \tanh(kh)$, may be expressed as $y = k_oh = X\tanh(X)$. The inverse relationship is provided here:

$$X^2 = y^2 + \frac{y}{1+\sum_{n=1} d_n y^n} \quad 0 \le y = {\omega^2 h}/{g} = k_0 h < \infty$$

Where the first six coefficients are:

d1=0.666	and	ω = wave frequency
d2=0.355		h = water depth
d3=0.161		g = gravity
d4=0.063		k_0 = deep water wave number
d5=0.022		
d6=0.007		

Wavelength calculations are computer over the marsh with a bottom elevation of 0 m. NAVD88 (2004.65)

Initial Design Wave Height Calculation

The Golden Triangle marsh acts as a surf zone, which, according to Goda, is defined as a region where $h/L_0<0.2$, where L_0 is the deepwater wavelength. Wave heights within the surf zone (local site conditions) were calculated using the following approximations (Goda, 1985):

$$H_{1/3} = \min\{(\beta_0 H_0' + \beta_1 h), \beta_{max} H_0', K_s H_0'\}: {h}/{L_0} < 0.2$$

$$H_{max} = H_{1/250} = \min\{(\beta_0^* H_0' + \beta_1^* h), \beta_{max}^* H_0', 1.8 K_s H_0'\}: {h}/{L_0} < 0.2$$

Were the coefficients for these approximations are given in Table 2 below:

Table 2. Coefficients for Design Wave Height Approximation

Coefficients for $H_{1/3}$	Coefficients for H_{max}
$\beta_0 = 0.028(H_0'/L_0)^{-0.38} \exp(20\tan 1.5\theta)$	$\beta^*_0 = 0.052(H_0'/L_0)^{-0.38} \exp(20\tan^{1.5}\theta)$
$\beta 1 = 0.52\exp(4.2\tan\theta)$	$\beta^* 1 = 0.63\exp(3.8\tan\theta)$
$\beta_{max} = \max[0.92, 0.32(H_0'/L_0)^{-0.29} \exp(2.4\tan\theta)]$, where θ = sea bottom inclination	$\beta^*_{max} = \max[1.65, 0.53(H_0'/L_0)^{-0.29} \exp(2.4\tan\theta)]$, where θ = sea bottom inclination

Wave Shoaling

Design waves, determined in accordance with the Goda (1985) approximation will traverse the marsh as they approach the IHNC surge barrier. Waves then cross the construction access channel, the MRGO, or the GIWW. These features are 4.6 m, 9.1 m, and 12.8 meters lower in elevation than the marsh, respectively. As the waves enter deeper water, they experience a modification of wave height resulting from a shoaling effect. The conservation of energy flux between two vertical planes that are perpendicular to the direction of wave propagation requires that $E_1C_{G1}b_1 = E_2C_{G2}b_2$ (Hudspeth, 2006). Substituting the following equations:

$$C_G = \frac{C}{2}\left[1 + \frac{2kh}{\sinh 2kh}\right] \qquad \text{and} \qquad E = V + T = \frac{\gamma H^2}{8}$$

Where

C= wave celerity
k = wave number
h = water depth
V= average potential energy
T = average kinetic energy
E = energy density
H = wave height
γ = specific weight of water

while assuming zero refraction, gives the following ratio between wave height, H_2 near the structure and wave height, H_1, located within the surf zone:

$$\frac{H_2}{H_1} = \sqrt{\frac{C_{G1}}{C_{G2}}\sqrt{\frac{b_1}{b_2}}} = \left\{\sqrt{\frac{L_1}{L_2}}\sqrt{\frac{1 + \frac{2k_1h_1}{\sinh 2k_1h_1}}{1 + \frac{2k_2h_2}{\sinh 2k_2h_2}}}\right\}\sqrt{\frac{b_1}{b_2}} = \{K_s\}K_r$$

As a result, the shoaling coefficient $K_s = \sqrt{\frac{L_1}{L_2}}\sqrt{\frac{1+\frac{2k_1h_1}{\sinh 2k_1h_1}}{1+\frac{2k_2h_2}{\sinh 2k_2h_2}}}$

Where L is the wave length, K_s is the shoaling coefficient, and K_r is the reflection coefficient.

DETERMINISTIC WAVE LOADS

Assumptions

Due to the complexity of wave loading calculations, some general assumptions have been made. Each assumption applied in the calculations was considered conservative.

- No wave refraction was assumed for waves leaving the marsh surf zone and entering channels.
- All waves were assumed to interact with the structure at a 90-degree approach angle.
- Impulsive horizontal wave conditions are unlikely (Goda, 1985).
- The construction trenches will be completely silted in for the 50-year condition.
- The calculated pressure intensities are assumed not to change even if wave overtopping occurs (Goda, 1985).

Using the recommended Goda formulation (USACE, 2007; Goda, 1985) for vertical "hard" structures, pressures resulting from wave interactions with the IHNC surge barrier structures are calculated. The trapezoidal wave pressure distributions, and related variables, for a typical vertical wall are presented in Figure 3.

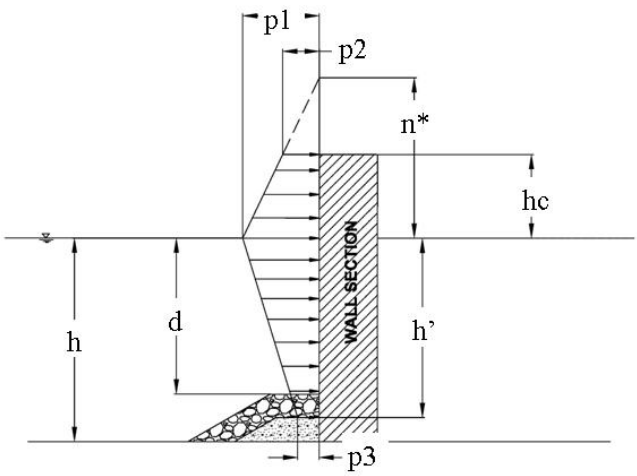


Figure 3. Typical cross section for wave pressure calculation (after Goda, 1985)

In the above figure, h represents water depth in front of the structure, d is the depth above the riprap armor layer (if present), h' is the exposed height of the structure from SWL (surge level) to the toe of the wall (or sand foundation of the riprap), and h_c is the freeboard elevation above SWL.

The elevation to which wave pressures are applied along the structure is determined by the following equation:

$$n^* = 0.75\ (1 + cos\beta)H_{max}$$

where H_{max} is the shoaled Goda-derived wave height at the structure, and β is the incident wave angle (assumed normally incident in all cases).

Wave pressures on the front of a vertical wall were calculated as follows:

$$p_1 = \frac{1}{2}(1 + cos\beta)(\alpha_1 + \alpha_2 cos^2\beta)\gamma_w H_{max}\ ; \qquad \alpha_1 = 0.6 + \frac{1}{2}\left[\frac{4\pi h/L}{\sinh(4\pi h/L)}\right]^2$$

$$p_2 = \frac{p_1}{\cosh(2\pi h/L)}; \qquad \alpha_2 = min\left\{\frac{h_b - d}{3h_b}\left(\frac{H_{max}}{d}\right)^2, \frac{2d}{H_{max}}\right\}$$

$$p_3 = \alpha_3 p_1; \qquad \alpha_3 = 1 - \frac{h'}{h}\left[1 - \frac{1}{cosh(2\pi h/L)}\right]$$

given that γ_w= specific weight of water and h_b = water depth at the location at a distance $5H_{1/3}$ seaward of the structure.

Note that the pressure values correspond to specific geometric locations along the wall. p_1 is located at the SWL, p_2 is located at the top of the wall structure, and p_3 is located at the toe of the structure. As these elevations change, so do the location of the pressure values (i.e. as the marsh bottom is silted in, the elevation of the p_3 value may rise with the bottom elevation).

The above formulas were used in calculating a 50th-percentile wave load across varying surge barrier features such as the typical surge barrier section, the MRGO closure, and the gates located at Bayou Bienvenue and GIWW. All calculations were conducted for present day and 50-year storm conditions. These calculations where then repeated 10,000 times through a probabilistic analysis applying the Monte –year Carlo approach to derive 90th-percentile wave loads. Table 3 presents the 50-year scenario 50th-percentile Goda pressures for two distinct features within the surge barrier, the typical surge barrier section and the GIWW sector gate.

Table 3. 1-Percent Exceedance, 50-year Goda Pressures

Section	50th-Percentile Pressures		
	p_1 (kPA)	p_2 (kPa)	p_3 (kPa)
Typical Surge Barrier	29	22	17
GIWW Sector Gate	27	19	16

DETERMINISTIC WAVE OVERTOPPING

The IHNC surge barrier was designed to protect against storm surge and waves, while allowing a predetermined amount of overtopping to contribute less than 0.46 meters

in water surface elevation behind the barrier – the protected side. This estimated amount of storage volume is 6.4 million m^3 (INCA/Gerwick, 2008).

The dominant parameters in estimating wave overtopping of coastal structures are significant wave height (H_s), structural freeboard (R_c), and the mean discharge (Q). Franco and Franco (1999) define the following dimensionless overtopping rate:

$$Q = 0.082\ exp\left[-1 * \frac{3R_c}{\gamma_{\beta\sigma}\gamma_{geom}H_{si}}\right]$$

Where

R_c = structural feeboard (m)
H_{si} = significant wave height at toe of structure (m)
$\gamma_{\beta\sigma}$ = 0.83 for short crested waves with 0° < β < 20°, where β = incident wave angle
γ_{geom} = 0.95 for vertical plain wall with minor roughness (Franco, 2008)
γ_{geom} = 0.75 for GIWW Gate structures (Franco, 2008)
3.0 = stochastic variable

Owen (1980) and Van der Meer (1992) defined the basic dimensionless parameter:

$$Q = \frac{q}{\sqrt{gH_{si}^3}}$$

Where q is the overtopping rate (m^3/sec/m), and g is the gravitational constant of 9.8 m/sec^2. This results in the formula used for calculation of the mean overtopping rate:

$$Q = \sqrt{gH_{si}^3}\ 0.082\ exp\left[-1 * \frac{3R_c}{\gamma_{\beta\sigma}\gamma_{geom}H_{si}}\right]$$

Franco and Franco (1999) further stated that the reliability of the stochastic coefficient 3.0 in the exponential function exhibits variability defined by a normal distribution with a standard deviation σ(3.0) = 0.26.

Overtopping calculations were performed for the ten-storm suite across six segments of the surge barrier due to differing geometry and foreshore conditions. A sensitivity examination determined that the 50-year scenario resulted in more overtopping than the present day scenario and was therefore used for design considerations. Similar to wave load calculations, these deterministic overtopping calculations were repeated 10,000 times in a Monte Carlo analysis to determine the 50^{th} and 90^{th} percentile total overtopping volumes across the surge barrier. Figure 4 presents the predicted overtopped volume across the surge barrier for the ten 1-percent chance exceedance storms with the 50-year condition. The dashed line in the figure represents the total available storage volume behind the surge barrier (0.46 meters of added water level).

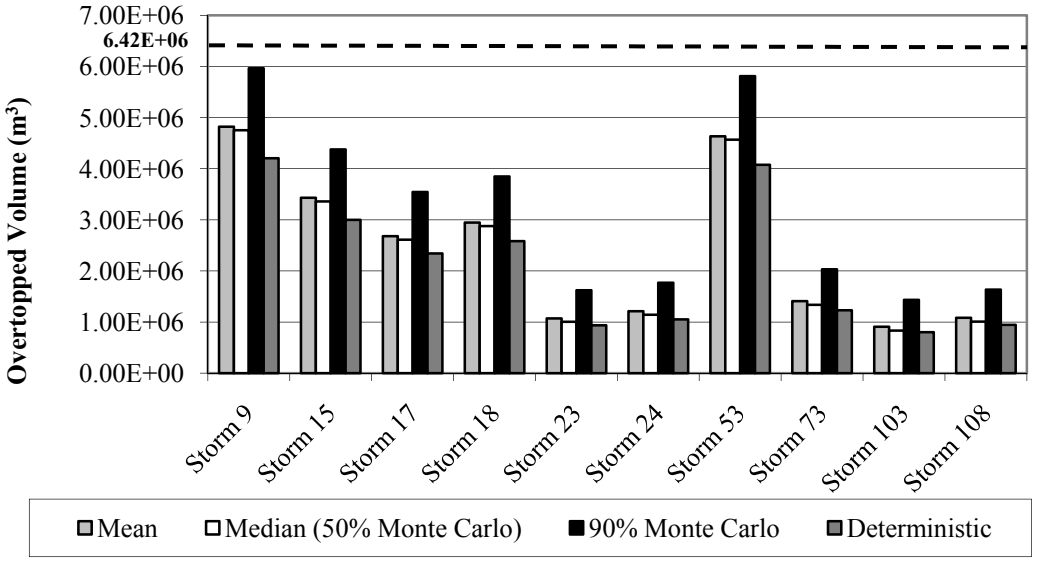


Figure 4. Total Overtopping Wave Volume for the 50-Year Condition.

VERIFICATION OF DESIGN THROUGH PHYSICAL MODELING

Verification of the deterministic hydrodynamic loading analyses was supported by two dimensional (2-D) and three dimensional (3-D) 1:20 Froude scaled physical model studies of the surge barrier and sector gates, respectively. The 2-D model additionally supported the selection of an appropriate armor size surrounding the vertical surge barrier through overtopping and scour observations. The model studies were performed in AECOM's Wave Lab near Redmond, WA.

Wave Loads

The verification of wave loading against the vertical surge barrier was performed using irregular wave tests, were a random wave time series was produced from a 1-percent chance exceedance TMA spectrum formulation (Bouws, 1984) using the initial hydraulic boundary conditions listed in Table 1. 2-D flume studies were conducted to compare with deterministic Goda pressures calculated for the typical surge barrier cross section. A 3-D wave basin study was conducted for the GIWW sector gates as this location of the surge barrier is geometrically complex. Table 4 presents a direct comparison between the 50^{th}-percentile Goda design pressures and experimental pressures obtain during physical modeling. Physical model results indicated quasi-steady pressures exist at the surge barrier and design pressures (90^{th}-percentile) were appropriate for structural design without modification.

Table 4. Comparison of Deterministic and Physical Modeling Pressures

Section	50th-Percentile Pressures		
	p_{1exp}/p_1	p_{2exp}/p_2	p_{3exp}/p_3
Typical Surge Barrier	1.9	3.3	1.6
GIWW Sector Gate	0.9	0.5	0.7

Reaction Forces and Vibration of GIWW Sector Gates

The GIWW sector gates include two main factors which increased the difficulty for designers to deterministically calculate accurate reaction forces or anticipated vibration. These factors are: (1) the sector gates and their surrounding monolithic structure and approach walls create a geometrically complex region for accurately anticipating hydrodynamics, and (2) the GIWW sector gates are neutrally buoyant structures which may result in vibrations related to wave loading.

In order to provide the design team with reaction forces for verification of design, the 3-D wave basin study included instrumenting hydroelastically scaled sector gates with force transducers at the actuating mechanism, the locking pin, and at the gate's pintle (lower bearing) and hinge (top bearing). Additionally, accelerometers were placed on the gate to sense the gate's movement. Analysis of these results helped the designers appropriately size bearing surfaces, size the actuator, and confirmed the gates are stable under transient wave loading and during gate opening sequences.

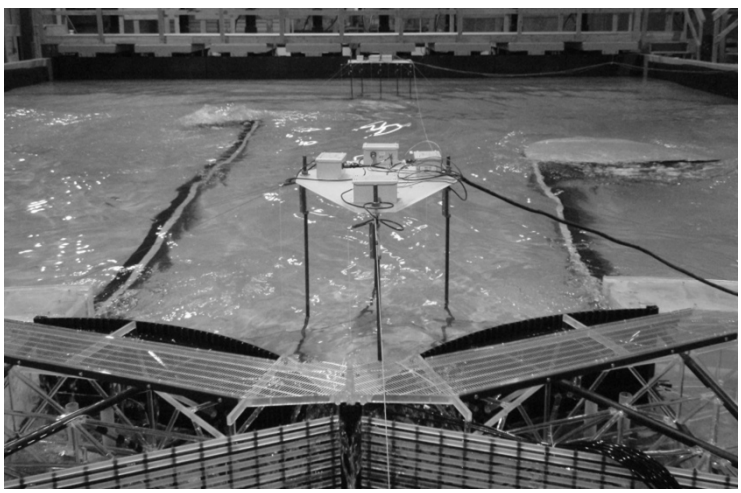


Figure 5. Photograph of Model GIWW Sector Gates – Looking Seaward

Wave Overtopping and Scour

Deterministic formula for selection of armoring the flood side of a bermed breakwater is well known and documented. Design guidance is very limited, however, for waves overtopping a vertical barrier into a plunge pool behind the structure (see Figure 6), where the armoring is submerged by a substantial depth – in

this case by a minimum of 4.6 meters. 2-D physical models of a typical surge barrier section and the MRGO closure were conducted to assist designers in confirming the characteristics of the plunging jet and the anticipated scour after a 1-percent chance exceedance hurricane.

The spilling jet created by an overtopping wave was found to be characterized well by a trajectory equation which includes the redirection of the water by the flat surface on the protected side of the surge barrier parapet. The trajectory may be calculated using the following relationship:

$$y = -g\left((\sec^2\theta)/2c^2\right)x^2 + x\tan\theta$$

Here, x is the horizontal displacement in meters from the seaward face of the surge barrier, g is the gravitational constant, y is the vertical displacement in meters, c is the overtopping wave celerity in meters per second, and θ is the angle of the jet measured from horizontal.



Figure 6. Characteristic Overtopping Jet Into Protected Side Polder

Deterministic methods do not exist for quantifying or characterizing the location of scour, both of which are important considerations in the design of coastal defenses. For these reasons, the designers selected to utilize physical modeling to provide a qualitative and quantitative analysis of scour with considered rock size combinations. Figure 7 illustrates a cross section of a bathymetric survey after an irregular wave test. Results from scour analyses assisted in the designer's selection of an appropriate stone armoring size.

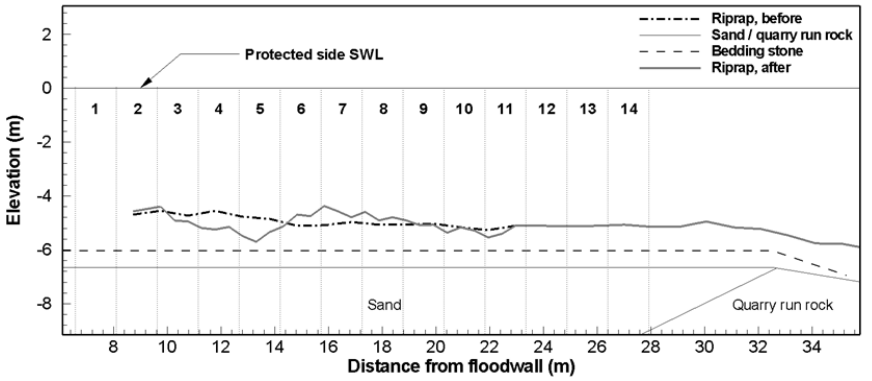


Figure 7. MRCO Closure Scour Results (LADOTD Class 440 Stone)

Numerical Modeling

Finally, in order to evaluate the change of flow patterns, velocities and scour potential due to the proposed construction of the IHNC surge barrier, the hydrodynamic model RMA2 was applied to Louisiana's Lake Pontchartrain and Lake Borgne, and extending into the Chandeleur Sound (see Figure 8). The model was utilized to provide predictions of hydrodynamics for the construction and final configurations within the channels and upstream and downstream of the barrier location. Channel velocities were predicted under a range of normal (non-flood) flow conditions. The model was calibrated and verified at eight different locations within the project area. In all scenarios, the model predicted increased velocities within GIWW. Predicted peak velocities ranged from 0.7 to 1.5 m/s for the proposed operating condition, and 1.2 to 2.4 m/s for the proposed construction conditions, compared with existing velocities, which ranged from 0.2 to 0.5 m/s.

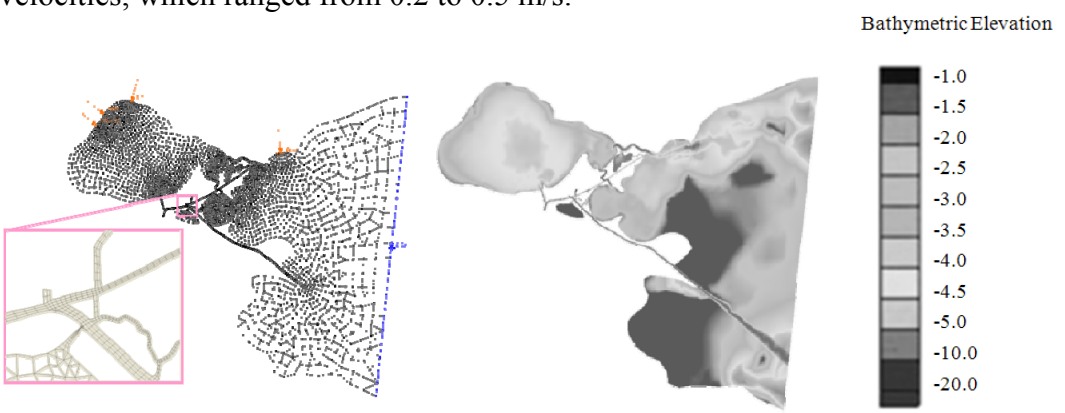


Figure 8. RMA2 Mesh and Bathymetric Conditions (meters NAVD88, 2004.65)

CONCLUSIONS

The hydrodynamic studies used to design this project provide an example of the combined application of state-of-the-art coastal engineering methodologies to infrastructure critical for the risk reduction of life and property.

ACKNOWLEDGEMENTS

The authors wish to acknowledge the project sponsor, the U.S. Army Corps of Engineers (USACE) Hurricane Protection Office, and the design-build project's prime contractor Shaw Environmental & Infrastructure (Shaw) and Shaw's subcontractors INCA Engineers, Inc., and Ben C. Gerwick, Inc. for their support on this important project.

REFERENCES

AECOM. 2009. *Hydraulic Storm Surge and Wave Design. Final Submittal. Inner Harbor Navigation Canal Surge Barrier Project.* August, 2009.

Bouws, E., Gunther, H., Rorenthal, W., and Vincent, C. L. 1984. *Similarity of the wind wave spectrum in finite depth water.* Part I – Spectrum form. JGR, 98:-986.

FEMA/USACE. 2008. *Flood Insurance Study: Southeastern Parishes, Louisiana, Draft, Intermediate Submission 2: Offshore Water Levels and Waves.* Vol. 1. Federal Emergency Management Agency and U.S. Army Corps of Engineers, New Orleans District. January, 2008.

Franco, C., and L. Franco. 1999. Overtopping Formulas for Caisson Breakwaters with Nonbreaking 3D Waves. *Journal of Waterway, Port, Coastal, and Ocean Engineering.* 125, no. 2:98-108.

Franco, L. 2008. Personal communication to Scott Emmons, ENSR, RE: Overtopping. July 22, 2008.

Goda, Y. 1985. *Random Seas and Design of Maritime Structures.* Tokyo: University of Tokyo Press.

Goda, Y., 2000. *Random Seas and Design of Maritime Structures*, World Scientific.

Hudspeth, R.T. 2006. *Waves and Wave Forces on Coastal and Ocean Structures.* Advanced Series on Ocean Engineering, Vol. 21. Hackensack, NJ:World Scientific Publishing Co. Pte.Ltd.

Hunt, J.N. 1979. Direct Solution of Wave Dispersion Equation. *Journal of Waterway, Port, Coastal, and Ocean Engineering.* Technical Note, 105(WW4):457-459.

INCA/Gerwick. 2008. *10% Submittal– Design Basis. Inner Harbor Navigational Canal Surge Barrier Project.* April 28, 2008

IPET. 2007. *Performance Evaluation of the New Orleans and Southeast Louisiana Hurricane Protection System. Final Report of the Interagency Evaluation Task Force. Interim Final.* Vol I-IX. March, 2007.

USACE. 2007. *Hurricane and Storm Damage Reduction System Design Guidelines. Interim.* U.S. Army Corps of Engineers, New Orleans District. October 23, 2007.

Sediment Nourishment at Orchard Beach, the Bronx, New York

Diane Rahoy, David Yang, Lynn Bocamazo, Shewen Bian, Frank Verga, Anthony Ciorra[1], Bill Tai[2], Project Manager[3]

1. US Army Corps of Engrs, NY District, 26 Federal Plaza, New York, NY 10278;
2. City of New York Parks and Recreation, Central Park, New York, NY 10021
3. Great Lakes Dredge and Dock Co., 2122 York Road, Oak Brook, IL 60521

ABSTRACT

Orchard Beach is a man-made, self contained sandy pocket completely dissimilar to the natural formation of the shoreline on which it is situated. The beach was created by connecting two rocky headlands with 4,000 feet of rock-filled crib seawall and concrete promenade, and backfilled with 1.2 million cubic yards of sand. Original construction was done between 1935 and 1937 by the City of New York, under the direction of Robert Moses. The beach was expanded 1,000 ft and two new rock terminal groins were added in 1949. Beach nourishments were performed in 1949 and 1964. The crescent shape beach is relatively stable due to low wave and current action; however, severe storms can overtop the berm and the crest of the promenade.

For nearly 50 years since the last nourishment, the beach retained its integrity; however, by the early 2000's the shoreline had shifted from north to south, resulting in a narrower and milder beach to the north and a wider and steeper beach to the south. In addition, formation of a large scour area with an abrupt drop-off slope presented a safety concern to swimmers. The beach is in the populated New York City metropolitan area and is frequented by 2.5 million visitors annually. During the summer season, the beach was overcrowded. Due to the gradual loss of sand to the north and a large 7 to 9 ft tidal range, beachgoers had little beach space during high tide and needed to wade out a long distance to reach the water during low tide. In 2009, USACE prepared the final construction plan for a beach nourishment and upgrade of the southern rock groin, and reached financial agreement with the New York City Parks & Recreation Department. The project was successfully bid by Great Lakes Dredge and Dock Co. (GLDD). Construction commenced on 30th October 2010 and was completed on 28th January, 2011.

SHORELINE HISTORY

In 1935, Robert Moses, then Commissioner of Parks, began construction of Orchard Beach. The beach was initially formed by joining Rodman's Neck and Hunter Island with a riprap dike capped with a concrete wall, and the pumping of sand and gravel to create a beach in front of it. Other facilities, including a promenade, were also built at this time (Figure 2). At the time of initial construction, Orchard Beach was approximately 4,000 feet long and did not have terminal groins. In subsequent years the New York City Parks Department planned and constructed various improvements at Orchard Beach to maintain its condition as a recreational

beach. These improvements included the construction of 1,000 feet of additional beach; a promenade extension, two terminal groins, and beach fill operations in 1938, 1949 and 1964. There have been no beach fill operations since 1964. Project location is shown in Figure 1.

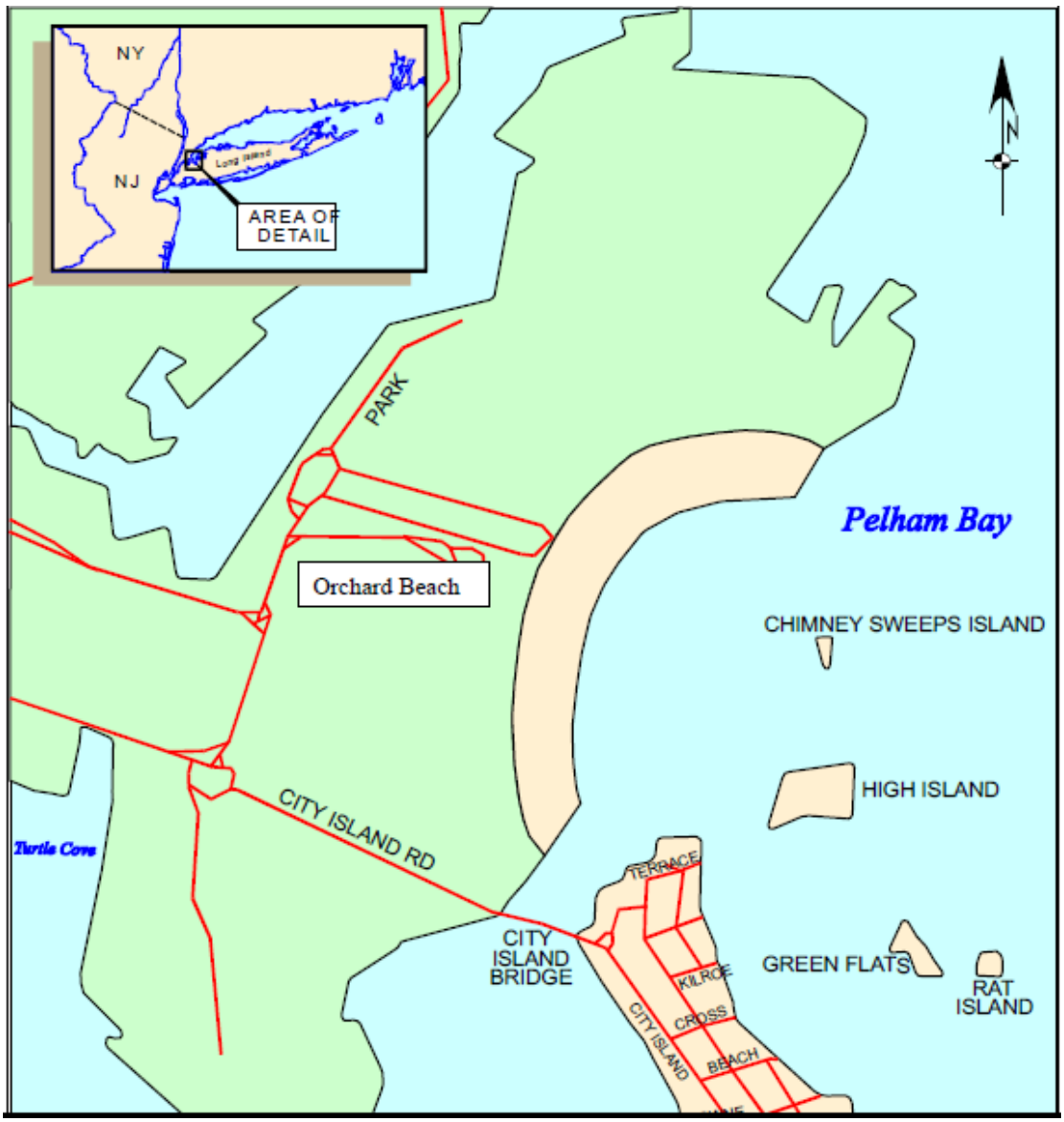


Figure 1. Project Location.



Figure 2. NYC Parks 1937 Orchard Beach Aerial Photo, looking south (NYCityMap 2011).

Terminal rubblemound groins were constructed in 1949 at the north and south ends of the beach in conjunction with the lengthening of the promenade and placement of beach fill. Based on the original design drawings obtained from the New York City Parks Department, the original lengths of the terminal groins were approximately 695 feet at the north groin (after extension) and 350 feet at the south groin (measured along the crest). Both the north and south groins are of similar rubble mound construction. The general nature of the shoreline in this locality precludes any regular littoral movement of sand; therefore, there is little sediment transport, influx or movement past Orchard Beach. Any sediment that is transported along the Orchard Beach shoreline originates from the Orchard Beach area and remains within this general area. The majority of beach sediment is lost directly offshore, with a small amount of material moving past the south groin, and lesser amounts removed by wind loss over the promenade, and removal by beach users.

Pelham Bay Park, where Orchard Beach is situated, is one of the largest New York City parks comprising over 2000 acres. Besides the Orchard Beach area, the park offers public facilities for golf, softball, picnicking, volleyball, nature walks, and various concessions. Orchard Beach is the only large public beach within two hours by public transportation for many of the local visitors. The Bronx is a very high density, urban area that needs the outlet provided by its recreational parks. Orchard Beach is considered its gem.

PRECONSTRUCTION CONDITION

Shoreline conditions at Orchard Beach vary with the changing tides. Tides in the area are semi-diurnal with a mean range of 7.2 feet and a spring range of 8.6 feet. At low tide, there is a broad expanse of dry land, which from a distance might give the impression of a wide beach. The beach is a mixture of wet fine sand and generally appears muddy. Due to gradual beach slopes, beach users must wade out a considerable distance. An unsafe condition exists because sudden drop-offs are located in an area of the nearshore zone. As the tide rises, this area quickly becomes inundated. The false beach quickly disappears, causing confusion and mass exodus from the area. Lifeguard stands that were once at the water's edge are now in the water over 2 feet deep, necessitating that they be pulled back to higher ground. Overcrowding from mid to high tide occurs because beach users are forced into the already overcrowded zone extending back from the high water line.

The existing condition mean high water line has receded since its historic extent in 1964. The average recession rate for the period 1966 to 1972 was approximately 6.8 feet per year. The annual recession rate has slowed down to approximately 2.7 feet per year (1966 to 2001) based on surveys taken in 2001 (Figure 3), possibly due to decreasing sand volume available on the beach (USACE, 2005).



Figure 3. Orchard Beach Aerial (2001).

The Orchard Beach vicinity has been a unique and popular recreational spot for over 100 years, with more than 2 million patrons returning year after year. Although the beach can be quite crowded on holidays and weekends, the attractiveness of a beach so close to an urban setting seems to outweigh the negative aspects of the crowding. On an average summer weekend day, this beach draws thousands of people for sunbathing, picnicking, swimming, and sport fishing. During the winter months the area is also used for recreational walks, nature study, and sport fishing. The waters off the beach are also popular for recreational boating.

CONSTRUCTION

Planning in the form of a Feasibility Study began in 2001. The Feasibility Study phase was completed in 2006, and preparation of plans and specifications for construction was completed in 2009. The construction contract was successfully bid by Great Lakes Dredge and Dock (GLDD). Construction officially started on October 30, 2010 and was completed on January 28th, 2011, within 90 days. Approximately 268,000 cubic yards sandfill, 4,000 tons of armor, core, and bedding rock were placed and 9.2 acres of underwater beach slope were re-graded. Details of construction methodologies are discussed below.

Borrow Site Determination

Finding a borrow source with sediment compatible to the native sand potentially required mixing stockpiled material which would then be transported to the beachfill site. In addition, a tight construction window from mid-October to mid-January for beach fill also limited possible methods of material handling and transportation. Several potential borrow sources were investigated to determine the suitability of the borrow material. The suitability requirements for borrow material includes compatibility to native beach grain size, amount of volume available, environmental and water quality permit considerations, and distance to the project site (USACE 2005). The following offshore sub-aqueous and upland sites, which are reasonably close to the project site, were investigated:

- Amboy Aggregates offshore mining area in Ambrose Channel, lower New York Harbor, approximately 45 miles from the project location;
- Long Island Sound, core 36, approximately 15 miles from the project location;
- An upland source located on the north shore of Long Island, approximately 10 miles by barge and 20 miles by truck from the project site;
- An upland source located on the northeast shore of New Jersey near South Amboy, approximately 45 miles by barge from the project site.

Several alternative schemes were developed based on the potential borrow sources and methods of construction as shown in Table 1 and Figure 4.

Table 1: Potential Borrow Schemes.

Borrow Location	Distance	Method of Construction	Borrow Restrictions
1. Amboy Aggregates Ambrose Channel site	45 miles	hopper dredge with pumpout facility	Need to confirm suitable sand at the borrow area
2. L.I. Sound Core 36	15 miles	hopper dredge with pumpout facility	Require dredging permit based on future testing
3. Upland North L.I.	20 miles	Trucked to site	Limited available volume
4. Upland North L.I.	10 miles	Towed barge to pumpout facility offshore of site	Limited available volume
5. Upland Northeast N.J. Amboy Aggregates	45 miles	Towed barge and pumpout	Potential high cost

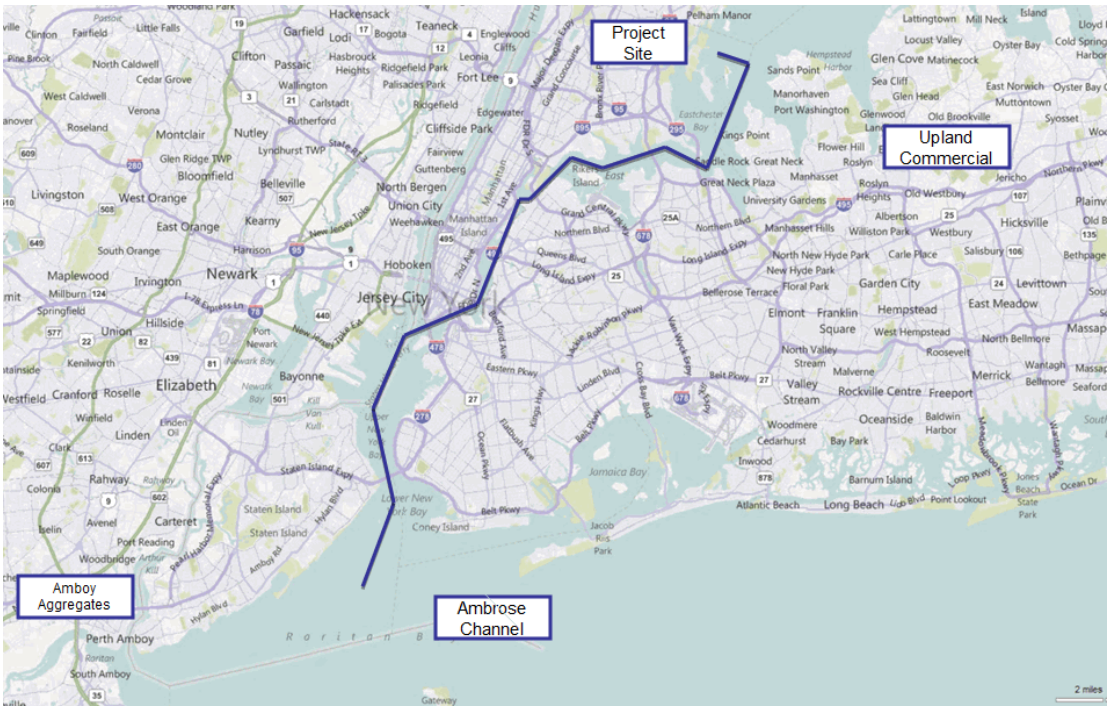


Figure 4. Potential Borrow Site Locations and Barge Route (blue line).

Only the borrow sites at Amboy Aggregates upland facility and in Ambrose Channel provided the necessary volume within economic transport distance. Beachfill using the upland material required double handling via barge, with resulting reduced production rate and increased cost. Use of the Amboy's Ambrose Channel borrow site would require sampling and grain size investigation to determine the suitability prior to placement.

Final Borrow Site and Beachfill Operations

After contract award, GLDD proposed pumping the beach fill material directly from Amboy's Ambrose Channel site via hopper dredge instead of barging and re-handling from the upland stockpile. This methodology saved both time and cost over re-handling. To transport the borrow material, two 20-ft loaded draft, 3,600 cubic yard hopper dredges were used. The dredges excavated and moved material from the offshore borrow site in lower New York Harbor via the East River to the site (Figure 4). The dredges were moored approximately 4,000 feet offshore in deep water within Long Island Sound and material was pumped onshore via an on-board 1,700 HP dredge pump with 30 inch steel pipeline (Figures 5 & 6). Including excavation, transit, and pump-out, the production rate achieved was approximately 2,500 cubic yards per dredge per day. Work was performed 24 hours per day. The beachfill operation was completed in 60 days from commencement of work and ahead of the sandfill deadline of 31 January imposed by NY State DEC. Two CAT D-7 dozers (one equipped with GPS for fine grading); one CAT 966H loader with Timber fork attachment (used to move shore pipes) (Figure 7) were used for re-grading and building the beach. The typical workday per 12-hour shift for shore crew included two equipment operators, fill foreman, one site security person, two

laborers, one safety officer, one QC manager, one site manager, one contract manager, the project engineer, one runner, the assistant project manager, and surveyors (not required daily). A typical beach cross section is shown in Figure 8.



Figure 5. Hopper Dredge Pumping Material Onshore.



Figure 6. Pumping on Beach via 30 inch Steel Pipe.



Figure 7. CAT Loader with Timber Fork Moving Pipe.

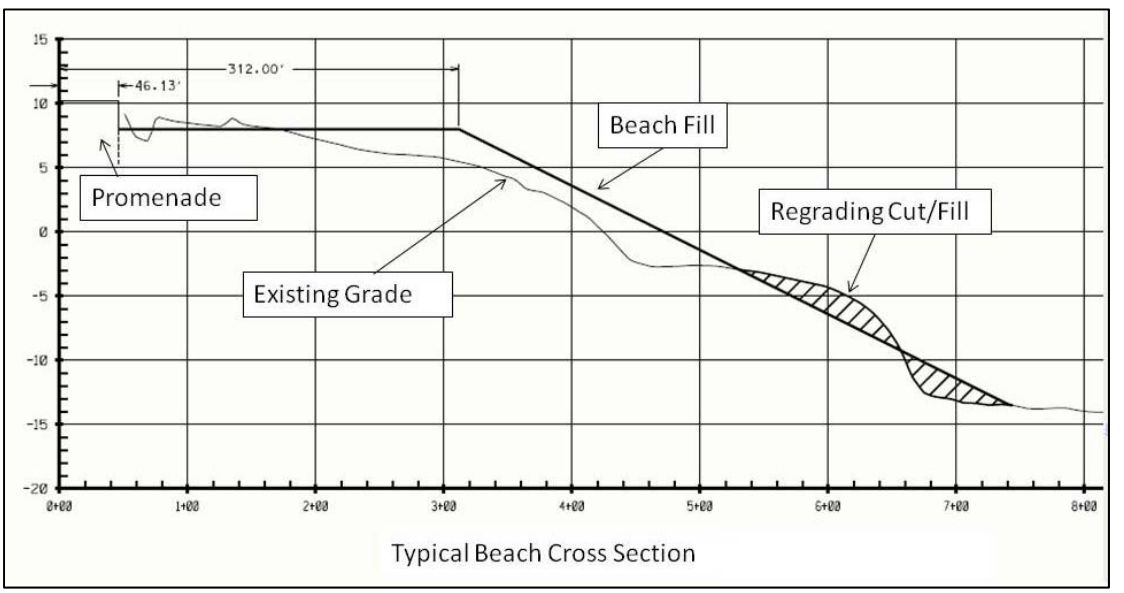


Figure 8. Typical Beachfill Cross Section With Offshore Regrading Cut/Fill.

Offshore Regrading

A large, 200-ft cross shore by 2,000-ft along shore drop-off zone formed naturally over time near the south side of the beach (Figure 9). This 9.2 acre zone presented a safety issue as non-swimmers waded offshore during low tide and suddenly lost the feel of solid ground. This area is located approximately 600 to 800 feet offshore, generally beyond the toe of the new beachfill. Selection of construction methodologies became a challenge due to the need for long-reach equipment underwater. Several construction methodologies were brainstormed to achieve re-grading, including towing a heavy flat steel plate along the slope, or bottom dragging of a long-reach crane-mounted bucket.

Ultimately, re-grading of the drop-off zone was achieved by applying a GPS equipped dozer and two 75-ft long-reach excavators. Material accumulated at the upper bump was excavated and pushed or placed further towards the lower trough offshore, then smoothed with a dozer during low tide, taking advantage of the large tidal range and mild beach slope (Figure 10). Two spud-barge-mounted long-reach excavators were able to smooth the area farther offshore via underwater cut and fill (Figures 11-12). The re-grading area was surveyed periodically to update grading progress. Re-grading started on 9 November 2010 and was completed within 80 days.

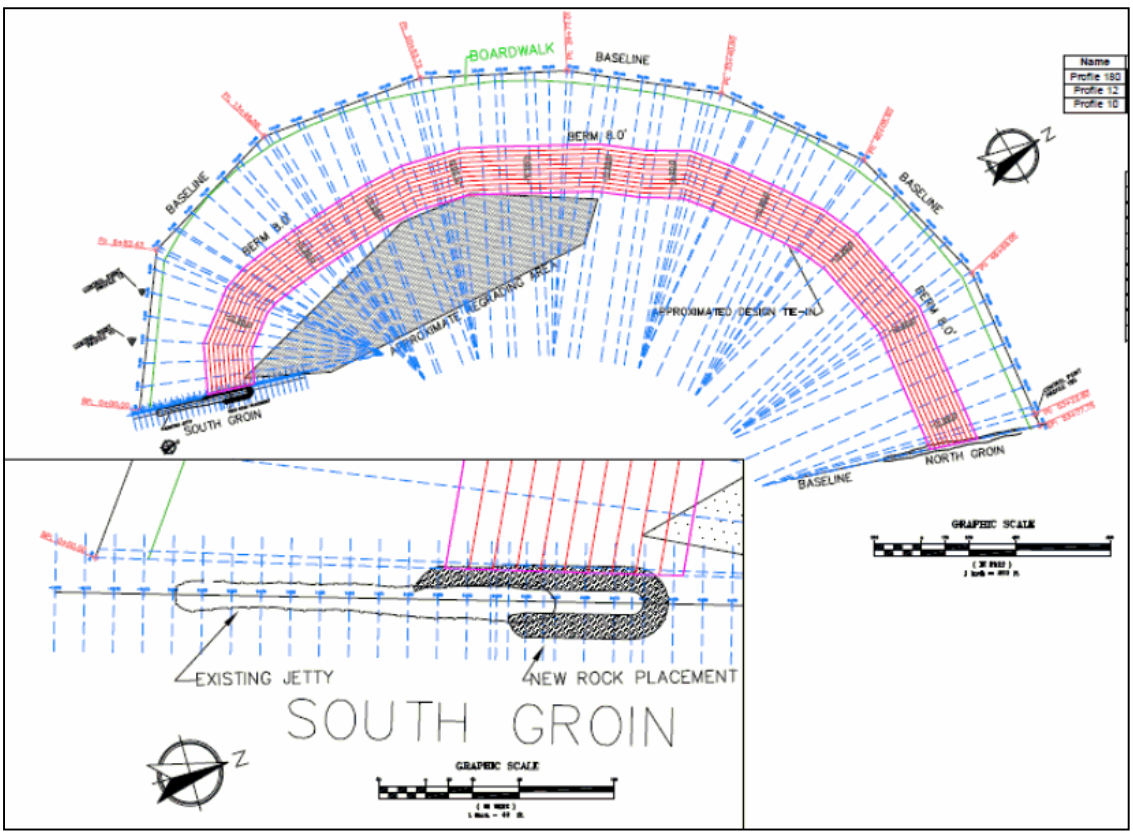


Figure 9. Plan View of Drop-off Zone, Shown in Gray Shaded Area.



Figure 10. Re-grading Nearshore Area with one Dozer and one Excavator.



Figure 11. Re-grading Offshore Area with two Spud-Barge mounted Excavators.



Figure 12. Spud Barge and Excavator Close-up.

Groin Repair

The 200-ft offshore section of the 400-ft south groin was rehabilitated to tighten the structure toe and to repair the head. Approximately 4,000 tons of rock was delivered and stockpiled on-site, including 2,500 tons of 1.0 to 3.5 ton armor stone, 700 tons of core/bedding stone, and 800 tons of underlayer stone. 40 cubic yard (60 ton) dump trucks were used to transport the rock material from Tilcon quarry in West Nyack, New York, approximately 26 miles from the project site. For construction, one CAT 320 Excavator with grapple attachment, one CAT 321C Excavator with bucket attachment; and one CAT 740 articulated dump truck were used (Figure 13). Due to the large tidal range, the crest elevation of armor units at the head section was raised from +5.0 ft to +8.0 ft NGVD via a construction modification to increase safety for boating and recreational use. Armor stone removed from the existing groin was re-used when it complied with specifications to save cost and limit required disposal. A typical design section for the groin head rehab is shown in Figure 14, and the completed structure is shown in Figure 15.



Figure 13. Groin Repair in Progress.

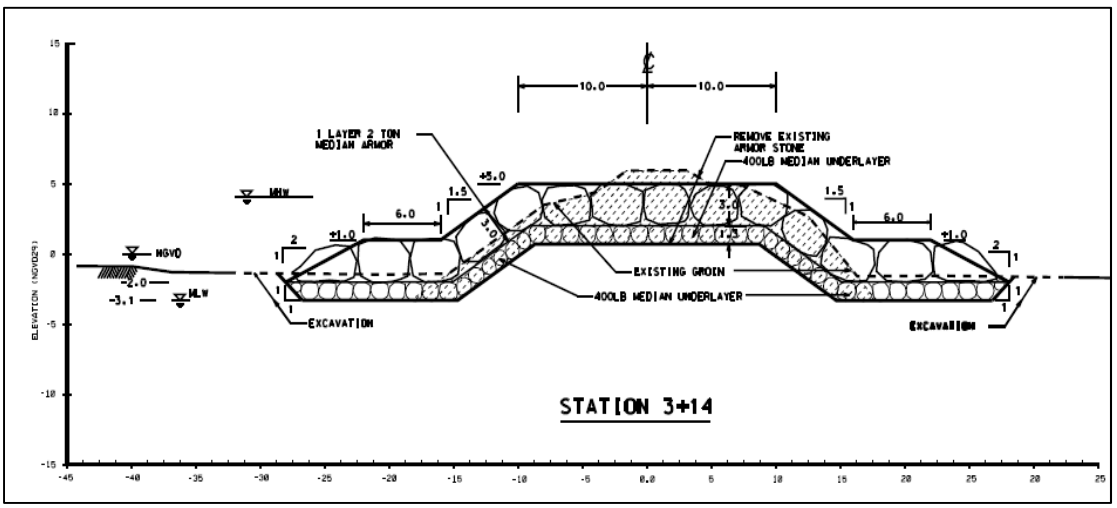


Figure 14. Typical Groin Head Cross Section.



Figure 15. Completed South Groin Head.

CONCLUSION

Based on innovative construction methodology and full partnering between contractor (GLDD), the designer (USACE) and owner (NYC Parks), the Orchard Beach construction project was able to be completed within a limited three month period, both on schedule and under budget. The choice of mobilizing two hopper dredges and excavation of borrow material directly from Ambrose Channel increased the production rate and lowered the beachfill cost. Application of both land-based and barge-mounted equipment plus taking advantage of the large tidal range allowed underwater grading to be accomplished successfully within the tight schedule. Both the beach grading and groin repair were completed by efficient use of standard construction equipment. A view of the completed beach fill is shown in Figure 16. The newly rehabilitated Orchard Beach is expected to continue to be a great recreational location for New York City residents for many years to come.



Figure 16. Completed Beachfill.

REFERENCES

NYCityMap, 2011. (http://gis.nyc.gov/doitt/nycitymap/) New York City Information Technology and Telecommunications, New York, New York.

U.S. Army Corps of Engineers, 1985. *Detailed Project Report Orchard Beach, Bronx, NY,* USAE District, New York, New York

U.S. Army Corps of Engineers, 2005. *Orchard Beach, New York, Re-evaluation Report and Environmental Assessment,* USAE District, New York, New York

Design and Construction of the Lake Borgne Surge Barrier in Response to Hurricane Katrina

Scott R. Huntsman, Ph.D., P.E., G.E., D.GE., CPESC, CPSWQ, QSD, F.ASCE[1]

[1]Shaw Environmental & Infrastructure Group, 4005 Port Chicago Highway, Concord, CA 94520-1122, PH (925) 288-2368; FAX (925) 288-2029; email: scott.huntsman@shawgrp.com

ABSTRACT

Following hurricanes Katrina and Rita in 2005, the U.S. Army Corps of Engineers (USACE) began to design and construct the Hurricane and Storm Damage Risk Reduction System (HSDRRS) for Southeast Louisiana. A key feature of the HSDRRS is the Inner Harbor Navigation Canal (IHNC) Lake Borgne Surge Barrier. The surge barrier is part of a larger program designed to provide a 100-year level of defense to a large portion of Orleans and St. Bernard parishes by reducing the effect of storm surge coming from the Gulf of Mexico and Lake Borgne.

The 10,000-foot (3050-meter) long, 26-foot (8-meter) high surge barrier includes three gate structures and a barrier wall. The project is being constructed approximately eight miles (13 kilometers) east of downtown New Orleans, near the confluence of the Gulf Intracoastal Waterway (GIWW) and the Mississippi River Gulf Outlet (MRGO). The entire barrier and all three gates are currently scheduled to be functional by June 2011.

This paper presents a description of challenges encountered by the design-build team, integration of design, procurement, and construction to meet an accelerated schedule and some of the unique methods used to construct the project.

INTRODUCTION

On Tuesday, August 23, 2005, Tropical Depression Twelve formed over the southeastern Bahamas. The storm reached hurricane strength (Hurricane Katrina) shortly before making landfall along the eastern Florida coast on the morning of August 25. After crossing over the southern tip of the Florida Peninsula, the storm entered the Gulf of Mexico and intensified to a Category 5 hurricane. At its peak strength, at approximately 1:00 p.m. on Sunday, August 28, the storm had a sustained wind speed of 175 miles per hour (282 kilometers per hour). Katrina made its second landfall on the morning of Monday, August 29 as a Category 3 hurricane with sustained winds of 125 miles per hour (201 kilometers per hour) near Buras-Triumph, Louisiana. At landfall, hurricane force winds extended outward 120 miles (193 kilometers) from the center. The center of the storm passed approximately 20 miles (32 kilometers) east of downtown New Orleans, traveled northward along

the Louisiana/Mississippi border, and was eventually downgraded to a tropical depression as it traveled north near Clarksville, Tennessee (see Figure 1).

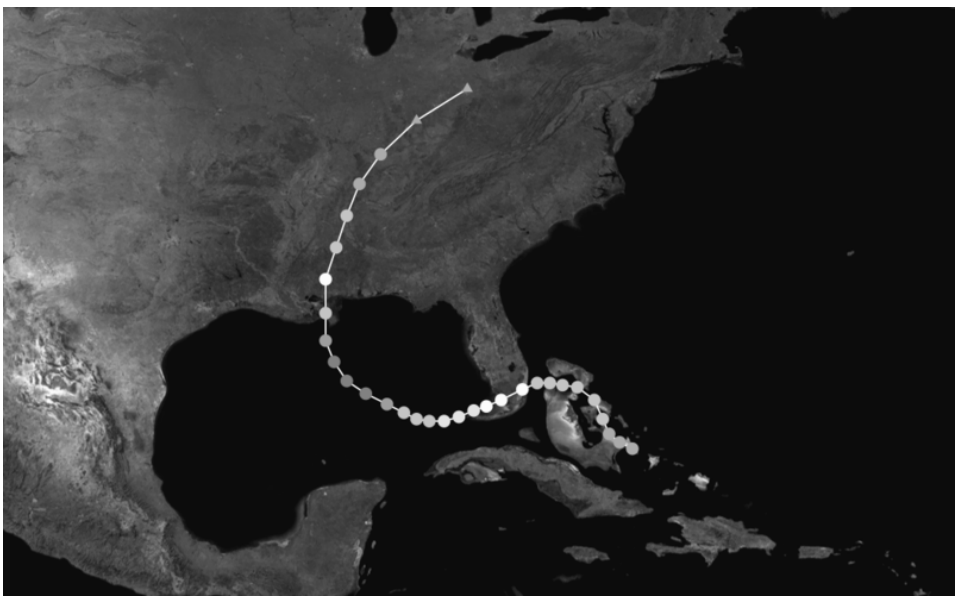


Figure 1. Path of Hurricane Katrina

On September 23, 2005, Hurricane Rita (another Category 5 hurricane) made landfall as a Category 3 hurricane near the Louisiana/Texas border. Rita caused further flooding and delayed cleanup and recovery efforts. The 2005 season was an unusually active year for Atlantic hurricanes (see Table 1).

Table 1. Comparison of "Average" Atlantic Season with 2005

	Tropical Storms	Hurricanes (category 1 through 5) >74 mph (119 km/h) winds	Intense Hurricanes (category 3 through 5) >111 mph (179 km/h) winds
"Average" Year	11	6	2
2005	28	15	7

Notes:

> greater than
km/h kilometers per hour
mph miles per hour

EFFECTS OF THE STORMS

As Hurricane Katrina passed New Orleans, a 26-foot (8-meter) high storm surge crippled the city's existing hurricane defense system. Levees and floodwalls along the perimeter of Lake Borgne, the IHNC, GIWW, MRGO, Lake Pontchartrain, and several drainage canals were either overtopped or failed, causing widespread flooding

throughout the city and surrounding areas. In a span of approximately 5 hours, 80 percent of the city was flooded; some of it to a depth of more than 10 feet (3 meters) (see Figure 2).

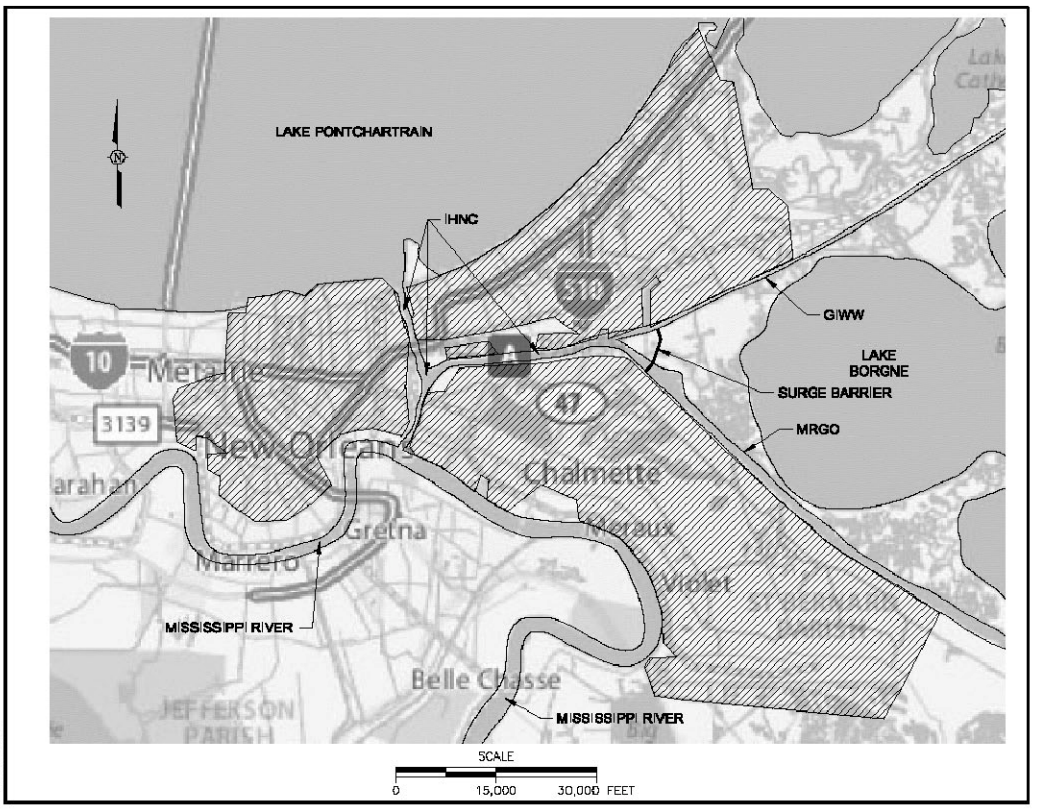


Figure 2. Greater New Orleans Area Showing Approximate Extent of Flooding

The hurricane, and the subsequent flooding, was responsible for approximately 1,850 deaths. Property damage has been estimated at $81 billion, making it the costliest U.S. hurricane on record; more than twice that of Hurricane Andrew. Approximately 1 million people were displaced. A large percentage of these people have not returned to New Orleans nearly six years later.

THE NEW ORLEANS HURRICANE PROTECTION SYSTEM

The New Orleans area is protected from flooding by a complex system of levees, walls, canals, and pumping stations. The system has undergone numerous modifications throughout history. Prior to the 2005 hurricane season the system was built to protect against the flooding caused by Hurricane Andrew in 1992, a Category 3 storm with 12-foot (3.5-meter) tides and 130-mile per hour (209-kilometer per hour) winds. To that end, several walls and levees were constructed to a height of 14 feet (4.3 meters) above mean sea level.

The IHNC, connecting the Mississippi River to Lake Pontchartrain was originally constructed between 1918 and 1923. The IHNC became part of the GIWW, authorized by the U.S. Congress in 1919 and constructed between the late 1930's and 1949. The GIWW is a navigable inland waterway running approximately 1,050 miles (1,700 kilometers) from Carabelle, Florida to Brownsville, Texas. The GIWW provides a protected route for barge transportation along the gulf coast.

The MRGO was a 76-mile (122-kilometer) long channel that extended from the confluence of the IHNC and GIWW southeastward to the Gulf of Mexico. Originally authorized by the U.S. Congress in 1956, the MRGO channel was constructed between 1960 and 1965. The purpose of the MRGO was to provide a deep draft channel for ocean-going ships to travel between New Orleans and the open waters of the gulf, avoiding the winding trip of approximately 80 miles (130 kilometers) along the Mississippi River. The MRGO never carried the traffic that its proponents envisioned, partly because the navigation gates at the junction of the IHNC and the Mississippi River were never enlarged to accommodate newer deep-draft ships.

As Hurricane Katrina passed by New Orleans in August 2005, the resulting storm surge traveled westward across Lake Borgne and entered the GIWW and MRGO. The surge caused extensive damage to levees and walls along the parishes neighboring the GIWW, IHNC, and MRGO. The storm surge also entered Lake Pontchartrain, to the north of New Orleans, and caused extensive flooding along the city's northern shoreline and several drainage canals that connect to the lake.

CORPS OF ENGINEERS RESPONSE

Following the hurricane season of 2005, Congress authorized the USACE to design and construct the HSDRRS for Southeast Louisiana. The 350-mile (564-kilometer) system, when completed, will consist of reinforced levees, T-wall floodwalls, surge barriers, pump stations, and floodgates at an estimated cost of more than $14 billion. The goal of the HSDRRS is to defend against the effects of a 100-year level storm by June 2011, thereby providing the greater New Orleans area with the best perimeter flood defense in its history. Figure 3 presents an illustration of the components of the overall system.

The USACE immediately began implementing the HSDRRS and, by June 2006, had accomplished the following repairs and enhancements to the damaged system:

- Pumped 250 billion gallons (9.5 million cubic meters) of water out of the city
- Built 2.3 miles (3.7 kilometers) of new floodwalls
- Built or repaired 22.7 miles (36.5 kilometers) of new levees
- Placed 195.3 miles (314.3 kilometers) of scour repair
- Completed three interim gated closure structures

A key feature of the HDRSS is the Lake Borne Surge Barrier project located near the confluence of the GIWW and MRGO channels east of the city of New Orleans.

During the early planning process, several alternative locations and configurations were considered for the construction of the barrier. Locations built farther to the west would have necessitated a greater amount of levee construction along the eastern perimeter of St. Bernard Parish and the southern shore of New Orleans East. Locations farther to the east would have required a longer barrier built in deeper, less protected waters. The location chosen included a barrier approximately 10,000 feet (3,050 meters) long with two gate complexes to allow for boat traffic. One gate was to be located approximately at midpoint of the barrier wall to allow for local recreational and fishing fleet traffic. The larger gates were to be located near the northern end of the wall to allow for barge commerce along the GIWW.

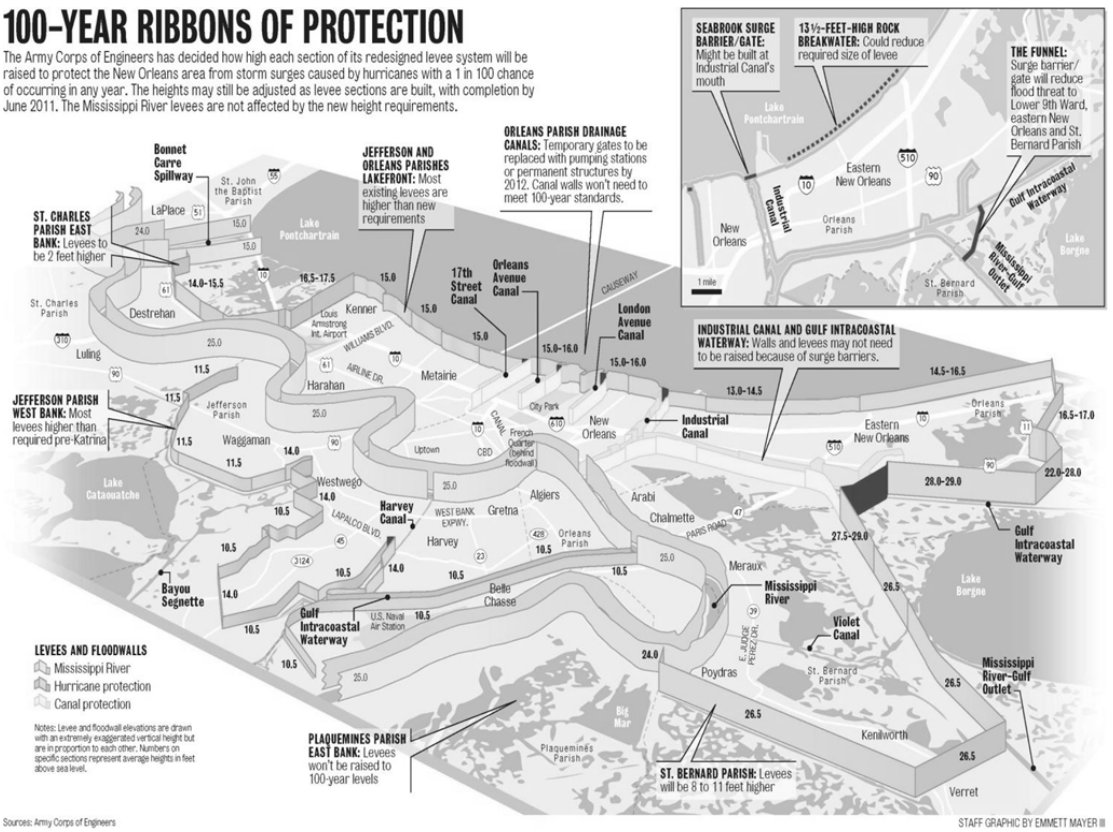


Figure 3. The HSDRRS for Southeast Louisiana

In April 2008, the USACE awarded a design-build contract to Shaw Environmental & Infrastructure Group for the Lake Borgne Surge Barrier, making this project the largest design-build civil works project in USACE history. Until this time, it was highly unusual for a civil works project to be designed and constructed simultaneously. The design-build process was necessary, however, given the very aggressive timeframe to achieve 100-year level of risk reduction in 2011.

ALTERNATIVES ANALYSES

The design-build team initially had to decide on the type of barrier wall and gates to be constructed. Figure 4 presents the evaluation criteria applied to the 12 options considered for the barrier wall. Each option was evaluated against the following criteria:

- Ability to Achieve Schedule: each alternative was rated Excellent, Good or Poor for the ability to achieve the two schedule milestones: Advance Measure Protection by June 1, 2010 and 100-year Protection by June 1, 2011.
- Ability to incorporate advance protection measures into final construction: All alternatives were rated Excellent.
- Cost: Costs for construction, operations and maintenance (O&M) and total lifecycle costs were rated Low, Medium or High for each alternative.
- Each Alternative was rated Excellent, Good or Poor for the "4Rs" criteria of resiliency, redundancy, repairability and reliability.
- Each alternative was rated Excellent, Good or Poor for the ability to be expanded in the future.
- Each alternative was rated Low Medium or High for its impact on the environment.
- Each alternative was rated Low Medium or High for complexity of design.
- Each alternative was rated Excellent, Good or Poor for constructability, local construction expertise and availability of local materials.
- All alternatives were rated to have a similar impact on navigation.

Figure 5 presents a description of the recommendations that were generated by the evaluation process and the alternative that was chosen to proceed into final design. The chosen alternative was a braced concrete pile wall utilizing large diameter cylindrical piles driven vertically at close spacing. The resistance to lateral loads was strengthened by steel batter piles driven on the western (protected side of the wall). The gaps between the vertical cylinder piles were closed by the installation of precast concrete piles into a column of grouted soil (see Figures 8 and 9).

Figure 6 presents the evaluation criteria applied to the seven options considered for the two required navigation gates. Each option was evaluated against the same criteria that were used to evaluate the barrier options. Figure 7 presents a description of the recommendations that were generated by the evaluation process and the alternative that was chosen to proceed into final design. The chosen alternative for the largest gate was for a radial sector gate constructed within a dewatered cofferdam. In order to maintain barge commerce during construction, it was decided to build this primary gate in two segments, with a secondary gate structure adjacent to (and built prior to) the sector gate. This gate was a concrete barge swing gate. After the barge gate was constructed, commercial barge traffic was routed through it and construction of the main sector gate began (see Figure 10).

Barrier System Alternative	Achieve Schedule		Incorporation into Advance Measures	Cost			OMRR&R*	4 Rs Criteria				Expandability	Environmental Impact	Team Confidence				Impacts to Navigation
	Advance Measures	100-Year Level of Flood Protection		Construction	O&M	Lifecycle		Resiliency	Redundancy	Repairability	Reliability			Design Complexity	Constructability	Local Construction Expertise	Local Material Availability	
Braced Concrete Pile Wall	G	E	E	M	L	M	L	E	G	G	G	G	L	M	G	E	E	L
Large (e.g. 56-foot diameter) Caissons	U	G	E	M	L	M	L	E	E	G	E	E	M	H	G	P	P	L
Dumbbell Caisson	U	G	E	M	L	M	L	E	E	G	E	E	M	H	G	P	P	L
Open Cell Sheet Pile	G	G	E	M	M	M	M	G	G	P	G	G	L	M	G	G	E	L
Earthen Levee	P	U	E	H	H	H	H	P	P	E	G	G	H	L	G	E	P	L
Pile-Supported Levee	P	U	E	H	H	H	H	P	P	E	G	P	H	L	G	E	P	L
Jet Grout Wall	P	G	E	H	L	M	L	E	G	G	G	G	L	M	G	G	E	L
New T-Wall	P	G	E	H	L	M	L	E	G	G	G	G	L	M	G	E	E	L
Braced Steel Sheet Pile Wall	G	E	E	M	M	M	M	G	G	P	G	G	L	M	G	E	E	L
Earth Levee with Soil Mixing	P	U	E	H	M	H	M	P	G	E	G	P	H	L	G	G	P	L
Hybrid Box Levee with T-Wall	P	G	E	M	M	M	M	G	G	G	G	G	M	M	G	G	G	L
Open Cell Sheet Pile with Earthen Levee	G	G	E	M	H	M	H	P	G	G	G	G	M	M	G	G	G	L

Notes:

**-Operation and Maintenance, Repair, Replacement and Rehabilitation*

E-Excellent, G-Good, P-Poor, H-High, M-Medium, L-Low, U-Unknown

Figure 4. Evaluation Matrix for 12 Barrier Options

Barrier System Alternative	Action/Decision
Braced Concrete Pile Wall	Retain as primary solution. Provides robust system that can be constructed by local resources. Low O&M
Large (e.g. 56-foot diameter) Caissons	Retain as alternate solution. Provides robust system with low O&M
Dumbbell Caisson	Dropped – variant of above. Can be re-evaluated if primary solution is not selected for further design
Open Cell Sheet Pile	Dropped – corrosion concerns with the sheet pile, high costs, and global stability concerns
Earthen Levee	Dropped – high cost for acquiring and placing the clay and high O&M cost for settlement. Also, resilience concerns from overtopping. Work will be significantly impacted by adverse weather
Pile-Supported Levee	Dropped – see above. Savings from smaller levee footprint offset cost for the piles
Jet Grout Wall	Dropped – high cost for jet grouting/deep soil mixing and concrete wall. Also, significant amount of site construction potentially affected by adverse weather
New T-Wall	Dropped – high cost for robust T-wall with piles, slow installation, and significant amount of site construction potentially impacted by adverse weather
Braced Steel Sheet Pile Wall	Dropped – corrosion concerns with the steel sheet piles
Earth Levee with Soil Mixing	Dropped – see "earthen Levee" Savings from smaller levee footprint offset by higher cost for deep soil mixing
Hybrid Box Levee with T-Wall	Dropped – difficult to attain Advance Measures, hybrid box cannot be cost-effectively built to an elevation to attain the Advance Measures so will still need T-wall. See "Earthen Levee" for sol placement concerns and "New T-wall:" for T-wall concerns
Open Cell Sheet Pile with Earthen Levee	Dropped – see "Open Cell Sheet Pile" and "Earthen Levee" for concerns

Figure 5. Evaluation and Decision Among Barrier Options

The gate structure located approximately midway along the length of the barrier was originally designed as a sector gate. However, after a value-engineering reanalysis, it was changed to be a steel vertical lift gate. This gate has a smaller draft requirement and is intended to primarily serve the local recreational and fishing fleet traffic. During construction, traffic was redirected through the recently completed barge gate at the GIWW.

The barrier wall was built in soft sediments resulting from thousands of years of deposition by the Mississippi River. To provide resistance necessary for the required protection against storm surge, the barrier and gates needed to be supported on piles driven deep below the mud line. The primary components of the wall were 1,271 cylindrical, 66-inch (1.7-meter) diameter vertical concrete piles driven to an elevation of -130 feet (-40 meters) below water level and spaced only 6 inches (15 centimerers) apart. The horizontal resistance was provided by 660 36-inch (91-centimeter) diameter steel batter piles driven to an elevation of -190 feet (98 meters) and connected to the vertical piles by precast and poured-in-place caps.

Concurrent with the evaluation of barrier and gate construction options, extensive numerical and physical modeling of navigational impacts was performed.

Gate System Alternative	Achieve Schedule		Incorporation into Advance Measures	Cost			OMRR&R*	4 Rs Criteria				Expandability	Environmental Impact	Team Confidence				Impacts to Navigation
	Advance Measures	100-Year Level of Flood Protection		Construction	O&M	Lifecycle		Resiliency	Redundancy	Repairability	Reliability			Design Complexity	Constructability	Local Construction Expertise	Local Material Availability	
Sector Gate – "Dry" Construction	G	G	E	M	M	M	M	E	G	G	E	G	M	M	E	E	G	M
Vertical Lift Gate	G	G	E	M	H	M	M	G	G	G	E	G	L	M	G	G	G	M
Sector Gate – "Wet" Construction	G	G	G	H	M	M	M	E	G	G	E	G	M	H	G	P	G	L
Steel Swing Gate	G	G	E	M	M	M	H	G	G	G	G	G	M	M	G	G	G	M
Concrete Swing Gate	G	G	E	M	L	M	H	G	G	G	G	G	M	M	G	G	G	M
Buoyant Roller Gate	G	G	E	M	M	M	H	G	G	G	G	G	M	H	G	G	G	M
Visor Gate	G	G	E	H	U	H	H	P	G	U	G	G	M	H	P	P	G	M

Notes:

**-Operation and Maintenance, Repair, Replacement and Rehabilitation*

E-Excellent, G-Good, P-Poor, H-High, M-Medium, L-Low, U-Unknown

Figure 6. Evaluation of Seven Gate Options

Barrier System Alternative	Action/Decision
Sector Gate – "Dry" Construction	Selected as primary solution. Proven design, proven construction, and proven performance
Vertical Lift Gate	Selected as alternate solution. Demonstrated at Olmsted. Concerns with wind loads with gate in up position.
Sector Gate – "Wet" Construction	Dropped – more costly than Dry Construction and local contractors are not proficient with this method
Steel Swing Gate	Dropped – does not meet operating timeframe or maintenance requirements. Concerns with opening under head.
Concrete Swing Gate	Dropped – does not meet operating timeframe. Concerns with opening under head.
Buoyant Roller Gate	Dropped – does not meet operating timeframe. Concerns with opening under head.
Visor Gate	Dropped – current designs are not believed to be resilient and would be difficult to construct.

Figure 7. Evaluation and Decision Among Gate Options

DESIGN-BUILD COORDINATION

Because of the aggressive project schedule, decisions regarding materials procurement and fabrication had to be made early. One of the most challenging decisions was to decide on the length of the large diameter concrete piles that were to be the primary structural component of the barrier. A 66-inch (1.7-meter) diameter spun-cast hollow concrete pile was selected as the primary element. Three locations near the barrier alignment were selected for full-scale pile load tests to gather the data needed to design the lengths of the 1,271 production piles. However, the fabrication and curing time for the piles did not allow for the completion of the pile load tests prior to beginning the pile fabrication. For this reason, the piles were constructed in 16-foot (4.9-meter) segments, and production of the segments commenced well before the pile load tests began in December 2008. As the pile load tests were completed, and design loads finalized, decisions were made regarding the required lengths of the piles (i.e., the number of segments needed). The previously manufactured segments were then joined together using a tendon pre-stressing and grouting system to form the full length piles. The final production length used nine pile segments for a total length of 144 feet (44 meters).

The need to limit on-site exposure to inclement weather conditions posed additional scheduling challenges. With construction continuing through the 2009 and 2010 hurricane seasons, the decision was made to store project components at the onshore fabrication facilities and transport them by barge to the project site on a very closely controlled delivery schedule. The subcontractors were required to continually update their contingency plans for demobilizing equipment and materials to "safe haven" sites in advance of upcoming storms.

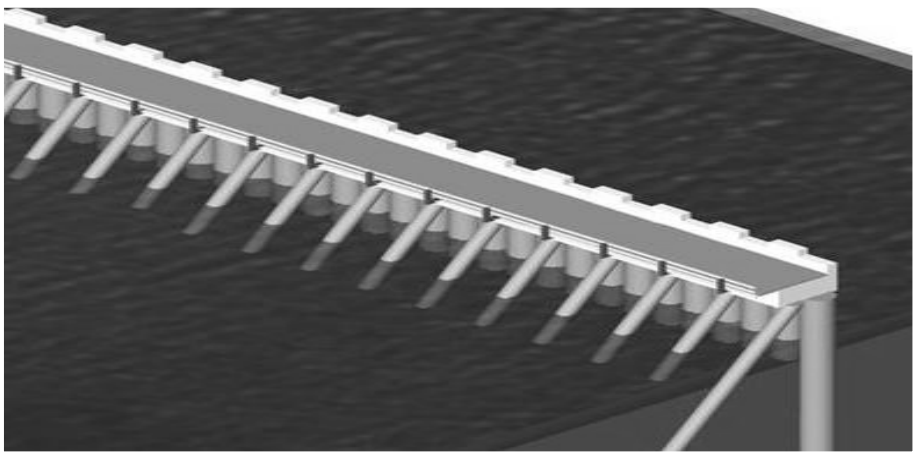


Figure 8. Illustration of Barrier Wall System. Flood Side of Barrier is Located to the Right Side of Illustration

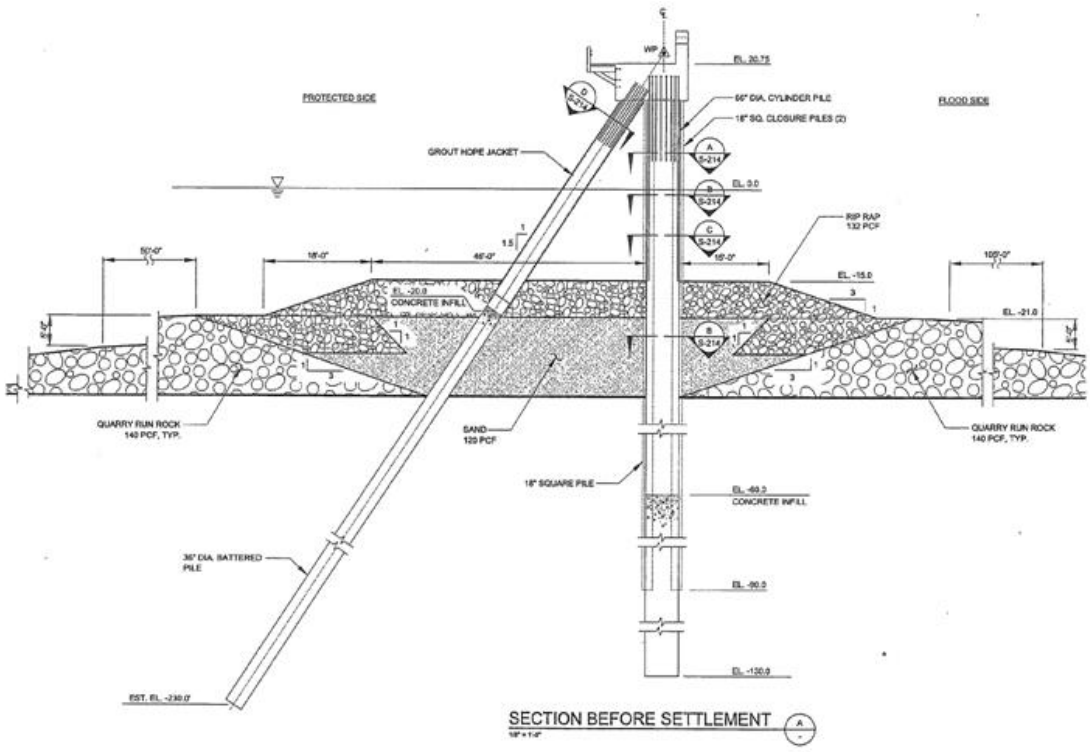


Figure 9. Cross-Section of Barrier Wall

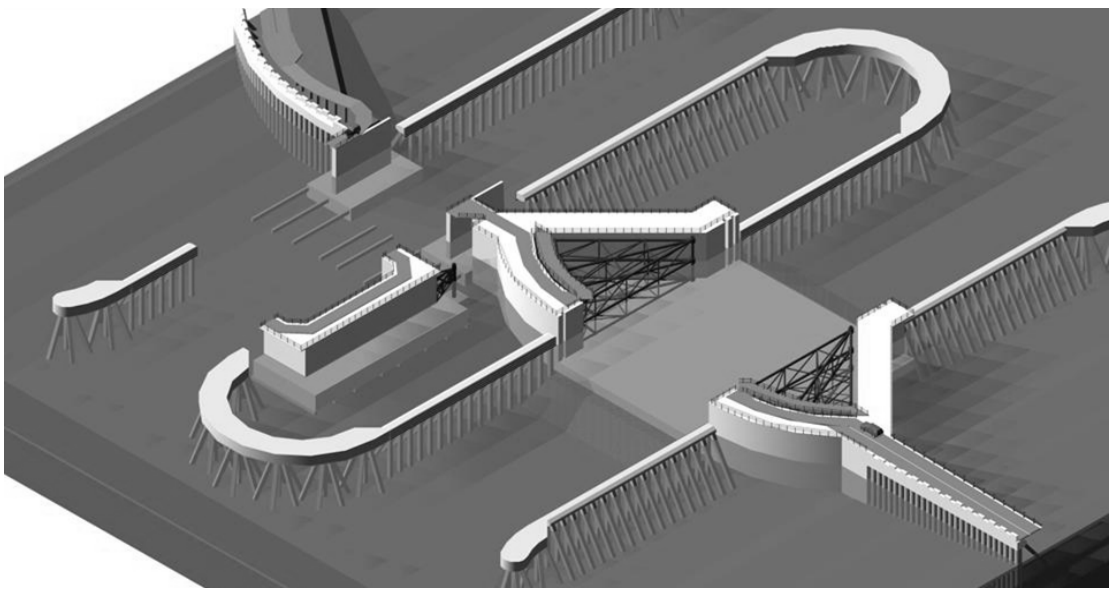


Figure 10. Illustration of Gate Structures at the GIWW (Each Gate is 150 Feet (46 Meters) Wide)

CONSTRUCTION SEQUENCING

In order to meet the demanding project schedule, multiple subcontractors and suppliers were used to build portions of the project concurrently on an around-the-clock schedule. The first production pile was installed on May 9, 2009. The surge barrier was complete and the gate structures were substantially complete by the start of the hurricane season on June 1, 2011.

Multiple marine subcontractors worked dual shifts at multiple locations within the project to complete the majority of the barrier wall in less than 12 months. The construction progressed in an "Assembly Line" fashion, with the construction equipment following each other in the following sequence:

- Dredging of the barrier alignment to allow for the construction to be performed with floating equipment. The dredge spoils were used to enhance nearby marsh areas.
- Closure of the MRGO. Congress de-authorized the MRGO for navigation and closed it to all traffic in April of 2009. Sand berms were built across the channel to provide for a stable construction site for the barrier wall to cross the former channel.
- Drive 66-inch (1.7-meter) diameter hollow concrete piles at close spacing along the barrier alignment. 1,271 piles were installed between May 9, 2009 and October 21, 2009. Each pile weighed 96 tons (87,000 kilograms) and was driven to 130 feet (40 meters) below the mud line.
- Install 12-inch (30-centimeter) concrete closure piles on both sides of the gap between the vertical piles. The piles were placed in pairs into jet-grouted columns of cement-treated soil (see Figures 11 and 12).
- Drive 36-inch (90-centimeter) diameter steel pipe piles at a 1:1.5 (H:V) batter on the "protected" side of the barrier. These piles were 240 feet (73 meters) long. They were installed in two segments, requiring field welding of each pile at the midpoint of driving.
- Clean out and fill concrete piles with steel reinforcing and concrete
- High-density Polyethylene sleeves were placed over the steel batter piles from the mud line to the top of the wall to protect against corrosion and to provide added protection in the event of a collision. The annulus between the piles and the sleeves was filled with cement grout.
- Clean out and place grout in the area between the main concrete piles and the closure piles to form a solid wall.
- Place precast concrete sections on top of the wall. Individual cap sections weighed 100 tons (91,000 kilograms) each and were grouted in place.
- Cast-In-Place cap closure sections were poured between precast cap sections.
- Construct parapet wall above the concrete pad.
- Install expansion joints, railing and finish details.

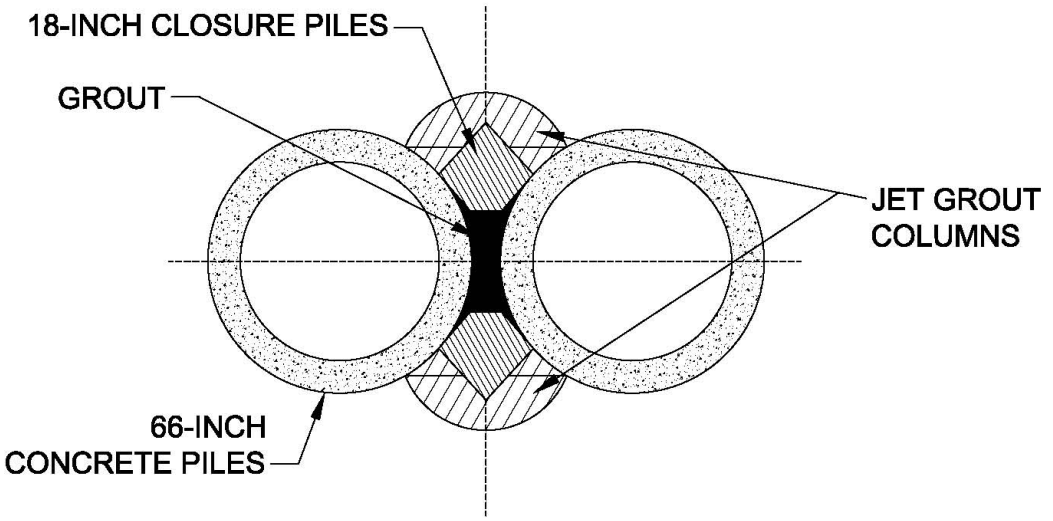


Figure 11. Plan View Detail of Closure Pile System

Concurrent with the construction of the barrier wall, work proceeded on the navigation gates. The foundations of the gates were constructed by driving hundreds of vertical piles through the water and below the mud line. After pile driving at each gate was complete, a steel sheet pile cofferdam was constructed around the perimeter of the gate structure and a thick concrete base slab was poured around the pile heads using tremie methods. The tremie slab was structurally connected to the foundation piles to resist the buoyancy uplift. The interior of the cofferdams was dewatered and the construction of the gate structures was completed "in the dry." The gates themselves were fabricated offsite and barged to the project site to be installed.

The barrier wall was connected with the adjoining levees on the north and south ends by a pair of pile-supported cast-in-place concrete transition walls. Control buildings for operation of the gate structures were built on top of the barrier wall adjacent to the gate structures.

The barrier and gates were constructed with minimal interruption to normal shipping operations, and with minimal impact to the surrounding wetlands environment.

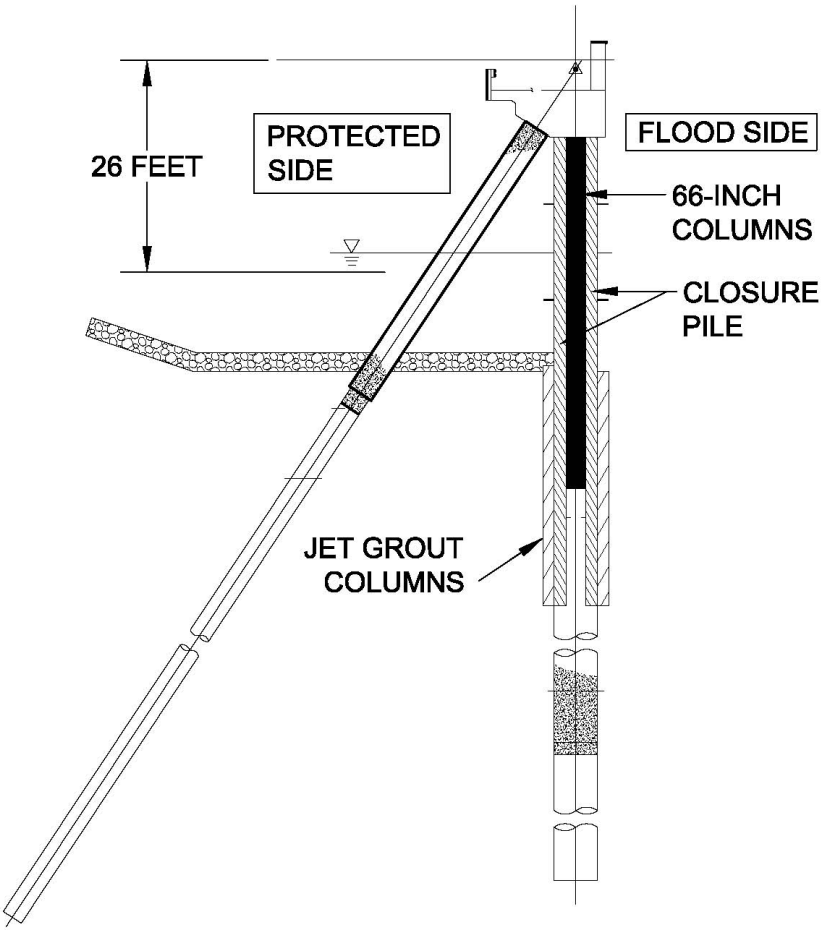


Figure 12. Profile View of Closure Pile System

The following statistics provide a summary of the overall construction of the Lake Borgne Surge Barrier System:

- Over 10,000 foot (3,050 meters) long project alignment
- Largest design-build project ever contracted by the U.S. Army Corps of Engineers
- Over 200,000 cubic yards (153,000 cubic meters) of concrete
- Over 100 linear miles (161 kilometers) of piles driven
- Over 27,000 tons (24,000 metric tons) of reinforcing bar used (enough to build eight Eiffel Towers)
- Approximately 700,000 tons (635,000 metric tons) of rock used as rip rap and scour protection
- Peak work force of 350 workers onsite
- Total work force of over 2,000 field and office personnel
- 17 barge-mounted cranes
- Over 2,000,000 work hours with 4 lost work days due to injuries
- 6 design subcontractors, 10 construction subcontractors, 55 small business subcontractors

LONG-TERM MONITORING AND EFFECTIVENESS OF SEDIMENT CAP, FORMER CAMPBELL SHIPYARD SAN DIEGO, CALIFORNIA

Rolf Schottle,[1] Larry McCauley,[2] and Bill Hays[2]

[1]AMEC Earth & Environmental, Inc., 9210 Sky Park Court, Suite 200, San Diego, CA 92123; PH (858) 300-4300; FAX (858) 300-4301; email : rolf.schottle@amec.com

[2]Port of San Diego, 3165 Pacific Highway, P.O. Box 120488, San Diego, CA 92112-0488; PH (619) 686 6597; FAX (619) 686-6467; email: lmccaule@portofsandiego.org and bhays@portofsandiego.org

ABSTRACT

In agreements reached with the Port of San Diego and the California Regional Water Quality Control Board (RWQCB), a 9.2-acre engineered (geotextile, sand, gravel, and rock armor) cap was constructed and completed in 2008 to isolate contaminated sediments at the Former Campbell Shipyard Site, San Diego Bay, San Diego, California. The cap included a special 1.6-acre eelgrass habitat cap. Using novel sediment and pore water monitoring stations installed in the cap, samples collected during the first 3 years of a 20-year mandated monitoring and reporting program indicate that the cap has been effective in retaining all constituents of concern (COCs). Monitored COCs include copper, lead, zinc, total PAHs, PCBs, total TPH, and butyltins.

1.0 INTRODUCTION

A long-term monitoring project is being conducted on behalf of the San Diego Unified Port District (Port) in support of compliance monitoring requirements at the Former Campbell Shipyard (Site) in San Diego, California. These requirements are specified in Cleanup and Abatement Order (CAO) 95-21 issued by the California Regional Water Quality Control Board San Diego Region (SDRWQCB, 1995) and the corresponding Order No. R9-2004-0295, Monitoring and Reporting Program (MRP) provisions (SDRWQCB, 2004). In agreements reached between the Port and the SDRWQCB, contaminated offshore bay sediments at the Site were capped, and a subsequent long-term monitoring program was implemented. Prior to construction of

the sediment cap, various remedial action alternatives were evaluated as part of the California Environmental Quality Act (CEQA) process to address contaminated sediments at the Site. As a result of the CEQA findings, the preferred and selected alternative was to isolate these sediments with an engineered cap. The 5-foot-thick engineered cap was completed in February 2008 and consists of a 2-foot thick sand base cap, a geotextile layer, and gravel and rock armored isolation cap. Within the capped area, a shallow 1.6-acre habitat cap consisting of sand over geotextile was constructed to support eelgrass beds. Figure 1 shows bathymetric contours of the habitat cap near a mole pier (white) at the approximate depth of 6 feet relative to mean lower low water (MLLW) (orange), and the engineered cap at the depth range of 10–25 feet MLLW (yellow to green) (Fugro-Pelagos, Inc, 2009). Figure 2 shows the approximate cap boundaries.

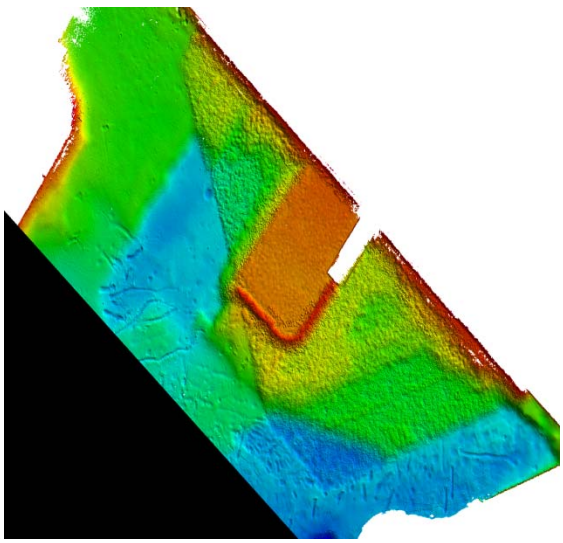


Figure 1. Bathymetric Chart of Cap Construction

The purpose of the 20-year-long monitoring program is to document the overall integrity of the engineered sediment cap over time, and ultimately assess whether the cap effectively isolates known constituents of concern (COCs) beneath its surface. The frequency of monitoring and testing is staggered with a greater frequency over the earlier life of the MPR. Monitoring since July 2008 has consisted of a total of eight surveys: the initial baseline survey, four quarterly monitoring events, and three annual monitoring surveys.

The on- and in-water monitoring tasks specified under the MPR and in the approved project work plan include multi-beam hydrographic surveys, visual dive inspections, and diver-collected samples. Media sampled to monitor for potential seepage of COCs from the impacted sediments beneath the cap include sediments from both the surface of the habitat cap and from within the engineered cap, pore waters from within the cap, and paired reference ambient water samples. The COCs for the Site are metals (copper, lead, and zinc), polycyclic aromatic hydrocarbons (PAHs), polychlorinated biphenyls (PCBs), total petroleum hydrocarbons (TPH), and

tributyltin (TBT). The CAO also specifies concentration-based action levels only for sediments that, if exceeded, may prompt further tiered investigation as defined in the monitoring provisions. Other requirements of the monitoring and reporting program include biennial benthic infauna analysis and bioaccumulation testing.

This paper focuses on chemical testing results for sediment and pore water during the first 3 years of monitoring to evaluate the effectiveness of the habitat cap and engineered cap in isolating COCs and meeting post construction monitoring requirements. Sediment concentrations are compared to CAO-defined action levels. The CAO does not specify action thresholds for pore water or ambient waters. However, the comparison of pore water results relative to concentrations of COCs in paired ambient bay water samples provides evidence of the effectiveness of the cap at isolating COCs.

2.0 METHODS

The cap design incorporates six monitoring stations (SS-1 through SS-6) installed within the engineered cap during construction to facilitate sediment and pore water sampling (Figure 2). Sample collection events occurred in July and November 2008; January, May, September, and November 2009; February 2010; and January 2011.

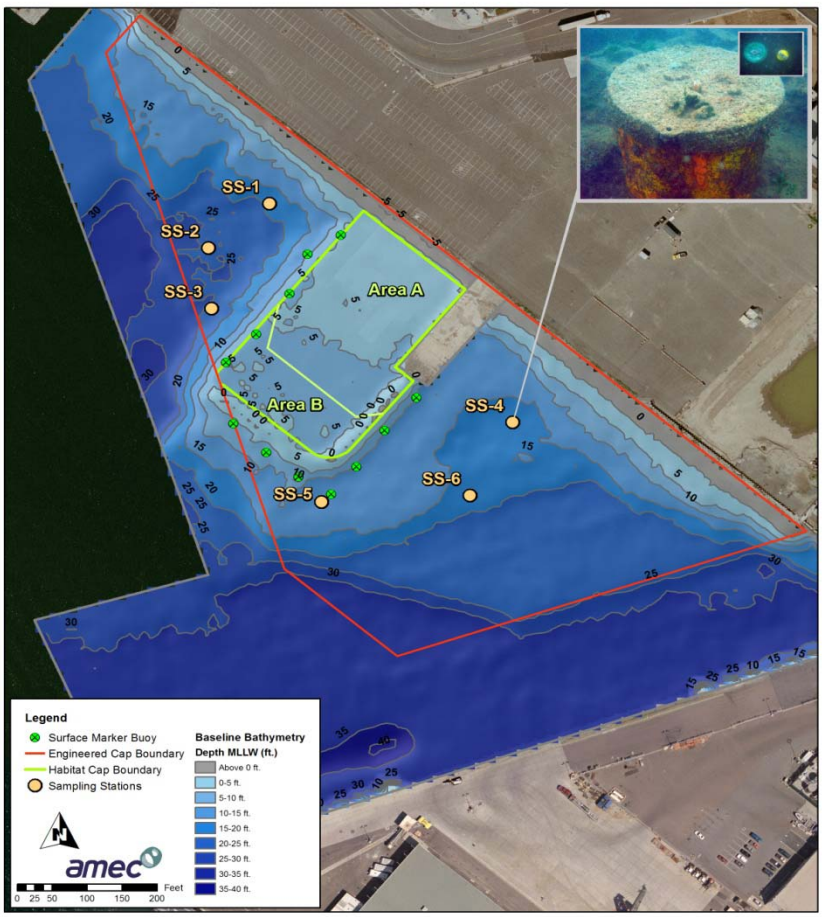


Figure 2. Engineered Cap Sampling Stations

Each "sampling station" consists of an embedded 12-inch-diameter steel cylinder, inside of which are two 3-foot-long polyvinyl chloride (PVC) well casings that were installed for pore water and sediment sampling (Figure 3, Ninyo and Moore 2005). Depths of the sampling stations vary between approximately -12 and -20 feet MLLW. Both PVC well casings are perforated at their bases, allowing connectivity to the underlying base cap/geotextile layer. The smaller 2-inch-diameter PVC well casing cap is plumbed with a semi-rigid tube, from which the isolated pore water can be withdrawn from the underlying base cap layer. The 4-inch PVC well casing provides access to a retrievable mesh bag of collocated test sediment. The test sediment is from the same sand source used for the clean capping material. This source sand was considered "clean" and is of similar grain size to the capping material, albeit containing background concentrations of COCs. This replacement and capping sand was obtained from Grand Caribe in the Coronado Cays, Coronado, California, a source located within San Diego Bay.

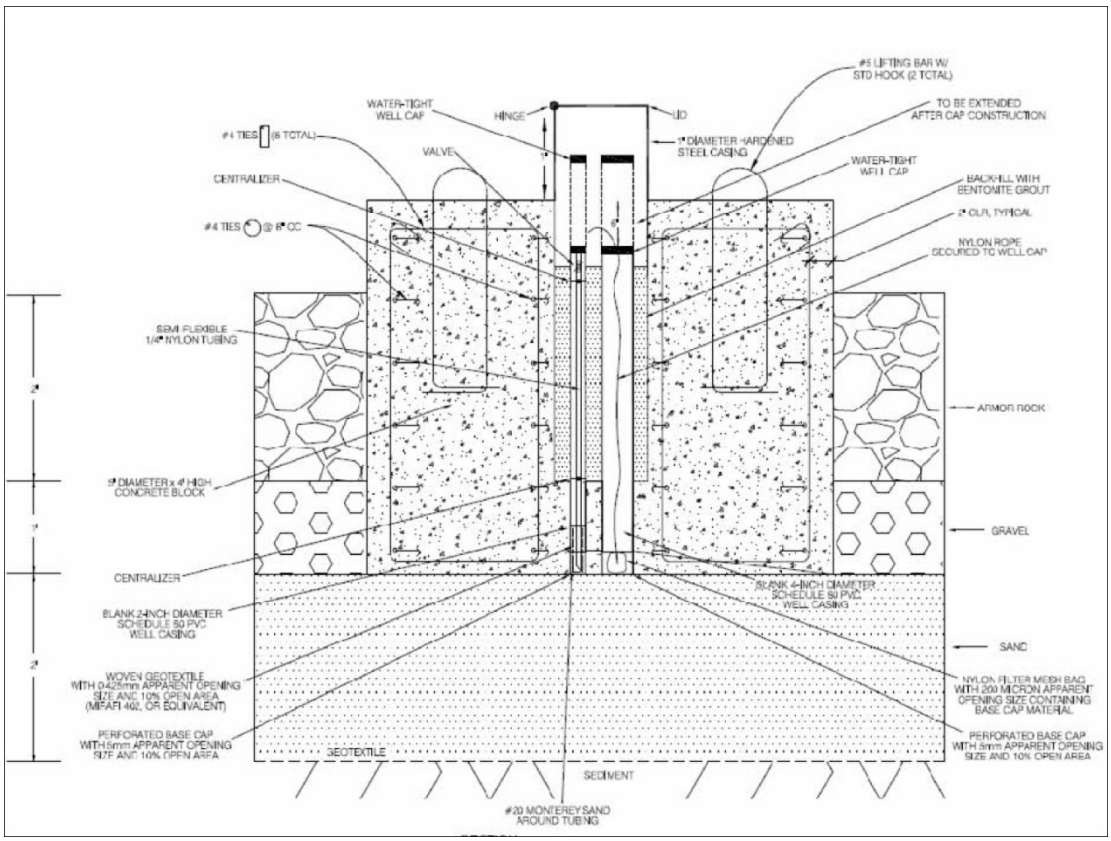


Figure 3. Monitoring Sampling Station Cross Section

Samples were collected using a boat moored at the sampling station. Divers plumbed a sampling tube from the surface to the sampling well cap, and opened the valve to collect the pore water samples from the 2-inch-diameter PVC riser. The wells were purged a minimum of three well volumes using a peristaltic pump and subsequently sampled on the boat. At the same time divers also retrieved the sediment sample from the 4-inch-diameter well casing, and replaced the removed sample volume with new

collocated sand samples that remained in place until they were collected during the next sampling event. Concurrently, ambient bay water was sampled by shipboard personnel using a Van Dorn bottle in the vicinity of the top of the well casing at each sampling station. Results of pore water chemical analyses for COCs were compared to concentrations of COCs in representative ambient bay water samples to discern if a potential release of COCs was occurring through the base chemical isolation layer. All ambient water and pore water samples were filtered (<0.45 µm) prior to analysis.

In addition to the engineered cap samples, surface sediment push cores were hand collected by divers to a depth of 1 foot at three randomized locations within the habitat cap during each event (Figure 4). Concentrations of COCs were measured in the top 2 to 3 inches of surface sediment of each core and compared to sediment action levels specified in the CAO to determine if post-construction deposition from the water column may be occurring. Results from the bottom 9- to 12-inch-depth sub-sample were similarly compared to action levels to determine if potential contamination is migrating to the surface from below the habitat cap.

All samples were collected, transported, and stored under customary chain-of-custody protocols. All samples were analyzed using low-level EPA methods modified for seawater and sediment by a California state-certified laboratory, Calscience Environmental Laboratories, Inc., located in Garden Grove, California.

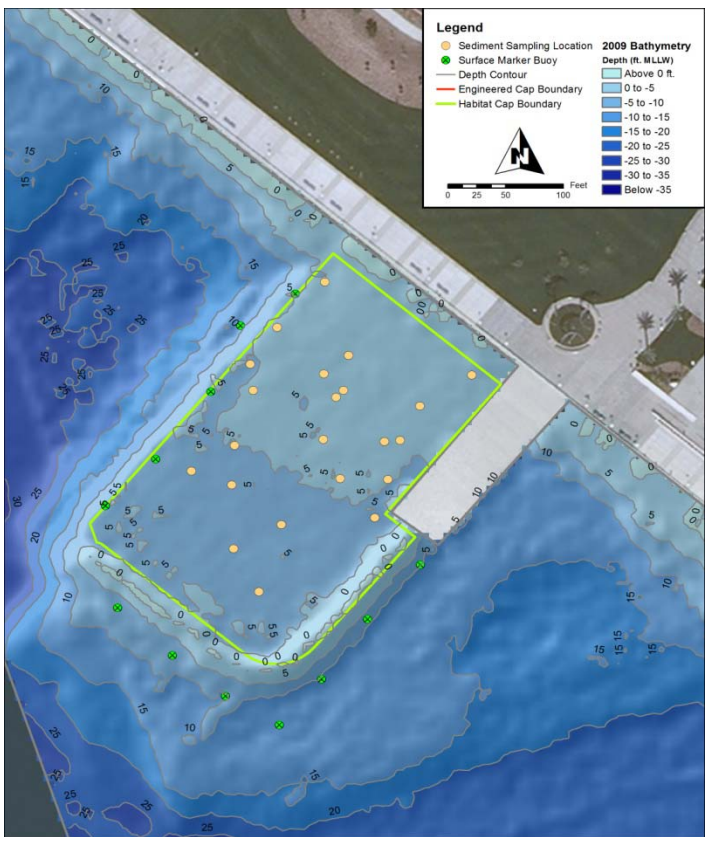


Figure 4. Habitat Cap Sampling Locations, July 2008–January 2011

3.0 RESULTS

A summary of the results for the eight sampling events is presented in Tables 1–4. Results are presented for individual metal constituents and for total summed concentrations for the remaining classes of organic constituents, including organotins. Because minimal temporal variability was observed in analytical results over the course of this study, the summary results presented in Tables 1–4 are average concentrations for all eight sampling events from July 2008 through January 2011. Results are summarized in Table 1 for the habitat cap sediment samples and in Table 2 for the engineered cap sediment samples. Results for pore water samples are presented in Table 3, and results for the corresponding ambient waters are presented in Table 4.

Concentrations of organic constituents for both sediment and waters were, with few exceptions, reported near or below method detection limits. Due to the preponderance of non-detectable and estimated results obtained below laboratory reporting limits, performing a rigorous statistical analysis was considered inappropriate, particularly for organic constituents for which greater than 95 percent of all results were reported as not-detected. For results reported at or below the method detection limit ("<" or ND), the absolute value of the reported method detection limit was used to estimate the total concentration for the corresponding class of organic constituents, and the summed constituents were reported in the tables as "less than" the summed method detection limits. Where one or more event results was reported as less than, the summed averages result was reported as less than, "<". The absolute value of the detection limit was selected to provide the most conservative estimate of COC concentrations relative to the action level thresholds prescribed in the CAO. Results for detected compounds (i.e., above the reporting limit) were included as reported in calculating the average concentrations so as to derive the total estimated concentration.

Concentrations of metals in sediments were generally well above method detection limits, thereby providing a quantitative indication that metals are binding to sediments. Concentrations of copper and zinc in ambient water samples were approximately 4–5 times greater than the method detection limits. Test methods used for organic constituents and lead yielded results that were generally below method detection limits.

Table 1. Concentrations of Sediments in Habitat Cap

			Habitat Cap Sample Location							
Compound Name	**Units**	**Action Level**	**HC-1-SB**	**HC-1-ST**	**HC-2-SB**	**HC-2-ST**	**HC-3-SB**	**HC-3-ST**	**AVG Bottom**	**AVG Top**
Copper	mg/kg	264	3.4	6.2	3.5	9.4	3.1	6.2	3.3	7.2
Lead	mg/kg	88	1.7	2.4	1.4	4.1	1.3	2.2	1.4	2.9
Zinc	mg/kg	410	15	22	16	30	16	20	15.6	23.7
TPH C6-C44 Total	mg/kg	14	<5.8	<7.0	<5.7	<8.6	<5.7	<5.8	<5.8	<7.1
Total PAHs	µg/kg	3,470	<660	<160	<410	<320	<130	<380	<401	<288
Total Butyltins	µg/kg	121	<4.1	<4.0	<4.1	<4.4	<4.1	<4.1	<4.1	<4.2
Total PCBs (Aroclor)	µg/kg	110	<29	<26	<27	<29	<28	<29	<27.9	<27.7

Note:

Calculated values are based on summed averages for n=8 sampling events (July 2008 through January 2011) and includes estimated and/or non-detect data.

These values are provided only as a basis for trend comparison and approximate level of detection, not as absolute concentrations. Reported on a dry weight basis.

HC= Habitat Cap, ST= sediment top, SB= sediment bottom, PAHs-Polyaromatic Hydrocarbons

TPH- Total Pretoleum Hydrocarbons, PCB- Polychlorinated Biphenyl

Table 2. Concentrations of Sediments in Engineered Cap

			Engineered Cap Sample Location						
Compound Name	**Units**	**Action Level**	**SS-1-S**	**SS-2-S**	**SS-3-S**	**SS-4-S**	**SS-5-S**	**SS-6-S**	**AVG**
Copper	mg/kg	264	1.7	2.5	1.7	2.1	1.7	1.9	1.9
Lead	mg/kg	88	1.4	3.2	1.3	1.2	1.2	1.4	1.6
Zinc	mg/kg	410	12	15	16	13	11	11	13
TPH C6-C44 Total	mg/kg	14	<6.4	<6.3	<6.2	<6.2	<6.2	<9.5	<6.8
Total PAHs	µg/kg	3470	<180	<170	<150	<170	<150	<150	<160
Total Butyltins	µg/kg	121	<4.6	<4.5	<4.5	<4.5	<4.6	<4.6	<4.6
Total PCBs (Aroclor)	µg/kg	110	<29	<31	<32	<31	<32	<32	<31

Note:

Calculated values are based on summed averages for n=8 sampling events (July 2008 through January 2011) and includes estimated and/or non-detect data.

These values are provided only as a basis for trend comparison and approximate level of detection, not as absolute concentrations. Reported on a dry weight basis

HC= Habitat Cap, SB= sediment bottom, SS= Sampling Station, S= Sediment (collocated in cap)

PAHs-Polyaromatic Hydrocarbons, TPH- Total Pretoleum Hydrocarbons, PCB- Polychlorinated Biphenyl

Table 3. Concentrations of Pore Water in Engineered Cap

		Pore Water						
COMPOUND NAME	**UNITS**	**SS-1-PW**	**SS-2-PW**	**SS-3-PW**	**SS-4-PW**	**SS-5-PW**	**SS-6-PW**	**AVG**
Copper	µg/L	<1.3	<0.96	<0.70	<0.53	<0.62	<0.77	<0.81
Lead	µg/L	<0.2	<0.20	<0.20	<020	<0.20	<0.20	<0.20
Zinc	µg/L	<9.8	<8.0	<5.7	<3.3	<3.5	<3.3	<5.6
Total TPH C6-C44	µg/L	<50	<52	<62	<45	<45	<72	<54
Total PAHs	µg/L	<0.40	<0.38	<0.46	<0.42	<0.38	<0.38	<0.40
Total Butyltins	ng/L	<4.3	<4.3	<4.3	<4.3	<4.3	<4.3	<4.3
Total PCBs (Aroclor)	µg/L	<0.26	<0.26	<0.26	<0.26	<0.26	<0.26	<0.26

Note:

Calculated values are based on summed averages for n=8 sampling events (July 2008 through January 2011) and include estimated and/or non-detect data.

These values are provided only as a basis for trend comparison and approximate level of detection, not as absolute concentrations.

PW=Porewater, SS= Sampling Station, PAHs-Polyaromatic Hydrocarbons, PCB- Polychlorinated Biphenyls

TPH- Total Petroleum Hydrocarbons

Table 4. Concentrations of Ambient Water on Engineered Cap

		Ambient Water						
COMPOUND NAME	**UNITS**	**SS-1-AW**	**SS-2-AW**	**SS-3-AW**	**SS-4-AW**	**SS-5-AW**	**SS-6-AW**	**AVG**
Copper	µg/L	2.8	<2.5	2.4	2.3	<2.3	2.6	<2.5
Lead	µg/L	<0.20	<0.086	<0.086	<0.086	<0.091	<0.089	<0.11
Zinc	µg/L	<7.5	<7.0	<6.8	<6.5	<6.9	7.6	<7.1
Total TPH C6-C44	µg/L	<45	<44	<44	<45	<49	<44	<45
Total PAHs	µg/L	<0.39	<0.20	<0.20	<0.20	<0.20	<0.20	<0.23
Total Butyltins	ng/L	<4.3	<3.2	<3.2	<3.2	<3.2	<3.2	<3.3
Total PCBs (Aroclor)	µg/L	<0.12	<0.097	<0.097	<0.097	<0.097	<0.097	<0.10

Note:

Calculated values are based on summed averages for n=8 sampling events (July 2008 through January 2011) and include estimated and/or non-detect data.

These values are provided only as a basis for trend comparison and approximate level of detection, not as absolute concentrations.

AW=Ambient Water, SS= Sampling Station, PAHs-Polyaromatic Hydrocarbons, PCB- Polychlorinated Biphenyls

TPH- Total Petroleum Hydrocarbons

4.0 DISCUSSION

Overall, the concentrations of COCs observed in sediments were well below action levels, providing the primary line of evidence that the cap is effectively containing COCs. Since testing results were predominately near or below method detection limits, in particular for organic constituents, the value of a robust statistical analysis was diminished. In addition, the variability of quantifiable results increases as values approach the method detection limits, thereby rendering significant differences difficult to discern. Subjective trend analysis (comparing any detected or estimated results at a given location to other strata at the same location) did not yield any significant or reproducible spatial trends. The prevalence of low and non-detected levels of COCs also made temporal trend analysis generally inconclusive. For this reason, summary tables averaging the results for all eight events were deemed the most useful presentation of data for establishing overall concentration trends spatially.

There were a few exceptions where a majority of the concentrations of COCs were above reporting limits, such as metals in sediments. In these cases, a standard deviation was calculated as an indicator of temporal variability, and to provide a better quantitative indicator of effectiveness of the cap at retaining COCs. These results are detailed separately by cap area and sample matrix below.

4.1. Engineered Cap: Sediments

Concentrations of all metals (copper, lead, and zinc) in the engineered cap sediments were above method reporting limits, but were generally 1–2 orders of magnitude below the CAO action levels (Table 2) and in the low parts per million (ppm) range.

Total butyltins and total PCBs were non-detectable in all samples analyzed. Approximately 10 percent of the samples contained low levels of PAHs, primarily naphthalene or methylated derivatives of naphthalene. Total PAHs were 20 times lower than action levels. Trace levels of naphthalene were found in several laboratory and field blanks, indicating possible low-level field and laboratory contamination. Approximately two percent of the samples had detectable levels of TPH. A single TPH concentration of 32 mg/kg for one of the baseline samples (SS-6-S) was above the sediment action level of the CAO for this measure (14 mg/kg). It is hypothesized that the TPH exceedance in the engineered cap represented either random contamination of the source sand or TPH introduced into the cap materials during the initial construction/installation of the sampling stations. No other TPH results were observed above the action level threshold during the subsequent seven sampling events.

4.2. Engineered Cap: Pore Water and Ambient Water

As noted, there are no action level thresholds for seawater constituents in the permit. Copper and zinc were detected much more frequently in ambient water (93 and

77 percent of samples analyzed, respectively) than in pore water (10 and 25 percent, respectively). This provides a second line of evidence that metals are effectively binding to sediments within the cap. Lead was not detected in either pore or ambient water samples.

Results for ambient water samples showed copper in 93 percent of samples, and detectable concentrations of zinc in 77 percent of samples. Concentrations of these metals were further evaluated for temporal variability. The average concentrations (in parts per billion [ppb]) and calculated standard deviation for these metals for all six stations for all eight sampling events was 2.50 ± 0.88 for copper and 7.06 ± 2.73 for zinc. Though these results represent field and laboratory variability, the ambient concentrations are statistically well above the average concentrations of pore water for copper and, to a lesser but notable degree, zinc. The low standard deviation of these metal concentrations over time also indicates relatively stable water column concentrations. These results support the assertion that sediments act effectively as a "sink" for copper and are consistent with studies measuring net losses of copper from the water column to the sediment (Chadwick et al., 2004).

No butyltins or PCBs were detected in ambient or pore waters. Detectable PAHs were present in approximately 10 percent of the pore water samples but in none of the ambient water samples. These results indicate the potential presence of trace concentrations of PAHs within the cap despite the overall lack of detectable concentrations in the sediments themselves. Similarly, TPH was detected at low frequency (21 and 5 percent) in pore water and ambient water, respectively. These results are consistent with the pattern of results for PAHs, indicating negligible residual fuel in the low (<0.4) parts per billion range.

4.3. Habitat Cap: Sediments

All metals (copper, lead, and zinc) were present in habitat cap sediment samples at concentrations above the reporting limits. Metal concentrations were 1.5–2.2 times higher in the habitat cap surface sediments (ST) when compared to the bottom (SB), -9 to -12 inch sediment push core segment. These higher concentrations at the surface likely result from surface sedimentation deposited from urban runoff and other well-documented metal loading sources, such as passive leaching of antifouling boat paints (SDRWQCB, 2005; D'Anna, 2010).

No PCBs or butyltins were detected in the habitat cap sediments. TPH was detected at generally low concentrations in approximately 10 percent of the samples. TPH concentrations did, however, exceed the sediment action level in the CAO of 14 mg/kg for this constituent in two samples over the course of eight sampling events. Two surface habitat cap samples (HC-1-ST, HC-2-ST) collected in February 2010 contained 16 and 24 mg/kg TPH, respectively. Stormwater runoff appears to be the likely source of TPH since significant rainfall occurred prior to this sampling event. The outlet from Switzer Creek is also located nearby, less than 700 feet southwest from the habitat cap.

5.0 CONCLUSIONS

Results of the monitoring lend several lines of evidence to suggest that the habitat cap and the engineered cap are effectively isolating known COCs. Concentrations of organic constituents for both sediment and pore waters were, with few exceptions, reported at or below method detection limits, and well below site-specific action thresholds for sediments. These data strongly support evidence that both the habitat cap and the engineered cap are effectively isolating known organic COCs. Concentrations of COCs in pore water were similar and, in cases of copper and zinc, lower than the average concentrations in ambient water, indicating that these metals are very strongly bound to the sediments within the cap. These results provide a second line of evidence that the cap is effectively binding COCs. Analytical results for habitat cap sediments show that concentrations of metals were 1.5-2.2 times higher in the "top" surface sediments of 1-foot cores than in the "bottom" sediments within the core. These results suggest that some surface deposition is occurring on the habitat cap, but below the surface metals concentrations are significantly lower and stable. These results provide a third line of evidence that metals are tightly bound in the sediments and are not migrating from the underlying fill through the cap and to the surface.

Analytical results from the engineered cap showed similar low concentrations as observed in the habitat cap sediments, possibly indicating that sediment within the cap is effectively isolating COCs. However, these results should be evaluated relative to the inherent background concentrations in each of these sediments and to varying exposure times. Therefore these results are not directly comparable and caution is warranted in comparing the results.

Over the course of eight sampling events conducted from July 2008 through January 2011, only three total petroleum hydrocarbon results were slightly above the action level threshold. These elevated TPH results appear to be associated with contamination introduced during construction of the engineered cap, or surface deposition on the habitat cap associated with seasonal urban stormwater runoff. None of the elevated TPH results appear to be related to sources emanating from the capped sediments.

6.0 REFERENCES

California Regional Water Quality Control Board, San Diego Region (SDRWCB), 1995. Cleanup and Abatement Order (CAO) 95-21 Campbell Industries, Marine Construction and Design Company, Campbell Shipyards, 501 East Harbor Drive, San Diego, California.

California Regional Water Quality Control Board, San Diego Region (SDRWCB), 2004. Monitoring and Reporting Program No. R9-2004-0295 For The Port of San Diego, Campbell Shipyard Bay Sediment Cap, Closure and Post Closure Maintenance, San Diego Bay.

California Regional Water Quality Control Board, San Diego Region (SDRWCB), 2005. *Total Maximum Daily Load for Dissolved Copper In Shelter Island Yacht Basin, San Diego Bay.* Resolution No. R9-2005-0019 Basin Plan Amendment and Technical Report.

Chadwick, D.B. Zirino, A. Rivera-Duarte, I., Katz, C.N., and Blake, A.C., 2004. Modeling the mass balance and fate of copper in San Diego Bay. *Limnology and Oceanography,* 49(2), 355–366.

Fugro-Pelagos, Inc. 2009. Hydrographic Bathymetric Survey, Former Campbell Shipyard, Non Baseline Survey, Year 1, San Diego, California.

D'Anna, H.J., 2010. "A spatial-temporal analysis of copper and zinc from antifouling paint in Pier 32 Marina, National City, California." Thesis, San Diego State University. San Diego, California.

Ninyo and Moore, 2005. Long Term Monitoring and Reporting Plan Sediment Remediation and Aquatic Enhancement Project, Former Campbell Shipyard, San Diego California. RWQCB No. LD: 06-0990.02.

Indian River County – Sector 3 Beach and Dune Restoration Project

Michael Walther, P.E., M.S., D.C.E.[1] and Tem Fontaine. E.I., M.S.[2]

[1] Coastal Tech, 3625 20th Street, Vero Beach, FL 32960; PH 772-562-8580; FAX 772-562-8432; email: mwalther@coastaltechcorp.com

[2] Coastal Tech, 3625 20th Street, Vero Beach, FL 32960; PH 772-562-8580; FAX 772-562-8432; email: tfontaine@coastaltechcorp.com

ABSTRACT

In 2010, Indian River County initiated restoration of the 6.6 miles of beach and dune known as the Sector 3 Project, which utilized previously untried technologies in that the Project:

- was innovatively designed to avoid impacts to nearshore hardbottom,
- was bid to allow construction via use of an offshore borrow area or upland sand mines as alternate sand sources, and
- employed innovative sand mining processes to construct the Project meeting stringent sand quality control specifications.

The Project is presented as a case study to demonstrate:

- the nuances of the design and construction,
- comparison of the predicted performance and that reflected in monitoring data, and
- conclusions in the form of lessons learned relative to coastal engineering practices for beach and dune restoration.

INTRODUCTION

As illustrated in Figure 1, Indian River County is located on Florida's east coast. The County's Atlantic coastline is a valuable natural resource that provides storm protection to upland property, recreation opportunities, and wildlife habitat. The beach and dune provide a natural buffer of protection to upland property during ocean storms. Recreation opportunities include beach use, fishing, and diving along the nearshore coquina and limestone rock outcrops or "hardbottom" that fronts most of the County's beaches. Wildlife habitat includes the beaches and dunes which provide for marine turtle nesting and the hardbottom which provide marine turtle foraging habitat. The northernmost 6 miles of Indian River County beaches are part of the Archie Carr National Wildlife Refuge which extends along 20.5 miles of beaches from Wabasso Beach in Indian River County to Melbourne Beach in Brevard County; the refuge was designated to protect sea turtle nesting habitat for the 15,000 to 20,000 sea turtles that annually within the refuge (DOI, 2008).

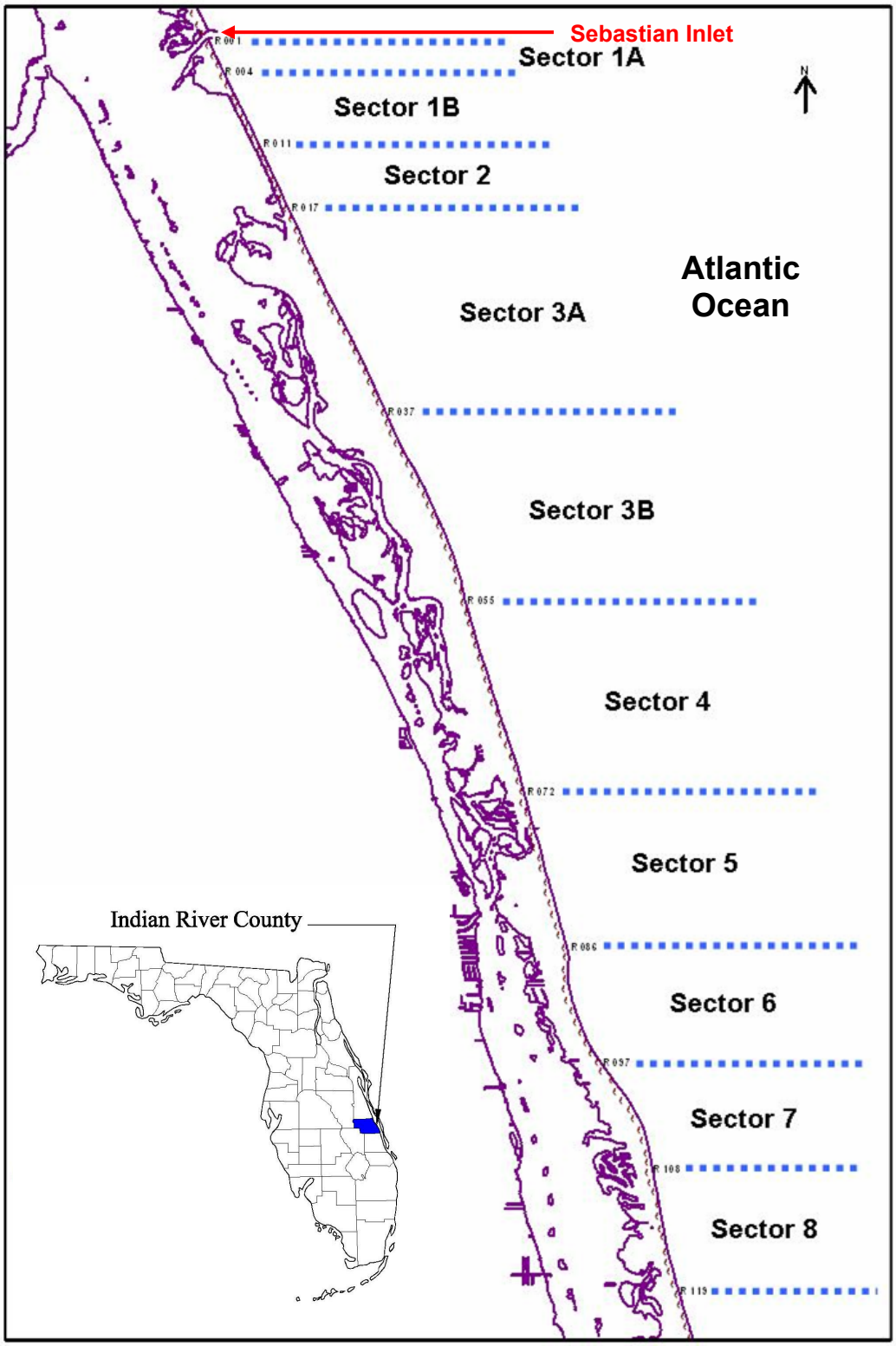


Figure 1. Location Map with Sector Boundaries

Indian River County developed and adopted its first *Comprehensive Beach Preservation Plan* in 1988; the Plan was updated in 1998 and again in 2008 (Coastal Tech, 2008a). The Plan identifies the placement of beach-compatible sand as the primary management strategy to address beach erosion. The Plan divides the County into eight planning Sectors to reflect physical and jurisdictional boundaries as illustrated in Figure 1.

The County's 22.4 miles of Atlantic Ocean beaches are located immediately south of Sebastian Inlet. Previous studies (FDEP, 2008) have identified that net longshore transport is directed to the south and that Sebastian Inlet creates a longshore transport deficit along County beaches on the order of 90,000 cubic yards per year which causes erosion of up to 55,000 feet of beach south of the inlet. From 1978 to 2002, about 2.1 million cubic yards of sand (≈ 56,000cy/yr) were placed on the beaches in Sector 1 via transfer of sand across Sebastian Inlet. To offset the long term beach erosion attributable to Sebastian Inlet, the beaches in Sectors 1 and 2 were initially restored in 2003 via placement of about 536,00 cubic yards of sand; Sector 1 and 2 beaches were re-nourished in 2007 via placement of about 536,00 cubic yards of sand; it is now anticipated that beaches in Sectors 1 and 2 will be maintained by sand transfer activities by the Sebastian Inlet District, which maintains the inlet and is now charged by Florida regulations to offset inlet effects. Sector 7 beaches were initially restored in 2007.

From 1978 to 2007, over 62,000 cubic yards of sand were placed in Sector 3 to restore dunes eroded during storm events. During 2004 and 2005, County beaches were again severely impacted by several hurricanes which caused significant beach erosion in Sector 3. The purpose of the Sector 3 beach and dune restoration project is to:

- offset the long-term sediment deficit attributable to Sebastian Inlet,
- restore and maintain recreational beach,
- restore/maintain beach habitat for marine turtles and shore birds, and
- provide storm protection for upland property and infrastructure.

AVOIDANCE OF HARDBOTTOM

In concert with the formulation of design criteria for the Sector 3 Project, Indian River County prescribed that the Project should have "no impact" upon nearshore hardbottom via burial by placed sand. Florida regulations mandate that unavoidable impacts to nearshore hardbottom attributable to beach restoration must be mitigated – commonly at cost exceeding $500,000 per acre of hardbottom impacts. By adoption of the "no impact" criteria, the County responsibly sought to preserve existing hardbottom and concurrently avoid mitigation costs. However, this "no impact" criteria also posed a limitation on the potential extent of sand fill placement and correspondingly limited the extent of upland protection afforded by the Project.

Throughout most of Indian River County, exiting hardbottom parallels the shoreline. In Sector 3, hardbottom commonly exists within a few hundred feet to 2,000 feet seaward of the shoreline. Based on interpretation of aerial photography, a total of 3,740 acres of nearshore hardbottom habitat are estimated to exist in the County. About 729 acres of nearshore hardbottom habitat are estimated to exist in Sector 3. Hardbottom is commonly dominated by benthic communities including wormrock, low-relief algal covered rock, and algal/sponge communities (Coastal Tech, 2008b).

The design of the Sector 3 Project is intended to not impact any hardbottom and is based upon a design process which limits the placed fill template so that after equilibration, the predicted seaward position of the Equilibrated Toe of Fill (ETOF) would not be seaward of the landward edge of hardbottom. To formulate a method for prediction of fill performance, post-construction monitoring surveys at five (5) survey reference monuments within the Sectors 1 and 2 beach restoration project were analyzed to assess the accuracy of ETOF predictive methods including:

- Historical Average Profile Translation,
- U.S. Army Corps of Engineers SBEACH cross-shore transport model, and
- Dean Equilibrium Profile.

The Dean equilibrium profile method is applicable to that portion of the beach profile below the "shoreline", therefore the chosen elevation of the "shoreline" effects the cross-shore location of the ETOF. A lower elevation "shoreline" would predict an ETOF landward of a higher elevation "shoreline". In order to further assess the Dean equilibrium profile method, four (4) different elevations were specified as the "shoreline" and the Dean equilibrium profile method was applied to each of these elevations for the five (5) Sector 1&2 profiles. The MLW, MSL, and MHW elevations were obtained from historical tide data maintained by NOAA Tides& Currents (2007) at the Vero Beach (Ocean) tide station 8722105. The following elevations are herein assessed as the shoreline for application of the Dean Equilibrium Profile:

- MLW (-1.34 ft NGVD) - at NOAA tide station 8722105
- -1.0 ft NGVD (as applied by ATM)
- 0.0 ft NGVD
- MSL (+0.35 ft NGVD) - at NOAA tide station 8722105
- MHW (+2.04 ft NGVD) - at NOAA tide station 8722105

Figure 2 illustrates the measured profile and the profile predicted by the Dean Equilibrium Profile method for the various assumed shoreline elevations.

Based on the analysis described above, on average:

- The Historical Average Profile Translation method under-predicted the measured ETOF by 24.3 feet.
- The SBEACH model under-predicted the measured ETOF by 20 feet.
- The Dean Equilibrium Profile method with the MSL "shoreline" provides the best estimate of the measured ETOF (within 0.2 feet) and was used to design the Project.

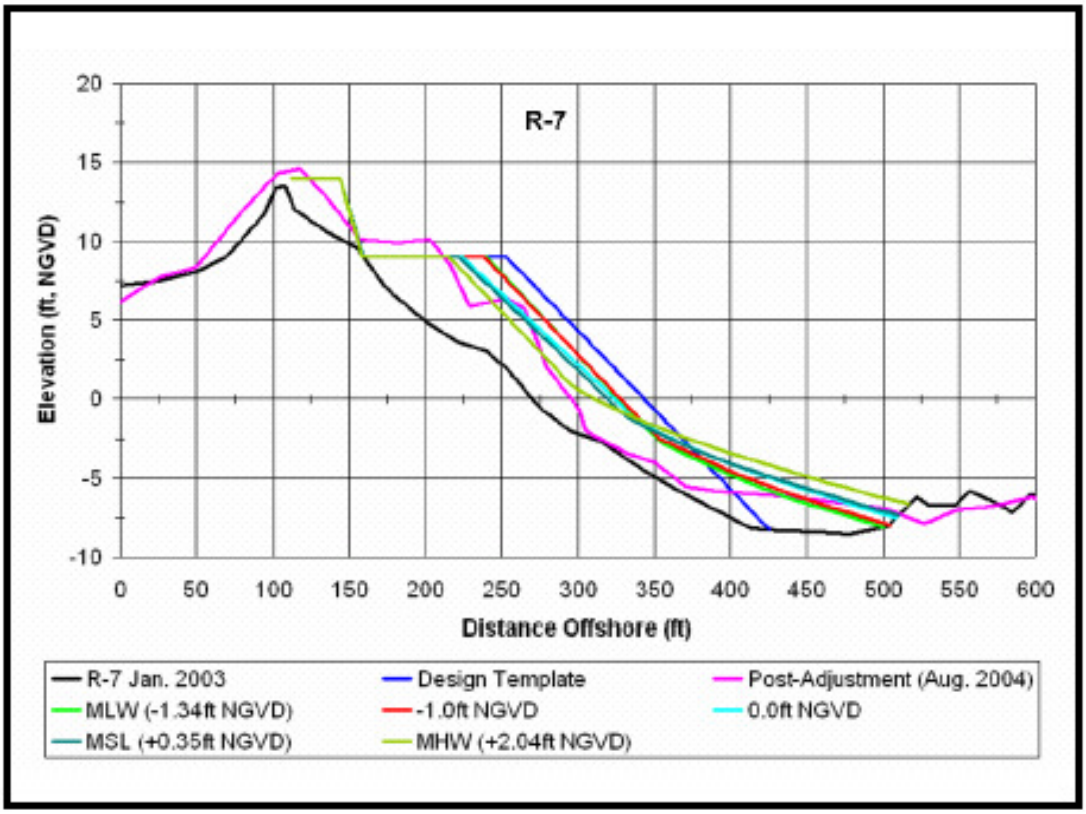


Figure 2. Sector 1 Design Template at R-7with Predicted & Measured Profiles

ALTERNATE SAND SOURCES

Native beach sand in northern Indian River County is characterized by medium-grained sand with 0.82 to 2.00% gravel, 0.27 to 1.68% fines, a mean grain size of 0.38 0.50mm, a median grain size of 0.43mm, 39.6 to 60% carbonate, 0.9% organics, and a Munsell color of white to pale brown (10YR 7/2-3 to 10 YR 8/1) (Coastal Tech, 2008b). The Sector 3 Project was originally designed to be constructed via placement of 472,000 cubic yards of sand obtained from an offshore borrow area as the sand source; this borrow area was previously used by the County for beach restoration and nourishment in Sectors 1, 2, and 7. This offshore borrow area is located about 10 miles offshore; sand within the borrow area is characterized by poorly sorted, medium-grained sand with 2.0% gravel <1% fines, a mean grain size of 0.48mm, a median grain size of 0.42mm, 55.7 to 80.2% carbonate, 1.5 to 2% organics, a Munsell color of light gray to light brownish gray (10YR 6/1 to 10 YR 7/1) and an overfill factor of 1.02 (Coastal Tech, 2008b).

During the process of seeking state and federal permits for the Project, local truckers and sand suppliers requested that the County allow construction via use of sand from an upland sand source to provide local jobs and a corresponding economic stimulus. In response to these requests, the Indian River County Board of County Commissioners voted to allow the Project to be constructed via use of either an

upland or offshore sand source. The state and federal permit applications were amended and the bid documents were developed to require any bidders proposing an upland sand source to include geotechnical data with their bid package to assess the compatibility of the proposed upland sand sources with the existing native beach. Although competitive bids were received for use of the offshore borrow area, the County Commission selected a contractor (Ranger Construction Industries, hereafter referred to as Contractor) to construct the project using two upland sand sources described as follows:

> The Ranch Road mine is located approximately 10 miles from the Project fill area and contained in situ material characterized by fine-grained sand including layers of well sorted and poorly sorted sand, with an average of 7.57% fines, a mean grain size of 0.36mm with an available volume of approximately 625,000 cubic yards of sand. The Ranch Road mine proposed via his bid to process the in-situ material to provide beach sand fill characterized by poorly sorted, medium-grained sand with 1.35% gravel, 0.55% fines, a mean grain size of 0.38mm, a median grain size of 0.33mm, 11% carbonate, a wet Munsell color of light gray (10YR 6/2 to 10YR 7/1.5) and an overfill factor of 1.10.
>
> The Fischer 86th street mine is located approximately 18 miles from the project area and contained an in situ sand characterized by well sorted, fine-grained sand with an average of 5.67% fines, a mean grain size of 0.32mm with a volume of approximately 4.9 million cubic yards of material. The Fischer 86th Mine proposed via his bid to process the in-situ material to provide beach sand fill characterized by poorly sorted, fine-grained sand with 1.88% gravel, 1.48% fines, a mean grain size of 0.39mm, 12.57% carbonate, 0.69% organic, a dry Munsell color of white (10 YR 8/1) and an overfill factor of 1.04.

As compared to the offshore borrow area, the more fine sand available from the upland sand mines would produce:

- a less steep adjusted slope with a more seaward ETOF, and
- undesirable hardbottom impacts – in conflict with the County's "no impact" design criteria.

To avoid impacts to the existing nearshore hardbottom, the more fine sand available from the upland sand mines – as bid - would require a reduced fill template and a corresponding reduction in the total fill quantity. It was determined that with use of the upland sand as bid, the total fill quantity of 472,000 cubic yards as originally proposed would be reduced by 26% to 350,000 cubic yards. This reduction in sand fill volume was determined to be unacceptable by the County Commission, who directed that the Project be constructed to the full template as originally proposed for the offshore borrow area. The proposed fill quantity was later increased to 586,000 cubic yards to address ongoing erosion as reflected in survey data obtained in late September 2009. In consultation with the Contractor, it was determined the only way to achieve the total proposed fill quantity would be for the Contractor is modify his mining processes to produce sand equivalent or better than that available in the offshore borrow area – relative to median grain size and overfill factor.

SAND MINING PROCESS

It was determined that the sand (89,482 cy) as bid from the Fischer mine could be used to construct the proposed landward dune features without any adverse impacts to nearshore hardbottom. To produce the desired beach quality sand for the balance of the proposed sand fill (496,518 cy), the Contractor developed a mining process for sand from the Ranch Road mine that employs (a) dredging to "wash" and remove the excess fines, and (b) screening to remove the coarse fraction.

As part of the negotiated Construction Contract and the state permits, the Contractor was held to a strict "Sediment QA/QC Plan" summarized in Table 1 (Coastal Tech, 2009). The Sediment QA/QC Plan also required a third party engineer to test the processed sand before it was transported to the beach at a frequency of one sample for every 3,000 cubic yards. As depicted in Table 1 below, the Sediment QA/QC Plan required the sand fill to have a mean grain-size between 0.33 mm and 0.55mm, contain less than 2% silt or shell where shell was prescribed by the percent retained on the #4 sieve. The Technical Specifications also required that the mean grain size and overfill factor of the sand fill be equivalent to or better than what was identified with the Contractor's revised bid.

Table 1. Sediment QA/QC Plan - Geotechnical Standards

Characteristic	Parameter Definition	Range	
		Minimum	Maximum
Mean grain-size		0.33 mm	0.55 mm
Carbonate Content		0%	50%
Silt Content	Passing #200 sieve	0%	2%
Shell Content	Retained on #4 sieve	0%	2%
Munsell Color	Based on moist sample	10YR 6/2	10YR 8/1

The Ranch Road revised their bid to process the in-situ material to provide beach sand fill characterized by poorly sorted, medium-grained sand with 1.48% gravel, 0.15% fines, a mean grain size of 0.51mm, a median grain size of 0.43mm, 42.35% carbonate, 0.81% organics, a wet Munsell color of light gray (10 YR 7/1) and an overfill factor of 1.0 – consistent with the Sediment QA/QC Plan.

As part of the dredging process, the Contractor first constructs a containment dike which directs the dredge slurry and excess fines back into the mine pit; Figure 3 depicts a typical containment dike at the start of dredging. To check and refine the mining process, the Contractor commonly dredged a small quantity of sand and then tested the dredged material to determine if further processing was required.



Figure 3. Dredging Process – Containment Dike

To remove the excess gravel content from the in situ sand, the Contractor utilized 3/8 inch screens and a screening machine as shown in Figure 4. The pile of material on the left in Figure 4 is the coarse fraction removed by the screen; the pile on the right is sand ready to be tested and pending favorable results, transported to the beach. Note that if the screened sand failed, the Contractor would selectively mix sand that had a high median grain size with material that had a low a median grain size to obtain beach compatible sand within the requirements of the Sediment QA/QC Plan.



Figure 4. Screening Process.

CONSTRUCTION

Once the processed sand has been tested and approved by the Contractors Third Party Engineer, the Contractor loaded the approved sand onto road trucks, and transported the sand to the Construction Staging and Access Areas. Figures 5 and 6 depict sand being unloaded from road trucks at the Wabasso Beach Construction Staging and Access Area and then loaded onto off-road trucks for hauling down the beach to the sand fill placement area.

Due to concerns relative to the potential impacts of the upland sand upon nesting marine turtles, Project construction was anticipated to occur in two phases – outside the May 1 to November 1 marine turtle nesting season. Phase 1 was expected to entail about 4.4 miles of beach fill area south of and including the mostly undeveloped portion of the Archie Carr National Wildlife Refuge; Phase 2 was expected to entail about 2.2 miles of beach fill area within the undeveloped portion of the Refuge – constructed after Phase 1 if no adverse impacts to turtle-hatchling-success were observed following Phase 1 construction.

Most of the Phase 1 fill area was constructed between February 9 and May 9, 2010; no adverse impacts to turtle-hatchling-success were subsequently observed. Phase 1 was subsequently completed between December 6 and December 16 in 2010. Phase 2 construction was initiated on February 28, 2011 and terminated on April 30, 2011 at the start of the marine turtle nesting season. In both phase of construction, a total of approximately 170,000 cubic yards of sand fill were placed. The Contractor was not able to complete 80,000 of fill placement over the northernmost 64,000 feet of the Phase 2 fill area. Indian River County is now considering options to complete the remaining portion of the Project construction between December 2011 and February 2012.

During construction, it became apparent that the processing of sand at the upland mine is the critical path for the Project construction employing upland sand sources. Trucking and grading operations were commonly on-hold while the upland mine processed sand consistent with the Sediment QA/QC Plan. Figures 7 and 8 depict the pre- and post-construction conditions near Wabasso Beach Park within the Phase 1 fill area; note the position of the Summerplace Seawall in each of these figures.



Figure 5. Road-Truck being Unloaded.



Figure 6. Off-Road Truck being Loaded.



Figure 7. Pre-Construction conditions at Wabasso Beach Park

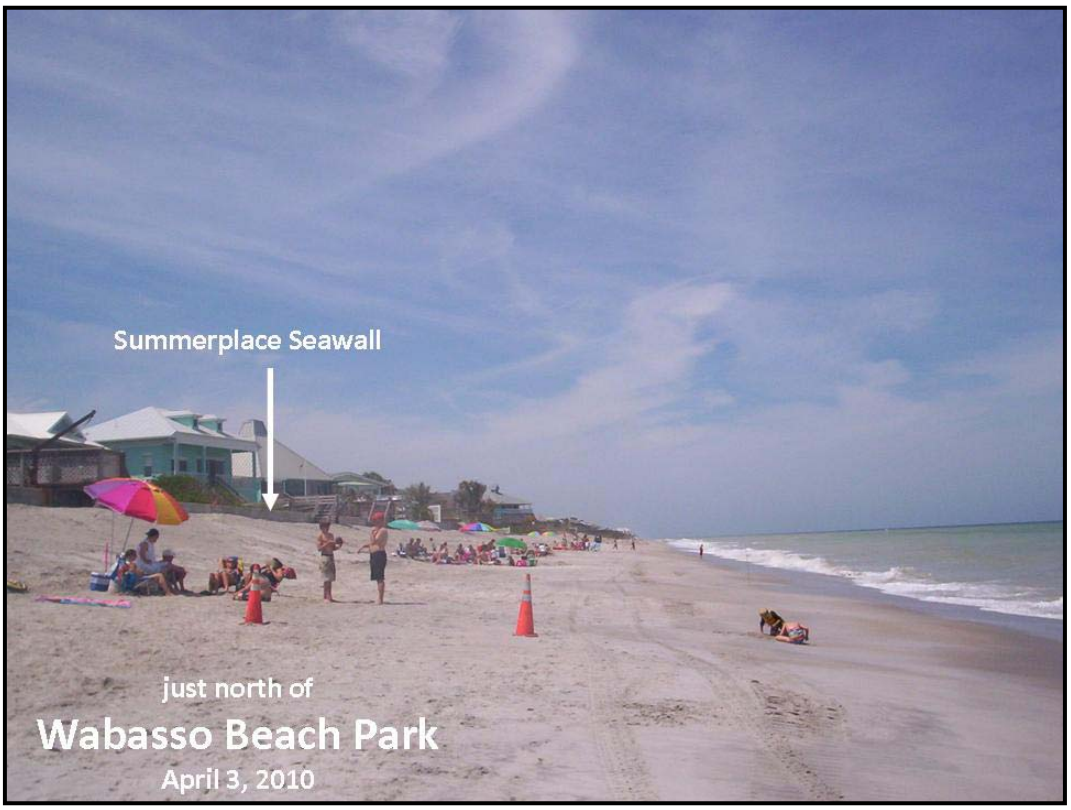


Figure 8 : Post-Construction conditions at Wabasso Beach Park

PERFORMANCE

Construction of the majority of the Phase 1 fill area was completed in May 2010. Post-construction beach profile surveys were performed in September 2010. Figure 9 illustrates the profile and ETOF as measured and predicted for survey reference monument R-37 – representative of the September 2010 surveys, which indicate:

- The entirety of the placed sand fill remained within the Phase 1 fill area boundaries.
- Over the approximately 20,000 feet of the completed Phase 1 construction fill area, the measured ETOF was (a) at or landward of the predicted ETOF with the exception of about 2,500 feet of beach, where up to 0.23 acres of hardbottom may have been impacted, and (b) on average, 9 feet further seaward that the predicted ETOF.

It is currently hypothesized that the more seaward measured ETOF is attributable to a slight change in shoreline orientation and the spreading of fill by longshore sediment processes. Hardbottom impacts will be assessed based upon surveys conducted in concert with 3 additional years of annual post-construction monitoring.

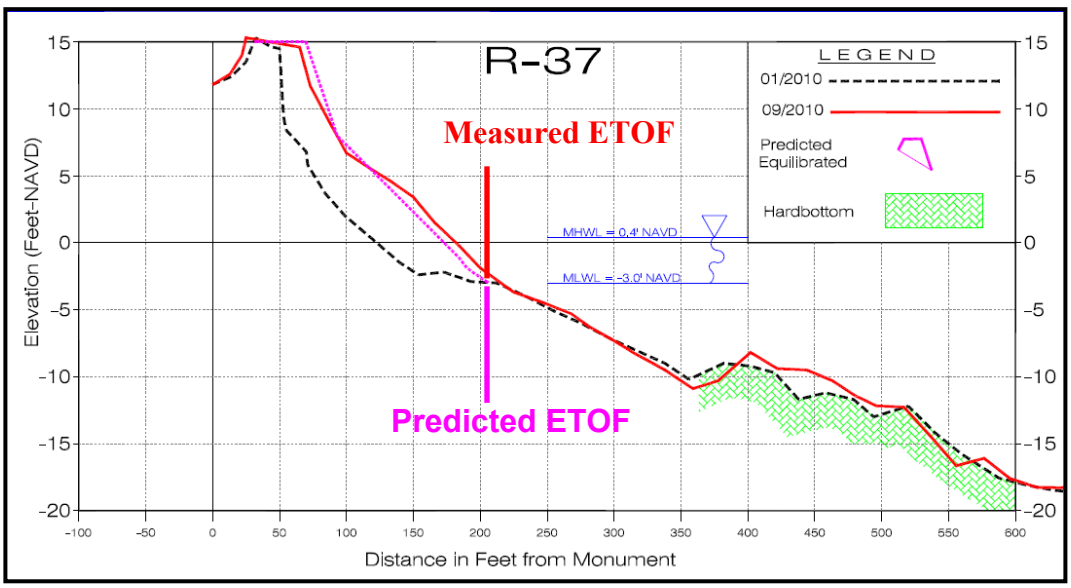


Figure 9. Measured/Predicted Profile & ETOF at R-37

CONCLUSIONS

The Sector 3 Beach and Dune Restoration Project points to the following learned lessons relative to coastal engineering practice:

- Sand from upland sand sources can be processed to remove excess silt and gravel to yield beach-compatible sand.
- The critical path for construction using processed upland sand is the mining and processing of sand at the upland source.
- The Dean Equilibrium Profile method with the MSL "shoreline" well predicts the ETOF – except where a change in shoreline orientation exists and longshore sediment transport processes may drive the ETOF further seaward.

REFERENCES

Coastal Tech (2008a). "Indian River County, Florida Beach Preservation Plan"

Coastal Tech (2008b). "Indian River County Sector 3 Beach & Dune Restoration Project Design Document"

Coastal Tech (2009). "Sector 3 Beach & Dune Restoration Indian River County, Sediment Quality Control/Quality Assurance Plan Upland Sand Source"

Dean, R.G., and Dalrymple, R.A. (2002). "Coastal Processes with Engineering Applications" Cambridge University Press. New York

Florida Department of Environmental Protection (FDEP, 2008). "Strategic Beach Management Plan"

U.S. Department of the Interior (DOI) Fish and Wildlife Service Southeast Region (November 2008). "Archie Carr National Wildlife Refuge Comprehensive Conservation Plan"

Sediment Transport Modeling and Application for Ocean Beach and San Francisco Bight, CA

H. Li[1], L. Lin[1], F. Wu[2], L. C. Andes[2], and J. G. Zoulas[2]

[1]U.S. Army Engineer Research and Development Center, Coastal and Hydraulics Laboratory, 3909 Halls Ferry Road, Vicksburg, MS 39180; PH: 601-634-2840; FAX: 601-634-3080; email: Honghai.Li@usace.army.mil, Lihwa.Lin@usace.army.mil

[2]U.S. Army Corps of Engineers, San Francisco District, 1455 Market Street, San Francisco, CA 94103; PH:415-503-6902; email: Frank.Wu@usace.army.mil, Lisa.C.Andes@usace.army.mil, James.G.Zoulas@usace.army.mil

ABSTRACT

The U.S. Army Corps of Engineers (USACE) San Francisco District (SPN) and Coastal Inlets Research Program (CIRP) are presently performing hydrodynamics, wave, and sediment transport numerical modeling study with the Coastal Modeling System (CMS) to evaluate a designated dredged-material placement site nearshore the beach erosion hot spot and onshore nourishment alternatives on Ocean Beach, California. Both model results and measurements reveal that tidal forcing is the main process in the nearshore area where the tidal current is predominantly along the shoreline. The calculated sediment transport shows more longshore movement than cross-shore shoreward the dredged-material placement site. The model result also indicates significant sediment erosion at Ocean Beach.

INTRODUCTION

Ocean Beach is located on the coast of San Francisco, California, to the south of the Golden Gate, and in the shadow of the San Francisco Ebb Tidal Delta (Figure 1). It is part of the San Francisco Littoral Cell that includes the outer ebb tidal bar of San Francisco Bay and the sandy waterfront on the north and west sides of San Francisco. High energy waves and human perturbation have induced significant sediment transport and resulted in periodic erosion at Ocean Beach adjacent to the southern-most lobe of the Ebb Tidal Delta. The erosion hotspot had threatened the structural integrity of the adjacent highway and ocean outfall pipe.

The SPN has designated a temporary nearshore dredged-material placement site located about 750 m offshore and slightly south of the erosion hot spot, in depths between approximately 9 and 14 m (Figure 1). This site, known as SF17, was chosen because strong tidal current and coastal waves in the area may have the potential to move the sediment toward the beach that was experiencing substantial erosion. The nearshore placement site can prevent further scour on the exposed outfall pipe. The U.S. Geological Survey (USGS) has monitored and studied the sediment transport and morphology change at the designated site since May 2005 (Barnard et al. 2009). Up to the present day, a total sediment load of about 700,000 m^3 has been placed in SF17, approximately

400,000 m^3 of which has remained within the placement site.

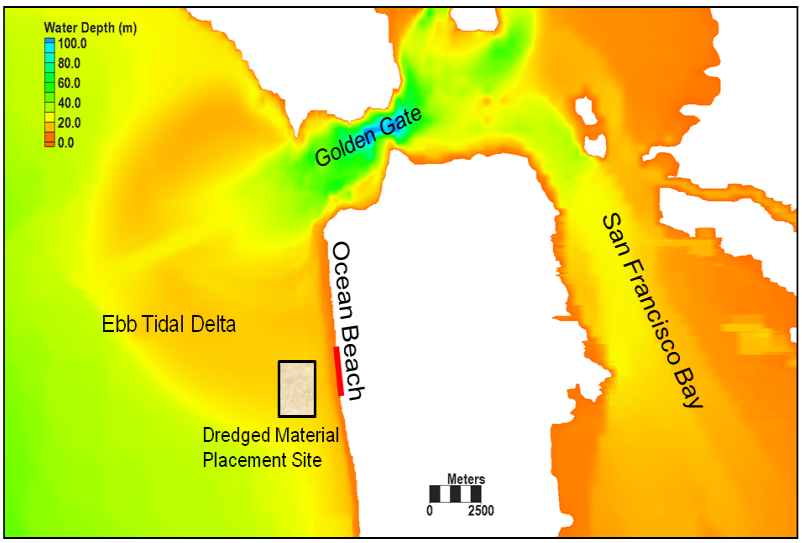


Figure 1. Study area.

OBJECTIVES

To remediate beach erosion and shoreline recession at Ocean Beach, it is necessary to designate a permanent nearshore placement location for a beneficial reuse of dredged material. USACE/SPN and USACE/CIRP are performing hydrodynamics, waves, and sediment transport numerical modeling study with the Coastal Modeling System (CMS) to evaluate the feasibility of such a placement site and the designated dredged-material placement site nearshore Ocean Beach. The offshore location was chosen because the strong tidal current and open-ocean waves in the area have the potential to feed sediment toward the beach experiencing erosion. The nearshore placement site may prevent further scour on the exposed outfall pipe.

FIELD DATA ASSEMBLY

A wide range of field data, including water levels, waves, current, and topographic mapping, have been collected by SPN and USGS at Ocean Beach and in San Francisco Bight from 2004 through 2010. The assembled data is applied for the CMS setup, and the model calibration and verification.

In January 2010, a set of bathymetric data were collected at Ocean Beach along 18 shore-normal transects by the Coastal Profiling System (CPS) (Barnard et al. 2009). Besides the CPS data, the offshore bathymetry data were extracted from GEOphysical DAta System (GEODAS) coastal grid (NGDC 2009) and multi-beam bathymetry surveys. Those data were used to configure the CMS models. Figure 2 shows the locations of the 18 transects and two CPS sample surveys of Transect 13.

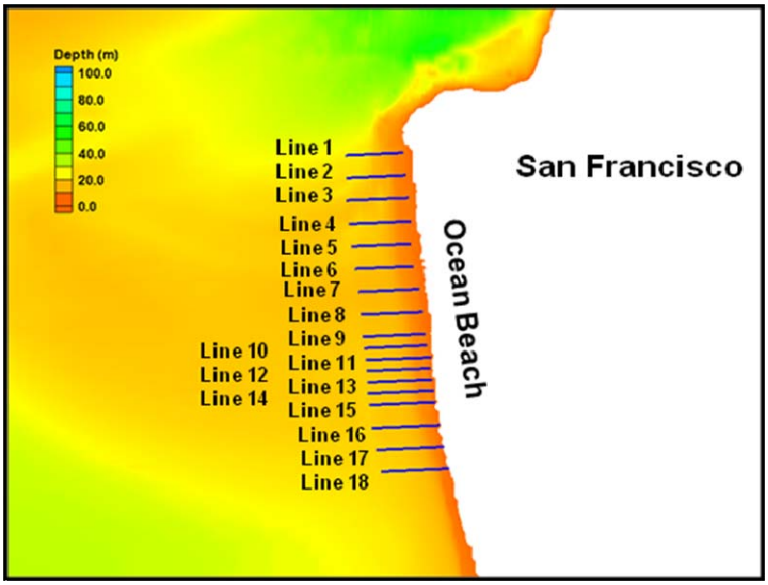


Figure 2. The CPS (18) transects and sample survey data of Transect 13.

Local water surface elevation data are available from two NOAA coastal stations 9415020 (Point Reyes) and 9415144 (Port Chicago), http://tidesandcurrents.noaa.gov (Figures 3 and 4). These water level data indicate a mixed, predominately semi-diurnal tidal regime at the study area. The mean tidal ranges (mean high water – mean low water) at Point Reyes and Port Chicago are 1.19 and 1.12 m, respectively.

Directional wave data are available from two Coastal Buoys No. 46026 and No. 142 maintained by the National Data Buoy Center (NDBC, http://www.ndbc.noaa.gov) and Coastal Data Information Program (CDIP, http://cdip.ucsd.edu), respectively (Figures 3). Figure 5 shows wave information collected at Buoy 46026 in June 20-29, 2005. The predominant waves are from the west-northwest direction. Extreme large waves are rare as more than 98 percent of the wave population shows a height less than 2 m. The average wave height and peak wave period are 0.9 m and 9 sec, respectively. Wind information is collected at Buoy 46026 and is characterized by the west-southwest direction. The mean wind speed is approximately 4 m/sec with an extreme value of 10 m/sec (Figure 6).

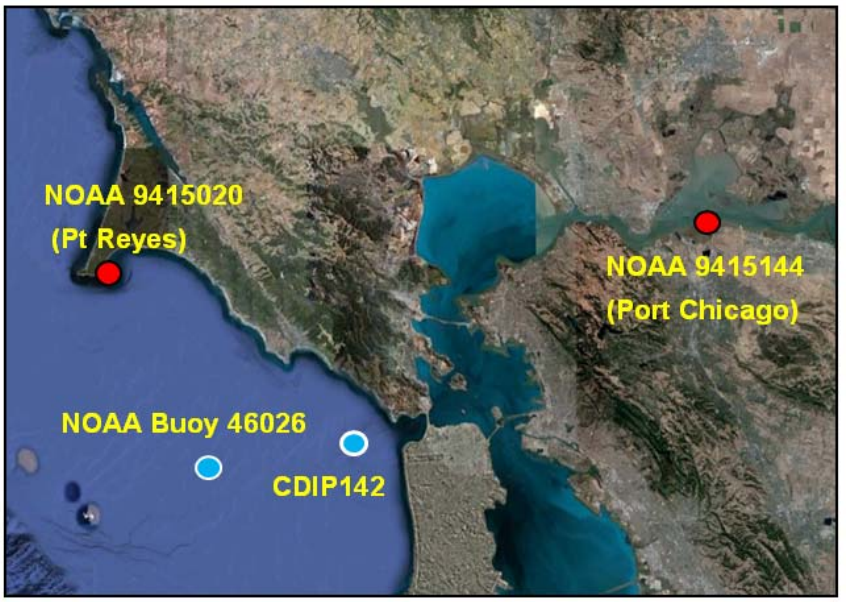


Figure 3. Locations of coastal buoys and tide gages.

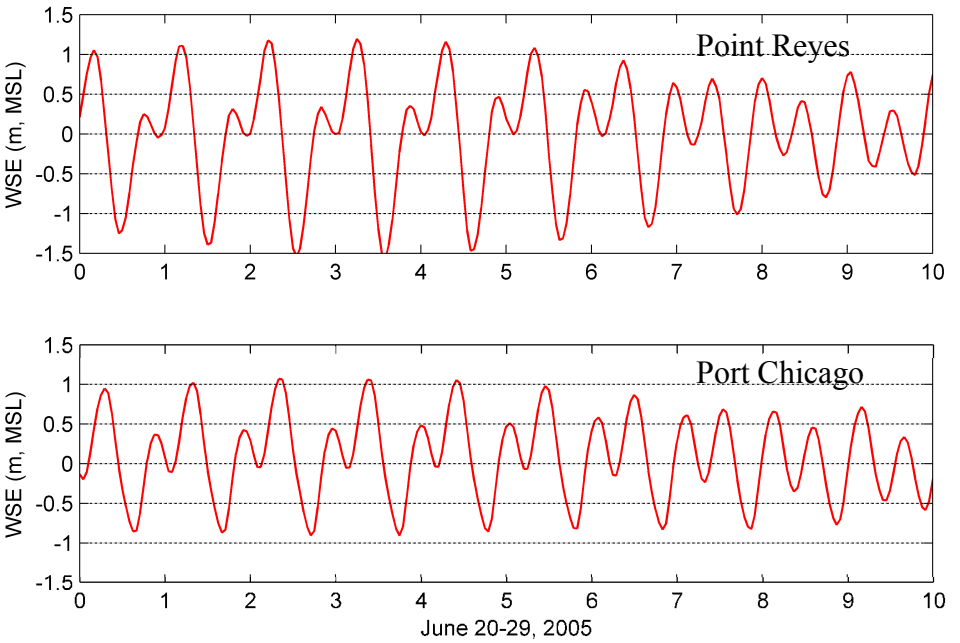


Figure 4. Water surface elevations at Point Reyes and Port Chiacago, CA.

Four Acoustic Doppler Current Profilers (ADCP) were deployed during the summer and winter of 2005 and 2006 (Barnard et al. 2009) to measure current, waves, and water levels. Current and water level data at three nearshore ADCPs (Sites 1, 2, and 3) were used to calibrate the CMS models (Figure 7). The offshore ADCP (Site 4) is too close to the CMS seaward boundary and, therefore, the data collected is not used in the study.

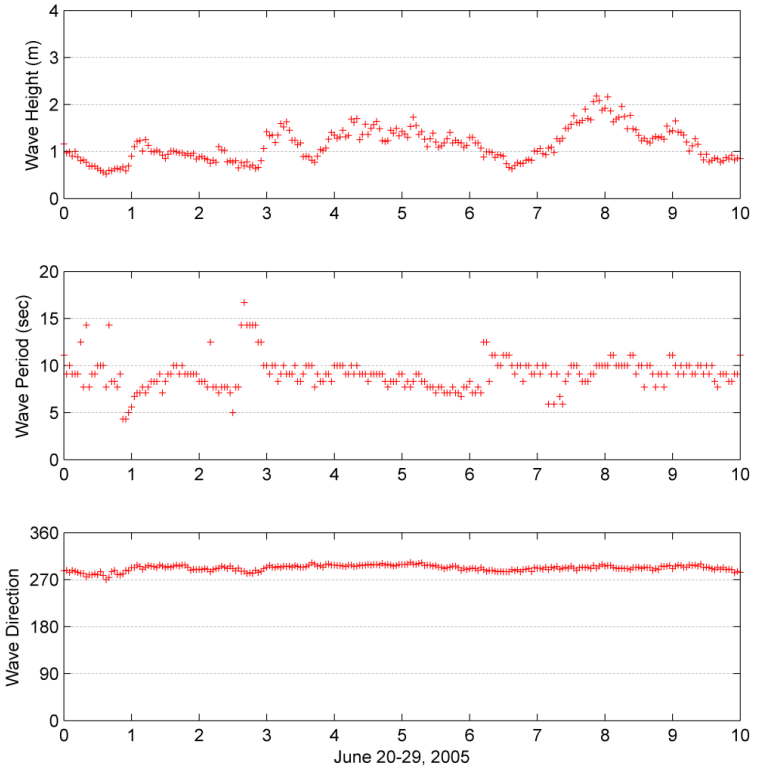


Figure 5. Wave information collected at NDBC Buoy 46026.

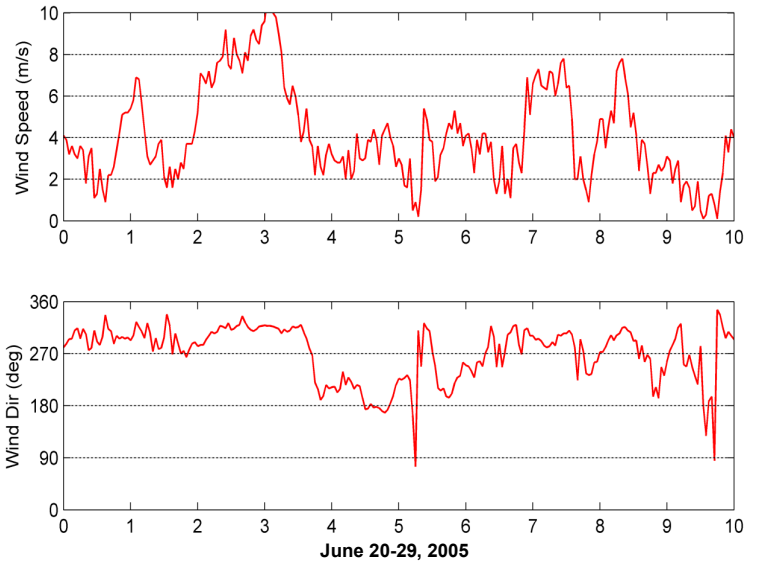


Figure 6. Wind data collected at NDBC Buoy 46026.



Figure 7. Locations of nearshore ADCPs.

COASTAL MODELING SYSTEM (CMS)

The CMS is a suite of hydrodynamics, wave, and sediment transport models including CMS-Flow and CMS-Wave, http://cirp.usace.army.mil/wiki/CMS. Physical processes calculated by CMS-Flow are circulation, sediment transport, and morphology change (Buttolph et al. 2006). CMS-Wave is a two-dimensional wave spectral transformation model that contains approximations for wave diffraction, reflection, wave transmission, wave run-up, and wave-current interaction (Lin et al. 2008). In the present study, CMS-Flow and CMS-Wave were applied to simulate coastal, estuarine, and wave-induced longshore and cross-shore mass transport processes, and to evaluate sediment transport and volume change at the nearshore placement site and Ocean Beach.

Figure 8 shows the CMS rectangular grid domain that consists of 300 × 541 cells, covering Ocean Beach and San Francisco Bay. The model domain extends approximately 50 km alongshore and 20 km offshore San Francisco Bight. The water depth at the offshore boundary is 80 m. The maximum water depth reaches to more than 100 m at the Golden Gate area. A variable-resolution grid system was created to discretize the nearshore and offshore regions, which permits coarser grid resolution of 400 m in the offshore and finer resolution of 20 m at Ocean Beach.

The CMS is driven by the forcing of the time-dependent open-boundary water surface elevations, offshore incident wave spectra, and buoy wind data. The water surface elevations were specified at open boundary using the data at Point Reyes (NOAA 9415020) and Port Chicago (NOAA 9415144). Wave spectra and wind forcing data were retrieved from NDBC Buoy 46026.

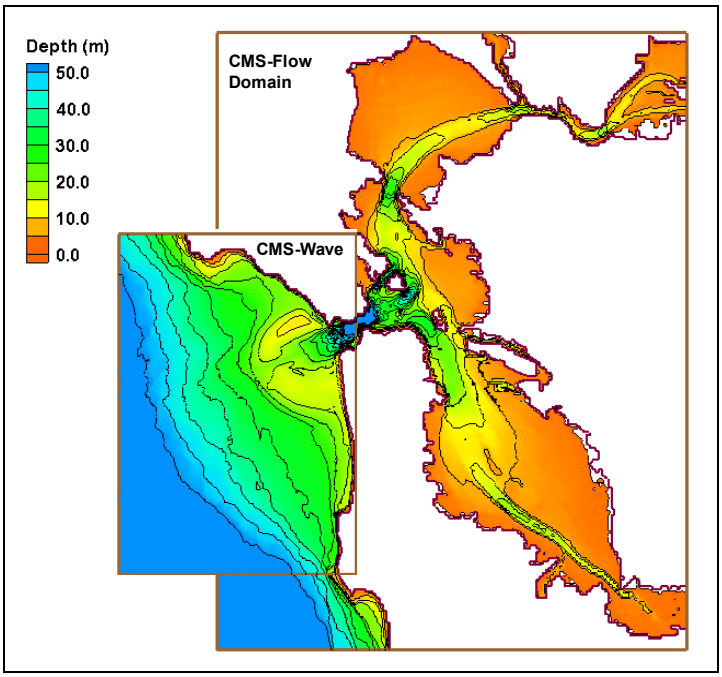


Figure 8. CMS-Flow and CMS-Wave domains.

RESULTS

The CMS simulation was conducted for a 10-day period of 20 to 29 June, 2005. CMS-Flow was calibrated against the ADCP measurements during this summer period, but the CMS-Wave calibration was performed against the CDIP142 buoy data during January 2009 because no wave data were available at this location before 2007. Figure 9 shows that the CMS-Wave results and the measured data at CDIP142 for January 2009. The wave transformation results show a good agreement with the measured wave parameters.

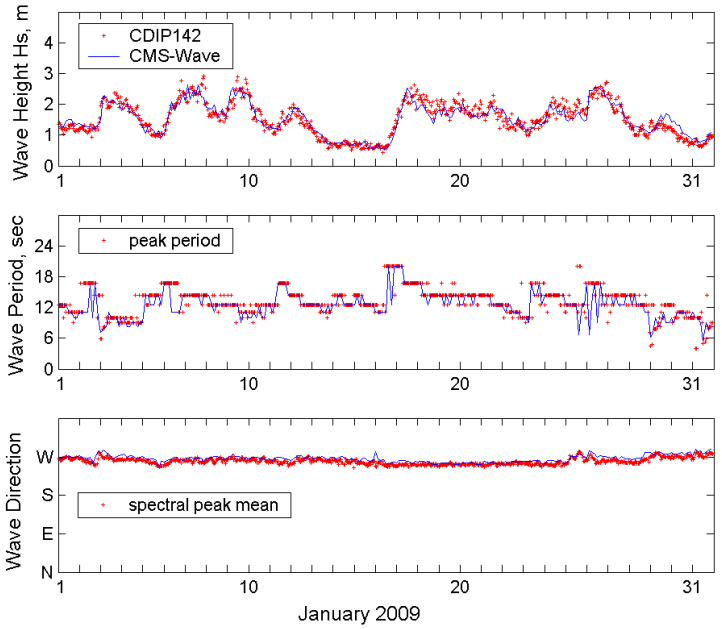


Figure 9. Measured wave parameters at CDIP142 and CMS-Wave results, January 2009.

Figure 10 shows water surface elevation comparisons at Site 3 from 20 to 29 June, 2005. The calculated water levels agree well with the measurements in amplitude and phase. The correlation coefficient between the CMS and the data is 0.99, the root mean square error (RMSE) is 0.11 m, and the relative RMSE (RMSE/Data Range) is 3.8%.

Figure 11 shows the current comparisons at Sites 1, 2, and 3. The tidal current is predominantly longshore and cross-shore component is relatively small. The depth-averaged current magnitude nearshore can reach 1.0 to 1.5 m/sec north of Ocean Beach adjacent to the Golden Gate entrance. The current magnitude decreases to south along Ocean Beach approximately 0.5 m/sec in the nearshore dredged-material placement site (SF17). The CMS reproduces well the current magnitude and direction at Sites 1 to 3. Table 1 presents the correlation coefficient, RMSE, and relative RMSE (RMSE/Data Range) between the calculated and measured currents.

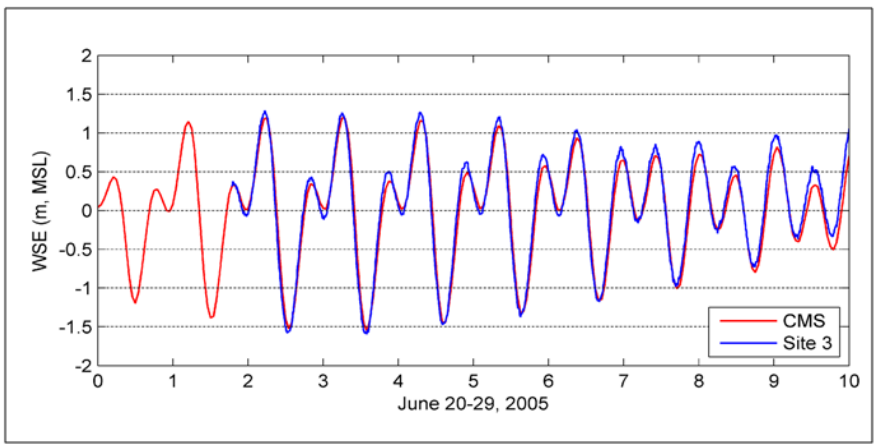


Figure 10. Calculated and measured water levels Ocean Beach, Site 3.

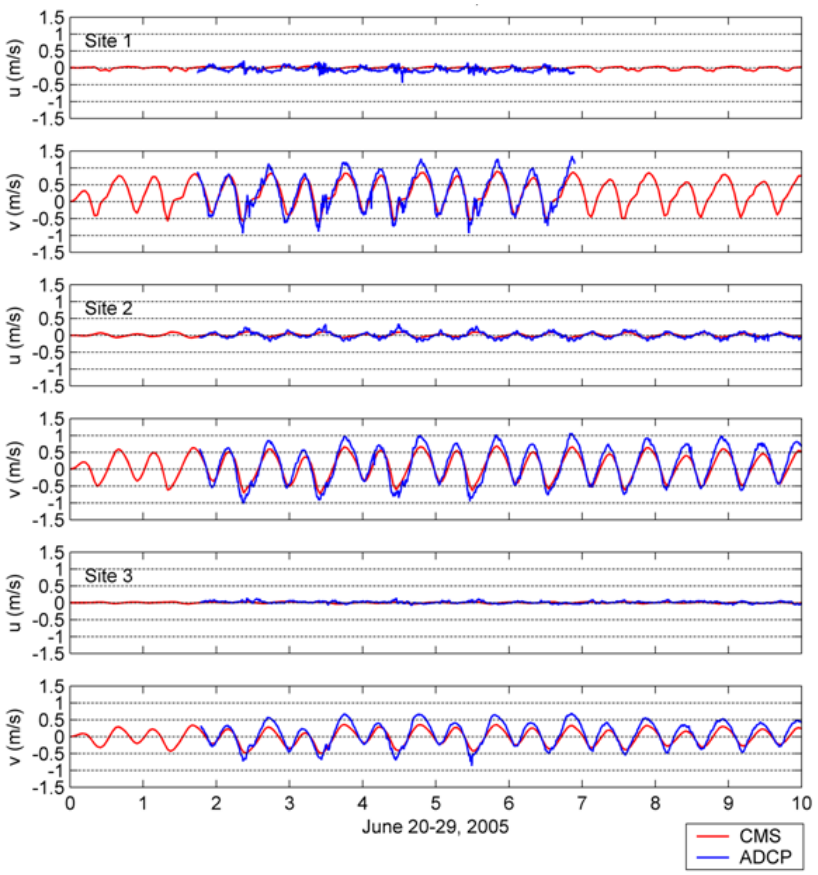


Figure 11. Calculated and Measured currents at Ocean Beach, Sites 1, 2, and 3.

Table 1. Correlation coefficients, root mean square errors (RMSE), and relative RMSEs for computed and measured longshore currents.

Site	Correlation Coefficient	RMSE (m/s)	Rel RMSE (%)
1	0.960	0.176	8.4
2	0.966	0.199	11.1
3	0.963	0.164	11.7

Figure 12 shows wave and wind data at NDBC 46013 and CDIP 142 in January 2010. With passages of winter storms from south and southwest in the study area, the peak wave height and peak wind speed are approximately 8 m and 20 m/sec around 20 January, 2010, respectively. The CMS is conducted to calculate the sediment transport and morphology change to compare with the bathymetry surveys in this period.

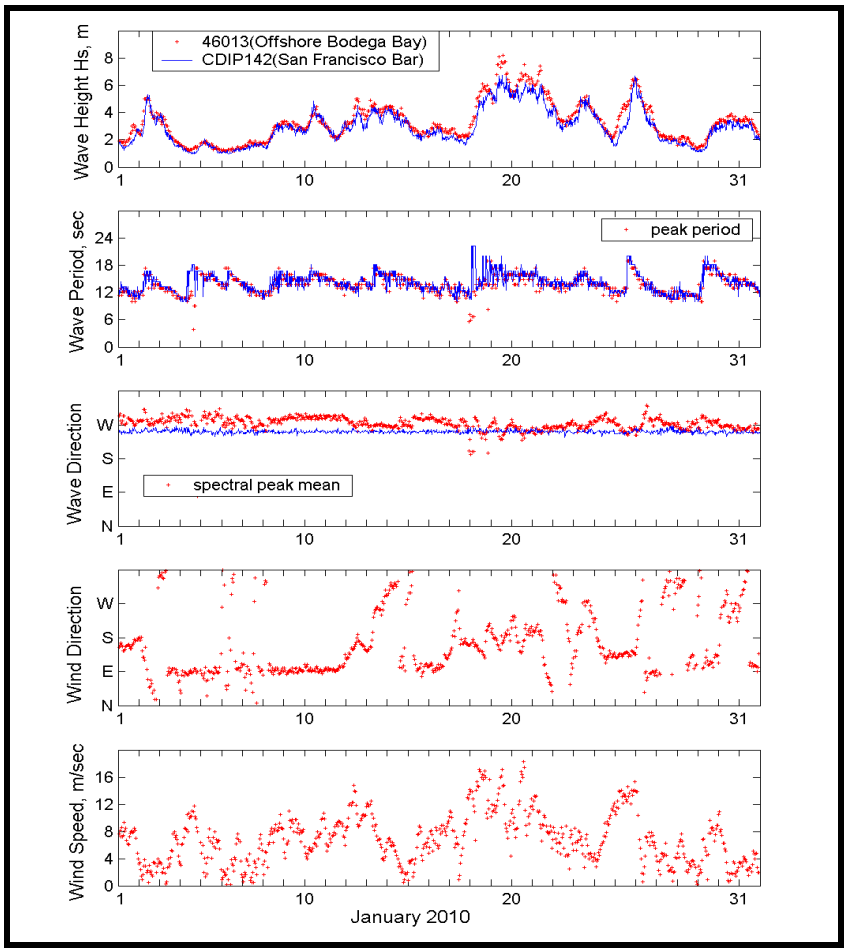


Figure 12. Wind wave data at NOAA 46013 and CDIP142 for January 2010.

Figure 13 shows the calculated morphology change nearshore Ocean Beach from a 25-day simulation of 3 to 28 January, 2010. The model result indicates that storms and coastal processes induce more erosion and accretion in the surf zone. There are clearly onshore and offshore bar movements in the nearshore coastal area. The maximum erosion and accretion are about 3 m along the shoreline. To estimate sediment volume balance, a polygon area was used for the calculation as shown in Figure 13. The calculated morphology change shows a net sediment loss of 790,000 m^3 within the area from the simulation. This calculated sediment volume loss is comparable to the CPS observation .

Sediment volume balance is calculated through the analysis within a rectangular area next to the erosion hotspot at Ocean Beach (Figure 14). The transport at the nearshore dredged-material placement site indicates the onshore sediment movement. Figure 14 shows a strong long-shore sediment transport from south to north. The sediment volume change analysis indicates that nearly half million cubic meters of materials are eroded during the winter storms. This local erosion provides primary source for the longshore transport.

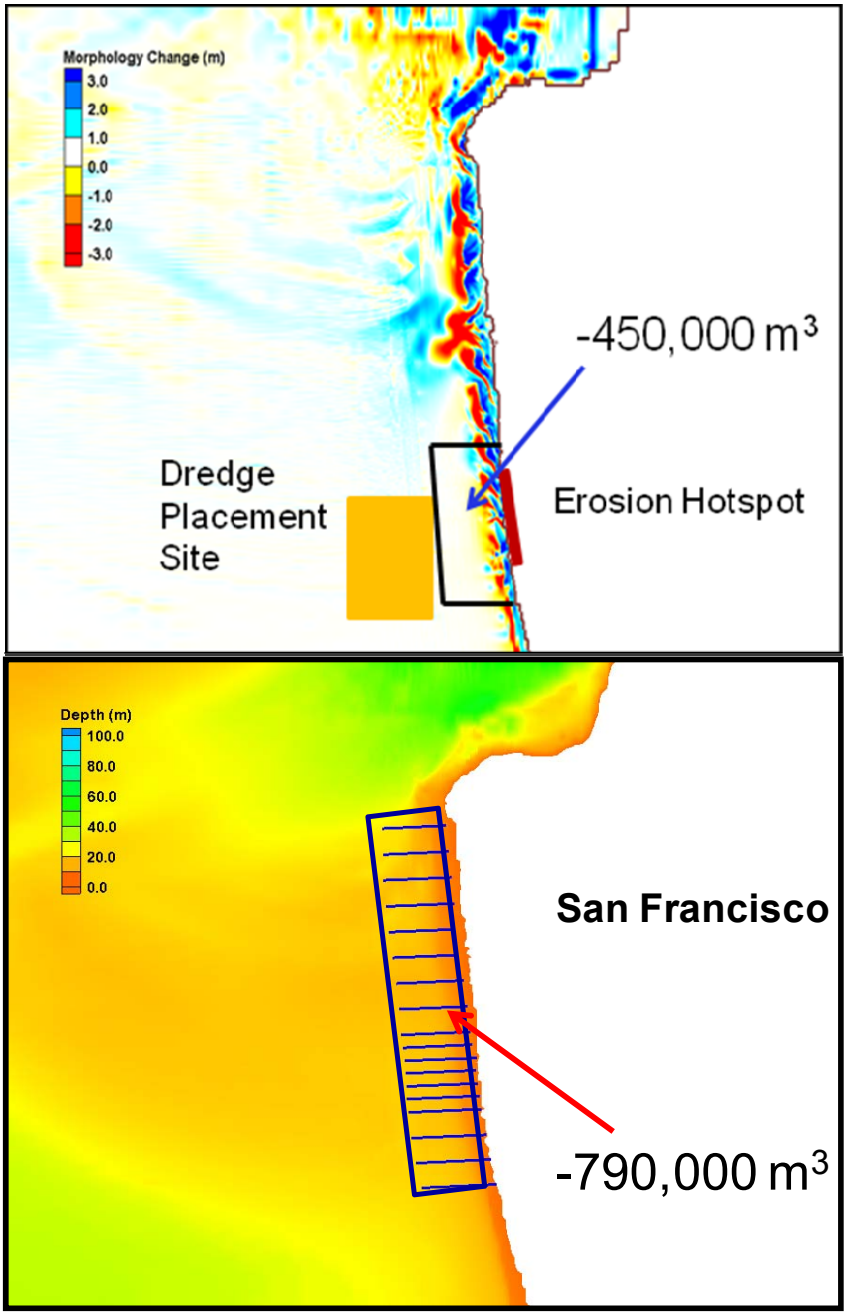


Figure 13. Morphology change and sediment balance after winter storms.

SUMMARY

A coupled wave, flow and sediment transport numerical modeling system, CMS, was applied to calculate sediment transport nearshore Ocean Beach in the San Francisco Bight. The CMS was calibrated against the measured waves, current, and water levels. The calculated sediment transport and morphology change were compared with the CPS observations.

The model results reflect a tide-dominated environment nearshore Ocean Beach during

the 10-day simulation from 20 to 29 June, 2005. The magnitude of tide-driven depth-average currents can reach 1 to 1.5 m/sec. Primary components of current are longshore whereas the cross-shore components are insignificant. Tidal currents carried sediment along the shoreline and generated significant transport from south to north during the winter month. Sediment volume change calculation indicates that sediment can move shoreward and greater erosion occurs between the Ocean Beach hotspot and the nearshore dredge placement site as winter storms passed the area. The sediment erosion rate obtained from the CMS results were validated via the sediment volume changes from the observations.

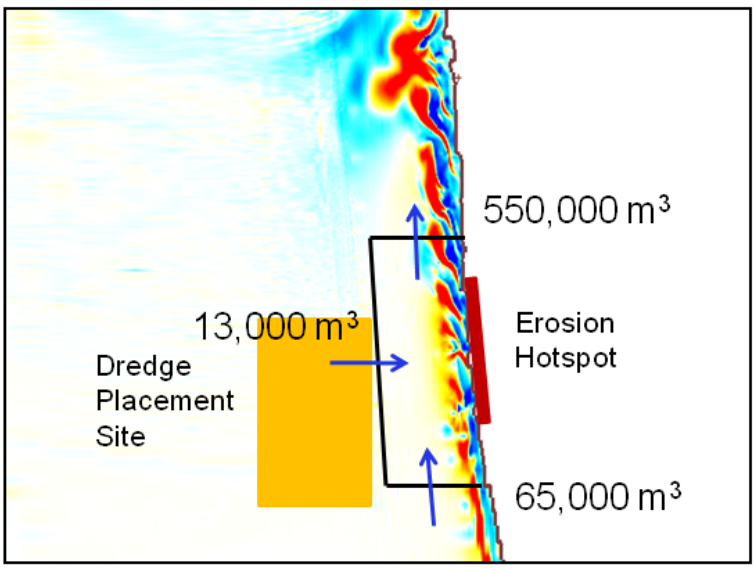


Figure 14. Sediment budget nearshore Ocean Beach.

REFERENCES

Barnard, P. L., L. H. Erikson, J. E. Hansen, and E. Elias. 2009. The Performance of nearshore dredge disposal at Ocean Beach, San Francisco, California, 2005-2007. U.S. Geological Survey Open-File Report 2008-13. http://pubs.usgs.gov/of/2008/1347/.

Buttolph, A. M., C. W. Reed, N. C. Kraus, N. Ono, M. Larson, B. Camenen, H. Hanson, T. Wamsley, and A. K. Zundel. 2006. Two-dimensional depth-averaged circulation model CMS-M2D: Version 3.0, Report 2, sediment transport and morphology change. Coastal and Hydraulics Laboratory Technical Report ERDC/CHL-TR-06-7. Vicksburg, MS: U.S. Army Engineer Research and Development Center.

Lin, L., Z. Demirbilek, H. Mase, J. Zheng, and F. Yamada. 2008. CMS-Wave: A near-shore spectral wave processes model for coastal inlets and navigation projects. Coastal and Hydraulics Laboratory Technical Report ERDC/CHL-TR-08-13. Vicksburg, MS: U.S. Army Engineer Research and Development Center.

National Geophysical Data Center. (2009). "*Bathymetry, topography and relief*," http://www.ngdc.noaa.gov/mgg/bathymetry/relief.html.

Regional Beach Restoration and Monitoring in San Diego County
A 10-Year Retrospective

Greg Hearon[1], Brady Richmond[2], and Shelby Tucker[3]

[1] Coastal Frontiers Corporation, 9420 Topanga Canyon Blvd, Suite 101, Chatsworth, CA 91311; PH: 818-341-8133; email: ghearon@coastalfrontiers.com.

[2] Coastal Frontiers Corporation, 9420 Topanga Canyon Blvd, Suite 101, Chatsworth, CA 91311; PH: 818-341-8133; email: brichmond@coastalfrontiers.com.

[3] San Diego Association of Governments, 401 B Street, Suite 800, San Diego, CA 92101; PH 619-699-1916; email: stu@sandag.org

ABSTRACT

The Regional Beach Sand Project, conducted by the San Diego Association of Governments in 2001, provided 1.6 million cubic meters of beach-quality sand to twelve receiver sites. Beach profile survey results were used to assess the shorezone changes and document the evolution of the San Diego County's beaches following the placement of the nourishment material. The analysis focused primarily on changes in shoreline position and sediment volume. The placement and subsequent dispersal of the beach nourishment material produced shoreline advances and sediment volume gains, some of which that have persisted to this day. Equally important, the RBSP demonstrated that San Diego County and its coastal cities can collaborate to implement a successful regional beach nourishment project.

INTRODUCTION

The coastline of San Diego County, California extends more than 60 miles between Orange County and the U.S.-Mexican border. The region includes parts of three littoral cells: the Oceanside, Mission Beach and Silver Strand Littoral Cells. The San Diego Association of Governments (SANDAG) conducted the Regional Beach Sand Project (RBSP) in 2001, a first-of-its-kind project that provided 1.6 million cubic meters (m^3) of beach nourishment to twelve receiver sites.

REGIONAL BACH SAND PROJECT

In 1993, SANDAG adopted the "Shoreline Preservation Strategy for the San Diego Region" as a comprehensive plan for erosion mitigation. An extensive beach building and maintenance program was proposed to provide for environmental quality, recreation, and storm protection in the coastal zone. After a number of mostly

modest beach nourishment projects were undertaken, the Regional Beach Sand Project was conceived as a more comprehensive approach to restoring the County's sand-starved beaches.

Nearly all of the pre-RBSP nourishment projects were opportunistic, utilizing sand that was derived from activities whose primary motive was other than beach replenishment. Lagoon restoration and harbor maintenance were the largest sources of this material. The non-RBSP nourishment projects conducted from 1993 to 2000 (corresponding the seven-year period between to the adoption of SANDAG's Shoreline Preservation Strategy and the inception of the RBSP) are summarized in Table 1.

Table 1. Pre-RBSP Beach Nourishment Summary, 1993 to 2000

Littoral Cell	No. of Projects	Nourishment Volume (m^3)	Average Annual Nourishment Rate (m^3/yr)
Silver Strand	5	508,000	56,000
Mission Beach	1	12,000	1,500
Oceanside	8	2,752,000	300,000

Source: Coastal Frontiers, 2010

The RBSP provided 1.6 million m^3 of beach-quality sand to twelve receiver beaches located between Imperial Beach and Oceanside. The project was conducted between April 6 and September 23, 2001. A trailing suction hopper dredge was used to excavate the borrow material from six offshore borrow areas (Noble, 2002). The sand was pumped onto each receiver beach and conventional earth-moving equipment was used to shape the fill to the design configuration. The median grain size (d_{50}) varied considerably among the borrow areas, ranging from 0.14 mm (fine sand) to 0.62 mm (coarse sand) (Noble Consultants, 2001).

The volume, dimensions, and median grain size of each beach fill is provided in Table 2. The majority of the sand (1.4 million m^3) was placed on ten receiver beaches in the Oceanside Littoral Cell. The fill quantities in the Oceanside Cell ranged from 322,000 m^3 at Oceanside to 77,000 m^3 at Cardiff. The Mission Beach and Silver Strand Cells each contained one receiver site. In the Mission Beach Cell, 115,000 m^3 were placed at Mission Beach. Approximately 92,000 m^3 were placed at Imperial Beach in the Silver Strand Cell.

The paucity of significant nourishment projects since the RBSP has led to a nourishment deficit relative to historical conditions in two of the three San Diego region littoral cells. The average annual nourishment rate in each littoral cell during the ten year period following the inception of the RBSP is shown in Figure 1. The diminishing impact of the nourishment material over time is apparent. A nourishment deficit was incurred in the Silver Strand Cell in 2002. The annualized nourishment rate remained below the pre-RBSP average until it was erased in 2005 by the

placement of approximately 230,000 m^3 derived from maintenance dredging in San Diego Harbor (Ryan, 2005). Despite additional small nourishment projects totaling approximately 34,000 m^3 conducted in 2008 and 2009, a net deficit of 16,000 m^3/yr persisted at the end of the period. In the Mission Beach Cell, declining rates persisted during the first nine years due to the lack of nourishment other than the RBSP. The rate increased in 2010 due to the influx of approximately 344,000 m^3 of material from a large navigation project conducted by the Corps of Engineers. At the end of the period, the nourishment rate in the Mission Beach Cell remained well above the comparatively small pre-RBSP rate. A trend of declining nourishment rates is evident in the Oceanside Cell despite several small nourishment projects totaling approximately 34,000 m^3 (Weldon, 2011). The net result in the Oceanside Cell was a deficit of 157,000 m^3/yr relative the pre-RBSP nourishment rate.

Table 2. RBSP Beach Fills

Littoral Cell	Receiver Beach	Fill Characteristics			
		Volume (m^3)	Length (m)	Width (m)	d_{50} (mm)[1]
Silver Strand	Imperial Bch	92,000	700	35	0.24-0.52
	Total Nourishment in Silver Strand Cell = 92,000 m^3				
Mission Beach	Mission Bch	115,000	700	60	0.52
	Total Nourishment in Mission Beach Cell = 115,000 m^3				
Oceanside	Torrey Pines	187,000	490	50	0.14
	Del Mar	140,000	975	35	0.14
	Fletcher Cove	112,000	580	20	0.14
	Cardiff	77,000	275	45	0.34
	Moonlight Bch	80,000	335	55	0.34-0.62
	Leucadia	101,000	825	35	0.62
	Batiquitos	89,000	455	55	0.62
	S. Carlsbad	121,000	610	55	0.62
	N. Carlsbad	172,000	945	30	0.14-0.62
	Oceanside	322,000	1340	55	0.62
	Total Nourishment in Oceanside Cell = 1,401,000 m^3				
Total RBSP Nourishment = 1,608,000 m^3					

Notes: [1] d_{50} represents median grain size of fill material. Source: Noble Consultants, 2001
[2] All nourishment activities were conducted in 2001

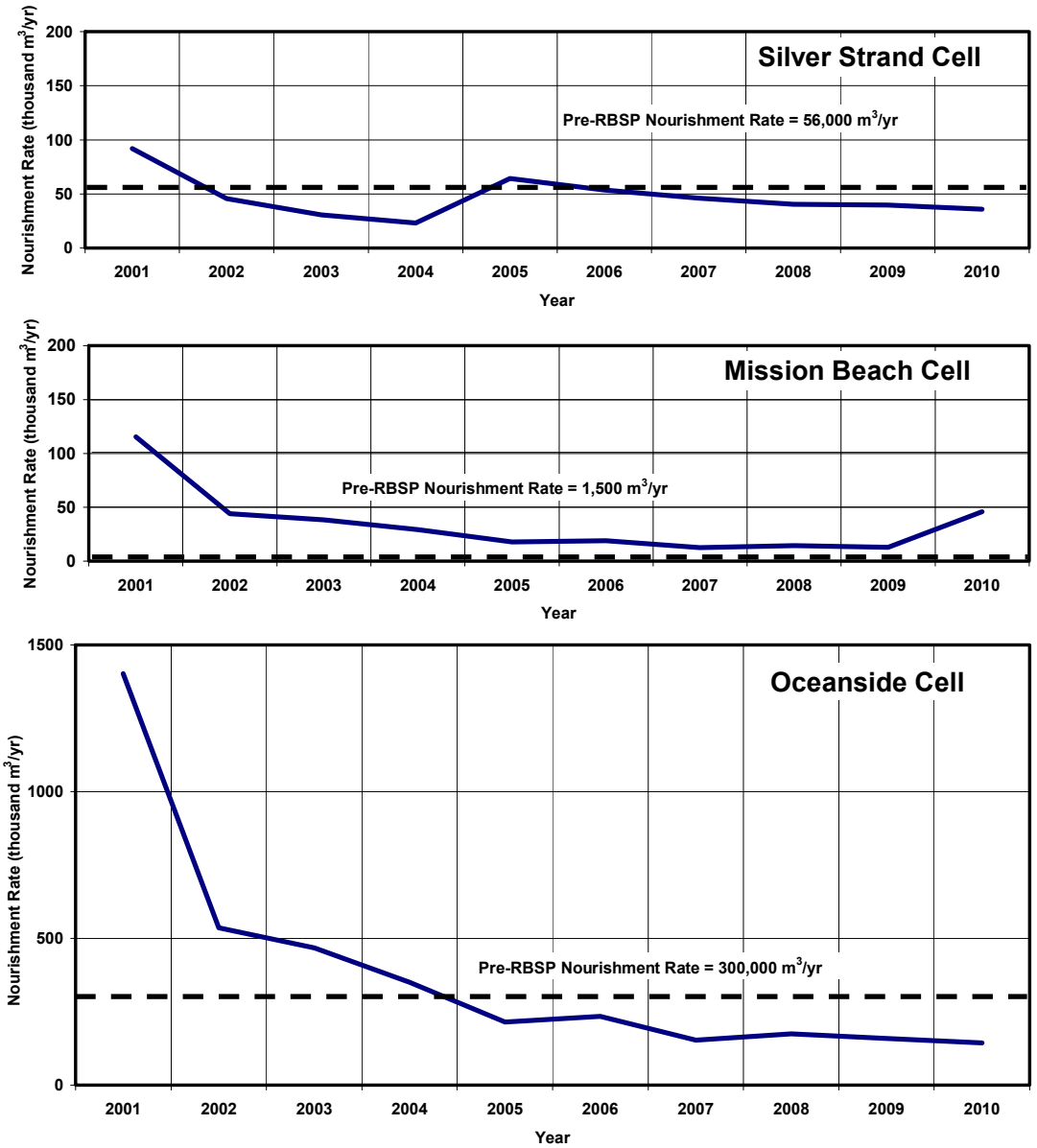


Figure 1. Time History of Nourishment Rates in San Diego Region , 2001-2010

SHORELINE MONITORING PROGRAM

SANDAG has sponsored a regional beach monitoring program since 1996. This effort is augmented by similar programs undertaken by several coastal cities. The general objective of the program is to obtain a quantitative understanding of coastal changes in the region. The fact that the program has been conducted without interruption for more that 15 years is a testament to SANDAG's philosophy that a shoreline monitoring should be sustainable on a continuous basis in preference to a larger effort that can not be maintained over the long-term (Leidersdorf, 1999).

The program consists primarily of semi-annual beach profile surveys conducted along shore-perpendicular transects with a typical alongshore spacing between transects of less than ½ mile. Data are obtained along each transect from the back beach to a location beyond the estimated depth of closure. The surveys are conducted in the spring and fall, corresponding with the beginning and end of the winter and summer wave seasons. Additional monitoring elements have included semi-annual oblique aerial photos of the receiver sites and monthly beach width measurements.

The program has evolved to meet changing needs and budgetary constraints. Most notably, the program was expanded in 2001 to develop more detailed information about the outcome of the RBSP nourishment activities. The underlying rationale was to provide coverage of each of the twelve receiver beaches and enhanced coverage of four of these sites. Beach profile data were obtained semi-annually at 61 sites, along with monthly beach widths measurements at four receiver beaches, and semi-annual oblique aerial photographs at each the twelve receiver sites. The program remained largely unchanged until 2005, when the agency mandated monitoring period ended. At that time the program was reduced by eliminating those elements deemed to be of marginal utility and reducing the beach profile locations to 55.

The beach profile survey results were used to assess the shorezone changes and document the evolution of the County's beaches following the placement of the RBSP nourishment material. Comparison of the Spring and Fall profiles provides an indication of seasonal changes, while comparison of consecutive Fall profiles shows the nature of inter-annual and long-term changes. A significant difference between the pre-RBSP envelope of changes and the post-nourishment profiles provides and indication of a an improvement that may have resulted from the RBSP nourishment activities. Changes in shoreline position and sediment volume also served as a primary analysis tool.

Beach widths were computed as the horizontal distance, in meters, between the landward limit of the sandy beach and the point at which the beach profile intersected the plane of Mean Sea Level (MSL) Datum. Although Mean Lower Low Water (MLLW) was used as the vertical datum for the profile data, MSL was adopted as the shoreline reference in the belief that it provides a more accurate indicator of changes in beach configuration.

The volume changes were computed for each transect for the entire width of the shorezone, from the back beach to the "statistical range of profile closure". This parameter represents the distance seaward of the back beach beyond which profile variations are smaller than the accuracy of the survey technique (Gadd, 2006). The statistical range of closure was adopted as the offshore boundary to separate the signal of true profile change from the noise of survey inaccuracy. Statistical closure was assumed to occur at the smallest range at which the standard deviation of the sea bottom elevations decreased below the survey accuracy of 15 cm, provided that the average value of σ remained less than or equal to 15 cm seaward of that point

(Coastal Frontiers, 2010). If this condition was not satisfied by the first downcrossing, the next downcrossing seaward of that location was checked.

ENVIRONMENTAL CONDITIONS

Environmental conditions that influence the condition of the shorezone, including precipitation, streamflow, and waves, were assessed to provide a general context for the monitoring data and to aid in evaluating the performance of the RBSP beach fills. Rivers and streams can transport substantial quantities of beach-quality sediment to the coast and flush coastal sediment from lagoon entrances during periods of heavy precipitation. Conversely, during dry periods riverine sediment input becomes negligible (Inman and Masters, 1991). The rate of coastal sediment transport is controlled by the nature and severity of the wave conditions, particularly in the case of storm events. The environmental data presented below are based on monitoring years, extending from November through October.

Rainfall data acquired at San Diego's Lindberg Field (Figure 2) were selected to represent precipitation for the study area, based on this station's nearly 100-year period of record (Western Regional Climate Center, 2011). Below- or near-average rainfall persisted in ten of the twelve years following the 1997-98 El Niño event, with 2005 and 2010 being the exceptions. During the ten years since the inception of the RBSP, the precipitation exceeded the long-term average (26 cm) on only two occasions. Below-average precipitation persisted for seven of the ten years, while average precipitation occurred during one year. The heavy rainfall during 2005 (46 cm) resulted in the fourth highest annual total on record.

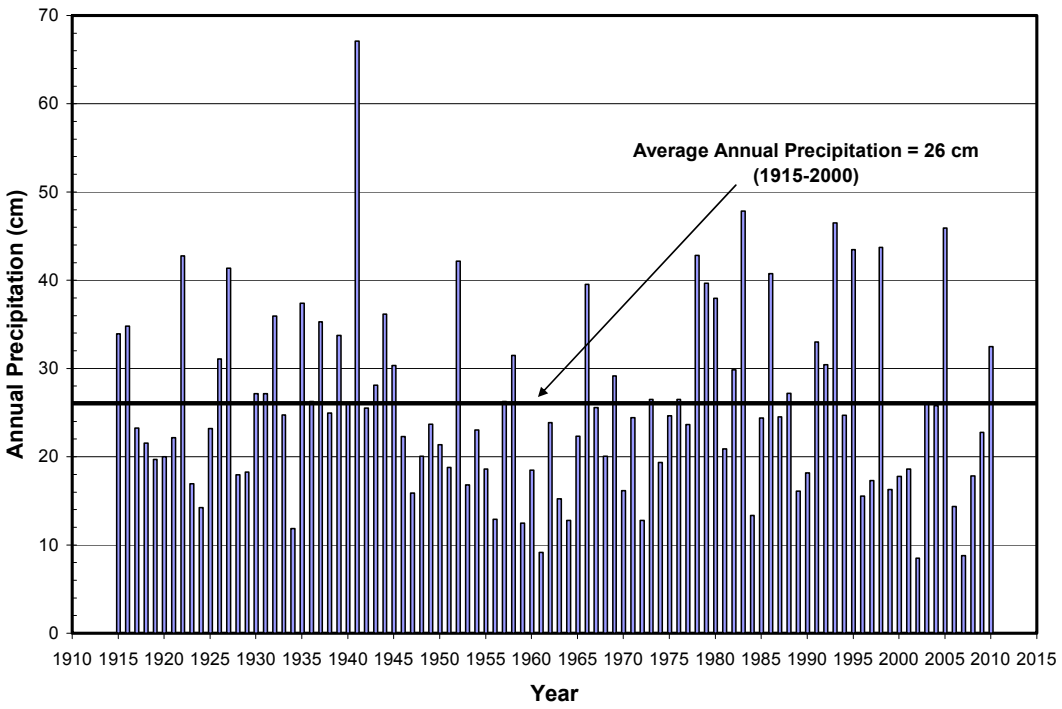


Figure 2. Annual Precipitation at Lindberg Field, 1915-2010

The annual mean streamflow measured in the San Luis Rey and San Diego Rivers between 1983 and 2010 is shown in Figure 3 (USGS, 2011). These rivers were selected for analysis because they are among the largest in the study area, and because streamflow data are available for an extended period of record that includes the period following the RBSP. Similar to the precipitation trends, the flow in both rivers remained below or near the long-term average for eight of the ten years following the RBSP. The highest values occurred in both rivers during 2005, corresponding with the heavy rainfall recorded that year.

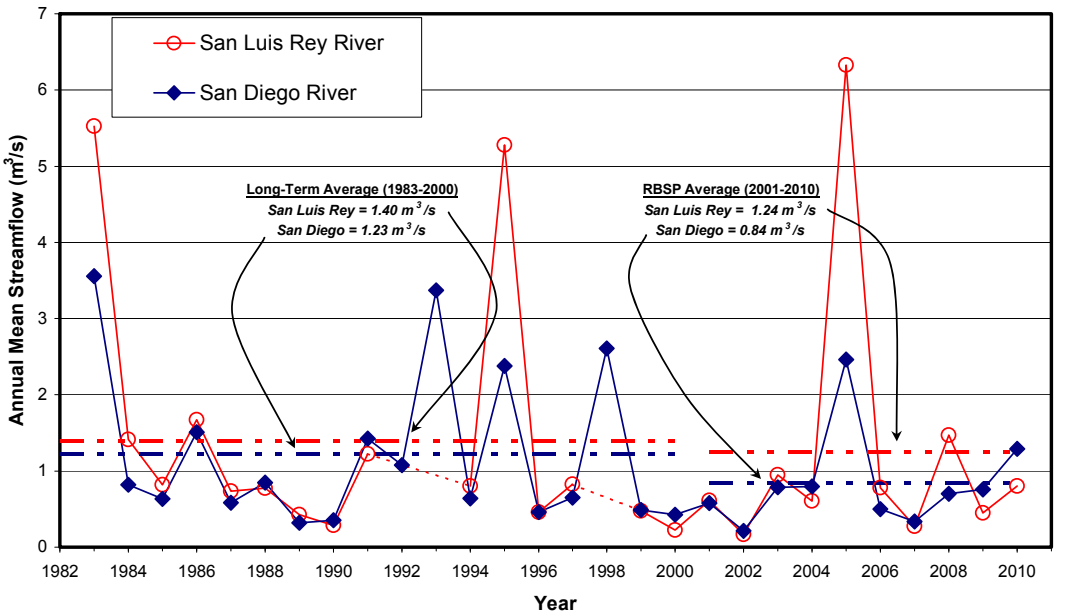


Figure 3. Annual Mean Streamflow in the San Luis Rey and San Diego Rivers, 1983-2010

Three measures of the wave climate were used to provide a first-order comparison of the potential for sediment transport during the post-RBSP period with that in previous years: (1) the number of storm events, (2) the duration of storm conditions, and (3) total wave energy. The assessment utilized wave measurements acquired offshore of Oceanside (Station 045) under the auspices of the Coastal Data Information Program (CDIP), which is operated by Scripps Institution of Oceanography (2011).

The total wave energy for each year from 1998 through 2010 was compared using the Relative Incident Energy Index (Er) developed by Seymour (1998). This index provides an approximation of the total energy per unit crest length delivered over the duration of the year.

The wave conditions at the Oceanside buoy during the 13-year period between 1998 and 2010 are summarized in Table 3. The highest values recorded during the period are shown in bold italics. The first six years following the inception of the RBSP (2001 to 2006) were characterized by relatively mild wave conditions. The

number of storms per year with H_s exceeding threshold values of 2.1 m (7 ft) and 3.0 m (10 ft) was highest in 2010 (a mild El Niño year), while the total number of days each year with H_s exceeding these thresholds was greatest in 1998 (a strong El Niño year). In keeping with the high storm frequency, severity and duration, the highest energy index values also occurred in 1998 and 2010. The highest measured significant wave height (4.8 m) was observed in 2007, a year characterized by mild El Niño conditions.

Table 3. Summary of Wave Conditions, 1998-2010

Monitoring Year	No. of Storms Exceeding Threshold		No. of Days with H_s Exceeding Threshold		Energy Index	Max. H_s (m)
	2.1 m	3.0 m	2.1 m	3.0 m		
1998	16	6	***42***	***11***	***149***	3.9
1999	8	3	12	3	121	3.9
2000	5	1	8	2	108	3.2
2001	6	2	7	2	99	3.6
2002	7	0	9	0	87	2.7
2003	7	2	12	3	103	3.2
2004	7	0	10	3	100	3.0
2005	7	2	12	2	105	3.4
2006	7	1	10	2	111	3.0
2007	12	4	38	9	103	***4.8***
2008	12	0	16	0	113	2.8
2009	11	4	17	5	100	3.5
2010	***18***	***9***	27	10	135	4.7

The implication of the scant precipitation and low streamflows following the RBSP is that significant quantities of beach-quality sediment were unlikely to be delivered to the coast in all but one year (2005) during the period following the RBSP. The mild wave conditions during the first six years following the RBSP (2001 to 2006) helped to prolong the life of the beach fills.

FINDINGS

Shorezone condition improvements relative to the pre-nourishment condition persisted for several years following the RBSP in each of littoral cells. The outcome was particularly favorable in the Oceanside Cell, where approximately 85% of the material was placed. The reasons for these improvements appears to have been the RBSP fills, and the relatively mild wave conditions that prevailed during the beginning of the period. A decade after nourishment, however, beach widths and shorezone volumes at the majority of sites have reverted back to near pre-RBSP levels.

Time series of the average shoreline change and average shorezone volume change at the time of each Fall Survey relative to the pre-RBSP condition (Fall 2000) are presented for each littoral cell in Figures 4 through 6. In the Oceanside Cell, substantial shoreline advance occurred in 2001 due to the RBSP. Additional gains were realized in 2002 as the RBSP fill material placed at the ten receiver sites dispersed alongshore. Shoreline retreat then persisted through 2005, consistent with the ongoing loss of the fill material from the above-water beach. This trend was unexpectedly reversed in 2006, with shoreline advance prevailing in response to wave conditions that were particularly favorable to onshore sediment transport (O'Reilly, 2007). Losses resumed in 2007, causing the beach widths to fall below the pre-RBSP values. Shoreline advance similar to that which occurred in 2006 predominated during 2008, followed by relative stability in 2009 and additional losses in 2010. At the end if the period, beach widths in the region had retreated to below pre-RBSP levels.

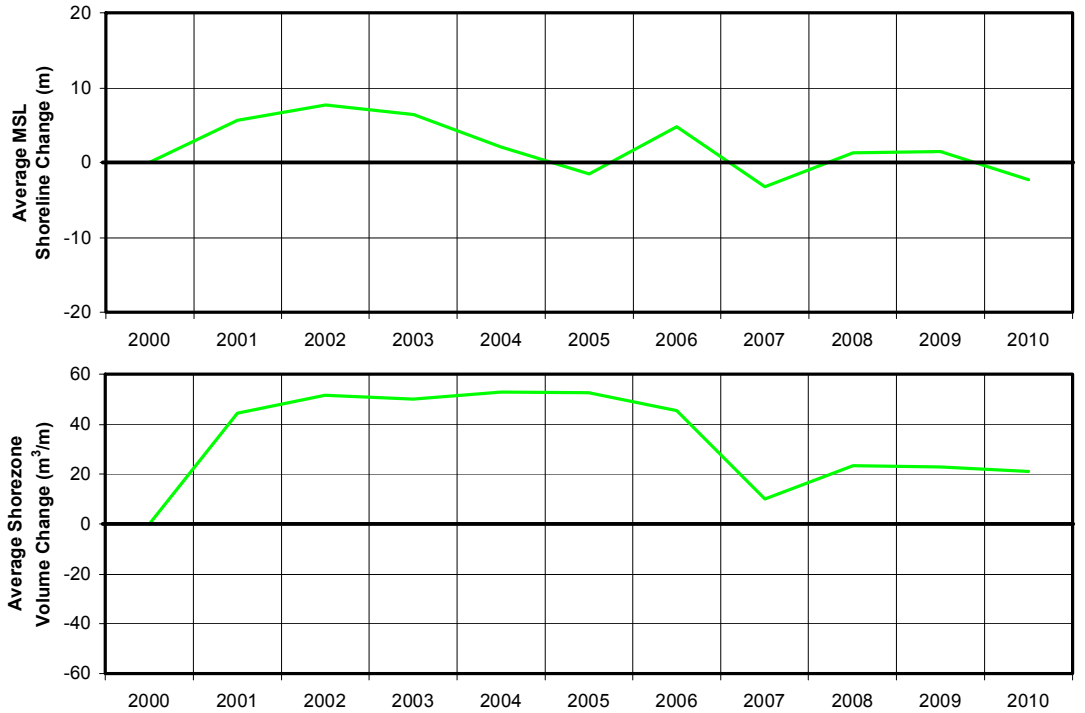


Figure 4. Average MSL Shoreline Position and Shorezone Volume Changes Relative to Pre-RBSP Condition, Oceanside Littoral Cell

The sediment volume gains that occurred in the Oceanside Cell following the RBSP persisted with minimal change through 2006. The shorezone volume decreased in 2007, corresponding to the occurrence of several severe winter storms (including the largest single event during the period). The volumes then remained relatively stable through 2010. At the time of the 2010 survey, the shorezone volume remained above the pre-RBSP value.



Figure 5. Average MSL Shoreline Position and Shorezone Volume Changes Relative to Pre-RBSP Condition, Mission Beach Littoral Cell

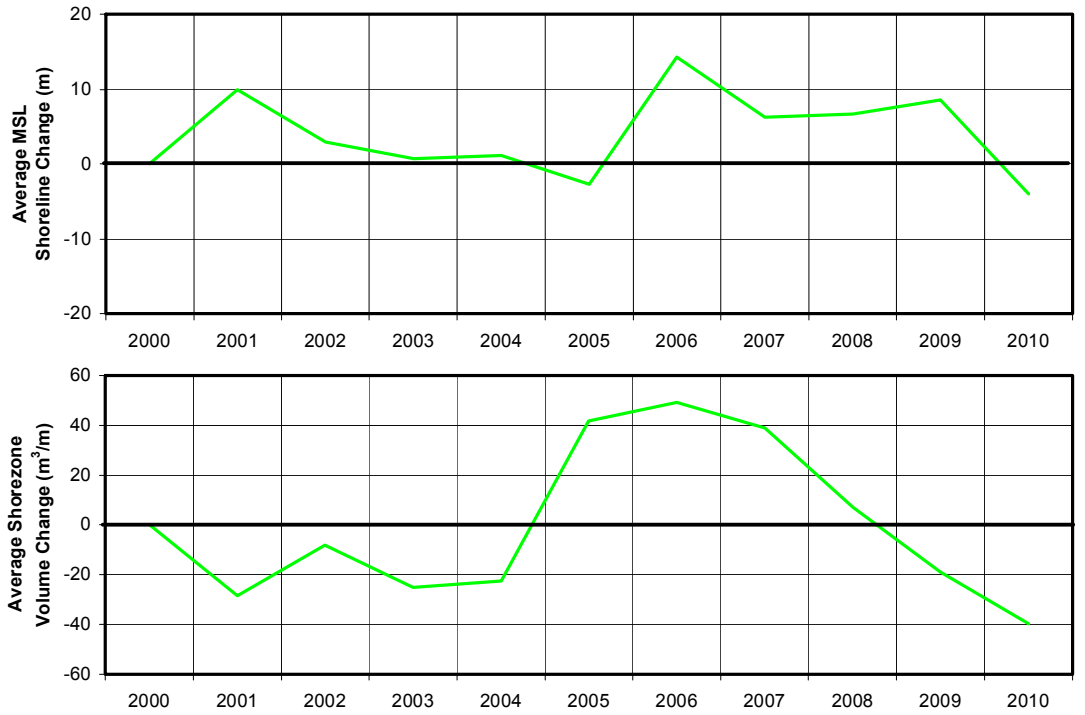


Figure 6. Average MSL Shoreline Position and Shorezone Volume Changes Relative to Pre-RBSP Condition, Silver Strand Littoral Cell

The RBSP nourishment in the Mission Beach Cell was limited to a relatively small quantity at one receiver site. The initial shoreline gains in this cell persisted through 2005. Similar to the Oceanside Cell, significant shoreline advance occurred in 2006. Despite these gains, the shoreline retreat that prevailed in 2007 was sufficient to cause a net loss in beach width relative to the pre-RBSP condition. Shoreline advance occurred in 2008 and 2009, followed by an even larger increase in 2010 attributable to placement of approximately 344,000 m^3 of material as part of the aforementioned Corps of Engineers navigation project.

Similar to the Oceanside Cell, the sediment volume gains that occurred in the Mission Beach Cell following the RBSP persisted with minimal change for several years. After 2005, a general trend of decreasing shorezone volume is evident. This trend was reversed in 2010, with significant shorezone volume gains occurring in response to the Corps sponsored nourishment. At the time of the 2010 survey, the shorezone volumes greatly exceeded pre-RBSP values.

The initial shoreline gain in the Silver Strand Cell was short-lived, diminishing to near pre-RBSP levels in 2003 and 2004. Shoreline retreat continued in 2005, followed by shoreline advance in 2006 similar to that observed in the other cells. These gains can be attributed, at least in part, to the onshore migration of the nourishment material placed in the nearshore at Imperial Beach during the previous year. Shoreline retreat in 2007 and 2010 reduced beach widths to below pre-RBSP values.

The shorezone volume in the Silver Strand Cell decreased following the RBSP and remained below the pre-RBSP value until placement of the nourishment material from San Diego Harbor in 2005. Because this material was placed in the nearshore, the shorezone volume gain was evident the year of placement, while the shoreline gains were delayed by one year. Losses prevailed from 2007 to 2010, reducing the shorezone volume to below the pre-RBSP value.

The outcome of the RBSP was evaluated for several sub-reaches in the region based on a combination of geographic and municipal boundaries. Tables 4 and 5 summarize the beach width and shorezone volume changes following the RBSP in selected sub-reaches within the region, respectively. The sub-reaches are categorized in terms of the initial persistence of post-RBSP gains. The persistence of post-RBSP gains was defined in terms of the number of consecutive years immediately following the RBSP in which the average change at the time of each Fall Survey relative to the pre-RBSP condition (Fall 2000) exceeded 3 m (10 ft) or 25.1 m^3/m (10 cy/ft) for beach widths and shorezone volumes, respectively. In recognition that shoreline and shorezone volume gains occurred in the Oceanside Cell during both the first and second year following nourishment as the RBSP fill material dispersed alongshore, the accounting of persistence was permitted to commence in 2001 or 2002. Three categories were adopted to classify the persistence of post-RBSP gains: Long-Term (5+ years), Transient (2 to 4 years), and Negligible (1 year or less).

Table 4. Post-RBSP Average Beach Width Gain Persistence in Sub-Reaches

Sub-Reach	Average Beach Width Gain Persistence	Fall 2010 Average Beach Width Change
Long-Term Beach Width Gains (5+ Years)		
North Carlsbad	10 years	15.5 m
Cardiff	10 years	13.7 m
Solana Beach	6 years	16.8 m
Transient Beach Width Gains (2 to 4 Years)		
Oceanside	4 years	-6.7 m
Leucadia/Encinitas	3 years	-7.0 m
La Jolla	2 years	-0.9 m
Imperial Beach	2 years	2.7 m
Negligible Beach Width Gains (1 Year or Less)		
South Carlsbad	<1 year	-13.7 m
Del Mar	1 year	-16.2 m
Mission Beach	1 year	17.7 m

Table 5. Post-RBSP Shorezone Volume Gain Persistence in Sub-Reaches

Sub-Reach	Average Shorezone Volume Gain Persistence	Fall 2010 Average Shorezone Volume Change
Long-Term Shorezone Volume Gains (5+ Years)		
Oceanside	6 years	0.0 m^3/m
North Carlsbad	10 years	87.8 m^3/m
Leucadia/Encinitas	6 years	17.6 m^3/m
Cardiff	10 years	200.6 m^3/m
Solana Beach	6 years	80.2 m^3/m
Mission Beach	5 years	75.2 m^3/m
Transient Shorezone Volume Gains (2 to 4 Years)		
Del Mar	2 years	20.1 m^3/m
Negligible Shorezone Volume Gains (1 Year or Less)		
South Carlsbad	<1 year	-115.4 m^3/m
La Jolla	<1 year	42.6 m^3/m
Imperial Beach	<1 year	-52.7 m^3/m

Long-term beach width gains prevailed at three sub-reaches in the Oceanside Cell. The gains at North Carlsbad and Cardiff persisted for the entire ten-year period. Transient beach width gains occurred at four sub-reaches, while the remainder of the sub-reaches were characterized by negligible gains.

When shorezone volume persistence is considered, the number of sub-reaches characterized by long-term gains doubles to six. All but one of the sub-reaches was located in the Oceanside Cell. As in the case of beach width gain persistence, the volume gains at North Carlsbad and Cardiff were sustained for the entire ten-year period. Negligible shorezone volume gains prevailed at three sub-reaches, while transient gains were limited to one location.

South Carlsbad was the only sub-reach where both the shoreline and shorezone volume persistence were categorized as negligible. Similarly, North Carlsbad, Cardiff, and Solana Beach were the only sub-reaches achieving the long-term gain category for both beach width and shorezone volume persistence.

CONCLUSIONS

In the absence of significant sediment to the delivery to the coast from rivers and streams, the improved condition of the County's shoreline during the first several years following the RBSP appears to be attributable to the nourishment material. In addition, the wave conditions were particularly mild during the first six years following the RBSP – a scenario that helped to prolong the life of the beach fills.

The outcome of the RBSP varied among the littoral cells. In the case of the Oceanside Cell (where material was placed at ten sites), the outcome differed by sub-reach. This was due partly to the individual fill characteristics and the relative locations of the placement sites. As expected, larger fills tended to last longer than smaller fills, and those comprised of coarser sand persisted longer than those with finer material. Closely spaced fills tended to merge and enhance larger areas. The beach width and shorezone volume gains at two of the sub-reaches (North Carlsbad and Cardiff) have persisted to this day.

A nourishment deficit relative to historical conditions currently exists in two of the three San Diego region littoral cells due to the paucity of significant nourishment projects since the RBSP. Only in the Mission Beach Cell, where the historical average nourishment rate was a paltry 1,500 m^3/yr and the recent opportunistic nourishment project provided 344,000 m^3 to the cell, has incremental nourishment been received (44,000 m^3/yr). The Oceanside Cell has incurred a deficit of 157,000 m^3/yr, while the Silver Strand Cell has incurred a deficit of 20,000 m^3/yr since the inception of the RBSP. The large deficits in these cells suggest that the benefits of the RBSP have been outweighed by a lack of sufficient nourishment from other sources. To address these shortfalls, SANDAG is using lessons learned from the RBSP to guide the design and implementation of the second regional program (RBSP II), scheduled for construction in 2012.

REFERENCES

Coastal Frontiers Corporation, 2010, "SANDAG 2009 Regional Beach Monitoring Program – Annual Report", Chatsworth, CA, 111 pp. + app.

Gadd, P.E., C. Leidersdorf, G. Hearon, A. Shak, J. Ryan, 2006, "Use of Statistical Depth of Closure to Resolve Historical Changes in Shoreline Position and Shorezone Volume in the Huntington Beach Littoral Cell", Proc. 30th Coastal Engineering Conference, San Diego, California, World Scientific, Singapore, p. 5302-5311

Inman, D.L. and P. Masters, 1991, "Budget of Sediment and Prediction of the Future State of the Coast", in USACE, 1991, "State of the Coast Report, San Diego Region", U.S. Army Corps of Engineers, Los Angeles District, Coast of California Storm and Tidal Waves Study, Volume I – Main Report, Los Angeles, CA.

Leidersdorf, C.B., R.C. Hollar and S. Sachs, 1999, "Technology in Support of Policy: The SANDAG Regional Beach Monitoring Program", *Proc. Sand Rights '99*, ASCE, New York, p. 261-272.

Noble Consultants, Inc., 2001, "Final Construction Management Documents, San Diego Regional Beach Sand Project", Irvine, CA.

Noble, R., 2002, "Beach Nourishment Construction at Twelve San Diego County, California Receiver Beach Sites," World Dredging, Mining, and Construction, February 2002, p. 7-20.

O'Reilly, W., 2007, personal communications, in Coastal Frontiers Corporation, 2010, "SANDAG 2009 Regional Beach Monitoring Program – Annual Report", Chatsworth, CA, 111 pp. + app.

Ryan, J., 2005, personal communication, in Coastal Frontiers Corporation, 2010, "SANDAG 2009 Regional Beach Monitoring Program – Annual Report", Chatsworth, CA, 111 pp. + app.

Ryan, J., 2010, personal communication, in Coastal Frontiers Corporation, 2010, "SANDAG 2009 Regional Beach Monitoring Program – Annual Report", Chatsworth, CA, 111 pp. + app.

Scripps Institution of Oceanography, 2011 "The Coastal Data Information Program", http://cdip.ucsd.edu.

Seymour, R.J., 1998, "Effects of El Niños on the West Coast Wave Climate", *Shore and Beach*, Vol. 66, No. 3. p. 3-6.

United States Geological Survey, 2010, http://waterdata.usgs.gov.

Weldon, K., C. Webb, and B. Leslie, 2011, " Implementation of San Diego Regional Sediment Management Objectives in the City of Encinitas, California", *Shore and Beach*, Vol. 79, No. 2. p. 2-8.

Western Regional Climate Center, 2010, http://wrcc.dri.edu.

Sustainable Concrete Mix Designs for 100-year Service Life for Bridges in San Diego County Coastal Environments

B.G. Smith PE[1], M. Creveling PE[2] , and J. W.Teig PE[3]

[1] Senior Engineer, San Diego Association of Governments (SANDAG) 401 B Street, Suite 800, San Diego, CA 92101-4231. Phone: 619-699-1907 Email: bsm@sandag.org
[2] Principal Design Engineer, Simon Wong Engineering (SWE), 9968 Hilbert Street, San Diego, CA92131; Phone: 858-566-3113; Email:mcreveling@simonwongeng.com
[3] Senior Professional Associate, HDR Engineering, Inc. (HDR), 8404 Indian Hills Drive, Omaha, Nebraska , 68114. Phone 402-399-105; Email: jeff.teig@hdrinc.com

Abstract.

Deterioration of reinforced concrete structures is a problem in coastal climates. Most of this deterioration is caused by chloride ingress through the concrete, which results in the corrosion of the reinforcing steel and spalling of the cover concrete. The practice of modeling chloride ingress to understand this deterioration process is increasing as engineers work to improve the durability of concrete. The authors present examples of deteriorated structures, modeling results for new structures and examples of current projects along the coastal LOSSAN rail corridor between Los Angeles and San Diego in San Diego County. The conclusion is that by specifying the addition of fly ash, silica fume and corrosion inhibitors in concrete, subject to temperate marine exposure conditions, we are able to increase the predicted service life of new structures to 100 years.

Part 1. Examples of Deterioration of Coastal Structures in Southern California. (B Smith & M. Creveling)

Example 1 North Torrey Pines Road bridge also known as Rail Bridge 245.7.

The 78-year-old North Torrey Pines Road Bridge, shown in Figure 1, is a 13-span concrete T-girder structure located on the Pacific Coast Highway between San Diego and Del Mar.



Figure 1. North Torrey Pines Road Bridge (Rail Bridge 245.7) in Del Mar, CA.

Bridge 245.7 has been labeled by the press as "the most structurally deficient bridge in San Diego County." With an FHWA Sufficiency Rating of 15 (out of 100), rehabilitation and retrofit of this historic bridge is underway after more than a decade of technical, seismic, and environmental studies.

The structure crosses the mainline rail tracks at LOSSAN Rail MP 245.7, was built in 1933, and the extensive studies provide good data on chloride ingress. The City of San Diego was proposing to demolish the bridge and build a new bridge to current design standards. The City of Del Mar protested and as a result the bridge was sold to Del Mar who have championed the rehabilitation and reconstruction of this historic structure.

Following 78 years of exposure to salty sea mist, the superstructure and columns have significant cracked, delaminated, and spalled concrete as illustrated in Figure 2. Studies determined extensive chloride intrusion requiring a combination of patch and repair, replacement, and cathodic protection to extend the service life a minimum 50 additional years, CTL 1999 and SWE 2006.



Figure 2. Deterioration of Bridge Beams and Deck in Del Mar, San Diego, CA.

Studies were initially undertaken by the City of San Diego who had the chloride ingress measured from 16 cores drilled in the deck by CTL in 1999. The results are shown in Figure 3.

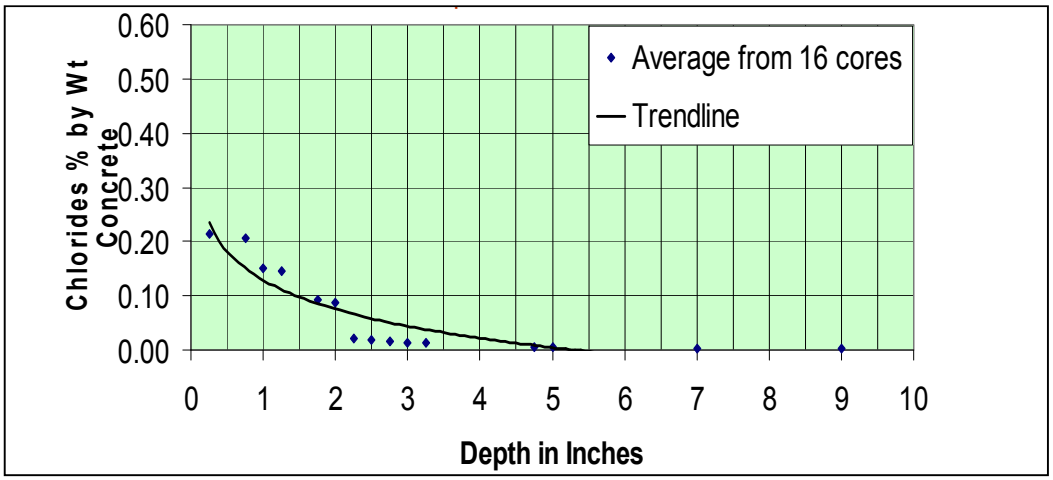


Figure 3. Chloride Ingress in Deck of Bridge 245.7 on coast after 66 Years.

Further studies were undertaken by the City of Del Mar and resulted in the chloride ingress being measured from 54 cores drilled in the columns in 2008 by SWE and the results are shown in Figure 4.

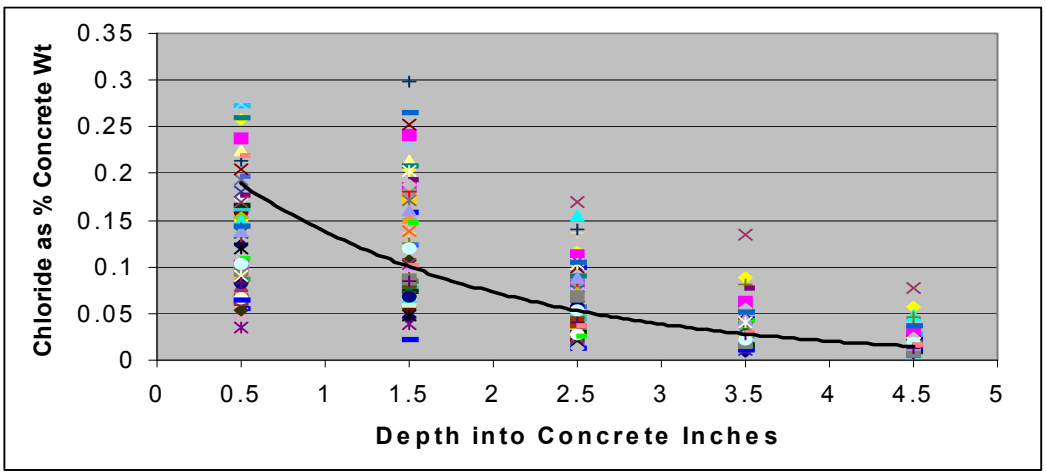


Figure 4. Chloride Ingress in Columns of Bridge 245.7 on coast after 75 Years.

The original 1933 drawings show that the bridge was specified with plain concrete and with 2-bar diameters and a minimum of 2 inches of concrete cover to the reinforcement. Field observations show that actual cover varies and has been observed as low as half an inch contributing to the deterioration.

Example 2. Rail Bridge 217.3 over Las Pulgas Rd and 218 over Las Pulgas Creek.

The 98-year-old Las Pulgas Creek rail bridge , shown in Figure 5, is a two span concrete arch structure located on the LOSSAN Rail Line at Mile Post 218 on Camp Pendleton. Bridge 217.3 at the Las Pulgas Road overcrossing is a steel thru plate gurder supported on concrete abutment walls built in 1927. A recent condition assessment was carried out to establish the remaining service life of these aging structures.



Figure 5. Rail bridge 218 over Las Pulgas Creek.

The condition survey has provided the chloride profile data shown in figure 6 on the chloride ingress into the structures over the last 84 to 98 years.

Design guides typically categorize structures as either being in the severe coastal exposure zone or in a more moderate zone within a set distance of the coastline. Exposed to moderate exposure conditions, half a mile from the coast, the chloride levels obtained from Br 218 and Br 217 confirm that chloride ingress from salty ground and sea mist is at lower levels that the Br 245.7 structure that is adjacent to the Pacific Ocean in the coastal dunes.

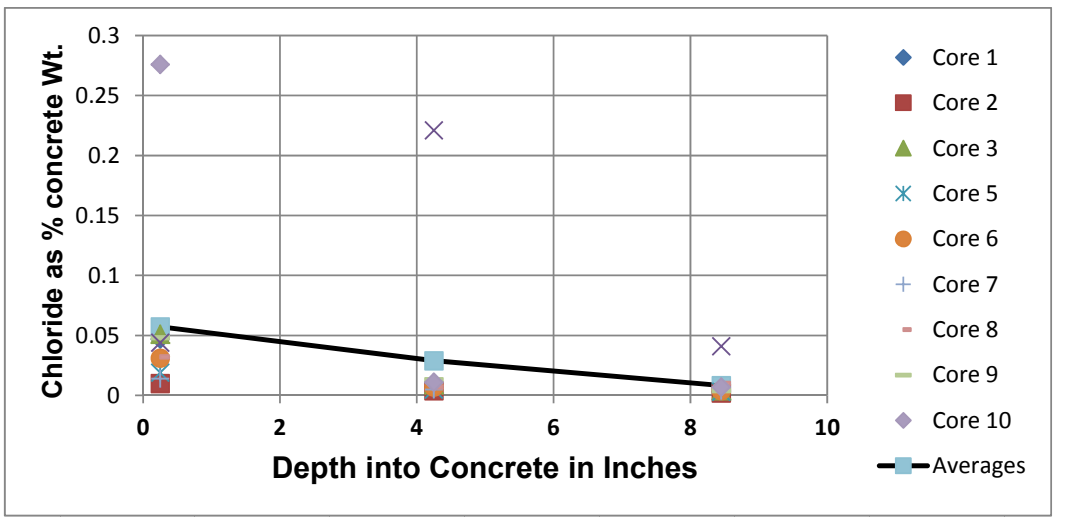


Figure 6. Chloride Profiles from Las Pulgas Creek(1913) and Las Pulgas Road (1927) Bridges, 0.5 mile from the Pacific Coast, Microchem 2010.

Part 2. Modeling Chloride Diffusion in Coastal Climates and Resulting Concrete Mix Designs to Obtain 100-years Service Life. (B. Smith)

2.1 Chloride Modeling. By making physical observations of structures built between 50 and 100 years ago with plain concrete, we conclude that these structures are unlikely to provide 100 years of service life when exposed to hot and temperate coastal environments, unless sufficient cover is provided.

Concrete mix design and reinforcement cover recommendations need to be made based on the results of chloride diffusion modeling. One method of modeling is based on the Fick's Second Law and the Fick's chloride profile equation:

$Cxt = Cs - (Cs-Co) * erf [x /\{ 2\sqrt{(Deff*T)} \}]$ where:

Cxt = Chloride concentration at a distance, x cm, inside the concrete after time T years, as % by mass of concrete

Co = Original chloride concentration in the concrete mix materials

Cs = Surface concentration of chloride

Erf = The error function from standard tables, Askeland 1989

Deff = Effective diffusion coefficient over time T. The diffusion coefficient over time which depends on time, temperature, and material properties.

Deff = Dei * Kti * Kte, in cm^2 / year where:

Dei = The initial diffusion coefficient from laboratory tests using 28-day-old sample over 90 days at 20°C, in cm^2 / year

Kti = Time-related effect on the diffusion coefficient

Kte = Temperature-related effect on the diffusion coefficient

2.2 Original Mix Chloride Concentration, (Co). Original mix concentrations of chloride, Co, are limited by codes of practice like ACI 222, Corrosion of Metals in Concrete. For reinforced concrete exposed to wet conditions Co<0.017% by weight of concrete (0.10% by weight of cement). For pre-stressed concrete Co<0.014% by weight of concrete (0.080% by weight of cement). Chloride concentrations are acid soluble chlorides to ASTM C1152. In this research paper Co=0.017% by weight of concrete has been used in the chloride modeling.

2.3 Surface Concentrations of Chloride, (Cs). Surface concentrations of chloride, Cs, are typically greatest in areas of wetting and drying immediately above mean sea level. Typically low exposures will result in CS <0.3% while severe exposure to sea water will result in 0.3%<Cs<0.6% in temperate climates.

2.4 Diffusion Coefficient (Deff). For further information on modeling diffusion coefficients the reader is referred to previous publications by Bruce Smith in the American Society of Civil Engineers Materials Journal in 2001 as listed in the references section of this paper.

2.5 Temperature Effect on Chloride Diffusion in Concrete (Kte). Temperature has a significant effect on the rate of chloride diffusion and should also be considered by designers. Chloride diffusion in tropical regions will occur twice as fast as in temperate regions as shown by the Kte values in Table 1. Under laboratory conditions Kte =1.

Table 1. Temperature Effect on Chloride Diffusion.

Location	Kte	Location	Kte
New York	0.56	Honolulu	1.41
San Francisco	0.63	Key West	1.50
San Diego	0.87	Aden	1.82

2.5 Corrosion Initiation. Chloride Modeling results in the comparison of concrete mix designs and the time to the start of corrosion for varying reinforcement covers. Figure 7 shows the predicted time to corrosion initiation for various covers for plain concrete in temperate climates. Figure 8 shows the increased service life obtained when silica fume and fly ash are added to the concrete mix. These figures provide a useful tool for design engineers when designing durable structures as they provide data for informed decision making. The modelling can be done for low and moderate exposures producing a set of design aids.

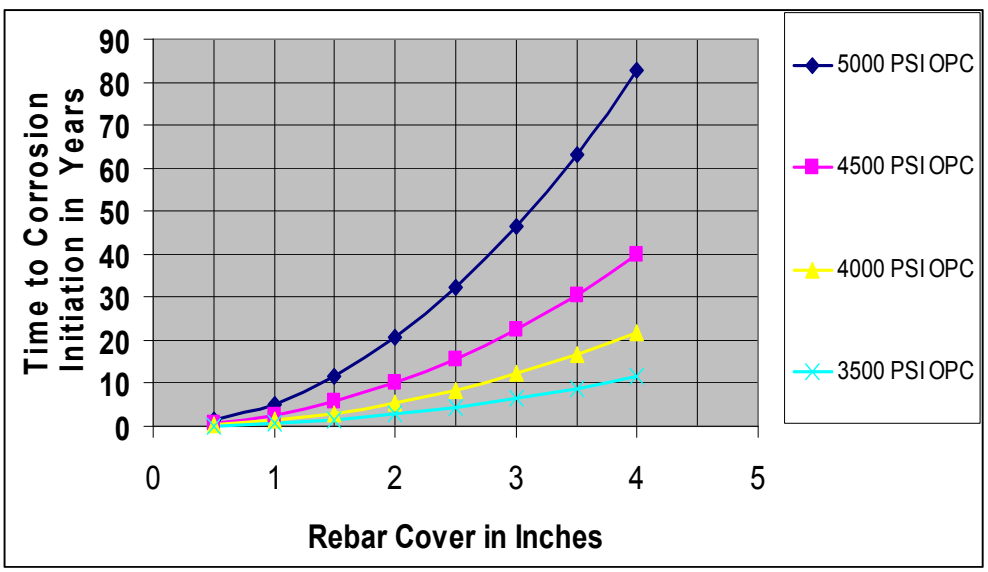


Figure 7. Time to Corrosion Initiation for Various Covers for Plain Type 1 Concrete in Temperate Climates at 67F with surface chloride of 0.6%.

Note that different cement types also effect the chloride diffusion rates for concrete. The use of Sulphate Resisting Cement (SRC) or Type 5 cement has been shown to significantly reduce the design life of structures subject to chloride exposure. In temperate climates for a structure made out of 5,000 PSI concrete with 3 inches of cover it is predicted that the initiation or reinforcement corrosion in a structure built in sea water will occur within 30 years if SRC or Type 5 cement is used and within 50 years if Type 1 Ordinary Portland Cement. Refer Smith 2001.

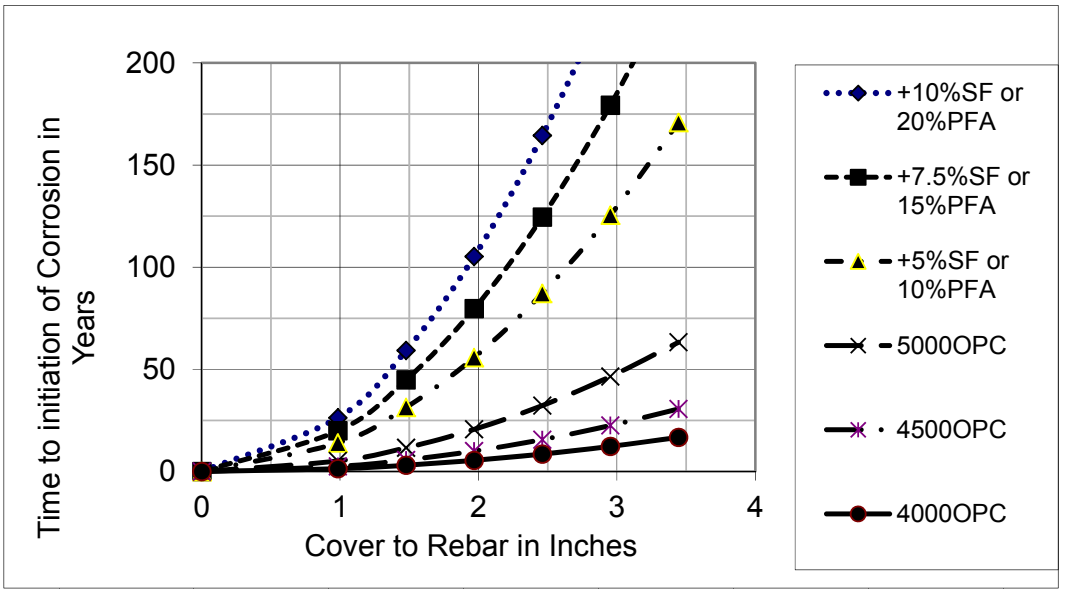


Figure 8. Time to Corrosion Initiation for Various Covers for Type 1 Concrete with Fly Ash or Silica Fume Exposed to Sea Water, Cs=0.6%, at 67F.

2.6 Chloride Modeling and Calcium Nitrite. Chloride modeling is also required to select the correct dose of Calcium Nitrite needed to be added to concrete to increase the threshold corrosion concentration and thus extend the life of a concrete structure. Figure 9 shows the predicted chloride levels at a depth of 2.5 inches for various concrete mix designs in seawater in temperate climates with an average annual temperature of 67 degrees Farenheit.

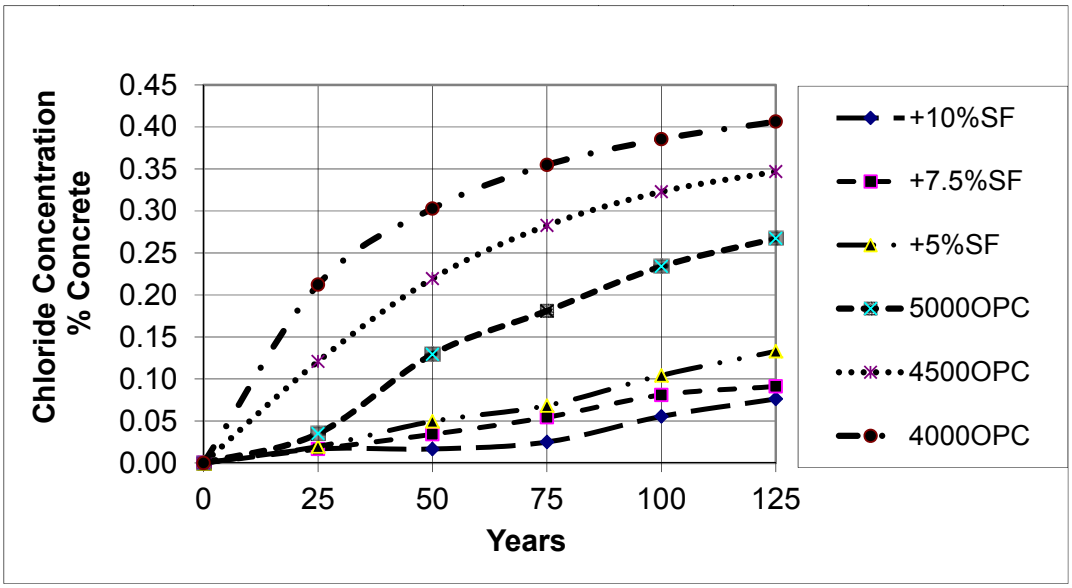


Figure 9. Predicted Chloride Ingress in Type 1 Concrete at a Depth of 2.5 Inches at 67 Degrees Farenheit with surface chloride =0.6%.

Manufacturers recommended dosing levels for 30% Calcium Nitrite for a cubic yard of concrete from literature provided by WR Grace and Co. are shown in Figure 10.

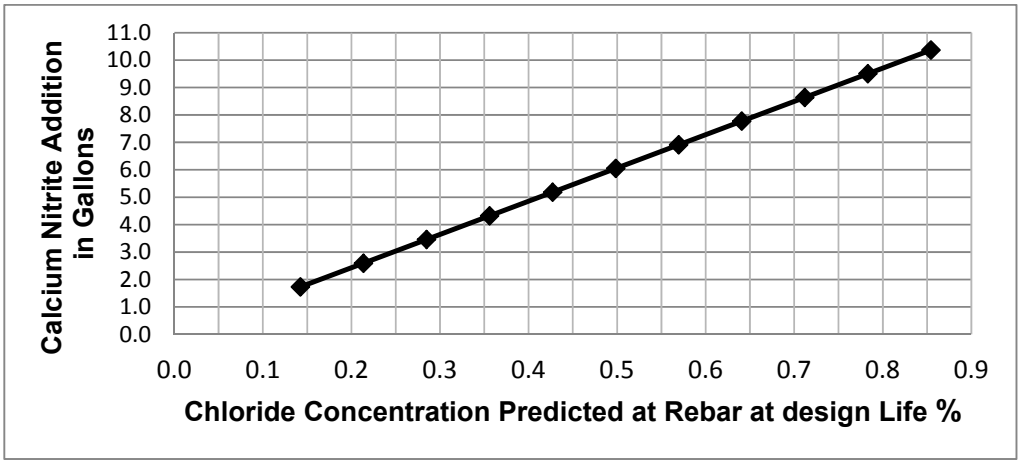


Figure 10. 30% Calcium Nitrite Addition Rates per Cubic Yard; Berk & Matta, WR Grace 1994.

Based on the chloride modeling prediction from figure 9, for 100 years of service life using a 4000 psi concrete made with Ordinary Portland Type 1 cement, the predicted chloride concentration is 0.38%. Using figure 10 the recommended dose of calcium nitrite would be 4.5 gallons per cubic yard of concrete having 2.5 inches of cover to the reinforcing steel.

Part 3. Examples of Projects using Pozzolins, Cathodic Protection and Corrosion Inhibitors to Extend Service Life along the LOSSAN Rail Corridor in San Diego County. *(M. Creveling)*

The design lifes of structures along the Los Angeles to San Diego Coastal Railway are being extended by using pozzolanic materials, like fly ash and or microsilica or corrosion inhibitors and epoxy coated rebar in the foundations and in those parts of the structures that are subject to chloride exposure as demonstrated in the following examples.

Example 3.1 – Rail Bridge 230.6 over Aqua Hedionda Lagoon.

Timber Piled Rail Bridge 230.6 on the LOSSAN Corridor spanning Aqua Hedionda Lagoon was replaced in 2006 with a new precast prestressed girder superstructure founded on cast-in-place piers and piles as shown in Figures 10 and 11. The corrosion mitigation measures used are shown in Table 2 and included increased clear concrete cover over the reinforcing steel, corrosion resistant concrete mix designs, and epoxy-coated reinforcing steel. These measures are intended to provide a bridge design life of 75 years, based on a global approach utilizing CALTRANS Memo to Designers 10-5 dated January 2002 and updated June 2010.

The construction of the new 214 long foot, single track rail bridge at mile post 230.6 occurred between September 2005 and October 2006 at a cost $5.5m.

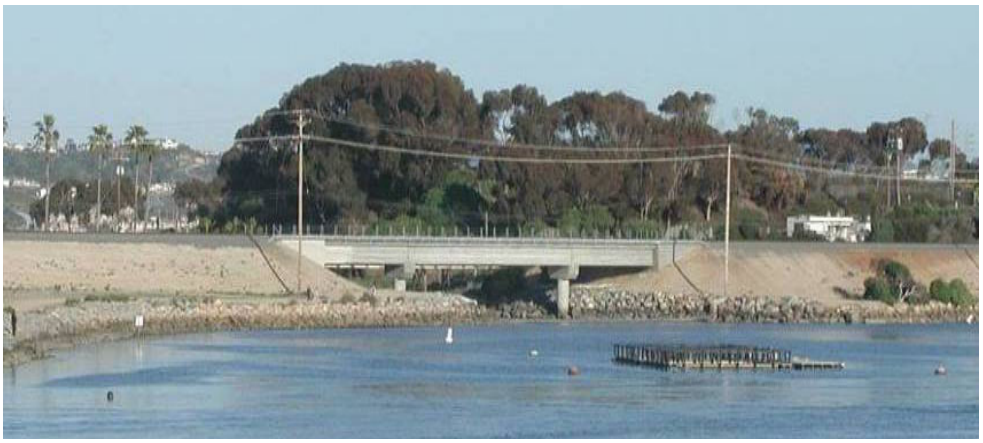


Figure 10. Rail Bridge 230.6 in Carlsbad -- Utilized Fly Ash, Silica Fume, and Epoxy-coated Rebar for a Extended Design Life.

Table 2 Corrosion Mitigation Measures used in Bridge 230.6.

Section	Mix additives	W/C	Rebar	Cover
Deck	25% Fly Ash	0.4	Epoxy Coating	2”
Abutments	25% Fly Ash	0.4	Epoxy Coating	3.5”
Stressed Beam	20% Fly Ash	0.3	Epoxy Coat Links	2”
Stressed Beam	20% Fly Ash (FA)	0.3	Stressing Strand	2.5”
Columns	20% FA & 5% Silica Fume(SF)	0.4	Epoxy Coating	3.5”
Piles	20% FA & 5% SF	0.4	Epoxy Coating	4”



Figure 11. Rail Bridge 230.6 in Carlsbad Utilized Epoxy-coated Rebar, Fly Ash, and Silica Fume to Extend the Design Life.

Example 3.2 – North Torrey Pines Road Bridge at Rail MP 245.7 in Del Mar.

For the North Torrey Pines Road Bridge on Highway 101 the rehabilitation methods included removal, replacement, and cathodic protection. The intent of the Corrosion

Management Plan (CMP) for Bridge 245.7 is to rehabilitate the bridge in order to extend its service life by 50 years. This will be accomplished through replacement of the superstructure, an extensive initial concrete repair scheme of the substructure in conjunction with an impressed current cathodic protection system, followed by an ongoing program of routine maintenance and inspections.

The following activities are currently under construction or planned for Bridge 245.7:

- Removal of all delaminated and unsound concrete from the substructure to sufficient depth so that all corroded steel is fully exposed below the affected bars
- Removal of concrete to the limits of corroded reinforcing steel
- Cleaning of all visible corrosion or other sources of bond-inhibiting materials from exposed steel
- Addition of supplemental reinforcement to patched regions for bars damaged during the removal process or with critical section loss
- Placement of appropriate patch materials
- Installation of a combination of mesh anodes, discrete anodes, and a deep anode well cathodic protection system
- Removal of existing superstructure deck, girders, railings, and bearing pads; replaced with new bearings, precast girders, and cast-in-place concrete deck with matching architectural treatments and a railing providing similar character
- Performance of regular inspections, maintenance, and scheduled routine repairs to delaminated areas

The construction contract for the rehabilitation of Bridge 245.7 for $13 million was approved by the City of Del Mar in October 2010. The reconstruction time is estimated at 2.5 years.

Part 4. Calcium Nitrite Admixture for Corrosion Protection. (Jeff Teig)

Maintenance and replacement of rail bridges can be a costly endeavor. The cost of performing the actual maintenance is usually far less than the cost of having a bridge out of service. When a rail bridge is out of service, freight and passengers cannot be moved along the line on which the bridge is located. Unlike highways, detouring rail traffic is expensive for additional mileage that the freight has to cover if an alternative route is available. For passengers, detouring is usually accomplished by busing the passengers around the bridge, which has a high cost, not only in the use of the buses and the drivers, but also in the loss of ridership during the outage. Bridge repairs involving concrete are a high cost maintenance item when we consider the time that is needed to have the bridge out of service to perform repairs on the concrete.

Because the maintenance costs and risks can be so high for concrete structures in marine environments, the Union Pacific Railroad contracted with HDR Engineering and Grace Construction Products to perform a life cost study to try to reduce or eliminate future concrete repairs in such environments. The study was titled, “Durability Report; Corrosion Protection Analysis, prepared by Grace Construction Products for HDR Engineering and Union Pacific Railroad (UPRR) Bridge 762.71”

dated February 11, 1998. The goal of the study was to develop a concrete mix design that would eliminate the need for concrete maintenance due to corrosion of the reinforcing steel and provide a 100 design life of bridges in a marine environment. Per AREMA, the design life of a steel and/or concrete bridge is 100 years. UPRR would use the recommended mix design for new bridges on their system that are exposed to salt and brackish water.

Four corrosion reduction aspects were considered during the study; reduced concrete permeability and corrosion rate, increased corrosion threshold, epoxy coating rebar and combinations of these methods. For the pile, an impervious membrane was also considered. Life cycle costs were also estimated to see which system provided the most economical solution.

Replacement of cement with silica fume or fly ash decreases the permeability of the concrete. The addition of calcium nitrite increases the threshold of the start of corrosion of the reinforcing steel. Epoxy-coated reinforcing steel delays the start of corrosion. All concrete mixes studied had a water to cement ratio of 0.45. The results of the study are shown in Table 3 and determined that the following admixtures added to a cubic yard of standard concrete mixes gave the best life cycle cost of the studied bridge elements:

Table 3. UPRR Durability Analysis Recommendations for Bridge 762.71

Bridge Member	Calcium Nitrite 30% /Yd	Silica Fume	Fly Ash	No. of Repairs	Cover
Pre-stressed Box Beams	6 gallons	7.5%	0%	3	1.5”
Cast-in-place Pile Caps	5 gallons	0%	20%	2	2”
Concrete Filled Pipe Pile	4 gallons	0%	0%	1	4”

The UPRR standardized the amounts of admixtures per cubic yard of concrete to keep the mixes consistent using 5 gallons of Calcium Nitrite in addition to 7 percent silica fume. All mild steel reinforcing is to be epoxy coated and pre-stressing steel would not be coated. The steel pipe piles were proposed to be coated with epoxy. The calcium nitrite and silica fume in the concrete mix design and epoxy-coated reinforcing all add to the life cycle cost and service life but reduce the number of repairs in all cases. The UPRR has successfully used the mix design at several bridge locations up and down the Pacific Coast in salt and brackish water. The UPRR previously had used 4 gallons of Calcium Nitrite for concrete in pipe piles but due to the low volume of cast-in-place concrete for piles versus all other bridge elements and to avoid confusion on construction sites the UPRR decided to use 5 gallons as a standard for all their mix designs.

In 2008 during design development of LOSSAN Bridge 207.6 and Bridge 223.1 meetings were held between HDR and North County Transit District and based on a consensus recommendation concrete mix designs using 4 gallons of Calcium Nitrite corrosion inhibitors were approved for use in Bridges 207.6 and 223.1. In high exposure elements like the CIDH Piles rebar cover was increased to 5” on Br 223.1. The cover on the pile caps on Br 207.7 was increased to 3 inches. With the increased cover the 4 gallons of calcium nitrite was believed to be sufficient to obtain 100 years of service life.

Example 4.1 Santa Margarita River Bridge 223.1 Replacement Project

The existing rail bridge over the Santa Margarita River, shown in figure 12, is to be replaced with a new double track bridge and two miles of second track for an anticipated construction cost of $26.3m. The main river crossing will be 200 feet long with 150ft cast in place end spans. The southern approach trestle is 252 feet long and consists of nine 28 foot precast double box beams. The existing bridge piers were built in 1916 with a 1:3:5 concrete mix and minimal reinforcement. They are in relatively good condition.



Figure 12. Existing Rail Bridge 223.1 across the Santa Margarita River

For the new main spans of Bridge 223.1 the specified concrete is 5,500 PSI and has four gallons per cubic yard of Calcium Nitrite (CaNi) corrosion inhibitor, and 3 inches of cover to the rebar of the entire superstructure to increase the service life. Corrosion Mitigation Measures for the main span are summarized below in Table 4.

Table 4. Corrosion Mitigation Measures for Bridge 223.1

Section	Mix additive	Mix	Rebar	Cover
Deck	4 gallons CaNi	5500 psi	Epoxy Coating	2”
Abutments	4 gallons CaNi	5500 psi	Epoxy Coating	3”
Stressed Box Girder	4 gallons CaNi	5500 psi	Epoxy Coat ing	3” outside 1” inside
Pile Cap	4 gallons CaNi	5500 psi	Epoxy Coat ing	3” sides & top, 6” bottom
Piers	4 gallons CaNi	5500 psi	Epoxy Coating	3”
CIDH Piles	4 gallons CaNi	5500 psi	Epoxy Coating	5”

Example 4.2 San Mateo Creek Rail Bridge 207.6

The northern portion of San Mateo Creek Rail Bridge 207.6 is being replaced with a pre-stressed concrete single track bridge with a construction value of $4.8m as shown in Figure 13.



Figure 13. LOSSAN Bridge 207.6 Replacement on San Mateo Creek.

HDR specified calcium nitrite be added at four gallons per cubic yard to extend the service life of the structure with appropriate allowances for rebar cover. In addition purple epoxy-coated reinforcement (ECR) was specified in the piles, pile caps deck. The Corrosion Mitigation Measures are summarized below in Table 5.

Table 5. Corrosion Mitigation Measures for Bridge 207.6

Corrosion Mitigation Measures used in San Mateo Creek Bridge 207.6				
Section	**Mix additive**	**Mix**	**Rebar**	**Cover**
Deck	4 gallons CaNi	6000 psi	Epoxy Coating	1.5”
Stressed 2 cell Box Beams	4 gallons CaNi	6000 psi	Epoxy Coat ing strand & rebar	1.5”
Abutments	4 gallons CaNi	4000 psi	Epoxy Coating	3”
Pile Caps	4 gallons CaNi	4000 psi	Epoxy Coating	3”
CIDH Piles	4 gallons CaNi	4000 psi	Epoxy Coating	Steel casing

4. Conclusions.

In temperate climates the addition of additives like fly ash, silica fume, and or corrosion inhibitors, like calcium nitrite, is required to achieve a service life of 100 years or greater, provided that adequate cover is obtained for reinforcement protection, as shown in figures 6 and 7. The predictions provided are for concrete made with type 1 cement which offers the greatest protection from chloride attack. Further research is needed for other cement types as used in this region.

New methods of modeling chloride ingress that are more computer friendly need to be developed. The iterative process of simulating Fick’s second law needs to be replaced with more user friendly methods.

SANDAG has engaged a service life modeling consultants to finalize our new concrete design criteria in San Diego for future LOSSAN Corridor Bridge structures to ensure that we invest in new structures that will still be in service in 100 years.

5. References;

Askeland D. 1989. "The Science and Engineering of Materials", Ch.5. PWS Publishing Co, Boston, 1989, p122.

Berke, N.S .& Matta G. 1994. "The use of Calcium Nitrite Corrosion Inhibiting Admixture to extend the life of Reinforced Concrete in the Gulf." Neal Berke WR grace Co, G Matta, Dr Matta &Associates. Proceedings of the 1st International Conference on Reinforced Concrete Materials in Hot Climates, UAE University, Alain, U.A.E., pp761-772.

Caltrans 2002. "Caltrans Memo 10-5 to Designers, Protection of Reinforcement Against Corrosion Due to Chlorides, Acids and Sulfates', California Department of Transportation, dated January 2002.

CTL 1999. "Petrographic and Chloride Test Results, North Torrey Pines Bridge", for City of San Diego by CTL Testing and Material Technology dated March 1999.

Grace 1998. "Durability Report; Corrosion Protection Analysis, Union Pacific Railroad (UPRR) Bridge 762.71", by Grace Construction Products, Cambridge Massachutes for HDR Engineering and, dated February 1998.

Microchem 2010. "Petrographic Examination and Chemical Analysis of Concrete Core Specimens for San Onofre Pulgas Double Track Project". SWE project No. 544-100. Marh 30, 2010.

Smith B.G. 2001. "Durability of Silica Fume Concrete, Exposed to Chloride in Hot Climates", The ASCE Journal of Materials in Civil Engineering, Volume 13 No.1, Jan/Feb2001 by Bruce Smith MASCE.

Simon Wong Engineering (SWE) 2006. "The Existing Condition and Rehabilitation Report for the North Torrey Pines Road Bridge at the San Diego Northern Railroad". Simon Wong Engineering Job No. 517-300 dated May 2006.

SWE 2009. "Corrosion Management Plan for Bridge 245.7", by Simon Wong Engineering, dated December 2009.

Maintenance of Navigable Depths at the Hawaii Kai Marina and Entrance Channel Oahu, Hawaii

Michael Whelan, P.E.[1], Rob Walker, P.E.[2], and Tracy Stofferahn[3]

Anchor QEA, L.P., 26300 La Alameda, Suite 240, Mission Viejo, CA 92691
[1]mwhelan@anchorqea.com; [2]rwalker@anchorqea.com;
[3]tstofferahn@anchorqea.com

ABSTRACT

The Hawaii Kai Marina (marina) is located on the southern coast of Oahu, approximately 12 miles east of downtown Honolulu. The entrance channel to the marina experiences significant sand deposition and shoaling, which interfered with navigation many times in past years, and requires repeated episodes of sand removal. Shoaling within the marina occurs at a much slower rate but, also requires attention. The case study presented herein presents the formulation of a plan to dredge both the entrance channel and the marina interior, while maximizing the beneficial reuse and on-site disposal of the dredged materials. This paper also discusses the ongoing investigation of sustainable management schemes for sand deposition in the entrance channel, and reviews some of the environmental and design challenges that are unique to this location in Hawaii.

SITE CONDITIONS AND HISTORY

The community of Hawaii Kai is located on the southern coast of Oahu, at the eastern end of Maunalua Bay, approximately 12 miles from downtown Honolulu (see Figure 1). The development now includes approximately 2,400 single- and multi-family residences, three commercial shopping centers, and a full-service marina. The marina is administered and managed by the Hawaii Kai Marina Community Association (HKMCA), and serves more than 1,000 registered vessels

while providing important public functions such as safe harbor for passing vessels and a base of operations for fire and rescue operations during times of emergency.

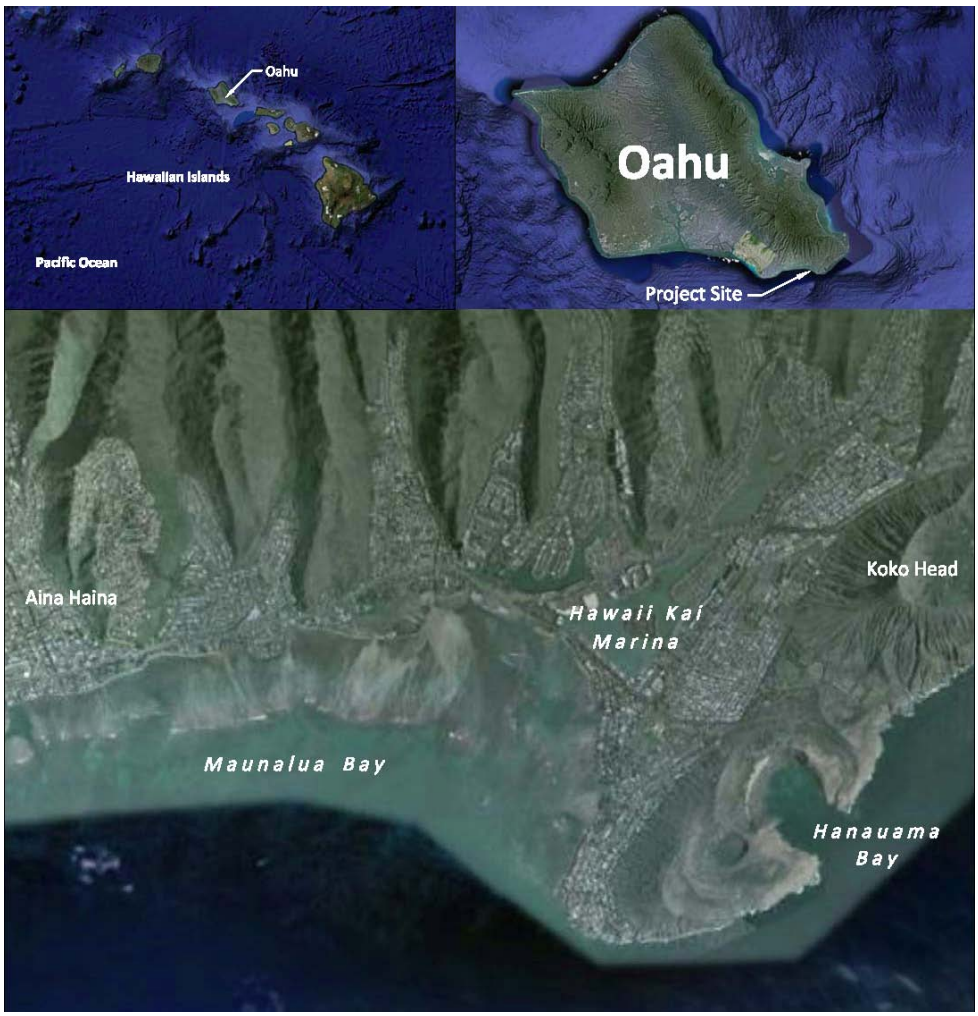
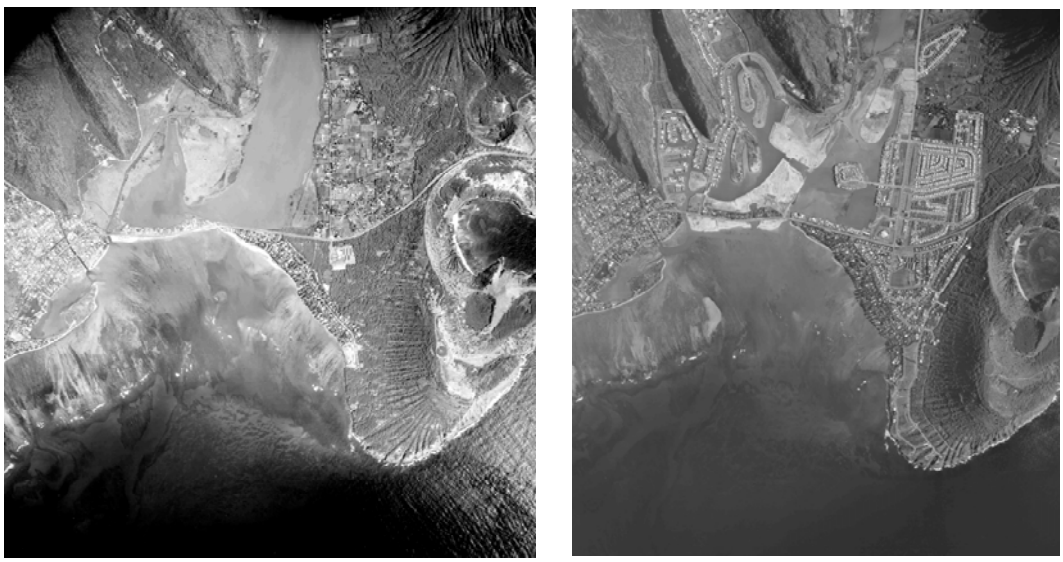


Figure 1. Vicinity map of the Hawaii Kai Marina located at Maunalua Bay, Oahu, Hawaii.

The marina and surrounding community are located within an area historically known as Kuapa Pond, a fishpond that dated back centuries. In the 1930s, the Kalanianole Highway was built along a rock and sand berm running along the perimeter of Maunalua Bay. In 1959, Henry J. Kaiser began development of the Hawaii Kai community on 6,000 acres that were, for the most part. untouched land. At that time, the marina was dredged to -6 feet Mean Sea Level (MSL), and a

navigable entrance channel was created by widening the existing inlet from 40 to 250 feet and deepening it to a depth of -8 ft MSL (Oceanit 1998).

Much of the original sediment removed during marina construction was used for the creation of upland areas for the Hawaii Kai community. In an attempt to provide a location for material dredged from the marina, dredged material disposal islands now referred to as Rim Island No. 1 and Rim Island No. 2 were constructed in the 1960s to provide additional sediment storage locations. Additional dredged material was used to modify the shoreline of Maunalua Bay Beach. Figure 2 depicts the layout of the area before and after development of the marina.



A. B.

Figure 2. Aerial photographs of Maunalua Bay depicting conditions before and after development of the Hawaii Kai Marina. North is toward top of photos. Photo credits: U.S. Geological Survey (USGS).

A. Photo from 1959 showing historic Kuapa Pond prior to development of the Hawaii Kai Marina.

B. Photo from 1968, approximately 9 years after construction began, showing islands and features within the marina created from dredging spoils. Shoreline modifications are apparent along Maunalua Bay beach.

DREDGING AND MANAGEMENT OF SEDIMENTS WITHIN MARINA

As previously stated, the marina is home to numerous private vessels. It receives inflow from a number of channels and creeks carrying sediment loads from upland areas and hillsides. As a result, it has been subject to ongoing sedimentation over the years. Last dredged in 1996, subsequent sedimentation and shoaling at the marina has reached a point where the existing mudline is at elevations above -4 feet mean lower low water (MLLW) in many areas (Figure 3), particularly those in closest proximity to points of water inflow. These relatively shallow depths are adversely impacting navigability for the various private boats in the marina. In 2008, the HKMCA started developing a plan for a new dredging event to return marina waters to the necessary depth of -4 feet MLLW or deeper. This would be done in conjunction with dredging the entrance channel below the Kalanainaiole Highway, as described in the next section.

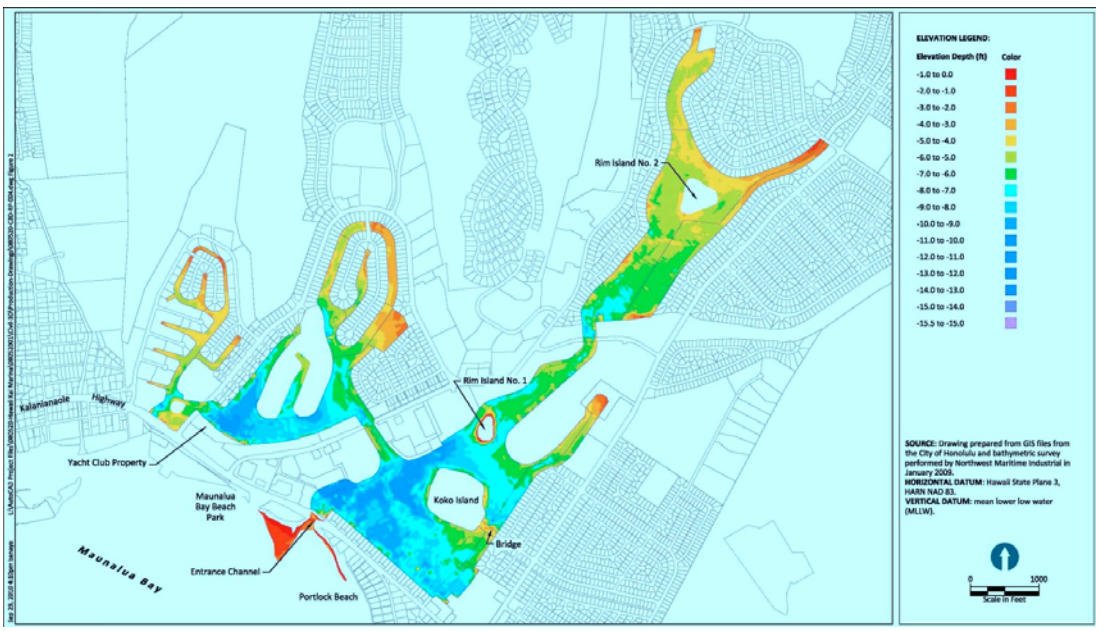


Figure 3. Color-contoured plot of bathymetry in Hawaii Kai Marina, depicting mudline elevations in early 2009.

Since the original construction of the marina, sediments dredged from the marina have been placed on the two Rim Islands, which were constructed expressly for that purpose. The most recent instance of sediment placement on the Rim Islands was in 1996. Since that time, shallow water and open mudflat areas in the interior of Rim Island No. 2—the larger of the two Rim Islands—were identified by the U.S. Fish and Wildlife Service (USFWS) as being suitable habitat for Hawaiian stilt, a federally-listed endangered species (USFWS 2003). As a result, Rim Island No. 2 was judged by the HKMCA to be a problematic candidate for sediment disposal, owing to the significant permitting hurdles and mitigation challenges that were likely to arise. The smaller island, Rim Island No. 1, remained available for sediment disposal uses, with an estimated capacity of 12,000 cubic yards.

The HKMCA commissioned a bathymetric survey of the entire marina area in early 2009 in order to more accurately delineate areas that would need dredging, and to determine the quantity of sediment that would need to be removed. The results of this survey indicated that the actual volume of sediment was well in excess of the 12,000 cubic yards of capacity provided by Rim Island No. 1. In total, up to approximately 110,000 cubic yards of material was projected to be removed from the marina by dredging approximately 37 acres of water area. This volume assumes a maximum planned dredge depth of -6 feet MLLW; based on a required dredging depth of -5 feet MLLW, plus 1 foot of allowable overdredging.

Needing to identify additional alternatives for sediment disposal, the HKMCA embarked on a sequenced search for sediment management options to accommodate the proposed dredged material, making use of the material as a beneficial resource to the greatest extent possible. Sediments dredged from the marina do not appear to contain a suitable percentage of sand to qualify for beach nourishment (unlike sediments in the entrance channel, as discussed in the next section). Off-site upland disposal options such as fill for upland development or landfill daily cover were explored, but no feasible or cost-effective upland disposal options have been identified.

After further evaluation of onsite disposal options, in addition to filling Rim Island No. 1 to full capacity (12,000 cubic yards), the HKMCA identified the planned Yacht Club Property, located north of the Kalanianaole Highway Bridge, as a location where dredged materials could be used as fill material for regrading purposes. This was estimated to contribute another 5,000 cubic yards of on-site sediment placement capacity. Together, these two on-site locations would therefore provide 17,000 cubic yards of capacity, still well below the total planned dredging volume of approximately 110,000 cubic yards.

Having exhausted the available upland sediment placement opportunities, the HKMCA chose to pursue potential sediment disposal at the South Oahu Ocean Dredge Material Disposal Site (SOODMDS), managed by the U.S. Environmental Protection Agency (EPA) and U.S. Army Corps of Engineers (USACE). A program of sediment sampling and analysis was designed to evaluate sediments for their chemical and biological suitability for open ocean disposal.

Table 1 summarizes the three different disposal locations for sediments dredged from within the marina.

Table 1
Disposal Locations for Marina Dredging*

Disposal Location	Approximate Volume (cubic yards)
Yacht Club Property	5,000
Rim Island No. 1	12,000
South Oahu Ocean Dredge Material Disposal Site	Approximately 93,000
TOTAL	**110,000**

*Sand removed from the entrance channel is not included in this table, and will be placed on adjacent beaches.

The proposed area to be dredged was sectioned into four separate areas (termed dredge units) for the purpose of sampling and analysis activities. Sediment cores were collected from multiple stations and combined to create one composite sample from each dredge unit for testing and analysis.

Testing for ocean disposal included physical, chemical, and biological analyses, per regional and federal guidance. Results of chemical analysis indicated that concentrations of contaminants were relatively low. Benthic and water-column toxicity tests indicated that sediments were not acutely toxic to benthic or water-column organisms. Bioaccumulation tests and tissue chemistry were conducted to evaluate the potential of benthic organisms to accumulate contaminants from the dredged material. Based on the results of sediment and tissue analysis, sediments from within the marina were indicated as being suitable for ocean disposal.

Although no specific upland disposal location had been identified, testing was also conducted for this potential option, using the Toxicity Characteristic Leaching Procedure (TCLP), used to evaluate contaminants in leachate produced after placement of dredged material at an upland site. TCLP testing indicated that sediment would be suitable for upland placement, if an available site were to be identified.

MANAGEMENT OF SAND SHOALING WITHIN ENTRANCE CHANNEL

Entrance to and exit from the marina is via a channel that was dredged when the Kalanianaole Highway Bridge was originally constructed. The channel is approximately 250 feet wide by 400 feet long, and was initially dredged to a depth of -8 feet MSL to allow boats from the marina to enter and return from the bay as well as to provide better drainage of the marina basin. Immediately west of this entrance channel is Maunalua Bay Beach Park; east of the entrance channel is Portlock Beach.

Ongoing accretion of sand in the entrance channel has gradually encroached on the channel's navigable width. The shoaling has repeatedly been apparent on the eastern edge of the channel adjacent to Portlock Beach, indicating that a key source of the accumulating sand is from this beach area, apparently in response to the prevailing westward longshore currents and wave action. Sand accumulates within the entrance channel inlet and under the highway bridge, such that over

time it has formed a large accreted area with submerged sandbars, partially blocking the entrance channel and hindering vessel navigation.

Although the entrance channel was previously maintained by the State of Hawaii, the HKMCA now carries responsibility for managing depths within the channel, and is developing a plan for dredging the channel in conjunction with the dredging of the marina interior.

Maintenance dredging of the marina's entrance channel will involve the removal of approximately 10,000 cubic yards of material down to a maximum dredge depth of -8 feet MLLW (see Figure 4). Dredging will be required to a depth of -7 feet MLLW with 1 foot of allowable overdredging. The dredge area is approximately 650 feet long, resulting in a total dredging footprint of approximately 3 acres.

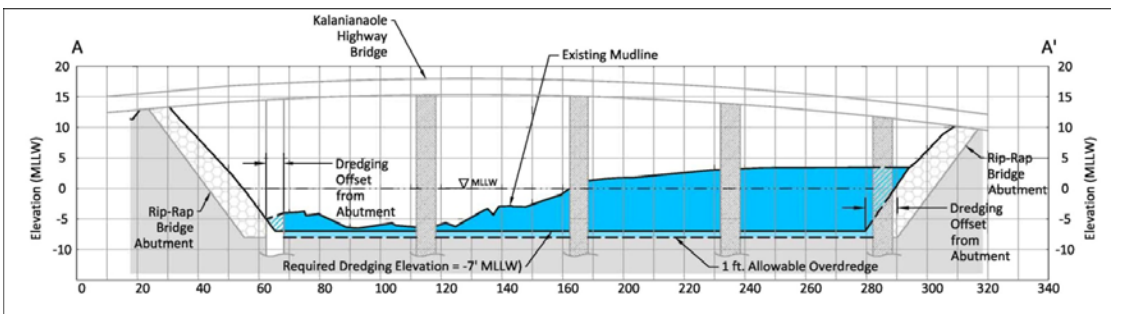


Figure 4. Profile across entrance channel (and Kalanianaole Bridge) showing planned dredging of accumulated sand.

HKMCA proposes to utilize the coarser-grained sandy sediment within the entrance channel shoaling area for placement along the adjacent shorelines of Portlock Beach and Maunalua Bay Beach Park (Figure 5). This beneficial reuse alternative is preferred to upland or offshore disposal options, as it returns needed material to the littoral system. The resulting beach nourishment offers benefits of increased habitat, protection of existing shoreline infrastructure, and a public recreation area to the eroding shorelines of Maunalua Bay.

State of Hawaii Department of Land and Natural Resources (DLNR) guidelines for beach nourishment projects dictate that the material proposed for dredging be tested for its suitability for beach placement. Sediment cores from the entrance channel dredging area were found to consist of sand and coarse-grained materials. All samples met DLNR guidelines of no more than 6 percent fines and no more than 50 percent material less than 0.125 mm. Based on these results, sediment from the entrance channel was determined to be suitable for beach nourishment.

Accordingly, sandy material dredged from the entrance channel is planned to be placed along the adjacent beach areas. The DLNR has clearly stated their preference that the sand be placed on the shorelines of both Maunalua Bay Beach Park to the west and Portlock Beach to the east to benefit both beach areas.



A. B.

Figure 5. Proposed beach nourishment locations.
A. Portlock Beach (east of entrance channel)
B. Maunalua Bay Beach Park (west of entrance channel).

PERMITTING FOR PROPOSED MAINTENANCE DREDGING ACTIVITIES

The HKMCA is in the process of obtaining permits in support of the upcoming round of maintenance dredging. These permits are similar to those required for most shoreline and in-water projects in the State of Hawaii, and are briefly summarized in Table 2.

Table 2. Key Federal, State, and Local Permits Required for Hawaii Kai Marina Maintenance Dredging Project

Regulatory Agency	Permit(s) and Related Consultation(s)	Environmental Issues or Reason for Permit
USACE	Standard Individual Permit - Consultation with NOAA Fisheries - Consultation with State Historic Preservation Office - National Environmental Protection Agency (NEPA) Environmental Assessment/ Finding of No Significant Impacts (FONSI)	- Clean Water Act (CWA) (Section 404) regulating discharge of dredged material - Rivers and Harbors Act (Section 10) regulating work in navigable waters
DLNR	Conservation District Use Permit - HEPA Final Environmental Assessment/FONSI	- Analyses to ensure there are no potential significant impacts to the environment or the public for projects on State-owned aquatic lands - Consistency with special Conservation District requirements to conserve, protect and preserve the natural resources of the state.
State of Hawaii Department of Business, Economic Development and Tourism	Coastal Zone Management Act (CZMA) Federal Consistency Determination	Consistency with zoning requirements for all projects in the coastal zone to conserve resources in a sustainable manner.
State of Hawaii Department of Health	- CWA Section 401 Water Quality Certification - CWA Section 402 Stormwater General Permit (NPDES)	Protection of surface waters during dredging and discharge of sediment, and Best Management Practices to control effects of runoff from on-land material placement activities

LONG-TERM MANAGEMENT STRATEGIES FOR ENTRANCE CHANNEL

Although the planned maintenance dredging event will provide for navigational use of the entrance channel for the immediate future, the causes of sand accumulation in the channel continue unabated. Review of historical shoreline imagery and data obtained from an erosion study conducted by the University of Hawaii Coastal Geology Group has shown that this accretion at the inlet has been ongoing since the channel was first dredged. Additionally, Portlock Beach appears to have gone through cycles of erosion and accretion, likely in response to various construction activities at the project site.

Historical shoreline records indicate that after beach nourishment from past dredging events, the sediments migrate back from the beach to the inlet at a fast rate (less than 5 years). Historical trends also indicate that without any outside influences, the Portlock Beach shoreline is attempting to reach its equilibrium shoreline location prior to development in the late 1950s. Likewise, unless intercepted and moved back to the south end of the beach, any sand placed on Portlock Beach will likely migrate back into the inlet over time.

In 1998, DLNR applied for permits to construct a "demonstration-level" sand retention structure consisting of a series of sand-filled polyester geotextile bags arranged to form a terminal groin extending approximately 90 feet into Maunalua Bay, immediately east of the entrance channel. The intended purpose of this installation was to block the migration of sand westward from Portlock Beach into the entrance channel, thereby reducing further siltation of the entrance channel. This sand bag retention system was installed in 2005, measuring approximately 12 feet in width, 4 to 5 feet in height and reaching from the shoreward vegetation line to an approximate depth of -3 feet MLLW. Each individual geotextile bag was approximately 8 feet long, 4 feet wide, and 1.5 feet thick, holding approximately 2.3 cubic yards of sand and weighting 3 tons. Figure 6 shows an illustration of this sand retention structure relative to the entrance channel.



Figure 6. Entrance Channel to Hawaii Kai Marina and approximate position of previous sand retention structure.

This retention system was intended to be used as a demonstration project and monitored over a 5-year period, with allowance for modifying the structure if necessary. The DLNR did not conduct any systematic monitoring program after it was installed, however. Based on a review of previous shoreline records, the sand bag retention structure appeared to be serving its intended purpose by limiting erosion of the shoreline east of its location, for a period of a few years. Within 5 years of its construction, however, the sand bag's capacity to retain migrating sand appears to have been reached due to continued westward sand migration towards the entrance channel. The sand bags are no longer effective as a barrier to impede sediment transport and sand is starting to migrate over the top of the structure and eventually settle out within the entrance channel limits. The sand bag feature is still visible at the time of this publication, although significant deterioration of the polyester bags is evident.

The HKMCA is currently in the process of investigating long-term management strategies for this ongoing issue, and is interested in developing a sustainable management scheme for marina operations, while minimizing impact to surrounding beaches and sensitive habitats. Sediment transport mechanisms within the adjacent portion of Maunalua Bay are currently being studied in an effort to identify a more sustainable long-term management scheme.

Options for long-term management of the entrance channel include, but are not limited to, the following options, which are currently being investigated by the HKMCA:

- Improvement or replacement of the remnant sand bag retention structure on the east side of the entrance channel
- Additional dredging alongside the entrance channel to form a depressed sediment deposition basin (the presence of limestone and rock rubble at shallow depths appears to post a hindrance to this concept)
- Design and installation of a more permanent sand retention feature, such as a rock jetty or groin

This investigation is being informed by sediment transport modeling, incorporating known shoreline conditions, physical properties of the carbonate sands, and historic wind and wave trends. Initial results of the modeling to date appear to support the concept that the primary source of sand to the entrance channel is indeed the adjacent Portlock Beach, and that transport rates are high enough to promote return of beach placement sand back to the entrance channel within a timespan of only a few years. The ongoing analyses will continue to focus on shoreline changes over time to estimate the impacts to the surrounding shorelines, as well as evaluate proposed alternatives and their anticipated shoaling response to assess the overall effectiveness of any particular management program.

REFERENCES

AECOS, Inc., 2010. *Draft Marine Biological and Water Quality Resources at Hawaii Kai Marina*, Hawaii Kai, Oahu. September 9, 2010.

Anchor QEA, L.P., 2010. *Sampling and Analysis Report*. Prepared for the Hawaii Kai Marina Community Association by Anchor QEA, L.P. December 2010.

EPA and USACE (U.S. Environmental Protection Agency and U.S. Army Corps of Engineers), 1991. *Evaluation for Dredged Material Proposed for Ocean Disposal – Testing Manual (OTM)*. EPA 503/8-91/001. EPA Office of Water (4504F).

Oceanit Laboratories, Inc., 1998. Final Environmental Assessment, Maunalua Bay Dredging, Oahu. Prepared for the Department of Land and Natural Resources. October 1998.

USFWS (U.S. Fish and Wildlife Service), 2003. *Letter to Lt. Colonel Ronald N. Light, District Engineer, U.S. Army Corps of Engineers*. 4 pp.

The Life and Death of North America's First Man-Made Surfing Reef

Craig B. Leidersdorf[1], Brady Richmond[1], and Chad E. Nelsen[2]

[1] Coastal Frontiers Corporation, Chatsworth, CA 91311; (818) 341-8133; cleidersdorf@coastalfrontiers.com; brichmond@coastalfrontiers.com

[2] Surfrider Foundation, P.O. Box 6010, San Clemente, CA 92674; (949) 637-2137; cnelsen@surfrider.org

ABSTRACT

This paper reviews the history of North America's first man-made surfing reef with the intent of informing the planning, implementation, and removal of man-made structures in the nearshore zone. The most positive outcome of the project was the recognition by regulatory agencies that natural surf breaks represent finite recreational resources worthy of preservation or, if necessary, mitigation. Conversely, the failure of Pratte's Reef to produce a sustained improvement in surf quality highlights the fact that nearshore reef structures are in the early stages of development. Until a substantial body of experience is acquired, they should be considered experimental and prone to unintended outcomes. A key lesson learned from Pratte's Reef relates to the difficulty and cost of removing geotextile containers from the nearshore environment. While geotextiles can be recovered with relative ease if they are located within reach of conventional earth-moving equipment operated from shore, the removal process is time-consuming, costly, and incomplete if the containers lie offshore. The result, in the case of Pratte's Reef, was a removal cost that matched the installation cost.

INTRODUCTION

In September 2000, the Surfrider Foundation initiated construction of an experimental surf-enhancement reef off Dockweiler State Beach in El Segundo, California (Figure 1). As mandated by the California Coastal Commission, the objective was to mitigate the impact on surfing that resulted from the construction of a shore-perpendicular groin at the El Segundo Refinery. The project was unique in that it not only produced the first man-made surfing reef in North America (and one of the first in the world), but also represented the first occasion on which a regulatory agency recognized a surf break as a natural recreational resource that warranted preservation or, in this case, mitigation.

Notwithstanding the excitement generated by permit approval, design and construction, Pratte's Reef failed to produce a permanent enhancement in surf quality. When periodic monitoring inspections revealed that the geotextile bags used

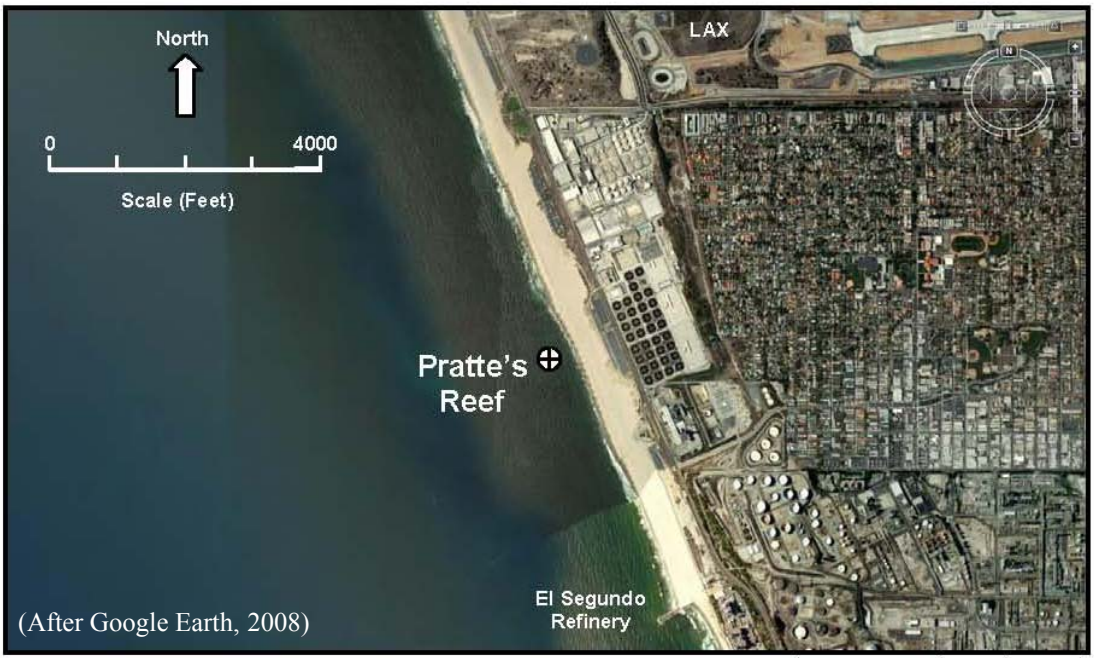


Figure 1. Location Map

to construct the reef had begun to deteriorate, the Surfrider Foundation commenced removal operations in the fall of 2008. A second and final phase of removal work followed two years later in the fall of 2010.

During the past decade, significant effort has been expended in the planning, design, and construction of "multi-purpose" reefs. In addition to improving surf quality, these structures are intended to address needs that include mitigating coastal erosion and providing hard-bottom habitat for nearshore organisms. Significant geotextile-based structures that have been constructed to date include Narrowneck Reef in Gold Coast, Australia (2001), Mount Reef in Mt. Maunganui, New Zealand (2005), Kovlam Reef in Western India (2009), and Bournemouth Reef in Boscom, U.K. (2009). In the United States, similar structures have been considered (but not constructed) in Florida and California.

The intent of this paper is to review the history of Pratte's Reef in a manner that will inform the planning, implementation, and removal of man-made structures in the nearshore zone. Particular emphasis is placed on removal – an activity that proved to be both difficult and costly in the case of Pratte's Reef, and that therefore warrants careful consideration when evaluating the desirability of such structures in the future.

DESIGN AND CONSTRUCTION

Permits to construct Pratte's Reef were issued by four entities: the California Coastal Commission, the U.S. Army Corps of Engineers, the California Regional Water Quality Control Board, and the City of Los Angeles Department of Recreation and

Parks. The permits identified the structure as an "experimental temporary (10-year) surfing reef" that would be dismantled if it caused unforeseen problems. Alternatively, if the reef proved to be successful in enhancing surf quality, its service life could be extended by amending the original permits.

Based on an agreement among Chevron Corporation (the owner of the El Segundo Refinery), the Coastal Commission, and the Surfrider Foundation, the budget available for reef design and construction was $300,000. This modest amount severely constrained the size of the structure, which in turn contributed to its inability to improve surf quality. As a point of reference, the recently-completed Bournemouth Reef reportedly cost more than $5.3 million (£3.2 million; Daily Mail, 2011).

The initial design consisted of 110 geotextile bags placed in a V-shaped configuration with the apex of the V facing offshore (Figure 2; Skelly Engineering, ca 1999). The bags were fabricated from woven polypropylene and fitted with nylon lifting straps to facilitate handling and placement. As reported by Borrero (2001a), each bag measured 10 ft long, 7 ft wide, and 4 ft high (3.0 x 2.1 x 1.2 m), and weighed approximately 14 tons (12.7 tonnes) when filled with sand (Figure 3). The sand fill was beach-compatible in terms of size and composition to minimize the impact if it were discharged from the bags.

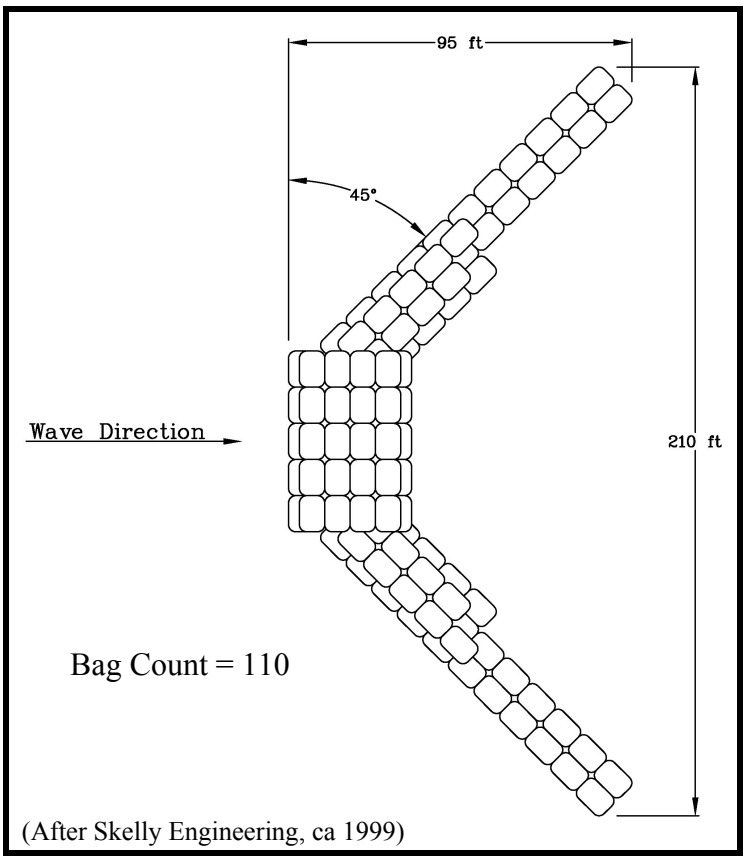
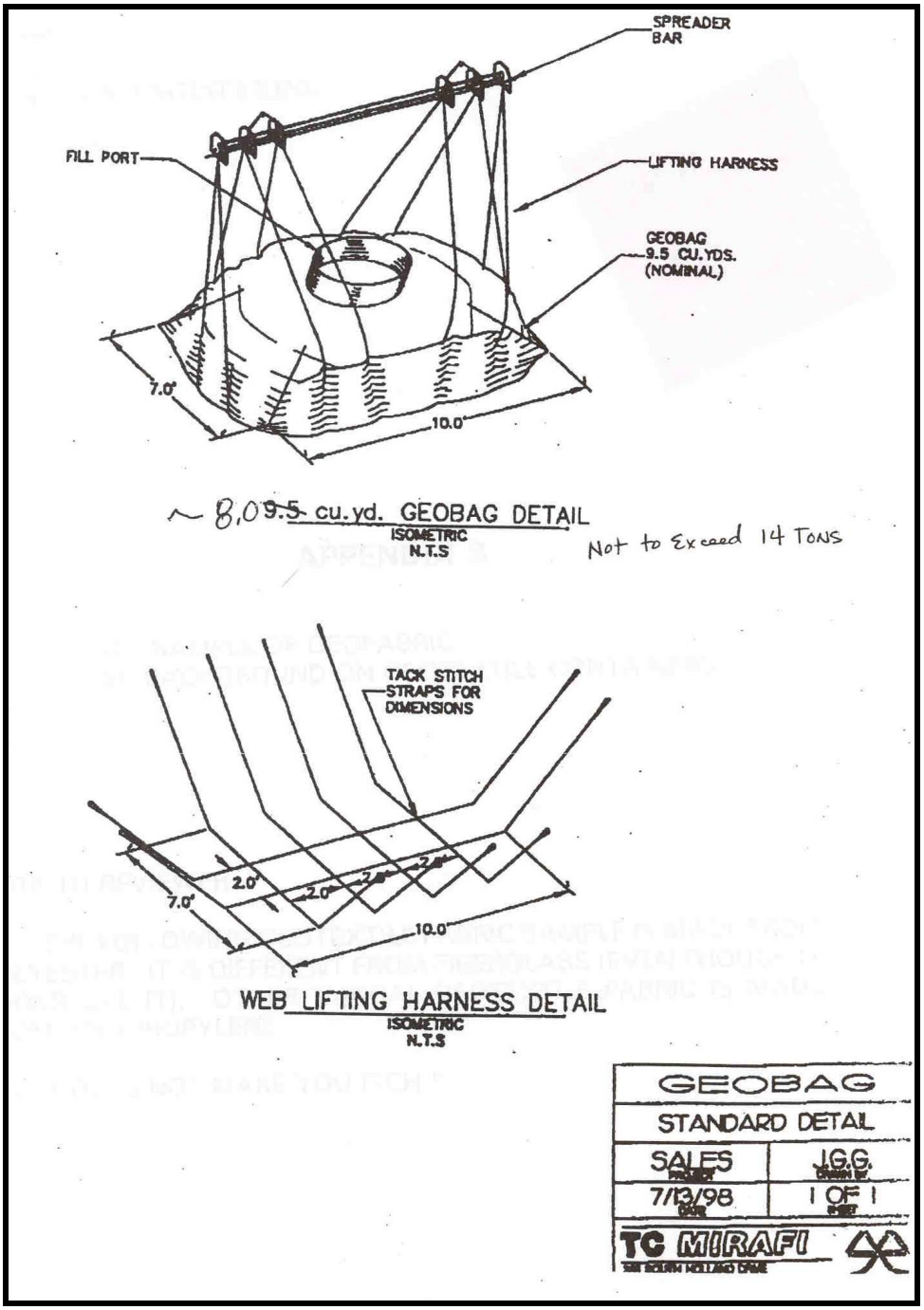


Figure 2. Design Configuration of Pratte's Reef



(Source: Skelly Engineering, 2000)

Figure 3. Geotextile Bag Design

Reef construction occurred in September 2000. As shown in Plate 1, the bags were placed using a crane operated from a barge. Approximately 15 bags were damaged during filling and placement, leaving about 95 bags for installation on the sea bottom. The natural water depth at the apex of the reef was approximately 10 ft (3.0 m) relative to Mean Lower Low Water ("MLLW", which represents the vertical

datum for all depths reported herein) at the time of construction, while the depth over the apex itself was reported to be approximately 6 ft (1.8 m; Borrero, 2001a). By the end of the following month (October 2006), a dive inspection revealed that scour had increased the water depth to as much as 13.5 ft (4.1 m) on the landward side of the structure.



(Source: Borrero, 2001a)

Plate 1. Reef Installation in September 2000

The inadequate size of the reef was recognized from the outset, leading to a second phase of construction in April 2001. Based on the availability of $250,000 in additional funding, 90 bags were added to increase the height and width of the structure. Construction losses were minimized by using high-strength polyester fabric with a wide-width tensile strength of 1,000 lb/in. (1,750 N/cm; ASTM D4595) to construct the bags instead of the lower-strength polypropylene employed for the original units.

The additional bags raised the elevation of the reef apex to about 3 ft (0.9 m) below MLLW while increasing the structure's footprint. For a brief period thereafter, the expanded reef was reported to produce marginally-rideable waves that tended to break briefly before dissipating in the lee of the structure (Borrero, 2001b).

PERFORMANCE

An extensive monitoring program was conducted for two years after completion of the construction work in 2001. The program included monthly beach profile surveys of the updrift, adjacent, and downdrift beaches, quarterly bathymetric surveys of the reef and surrounding sea bottom, quarterly dive inspections of the reef itself, and near-daily observations of the surf conditions. Additional dive inspections were undertaken in 2004 and 2005, and twice in 2007.

In the year that followed reef expansion, the maximum elevation of the apex decreased by approximately 5 ft (1.5 m; Borrero, 2002). Although the cause was not

definitively established, observations made during reef removal suggested that contributory factors included the displacement of stacked bags, compaction of the bag fill, and settlement resulting from scour of the sandy sea bottom. The net result was a permanent loss of the reef's ability to enhance surf quality (Borrero, 2004). Its diminished size also contributed to a finding of no discernible impact on the adjacent beaches.

With respect to structural integrity, the dive inspections documented progressive deterioration of the geotextile bags. When the final monitoring inspection was performed in November 2007, intact bags were found to be interspersed with debris that included flaps of torn fabric and knotted nylon webbing (Valor, 2007). Some of the bags were partially buried, while gaps in the structure suggested that others had been either carried away or completely buried beneath the sea floor.

To prevent further degradation of the structure, including the possible loss of geotextile fabric into the marine environment, and to fulfill the requirement for removal that was included in the original permits, the Surfrider Foundation resolved to dismantle Pratte's Reef commencing in 2008.

REMOVAL

To facilitate the development of a reef removal plan, two detailed site inspections were undertaken. The first was conducted in April 2008 to determine if eelgrass (*Zostera marina*) had colonized the structure (Shuman, 2008). Eelgrass beds tend to develop in protected and semi-protected areas of shallow water, where they provide habitat for both fish and invertebrates (Hoffman, 1986). The dive team observed patches of red and brown algae growing directly on the geotextile bags, with the growth concentrated in areas that were sufficiently far above the sea bottom to prevent burial during periods of sediment accumulation. Invertebrates (primarily barnacles) also were present, but eelgrass was absent both from the reef itself and from the surrounding sea bottom. As a result, it was concluded that reef removal could proceed without significantly impacting the nearshore habitat.

The second site visit, conducted in May 2008, included a wading survey to document the configuration of the reef and a dive inspection to assess the quantity and condition of the geotextile bags. Soundings were obtained using an electronic total station and a submersible survey rod, with data acquired on a shore-perpendicular transect through the center of the reef as well as on the reef itself. As shown in Figure 4, the structure's plan form was found to resemble the design configuration (Figure 2). The exposed bags extended approximately 240 ft (73 m) in the alongshore direction and 90 ft (27 m) in the cross-shore direction, with the apex located more than 260 ft (79 m) from the MLLW shoreline. The water depths over the bags were substantially greater than those reported after reef installation, with values ranging from 6.8 to 11.2 ft (2.1 to 3.4 m).

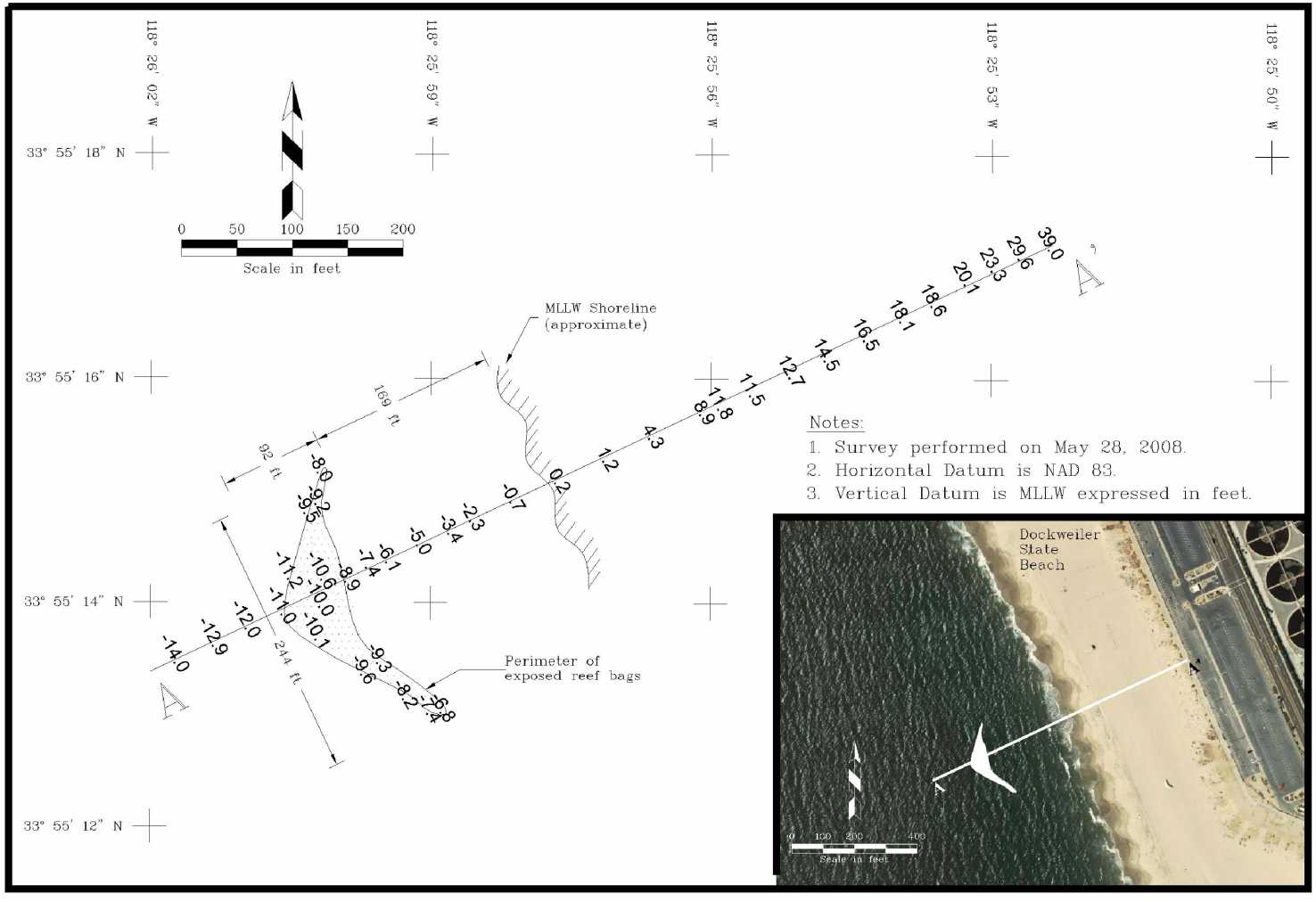


Figure 4. Configuration of Exposed Reef Bags in May 2008

During the dive inspection, approximately 50 geotextile bags and bag fragments were observed protruding up to 1 ft (0.3 m) above the sea bottom. The bags typically occurred in clusters separated by areas of sandy sea bottom, with many of the bags partially buried in the sediment. Torn fabric and severed nylon lifting straps were observed at numerous locations, suggesting that many of the exposed bags had sustained damage (Plate 2). While the white polyester bag fabric was found to be in relatively good condition, some of the black polypropylene fabric had degraded to the point that it could be torn by hand.



Plate 2. Torn Polyester Fabric Noted during Dive Inspection

No prior experience with the recovery of geotextile reef structures from the surf zone was available to guide the removal of Pratte's Reef. Significant insight was available, however, from more than two decades of experience with the removal of geotextile armor systems from man-made islands in the Alaskan Beaufort Sea. As discussed by Leidersdorf, *et al.* (2008), gravel-filled bags with capacities of 2 and 4 cubic yards (1.5 and 3.1 cubic meters) have been removed from the side slopes of ten islands located in water depths ranging from 4 to 50 ft (1.2 to 15.2 m).

The Alaskan island experience indicates that geotextile bags and any underlying filter fabric can be removed from subaerial slopes and the water line area using a conventional hydraulic excavator (Plate 3). Provided that the bags are exposed, virtually all of the fabric can be recovered in an expeditious manner (Anderson and Leidersdorf, 1988). If the bags are covered with sediment or located on submerged



Plate 3. Removal of Subaerial Bags with Hydraulic Excavator

slopes beyond the reach of an excavator, however, the effectiveness of the removal process diminishes while the time and cost increase dramatically. The problem is particularly acute on submerged slopes, where a crane equipped with a clamshell or a dragline must be used instead of an excavator. In either case, the fabric is randomly torn and the bags are recovered in pieces. Notwithstanding repeated cycles of dredging and diver inspection, some pieces of fabric inevitably become buried in the slope while others are lost into the water column.

An additional finding from the Alaskan experience is the importance of emptying the contents of the geotextile bags away from other bags awaiting removal. If the fill material from one bag is allowed to spill onto another bag, removal of the second bag will be compromised.

Based on the foregoing experience as well as the results of the May 2008 dive inspection, dredging (whether by clamshell or dragline) was eliminated from consideration due to the potential for widespread disturbance of the sea bottom, turbidity, and incidental discharge of geotextile fabric into the marine environment. Similarly, cutting the bags open and jetting out the sand fill was ruled out due to the generation of turbidity as well as the difficulty a diver would experience in controlling a high-pressure water jet near the surf zone. The recovery of individual bags using the original nylon lifting straps also was eliminated from consideration in recognition of the deteriorated condition of the straps.

Two approaches were identified as offering the greatest potential for recovering the bags in an environmentally-responsible manner while minimizing the risk to

personnel and equipment: (1) vessel-based removal, in which a large vessel is used to extract individual bags with a deck winch (Figure 5; Plate 4); and (2) shore-based removal, in which a bulldozer equipped with a winch is used to drag individual bags ashore (Figure 6; Plate 5). In both cases, a commercial diver is needed to attach each bag to the removal cable using a nylon sling or net, and to cut the bag open during removal in a manner that allows the sand fill to escape without burying the adjacent bags.

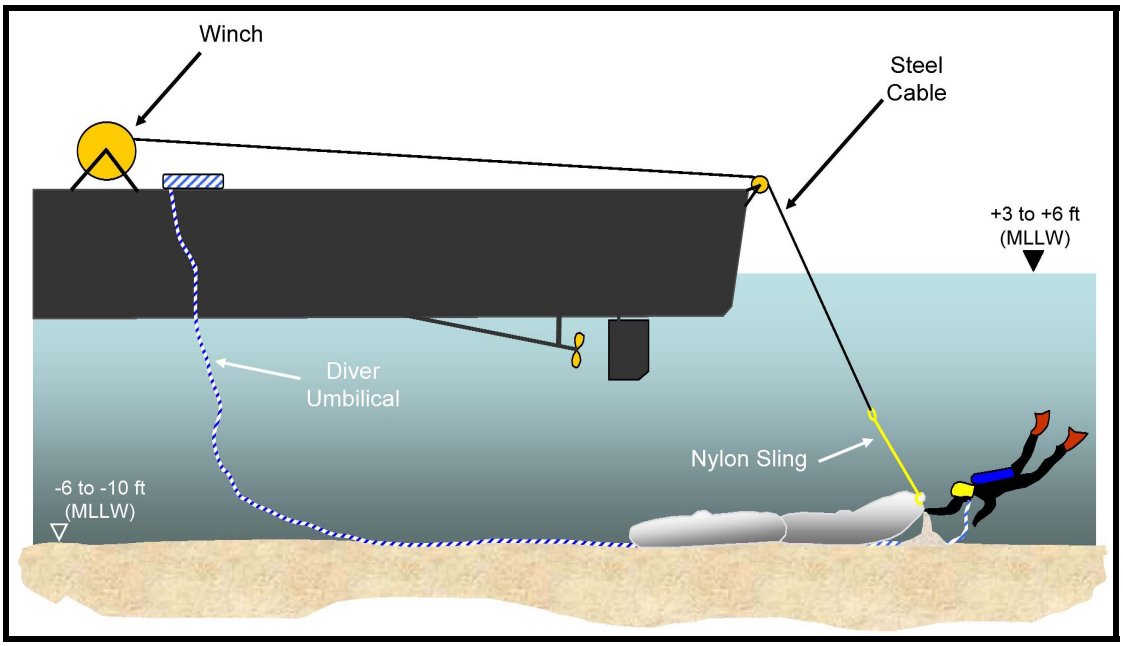


Figure 5. Vessel-Based Removal

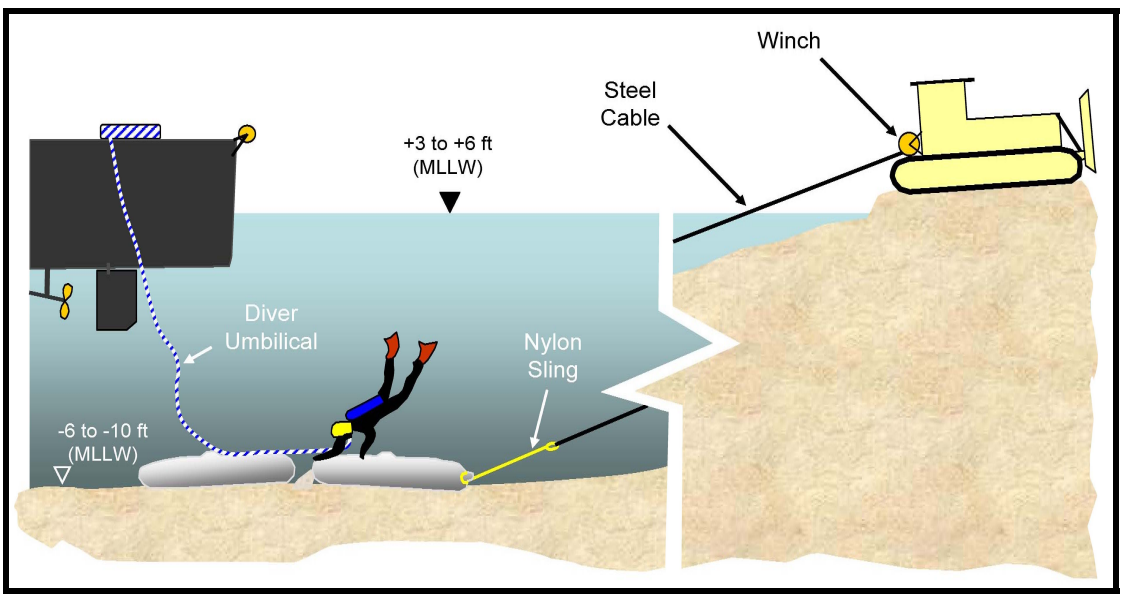


Figure 6. Shore-Based Removal



Plate 4. Vessel-Based Removal



Plate 5. Shore-Based Removal

The removal plan was implemented in the fall of 2008. This time of year was selected for three reasons: (1) the surrounding sea bottom is likely to attain its minimum elevation, thereby maximizing the exposure of the reef, (2) large wave events tend to occur infrequently, and (3) the impact on species such as whales, grunion and sea birds is minimized.

The budget available for reef removal, $285,000, covered mobilization and demobilization expenses, 12 days of on-site operations, and four days of weather downtime. Despite the diligent efforts of a professional dive team with extensive experience in the removal of geotextile armor systems, a 70-ft (21.3-m) supply vessel with a seasoned crew, and a well-equipped civil contractor on the beach, the 12 days of operations yielded only 76 bags and bag-equivalents (6.3 bags/day). Vessel-based removal proved to be more efficient than shore-based removal, with an average yield of 7.8 bags/day for the former and 3.5 bags/day for the latter. Additional advantages of vessel-based removal included reduced risk to the divers (by virtue of their remaining outside the surf zone) and negligible impact on beach users.

Nylon slings outperformed nets in connecting the bags to the steel removal cable. The most secure connection resulted from using the sling as a choker on a corner of the bag. Typically, the diver was required to re-establish the connection repeatedly before a bag fragment or, rarely, a whole bag, could be extracted from the reef and winched aboard the supply vessel or onto the beach.

Another significant finding in 2008 was the critical importance of the prevailing water level. Due to the reef's proximity to the surf zone, the divers' ability to work was impaired by wave heights as low as 2 to 3 ft (0.6 to 0.9 m) when the still water level approached the lower end of the 5.4-ft (1.6-m) diurnal tide range, versus 4 to 5 ft (1.2 to 1.5 m) at the upper end of the range. Wave period also proved to be important, in that long-period swell tended to preclude dive operations at lower wave heights than short-period wind waves.

When a dive inspection was conducted at the end of the budget-constrained removal period, approximately 50 bags were evident on the sea bottom – the same quantity as at the outset. This finding, which resulted from additional bags becoming exposed as the work progressed, necessitated a second phase of reef removal work.

Following a two-year hiatus that was used to secure additional funding, the Surfrider Foundation initiated the second phase of the removal operations in the fall of 2010. Based on the lessons learned during the first phase, the shore-based method of removal was abandoned in favor of the vessel-based method (Figure 5), and the work was scheduled during periods when the predicted still water level exceeded +3 ft (+0.9 m).

Despite the experience gained during the first phase of the project, progress was slowed by the fact that many of the remaining bags were partially buried in the sea bottom. Persistent long-period swell and poor visibility underwater also hampered productivity. As a result, during a 19-day work period that included 18 days on site and only one day of weather downtime, 66.5 bags and bag-equivalents were recovered at the appallingly slow rate of 3.7 bags/day. On a more positive note, only

one deeply-buried bag was evident in the sea bottom at the conclusion of the work, the total cost of which was $266,000.

When the two phases of reef removal are considered together, 142.5 bags and bag-equivalents were recovered and one bag was left in place. Of the remaining 42.5 bags that comprised the original total of 185, it is likely that some sustained damage and were carried away by wave agitation while others remain buried in the sea bottom. The total cost of removal, $551,000, was nearly identical to the installation cost of $550,000.

SUMMARY AND CONCLUSIONS

As the first man-made surfing reef to be constructed in North America, Pratte's Reef offers a number of lessons that may benefit the planning, implementation, and removal of similar structures in the future. Without question, the most positive outcome of the project was the recognition by regulatory agencies that natural surf breaks represent finite recreational resources worthy of preservation or, if necessary, mitigation.

From the standpoint of performance, the failure of Pratte's Reef to produce a sustained improvement in surf quality highlights the fact that nearshore reef structures are in the early stages of development. Until a substantial body of experience is acquired, such structures (whether intended for surf enhancement, erosion mitigation, or a combination thereof) should be considered experimental and prone to unintended outcomes. To minimize the chances of failure, ample funds should be allocated for design and scale model testing.

Perhaps the most important technical lesson to be learned from Pratte's Reef relates to the difficulty and cost of removing geotextile containers from the nearshore environment. Unfortunately, a misconception currently exists that removal can be accomplished simply by cutting the containers open and allowing the fill material to spill out as the fabric is withdrawn. While geotextiles can be recovered with relative ease if they are located within reach of conventional earth-moving equipment operated from shore, the removal process is time-consuming, costly, and incomplete if the containers lie offshore. The result, in the case of Pratte's Reef, was a removal cost that matched the installation cost despite the best efforts of an experienced crew.

Based on the life-cycle experience acquired in connection with Pratte's Reef, two general guidelines are recommended for the planning and design of man-made reefs in the nearshore environment:

1. Notwithstanding the high hopes that often accompany the prospect of surf enhancement or erosion mitigation, each reef proposal should receive careful scrutiny with respect to construction feasibility and cost, long-term durability, and the probability of accomplishing the design objectives without unintended consequences.

2. As man-made reefs remain in the experimental stage, and as geotextile-based structures cannot be considered permanent, the assessment of each prospective project should include consideration of the techniques and funding necessary for removal at the end of the service life.

REFERENCES

Anderson, L.M., and C. B. Leidersdorf, 1987, "Arctic Island Abandonment: Planning and Implementation for Mukluk Island", *Proc. 1988 Offshore Technology Conference*, OTC 5686, Houston, TX p. 49-60.

Borrero, J.C., 2001a, "Pratte's Reef 1st Quarter Monitoring Report", Surfrider Foundation, San Clemente, CA.

Borrero, J.C., 2001b, "Pratte's Reef 3rd Quarter Monitoring Report", Surfrider Foundation, San Clemente, CA.

Borrero, J.C., 2002, "Pratte's Reef 4th Quarter Monitoring Report", Surfrider Foundation, San Clemente, CA.

Borrero, J.C., 2004, "Pratte's Reef 2004 Supplemental Monitoring Report", Surfrider Foundation, San Clemente, CA.

Daily Mail, 2011, "Wave goodbye! Britain's £3.2 million artificial surf reef closed after only two years as it's unsafe", http://www.dailymail.co.uk/news/article-1372879/Britains-3-2m-artificial-surf-reef-closed-2-years-unsafe.html.

Google Earth, 2008, www.earth.google.com.

Hoffman, R.S., 1986, "Fishery Utilization of Eelgrass (*Zostera marina*) Beds and Non-Vegetated Shallow-Water Areas in San Diego Bay", National Oceanic and Atmospheric Administration, National Marine Fisheries Service, Southwest Region, Administrative Report SWR-86-4, 29 pp.

Leidersdorf, C.B., P.E. Gadd, G. E. Hearon, J.D. Hall, and C.J. Perry, 2008, "Coastal Engineering Design of the Oooguruk Project", Proc. 2008 Offshore Technology Conference, OTC 19369, Houston, Texas, 17 pp.

Shuman, C.S., 2008, "Pratte's Reef Eelgrass Survey", Surfrider Foundation, San Clemente, CA, 6 pp.

Skelly Engineering, ca 1999, in Borrero, J.C., 2001a, Borrero, J.C., 2001a, "Pratte's Reef 1st Quarter Monitoring Report", Surfrider Foundation, San Clemente, CA.

Skelly Engineering, 2000, personal communication to Surfrider Foundation, Carlsbad, CA.

Valor, S.H., 2007, "Pratte's Reef 2007 Final Monitoring Report", Surfrider Foundation, San Clemente, CA.

Capacity Enhancement at Coastal Disposal Sites

by R. David Espinoza, Ph.D[1]*., P.E.; and Michael F. Houlihan, P.E., F.ASCE*[2]

[1] Geosyntec Consultants Columbia, MD, 10220 Old Columbia Road Suite A, Columbia, MD 21046, Ph: (410) 381-4333; Fax: (410) 381-4499; email: despinoza@geosyntec.com

[2] Geosyntec Consultants Columbia, MD, 10220 Old Columbia Road Suite A, Columbia, MD 21046; Ph: (410) 381-4333; Fax: (410) 381-4499; email: mhoulihan@geosyntec.com

ABSTRACT

The coastal environment is host to a large number and variety of disposal facilities, including dredge disposal sites and landfill sites. Because these sites are commonly located over weak foundation soils, it is difficult to maximize the disposal capacity without risking foundation instability or general instability and, as a result, the disposal capacity of these sites is often not maximized. Recent advances in foundation improvement and design, though, have made it possible to significantly, and reliably, extend the service life of coastal disposal sites. The purpose of this paper is to describe the challenges faced by disposal facilities that are designed in coastal environments and to present a case history of a recent construction project at the confluence of two rivers in which substantial additional service life was provided using innovative design techniques and comprehensive construction oversight which resulted in construction cost savings well over ninety percent when compared to the original conventional design. The successful design and construction over extremely soft dredge using innovative design and construction techniques described in this paper opens opportunities not only for extending the life of disposal facilities next to riverfront environments but also for raising levees and dikes cost effectively at critical locations that are prone to flooding.

INTRODUCTION

Earth structures have been developed along waterways in the United States throughout our nation's history for many purposes, including dredge material management, flood control, and waste containment. The U.S Army Corps of Engineers (USACE), which is involved in nearly all navigation dredging operations performed in the Unites States, serves over about 40,000 Km of navigable rivers and manages approximately 327 million cubic yards of dredge per year. USACE serves approximately 400 ports, 130 of which are located in the country's largest cities, at an average annual cost of about $400 million (Hales, 1995). Another important application of constructing berms over soft soils is flood protection. Inland flooding of rivers causes billions of dollars in losses every year in the United States; earth levees constructed along waterways are a key component of protection against such flooding. Finally, waste management facilities have historically been developed along waterfront locations in areas having the same foundation conditions and environmental sensitivity as dredge and levee structures. All of these structures are important to protecting the commerce and resources of the nation.

Siting and permitting new dredge disposal facilities, flood control structures, and other waterfront earthen structures are becoming increasingly difficult due to natural resources damage concerns and because of the large areas of land needed to develop these facilities. Also, development of new disposal facilities can be very time consuming and expensive. Hence, design and construction methods that can provide cost-effective increases in the available capacity at existing facilities can prove invaluable for planning and budgeting purposes.

The focus of this paper is on one example of a waterfront earth structure that was developed over very soft soils, as many of the dredge management, levees, and other waterfront earthen structures. The facility is the Cherry Island Landfill, located in Wilmington, Delaware, along the Delaware and Christina Rivers. The successful design and construction of large Mechanically Stabilized Earth (MSE) Berm over extremely soft river-dredge material at the site demonstrates the opportunities for raising levees and dikes cost effectively at critical locations that are prone to flooding and that present significant challenges for foundation design. This pioneering project, which is described in detailed below, was made possible through innovative design and construction techniques developed by Espinoza et al (2011).

CASE STUDY: THE CHERRY ISLAND LANDFILL

Project Description

The Cherry Island Landfill (CIL), located in Wilmington, Delaware, was constructed over an area that was partly reclaimed from the Delaware River in the early 1900s (see picture below) and that had been used for many years as a dredged material

disposal site for the U.S Army Corps of Engineers (USACE). The USACE had placed dredge within several cells from about elevation 0 ft-msl up to elevations ranging from 20 ft-msl to 40 ft-msl. Under the dredge layer lies an alluvium deposit that has similar physical as well as strength characteristics to the overlying dredge. As a result, the subsurface characteristics at the site consist of unconsolidated, very soft, low permeability and extremely compressible materials with undrained shear strengths as low as 200 psf and thickness ranging from 60 to 100 feet. Under the alluvial deposit lies, from top to bottom, the Columbia Formation, the Potomac Formation, and weathered bedrock. The Columbia Formation would typically be considered the uppermost load-bearing until, as it is characterized by dense sands underlain by a dense clay layer of the Potomac Formation.

To meet the growing demands for waste disposal, the Delaware Solid Waste Authority (DSWA) evaluated the feasibility of vertically expanding the existing Cherry Island Landfill facility to provide, at a minimum, an additional 22.7 million cubic yards (mcy) of waste disposal capacity (20+ years capacity at the disposal rates at the time). The feasibility depended on overcoming the constructability issues associated with earth construction over very weak soils. . Because of its location near the rivers, the potential for a horizontal expansion was limited, hence the main alternative to obtain additional capacity at this facility was to expand vertically. In order to obtain 22.7 mcy of capacity, the only option available that would provide the additional disposal capacity was to build an 8,000-ft long and 70-ft high perimeter mechanically stabilized earth (MSE) berm around the facility. The preliminary feasibility study indicated that, in order to build the 70-ft high MSE berm, the foundation undrained shear strength needed to be improved from 200 psf to 3,200 psf. The preliminary conceptual solution for achieving this strength gain was to use deep soil mixing (DSM), a technique that consists of mixing soil with cement. Because of the depth of the soft soils that needed to be improved, the volume of soil that needed to be treated was approximately 2.5 mcy. The estimated cost for this soil improvement option was estimated to be $170 million (2011 dollars).

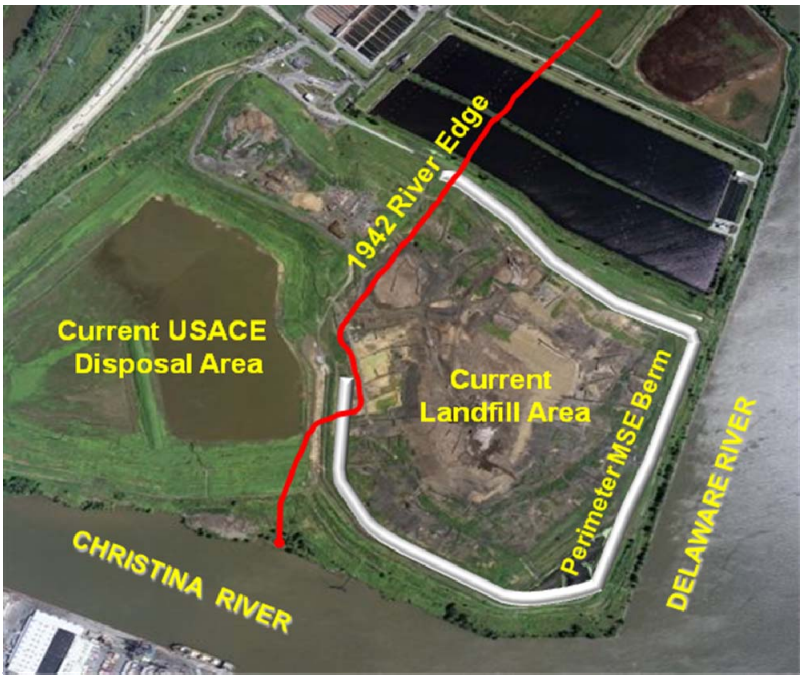


Photo 1 – Site Location

Proposed Solution

Several alternatives to deep soil mixing were evaluated, and prefabricated vertical drains (PVDs) were found to be the most cost-efficient foundation improvement techniques to take advantage of the substantial weight of the MSE berm to improve the foundation strength. However, based on projects where PVDs are used in combination with a surcharge load (i.e., the MSE berm), the maximum height of the berm is dictated by the undrained strength of the underlying soft material after loading. At the CIL facility, the maximum height that could have been built using standard analysis techniques that only takes into account the undrained shear strength would have been on the order of 25-ft high (i.e., about 45 ft shorter than required to achieve the target airspace).

In the design, the 70-foot high, 8,000-foot long MSE berm plays a dual role, compressing and consolidating foundation soils while at the same time providing new disposal space. The MSE berm consists of two million cubic yards of fill, and is one of the highest and most massive reinforced structures constructed over soft soils in the United States. The MSE berm was designed to provide a counterweight at the toe of the landfilll, whereas the PVDs were designed to dissipate pore pressures during berm construction and subsequent waste placement. Because of the low permeability of the dredge/alluvium foundation soils, approximately 6 million linear feet of prefabricated vertical drains (PVDs) were installed at a 5-ft spacing to allow dissipation of the excess pore-water pressures that were generated during construction of the overlying MSE berm. In addition, because large settlement were expected to take place

along the perimeter MSE berm, special design considerations for the stormwater management system, were taken into account (as described below). The recorded maximum vertical and horizontal displacements were approximately 14 ft and 5.5 ft, respectively. An extensive geotechnical monitoring network was required to monitor the stability of the berm as it was built.

Berm Construction

Contrary to most fill construction jobs, the design documents indicated that the MSE berm could not be built as fast as logistics would allow but, instead, would require staged construction with specific performance requirements and instructions from Geosyntec's engineers at each stage of construction. In order to prevent unacceptably high pore pressures from developing, each stage of berm construction was limited to a 10-ft thick lift followed by a 3-month pore pressure dissipation period. To monitor the performance of the foundation during the stages of construction, Geosyntec developed several finite element models for critical cross sections. The soil strength parameters obtained from the laboratory and pilot test were used as an initial model calibration. The parameters were adjusted during the initial 10-ft lift placement and then used to predict pore pressures, lateral vertical displacements during construction for subsequent lifts. During construction of each stage, measurements were made of the foundation pore pressure, settlement, and lateral displacement at the selected cross sections along the berm. This data was carefully evaluated and compared to predicted values to verify that the berm was performing as expected. The construction schedule was initially established based upon estimated rates of pore pressure generation and subsequent dissipation using a simplified drainage model, but the schedule was continually adjusted during construction as readings from geotechnical monitoring instruments were collected as frequently as daily in areas of active construction. Figure 1 shows an example of the comparison between the measures pore pressures and estimated ones using final element models.

Close interaction between the designer (Geosyntec) and the contractor (Sevenson) and DSWA, allowed timely geotechnical review and interpretation of monitoring data and communication of findings. By providing clarity to all parties on when subsequent berm lifts were likely to be feasible in any particular location, this provided flexibility in construction task management and minimized disruption to the overall construction schedule. MSE berm construction began in August 2007. Following two lifts of construction over each of the three sides of the berm, it became apparent that the rate of pore pressure dissipation for each side varied. On the Christina River side the pore pressures consistently dissipated over three months. However, pore pressure along the Delaware River side (see Picture below) dissipated more quickly, on the order of 45 days. Upon review of this condition, the existence of the stiff sand lenses which had been a problem during PVD installation were now found to be a benefit to berm construction. These same sand lenses were typically several orders of magnitude more permeable than the surrounding fine grained dredge

materials and, as a result, they became conduits for fast transport of pore water to the PVDs. On the North side, however, observed pore pressure dissipation took significantly longer than predicted, on the order of five months.

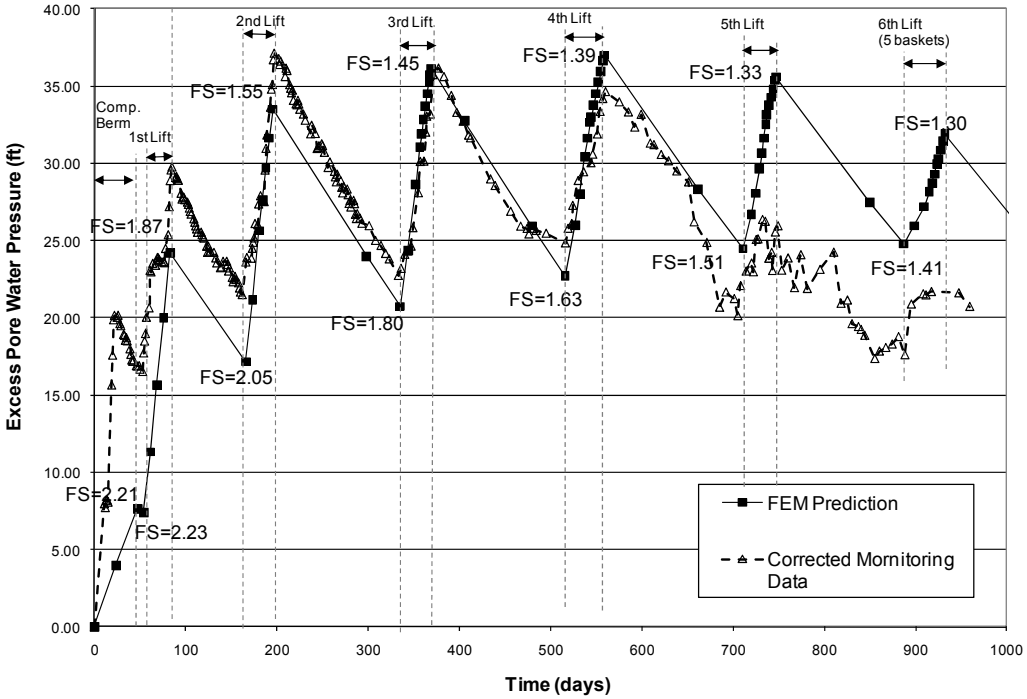


Figure 1 – Example of monitoring results

As a result of these conditions, the contractor was required to significantly alter its original construction sequence for the berm. Rather than move at a steady pace along the entire 8,000-ft long berm, pore pressure conditions required the contractor to move back and forth between the Christina River, Delaware River, and North sides. With daily review of geotechnical data and frequent review of finite-element modeling output prepared for numerous berm cross sections, Geosyntec was able to identify areas of construction on a "just-in-time" basis for Sevenson to continue uninterrupted work. Eventually, the original plan of building a 10-ft thick lift over 2,000 to 3,000 ft length of the berm every 90 days evolved into construction of lifts in thicknesses as thin as three feet and/or berm lengths as short as 1,000 feet which were patched together as review of geotechnical data would allow. Sevenson's ability to reorganize its efforts to construct the various sections of the berm based on week-to-week feedback from Geosyntec became a critical piece of the success of the project. In this way, by August 2010, 36 months after starting, MSE berm construction was completed.



Photo 2 – Construction of MSE berm along the Delaware River

Stormwater Management Culverts

One of the most significant project challenges was the design and construction of the stormwater management system for the landfill. Stormwater runoff from the vertically expanded landfill will flow to the top of the berm, where drop inlets are provided to transmit stormwater runoff down through the berm to discharge points along the Delaware and Christina Rivers, a vertical drop in elevation of about 80 feet. To manage the expected volume of stormwater runoff, the design required concrete culverts as large as six feet in diameter. Because of the overburden pressures resulting from the weight of the overlying fill, Class V reinforced concrete pipes (RCP) were required. However, because up to 14 feet of settlement was expected, maintaining the integrity of a rigid RCP within the berm was a major concern. The issue of settlement was addressed recognizing that, the type of settlement to be addressed would not result in abrupt shearing but, instead, gradual differential settlements across the width of the berm as depicted in Figure 2.

To accomodate this settlement, the design strategy involved the use of 8-ft long RCP sections fitted with bell and spigot joints. Each joint provides a modest ability for rotation without pipe damage, such that the sum of all joint rotations could address the expected total differential settlement. Each of the culverts was modeled using finite element techniques to estimate the differential settlement and the expected rotation between RCP sections. The analysis indicated that the RCP joints would accomodate the expected rotations and differential settlements. In order to further force any rotations to occur at the RCP joints, a reinforced concrete cradle was installed beneath the RCP within the MSE berm.

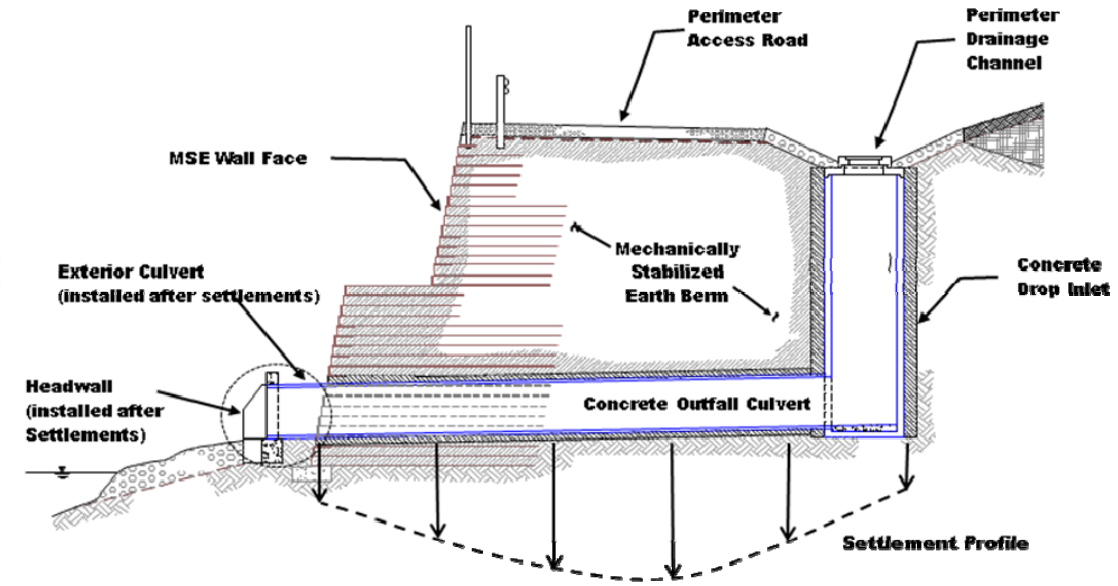


Figure 2 – Sketch of settlement profile across RCP culverts

Steel reinforcing for the cradle was designed to be discontinuous at each RCP joint, thereby forcing differential settlement to be expressed as joint rotation. To avoid grade reversal of the pipe, the pipe was constructed at a steeper slope and a higher elevation than required. The outlet pipes at the face of the MSE berm were installed about 10 feet above the final elevation. To minimize stress concentration on the outlet pipes, the final connections to the discharge point were not installed until after the MSE berm was complete and most of the anticipated settlement had already taken place. Following MSE berm construction, a detailed inspection of the RCP stormwater culverts was conducted. The inspection indicated that the RCPs had performed as designed.



Photo 3 – RCP culvert installation

CONCLUSIONS

The completion of this two-million-cubic-yard MSE berm (see picture below) represents a significant engineering achievement considering the size of the embankment and the deep layer of very soft soils over which the berm was constructed. The successful design and construction of a 8,000-ft long, 70-ft high MSE berm over extremely soft dredge using innovative design and construction techniques opens opportunities not only for extending the capacity of existing disposal facilities over dredge disposal sites but also for raising levees and dykes very cost effectively at critical locations that are prone to flooding.



Photo 4 – View of Completed MSE berm

REFERENCES

Espinoza R.D., Houlihan M.F. and Ramsey, T.B. Design of High Soil Berms over Soft Soils. *Geo-Strata*, March-April 2011, pp. 52-54.

Hales, L. Accomplishments of the Corps of Engineers Dredging Research Program. *Journal of Costal Research*, Vol. 11, No. 1, pp. 68-88, Fort Lauderdale, Florida.

Operation, Maintenance, and Repair of Coastal Wastewater Outfalls: San Francisco, Boston, Los Angeles County, and San Diego

Brian J. Van Weele[1] and Donald D. Treadwell[2]

[1] Parsons Brinckerhoff, San Francisco, California; vanweele@pbworld.com
[2] Consulting Engineer, Sausalito, California; ddtreadwell@comcast.net

ABSTRACT

Information regarding the operation, maintenance, and repair of a number of major coastal wastewater outfalls has been provided to the authors by representatives of the responsible operating organizations. The outfalls for San Francisco, Boston, Los Angeles County, and San Diego are discussed herein.

INTRODUCTION AND BACKGROUND

Since the middle of the 20th century, hundreds of coastal wastewater outfalls (Grace, 1978; Gunnerson, 1986; Treadwell, Van Weele, and Eisenberg, 2004; Grace, 2009; Roberts et al, 2010) have been constructed around the world to dispose of treated effluent from coastal metropolitan areas. The construction and performance goals of coastal wastewater outfalls include:

- minimal impact on the affected coastal environment
- minimum "mixing zone" length and high initial dilution
- designed for protection from ship-related possible damage
- designed for long life and hydraulic efficiency
- constructability ease and reasonable construction cost
- minimum operations and maintenance requirements

The design and construction of these outfalls have, in the main, incorporated the best materials and practices to minimize the likelihood of negative system impacts. These impacts include structural failures, corrosion and biofouling problems, sediment intrusion, degradation of hydraulic performance, and costly operational and maintenance issues.

The authors were directly involved in the design of the outfall systems for San Francisco and Boston. In regard to the Whites Point Ocean Outfall on the Palos Verdes Peninsula and the Point Loma Ocean Outfall in San Diego, the authors are familiar with the systems and with the owner's design and operations staff.

In order to facilitate the collection of current information on the operation and maintenance and repair of the outfalls, representatives were asked to provide details on location and outfall diameter, length and capacity, and materials comprising the system. In addition, along with a request for any relevant discussion of causes of and solutions for problems, eight specific questions were asked:

- Have there been any structural problems (such as anchor drag or drop)?
- Has the material had corrosion issues?
- Has sediment intrusion affected performance?
- Have there been any hydraulic performance problems?
- Have there been any significant operation issues?
- Have there been any significant maintenance issues?
- What has worked the best on the outfall system?
- What needs improvement on the outfall system?

Important aspects of coastal wastewater outfall operation include capacity, inspection and maintenance, and the ability to fail in a safe manner. In particular, the outfall and diffuser must be capable of conveying the maximum hydraulic flow from the wastewater treatment plant at the mean high water tide level taking into account waves and storm surge. The outfall and diffuser must also operate satisfactorily at minimum projected flow rates.

Inspection, maintenance, and repair of these types of facilities is dangerous and potentially disruptive to nearby marine operations, such as ports and harbors. Inspection is facilitated by the design, and the need for maintenance and repair reduced through the robustness of the facility, the durability of the selected materials, and the simplicity of the construction details.

SOUTHWEST OCEAN OUTFALL
San Francisco, California

The Southwest Ocean Outfall (Figure 1) extends more than 4.5 miles offshore from the Oceanside Wastewater Treatment Plant located in the extreme southwest corner of San Francisco near Lake Merced (Eisenberg and Treadwell, 1982). The outfall owner is the Public Utilities Commission of the City and County of San Francisco.

The outfall pipe is constructed of reinforced concrete with an inside diameter of 12 feet and is embedded as much as 20 feet beneath the seabed. In the diffuser section, the outfall pipe inside diameter reduces from 12 to 10 to 8 feet. There are 85 diffuser risers that extend from the pipe invert to about 6 to 8 feet above the seabed.

Offshore, the outfall pipe crosses the San Andreas Fault (Treadwell et al, 1980). It was determined that if an 8.0 or larger earthquake occurred (the 1906 San Francisco earthquake is estimated to have been about 8.0 on the Richter scale), the fault could offset 20 feet horizontally and 2 feet vertically.

There is no way for the outfall pipeline to withstand this major seismic force so the design team incorporated features to protect against smaller quakes and to facilitate repair after a catastrophic failure (Gilbert, Eisenberg, and Treadwell, 1981). The pipeline has a slight S-curve in the alignment to accommodate realignment and the joints are of a special bell and spigot design allowing substantial movement.

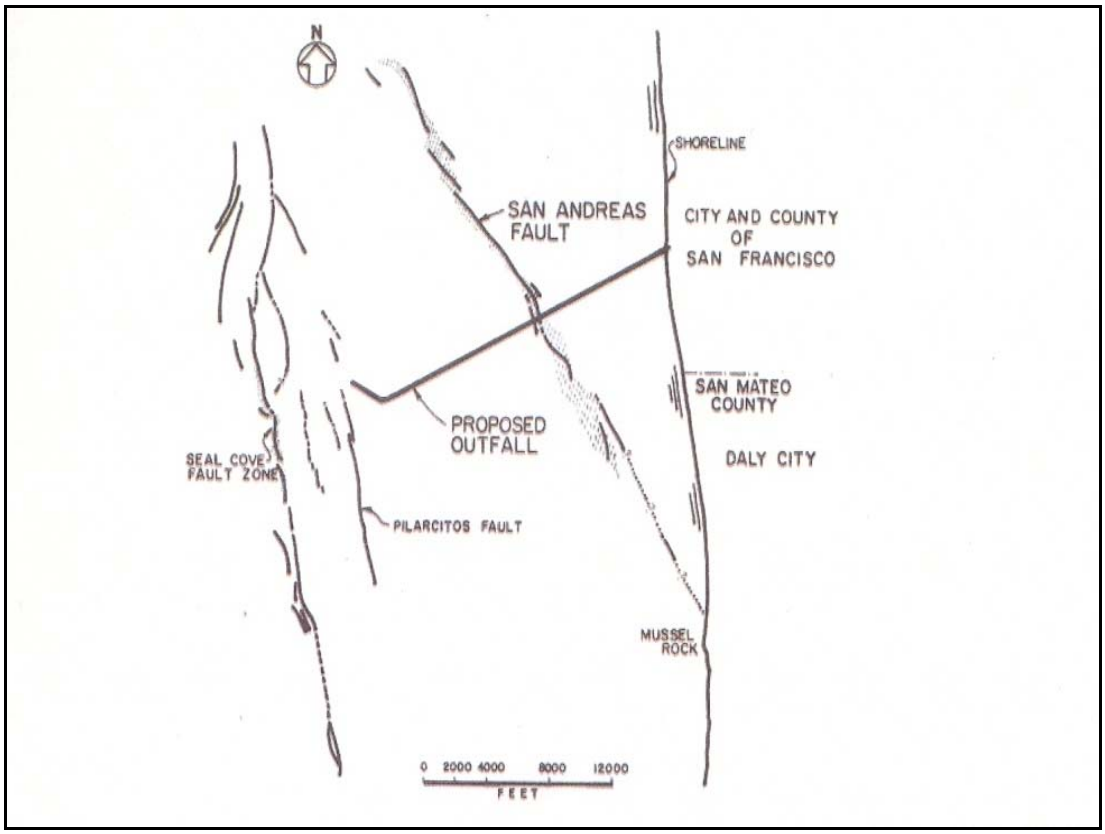


Figure 1. Location of Southwest Ocean Outfall, San Francisco

Even during the outfall design phase in the late 1970s, there had been a concern that sand might enter the pipe through the diffuser ports due to low initial flows of the entire outfall system. During a more recent scheduled permit inspection, the outfall end gate fell off its hinges as it was opened. A temporary bulkhead was installed to meet permit requirements until the end gate could be repaired.

During the end gate repairs, the gate was upgraded with a small door and two duckbill check valves. The small door can be opened for inspection instead of lifting the entire gate. Some sand was observed in the outfall diffuser; however, because of the bottom takeoff design (Figure 2) of the diffuser risers, there was no discernible effect on the hydraulic performance.

The operation and maintenance manual (CCSF, 1986) did have a procedure identified to open the 1,600 pound end gate with an "A-frame" hoist to be set on the seabed to lift the gate into the open position by attaching a cable to the lifting eye on the gate. However, the contractor employed to assist in the gate opening, elected to use an air filled bag to lift the gate, which led to the hinge separation.

One of the value engineering decisions significantly impacted on future operations and maintenance procedures and costs. Originally, there were 50 manholes planned to rise to up to the seabed over the length of the outfall. It was decided to save on

construction costs by providing a stub for the manhole riser and providing a capped pipe manhole marker to rise to the seabed to allow for locating the manhole stubs. Years later, it became clear that locating these small pipe markers was virtually impossible and that the cost of excavating through the armor stones to provide access to the manhole stubs was prohibitive.

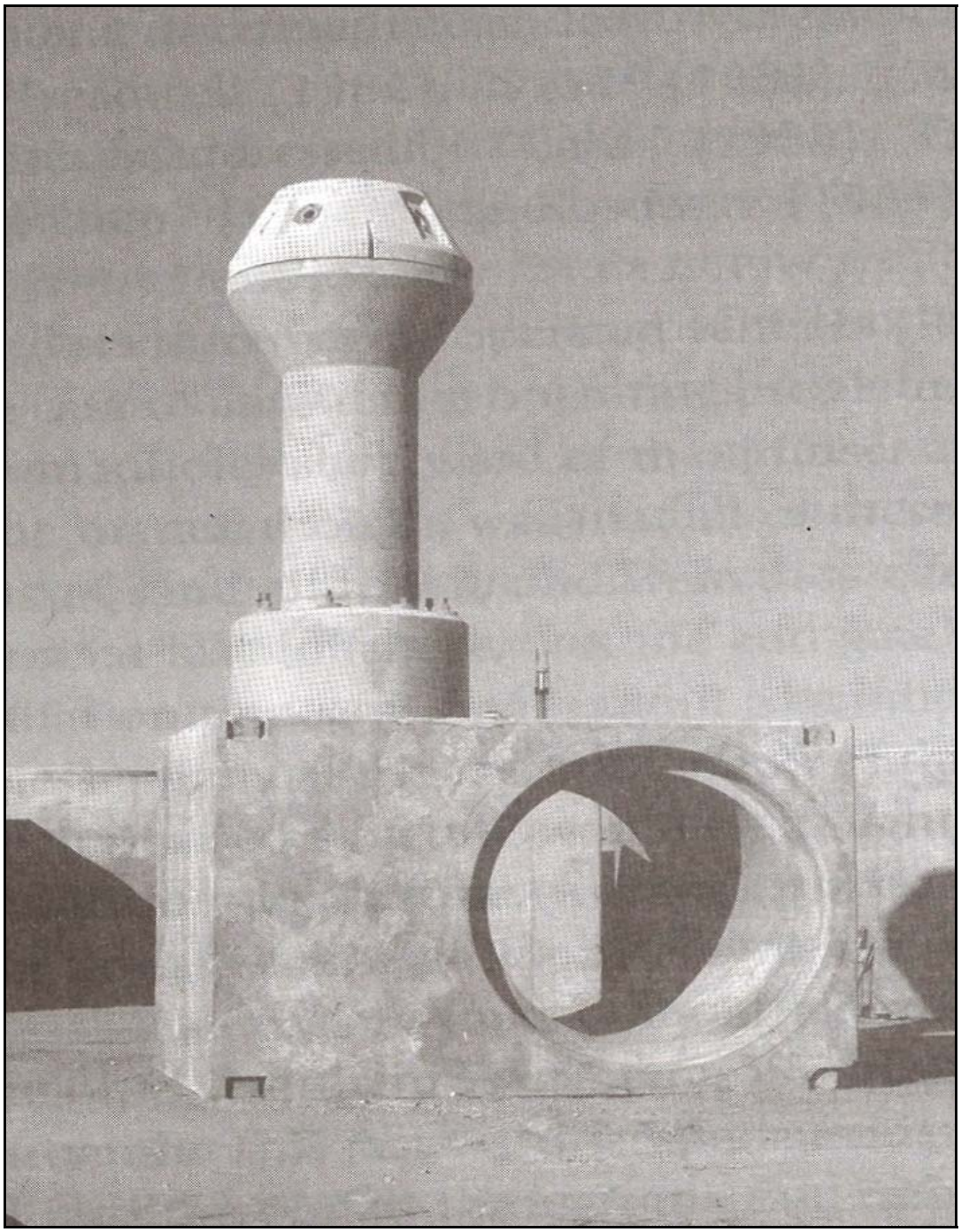


Figure 2. Diffuser Section of Southwest Ocean Outfall, San Francisco

DEER ISLAND OCEAN OUTFALL
Boston, Massachusetts

The Deer Island Ocean Outfall (Eisenberg and Brooks, 1992; Brocard, Van Weele, and Williamson, 1994) is owned by the Massachusetts Water Resources Authority (MWRA). The shoreward end of the outfall is located at the MWRA's Deer Island Treatment Plant (Figure 3).

The outfall extends 9.5 miles from Deer Island into the Atlantic Ocean to a depth of approximately 100 feet. The outfall tunnel is in rock and has an inside diameter of 24 feet for approximately 8 miles and then begins to taper at the diffuser portion. Flow is discharged through 55 diffusers over the final 1.25 miles of the system. Each diffuser has up to 8 ports that can be opened.



Figure 3. Deer Island Wastewater Treatment Plant, Boston

The tunnel and most of the diffuser sections have pre-cast reinforced concrete liners. The 55 risers were drilled to the tunnel depth in rock and connected from inside the tunnel. The risers are lined with fiberglass pipe.

The diffusers were designed with bottom takeoff from the tunnel to the risers to prevent any sediment that might get into the outfall from building up on the bottom of the diffuser (Figure 4). The outermost riser was connected from the top of the diffuser pipe to allow any entrapped air to escape.

The MWRA maintenance team makes regular inspections of the diffuser sections which sit on the seabed. In particular, they look for evidence of excessive marine growth and/or damage.

To date, there have been no records of excessive marine growth, damage from corrosion, or sediment intrusion. There have not been any hydraulic performance problems. However, during combinations of high flows and extreme high tides there may be temporary tank flooding should the weirs become submerged.

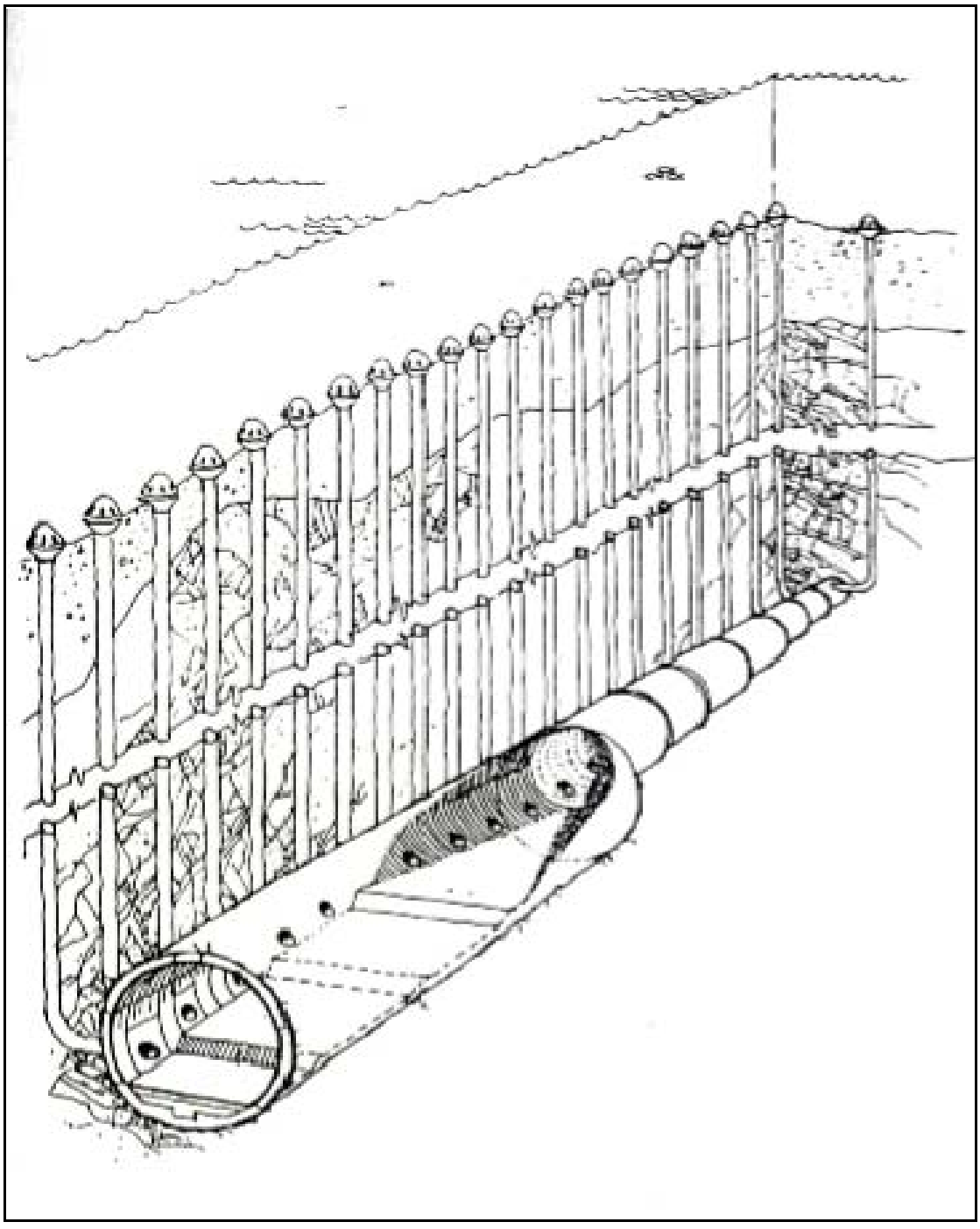


Figure 4. Diffuser Section of Deer Island Ocean Outfall, Boston

WHITES POINT OCEAN OUTFALLS
Los Angeles County, California

The owner of the Whites Point Ocean Outfalls is the Sanitation Districts of Los Angeles County. The outfalls are located in the Pacific Ocean on the Palos Verdes Shelf offshore of Whites Point on the Palos Verdes Peninsula (Figure 5).

The Sanitation Districts operate four outfalls which vary in size and length. The two continuously operated outfalls are 120-inches and 90-inches in inside diameter. The other two outfalls, 60- and 72-inches in diameter, are used for additional hydraulic capacity during high flow conditions.



Figure 5. Service Area of Whites Point Ocean Outfalls, Los Angeles County

The 60-inch outfall was placed into service in 1937 and is approximately 5,000 feet in length, including the 400 feet of main barrel diffuser section. The outfall is of reinforced concrete pipe with cast iron bell and spigot joints. The diffuser section consists of a pair of ports spaced every 18 feet at the pipe spring line. There are nine pairs of 9-inch diameter and thirteen pairs of 8.38-inch diameter ports. The outfall terminates at a water depth of about 110 feet.

The 72-inch outfall was initially placed into service in 1947 with a discharge depth of 110 feet; the outfall was extended in 1953 to a water depth of 160 feet. The main barrel of the outfall is approximately 6,480 feet in length, not including the diffuser section. The diffuser section is wye-shaped and contains two 48-inch diameter,

225-foot long legs spaced 127 degrees apart and 216 feet of the main barrel. The outfall and diffusers are reinforced concrete pipe with cast-iron bell and spigot joints. The diffuser section consists of a pair of bell-mouthed ports at the pipe springline spaced every 24 feet. The 72-inch diameter pipe has eighteen 8-inch diameter ports and both 48-inch diameter pipes have eighteen 9-inch diameter ports.

The 90-inch outfall was placed into service in 1957. The main barrel of the outfall is about 7,980 feet long, not including the wye-shaped diffuser section. The diffuser section consists of two 60-inch diameter 1,208-foot long legs spaced 127 degrees apart. The outfall and diffusers are reinforced concrete pipe with cast-iron bell and spigot joints. The diffuser section consists of bell-mouthed ports, alternating sides every 24 feet. Each of the legs contains sixteen 7.5 inch and thirty-four 6.5 inch diameter ports. The outfall terminates at a water depth of about 210 feet.

The 120-inch outfall was placed into service in 1967 and is about 11,880 feet long, including the approximately 4,440 foot long main barrel diffuser section. The outfall is “L” in shape and constructed of reinforced concrete pipe with bell and spigot joints. The diffuser section contains approximately 768 feet of 120-inch diameter, 2,300 feet of 102-inch diameter, and 1,370 feet of 72-inch diameter pipe. The bell-mouthed ports are located approximately 12 inches above the pipe spring line. The ports on the 120-inch and 102-inch diameter pipes have a 5 degree downward angle. The ports on the 72-inch diameter pipe have no angle. The outfall terminates at a water depth of about 190 feet.

With regard to structural problems, Army personnel disposing of surplus ordnance in the 1950s set off explosions along the 60-inch outfall that caused minor cracking in the concrete coverings of ten of the cast iron joints. These joints were encased in concrete collars. The collars have deteriorated over the decades, but the cast iron joints are in a similar condition as the remaining joints. In 1994, thirteen joints on the 72-inch outfall were encased with concrete collars.

With regard to corrosion, some deterioration of the 60-inch outfall concrete pipe has been observed since the 1980s. Concrete spalls and rebar are visible in several locations.

Sediment intrusion has not been a problem but a grit mound has formed around a portion of the 120-inch outfall that has plugged a few ports. With the reduced flows resulting from current drought conditions, performance of the outfall has not yet been affected. Major maintenance efforts primarily involved reballasting the 72-inch, the 90-inch, and the 120-inch outfalls in 1997 and 1999 (Figure 6).

What has worked best for the Whites Point Ocean Outfalls is having the flexibility to increase the hydraulic capacity during high flow conditions by opening the 72-inch and 60-inch outfalls. This is a significant benefit to the daily operations of the system.

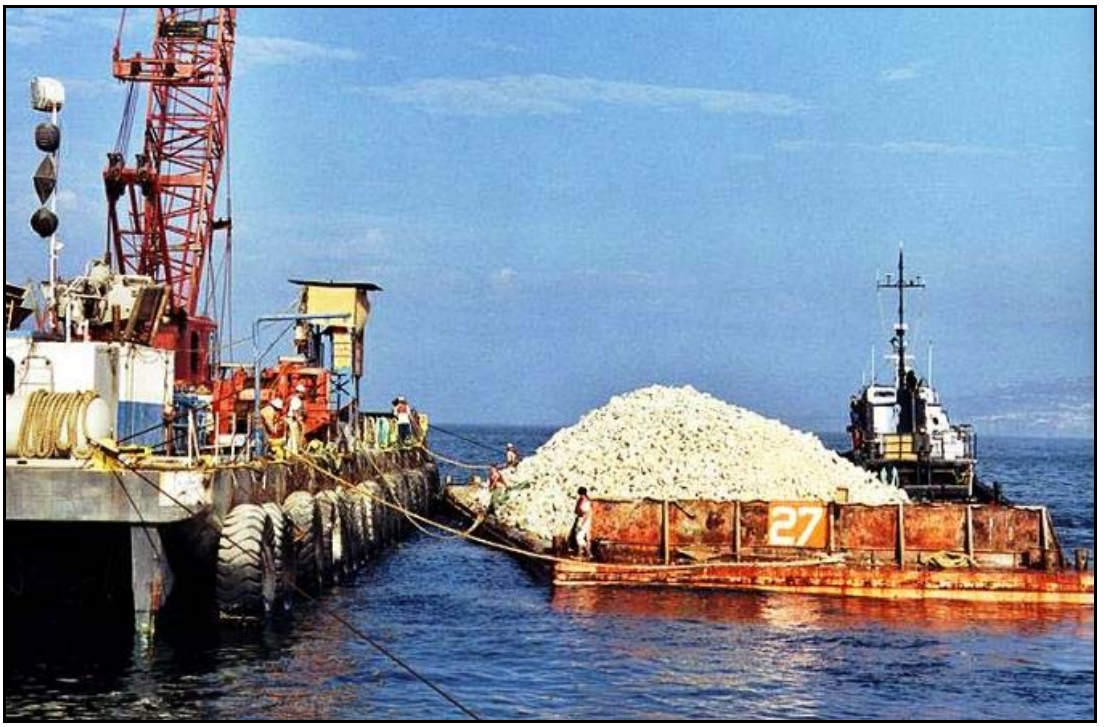


Figure 6. Reballasting the Whites Point Ocean Outfalls, Los Angeles County

POINT LOMA OCEAN OUTFALL
San Diego, California

The owner of the Point Loma Ocean Outfall is the Public Utilities Department, City of San Diego. The outfall is located in San Diego near the tip of the Point Loma Peninsula and extends from the Point Loma Treatment plant (Figure 7) into the Pacific Ocean.

The inside diameter of the outfall is 108 inches for the first 11,300 feet; the outer 12,500 feet has an inside diameter of 144 inches. The entirety of the offshore outfall is constructed of concrete reinforced cylindrical pipe.

The outfall discharges in 300 feet of water about 4.5 miles offshore. The discharge is through wye diffusers that transition the 144-inch pipe into two 84-inch pipes. The inside diameter of the two diffuser legs reduce from 84 inches to 48 inches over a length of about 2,500 feet. There are discharge ports every 24 feet along the crown of the diffuser pipes. These ports range in diameter from 3.75 inches to 4.75 inches at the end of the diffuser legs.

The original outfall had a structural failure to the pipe in February 1992 which was believed to be caused by air entrainment. The failure was located about three-fourths of a mile from the onshore vortex structure. This vortex structure provided for vertical drop of 90 feet to the beginning of the 108-inch pipe discharge. Air is entrained by the circular motion imparted by the vortex and the fine bubbles rise to

the pipe crown and then to get trapped at high points within in the pipe. When the air blowback occurs, pressure differentials are created that cause structural stress.

The South Effluent Outfall Connection (SEOC) was constructed in 1993 to 1997. The SEOC was constructed to minimize introduction of air in to the outfall and to allow for the shutdown of the north effluent system for maintenance. The SEOC allowed the water to entry the discharge pipe through a lower angle with the head being controlled by thee 84-inch sleeve valves. The north effluent system and the SEOC are the two methods used to transport treated wastewater flow to the outfall pipe. The vortex structure is no longer used on a regular basis.

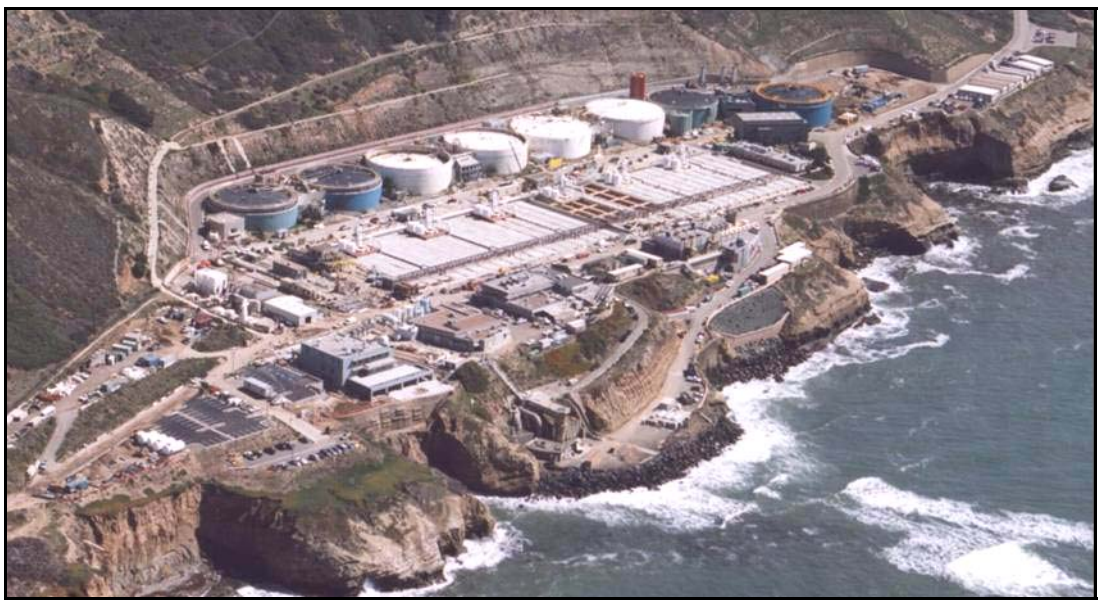


Figure 7. Point Loma Wastewater Treatment Plant, San Diego

There have not been corrosion issues**,** but the joints on the first 3,000 feet of pipe inspected have been found to be worn. This was the portion constructed in the early 1960s. The inspection was done by divers, who confirmed it by feel.

Presently there are no issues to be addressed with the outfall. It is inspected regularly in accordance with the requirements of the discharge permit.

The exterior is inspected yearly with remote cameras to view the ballast, the crown of the pipe, and the diffusers. The first 3,000 feet of the pipe interior seaward from the shore is inspected by divers every 7 years. Visibility in the pipe is not possible due to the black water; the interior inspection takes place during early morning shutdowns of 3 to 5 hours in length. The divers feel along the top of the pipe and check the joints for corrosion and movement.

The steel onshore portion of the outfall between the vortex structure and the ocean (about 100 feet) was lined and coated on the exterior in 1998. Exterior pitting of the

steel pipe was noticed during the construction of the SEOC. This exterior portion was exposed, patched where necessary, then wrapped in PVC. Reinforcing steel was placed and concrete poured around the 108-inch steel pipe (Figure 8). This method allowed the outfall to stay in service while implementing repairs. If the steel pipe ever corrodes, the surrounding reinforced concrete will be there to take its place.



Figure 8. Repairing Onshore Portion of the Point Loma Ocean Outfall, San Diego

OBSERVATIONS AND CONCLUSIONS

As the present century unfolds, developed nations are scrambling to rebuild their decaying infrastructure as well as continuing to build new projects while many developing nations are investing in substantial infrastructure for the first time (Treadwell et al, 2008). The major infrastructure investments seen around the world typically involve transportation networks, energy pipelines, water supply systems, communications networks, and sewers and wastewater treatment systems. As more and more of us now live at or near the coastlines of the world, a majority of these projects are at the coast.

Infrastructure assets are typically large in scale and they come with high initial costs and their true value can often be difficult to determine. Built to last for many decades and even a century or more, these assets require long-term commitments from the companies and governments that build and operate them.

History has taught that design, value engineering, and construction must not overlook the critical aspects of operation, maintenance, and potential repair. The need for these missions to be carried out over time by dedicated and experienced personnel is particularly important for marine structures because of the harsh environmental conditions and the difficulty and expense of inspection, maintenance, and repair operations. Durable and well-maintained structures clearly improve the sustainability of vital infrastructure elements.

ACKNOWLEDGMENTS

The authors particularly appreciate the coastal wastewater outfall system information provided by the following owner's representatives:

- Southwest Ocean Outfall --- Tommy Moala, Assistant General Manager, Wastewater Division, San Francisco Public Utilities Commission.
- Deer Island Ocean Outfall --- Daniel O'Brien, Director, Deer Island Treatment Plant, Massachusetts Water Resources Authority.
- Whites Point Ocean Outfalls --- David Haug, Senior Engineer, Wastewater Design Section, Sanitation Districts of Los Angeles County.
- Point Loma Ocean Outfall --- F. Stuart Seymour, Associate Civil Engineer, Public Utilities Department, City of San Diego.

The work reported herein was supported in part by Parsons Brinckerhoff through their professional development program. The authors appreciate this support and the support, encouragement, and enthusiasm of their colleagues, friends, and families.

REFERENCES

Brocard, D. N., Van Weele, B. J., and L. A. Williamson (1994), The New Boston Outfall, Journal of the Boston Society of Civil Engineers, Volume 9, Number 1, Spring/Summer 1994, pages 33-48.

CCSF (1986), *Southwest Ocean Outfall: Operation and Maintenance Manual*, Clean Water Program, Department of Public Works, City and County of San Francisco, San Francisco, California.

Eisenberg, Y. and D. D. Treadwell (1982), San Francisco's Southwest Ocean Outfall, Proceedings, 18th International Conference on Coastal Engineering, ASCE, Cape Town, South Africa, pages 2418-2435.

Eisenberg, Y. and P. Brooks (1992), Design and Construction of the Boston Outfall, Proceedings, 23rd International Conference on Coastal Engineering, ASCE, Venice, Italy, pages 3285-3304.

Gilbert, O. H., Jr., Eisenberg, Y., and D. D. Treadwell (1981), Seismic Design of the San Francisco Ocean Outfall, Proceedings, International Conference on Recent Advances in Geotechnical Earthquake Engineering and Soil Dynamics, ASCE, St. Louis, Missouri, pages 1133-1138.

Grace, R. A. (1978). *Marine Outfall Systems: Planning, Design, and Construction,* Prentice-Hall, Englewood Cliffs, New Jersey.

Grace, R. A. (2009), *Marine Outfall Construction: Background, Techniques, and Case Studies,* ASCE Press, American Society of Civil Engineers, Reston, Virginia.

Gunnerson, G. C., editor (1988), *Wastewater Management for Coastal Cities: The Ocean Disposal Option*, World Bank Technical Paper No. 77, Washington, DC, 426 pp.

Roberts, P. J. W., Salas, H. J., Reiff, F. M., Libhaber, M., Labbe, A., and J. C. Thompson, J. C. (2010), *Marine Wastewater Outfalls and Treatment Systems*, IWA Publishing, London, U. K.

Treadwell, D. D., Rietman, J. A., Weaver, K. D., and G. J. Murphy (1980), Offshore Faulting in the Gulf of the Farallones, Proceedings, Paper OTC 3916, 12th Offshore Technology Conference, Houston, Texas, pages 611-616.

Treadwell, D. D., Van Weele, B. J., and Y. Eisenberg (2004), Wastewater Outfalls for Coastal Cities, Proceedings, ICCE 2004, 29th International Conference on Coastal Engineering, Lisbon, Portugal, September 2004, pages 3239-3250.

Treadwell, D. D., Van Weele, B. J., Magoon, O. T., and Y. Eisenberg (2008), Improved Longevity of Coastal Structures, Proceedings, ICCE 2008, 31st International Conference on Coastal Engineering, Hamburg, Germany, 31 August through 5 September 2008, pages 3393-3402.

Numerical Modeling Studies of San Elijo Lagoon Restoration Project

Weixia Jin, PhD, PE[1], Xiuying Xing, PhD, PE[2], Chris Webb[3], and Doug Gibson[4]

[1]Senior Coastal Engineer, wjin@moffattnichol.com; [2]Coastal Engineer, xxing@moffattnichol.com; [3]Senior Coastal Scientist, cwebb@moffattnichol.com; Moffatt & Nichol, 3780 Kilroy Airport Way, Suite 600, Long Beach, CA 90806; PH 562-426-9551; FAX 562-424-7489

[4]Executive Director, dg@sanelijo.org, San Elijo Lagoon Conservancy, P.O. Box 230634, Encinitas, CA 92023; PH 760-436-3944; FAX 760-944-9606

ABSTRACT

The San Elijo Lagoon Ecological Reserve is located within the City of Encinitas in San Diego County, California. The Reserve provides habitat for sensitive, threatened, and endangered species, as well as recreational opportunities. Due to development, the ecological function of the lagoon has been degraded. The San Elijo Lagoon Restoration Project is an effort to restore the lagoon functions and values. Four new alternatives are proposed. Two of them will use the tidal inlet at its current location and the other two will have a new, wider and deeper tidal inlet located south of its current location. RMA2 tidal and flood hydrodynamic modeling studies were performed. The results indicate that alternatives with the new tidal inlet can provide better tidal flushing, support a broader vertical range of salt marsh habitat, significantly lower the flood water level, and avoid flooding of a perimeter road during the 100-year storm event. RMA4 water quality modeling results indicate that alternatives with the new inlet would dramatically reduce the residence time, the duration of bacteria exceedance in the Lagoon and nearshore ocean, the salinity concentration recovery time after rain events, the travel time of nutrients and fine sediment through lagoon, and sedimentation in the Lagoon.

INTRODUCTION

The San Elijo Lagoon Ecological Reserve is a 915 acre site located within the City of Encinitas in San Diego County as shown in Figure 1. It is owned and managed by the California Department of Fish and Game, the County Department of Parks and Recreation, and the San Elijo Lagoon Conservancy (SELC). The Lagoon is traversed by Highway 101, the North County Transit District (NCTD) railroad, and Interstate 5 (I-5). The Lagoon provides habitat for sensitive, threatened, and endangered plants and animals. In addition, the Lagoon provides recreational opportunities such as hiking and bird-watching. Due to encroachment by development and infrastructure located inside the Lagoon as well as within the watershed, the ecological function of the Lagoon has been compromised through reduced tidal circulation and degraded water quality. The San Elijo Lagoon Restoration Project (SELRP) is an effort to restore the lagoon functions and values given historic development and constraints

placed on it by surrounding development activities. The project aims to enhance the tidal prism of the Lagoon by proposing lagoon dredging and modifications to hydraulic constraints.



Figure 1. Project Location Map

Preliminary engineering is being performed that consists of conceptual alternative designs and a series of numerical modeling studies to evaluate their performance. The inlet location is an importance factor in alternative selection as it associates with changes to existing beach activities if a new inlet location is selected, replacement costs of the existing infrastructures, and future project maintenance cost. Also, the selected inlet needs to be able to provide sufficient tidal flushing and inundation to achieve project objectives. This paper compares flood conveyance, tidal flushing, and pollutant transport/dilution between alternatives with the new tidal inlet and alternatives with inlet at its current location based on flood and tidal hydrodynamic and water quality numerical modeling results.

ALTERNATIVE DESCRIPTION

Five project alternatives have been identified by the Stakeholder Committee as likely to be included in the environmental document. They include: No-Project-Existing Conditions, Alternatives 1a and 1b with inlet at its existing location, and Alternatives 2a and 2b with inlet located approximately 0.7 miles south of the existing inlet. Alternatives 1a and 1b will use the existing inlet as the source of seawater. The tidal muting, inlet stability and flood shoal development are expected to be similar to the existing lagoon conditions. Alternatives 2a and 2b will be connected to the ocean via a new, wider and deeper tidal inlet. The tidal muting, inlet stability and flood shoal

development are expected to be very similar. Although Alternatives 1b and 2a will be connected to the ocean at different inlet locations, they will create similar diversified habitats. Therefore, numerical modeling results of these two alternatives are discussed and compared in the following sections to assist the inlet location selection.

No Project – Existing Conditions. No Project assumes existing conditions remain into perpetuity. The Lagoon presently experiences mouth constriction and manual re-opening annually, and sometimes more frequently. Tidal flushing is restricted, and water quality conditions are impaired for nutrients and fine sediment.

Alternative 1b – Maximum Habitat Diversity, Existing Inlet Location. Alternative 1b provides a substantial change to the existing site to create a greater diversity of habitats than currently exists. The existing tidal inlet remains the source of seawater, and the main tidal channel extends throughout the Lagoon. A new subtidal basin off the main channel is created in the Central Basin. The main feeder channel is redirected just west of I-5, and extended farther into the East Basin. The channel in the East Basin is significantly enlarged in cross-sectional area to promote more tidal exchange east of I-5. The tidal prism of Alternative 1b will be significantly increased compared to No Project and Alternative 1a. Figure 2 shows Alternative 1b.

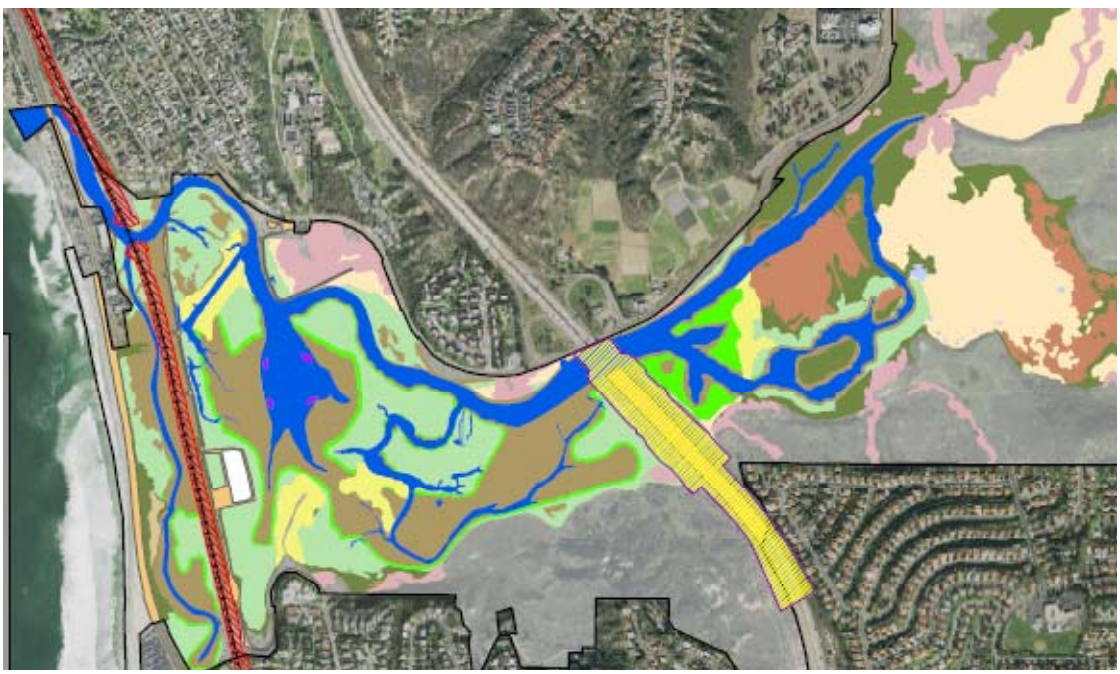


Figure 2. Alternative 1b

Alternative 2a – Maximum Habitat Diversity, New Inlet Location. Alternative 2a also provides changes to the existing site to create a greater diversity of habitats than presently exists. Seawater would enter the Lagoon via a new tidal inlet located south of the existing inlet and a new subtidal basin would be created just landward of the new inlet in the West and Central Basins. The main tidal channel would extend throughout the Lagoon and be redirected just west of I-5. The channel in the East

Basin is identical to that for Alternative 1b. The tidal prism of Alternative 2a will increase compared to Alternative 1b. Figure 3 shows Alternative 2a.

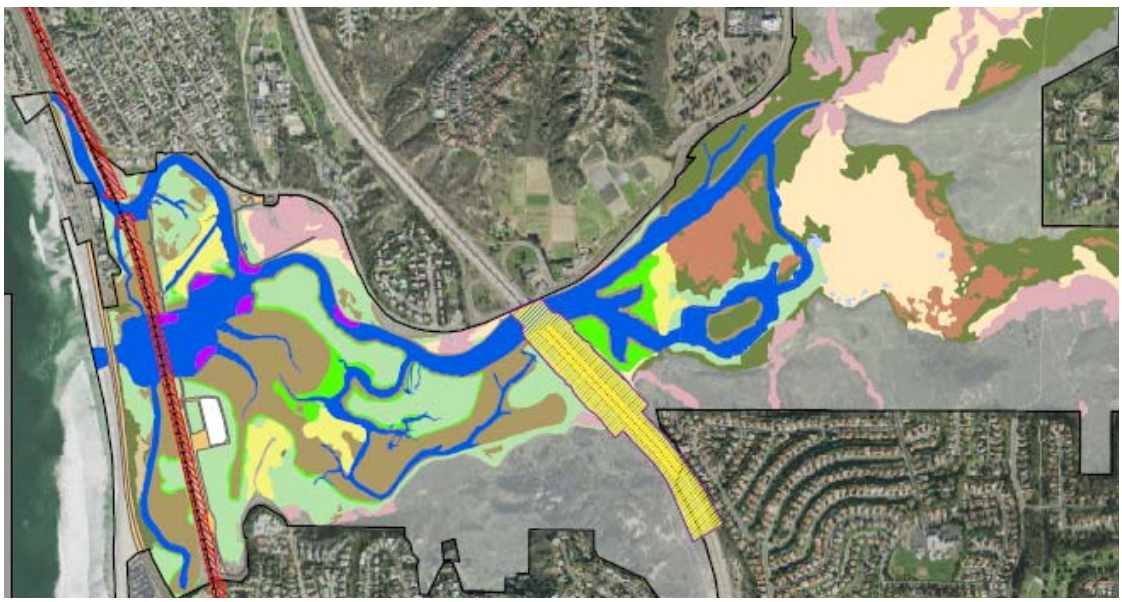


Figure 3. Alternative 2a

Summary of Inlet and Channel Dimensions. The channel cross-section dimensions at each bridge constraint are shown in Table 1. Both Alternatives 1b and 2a assume wider and deeper channels at each bridge location for further improved hydraulics. All bridges would need to be replaced under these alternatives.

Table 1. Summary of Inlet and Channel Dimensions

Alternative	HW101/Inlet		Railroad Trestle		I-5 Bridge	
	Bottom Width (ft)	Invert (ft, NGVD)	Bottom Width (ft)	Invert (ft, NGVD)	Bottom Width (ft)	Depth (ft, NGVD)
Existing	105	-0.87	165	-0.87	130	0.74
Alt. 1b	130	-4.0	165	-5.5	260	-6.0
Alt. 2a	200	-6.5	590	-7	260	-6.5

HYDRODYNAMIC MODELING

The 2-D vertically averaged finite element hydrodynamic (RMA2) and water quality (RMA4) models were used in the studies. The purposes of hydrodynamic modeling were to: 1) evaluate wetlands hydraulics by predicting tidal ranges and tidal inundation frequencies; 2) predict the maximum water level for flood protection and infrastructure design; 3) optimize tidal inlet dimensions; 4) estimate tidal inlet flow velocities for inlet stability analyses, and 5) generate flow fields to drive the RMA4 water quality model. The RMA2 model was calibrated with tides recorded at the NCTD Bridge and the I-5 Bridge in the summer of 2002 by the SELC. Numerical modeling parameters of Manning's roughness coefficient (n), peclet numbers, and marsh porosity were determined during the calibration process. The calibrated model

was then verified with a data set collected in January 2008 also by the SELC. The calibration and verification processes and results are included in hydrology and hydraulic report prepared by Moffatt & Nichol (M&N 2010a).

Alternative Modeling. The modeling parameters calibrated for existing conditions were assigned for the alternative modeling. Numerical model grids in the wetland area and virtual gage locations where modeling results are analyzed are shown in Figure 4 for the existing and Alternative 1b and in Figure 5 for Alternative 2a. These locations are fixed except at the tidal inlet, depending on inlet location.

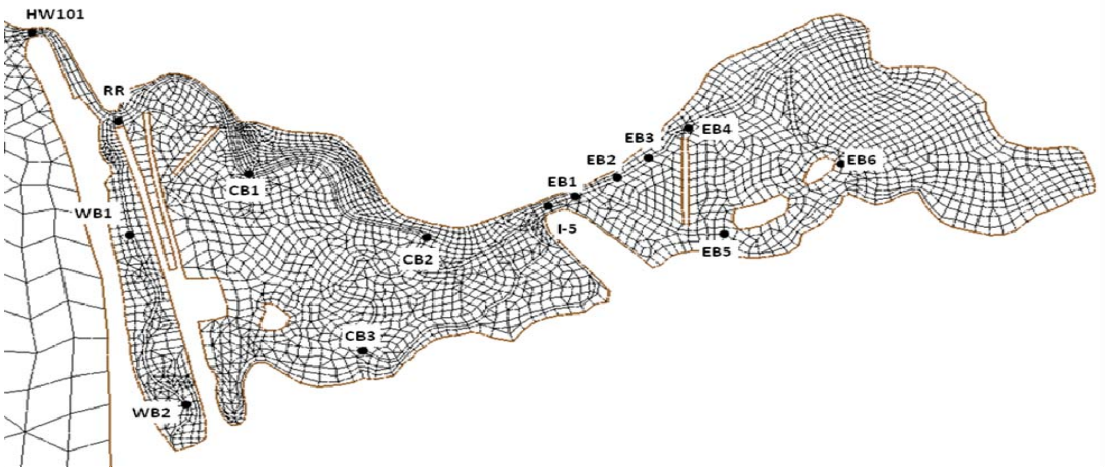


Figure 4. Virtual Gage Locations for Existing Conditions and Alternative 1b

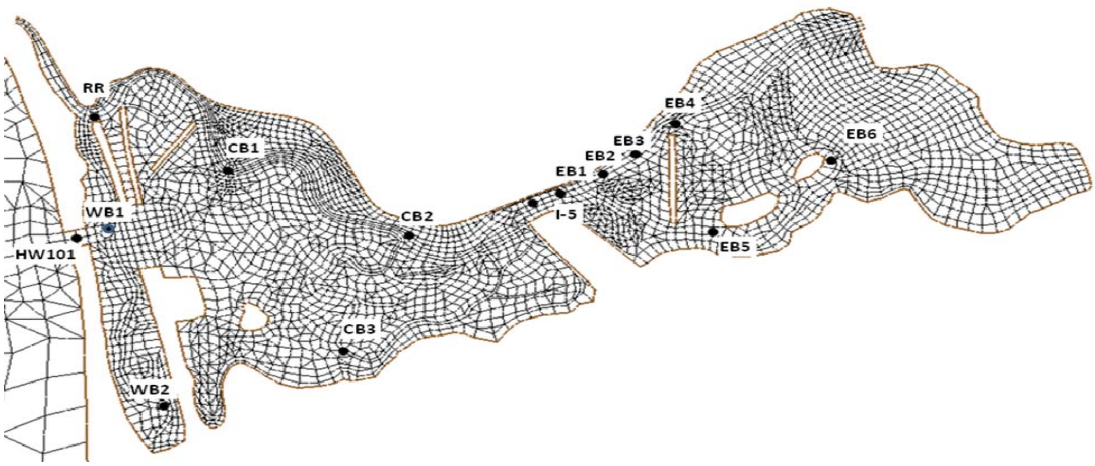


Figure 5. Virtual Gage Locations for Alternative 2a

Flood Hydraulic Modeling Results. The purpose of the flood hydraulic analyses is to determine the maximum water levels throughout the Lagoon to quantify impacts of restoration on potential flooding of adjacent areas. The hydrodynamic model runs were conducted under the 100-year flood combined with the extreme high spring tide. The spring tidal series was shifted upward to match the FEMA base flood elevation of

+7 feet (ft) NGVD (FEMA FIRM Panel No. 06073C1044F) along the shores of the Lagoon.

The Lagoon is the estuary of both Escondido and La Orilla Creeks. A statistical analysis was performed by Exponent Inc. (2000) to determine the 100-year flood flow based on data from a neighboring stream gage on Las Flores Creek near Oceanside Harbor, as the stream gage record for Escondido Creek is too short to generate statistics and no stream gage exists on La Orilla Creek. The 100-year peak flood was determined to be 21,000 cubic feet per second (cfs) for Escondido Creek, which is the flood flow rate used by FEMA for the National Flood Insurance Program. The watershed area of La Orilla Creek is about 10 percent of that for Escondido Creek; therefore the combined peak flow from both creeks is estimated to be 22,255 cfs. A synthetic hydrograph was developed by Exponent Inc. (2000) and was raised to the peak flow rate of 22,255 cfs to represent the 100-yr flood into the Lagoon.

For a specific location, the highest water level occurs when the extreme high tide and the peak flood occur simultaneously. Table 2 summarizes numerical modeling results under post-construction bathymetry conditions. The flood water level will be higher if shoals build up in the tidal inlet and wetland basins without proper maintenance (periodic removal).

Table 2. Maximum 100-Year Flood Elevation in the Wetlands (ft, NGVD)

Gage Locations	HW101	RR	CB1	CB2	I-5	EB1	EB3	EB3	EB4
Manchester Ave.	N/A	N/A	16.6	9.5	14.0	13.5	9.4	9.8	10.0
Existing	6.7	8.1	9.6	9.6	11.0	13.0	13.2	13.2	14.2
Alt. 1b	6.9	7.8	10.0	10.0	10.1	10.1	10.2	10.3	10.5
Alt. 2a	6.9	7.6	7.8	7.9	8.2	8.5	8.9	9.0	9.5
Note: Values in italics indicate elevations above the roadway and represent flooding.									

The main roadway of concern is Manchester Ave. that extends along the entire northern boundary of the Lagoon. Other important features are the three bridges at Highway 101, the NCTD Railroad, and I-5. These features have been the focus of flood studies over time by Caltrans. Results indicate that for Alternative 1b a reach of Manchester Ave. in both the Central and East Basins will be flooded during the combined high tide and 100-yr flood event. The table also shows the current surface elevation of Manchester Ave. for comparison. In contrast, the 100-yr flood levels are at least 0.5 ft lower than the road surface for Alternative 2a with the proposed new inlet. Alternative 2a may not provide a 3-foot freeboard required by FEMA, but the future condition should be an improvement over existing flood conditions.

Tidal Hydraulic Modeling Results. The purposes of the tidal hydraulic studies are to: 1) Predict tidal elevations and flow velocities; 2) Determine the tidal inundation frequency in the wetlands; and 3) Predict statistics of tidal inlet hydraulics for the inlet design and stability analyses. Figure 6 shows the predicted tidal series in the wetlands and ocean for Alternative 1b. Table 3 presents predicted tidal ranges for conditions representing immediate post-construction. The ocean tidal range is also included for comparison. The tidal range difference between a wetland and the ocean represents the

potential tidal muting in that specific location. Table 4 presents the model-predicted spring high and low tide elevations and provides detailed information on whether the tidal muting occurs for high tides, low tides, or for both tidal conditions. The results are summarized below.

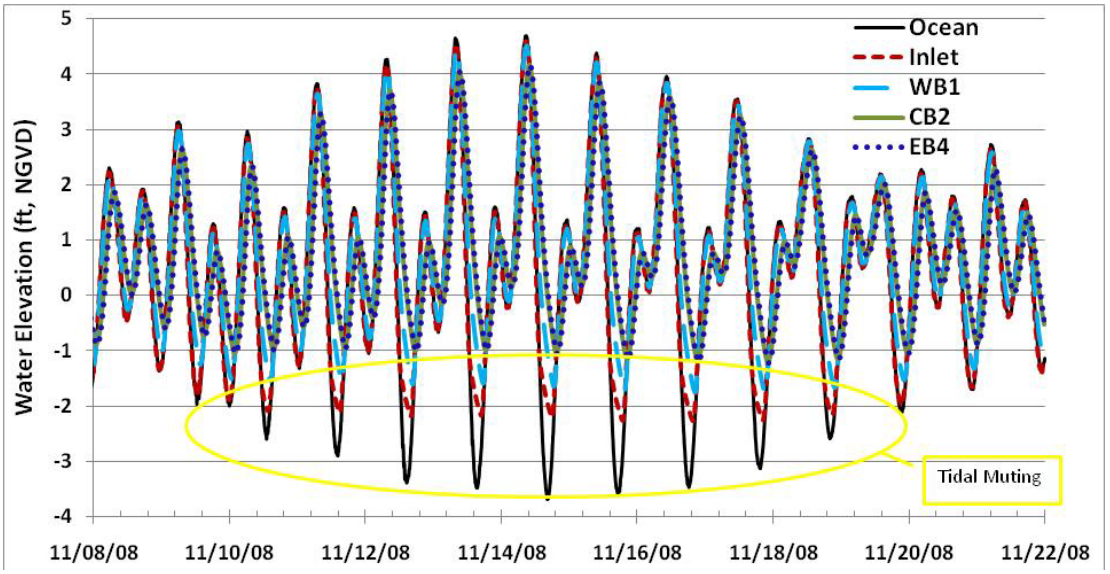


Figure 6. Predicted Tidal Elevations for Alternative 1b

Table 3. Predicted Tidal Ranges

Alternative	Tidal Range (ft)					
	Ocean	HW101	WB1	CB2	I-5	EB4
Existing	8.37	5.13	4.25	3.49	3.30	3.16
Alt. 1b	8.37	6.87	6.25	5.38	5.38	5.38
Alt. 2a	8.37	8.39	8.29	8.10	8.08	8.07

Table 4. Predicted Spring High and Low Tidal Elevations

Alternative	High and Low Tidal Elevations (ft, NGVD29)											
	Ocean		HW101		WB1		CB2		I-5		EB4	
	High	Low	High	Low	High	Low	High	Low	High	Low	High	Low
Existing	4.69	-3.68	3.69	-1.45	3.49	-0.76	2.96	-0.53	2.80	-0.50	2.68	-0.47
Alt. 1b	4.69	-3.68	4.60	-2.26	4.51	-1.74	4.16	-1.22	4.16	-1.22	4.16	-1.22
Alt. 2a	4.69	-3.68	4.68	-3.71	4.68	-3.61	4.69	-3.42	4.69	-3.40	4.68	-3.39

For No Project, the inlet is narrow and long, and the inlet depth is limited by a bedrock and cobble sill at the mouth. Both high and low tides in the West Basin are muted by more than 1 ft compared to the ocean tides. The tides are further muted in the Central Basin due to the constriction of the Railroad Bridge, and then even further muted in the East Basin by the narrow channel under the I-5 Bridge. Therefore, the vertical range of intertidal habitat is approximately 3 to 4 ft and much narrower than that under the open-ocean condition. A range of salt marsh habitats can occur on-site, but their areas will be constrained by the tidal range, and the habitat distribution on-site may be dominated by fewer species more suited to the tidal elevations.

For Alternative 1b, the overall hydraulics is controlled by the constriction at the mouth as with existing conditions. Both high and low tides are muted, with low tides muted by more than 2 ft in the Central Basin. Both the inlet and Railroad Bridge restrict flow to the Central Basin. The predicted tidal range in the East Basin is similar to that in the Central Basin, which indicates that the proposed channel cross-section under the I-5 Bridge is sufficient to not cause further muting in the East Basin. Therefore, the vertical zonation of intertidal habitat is more extensive than for existing conditions, ranging from 6.2 ft in the West Basin, to 5.4 ft in the Central and East Basins, but their areas will still be constrained by the tidal range. Any tidal muting could further constrain the elevations and distribution of salt marsh habitat.

For Alternative 2a, with the proposed new tidal inlet location, the high tide is not muted and the low tide is muted approximately 0.3 ft in both the Central and East Basins due to retarding effects of the meandering main channel in the Central Basin. Hydraulically, Alternative 2a reduces tidal muting and improves circulation in the wetland basins. The inundation frequencies in the wetland basins closely mimic that in the ocean, and the vertical zonation of intertidal habitats is maximized at 8.3 ft in the West Basin and 8.0 ft in the Central and East Basins. This situation indicates that the tidal inlet design is sufficient to approximately convey full tidal circulation in all wetland basins. As a result, the full range of salt marsh habitats should occur on-site. As with previous alternatives, any tidal muting from shoaling would constrain the tidal range and distribution of habitats, thus maintenance dredging would be important in preserving habitat areas.

In summary, Alternative 2a with the proposed new wider and deeper tidal inlet would result in the least tidal muting and circulation is most improved in the wetland basins. Also, a greater range of salt marsh habitat would occur on a broader vertical elevation range as result of nearly fully tidal exchange with the ocean compared to the existing condition and Alternative 1b with the inlet at its current location.

WATER QUALITY MODELING

The Lagoon is 303d listed for indicator bacteria, nutrients, and fine sediment siltation. The SELRP is intended to improve water quality for lagoon habitat and for beach recreation near the tidal inlet. The purpose of water quality modeling is to evaluate water quality conditions in the Lagoon, the tidal inlet, and the nearshore-ocean associated with the proposed alternatives during both dry and wet weather conditions. The RMA4 water quality model was applied to evaluate:

- Tidal circulation efficiency and seawater residence time within different areas of the Lagoon. Daily water quality is dependent on tidal circulation.
- Dispersion and dilution of bacteria and/or other potential pollutants of concern. Ocean water quality may be a concern to certain stakeholders if the ocean inlet is relocated.
- Dilution and dispersion of freshwater storm flows within the Lagoon from upstream. Salinity levels vary during storms and may affect habitat. Model results will be useful to show potential stresses to habitat during the wet season.

- Potential sedimentation within the Lagoon from upstream sources based on projected sediment yield and predicted hydraulic conditions.

The RMA4 numerical model was calibrated with salinity data measured throughout the Lagoon in summer 2002 by the SELC. Dispersion coefficients were determined during the calibration process. The calibrated model was then verified with another salinity data set collected in January 2008. The calibration and verification processes and results are included in the water quality study report by Moffatt & Nichol (M&N 2010b).

A wet season storm event in January 2008, which will be referred to as the 2008 rain event in the following text, was selected to represent a typical 2- to 5-year storm, as this event is one of the three wet weather events monitored for TMDL development (MACTEC 2009). Valuable water quality data were collected during the monitoring period.

Residence Time Analyses. Residence time (i.e., average time a particle resides in a hydraulic system) provides a useful measure of the rate at which waters in the hydraulic system are renewed. Accordingly, residence times provide a means for assessing the water quality of the hydraulic system. A 15-day modeling tidal series, representing the average spring and neap tidal cycle was taken as the offshore driving tide. No runoff from the fresh water boundary was considered, as the base flow of creeks is negligibly small.

Based on RMA4 numerical modeling results, residence times are calculated at representative gage locations shown in Figure 4 for existing and Alternative 1b and in Figure 5 for Alternative 2a. Results of residence time analyses are summarized in Table 5. Both proposed alternatives reduce residence times significantly compared to the existing condition. Residence times under Alternative 2a with the new inlet are further reduced to less than half of those under Alternative 1b. Residence time is an indicator of tidal flushing efficiency. A short residence time means good flushing and circulation. With short residence times such as those created by conditions in Alternative 2a, contaminant constituents such as nutrients and fine sediments can be quickly diluted and/or flushed out to the ocean. A long residence time often indicates stagnation and poor circulation and results in a poor water quality condition.

Table 5. Residence Time Comparison

Gage Locations	West Basin		Central Basin			I-5	East Basin	
Alternative	WB1	WB2	CB1	CB2	CB3		EB4	EB6
Existing	5.9	8.0	2.4	7.3	7.2	15.1	n/a	n/a
Alt. 1b	1.2	1.8	1.3	3.6	3.6	6.1	9.3	11.3
Alt. 2a	<0.5	1.1	1.1	1.9	2.0	2.7	3.3	3.3
n/a-residence time is not calculated since there is no tidal circulation in East Basin under the existing conditions								

Bacteria Analyses. Enterococcus bacteria were selected as the type of indicator bacteria for the modeling study and results are analyzed with regard to recreational water contact activities in the ocean. Enterococcus concentrations were monitored at

three locations within the Lagoon during the 2008 rain event. Concentrations measured at the I-5 Bridge were used as model boundary input. Being conservative, the highest measured concentration of 8,400 Most Probable Number per 100 milliliters (MPN/100 ml) during the storm event was selected to represent the entire rain event, and the highest concentration of 168 MPN/100 ml measured over a one week period after the rain event was applied as the pre- and post-rain storm condition concentration input. Zero concentration is applied at the model offshore ocean boundary, assuming that seawater is uncontaminated. Model calibration under existing lagoon conditions was performed to determine the average die-off rate of enterococcus bacterium. The results indicate that the simulated concentrations match the measured concentrations well when the die-off rate equals 0.2 day^{-1}, or when the T_{90} is 120 hours.

Enterococcus was modeled with the RMA4 model for each alternative during the 2008 rain event. The modeling results are extracted at the inlet and the nearshore ocean where routing water quality samples have been taken by the San Diego County Department of Environmental Health and the San Elijo Lagoon Joint Powers Authority. Figure 7 shows the nearshore sampling locations. Table 6 summarizes days of exceedance in the Central Basin and the nearshore ocean. One day exceedance is defined if the enterococcus concentration tips over the instantaneous criterion of 104 MPN/100ml over a 24-hour period. The results are primarily provided for the purpose of alternatives comparison. The days of exceedance are separated into two periods: during the three day rain event and the post-rain period. Locations near the lagoon outlet exceed the criterion during the rain event, specifically, at SE-06 for existing and Alternative 1b; and at SE-03 and SE-04 for Alternative 2a. After the rain event, there are multiple days of exceedances for existing and Alternative 1b since the bacteria are trapped in the Lagoon and being discharged slowly. However, there is no exceedance for alternatives with the new inlet location due to improved circulation. Overall, Alternative 2a will result in fewer potential beach closures after storm events. Inside the Lagoon, the exceedances occur even one week after the rain event for existing and Alternative 1b compared to the first three days for Alternative 2a.

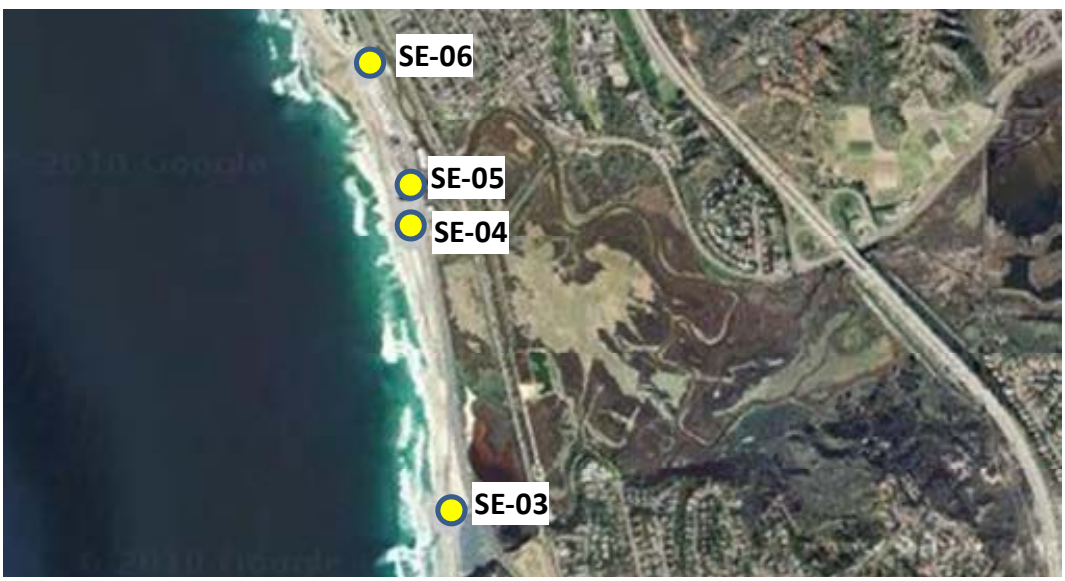


Figure 7. Water Quality Sampling Locations (Based on Google Image, 2010)

Table 6. Days of Enterococcus Bacteria Exceedance

Time	Location	Existing	Alt. 1b	Alt. 2a
During the 3-day Rain Event	SE-03, Seaside	2	0	1
	SE-04, Las Olas	2	1	3
	SE-05, Charthouse	2	1	3
	SE-06, SEL Outlet	3	3	1
	Central Basin	3	3	3
Post Rain Event	SE-03, Seaside	0	0	0
	SE-04, Las Olas	0	1	0
	SE-05, Charthouse	0	1	0
	SE-06, SEL Outlet	6	4	0
	Central Basin	8	7	3

Salinity Modeling. Salinity levels in the water column within the Lagoon during the 2008 rain event were modeled using the RMA4 model. Wetlands fed by upstream tributaries typically experience a flush of freshwater to varying degrees during rain events. Salinity levels can fluctuate from an ocean salinity concentration of 34 parts per thousands (ppt) to freshwater conditions with salinity levels of less than 5 ppt. Conditions of low salinity can stress salt marsh habitat. The purpose of the modeling is to show the duration of low salinity within the Lagoon during a typical rain event, and to quantify how rapidly salinity levels return to certain threshold levels. This information enables a comparison between alternatives. A typical salinity level of 34 ppt is applied at the model ocean boundary and a storm water salinity level of 1.2 ppt is applied at the upstream flood flow boundary.

Salinity modeling results are provided by the numerical model at specified locations. The locations specified for the results are shown in Figure 4 for existing and Alternative 1b and in Figure 5 for Alternative 2a. Salinity criteria of 10 ppt and 25 ppt, which represent 30% and 75% of normal seawater salinity, are used to assess impacts of excessive freshwater. The first criterion was developed primarily to protect the less mobile marine invertebrates (Sanders et al 1965), and the second one was developed to protect certain fish species (Baczkowski 1992). The salinity recovery times are summarized in Table 7.

Table 7. Maximum Salinity Recovery Time in Hours

Salinity Drops Below	West Basin (WB1)			Central Basin (CB2)			East Basin (EB4)		
	Exist	Alt1b	Alt2a	Exist	Alt1b	Alt2a	Exist	Alt1b	Alt2a
10 PPT	1	1	8	67	17	7	>240	168	91
25 PPT	24	23	10	69	46	10	>240	>240	>240

The East Basin is completely filled with fresh water during the rain event for all scenarios. Under Alternative 2a with the new wider and deeper inlet, salinity recovers to 10 ppt much faster than Alternative 1b and existing conditions with the existing narrower and shallower tidal inlet. The recovery times to 25 ppt are longer than the simulation duration of 10 days after the rain for all scenarios.

The Central Basin is nearly completely filled with fresh water. The recovery times for both criteria are less than one day for Alternative 2a, one to two days for Alternative 1b, and about 3 days for existing conditions.

In the West Basin, the salinity is oscillating between seawater and freshwater due to its closeness to the inlet. The recovery time is less than half of a day for Alternative 2a. For Alternative 1b and existing conditions, the West Basin is connected with the inlet channel with a small feeder channel; therefore, the basin is not completely filled with fresh water and the salinity is rarely drops below 10 ppt.

Overall, the salinity levels depend on tidal circulation efficiency, with the better circulation resulting in more rapid salinity recovery. Alternative 2a with the new and inlet provides better circulation and faster salinity recovery than Alternative 1b with a narrower and shallower inlet remaining at its current location.

Sedimentation. The Lagoon is 303d listed for fine sediments. Stakeholders expressed concerns about potential future sedimentation at the Lagoon. This effort is to analyze the potential for sedimentation from upstream sources. Analyses are based on estimating flow velocities through the Lagoon and the resulting sediment transport and patterns of deposition during a 100-yr storm event and a typical 2-5-yr storm event. The numerical model predicts the spatial distribution of flow velocities as a time series over the storm event. All analyses use a threshold flow velocity of 0.6 ft per second (fps) to represent the velocity required to maintain sediment transport of sand-sized material and unconsolidated clay and silt materials (Hjulstrom 1935). Velocities below this threshold result in sedimentation. Typically the larger grain-sized material, such as sand, will settle out first, followed by the finer grain sizes such as silt and clay. While sand may settle out with flows under 0.6 fps, silts and clays may not settle out until flow velocities drop below 0.3 fps.

Under the existing conditions, the peak flow velocity in the Central Basin drops below 0.3 fps during the low flow event and below 0.6 fps during the 100-yr storm event. These results indicate that the silts and clay material will settle in the Lagoon during frequent low flow storm events and may be carried through the Lagoon to the ocean during major storm events.

Under Alternative 1b, the peak flow velocity maintains 0.3 fps, but less than 0.6 fps during both the low flow event and the 100-yr storm. These results indicate that silt and clay materials may be able to pass through the Lagoon without settling; however, fine sandy materials are still expected to settle in the Lagoon during both smaller and larger storm events. However, overall rates of sedimentation will be lower than those under the existing conditions.

Under Alternative 2a, the peak flow velocity maintains above 0.6 fps during both the low flow and 100-yr storm events. These results indicate sand and finer sediments should be transported through the Lagoon and to the ocean under most storm conditions. Sedimentation from upstream will be significantly reduced under this alternative compared to existing conditions and Alternative 1b. Also, the drainage of storm flow through the Lagoon is more efficient for Alternative 2a compared to

existing and Alternative 1b as shown in Table 8. Alternative 2a reduces the drainage duration that leads to less opportunity for sedimentation.

Table 8. Duration of Storm Flow Drainage

Alternative	From Upstream Lagoon Boundary to Highway 101	
	2- to 5-Year Storm	100-Year Storm
Existing	4 hours, 30 minutes	3 hours, 30 minutes
Alt. 1b	2 hours, 20 minutes	1 hours
Alt. 2a	1 hour, 6 minutes	0 hours, 30 minutes

CONCLUSION

The RMA2/RMA4 numerical modeling suite was applied in hydrodynamic and water quality modeling studies. The RMA2 tidal and flood hydrodynamic modeling results indicate that alternatives with the new wider and deeper tidal inlet will:

- Lower the 100-yr flood water level below the road along the northern boundary of the Lagoon;
- Provide more efficient tidal flushing; and
- Support a broader vertical range of salt marsh habitat as a result of nearly fully tidal exchange with the ocean compared to the existing conditions and alternatives with the inlet at its current location.

The RMA4 water quality modeling results indicate that alternatives with the new tidal inlet would dramatically reduce:

- Residence time in the Lagoon;
- Storm associated bacteria exceedance and salinity concentration recovery time;
- Fine material travel time through the Lagoon; and
- Sedimentation in the Lagoon.

In summary, alternatives with the proposed new tidal inlet would perform better than alternatives with the inlet at its current location based on hydrodynamic and water quality modeling results.

ACKNOWLEDGMENT

We wish to thank and acknowledge the Stakeholder Committee, made up of representatives of the resource and regulatory agencies involved in the management and oversight of the project development, and affected landowners and land managers. In particular, we wish to acknowledge the San Elijo Lagoon Conservancy for their direction and guidance, and the San Diego Association of Governments and California Coastal Conservancy, under whose funding the project was undertaken.

REFERENCES

Baczkowski, S.L. (1965). *The Effects of Decreased Salinity on Juvenile California Halibut, Paralichthys californicus*. Masters Thesis, San Diego State University.

Exponent Inc. (2000). Feasibility Study and Conceptual Plan for the Relocation of the San Elijo Lagoon, Progress Report #6 - Hydraulic and Sedimentation Study. Prepared for City of Encinitas.

Google Earth. (2010). "San Elijo Lagoon, Encinitas, California." 33^{o} 00' 31.55" N and 117^{o} 16' 28.84" W. Image Date: August 24, 2010.

Hjulstrom, F. (1935). "Studies of the Morphological Activity of Rivers as Illustrated by the River Fyris," *Bulletin,* Geological Institute of Upsala, Vol. XXV, Upsala, Sweden.

MACTEC Engineering and Consulting, Inc. (2009). Carlsbad Hydrologic Unit (CHU) Lagoon Monitoring Report.

Moffatt & Nichol. (2010a). *San Elijo Lagoon Restoration Project - Hydrology/Hydraulic Study,* Draft Report, prepared for The San Elijo Lagoon Conservancy.

Moffatt & Nichol. (2010b). *San Elijo Lagoon Restoration Project – Water Quality Study,* Draft Report, prepared for The San Elijo Lagoon Conservancy.

Sanders, H.L., P.C. Mangelsdorf, Jr., and G.R. Hampson. (1965). "Salinity and Faunal Distribution in the Pocasset River, Massachusetts", *Limnology And Oceanography*, 10, 216-228.

Modeling study of bacterial dispersion for marine-coastal waters, according with the European Directives

I. Scroccaro[1], L. Colugnati[1], G. Umgiesser[2] and G. Mattassi[1]

[1]Isabella Scroccaro, ARPA FVG, Via Cairoli 14, 33057 Palmanova (UD), Italy; PH (0039) 0432 922628; FAX (0039) 0432 922626; email: isabella.scroccaro@arpa.fvg.it
[1]Luigi Colugnati, ARPA FVG, Via Cairoli 14, 33057 Palmanova (UD), Italy; PH (0039) 040 9494903; FAX (0039) 040 9494944; email: luigi.colugnati@arpa.fvg.it
[2]Georg Umgiesser, Oceanography, ISMAR-CNR, Arsenale Tesa 104, Castello 2737/F 30122 Venice, Italy; PH (0039) 041 2407943; FAX (0039) 041 2407940; email: georg.umgiesser@ismar.cnr.it
[1]Giorgio Mattassi, ARPA FVG, Via Cairoli 14, 33057 Palmanova (UD), Italy; PH (0039) 0432 922619; FAX (0039) 0432 922626; email: giorgio.mattassi@arpa.fvg.it

Abstract

In this paper an overview of the numerical modeling applications for marine-coastal waters, carried out at ARPA FVG, the Environmental Protection Agency of the Friuli Venezia Giulia Region, is given according with the European Directives. The aim of these modeling applications is to identify andd assess the critical factors (pressure sources) that may condition water quality from the microbiological point of view and to investigate the impact on the marine-coastal waters and on the shellfish farmings and bathing activities that are present along the coast of the Friuli Venezia Giulia, in the north-eastern part of Italy.
The finite element model SHYFEM, developed at ISMAR-CNR in Venice, has been implemented and applied to investigate the bacterial dispersion, taking into account *Escherichia coli* as a tracer. Results of modeling and data analysis are discussed in order to better understand the mechanisms that may influence water quality.

Introduction

The Water Framework Directive 2000/60/EC (WFD) establishes the quality objectives of water bodies: a good ecological status and good chemical status across European waters need to be achieved within 2015. To reach this goal the European Directive 2000/60/CE requires monitoring programs to be applied to evaluate the status of environmental quality of water bodies of European Member States.
EAA, the European Environmental Agency, developed a conceptual model, called DPSIR model, that represents a link among these elements: Drivers, Pressures, State, Impacts and Response. This conceptual model indicates the existence of driving forces (Drivers) that cause the pressures on the environment. Pressures may determine modification and/or loss of environmental quality and biodiversity, that is expressed by the State. Modifications of the State are represented by the Impacts, understanding in negative sense as effects on human health and ecosystems. The operations and measures adopted to reduce the impacts are represented by the Response. According with the DPSIR model, the use of indicators is necessary to

provide information on the environmental status of the water bodies. To achieve these aims, the WFD contemplates the classification of coastal systems first in typologies, defined on the basis of abiotic factors (including salinity, temperature, oxygen and nutrients) to describe a group of specific environments. Further the Directive 2006/7/EC on bathing waters aims to establish a new approach based on an integrated management of water quality, according with the general objective of "good ecological status" of the Directive 2000/60/EC, to be achieved with specific plans and programmes of measure.
In particular, the Directive 2006/7/EC requires an identification and assessment of causes of pollution that might affect bathing waters and impair bathers' health.
In this context modeling may be used as a technical tool with high scientific content to support with simulations the evaluation of the water quality classification and the achievement of the objectives through specific measures.
The case of the submarine wastewater pipelines discharging into the Gulf of Trieste in the Northern Adriatic sea till about 7 km from the coast, is reported as an attempt to assess and explain the microbiological pollution events that sometimes occur. The study consisted both of data collection and laboratory analysis, performed by ARPA FVG for the microbiological parameter Escherichia Coli, and numerical simulations. The application of the 3D numerical model SHYFEM, developed at ISMAR-CNR in Venice, has been realized to support the traditional monitoring methods in order to connect the information concerning the hydrodynamic circulation and the microbiological features, to evaluate possible health risks associated with recreational and coastal shellfish farming activities, located along the regional coast.
In general, the aim of these modeling applications, starting from the classification data of surface water from available monitoring data, has been to identify the external critical factors (pressure sources) that may condition the water quality.

Area of study and pressure sources
The area of study consists of the coastal-marine waters of the Friuli Venezia Giulia Region, in the north-east part of Italy, enclosing the Gulf of Trieste, in the Northern Adriatic Sea (figure 1).
The pressure sources taken into consideration in this study are surface sources and submarine sources and are listed below:

- the submarine outfalls that discharge wastewaters into the marine environment with different wastewater treatment mechanisms;
- the rivers Isonzo and Tagliamento that discharge into the northern Adriatic Sea the contribution of different sewage systems;
- the main inlets of the Marano and Grado lagoon;
- the port area of Monfalcone, affected by the contribution of different sewage systems.

The submarine outfalls belong to the wastewater treatment plants presented in table 1, in clockwise sense. Figure 2 shows the location and length of the pipelines. See Scroccaro et al., 2009 and Mattassi et al., 2009 for details on the waste water

treatments plants and their submarine pipelines. In the same picture also the monitoring points for the bathing waters and the water bodies polygons are indicated.

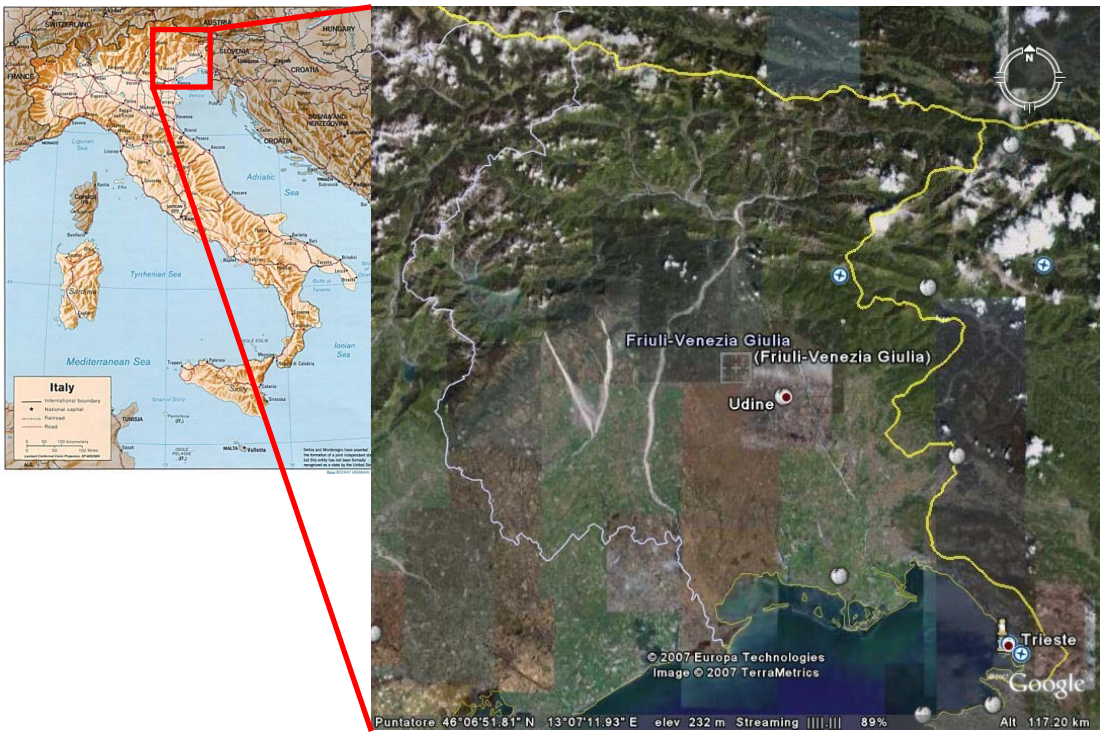


Figure 1. The area of study in the Northern part of Italy (from Google maps).

The microbiological parameters required for the bathing waters are: *Escherichia coli* and *Intestinal Enterococci*. At the moment only *Escherichia coli* has been taken into account for the modeling study.



Figure 2. Location of the submarine pipelines (lines) in the Gulf of Trieste, monitoring points for bathing waters (circular points) and subdivision of water

bodies for coastal-marine waters of Friuli Venezia Giulia (polygons).

The survival time of micro-organisms in the water environment depends on many factors, mainly on temperature and weather conditions. The survival time is measured with the T90, which is the time observed for a 90% decrease of the concentration of the bacteria or virus. The survival time for marine waters is shown in table 2 and it is expressed in hours: minimum-maximum according to depth and intensity of light and turbidity), with the value indicated in the most recent literature.

Table 1. WWTPs with submarine outfalls in Friuli Venezia Giulia region taken into account in the study (Source: ARPA FVG).

WWTP	Localization (region and town)	Distance from the coast (km)	Potentiality (Equivalent Inhabitants as BOD_5)	Disinfection system
Lignano	FVG – Udine Lignano	6	180.000	none
S.Giorgio	FVG – Udine S.Giorgio di Nogaro	6	225.000	none
Grado	FVG – Gorizia Grado	5	35.000	CH3COOOH
Staranzano	FVG – Gorizia Staranzano	8	68.000	CH3COOOH
Sistiana	FVG – Trieste Duino Sistiana	2,5	8.000	CH3COOOH + NaClO
Barcola	FVG – Trieste Barcola	0,9	12.000	none
Servola	FVG- Trieste Servola	7	250.000	none

Table 2. Value of "T90" , time for decay of 90 % of a bacterial population in sea water) depending on temperature: 20°C - (5°C) and weather.
(Source: IFREMER-M. Pommepuy, 2005).

T. 90 (hours)	SUNNY	CLOUDY
	(UV rays)	
Escherichia Coli	5 - (50)	35
Intestinal Enterococci	15 -(100)	70 - (300)

Finally, the classification and monitoring for shellfish farming activities in the Friuli Venezia Giulia Region, as defined by D.G.R. 2010, is presented in figure 3.

The data and the model

The regional environmental protection agency has the responsibility of the monitoring of water bodies and of the verification of the respect of limit values. For

the purposes of the study it was decided to consider data of the year 2007 produced by ARPA FVG in the institutional control activity (e.g. in figure 4).

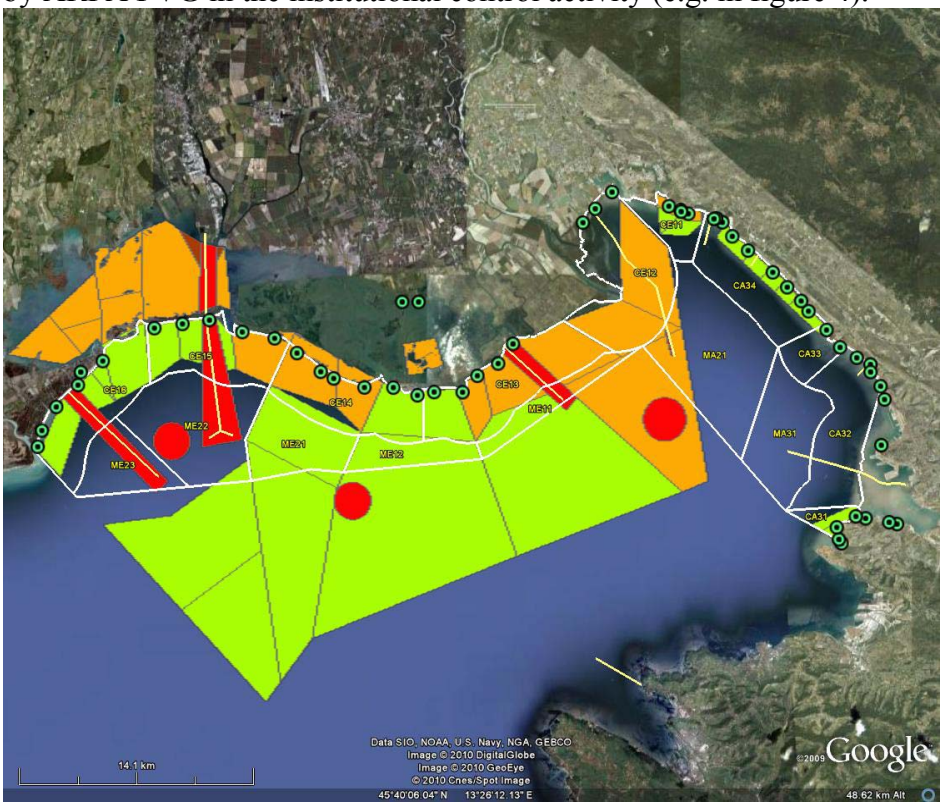


Figure 3. Map with th classification and monitoring for shellfish farming activities for coastal-marine waters in the Friuli Venezia Giulia Region.

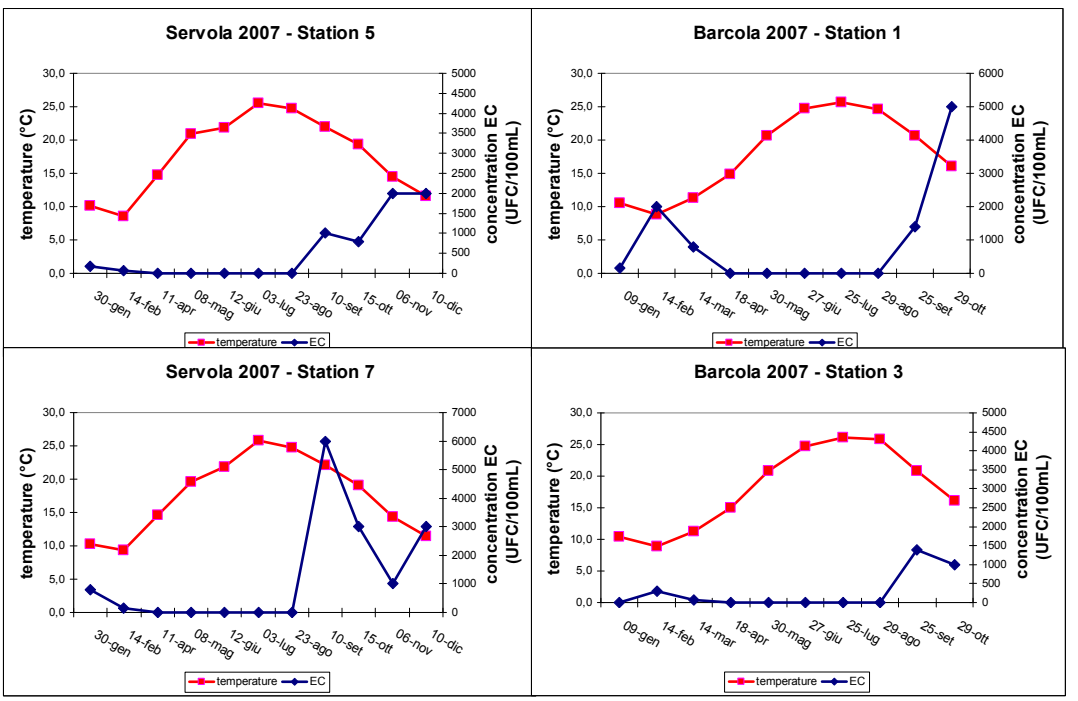


Figure 4. Temperature and concentration data collected in sampling stations of Servola and Barcola submarine outfalls (primary treatment, only).

2.1. The 3D Hydrodynamic model

The 3D SHYFEM model has been implemented to simulate the hydrodynamics in the North Adriatic Sea. The model, in its 2D versions, has been applied in many studies to the Venice Lagoon area (Umgiesser et al. 2004; Cucco & Umgiesser 2006; Umgiesser 2000). It is a primitive equation model, based on the solution of momentum and continuity shallow water equations. The complete equations, after dividing the water column in vertical layers, are:

$$\frac{\partial u_l}{\partial t} + u_l \frac{\partial u_l}{\partial x} + v_l \frac{\partial u_l}{\partial y} + w_l \frac{\partial u_l}{\partial z} - f v_l = -g \frac{\partial \zeta}{\partial x} - \frac{1}{\rho_0} \frac{\partial p_a}{\partial x} - \frac{g}{\rho_0} \frac{\partial}{\partial x} \int_{-H_l}^{\zeta} \rho' dz$$

$$+ v_t^H \left(\frac{\partial^2 u_l}{\partial x^2} + \frac{\partial^2 u_l}{\partial y^2} \right) + \frac{1}{\rho_0} (\tau_x^{l-1} - \tau_x^l)$$

$$\frac{\partial v_l}{\partial t} + u_l \frac{\partial v_l}{\partial x} + v_l \frac{\partial v_l}{\partial y} + w_l \frac{\partial v_l}{\partial z} + f u_l = -g \frac{\partial \zeta}{\partial y} - \frac{1}{\rho_0} \frac{\partial p_a}{\partial y} - \frac{g}{\rho_0} \frac{\partial}{\partial y} \int_{-H_l}^{\zeta} \rho' dz$$

$$+ v_t^H \left(\frac{\partial^2 v_l}{\partial x^2} + \frac{\partial^2 v_l}{\partial y^2} \right) + \frac{1}{\rho_0} (\tau_y^{l-1} - \tau_y^l)$$

$$\frac{\partial \zeta}{\partial t} + \frac{\partial}{\partial x}(u_l h_l) + \frac{\partial}{\partial y}(v_l h_l) = 0$$

with l the vertical layer, (u_l, v_l, w_l) horizontal velocities in (x,y,z) direction, p_a atmospheric pressure, g gravitational acceleration, f the Coriolis parameter, ζ sea level, $\rho=\rho_0+\rho'$ water density, H_l depth of the vertical layer l, h_l the layer thickness, and v_t^H, horizontal eddy viscosity.

The stress terms for each vertical interface are written as

$$\tau_x^l = v_t^V \left(\frac{\partial u}{\partial z} \right)_l \text{ and } \tau_y^l = v_t^V \left(\frac{\partial v}{\partial z} \right)_l$$

with v_t^V being the vertical eddy viscosity. Boundary conditions for the stress terms are the usual quadratic bulk formula for the wind drag and the bottom friction.

The equation for the dispersion of a general property A_l at level l (e.g.: a dissolved tracer or concentration) is:

$$\frac{\partial A_l}{\partial t} + u_l \frac{\partial A_l}{\partial x} + v_l \frac{\partial A_l}{\partial y} + w_l \frac{\partial A_l}{\partial z} = K_H \left(\frac{\partial^2 A_l}{\partial x^2} + \frac{\partial^2 A_l}{\partial y^2} \right) + K_V \frac{\partial^2 A_l}{\partial z^2} + S$$

where K_H and K_V are the horizontal and vertical diffusivities, respectively, and S represents the sources and sinks for concentration, that can be applied in any layer, also in the bottom layer.

The SHYFEM model applies a finite element Arakawa B grid for the horizontal and z-layers for the vertical discretization. The barotropic pressure gradient, the Coriolis term and the divergence terms in the continuity equation are semi-implicitly discretized, while the bottom friction and the vertical stress terms are fully implicit. The baroclinic, advective and horizontal diffusion terms are explicitly discretized. The model is therefore unconditionally stable with respect to fast gravity waves, Rossby waves, vertical diffusion and bottom friction. The boundary conditions are free slip on material boundaries. On the open boundaries (rivers) either fluxes or water levels have to be prescribed.

The horizontal diffusion coefficients are computed through a Smagorinsky type turbulence closure that takes into account the horizontal shear and the size of the elements. In the vertical a k-e turbulence closure model has been used that uses turbulent kinetic energy and dissipation rate to compute the vertical diffusivities and viscosities. The GOTM library (Umlauf and Burchard, 2005) has been included and linked into the 3D code.

2. Implementation of the hydrodynamic model

3.1. Grid construction

The modeling of the investigated area in the Northern Adriatic Sea is performed by taking into account the whole Adriatic basin, down South to the open boundary of the Strait of Otranto, in order to obtain better conditions. The spatial domain is divided in triangles varying in form and size and the computation grid contains 14388 nodes and 26410 elements (see figure 5).
The horizontal resolution ranges from about 100 meters along the regional coastline of Friuli Venezia Giulia up to 60 km in the central Adriatic Sea. The bathymetric data have been derived from the NOAA 1:250000 for the Adriatic Sea, while they have been obtained, with higher resolution, from ARPA-FVG for the Gulf of Trieste.
The model grid is constructed with an automatic mesh generator, starting from the coastline of the whole basin of the Adriatic Sea, and it is represented in figure 5. In particular, a higher grid resolution has been imposed in the zones of major interest for the research, such as the whole northern coast of the Adriatic Sea, close to the Friuli Venezia Giulia region coastline. The grid has been created ad hoc in order to position the nodes exactly on the coordinates of the submarine outfalls. For the three-dimensional application 16 levels have been chosen to divide the water column into (0-3, 3-7, 7-12, 12-17, 17-22, 22-26, etc…).

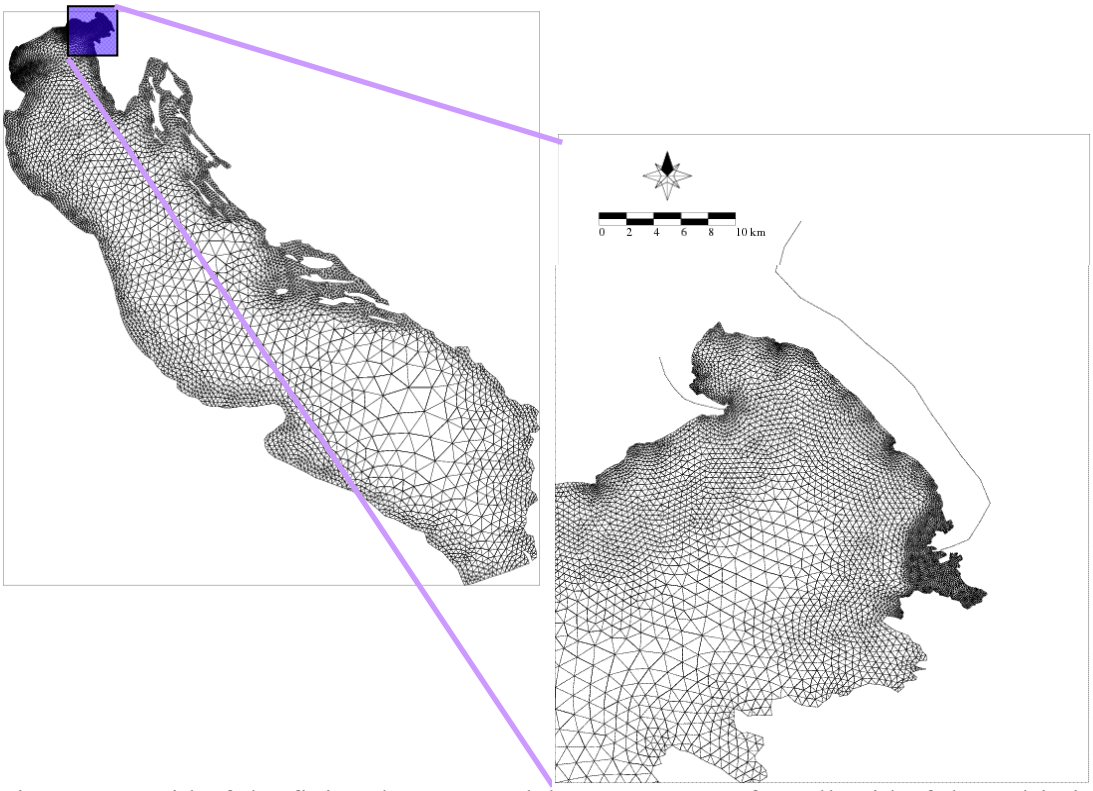


Figure 5 - Grid of the finite element model SHYFEM. Left: Full grid of the Adriatic Sea. Right: Zoom on the area of the Gulf of Trieste.

3.2. Decay of concentration

The concentration used as a tracer has an intrinsic decay rate that is simulated with a simple exponential decay. If the e-folding time for the decay of the substance τ is known, then the decay is described by the formula

$$c(t) = c_0 e^{t/\tau}$$

where t is the time step used. In case the decay rate τ_90 is known (decay of 90 % of the substance), the decay time scale τ can be computed as τ= τ_90/ln(10).

For the various inputs a different decay rate can be used, independently from each other.

3.3. Maps of influence

Influence maps have been computed as follows: for each node of the numerical grid the total concentration of all inputs is computed. If this total concentration is higher than a threshold concentration, and if the tracer with the highest concentrations has a percentage higher than 30 % of the total concentration, than the node will be counted as influenced by this tracer. In this way it is assured that only with a significant level of total tracer concentration the node is colored, and only if one tracer is much higher

than the other tracer concentrations.

3.4. Simulation setting up

The model has the capacity of simulating parameters such as flow velocities, flow orientation, temperature, salinity and concentration. One of the most important parameters to be set is the value of the bottom friction coefficient. In this study, the default value for the friction parameter of 2.5×10^{-3} is applied to the whole basin. The parameters dealing with the wind stress affect the surface of the water. For the wind drag coefficient C_D, a constant value of 2.5×10^{-3} has been used. As initial conditions, all velocities and water levels are set to zero. At the closed boundaries, the normal velocity was set to zero. The tangential velocity is a free parameter corresponding to a full slip conditions (Ferrarin & Umgiesser, 2005).

All simulations presented in this work have been carried out for 3 months during autumn 2007, using a time step of 300 seconds for the whole finite element model. A spin-up time of 30 days has been used. This time period was enough to damp out the noise introduced through the initial conditions.

Results and discussion

Many simulations have been performed taking into account different input concentration values and different survival times (T90) for the microbiological parameter *Escherichia coli* to investigate the impact of the bacterial dispersion.

Wind and pressure data have been used coming from the global atmospheric model of the European Centre for Medium Range Weather Forecast (ECMWF) of Reading, UK, available for the whole Mediterranean area with a spatial step of ¼ degrees in latitude and longitude.

At the open boundary (strait of Otranto) an astronomical tide has been prescribed, taking into account the main astronomical components, 4 semi-diurnal (period of 12 hours) M2, S2, N2 and K2 and 3 diurnal (period of 24 hours), K1, O1 and P1.

For the microbiological parameters, data collected by ARPA FVG have been used. Data provided by ARPAV, ARPA EMR and by the Regional Civil Defence of Friuli Venezia Giulia have been used for the discharges of the rivers.

Instantaneous pictures of bacterial dispersion have been produced by the output of the simulations (see figures 6, 7 and 8). Results have also been elaborated to assess the area of influence of the pressure sources (not shown).

The discharges of the Gulf of Trieste (in particular the Servola and Barcola ones) can be seen nicely, as expected, since they have no biological stage. Results show that, maybe under particular meteo-marine forcing conditions and due to high input concentration values, the submarine discharges may influence the water quality of the shellfish farming areas along the coast of Trieste. This confirms what has been observed all along the years during actual monitoring of water and shellfish quality.

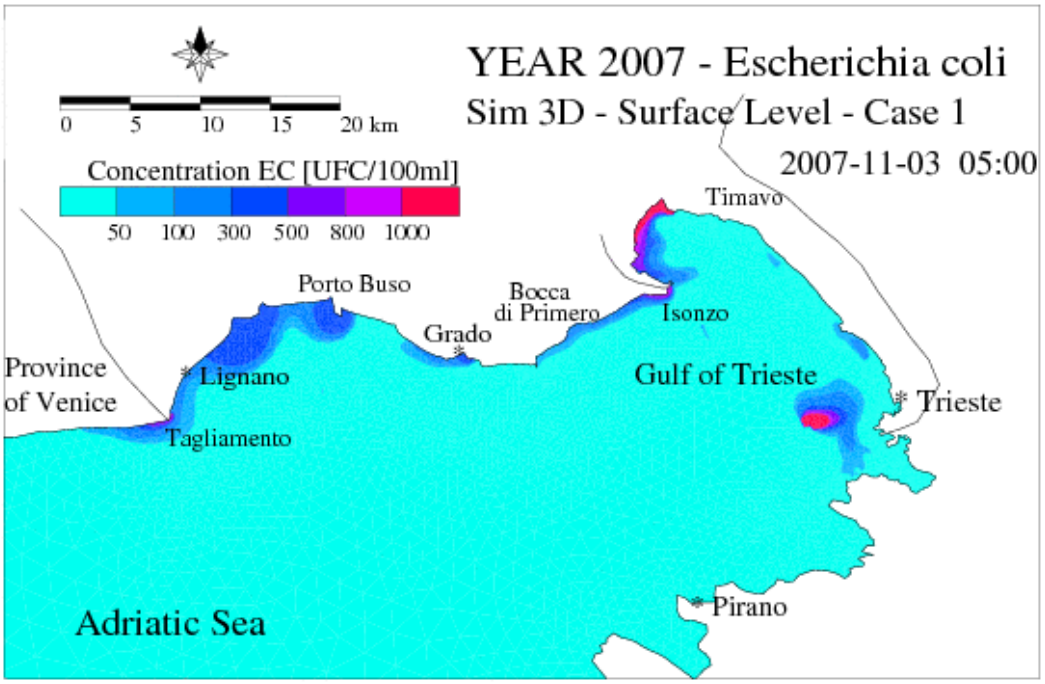


Figure 6. Instantaneous picture of bacterial dispersion from different sources during autumn time (3rd November 2007, h. 5:00). Case 1: Continuous release from all the sources taken into consideration.

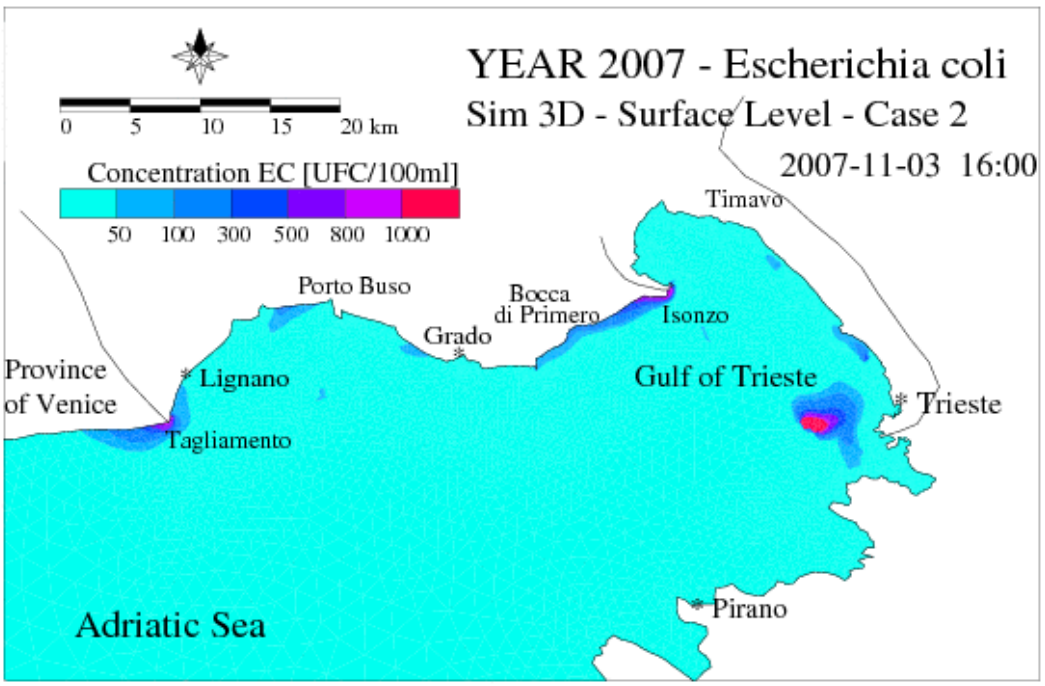


Figure 7. Instantaneous picture of bacterial dispersion from different sources during autumn time (3rd November 2007, h. 16:00). Case 2: Continuous release from the submarine pipelines and instantaneous release from rivers and inlets.

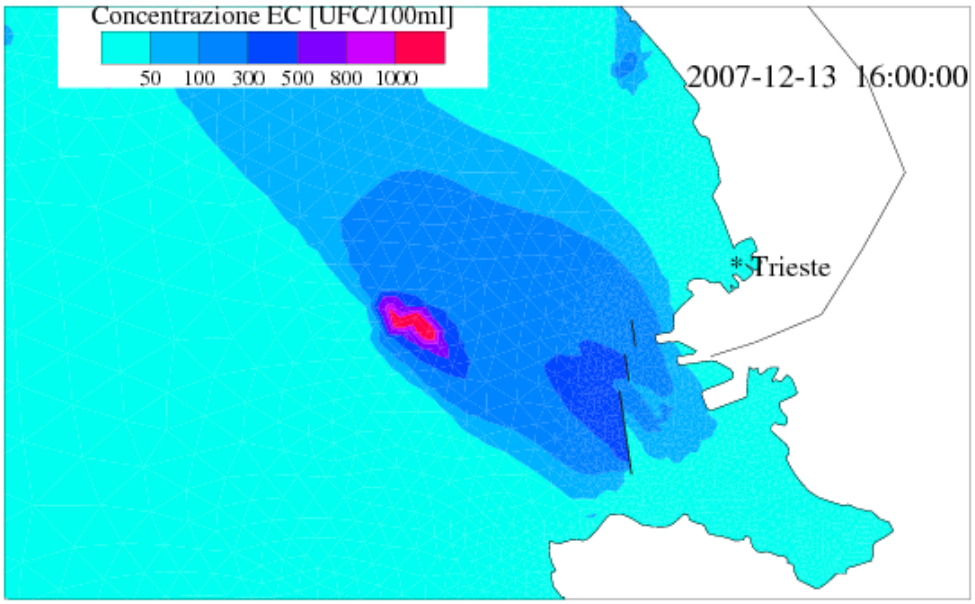


Figure 8. Zoom of modeling results on the area of the Muggia Bay, in the Gulf of Trieste. Bacterial dispersion from the submarine outfall of Servola and Barcola during autumn time (instantaneous picture of 13th December 2007, h. 16:00).

Conclusion

In this paper a brief overview of the numerical modeling applications for marine-coastal waters, carried out at ARPA FVG is given according with the European Directives. Different sources of bacterial dispersion, both surface and submarine sources, have been prescribed to assess the impact of bacterial pollution on the Friuli Venezia Giulia context, taking into account *Escherichia coli* as a tracer.

The 3D version of the finite element model SHYFEM, developed at ISMAR-CNR in Venice, has been implemented and applied. In this case, a 3D model is needed, even if it is more costly and time consuming for computer calculation, because of the complex features of the investigated area, in which stratified waters, changing currents and microbes concentration in the water column, are present. Further it is necessary to depict the results in clear explicative coloured maps for stakeholders understanding and decision making.

The SHYFEM model may represent a versatile modelling tool that may be used for describing pollutions sources and bacterial dispersion. Continuous improvements and upgrade of the 3D version are in progress to take into account the physical and ecological processes that occur in the marine ecosystems and the different pressure sources.

Acknowledgements

The authors wish to acknowledge the ARPA FVG Laboratory personnel for the analytical activities. In particular the authors wish to thank the Meteorological Observatory (OSMER) of ARPA FVG for the ECMWF data, ARPAV, ARPA EMR and the Regional Civil Defence of Friuli Venezia Giulia for the discharge data of the rivers.

References

Cucco, A.; Umgiesser, G. (2006). "Modeling the Venice Lagoon Residence Time." Ecol Modell., vol. 193(1-2), 34-51.

European Community (2006). Directive 2006/7/EC 15/02/2006, concerning the management of bathing water quality and repealing Directive 76/160/EEC, OJ of the European Communities 4/03/2006 n. L 64.

European Community (2000). Directive 2000/60/EC 23/10/2000, establishing a framework for Community action in the field of water policy, OJ of the European Communities 22/12/2000 n. L 327.

Ferrarin, C.; Umgiesser, G. (2005). "Hydrodynamic modelling of a coastal lagoon: The Cabras Lagoon in Sardinia, Italy." Ecol Modell., vol. 188, 340-357.

Mattassi G., Scroccaro I., Umgiesser G., Colugnati L., Ostoich M., Vazzoler M., Cuomo M. (2009). "Dispersion modeling of submarine wastewater discharges in the Northern Adriatic sea along Friuli Venezia-Giulia and Veneto regions' coasts." *Proceedings of MWWD 2008 - 5th International Conference on Marine Waste Water Disposal and Marine Environment*. Dubrovnik, 27-31 October 2008.

Scroccaro I., Colugnati L., De Pascalis F., Umgiesser G., Mattassi G. (2009). "3D Modeling of submarine discharges in the Gulf of Trieste." *Proceedings of MWWD 2008 - 5th International Conference on Marine Waste Water Disposal and Marine Environment.* Dubrovnik, 27-31 October 2008.

Scroccaro I., Ostoich M., Umgiesser G., De Pascalis F., Colugnati L., Mattassi G., Vazzoler M., Cuomo M. (2010). "Submarine wastewater discharges: dispersion modeling in the Northern Adriatic sea." *Environmental Science and Pollution Research*, 17:844-855.

Umgiesser G., and Bergamasco A. (1995). "Outline of a Primitive Equations Finite Element Model." *Rapporto e Studi, vol. XII, Venice, Italy: Istituto Veneto of Scienze, Lettere ed Arti*, 291-320 pp..

Umgiesser, G. Modeling residual currents in the Venice Lagoon.In: Yanagi, T. (Ed.), Interactions between Estuaries,Coastal Seas and Shelf Seas Tokio: Terra Scientific Publishing Company (TERRAPUB), JP. 2000, 107-124

Umgiesser G., Melaku Canu D., Cucco A., Solidoro C. (2004). "A finite element model for the Venice Lagoon. Development, set up, calibration and validation." *Journal of Marine Systems*, 51, 123-145.

Umgiesser G., Mattassi G., Scroccaro I., Ostoich M., Vazzoler M. (2008). "The use of numerical modeling in Italian watershed management." *I.E. Gönenç et al. (eds.), Sustainable Use and Development of Watersheds*, 243–261.© Springer Science + Business Media B.V.

Masonville Dredged Material Containment Facility: Mitigation Design Including Shore Protection, Reef Creation and Wetlands Restoration

Peter W. Kotulak, P.E.[1] and Kristen Piggott, P.E.[2]

[1] Moffatt & Nichol, 2700 Lighthouse Point East, Suite 501, Baltimore, MD 21224, PH (410) 563-7300; FAX (410) 563-4330; email: pkotulak@moffattnichol.com

[2] Moffatt & Nichol, 2700 Lighthouse Point East, Suite 501, Baltimore, MD 21224, PH (410) 563-7300; FAX (410) 563-4330; email: kpiggott@moffattnichol.com

ABSTRACT

As a component of the Masonville Dredged Material Containment Facility (DMCF) project, the Maryland Port Administration (MPA) was required to develop a compensatory mitigation package to offset impacts associated with filling approximately 53 hectares (130 acres) of open water in the Patapsco River, which is a major tributary to the Chesapeake Bay. The mitigation is a comprehensive package of inwater and upland projects totaling over $20 million. The majority of mitigation is located adjacent to the DMCF in the 29 hectares (71 acres) of open water and 22 hectares (54 acres) of uplands that comprise Masonville Cove. The projects serve to enhance existing resources and provide improved habitat and increased wildlife use of the area, in addition to remediating contamination from historical industrial usage and dumping. The project will also provide opportunities for community-based environmental education to promote stewardship of the Bay waters for the local citizens. The mitigation projects discussed in this paper include shoreline stabilization and erosion control, reef creation and substrate improvement, and creation and enhancement of tidal and non-tidal wetlands. Design development concepts for these projects are presented. Following construction of the mitigation projects within the Cove, the area will be placed into a conservation easement and opened as an urban wildlife conservation area, environmental education center and natural park. The size and location of the Cove within Baltimore City make it a unique site for wildlife habitat and opportunity for the public to connect with the natural environment. The area is also a designated habitat protection area in the City and is in the Critical Area Resource Conservation Area.

INTRODUCTION

The MPA began developing the mitigation plan for the DMCF by working with the surrounding community to identify potential projects in the immediate vicinity of Masonville. Additional input and comments were obtained from the Bay Enhancement Working Group (BEWG), the Joint Evaluation Committee (JE), and local, state, and federal agencies. The BEWG and JE are composed of scientists and policy makers who are knowledgeable about the Chesapeake Bay and tributaries. These suggestions were incorporated into the "Tier I" mitigation plan which was

developed to include sufficient environmental improvements to compensate for the impacts associated with the construction of the DMCF. The Habitat Conditions Analysis used to demonstrate the sufficiency of the mitigation package is described in Boraczek et al. (2008). A Tier II list of projects was developed as alternates should one of the original projects prove infeasible or unsuccessful. The Tier I plan focuses on enhancement of the Masonville Cove, which is adjacent to the recently constructed DMCF (Figure 1). This paper will present some of the major components of the projects in the Cove, including shoreline stabilization and erosion control, reef creation and substrate improvement, and creation and enhancement of tidal and non-tidal wetlands.



Figure 1. Masonville DMCF project site.

Masonville Cove is located in Baltimore City along the southern shore of the Patapsco River in Baltimore Harbor. The Cove is comprised of 29 hectares (71 acres) of open water and 22 hectares (54 acres) of uplands. The area was historically mined for sand and gravel and was the site of unauthorized waste disposal and filling for over 100 years (USACE 2007). The years of waste disposal within the upland and in-water areas of the Cove has resulted in extensive debris throughout the site and areas of metals and semi-volatile organic compound (SVOC) contamination. Debris including tires, ceramic insulators, railroad ties, and trash is present in the shallow

water and shoreline within the Cove. The substrate consists primarily of fine grained material (silts and clays) with isolated sand pockets.

During feasibility studies, it was observed that the water within Masonville Cove provides refuge and forage opportunities for a variety of fish species including juvenile anadromous species, such as white perch (*Morone americana*), striped bass (*Morone saxatilus*), yellow perch (*Perca flavescens*), and river herring (*Alosa pseudoharengus* and *Alosa aestivalis*), and forage species such as minnows, shiners, and silversides (USACE 2007). The Cove also provides foraging and resting opportunities for many bird species. Waterfowl are common during the winter months and herons and egrets are common in warmer months.

The mitigation projects within the Cove were selected to enhance the existing resources and provide improved habitat and increased wildlife use of the area. Following construction of the mitigation projects within the Cove, the area will be placed into a conservation easement and opened as an urban wildlife conservation area, environmental education center and park. The size and location of the Cove within Baltimore City make it a unique site for wildlife habitat and opportunity for the public to connect with the natural environment. The area is also a designated habitat protection area in the City and is in the Critical Area Resource Conservation Area.

Table 1 contains components of the mitigation plan as presented in the Environmental Impact Statement (USACE 2007). This plan is subject to change during the life of the project should some of the projects be unsuccessful, fall short of the goal, or if the project is removed from consideration for other reasons (e.g. changed site conditions).

SHORELINE STABILIZATION AND EROSION CONTROL

Shoreline stabilization is part of a series of improvements to Masonville Cove and the surrounding land to serve as mitigation for the construction of the Masonville DMCF. Much of the cove shoreline is scarped and eroding. Erosion is of particular concern because the cove uplands were used as a disposal site for various wastes, resulting in widespread soil contamination. Without some type of stabilization, contaminated soils will continue to enter the cove and potentially impact vegetation, fish, and wildlife of Masonville Cove and the Patapsco River.

The Masonville uplands have been divided into three phases; each phase will require soil encapsulation of all contaminated areas. Shoreline stabilization will consist of creating a stable slope to prevent erosion and release of contaminants. Once a stable grade has been established, the slope will receive a 0.6 m (2-ft) layer of soil to serve as a cap. Both riprap and sand beaches will be employed for the stabilization. Figure 2 shows the limits of soil encapsulation and the adjacent shorelines to be stabilized, an area of about 10.5 hectares (26 acres). Timbers, concrete, scrap metal, and other debris have been removed from the uplands yet some waste materials still remain on the shorelines. Common materials which will require removal prior to stabilization

include scrap metal, steel rebar protruding from concrete rubble, bricks, and other general trash. Concrete without rebar may be incorporated into the riprap shoreline protection or used in the reef creation project in the Cove.

Table 1. Masonville mitigation plan.

Aquatic Projects		
Wetland Enhancement	0.8 hectares	(2 acres)
Wetland Creation	1.3 hectares	(3.1 acres)
Non-Tidal Wetland	4 hectares	(10 acres)
Reef and Fish Habitat (subtotal)	39 hectares	(96 acres)
Reef and Fish Habitat	30 hectares	(74 acres)
SWH Substrate Improvement	9 hectares	(22 acres)
Fringe Wetland Creation (along dike)	0.8 hectares	(2 acres)
Eel Passages (3 Dams)	3 projects	
Shad and Herring Restoration	1 project	
3 Trash Interceptors	3 projects	
Biddison Run (Reach O)	1 project	
Biddison Run (Reach P)	1 project	
2 Trash Interceptors	2 projects	
Western Run (6 Reaches)	1 project	
Aquatic Related Projects		
WQ Monitoring in Cove	1 project	
Landside and In-Water Cleanup	10 hectares	(25 acres)
Non-Aquatic Projects		
Terrestrial Habitat Enhancement	4 hectares	(10 acres)
Education Center/Trails (Allocation)	1 project	project
Education / Research $500,000 Allocation	1 project	project
Conservation Easement	10 hectares	(25 acres)

Phase 1 is the largest phase at 15.5 hectare (38.5 acres) and contains 11.3 hectares (28 acres) of area that will not require encapsulation, leaving 4.2 hectares (10.5 acres) for capping. Shorelines will be stabilized in areas which require remediation or removal of physical hazards. A fixed pier and a floating dock are proposed near the middle of the shoreline (see Figure 2). The shoreline in the pier area will be stabilized with riprap. Shoreline west of the pier is currently at a stable slope but will require encapsulation. Approximately 114 m (375 ft) of shoreline east of the pier is scarped and will need stabilization and encapsulation. Additionally, over 70 m (230 ft) of shoreline adjacent to the capping area in northwest Phase 1 will require stabilization and encapsulation. Phase 1 contains two large box culverts which transport water from a tributary with a watershed of approximately 310 hectares (1.2 sq mi). Water

flows through a short stream before entering the Masonville Cove. This stream can experience relatively high flow rates during storms, so the banks will need to be stabilized through several approaches involving excavation and riprap protection. Stabilization methods used for the stream banks are unique to this area and will not be applied to cove shorelines.

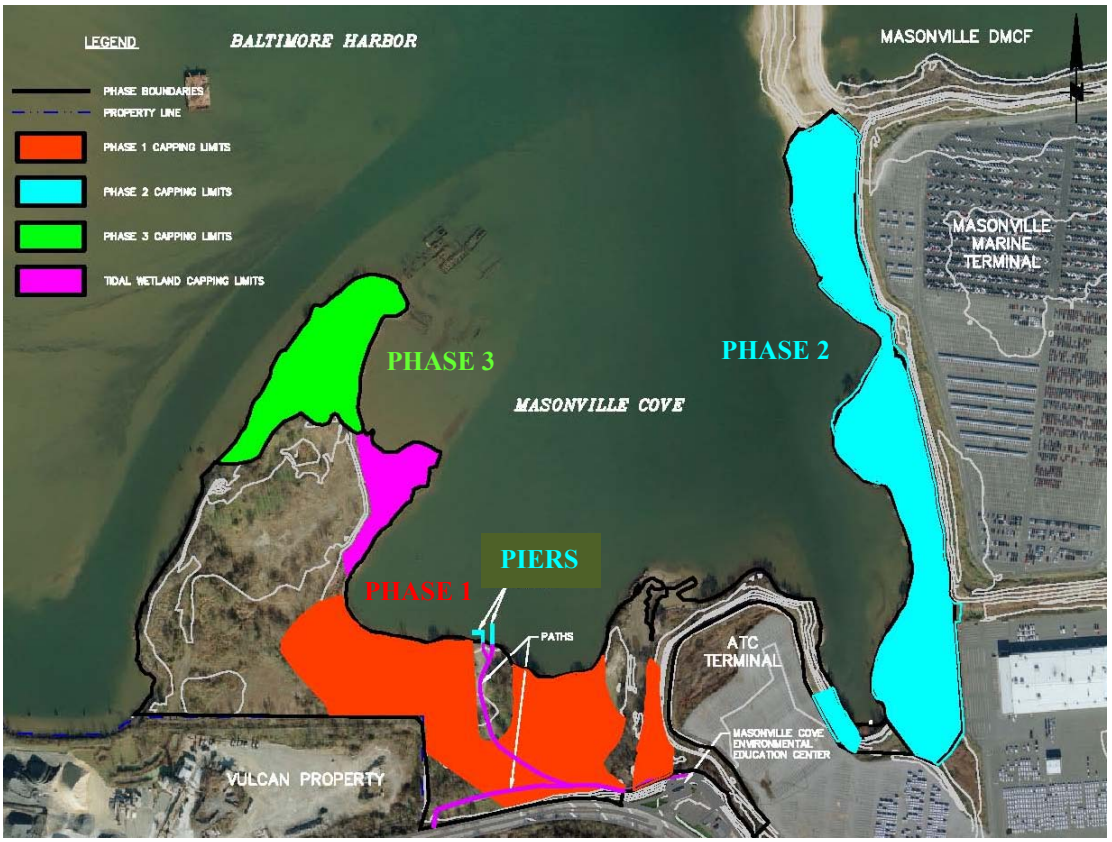


Figure 2. Masonville Cove Soil Cap and Shoreline Stabilization Areas.

Phase 2 comprises the entire eastern shoreline of Masonville Cove, all of which will require remediation. This includes approximately 5 hectares (12 acres) of uplands and over 914 m (3,000 ft) of shoreline. Phase 2 uplands are at the highest elevations of the site and most of the shoreline is scarped. Therefore, greater quantities of excavation or fill will be necessary to achieve stable slopes. Additionally, the cove is steep along the northern part of the shoreline, so any approaches using fill will require larger volumes and extend further into the cove in this area. Two tidal wetlands are proposed in Phase 2, which are designed to tie into the base of the stabilized shoreline. Alternatively, a stabilization method creating an entire "living shoreline" of wetlands could be implemented.

Phase 3 is the smallest phase, comprised of slightly more than 1.4 hectares (3.5 acres), yet has almost 400 m (1,300 ft) of shoreline. Most of Phase 3 was used as a dump and the entire site requires encapsulation. Currently, approximately 107 m (350 ft) of the shoreline has stable slopes, however, the topography of Phase 3 is

undulating and will likely require grading prior to cap installation. Grading will alter the stable slopes at lower elevations, so the entire shoreline is planned for stabilization as a shoreline cap is required even where it is stable. The western shore of Phase 3 is scarped and eroding, which is of particular concern due to high concentrations of contaminants which may be entering the Patapsco River.

In total, over 1,700 m (5,500 ft) of shoreline require stabilization at the Masonville Cove site. Stabilization will be achieved through establishing a suitable slope and using both riprap and a stable beach for protection from wave action. Varying methods will be used to prevent further shoreline erosion and facilitate the encapsulation of contaminated soils. Some methods minimize fill in open water by excavating to create a stable slope; others fill into the cove to stabilize the slopes thereby eliminating potential transport concerns, exposure risks, and offsite disposal costs that may be encountered during excavation. The methods include both traditional revetments and a "living shoreline" with both excavation and fill approaches.

Revetment with Excavation

One method for stabilization will be a traditional revetment constructed by cutting into the existing grade, installing the soil cap, and armoring with riprap. The cut will begin at the base of the scarp and continue through the existing grade at a 3:1 slope. All suitable cut material will be relocated upland and graded. Any unsuitable material, such as large timbers, concrete, or metal will be removed and disposed. Geotextile fabric will be installed over all impacted areas and a 0.6 m (2 ft) layer of soil will be placed over the geotextile. The 0.6 m (2 ft) soil cap layer will continue down the 3:1 slope to mean high water (elevation +0.4 m [1.36 ft]). The cap will then transition down 0.2 m (7 in) in depth at mean low water (elevation +0.07 m [0.22 ft]) to tie into the substrate improvement layer in Masonville Cove. The slope will be armored with a 1 m (3 ft) layer of Class II riprap from the base of the slope up to elevation +2.1 m (7 ft). Impacted areas above this elevation will be planted to stabilize the slope.

Revetment with Fill

Another method for stabilization will be placing fill material into the cove, and protecting the fill with armor stone. All impacted areas will be covered with a geotextile fabric and approved fill will tie into the soil cap at the top of the scarp and extend to the cove surface at a 3:1 slope. The face of the 3:1 slope will be armored with a 1 m (3 ft) layer of Class II riprap from the base of the slope up to elevation +2.1 m (7 ft). Unarmored areas of the slope will be planted. Costs associated with this option are higher due to the fill material that will be required. However, this method is more protective of health and safety or transport concerns because no excavation or handling of contaminated material is required. All contaminated soils will remain in place and not be disturbed, however, a large volume of fill material will be placed in the cove, filling or impacting 0.8 hectares (2 acres) of shallow water.

Living Shoreline with Fill

A third option for stabilization will be to create a marsh along the shoreline of Masonville Cove based on Maryland Department of the Environment (MDE) guidelines. The existing shoreline will be either excavated or filled to tie into the living shoreline. Impacted areas will be covered with a geotextile fabric. Fill material will tie into the soil cap at the top of the scarp and extend to elevation +1.2 m (4.0 ft) at a 3:1 slope. The slope will then decrease to a 10:1 slope to elevation +0.0 (MLLW) where it will meet a riprap sill. The sill will be comprised of Class II riprap with 1.5:1 side slopes. The crest of the sill will be 1 m (3 ft) wide at elevation +0.8 m (2.5 ft), approximately 0.3 m (1 ft) above mean high water. Fill material will be appropriate for wetlands and wetland plants will be planted throughout the entire fill area.

The Living Shoreline has the benefit of creating tidal wetlands and will not only stabilize the cove shoreline, but also provide habitat for many plant and animal species and improve water quality in the cove. Similar to the revetment with fill, this option does not present exposure and transport concerns because all contaminated material will remain in place and not be disturbed. However, this method would have the largest impact on shallow water habitat and require the most fill to be added to the cove. Additional sediment controls may be required to limit the release of fill into the cove during construction.

REEF CREATION AND SUBSTRATE IMPROVEMENT

The substrate within the Cove consists primarily of fine grained material (silts and clays) with isolated sand pockets. The Outer Cove area has a marginal-to-poor benthic condition and low-to-average fish utilization for the Baltimore Harbor. The Inner Cove area contains some areas that are severely degraded. Seining studies indicated that fish utilization in the Inner Cove is consistent with other areas of the Baltimore Harbor. White perch and young striped bass dominated the open water collections in the proposed reef area outside the Cove. The substrate consists primarily of fine grain material.

Submerged aquatic vegetation (SAV) is sparse throughout Baltimore Harbor. Environmental studies performed in the summer of 2003 identified a very small patch of SAV in the southern part of Masonville Cove; the species was identified as the non-native Eurasian watermilfoil (*Myriophyllum spicatum*). The SAV patch had expanded significantly by the summer of 2004, comprising approximately half an acre of moderately dense growth. The June 2006 survey observed two species of SAV, one native [horned pondweed (*Zannichellia palustris*) and one non-native [Eurasian watermilfoil (*Myriophyllum spicatum*)]. Horned pondweed was observed at 18 of the 109 locations surveyed within the Cove and Eurasian watermilfoil was found at two of the locations. No SAV was observed in Masonville Cove during the August 2006 survey. It is hoped that reef creation and substrate improvement may serve to provide conditions where SAV could re-establish in the Cove.

Prior to reef creation, debris removal will take place and improvement of substrate will occur through spreading and creating underwater mounds of sand and gravel and placement of reef balls, rock piles and concrete rubble. The sand and gravel used to create the reef structures will come from an upland source approved for in-water placement. Additional shallow water habitat will be created in the Outer Cove along the eastern shoreline fringe marsh by placing sand from the MLLW water line down to the Cove bottom at a 15:1 slope. Figure 3 shows the plan of the reef creation and substrate improvement.

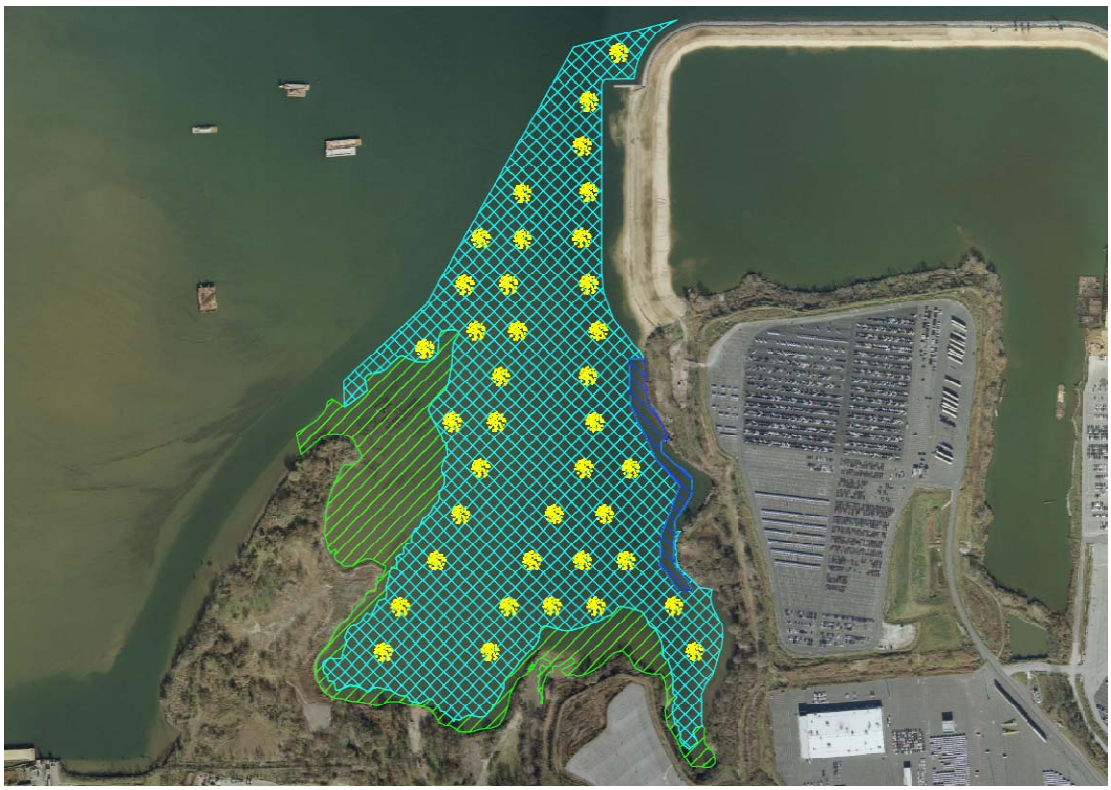


Figure 3. Masonville Cove reef creation and substrate improvement area.

This project will improve substrate conditions, in-stream habitat, create shallow waterhabitat (SWH) and provide vertical structure. Granular substrate material will improve the benthic conditions, which will lead to higher densities of benthic organisms and/or greater diversity of benthic species. An improved benthic community combined with substrate enhancements will improve fish foraging opportunities, and benefit many of the fish species known to use Masonville Cove. Increase of in-stream three-dimensional structure will provide additional habitat for epibenthic colonization, cover for crabs, juvenile and small fish, and foraging sites for larger fish species. Many of the fish species known to use the cover are species that will benefit from the improved in-stream refugia. The hard vertical structure will provide substrate for encrusting bivalves such as platform mussels, which are known to occur within the cove, or oysters, which are found elsewhere in the Harbor. Once bivalve colonies establish themselves in the area, their filter feeding is expected to

improve water clarity. The proposed shallow water substrate improvement is located in and adjacent to Masonville Cove in the Patapsco River. The area of depth less than two meters is considered SWH. Approximately 11 hectares (27 acres) of area within the Cove or adjacent to the DMCF is of this suitable depth, and the plan is to improve approximately 8.9 hectares (22 acres) of the available area. In addition to the 8.9 hectares (22 acres) of improvement, SWH will be created over 0.3 hectares (0.8 acres) within the Cove.

TIDAL WETLANDS

Tidal wetland creation and enhancement projects are located along the shore on the east and west sides of Masonville Cove (Figure 4). The western tidal wetland consists of both creation and enhancement. The wetland area included in the enhancement project on the west side of the Cove is dominated by *Phragmites australis*.

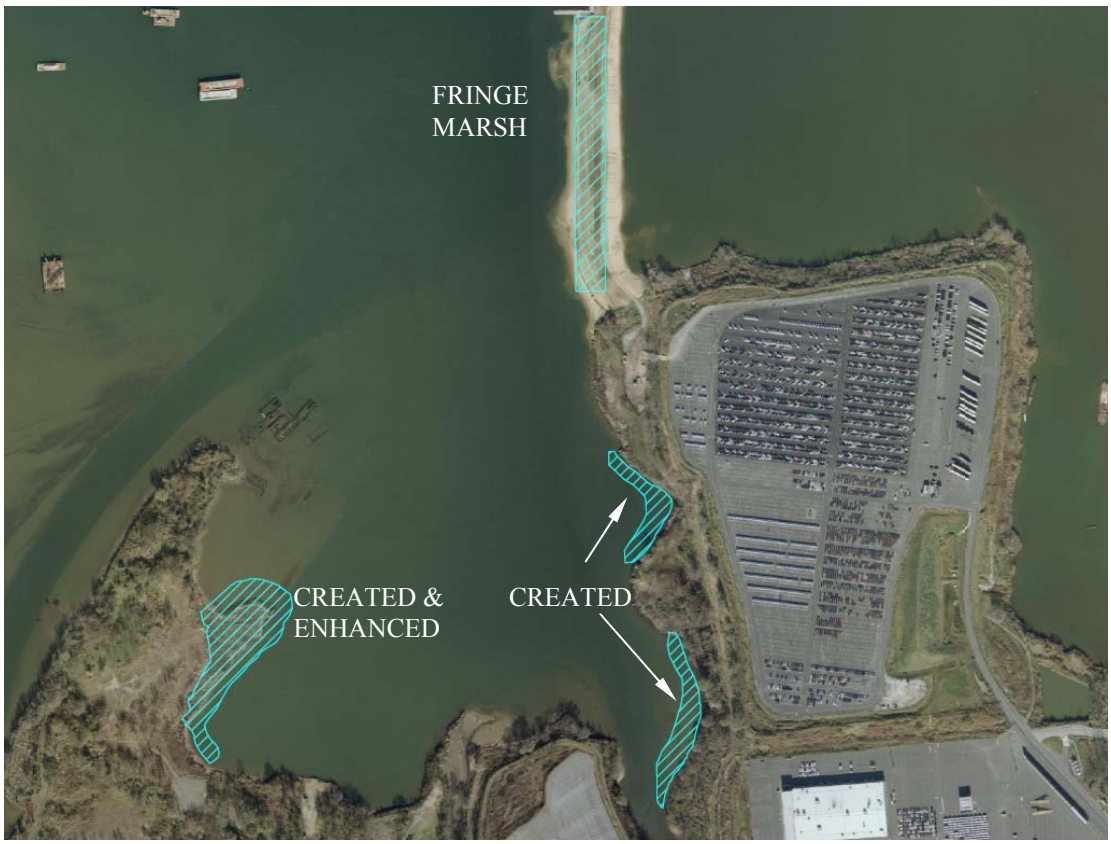


Figure 4. Masonville tidal wetlands project planned locations.

The western tidal wetland totals 1.4 hectares (3.5 acres) and consists of 0.8 hectare (2 acres) of enhancement and 0.6 hectare (1.5 acres) of creation. The 0.8 hectare (2-acre) enhancement portion includes excavation of soil down to -0.6 m (-2 ft) mean lower low water (MLLW) to remove the root mat of the *Phragmites*, followed by placement of sand to appropriate elevations [+0.3 m to +0.6 m (+1 to +2 ft) MLLW], construction of channels and inlets for hydrodynamic function, and the planting of

several different species of native vegetation. The 0.6 hectare (1.5-acre) creation portion of the western tidal wetland will include placement of sand to appropriate elevation [+0.3 m to +0.6 m (+1 to +2 ft) MLLW], construction of channels and inlets for hydrodynamic function, and planting of native vegetation. The 1.4 hectares (3.5 acres) of sand placement will be constructed as one project. The 0.6 hectare (1.6-acre) eastern creation project will include placement of sand to the appropriate elevation [+0.3 m to +0.6 m (+1 to +2 ft) MLLW], construction of channels and inlets for hydrodynamic function, and planting of native vegetation.

The western dike of the DMCF is exposed to smaller waves and coastal engineering design analysis indicated that this dike could function without armor stone protection. The dike was designed to function as a fringe marsh with a flat beach slope to the bottom. This feature will improve habitat through placement of sand material to create a fringe marsh with a 6 m (20 ft) wide berm at elevation +0.3 m (+1 ft) MLLW and a slope into the water at 15:1 until elevation -0.6 m (–2 ft) MLLW. The berm will be planted with *Spartina patens*, the slope will be planted with *Spartina alterniflora* where appropriate, and the DMCF dike slope above the berm will be planted with saltbush community vegetation. The fringe marsh will have a length of about 375 m (1,230 ft) along the DMCF dike (see Figure 2).

The tidal wetlands projects will increase the acreage of wetland habitat in the area, as well as improve conditions of the existing *Phragmites*-dominated wetland through the diversification of vegetation and improved tidal flushing. There will be an increase in fish forage and refuge opportunities along the south shore of the Patapsco River, which is known to be an important anadromous fish nursery area within the River. The projects will also enhance the Cove habitat by improving the shore conditions and providing better habitat for SAV expansion. They will also provide wading bird, shorebird and waterfowl foraging opportunities. Shorebird habitat, in particular, is currently lacking in Baltimore Harbor.

NON-TIDAL WETLANDS

The non-tidal wetlands were originally scoped as a creation project of 4 hectares (10 acres) that would use groundwater to achieve appropriate hydrologic conditions. After more detailed design analysis and chemical characterization of site soils and groundwater, the project was sub-divided into two separate areas for creation of wetlands having areas of 1.0 hectare (2.4 acres) and 1.1 hectares (2.7 acres), and one restoration wetland having an area of 0.2 hectares (0.5 acres), see Figure 5. The three creation wetlands will use surface water to achieve appropriate hydrological conditions. The wetlands will be constructed by excavating existing soil material to achieve appropriate grades, installing water level maintenance structures, and planting native non-tidal wetland vegetation. The species used for the wetlands planting will be consistent with those recommended by U.S. Fish and Wildlife Service for wet and moist areas of the Maryland Coastal Plain, which is the physiographic province including the Cove. Plant species that have been successful in similar wetland creation projects include: switchgrass (*Panicum virgatum*),

gamagrass (*Tripsacum dactyloides*), rose mallow (*Hibiscus moscheutos*) and rush species. Plants will be selected to be consistent with the other terrestrial habitat improvements proposed for the Cove area to minimize the potential for invasive species and to accommodate an ecosystem-level restoration of the floodplain.

Masonville Cove lies in the upper reach of the Patapsco River within the floodplain of the river. There is currently little wildlife use of this part of the site. Creation of non-tidal wetlands will enhance the existing area through diversification of vegetation and floodplain habitat. The wetlands will provide refuge and forage opportunities for freshwater fish species that are known to occur in the area, such as shiner and sunfish species. Non-tidal wetlands will also provide additional forage areas for wading and shorebirds and nesting opportunities for floodplain and wetland nesting waterfowl species. These functions are an improvement over the functions of most of the open water habitat within the proposed DMCF footprint which is too deep for wading or shorebird utilization, provides provide habitat for fish species, and provides no nesting habitat. Creation of a freshwater wetland will have the additional benefit of providing a freshwater (drinking) source for birds and terrestrial wildlife in the area.



Figure 5. Masonville non-tidal wetlands project locations.

CONCLUSIONS

As a component of the Masonville DMCF project, the MPA was required to construct several environmental mitigation projects to offset impacts to 53 hectares (130 acres) of open water and 0.4 hectare (1 acre) of vegetated wetlands in the Chesapeake Bay watershed. The mitigation is a comprehensive package of in-water and upland projects. Most of the mitigation projects are located adjacent to the DMCF in the 29

hectares (71 acres) of open water and 22 hectares (54 acres) of uplands that comprise Masonville Cove. The projects serve to enhance existing habitat and remediate contamination from historical dumping, as well as provide opportunities for community-based environmental education to promote stewardship of the Bay waters for the local citizens. The mitigation projects include the creation and enhancement of tidal and non-tidal wetlands, reef creation and substrate improvement, upland remediation, terrestrial habitat enhancement, and construction of an environmental education center and trails. Implementation of the mitigation package required integration of the remedial activities with the habitat enhancements and coordination with stakeholders and community members. Following construction of the mitigation projects within the Cove, the area will be placed into a conservation easement and opened as an urban wildlife conservation area, environmental education center, and park. The size and location of the Cove within Baltimore City make it a unique site for wildlife habitat and opportunity for the public to connect with the natural environment.

REFERENCES

Boraczek, J. A., K. E. McCormick, and N.K. Brown. (2008). "Habitat Conditions Analysis to Justify Wetlands Mitigation." Conference on Coastal and Estuarine Habitat Restoration, Providence, RI.

U.S. Army Corps of Engineers (USACE) (2007). Final Environmental Impact Statement for the Proposed Masonville Dredged Material Containment Facility.

Influence of small rivers runoff on the hydrochemical structure of coastal waters of the north-eastern Black Sea.

A.V.Kostyleva[1], O.I.Podymov[2], P.N.Makkaveev[3] and A.A.Polukhin[4]

[1] Laboratory of Marine Chemistry, Southern Branch of P.P.Shirshov Institute of Oceanology, RAS, P.O. Box 353467, Prostornaya 1g, Gelendzhik, Russia; PH (8918) 3360155; FAX (886141) 28089; email: ventis-ire@yandex.ru

[2] Laboratory of Informatics and Applied Hydrophysics, Southern Branch of P.P.Shirshov Institute of Oceanology, RAS, P.O. Box 353467, Prostornaya 1g, Gelendzhik, Russia; PH (8928) 2827237; FAX (886141) 28089; email: huravela@yahoo.com

[3] Laboratory of Biogeochemistry, P.P.Shirshov Institute of Oceanology, RAS, P.O.Box 117851 Nakhimovskiy prospect 36, Moscow; PH (8499) 1247742; FAX (8499) 1245983; email: makkaveev55@mail.ru

[4] Laboratory of Biogeochemistry, P.P.Shirshov Institute of Oceanology, RAS, P.O.Box 117851 Nakhimovskiy prospect 36, Moscow; PH (8499) 1246149; FAX (8499) 1245983; email: desandr@rambler.ru

ABSTRACT.
River runoff is the main source of nutrients and man-made pollutants that affects functioning of biological communities. About a thousand small and medium rivers flow into the Black Sea, and while their contribution in total sea balance is significant, there are no systematic observations on that matter. This work presents the studies carried out in 2006-2010 in coastal area of the north-eastern Black Sea. Attention is focused on studies in 2009 near the Greater Sochi region, since two major local rivers, Kudepsta and Mzymta, significantly differ in composition, which allows tracing the inflow of each individual river and estimating their fractional contribution to formation of surface water structure. Influence of river runoff on hydrochemical balance of nearshore water is demonstrated, with estimations of amount of dissolved carbon, alkalinity, silicate, dissolved oxygen and pH. Development of the river plume is traced, along with its reaction on wind direction and shelf circulations.

Introduction.

Continental inflow brings significant amount of fresh water, buoyancy and heat into the ocean. It is also a main source of suspended and dissolved terrigenous substances, nutrients and - very often - products of man-made pollution. Role of the continental inflow for certain ocean shelf areas, as well as for inland and marginal seas, may be up to ten times higher than for ocean in general. For example, annual river inflow for the Black Sea (338 km^3) exceed atmospheric precipitation (238 km^3) and is comparable to the amount of evaporation (396 km^3) (Hydrometeorology and Hydrochemistry of seas of USSR, 1991). Waters of continental origin are also considered responsible for strong density stratification in the Black Sea.

Specific river-sea contact zone forms in nearshore areas that neighbor river mouths. Until recently, major attention was paid to the large rivers and the processes taking place in their contact zones. Meantime, small and average watercourses can also play a significant role in formation of hydrochemical regime and transfer of matter in coastal areas. The goal of this work is to study influence of small and medium rivers on nearshore areas of north-eastern part of the Black Sea.

Subject of the study.

When continental waters enter the sea, they form mesoscale structures near river mouth with decreased salinity, temperature different from that of the environment, increased turbidity, large amount of suspended and dissolved organic matter. Such structures are usually called plumes. Spatial scales of plumes from the large rivers can reach hundreds of kilometers; their boundary with surrounding sea waters, however, remains sharp (about several centimeters). Plumes are characterized with a decreased water density, and thus are always confined to the surface. Thickness of that upper layer depends on strength of inflow and intensity of mixing. Observations, especially from satellites, confirm that river plumes are characterized with a vast variety of morphological forms and types of dynamic behavior. The plumes have their own inertia; they interact with bathymetry and vertical formations on shelf and are carried by wind and nearshore background circulation. Only after all that the plumes mix with the surrounding waters and convey terrigenous impact to the sea. Therefore key to understanding distribution mechanisms of coastal inflow lies exactly in plume dynamics. Meanwhile, regularities of plume behavior for small and large rivers in different conditions are studied insufficiently.

As an inland basin, the Black Sea is particularly susceptible to the influence of continental freshwater inflow. Total amount of rivers flowing into the sea is about 1000, but only 10 of them are considered major (i.e. with drainage basin larger than 10000 km^2). Most authors estimate average annual runoff into the Black Sea being about 350 km^3, with more than 80% of this volume from the mentioned 10 rivers, first of all the Danube (200 km^3), Dniepr (44 km^3), Rioni (13 km^3) and Dniestr (9 km^3) (Hydrometeorology and Hydrochemistry of seas of USSR, 1991). An extensive literature is dedicated to inflow of these rivers, especially Danube. However, there are no systematic observations on most of the small and medium rivers of the Black Sea, while their contribution is quite significant. Different authors (Mikhailov, Mikhailova, 2008, Altman and Kumysh, 1986, Jaoshvili, 2002) estimate it from 40 to 120 km^3 of average annual runoff. There are about 20 small rivers along the Russian

coast and several medium: the Pshada, Vulan, Tuapse, Psezuapse, Sochi. The medium rivers are characterized with annual average stream flow about 10-15 $m^3 s^{-1}$ and yearly runoff about 0.3-0.5 km^3. There are also two larger-scale rivers, Shakhe (37 $m^3 s^{-1}$, 1.2 $km^3 year^{-1}$) and Mzymta (49 $m^3 s^{-1}$, 1.6 $km^3 year^{-1}$) at the eastern part of Russian coast. Total average annual runoff from the territory of Russia is about 7 km^3. It is about only 2% from all freshwater inflow into the Black Sea, which may be the reason why so little attention was paid to small and medium river effect so far. This inflow, while rather insignificant for the entire sea, can still cause noticeable impact on ecosystem of the Black Sea shelf on a local scale.

To estimate influence of river inflow on the Black Sea coastal ecosystems, P.P.Shirshov Institute of Oceanology of Russian Academy of Sciences had launched annual field observations since 2006. Expedition program included hydrophysical, hydrochemical and hydrobiological studies.

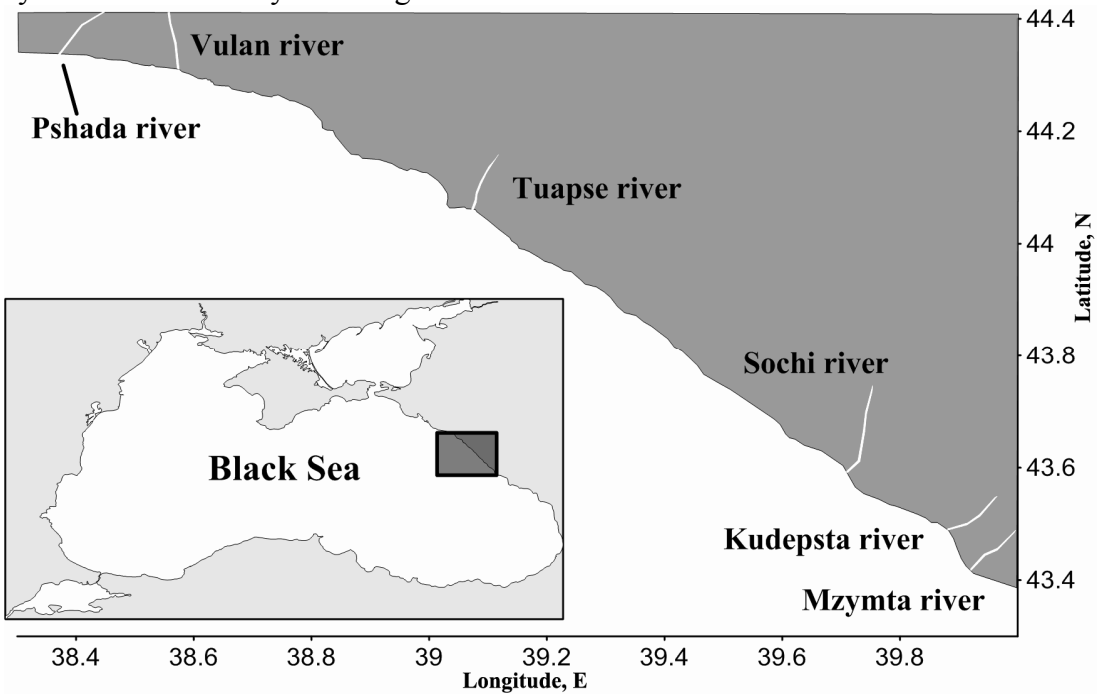


Fig. 1. Region of studies in 2006-2010 and studied rivers.

In first part of June 2006 (period of relatively high inflow) investigations in river mouth areas of the Pshada and Vulan rivers were carried out. These studies were considered pilot, with additional goals of developing methods for similar observations in the future, with wider spatial and time coverage of river influenced coastal areas.

In 2007, from 30 April to 5 May expedition on a research vessel “Akvanavt” performed studies on five sites in mouth areas of the following rivers: Mzymta (town of Adler), Tuapse (town of Tuapse), Vulan (township of Arkhipo-Osipovka) and Pshada (village of Krinitsa).

In 2008, from 7 to 13 November detailed studies had taken place in the Vulan bay (township of Arkhipo-Osipovka).

In 2009 from 20 to 27 May and in 2010 from 26 to 30 May expeditions studied the nearshore area between river mouths of Kudepsta and Mzymta rivers (the Greater Sochi district).

Materials and methods.

Every expedition included hydrophysical and hydrochemical studies. Continuous measurements of temperature and salinity were performed with running CTD system (SBE 911 CTD probe with a deck unit and a centrifugal pump running outside water through the probe).

Vertical CTD profiling was carried out with SBE 19plus probe.

Anchored stations equipped with current meters were used for current velocity measurements. Near bottom currents were studied with the SeaHorse current meter, and the acoustic current meter Nortek Aquadopp was used for surface measurements.

Continuous measurements of meteorological parameters (wind speed and direction, temperature, humidity, atmospheric pressure) were carried out on two portable weather stations about 8 km distanced from each other.

Concentrations of pH and dissolved oxygen were continuously registered all along the expedition route. Outside water was pumped during the boat movement into a flow-through cell with a pH electrode and sensors of oxygen and temperature. Measured parameters and boat coordinates were recorded every 10-30 seconds (more frequently near the shore). Four channel ion meter "Econix-Expert 001" and amperometric temperature and dissolved oxygen sensor DKTP-02.4 (manufactured by NPP "Econix Expert", Russia) were used for these measurements. Modified water feeding system removed air bubbles and allowed continuous sampling with boat speed of 5-6 knots (2-3 knots in preceding years), thus average 20 seconds sampling rate allowed spatial observation resolution of 50-60 meters.

Bottled samples were analyzed in an onshore makeshift laboratory no later than 12 hours. Analyzed species included silica and total alkalinity.

Measurement of oxygen and pH on individual stations were processed correspondingly with Winkler method and potentiometric method according to Grasshof et al (1999).

Main nutrients (silica, phosphorus, nitrate, nitrite and ammonia) were analyzed according to Grasshof et al (1999).

Total alkalinity was determined using modified Bruevich method of direct titration (Bordovsky and Chernyakova, 1992).

Due to high turbidity, especially in river mouth areas, nutrient samples were filtered with 0.45 μm Millipore filters under external pressure.

Results.

The site near Greater Sochi studied in 2009-2010 proved to be a most interesting subject. First of all, this area is under strong man's impact because of residential and industrial drainage of Sochi agglomeration. Second, two major local rivers, Kudepsta and Mzymta, significantly differ in composition (Table 1). It allows tracing distribution of inflow for each individual river and estimating their fractional contribution to formation of surface water structure. The results acquired in this zone

will be the main focus of this article, but first we will briefly overview the field studies in 2006-2008.

Pilot studies in 2006 carried out in the area of Pshada and Vulan rivers and primary aimed at developing investigation methods, had shown significant influence of river inflow on hydrochemical water structure. Zone of impact of all studied rivers was characterized with increased total alkalinity, increased concentrations of dissolved inorganic silica and decreased pH. Behavior of other hydrochemical parameters depended on individual properties of a particular river. Influence of river inflow on hydrochemical regime was traced on a distance from 0.5 to 3 km in the direction of prevalent water transfer. The affected area is characterized – at least during spring-summer season – with increased biological activity.

Focus of studies in 2007 was shifted from wide surface surveys to vertical distribution of hydrochemical parameters along cross-sections from 8-10 meter depth to isobaths of 50-100 meters. It was discovered that rivers of Tuapse-Sochi region are under greater anthropogenic impact than rivers of Pshada-Vulan region. Concentrations of ammonia and phosphate in river-influenced nearshore areas of the first region were significantly higher.

Investigations in 2008 were concentrated near the Vulan river mouth area. The goal of these studies was to trace the nature of continental inflow on hydrophysical fields of the shelf under conditions of weak inflow of low water in autumn. It was found that even weak winds of southern bearing during low water period can effectively "lock" the runoff and even drive sea water into river mouths. Intensive background circulation along the coast, probably related to the Rim Current, was another factor that limited distribution of river water on the shelf. The river plume under such circumstances had highly constrained area and was shaped into a thin strip, pressed to the shore and stretched out westward. Influence of the river inflow is still significant under such conditions; however, its quantitative characteristics (horizontal and vertical scales of fresh water areas, amount of decreased salinity, concentrations of dissolved and particulate matter) are 3-5 times lower than during springtime high water.

The site of studies in 2009-2010 near the Greater Sochi region included five cross-sections about 1.5-mile length each. The most southern cross-section was in the Imeretinskaya bay area, second one from the south was related to the Mzymta river mouth, and the others were situated between Mzymta and Kudepsta river mouths (fig. 2). Continuous sampling during the boat movement between cross-sections was performed as well. Total route length during the expedition of 2009 was more than 150 miles.

The discussion below is related to studies on this observation site in May 2009.

High variability of river plume was registered during observation period. Its alongshore extension differ in less than a week from a few hundred meters to 8.5 kilometers. Decrease of salinity in the river mouth area of the plume (control point at the Mzymta river mouth) changed from 0.8 to 3.5 psu. Vertically the plume was confined withing the top 1-meter layer, with a sharp pycnocline formed at the bottom boundary (fig. 3).

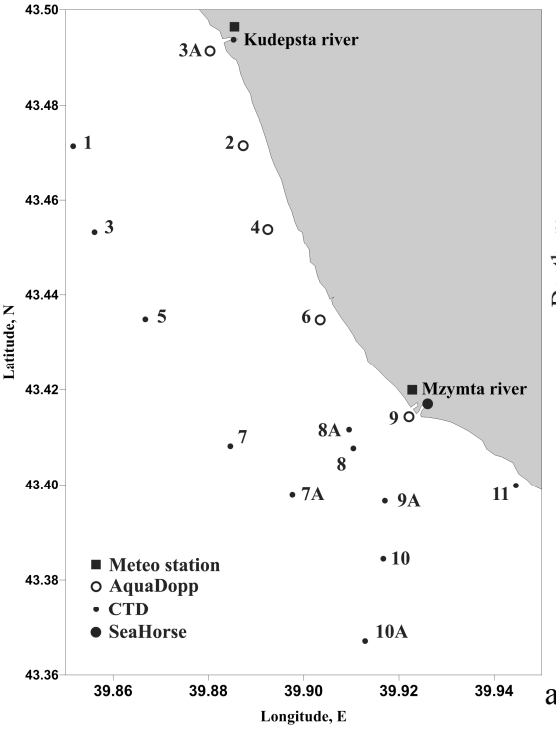


Fig 2. Scheme of daily measurements on the Greater Sochi site during 21-27 May, 2009.

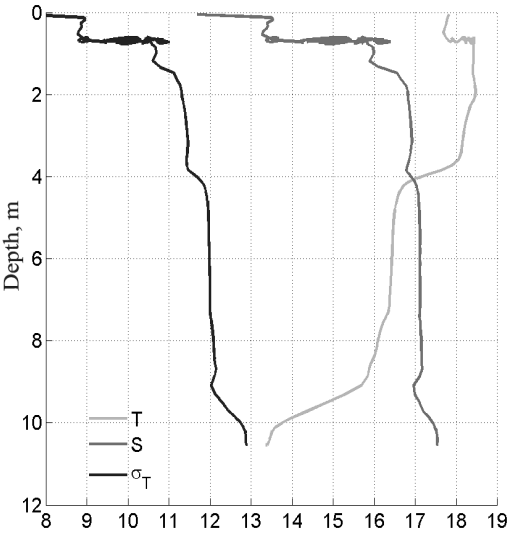


Fig 3. Vertical profiles of salinity, temperature and density (σ_θ) in the Mzymta river mouth area. Horizontal axis is used for all three of the mentioned parameters (psu, ^oC and kg m^{-3} correspondingly).
Station 9 (see fig.2), 23 May, 2009.

Area of desalination from the Mzymta river inflow reached maximum spatial extension during downwelling wind of southern and eastern bearings (see fig.4 for variability of wind strength and direction during observation period).

So, what external factors determine the plume development in the first place? Acquired data show that plume area and salinity anomaly increase with intensification of alongshore wind stress components. Similar dependence is noted for the alongshore current velocity. Stronger vertical stratification also contributes to plume development in near-surface layer, so it is possible to conclude that increased salinity anomaly mainly increases plume area, rather than thickness.

Finally, while the intensity of river inflow is an obvious factor, its strength during the observed period changed no more that twice the initial volume, while plume area and salinity anomaly varied in more than 10 and 15 times correspondingly. It seems that oceanological factors determining distribution of plume and fresh water efflux are more important in this case than velocity of fresh water inflow. Figure 5 shows series of alongshore component of surface and bottom current velocities on the anchored station that was set 300 m westward of the Mzymta river mouth, near the “beginning” of the plume.

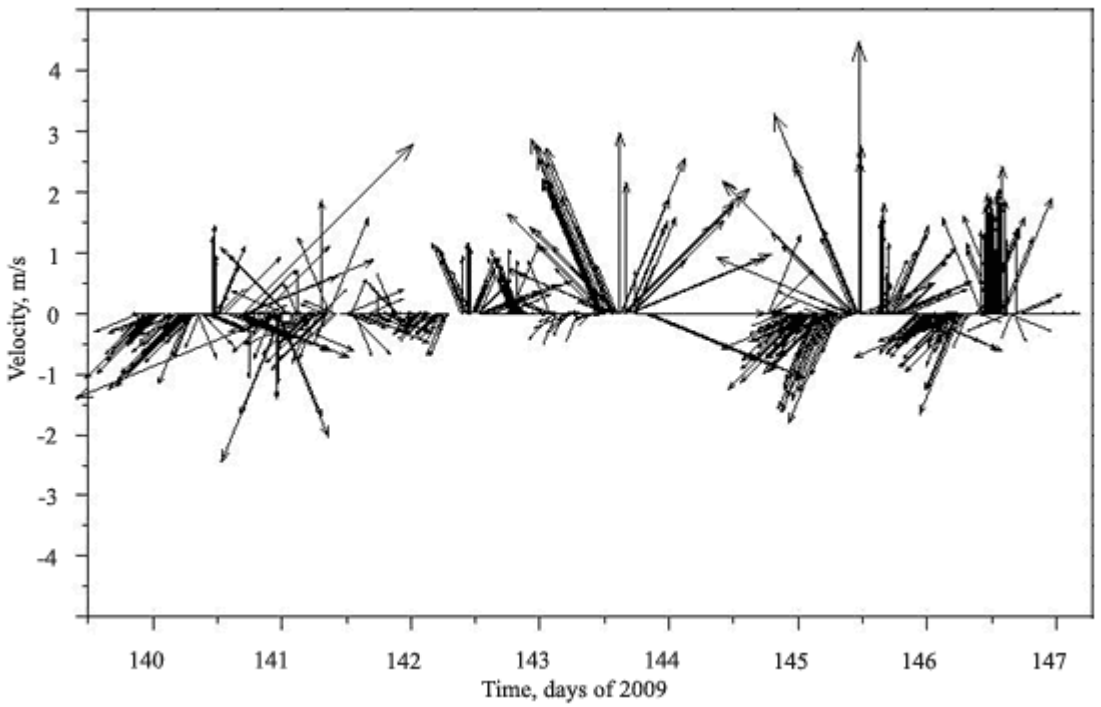


Fig. 4. Wind velocity vectors during 20-27 May, 2009. Horizontal axis represents day number (day 140 corresponds to 20 May). Portable meteorological station was set up near Kudepsta river mouth.

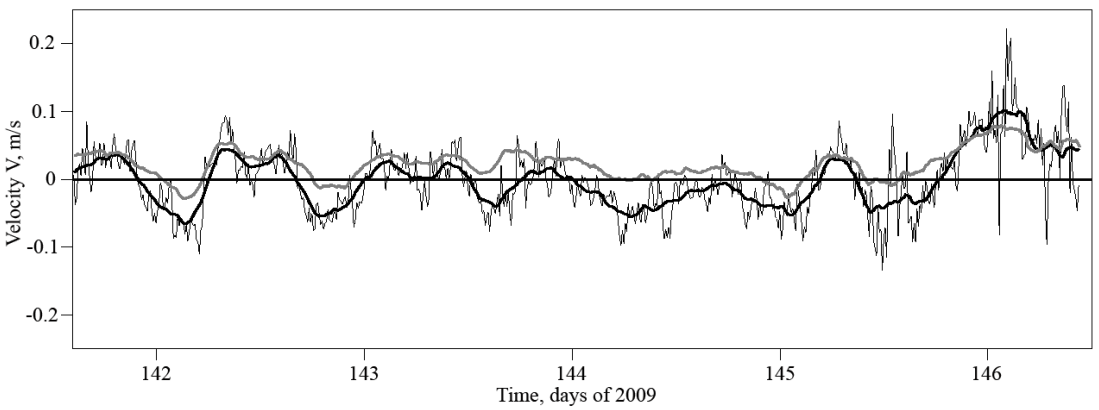


Fig 5. Variability of alongshore component of current velocity on the anchored station set up 300-meters westward of the Mzymta river mouth at 8-meter depth. Black curves correspond to 1-meter depth, grey curve – to bottom layer. Thin line represents raw data of 10 minutes interval; thick lines are data, filtered with moving average window of 4 hours. Positive direction is to the north.

Dissolved oxygen.

The studied area in 2009 and 2010 was characterized with decreased values of dissolved oxygen (230-260 μM l^{-1}) in the surface layer compared with the average Black Sea values (280-320 μM l^{-1}). It may be due to high intensity of oxidation processes, since river waters bring a large amount of the suspended matter into the

sea. Nevertheless, results of continuous records of oxygen concentrations have shown that each river mouth area was characterized with increased oxygen. It appears that despite the oxidation processes, the biological activity, supplied with the inflowing nutrients, is increased in this area. Boundary of this zone is located at 1.5 – 2 km from the river mouth. Fig. 6 (left part) shows dissolved oxygen distribution in the region between the Mzymta and Kudepsta rivers.

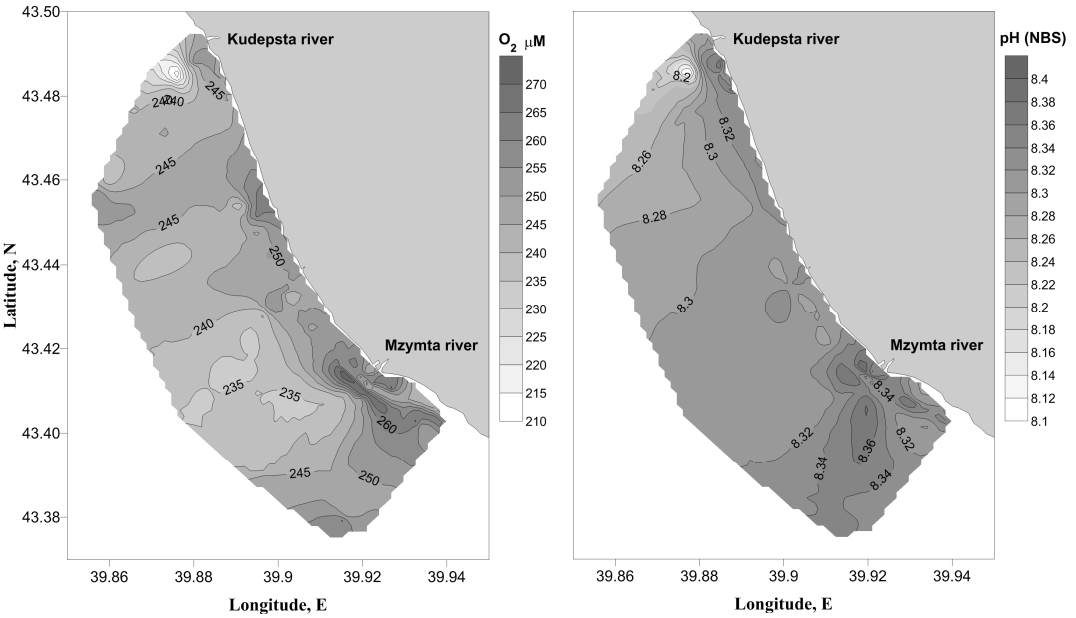


Fig. 6. Distribution of oxygen concentrations and pH values on the studied site in 23 May, 2009.

pH.

Measured pH values in the surface layer varied from 8.13 to 8.40 (NBS scale), which is lower than the average Black Sea values (8.4-8.6). Fig. 6 (right part) shows distribution of pH in the surface layer. Immediate vicinity of the Mzymta river mouth was characterized with increased pH values, confirming the expedition results of 2006 – 2008. pH values were decreased in the area of Kudepsta river mouth.

Total alkalinity and carbonate.

Amount of alkalinity is one of the most sensitive indicators of river inflow. With it, influence of Mzymta river inflow can be easily traced in 3-4 km distance into the sea and 10-12 km along the shore.

Alkalinity variability range was very high, changing from river to river (921 μM l^{-1} in Mzymta, 4200-4400 μM l^{-1} in Vulan). High alkalinity (3419 μM l^{-1}) was also detected in the Kudepsta river water in 24 May after rains in both the studied area and river drainage area. Average alkalinity of the surface sea waters is 3200-3300 μM l^{-1}.

Influence of the Mzymta river results in decreased contents of carbonate, which makes up major part of total alkalinity. Similar result was observed in 2007 during RV "Akvanavt" cruise. Influence of river inflow can be traced almost anywhere on the studied site. Alkalinity of the Kudepsta river was close to the one of

surface sea water, only slightly higher on several occasions. As a result, distribution of alkalinity in north-eastern part of the studied area is smoother, without noticeable extremums. It is also related with far lesser amount of inflowing water in Kudepsta river in contrast with the Mzymta and, as a result, its weaker impact on hydrochemical parameters in the nearshore area.

Table 1. Hydrochemical characteristics of Kudepsta and Mzymta river inflow measured in 2009-2010.

Kudepsta river				
Date	Distance from the river mouth, m	pH NBS	Alk, μM/l	Si, μM/l
24.05.09	90	8.16	3420	80.70
24.05.09	550	8.19	3066	93.10
26.05.09	90	8.40	3010	-
26.05.09	550	8.38	3165	84.48
26.05.10	90	7.69	3200	105.83
29.05.10	90	8.3	3200	24.03
29.05.10	700	8.14	3654	94.43

Mzymta river				
Date	Distance from the river mouth, m	pH NBS	Alk, μM/l	Si, μM/l
26.05.09	100	8.31	921	86.05
26.05.09	500	8.50	929	86.12
26.05.09	750	8.37	970	81.13
26.05.10	750	7.93	991	100.85
27.05.10	100	8.68	1042	98.53
29.05.10	100	8.28	916	93.61
29.05.10	500	8.14	924	91.29

Silicate.

Content of dissolved organic silica in the water, like total alkalinity, is a good tracer of river water intrusion. Variability range of silica in studied area was high enough, a typical feature of mixing zones. Si concentrations varied from 0.09 до 93.1 μM. River mouth areas of all studied rivers content of silicate is increased compared with marine part of the studied area. Both Mzymta and Kudepsta rivers carry out significant amount of silica.

Distribution of river waters.

Contribution of individual rivers into surface water formation was estimated for the Greater Sochi area. Presuming that parameter C_o is conservative (or quasi-conservative), its concentration during water mixing will be described with a following equation:

$$C_o \cdot V_o = C_1 \cdot V_1 + C_2 \cdot V_2 + C_3 \cdot V_3 + \ldots.$$

where V_i is water volume, and C_i – amount of certain parameter in particulate volume. Since total water volume, $V_o = \sum_i \mathbf{V}_i$, relative contribution of each water mass can be described as $K_i = V_i / \sum_i \mathbf{V}_i$. The initial equation can be rewritten as followed: $\mathbf{C_o} = \sum_i (\mathbf{C}_i V_i / \sum_i \mathbf{V}_i) = \sum_i (\mathbf{K}_i \mathbf{C}_i)$. Since sum of relative contributions of every water mass $\sum_i \mathbf{K}_i = 1$, we have a system of linear equations that with knowledge of C_i parameters can be solved relative to K_i, and with N parameters it is

possible to make calculations for N+1 water masses. Numerical solution was acquired for 2, 3 and 4 water masses.

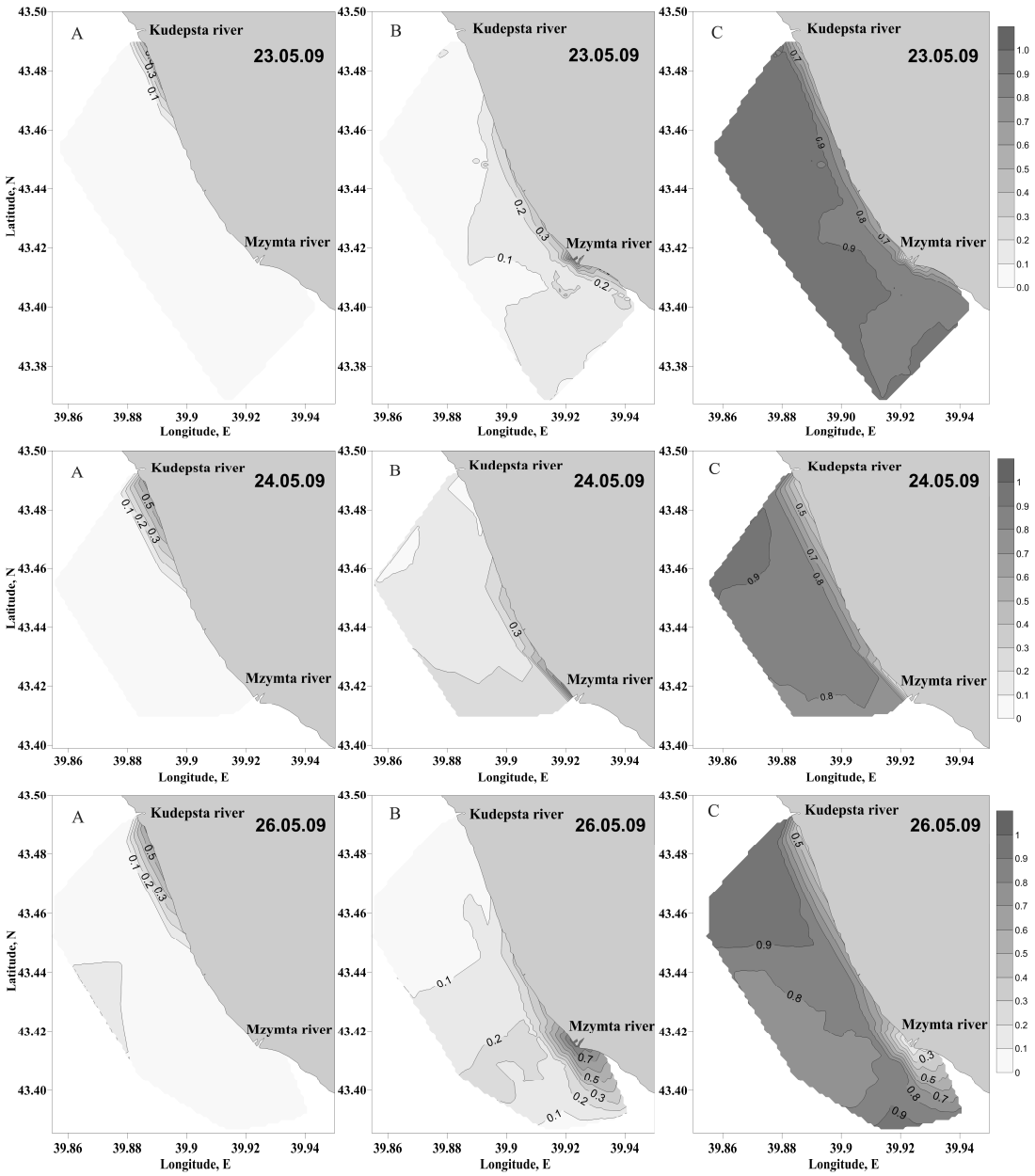


Fig. 7. Relative content of Kudepsta river (A), Mzymta river (B) and sea (C) waters in formation of hydrochemical structure of surface waters on the studied site in May, 2009. These values were calculated assuming linear mixing of three water masses. Salinity and total alkalinity values were set with the data measured in river mouths of both rivers and in the open sea.

Program for K_i calculation was written, with salinity, silica and total alkalinity taken as parameters. Since biological activity in the studied area is relatively low and amount of dissolved carbon involved in photosynthesis is only 1-

10% of its total sum, total alkalinity, with certain assumptions, can be regarded as quasi-conservative parameter, especially for a short time period.

Fig. 7 shows relative contents of Mzymta and Kudepsta waters, along with "background" marine waters in top 1-meter surface layer of the studied site for separate daily cruises in 2009. These values were calculated with assumption of linear mixing of three water masses with values of salinity and total alkalinity set by sampling in river mouths of both rivers and in the open sea, far off them. As it seen, Mzymta waters contribute up to 30% in nearshore strip, extended about 6-7 km north-west. Kudepsta waters contribution is more localized (with the exception in 26 May, when lens of its waters was observed on a significant distance from the river mouth).

Conclusions.

During field studies on the north-western coast of the Black Sea in 2006-2010 qualitative characteristics of processes of distribution of small and medium rivers inflow (Mzymta, Kudepsta, Vulan, etc), their transfer of organic pollution and large mass of suspended matter in the nearshore zone were acquired. It was found that affected area is stretched from 3 to 11 km alongshore and 1-3 km into the sea. Maximum concentrations of dissolved organic matter in this zone are increased 6 times, suspended matter – 70 times. Observed river plume area differ from 2 to 42 km^2, maximum salinity anomaly – from 0.8 to 3.5 psu.

River plume dynamics and variability under hydrometeorological factors were observed with direct instrumental measurements during several consecutive days. It was shown that areal characteristics of plume are increased with alongshore wind stress component, which corresponds to downwelling conditions. Similar dependence was observed in connection of plume development with alongshore component of background current velocity. No significant connection of river plume area and its salinity anomaly with current vorticity and transverse to coast line wind component and current velocity was found.

Influence of river inflow on hydrochemical structure during studied period was clearly traced. Amount of total alkalinity and dissolved silica were found to be the most sensitive indicators of river inflow influence. Expeditions of 2009-2010 found an interesting fact that the Kudepsta river waters contained significant amount of carbonate. In 2006-2008 high amount of carbonate (and, consequently, total alkalinity) was observed only in rivers located westward of the Vulan river. However, alkalinity in the Mzymta river waters, located practically in the same drainage area as the Kudepsta river, was 3-4 times lower.

Results of continuous records of hydrophysical parameters, dissolved oxygen and pH have shown that river mouth areas of all studied rivers are characterized with increased values of dissolved oxygen and pH. It can be supposed that biological activity, supplied with the inflowing nutrients, is increased in this area. Under impact of dynamic factors this area can drift or disappear for some time. Outer boundary of this zone is usually located 1.5 – 2 km from the river mouth.

From methodological point of view, these studies confirmed that discreteness of observations plays an important role in such field experiments. Traditional approach (working on individual hydrological stations) may miss or misrepresent

many characteristics of interaction zone of river and marine waters because of high time and spatial variability of hydrological and hydrochemical parameters. Use of flow systems with continuous registration of measured parameters seems to be more perspective for this kind of studies.

References.

Altman A.M., and Kumysh N.I. (1986) "Perennial within-year variability of the Black Sea fresh water balance." *Trudy GOIN* 176, Gidrometeoizdat, Leningrad, 3-18 (in Russian).

Bordovsky O. and Chernyakova A. (Eds). (1992) *Modern Methods of Ocean Hydrochemical Investigation*. SIO RAS, Moscow (in Russian).

Bruevich C.V. (1944). "Determination alkalinity of small volumes of seawater by direct titration." *Instruction of chemical investigation of seawater*. Glavsevmorput, Moscow (in Russian).

Grasshof K., Ehrhard M. and Kremling K. (Eds.) (1999). *Methods of Seawater Analysis*, 3rd ed., Wiley-VCH, Weinheim.

Ivanenkov V. and Bordovsky O. (1978). *The methods of hydrochemical investigation of the ocean*. Nauka, Moscow (in Russian).

Jaoshvili Sh.(2002). "The rivers of the Black Sea." *European Environmental Agency. Technical report no. 71*. http:// reports.eea.eu.int/technical_report_2002_71/

Levy G. and Brown R.A. "A simple objective analysis scheme for scatterometer data". *J. of Geophysical Res.*, 91, 5153-5158.

Lisitsyn A.P.(1974). *Sediment formation in oceans*. Nauka, Moscow (in Russian).

Lopatin G.V. (1952). *Sediments in the rivers of the USSR*. Geografizdat, Moscow (in Russian).

Makkaveev N.I. (1981). "Some peculiarities of erosion and accumulation process". *Soil erosion and river mouth processes*, (8), MGU, Moscow, 5-16(in Russian).

Mikhailov V.N. (1997). "*River mouths of Russia and neighboring countries: Past, present and future*". GEOS, Moscow (in Russian).

Mikhailov V.N. and Mikhailova M.V. (2008). "River mouths". *The Black Sea Environment*, edited by A.G. Kostyanoy, A.N. Kosarev, Springer-Verlag: Berlin-Heidelberg, 93–133.

Milliman J. and Syvitski J. (1992). "Geomorphic/tectonic control of sediment discharges to the sea : The importance of small mountainous rivers". *J. of Geology*, 100, 525-544.

Solyankin E.V. (1963). "Water balance of the Black Sea". Oceanology, 6, 986-993.

Sorokin Yu. I. (2002). *The Black Sea Ecology and Oceanography*. Backhuys Publ. Leiden.

"The Black Sea."(1991). *Hydrometeorology and hydrochemistry of seas of USSR,* (4), Gidrometeoizdat, Leningrad (in Russian).

Zavialov, P. O., A.G. Kostianoy, and O. O. Moller Jr. (2003). "SAFARI cruise: Mapping river discharge effects on Southern Brazilian shelf". *Geophysical Research Letters*, 30 (21).

Restoring Malibu Lagoon: A Case Study in Collaborative Coastal Restoration

Marc Beyeler[1], Steve Seville, PE[2], Mark Abramson[3]

1 University of California, Santa Cruz, MBA Consultants, 111 El Camino Real, Berkeley, CA 94705; 510 316-6095; 510 652-7274; marcbeyeler@mac.com.
2 ICF International, 75 E Santa Clara Street, Suite 300, San Jose, CA 95113; 408-216-2821; sseville@icfi.com.
3 Santa Monica Bay Restoration Commission, 320 West 4th Street Suite 200 Los Angeles, Ca 90013; PH; 310-961-4871; email. mabramson@santamonicabay.org

ABSTRACT (Limit 150 Words)

The restoration of Malibu Lagoon is an excellent case study example of the important and critical role that engineers can, and very often do, play in coastal restoration efforts in California. This case study analysis offers many lessons learned for the engineer that can inform how best to be involved in the development and implementation of coastal restoration projects. These lessons learned can be applied to other coastal restoration projects in California and nationally.

This paper focuses on the roles and services that coastal engineering can provide in larger interdisciplinary restoration teams and in efforts to restore coastal resources and the many challenges faced in attempting to provide value-added services. It examines the complex project management structure required to be in place to plan for and implement the restoration project, focused on the need for, and roles, engineers have played in the distinct planning and implementation phases, and it documents and analyzes the specific factors contributing to successful restoration planning and implementation efforts, including importantly the role of technical expertise and the contribution that engineers make to project success.

Malibu Lagoon

Malibu Lagoon remains one of Southern California's most important remaining coastal wetlands. The small, 31-acre Lagoon is located at the mouth of Malibu Creek and the 109 square-mile Malibu Creek Watershed. The Malibu Creek Watershed, with about two-thirds of natural vegetation still intact, anchors a 170,000-acre oasis of open space and nature in the heart of the larger Santa Monica Mountains, bordering the Los Angeles basin to the east and forming the northern rim of Santa Monica Bay.

Malibu Lagoon empties into the Pacific Ocean at world famous Malibu Surfrider Beach, renowned as a surfing and recreational destination, hosting approximately 1.5 million visitors every year. Malibu Lagoon provides vital habitat for a combination of aquatic, avian and terrestrial species, including several endangered and threatened species, such as the tidewater goby and the southern steelhead trout. The area is also home to several threatened and endangered birds, including the Brown pelican, California least tern, and the snowy plover, and represents a vital stopover for migratory birds along the Pacific

Flyway. An estimated ninety percent of historic coastal wetlands in southern California that have been filled, drained, or otherwise altered. Over several decades, the area of Malibu Lagoon and its associated wetland habitats has been significantly reduced. Despite the alterations to the wetlands and the many changes to the lagoon environment, Malibu Lagoon provides a unique opportunity to restore a vital portion of the state's remaining historic coastal wetland habitat.

Figure 1: Map Image-Malibu Lagoon and Lower Malibu Creek and Northern Santa Monica Bay



Historic coastal maps depict a much larger lagoon and wetland complex that extended north behind an expansive barrier beach. Anthropogenic influences to the landscape have significantly altered the lagoon footprint. Originally, Low lying areas were filled to "reclaim" usable land. Eventually, coastal thoroughfares were established and coastal development ensued. Developers continued to fill the historic lagoon area to create housing and commercial and recreational development. With the construction of the Pacific Coast Highway (PCH, SR-1), the California Department of Transportation (Caltrans) established operation and maintenance facilities along the highway near the edge of the lagoon. Caltrans had created a dumpsite that was operated through the 1960's. In 1968, one of the early Malibu residences was purchased and demolished to create a parking area and public access point for surfrider beach. By the late 1970's, the last

remnant of the historic lagoon extending to the west had been filled and was now the site of two baseball fields. The lagoon complex that had once extended west as far as ¾ of a mile was now reduced to approximately 20 acres and confined to the Malibu Creek channel downstream of the PCH bridge.

California State Parks acquired the lagoon and wetland properties in 1978. In 1983, The California Department of Parks and Recreation undertook restoration efforts for a portion of the western complex that resulted in the removal of the baseball fields and carved 3 separate tidal channels from the edge of Malibu Creek to the western boundary of the State Park. While the restoration effort was a step in the right direction, the configuration of the channels, their lack of ability to interconnect and circulate flows, and the influences of urban and agricultural uses upstream in the watershed produced several negative impacts to the lagoon's ecology and water quality including increased fresh water inputs into the lagoon and increased toxic pollutant loads.

The lagoon is currently listed as impaired under the Clean Water Act Section 303(d) for benthic impacts, pathogens, nutrients, eutrophication, swimming restrictions, and shellfish harvesting. Studies have indicated high pathogen concentrations in the lower Malibu Creek, the lagoon and surf zone that could potentially impact the health of swimmers and surfers. The current configuration of channels causes poor circulation, eutrophication, and low dissolved oxygen levels in the lagoon.

Efforts to study the lagoon and develop strategies to improve its overall health have been ongoing since the first efforts that led to the restoration construction in 1983. Restoring coastal resources and managing coastal restoration projects, especially coastal wetland restoration projects, is often very time consuming and very staff intensive. State Parks, NGOs, and local activists are engaged and vocal whether it be maintenance and operation of the existing facilities, studies to better understand the lagoon and it's interaction with Santa Monica Bay, or efforts to improve its restoration. Like similar habitat restoration projects Malibu Lagoon has very unique environmental and social conditions that must be planned for and taken into account in the restoration planning process.

Collaborative Restoration Project Management

Mirroring similar efforts nationwide, a great deal of social investment has been focused on building more cooperative and collaborative social network-based governance and management structures to facilitate natural resource restoration within Santa Monica Bay, and specifically Malibu Lagoon. In this presentation, collaboration is recognized as a principal foundation to address the complex coastal restoration implementation and management needs and goals.

Part of any collaborative efforts involves the participation of, and the data and information generated and interpreted by engineers. Assembly of a multi-disciplinary team of staff, scientists, and consultants spanning a range of expertise is most often required to develop and manage the many phases of the restoration planning and the implementation process. Starting with conceptual restoration planning alternatives and cost estimates of alternative designs to development and production of bid documents,

engineers must provide the integral function to ensure the design intent for restoration is maintained throughout the process and that all restoration efforts are feasible and meet the goals and objectives of the project.

Restoration projects are particularly challenging from a purely technical perspective. Designing a project to restore habitats that have been absent from the landscape for decades is difficult at best. Typically, disturbed landscapes are no longer capable of supporting the diversity or functionality that originally existed. Elements of the historic ecosystem must be reintroduced within the confines of the restoration that can be achieved in the new landscape and land use setting.

Beyond the complexities of designing a functioning and appropriate ecosystem, each project also requires the cooperation of a number of involved agencies that require specific inclusions to the project. Coordination of the restoration concept elements, review of environmental impacts, and permitting requirements generally extends the overall life of a project from conception to implementation. Figure 2 illustrates some of the governance and management parts of collaborative restoration project management, including formal project partnerships, watershed stakeholder groups, science and technical advisory bodies, project funders, and other project management oversight groups.

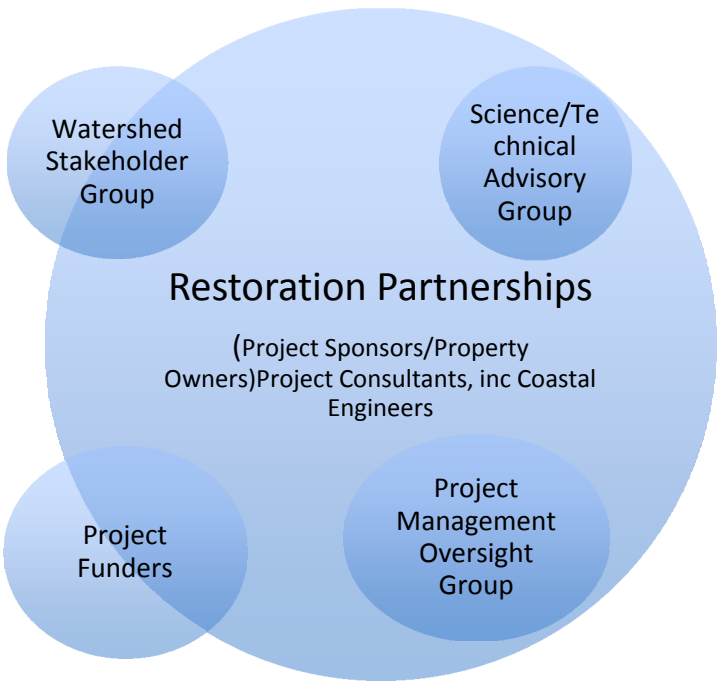


Figure 2. Collaborative Restoration Project Management

Each of these parts of the restoration management collaborative plays a slightly different role and function. Each is an essential pre-condition of successful restoration planning, understanding that the restoration process must be built on a solid foundation that develops public trust and acceptance through its transparency.
While this does not in and of itself guarantee success, in its absence even meritorious restoration projects can be delayed by very small groups of willful and determined opponents. At the same time it is essential to emphasize the importance of technical and scientific expertise in assisting in both design and in decision-making, and not just target appeasement of all stakeholders.

Collaborative Coastal Restoration Projects and Coastal Engineering

There are several important and often very distinct stages of restoration planning design engineering and construction involved in completing a successful coastal restoration project. At each stage there are one or more roles that the civil engineers can play to assist in moving the restoration goals forward to project completion.

Each restoration project is process intensive. Projects are very long-term, complex, often halting and time consuming, labor intensive, and include discreet citizen and stakeholder involvement stages, and multiple and multi-layered permit and approval requirements.

In addition the projects are frequently expensive, with budgets that focus on land acquisition, extensive landform alteration to return the historic condition to the landscape, and temporal disturbance to terrestrial and aquatic resources that have subsisted in the degraded habitat that is the focus of the project.

It is the impairment of these resources that sparked the want or need for any sort restoration effort in the first place, and it is often the protection of these scarce resources that forms the case to forego any restoration project at all for fear or harming what remains.

We summarize below some of the more important topics and roles that civil engineers should be familiar with and trained to address in order to effectively participate on a restoration project team. The form of the restoration project "coastal engineering related" product within each stage is identified and the important role for the engineer is described.

1. **Planning Concept and Concept Alternatives**: Often contained in larger scale watershed or river drainage plans or in jurisdictional comprehensive coastal plans, or in sub-area plans, such as the Lower Malibu Creek Restoration Plan.

2. **Restoration Planning Alternative Designs**: Often contained in Restoration Plans for larger areas or in specific area Restoration Plans, such as the Malibu Lagoon Restoration and Enhancement Plan.

3. **Preferred Project Design**: Must have done sufficient engineering and project

design to state a preferred alternative (or equivalent). Must be completed to go to the Environmental Review Stage. Such as hydrology technical reports, hydrodynamic and water quality modeling, tidal and survey datum comparison, sea level rise considerations, and tidal exchange calculations.

4. **Environmental Impact Report Design Mitigations and Requirements**: As a result of the Environmental Review Stage an approved final design for final permitting and approvals and bid specifications for advertising and awarding and constructing. Mitigations themselves can often result in greater restoration project management requirements and needs.

5. **Project Design for Permits and Approvals**: In the case of a multi-purpose restoration project no less than six permits and eleven different monitoring and reporting programs or protocols.

6. Project Final Engineering Drawings and Specifications (at all percentage design milestones): At each mini-milestone (30 Percent Drawings; 60 Percent Drawings) additional value and ecological engineering can be applied to final design.

7. Final Bid Specifications: Based on all project design factors, finished work to be used for active contract bidding. Matching the right level of engineering detail and the right engineering details can entail a great deal of planning time at this stage much of it involving the coastal engineer.

8. Final Contract/Construction Specifications: Depending on the bid rec'd a revised design specification. Often requires values engineering but could also require additional ecological engineering.

9. Project and Construction Management Stage (inc all Change Orders and "As-Builts"): With restoration being soil and water intensive environments in dynamic environments this stage of advice and direction can be critical to overall project long-term success and critical to budget success and project management success.

Table 1 provides the cross-walk between the full sequence of Restoration planning design engineering and construction stages and the important roles engineers and engineering firms can play in assisting in the successful implementation.

Table 1. Important Restoration Planning Stages

	Restoration Planning Design Engineering and Construction Stage	Role for Coastal Engineer/Firm
1	Planning Concept and Concept Alternatives	Engineering/Technical/Ecological Feasibility
2	Restoration Planning Alternative Designs	Engineering/Technical/Ecological Feasibility
3	Preferred Project Design	Cost Estimation and Project Feasibility Analysis
4	Environmental Review and Certification Design with M/C	Value Engineering; Feasibility Analysis; Ecological Analysis and Ecological Engineering
5	Project Design for Permits and Approvals	Value Engineering; Feasibility Analysis; Ecological Analysis and Ecological Engineering
6	Final Engineering Drawings and Specs	Value Engineering; Ecological Analysis and Ecological Engineering
7	Final Bid Specifications	Bid Spec Advice; Value Engineering
8	Final Contract Specifications	Contract Spec Advice; Value Engineering
9	Construction Management (As-Built)	Value Managing; Contract Managing

The Malibu Lagoon Restoration Project

While efforts to restore Malibu Lagoon within Santa Monica Bay have been ongoing for more than thirty years, starting a little more than a decade ago, a renewed effort by a "collaborative ensemble" of state, regional, and local agencies and stakeholders increased efforts to plan for and implement restoration of Malibu lagoon. To address the many long-standing conditions, a broad range of local and state agencies collaborated, led by the California State Coastal Conservancy and Heal the Bay.

These two collaborators joined in an effort with the California Department of Parks and Recreation, and together coordinated the preparation of a restoration plan for Malibu Lagoon. The purpose of the Malibu Lagoon Restoration and Enhancement Project is multi-fold, focused on several critical objectives including enhancing existing water quality conditions and restoring and enhancing habitat areas that have diminished functions or are in a currently degraded state.

As noted, restoration projects are particularly challenging, requiring the cooperation of a number of affected agencies and stakeholders and involving a very long time to plan and implement. Recent efforts at coastal restoration at Malibu Lagoon in Santa Monica Bay reflect this planning reality. Figure 3 below illustrates the complex restoration management structure involved in implementing the Malibu Lagoon Restoration Project.

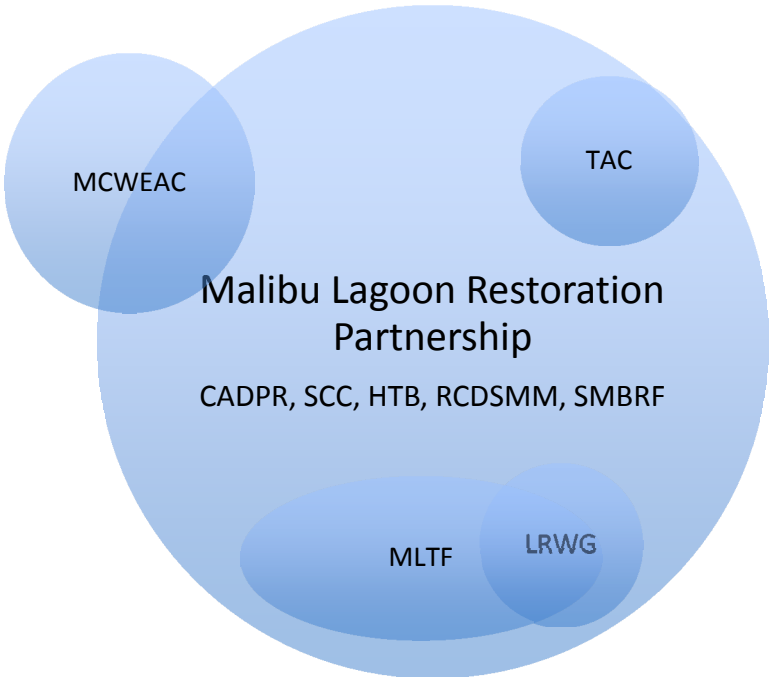


Figure 3. Collaborative Management for Malibu Lagoon Restoration

The Malibu Lagoon restoration effort has involved many actors and many different actions over many years. The Malibu Creek Watershed Executive and Advisory Council (MCWEAC) and the Malibu Lagoon Task Force (MLTF) have been long-standing components of watershed, creek and lagoon planning for the past two decades. In a stakeholder driven process, 85 members participated in the Malibu Lagoon Task Force, part of the greater Malibu Creek Watershed Advisory Council. The 85 Task Force members included residents, local homeowners associations, business owners, natural resource management agencies like State Parks and the Department of Fish and Game, and several environmental groups, including the local Surfrider chapter.

The goal of the project is to create a more natural self- sustaining system that minimizes future operations maintenance and stewardship requirements. Restoration activities have been designed to meet objectives that target the project goal. Improved water circulation, increased tidal inundation, improvement and expansion of critical habitat for tidewater goby and steelhead trout are achieved through alteration of the lagoon bathymetry in channelized area and expansion of open water habitat that considers wind fetch. Removal of non-native vegetation and reintroduction of native vegetation creates appropriate tidal and upland foraging and refugia zones for both aquatic and terrestrial species. Minimizing human disturbance, and domestic and feral animal access to the lagoon's

interior islands promotes natural wildlife diversity within the lagoon proper. All of this can be achieved while maintaining public beach access, lagoon wildlife viewing opportunities, and maximizing educational and recreational use of the site with the emphasis of ecosystem health as the overarching goal.

The current Malibu Lagoon Restoration and Enhancement Project took many years to conceive and design, taking final shape in 2005 with Restoration Alternative 1.5 Conceptual Plan illustrated in Figure 4 below as part of the approved plan.

Figure 4. Preferred Restoration Alternative Design
Restoration Alternative 1.5



Malibu Lagoon is created through the complex interaction of littoral drift of sand deposits along the California coast, the hydrology and sediment transport capacity of Malibu Creek, and the diurnal tides of Santa Monica Bay. In general, the flows of Malibu Creek maintain a natural breach in the barrier beach until tidal action and littoral drift can overcome the flow rate from the Malibu Creek Watershed. The restoration design must consider two basic separate habitat regimes; one as a brackish tidally influenced estuary with a 6 foot tidal exchange that floods and drains twice a day called the “open condition”, and a second that floods with poorly mixed, slow moving freshwater influenced by the surface flows of the creek and groundwater inputs that inundate the lagoon area called the “closed condition”. To further complicate the design

considerations, the closed condition generally floods the lagoon to elevations that are 3 feet higher than the tidally connected open condition.

The existing Lagoon configuration is not functioning properly and has several issues that will be addressed through landscape changes proposed in the restoration plan. The existing lagoon has three separate tidal channels that connect to the main lagoon perpendicular to the general alignment of the flow path created by Malibu Creek. Whether the creek is flowing or tidal exchange is influencing the lagoon, the alignment of the channels minimizes their ability to flood and flush efficiently. The tidal signal in the upper ends of the channels is muted, encouraging sediment deposition, stagnation, and reduced water quality conditions.

Overall the Lagoon has reduced tidal influence because of how the original channels were built. The existing topography of the tidal channels is significantly above sea level, exacerbating the lack of tidal inundation and scouring. It takes a moderate- to high-high tide to completely inundate the lagoon and a very low tide to adequately drain the lagoon. This also means that as normal tides push in and out of the Lagoon, the same water continually moves in and out of the tidal channels, without being refreshed by new ocean water. High topography also prevents saline water from contacting the land and vegetation as it would in a healthy salt marsh, leading to low diversity of vegetation at the site. During the implementation of the 1983 restoration effort, vegetation native to the Channel Islands and not the Malibu Creek watershed was introduced, further disrupting the native ecosystem and hindering a successful restoration attempt. Currently, Malibu Lagoon suffers from low species richness of bi-valves (clams, mussels), crustaceans, fish, and benthic invertebrates as compared with similarly sized southern California coastal estuaries. While the efforts put forth in 1983 were targeting restoration of the lagoon, much has been learned since this early effort.

Issues of concern in the lagoon and creek include excessive freshwater inputs from urban runoff and imported water; high nutrient, pathogen, and bacteria levels; sedimentation; contaminated runoff; loss of habitat; and invasive species. Excessive freshwater inputs from both the Tapia wastewater treatment plant and urban runoff, along with the occasional mechanical breaching of the lagoon/ocean barrier beach, disrupt the natural hydrologic cycle and subject the lagoon to sudden, drastic changes in salinity. While natural breaches create sudden changes in the ecosystem of the lagoon, they generally occur on a hydrologic cycle that has developed over centuries and species have evolved to accommodate the events. Mechanical breaches create these sudden changes at inappropriate times during any particular species life history and place enormous stress on the biotic community. Additionally, urban inputs to the watershed contribute to high nutrient concentrations in the creek can create eutrophic conditions in the lagoon. Elevated levels of bacteria and pathogens from a variety of potential sources (including malfunctioning septic systems, animal waste, storm drains and treatment plant discharges) adversely affect human health, increasing the risk of illness for swimmers and surfers. The lagoon ecosystem is highly disrupted and unhealthy as compared to its historic pre-anthropogenic condition.

The current function of the lagoon and species that reside in the habitat that does exist must be considered of paramount importance. Several aquatic and terrestrial species rely on the small and fragile lagoon habitat for their survival. Breeding seasons and critical habitat must be accommodated in the design and implementation of any project. In order to minimize construction disturbance and avoid critical time periods for a variety of species, the overall restoration project was segmented into 2 phases.

Phase 1 created a completely redesigned parking lot. The Malibu Lagoon parking lot within the State Park was reconfigured to move it away from the open water area of the lagoon. This maximizes the available space for Phase 2, allowing restoration planning for an additional 2 acres. The parking lot construction maintained the original parking capacity, incorporated low impact design (LID) elements, created stormwater infiltration and treatment technologies, and created a planting palette for the restoration and establishment of native and appropriate watershed species. Finally, Phase 1 has incorporated educational elements that serve as a foundation for a better understanding of the lagoon and launching point for the interpretive and educational elements that will be incorporated during Phase 2.

Phase 2 represents a majority of the western lagoon restoration design and implementation. Wetland Restoration, including removal of polluted soils, reconstruction and re-contouring of wetland elevations and replanting of wetland aquatic and upland vegetation. The restoration proposal will create a single meandering channel, similar to other less impacted southern California coastal estuaries. This will improve tidal inundation and scour. The goal is to improve circulation on the incoming tides and to better scour fine sediments and organic matter out to the ocean, decreasing the potential for low dissolved oxygen at the bottom and throughout the Lagoon. Unlike the efforts attempted in the 1983 restoration effort, the Phase 2 design establishes a primary tidal channel with tributary arms. This approach increases the overall available tidal prism, focuses tidal exchange and flow velocities to the western edge of the barrier beach to maximize the benefits of the open condition, and better connects shallow water habitats to upland lagoon elements with appropriate slopes and grades.

It will also remove the pedestrian bridge “pinch points”. The public access trail will be directed around the lagoon perimeter for improved habitat connectivity within the western lagoon and create an interpretive user experience for travelers between the parking area and the beach. The open area of the western lagoon will continue without restriction or interruption to the main lagoon area. This allows uninterrupted wind patterns to increase wave action and circulation over a longer and more natural fetch even when the natural sand bar closes the Lagoon off from the ocean. Finally, the restoration plan will remove improper vegetation that was planted during the initial 1983 restoration. Many of the species are native to the Channel Islands and inappropriate for this site. Also, removing invasive vegetation, which is persistent on the current site, will allow creation of additional salt marsh habitat and lessen upland scrub type habitat.

Table 2. outlines the timeline of the various stages and differing engineering designs for the Malibu Lagoon Restoration project. At each step in this sequence the best

professional judgment of the engineer was called upon affecting both engineering and ecological designs. Several aspects of eco-engineering were applied at different stages during the design permitting and implementation stages.

The Phase 1 of restoration was recently completed in 2008, resulting in a larger wetland footprint and providing the basis for a larger scale lagoon restoration to be completed in this year. The project was stalled for almost a year during a state budget freeze from December 2008 through June 2009 in California.

Table 2. Timeline of Important Restoration Planning Stages For the Malibu Lagoon Restoration Project

	Planning Design Engineering and Construction Stage	Malibu Lagoon Restoration Project (By Date)
1	Planning Concept and Concept Alternatives	Phases 1 & 2- 2003-2005 (Final Plan Concept 6-17-2005)
2	Restoration Planning Alternative Designs	Phases 1 & 2- 2004-2005
3	Preferred Project Design; Environmental Review and Approval Design with Mitigations	Phases 1 & 2- 2005-2006 (Final EIR 4-3-2006)
5	Project Design for Permits and Approvals	Phase 1-2006; Phase 2- 2007-2011
6	Final Engineering Drawings and Specs	Phase 1-2007; Phase 2- 2008-2010
7	Final Bid Specifications	Phase 1-2007; Phase 2- 20082011
8	Final Contract Specifications	Phase 1-2007; Phase2- 2011
9	Construction Management (As-Built)	Phase 1-2008 (Complete 4-16-2008); Phase 2-2011

Final permits and approvals for Phase 2 took nearly 3 years with the project receiving its needed coastal permit in October 2010. The project has strong and broad support among a diverse and very large group of stakeholders and permitting and approving agencies. The second phase of wetland restoration is currently in construction and expected to be completed this calendar year. A multi-media project monitoring program with varied protocols has been developed to track project effectiveness.

Conclusion

Through the development and design of the restoration plans for Phase 1 and 2 of the Malibu Lagoon Restoration Project, the overall engineering effort and involvement was anything but trivial. Through the conceptual design phase that incorporated hydrodynamic modeling of the existing and alternative conditions, to the analyses of the Malibu Creek hydrology and tidal datum corrections and epoch adjustment, each step

presented a new challenge.

The Phase 1 parking lot improvements incorporated specific water quality improvement technologies, review under a variety of permitting agency criteria, and field adjustment strategies developed during construction. Phase 2 bid package development incorporated additional review and adjustment to accommodate increasing permit requirements and stakeholder suggestions. Each additional requirement created a need for more rigor in design. Repetitive efforts to verify survey data, hydrology, tidal, topography, grading design, construction quantities, and project cost created the need for continuous refinement and improvements informed by the project team of technical experts in their respective fields.

Successful coordination of the many related planning, design, and engineering efforts ultimately rested with the issuance of the required permits and the stamp and approval of the engineer. This is not an easy task, considering that a restoration project is intended to return part of the landscape back to the natural environment, an environment that will not be static and will evolve toward equilibrium and perhaps away from your best efforts to predict and restore.

This case study analysis offers many lessons learned for the civil engineer that can inform how best to be involved in the development and implementation of coastal restoration projects. These lessons learned can be applied to other coastal restoration projects in California and nationally.

The demand for engineering solutions to ecosystem–level problems has increased across the United States. The evolving science of restoration ecology has been evolving to address many critical ecosystem management issues. At the same time, the high degree of complexity and uncertainty associated with these issues often demands a range of quantitative approaches and technical expertise to assist in the design, engineering, and implementation of successful restoration projects.

Ecological engineering approaches using science-based quantification of ecological processes to develop and apply engineering-based design criteria are increasingly being employed to restoration projects. The civil engineer and the engineering firm can play a leading role in promoting sustainable coastal design.

There are several steps the coastal engineer and the civil engineering firm can continue to take to best ensure that they can contribute to successful restoration projects. The most important steps are described below, including:

Build interdisciplinary professional and technical team skills- Using existing resources and network collaborations, the individual engineer and engineering firm can leverage results by broadening team opportunities for interdisciplinary projects.

Build restoration science and ecological engineering capabilities- Engineering sciences approaches must be informed by and integrated with biological and physical sciences to create sustainable and feasible restoration projects.

Build planning and project management capabilities- Focusing additional attention on traditional project management core area strengths is becoming even more important, particularly the intersection of planning and project management, where both engineering and ecological creativity and innovation can be applied.

Build project finance and implementation capabilities- Most restoration projects of any size are expensive, increasingly so. The Malibu Lagoon Restoration Project Phase 2 is more than $5 million. Phase 1 was more the $1.75 million. Both projects benefited from a great deal of agency in-kind staff services and other administrative and project management supporting services.

Build Long-Term Restoration Project Partnerships- Most, if not all, restoration projects are multi-stage, multi-year, or even multi-decade, in their planning, design and construction. The most successful engagements will be the partnerships that can span the many project life stages.

Sources and Bibliography

Abramson et al, 1998 "The Malibu Creek Watershed: A Framework for Monitoring, Enhancement, and Action." California State Polytechnic University, Pomona for the California State Coastal Conservancy: Oakland, Ca.

Ambrose, Richard F., and Douglas J. Meffert. 1999. Fish-Assemblage Dynamics in Malibu Lagoon, A Small, Hydrologically Altered Estuary in Southern California, *Wetlands,* Vol. 19(2).

Beyeler, Marc. 2000. "Dangerous Currents: The Questionable Quality of our Coastal Waters," California Coast and Ocean. Vol.16, No. 3, Autumn, 2000. California State Coastal Conservancy: Oakland, Ca.

California State Coastal Conservancy. 2008. Final Project Report: Malibu Lagoon Restoration and Enhancement Project, Phase 1. April 14, 2008. California State Coastal Conservancy: Oakland, Ca.

California State Parks Department, 2006. Final EIR-Malibu Lagoon Restoration and Enhancement Plan. California State Department of Parks: Sacramento, Ca.

Moffat and Nichol. 2005. Final Malibu Lagoon Restoration and Enhancement Plan. Prepared for the California Coastal Conservancy and California Department of Fish and Game. June 2005.

Resource Conservation District of the Santa Monica Mountains. 2008. Final Project Report. Malibu Lagoon Restoration and Enhancement Plan, Phase 1. Topanga, California.

Water Quality Study for a Coastal Development at the Bahia de los Sueños, Baja California, Mexico

Wenkai Qin[1] and Ronald M. Noble[2]

[1]Noble Consultants, Inc. 2201 Dupont Drive, Suite 620, Irvine, CA 92612; PH (949) 752-1530; Fax (949) 752-8381; email:wqin@nobleconsultants.com

[2]Noble Consultants, Inc. 2201 Dupont Drive, Suite 620, Irvine, CA 92612; PH (949) 752-1530; Fax (949) 752-8381; email:rnoble@nobleconsultants.com

ABSTRACT

Detailed hydrodynamic and water quality modeling studies were conducted for the purpose of evaluating the waterfront development alternatives that the Bay of Dreams LLC (Owner) was contemplating for their real estate development at the Bahia de los Sueños, Baja California, Mexico. The Corps approved RMA2 and RMA4 models were used, and a tidal hydraulic model was developed in the studies. The water quality between different lagoon alternatives was evaluated based on the two indicators including the water exchange time and the constituent residence time. The environmental impact of a brine discharge from the planned Reverse Osmosis (RO) seawater desalination plant on the marine environment was assessed.

INTRODUCTION

A series of investigations and studies were conducted on behalf of the Bay of Dreams LLC (Owner), with the objective of evaluating, from a coastal engineering perspective, the feasibility of six waterfront development alternatives that the Owner was contemplating for their real estate development at the Bahia de los Sueños, Baja California, Mexico. The six alternatives consist of (1) an open deep water lagoon alternative, (2) an open shallow water lagoon alternative, (3) a closed salt water lagoon alternative, (4) the open moorings facility, (5) the docking facilities at "El Manglito", and (6) a desalination plant. The project location is shown in Figure 1.

As part of the coastal engineering feasibility study, detailed hydrodynamic and water quality modeling studies were conducted (1) to evaluate the lagoon water quality conditions for the proposed lagoon alternatives and (2) to assess the environmental impact of a brine discharge from the planned Reverse Osmosis (RO) seawater desalination plant on the marine environment.



Figure 1. Project Location

MODEL DEVELOPMENT

The RMA2 and RMA4 models were used in the hydrodynamic and water quality study for the four proposed open water lagoon alternatives, in which the lagoon will be connected to the ocean through an entrance channel, and for an existing lagoon/marina in the adjacent area, and for the environmental impact evaluation for the desalination plant offshore concentrate discharge. A tidal hydraulic model was developed for the closed salt water lagoon alternative in which the lagoon would be connected to the ocean through pipes.

RMA2/RMA4 Model Description. The RMA2 model was developed by the U.S. Army Corps of Engineers (USACE, 2003) to compute the water surface elevation and horizontal velocity for sub-critical, free-surface flow in two-dimensional flow fields. This model module is well suited for and has been extensively applied to the simulation of complex riverine and tidal hydrodynamics of rivers, bays and estuaries. RMA2 computes a finite-element solution of the Reynolds form of the Navier-Stokes equations for turbulent flows (Norton and King, 1977).

RMA4, developed by the U.S. Army Corps of Engineers (USACE, 2003), is a two-dimensional finite element water quality transport model for simulating depth-average advection-diffusion processes in an aquatic environment. For most applications, RMA4 utilizes the depth-averaged hydrodynamic parameters computed from RMA2. The RMA4 model has been extensively applied to simulating the concentration of non-conservative substances in an aquatic environment, calculating residence time and evaluating water quality of a harbor or basin, modeling horizontal salinity distribution, defining mixing zones, and optimizing the placement of outfalls.

Modeled Alternatives. The water quality study was conducted for the three proposed lagoon alternatives. Two additional alternatives, which included slight modifications to the original open deep water lagoon alternative, were also modeled

for the purpose of investigating the feasibility of improving lagoon water quality with limited modifications to the deep water plan.

The open deep water lagoon alternative consisted of a basin, including island, covering approximately 40 acres and connected to the ocean through an entrance channel. The bottom elevation is –2.5 meters, MSL for the lagoon basin and is –3.0 meters, MSL for the entrance channel. One modified deep water lagoon alternative (referred as M1) has the same layout as the proposed alternative, except that the bottom of the inner lagoon basin elevates from –2.5 meter, MSL to –1.5 meters, MSL. The other modified deep water alternative (referred as M2) has the same lagoon basin layout as the proposed alternative, except the entrance channel being widened by 20 meters. The proposed shallow water lagoon alternative has the same lagoon layout as the open deep water lagoon alternative, however the bottom of the lagoon basin and the entrance channel will be elevated to –1.5 meters, MSL for both the lagoon basin and entrance channel. As examples, Figure 2 shows the lagoon layout and bathymetry for the open deep and shallow water lagoon alternatives.

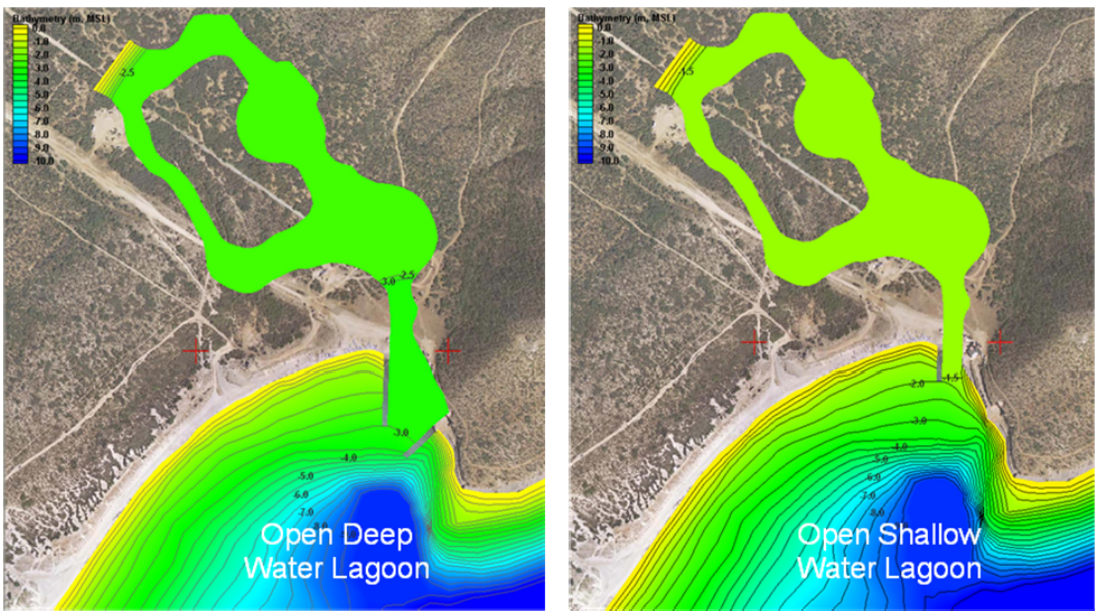


Figure 2. Lagoon Layout for Deep and Shallow Water Lagoon Alternatives

Given that no quantitative water quality standards exist for marinas and lagoons, the water quality conditions of the proposed alternatives were compared between the different lagoon alternatives and an existing marina adjacent to the project site, known as Marina Costabaja near La Paz. Therefore, the water quality study was also conducted for Marina Costabaja.

While the RMA2 and RMA4 models were used to model the water quality for the four open lagoon alternatives and for Marina Costabaja, a tidal hydraulic model was developed to model the closed salt water lagoon alternative.

In addition, the RMA2 and RMA4 models were also used to model the salinity distribution in the vicinity of the concentrated discharge of a proposed Reverse Osmosis (RO) seawater desalination plant.

The modeled scenarios/alternatives are summarized in Table 1. The models being applied and the parameters being investigated for these scenarios are also summarized in this table.

Table 1. Modeled Alternatives.

Modeled Scenarios	Modeled Parameters	Models Used
Open Deep Water Lagoon	Water Circulation & Quality	RMA2/RMA4
Open Deep Water Lagoon (M1)	Water Circulation & Quality	RMA2/RMA4
Open Deep Water Lagoon (M2)	Water Circulation & Quality	RMA2/RMA4
Open Shallow Water Lagoon	Water Circulation & Quality	RMA2/RMA4
Costabaja Marina (Reference)	Water Circulation & Quality	RMA2/RMA4
Closed Salt Water Lagoon	Water Level Fluctuation	Hydraulic Model
Desalination Plant Discharge	Water Circulation & Salinity	RMA2/RMA4

Finite Element Mesh for Open Water Lagoon Alternatives. The area of interest in evaluating the lagoon's water quality is the entire proposed area of the lagoon. However, the modeled domain was significantly expanded to cover the lagoon, the Bay of Dreams and the portion of the Gulf of California in the vicinity of the proposed lagoon. The expanded model domain was selected so that the boundary conditions would be placed away from the area of interest. This will eliminate or minimize the unduly influence by the values assigned at the boundaries of the modeled domain.

As an example, Figure 3 shows the finite element mesh that was used in the RMA2/RMA4 models to characterize the modeled domain for the open deep water lagoon alternative, and the detailed view for the project area. Although the area of the proposed lagoon was less than 14 hectares, the whole modeled domain covered an area of approximately 2,020 hectares, which extended as much as 5.5 kilometers offshore from the shoreline with the alongshore width of approximately 2.7 kilometers at the offshore boundary. The cross-shore and bi-lateral boundaries of the modeled domain were determined based on a previous modeling study of the tidal hydrodynamics in the Gulf of California (COGA, 2004), in which the tidal ellipses were predicted.

The bathymetry of the modeled domain was developed based on: (1) the proposed open lagoon alternatives for the lagoon basin and entrance channel, (2) the bathymetric survey to a water depth of –34.38 meters, MSL, and (3) the navigational chart (Chart No. 21014) for the ocean area that is beyond the bathymetric survey coverage. As an example, Figure 4 shows the bathymetric contour of the modeled domain for the open deep water lagoon alternative and the detailed view for the

project area. The bathymetry ranges from a depth deeper than –400 meters, MSL at the offshore boundary to above MSL at the shoreline.

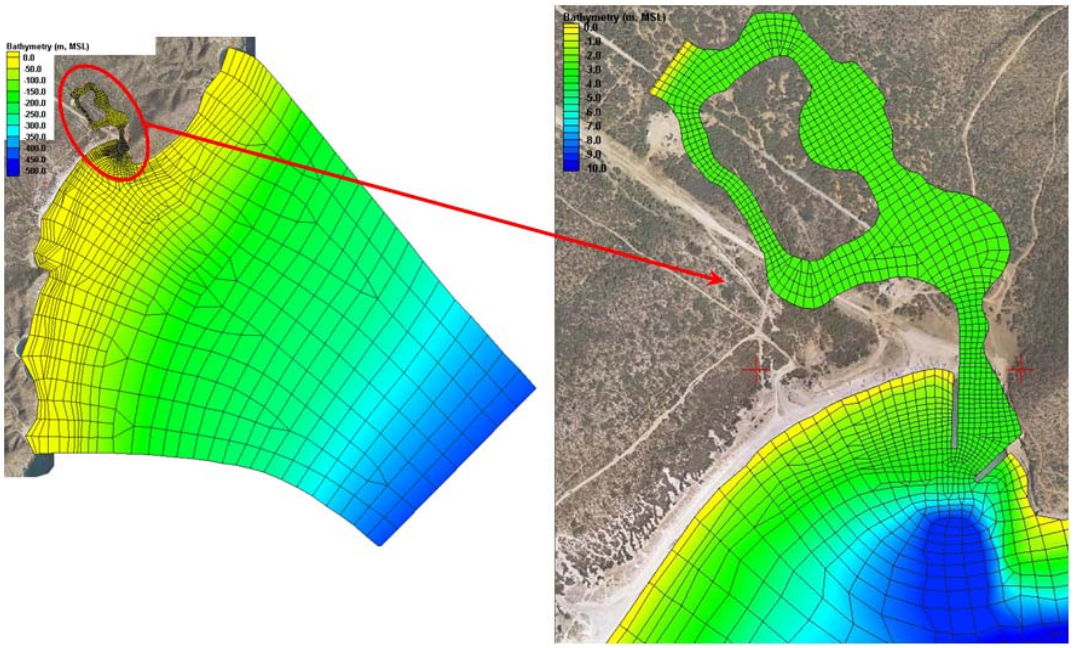


Figure 3. Finite Elements for the Modeled Domain (Open Deep Water Lagoon)

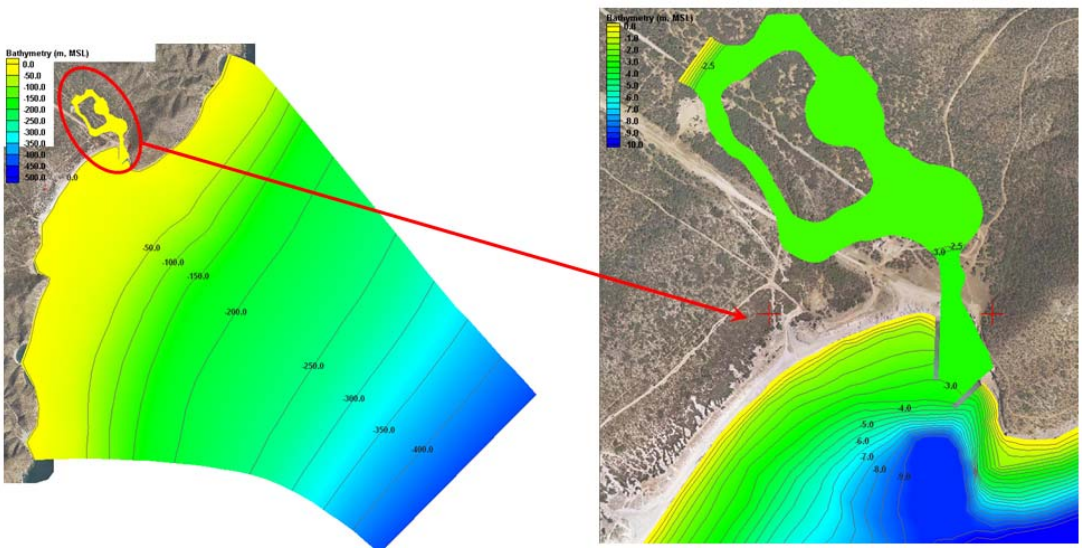


Figure 4. Bathymetry of the Modeled Domain (Open Deep Water Lagoon)

The finite element mesh and the bathymetry that were used for the offshore ocean portion of the modeled domain were the same for the four modeled lagoon alternatives. However, the finite elements and the bathymetry for the lagoon basin and entrance areas were different for various lagoon alternatives in order to accommodate the different lagoon designs.

The numbers of elements and nodes used to characterize the modeled domain are summarized in Table 2 for the four modeled lagoon alternatives and for Marina Costabaja.

Table 2. Numbers of Finite Elements and Nodes.

Lagoon Alternative	Element	Node
Open Deep Water Lagoon	2,160	6,850
Open Deep Water Lagoon (M1)	2,169	6,881
Open Deep Water Lagoon (M2)	2,211	7,001
Open Shallow Water Lagoon	2,066	6,538
Costabaja Marina (Reference)	609	1,978

RMA2/RMA4 Boundary and Initial Conditions. The boundary conditions required in the RMA2 hydrodynamics simulation include the upstream flow discharge and the downstream (offshore) water surface elevation. Since no water influx will be directed to the proposed lagoon other than through the lagoon entrance, a flow discharge of zero was specified at the land (upstream) end of the lagoon. The offshore water level boundary condition, which is the driving force for the tidal currents in the modeled domain, was specified based on the tidal elevation predicted for the Bay of Dreams. The tidal prediction of twenty days from June 22 to July 12, 2006, as shown in Figure 5, was used to represent the typical offshore water level boundary condition. This particular period spanned at least one spring tide cycle and one neap tidal cycle.

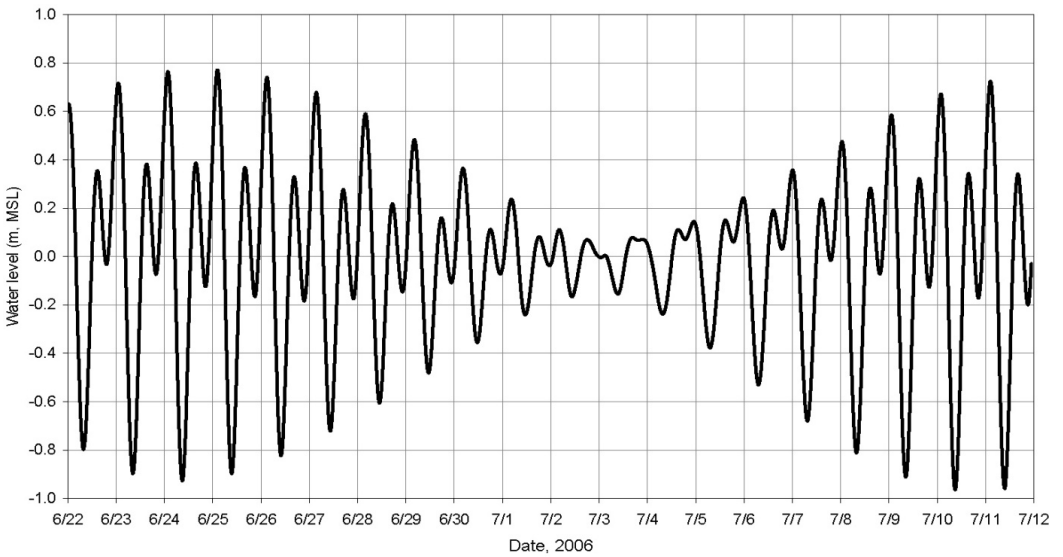


Figure 5. Representative Water Surface Elevation at Offshore Boundary.

The boundary conditions required by the RMA4 model include the constituent concentration at the boundaries. Because the water quality in the Gulf of California is

considered good, the constituent concentration was assigned to zero at the offshore boundary of the modeled domain, which is located approximately 5.5 kilometers from the proposed lagoon. Since no water will be directed into the lagoon through the upstream (land) boundary, no concentration was specified at this boundary.

The initial value of the offshore water level boundary condition was specified as the initial condition in the RMA2 hydrodynamic simulation. In the RMA4 water quality modeling, the initial constituent concentration was specified as zero for the ocean that is outside of the lagoon entrance channel, and 100 for the entire lagoon basin and entrance channel. This represents the scenario when the entire lagoon basin is initially polluted, while the ocean has good water quality.

It is noted that the same boundary conditions and the same initial conditions were specified in the water quality modeling studies for the four open lagoon alternatives and for Marina Costabaja. By specifying the same boundary conditions and initial conditions for different model scenarios, the modeled results can be compared among the alternatives and the relative difference in water quality can be assessed.

RMA2/RMA4 Model Parameters. Three major model parameters required by the RMA models include the Manning's roughness coefficient (n) and the turbulence eddy viscosity (E) in RMA2, and the constituent diffusion coefficient (D) in RMA4. Ideally, these model parameters should be calibrated using measured data in the field. However, no existing lagoon with any measurement data is available in this region. Therefore, the model parameters were selected in the modeling studies based on the values recommended in the RMA documentation (USACE, 2003) and on our past experience with RMA modeling studies (NCI, 2005 & 2002, USACE, 2003). The model parameters are summarized in Table 3.

Table 3. RMA2/RMA4 Model Parameters.

Lagoon Alternatives	Manning Coefficient (n)	Eddy Viscosity (E) (Pa-sec)	Diffusion Coefficient (D) (m^2/s)
Open Deep Water Lagoon	0.02	2,500	1.0
Open Deep Water Lagoon (M1)	0.02	2,500	1.0
Open Deep Water Lagoon (M2)	0.02	2,500	1.0
Open Shallow Water Lagoon	0.02	2,500	1.0
Costabaja Marina (Reference)	0.02	2,500	1.0

Tidal Hydraulic Model for the Closed Water Lagoon Alternative. For the closed salt water lagoon alternative, the lagoon will be connected to the ocean through pipelines instead of an open entrance channel. The inlet and outlet structures for the proposed closed salt water lagoon was designed after investigating several existing closed lagoon systems located within the San Francisco area. Based on the preliminary hydraulic model results, the lagoon bottom was designed to be at –1.0

meter, MSL. The lagoon bottom will be lowered down to –2.0 meters, MSL at the areas of the inlet and outlet structures. High-density polyethylene (HDPE) material was chosen for the proposed inlet and outlet pipelines. The layout of the proposed closed water lagoon is shown in Figure 6.

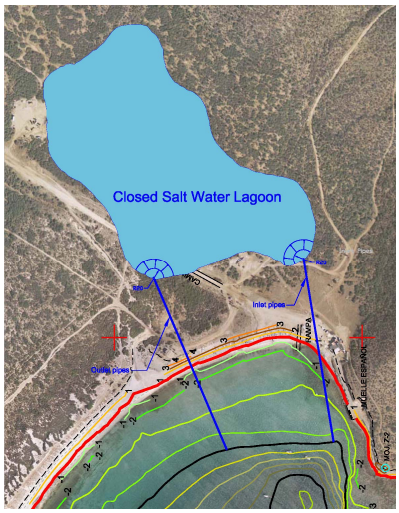


Figure 6. Layout of the Proposed Closed Salt Water Lagoon

The pipe flow, particularly when it is pressured, is beyond the capability of the RMA2/RMA4 models, which were used for the open lagoon alternatives. Therefore, a hydraulic model was developed for this closed water lagoon alternative in order to estimate the water exchange between the lagoon and the ocean via the pipelines. The hydraulic model developed for this alternative was based on the culvert/pipe hydraulics, using the energy equation together with the Manning formula. All of the flow patterns that can possibly occur in this lagoon-ocean system were considered in the hydraulic model. The duration of the hydraulic modeling conducted for this closed lagoon alternative was ninety days.

LAGOON WATER QUALITY ASSESSMENT

RMA2/RMA4 Model Results. The hydrodynamics and constituent transport were modeled for twenty days from June 22 to July 12, 2006. The modeled period spanned at least one spring tide cycle and one neap tidal cycle. The RMA2 model computed the flow field, including the water surface elevation, water depth and current velocity components, and provided flow parameters for the water quality model RMA4. The RMA4 model computed the temporal variations and spatial distributions of constituent concentrations. As examples, Figure 7 shows the snapshot of the flow field (flow velocity vectors and water depth) for a peak ebb tide for the open shallow water lagoon alternative. Figure 8 shows the snapshot of the lagoon constituent (relative) concentration in one day after releasing the constituent (concentration of 100) in the lagoon during a spring tidal cycle for the open shallow water lagoon alternative.

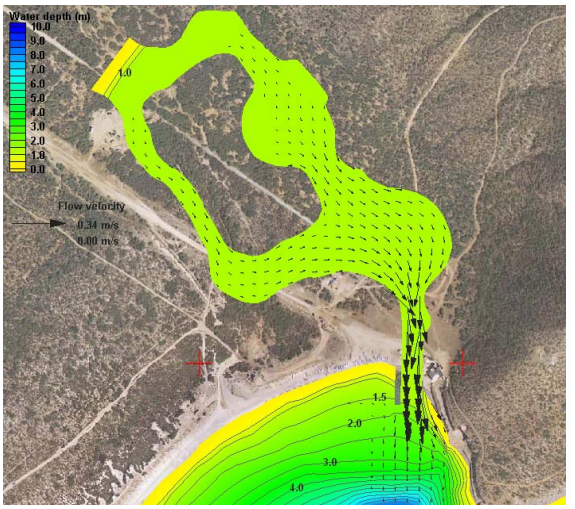


Figure 7. Flow Field at a Peak Ebb Tide.

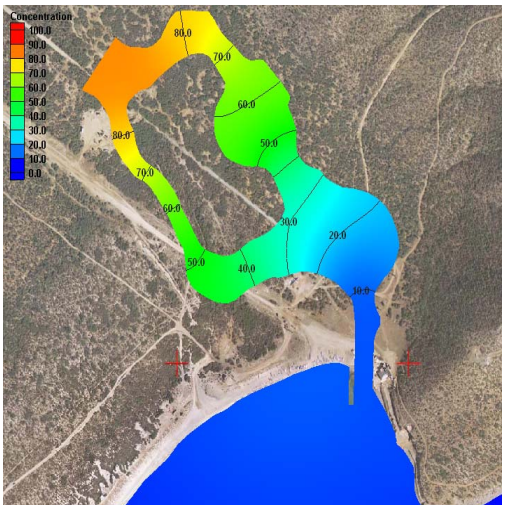


Figure 8. Constituent Concentration at Day 1.

Criteria for Water Quality Assessment. Two water quality indicators, the water exchange time and the constituent residence time, were used for the lagoon water quality evaluation. The water exchange time defines how long it takes for the water body in the lagoon to be replaced by the ambient water in the ocean. The residence time indicates how long it takes for a constituent, if present in the lagoon, to be flushed out of the lagoon.

The water exchange time was defined herein as the ratio of the lagoon storage volume at the lagoon Mean High Water level (MHW) to the water exchange volume between the ocean and the lagoon, i.e.,

$$Water\ Exchange\ Time\ (day) = \frac{Lagoon\ Storage\ Volume\ (m^3)}{Water\ Exchange\ Volume\ (m^3/day)}$$

Assuming the ocean water is brought into the lagoon by the flood tides and stays in the lagoon, and only the water originally stored in the lagoon is flushed out of the lagoon during the ebb tides, the water exchange time is the minimum time that is required for the water in the lagoon to be totally replaced by ocean water. A longer water exchange time implies that the water in the lagoon is replaced less readily by the ocean water, leading to a potentially less desirable water quality.

The residence time is another important indicator of how fast the lagoon water is renewed, and thus provides a means for assessing the lagoon water quality. A typical application to calculate the residence time across the lagoon is to hypothetically release a constituent with initially uniform concentration throughout the lagoon. The diffusion and advection process will gradually transport the constituent out of the lagoon, and thus the constituent concentration will drop with time. Quantification of the residence time at a given location is typically defined as the time for the constituent concentration to drop to *exp(-1),* or 37 percent of its initial value. A

longer residence time indicates that the lagoon water is renewed less readily by ocean water, leading to a less desirable water quality.

Water Quality Assessment and Recommendation. The water exchange time was computed based on the RMA2 model results for the open water lagoon alternatives and for the existing Marina Costabaja, and was computed based on the tidal hydraulic model results for the closed water lagoon alternative. The constituent residence time was computed based on the time series of the constituent concentration predicted by the RMA4 model for the open water lagoon alternatives and for the existing Marina Costabaja. The computed water exchange time and constituent residence time were compared between the different lagoon alternatives and the existing Marina Costabaja, from which the water quality was evaluated for different alternatives.

The basic lagoon characteristics, including lagoon size, basin bottom elevation and average water volume, are summarized in Table 4 for the proposed lagoon alternatives. Compared to Marina Costabaja, the proposed lagoons have larger sizes with shallower water depths. While the closed salt water lagoon has a smaller water volume than Marina Costabaja, the lagoon water volume for the open lagoon alternatives will be larger than Marina Costabaja.

Table 4. Comparison of Lagoon Characteristics.

Lagoon Alternative	Surface Area (hec)	Bottom Elev. (m, MSL)	Water Vol. (MSL, hec-m)
Open Deep Water Lagoon	13.4	-2.5	33.1
Open Deep Water Lagoon (M1)	13.4	-1.5 to -2.5	30.0
Open Deep Water Lagoon (M2)	13.4	-2.5	33.1
Open Shallow Water Lagoon	13.4	-1.5	19.9
Closed Salt Water Lagoon	15.3	-2.0 to -1.0	15.5
Marina Costabaja (Reference)	5.7	-3.0 to -3.6	19.5

The MWL, MHW, MLW and mean tidal range (MHW-MLW) within the proposed lagoon are summarized in Table 5 for the proposed lagoon alternatives, compared to the Marina Costabaja. Except for the closed salt water lagoon alternative, in which the fluctuation of lagoon water level will be significantly muted, no tidal muting will occur in the lagoon for the other alternatives. For the closed lagoon alternative, the MWL will be elevated to 0.20 meters, MSL, and the mean tidal range within the lagoon is merely 0.13 meters, less than 20 percent of the tide in the ocean. For the open lagoon alternatives, the tidal range will be the same between the lagoon and the ocean. This implies that the design entrance channel is large enough to provide the full water exchange potential. Enlarging the entrance channel will not facilitate the water exchange between the lagoon and the ocean.

Table 5. Comparison of Lagoon Water Levels.

Lagoon Alternative	MWL (m,MSL)	MHW (m,MSL)	MLW (m,MSL)	MHW-MLW Tidal Range (m)
Open Deep Water Lagoon	0.00	0.39	-0.37	0.76
Open Deep Water Lagoon (M1)	0.00	0.39	-0.37	0.76
Open Deep Water Lagoon (M2)	0.00	0.39	-0.37	0.76
Open Shallow Water Lagoon	0.00	0.39	-0.37	0.76
Closed Salt Water Lagoon	0.20	0.26	0.13	0.13
Marina Costabaja (Reference)	0.00	0.39	-0.37	0.76

The lagoon water volume at the MHW, the mean tidal prism and the computed average water exchange time are listed in Table 6 for the different lagoon alternatives. While the proposed closed salt water lagoon will have a water exchange time longer than the Marina Costabaja, the water exchange time for the proposed open lagoon alternatives will all be less than the water exchange time estimated for the Marina Costabaja. A shorter water exchange time will potentially lead to an overall better water quality within the lagoon.

Table 6. Comparison of Lagoon Water Exchange Time.

Lagoon Alternative	MHW Water Vol. (hec-m)	Tidal Prism (hec-m)	Water Exchange Time (Day)
Open Deep Water Lagoon	38.3	10.2	1.9
Open Deep Water Lagoon (M1)	35.2	10.2	1.7
Open Deep Water Lagoon (M2)	38.3	10.2	1.9
Open Shallow Water Lagoon	25.1	10.2	1.2
Closed Salt Water Lagoon	19.6	1.9	5.1
Marina Costabaja (Reference)	21.7	4.3	2.5

The predicted constituent residence times, after releasing the constituent in the entire lagoon, are summarized in Table 7 for the proposed alternatives. As an example, Figure 9 shows the spatial distribution of the residence time within the lagoon for the open shallow water lagoon alternative during the spring and the neap tidal cycles, respectively. Compared to the existing Marina Costabaja, the residence time for the open shallow water lagoon alternative is shorter during the spring tidal cycle and is comparable during the neap tidal cycle. For the open deep water lagoon alternatives, including the two modified alternatives, the residence time will be longer than that for the Marina Costabaja, and the difference will be larger during the neap tidal cycle. Among the three open deep water alternatives, the modified alternative M1 will have a shorter residence time than the two other alternatives.

Table 7. Comparison of Constituent Residence Time.

Lagoon Alternative	Residence Time (Days)	
	Spring Tide Cycle	Neap Tide Cycle
Open Deep Water Lagoon	5.6	8.6
Open Deep Water Lagoon (M1)	4.9	8.0
Open Deep Water Lagoon (M2)	5.6	8.2
Open Shallow Water Lagoon	3.1	6.6
Closed Salt Water Lagoon	N/A	N/A
Marina Costabaja (Reference)	4.3	6.5

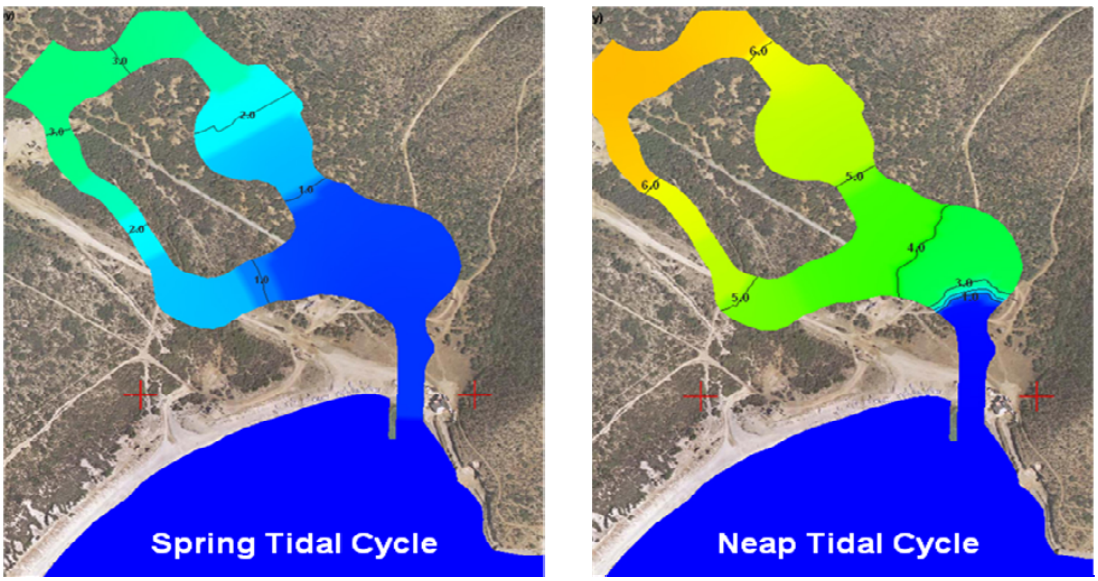


Figure 9. Residence Time (Open Shallow Water Lagoon Alternative)

Based on the comparisons of the water exchange time and the residence time estimated for the different alternatives, it was concluded that the open shallow water lagoon alternative would result in the best lagoon water quality. The lagoon water quality for this alternative will be better than the water quality of the Marina Costabaja. The water quality for the open deep water lagoon alternatives will probably be comparable to or slightly worse than the Marina Costabaja. Although the improvement to the lagoon water quality will be limited by modifying the open deep water lagoon design, elevating the lagoon bottom at the inner lagoon, as done in the M1 alternative, is recommended in order to achieve a better water quality. The closed salt water lagoon will have less lagoon water quality when compared with the open lagoon alternatives, because of the decreased water exchange capability of the pipes.

Mechanical mixing measures are recommended in order to improve the water quality for either the closed salt water lagoon or the open deep water lagoon alternative. As

the model results indicate, the water quality at the inner lagoon basin, which is furthest from the lagoon entrance or inlet/out structures, will be worse than for the outer lagoon, where the water and the constituent, if present, can be exchanged more easily with the ambient water of the ocean. Therefore, mechanical mixing equipment was recommended to be installed within the inner lagoon basin. This equipment will provide an auxiliary means to improve the local water circulation and intensify flow turbulence, and thus facilitate the advection and diffusion process of the constituent, resulting in an improved water quality within the inner lagoon basin.

ENVIRONMENTAL IMPACT OF DESALINATION PLANT DISCHARGE

A Reverse Osmosis (RO) seawater desalination plant is proposed as part of the real estate development in order to produce freshwater with a maximum production rate of 2 million gallons per day (MGD). The concentrated seawater, as the byproduct of the RO seawater desalination facility, will be directly discharged to the ocean at a discharge rate of 3 MGD. After the preliminary analysis, the design salinity of the concentrated seawater was set to 70 grams per liter, or 70 parts per thousand (ppt).

The average ambient salinity in the lower Gulf of California is approximately 35 ppt. Salinities ranging from 32 ppt to 34 ppt were measured during an oceanographic investigation conducted immediately offshore of the proposed desalination facility. Since the marine species may be sensitive to the salinity change, it is useful to estimate how fast the concentrated salinity is diluted and define a zone where noticeable impact may exist to the environmentally sensitive habitats. Therefore, a water quality modeling study was conducted, using the RMA2 and RMA4 models, to predict the distribution of salinity when the concentrate with a salinity of 70 ppt is constantly discharged to the ocean.

Without an oceanographic investigation of the aquatic life in the offshore area of the desalination plant, the discharge was assumed to be located at a water depth of –19.38 meters, MSL in this modeling study. The location of the discharge was selected because: (1) the offshore bottom slope starts to steepen as the water depth becomes deeper, and (2) this location is away from the rocky and reef area where more marine species may be present.

As examples, Figure 10 and Figure 11 show the snapshots of the predicted salinity distribution in the vicinity of the concentrated discharge at a low tide condition and at a peak tidal current condition, respectively. The model results indicate that the proposed brine discharge will have an impact on the marine environment within a 60-meter diameter area, where salinities will be higher than 40 ppt, and an insignificant impact within a 200-meter diameter area where salinities vary between 36 ppt and 40 ppt. It is noted, for reference purposes, that salinities at the bay range between 32 ppt and 34 ppt. The optimal location for the outfall has yet to be defined, where a compromise between minimum environmental damage can be achieved at the same time capital investment is reduced by locating the outfall closer to the shore. A

complete inventory and map of the marine life in the bay was recommended to guide this process.

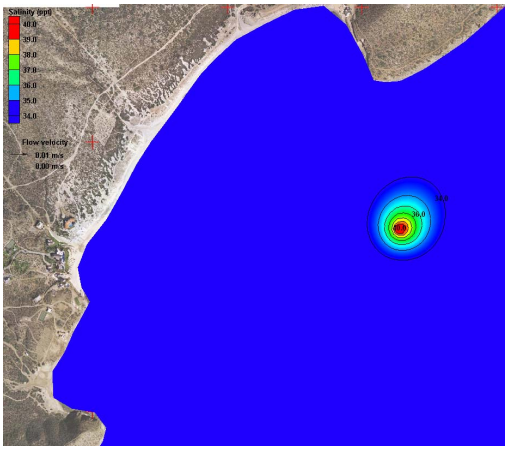


Figure 10. Salinity Near Discharge (Low Tide)

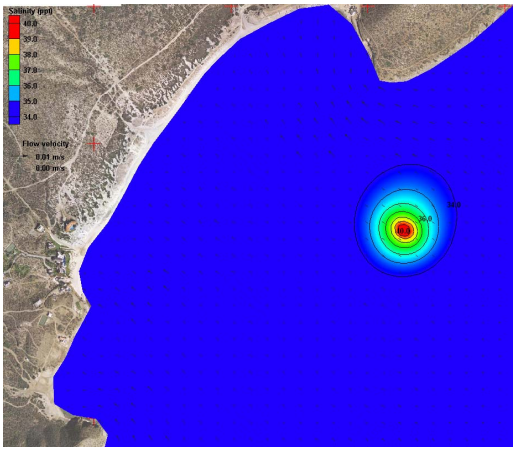


Figure 11. Salinity Near Discharge (Peak Flood Tide)

REFERENCES

COGA Consultoria Ambiental, 2004: Informe Ensenada de Los Muertos.

Noble Consultants, Inc, 2005. "Numerical Modeling Study for Yosemite Canal Wetlands Restoration", prepared for California Park and Recreation.

Noble Consultants, Inc, 2002. "Constructed Treatment Wetland Feasibility Study, Chapter 6" prepared for Marine Corps Base Camp Pendleton, California.

Norton, W. R. and King I. P., 1977. "Operating Instructions for the Computer Program RMA2-2V", Resource Management Associates, Lafayette, CA.

USACE-LAD, 2003. "Engineering Design and Evaluation of San Onofre Lagoon Enhancement", Camp Pendleton, California, prepared by Noble Consultants Inc.

USACE, 2003. "Users Guide to RMA2 WES Version 4.5".

USACE, 2003. "Users Guide to RMA4 WES Version 4.5".

HYDRAULIC EFFECTS OF PROPOSED KNIK ARM CROSSING

J. Colonell, PE, PhD., F.ASCE[1], P. Mineart, PE, M.ASCE[2], and J. Gambino, PE[2]

[1]ERM, 341 W. Tudor Rd., Suite 206; Anchorage, AK; *Jack.Colonell@erm.com*
[2]URS Corporation, 1333 Broadway, Suite 500; Oakland, CA;
Phillip_Mineart@urscorp.com, *Jeanne_Gambino@urscorp.com*

1.0 ABSTRACT

Knik Arm, an extension of Upper Cook Inlet, with the world's second highest tides, seasonal ice cover, and prodigious sediment load, presents unique challenges to the design and construction of a highway crossing. The current concept for a proposed Knik Arm Crossing (KAC) structure includes earthen-fill approaches from either side, connected by an 8,180 ft (2,493 m) pile-supported bridge, to span the 12,500-ft (3,810 m) width of Knik Arm at the preferred alignment. Described herein are the methods, results and conclusions of analyses performed for an assessment of the effects of KAC on the hydraulic environment of Knik Arm. Principal effects include increases in maximum current speed of ≤10% within 1.3 mi. (2.2 km) of KAC. Except for expected sediment accumulations on both sides of the earthen-fill portions of KAC, no significant changes in sedimentation processes are expected beyond the immediate vicinity of KAC.

2.0 INTRODUCTION

Knik Arm Crossing Project: More than 80 years of transportation, land use, and economic plans and studies for the Upper Cook Inlet region of Alaska have identified the need to connect Anchorage with the Matanuska-Susitna Borough on the north side of Knik Arm. In 2003 the Alaska State Legislature established the Knik Arm Bridge and Toll Authority (KABATA) as a public corporation of the State of Alaska within the Department of Transportation and Public Facilities. The legislative mandate for KABATA is to "… further the development of public transportation systems in the vicinity of the Upper Cook Inlet with construction of a bridge to span Knik Arm and connect the Municipality of Anchorage and the Matanuska-Susitna Borough."

The Knik Arm Crossing project (KAC) is being developed to meet the current and projected transportation needs of the Municipality of Anchorage and the Mat-Su Borough. KABATA's goal is to construct a cost-affordable, vehicular

toll bridge of about 2.7 miles (4.3 km) across Knik Arm to join the Port of Anchorage area and Port MacKenzie area, as well as 19 miles (30 km) of road to support the bridge's accessibility (Figure 1).

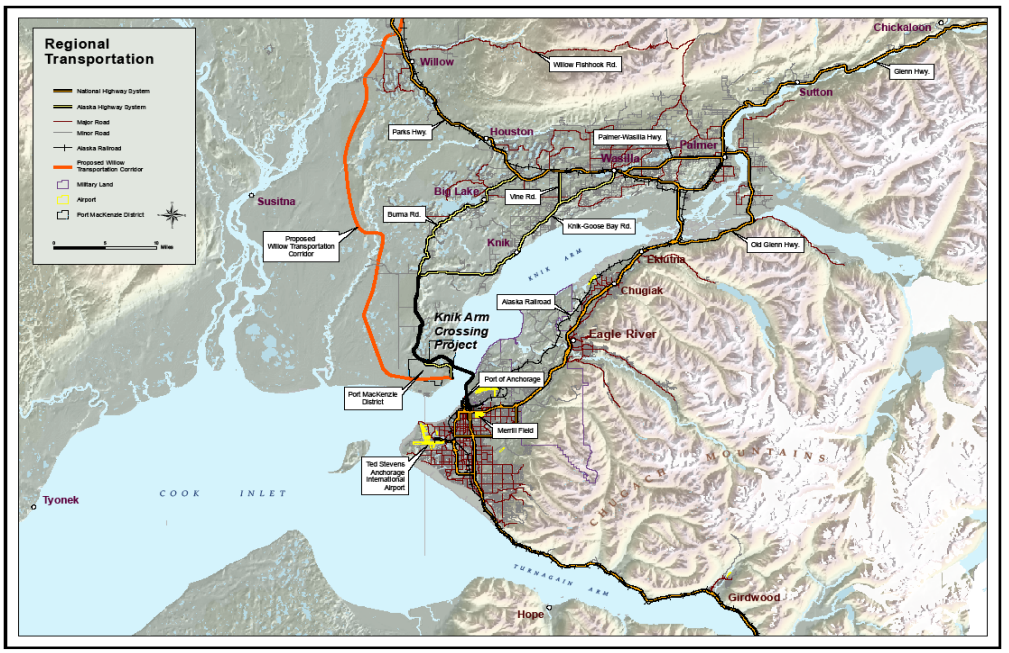


Figure 1. Knik Arm Crossing Project Location

Responding to the requirements of the National Environmental Policy Act (NEPA) of 1969, the Federal Highway Administration (FHWA) undertook preparation of an Environmental Impact Statement (EIS) to evaluate the proposed KAC. In accordance with the NEPA process, the EIS addressed all effects of highway approaches, as well as the effects of the KAC on the water body of Knik Arm. While the hydrodynamic effects of KAC were summarized in the EIS (FHWA 2007), the entire study was addressed in a separate report (HHEKA 2007), which was one of many prepared in support of the overall EIS.

Two alternatives have been proposed for the configuration of KAC: Alternative 1 (Figure 2) consists of earthen-fill approaches extending from either side of Knik Arm, connected by a pile-supported 8,180 ft (2,493 m) roadway. Alternative 2 would have same alignment but would consist entirely of a pile-supported roadway with a total length of approximately 14,000 ft (4,270 m), including the curved portions of the roadway on both sides of Knik Arm. This paper describes the methods, results and conclusions of analyses performed for an assessment of the effects of the KAC Alternative

1 on the hydraulic environment of Knik Arm. As hydraulic effects of Alternative 2 are benign, all subsequent discussion refers to Alternative 1, and then simply as KAC.

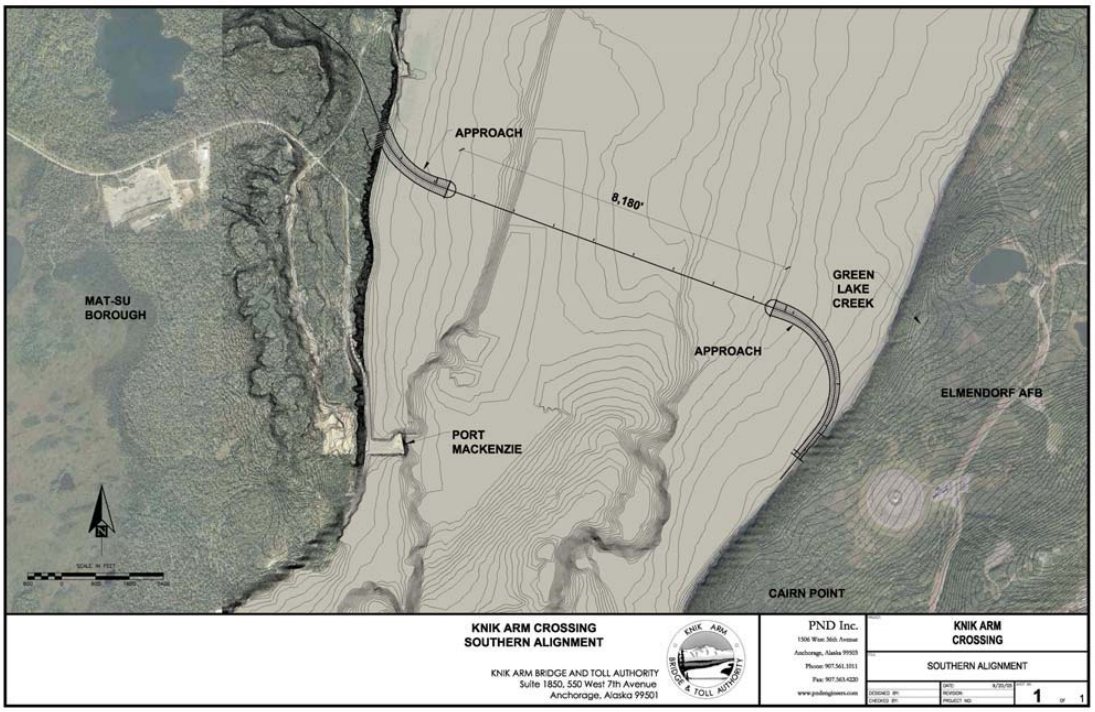


Figure 2. Knik Arm Crossing Project - Alternative 1

Study Objective: KAC is capable of altering flow patterns in its immediate vicinity, as well as altering sedimentation processes in Knik Arm. The objective of this study was to implement analytical methods that would address all reasonable environmental concerns and to provide quantitative measures of changes (potentially) induced by each alternative. Environmental effects that are required to be addressed by NEPA can be categorized as *direct, indirect* and *cumulative.*

Direct effects of the KAC on the physical environment of Knik Arm include potential alterations of the following large-scale processes: (1) Tide stage and phase; i.e. amplitude and timing of water surface elevation (WSE) changes due to tidal action; and (2) Flow velocities, especially beneath bridge but also "downstream" of bridge to the extent that such alterations are "significant" and of environmental concern.

Indirect physical effects of the KAC include alterations of the sedimentation environment (erosion and accretion), as a result of changes in the hydraulic

regime of Knik Arm. Other indirect effects of altering Knik Arm hydraulics are those that might be experienced by the biota of Knik Arm, and are addressed in the biological technical reports.

Cumulative effects of KAC would be those that either enhance, or are enhanced by, similar effects of past, present, or reasonably foreseeable future actions within Knik Arm. For KAC, only those projects capable of altering the hydraulics of Knik Arm were considered for cumulative effects analysis. Construction of Port MacKenzie is an existing "recent past" project of concern, while the planned expansion of the Port of Anchorage (POA) is a "future" project of concern for cumulative effect analysis.

3.0 KNIK ARM ENVIRONMENT

Bathymetry: Knik Arm is a northeasterly extension of Upper Cook Inlet. Central Knik Arm deepens from the adjacent seabed of Upper Cook Inlet, especially at the constriction between Point MacKenzie and Point Woronzof (Figure 1), where depths in the central channel are 50-100 ft (15-30 m), being generally greater on the north (Pt. MacKenzie) side. Another constriction occurs near Cairn Point, about 1.4 mi. (2.2 km) southwest of the KAC alignment (Figure 2). The channel deepens to as much as 177 ft (54 m) near Cairn Point, then shoals northeastward to 60-70 ft (20 m) at the KAC alignment. A trench in the middle of Knik Arm broadens north of the depression near Cairn Point and shoals northward.

To the northeast the channel shallows further and broadens into extensive tidal flats where maximum depths are 10-15 ft (3-4 m). The tidal flats extend for a distance of over 15 miles (28 km) to where the Knik and Matanuska Rivers discharge into Knik Arm. An analysis of bathymetric data for Knik Arm, collected over six decades suggests that the seabed is relatively stable (HHEKA, App. II)

Several rivers and creeks provide substantial quantities of sediment to Knik Arm, although quantitative information is sparse. The major contributors are the Knik and Matanuska Rivers, for which limited data exist. Both of these rivers carry suspended sediment concentrations (SSC) that exceed 1,000 – 2,000 milligrams per liter (mg/L). Mobile sediments near the proposed KAC alignment exist in two regimes: a sandy mobile bed saltation, and finer silt and clay particles in suspension above. The characteristics of these two

regimes of sediment in Knik Arm were investigated during extensive field studies (HHEKA, Apps. I, V).

Tides and Tidal Currents: Tides in Knik Arm are semi-diurnal with a substantial inequality between two high water and two low water levels that occur each day. The NOAA tide recorder at POA has a 29 ft (8.9 m) diurnal range and recorded extremes as high as 34.5 ft (10.5 m) above and 6.4 ft (1.9 m) below MLLW. The tidal range increases north of Cairn Point with currents modified by the changing bathymetry. Measurements performed for this study show that ebb flows are stronger than flood flows in the vicinity of the proposed bridge alignment, and that current speeds of over 12 ft/s (3.6 m/s) are common (HHEKA, App. V). Velocity transects generated with an acoustic Doppler current profiler (ADCP) indicated maximum ebb flows of about 4 million ft^3/s (11,300 m^3/s).

Water Properties: In upper Knik Arm, summertime salinities range from 4 to 8 PSU (Practical Salinity Units, equivalent to grams of dissolved solids per kilogram of sea water). In winter salinities are higher, but liquid water remains brackish. Temperatures vary seasonally but, during summer, generally remain less than 50° F (10° C.) in upper Knik Arm near the proposed bridge alignment. In winter rafts of sea ice form during prolonged periods of subfreezing temperatures.

Suspended sediment concentrations (SSC) measured during site investigations (HHEKA, Apps. I, V) using optical backscatter (OBS) instruments, showed SSC as high as 5,000 mg/L. OBS measurements were calibrated with SSC in water samples, which were collected nearly simultaneously. Vertical profiles of OBS were collected from a survey vessel in conjunction with water property profiles throughout the project area (HHEKA, App. V). Also, OBS measurements were obtained at a stationary position near the surface for one month (July 10 to August 16, 2005) as a component of measurements on a tethered mooring.

Additional samples of Knik Arm seawater were collected during supplemental field studies in September 2006, for the purpose of determining extent of spatial and temporal variations of SSC at the seaward boundary of the study area. The SSC samples were also used for measurements of sediment settling velocities (HHEKA, App. IX). The latter were subsequently used to define boundary conditions for input to the sediment transport model.

4.0 ANALYSIS

Approach: The usual approach to analysis of large-scale effects (i.e. length scales > 500 ft [150 m]) in a hydraulic regime such as Knik Arm is to construct a model of the base case (i.e., the unaltered environment), into which the proposed KAC can be introduced to observe how it alters the hydrodynamic environment.

An extensive list of criteria for an appropriate modeling approach resulted in selection of the Danish Hydraulic Institute (DHI) MIKE 21 suite of hydrodynamic models (*http://www.dhi.dk*). A key factor in the selection of these DHI programs is that Knik Arm, because of its vigorous tides, is a well-mixed water body, so flow patterns can be represented adequately by vertically averaged velocities within the water column.

A further consideration in the selection of MIKE 21 was our experience in assessing effects of the expansion of San Francisco Airport (SFO), which included extension of runways into south San Francisco Bay. Utilization of MIKE 21 was monitored and critiqued at every step of the analysis by a blue-ribbon panel of experts assembled by the National Academy of Science for the specific purpose of overseeing this aspect of the EIS prepared by the Federal Aviation Administration for the SFO expansion (FAA 2003).

Model Description and Application: MIKE 21 is a two-dimensional, free-surface flow modeling system that simulates hydraulics and hydraulics-related phenomena in estuaries, coastal waters and seas where stratification can be neglected. It simulates the changes in water levels and velocities in response to tides, wind, and freshwater inflows. It solves the time-dependent, vertically integrated equations of continuity and conservation of momentum in two horizontal dimensions, which are solved by a finite difference method. Water levels and flows are resolved on a rectangular grid covering the area of interest. Inputs include bathymetry, bed resistance, wind velocities, and hydrographic boundary conditions (e.g., tides and inflows).

A nested grid was used to model Knik Arm. The largest grid covered the entire domain and consisted of more than 36,000 135 m (443 ft) square grid cells. Along the KAC corridor, a denser grid of 45 m [148 ft]) cells was nested within the larger grid. Near the distal ends of the earthen berms, the computational grid was further subdivided into 15 m (49 ft) cells.

The seaward boundary of the model was initially placed on a line that connects Point MacKenzie to Point Woronzof, but was subsequently moved to the west end of Fire Island (Figure 1) in response to a review by the USACE Coastal Hydraulics Laboratory (HHEKA, Apps. VIII, IX). The model domain extends northeasterly direction to the bridges over the Matanuska and Knik Rivers.

The model was driven by tidal records obtained from the NOAA tide gauge at POA, transferred to the Fire Island boundary. Water surface elevation, current velocities, and SSC were calibrated and validated to Knik Arm conditions with extensive data sets developed during 2002, 2004, and 2005. The validated model then served as the base case against which perturbations to the marine environment, as introduced by KAC, could be evaluated for their potential environmental impacts. Figure 3 is an example of the comparison between predicted and measured current speeds from one of the tethered moorings.

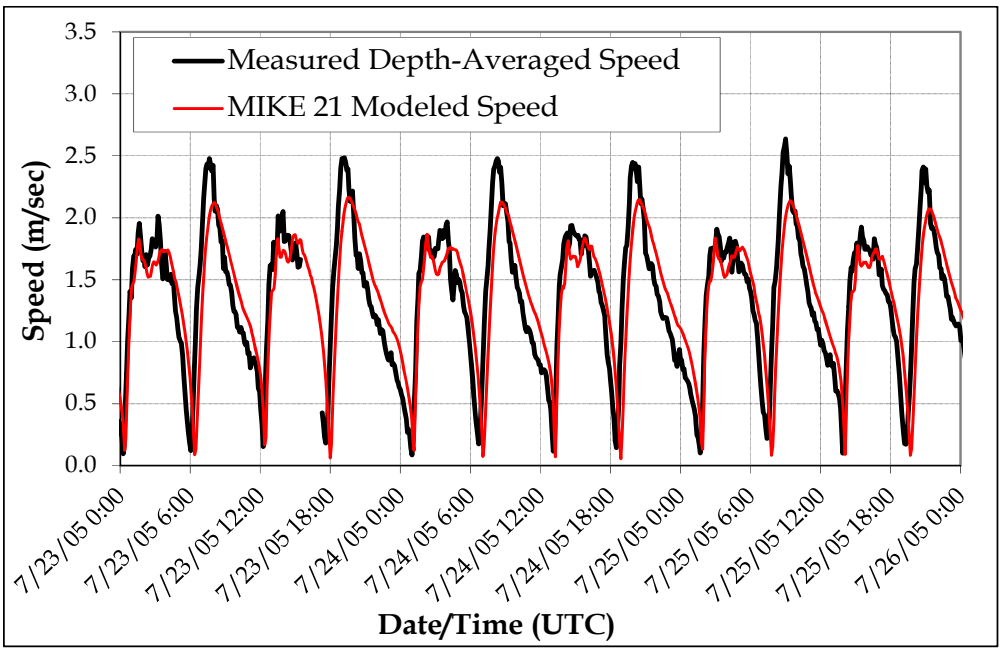


Figure 3. Comparison of Modeled and Measured Current Speed at the West Bridge Mooring During a High Spring Tide.

Comparison of the unperturbed ("Base Case") conditions to those as altered by introduction of KAC into the model then provided the basis for evaluation of the changes to the environment. Model selection criteria, details of model setup, application to Knik Arm, model performance, presentation and interpretation of computational results are all described in detail in the hydrodynamic modeling report (HHEKA, Apps. III, IX).

5.0 RESULTS

Tide Amplitude and Phase: The approach embankments of KAC will impede the flow past the bridge location, resulting in a slight decrease in the WSE and a lag (delay) in the tide north of the bridge. This was computed in terms of the differences in M2 amplitude and M2 phase, between Base Case and KAC. M2 is the major tidal component, accounting for about two-thirds of the total tidal fluctuation and, as such, provides a convenient metric for project effects on tides within Knik Arm.

During maximum spring flood tide the reduction in M2 amplitude diminishes northward from about 15 cm (0.5 ft) at the bridge to about 5 mm (0.002 ft), within 3 km (2 mi) of the bridge alignment. The decrease in WSE at the bridge is due primarily to the increased flow velocity through the bridge opening. North of the bridge, the decrease reflects a slight reduction in the tidal prism due to the narrowing of the channel cross-section at the bridge. The tide lags by about 1 minute north of the bridge, reflecting the slight decrease in conveyance capacity through the bridge, which in turn, delays the draining of the area north of the bridge. At the bridge location the tide is lagged by about 1 to 3 minutes, reflecting the increased time needed to drain the area behind the embankments.

Tidal Currents: During both flood and ebb tides, the modeling showed as expected that there is an acceleration of the flow through the proposed bridge alignment due to reduction in cross-section of the available flow channel. However, this effect is greater during ebb tide because the southward flow is laterally constrained until it passes Cairn Point. With KAC this effect is enhanced somewhat, and modeling results indicate that both of the eddies that flank the main channel flow would be strengthened slightly.

During flood tide, there is a net increase in maximum current speed north of the bridge of 0.2 to 0.3 meters per second (m/s) (0.6-1.0 feet per second [ft/s]). Behind the approach embankments there is a decrease in maximum current

speed of over 1 m/s (3.3 ft/s), mostly north of the bridge. As with the Base Case, effects during ebb tide are greater than during flood tide (Figure 4).

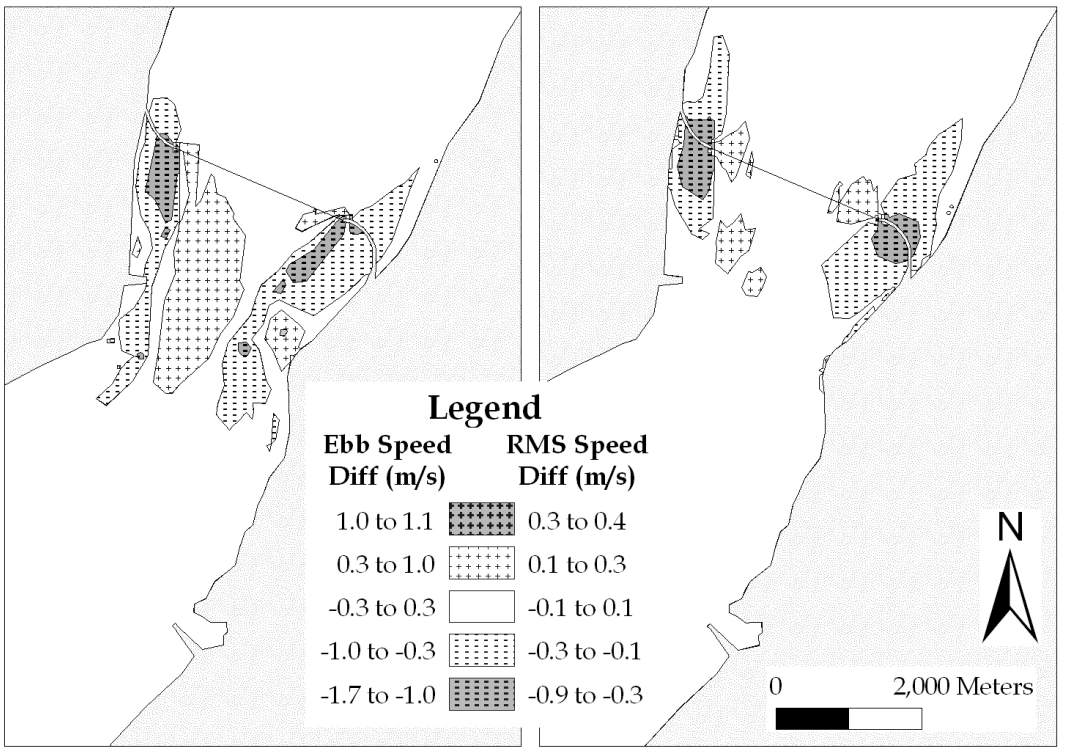


Figure 4. KAC effects on maximum spring ebb currents (left) and root-mean-square current speeds (right).

The modeling results depicted in Figure 4 (left) are the *maximum* effects of KAC on typical *spring* tide events, and are thus indicative of conditions that occur during peak flood and ebb, which have durations of 2-3 hours for only a few days each month.

A long-term measure of KAC effects on Knik Arm tidal flows is provided by differences in the root-mean-square (RMS) tidal flow speeds, which are also more meaningful for consideration of potential sedimentation effects because they represent time-averaged changes in the current speed. Figure 4 (right) indicates that the greatest RMS speed changes would be near the distal ends of the approach embankments (0.1 to 0.3 m/s [0.4-1.0 ft/s]). Meanwhile, it is expected that midchannel RMS current speeds would increase by generally less than 0.1 m/s (0.4 ft/s). The implications of these impacts on Knik Arm hydraulics would mostly be related to erosion and accretion of sediment and suggest that, overall, the long-term effects of an 8,200-foot alternative on tidal currents would be very localized (HHEKA 2007).

Sedimentation: Figure 5 shows the changes in sedimentation rates attributable to KAC as calculated over a period 30 days using tidal input from 5/11/04 to 6/11/04. Since the seabed morphology was not updated during the model simulations, these represent only the changes in maximum sedimentation *rates* that would be expected. That is, *positive* rates could be expected to decrease over time, as the channel deepens, causing flow speeds to increase and sediment to remain in suspension longer. Conversely, *negative* rates would imply erosion of the channel as it achieves a new sedimentation equilibrium. This feedback was not included in the model simulations.

These results suggest that the KAC would cause increased rates of deposition on either side of the bridge embankments, as well as near Port MacKenzie and at the northern end of the POA. The rate of deposition would generally decrease starting from the midpoint of the dock face at the POA and would continue to decrease along the shoreline to Point Woronzof. As already noted, these computed rates are most appropriately considered as *trends* in sedimentation processes because they do not represent the complex process of the channel's adjustment to a new sedimentation equilibrium.

Cumulative Effects: Cumulative effects of the proposed KAC would be those that either enhance, or are enhanced by, similar effects of past, present, or reasonably foreseeable future actions within Knik Arm. For the proposed KAC, only those projects capable of altering the hydraulics of Knik Arm were considered for cumulative effects analysis. Port MacKenzie is an existing "past" project of concern, while the current expansion of the POA is a "future" project of concern for cumulative effect analysis. Modeling performed to analyze cumulative effects followed the same approach as previously described for determining the direct effects of KAC; namely, the differences between selected hydrologic measures (e.g. tides, currents, and sedimentation) were determined quantitatively by calculating differences between Base Case (no KAC) and with KAC in place. While modeling can produce numerical results for current speed changes, state-of-the-practice modeling of sedimentation rates is limited to qualitative predictions of changes.

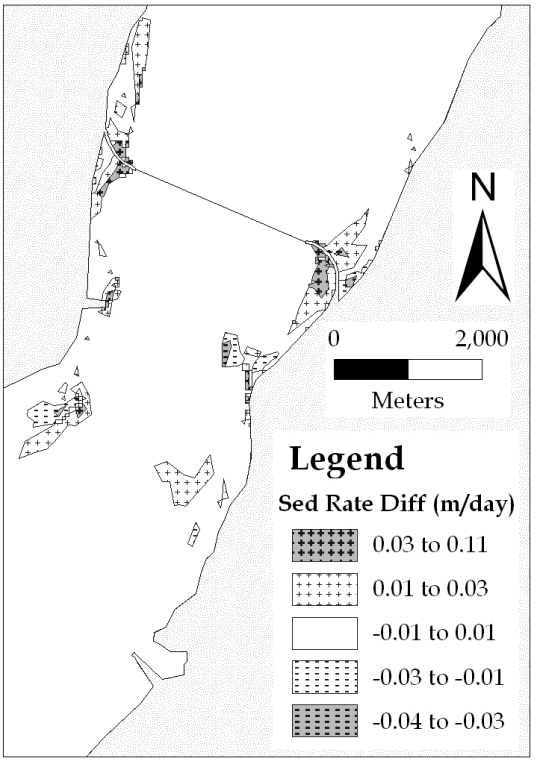


Figure 5. Differences in Maximum Sedimentation Rates Between the Base Case and KAC Alternative 1 (KAC rates – Base Case rates).

Port MacKenzie: Located on the west shore of Knik Arm approximately 1.2 mi. (1.9 km) south of the proposed west terminus of KAC, Port MacKenzie is an 800 x 400 ft (240 x 120 m) gravel-fill dock that extends into Knik Arm to a water depth of –20 ft (6 m) (re: MLLW). Changes in peak current speeds, which occur during spring tide conditions, are of interest although these changes manifest for only a few hours each month. Of greater significance are long-term average changes to current speeds, computed as RMS values, because these are more relevant to changes in sedimentation processes. Results for Port MacKenzie are as follows.

- Peak ebb tide current speed (< 2 hr duration): Decrease of 2 ft/s (0.6 m/s);
- Peak flood tide current speed (< 2 hr duration) : ≤ 0.5 ft/s (0.15 m/s);
- RMS (28-day) speed: ≤ 0.5 ft/s (0.15 m/s) decrease; and
- Sedimentation rate: Expect increase (minimal) due to RMS speed decrease.

Port of Anchorage: The expansion of the POA was initiated in 2007 and is planned for completion by 2012. By placing gravel fill along the present dock face in several separate stages, the dock face of the port will be moved 500 to 1,000 ft (150 – 300 m) seaward. When completed, the port dock face will extend approximately 1.6 mi. (1.9 km) from the south end of the present port facility northward nearly to Cairn Point. Numerical results are the result of subtracting the Base Case from the KAC case with following results.

- Peak ebb current speed (< 2 hr duration); Increase of 1.6-2.5 ft/s (0.3-0.8 m/s)
- Peak flood current speed (< 2 hr duration); Increase of 0.3-0.7 ft/s (0.1-0.2 m/s);
- RMS (28-day) speed: 1-2 ft/s (0.3-0.6 m/s) increase; and
- Sedimentation rate: Expect decrease due to RMS speed increase.

6.0 CONCLUSIONS

Hydraulic Effects of Knik Arm Crossing:

Tide stage (water surface elevation) and phase (timing): Project will slightly impede flow past bridge location, resulting in a slight decrease (~0.05 ft / 0.02 m) in the water surface elevation (WSE) and a lag (~ 1 min.) in the tide north of the bridge.

Current velocities (maximum values): During both flood tide (northward flow) and ebb tide (southward flow), the flow will accelerate as it passes between the embankments. This effect will be greatest during the maximum spring ebb, when increased current speeds may extend 0.8 mi. (1.3 km south of Cairn Point (see figure above for location) before the speed increment attributable to the project diminishes to pre-project conditions. The largest increase in current speed would be about 2 ft/s (0.6 m/s), occurring mostly in the west half of Knik Arm about 0.5 mi. (0.8 km) north of Cairn Point. During maximum (spring) flood tide conditions, the maximum current speed increment would be about 1 ft/s (0.3 m/s) and confined to less than 0.5 mi. (0.8 km) north of the KAC alignment. Base Case (no project) maximum current speeds in these areas are ≥ 10 ft/s (3 m/s).

Current velocities (mean values): The maximum effects described above would occur only during the higher spring tides that occur *once in each*

monthly tidal cycle. Root-mean-square (RMS) values of current speed changes provide more meaningful measure for consideration of sedimentation effects that are time-averaged effects of the current speed changes. The *largest* changes in RMS values of current speeds would be less than 1.0 ft/s (0.3 m/s), occurring near the distal ends of the embankments.

Sedimentation Effects of KAC Alternative 1: Knik Arm has a large suspended sediment load with maximum concentrations ≥ 5,000 mg/L. Additionally, deposition rates can be large, sometimes amounting to several feet occurring during spring and summer months near the Port of Anchorage, thus necessitating annual dredging by the Corps of Engineers. However, limited data on sediment transport in Knik Arm necessitated application of the model for prediction of changes in sedimentation *rates* only, rather than absolute quantities of erosion or deposition.

Rates of deposition would increase substantially on both sides of the approach embankments, resulting in sediment "fillets," similar to those observed at the Port Mackenzie dock.

Rates of deposition are expected to *decrease* slightly along the east shore of Knik Arm, south of Cairn Point, although along the west shore some *increase* in depositional rates would be expected north and south of the headland opposite Cairn Point. However, the rates predicted for both sides are likely within the margin of error for such computations.

Rates of sedimentation in the vicinity of the Port of Anchorage were predicted to be affected very minimally and not likely measureable.

Environmental Impacts: Environmental impact evaluations were obtained by comparision of analytical results for Base Case (i.e. no bridge) against KAC alternatives:

Hydraulic effects of KAC Alternative 1 (earthen approach embankments, with 8,200-ft bridge), while possibly measureable, would be benign.

Sedimentation effects of KAC Alternative 1, would appear mainly as "fillets" on both north and south sides of the approach embankments.

Athough minor changes in sedimentation rates are predicted by the model along both shores of Knik Arm south of Cairn Point, these changes are small and likely within the margin of error for such computations.

7.0 REFERENCES

FAA (Federal Aviation Administration). 2003. Proposed SFO Runway Reconfiguration Project: Predicted Changes in Hydrodynamics, Sediment Transport, Water Quality, and Aquatic Biotic Communities. Final Technical Report prepared by URS Corporation. Burlingame, CA.

FHWA (Federal Highway Administration). 2007. Knik Arm Crossing: Final Environmental Impact Statement and Final Section 4(f) Evaluation. Prepared for Federal Highway Administration. Prepared by Knik Arm Bridge & Toll Authority and Alaska Department of Transportation & Public Facilities. Available at *http://knikarmbridge.com/project_docs.html*

HHEKA (Hydrology and Hydraulic Environment of Knik Arm). 2007. Prepared for Knik Arm Bridge and Toll Authority, Alaska Dept. of Transportation and Public Facilities, and Federal Highway Administration. Prepared by HDR Alaska, URS Corporation, and ENTRIX, Inc. 72 p. + 9 app. *http://knikarmbridge.com/Tech_Reports/start.html*

A Joint Hydraulic/Structural Methodology for the Rehabilitation of the Crescent City Marina

J. O. Toilliez, PhD, PE†‡ and M. P. Jorgensen, PE†

†Marine and Coastal Engineers, Ports and Terminals Department, Ben C. Gerwick, Inc. COWI USA, 1300 Clay St Suite 700 Oakland, CA 94612; PH (510) 839-8972
‡ Author to whom correspondence should be addressed. email: jnot@gerwick.com

ABSTRACT

To date, proper design guidelines and codes are somewhat incomplete with respect to addressing natural coastal hazards such as tsunamis in the design of marine projects. This paper illustrates how a way forward was devised by specifically elaborating on tsunami-induced loads within the context of the Crescent City marina rehabilitation.

Specifically, the methodology implemented herein focuses on defining a set of reasonable design hydrodynamic loads for floating and fixed structures in the Crescent City harbor. This task is part of an on-going master plan initiated after the 2006 Kuril Island tsunami. The technical focus is on establishing the direct effects of a tsunami wave upon moored vessels, floats, and pilings. The purpose is to mitigate tsunami damage by adequately designing all constitutive elements of the rehabilitated marina. This analysis is at the interface between large-scale models of tsunami propagation and the need of marine structural designers for robust loading constraints. To do so, a Boussinesq model is deployed. An overview of the results gathered from the numerical simulations is presented, along with a summary of structural solutions retained to mitigate future damage.

More broadly, the work and analysis described in this paper show that the application of a judiciously parameterized conventional numerical model is capable of delivering readily-useable loads that are in good agreement with observed eyewitness measurements of tsunami action. In doing so, we hope to show that the inclusion of tsunami loads within design codes can be achieved efficiently.

INTRODUCTION

The March 2011 Tsunami

On March 11, 2011, a 9.0-magnitude underwater earthquake triggered a massive tsunami causing extensive damage to the northern shore of Japan and claiming over 13,000 lives. The "Great East Japan Earthquake" [1] radiated waves of historic proportions all across the Pacific causing the Hawai'i-based Pacific Tsunami Warning Center to issue a Pacific-wide tsunami warning. On the North American Pacific coast, significant surges were recorded in British Columbia, California and Oregon. In

particular, Crescent City was severely hit. Despite the distance separating it from the epicenter, waves exceeding 8ft (per NOAA tide gauge ID 9419750) in height formed a powerful river-like current in the marina, tearing apart docks, gangways and floats. Four people were swept out to sea and one fatality was reported; 16 vessels sank and 47 others were damaged. Final estimates bring the damage to about $20.5M, or about half of the statewide damage exceeding $40M [2][3][4]. This tsunami follows a long history of similar events at Crescent City. One of them, the 8.3-magnitude sub-sea earthquake originated in the Kuril Islands in 2006 (prompting over $22.5M in damage, see [5] by Dengler et al. and Barberopoulou et al. [6]) is at the origin of a master plan to retrofit the marina against tsunamis hazard, from which the present study stems.

The Mendocino Escarpment

Crescent City has a long documented history of tsunami-induced damage. Such vulnerability can be directly correlated to the specific configuration of its off-shore bathymetry. The Mendocino escarpment is particularly conducive to carrying wave energy toward the city and its harbor [7]0. Through refraction, the wave direction rotates so as to line up with the region near Crescent City, a phenomenon that is clearly visible in the work by Kowalik and Horrillo [9]. This puts Crescent City in a particularly vulnerable position because regardless of where a tsunami originates, some significant wave action is to be expected[1].

Because of this funneling mechanism, Crescent City is thus subject to a wide array of potential tsunamis sources, all located on a system known as the Pacific Ring of Fire[2]. A 2010 report issued by the National Center for Tsunami Research (NCTR) analyzes these tsunami sources and evaluates their risk [10] for Crescent City, with a focus set on identifying offshore amplification and providing inundation estimates on dry land. This report is used to assess the design tsunami wave height, as explained later in the text.

Framework and Objectives

Protecting the City of Crescent City against very large and inundating tsunamis is not within the scope of this rehabilitation effort. Rather, its focus is to mitigate the repeated action of lesser events that damage floating docks and boats in the marina. This study is at the interface between offshore tsunami mechanics and the need of structural planners and designers for realistic, ready-to-use structural loads. Such

[1] For example, the March 2011 tsunami was recorded as a 1.12m (3.68ft) disturbance by DART II station 21413 off the coast of Japan and generated 8ft waves at the Crescent City harbor.

[2] The primary exposure is due to earthquakes originating in the upper part of the Pacific along the Kuril Islands, Aleutian Islands, and Alaska; in the Cascadia Subduction Zone (extending from Cape Mendocino in Northern California past Oregon and Washington into British Columbia); and the Gorda Plate making up its southern portion presents the nearest subsea fault region in proximity to Crescent City, capable of producing large earthquakes and potentially very large tsunamis.

considerations are articulated in the section below. A presentation on the selection of the performance level input parameters used to model the tsunami wave follows. Later, structural solutions adopted in response to the tsunami are briefly described.

MODEL SELECTION

While the timing and propagation of a tsunami are better handled with a global model, a functional sketch of its localized behavior in the Crescent City harbor was successfully established using a Boussinesq model, upon which the following shall elaborate.

Global Models

Global models such as the Method of Splitting Tsunami (MOST) code by NCTR [11] are successful at simulating the three processes of tsunami evolution: earthquake, transoceanic propagation, and coastal flooding, all of which occur on very large scale. However, a potential shortcoming, as seen from a structural engineer's point of view, may be that these are not optimized to resolve more localized effects in a computationally efficient manner. Again, the goal here is not to address inundation of large areas of dry land. Instead, it is to resolve detailed quantities, e.g. velocity distribution, over small scale features such as a harbor, or a marina.

A Local Model

This paper is thus motivated by a desire to fill this gap by leveraging a Boussinesq-type equation solver to estimate wave-induced current during tsunamis in the marina.

The model retained for the present study is BOUSS-2D, initially developed by Nwogu [12] and maintained by Demirbilek (see [13]; and on future parallelization of the model, [14]) from the Coastal Hydraulic Laboratory. This time-domain solver is capable of describing highly asymmetric waves in shallow water, wave-induced currents, wave setup close to the shoreline and wave-current interaction. As such, this model is more readily geared toward the needs of marine structural engineers and planners. Tsunami-specific models also include the FUNWAVE package spearheaded by J. Kirby in 1998 [15][16][17].

The model is fitted to a 1 arc-second Crescent City digital elevation model (DEM) provided by the National Geophysical Data Center (NGDC) [18]. The grid is lined up with the marina in order to achieve a good compromise between resolution and computational efficiency. The 3000m × 3500m grid is subdivided in 10m square cells. Datum is MLLW; proper water level adjustments are made in the computations based on tidal records as needed. A perspective of that domain is shown in Figure 1. The main breakwater, the marina and shallow regions inside the main harbor are augmented using detailed hydrographic surveys to allow for accurate computations.

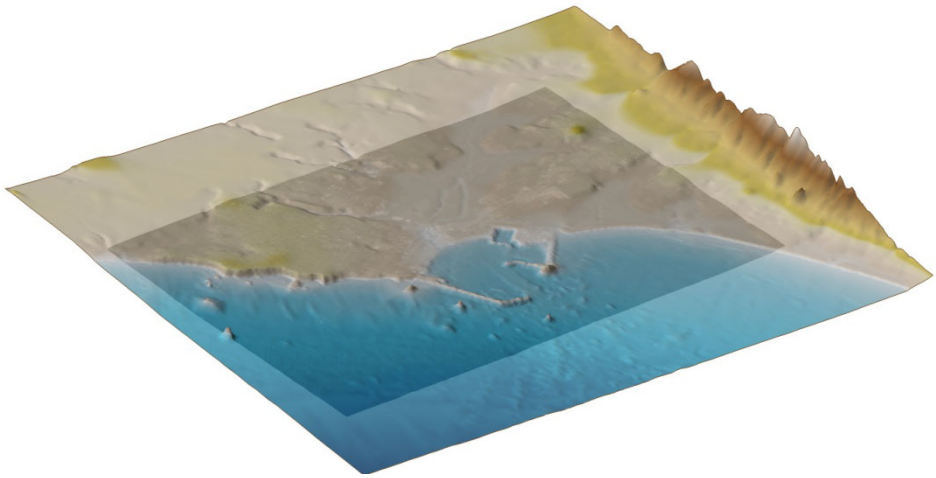


Figure 1 Perspective view from the Northwest of the 1 arc-second Crescent City NGDC DEM (MHW). Vertical exaggeration–times 5. Data courtesy of NGDC/NOAA

DESIGN LIFE AND RETURN PERIOD

Design Life

Existing international standards for small boat installations and marinas provide guidelines with respect to expected design life, ranging from 25 (European code R46) to 50 years (British Code BS6349-1:2000; Engineering Manual 1110-2-1615). Given the heavy use expected from the marina, agreement was reached over a 25-year useful lifetime, in concert with all stakeholders in this project. The required performance level, however, is not readily defined and must be independently developed.

Performance Level and Return Period

Australian Code AS3962-2001 suggests that "strength limit-state loads should be calculated for a 1 in a 50 year return period for wind, wave, surge and flooding loads". Article 11 of the Hawaiian State standards provides guidelines on surge hazard on vertical walls. Nonetheless, no tsunami-specific standards for small-craft installations are provided, and no provisions are made for the design of floating elements.

The choice of design load is directly connected to the selection of an adequate tsunami return period. This translates into a more complex and costly design. To protect against a 0 to 10-year return period (YRP) tsunami event, conventional concrete piles are sufficient. A 10 to 25-YRP tsunami design limit imposes the use of 2-ft steel pipe piles at the most exposed docks, as determined by the numerical model. Beyond the 25-YRP design level, steel pipe piles use is extended to several docks located in the wake of Dock H, first in line in the high-current region.

This initial cost increase incurred by a heightened bending demand on the structural elements (piles and floats) is balanced by a sharp performance improvement and a significant risk reduction for the marina installation. In effect, considering a design event with recurrence interval F = {10, 25, 50} years; and a design life of 25 years, the probability of occurrence reads P_{25} = {93%, 64%, 40%}, respectively.

Therefore the cost premium turns into a net gain over time stemming from a lower need for maintenance. Essentially, no significant costs for replacement are expected at the expiration of the 25-year design life period; only incremental maintenance steps need be taken. On the other hand, limiting the design load limit to a lower 10-year tsunami implies costly future upgrades — or most likely a complete replacement, as shown above by a near 100% probability of occurrence of such event. That problem is further exacerbated by the presence of socketed piles that make future driving of additional piles technically challenging. This reasoning weighs in favor of the decision to provide for a 50-year design limit load.

HYDRAULIC MODELING

Definition of the 50-Year Tsunami

With a performance level established, a set of design parameters is then devised to model the tsunami. Physically, an incoming tsunami wave resembles a tidal surge as it rushes through the access channel. Because the framework is local, such topics as the initial earthquake formation or offshore transformations are taken out of the analysis; they are best handled by global models. Instead, for the purpose of this analysis, the tsunami wave shall be simplified as a long monochromatic wave whose key parameters are adjusted based on global model results (e.g., the wave angle at the harbor is obtained by studying offshore wave refraction and NESDIS iso-lines, [7]) or by collecting data from previously published studies.

To do so, a growing body of tsunami wave height and maximum run-up height records at Crescent City is leveraged. According to past studies (see Wiegel, [19]) such return period corresponds to a design wave height of approximately 15ft (4.6m). Figure 2 shows Wiegel's 1965 original data points (brown dots) along with more recent data (blue dots) 0. Some uncertainty in the records appears as wave height ranges. For comparison, the amplitude and frequencies of the synthetic mega-tsunamis developed by NCTR [10] are shown on the rightmost part of the plot. Because these events are synthetic, they were not included in the return period estimate; yet, it can be observed that only 3 of the NCTR tsunami scenarios are above the 15-ft mark, used as design wave height in this analysis. This confirms that the level of protection retained in this design is reasonable and adequately conservative.

The wave period is based on a compilation of eyewitness accounts and collected data [19][6]0. Further statistical considerations support a typical period of 24 minutes. It was later verified (but not shown) that, in general, for a wave period larger than 10 minutes, the maximum flow velocity amplitude seldom varies past this point. That is because, in the access channel, the velocity is driven by the surge height rather than by the frequency of the forcing. Additional input parameters and calibration data are obtained from the NGDC and tidal gauge 9419750, located in the Crescent City harbor.

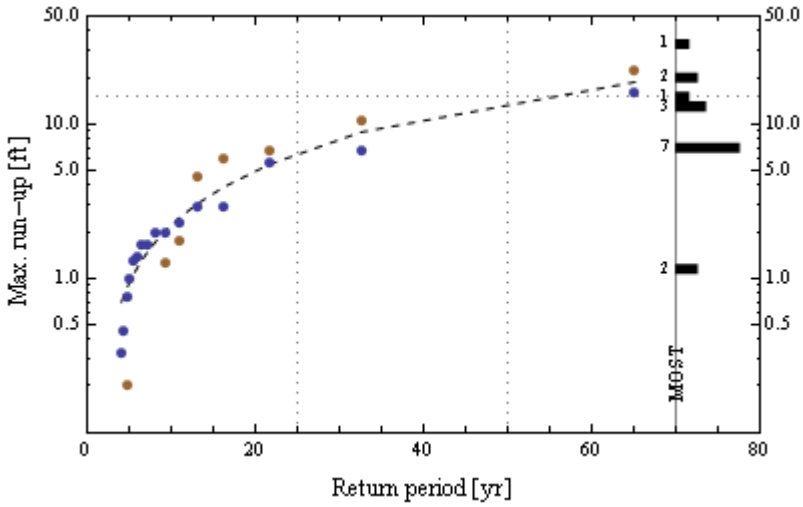


Figure 2 Estimated average return period of tsunamis of equal or greater wave height at Crescent City, CA. Wiegel's data (brown dots) and recent data (blue dots) are shown. Predicted mega-tsunamis devised by Arcas and Uslu (MOST) are shown on the rightmost part of the plot, in the form of an histogram. These theoretical events were not included in the return period estimate.

Tsunami Surge Mechanics

Of importance to the structural designers and planners is understanding how the current velocity distribution develops in the harbor and in the marina. The sequence of snapshots shown in Figure 3 illustrates the fate of a modeled tsunami wave in the harbor. The velocity amplitude is color coded as indicated in the color bar of Figure 4. For this synthetic 50-year tsunami event, velocities of up to 6 m/s (20 ft/s) are recorded. The sequence of plots can be summarized as follows.

First, the tsunami wave swells up outside the harbor (leftmost figure). Large velocity occurs where the flow section contracts, such as the tip of the main outer breakwater. The large body of water incurred by the approaching tsunami wave penetrates the harbor where an intense jet forms at the access channel (middle figure). This jet eventually reaches the marina where it forms a clockwise circulation pattern (rightmost figure); that phenomenon is well explained using the principle of conservation of mass. This cycle repeats itself over hours in the case of an actual tsunami. While the mechanics of harbor resonance offer opportunities for further

research (see part two of the work done by Horillo and Kowalik [20]), this paper is specifically vested in the assessment of the circulation patterns in the port basin.

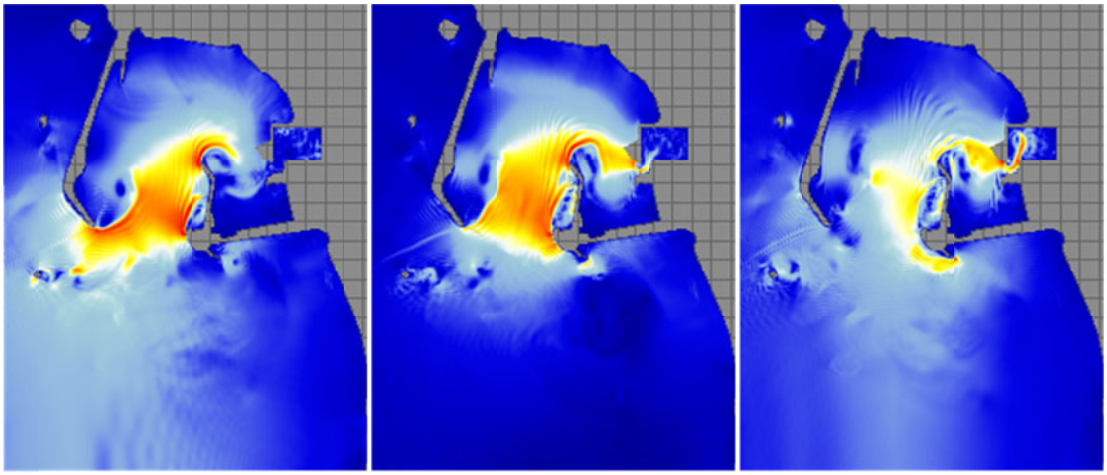


Figure 3 From left to right: snapshots of current intensity taken 2 minutes apart from 46m to 50min (time origin is arbitrary) for a 24 min wave period. The strong jet developing in the marina is clearly visible at 50min. Contour levels are those of Figure 4, below.

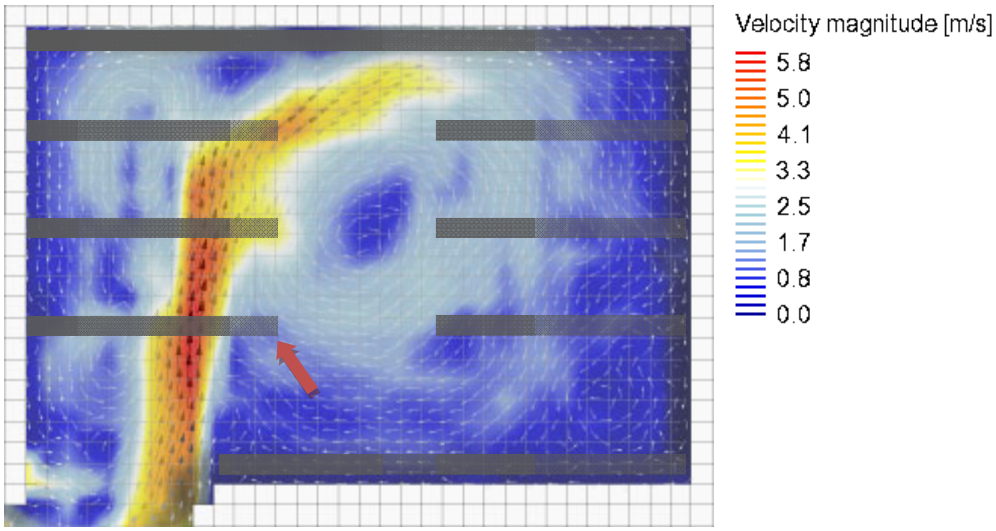


Figure 4 Velocity distribution in the marina at 50 minutes (corresponding to the second tsunami wave). Vectors indicate direction and amplitude of the flow velocity. The clockwise circulation pattern is visible in the center of the marina, in line with witness accounts obtained for the 2006 and 2011 tsunamis. Approximate position of Dock H is indicated by the red arrow; remaining elements are shown as gray rectangles (locations are for reference only)

Marina Currents

A close inspection of the velocity field reveals that, for the design wave height defined earlier, the peak velocities developing near the floating docks is in some instances as high as 20 ft/s (6 m/s). Detailed direct measurements of current velocity in the marina were not available. However, eyewitness accounts and video of the event confirm that the model matches well with observations, with the 2006 tsunami peak velocity reaching 20.24 ft/s [6]. The grid resolution selected for this project

provides a detailed picture of the evolution of the currents developing near and inside the marina. As the jet enters the marina, it forms a region of high velocity right in front of the Dock H. As the tidal wave recedes, two opposite circulation patterns survive, the largest of them rotating in a clockwise direction, as reported in earlier witness accounts. It is then that any loosened dock, free-floating debris or untied vessel is literally flushed out of the marina. Modifying the boundaries of the marina are the only conclusive methods to appreciably change the fate of the flow. However, such measures are beyond the scope of the plan implemented here.

Marina Modifications

The BOUSS-2D model is versatile and robust. As such, it lets us investigate the feasibility of some tentative marina reconfigurations with ease. Specifically, the following section shall focus on the impact of a solid wall in lieu of Dock H (shown in Figure 4 by the red arrow) and the impact of sediment transport on hydrodynamic loads.

Among the solutions retained to tame the high-speed currents is the addition of solid wall to deflect the flow. By comparing the wall case with the actual case it was determined that the addition of this structural element did not effectively eliminate or protect the marina against these currents. The wall does little but displace the high velocities to another region of the marina, exposing other initially sheltered floating structures to newly-formed strong currents. Given the cost of a solid wall and the findings of this test, this solution was not retained. Instead, a choice was made to create a more open layout with shallower floats, capable of vertical motion to ride out the tsunami waves and allow currents to vent underneath, offers a more tsunami-resistant solution.

The bathymetry investigated here is not definitive. Sediment transport and dredging are expected to occur over the life of the project and their effect on flow velocity was evaluated. Based on the various cases tested in this project, it was determined that long tsunami waves are seldom sensitive to relatively small change in depth. Sensitivity analyses were conducted to confirm that the impact of dredging on velocity distribution is minimal; overall, the mean momentum acting on the floating elements remains similar. Nevertheless, while sediment deposition near the marina does not change the outcome of velocity magnitude, special care should be paid when calculating the current load on the floating elements. Indeed, the presence of suspended sediments increases the effective water density. Calculations [21] show that a 10% increase in density is to be expected. Note that sediment transport by tsunami on dry land is a different story altogether, and is beyond the scope of this study.

MARINA REHABILITATION

Hydrodynamic Loads

A peak load is established for each element present in the inner boat basin, including piles and floating docks. Time series are extracted by judiciously geo-positioning a map of the marina on the model grid. A velocity envelope can then be assessed (Figure 5). The hydrodynamic loads are calculated using a Morrison equation, where the force acting on the element depends on the current velocity magnitude, acceleration drag and inertia properties of that element. While the fluid motion cannot be easily controlled, the hydrodynamic properties of a given element can be optimized by selecting more slender floats positioned in an open fashion.

Marina Replacement Features

The most exposed modules are made longer than the typical floats in the marina, thereby reducing the number of connection points and providing a more robust dock. Floating elements are also built with thicker walls and slabs and are reinforced with steel bars instead of welded wire fabric, which provide more robustness to floats. Piles are designed as capacity-protected elements, using steel pipe piles at the most exposed docks, leveraging their greater capacities compared to regular concrete precast piles. This in effect reduces the number of piles needed to be installed, and further improves construction cost-effectiveness.

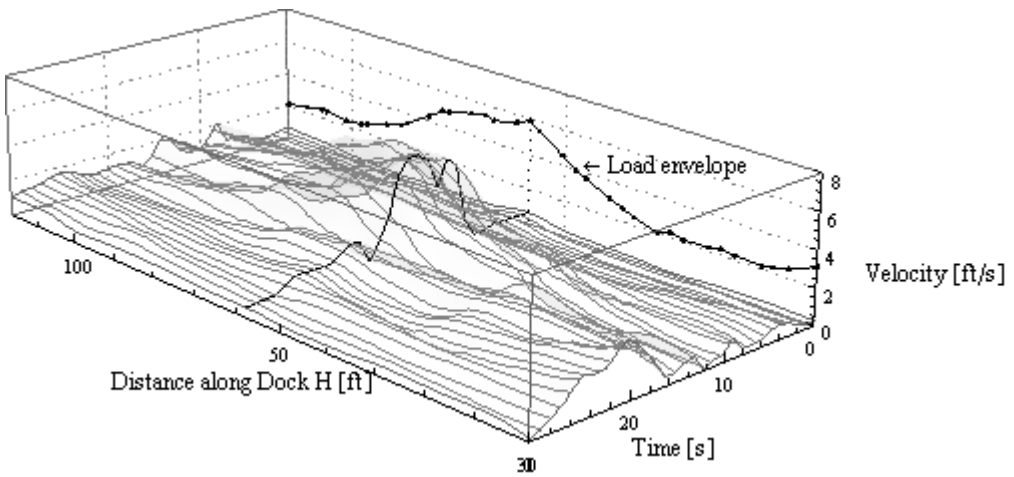


Figure 5 Velocity profiles (gray lines) are extracted over a time window; a load envelope (solid line and dots) is obtained by taking the maximum velocity at each point along Dock H. The location of maximum velocity is approximately 60ft from the East end of the dock, corresponding to the jet trajectory shown in Figure 4.

In addition to covering typical loads (e.g. dead loads, wind, impact from floating objects and vessels, berthing and mooring) provisions were made to design for floats capable of riding large tsunami waves and to also ensure that sufficient clearance is maintained at all times between the keel and riprap protection around the marina. In

effect, while the tsunami is typically represented as a surge, it may just as likely dry out the marina, if it occurs during a low tide. If unaccounted for, such situations may subject the piles and floating docks to undue bending stresses. Furthermore, the design takes into account the possibility that not all existing piles can be entirely removed, which may require that new piles be offset as needed.

CONCLUSION AND REMARKS

The analysis presented herein is part of a planning effort designed to rehabilitate the Crescent City marina, which began in the aftermath of the 2006 Kuril Islands tsunami. The new marina layout and elements are designed to withstand a 50-YRP tsunami wave. Strong current action is mitigated by the placement of concrete-filled steel piles. To further ease out current loads, slender, reinforced concrete floats are laid out in an open fashion. In absence of directly applicable tsunami-specific design guidelines, research was conducted to establish a reasonable marina performance level. Lastly, a sensible tsunami wave height was substantiated by a sizable set of historical run-up data.

The analysis herein serves as an example application of how conventional techniques can be successfully applied to address an unusual coastal hazard such as a tsunami. It shows that, with a set of judicious simplifications and the right set of working assumptions, a commercial model can be adequately deployed to establish a set of ready-to-use structural loads, while delivering results that are in good agreement with observed phenomena. As such, this study opens an implicit pathway for the establishment of structural design standards that specifically address tsunamis.

REFERENCES

[1] “Press Conference by Prime Minister Naoto Kan”. Prime Minister of Japan and His Cabinet. Archived from the original on 2011-04-18.
[2] “My Heart is in Crescent City”. The Daily Triplicate (Crescent City, CA, March 16, 2011).
[3] “Crescent City tsunami costs estimated at $12.5 million; assessment of harbor continues,” The Contra Costa Times, March 19, 2011.
[4] “Federal damage threshold met,” The Daily Triplicate (Crescent City, CA, April 5, 2011).
[5] L. Dengler et al., “The November 15, 2006 Kuril Islands-Generated Tsunami in Crescent City, California,” Pure and Applied Geophysics 166, no. 1-2 (2009): 37-53.
[6] A. Barberopoulou, B. Uslu, and L. Dengler, “Lessons for California from the November 2006 Tsunami in Crescent City, California,” in Proceedings of Solutions to Coastal Disasters (presented at the Tsunamis 2008 Conference, Turtle Bay, Oahu, HI: COPRI of ASCE, 2008).
[7] Tsunami Travel Times. National Environmental Satellite, Data and Information Service (NESDIS). NOAA Satellite and Information Service. http://map.ngdc.noaa.gov

[8] Tsunamis Affecting the West Coast of The United States 1806-1992. James F. Lander, University of Colorado, Cooperative Institute for Research in Environmental Sciences (CIRES); Patricia A. Lockridge, National Oceanic and Atmospheric Administration, National Geophysical Data Center; Michael J. Kozuch, University of Colorado, CIRES and Department of Geological Sciences. United States Department of Commerce, National Oceanic and Atmospheric Administration. National Environmental Satellite, Data, and Information Service, December 1993.

[9] Z. Kowalik et al., "Kuril Islands tsunami of November 2006: 1. Impact at Crescent City by distant scattering," Journal of Geophysical Research 113, no. 1 (2008).

[10] D. Arcas and B. Uslu, A tsunami forecast model for Crescent City, California, NOAA OAR Special report, PMEL Tsunami Forecasts (NOAA Center for Tsunami Research (NCTR). Pacific Marine Environmental Laboratory, March 2010).

[11] Titov, V.V., and C.E. Synolakis (1998): Numerical modeling of tidal wave runup. J. Waterw. Port Coastal Ocean Eng., 124(4), 157–171.

[12] Okey Nwogu, "Alternative Form of Boussinesq Equations for Nearshore Wave Propagation," Journal of Waterway, Port, Coastal and Ocean Engineering, ASCE 119, no. 6 (1993): 618-638.

[13] O.G. Nwogu and Z. Demirbilek, BOUSS2D: A Boussinesq Wave Model for Coastal Regions and Harbors, Theoretical background and user's manual (Vicksburg, MS: US Army Corps of Engineers. Engineer Research and Development Center, September 2001).

[14] S. W. Bova et al., "Dual-Level Parallel Analysis of Harbor Wave Response Using MPI and OpenMP," International Journal of High Performance Computing Applications 14, no. 1 (2000): 49-64.

[15] J.T. Kirby, "Chapter 1 Boussinesq models and applications to nearshore wave propagation, surf zone processes and wave-induced currents," Advances in Coastal Modeling 67, Elsevier Oceanography Series (2003): 1-41.

[16] P. Watts et al., "Landslide tsunami case studies using a Boussinesq model and a fully nonlinear tsunami generation model" (2003), http://hal.archives-ouvertes.fr/hal-00299049/en/.

[17] J.T. Kirby et al., FUNWAVE 1.0 Fully Nonlinear Boussinesq Wave Model Documentation and User's Manual, Research Report (Newark, DE: Center for Applied Coastal Research. Department of Civil Engineering. University of Delaware, September 1998).

[18] P.R. Grothe et al., Digital Elevation Models of Crescent City, California: Procedures, Data Sources and Analysis. Prepared for the Pacific Marine Environmental Laboratory (PMEL) NOAA Center for Tsunami Research (Boulder, Colorado: NOAA National Geophysical Data Center (NGDC), June 3, 2010).

[19] R.L. Wiegel, Protection of Crescent City, California from Tsunami Waves (Crescent City, CA: Redevelopment Agency of the City of Crecent City, March 5, 1965).

[20] J. Horrillo, W. Knight, and Z. Kowalik, "Kuril Islands tsunami of November 2006: 2. Impact at Crescent City by local enhancement," Journal of Geophysical Research 113, no. 1 (2008).

[21] Jørgen Fredsøe, Mechanics of coastal sediment transport (Singapore ;;New Jersey: World Scientific, 1992).

Operational Oceanographic System for the Southern Coastal Waters of Korea

Hak Soo Lim[1], Chang S. Kim[2], Kwang Soon Park[3] and Jae Seol Shim[4]

[1]Department of Marine Environment and Pollution Prevention Research, Korea Ocean R&D Institute, 454 Haeanro, Ansan 426-744; PH (82) 31-400-6334; FAX (82) 31-400-7873; email:hslim@kordi.re.kr

[2]Department of Marine Environment and Pollution Prevention Research, Korea Ocean R&D Institute, 454 Haeanro, Ansan 426-744; PH (82) 31-400-6340; FAX (82) 31-400-6340; email:surfkim@kordi.re.kr

[3]Department of Climate Change and Coastal Disaster Prevention Research, Korea Ocean R&D Institute, 454 Haeanro, Ansan 426-744; PH (82) 31-400-6343; FAX (82) 31-400-5827; email:kspark@kordi.re.kr

[4]Department of Climate Change and Coastal Disaster Prevention Research, Korea Ocean R&D Institute, 454 Haeanro, Ansan 426-744; PH (82) 31-400-6344; FAX (82) 31-400-5827; email:jsshim@kordi.re.kr

ABSTRACT

We have developed an operational oceanographic system for the southern coastal waters of Korea as a part of the development of Korea Operational Oceanographic System (KOOS). The operational oceanographic system consists of atmospheric and hydrodynamic models coupled with three-dimensional hydrodynamics, wave, sediment transport and water quality modules. The forecasting system focuses on the southern coastal waters of Korea which are very shallow with complex coastal lines and hundreds of islands. The operational modeling system of the southern coastal waters of Korea uses 3-D operational model ROMS (Haidvogel et al., 2008) which is 2-way coupled with SWAN for waves, nested with WRF for meteorological surface forcing, internally linked with sediment transport (Warner et al., 2008), and externally linked with CE-QUAL-ICM (Cerco and Cole, 1993, Kim et al., 2011) for water quality etc. The forecasting system provides predicted oceanographic data and warning of storm surge occurrence two times a day in the 72-hours base for the public through a web-GIS based coastal information system.

INTRODUCTION

Korea Operational Oceanographic System (KOOS) is a research project funded by the Minister of Land, Transport and Maritime Affairs (MLTM) in Korea. The main objective of this project is to produce and give users the forecasted information which is needed to support ocean activity and to resolve various concerned problems. KORDI (Korea Ocean Research and Development Institute) has been carrying out the KOOS program since August, 2009 and is supposed to finish its 1st stage until 2013. Presently the major efforts are focused on the setting and testing operational system with data management including information service. With the real-time observing networks, KOOS has developed the coastal/ocean forecasting system around the Korea waters. Now, 10 numerical models are under testing; two numerical weather models (WRF and UM), two wave models (SWAN, WAM) and six ocean/coastal models (ROMS, MOM3, KOSY (Park et al 2009), FVCOM (Chen et al., 2006), MOHID (MOdelo HIDrodinamico), ADCIRC).

As a part of KOOS system, we have developed an operational oceanographic system for the southern coastal waters of Korea. The operational modeling system consists of atmospheric and hydrodynamic models coupled and nested with three-dimensional hydrodynamics, wave, sediment transport and water quality modules etc. The operational oceanographic system focuses on the southern coastal waters of Korea which are very shallow with complex coastal lines and hundreds of islands. Along the coast there are many ports and harbors that are located mainly in the landward side of the embayment. The southern coastal waters are connected with Jeju Strait in the west and Korea Strait in the east.

The operational modeling system of the southern coastal waters of Korea uses operational model ROMS (Haidvogel et al., 2008) which is 2-way coupled with SWAN for waves, nested with WRF for meteorological surface forcing, internally linked with sediment transport (Warner at al., 2008), externally linked CE-QUAL-ICM (Cerco and Cole, 1993, Kim et al., 2011) for water quality etc. The model uses two different domains; one is coarse orthogonal domain covering the entire southern coastal waters of Korea, and the other is the high resolution orthogonal curvilinear domain with cell size of 300 m in the ports such as Yeosu and Masan which are recognized as very vulnerable to the attack of the storm surge by typhoon. The operational system starts from atmospheric forcing forecasted in 72-hours advance with either the WRF (Weather Research and Forecasting Model) in normal case or CE (US Army Corps of Engineers Wind Model) in the case of Typhoon approach. The input data of boundary condition and surface forcing to the 3-D hydrodynamic model ROMS is automatically provided through FTP transmission and converted with shell script at 12-hourly interval. Then, the model uses the previous result simulated 12 hours before for an initial condition with predicted boundary and surface data to forecast twice a day for 72 hours such as sea surface height, tidal currents, wind-driven currents, temperature, and salinity. The predicted results are exported to the web-GIS based coastal information system for real-time public dissemination.

THE OPERATIONAL MODEL

The Regional Ocean Modeling System (ROMS) is used as an operational coastal circulation and storm surge model. Originally the ROMS has been developed as a community model by the Rutgers University USA (Haidvogel et al., 2008). The model uses a horizontal curvilinear grid system and stretched terrain-following coordinate in vertical array. It has been widely used for a diverse range of application such as coastal/ocean prediction of hydrodynamic variables as well as sediment transport study with highly resolving tidal flat dynamics (Kim and Lim, 2007, 2009, Warner et al., 2008) etc. the wave coupled model ROMS enhances the current related bottom stress due to the wave induced oscillatory boundary layer, and wave friction is also increased due to the currents (Warner et al., 2008). Being module-based model system, the ROMS is to be operational with easy link or coupling with other models such as weather model WRF for meteorological surface forcing, wave model SWAN for waves, internally linked sediment transport, externally linked CE-QUAL-ICM for water quality, and even with nonlinear processes.

For the operational oceanographic modeling system focusing on southern coastal waters of Korea, we use two different domains; one is coarse orthogonal domain with cell size of 1.5km covering 125.0 – 130.5°E, 32.8 – 35.8°N for the circulation of southern coastal waters of Korea, and other one is high resolution orthogonal curvilinear domain with cell size of 300 m in the northern land-side such as Yeosu and Masan Bays which are recognized as very vulnerable to the attack of the storm surge by typhoon. We use 20 levels in the vertical array with significant stretching near the surface and bottom. For the tides at open boundary, we use major 8 tidal constituents with semi-diurnal tidal constituents (M2, S2, N2, K2) and diurnal tidal constituents (K1, O1, P1, Q1) derived from the regional ocean tide model NAO.99jb with 5′resolution (Matsumoto et al., 2000). The initial condition of the model are computed with 2 years simulation using monthly mean temperature and salinity derived from the World Ocean Atlas 2005 (WOA2005) and monthly mean surface forcing derived from the Comprehensive Ocean-Atmosphere Data Set (COADS). Recently, this regional ocean modeling system is nested with Yellow Sea operational modeling system with 9km grid covering the entire area of the Yellow Sea and predicts tides, wind-driven circulation, temperature and salinity two times a day for 72 hours. The hydrodynamic data derived from the predicted results from the Yellow Sea operational model is converted into boundary condition of the model. The surface forcing including wind stress, heat flux and water flux obtained from the operational weather model WRF with 4km fine mesh covering entire Yellow Sea simulated by KORDI is automatically converted into atmospheric forcing for the operational model. For the restart of the operational system, the model uses the previous result simulated 12 hours before as an initial condition. With predicted atmospheric forcing and boundary condition, the model ROMS forecasts tides, wind-driven currents, temperature and salinity twice a day (05:00 and 17:00 Local Standard Time) for 72 hours. In case of typhoon approach, the operational model use weather model CE for accurate wind forcing which is changed with its typhoon track and wind strength.

RESULTS AND DISCUSSION

The regional operational oceanography system of KOOS comprises of atmospheric and hydrodynamic models coupled with 3-D hydrodynamics, wave, sediment transport and water quality modules. The hydrodynamic variables including storm surge are forecasted in the 72-hours base. The predicted results are exported to the web-GIS system for real-time dissemination to the public. The boundary condition of the regional model uses the predicted results derived from the Yellow Sea operational modeling system simulated before. Atmospheric forcing including surface wind stress, net heat flux and water flux obtained by operational atmospheric model WRF has been used. The model use previous result simulated 12 hours before for an initial condition with nested boundary condition and surface forcing and forecasts tides, wind-driven circulation, temperature and salinity 2 times a day for 72 hours.

For the validation of the operational model, real-time monitoring data from the real-time observing networks such as remote Buoy system, ocean observatory tower and HF-Radar system near the coastal area is generated through web-GIS based coastal information network system which provides real-time visualization of simulated results and analysis tools for comparison of predicted result and observed data. Figure 1 shows real-time observing networks for the validation and data assimilation of operational model. The operational model ROMS uses nested boundary and surface condition from Yellow Sea operational models obtained twice a day (05:00 and 17:00 Local Standard Time) from the operational ROMS and WRF model simulated by KORDI. Figure 2 shows process of regional operational oceanographic system for the southern coastal waters of Korea. The boundary and atmospheric data derived from the operational ocean and atmospheric models are automatically downloaded from FTP server system and converted into boundary condition and atmospheric forcing for the operational regional ROMS. The model uses previous result simulated at 12 hours before as an initial condition to restart model and forecasts tides, wind-driven currents, temperature and salinity twice a day (07:00 and 19:00) for 72 hours. Then, the predicted results are exported to the web-GIS based coastal information system for the validation of model and the application of KOOS system. Figure 3 shows maximum storm surge distribution simulated by nested operational model ROMS when the typhoon Maemi hit the southern coast of Korea on September 12, 2003.

The coastal information system is based on web-GIS system to provide hydrodynamic environment data such as real-time monitoring data, periodically observed data and predicted model result effectively to the public and carry out complex analysis of the information for the other application. We use different visualization methods and web service configurations appropriately according to each data properties considering observation items. For improving web service speed and effective visualization of spatio-temporal coastal environmental data, we us Flex API based on ArcGIS engine (Lim et al., 2011).

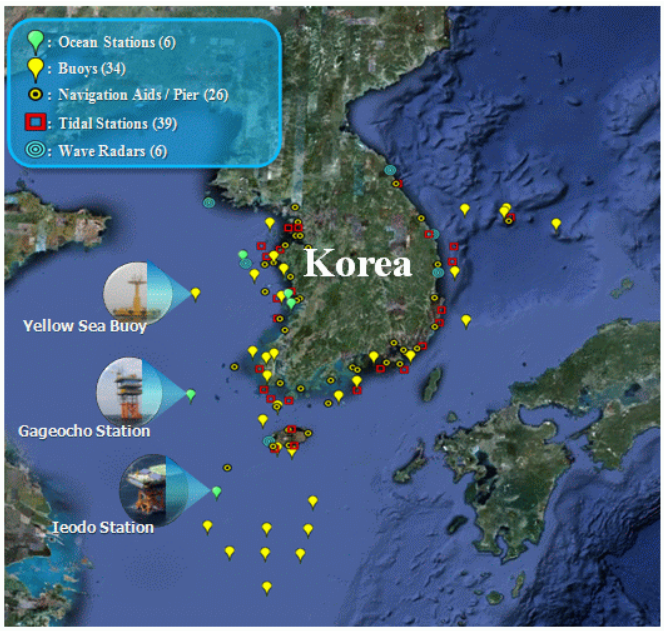


Figure 1. Real-time observation system for the validation and data assimilation of operational model.

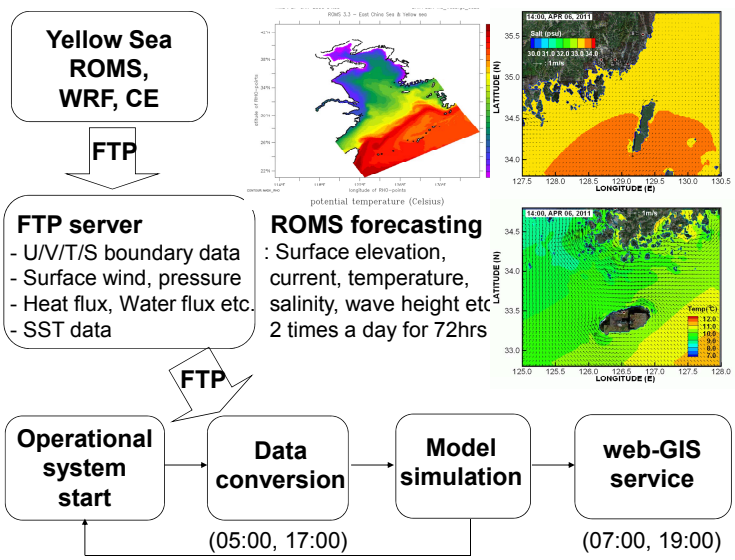


Figure 2. Process of operational oceanographic system for the southern coastal waters of Korea.

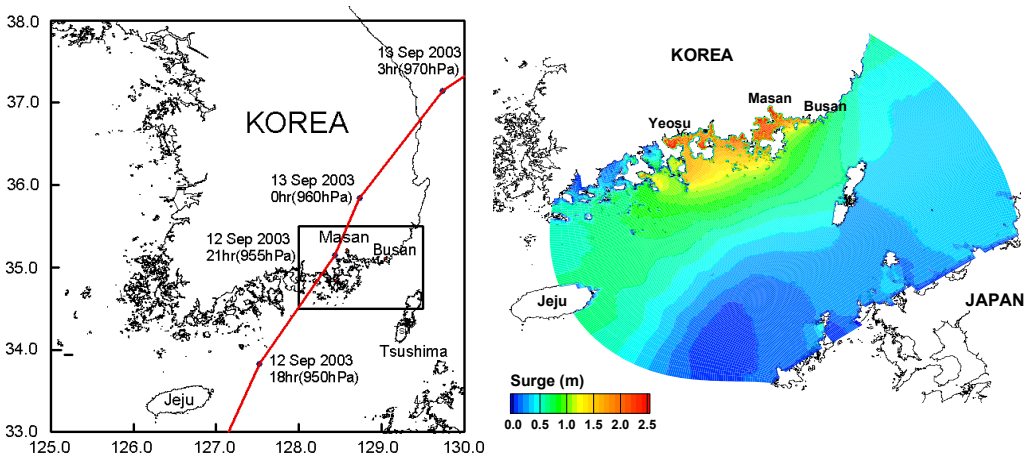


Figure 3. Maximum storm surge distribution simulated by operational model ROMS when the typhoon Maemi hit the southern coast of Korea on Sep. 12, 2003.

CONCLUSIONS

The main purpose of KOOS program is developing and operating operational oceanographic system for the Korean waters to solve various problems, coastal disasters, marine pollution, safe navigation and to provide necessary information of sea states and prediction for governments, industries, publics. As a part of KOOS system we have developed a high-resolution operational oceanographic system for the southern coastal waters of Korea. The operational oceanographic system consists of atmospheric and hydrodynamic models coupled with three-dimensional hydrodynamics, wave, sediment transport and water quality modules. We forecast predicted results two times a day in the 72-hours base including sea surface elevation, currents, temperature, salinity, and waves etc. for the southern coastal waters of Korea. The predicted results are exported to the web-GIS based coastal information system for the real-time dissemination to the public.

The operational modeling system for the coastal waters of Korea uses hydrodynamic model ROMS which is coupled with SWAN for the waves and nested with WRF for the meteorological surface forcing, regional tide model NAO.99jb for tidal boundary condition, and externally coupled CE-QUAL-ICM for the water quality. For the open boundary condition the operational model is nested with another operational model ROMS which has been operated for the Yellow Sea. The model ROMS has been calibrated with observed tidal elevation, then the model verified with current data observed by bottom mounted AWAC near the coastal waters. To validate the operational model we use real-time monitoring data provided by remote Buoy system, ocean observatory tower, and HF-radar system installed by KORDI comparing with predicted hydrodynamics of coastal waters of Korea.

In this study, we have developed an operational oceanographic system for the southern coastal circulation and hydrodynamics in Korea. The operational model forecasts hydrodynamics and wave information twice a day for 72 hours. The predicted result validated by real-time monitoring data is visualized effectively through the web-GIS system to provide 72-hours predicted coastal hydrodynamic information in Korea to the public. This coastal operational oceanographic system has been used as a part of the development of Korea Operational Oceanographic System (KOOS) with other operational system.

REFERENCES

Kim, C.S. and Lim, H.S. (2007). "Safety criteria on water depth, offshore distance and dredging volume in marine sand mining operation in Kyunggi-Bay, Korea." *Journal of Coastal Research*, SI50: 507-510.

Kim, C.S. and Lim, H.S. (2009). "Sediment dispersal and deposition due to sand mining in the coastal waters of Korea." *Continental Shelf Research*, 29: 194-204.

Cerco, C.F. and Cole T. (1993). "Three-dimensional eutrophication model for Chesapeake Bay." *Journal of Environmental Engineering,* 119(6): 1006-1025.

Chen, C., Beardsley, R.C., Cowles, G. (2006). "An unstructured grid, finite-volume coastal ocean model (FVCOM) system." *Oceanography*, 19(1): 78-89.

Haidvogel, D.B., Arango, H., Budgell, W.P., Cornuelle, B.D., Curchitser, E., Lorenzo, E.D., Fennel, K., Geyer, W.R., Hermann, A.J., Lanerolle, L., Levin, J., Mcwilliams, J.C., Miller, A.J., Moore, A.M., Powell, T.M., Shchepetikin, A.F., Sherwood, C.R., Signell, R.P., Warner, J.C., and Wilkin, J. (2008). "Ocean forecasting in terrain-following coordinates: Formulation and skill assessment of the Regional Ocean Modeling System." *Journal of Computational Physics*, 227: 3595-3624.

Kim, C.S., Lim H.S., and C.F. Cerco (2011). "Three-dimensional water quality modeling for tidal lake and coastal waters with ROMS-ICM." *Journal of Coastal Research*, SI64, *(accepted)*.

Lim H.S., Kim, J.A., Kim, C.S., and Park, K.S. (2011). "SOON: The Saemangeum operational oceanography networks." *Journal of Coastal Research*, SI64, *(accepted)*.

Park, K.S., Lee, J.C., Jun, K.C., Kim, S.I., and Kwon J.I. (2009). "Development of an operational storm surge prediction system for Korean coast." *Ocean and Polar Research*, 31(4): 369-377.

Warner, J.C., Sherwood, C.R., Signell, R.P., Harris, C.K., and Arango, H.G. (2008). "Development of a three-dimensional, regional, coupled wave, current, and sediment-transport model." *Computers & Geosciences*, 34: 1284-1306.

ACKNOWLEGEMENTS

This research was supported by the project entitled “Development of Korea Operational Oceanographic System (KOOS)” and partially supported by the project entitled “Core Engineering Technology Development of Super Long Span Bridge R&D Center” funded by Ministry of Land, Transport and Maritime of Korean government (grant no. PM55991 and PM56350). In-House Program (grant no. PE98573) entitled “Estimation of Storm Surge Inundation and Hazard Mapping : Busan, Masan, Yeosu” is greatly appreciated. The authors also thank to the US Army Corps of Engineers (USAE ERDC) for the cooperative partnership with KORDI.

Application of Coastal Engineering Principles in Response to the Deepwater Horizon Disaster: Lessons Learned in Coastal Alabama

Bret M. Webb[1], Scott L. Douglass[2], Caren R. Dixon[3], Beau Buhring[4]

[1]University of South Alabama, Department of Civil Engineering, 6021 USA Drive South, Suite 280, Mobile, AL 36688; PH (251) 460-6174; FAX (251) 461-1400; email: bwebb@usouthal.edu

[2]University of South Alabama, Department of Civil Engineering, 6021 USA Drive South, Suite 280, Mobile, AL 36688; PH (251) 460-6174; FAX (251) 461-1400; email: sdouglass@usouthal.edu

[3]South Coast Engineers, LLC, PO Box 72, Fairhope, AL 36533; PH (251) 510-2903; email: caren@southcoastengineers.com

[4]South Coast Engineers, LLC, PO Box 72, Fairhope, AL 36533; PH (251) 510-2903; email: beaubuhring@gmail.com

ABSTRACT

The explosion of the Deepwater Horizon drilling rig on April 20, 2010, and the subsequent events leading to the nation's largest oil spill in recorded history, illuminated a threat not typically included in any practitioner's list of coastal hazards: oil fouling thousands of miles of gulf coastline, habitat, fisheries, and recreational areas. Much uncertainty paralyzed early efforts to contain the spill at the source, and it soon became evident that containment strategies would be focused on preventing surface oil from fouling marshes, wetlands, beaches, bays, bayous, and estuaries. A number of containment strategies and efforts were employed to protect Alabama's 1000 km of tidally influenced shoreline. Some strategies actively contained surface oils (e.g. booms, skimming), others were more passive (e.g. beach cleaning), and still others modified the properties of the oil to enhance degradation (e.g. dispersant). A considerable amount of time, effort, and money was spent on containment efforts and coastal defenses in Alabama during the nearly three-month period following the initial explosion and leak of the Macondo well. The benefit of hindsight affords an opportunity to look back at some of the coastal projects and identify areas for improvement, as well as compare the relative efficacy of proactive and reactive strategies. Along with a general discussion of various impacts to Alabama's coastal resources as a result of the oil spill, four unique coastal projects will be highlighted: the construction of containment measures on Dauphin Island; the closure of a barrier island breach; the closure of a tidal inlet; and the implementation of a novel, robust boom system for Perdido Pass.

INTRODUCTION

The explosion and subsequent sinking of the Deepwater Horizon drilling rig on April 20, 2010, and the leaking of more than 206 million gallons of crude oil into the Gulf of Mexico, illuminated a threat not typically included in any practitioner's list of coastal hazards. Much uncertainty paralyzed early efforts to contain the spill at the source, and it soon became evident that containment strategies would be focused on preventing surface oil from fouling marshes, wetlands, beaches, bays, bayous, and estuaries. A number of containment strategies and efforts were employed to protect Alabama's 1000 km of tidally influenced shoreline, 100 km of beaches, and arguably one of the most productive estuaries in the world, Mobile Bay.

The Mobile Bay estuary covers approximately 1000 km^2 of water, representing the nation's sixth largest watershed by area and contains seven endangered ecosystems. In addition to the 49 species of mammals, 126 species of reptiles and amphibians, 337 species of fresh and saltwater fish, and 355 species of birds found there, the estuary also provides foraging grounds for the threatened Gulf Sturgeon and West Indian manatee. The bay is a highly productive fishery and shellfishery with an annual harvest of 30 million pounds at a value of $47 million. The associated sport-fishing industry contributes $260 million annually to the local economy. At the onset of the oil spill, the biological and economic productivity of the estuary seemed at risk of an environmental disaster of unfathomable proportion, particularly as the forecast for an active tropical season loomed in the not too distant future.

What follows is a rather non-technical synopsis of a few coastal projects conceived of and implemented in response to the gulf oil spill including: the construction of two, shore-parallel protective sand barriers on Dauphin Island; the filling of a 2.5-km-long barrier island breach; the filling of the nation's second smallest tidal inlet at Little Lagoon; and the deployment of a novel containment boom at Perdido Pass. First, a general overview of the impacts of the oil spill on Alabama's coastal resources is provided for context.

COASTAL IMPACTS IN ALABAMA

Response. On a single day in July 2010, over 700 km of gulf shoreline was oiled: over 400 km of that was in Louisiana, while roughly 83 km was found in Alabama. Compared to Alabama's four gulf coast neighbors, the state's physical coastal resources, mainly its beaches, waterways, and salt marshes, were in many cases spared from a daily battering of thick, crude oil at the surface. By the time they reached Alabama's coastal waters, the surface oils had been weathered significantly, resulting in mostly emulsifications, sheen, and tarballs. The weathering process, however, made containment and cleanup every bit as difficult along Alabama's 100 km of white, sandy beach. At one point during the spill there were more than 700 cleanup workers in Mobile and Baldwin County, another 450 workers involved with deep cleaning projects on the state's beaches, and approximately 125 staff at the central command office in Mobile, Alabama. According to BP statistics, the company had over 1300 workers and 370 pieces of heavy equipment deployed to Alabama's

beaches during the cleanup process. By comparison, the state of Mississippi had 2300 cleanup workers focused on shorelines and barrier islands at one point during the spill. In terms of the water-based response, there were approximately 1900 vessels involved with skimming operations between the states of Mississippi, Alabama, and Florida.

Beach Cleaning. It is safe to say that over the period May 2010 – May 2011, the entire length of Alabama's gulf-fronting beaches had been cleaned by some sort of means. On Dauphin Island, response teams mainly employed sifting nets to remove tarballs and oil-laden sand from the beachface. The beaches of Baldwin County, namely Gulf Shores and Orange Beach, received a different treatment in response to a higher level of contamination across the beach. These beaches received a "deep cleaning" to remove oil, tarballs, and tar mats buried as deep as 1 m below the surface of the subaerial beach. This process was performed using what came to be known as the "Sand Shark." The Sand Shark, a $300,000 USD machine generally employed for road resurfacing, consisted of a powered vehicle with an excavator, and a tow-behind conveyor and sieve. The Sand Shark screened and retained all material larger than 2 mm. A single crew and machine could cover 450 m in a 12-hour workday. Crews worked seven days per week between October 2010 and March 2011 to complete the beach-cleaning process in Baldwin County. And although a mid-February 2011 federal report stated that as much oil had been removed from beaches and shorelines of the five affected gulf states as practical, more than 4300 kg of tarballs were collected along the beaches of Baldwin County over a two-week period that same month.

General Numbers. According to BP statistics, a total of 48,000 people were mobilized in response to the gulf oil spill. There were 6500 vessels involved in water-based cleanup and response activities, some of which placed and tended the more than 4000 km of containment or absorbing boom. Controlled burns of surface oils at sea were estimated to destroy 265,450 barrels of oil, and 7 million liters of dispersant were applied to surface waters further than 4.8 km from shore. A total of 11,000 workers were trained to monitor and clean the beaches and shorelines of the five affected states. The U.S. Army Corps of Engineers, Mobile District, issued a total of 91 emergency permits along the gulf coast during the oil spill in the summer of 2010. Eight of those emergency permits were issued for coastal projects in Mississippi and Alabama. Of those eight permitted projects, two were never implemented, and two remain intact as of May 2011 with the goal of seeking a permanent permit, one of which is the closure of Katrina Cut, a 2.5-km-wide breach through Dauphin Island, Alabama.

CONTAINMENT MEASURES ON DAUPHIN ISLAND

Dauphin Island is a dynamic, microtidal barrier island approximately 22.5 km in length located 7 km south of mainland Mobile County (see Figure 1). The easternmost 10 km of the island is home to approximately 1300 permanent residents, while the westernmost 12.5 km is largely undeveloped. The width of Dauphin Island

varies from about 3000 m at its widest point near the east end, to less than 300 m along most of the lightly-developed west end. While the east end of the island boasts 10 – 15 m dunes and a maritime forest, much of the west end has a nominal elevation of 2 m or less. The long, thin, low-elevation portion of Dauphin Island's west end makes it particularly susceptible to storm surge and even milder shelf setup events, and is continually shaped by the wave-driven longshore sand transport processes immediately downdrift of a federally managed navigation channel, Mobile Pass.

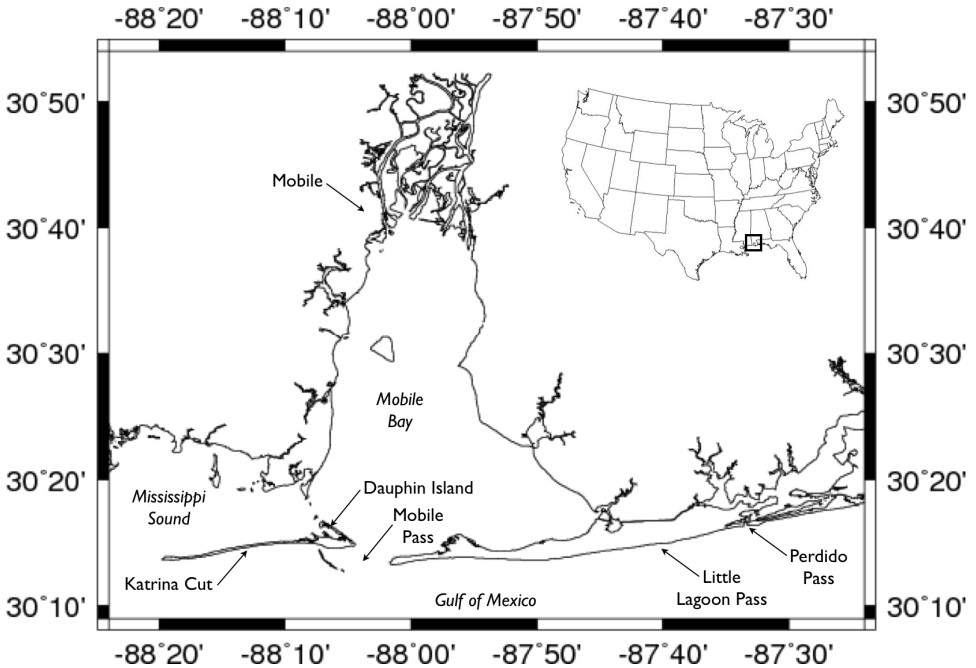


Figure 1. Location overview.

Dauphin Island artificially manipulated its beach profile, and island-wide cross-shore transect, in response to the oil spill. This artificial manipulation, described below, succeeded in keeping oil from overwashing the island and thus, succeeded in keeping oil both from depositing under elevated houses and from overwashing the island into Mississippi Sound. The emergency manipulations restricted all oil to a narrow area on the beachface. This success is certainly also attributable to the mild waves and storms in the critical months of June-August 2010.

Background. By May 1, 2010, it became obvious that there was a major surface oil slick drifting toward Dauphin Island, Alabama (Figure 2). On May 2, 2010, the combination of a spring tide and strong southeasterly winds produced a mild overwashing event on the west end of Dauphin Island (Figure 3). The "west end" here refers to the western 6.5 km of the inhabited portion of the island. A typical elevation on this part of the island was roughly +1.5 m NAVD, although the crest of the beach storm berm was slightly higher in some locations.



Figure 2. Aerial imagery of Dauphin Island, Alabama taken January 2010. Approximate scale provided for reference. Note that an additional 6 km of the island, located to the west of the breach shown on the left side of the image, is not shown here.



Figure 3. Overwashing event on Dauphin Island, Alabama. This photo was taken on May 2, 2010 on the crown of Bienville Boulevard looking east-southeast toward the Gulf of Mexico (at right). The maximum observed tide on this day was +0.7 m NAVD at the Dauphin Island CO-OPS station.

This portion of the island is so susceptible to overwashing—usually through a combination of astronomical tides, wave setup, and wave runup—that the west end had been overwashed at least six times in the twelve-month period preceding the oil spill; and it had been partially or completely overwashed dozens of times including most tropical storm events during the past 15 seasons. Essentially, this period of repeated overwashing corresponds with the increased storminess since 1995 (Hurricane Opal).

Strategy. A decision was made by the officials of Dauphin Island, in consultation with the authors, to construct two protective sand barriers (essentially linear sand

piles) on the island as a primary strategy for protection and oil containment: the first to prevent complete overwashing during a weak tropical storm, and the second for containment on the beachface under typical conditions. At the time, a means of stemming the oil leak was unavailable, a growing slick of surface oil had begun its translation toward the north-central gulf coast, and the forecast of an active hurricane season suggested that the island's west end could potentially be covered in oil during the next overwash event.

The first protective sand barrier/pile was constructed just south of Bienville Boulevard extending from St. Stephens Street to the public park on the west end, a distance of approximately 4 km. It was completed in several days as a stopgap measure to prevent a complete overtopping event. It was not extended across roads or driveways but additional sand was placed near those gaps with the intent that should oil start to wash across the island, bulldozers could close the gaps fairly quickly. That sand barrier pile initially had a height of 2 to 3 m above grade (thus the crest elevation was typically +3.5 to +4.5 m NAVD). The width of the base of the pile was controlled mainly by the angle of repose and varied from 5 to 7 m. The contractor was instructed to not smooth the surfaces but just dump it to "make it look like the Rocky Mountains."

Guidance provided in Hallermeier and Rhoades (1988) was used to determine the amount of sand in this first (northern) sand barrier/pile. The initial volume density of the northern sand barrier afforded protection against a storm having a recurrence interval of roughly 10 years. It was subsequently expanded with placement of more sand, where there was room for expansion amongst the existing houses, to increase the level of protection to a 20-year storm event.

Construction of a second, southern, protective sand barrier/pile commenced shortly after initial construction of the northern pile was completed. The second, southern sand pile was placed on the beach at or near the highest elevation (the existing storm berm) of the subaerial beach with the goal of containing the oil on the beachface. It was originally envisioned that this small pile of sand would likely be eroded in the next high tide event. However, due to the mildness of the winds and waves, and the addition of more sand by the contractor, this southern sand barrier/pile survived along most of the island for the summer. Approximately 267,000 m^3 of sand was used in the construction of the two protective sand barriers, and placed on the island between the months of May and July 2010.

Results. Oil was contained successfully on the beachface throughout the summer and fall by the second, southern, sand barrier/pile. Regular beach patrols quickly removed tarballs and emulsifications. The summer and fall of 2010 was a relatively mild period with natural, seasonal, beach accretion south of the southern sand barrier.

It should be noted however, that neighboring beach communities that opted to forego any beach profile manipulation had a much more serious oil problem. There were a few days in the summer of 2010 when storms raised the Gulf sea level over the

natural berm elevations, but not the manipulated profile on Dauphin Island, and oil was deposited across 20 to 30 meters of beach width in the neighboring beach communities. These photographs, of extensive black oil deposited on the native white beaches, were broadcast nationally and contributed to the temporary collapse of the beach tourism economy. The cleanup of these neighboring oiled beaches also included excavation and mechanical sieving of the top 1 m of beach material. Dauphin Island avoided these problems in large part because of the beach profile manipulations described here.

The elevation of the second, southern sand barrier/pile was reduced in the winter of 2010-2011 after the oil spill was contained and the threat of large surface oil slicks washing ashore was gone. The sand in that barrier, essentially a sand pile along the beach berm crest, was sifted and redistributed into a much flatter, more naturally-shaped beach berm. Figure 4 shows a comparison of photos of this feature during and one year after placement.

The first, northern sand barrier/pile remains today and the Town has decided to maintain it as a sand dune. It was planted with native sand dune species in the summer of 2010 with the goal of stabilizing the sand. The vegetation has survived (see Figures 5 – 6), and six months of weathering has resulted in a much more natural looking feature.



Figure 4. Photos taken of the frontal sand barrier on Dauphin Island (a) in May 2010 during placement, and (b) May 2011 one year after placement.



Figure 5. Photos taken of the initial, larger roadside sand barrier on Dauphin Island (a) in May 2010 during placement, and (b) May 2011 one year after placement.

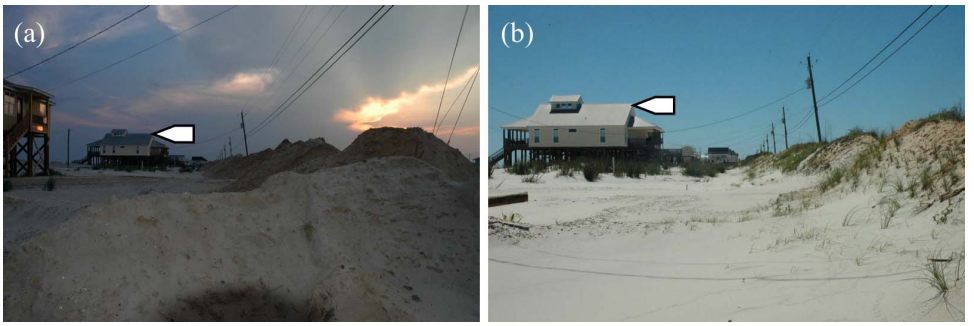


Figure 6. Photos taken of the initial, larger roadside sand barrier on Dauphin Island (a) in May 2010 during placement, and (b) May 2011 one year after placement.

Obstacles. A number of issues were encountered in the construction of these sand barrier/pile features that were addressed with what might be called "incremental field engineering." Siting issues, homeowner concerns, overhead utilities clearances, water and sewer infrastructure, fire hydrants, and the availability of suitable fill material all dictated an immediate design modification at one time or another. Regular communication and coordination with the US Fish and Wildlife Service was a necessity, particularly in light of premature turtle activity in the area. Routine morning patrol volunteers searched the beachface for turtle crawls and any other signs of turtle activity.

BREACH CLOSURE: KATRINA CUT

Background. Due to its relatively narrow width and low elevation, the western end of Dauphin Island has been overtopped and breached many times in the past 160 years of well-documented history. Over that same period of time, the western end of the island has actually migrated northward one entire island's width. In September 2004, Hurricane Ivan's storm surge and waves created multiple breaches through the undeveloped western portion of the island (Froede, 2006). Such breaches had historically healed through wave-driven longshore sand transport, but Hurricane Katrina in 2005 widened and stabilized the breach, growing to more than 2.5 km in width with an average depth of 2 m during the 5 years that followed (Froede, 2008). The breach was given the moniker Katrina Cut by the locals (see Figures 1 and 7).



Figure 7. Tiled aerial imagery of Katrina Cut (Dauphin Island, AL) taken on May 9, 2010.

For a number of reasons, including concern over a declining oyster population in Mississippi Sound thought to be partially due to increased salinity levels as a result of Katrina Cut, many have proposed filling the breach and fusing the two ends of Dauphin Island back together. This potential project was given substantial relevance during the oil spill, as blocking the breach would relieve one point of ingress for surface oils into the sensitive habitats of Mississippi Sound and Mobile Bay.

Strategy. The strategy adopted and implemented for closing Katrina Cut was to use a combination of rock and sand fill to create a sand-tight rubble mound structure in the 2.5 km gap. The project was designed and constructed by a local engineering firm under an emergency permit issued by the U.S. Army Corps of Engineers, Mobile District. Project construction began in early July 2010, and a final inspection was completed in April 2011. Under the existing emergency permit, the structure must be removed by June 2011. A permanent permit is being sought for the project.

Results. A sketch of the structure cross-section is provided in Figure 8. The rubble mound structure was built in stages: two, parallel internal sections were built first; good quality sand fill from a nearby borrow area was then pumped in between the rock structures and sealed within a geotextile fabric; finally, a nearly 1-m-thick layer of armor stone was applied and choked at the crest with a 0.3-m-thick layer of smaller stone. Placing 60 – 90 m of rock per day, the original construction timeline called for completion in 100 days. The two internal sections were completed in early November 2010, effectively sealing the breach.

The crest of the structure is approximately +2.4 m NAVD. The armor stone is specified as an ALDOT Class 5 riprap, which has a median weight of 454 kg (1000 lbs). Assuming some nominal values and considering the 2:1 structure side slopes, the median weight of the armor stone should accommodate wave heights up to 1.5 m according to Hudson's equation (USACE, 1984). The structure base is 26 m wide in some locations and rests on a Tensar BX 1200 geogrid. A total of nearly 215,000 metric tons of rock were used to build this structure. Other structure quantities include: 54,000 m^2 of geogrid; 47,000 m^2 of geotextile fabric; 100,000 metric tons of armor stone; 20,000 m^3 of sand fill; 108,000 metric tons of stone for the two internal structures; and 7,000 metric tons of #57 stone to choke the structure crest. A Type III floating turbidity barrier was used throughout the project.

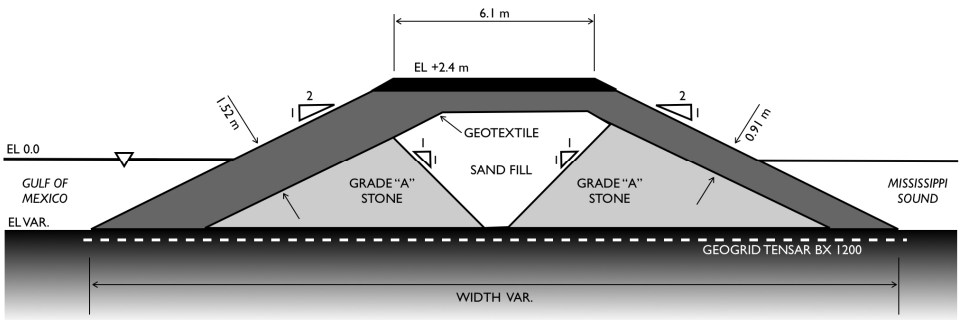


Figure 8. General cross-section sketch of the rubble mound structure constructed to close Katrina Cut.

TIDAL INLET CLOSURE: LITTLE LAGOON PASS

Background. Little Lagoon is a 9 km^2 estuary separated from the Gulf of Mexico by the beaches of Gulf Shores (see Figure 1). The estuary has a large freshwater input from a nearby freshwater lake and serves as an aquatic nursery for octopus, squid, speckled trout and flounder. Little Lagoon has a very small tidal connection to the Gulf of Mexico that is maintained through regular dredging to ensure adequate flushing and provide a navigable waterway for those living on the lagoon. The tidal connection, called Little Lagoon Pass, is stabilized by a combination of steel sheetpile and reinforced concrete seawall. The width of the pass as it cuts across the beach is only about 15 m.

Strategy. Although the tidal connection of Little Lagoon is highly restricted, officials in the City of Gulf Shores were concerned about the potential environmental impacts and the difficulty of cleaning large amounts of oil from within the estuary. City officials elected to plug the tidal pass with sand rather than battle what may have been a continuous tending of ocean boom on the gulf side of the pass. The pass was initially plugged in early May using over 4500 m^3 of sand fill, as shown in Figure 9.



Figure 9. Aerial photo of the sand barrier in Little Lagoon Pass. The estuary is in the foreground while the Gulf of Mexico is in the background. The road visible is West Beach Boulevard, AL 182. Photo courtesy: Mark Acreman, City of Gulf Shores.

Results. City officials were very pleased with their decision to plug the pass. The estuary did not receive any reports of visible oiling with the barrier in place. Indeed, the barrier was installed prior to Baldwin County beaches receiving their first major oiling. As seen in Figure 9, some boom was deployed on the gulf side of the sand

barrier to train oil to an extraction location. The final restoration of Little Lagoon Pass was initiated in February 2011.

Obstacles. Precipitation, the seasonal groundwater table, and inflows from a nearby freshwater lake primarily control water levels in Little Lagoon owing to the small 0.4 m tide range in the area. As a result, the sand barrier was mechanically breached in August 2010 to relieve an accumulation of water due to precipitation that increased lagoon waterlevels by about 0.5 m above their normal levels. An earlier breaching was conducted during an ebb tide in July 2010 to allow flushing of the estuary. A secondary diversion channel was excavated through the subaerial beach in an "S" shape to control the exchange of estuary and gulf water during these mechanical breaches.

CONTAINMENT BOOM

Background. Perdido Pass, located in Orange Beach, Alabama, provides a tidal connection and navigable waterway between the Gulf of Mexico, Perdido Bay, Wolf Bay, and the Gulf Intracoastal Waterway (see Figure 1). The pass itself is stabilized with rubble mound jetties and reinforced concrete seawalls. A fixed bridge carries Perdido Beach Boulevard (AL 182) over the pass to Escambia County, Florida immediately to the east. It is not uncommon to have boat traffic numbering in the thousands in this pass on a single day during tourist and sportfishing seasons. The pass itself is a dynamic place: tidal currents in the pass routinely exceed 4 m/s (8 kt).

On June 9, 2010, a concentrated slick of surface oil entered Perdido Pass on a flood tide, subsequently soiling shoreline as much as 5 km away from the pass. Hundreds of meters of existing boom deployed to waterways north of the pass were oil-laden. Two days later, waters near Perdido Pass were closed to all recreational and commercial boat traffic not involved with oil response operations.

Strategy. An early idea for preventing another widespread oiling of the bays was to plug Perdido Pass with a large volume of rock and sand fill. For a number of reasons, navigation included, this plan was never implemented. Similarly, any complete closure of the pass would create a significant hardship for recreational and commercial boaters in the area, as well as reduce the flushing capacity of the tidal inlet. And due to the strong tidally induced flows through the pass (> 4 m/s), the deployment of standard ocean boom was not possible owing to its practical limitation of about 0.4 m/s (0.7 kt).

A local engineering firm was contracted to design, build, and install a boom system that would train surface oils to extraction locations while allowing for safe navigation through the pass. The plan called for nearly 1000 m of 1 m diameter steel dredge pipe to be filled with polystyrene foam to aid in flotation, and to be anchored with chains affixed to a number of 1 m diameter steel pipes driven into the seabed. A photo of the boom during construction is provided in Figure 10. The system also included a steel

curtain and dampers affixed to the bottom of the floating pipe to capture and train oil entrained in the upper portion of the water column to extraction points.



Figure 10. Photo of the polystyrene foam-filled 1 m dredge pipe used as oil training boom in Perdido Pass, Alabama. The Gulf of Mexico is in the background and the image is shot looking toward the west-southwest. Orange ocean boom can be seen in the distance below the horizon. Photo courtesy: Phillip West, City of Orange Beach.

Results. Construction of the novel boom system began in mid-June 2010 and was completed in the first weeks of July 2010. The system sustained some minor damage from increased wave heights during Hurricane Alex prior to completion ($H_s \sim 2$ m, $T_p \sim 10$ s in 25 m of water south of Orange Beach). The boom system was disassembled on July 23, 2010 as a precaution ahead of a strengthening Tropical Storm Bonnie in the Gulf of Mexico. Days later, the Macondo well was capped, and the infrequent presence of oil near the pass did not justify replacement of the system. The total project cost was about $5.3 million USD, where $4.8 million USD was used for construction, and the remaining for removal and disassembly. By comparison, the unit cost of ocean boom during the height of the oil spill crisis was approximately $330/m.

Obstacles. Although the complete system was only in place for a few weeks during the oil spill, officials with the City of Orange Beach stated that the system performed as designed. The boom could be seen training oil to the extraction points on the flood tide, and even captured some surface oils that had been communicated through the coastal waterways on the ebbing tide. Its premature disassembly in light of tropical storm activity may point to a possible future improvement of the system: to be able to

flood and sink the boom during rough weather as opposed to complete disassembly. One idea was to use pressurized tubes as opposed to the foam-filled steel dredge pipe.

CONCLUSIONS

The 2010 oil spill in the Gulf of Mexico had a tremendous impact on the coastal resources and economies of Texas, Louisiana, Mississippi, Alabama, and Florida. In the state of Alabama, 100% of the beaches were impacted by oil in some form during the one-year period May 2010 – May 2011. A number of strategies were implemented to eliminate, capture, skim, train, and contain surface oils in order to mitigate damage to shorelines, salt marshes, and other coastal habitat. Even within the state of Alabama, some novel approaches were considered and taken to minimize the impacts of oil, particularly on its 100 km of sandy beaches. While the beaches of Baldwin County endured a rather lengthy cleaning process that included tilling of the uppermost 1 m of sand across the subaerial beach, Dauphin Island chose to erect two shore-parallel protective sand barriers to contain oil on the beachface. A small tidal inlet was effectively plugged with sand to prevent the oiling of a sensitive estuary; a novel boom system was designed and implemented to withstand the strong 4 m/s current in a dynamic tidal inlet; and a barrier island breach was sealed with a 2.5-km-long sand-tight rubble mound structure. In most cases, sound coastal engineering principles were applied in the design and implementation of oil spill response projects, but a number of lessons were learned that highlight areas for improvement. The identification of an oil spill as an ever-present coastal hazard for much of the shoreline of the Gulf of Mexico should serve to stimulate continued discussion within the coastal engineering community on how best to respond to such a disaster in the future.

ACKNOWLEDGEMENTS

The authors would like to recognize and thank Phillip West, Coastal Resource Manager for the City of Orange Beach, and Mark Acreman, Public Works Director for the City of Gulf Shores, for contributing to this article.

REFERENCES

Froede, C. R. Jr. (2006). “The impact that Hurricane Ivan (September 16, 2004) made across Dauphin Island, Alabama.” *Journal of Coastal Research*, 22(3), 561 – 573.

Froede, C. R. Jr. (2008). “Changes to Dauphin Island, Alabama, brought about by Hurricane Katrina (August 29, 2005).” Journal of Coastal Research, 24(3), 110 – 117.

Hallermeier, R. J., and P. E. Rhodes. (1988) “Generic Treatment of Dune Erosion for 100-Year Event,” Proceedings, Twenty-First International Conference on Coastal Engineering, ASCE, pp. 1121-1197.

U.S. Army Corps of Engineers (1984). *Shore Protection Manual, 4th Ed.* Waterways Experiment Station, Vicksburg, MS.

Sea Level Rise Impact Assessment and Mitigation Alternatives Development for Balboa Island and Little Balboa Island, City of Newport Beach, California

Ying Poon[1], Brett Sanders[2], Randy Mason [3], and Robert Stein[4]
[1]Everest International Consultants, Inc., 444 West Ocean Blvd, Suite 1104, Long Beach, CA 90802, USA; Ying.Poon@EverestConsultants.com;
[2]Civil and Environmental Engineering, University of California, Irvine, Irvine, CA 92697
[3]URS Corporation, 5772 Bolsa Avenue, Suite 100, Huntington Beach, CA 92649
[4]City of Newport Beach, 3300 Newport Boulevard, Newport Beach, CA 92663

Abstract: *The City of Newport Beach (City), a highly developed, densely populated coastal city in southern California is periodically subject to flooding from coincident high tides and waves. To prepare for sea level rise and potential flood damages, the City initiated a study to assess the potential flood impact to Balboa Island and Little Balboa Island. A recently developed 2D flood simulation model is utilized to investigate the effect of high tides occurring with increased sea levels. Additionally, a simple wave overtopping model is proposed to account for the effect of wind waves and ocean swells. The results of the flood model simulations were used to help the City to formulate flood inundation mitigation alternatives.*

Keywords: *Coastal flooding, Inundation modeling, Flood mapping, Urban flooding, Wave overtopping, Sea level rise*

1. Introduction

The City of Newport Beach (City) has been dealing with localized flooding for several decades due to lower-than-optimum seawall and land mass heights in various locations around Newport Harbor. Flooding of streets and walkways has occurred on Balboa Peninsula, Balboa Island and other localized areas as a consequence of high tides and waves. The challenge of flood control is compounded by City storm drain lines that empty by gravity into the Bay and therefore do not provide flood relief when the bay water level is high. To a lesser extent, distress in the form of concrete cracks and construction joints allows water to breach the protection of these walls and contribute to localize flooding.



Figure 1. Site Location

To prepare for sea level rise and potential flood damages, the City of Newport Beach initiated a study to assess the potential flood impact to Balboa Island and Little Balboa Island. The study includes: 1) evaluation of conditions of existing seawalls protecting the islands, 2) prediction of flood water overtopping and resulting inundation due to sea level rise and storm events over the next 100 years, and 3) evaluation of flood hazard mitigation alternatives.

2. Balboa Island and Little Balboa Island

Balboa Island and Little Balboa Island are two adjacent islands located in Lower Newport Bay in the City of Newport Beach in Orange County, California (Figure 1). These two islands are also collectively known as the Balboa Islands. Both islands are encircled by concrete seawalls that provide protection from flooding during periods of high tides and waves. Under present-day conditions, wave overtopping and flooding do occasionally occur on Balboa Island during high tide and high wave events, but in general do not cause damage to residences, businesses, vehicles or public infrastructure. The higher seawalls around Little Balboa Island protect it from seawater overtopping.



Figure 2. City personnel pumping storm water

During high water events, the City closes the storm drain outlets to the Bay to prevent sea water from flowing backwards through the storm water outlets and inundating Balboa Island. Figure 2 shows a picture of City personnel pumping out water that was collected at the storm drain outlet junction structure located at a bay-front street in a high water, high wave event in December 22, 2010.

During high water and high wave events, there are four areas on Balboa Island that are particularly susceptible to flooding; they are: the Balboa Island ferry boat landing and its surroundings, and the three bridges on the Island - the Marine Avenue Bridge, the Park Avenue Bridge, and the Collins Island Bridge. If an extension or reconstruction of the existing seawall is to be performed, these four areas need to be modified to prevent them from acting as openings in an otherwise solid



Figure 3. Flooding at Balboa Island Ferry Landing

seawall fortification around the island. Figure 3 shows flooding of the Balboa Island ferry landing area during the December 22, 2010 flood event.

3. Flood Modeling

An unstructured, variable grid, Godunov-type finite volume model, based on the shallow water equations, BreZo, was applied to Newport Harbor to map present-day (2010) and future flood zones on Balboa Island and Little Balboa Island. The model incorporated scenarios for sea level rise projected for 2025, 2050 and 2100, as well as proposed improvements. The model was developed to account for both wave- and tide-driven sea wall overtopping. Moreover, overtopping flows are predicted to spread in accordance with local topography and the effects of gravity and friction. Detailed descriptions of the Brezo model used for this study can be found in Sanders (2008) and Schubert et. al. (2008).

A variable-resolution computational mesh was developed for this study. In preparing the mesh, special attention was paid to Balboa and Little Balboa islands. Edges of the mesh were aligned with sea walls around these islands, and flagged with unique identifiers that allowed the model to easily incorporate surveyed wall height data and the wave-driven overtopping data. The mesh was locally refined on Balboa and Little Balboa islands for flood mapping precision, an intermediate resolution was used within the embayment, and a coarser resolution was used offshore. The finest and coarsest resolution corresponds to approximately 10 feet and 1000 feet, respectively. In total, the mesh consisted of 282,935 cells.

Several datasets were relied upon to implement BreZo, including topographic and bathymetric data, seawall and house first-flood elevation data, ocean tide height data (including sea level rise projections), and wave-driven overtopping rates. These are briefly described in the following.

Topographic and Bathymetric Data

Several sources of data were obtained and organized to provide a seamless terrain map that synthesizes available topographic (above sea level) and bathymetric (below sea level) ground elevation data in the vicinity of Newport Harbor. The data sources include the following:

1. Light Detection and Ranging (LiDAR) topography data;
2. Upper Bay bathymetry resulting from a multi-beam survey for the U.S. Army Corps of Engineers, Los Angeles District;
3. Lower Bay bathymetry data resulting from a multi-beam survey for the U.S. Army Corps of Engineers, Los Angeles District; and
4. Offshore bathymetry data from the National Geophysical Data Center (NGDC) 3 Arc-Second Coastal Relief Model accessed from the Southern California Coastal Ocean Observing System (SCCOOS) website.

Seawall Elevation and House First Floor Elevation Data

Balboa and Little Balboa Islands are encircled by concrete seawalls that provide protection from flooding during periods of high tides and waves. Because elevations of the seawall represent a threshold for overtopping, it is critically important that they are surveyed with 0.1 foot accuracy or less. The seawall elevations used for setting up the BreZo Model were surveyed for this study with a vertical accuracy of approximately 0.01 feet

Ninety-one houses along three streets were also surveyed for their first-floor elevations. The data were used to generate a probability distribution representing the first floor elevations for the Balboa Islands which are used for assessing potential flood impacts to the houses on the Islands under different flood model scenarios (see Section 4).

Water Level Description

Extreme high tide scenarios are needed to support hydraulic modeling of coastal flooding and plan for sea level rise. The hydraulic model uses Equation 1 below to simulate the rise and fall of the ocean height, h(t), which in turn causes the tide to rise in the embayment and potentially flood low lying areas.

$$h(t) = H_0 + a\cos\left(\frac{2\pi(t-t_1)}{t_2}\right) + b\sec h^2\left(\frac{t-t_3}{t_4}\right) \qquad \text{[Eq. 1]}$$

In this equation, t represents time, H_0 represents the mean sea level, a represents the amplitude of a periodic wave with phase t_1 and period t_2, and b represents the amplitude of a solitary wave with phase t_3 and duration parameter t_4. Equation 1 allows the hydraulic model to account for increases in sea level and the probability of an extreme high tide. The value of H_0 is varied by year to account for higher sea levels projected for the future. The remaining tide-height parameters (a, b, and time constants) are specified to simulate either a 10 percent or 1 percent annual exceedance probability tide. Two sources of information were merged to parameterize Equation.1: hourly tide measurements and sea level rise projection.

Over 80 years of hourly tide measurements at Los Angeles (NOAA Station ID: 9410660) were analyzed for this study. Using the hourly record, the mean and maximum value of the tide height from each year was computed, and a linear model was least-squares fit to each of the time series. These tide heights and trends are shown in Figure 4.

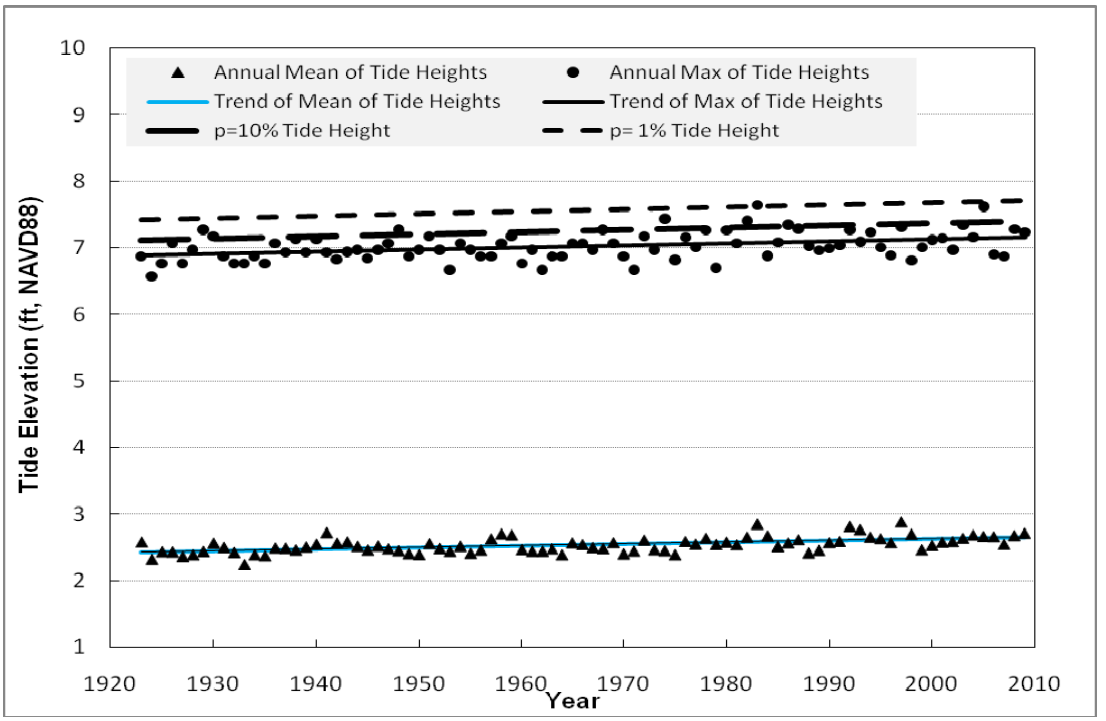


Figure 4. Mean and annual maximum tide elevations, and trends of mean, maximum, 10% and 1% annual exceedance-probability tide heights, Los Angeles, 1923 – 2009

As shown in the Figure, the maximum tide heights exhibit considerable inter-annual variability on the order of one foot. For this study, this variability is treated by considering the extreme tide height to be a random variable and probability analysis was performed to obtain the 1% and 10% extreme high tide trends shown in the figure. Based on the analyses of the historical data, mean sea level for 2010 is 2.65 feet NAVD88, and the 10% and 1% probability of occurrence extreme tide heights for 2010 are 7.41 and 7.71 feet NAVD88, respectively.

Future mean sea levels are estimated by applying the methodology recommended by the U.S. Army Corps of Engineers (USACE 2009). This gives sea level rise, SLR (in feet), between years y_1 and y_2 as follows,

$$SLR(y_1, y_2) = 0.0056(y_2 - y_1) + 3.2964 \times 10^{-4}\left((y_2 - 1986)^2 - (y_1 - 1986)^2\right) \quad \text{[Eq. 2]}$$

Figure 5 show projections of future tide heights based on the sea level rise trends given by Eq. 2, assuming the trend for extreme high tide follows the trend for mean sea level. Projections point to a rapid increase of sea level over the next decade, compared to the historical rate of rise. The projections also show that the differences between 10% and 1% extreme tide events is very important in the near term, but less important in the long term compared to sea level rise.

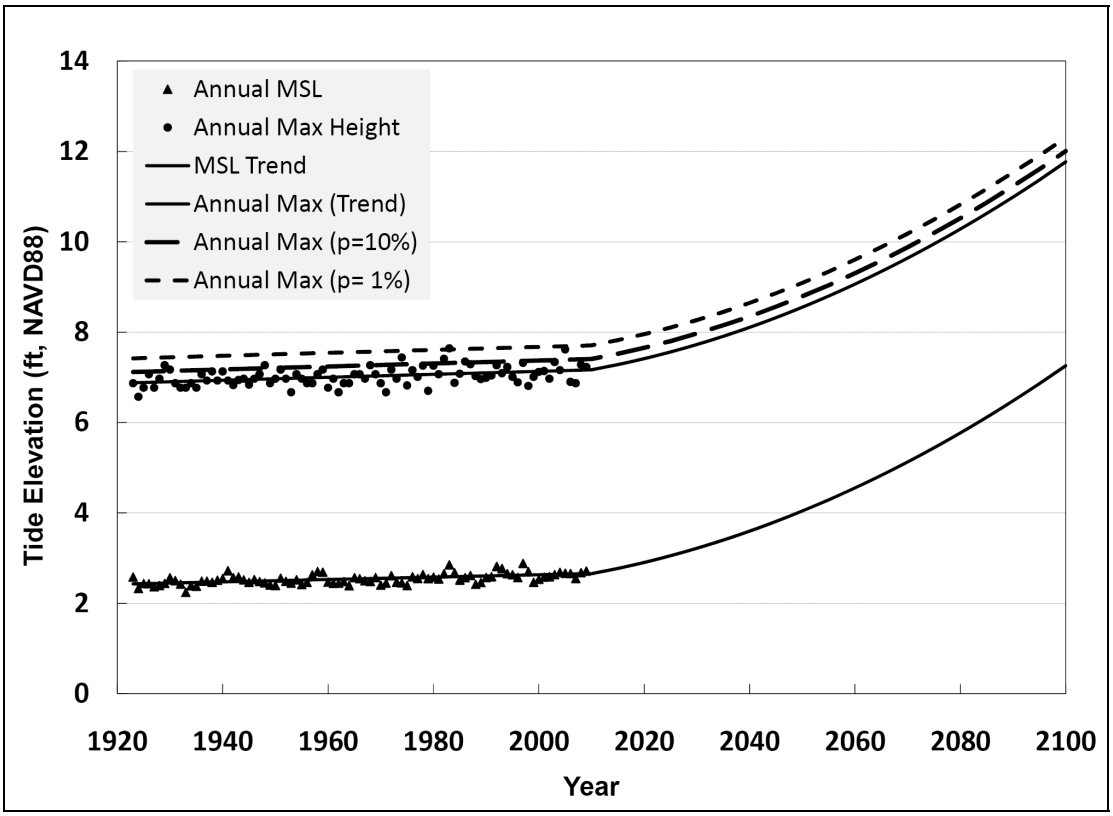


Figure 5. Projections of mean sea level and extreme tide heights through Year 2100

Wave-driven Overtopping Rates

Waves are an important driver of embayment flooding when the tide level approaches the crest of a flood barrier. Wave action provides the necessary energy for water to rise up above the tide level and spill over the barrier. The rate at which this occurs is dependent on many factors such as the wave height, period, water depth at the toe of the wall, the height of the tide, and the height of the wall. Figure 6 shows an example of wave overtopping a seawall at Balboa Island during the December 22, 2010 flood event.



Figure 6. Waves Splashing over the Balboa Island Seawall (December 22, 2010)

It can be expected that as the tide height, *h*, rises, the rate of wave overtopping will commence once the tide reaches a height that allows the first drops of water to spill

over the wall. As the tide continues to rise, the rate of overtopping can be expected to increase until the tide height surpasses the height of the wall. Thereafter, weir-like flow can be expected to dominate the overtopping rate and wave-driven flow can be ignored. BreZo was modified to account for the mode of wave overtopping described here. The following formula was used to specify the volumetric flow rate along sea walls where wave overtopping is expected:

$$q_{wo} = \begin{cases} q_{wo}^{\max}\left(\dfrac{h - h_{q0}}{h_{wall} - h_{q0}}\right) & if \quad h_{q0} \le h \le h_{wall} \\ 0 & otherwise \end{cases} \qquad \text{[Eq. 3]}$$

where $q_{wo}^{\max}$ represents the maximum rate of wave overtopping based on all possible water levels, h_{wall} represents the height of the wall, and h_{q0} represents the tide height corresponding to the onset of overtopping.

Wave overtopping rates were calculated using the ACES program within the CEDAS (version 4.03) suite of programs developed by the U.S. Army Corps of Engineers (Veri-Tech, Inc., 2009). The parameters controlling the onset of wave overtopping and the overtopping rate include structure type and structural slope, beach slope, water depth, and wave characteristics (height and period). Based on the wall types, mudline elevations, and wave conditions for Balboa Island, wave overtoppings were calculated for three different reaches. Reach 1 and 2 correspond to the southwest and south sides of Balboa Island, respectively, and Reach 3 corresponds to the south side of Little Balboa Island. All other sides of these islands were ignored, relative to wave overtopping, due to a negligible wind fetch.

4. Model Scenarios and Results

The model was used to compare flood zones based on present-day seawall heights, a future sea wall raised uniformly to a 9.8 feet NAVD88 height, and an interim extension of the sea wall height by 6 to 8 inches (replacing existing seawall cap with a taller cap, add an extension to the existing cap, or deployment of sandbags). A total of 17 different modeling scenarios were considered to account for the varied effects of high tides, waves, sea levels, and sea wall heights. These model scenarios and model results are shown in Table 1. In the table, the number of flood impacted buildings for each model scenario is estimated by comparing the modeled flood water depth at each parcel with a randomly generated first floor elevation for that parcel based on the first floor probability distribution described earlier.

The model results show that Balboa Island is presently vulnerable to extensive flooding because of low points in the seawall at the Balboa Ferry ramp, the Collins Island bridge crossing, and the relatively low height of its seawall. The sea wall around Little Balboa Island is higher than the Balboa Island sea wall and therefore offers better protection against present-day flood risks. Modeling shows that present-day flooding may occur from a combination of high tides and high waves, and the

southwest boundary of the island is particularly vulnerable to overtopping due to its exposure to southerly and westerly winds. Modeling also shows that a combination of high tides and ocean swell may cause overtopping of the southern seawall due to its orientation towards the harbor mouth. Figure 7 shows an example of flood model results for the existing seawalls with and without the effects of wave overtopping under a 10% exceedance tide (Scenario 1 versus Scenario 3).

Table 1. Model Results for 17 Scenarios

Scenario	Year	Tide Height (Annual Exceedance Probability)	Wave Scenario	Average Flood Depth (ft)	Impacted Parcels (Number)	Parcels Impacted (%)	Impacted Buildings (Number)	Impacted Buildings (%)
Existing Condition Scenarios								
1	2010	10%	No Waves	0.26	61	4.0	3 ± 2	0.2
2	2010	10%	Wind Waves	0.26	61	4.3	3 ± 2	0.2
3	2010	10%	Ocean Swell	0.29	514	36.5	24 ± 5	1.7
4	2010	1%	Wind Waves	0.36	324	23.0	22 ± 4	1.5
5	2025	10%	Wind Waves	0.48	681	48.3	66 ± 7	4.7
6	2025	10%	Ocean Swell	0.79	1,176	83.4	235 ± 13	16.6
7	2025	1%	Wind Waves	1.16	1,179	83.6	420 ± 14	29.8
8	2050	10%	No Waves	1.84	1,410	100.0	894 ± 17	63.4
9	2050	1%	No Waves	2.15	1,410	100.0	1047 ± 15	74.3
10	2100	10%	No Waves	5.02	1,410	100.0	1410 ± 1	100.0
6-inch Extension Scenarios								
11	2010	1%	Wind Waves	0.03	0	0.0	0	0.0
12	2025	1%	Wind Waves	0.12	12	0.9	0-1	<0.1
10-foot Seawall Scenarios								
13	2010	1%	Wind Waves	0	0	0.0	0	0.0
14	2025	1%	Wind Waves	0	0	0.0	0	0.0
15	2050	1%	Wind Waves	0	0	0.0	0	0.0
16	2050	10%	Wind Waves	0	0	0.0	0	0.0
17	2100	1%	Wind Waves	5.30	1,410	100.0	1410 ± 1	100.0

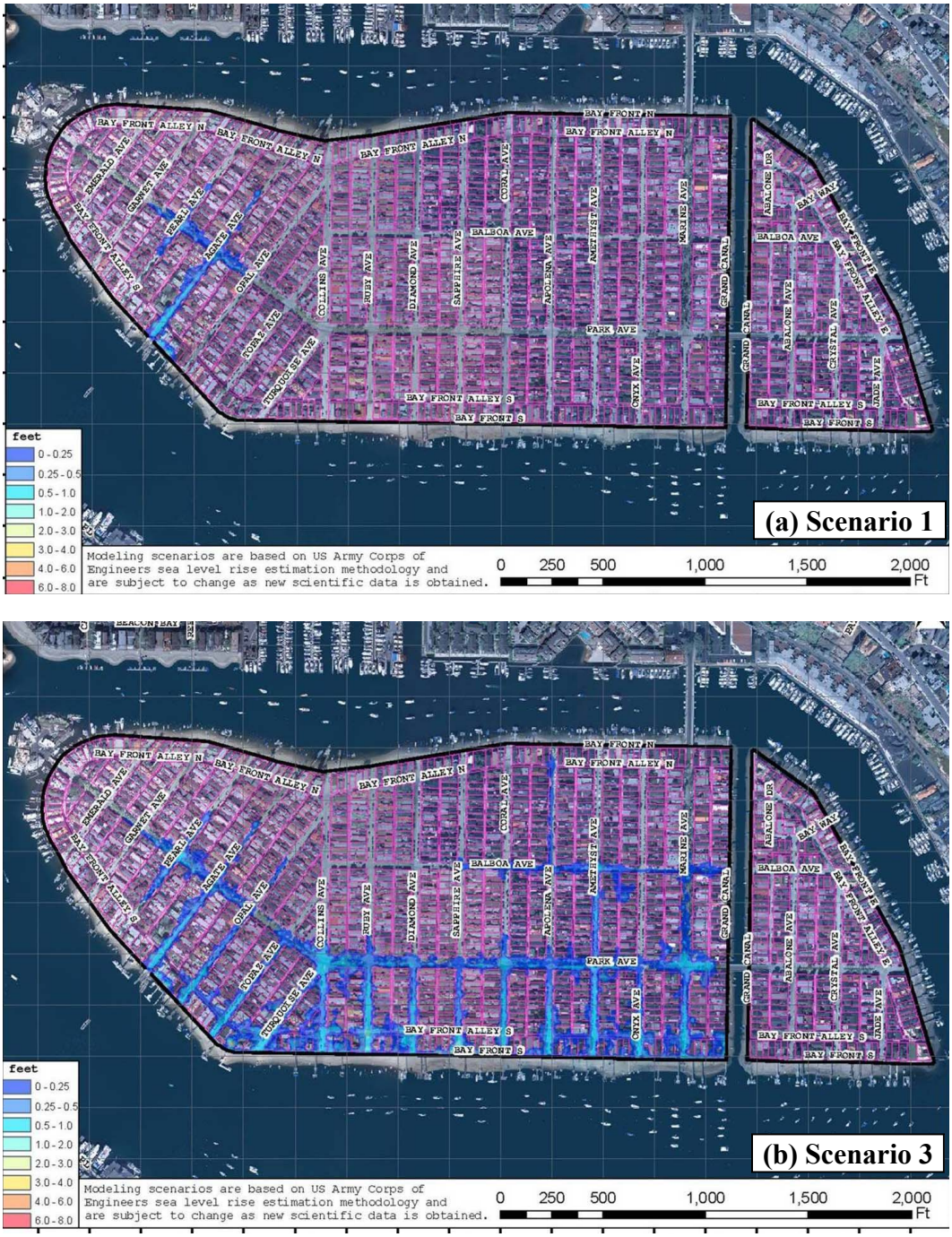


Figure 7. Modeled flood depths for existing condition (a) Scenario 1 – without waves; and (b) Scenario 3 – with waves

Modeling also shows that by extending the existing seawall cap by 6 inches and raising the height of the Balboa ferry ramp and Collins Island bridge crossing to the height of adjoining sea walls, both islands would be protected through 2025 from a flood event caused by the combined effects a 1% exceedance probability storm tide and 10% exceedance probability wind waves. However, the islands would not be protected far past 2025 based on current sea level rise projections. The effectiveness

of extending the existing seawall cap by 6 inches is illustrated in Figure 8, which compares the flood model results for Scenario 7 (existing seawall, year 2025, 1% exceedance tide and wind waves) with Scenario 12 (same environmental condition as Scenario 7 but with 6 inch extension of seawall).

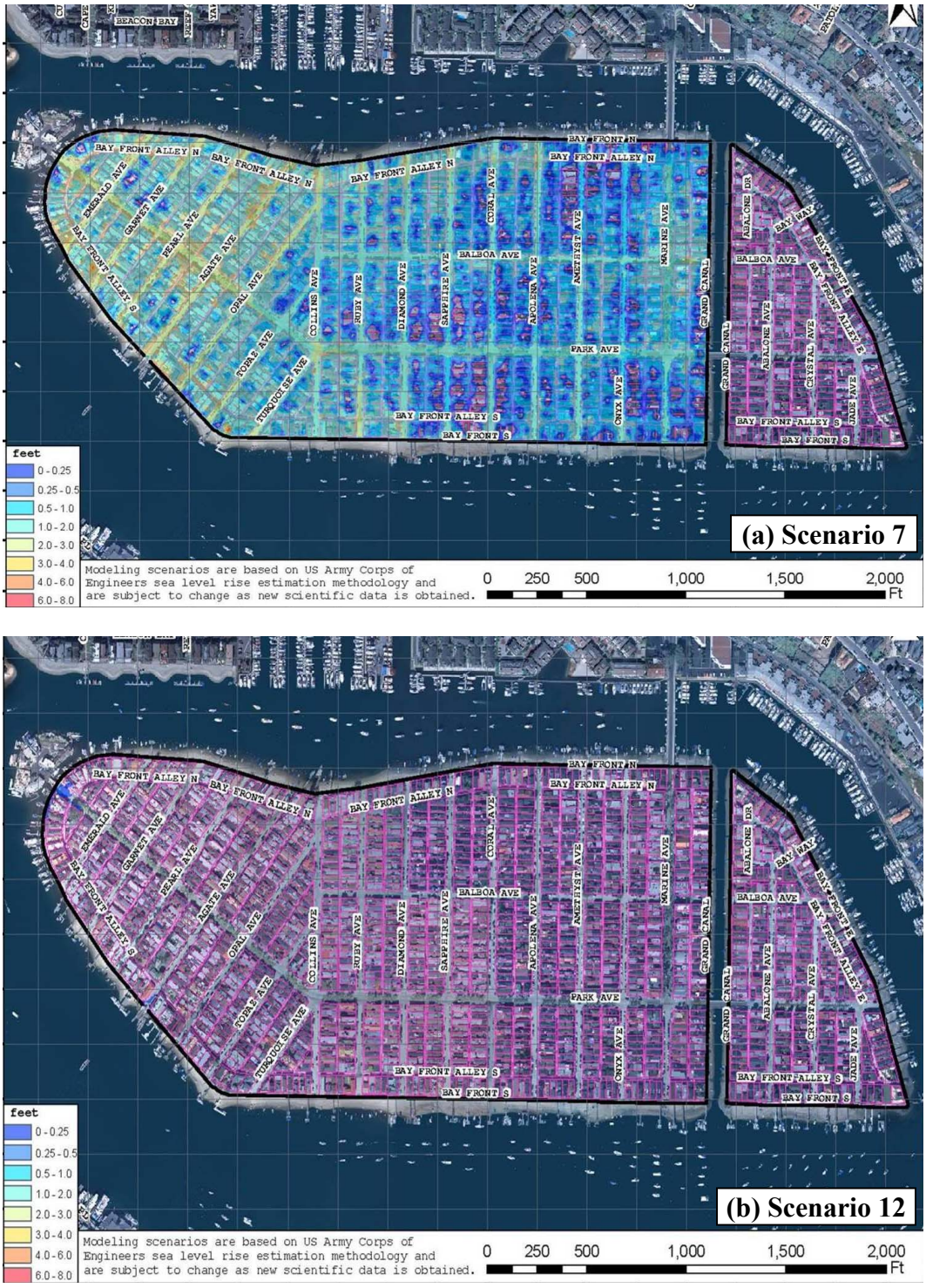


Figure 8. Modeled Year 2025 flood depths for 1% exceedance tide and wind waves (a) Scenario 7 – existing seawall and (b) Scenario 12 – 6-inch extension

Modeling also shows that a seawall constructed to a height of 9.8 ft NAVD88, uniformly around the islands including all road crossings, would provide protection from flooding from the 1% storm tide and 10% waves scenario through 2050. The islands' seawalls would need to be raised 3 or 4 feet to protect the islands after 2050, based on current sea level rise projections.

5. Flood Inundation Mitigation Solutions

Review of available documents, reports and drawings revealed that most of the existing concrete seawalls were constructed in the 1930s to replace earlier timber seawalls. Site observations determined that an undocumented extension of 6 to 12 inches was added to the seawall cap around Little Balboa Island. The site observations also found universal distress in the caps, specifically multiple cracks, coinciding with the locations of the soldier piles. In addition, common and continuous cracks were observed along the seawall approximately 2- to 4-inches above the boardwalk behind the seawalls. Based on the review of construction documents, assessment of the construction practices in the 1930s, and site observations of the existing seawall conditions, it is estimated that the remaining useful life of the seawalls is between 10 to 25 years.

Even though it is possible to either replace the existing cap with a taller cap or extend the existing cap to a taller height to prevent flooding from high water levels and wave overtopping, it is not recommended because the existing seawalls at Balboa Island and Little Balboa Island only have a remaining usable life of between 10 to 25 years. In addition, the flood modeling results indicate that properly maintained sandbag extension would be sufficient to prevent overtopping from high tides and waves for the remaining usable life of the seawalls. Hence, instead of fixing the cap, a replacement seawall with top elevation at +9.8 feet NAVD88 is recommended. The new seawall should have a flexible design such that it can easily be further extended by 3- to 4-feet if and when rising sea level dictates. For the Balboa ferry terminal, solutions include either raising the dock and launch ramp, or shifting the launch ramp further into the main channel so that existing properties can remain unchanged. Finally, to limit future damages, the City should establish appropriate minimum lowest first floor elevation in accordance with the federal Base Flood Elevation (BFE).

6. References

Sanders, B.F. (2008) Integration of a shallow-water model with a local time step, Journal of Hydraulic Research, 46(4) 466-475.

Schubert, J.E., Sanders, B.F. Smith, M.J. and Wright N.G. (2008) Unstructured mesh generation and landcover-based resistance for hydrodynamic modeling of urban flooding, Advances in Water Resources, doi:10.1016/j.advwatres.2008.07.012.

U.S. Army Corps of Engineers. 2009. Water Resources Policies and Authorities Incorporating Sea-Level Change Considerations in Civil Works Programs.

Veri-Tech, Inc. 2009. Coastal Engineering Design and Analysis System (CEDAS) 4.03. http://www.veritechnic.com/products/cedas/index.php.

Comparison of Two Severe Storms in Terms of Wave Characteristics Based On Recorded Field Data

Alireza Jafari[1] , Nick Cartwright[2] , Peter Nielsen[3]

[1]Griffith School of Engineering, Gold Coast Campus, Griffith University, Southport QLD 4215, Australia, a.jafari@griffith.edu.au

[2]Griffith School of Engineering, Gold Coast Campus, Griffith University, Southport QLD 4215, Australia, n.cartwright@griffith.edu.au

[3] School of Civil Engineering, The University of Queensland, Brisbane St Lucia, QLD 4072,Australia, p.nielsen@uq.edu.au

Abstract

Understanding of storm wave behaviour is critical to the development of appropriate coastal hydrodynamic models to assess risk management and mitigation strategies in response to problems such as coastal inundation and erosion. This is becoming increasingly important in the present age of accelerated global warming where it is expected that there will be an increase in the intensity of severe weather events such as tropical cyclones. One of the main problems in storm wave predictions is the lack of availability of sufficient field data for used in calibrating and verifying models. Most of the existing models have been validated based on laboratory works and as such are not entirely representative of storm wave conditions experienced in the field. This paper, presents a novel approach to the collection and analysis of field data under two different storm events which hits south-east Queensland in 2009, namely Tropical Cyclone Hamish and an East Coast Low. Results of these two severe storms are added to a data set collected in calm condition and in order to extracting new formulation of γ_s.

Key Words: Storm Surge, Tropical cyclones, Monometer Tubes, Wave Setup

INTRODUCTION

This paper presents field data collected under storm conditions. All of the field work was done at `The Spit on the Gold Coast, Australia. The Gold Coast has a sub-tropical climate located in south east Queensland and experiences tropical cyclones and East Coast Lows during the summer months. The research facility at The Spit (see Figure 1) provides the opportunity of collecting surfzone water level and wave data even under harsh storm conditions. “The Bunker” utilises an array of permanently deployed manometer tubes to observe both time-averaged (mean) water levels (MWL) and high-frequency pressure fluctuations due to wave action at

12 locations extending from 500m offshore in to 60m through the surfzone (Figure 2). Theoretical details of the system can be found in Nielsen and Dunn (1998) and a description of Research Bunker can be found in Cartwright et al. (2009) .



Figure 1. Research Bunker in The Spit, Gold Coast

METHODOLOGY

The manometer tube system is a simple but very robust means of measuring and monitoring wave trains while they travel from 500m offshore through the inner surfzone.

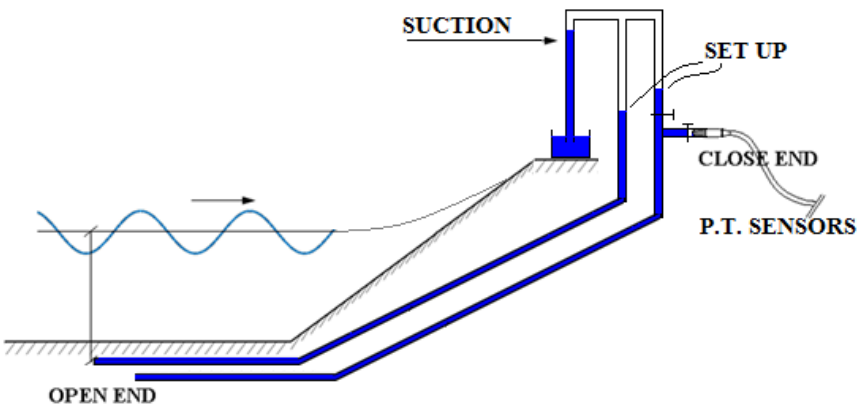


Figure 2. Sketch of manometer tube array, exerting suction make it possible for reading

Generally, the mean water surface level in the ocean is below the ground level at the land based monitoring station and so suction is applied in order to draw the water levels above ground. This is done in an enclosed system with each tube being subjected to the same degree of suction thus preserving the relative water level differences between each tube. The absolute level of all tubes is then converted to

the Australian Height Datum (AHD) by including a surveyed static water level into the manometer board system so that it also experiences the applied suction. The water level in water reservoir is exposed to atmospheric pressure, thus the column of water which climbed inside the reference board shows the amount of suction inside manometer system (see Figure 2).

High frequency water level fluctuations due to wind waves are recorded by connecting pressure transducers directly to the landward end of the tube system (Figure 2). The raw voltage output from each of the sensors is logged at 10 Hz using a data acquisition card connected to a laptop computer. The raw voltage data is then converted to a pressure head by means of a calibration equation derived from laboratory tests. However, the manometer tube systems behaves as a resonating system with one end of the tube open to the wave fluctuations and the other blocked by a pressure transducer (cf. Nielsen et al. (1993)). In order to correct for resonance effects, a gain function introduced is applied to convert the pressure observed at the landward end of the tube to a pressure at the seaward end of the tube. Nielsen et al. (1993) performed laboratory tests to establish the following empirical gain function for a similar tube system,

$$G = \frac{1}{\sqrt{\left(\cos^2\left(\frac{\pi \times f}{2 f_o}\right) + \left[B_1 \frac{L \times f}{c}\left(1 + B_2\sqrt{\frac{\nu}{f \times d^2}}\right)\right]^2\right)}} \qquad (1)$$

where, ν is fluid viscosity (for water $\nu = 1.0\times10^{-6}\ m^2/s$), f_0 is the lowest resonance frequency, i.e., $f_0 = 0.25 \times c/L$, c is speed of waves sound in flexible tubes which can define as

$$c = \frac{1}{\sqrt{\rho(K + D)}} \qquad (2)$$

where, K is the compressibility of the fluid and D is the distensibility of the tube. B_1 and B_2, are two dimensionless factors which initially introduced to be $B_1=0.58$ and $B_2=5.0$ by curve fitting over data obtained from 120m and 50m tubes. However, these two empirical factors, improved by performing extensive sets of laboratory test over 9 different tubes varying in length from 10m to 900m. Applying new dimensionless factor, B_1 and B_2, and replot the GF, result shows very good agreement with Laboratory data. By curve fitting (see Figure 3) following relations can be extract from B_1 and B_2 in term of length over outer diameter ratio of tubes:

$$B_1 = \pi \times \left(L/OD\right)^{-\frac{t}{ID}} \qquad (3)$$

$$B_2 = \left(2 \times OD/t\right) \times e^{-6\times10^{-6}\times\left(L/OD\right)} \quad (4)$$

where, L is tube length, OD is tube outer diameter, ID is tube inner diameter, t is tube thickness.

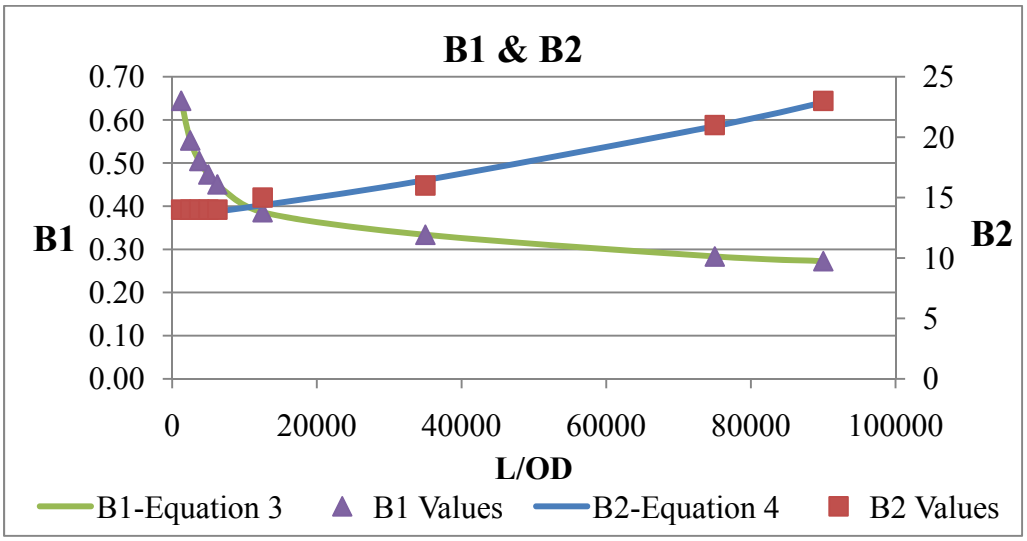


Figure 3. B_1 and B_2 Values against Equations (3) and (4) respectively

After applying the Gain Function to the recorded data, seabed pressure obtained. The seabed pressure is then converted to a free surface fluctuation using the local approximation approach of Nielsen (1989) .

Nielsen (1989) used the concept of most existing wave theories that all surface waves are harmonic and can be define by a combination of suitable harmonic functions. Then for an irregular wave in the ocean, a local frequency for each individual point in time series of water elevation can be defined. For example, for linear wave theory which assumes waves to have sinusoidal shape like $y(t) = A_n \sin(\omega_n t - \varphi_n)$, by considering three points y_{n-1}, y_n, and y_{n+1} the angular frequency for n^{th} point can be approximated by,

$$\omega_n^2 = \frac{-y_{n-1} + 2y_n - y_{n+1}}{\delta^2 y_n} \quad (5)$$

where δ is sampling time interval. Considering p as recorded dynamic pressure below water surface, the semi-empirical function for transferring dynamic pressure to water surface elevation defined as:

$$\hat{\eta}_n = \frac{p_n}{\rho g} \exp\left[A\left(\frac{z}{h}\right)\frac{-p_{n-M} + 2p_n - P_{n+M}}{g(M\delta)^2 p_n}\left(h + \frac{p_n}{\rho g} - z\right)\right] \quad (6)$$

with experimental factor related on depth of recording dynamic pressure

$$A\left(\frac{z}{h}\right) = 0.67 + \frac{0.34z}{h} \tag{7}$$

where, h is water depth, z is the elevation of the sensor used to measure the dynamic pressure and M is a smoothing factor whereby instead of using the first neighbours of n^{th} point to estimate the free surface elevation, the M^{th} neighbours are used to smooth out numerical noise introduced by the finites difference expression in equation (6).

DATA VERIFICATION

The recorded data is verified against data from a nearby wave rider buoy and tide gauge. For example, Figure 4 shows the comparison between the mean water level recorded by the monometer tubes and the nearby Maritime Safety tide gauge data. It is seen that the deeper water tubes closely match the observed tide levels and then the tubes in shallow water sit above the tide as expected due to the upward curving mean water surface caused by wave setup.

Wave characteristics were extracted using both spectral and zero-crossing approaches. Both approaches generally show good agreement with the buoy data (see Table 1). Considering the depth and offshore distance where wave rider buoy is located (1200m offshore and 18m depth) and also the fact that the waves are subjected to transformation process (e.g. refraction, shoaling) while they travel between the buoy and the tubes, it is expected that some differences between the tube and buoy data sets will exist. The comparison between the Gold Coast Buoy and tube system for different time-block data is shown in Table 1. Significant wave height (H_s) and maximum wave height (H_{max}) are derived from the zero-crossing method and the represented peak period (T_p) in right hand side of Table 1obtained from Spectral method to show the general conformity of both methods with Buoy data.

Table 1. Wave characteristics of Gold Coast Buoy against Manometer Tube System

Tube / Length / Time-Block	H_{sign} (Zero-up)					H_{max} (Zero-up)					T_p (Spectral)				
	400	300	250	200	GCB	400	300	250	200	GCB	400	300	250	200	GCB
9:00 AM	0.87	1.1	1.36	1.1	**1.05**	1.44	1.64	1.91	1.62	**1.8**	8.03	7.95	7.95	8.03	**8.33**
9:30 AM	0.92	1.16	1.42	1.18	**1.09**	1.49	1.77	2.04	1.82	**1.66**	7.55	7.55	7.66	7.66	**8.33**
10:00AM	0.89	1.12	1.42	1.21	**1.11**	1.27	1.77	2.46	1.89	**2**	7.95	7.31	7.52	7.25	**8.33**
10:30AM	0.92	1.15	1.3	1.14	**1.09**	1.32	2.05	1.95	1.83	**1.56**	7.84	7.88	7.84	7.73	**8.33**
11:00AM	0.95	1.18	1.38	1.17	**1.01**	1.34	1.95	2.28	1.99	**1.77**	8.03	7.99	7.95	8.07	**7.69**
11:30AM	0.89	1.08	1.32	1.16	**1.08**	1.44	1.64	2.16	1.85	**1.74**	7.76	7.76	7.8	7.76	**8.33**
12:00PM	0.96	1.15	1.36	1.15	**1.08**	1.29	1.75	2.07	1.83	**1.77**	5.85	5.77	5.65	5.77	**8.33**

DATA ANALYSIS AND DISCUSSION

All continuous data break in to 30 min block to make consistency with Gold Coast wave rider buoy. Figure 5 and Figure 6 represent the spectral and zero crossing analysis of the first block of TC Hamish data respectively.

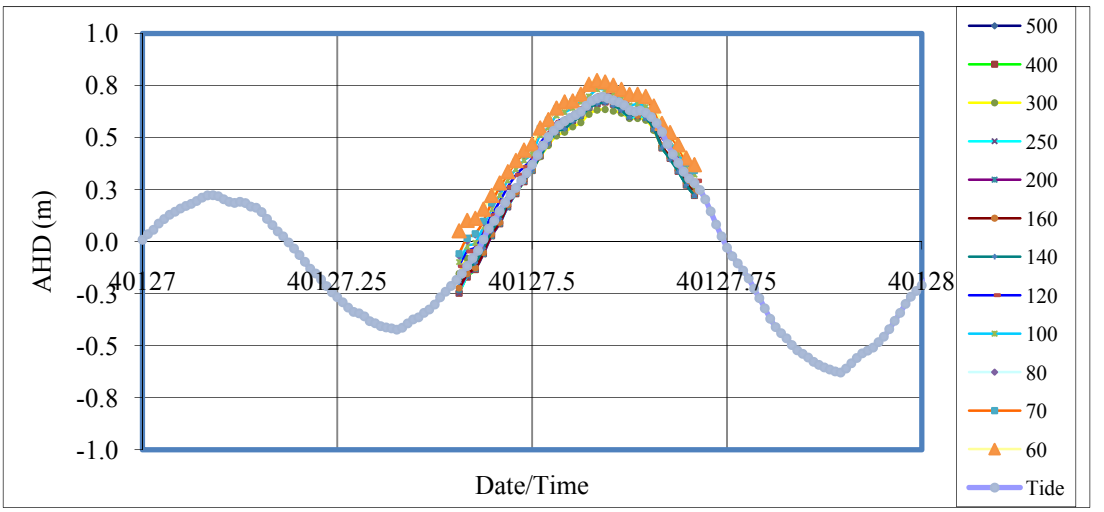


Figure 4. Verifying water level against Maritime Safety Gauge data

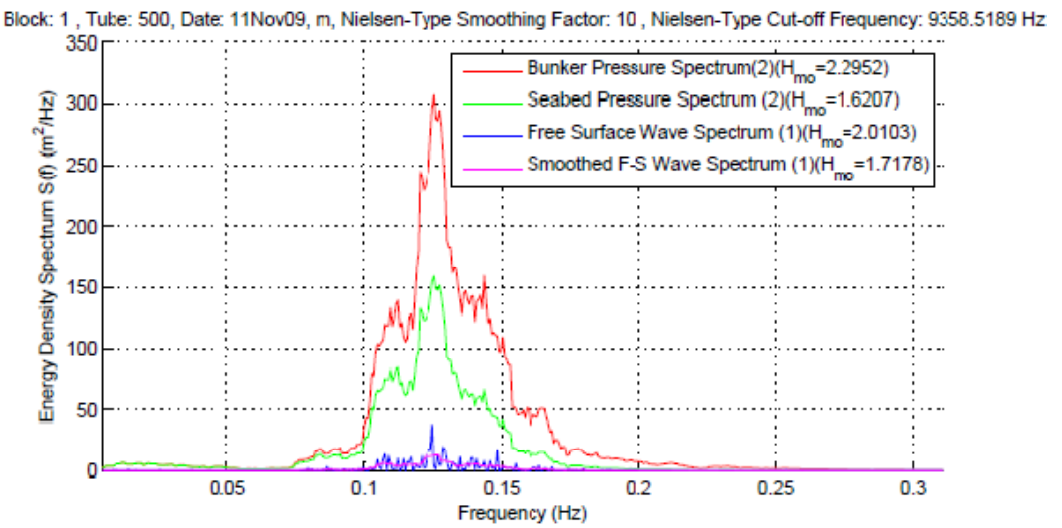


Figure 5. 500m tube Energy Density Spectrum, in first 30min block of data

Table 2.General conditions of each event (BoM (2009); DERM (2009))

Event	Date	Record Duration	Max Wind Speed	Wind Direction	H_{sign}	H_{max}	Damage to Beaches
Tropical Cyclone Hamish	March 2009	3 Days	215 km/hr	East to Northeast	4.7m	8.4m	Moderate erosion
East Coast Lows	May 2009	1 Day	117 km/hr	East to Southeast	6.2m	10.6m	Significant erosion

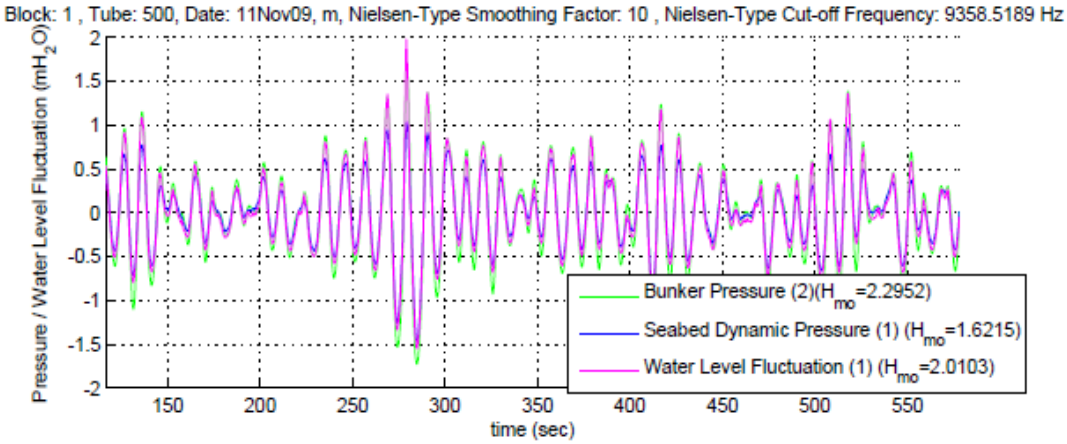


Figure 6. Part of time series data for 500m tube in first 30min block of data

General Observations

General conditions experienced in the two stormy events are presented in Table 2. Also, Figure 7 provides some example data of the significant wave height profile for each of the events which indicates that the offshore wave height in the ECL was larger than TC Hamish. Moreover, Figure 7 shows that the rate of energy dissipation in ECL is higher than TC Hamish (i.e. in ECL 3m offshore wave height reaches 0.5m near shoreline, however, in Hamish it changes from 2m offshore wave to 1.4m nearshore), which the surfzone bathymetry can explain the differences (see Figure 8). Inspection of Figure 7 indicates the presence of two breakpoints, an offshore and nearshore breaker line, at approximately 400m and 160m respectively.

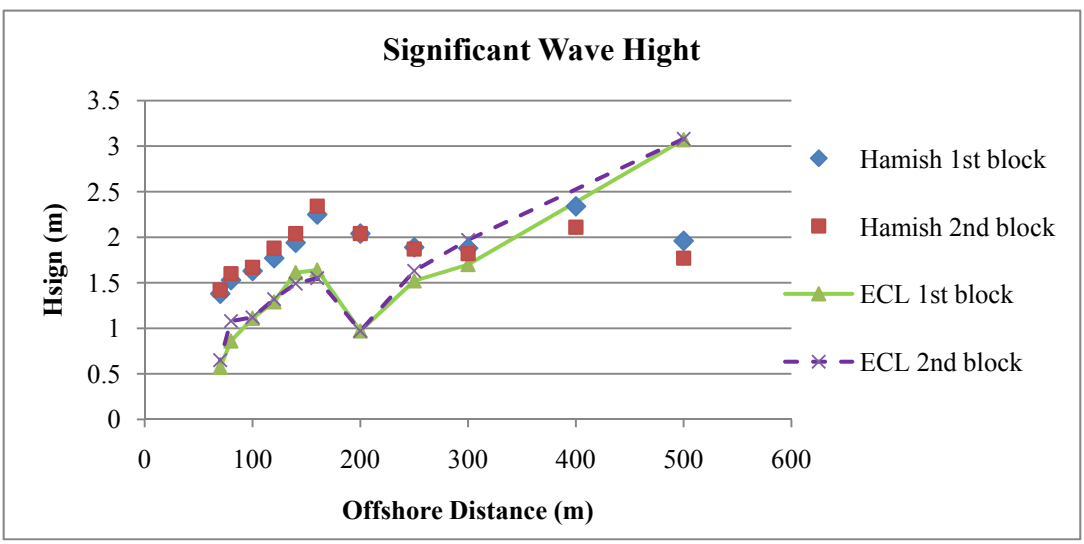


Figure 7. Wave height of first two blocks of each events

Beach Profiles

Beach profile differences are illustrated in Figure 8. Comparing the beach profile before and after Hamish, there were no considerable changes in the profile. A small amount of erosion occurred in swash zone at about 50m, and also the offshore bar moved about 50m offshore as it can be seen in Figure 8. However, the ECL event caused massive changes in beach profile. Enormous amount of sands was eroded from the beach dunes and consequently the beach profile became much flattened in next 80m after shoreline.

Table 3. Surf similarity parameter for each events

Offshore distance of breaker line		400 (m)	160 (m)	Throughout Surfzone
TC Hamish	Local Surf Similarity ξ	0.149	0.113	0.141
ECL	Local Surf Similarity ξ	0.243	0.231	0.265

Surf Similarity Parameter

Considering the beach profiles (Figure 8) and the result of wave analysis, the surf similarity parameter (ξ) corresponding to each event is provided in Table 3. During TC Hamish ξ was about 0.141, however, it increases about 90% in ECL which is 0.265. According to CEM (2002) and considering these values, dominant type of breaking expected to be spilling however visual observations during both events saw a significant proportion of plunging type breakers. Hence, CEM (2002) criteria for defining the breaker type doesn't seems accurate enough for defining the in breaker type in The Spit under these two stormy events.

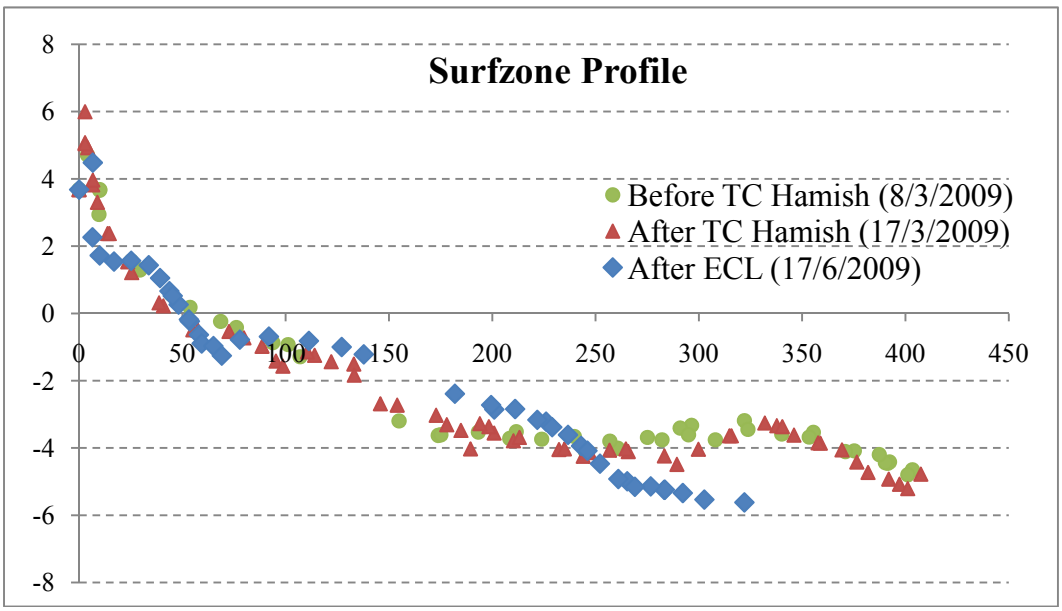


Figure 8. Beach profile changes

Wave height to water depth ratio, γ

The present data has been used to test the ability of existing expressions from the literature to predict the behaviour of γ_s, the ratio of significant wave height to water depth. Thornton and Guza (1983) measured wave transformation at Torrey Pines Beach, California, during November 1978. Sensors located along an on-offshore transect from 10m depth to the inner surf zone. This measurement conducted in calm situation which the offshore wave height varied between 0.6m to 1.6m and the average peak frequency of the incident wave spectra varied little during the experiments and was about 0.07 Hz. There was no stormy wave recorded. Based on their observation they suggested that γ_s is about 0.6 (see Figure 9).

Sallenger and Holman (1985) based on collected data during storm, $1.96 < H_o < 2.4$; $6.9<T_p<16.8$, said that γ_s is related to beach profile (i.e. $\gamma_{rms}=3.2\tan\beta+0.3$). in th other hand, Combining low and high wave steepness data collected on barred and unbarred beaches in the laboratory and field, Nairn (1990) suggested that γ_s increases with increasing offshore wave steepness. The data used by Nairn (1990) were collected in the Grossen Wellenkanal (Big Wave Flume) at Oranjemund in Namibia and during hurricane Eloise on the Florida coast. H_{rms} and peak period vary between 1m to 2.6m and 6s to 14s respectively. However, these data were collected just in inner surfzone area.

Vincent (1985) presented laboratory and field observations in which the significant wave height was proportional to $\gamma_s \propto h^{-1/2}$ in the outer surf zone but γ_s was approximately constant in the inner surf zone. Field data used by Vincent (1985) were collected during storm on October 25, 1980 in which significant wave height reach 5m in 36m depth buoy. He studied collected data in six different points from relatively depth water (36m) to shallow water (2.7m). However, Vincent did not proposed specific formulation purely for storm condition in his work.

As illustrated in Figure 9, Thornton and Guza (1983) doesn't show good agreement with the present data. Moreover, Nairn (1990) expression doesn't agree with the data at all which is γ_s increases with increasing offshore wave steepness. However, Sallenger and Holman (1985) expression has a good agreement with the offshore data but still doesn't satisfy the inner surfzone. Vincent (1985) qualitatively predicts the trend of increasing γ_s with decreasing depth. However, Vincent (1985) expression needs to be modified since the recorded γ_s values first, haven't shown constant values in inner surf zone and second, variation range of this expression hardly covers all the γ_s values extracted from field data. In addition in outer surf zone, it isn't delicate enough to mention that $\gamma_s \propto h^{-1/2}$.

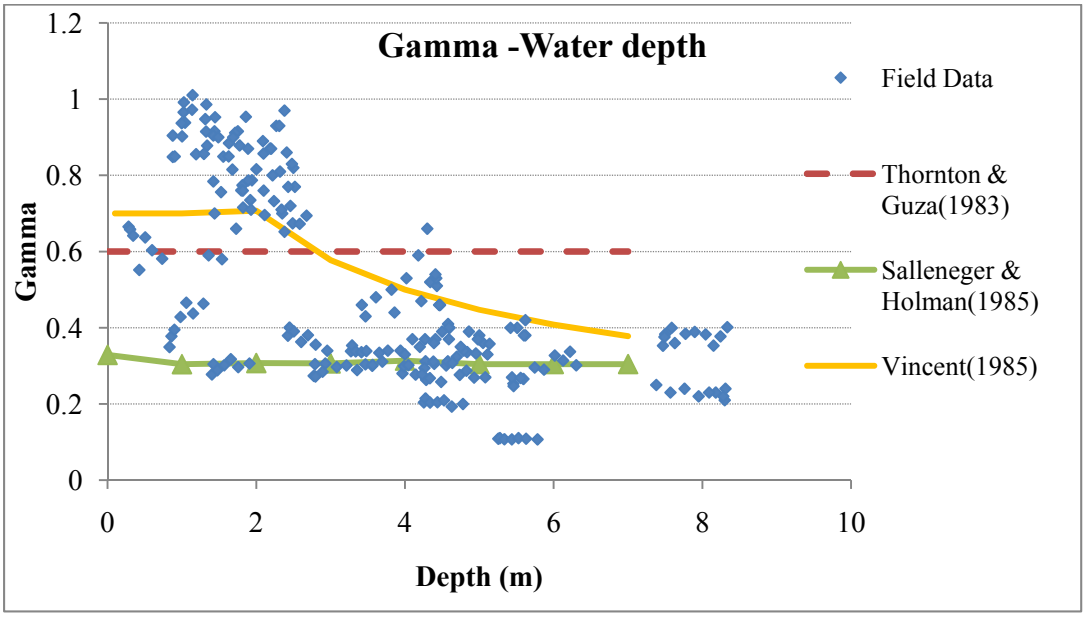


Figure 9. Comparison of existing model against collected data

Field data mentioned in both Figure 9 and Figure 10 include two different stormy events (i.e. TC Hamish, ECL) as well as calm condition one. Therefore, this data scatter is elaborate enough to cover almost all the wave conditions in this area.

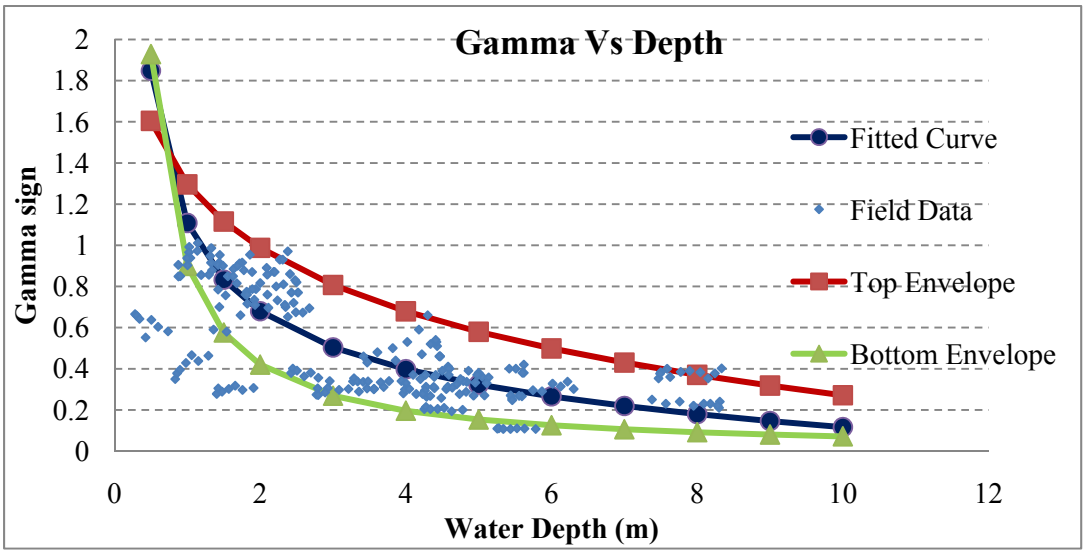


Figure 10. Curve fitting for extracting more accurate relation for γ_s

In order to develop and accurate model of energy dissipation based on actual field data, it is essential to represent γ_s as simple and accurate as possible. By drawing the envelops of data (see Figure 10) and extracting the equation of average amount of envelopes the following empirical equation for γ_s is suggested:

$$\gamma_s = \pi^2 \left(\frac{4.6 - h^{1.1} \times ln(h)}{70h^{1.1}} \right) + 0.46 \quad (8)$$

where, h is water depth.

CONCLUSION

Analysis and comparison of stormy wave data from two severe storms which hit the South-east coast of Queensland in 2009 have provided an opportunity to test the performance of existing predictors of the behaviour of γ_s against storm data. The result of this paper indicates that, the existing expressions for the experimental wave height to water depth ratio, γ_s, don't reflect exactly what happened while storm wave trains travel from offshore toward inner surf zone. Study two severe events plus calm condition data reveals that the exponential function is the best fitting formula for γ_s changes against water depth throughout the surfzone. Moreover, Current criteria of breaking type in existing literatures doesn't describe the breaker type under storm condition at all.

REFERENCES

BoM, (2009). *Significant Weather– May 2009*, Bureau of Meteorology, Australian Government.

Cartwright, N., Callaghan, D.P. and Nielsen, P., (2009). *Coastal Field Research Facility: The Spit, Gold Coast, Australia*, The University of Queensland.

CEM, U.S.A.C.o.E., (2002). *Coastal Engineering Manual* Estimation of nearshore waves U.S. Army Corps of Engineers, Washington, D.C.

DERM, (2009). *Factsheet – Tropical Cyclone Hamish*, Department of Environment and Resource Management, Queensland Goverment.

Nairn, R.B., (1990). *Prediction of cross-shore sediment transport and beach profile evolution*, University of London, London, England.

Nielsen, P., (1989). *Analysis of Natural Waves by Local Approximations.* Journal of Waterway, Port, Coastal, and Ocean Engineering, 115(3): 384-396.

Nielsen, P. and Dunn, S.L., (1998). *Manometer tubes for coastal hydrodynamics investigations.* Coastal Engineering, 35: 73-84.

Nielsen, P., Hanslow, D.J. and Apelt, C.J., (1993). *A new type of nearshore wave*

gauge. 11th Aust. Conf. Coastal Ocean Eng. Townsville.: 247-251.

Sallenger, A.H. and Holman, R.A., (1985). *Wave energy saturation on a natural beach of variable slope.* Journal of geophysical research: 11,939-11,944.

Thornton, E.B. and Guza, R.T., (1983). *Transformation of Wave Height Distribution.* Journal of geophysical research, 88: 5925-5938.

Vincent, C.L., (1985). *Depth-controlled wave height.* Journal of Waterway, Port, Coastal and Ocean Engineering, iii: 459-475.

Estimation of storm surge inundation and hazard mapping

Jae Seol Shim[1] and Jong Joo Yoon[2]

[1]Climate Change & Coastal Disaster Research Department, Korea Ocean Research Development Institute, Ansan P.O. Box 29, Seoul 425-600, Korea; PH (82)31-400-6344 ; FAX (82)31-408-5827; email: jsshim@kordi.re.kr

[2]Climate Change & Coastal Disaster Research Department, Korea Ocean Research Development Institute, Ansan P.O. Box 29, Seoul 425-600, Korea; PH (82)31-400-7815 ; FAX (82)31-408-5827 ;email: jjyoon@kordi.re.kr

ABSTRACT

Typhoon is the most serious natural disaster in Korean coastal area. Many peoples died by storm surge inundation every year. And typhoon caused a lot of damage to property. Climate changes due to global warming are producing a stronger natural disaster. Coastal zones have been damaged by typhoons and accompanying storm surge. Especially, the most serious loss of life and terrible propertydamage caused by typhoon Maemi in 2003. After then, there has been an increased interest in these coastal zone problems. If storm surges coincide with high tides, the loss of life and property damage due to high waters arc even worse. Therefore it is desirable to accurately forecast the amount water level increase. In this study, using a numerical model FVCOM(finite volume coastal circulation model, Chen et al.,2004), storm surge was simulated to examine its fluctuation characteristics for the coastal area behind Masan, Yeosu and Busan city in Korea. In the numerical model, a moving boundary condition(wet-dry treatment) was incorporated to explain wave inundation. Numerically predicted inundation regimes and depths were compared with measurements from a tidal gage each area. Comparisons of the numerical results and measured data shows a good correlation. The numerical model adopted in this study is expected to be a useful tool for analysis of storm surges, and for predicting inundation regimes due to coastal flooding. Many coastal cities including low-lying areas were flooded during strong typhoon. So it is necessary to consider detailed evacuation planning, including hazard map, preparation of evacuation site, and sustainable city planning against storm surge inundation problems. For this study, we used 201 typhoon passing through Korea during the past 55 years since 1950. Typhoon wind model was used to estimate wind forcing and air pressure data for each typhoon. We estimated the spatial statistical analysis for inundation level as each return period. And finally we suggest the example of coastal hazard map in the Korean coast(Masan, yeosu and Busan city)

1. Introduction

Setup (sea-level rise) due to weather change following the global warming and the increased intensity and return period of typhoon is magnifying inundation hazards up to the unpredictable level, resulting from the typhoon surge in Korea and other coastal states around the world.

It is predictable that in Korea, where the area of the national territory is narrow and the natural resources poor, damages resulting from the natural disaster will increase widely according to the increased number of industrial complexes and development of the residential facilities through costal development like reclamation projects and the increased utilization and scope of activities in the coastal zone. Development of technologies to cope with the natural disasters like coastal inundation and for the vulnerable areas is therefore required to minimize such damages and to plan and manage the coastal development thoroughly. It is imperative to establish a countermeasure to protect the properties and lives of the people from the natural disasters of the coast since the damages to the lives and properties are on the rapid trend of increase (in 2003, the typhoon "Maemi" invaded Korean Peninsula leaving property loss of $ 4 Billion and killing 131 people) due to the increased intensity and return period of the typhoon following recent weather change. We shall be able to minimize damages resulting from inundation by the typhoon surge and counteract more scientifically and systematically if only we can predict the damages from disasters, since it is impossible to entirely defend with the costal defensive structures like revetment and levee from the surges or inundations. Since understanding the exact regional distribution characteristics of the surge-heights due to the typhoons invaded in the past is indispensable to establish the regional disaster prevention plan, it is necessary to fully analyze the data and establish the estimation technique.

In order to precisely estimate the inundation area due to storm surge at the coast, the costal fine-grid storm surge model in consideration of the numerical weather forecasting model by the fine grid and other diverse marine elements should be established in combination and, the DB/GIS of the costal geomorphology should be established by developing a technology that links the overland altitude and the depth of water systematically. They are producing precise DEM data in the advanced countries in application of diverse survey techniques such as aero- LiDAR survey, aerial photogrammetry, landsat image, SHOALS, etc., which are the up-to dated technologies to predict the area inundated at the coast and to prepare the hazard mapping and, such basic technologies were also introduced to Korea and applied to many research works.

In order to minimize the inundated area by the surges and to protect the human lives and properties from such costal disasters, it is necessary to install facilities like the coastal defense structures to prevent disasters, and considering the reality of our country where there is no nameable disaster preventive facilities at present, securing the base technology for such facilities is also imperative.

The predictive modeling of the respective components inducing the sea-level rise at the coast (tide, surge and wave, etc.) is comparatively well established but the technology to integrate and apply them by linking with the weather input data is still vulnerable. In addition, the data on sea level pressure and sea surface wind at the fine grid to forecast the storm surge at the time of typhoon is required as well. At present,

a study on 'technology to predict storm surge inundation area and to prepare hazard mapping' ("Estimation of storm surge inundation and hazard mapping") for practical application is intended to secure vertically (How much high the surge will approach?) precise forecasting system for the regional surges at the coastal area and to solve the core of the issues by application to the practical use, but the prediction of storm surge inundation area should consider the effect of horizontal (How much wide and deep the surge will immerse?) influence importantly in addition. Accordingly analysis by the diverse statistical techniques, etc. is a subject of research required together with the analysis on the examples of the past inundation and the comprehensive numerical model experiment. In the technology to predict the storm surge inundation area and to prepare a hazard mapping, establishment of the DB on costal geomorphology combining the map and the nautical chart is taking a large portion determining the outcome of the research, but the current real state in Korea is so poor that it is urgently required to develop a mapping technique to combine them. In addition, the coastline should be arranged well at the areas where there are wide tidal ranges.
In this research, in order to predict the storm surge inundation area together with calculation of the surge heights due to the storm surge, the areas vulnerable to inundation in Masan, Busan and Yeosu regions were designated as an example by establishment of DB on the long-term estimation data on the surge heights/inundated areas through precise reproduction of the past typhoons and in application of the statistical process technique by each return period, and executing a study to prepare a manual on the storm surge inundation prediction. Also, for the above, development of the precise combination technique of the map and the nautical chart, and development for accuracy of the verification data on the surges and simulated inundation, as well as their estimation technique is ongoing.

2. Precision Topography/ Water-depth Survey in application of the Ground LiDAR and MBES, and Preparation of the precision Topographical Map through Combination of the Intertidal Zone (Malipo)

Malipo, located at the macrotidal range coast, was selected as a model research area to prepare a precision and high-resolution topographical map through combination of the map and the nautical chart of the coastal area. Precision topographical and water-depth survey was carried out in application of the ground LiDAR and the Multi-Beam Echo Sounder, and the precision topographical map of Malipo, located at the macrotidal range coast, was prepared through combination of the map and the nautical chart of the intertidal zone(see figure 1). In order to acquire sufficient topographical information on the intertidal zone within the restricted time, topographical information on the coast was collected through repetition of moving, stopping and scanning with the ground LiDAR and DGPS mounted on the roof of a vehicle during the ebb tide, and at the same time, water-depth survey was carried out through MBES during the high tide, and the tide level observation through tide gauge installation and visual measurement was parallelly carried out to be used as the water-depth compensation data and data to estimate the mean sea level of Malipo. The reference plane of the Cartesian Coordinates of the topographical and water-depth information was unified to the mean sea level of Incheon to adjust the intertidal zone, and the average nested error of the intertidal zone showed

approximately less than 2~6 cm. Also, RTK-DGPS survey was carried out simultaneously to verify the accuracy of the ground LiDAR data, and the compared result of the Cartesian Coordinates value showed the average square root error is approximately less than 5~7 cm. Preparation of the precision topographical map has produced a digital elevation model (DEM) having 50cm of resolution through GIS-based data process, which is presently utilized as a precision input data on the prediction model of storm surge inundation to predict the inundation at the coastal area.

In order to combine the map and the nautical chart, the ground and the sea should indicate the topography and the water-depth calculated by the same vertical reference plane, requiring unification of the control point of the Cartesian Coordinates. In this research, combination of two kinds of data was executed by converting the reference point of the Cartesian Coordinates to the average mean sea level of Incheon when converting the topography and the water-depth to the geological coordinates. Moreover, to ensure more accurate combination, the timing of survey was pointed to the ebb tide during the spring tide and during the high tide to acquire fully overlapping topographical information and water-depth data in the intertidal zone. The result of mutual comparison for the overlapping area of LiDAR and MBES for the data of September 2008, December 2008 and March 2009 showed approximately 2~6cm of the average error and more than 95% of the overlapping area was distributed between +2cm at approximately -2 of the margin of error.

In case of predicting the storm surge and inundation, inundation area should be predicted based on the mean sea level of that area because the locally incurring inundation area should be predicted. Accordingly, it is necessary to find out the correlation between the average mean sea level of Incheon and the average mean sea level of Malipo in order to convert the altitude and water-depth based on the average mean sea level of Incheon to that of the average mean sea level of Malipo. For this, the difference between the average mean sea level of Malipo calculated by observation of the tidal level through installation of the wave height gauge at Malipo and the average mean sea level of Incheon was converted to the average mean sea level of Malipo to be used as the input data of the prediction model. At present, the average mean sea level of Malipo calculated through the tidal observation for approximately 7 months showed about 14.45 Cm of height difference from the average mean sea level of Incheon, but it is planned to calculate more accurate average mean sea level of Malipo through long-term tidal observation because height of the mean sea level varies according to the observation period and season.

The precision topographical map obtained though combination of the map and the nautical chart shall have 5 points of resolution per 1㎡ in case of the water-depth information, and shall have 5 cm ~ 1 m of radial and variable resolution as the characteristics of radial data acquisition of the laser scanner. In processing each LiDAR data and MBES data, RiScan Pro and Hypack program, which are the exclusive data processing software, were applied, and ArcGIS was applied to combine and verify the processed data and for 3D spatial analysis. The final precision topographical map prepared through GIS based data processing was prepared into a digital elevation model (DEM) having 50 cm of resolution.

The precision topographical map prepared through combination of the map and the

nautical chart is in use as a precision input data to enhance accuracy of the prediction model of the storm surge and inundation, showing improvement in the prediction result following enhancement of accuracy of the input data. Further, by examining the morphological change through calculation of the inclination and the volume change by GIS based 3D spatial analysis, it is anticipated that the precision topographical map shall be effective utilized in management and monitoring of the coast by the analysis linked with the observation result of the marine environment.

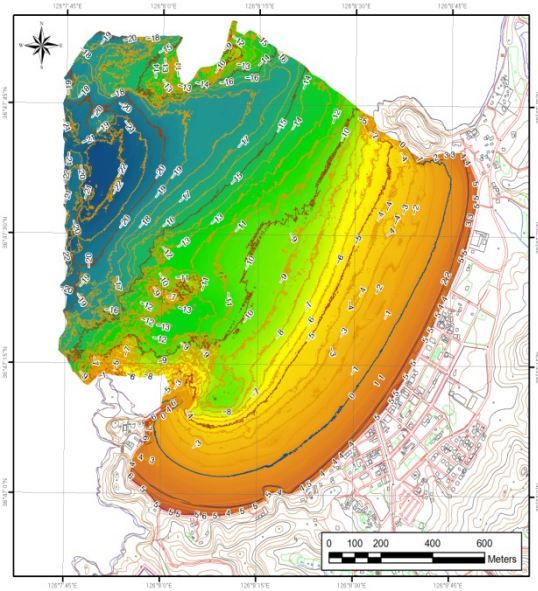


Figure 1. Topographical Map through Combination of the Intertidal Zone (Malipo)

3. Calculation of Storm Surge Height

In case of the storm, there is a wide range of temporal and spatial variations. There are errors in estimating the perpendicular profile and shear stress of the lower atmosphere due to stability and sea surface roughness at the boundary layer of the lower atmosphere, and such can be increased in case of the storm that moves fast in particular.

It is required to choose a model to well reproduce the temporal and spatial changes according to the typhoon models and to accurately estimate as much as possible the parameter of the typhoon required by its input. Since the observation data is exceedingly insufficient in the sea, it is necessary to analyze the typhoon accurately in application of all data available such as the satellite data and the numerical model result, etc. Spatial variation of the storm surge will increase due to the local influence in the complicated coasts like the southern coast of Korea and the fine grid water-depth data is required to adequately consider this. It is important to accurately plan the bathymetric grid system in proper application of the available water-depth information.

It is necessary to estimate the tidal information of the sea surface accurately because of the mixed influence of the tides and the storm surges, and to properly understand the mutual influence between the tides and the surges. It is advantageous to examine the storm surges by classifying the part due to the sea wind from the part due to the atmospheric pressure because interactions of the tides and the storm surges are appearing complexly at the non-linear advection term, friction dissipation term and shallow water term, etc. in the long-wave equation. Moreover, the sea surface is widely influenced by the waves as well. Since the effect of wind at the storm surge model varies according to roughness of surface layer of the sea by the waves, data on the waves is required to properly estimate it. For the area influenced by the wave setup due to wave breaking according to the location of the structures at the coast, the information on the waves is required to estimate it. Such influence can be considered in application of the past long-term wave calculation result DB. In order to reduce the error of the extreme statistics, it is required to calculate the storm surges for sufficiently long duration, but it is not feasible to extend the application period endlessly because reliability of the past weather input data is considerably lower compared with the present one. Accurate estimation is required for such typhoons after the past 1950th. The most critical element in occurrence of error is the issue of reliability of the numerical model of the storm surge. Enhancing reliability of estimation by the numerical model is more important than anything else by sufficiently making compensations from the observation data to the estimated values obtainable by the weather data.

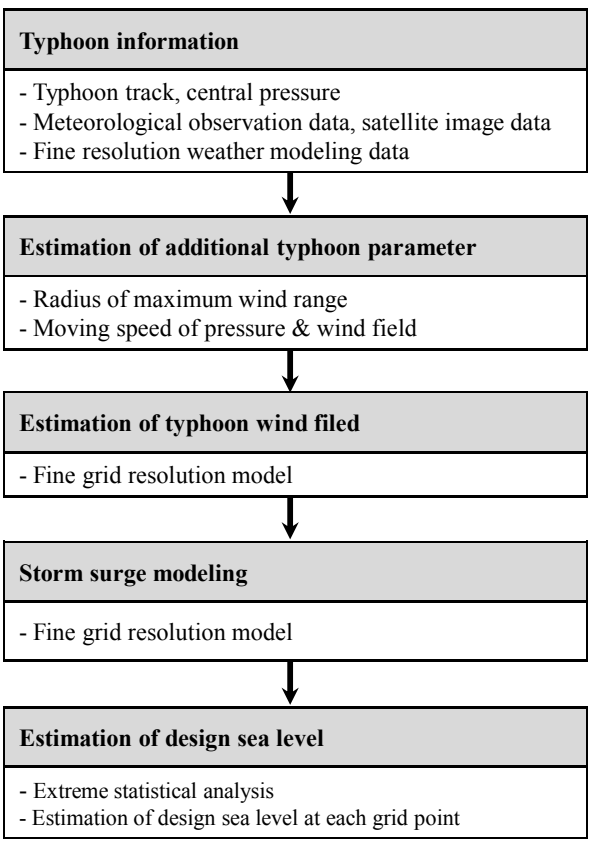


Figure 2. Flow chart of design sea-level estimation

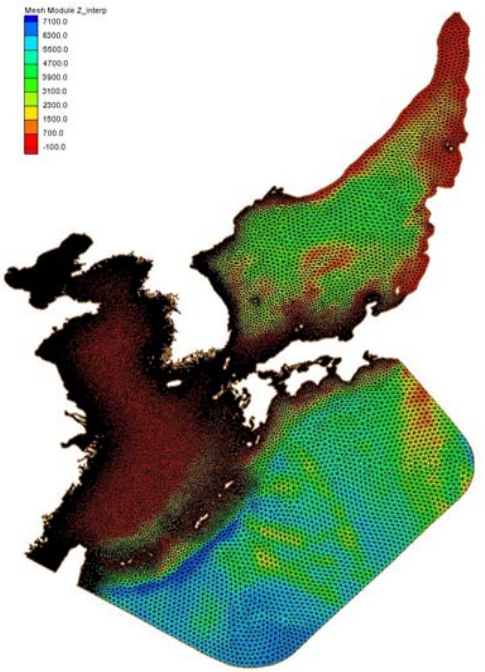


Figure 3. Grid system and bathymetry of FVCOM model

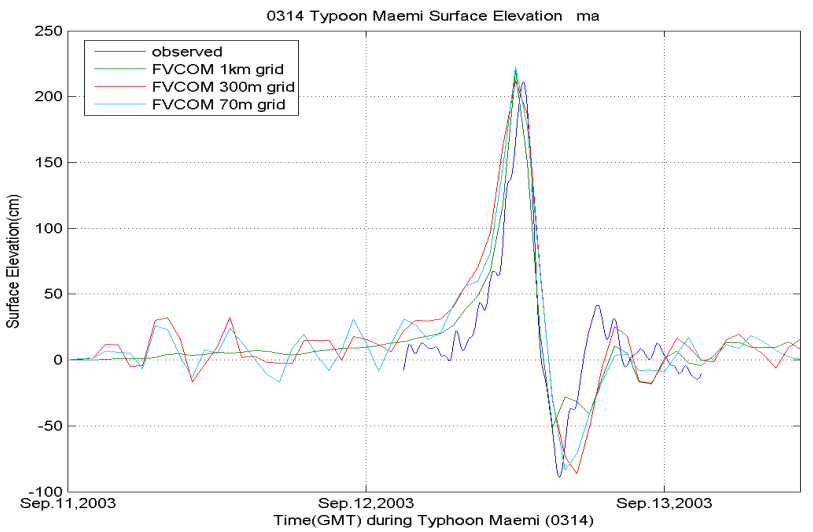
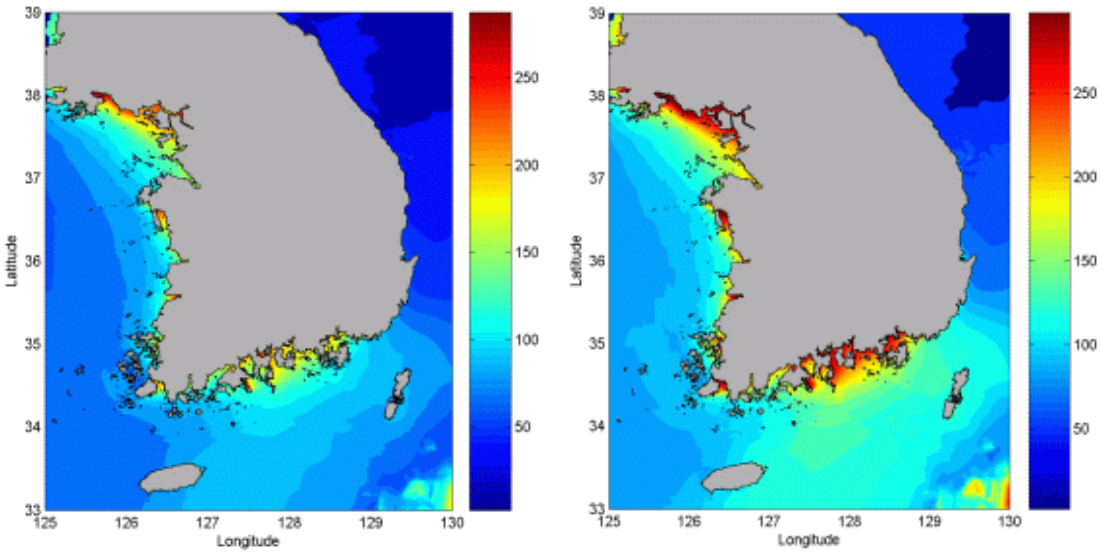


Figure 4. Comparison of surge height between observed and simulated data (Masan tidal station)

In order to calculate the extreme sea level through long-term simulation, the storm surges were calculated for the typhoons that has given influence on Korea over the past 56 years. All 201 typhoons for 58 years from 1951 to 2006 were selected, and the fields of pressure and wind were calculated at the time of passing of the typhoons in application of the sea surface wind model of the typhoon. The unstructured fine grid model FVCOM (Finite-Volume Coastal Ocean Model) 3D model was applied to calculate the storm surge with the calculated fields of pressure and wind as the input

data. Beforehand, the storm surge test according to the sizes of grids in application of FVCOM was implemented at the minimum grid gap of 1 km, 300 m and 70 m respectively. The depth of water by each grid has applied the same data and the numerical experiment was executed while allowing the different sizes of the grids only in this simulation. Only the surge height was simulated except for the tides at the time of invasion of the Typhoon "Maemi", and the wet-dry treatment module was applied and simulated in 3D for all. As shown in Figure 4, FVCOM model is very accurately and properly reproducing the observed value, and it was proved that the 300 m grid system is objectively most effective, considering the operational benefit and accuracy in general in consideration of the counting time of the model, among the 3 types of the grid systems applied in this research. Large unstructured grid of approximately 1~10 km was applied at the open sea including the surrounding seas of Korea and the East China Sea, and the storm surge height from the fine grid system (see figure 3) of the resolution of approximately 300 m of the minimum grid gap at the coast was obtained, and the surge height by each return period according to the extreme value analysis was calculated (see figure 2 and 5).



(a) (b)

Figure 5. design storm surge height at Korean coast,
(a) returen period : 50years, (b) returen period : 200years

The statistical models applied to the extreme statistical analysis are Gumbel Distribution, Weibull Distribution and GEV (General Extreme Value) Distribution, etc., but Weibull Distribution, which is applicable to the extreme value analysis for the waves and surface of the sea, was applied here. Weibul extreme value model includes 3 parameters that should be determined from the observed data. There are Least Square Method (LSM), Conventional Moment Method (CMM), Probability Weighted Method (PWM), (Maximum Likelihood Method (MLM) and Bayesian Method (BM), etc. in estimation method of the parameters, but LSM, CMM and PWM, which are widely used due to their comparative easy application, were applied

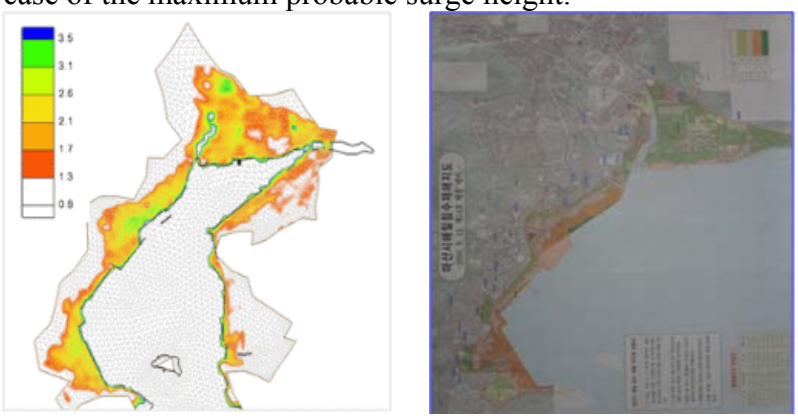
here. Accordingly, even though the design sea level was calculated by 3 kinds of the extreme probability method in this task, LSM was applied to calculate storm surge height by each return period because the result of LSM showed the best interrelationship. In the Tables 1, the calculated values for the design sea level by each major return period about the 28 main trade port in Korea according to the long-term calculation of the storm surges are presented together with the average sea level value of each port.

Table 1. The design sea level by each major return period about the 28 main trade in Korea

Port name	Design sea level(m)					Mean sea level(m)
	10yr	30yr	50yr	100yr	200yr	
Incheon	1.35	1.77	1.97	2.24	2.52	4.64
Pyyongtak	1.18	1.49	1.64	1.83	2.03	4.65
Daesan	0.90	1.11	1.20	1.33	1.45	4.14
Taean	0.81	0.98	1.06	1.17	1.27	3.85
Boryoung	1.17	1.57	1.77	2.03	2.31	3.83
Janghang	1.18	1.55	1.73	1.97	2.22	3.74
Gunsan	1.23	1.63	1.82	2.07	2.33	3.71
Mokpo	0.85	1.11	1.23	1.40	1.58	2.43
Wando	0.90	1.12	1.22	1.35	1.48	2.43
Yeosu	1.34	1.91	2.20	2.61	3.03	1.81
Gwangyang	1.47	1.97	2.21	2.55	2.89	1.91
Samcheonpo	1.20	1.69	1.94	2.29	2.65	1.65
Tongyoung	1.05	1.50	1.73	2.05	2.38	1.41
Gohyun	1.04	1.49	1.72	2.03	2.36	0.98
Jangseongpo	0.80	1.16	1.34	1.59	1.86	0.94
Okpo	0.83	1.22	1.41	1.68	1.96	1.07
Masan	1.24	1.80	2.07	2.46	2.87	0.98
Jinhae	1.09	1.59	1.83	2.18	2.55	1.00
Busan	0.66	0.95	1.10	1.31	1.52	0.95
Ulsan	0.46	0.65	0.74	0.88	1.02	0.30
Pohang	0.58	0.86	0.99	1.19	1.40	0.12
Samchuk	0.26	0.37	0.42	0.49	0.57	0.17
Donghae	0.27	0.37	0.43	0.50	0.58	0.19
Mukho	0.30	0.43	0.50	0.59	0.69	0.20
Okgye	0.26	0.36	0.41	0.48	0.55	0.19
Sokcho	0.25	0.35	0.41	0.48	0.56	0.20
Jeju	0.58	0.76	0.85	0.96	1.08	1.42
Seoguipo	0.56	0.74	0.83	0.95	1.07	1.52

4. Demonstrative estimation of the probable inundation area

In order to simulate the maximum probable inundation scenario, the event of typhoon invasion at the time of approx. highest high water was selected and applied to the semi-diurnal tide M2 with the 8 input harmonic amplitudes of the open boundary for this. This is the case of the spring tide when all of the amplitudes of all 8 harmonic constituents are applied to their maximum and the probability of such actual invasion is very scarce. However, even though the probability is very scarce, this was applied to the extreme case for simulation of the maximum inundation area because this is the case of the maximum tide with probable invasion in reality. Invasion of typhoon "Maemi" was simulated to be used as a scenario to calculate the virtual maximum inundation area in accordance with the invading condition of such maximum tides. To simulate the inundation scenario, the model grids were extended up to the area inside the lowland in application of the digital elevation data (DEM) made by precisely combining the aero-LiDAR survey data and the nautical chart data of the 3 demonstration regions of Busan, Masan and Yeosu to allow simulation of the inundation. Minimum grid of 300 m unstructured triangular mesh applied to calculate the storm surge was adopted as a grid system, and the minimum grid size of 30 m was built near Busan, Masan and Yeosu area which are the fine coastal regions and where the inundation is simulated. Prior to simulating the maximum probable inundation scenario, inundation of the Masan Bay where there was an extensive damage from inundation by typhoon "Maemi" was simulated beforehand. In the Figures 6, result of simulation of the inundation area at the time of typhoon "Maemi(2003)" and the actual hazard map of surge inundation over Masan city made after typhoon "Maemi" according to FVCOM are presented. It was proved that the result of simulation for the inundated area according to the model has pretty accurately reproduced the damaged area appeared in the hazard map. Figure 7 shows the calculation result of the maximum surge height according to the scenario at the Masan seas, and the red line is the probable maximum surge height at the maximum spring tide, the violet line is the result of the coupled model of the tides at the time of actual typhoon "Maemi" and the storm surge, while the green line is the result of the model of storm surge at the time of actual typhoon "Maemi". It shows that the surge of higher than approx. 1 m in height compared with the existing result that can be generated in case of the maximum probable surge height.



(a) (b)

Figure 6. (a) Inundation simulation result, (b) hazard map of surge inundation

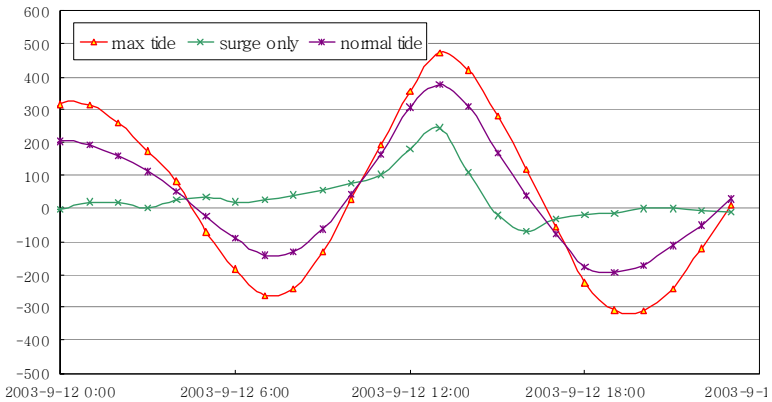
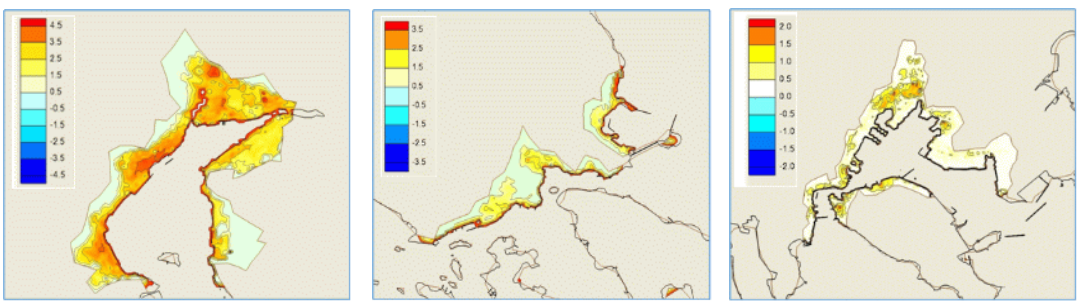


Figure 7. Calculation result of the maximum surge height according to the maximum tide scenario at the Masan seas

When we see the result of calculation for the inundated area of the subject seas, and when it comes to the case of Masan where the previous invasion of typhoons like typhoon "Maemi" had inflicted comprehensive damage, it had proved that the surge height combining the tide of approx. 4.7 m and the storm surge could have been generated in case of the probable maximum inundation in application of the combination of the 8 harmonic constituents. Damages from such inundation were, as shown in the Figure 8(a), simulated to be present comprehensively across the lowlands with altitude lower than 3 m.



(a) (b) (c)

Figure 8. Probable maximum inundation height at Masan(a), Yeosu(b) and Busan(c)

And, as for the case of Yeosu(Figure 8(b)) and Busan(Figure 8(c)), where the damages from inundation are simulated comparatively less by the simulation of the previous invasion of typhoons, it was also simulated that there are areas damaged by inundation with the lowlands along the coast at its center when the maximum probable inundation scenario in this research was applied.
It can be said that the above is showing the probable area of inundation damage that may occur in case that the extremely powerful typhoon is to invade together with the high tide at the time of spring tide in the future.

5. Future Research Project and Proposal

Till present, in calculating the design conditions (design wave, design water level,

etc.), which are the core data for disaster prevention of the costal structures, they are estimating the waves and storm surges for a long period to calculate the design conditions through the extreme statistical process under the assumption that the global weather will remain normal with its statistical characteristics unchanged during the comparatively short period of time compared with the geological time. Recently many experts are warning that the damages from typhoon will become more serious due to the increased strength and frequency of the typhoons because of the global warming. Accordingly, there are opinions raised to consider the impact of the global warming in estimating the design wave and design water level. Among the many phenomena from the global warming, the change in external force of the coastal structures following change of the sea level rise and the intensity of typhoons are affecting the safety of the harbor structures. As for the water level rise, most experts are in the same opinion for the fact that the water level is rising by increase of the atmospheric and sea water temperature following the global warming, even though slightly different in its intensity. Since the sea level rise is progressing gradually, adaptation for it is also gradually required. However, so far, the scientific technology cannot reach up to the level to quantitatively estimate the change in strength of typhoon and the sea level rise, etc., following the global warming. Accordingly, there are a lot of difficulties in establishing the countermeasures to reduce disasters to the costal ports following the weather change because there can be waste of budget due to excessive design if the costal structures were to be designed and built in application of the uncertain prediction, and in case of the opposite, there can be a considerable damage to be sustained.

Damages from the natural disasters at the coast comprise damages solely by the inundation without mechanical destructive power due to sea level rise by the astronomical tide, meteorological tide and wave, etc., and damages like coastal erosion and destruction of the structures due to the works of wave force because the waves that didn't reach at normal times give influence following the raised sea level. Countermeasures to prevent such disaster at the coast are; first, reduction of damage through evacuation, etc., by the short-term forecasting; second, construction of the disaster prevention facilities like seawall by the long-term forecasting, moving-out from the lowland, adequate design of the coastal disaster prevention facilities at the time of each kind of construction works or developments; and through the above, damages from disaster can be either prevented or minimized. As for the countermeasure to prevent disasters due to the abnormal sea level rise, the advance countermeasure by the long-term forecasting, which is corresponding to the above second, is the main issue. In addition, since the sea level is receiving the combined influence of the tide and the storm surge, it is required to accurately estimate the tidal information and to properly understand the mutual effect of the tide and surge. Development of the abnormal sea level estimation model, in which the wave, tide and surge models are complexly operated, is indispensable since the wave, tide and storm surge are interacting powerfully at the coast and all of them has to be calculated accurately in order to estimate the local sea level rise to establish disaster prevention measures accordingly.

Recently, a storm surge calculation model by the unstructured grid models like ADCIRC model and FVCOM model, etc. was developed and put to practical use, and this model was combined with the wave model so as to enable estimation of the sea level from the finer grid system. Even though the wave complex model is not applied from the fine grid in this research, a research is underway to establish a fine storm surge forecasting system by the complex model of the wave, tide and surge, where SWAN (Simulating WAves Near-shore, SWAN Team, 2006a) model is combined with FVCOM. In particular, there was a numerical experiment on the storm surge height where the wave model was combined for the Typhoon Maemi (2003) and Typhoon Kompasu (2010). It was revealed that there was an effect of rise in the surge height up to the maximum 25% according to the regions when the influence of the waves was considered. In addition, it showed improvement of the result of wave model due to the wave-current interactions according to the tidal current and the wind-driven current, etc. It reminds us that the effect of the waves should not disregarded when estimating the inundation precisely.

There has been an on-going research to forecast the inundation areas by forming a scenario according to the virtual typhoon and calculating the probable inundated area accordingly. However, in this research, we have carried out a long-term analysis on the actual typhoons invaded in the past and through this, tried to present the probable inundated area by each return period as a statistical approach. The final target of this research is to properly supplement the research to predict the inundated area according to the existing virtual typhoon scenario, and properly link the aforesaid with the real-time ocean forecasting system provided by the "Development of Korea Operational Oceanographic System (KOOS)" which is under execution by Korea Ocean Research and Development Institute (KORDI) so as to finally establish a forecast and warning system of 72 hour inundation at the major coastal area vulnerable to inundation.

The past long-term typhoon fine analysis data secured to estimate the storm surge for long-term and the fine grid weather input data are utilized as an indispensable data to prepare a hazard map according to the lowland inundation by the storms in the future. They shall become the basic data for the fine storm surge forecasting system to establish countermeasures to reduce disasters from the coast by the typhoons. Fine storm surge forecasting system is utilized to establish short-term fine storm surge forecasting system after linking with the short-term weather forecast data. This system can be utilized to forecast the fine grid storm surge for the nationwide coasts and ports. The 3D ocean circulation model established here can be utilized; to support sailing of the vessels at the coasts and in the ports; to transport the suspended loads during construction works; to forecast dissipation of oil contaminants at the time of marine accidents; to establish a supporting system for search and rescue, and forecasting; and to establish an inundation forecast and warning system, etc. so as to be applicable to establishment of the long-term plan to correspond to the nationwide natural disasters by the severe weather like typhoon, etc.

REFERENCES

Chen, C., Liu, H., Beardsley, R.C., 2003. An unstructured, finite volume, threedimensional, primitive equation ocean model: Application to coastal ocean and estuaries. J. Atmos. Oceanic Technol. 20, 159–186.

Chen, C., Beardsley, R.C., Cowles, G. 2006a. An unstructured grid, finite-volume coastal ocean model (FVCOM) system. Special Issue entitled "Advances in Computational Oceanography". Oceanography, 19(1), 78–89.

Chen, C., Beardsley, R.C., Cowles, G. 2006b. An unstructured grid, finite-volume coastal ocean model FVCOM user manual. SMAST/UMASSD, 2006.

Chen, C., Huang, H., Beardsley, R.C., Liu, H., Xu, Q., Cowles, G., 2007. A finite-volume numerical approach for coastal ocean circulation studies: comparisons with finite difference models. J. Geophys. Res. 112, C03018. doi:10.1029/2006JC003485.

Cho, Y.-S. and Kim, H.-J., 2006. Sea level change due to typhoons in Korean Peninsula, Journal of Coastal Research, Vol. 22, No. 3, pp. 678-682.

Choi, B.-H., Hong, S.-J. and Pelinovsky, E., 2006. Distribution of runup heights of the December 26, 2004 tsunami in the Indian Ocean. Geophysical Research Letters, Vol 33, No. 13, L13601.

Emanuel, K., R. Sundararajan, and J. Williams, 2008: Hurricanes and global warming: Results from downscaling IPCC AR4 simulations. Bull. Amer. Meteor. Soc,, 89, 347-367.

IPCC, IPCC AR4 Synthesis Report, 2008.

Coastal Engineering for Veterans Drive Improvements

Manish Aggarwal[1] and Jerald Ramsden[2]

[1]145 Sanskriti Apartments Sector 19B, Dwarka, New Delhi 110058; PH +91-9967779663; manish.agg@gmail.com
[2]Parsons Brinckerhoff, Ports & Marine Division, 400 SW 6th Ave., Portland, Oregon 97204; PH (503) 274-8772; FAX (503) 274-1412; ramsden@pbworld.com

ABSTRACT

The Department of Public Works of the Government of the Unites States Virgin Islands has undertaken engineering design for widening of Veterans Drive along the waterfront of Charlotte Amalie on the island of St. Thomas. This proposed widening will include a revetment and bulkheads to protect the fill associated with the proposed widening. An alternative under consideration includes a low lying bridge along a historic section of the rock shoreline to protect it from the proposed fill. Hurricane surges, wave transformation, scour and wave loads were analyzed for various elements of the proposed infrastructure improvements. Design conditions at the site are characterized by moderate waves and storm surge due to its location at the head of a semi-enclosed embayment and a relatively narrow shelf south of St. Thomas terminating in a deep trench of the Caribbean Sea.

INTRODUCTION

The Department of Public Works (DPW) of the Government of the Unites States Virgin Islands (USVI) has undertaken environmental and engineering studies for widening Veterans Drive along the waterfront of Charlotte Amalie on St. Thomas in the USVI. The proposed widening will include a revetment and bulkheads to accommodate the four lane road and a 20-foot promenade between the roadway and the bay within the project site shown in Figure 1.

Near the western end of the project at Kings Wharf the road will be routed south of the Coast Guard Station and Legislature Building as shown in Figure 1. Alternatives for this section of the roadway include fill and a low-lying bridge. The bridge alternative would locate the roadway offshore of a historic section of the rock shoreline to preserve it from being covered by fill. The harbor contains seagrass beds and coral resources as well. Project features such as the road alignment, bulkhead and revetment are configured in order to avoid impacts to the marine resources to the extent practicable. However, another project constraint involves the current location of the two lane road located between the Legislature Building and historic Fort Christian located immediately east and northeast of the Coast Guard Station, respectively. Road widening to accommodate four lanes would encroach into the footprint of one or both historic structures. Thus, planned expansion of the roadway is located south of the historic buildings at this location.

Several coastal engineering analyses were conducted for this project and are the subject of this paper including hurricane surge and associated currents, nearshore wave transformation, wave loads and scour. The project site is located along the northern shore of St. Thomas Harbor and is moderately protected from waves due to the narrow harbor entrance to the south shown on the vicinity map in Figure1. Storm surge at the project site is not large since the offshore bathymetry lacks a low-gradient shelf of sizeable width. However, significant storm waves can reach the site when propagating in a northerly direction.

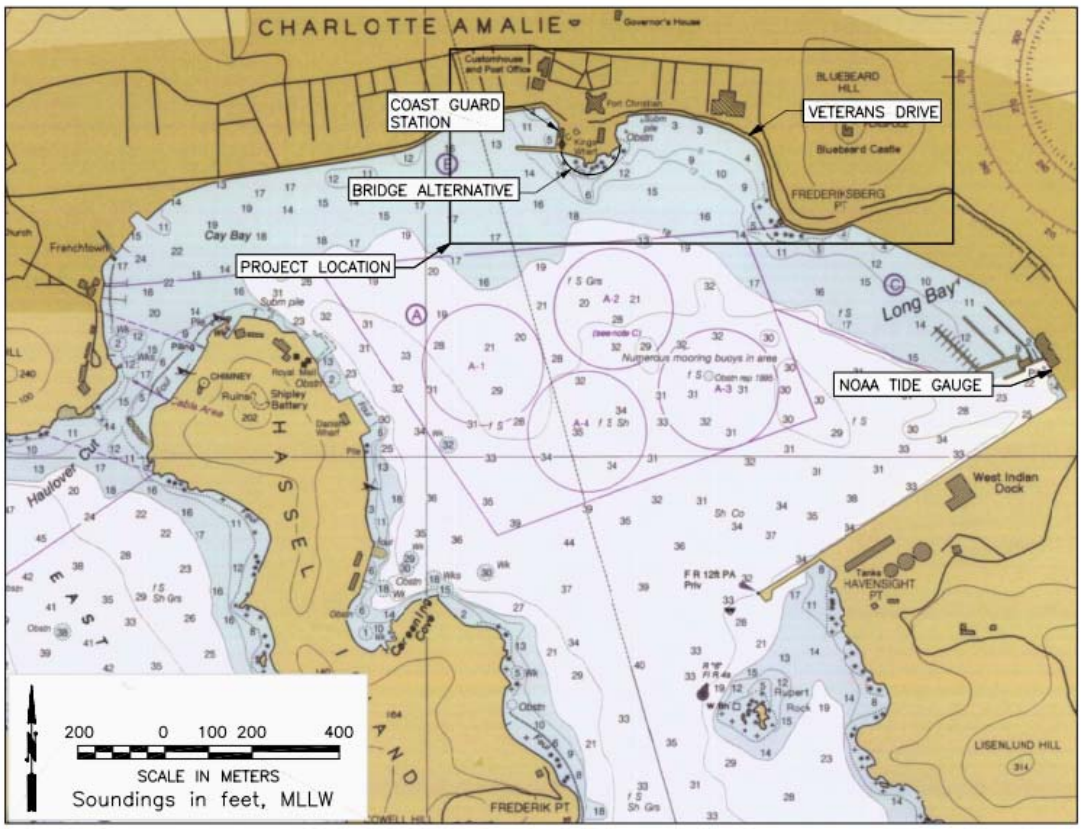


Figure 1. Charlotte Amalie and project location (excerpt from NOAA Chart No. 25649).

COASTAL HYDRAULICS

Storm surges, currents and wind waves were calculated in the vicinity of the project site using hydrodynamic and wave transformation models. Several sources of data were obtained for use in the study including bathymetric data from various sources, tide data from the four gauges maintained in the region by the National Ocean Service (NOS), hurricane data from the North Atlantic hurricane database, HURDAT (Jarvinen, et al., 1988)), and existing hindcast wave data available through the Wave Information Study (WIS) (Hubertz, 1992). Bathymetric data included project specific

hydrosurveys, National Oceanographic & Atmospheric Administration (NOAA) navigation charts, regional data from the National Geophysical Data Center and an Atlantic Ocean grid developed by the U.S. Army Corps of Engineers.

Storm Surge

A finite element hydrodynamic model ADCIRC (Advanced Circulation Model), (Luettich et al., (1992)), was developed for the project site to simulate water levels and currents for typical conditions and selected historical hurricanes summarized in Table 1. The ADCIRC model domain included the region surrounding St. Thomas and extended eastward significantly offshore of the West Indies in order to allow sufficient distance for development of storm induced wind and hydraulic conditions well in advance of storm arrival in the St. Thomas region. The model domain in St. Thomas Harbor has a minimum grid spacing of about 20 m near the shoreline.

The model results were compared against several regional NOS tide gauges including Charlotte Amalie on St. Thomas, Lime Tree Bay in St. Croix, Lameshur Bay on St. John and Vieques Island, Puerto Rico. An example of a tide comparison between the calibrated model and the tide measurement at the Charlotte Amalie tide gauge is shown in Figure 2. The root mean square error (RMS) error between the ADCIRC model and NOS predicted tides shown in Figure 2 is 3.5 cm or about 10% of the predicted spring tide range. For the NOS observed tides and ADCIRC results the

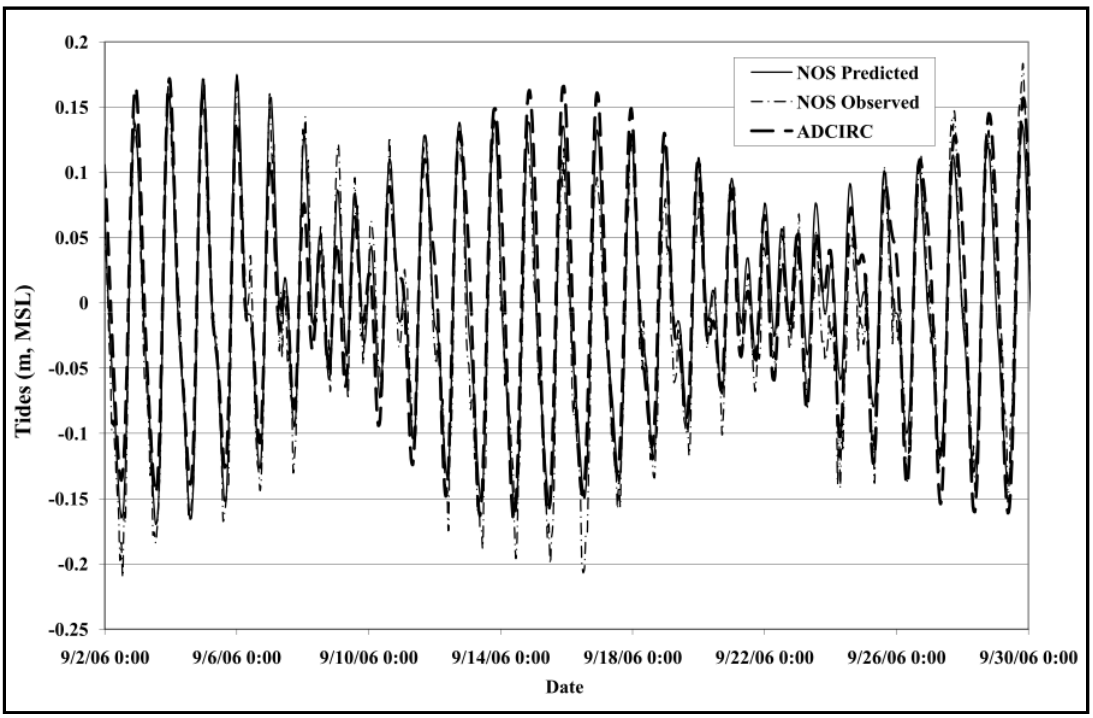


Figure 2. Comparison of observed and modeled tide induced water levels at the Charlotte Amalie tide gauge

Table 1: Observed and Modeled Water Levels for Historical Storm Events

Storm Number	Hurricane	Date	Bridge Location			Charlotte Amalie Tide Gage			
			Modeled Surge (m)	Wave Setup (m)	Modeled Water Level (m)	Modeled Surge (m)	Wave Setup (m)	Modeled Water Level (m)	Observed Water Level (m)
101	Un-named	09/24/1866	0.18	0.30	0.47	0.18	0.31	0.48	NA
111	Un-named	10/27/1867	0.60	0.34	0.94	0.60	0.36	0.96	NA
302	Un-named	10/12/1891	0.38	0.12	0.50	0.40	0.13	0.52	NA
330	Un-named	10/11/1894	0.15	0.21	0.35	0.17	0.21	0.39	NA
384	Un-named	9/9/1901	0.22	0.11	0.33	0.22	0.12	0.34	NA
418	Un-named	8/25/1906	0.32	0.22	0.54	0.36	0.23	0.58	NA
483	Un-named	7/10/1916	0.23	0.15	0.37	0.22	0.16	0.39	NA
486	Un-named	8/21/1916	0.27	0.05	0.32	0.26	0.05	0.31	NA
493	Un-named	10/6/1916	0.37	0.22	0.59	0.37	0.23	0.60	NA
559	Un-named	9/6/1928	0.27	0.30	0.57	0.24	0.31	0.55	NA
572	Un-named	9/8/1931	0.36	0.16	0.52	0.35	0.17	0.52	NA
582	Un-named	9/25/1932	0.53	0.31	0.84	0.51	0.33	0.84	NA
744	Un-named	8/23/1949	0.20	0.17	0.37	0.21	0.18	0.39	NA
915	FAITH	8/21/1966	0.23	0.19	0.42	0.24	0.20	0.43	NA
969	DORIA	8/20/1971	0.13	0.31	0.44	0.12	0.33	0.45	NA
1094	KLAUS	11/5/1984	0.26	0.13	0.38	0.26	0.14	0.39	NA
1139	HUGO	9/10/1989	0.63	0.24	0.86	0.59	0.25	0.84	0.72
1199	MARILYN	9/12/1995	0.60	0.27	0.87	0.59	0.28	0.87	1.10
1207	BERTHA	7/5/1996	0.31	0.31	0.61	0.31	0.31	0.63	0.53
1233	GEORGES	9/15/1998	0.23	0.17	0.40	0.21	0.19	0.40	0.61
1250	JOSE	10/17/1999	0.17	0.17	0.34	0.17	0.18	0.35	0.26

NA=Not Available

RMS error is slightly higher at 4.6 cm. For the other tide stations the RMS error between the ADCIRC results and the NOS predicted tides varies up to a maximum of 4.3 cm for similar tide ranges. The smallest RMS error for Charlotte Amalie is not unexpected due to the more refined model grid in the bay which was not the case at the other tide station locations.

The hurricanes considered included all that travelled past the project site within a 370 km (200 nm) radius between 1856 and 2006. Of these 213 storms only about two dozen had a combination of storm path and proximity to cause significant storm surge and/or wave conditions at the project site. The 21 storms used in the analysis are shown in Table 1 along with tide gauge measurements for several of the more recent hurricanes including Hugo and Marilyn. The Planetary Boundary Layer (PBL) model (Cardone, 1992) was used with ADCIRC to generate the wind fields based on storm trajectory and pressure information available in the HURDAT database. Figure 3 shows a comparison of the ADCIRC model results with the NOS measured water surfaces during Hurricane Hugo. Note the water surface shown for ADCIRC does not include the wave setup. As noted in Table 1, the wave setup is included with the ADCIRC results for comparison against the measurements from the tide gauge.

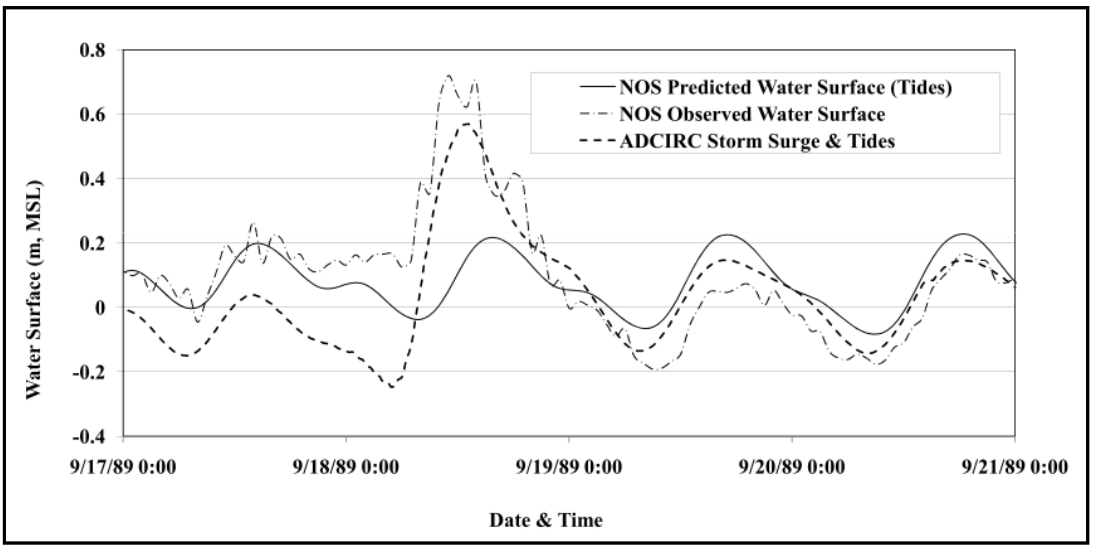


Figure 3. Comparison of observed and modeled water levels during Hurricane Hugo at the Charlotte Amalie tide gauge

Waves

Waves at the project site were calculated using an energy-based model for nearshore wave transformations called SWAN (Simulating WAves Nearshore), Ris (1997). A nested model was configured to allow extension offshore to deep water and adequate resolution in the relatively shallow bay at the project site. The outline of the nested model is shown in Figure 4.

Ocean waves were specified as a boundary condition and wind stress was applied over the domain of the SWAN wave model. The winds used in the SWAN model were calculated from the PBL model. The method outlined in the Shore Protection Manual (SPM) (USACE, 1984) was used to calculate the maximum wave height and wave period for a given storm condition. To determine the variation of wave height and direction within the storm a nomograph available in the Coastal Engineering Manual (CEM) (USACE, 2006) was used. This methodology was checked by calculating the maximum wave conditions for several hurricanes as they passed WIS Station 61012. Wave heights and wave periods for the hurricanes that fall within the WIS 20-year hindcast time series are shown in Table 2 illustrating agreement between the two methods.

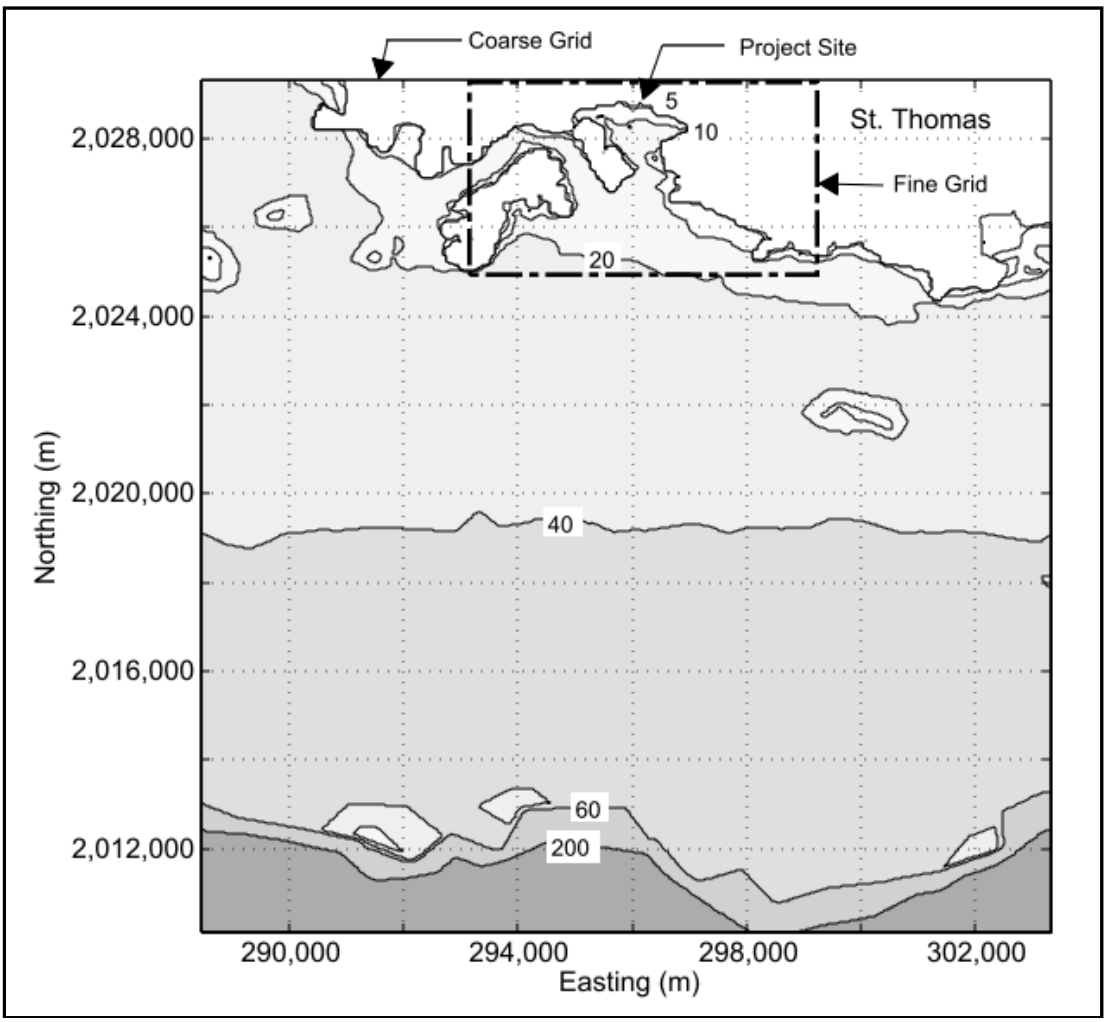


Figure 4. Coarse and Fine Grid Wave Model Domain and Depth Contours (m, MSL).

An example of the modeled wave heights are provided in Figure 5 for Hurricane Marilyn which had one of the largest wave conditions inside the bay of any of the historic hurricanes. Figure 5 shows the modeled wave height contours within the fine grid portion of the SWAN model.

Design Events

Storm surge and currents from the ADCIRC model and waves from the SWAN model were analyzed using the Empirical Simulation Technique (EST) (Borgman,

Table 2. Offshore Wave Parameters for Historical Storm Events

		Calculated		Hindcast - WIS Station 61012	
Hurricane	**Date**	**Hs (m)**	**Tp (sec)**	**Hs (m)**	**Tp (sec)**
KLAUS	11/5/1984	4.7	10.9	4.8	9.1
HUGO	9/10/1989	11.0	14.3	11.9	14.3
MARILYN	9/12/1995	9.1	11.6	10.4	12.5
BERTHA	7/5/1996	7.7	12.4	7.9	12.5
GEORGES	9/15/1998	7.9	12.2	7.9	11.1
JOSE	10/17/1999	6.3	10.9	6.1	11.1

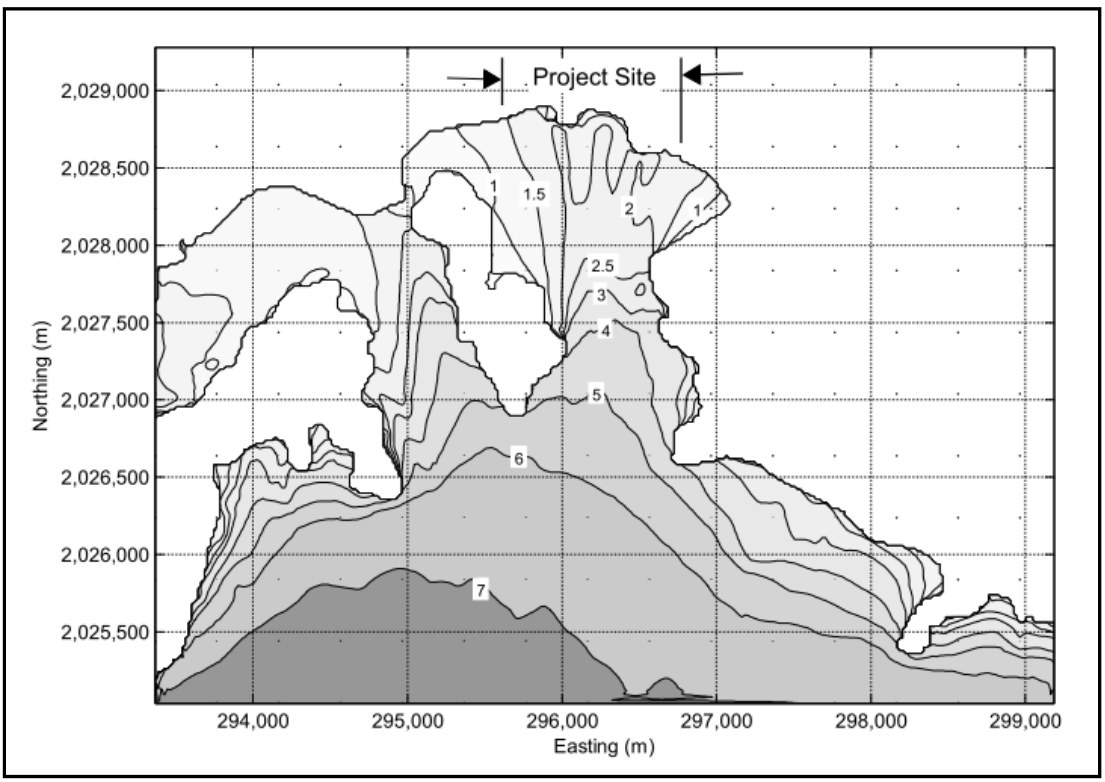


Figure 5. Significant wave height contours (m) for Hurricane Marilyn.

et al., 1992 and Scheffner, et al., 1999) model to calculate the probabilities of extreme events and associated recurrence intervals. Seventeen locations of interest were selected along the project site to adequately characterize the variation of results due to shoreline features. For each location, results from the ADCIRC and SWAN models were used in EST along with the storm frequency based on the number of storms (213) passing within a 370 km (200 nautical-mile) radius of the site between 1851 and 2006. This yields a frequency of 1.37 storms per year and is generally consistent with the methods used for the EST analysis conducted as part of the currently effective Federal Emergency Management Agency (FEMA) Flood Insurance Study (FIS) (FEMA, 2007). The results obtained from this study and those of FEMA from the FIS study shown in Table 3 are in agreement to within 5% for the 50-year and 100-year events but as can be seen there is a 1/3 m difference in the 500-year levels. This may be due to the FEMA FIS being taken at the shoreline where larger values of the wave setup would occur relative to the offshore locations where the wave setup was evaluated in this study.

Table 3. EST results for this study and water levels from the FEMA FIS

Annual Probability of Occurrence (%)	Average Return Period (yrs)	FEMA FIS Water Level (m)	Water Level at FEMA station (m)	Current at the proposed bridge (m)	Significant Wave Height at the proposed bridge (m)
2	50	1.62	1.62	0.83	2.61
1	100	1.83	1.74	0.95	2.75
0.2	500	2.34	2.01	1.22	3.07

Sea level rise

At the time of this work in 2007, the projected sea level rise was calculated based on a sea level trend analysis at the Charlotte Amalie tide gauge and the projected global increase in sea level rise based information available in the report on Global Climate Change (Bindoff, et al., 2007). From sea level trend predictions and historic values of sea level rise (Bindoff, et al., 2007) a ratio of global sea level rise was calculated. This ratio was obtained by dividing the average future projected global sea level rise for the next 75 years by the rate from the previous 25 years of global sea level rise. This ratio (1.62) was then multiplied by the sea level rise calculated from the previous 25 years of Charlotte Amalie tide gauge reported by (NOAA, 2001). A 90% confidence interval applied to the reported MSL trend (+0.5 mm/yr) and standard error (0.74 mm/yr) from the Charlotte Amalie data yields a rate of 1.7 mm/yr. Multiplying the ratio from the global sea level rise by the Charlotte Amalie trend yields 1.62 * 1.7 mm/yr or 2.8 mm/yr. Over the 75-year life of the structure this yields a sea level rise of 0.21 m which was used in the analyses described below.

SCOUR

Scour due to the combined action of waves and current was analyzed based on methods outlined in Sumer and Fredsoe (2002). The bridge piers consist of three 1.5 m diameter piles at each bent. The distance between bents along the curved bridge was approximately 18 m and the width of the proposed bridge is approximately 24 m including four lanes for traffic and a promenade for pedestrian access between the road and the bay.

Scour was calculated for both the 100-year and 500-year cases including the water levels, current and wave conditions. Significant wave heights ranged from 2.8 m to 3.6 m and currents ranged from 0.67 m/s to 1.07 m/s depending on the design event and location along the bridge. Scour was calculated for both the local pile scour and the pile group effect accounting for neighboring piles. Predicted scour depths ranged from about 1.0 to 1.6 times the pile diameter for the local pile scour to a range of 1.4 to 2.0 times the pile diameter for scour that includes both the local pile scour and the pile group effect. At each bent neighboring piles are located within about 7 m of each other center to center. Relatively small sand to gravel and small rock exists at all piles to the full depth of the calculated scour.

WAVE LOADS

Wave loads on the bridge deck included slamming, uplift and horizontal forces as well as associated moments. These loads were calculated using the published Guide Specification for Bridges Vulnerable to Coastal Storms (AASHTO, 2008). The bridge also has a façade on the seaward side for a pedestrian walkway which was analyzed using the empirical relationships outlined by (Cuomo et al., 2007). Stream Function Wave Theory (Dean, 1974) and Morison's Equation were used to calculate the wave loads on the piles. Time series of the stream function wave theory kinematics were calculated using a numerical code (Chaplin, 2007) in order to resolve the phase of the wave loading on each pile during propagation of the wave past the bridge.

Water levels at the bridge were determined based on a combination of sea level rise, tides, storm surge and wave setup. Wave setup was calculated across the entire shoreline at the bridge locations using the ACES program (Leenknecht, et al., 1992). In addition, the Direct Integration Method (DIM) (MacArthur, et al., 2006) was used to calculate the static plus dynamic wave setup at the shoreline. The ratio of the DIM wave setup (including both static and dynamic components) to the ACES wave setup at the shoreline was calculated. This ratio was then multiplied by the ACES wave setup profile to account for the dynamic component of wave setup. This typically increased the ACES wave setup by about 30%.

Wave loads were evaluated for each of three bridge elevation options including a minimum low chord elevation of 3.7 m above MSL. The other two alternatives include a low chord equal to half the height above MSL (i.e. 1.85 m) and another

higher elevation such that the low chord is above the maximum water surface elevation to prevent wave induced loading on the bridge deck. The proposed bridge configuration included a smooth surface under the deck. For the low level bridge option the wave load methodology predicts a deck uplift force of 430 kN/m with a moment of 5500 kNm/m. The maximum wave loads for the three piers range from 37 kN to 71 kN depending on the pier locations and the deck elevation.

Physical modeling studies are scoped as part of the final design effort, due in part to the location of the proposed bridge on a sloping seabed and the 3-dimensional aspects of the curved bridge around the associated headland.

CONCLUSIONS

A low level bridge is under consideration to minimize environmental impact to the historic beach from fill. The motivation to locate the road south of the Legislature building is to avoid impacts to two historic structures in an area where roadway widening to four lanes would encroach on the historic structures necessitating some demolition.

The project site is located within a moderately protected embayment. The location of this embayment on the south side of St. Thomas prevents the development of large storm surges due to the relatively narrow offshore shelf in this location. From a coastal engineering perspective these two effects yield a site where moderate storm surge coupled with moderate wave action leads to water levels that are influenced by both storm surge and wave setup. Storm induced currents are also low and generally limited to within a meter per second.

Analysis results are in general agreement with the currently effective FEMA Flood Insurance Study as well as NOAA tide gauge records.

REFERENCES

American Association of State Highway and Transportation Officials (AASHTO), (2008). “Guide specifications for bridges vulnerable to coastal storms.” AASHTO, Washington, D.C.

Bindoff, N.L., J. Willebrand, V. Artale, A, Cazenave, J. Gregory, S. Gulev, K. Hanawa, C. Le Quéré, S. Levitus, Y. Nojiri, C.K. Shum, L.D. Talley and A. Unnikrishnan, (2007). “Observations: Oceanic Climate Change and Sea Level.” *Climate Change 2007: The Physical Science Basis*. Contribution of Working Group I to the “Fourth Assessment Report of the Intergovernmental Panel on Climate Change.”[Solomon, S., D. Qin, M. Manning, Z. Chen, M. Marquis, K.B. Averyt, M. Tignor and H.L. Miller (eds.)]. Cambridge University Press, Cambridge, United Kingdom and New York, NY, USA.

Borgman, L.E., Miller, M.C., Butler, H.L., and Reinhard, R.D. (1992). "Empirical simulation of future hurricane storm histories as a tool in engineering and Economic Analysis." *ASCE Proc. Civil Engineering in the Oceans V*. College Station, TX. 2-5 Nov. 1992.

Cardone, V.J., Greenwood, C.V., and Greenwood, J.A., (1992). "Unified program for the specification of hurricane boundary layer winds over surfaces of specified roughness." Contract Report CERC-92-1, US Army Corps of Engineers, Waterways Experiment Station, Vicksburg, MS.

Chaplin, J. R. (2007). "Downloadable Software for Waves." http://www.civil.soton.ac.uk/hydraulics/download/downloadtable.htm, accessed 2007, University of Southampton, Southampton, U.K.

Cuomo, G., Tirindelli, M. and Allsop, W. (2007). "Wave-in-deck loads on exposed jetties." Coastal Engineering, Elsevier B. V., (54), pp. 657-679.

Dean, Robert, (1974). "Evaluation and development of water wave theories for engineering applications." Special Report No. 1, U.S. Army Corps of Engineers, Coastal Engineering Research Center, Fort Belvoir, VA. (in two volumes).

Hubertz, J.M., (1992). ""User's Guide to the Wave Information Studies (WIS) Wave Model, Version 2.0. WIS Report 27(AD A254 313)," U.S. Army Engineer Waterways Experiment Station, Vicksburg, MS 39180-6199.

Jarvinen, B.R., Neumann, C.J., and Davis, M.A.S., (1988). "A Tropical Cyclone Data Tape for the North Atlantic Basin," NOAA Technical Memorandum NWS NHC 22. Leenknecht, D. A., Szuwalski, A., and Sherlock, A. R. (1992). "Automated Coastal Engineering System Technical Reference." Coastal Engineering Research Center, Department of the Army, Vicksburg, MS, Version 1.07, September.

Leutich, R.A., Westerlink, J.J., and Scheffner, N.W., (1992). "ADCIRC: An Advanced Three-Dimensional Circulation Model for Shelves, Coasts, and Estuaries Report 1: Theory and Methodology of ADCIRC-2DDI and ADCIRC-3DL." Technical report DRP-92-6, Nov. 1992, U.S. Army Engineer Waterways Experiment Station, Vicksburg, MS.

MacArthur, R. C., Dean, R. G. and Battalio, R. (2006). "Wave processes in nearshore environment for hazard identification." *Proceedings of the 30th International Conference on Coastal Engineering*, Ed. McKee, J. S. World Scientific, New Jersey.

National Oceanic and Atmospheric Administration (NOAA), (2001). "Sea Level Variations of the United States 1854-1999." NOAA Technical Report NOS CO-OPS 36, Silver Springs, MD, July.

Ris, R., (1997). "Spectral modeling of wind waves in coastal areas." Report no 97-4, Communications on Hydraulic and Geotechnical Engineering, Department of Civil Engineering, Delft University of Technology, 160 pp.

Scheffner, Norman W., Clausner, James E., Militello, Adele, Borgman, Leon E., Edge, Billy L., and Grace, Peter E, (1999). "Use and application of the Empirical Simulation Technique: Users Guide." Technical Report CHL-99-21, December 1999, U.S. Army Engineer Waterways Experiment Station, Vicksburg, MS.

Sumer, B. Mutlu and J. Fredsoe, (2002). *The Mechanics of Scour in the Marine Environment*, World Scientific, New Jersey.

U.S. Army Corps of Engineers (USACE), (2006). *Coastal Engineering Manual*. U.S. Army Corps of Engineers, Washington, D.C. (in 6 volumes).

U.S. Army Corps of Engineers (USACE), (1984). *Shore Protection Manual*. U.S. Army Corps of Engineers, Washington, D.C. (in 3 volumes).

Vulnerability Assessment of Climate Change Impact on Groundwater Salinity in the Nile Delta Coastal Region-Egypt

Elshinnawy, I.A.[1], and Abayazid, H. O.[2]

Abstract

Though gifted with the Nile River, limitation in fresh water resources compared to expanding development activities add pressure to groundwater for fulfilling essential supply in Egypt. Therefore, attention is paid in groundwater management in facing development process pressures as well as initiated extra concerns of climate changes.

Being hydraulically connected with the sea, groundwater in coastal aquifer has special water characteristics and flow conditions. This study presents a vulnerability assessment for a study area that acquires a strategic environmental and socio-economic importance, located in the North-Eastern sector of the Nile Delta, with special reference to the impact of Climate Change-related Sea Level Rise (SLR) on salt water intrusion into aquifer.

The study tracks changes in sea water intrusion in terms of advancement of saltwater/freshwater interface inland. Analytical methods as well as numerical modeling approaches have been considered for modeling saltwater/freshwater interface behavior. Accordingly, interface dynamics and potential lateral and upward groundwater movements in the region of study in face of predicted SLR in years 2025, 2050, 2075 and 2100 have been investigated. Results showed that saltwater/freshwater interface advancement of 35 meters by year 2025, 180 meters in 2050, 509 meters in 2075, and 1065.8 m by year 2100 are predicted within the study area as a result of projected climate change and SLR; if no adaptation measures are implemented.

While considering ground levels, soil characteristics and land-use patterns, vulnerability analysis for the study area highlighted particular sub-regions at risk within the study area as being more susceptible to difficulties and deserves priority in precautionary management actions. In view of the concluded results, a review of prospective adaptation measures to be considered for alleviating adverse impact of Climate Change-related SLR are discussed in order to safeguard socio-economic assets and environmental state. However, it is recommended to investigate potential effectiveness and viability of alternative measures with periodic monitoring.

[1] Director of the Coastal Research Institute, National Water Research Center, 15 El-Pharaana str., El-Shallalat, Postcode 21514 Alexandria, Egypt; Tel (203) 4844614/5/6; Fax (203) 4844614/5, E-mail: coriegypt@gmail.com

[2] Researcher / Head of the Technical Office, Coastal Research Institute, National Water Research Center, 15 El-Pharaana str., El-Shallalat, Postcode 21514 Alexandria, Egypt; Tel (203) 4844614/5/6; Fax (203) 4844614/5, E-mail: halazid@yahoo.com

1. Introduction

Environment in coastal areas is custom to continuous cyclic changes. Yet predictions of climate changes give wider range of effects with different levels of risk. Therefore certain precautionary preparations are required in coastal regions in order to safeguard socio-economic assets and environmental state.

Early studies investigated predictions of climate change impact in the Egyptian coastal zone. Results showed that the area located in the North-Eastern sector of the Nile Delta is one of the most vulnerable regions to climate change adverse impacts. This study presents vulnerability assessment for the study area with special reference to the impact of sea level rise on groundwater elevation and salinity intrusion. Issues such as unprecedented changes, limitation in groundwater as a supplementary fresh water resource, alteration of salinity level in agricultural lands as well as difficulties to drainage system are among the concerns threaten progress in development processes.

This paper presents a review of approaches for following saltwater/freshwater interface behavior and modeling concepts. Then, predicted advance of saltwater/freshwater interface and change in groundwater levels, as a result of climate change and consequent Sea Level Rise, are demonstrated. Accordingly, and while considering land levels and soil characteristics, vulnerability assessment for the study area and possible adaptation measures are presented.

2. Background

As a semi arid country, Egypt suffers from limited resources of fresh waters compared to its needs for uses and development activities. While the River Nile plays a major role in supplying freshwater, however certain regions are mainly depending on groundwater for fulfilling essential beneficial uses. Therefore, attention is paid to maintain acceptable level of both quantity and quality of groundwater while conducting water resources management programs for sustainability of irrigation and land reclamation purposes (Anon, 1980).

The Nile Delta acquires a special importance and witnesses a variety of activities. The Delta ground water aquifer underlies about 3 million acres of fertile lands, while the aquifer systems are increasing in thickness from about 250 meters in the south to about 900 meters near the Mediterranean Sea (Kashef, 1983). However, the Nile Delta base meeting the Mediterranean Sea in about 240 km, which raise concerns of salt water intrusion into aquifer.

The area under consideration “Gamasa-Ras al Bar” is located in the north-eastern part of the Nile Delta and, while hosting the confluence of a major Nile branch “Damietta” with the Mediterranean Sea, witnesses an active hydrological cycling, (figure 1). This region is highly populated and hosting a variety of development activities. Therefore, groundwater is used to supplement available surface water to meet the ever increasing water demands.

Evidently, impact of predicted Sea Level Rise would go beyond inundating parts of the region adjacent to the shoreline. Advancing saltwater/freshwater interface, elevating groundwater levels as well as increasing ambient salinity degree are among major concerns to address.

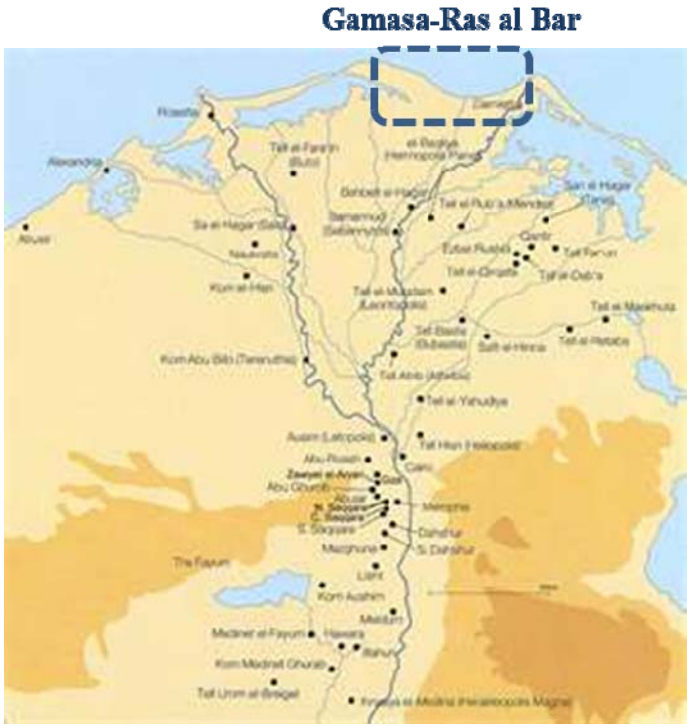


Figure 1: Location of the study area within the Nile Delta coastal zone

3. Research Objectives

With the main goal of tracking changes in salt intrusion into ground water as a result of sea level rise, this study seeks covering the following objectives:

- Define the inland advancement of saltwater /freshwater interface and, consequently, assess potential elevation in groundwater levels within the study area
- Highlight spots at risk within the study area
- Present vulnerability analysis and prospective adaptation measures

4. Sea Water Intrusion in Coastal Aquifer

4.1. Theory of Sea Water Intrusion

Being hydraulically connected with the sea, groundwater in coastal aquifer has special characteristics and flow conditions. Basically the denser saltwater tends to lay under the less in density freshwater with a zone of mixing known as the transition or dispersion zone formed between the two fluids. Equilibrium of the fluids dynamic

pattern is principally governed by, given certain medium/soil characteristics, rates of groundwater recharge/withdrawal and sea level. However, under normal conditions, fresh water flows from inland aquifers to the sea.

Early researches have commonly dealt with position movement of the saltwater/freshwater interface in relation to freshwater recharge into the aquifer versus withdrawals and resulting advance or retreat in position. Recently, however, climate change and potential sea level rise added a new dimension to consider in this arena. Climate change is likely to have impressive effects on the hydrologic cycle through altered precipitation, evapotranspiration, runoff and soil moisture patterns…etc. These changes will lead to altered groundwater recharge and flow regime as well as rate of saltwater intrusion in coastal aquifers.

4.2. Saltwater/Freshwater Interface Dynamics

Early studies on salt water intrusion were raised from concerns of over extraction of fresh ground water near coastal region. Main objective has been to reach safe withdrawal level that balances the recharge rates so that saltwater/freshwater interface advancement inland, along with accompanied threats of increased salinity levels, can be avoided. Among the reviewed approaches, following is a brief of selective ones considered in this report.

4.2.1. Ghyben-Herzberg Formula for Interfaces Dynamics

This Equation is considered a simplified representation of interface behavior as Ghyben-Herzberg model assumes that both freshwater and saltwater are static. Ghyben-Herzberg relation is based on satisfying hydrostatic equilibrium between the two fluids, freshwater and saltwater, with their different densities (Reilly and Goodman, 1985, and Sakr, 2005). The interface elevation is estimated for a given freshwater head at any point in the aquifer using the following relationship:

$$Z = \delta\, h_f \qquad \text{Eq. 1}$$

Where Z is the interface elevation measured downward from the mean sea level, h_f is the freshwater head measured above the mean sea level and δ is given by:

$$\delta = \left(\frac{\rho_f}{\rho_s - \rho_f} \right) \qquad \text{Eq. 2}$$

ρ_f and ρ_s in (Eq.2) are the freshwater and saltwater density respectively.

While assuming the hydrostatic equilibrium between the freshwater and saltwater, a sea level rise of (Δh_s) would have an impact on the interface movement (ΔZ):

$$\Delta Z = Z_o - Z_n = \delta (h_{f_o} - h_{f_n}) \cong \delta\, (\Delta h_s) \qquad \text{Eq. 3}$$

Where $(_0)$, $(_n)$ subscripts refer to present situation and situation with the sea level rise respectively.

4.2.2. Hubbert Theory

Hubbert Theory assumes equilibrium conditions, either in case the saltwater is stationary or when both fluids are in motion. The theory is conceptually based on maintaining the continuity of pressure in a flow field across an assumed interface. Governing equation of Hubbert for Interface dynamic (Eq. 4) is presented with reference to freshwater head (h_f), saltwater head (h_s), and Z the elevation above the datum of the point at which the head is measured.

$$Z = \frac{\rho_s}{\rho_s - \rho_f} h_s - \frac{\rho_f}{\rho_s - \rho_f} h_f \qquad \text{Eq.4}$$

4.2.3. Glover Formula

Glover analytical model accounts for the freshwater movement towards the sea while considering the saltwater remains static, (Glover, 1959). The developed model computes the interface elevation Z in coastal aquifers at any point X measured from the shoreline as a function of the net ambient fresh groundwater flow (Q), the density ratio between the freshwater and the saltwater (δ) and the aquifer hydraulic conductivity (K):

$$Z^2 - \left(\frac{2\delta Q}{K}\right) X - \frac{\delta^2 Q^2}{K^2} = 0 \qquad \text{Eq. 5}$$

4.2.4. Numerical Modeling

The above mentioned analytical solutions assume sharp interface with steady state flow conditions and fairly simplified aquifer characteristics, geometry, heterogeneity, anisotropy and boundary condition. However, in real situations both freshwater and saltwater are in motion and the aquifer characteristics are complicated (Sakr, 2005). While many approaches follow the assumed sharp interface for simplifying computations, yet considering that the boundary between saltwater and freshwater is not sharply distinct and a zone of dispersion or transition zone exist have been covered in certain researches.

A number of studies have presented numerical modeling approaches for seawater intrusion, while considering either fully mixed or sharp saltwater/freshwater interface condition (details can be found in Sakr, 1992 and Sakr, 2005). First consideration of the impact of advection-dispersion, density differences and mixing processes on seawater-freshwater interface has been introduced by Henry (Henry, 1959). The model deal with flow equations and the transport equations linked through fluid density and concentration state. Governing equations are customary simultaneously solved using numerical methods such as finite difference, finite element and boundary integral equation methods (Sakr, 2005). In 1992, another numerical model for saltwater/freshwater interface predictions (GWCH2O) has been introduced by Sakr, using the Finite Element method. Applications of GWCH2O model in Nile Delta aquifer have been presented in studies by Sakr et al. (Sakr et al., 2004 and Sakr 2005).

The simplified analytical solutions are widely-applied and found satisfactory in many early researches. Therefore, and with the limitation in historical field data, this research study is presenting an application of potential saltwater/freshwater interface

movement and groundwater level elevation resulting from predicted sea level rise, using Ghyben-Herzberg and Glover approaches.

5. Prediction Results and Vulnerability Analysis for the Study Area

As presented in early reports by the Egyptian National Water Research Center' institutes; Coastal Research Institute (CoRI), Drainage Research Institute (DRI) and Research Institute of Ground Water (RIGW), the current land elevation of the study area varies from 0.20 m below Mean Sea level (MSL) to 2.5 m above (MSL). The Groundwater flow is directed from south to north where the Piezometric level decreases gradually from more than 15m + MSL in Cairo city to less than 1m + MSL near the Mediterranean coast (Sakr, 2005 and RIGW, 2002). Figure (2) shows contours of land levels and present depth to groundwater in the study area.

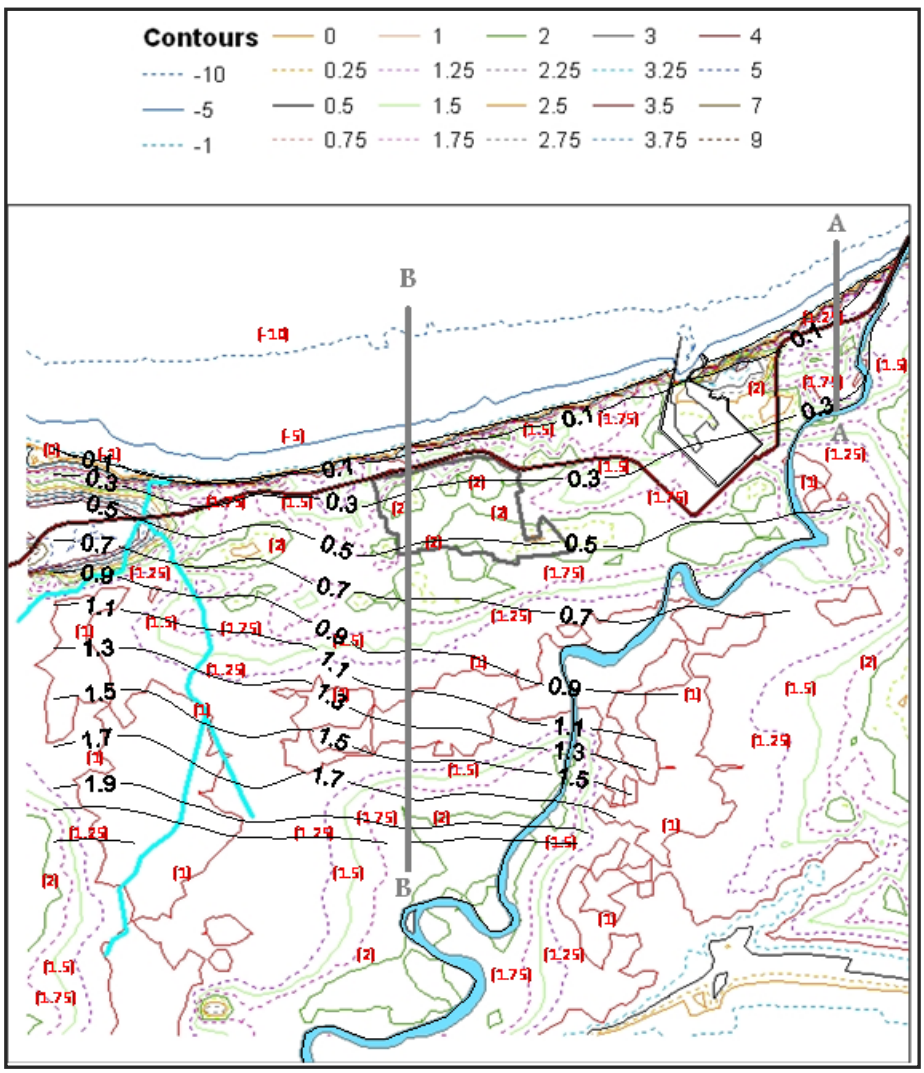


Figure 2: Land levels and present depth to groundwater

To investigate the potential impact of Sea Level Rise (SLR) on shifting saltwater/freshwater interface position and consequent elevation of groundwater levels, predicted rise in sea levels for years 2025, 2050, 2075 and 2100 have been considered. According to the Intergovernmental Panel on Climate Change Fourth Assessment Report (IPCC-AR4, 2007), results of worst case scenario of climate modeling, A1F1 scenario for Sea Level Rise, expect rise of 13.25cm, 30.50cm, 51.75cm and 73cm by years 2025, 2050, 2075, and 2100, respectively. Predictions of Sea Level Rise have been used in applying the analytical methods and concluding inland/upward movement of the saltwater/freshwater interface. With the predicted Sea Level Rise, shoreline is expected to move inland at variable rates in relation to the topography and, accordingly, new boundary conditions are formed.

For purpose of demonstration, results of two profiles are presented; profile "A" in eastern side of the study area that meet with the Damietta branch in distance less than six kilometers from shoreline, and profile "B" in the middle of the study area that stretch inland till its boundaries, [locations of profiles "A" and "B" are defined in figure (1)]. Results showed that sea water intrusion and interface shifting of 35 meters by year 2025, 180 meters in 2050, 509 meters in 2075, and 1065.8 m (more than 1 kilometer) by year 2100 are expected, if no adaptation measures are implemented. Illustrations are found in figures (3-6) and figure (7) for results in profiles "A" and "B", respectively.

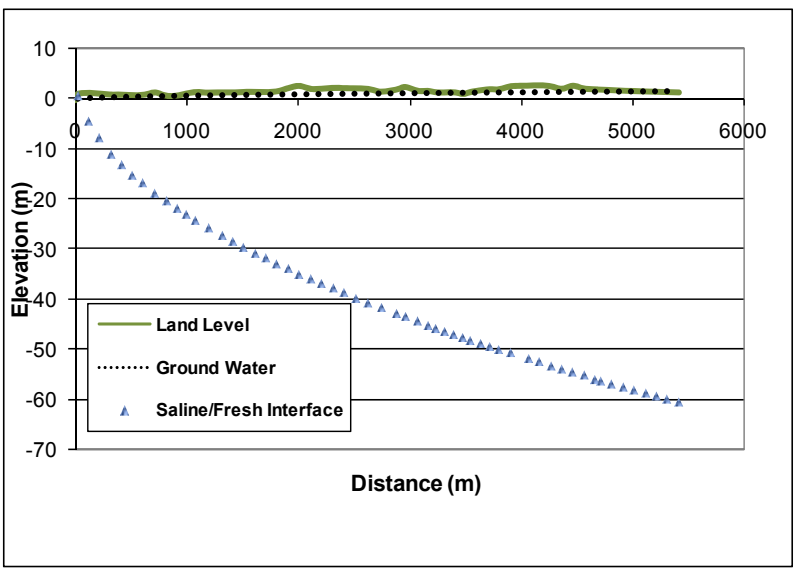


Figure 3: Predicted interface movement and groundwater elevation in 2025 [Profile A]

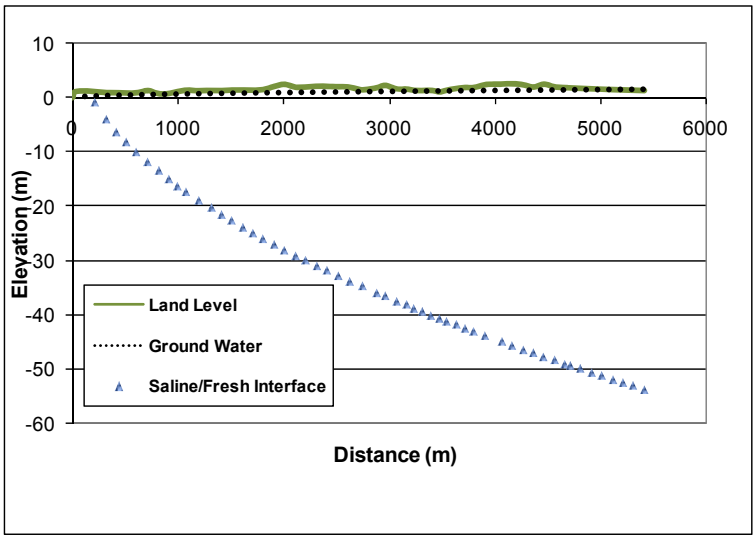


Figure 4: Predicted interface movement and groundwater elevation in 2050 [Profile A]

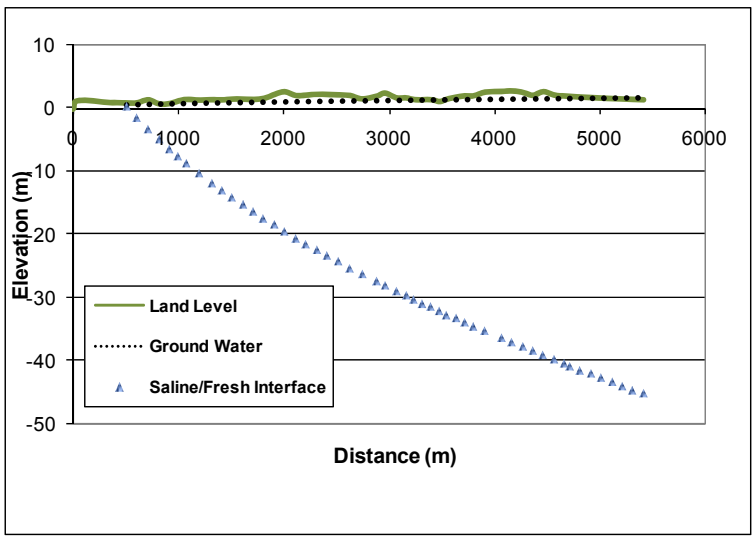


Figure 5: Predicted interface movement and groundwater elevation in 2075 [Profile A]

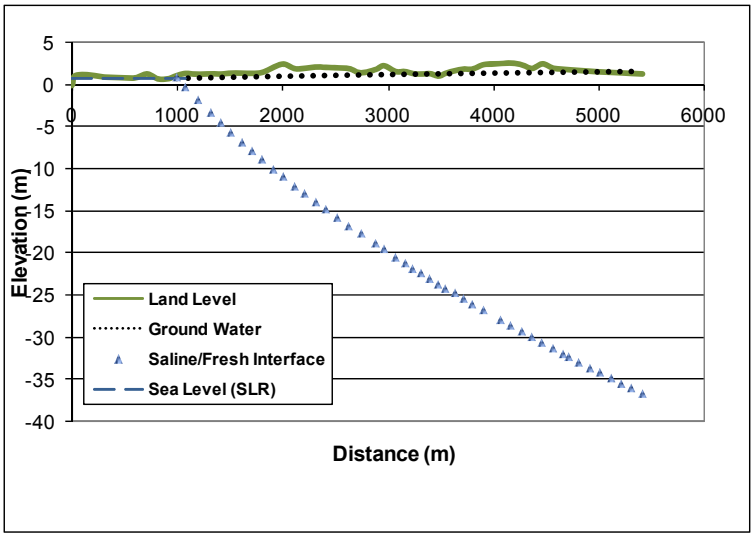


Figure 6: Predicted interface movement and groundwater elevation in 2100 [Profile A]

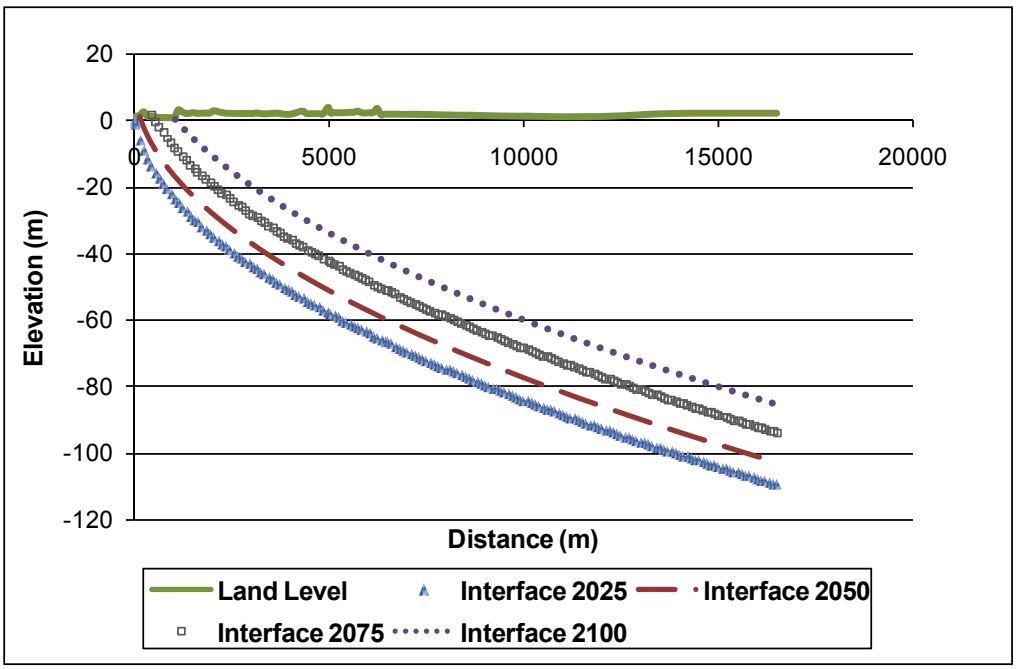


Figure 7: Predicted sea water intrusion and saltwater/freshwater interface shifting for years 2025, 2050, 2075 and 2100 [Profile B]

As discussed above, prediction of lateral and upward movement of saltwater/freshwater interface resulting from saltwater intrusion into coastal aquifers showed that an increase of 73 cm of sea level by year 2100 would cause intrusion of saltwater by about 1 kilometer into aquifer. Furthermore, elevation of groundwater table would cause vulnerable areas to have near surface groundwater causing serious cultivation and drainage difficulties, or even be inundated.

6. Vulnerability Analysis: Risks of Sea Level Rise on Coastal Aquifer

Implied concerns of Sea Level Rise on coastal aquifer can be summarized as:
Advancement of saltwater/freshwater interface inland
Saltwater intrusion and potential elevated salinity in water and soil
Vulnerability to inundation of Lowland regions
Shortage in fresh groundwater availability for beneficial uses
Elevation in groundwater levels
Concerns on agricultural land productivity and pressure on drainage systems
Impact on natural resources, fisheries and ecosystem sustainability
Impact on development process and socio-economic activities, and safety of populated areas

Survey results and collected data, reported from the Drainage Research Institute, revealed that soils of the study area are predominantly compact clay soils overlying subsurface strata of varying texture and nature, while only small parts of the area have loamy soils. As figures (8) and (9) show, clay cap thickness varies between 2m and 18 m. Also, the Pizometric head varies between (-1.25m) to (+0.25m) with reference to land surface. Thus, it is noteworthy that certain hydrological units raise concerns of being more susceptible to inundation as a result of reduces thickness of clay cap that coincide with Pizometric Head reaching land level in present conditions. These vulnerable units are highlighted in figures (8) and (9). As a result, these sub-regions are expected to have serious problems with predicted Sea Level Rise; in terms of cultivation drainage problems, elevated soil salinity in agriculture land as well as inundation to community settlements. Based on that, measures to alleviate potential adverse effects should be sought while giving priority to most vulnerable sub-regions, environmental factors as well as socio-economic importance.

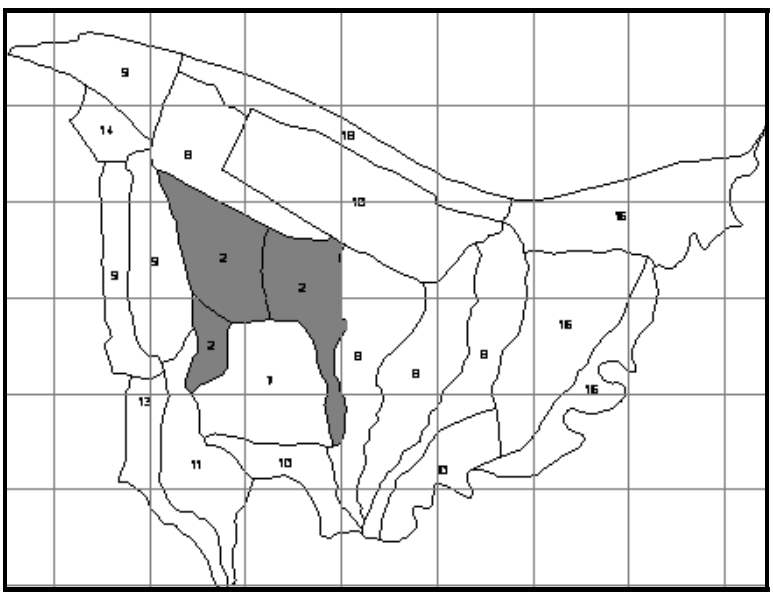


Figure 8: Clay Cap thickness for the hydrological units (m)

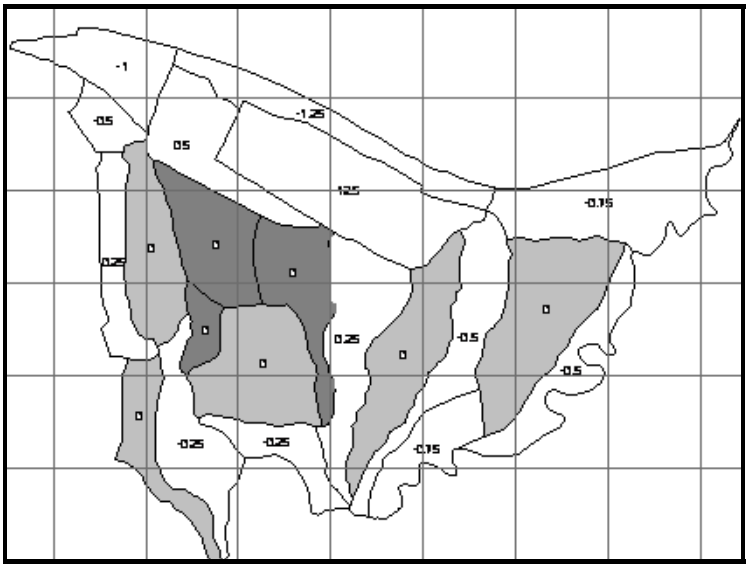


Figure 9: Pizometric head for the hydrological units (± Land Surface)

7. Managing Saltwater Intrusion: Adaptation /Mitigation Measures

7.1. Mitigation Based on Analytical Methods

The strategy of alleviating impact of lateral/upward movement of saltwater-freshwater interface is mainly based on minimizing the change in the interface position (Sakr, 2005). According to Ghyben-Herzberg Formula, the proposed mitigation strategy to stabilize the saltwater/freshwater interface can be achieved by increasing the freshwater head (Piezometric surface) by the same magnitude equivalent to the sea level rise value (i.e. in this case study 13.25 cm, 30.50, 51.75 and 73 cm by years 2025, 2050, 2075, and 2100, respectively).

Meanwhile, Glover model link the minimized interface movement by balancing the two sides of equation (Eq. 6):

$$\left(\frac{2\delta Q_{slr}}{K}\right)X_{slr} - \frac{\delta^2 Q_{slr}^{\ 2}}{K^2} = \left(\frac{2\delta Q_i}{K}\right)X_i - \frac{\delta^2 Q_i^{\ 2}}{K^2} \qquad \text{Eq. 6}$$

Where ($_i$) *and* ($_{slr}$) subscripts refer to present situation and situation with the sea level rise, respectively. Assuming constant hydraulic conductivity and density difference ratio, the following conditions would ensure balanced equation:

The shoreline position should remain at its present location ($X_{slr} = X_i$)
The net ambient fresh groundwater flow is kept constant ($Q_{slr} = Q_i$)

In Hubbert theory, the change in the interface position as a function of the sea level rise is directly related to densities, h_s, and h_f. Minimizing the interface changes for potential sea level rise is governed by the following equality condition.

$$\frac{\Delta Z}{\Delta h_s} = \frac{\rho_s}{\rho_s - \rho_f} - \frac{\rho_f}{\rho_s - \rho_f}\frac{\Delta h_f}{\Delta h_s} = 0 \qquad \text{Eq. 7}$$

$$\Delta h_f = \left(\frac{\rho_s}{\rho_f}\right).\Delta h_s \cong 1.025(\Delta h_s) \qquad \text{Eq. 8}$$

Accordingly, the present interface position would be stabilized with sea level rise when freshwater head or the Piezometric surface is increased with a value equal to 1.025 of the sea level rise value (i.e. in this case 13.58, 31.26, 53.04, 74.83 cm by years 2025, 2050, 2075, and 2100, respectively).

7.2. Mitigation Based on Modeling Methods

Modeling approaches are principally based on relating interface elevation at any point in the aquifer to the aquifer characteristics, fluid properties, groundwater extraction, boundary conditions and initial conditions. With rising sea levels, and while assuming constant aquifer and fluid properties, the impact of the changes in conditions resulting from the sea level rise would principally be alleviated by controlling freshwater and the saltwater pumping processes.

7.3. Mitigation Strategy: Alternative Measures for Adaptation

Measure in this arena should be multi-disciplinary because of the variability of strains attached. A comprehensive planning for adaptation strategy in coastal areas is required to cover aspects such as socio-economic and environmental status, available technologies, legal and administrative procedures...etc. However, with certain focus on alleviating negative effects on aquifer and related activities, precautionary alternatives and adaptation measures could be recommended hereby.

Earlier in a study by Kashef (1977), alternative control measures were suggested to control salt water intrusion by using physical barriers (e.g. curtains of injected soil, backfilled trenches with compacted soil) and/or hydraulic barriers formed by well or drain recharge. Also precautionary measures were recommended; such as, changing some irrigation procedures, planning ahead for industry and urban development in relation to water supply/demand, and change in activities whenever applicable, as well as reconsideration of groundwater withdrawal stations and their operational pattern.

Mitigation strategies for alleviating the impact of sea level rise on the Nile Delta aquifer is based on the concept of stabilizing piezometric surface and interface position as possible using controlling measures such as:

- Pumping of brackish/saltwater from the vicinity of the shoreline and Northern part of the Delta in order to reduce the saltwater head and help the freshwater to push the interface seaward (Sakr, 2005)
- Compensating lowered recharge rates in areas with increased urbanization and thus impervious surfaces

- Artificially recharging the groundwater table by means of injection wells of freshwater or primarily treated sewage along the shoreline
- Restricting, via quantitative rates, withdrawals from coastal aquifers especially in the areas located within the interface boundaries
- Constant monitoring system for groundwater level and saltwater/freshwater interface for continuous status observation and restoration planning

Meanwhile it is recommended to reconsider certain Land-uses in the study area; for instant, altering vegetation patterns (i.e. cultivating salinity tolerant crops), and applying management practices that have direct impact on hydrological processes through evapotranspiration and surface runoff. Changing in these components can be employed to maintain certain stability of groundwater as well as freshwater/saltwater interface in the study area.

8. Conclusion and Recommendation

The study presented methodologies of tracking potential changes in salt water intrusion into the Nile Delta coastal aquifer, resulting from IPCC projected Sea Level Rise in years 2025, 2050, 2075 and 2100. Predicted lateral/upward movement of saltwater-freshwater interface raised concerns in salt water intrusion and groundwater elevations in the study area. The study also highlighted certain sub-regions with high vulnerability that are expected to have serious problems with predicted Sea Level Rise; in terms of cultivation drainage problems, elevated soil salinity in agriculture land as well as inundation to community settlements. Based on that, measures to alleviate potential adverse effects should be sought while giving priority to most vulnerable sub-regions, environmental factors as well as socio-economic importance.

Finally, a review of adaptation measures to be considered for alleviating adverse impact of sea level rise-related salinity intrusion was presented. However, it is recommended to investigate potential success, effectiveness and viability of alternative measures with periodic monitoring, evaluation and update in application.

9. References

- Anon, 1980, Investigation project of sustained yield of aquifers, Part 1, Groundwater Research Institute, Cairo, 342 pp.
- Glover, R. E., 1959, The pattern of freshwater flow in a coastal aquifer, Journal of geophysical research, 64 (4): 457-459.
- Henry, H. R. 1959, Salt intrusion into freshwater aquifers, Journal of geophysical research, 64 (11), 1911-1919.
- Intergovernmental Panel on Climate Change, Fourth Assessment Report, IPCC-AR4, 2007
- Kashef, A. I., 1977, Management and control of salt-water intrusion in coastal aquifers, CRC Critical Reviews in Environmental Control, Ohio, USA , pp. 217-275.
- Kashef, A. I., 1983, Salt-Water intrusion in the Nile delta, ground water, vol. 21, no. 2.
- Reilly, T. E. and Goodman, A. S., 1985. Quantitative analysis of saltwater-freshwater relationships in groundwater systems - A historical prospective. Journal of hydrology, 80: pp. 125-160.
- RIGW, 2002, Nile delta groundwater modeling, Research Institute for GroundWater, El-Qanatir, Egypt.
- Sakr, S. A., 1992, Vertically integrated two-dimensional finite element model of seawater intrusion in aquifers, M. Sc. Thesis, Faculty of Engineering, Colorado State University, Fort Collins, Co. 80521.
- Sakr, S. A., Attia, F. A. and Millette, J. A., 2004, Vulnerability of the Nile delta aquifer of Egypt to seawater intrusion, International conference on water resources of arid and semi-arid regions of Africa- Issues and challenges. Gaborone, Botswana.
- Sakr, S. A., 2005, Impact of the possible sea level rise on the Nile delta aquifer, A study for Lake Nasser Flood and Drought Control project (LNFDC/ICC), Planning Sector, Ministry of Water Resources and Irrigation

Seawall-Waves Interaction and Impact on Sediment Morphology

Nabil M. Ismail 1, M.ASCE and Walid El-Sayed 2

1 Prof. of Coastal Engineering, Maritime Academy for Science and Technology and Maritime Transport, Miami, Alexandria, Egypt; formerly, Director of Eng. & Tech., Wellstream Int'l, Panama City, FL, USA; email: nbismail@usa.net

2 Manager of Rosetta Research Station, Coastal Research Institute, Alexandria, Egypt; email: walidelsayd@yahoo.com

ABSTRACT

A study was conducted to investigate hydrodynamic and sediment transport mechanisms induced by the interaction of seawalls or breakwaters and the incident wave field. Use has been made of field data of two case studies and the numerical predictions of Genesis. The main case study examines the seabottom morphology and cross shore profiles in front of Rosetta seawalls, constructed in 1990, on the Nile Delta coastline to decelerate coastal erosion of the headland after the operation of the Aswan high dam in 1965.

The analysis of the field data indicated lowering of the cross shore beach profiles, an increase of scour depth and an increase of the longshore sediment transport rate in front of the seawalls followed by downdrift accretion. These results are inline with the analysis of the second case study conducted to investigate the bathymetric changes, 1998-2004, at the Véran seawall located at the Gulf of Lions at the French Mediterranean coast. The modifications of sediment transport rates are attributed to the generated short-crested wave pattern in front of the seawalls and the modifications of long shore current. Further, the present analysis indicates that a significant component of sediment scour, in front of the seawall, is manifested as an offshore sediment transport current. Thereafter this offshore current is deflected alongshore contributing to sediment accretion down drift the seawall. Implications of these results to the design steps for coastal zone management and optimization of breakwater design, to minimize sediment accretion at entrances of small craft-harbors, are discussed.

INTRODUCTION

Most modeling and design activities do not take into consideration the impact of the structure- ocean wave interaction on sediment transport rates. The modified rates are responsible for the observed accelerated shoreline erosion at seawalls and subsequent down drift sediment accretion at the end of seawall or breakwater trunk. Figure 1 shows the morphological changes subsequent to the construction of Rosetta seawalls to mitigate coastal erosion after the operation of Aswan high dam in 1965.

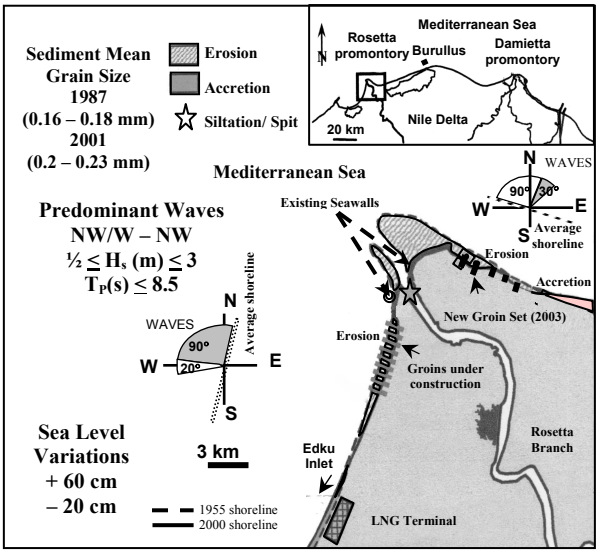


Figure 1. Morphological changes at Rosetta promontory headland.

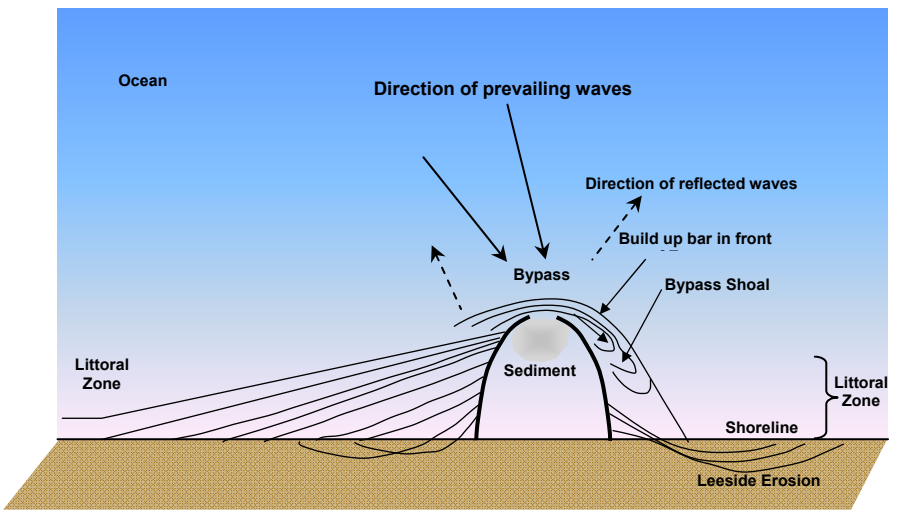


Figure 2. Schematic of the effect of wave patterns on sediment transport at harbor entrances

At the breakwater or seawall itself scouring can be dramatic, and if extensive enough, contributes to the failure of the structure through slumping or overturning. The loss of protection to the harbor and the coast and the subsequent cost of repair make good engineering design important. Thus, the knowledge of transport mechanisms at or in front breakwater and seawalls will contribute to the enhancement of models to determine patterns of erosion and scour along the protective shoreline structures and to estimate sediment accretion at harbor entrances.

Maintaining sufficient navigation depth in front of the entrance at harbors on littoral transport coasts is a major operational challenge for many harbor authorities, especially for small craft and fishery harbors located at exposed or moderately exposed sandy coasts. Sedimentation in harbor entrances cannot be completely avoided due to longshore currents, tidal currents and turbulent mixing processes. Reducing sedimentation in harbors can significantly decrease maintenance dredging costs. Different parametric studies are usually conducted to develop solutions to reduce sediment accretion at the harbor entrances and within harbors. These studies which use physical models and numerical 3D-models are aimed to arrive at an optimum harbor design and cost. One of the typical recommended solutions for the main up drift breakwater is to be extended further offshore. The extended breakwater will reduce the sediment accretion and allows for more sediment bypass to the downdrift coast. Figure 2 shows a schematic for development of the longshore sediment accretion adjacent to a small craft harbor located on a typical coast line after the extension of the harbor breakwater.

Seawalls and Ocean Waves Interaction

It is for the above reasons that we need to understand the sediment transport mechanisms (waves and currents) in shallow waters - especially at and near the structure. Wave mechanisms have been studied extensively, but little has been done to examine the impact of seawalls on the longshore and offshore currents. Among the few theoretical models, a numerical model was developed by McDougal et al in 2001 and a comparison of the cross shore profiles of long shore currents for a case of a seawall-protected beach and for an unprotected beach. It was found that the current profile for the seawall-protected beach was slightly higher near the breaker line. However the extent of current velocity variations would depend on the location of the seawall within the surf zone.

The construction of seawalls at the shoreline or surf zone and their impact on the shoreline, in front of the wall and, at the downdrift ends, has been a topic of considerable controversy for many years. It is becoming imperative to review and analyze in some varying detail field monitoring studies of coastal morphology modifications for seawall design cases, which would reflect the opposite impacts of seawalls. In this paper three case studies are considered which are located in California, USA, the Gulf of Lions, France, and the Rosetta headland estuary on the Nile Delta Coast.

Several long-term field studies such as that conducted by Griggs et al (1997) on the Aptos Seascape Seawall, located near Santa Cruz in Monterey Bay, California, showed that a seawall does not notably increase the erosion of the submerged part, except some local erosion at the foot of the seawall. In addition there were no significant differences between cross shore profiles for armored and non-armored beaches were reported in the studies. In some other cases such as seawalls located on the coastline of Monterey City, California, the seawalls were only impacted during the largest winter storm waves. These reported positive impacts of seawalls are attributed to the position of the seawall, within the surf zone, which is on the shoreline and the natural protection of the seawall provided by its location in Monterey Bay.
On the other side of seawall impact, the analyses conducted by Olivier et al (2005) of seabottom bathymetric profiles in front and on either side of the Véran Seawall (Fig.3), located on the sandy shoreline coast, Gulf of Lions, France, indicated an increase in longitudinal sediment transport rate and a deepening of the trough at the foot of the seawall structure. The details of the morphological responses to the construction of the Véran Seawall (1998-2004) will be addressed in the following section.

A notable case study of the drastic modifications which occur to the cross shore profiles and adjacent shorelines at seawalls is the case of the two seawalls constructed at the Rosetta Promontory between 1989-1990 (Fig.1) to decelerate the Rosetta headland rapid retreat after the operation of the Aswan High Dam in 1964. Figure 3 show the historical evolution of the Rosetta headland and shoreline modifications after the completion of the two seawalls which were constructed inland. The Rosetta case study is the prime focus of this research work and will be presented subsequently. It should be highlighted that the above mentioned three case studies deal with seawalls constructed where tidal range is small (microtide). However, as pointed out by Ilic et al (2007), in coastal areas with large tidal ranges, such as the west coast of the UK, beach lowering and scour in front of seawalls might be short-duration features taking place only during storm conditions. However, she recommended further work using Argus Video Images system coupled with conventional surveying methods to arrive at conclusive deductions on the impact of seawalls in these coastal areas.

SEABOTTOM EROSION IN FRONT OF VÉRAN SEAWALL AT THE GULF OF LIONS, FRENCH MEDITERRANEAN COAST

This case study demonstrates the major problems of coastal erosion and coastal management of the littoral zone at the seawall constructed at the Véran site, Gulf of Lions, Mediterranean Coast. The results of the study are based on a bathymetric monitoring program carried out by Olivier et al (2005) in front of the seawall, on a barred sandy coast in a microtidal setting. The Véran project is located on the shoreline of the Rhone delta (Fig.4). The beach profile (D_{50} = 0.2mm) forms a barred coast of France. The net longitudinal sediment transport is predominantly towards the west. In this microtidal context (<0.3m), the wave storms approach from SE quadrant (H_{sig}=3m, T= 7s annual, with a 6m maximum wave height). The seawall extends along the shore a distance of 2.7km.

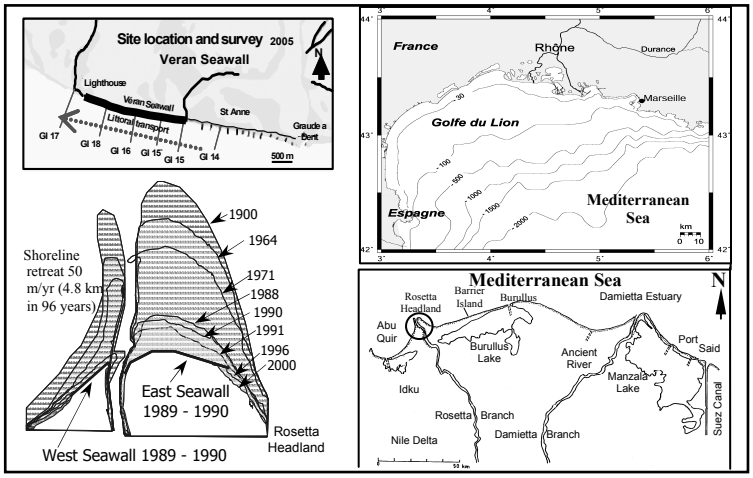


Figure 3. The Rosetta headland of the Nile Delta, Egypt and location of Rhone river case study in the Gulf of Lion, France

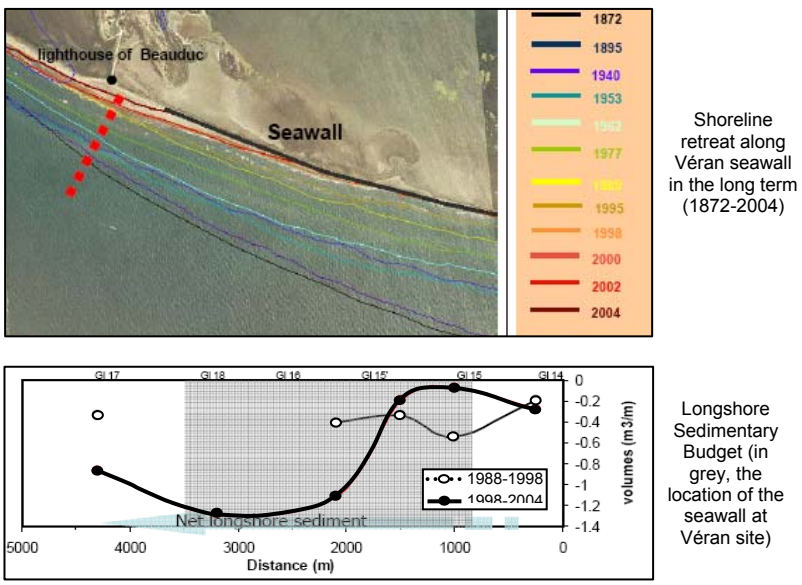


Figure 4. Longshore sedimentary budget: in grey, the location of the seawall, at Véran site, Gulf of Lions, France, Mediterranean (Olivier et al, 2005-2007)

Before the construction of the seawall in 1998, the shoreline was retreating at rates ranging between 3m and 8m per year, which is somewhat similar to the case study of Rosetta headland retreat. The environmental conditions produce a pattern of intense long shore erosion with a net long shore transport from east to west as demonstrated in Figure 4. Further, the field data showed the increase of the width of the surf zone and the closure depth in front of the seawall. This negative impact of the seawall was argued by the authors to be due to wave reflection.

NILE DELTA PROJECT - ROSETTA HEADLAND

The Rosetta promontory on the western coast of the Nile delta has been subjected to the most severe erosion of the delta coastline. The Nile delta coast including Abu Quir Bay forms a unique depositional environment, in which sedimentation is controlled by a combination of environmental factors such as waves, current, tides and river discharges as well as effects of mean sea level rise due to global warming. (Fanos et al, 1991)

Similar to other worldwide deltas, the Nile delta is presently subjected to significant coastal changes due to a combination of several factors. The main factors are the general decrease and current absence of the Nile discharge and sediment load to the Nile promontory mouth due to the construction of water control structures. The last structure was the Aswan High Dam which started operation in 1964 (Inman et al, 1984).

The absence of river currents modified the nearshore circulation induced by wave-current interaction which maintained the delta shape for many centuries. Such effects of the combined wave-current flow are well detailed in the studies made by Ismail (1982) and Ismail and Wiegel (1983, 2003). Subsequently, the continued action of waves and currents acted to induce beach and coastline erosion resulting in major reorientation of the coastline as some beaches eroded while others accreted.

A comprehensive program has been underway by the government coastal protection agencies for more than three decades to collect nearshore data related to coastal erosion problems along the Nile Delta. The data included daily measurements of deep water wave conditions, twice-yearly surveying of cross shore beach profiles, the measurement of mean sea levels, long shore currents and the mineralogical analysis of shoreline materials. Review of major existing coastal problems along the Nile delta coast and general description of the protective structures that have been implemented to address these problems are given by Mobarak (1972), Fanos et al (1995) Kadib et al (1986), and Khafagy et al (1992).

Rosetta Headland Shoreline Protection

To reduce the impact of the shoreline retreat at Rosetta promontory, two dolos seawalls (4-7 tons) were constructed between 1989 and 1990 on both sides of the Rosetta Nile branch mouth (Fig. 5). The western and eastern seawalls were constructed inland and extend alongshore to a length of 1.5km and 3.35km, respectively. Details of the seawall design are given in Figure 6. The rate of shoreline

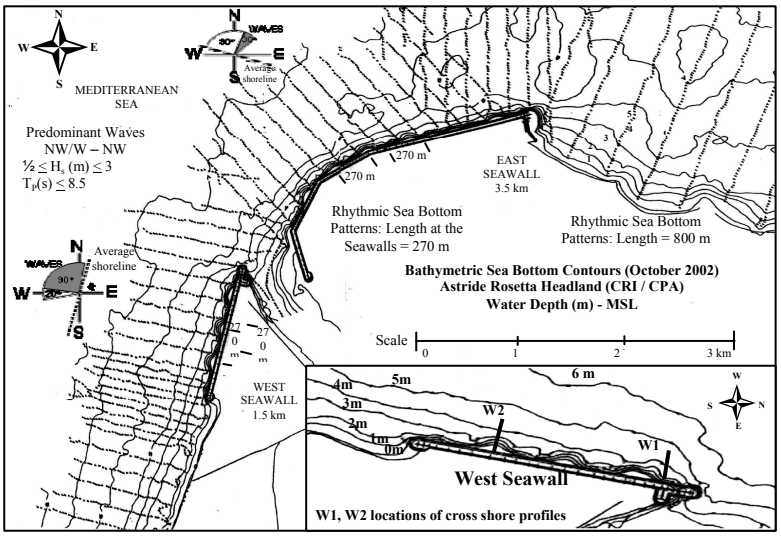


Figure 5. Rhythmic sea bottom bathymetry patterns at Rosetta seawall

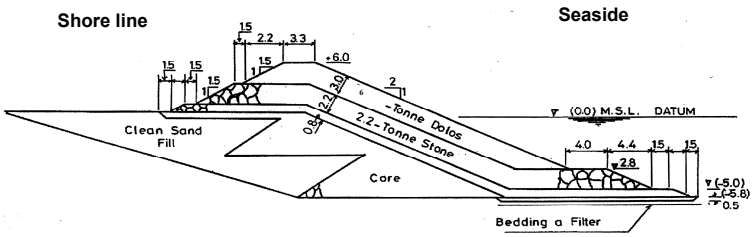


Figure 6. Cross section of rubble- mound seawall at Rosetta headland (1990)

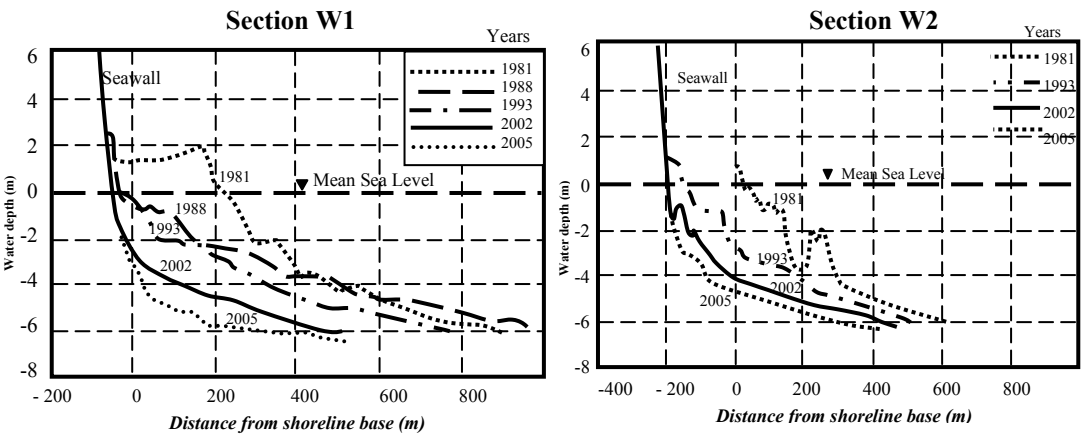


Figure 7. Evolution of cross shore beach profiles-west of Rosetta headland at the western seawall– sections W1and W2

changes after the construction of the seawalls revealed that the protection had succeeded in stopping retreat and flooding of the headland. However, coastal changes have shifted to shoreline modifications (erosion & accretion) to downdrift areas at the end of the seawalls. Consequently, groin systems were built at the eastern side and are being constructed on the western side, to combat the erosion that resulted at the downdrift areas (Fig. 1).

Morphological Changes at Rosetta Seawalls

Analysis of field data taken by the Coastal Protection Authority for the seabottom bathymetry in front of the seawalls in 2002 shows interesting features due to seawall-shore interaction. The bathymetric data shown in Figure 5 indicate that not only the shoreline in front of the seawall has eroded, but also a rhythmic seabottom pattern has formed along the walls. This rhythmic pattern has the appearance of "Beach Cusps". This persistent formation along the western and eastern seawalls occurs at a uniform distance of 270m. It is interesting to notice that the periodicity of this uniform distance appears to match the length of standing edge waves or low frequency oscillations which might be generated along the seawalls. Basic characteristics of the generated standing short-crested waves are given by Wiegel (1992).

As far as the cross shore beach profiles, two locations of beach profiles were identified and selected for analysis. The field data of the two cross shore profiles were compiled for comparison and presented in Figure 7. The location of these profiles was taken at the trough W1 and crest W2 of the seabottom rhythmic pattern (Fig. 5). The evolution of the beach profiles indicates beach lowering, increase in scour depth and the formation of a scour trough at W2 location.

DISCUSSION AND ANALYSIS

The results obtained on the morphological modification of the coastal zone at Rosetta headland after the construction of the two seawalls in 1990 indicate strong long shore and cross shore mechanisms contributing to the sediment transport processes.

These findings confirm the previous results highlighted by Olivier et al (2005) for the Véran seawall. Inspection of the cross shore beach profiles at W1 and W2 demonstrates that the beach responds to wave-seawall interaction through several mechanisms. An argued hypothesis is that wave reflection of incident waves at seawalls makes a significant contribution to wave pattern (McDougal et al, 2001) and morphology changes set at the walls. Figure 9 shows a photo of the wave pattern at Rosetta western seawall and generated offshore return currents. Wave reflection was also shown in many laboratory experiments to affect the pattern of the incident wave field and wave return currents. Among these experiments are that reported by Ismail and Wiegel (2003), and of which some results are shown in Figure 8.

Further, a field test was conducted in 2007 at Rosetta seawalls using surface floats and showed an average longitudinal spacing between return offshore currents (Fig. 8) which coincided approximately with the uniform rhythmic pattern observed on the seabottom bathymetry (Fig. 5). The generation of these cross offshore currents enhances the potential to increase the offshore sediment transport rate.

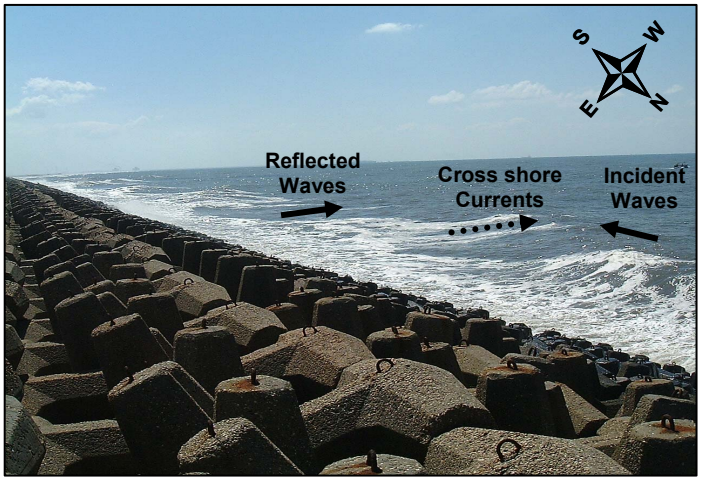


Figure 8-a. Wave patterns at Rosetta western seawall (March 2007)

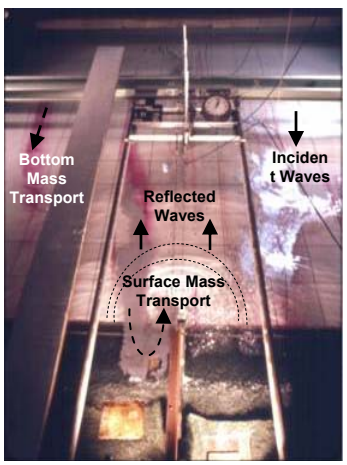


Figure 8-b. Reflected waves at a vertical wall and return surface flow: large wave steepness (Ismail, 1982)

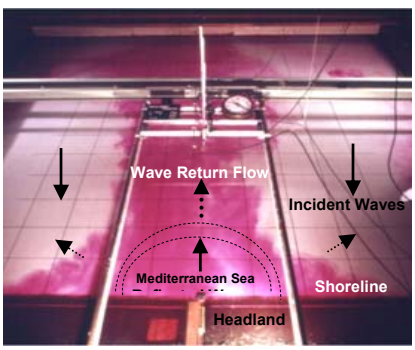


Figure 8-c. Reflected waves at a vertical wall and return flow: small wave steepness (Ismail & Wiegel,1983)

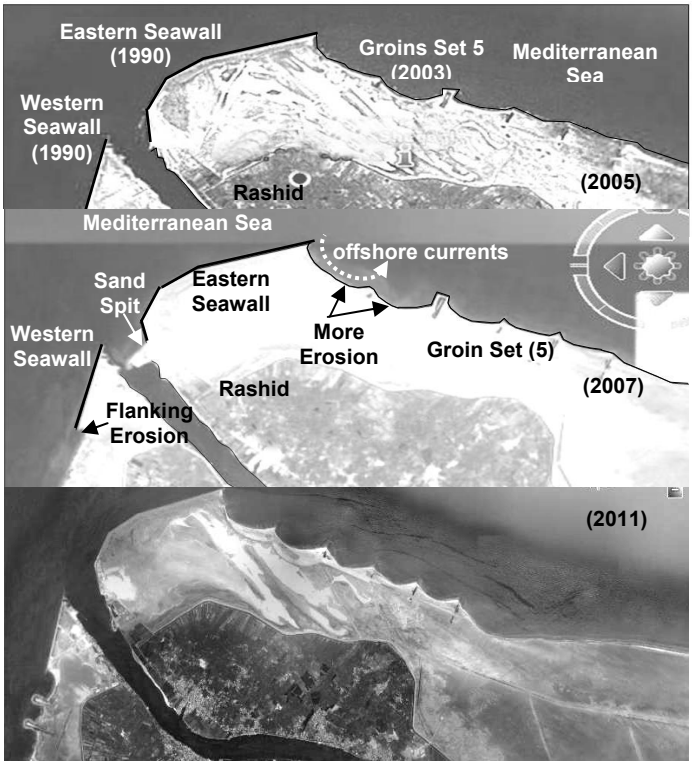


Figure 9. Comparison of satellite images of Rosette headland and coastal zone in the years 2005, 2007 & 2011 (Google Earth)

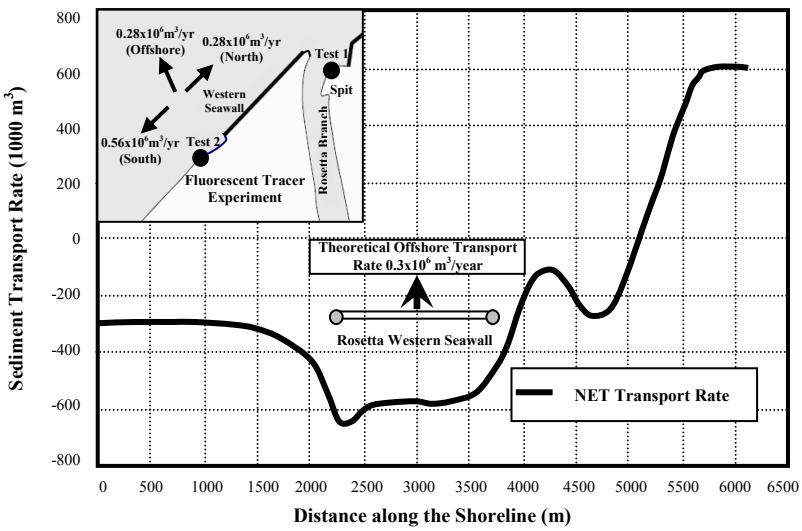


Figure 10. Sediment transport rate (Genesis) along the shoreline at west Rosetta headland for one year period (2003 – 2005 wave data)

This argument is confirmed by the field measurements of offshore sediment transport conducted by Miles et al (2001) at a seawall test rig in the UK.
Moreover, the impact of the seawall on the downdrift regions of the seawall are quite recognized from the satellite images of the Rosetta headland for the years 2005 , 2007 and 2011 as can be seen in Figure 9. The satellite image data show an increased rate of the scour between the groins existing on the eastern side of the Rosetta headland.

To obtain an estimate of the rates of long shore and cross shore sediment transport in front of the Rosetta headland seawall, and thus confirm our hypothesis of the hydrodynamic mechanisms, predictions of Genesis computer model (version 3) and the results of the fluorescent sand tracer were used to confirm the offshore sediment transport rate. An estimate of the rate of beach erosion at location W1 and W2 was calculated from the beach profiles and the results are given in Table 1. Figure 10 shows the numerical predictions using Genesis for the long shore sediment transport rate. Making use of the beach scour rate given in Table 1, the offshore sediment transport rate could be deduced at the western seawall, which is equivalent to that obtained using tracer field data. (Abou Zed et al, 2005).

Table 1. Rate of erosion at the Rosetta western seawall site for cross shore profiles W1, W2 (1998-2005)

Year	Erosion rate m^3/year/m'	
	Section W1	Section W2
1981-1988 Pre-Construction	93	93
1998-2002 Post Construction	125	115
2002-2005 Post Construction	140	100

CONCLUSIONS

Wave reflection of incident waves at seawalls or breakwaters makes a significant contribution to wave pattern (McDougal et al, 2001) and morphology changes set at the walls. This mechanism is confirmed by the generated wave pattern in front of Rosetta headland seawall on the Nile Delta Coast enhance the rate of offshore sediment transport as well as the long shore transport rate. These deductions are based on the detailed analysis of the field data collected from 1981 until recently by the Coastal Research Institute in Alexandria and the Coastal Protection Authority in Cairo. Use had been made of numerical predictions of Genesis as well as rate of scour, calculated based on the measured cross shore beach profiles in front of the seawalls. The semi-theoretical estimate of the along shore and cross shore sediment transport rates agree with the corresponding values obtained from the results of fluorescent tracer experiments conducted at the Rosetta western seawall. The above results agree qualitatively with the analyses carried out by previous investigators on field monitoring of morphological changes occurring in front of the Véran Seawall located on the French Mediterranean Coast.

The observed accelerated erosion (Fig.9) between the groins on the eastern side of Rosetta headland would suggest the use of efficient sediment retraction structures such as T-head groins.

Further field experiments are recommended to examine the wider spatial and temporal distributions of all relevant oceanographic, seawall geometry and shoreline parameters. These field experiments should take into consideration the interaction of waves and non-uniform return offshore currents at the seawalls or breakwaters (Ismail, 2007). The current research highlights that seawall-waves interaction modifies longshore and cross shore sediment transport rates along coastal structures. Thus there is a necessity of evaluating harbor breakwater layouts as well as the breakwater design with the objectives of minimizing wave reflection and reducing sediment accretion at harbor entrances.

ACKNOWLEDGEMENTS

The senior author wishes to express his deep appreciation to Professor Emeritus R.L. Wiegel of the University of California at Berkeley, who stimulated the senior author interest in coastal processes during his PhD graduate work and who gave him inspiring comments during the model study of PG&E Diablo Canyon Project which was successfully completed by the University of California and Bechtel Corporation in San Francisco in 1988.

REFERENCES

AbouZed A.I., and Shereet S.M., (2005). "Dynamics of Near Shore Sediments and Coastal Changes Astride Rosetta Branch, Egypt". *Emirates Journal for Engineering Research,* vol.10, No.2, 51-61.

Fanos, A.M., Frihy, O.E., Khafagy, A.A. and Komar, P.D., June 25-27, (1991). "Processes of Shoreline Change along the Nile Delta Coast of Egypt". *Proc. Coastal Sediments 91,* ASCE, vol. II, Seattle, Washington, 1547-1557.

Fanos, A.M., Khafagy, A.A. and Dean, R.G.,(1995). "Protective Works on the Nile Delta Coast". *Journal of Coastal Research,* vol. 11, No. 2, 516-528.

Griggs, G.B., Tait, J.F., Moore, L.J., Scott, K., Corona, W. and Pembrook, D., (1997). "Interaction of Seawalls and Beaches: Eight Years of Field Monitoring, Monterey Bay, California". *Technical Report CHL-97-1, US Army Corps of Engineers.*

Ilic, S., Ruzic, I., de Alegria, A.R. and Kingston, K., (2007). "Evolution of the Beach in Front of a New Seawall: Cleveleys, UK". *Proc. 7th. Int. Conf. Coastal Structures,* Venice, Italy.

Inman, D.L., and Jenkins, S.A., (1984). "The Nile Delta Littoral Cell and Man's Impact on the Coastal Zone of the Southeastern Mediterranean". *Proc. 19th Int. Conf. Coastal Engineering,* ASCE, vol. II, Houston, Texas, 1600-1617.

Ismail, N.M., (2007). "Discussion of Reynolds Stresses and Velocity Distributions in a Wave-Current Coexisting Environment". *Journal of Waterway, Port, Coastal and Ocean Engineering,* vol.133, ASCE, NY, 168-170.

Ismail, N.M. and Wiegel, R.L., (2003). "Secondary Flows and Sediment Problems Near Coastal Marine Outfalls". *Proc.3rd Int. Conf. Coastal Structures,* ASCE, Portland, Oregon, USA, 764-776.

Ismail, N.M. and Wiegel, R.L., (1983). "Opposing Waves Effect on Momentum Jets Spreading Rate", *J. Waterways, Port, Coastal and Ocean Division, Proc.*, ASCE, vol. 109, No.4, 465-483.

Ismail, N.M., (1982). "Effect of Wave-Current Interaction on Littoral Drifts", *Shore and Beach, J. American Shore & Beach Preserv. Assoc.,* vol. 50, No. 1, 35-38.

Kadib, A.L., Shak, A.T., Mazen, A.A. and Nadar, M.K., (1986). "Shore Protection Plan for the Nile Delta Coastline". *Proc. 20th Int. Conf. Coastal Engineering,* vol. III. Taipei, Taiwan, 2530-2544.

Khafagy, A.A., Nafaa, M.G., Fanos, A.M. and Dean, R.G., (1992). "Nearshore Coastal Changes Along the Nile Delta Shores", *Proc. 23nd Int. Conf. Coastal Eng*., ASCE, vol. II, Venice, Italy, 3261-3272.

McDougal, W.G. and Ruggiero, P., (2001). "An Analytical Model for the Prediction of Wave Setup, Longshore Currents and Sediment Transport on Beaches with Seawalls". *Coastal Engineering,* vol. 43. 161-182.

Miles, J.R., Russel, P.E. and Huntly D.A., (2001). "Field Measurements of Sediment Dynamics in Front of a Seawall". *Journal of Coastal Research,* vol. 17, No. 1, 195-206.

Mobarak, I.E., (1972). "The Nile Delta Coastal Protection Project", *Proc.13th Int. Conf. Coastal Eng.,* ASCE, vol. II, Vancouver, B.C., Canada, 1409-1426.

Olivier, S., Francois, S., and Lambert, A. (2005). "Erosion of the Sandy Bottom in front of a Seawall Véran site, Gulf of Lions, Mediterranean". *Proc. Specialty Conf. on Coastal Dynamics,* ASCE, Barcelona, Spain. Also, personal communication (2007); http://paralia.fr/Files/08_32__6p__samat.

Wiegel, R.L., (1992). "*Oceanographical Engineering*", Prentice-Hall, Englewood Cliffs, NJ, 532 pp. and reprint (2005), Dover Publication, NY.

Coastal Structures & Sea Level Rise: Adaptive Management Approach

John R. Headland[1], Dilip Trivedi[2], Russell H. Boudreau[3]

[1] Moffatt & Nichol, 104 West 40th St., New York, NY 10018; PH (212) 768-7454; FAX (212) 768-7936; email: jheadland@moffattnichol.com
[2]Moffatt & Nichol, Walnut Creek, CA, 2185 N. California Blvd., Walnut Creek, CA 94596; PH (925) 944-5411; FAX (925) 944-4732; email: dtrivedi @moffattnichol.com
[3]Moffatt & Nichol, 3780 Kilroy Airport Way, Long Beach, CA 90806; PH (562) 426-9551; FAX (562) 424-7489; email: rboudreau@moffattnichol.com

ABSTRACT

There is an impetus by the scientific community in general, and federal agencies like the U.S. Army Corps of Engineers and the U.S. Environmental Protection Agency in particular, to include the effects of global warming and sea level rise (SLR) within the design life of all federally funded projects. However, no mandates or policies have been issued. In many coastal states, specific policies and mandates have been issued to agencies to include the effects of climate change, which has resulted in relevant coastal management agencies taking on the mantle of addressing sea level rise issues in terms of development permits for new projects, and some on existing projects.

Since there is no generally-accepted, specific guidance on ranges of SLR or management strategies for the future, coastal developments are seeking guidance for an understanding of the issues and associated economic implications and other risks. An illustrative example of an adaptive management strategy for a typical coastal protection structure (seawall) is presented including a net present value analysis of various strategies. Finally, an implementation strategy that integrates Adaptive Management and a Monitoring Framework based on recent experience in San Francisco Bay is presented. Scientific projections, illustrative cases, and the evolving nature of SLR projections are discussed.

INTRODUCTION

A plethora of projected sea level rise (SLR) scenarios have been developed. The challenge is to plan/design coastal protection works for SLR. One approach is to select a target number (e.g., a medium SLR scenario 50 years hence) and design (or improve an existing design) ahead of time for this SLR. The other approach is to design for a shorter period (say 20 years) and adapt the design to accommodate SLR over time. This paper focuses on the A*daptive Management Approach*.

SEA LEVEL RISE SCENARIOS

Figure 1 shows modified NRC (USACE, 2009) and Rahmstorf (2007) scenarios for 2010-2060. Occurrence probabilities are not given for any of the scenarios.

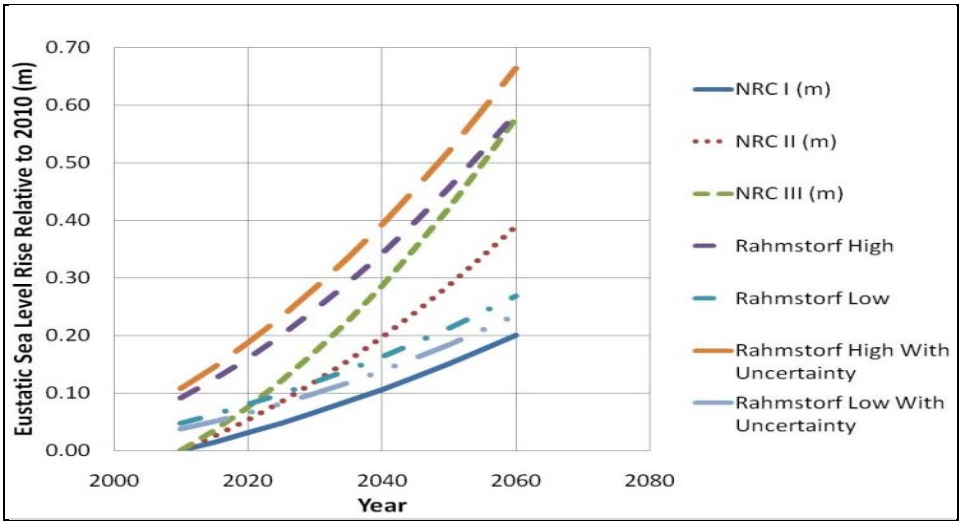


Figure 1. Modified NRC and Rahmstorf (2007) Scenarios

Figure 2 schematically shows the Adaptive Management Approach. In this example, the initial structure is designed for the existing SLR rate. After the initial period, observation of SLR will make is possible to determine how much the structure should be adapted to accommodate the SLR elevation at the end of the second period. Additional periods would be accommodated in the same way.

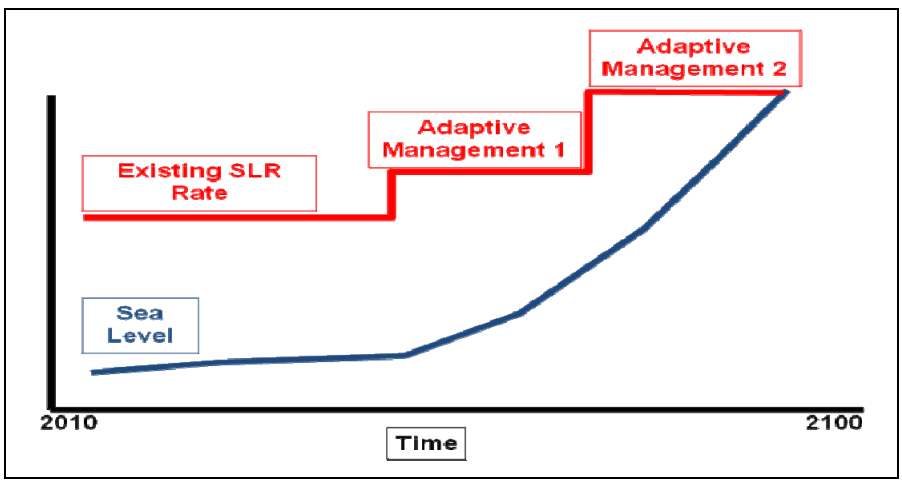


Figure 2. Adaptive Management Approach

The next step is to evaluate the total cost of the adaptive management and compare those costs to a scenario where the structure is built in year one to accommodate the full-period SLR. The costs are simply evaluated using net present value (NPV.) This is the basic framework for the Adaptive Management Approach. The following demonstrate the methodology for a simple rubble mound seawall example.

SEAWALL EXAMPLE

This example considers design of a new rubble mound seawall shown in Figure 3. The seawall is comprised of rock armor, a concrete crown wall, and rock under-layers. Assumed unit costs for these elements are given in Table 1. The design conditions for this example are also provided in Figure 3. The design conditions

constitute a case where a change in water depth owing to SLR would cause a meaningful change in wave heights reaching the structure. In deeper water, a change in water level would not have as large an impact on wave heights reaching the structure.

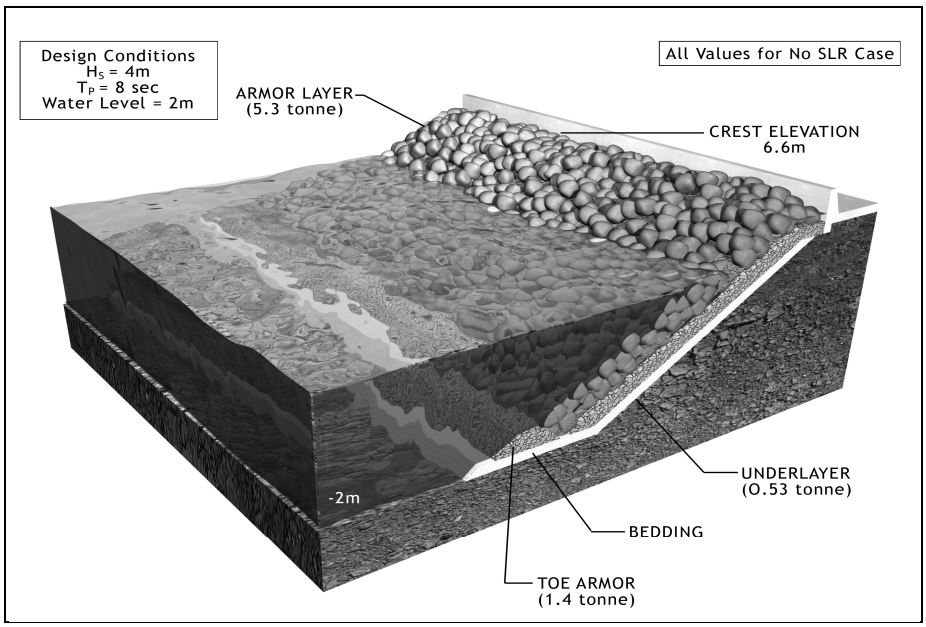


Figure 3. Example Rubble Mound Seawall

Seawall geometry (armor sizes, crest elevation, etc) is increased for SLR ranging from 0m-0.66m. Table 1 shows the unit costs for materials (rock, filter fabric, etc) that were used to estimate total structure costs.

Table 1. Rubble Mound Seawall Unit Costs

Item	Unit	Unit Rate ($)
Armor Stone	tonne	$80
Under Layer	tonne	$60
Quarry Run	tonne	$45
Geotextile	m^2	$30

Figure 4 summarizes changes in various structural design parameters with SLR. These parameters are used to develop costs for each SLR scenario. The total costs per meter of structure length are provided in Table 2, including the differential costs for various SLR levels.

Table 2. Seawall Cost per Meter Length

SLR (m)	Seawall Costs ($/m)	Differential Cost ($)
0	$ 12,333	-
0.2	$ 14,141	$ 1,808
0.4	$ 15,091	$ 950
0.58	$ 15,977	$ 866
0.66	$ 16,626	$ 650

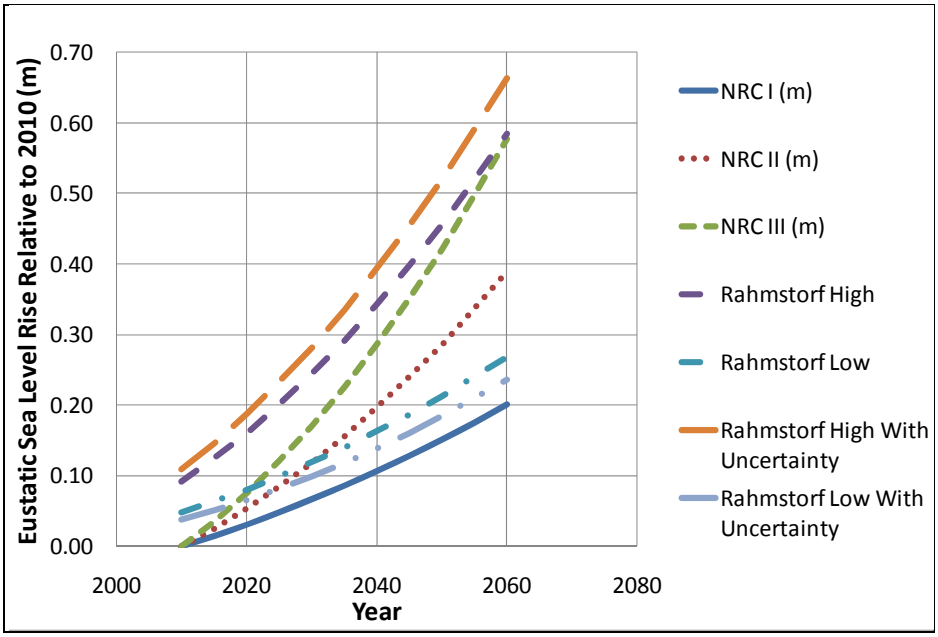


Figure 4. Summary of Seawall Design Parameters for Various SLR Levels

ADAPTIVE MANAGEMENT APPROACH

The technique here is to construct an initial structure designed for an initial period of SLR. The length and rise of the initial and subsequent periods depend on the SLR scenario, the higher the rise rate, the shorter the periods. The intent is to minimize the adaptive steps while keeping pace with SLR. Table 3 and Figures 5 and 6 summarize an Adaptive Management Approach for the Modified NRC (2009) scenario.

Table 3. Adaptive Management Plan for Modified NRC SLR Scenarios

	Scenario (4% Interest Rate)			
Year	**No SLR**	**NRC I**	**NRC II**	**NRC III**
1/1/2010	$ 12,333	$ 14,141	$ 14,141	$ 14,141
1/1/2015	$ -	$ -	$ -	$ -
1/1/2020	$ -	$ -	$ -	$ 950
1/1/2025	$ -	$ -	$ -	$ -
1/1/2030	$ -	$ -	$ -	$ -
1/1/2035	$ -	$ -	$ -	$ -
1/1/2040	$ -	$ -	$ 950	$ -
1/1/2045	$ -	$ -	$ -	$ 886
1/1/2050	$ -	$ -	$ -	$ -
1/1/2055	$ -	$ -	$ -	$ -
1/1/2060	$ -	$ -	$ -	$ -
Total NPV	**$ 12,333**	**$ 14,141**	**$ 14,434**	**$ 15,007**
% Difference	**100%**	**115%**	**117%**	**122%**

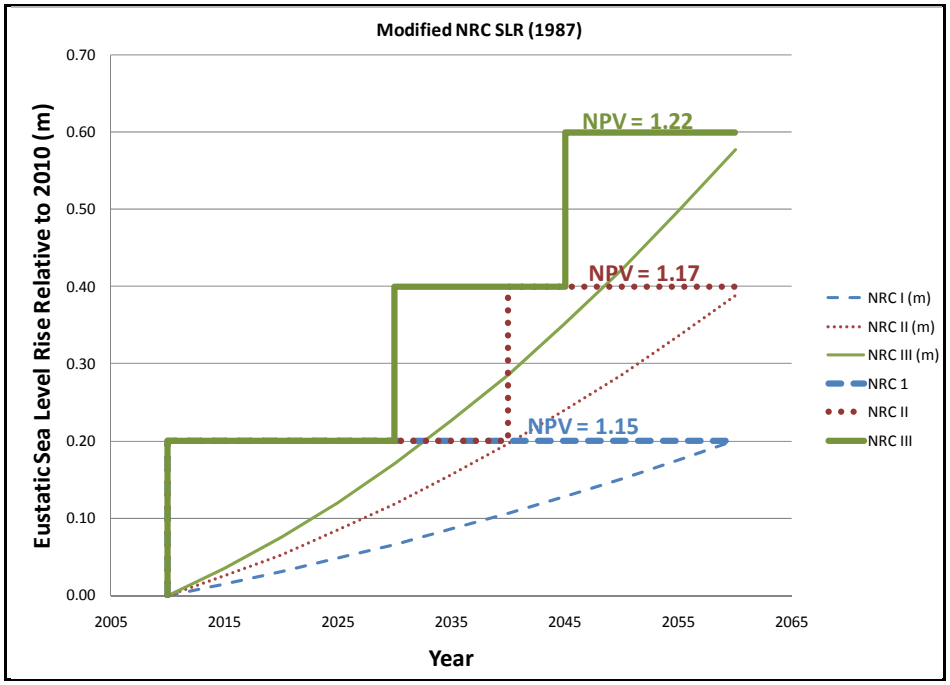


Figure 5. Adaptive Management Plan for Modified NRC SLR Scenarios

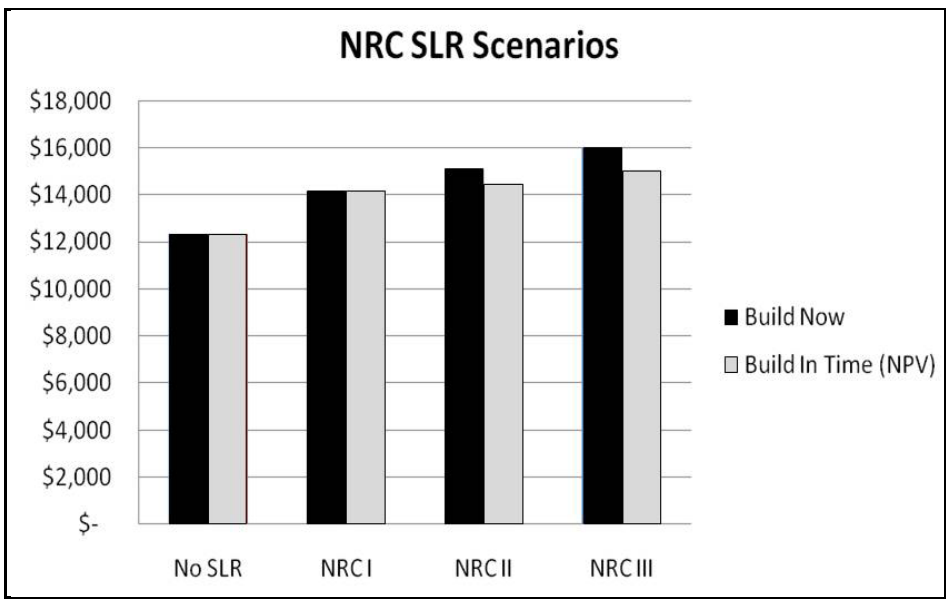


Figure 6. Relative Costs Adaptive Management Plan for Modified NRC SLR Scenarios

Figures 5 and 6 show the cost of the adaptive management approach scenarios relative to a base case designed for the full 50 years of SLR in the first year. Table 5 shows that it would be reasonably economical to design the structure for the full 50 years in year 1 for the lowest scenario (NRC1). The NRC III scenario can be accommodated in three steps. Figure 6 shows that it is more economical to take an Adaptive Management Approach for NRC II and III.

Table 4. Adaptive Management Plan for Rahmstorf SLR Scenarios

	Scenario (4% Interest Rate)				
Year	**No SLR**	**Rahmstorf Low (m)**	**Rahmstorf Low with Uncertainty (m)**	**Rahmstorf High (m)**	**Rahmstorf High with Uncertainty (m)**
1/1/2010	$ 12,333	$ 14,141	$ 14,141	$ 14,141	$ 14,141
1/1/2015	$ -	$ -	$ -	$ -	$ -
1/1/2020	$ -	$ -	$ -	$ 950	$ 950
1/1/2025	$ -	$ -	$ -	$ -	$ -
1/1/2030	$ -	$ -	$ -	$ -	$ -
1/1/2035	$ -	$ -	$ -	$ -	$ -
1/1/2040	$ -	$ -	$ -	$ 886	$ 886
1/1/2045	$ -	$ 950	$ -	$ -	$ -
1/1/2050	$ -	$ -	$ 950	$ -	$ -
1/1/2055	$ -	$ -	$ -	$ -	$ 650
1/1/2060	$ -	$ -	$ -	$ -	$ -
Total NPV	**$12,333**	**$ 14,382**	**$ 14,339**	**$ 15,056**	**$ 15,167**
% Difference	**100%**	**117%**	**116%**	**122%**	**123%**

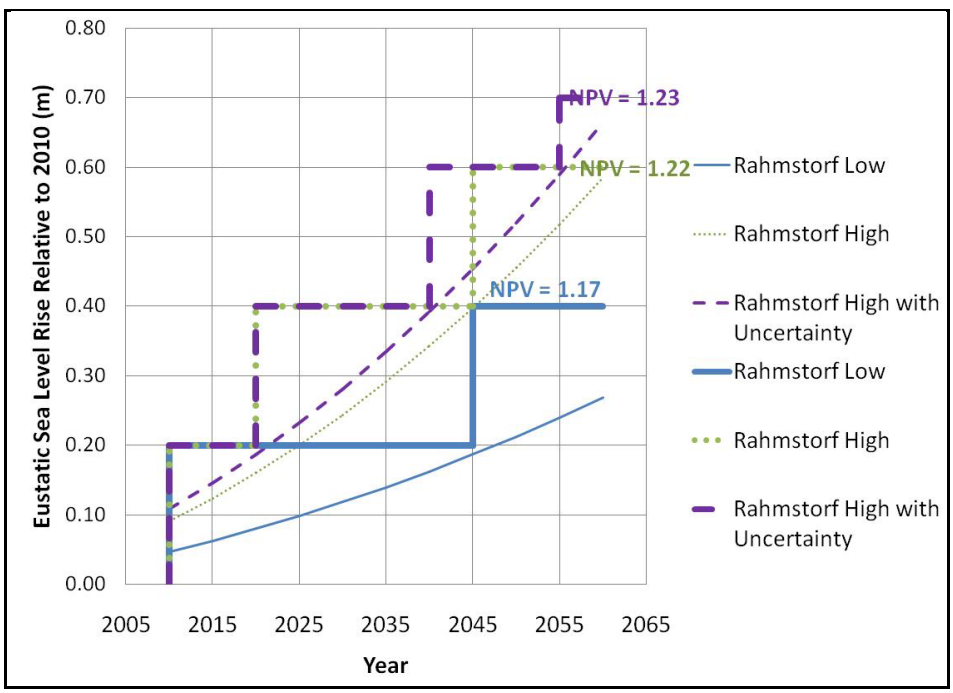


Figure 7. Adaptive Management Plan for Modified NRC SLR Scenarios

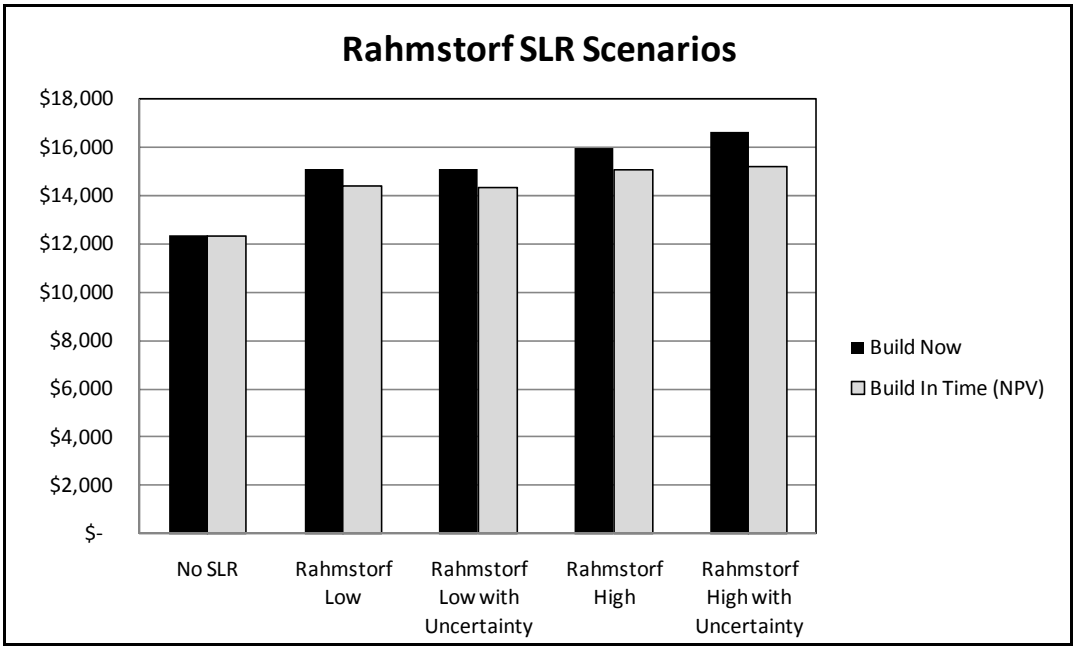


Figure 8. Relative Costs Adaptive Management Plan for Modified NRC SLR Scenarios

Figures 7 and 8 show that the lowest Rahmstorf scenario could be accommodated with one adaptive step; the highest Rahmstorf scenario, could be accommodated with three adaptive steps. Figure 8 shows that it is more economical to take an Adaptive Management Approach.

Overall, the above example demonstrates the utility of the Adaptive Management Approach. An example of such an approach is provided in the following section.

PROJECT EXAMPLE – TREASURE ISLAND DEVELOPMENT, SAN FRANCISCO, CALIFORNIA

Treasure Island was constructed using sand mined from San Francisco Bay in 1936 for the Golden Gate International Exposition. The Treasure Island Development Authority (TIDA), which is a Redevelopment Agency in San Francisco, and Treasure Island Community Development (TICD) are working together in a public-private partnership towards the redevelopment of Treasure Island. Development plans for Treasure Island include 6,000 new residential units, three hotels, a 400-slip marina, restaurants, retail and entertainment venues, and nearly 300 acres of parks and open space.

Sea Level Rise. The traditional approach to designing non-levee protected coastal developments, per FEMA guidance, is to set interior grades throughout a community such that finished floor elevations for buildings would be above the present-day base flood elevation (BFE, or the 100-yr return period water level). Improvements along the shoreline are required only to protect against storm wave run-up and overtopping. The modest amount of historic SLR (about 8 inches over the past century) was within the allowances that traditional coastal developments included in their design. However, recent projections of accelerating SLR necessitated its inclusion in the planning process for coastal developments to

prevent future flooding or loss of infrastructure resulting from shoreline erosion. Treasure Island's location in the Bay and typical low lying terrain makes the proposed development a perfect example of the need to plan for SLR.

Incorporating SLR into Development Plan. SLR estimates in the literature vary widely, from an observed value of 8 inches per century to about 33 inches per century based on IPCC high estimates. High-resolution global altimetry data, through the end of 2009, suggest that in the last two decades, global mean sea level has increased at a rate close to the upper end of the IPCC projections. This corresponds to an increase in global mean sea level of around 10 inches by 2050 and 30 inches by 2100. Semi-empirical studies by Rahmstorf and news articles have stated that SLR over the next 100 years could be substantially higher than that suggested by IPCC and could be as much as 55 inches by 2100. This SLR estimate was adopted by the CALFED Independent Science Board as a plausible, albeit high, value. It is also the basis for the long-term estimate recommended by BCDC and SCC.

What is clear is that the science of climate change and SLR is evolving, implying that it is prudent to develop community designs that can accommodate various levels of SLR over the planning horizon rather than design to a specific report or estimate. Since building structures are generally "immovable," whereas a shoreline protection system and/or storm drain system can be adapted to keep up with changing sea levels, various planning horizons were adopted for different elements of this project.

The first step was a study to develop planning and design guidance through the various phases of the project. The study was based on an exhaustive review of the literature, recent guidance from regional agencies, and extensive modeling of tidal, wind-wave, and storm-wave processes for the Central Bay. Based on the study results and numerous discussions with TIDA, TIDC, and other City agencies, the following strategy for protection against SLR was adopted for the Treasure Island project. It is comprised of four separate components:

1. Construction of a shoreline protection system that is initially built to accommodate a mid-term rise in sea level of 16 inches, with a design that is adaptable to meet higher than anticipated values in the mid-term as well as for the long-term;
2. Designing a storm drainage system that is initially built to accommodate a mid-term rise in sea levels with a design that is adaptable to meet higher than anticipated SLR values (similar to 1 above);
3. Construction of buildings and vital transportation infrastructure at elevations that would not be exceeded by flood waters in the event of failure along the shoreline, for present conditions as well as over a longer-term compared to 1 and 2 above. It is obvious that while the shoreline protection and storm drain system could be upgraded over time, habitable structures cannot be raised;
4. Implementing an Adaptation Strategy that would include a funding mechanism that pays for infrastructure improvements necessary to adapt to higher than anticipated sea levels.

In almost all of the science reports reviewed, a 36-inch SLR value is not reached until after 2100. Even with a more aggressive projection of SLR (55 inches), the increase in sea level reaches 36 inches between 2075 and 2080.

The strategy for development of Treasure Island is founded on raising grades for the new development to accommodate 36 inches of SLR, combined with an Adaptation Strategy for long-term improvements to the drainage and shoreline protection system in the event that actual SLR exceeds that value. Specific implementation strategies are discussed below.

All buildings and entrances to subterranean parking and streets would be set at an elevation that is 36 inches higher than the present day 100-yr return period water level in the Bay. This 36-inch SLR allowance plus a freeboard of 6 inches is proposed to be used for finished floor elevations of all buildings. This will ensure that even if no shoreline protection improvements are undertaken, or in the event of a slope failure along the shoreline, buildings and transportation infrastructure would not be flooded for water levels 42 inches higher than current BFE. This would put it beyond the 2080 time frame according to the most aggressive SLR, and well beyond 2100 according to the highest IPCC projection.

The storm drain system will be constructed with an initial SLR allowance of 16 inches, and will be adaptable to higher levels of SLR with minimal intervention. It will thus function as a gravity-drained system until about 2050, beyond which the Adaptation Strategy will be implemented consisting very likely of installing storm drain pumps.

It is not practical to build a high wall around the project for a design condition that may not happen for several decades, as it would pose a visual obstruction and severely limit public access. At the same time, it is not practical to build to present sea level conditions and keep raising it as sea levels rise. Therefore, an allowance of 16 inches of SLR will be built into the initial construction, and the design will be adaptable to higher levels of SLR by leaving a significant development setback such that improvements can be made. A stream of funding to construct these improvements will be part of the Adaptation Plan.

Adaptation Strategy. A project-specific Adaptation Strategy was implemented to provide guidance, identify relevant stakeholders, define appropriate management actions and triggers, and establish a project-specific funding mechanism. The strategy envisions incorporating ongoing measurements of SLR from the scientific community into Monitoring and Adaptive Management Plans that would guide the decision making process for future improvements. It will be administered by an entity created for Treasure Island which would have taxing authority and funding responsibility. A Monitoring Program will be put in place to compare observed changes in sea level with the crest elevations of the shoreline protection system.

The Adaptive Management Strategy will define specific triggers for action based on the observed changes in sea level. Future phases of construction that may be needed to respond to SLR are as follows:

- When a sea level increase of 16 inches is reached, the crest elevation of the shoreline protection system would be raised and storm drain system pumps installed.
- When a sea level increase of 36 inches is reached, the shoreline protection system would be improved to act as a flood barrier (levee or floodwall).

The elevation and structural characteristics of the island's perimeter are key components of Treasure Island's Adaptation Strategy. The proposed development setback distances will enable a variety of future modifications along the shoreline protection system to accommodate at least 55 inches, as recommended by the CALFED Panel, with the ability to accommodate even higher values of SLR if necessary. Adaptations would likely include a combination of the following components in response to varying land use and wave runup characteristics at different locations around the island:

- Raising the shoreline embankment in place to function as a storm surge or flood barrier;
- Constructing a series of embankments of increasing heights away from the water. Land between sets of embankments can hold periodic wave overtopping that drain out between high tides;
- Constructing sea walls – particularly at the proposed ferry quay and along Clipper Cove where they would also function as a public amenity; and
- Laying back the shoreline to create cobblestone beaches to limit wave runup and overtopping, rather than increasing embankment heights.

Figure 9 shows an illustration of the adaptive SLR strategy for the Treasure Island Development.

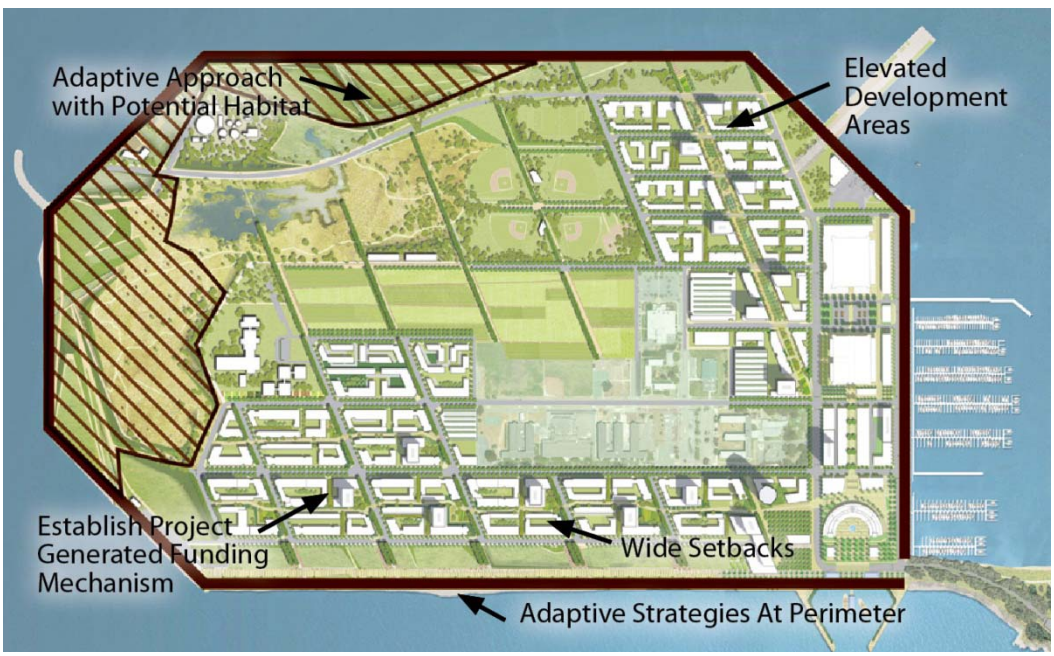


Figure 9. Treasure Island – Sea Level Rise Adaptive Strategy

CONCLUDING THOUGHTS

- The coasts of the United States are not equal; some will be impacted by SLR more than others.
- Adaptive management appears to be an expedient approach given the significant uncertainties in SLR forecasts.
- NPV analysis for generic example of a rubble mound seawall shows there is little practical difference in the forecast range of SLR scenarios and the costs to mitigate the effects of those scenarios.
- SLR and climate change may be a great challenge, but there will likely be tractable solutions in many cases.

REFERNCES

California State Coastal Conservancy. *Policy Statement on Climate Change*. Adopted at the June 4, 2009 Board Meeting.

Cayan, D., P. Bromirksi, K. Hayhoe, M. Tyree, M. Dettinger, and R. Flick, 2006. *Projecting Future Sea Level*. California Climate Change Center report number CEC-500-2005-202-SF, March 2006.

Intergovernmental Panel on Climate Change, 2007. *Climate Change 2007: The Physical Science Basis. Contribution of Working Group I to the Fourth Assessment Report of the Intergovernmental Panel on Climate Change*. Solomon S., D. Qin, M. Manning, Z. Chen, M. Marquis, K.B. Averyt, M. Tignor, and H.L. Miller (eds.). Cambridge University Press.

Moffatt & Nichol, *Treasure Island Development Project, Planning For Sea Level Rise, Part I – Background and Projections*, prepared for Treasure Island Community Development, July 2008.

National Research Council (NRC), *Responding to Changes in Sea Level: Engineering Implications*, 1987.

Rahmstorf, Stefan, "A *Semi-Empirical Approach to Projecting Future Sea Level Rise*, Science, 2007.

San Francisco Bay Conservation and Development Commission, *Living With A Rising Bay, Vulnerability and Adaptation in San Francisco Bay and on its Shoreline,* April 2009.

U.S. Army Corps of Engineers, *Incorporating Sea-Level Change Considerations in Civil Works Programs*, EC 1165-2-211, July 2009.

Subaqueous cohesive sediment gravity flows from open water pipeline dredge disposal: laboratory experiments and mathematical modeling

M. R. Chowdhury and F. Y. Testik*

Department of Civil Engineering,
College of Engineering and Science, Clemson University
Clemson, SC 29634, USA, E-mail: ftestik@clemson.edu

ABSTRACT

Subaqueous sediment gravity flows generated in open water pipeline dredge disposal operations were investigated through laboratory experiments and mathematical modeling. Three laboratory experiments that simulate typical open water pipeline dredge disposal operations in the coastal environment were conducted by discharging mud slurries with three different initial concentrations in a large pool. The discharged mud slurries descended as vertical buoyant jets through the water column. After impinging the bottom, they formed a short-lived momentum-driven axisymmetric horizontal flow that transformed into an axisymmetric gravity flow soon after. The analysis of the radial spreading of those fluid mud gravity flows showed that their flow dynamics were governed by a balance between the driving buoyancy force and the resisting inertia force. A simple mathematical model (compositional box model) that does not consider the presence of suspended sediment was used to predict the experimental observations. The predictions of the box model solution were observed to be notably in good agreement with experimental observations, despite the box model exhibiting several simplifying assumptions. It is concluded that the radial propagation of fluid mud gravity flows in the inertia-buoyancy propagation phase can be modeled by a compositional box model solution. This study is motivated by the need for deterministic predictive modeling capabilities for coastal dredging operations.

Keywords: gravity flows, pipeline dredge disposal, box model, fluid mud, cohesive sediment transport

1. INTRODUCTION

Each year large volumes of sediments are dredged from rivers, waterways, ports and harbors around the world primarily to maintain and enlarge their navigability. It is estimated that an average of 230 million cubic-meters of sedimentary materials are dredged by the U.S. Army Corps of Engineers in the United States annually (Hales, 1996). Among the different dredging methods employed in removing those sedimentary materials, the hydraulic pipeline dredging method is one of the most common and economical methods for maintenance dredging of rivers, estuaries or channels (Barnard, 1978). In this method, the hydraulically dredged cohesive sediments are generally pumped as slurries (i.e. mixture of cohesive sediments and water, often called fluid mud) and transported through a suitable pipeline to dispose into a designated open water disposal area (Thevenot et al., 1992). As the slurries are discharged from the discharge port (i.e. end of the pipeline) into the open water, they may flow away from the discharge point in the form of a sediment gravity flow on the sea floor due to the density difference of the slurry and the ambient water (Nichols et al., 1978). In this study, the propagation dynamics of such subaqueous sediment gravity flows of dredged slurries is studied in a laboratory experimental setup.

In open water pipeline dredge disposals, the discharged dredged fluid mud slurries start to descend in the water column by forming a buoyant jet. The buoyant slurry jet is formed due to the high initial momentum of the discharged slurry as well as the density difference between the slurry and the ambient seawater (Hall et al., 2010). Once the buoyant slurry jet impinges on the sea bottom, it may radially flow away from the impingement point (Teeter, 2000; 2002). The radial spreading from the impingement point may initially occur as a momentum-dominated wall jet which then transitions into a buoyancy-dominated radial gravity flows (Chen, 1980; Papakonstantis and Christodoulou, 2010). The momentum-dominated radial wall jet is typically either short-lived or absent (see Papakonstantis and Christodoulou, 2010; Kotsovinos, 2000). Therefore, the subsequent phase of gravity/buoyancy driven fluid mud flow plays a major role in governing the spreading characteristics of pipeline dredge disposals, and this study focuses on this gravity driven flow phase. It is estimated that 99% of the disposed sediments in an open water pipeline disposal operations are transported in the form of gravity flows (Nichols et al., 1978; Teeter, 2001). The subaqueous fluid mud gravity flows are highly dispersive in nature and may propagate several kilometers away from the source depending upon a number of factors, such as the density of the slurry, bottom slope, ambient flow field, and discharge flow rate of the slurry. Hence, there are a number of environmental concerns associated with the radial spreading of fluid mud gravity flows (Teeter, 2001). For example, as the gravity flow spreads, it may overrun everything in its path, killing benthos such as clams and oysters (Nichols et al., 1978). If there is a high bed shear stress, entrainment of the gravity flows by the ambient water can generate a turbid plume of suspended sediment in the water column (Teeter, 2001). This turbid plume may pollute the water quality and block sunlight, harming underwater flora and fauna. Therefore, it is of great environmental importance to investigate the propagation of such sediment gravity flows.

There have been very limited analytical, laboratory or field investigations that thoroughly investigate the behavior of radial fluid mud gravity flows such as those generated in open water pipeline disposal operations. Laboratory and field studies had been carried out by Neal et al. (1978), Nicholes et al. (1978), and Thevenot et al. (1992) on the short and long term fate of discharged slurry in open water pipeline disposal operation. Those studies mostly focused on the estimation of turbidity generation by fluid mud dispersion in open water pipeline disposal operations. Recently, Teeter (2002) conducted field experiments to evaluate their proposed model for predicting dispersion in open water pipeline disposal operation in Teeter (2001). However, their experimental data did not provide information on the time-dependent spreading of radial gravity flows, which is the focus of this study. Van Kessel and Kranenburg (1996) and Chowdhury and Testik (2011) in investigated the fluid mud gravity currents extensively. However, their experiments were conducted in two-dimensional setups, incorporating a simplified representation for the 3D nature of radially spreading gravity flows generated in open water pipeline disposal operations.

In the initial propagation stage (henceforth, inertia-buoyancy stage), the driving buoyancy force of the gravity flows is balanced by the inertia force and viscous force is negligible. As the gravity flows propagates, it starts experiencing an increasing viscous force, and after some time, depending on the rheological properties of the slurries, the viscous force may become comparable to the inertia force. After this point, propagation dynamics is governed by the viscous and buoyancy force balance (henceforth, viscous-buoyancy stage). The experiments conducted in this study were found to be governed by inertia-buoyancy balance. The viscous forces are expected to govern the propagation dynamics after sufficient propagation distances, which we were not able to attain due to the physical limitations of our laboratory setup. There are various mathematical modeling approaches characterized by different levels of complexities to approximate the spreading characteristics of axisymmetric radial gravity current governed by inertia-buoyancy balance. Some commonly used approaches are: force-balance models based on dimensional arguments (e.g. Chen, 1980), box models based on simplifying assumptions on the current geometry (Huppert and Simpson, 1980; Dade and Huppert, 1995), and shallow water models based on approximate solutions of Navier-Stokes equations (e.g. Bonnecaze et al., 1995). In this study, we have chosen the widely used box model approach due to its simplicity to predict the spreading characteristics of our experimental observations of fluid mud gravity flows.

Theoretical background for the buoyant jets and the axisymmetric gravity flows formed by the discharged mud slurries are given in Section 2. The experimental set-up and methodology are described in Section 3. Results of this study are presented in Section 4, and the conclusions are given in Section 5.

2. THEORETICAL BACKGROUND

In this study, the problem under consideration is the time dependent spreading of subaqueous sediment gravity flows generated by the impinging buoyant jet of mud slurries. The buoyant jet of mud slurries generated from a round discharge port has jet like characteristics depending on its discharge volume flux $Q_{0,}$ discharge momentum fluxes M_0 and plume like characteristics depending on its discharge buoyancy flux, B_0 (Fischer, et al., 1981). These fluxes are defined for the pipeline discharge of the slurry as follows.

$$Q_0 = \frac{1}{4}\pi d_0^2 u_0; \quad M_0 = \frac{1}{4}\pi d_0^2 u_0^2; \quad B_0 = g_0' Q_0 \tag{1}$$

Here, $g_0' = \frac{|g(\rho_a - \rho_m)|}{\rho_a}$ is the buoyancy gradient at the source where g is the acceleration due to gravity, u_0 is the discharge velocity of the slurry, ρ_m and ρ_a are the densities of the discharge mud slurry and the ambient water respectively. From dimensional analysis, an important characteristics length scale describe the relative importance of the buoyancy and momentum flux, l_M, can be defined as:

$$l_M = M_0^{3/4} B_0^{-1/2}$$

The dimensionless distance of the bottom from the discharge port, h/l_M (here, h is the distance between the discharge port and the bottom, see Fig. 1) of the buoyant slurry jet can be used to assess whether the flow of the slurry is buoyancy or momentum driven at the impingement point at the bottom (Fischer et al., 1979). According to Papanicolaou and List (1988) a vertical buoyant jet behaves as a pure jet for $h/l_M < 1$ and as a pure plume for $h/l_M > 5$. For $1 < h/l_M < 5$, it is dynamically intermediate between a jet and a plume.

In box modeling approach for gravity flows, the gravity flow is considered to evolve as axisymmetric cylinder that has uniform properties at any instant in time. It incorporates expressions for the conservation of volume and a Froude number condition at the current front (Dade and Huppert, 1995). The box model solution for the spreading of compositional axisymmetric gravity currents can be expressed as(Huppert and Simpson, 1980; Dade and Huppert, 1995; Ungarish, 2009):

$$r_n(t) = \left(\frac{4Fr}{3}\right)^{\frac{1}{2}} (2g'q)^{\frac{1}{4}} t^{3/4}. \tag{2}$$

Here, r_n is the radial front position of the current head from the volume source as a function of time, t, q is the volume flow rate per radian at the source of gravity flows, Fr is the Froude number defined as $Fr = u_n / \sqrt{g' h_c}$ where u_n and h_c are the velocity of

the front and height of the gravity current and g' $(= g(\rho_c - \rho_a)/\rho_a)$ is the reduced gravity with ρ_c and ρ_a being the density of the spreading fluid and the ambient fluid, respectively.

In order to calculate the predictions of mathematical models for radial gravity flows, typically the local parameters at the impingement point (M, Q, g') are used rather than the discharge parameters (ρ_c, Q_0, M_0, g') (see Papanicolaou and List, 1988). This is because the source of the radial spreading of the fluid mud gravity flows is considered to be at the impingement point. The local parameters are estimated in terms of discharge parameters using well-established integral models or analytical solutions of buoyant jets (e.g. Wang and Law, 2002; Jirka, 2004; Papanicolaou and List, 1988).To employ those models, it is necessary to determine whether the buoyant jet behaves as a jet or a plume at the impingement point since the expression for jets and plumes differ in those models. In our calculations presented in Section 4, the discharge parameters are employed due to simplicity considerations. It is important to note that Eq. (1) represents the box model solution for axisymmetric compositional gravity flows and hence, settling of the particles is not included. However, Chowdhury and Testik (2011) showed that cohesive particle-driven gravity flows, specifically fluid mud, behaves as a compositional gravity flow in the inertia-buoyancy stage of propagation. As will be shown in Section 4, it is also adequate to model the gravity driven axisymmetric slurry flow using a compositional box model solution in the inertia-buoyancy stage

3. EXPERIMENTAL SETUP AND METHODOLOGY

The experiments were conducted by discharging mud slurries with varying concentrations in an experimental pool (3.6 m - length, 3.6 m - width, 1 m – height), three sides of which are made of Plexiglas for visualization purposes. The bottom floor of the pool was marked by reference concentric circles of in 20 cm increment from its center. A schematic of the experimental setup is shown in Fig. 1. The experimental setup also includes a mixing tank placed beside the pool to form homogeneous fluid mud slurries. An overhead tank is placed approximately, H_o=3.2 m above from the bottom of the pool that provides a constant head of fluid mud. Homogeneous fluid mud slurries were prepared by vigorously mixing cohesive Kaolinite clay particles with tap water in the mixing tank. The mean particle size and the average density of the clay particles are 0.7 μm and 2620 kg m^{-3}, respectively. Fluid mud slurry was first pumped up from the mixing tank to the overhead tank; the fluid mud overflow is then returned to the mixing tank via a side pipe attached to the overhead tank which ensures a constant overhead tank of fluid mud slurries (see Fig. 1).

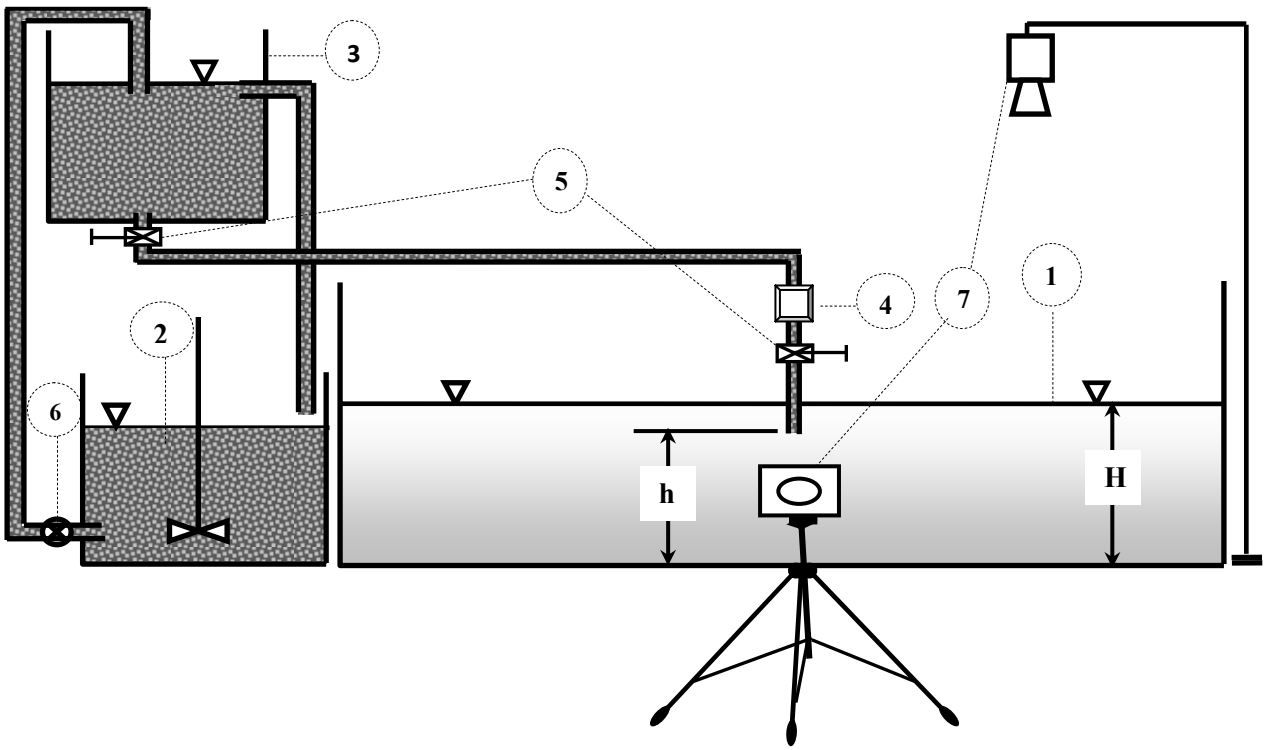


Fig. 1. Schematic of the experimental set-up: 1 - pool with tap water, 2 - mixing tank with slurry, 3 –overhead tank with constant head of slurry, 4 - electromagnetic flowmeter, 5 - adjustable valves, 6 – pump, and 7 - video cameras.

Before each experiment, the pool was filled with tap water to a depth of, H=60 cm. The delivery of the slurry was then introduced from the overhead tank at the center of the pool through a 2.54 cm diameter discharge pipe. The discharged pipe was aligned perpendicular to the center of the bottom floor and positioned 20 cm below the free surface of the water in the pool. To control and measure the discharge flow rate, two valves and an electromagnetic flowmeter were attached to the discharge pipeline. The discharge flow rate, water depth and the position of the discharge pipe were chosen from an appropriate scaling analysis of typical pipeline disposal field conditions. Throughout each experiment, the discharge volume flow rate, Q_0 is acquired at 1 Hz using the electromagnetic flowmeter connected to a computer. Before each experiment, the density of the prepared fluid mud mixture was measured by an Anton Paar DMA-35 densitometer with an accuracy of 0.001 g cm^{-3}. It is important to note that fluid mud slurries exhibits profound non-Newtonian behavior, the rheological behavior of which can be approximated as Ostwald power-law model (Chowdhury and Testik, 2010). Hence, this non-Newtonian viscous rheology of the slurry influences their spreading in viscous-buoyancy propagation stage. However, the experiments conducted in this study were found to be governed only by inertia-buoyancy balance. The viscous forces are expected to govern the propagation dynamics after sufficient propagation distances, which we were not able to attain due to the physical limitations of our laboratory setup. Therefore, non-Newtonian

rheological behavior of fluid mud will not be discussed further in the present study. Our two-dimensional investigation (Chowdhury and Testik, 2011) on fluid mud gravity current discusses this behavior in detail.

Each experiment was recorded by two Sony high definition camcorders: one from the side and the other from the top. The top camera was placed high enough to reduce any parallax error. The recorded video signals were then fed into a computer and digitized using commercial software to obtain 30 individual images per second of recording. A systematic approach was used to determine radial propagation distance measurements of current fronts as a function of time from the digitized images. First, optical calibration factors (total of 8 calibration factors) between the concentric reference circles on the floor were calculated for using them in converting geometric characteristics of a current from pixels to real world units. The reason for calculating more than one calibration factor is simply to minimize any optical distortion errors that are associated with such large field of view (≈ 160 cm for top camera). The experimental radial front positions, r_n were then obtained by summing the distance of the current front from the closest concentric reference circle upstream of the front and the absolute position of that reference line. The distance of the front from the reference circle was calculated by multiplying the total number of pixels between the front and the reference circle, and the respective calibration factor for that position.

4. RESULTS AND DISCUSSIONS

Three experiments with different initial concentrations of fluid mud slurries were performed. The experimental conditions are tabulated in Table 1. In this table, initial values of slurry volume concentration (C_v) [$C_v = V_s/(V_s + V_w)$, where V_s and V_w are the volume of sediment particles and water in the prepared slurry, respectively], density (ρ_m), initial volume flux (Q_0), momentum flux (M_0), buoyancy flux (B_0) of the discharged slurry and the dimensionless distance (h/l_M) are given. As can be seen from the tabulated value of h/l_M, the vertical buoyant jets in the three experiments were dynamically intermediate between jet- and plume-like behaviors at the impingement point (see Section 2).

Fig. 2 presents two photographs of the subaqueous axisymmetric sediment gravity flows propagating over a horizontal bottom. As is evident, the fluid mud gravity flow propagates by forming a distinct dividing line between the propagating gravity flows and ambient fresh water. The shape of the radial gravity flows is axisymmetric which confirmed earlier observation of Papakonstantis and Christodoulou (2010) in similar experiments for compositional gravity flows (i.e. gravity flows of saline solution). In Fig. 3, experimentally measured radial front positions, r_n, of axisymmetric sediment gravity flows for the experiments listed in Table 1 as a function of propagation time, t, are presented. As is evident, the initial front propagation velocities of gravity flows with higher initial concentrations are larger due to the larger driving gravitational/buoyancy force. However, all propagation curves have a similar trend.

Table 1. Experimental conditions for subaqueous fluid mud gravity flows. All the values except z/l_M is at the discharge port.

Exp. # [a]	C_v (%) [b]	ρ_m (g/cm^3) [c]	Q_0 (cm^3/s) [d]	M_0 (cm^4/s^2) [e]	B_0 (cm^4/s^3) [f]	z/l_M
1	4.6	1.075	550	59729	40736	2.11
2	9.7	1.1576	600	71082	92763	2.79
3	13.2	1.215	770	117069	162404	2.54

[a] Exp. # - Experiment number
[b] C_v - Volume concentration of the fluid mud slurry
[c] ρ_m - Density of the fluid mud slurry
[e] Q_0 – Volume flux of the slurry at the discharge port
[e] M_0 – Momentum flux of the slurry at the discharge port
[f] B_0 – Buoyancy flux of the slurry at the discharge port
[g] z/l_M – Dimensionless distance of the bottom from the discharge port.



Fig. 2. Photographs showing the propagation of a typical axisymmetric subaqueous gravity flows from side (left picture) and from top (right picture). Experimental conditions: Exp. #1, t = 11.75 s, r_n = 77 cm.

In order to determine the propagation dynamics of gravity flows presented in Fig. 3a, scaled radial front positions of the experimental gravity flows ($R = r_n/h$) as a function of scaled time ($T = \frac{t}{\sqrt{h/g'_a}}$) are plotted as a log-log plot in Fig. 3b. Note that

similar form of scaling was used in Rottman and Simpson (1983) and Chowdhury and Testik (2011) for two-dimensional gravity currents.

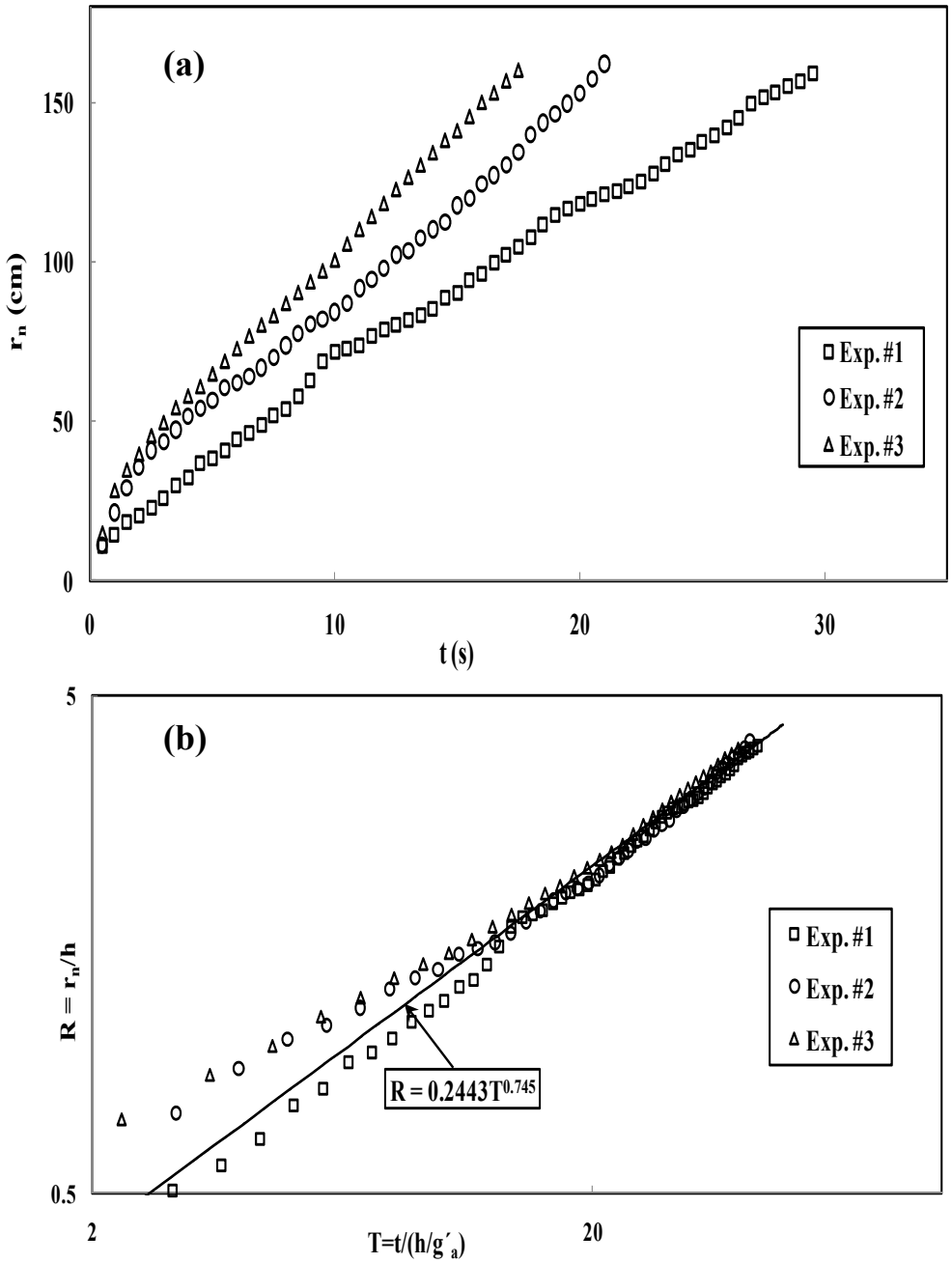


Fig. 3. Radial front position of the subaqueous axisymmetric fluid mud gravity flows as a function of elapsed propagation time. (a) Linear plot of radial front position, r_n, versus time, t, (b) Log-log plot of dimensionless radial front position, R, versus dimensionless time, T. Symbols represent the data from the experiments tabulated in Table 1 and are defined in the legend.

As is seen in Fig. 3b, the log-log plot of the curves for the three experiments collapse on a best-fit line of slope 0.745 which agrees well with the inertia-buoyancy stage represented by Eq. (1). Note that a log-log slope of 0.75 is predicted by Eq. (1). However, the initial portions of the curves deviated from the line. This is because the deviated points correspond to the momentum-dominated radial wall jet phase as described in Section 1. It is evident from Fig. 3 that the fluid mud gravity flows are governed by the inertia-buoyancy balance for most of their propagation before hitting the side walls of the pool for the experimental conditions studied.

As mentioned in Section 2, the local parameters (M, Q, g') at the impingement point are usually used to calculate the prediction of mathematical models in similar experiments to the present study. However, in this study, the initial conditions at the source at the source are used in estimations since they are the measured values and are easier to obtain. In addition, since the dimensionless distance, h/l_M, is low, the buoyant jet would not experience much of a change of the source parameters until the impingement point at the bed. In Fig. 4, comparisons of the current radial front position observations and the corresponding box model predictions are presented. Note that we used Fr =1.19 in calculating the radial front positions using Eq. (2) suggested by of Huppert and Simpson (1980) when $\frac{h_c}{H} \le \frac{1}{13.3}$. We have estimated the ratio h_c/H for the three experiments from the digitized image of the recorded video from the side which is approximately 1/10.

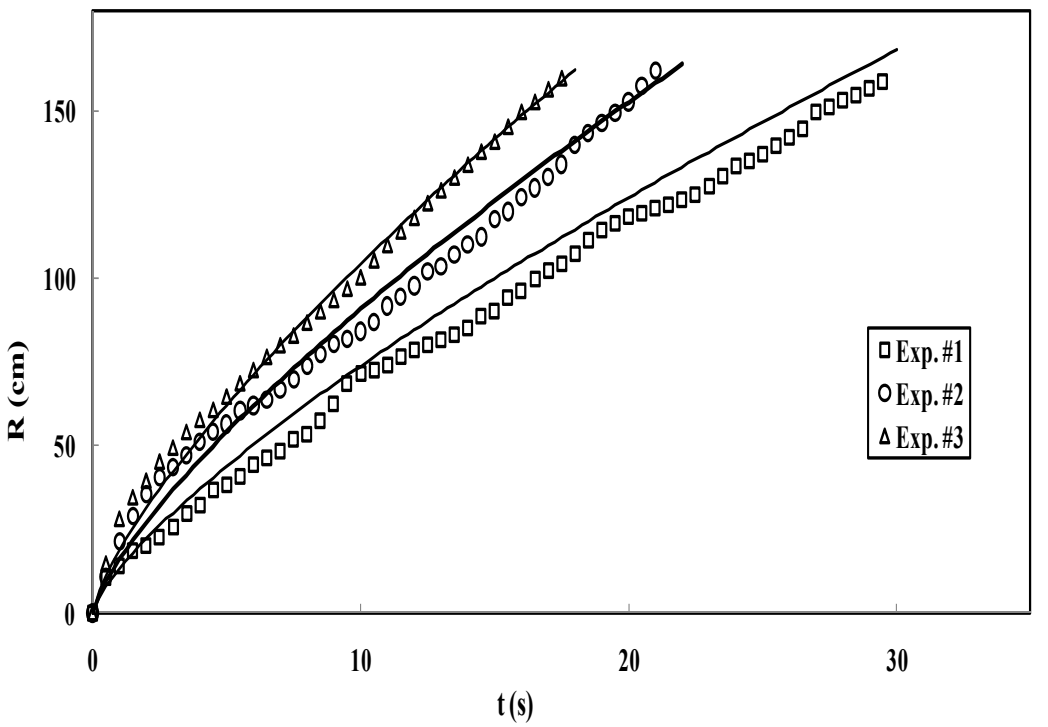


Fig. 4. Comparison of the radial front position predictions by the compositional box model solutions (solid lines, Eq. (2)) with the experimental data. Symbols represent the data from the experiments tabulated in Table 1 and are defined in the legend.

Huppert and Simpson (1980) determined this Froude number condition for two-dimensional gravity current. However, they also used the same Froude number for axisymmetric gravity current considering the head of axisymmetric gravity current is locally two-dimensional. Comparisons presented in Fig. 4 show that predictions of the box model solution are in good agreement with the experimental observations. However, predictions underestimate the initial portions of the experimental propagations since these initial portions represent the momentum-dominated radial buoyant jets. For the remainder portions of the propagation curves where the flow is buoyancy-dominated, the predictions systematically overestimate the observations which may be caused by the simplifying assumptions embedded in the box model solution. In the compositional box model approach, entrainment of ambient fluid in the current and settling of cohesive particles, both of which may slow down the current front propagation, are not considered. The use of discharge condition at the source instead of local conditions and the Froude number condition by Huppert and Simpson (1980) for two-dimensional gravity current may also affect the accuracy of the predictions. However, the coefficient of correlation, R^2-values between experimental data and model predictions are over 0.9 for all three experiments. Hence, compositional box model solution can be employed to predict the spreading of subaqueous axisymmetric fluid gravity flows.

5. CONCLUSIONS

In this study, the subaqueous sediment gravity flows generated in open water pipeline dredge disposal operations were investigated experimentally and theoretically. To elucidate the propagation dynamics of subaqueous sediment gravity flows, laboratory experiments were conducted by discharging fluid mud slurries from a submerged pipe in a large pool. The discharged mud slurries descended as vertical buoyant jets through the water column. After impinging the bottom, they formed short-lived momentum-driven axisymmetric horizontal flows which then transformed into axisymmetric sediment gravity flows soon after. Then flow dynamics of the radial axisymmetric fluid mud gravity flows were governed by the inertia-buoyancy balance in our limited experimental propagation distances. A compositional box model solution was used to predict the experimental current propagation distance observations. The predictions of the box model solution are observed to be notably in good agreement with experimental observations, despite the box model exhibiting several simplifying assumptions. It is concluded that the radial axisymmetric propagation of sediment gravity flows can be modeled by compositional box model solution.

ACKNOWLEDGMENTS

This research was supported by the funds provided by the USACE Grant W912HZ-09-C-0068 to the second author. The first author is a graduate student under the guidance of the second author.

REFERENCES

Barnard, W., (1978). Prediction and control of dredged material dispersion around dredging and open water pipeline disposal operations: Dredged Material Research Program Synthesis Report. *Technical Report DS-78-13, US Army Engineer Waterways Experiment Station,* Vicksburg, MS.

Bonnecaze, R., Hallworth, M., Huppert, H., and Lister, J. (1995). Axisymmetric particle-driven gravity currents. *Journal of Fluid Mechanics , 294*, 93-121.

Chen, J., (1980). Studies on gravitational spreading currents. *PhD thesis, California Institute of Technology*, Pasadena, California.

Chowdhury, M. R. and Testik, F. Y., (2011). Laboratory testing of mathematical models for high-concentration fluid mud turbidity currents. *Ocean Engineerig, 38*, 256-270.

Dade, W., and Huppert, H., (1995). Runout and fine-sediment deposit of axisymmetric turbidity currents. *Journal of Geophysical Research, 100*, 18597-18609.

Fischer, H., List, E., Koh, R., Imgerger, J., and Brooks, N., (1981). *Mixing in inland and coastal waters*. Academic Press, Orlando, Florida, p. 489.

Hales, L., (1996). Analysis of dredged material disposed in open water: summary report for technical area 1. *Technical Report DRP-96-4, US Army Engineer Waterways Experiment Station, Vicksburg, MS*, 115.

Hall, N., Elenany, M., Zhu, D., and Rajaratnam, N., (2010). Experimental Study of Sand and Slurry Jets in Water. *Journal of Hydraulic Engineering*, *136*(10), 727-738.

Huppert, H. E. and Simpson, J. E., (1980). The slumping of gravity currents. *Journal of Fluid Mechanics, 99*, 785-799.

Jirka, G., (2004). Integral Model for Turbulent Buoyant Jets in Unbounded Stratified Flows . Part I : Single Round Jet. *Environmental Fluid Mechanics*, 1-56.

Kotsovinos, N., (2000). Axisymmetric submerged intrusion in stratified fluid. *Journal of Hydraulic Engineering*, *126*(6), 446-456.

Neal, R., Henry, G. and Greene, S., (1978). Evaluation of the submerged discharge of dredged material slurry during pipeline dredge operations. *TR D-78-44, US Army Engineers Waterways Experiment Station*, Vicksburg, Mississippi, 176 p.

Nichols, M., and Thompson, G., (1978). A field study of fluid mud dredged material: its physical nature and dispersal. *Technical Report D-78-40, US Army Engineers Waterways Experiment Station*, Vicksburg, Mississippi, p 91.

Papakonstantis, I., and Christodoulou, G., (2010). Spreading of round dense jets impinging on a horizontal bottom. *Journal of Hydro-environment Research*, *4*, 289-300.

Papanicolaou, P., and List, E.,(1988). Investigations of round vertical turbulent buoyant jets. *Journal of Fluid Mechanics*, *195*, 341-391.

Rottman, J., and Simpson, J., (1983). Gravity currents produced by instantaneous releases of a heavy fluid in a rectangular channel. *Journal of Fluid Mechanics , 135*, 95-110.

Teeter, A., (2000). Underflow spreading from an open-water pipeline disposal. *Technical Note TN-DOER-N7, US Army Engineer Waterways Experiment Station, Vicksburg, MS*.

Teeter, A., (2001). Simulating underflow spreading from a shallow-water pipeline disposal. *Technical Note TN-DOER-N11, US Army Engineer Waterways Experiment Station, Vicksburg, MS*.

Teeter, A., (2002). Sediment dispersion near dredge pipeline discharge in Laguna Madre, Texas. *Technical Note DOER-N-16, US Army Engineer Waterways Experiment Station, Vicksburg, MS* .

Thevenot, M., Prickett, T., and Kraus, N., (1992). Tyler's beach virginia, dredged material plume monitoring project, 27 September to 4 October 1991. *Technical Report DRP-92-7, US Army Engineers Waterways Experiment Station*, Vicksburg, Mississippi.

Ungarish, M., (2009). *An introduction to gravity currents and intrustions*. Chapman and Hall/CRC Press, Boca Raton, Florida,. p 489.

Wang, H., and Law, A., (2002). Second-order integral model for a round turbulent buoyant jet. *Journal of Fluid Mechanics*, *459*, 397-428.

Modeling regional sediment transport and barrier elongation at Long Island coast, United States

Le Xuan Hoan[1,2], Hans Hanson[3], Magnus Larson[3], Shigeru Kato[1] and Shin-ichi Aoki[1]

[1.] *Department of Architecture and Civil Engineering, Toyohashi University of Technology, 1-1 Tempaku-cho, Toyohashi, Aichi 441-8580, Japan.(Hoan, L.X.: Tel. +81-532-44-6860, Fax +81-532-44-6831, email lxhoan99@yahoo.com; Kato, S.: Tel. +81-532-44-6853, Fax +81-532-44-6831, email s-kato@ace.tut.ac.jp; Aoki, S.: Tel. +81-532-44-6850, Fax +81-532-44-6831, email aoki@jughead.ace.tut.ac.jp).*

[2.] *Institute of Mechanics, Vietnam Academy of Science and Technology, 264 Doi Can, Hanoi, Vietnam.*

[3.] *Water Resources Engineering, Lund University, Box 118, SE-221 00 Lund, Sweden. (Hanson, H.: Tel. +46-46-222-8987, Fax +46-46-222-44-35, email Hans.Hanson@tvrl.lth.se: Larson, M.: Tel. +46-46-222-8729, Fax +46-46-222-4435, email magnus.larson@tvrl.lth.se)*

ABSTRACT

A new numerical model of regional sediment transport and barrier elongation, supplied by sediment coming from longshore sediment transport (LST), was developed. The spit growth and barrier elongation model was based on the model proposed by Kraus (1999). The LST rate used as input for the spit growth and barrier elongation model was simulated by the one-line model of shoreline change (Hanson, 1987) combined with the inlet reservoir model (Kraus, 2000; Larson *et al.*, 2006). The model was applied to field data from the south coast of Long Island, United States. The simulation results were compared with measurements of the annual net LST rate and the barrier elongation. Overall, the model simulations were in good agreement with the measured data.

INTRODUCTION

Spits are common morphological features at tidal inlets, entrances, river mouths, and barrier islands. A primary mechanism for spit development is accretion by longshore sediment transport (LST) in the shelter of a promontory, structure, or island. A second mechanism for spit elongation is associated with the migration of a tidal inlet where one spit elongates and the other spit shortens as the inlet migrates (Aubrey and Gaines, 1982; Petersen *et al.*, 2008).

Spit growth is often categorized into restricted and unrestricted growth. Spit development can result in changes of the hydrodynamic conditions and geomorphological features at the tidal inlet, such as decreasing the cross-sectional area of the inlet and consequently causing the tidal jet to become gradually stronger. Therefore, the spit growth is, in turn, modified by the hydrodynamic forces. Under these conditions, the spit is expected to develop towards an equilibrium state, where the entire sediment feeding the spit is removed by the inlet flow. In this case, the spit elongation will be limited by the presence of the channel (Kraus, 1999). If the spit forms at an inlet with weak hydrodynamic forcing, the tidal channel may close due to the spit elongation. Thus, the spit growth will eventually be limited by the facing coast or by the opposite spit (if spit growth on both sides of the inlet prevails). In this study, spit elongation limited by the presence of an inlet channel or by an obstacle is classified as a restricted spit growth. A spit may also form in the shelter of headlands,

barrier islands, or structures, where the spit growth is oriented towards an open area and growing without any restriction during the period under consideration. In such cases, spit elongation is classified as an unrestricted spit growth.

Kraus (1999) developed a mathematical model of spit growth due to LST. In the work of Kraus, an attempt was made to estimate the amount of sediment bypassing the spit in the two cases of restricted and unrestricted spit growth. For an unrestricted spit growth, he assumed that no sediment was lost from the spit, implying that the entire LST from the updrift side feeds the spit. For a restricted spit growth, Kraus analyzed a case of spit growth influenced by the presence of an inlet channel. The amount of sediment bypassing the spit is calculated based on a reservoir analogy using the ratio of the spit length at a particular time to that at equilibrium. Thus, an initial location of the spit must be specified to quantify the spit length. Since there is no explicit expression to locate the initial position of spit, specifying the initial conditions for the model by Kraus is one of its greatest challenges. In addition, several factors expected to modify the spit growth rate are not included in the model, such as the channel depth (adjusts the sediment transport bypassing the spit), channel scour by tidal and river flow, and dredging works to maintain channel navigation.

In this study, a mathematical model to simulate spit elongation due to sediment coming from LST for two different cases, restricted and unrestricted spit growth was developed. The governing equation is primarily based on the sand volume conservation equation suggested by Kraus (1999) under the assumption that the width of the spit is constant. The ratio of the depth of the inlet to the depth of active LST, together with an assumption of uniform cross-shore distribution of LST suggested by Hanson (1987), are employed to estimate the amount of sediment bypassing the spit. In addition, the sediment transport going out from the channel due to the channel flow, as well as other sinks or sources of sand, were included in the model. For an unrestricted spit growth, the entire LST feeds the spit, and no sediment is lost from the channel. The model was applied to simulate the spit growth at Fire Island Inlet, New York, United States, as an example of restricted spit growth.

The spit growth model requires the calculation of LST rates, which are used as input data for the model. For the Fire Island case, a shoreline change model combined with the inlet reservoir model (Hoan *et al*., 2011) was employed to represent the LST along the coastline stretch from Mountauk Point to the Fire Island Inlet, including Shinnecock and Moriches Inlets.

SPIT GROWTH MODEL

The governing equation of the model is primarily based on the sand volume conservation equation suggested by Kraus (1999). In this study, an attempt is made to estimate the amount of sand, coming from the LST, bypassing the spit, and take other sinks or sources of sand into account. The model mainly focuses on two typical types of spit growth. First, spit elongation is restricted by the presence of an inlet channel or by an obstacle, and second, the spit elongates without restriction over the time period of consideration.

Restricted spit growth. Natural bypassing of sediment at inlets occurs mainly through two processes: the LST can be bypassed through the ebb shoal complex or fall into the inlet channel and then be directly flushed out of the inlet to the downdrift beach (Bruun and Gerritsen, 1959). The hydrodynamic conditions at the inlet govern the fraction of the sediment falling into to the channel. Weak hydrodynamic forces promote deposition of sediment in the channel, which may be the case at inlets or entrances with a large cross-sectional area or with a small tidal prism. This deposition results in spit development together with shoaling of the inlet channel. Spit elongation can decrease the inlet cross-sectional area, gradually increasing the hydrodynamic forces in the channel. The stability of a spit depends on the balance between the LST rate coming into the channel and the tidal (and/or river) flow that scours the channel.

In order to derive a spit growth model, the following assumptions are made (compare Kraus, 1999),

- spit growth is sustained by the LST,
- spit elongation is in the same direction as the regional shoreline trend,
- spit width is constant,
- contours of the spit move in parallel.

Assuming that the LST (Q_{LST}) is coming to the inlet in the positive x-direction (see Fig. 1), the sand volume conservation equation that governs spit growth can be expressed as,

$$\frac{d}{dt}\left[\left(h+B_s\right)x\right]=\frac{1}{W}\left(Q_{in}-Q_c+Q_s\right) \tag{1}$$

where t= time; x = spit length; h = channel depth; B_s = average berm elevation of the

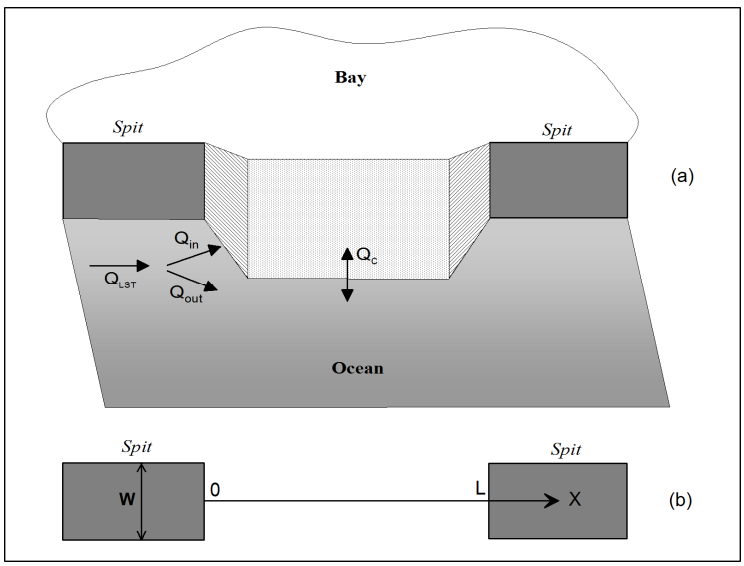


Fig. 1. Definition sketch for spit growth and sediment pathway: (a)- overview, (b)- plan view and coordinate axis.

spit; W = spit width; Q_{in} = sediment transport entering the channel; Q_c = sediment transport going out from the channel; and Q_s = sources or sinks of sand associated with the channel.

Kraus and Seabergh (2002; see also Kraus, 1999) proposed an approach to calculate Q_{in} for spit growth restricted by the presence of an inlet channel. In their approach, the portion of the LST rate that is transported away by the channel depends on how far the spit is from the center line of the inlet channel with respect to an initial condition for the spit position located far updrift of the channel where the LST is unrestricted. Thus, the definition of the initial condition presents some difficulties and contains an element of subjectivity.

In this study, another method is employed to calculate Q_{in} and Q_c in Eq. 1, where the sediment pathways are taken into account. The sediment that falls into the channel (Q_{in}), contributing to the spit growth, is estimated based on the relationship between the maximum depth of the channel and the depth of active LST. If the maximum depth of the channel (D_M) is deeper than the depth of active LST (D_{LT}) it is expected that the entire LST falls into the channel (Fig. 1). Otherwise, if the maximum depth of the channel is smaller than the depth of active LST, a fraction of the LST is directly transferred to the ebb shoal complex and then bypassed downdrift (or possibly lost into deep water). If the cross-shore distribution of the LST is assumed to be uniform (Hanson, 1987), Q_{in} is expressed through the ratio between D_M and D_{LT} according to,

$$Q_{in} = \frac{D_M}{D_{LT}} Q_{LST} \tag{2}$$

where D_{LT} is estimated from an empirical equation (Hanson, 1987) as $D_{LT} = 1.6H_b$, where H_b = breaking wave height.

The sediment transport rate (Q_c) produced by the inlet flow is given by (Kraus, 1998),

$$Q_c = \omega \frac{(\tau_m - \tau_{cr})}{\rho g} U_c w_c \tag{3}$$

where ω = an empirical coefficient (on the order of unity); τ_m = bottom shear stress; ρ = density of water; U_c = mean velocity of the inlet channel flow; w_c = channel width; and τ_{cr} = critical shear stress for sediment transport calculated from (Van Rijn, 1993), $\tau_{cr} = \theta_{cr}(\rho_s - \rho) g d_{50}$; ρ_s = density of sand; d_{50} = medium grain size; and θ_{cr} = critical Shield's parameter given by (Soulsby, 1998),

$$\theta_{cr} = \frac{0.30}{1 + 1.2D_*} + 0.055\left[1 - \exp\left(-0.020D_*\right)\right] \tag{4}$$

where $D_* = d_{50}\left[\frac{(s-1)g}{\upsilon}\right]^{1/3}$; $s = \rho_s/\rho$; and υ = viscosity coefficient.

The bottom shear stress due to the mean current is expressed as (Kraus, 1998),

$$\tau_m = \rho c_f U_c^2 \tag{5}$$

where c_f = bottom friction coefficient, estimated following Kraus (1998),

$$c_f = gm^2/\bar{h}^{1/3} \tag{6}$$

where g = acceleration due to gravity; m = the Manning coefficient; and $\bar{h}$ = average depth of the channel. Mean current velocity in the inlet channel is calculated based on the tidal prism (P), the tidal period (T), and the cross-sectional area of the inlet (A_c) according to Keulegan and Hall (1950),

$$U_c = \frac{\pi C_k P}{T A_c} \tag{7}$$

where C_k = a coefficient to account for a non-sinusoidal tide, having a value in the range of 0.81 to 1.0 (Kraus, 1998), and

$$A_c = \int_{x_t}^{L} h dx \tag{8}$$

where x_t = length of the spit at any given time, and L = maximum length of the spit from the initial spit position (Fig. 1).

Using Eqs. (3), (5), and (6), Eq. (1) may be written,

$$\frac{d}{dt}\left[(h+B_s)x\right] = \frac{1}{W}\left[Q_{in} - \omega U_c w_c \left(\frac{m^2}{\bar{h}^{1/3}}U_c^2 - \frac{\tau_{cr}}{\rho g}\right) + Q_s\right] \tag{9}$$

Spit elongation can gradually decrease the entrance cross-sectional area, increasing the mean current velocity in the inlet. Equilibrium conditions for the spit occur when $d/dt\left[(h+B_s)x\right] = 0$, that is,

$$Q_{in} = \omega U_c w_{ce}\left(\frac{m^2}{\bar{h}^{1/3}}U_c^2 - \frac{\tau_{cr}}{\rho g}\right) - Q_s \tag{10}$$

where w_{ce} = width of the inlet at equilibrium. Under conditions of strong inlet flow at equilibrium, τ_{cr} may be neglected (Kraus, 1998). If the channel depth is assumed to be constant, and neglecting sand sources or sinks, substituting (7) and (8) into (10), the equilibrium length of the spit is obtained as:

$$x_e = L - \frac{\omega^{1/2} m}{h^{5/3}}\left(\frac{\pi C_k}{T}\right)^{3/2}\frac{P^{3/2}}{Q_{in}^{1/2}} \tag{11}$$

Eq. (11) shows that the length of a spit at equilibrium is directly proportional to the LST rate supplied to the channel to a power 1/2 and inversely proportional to the

tidal prism to a power 3/2. This means that, for the same magnitude of LST, a lower inlet flow will produce a longer spit at equilibrium than that produced by a stronger flow.

Unrestricted spit growth. Unrestricted spit growth occurs if there is nothing preventing its elongation, for example, at a headland or a large entrance. In such cases, the cross-sectional area of the entrance is assumed to be large enough so that the inlet current velocity is causing negligible sediment transport, implying that $Q_c \approx 0$. Thus, Eq. (1) simplifies to:

$$\frac{d}{dt}\left[\left(h+B_s\right)x\right]=\frac{1}{W}\left(Q_{in}+Q_s\right) \tag{12}$$

If a spit grows without restriction in time, the entire LST is expected to fall into the channel and feed the spit (Kraus and Seabergh, 2002), yielding $Q_{in}=Q_{LST}$, and:

$$\frac{d}{dt}\left[\left(h+B_s\right)x\right]=\frac{1}{W}\left(Q_{LST}+Q_s\right) \tag{13}$$

SEDIMENT TRANSPORT AND SHORELINE CHANGE MODEL

A LST and shoreline change model may be employed to compute Q_{LST} and how it varies in time, which is then used as input data to the spit model. The regional sediment transport and shoreline change model is based on the one-line theory (Pelnard-Considere, 1956), employing algorithms for the numerical solution developed by Hanson (1987). Conservation of sediment volume together with a relationship for the LST rate yield the fundamental equations to solve for obtaining shoreline change. Employing a coordinate system where the *y*-axis points offshore and the *x*-axis is oriented parallel to the trend of the shoreline, the conservation of sediment volume is expressed as,

$$\frac{\partial y}{\partial t}+\frac{1}{(D_B+D_C)}\left[\frac{\partial Q_{LST}}{\partial x}+q\right]=0 \tag{14}$$

where x = longshore coordinate; y = shoreline position; t = time; D_C = depth of closure; D_B = average berm elevation; and q = source or sink of sand.

The empirically based predictive formula for the total LST rate developed by Hanson *et al*. (2006) that exhibits sensitivity towards grain size and includes other currents than wave-generated ones was used,

$$Q_{LST}=\frac{\varepsilon}{8\left(\rho_s/\rho-1\right)\left(1-p\right)w_s}H_b^2C_{gb}\cos\alpha_0\left[K_1\left(a_1\sin\alpha_0+\overline{U}_{ex}\right)-K_2a_2\right] \tag{15}$$

in which, $a_1=\frac{5}{32}\frac{\pi\chi}{c_f}\sqrt{g}A^{\frac{3}{2}}$; $a_2=\frac{\pi}{c_f\chi^2}\sqrt{gd_b}\frac{\partial H_b}{\partial x}$ and $A=2.25\left(\frac{w_s^2}{g}\right)^{\frac{1}{3}}$

where d = water depth; C_g = wave group celerity; b = subscript denoting breaking wave conditions; K_1, K_2 = empirical coefficients (treated as calibration parameters); p = porosity of sand; w_s = fall velocity; $\overline{U}_{ex}$ = external surf-zone average longshore

current velocity generated by tide or/and wind; A = shape parameter in equilibrium beach profile equation; χ = breaker index; ε = transport coefficient expressing efficiency of the waves keeping sand grains in suspension; and α_0 = angle of breaking waves to the local shoreline orientation given by,

$$\alpha_0 = \alpha_b - \arctan\left(\partial y/\partial x\right) \tag{16}$$

The effect of a regional shoreline shape may be included in Eq. (16), assuming that the local shoreline evolves with respect to the regional shoreline (Larson *et al*., 2002), yielding a new expression for α_0 according to, $\alpha_0 = \alpha_{br} + \alpha_b - \arctan\left(\partial y/\partial x\right)$, where $\alpha_{br} = \arctan\left(\partial y_r/\partial x\right)$ and y_r denotes the regional shoreline shape, which is taken to be constant over the time period studied.

INLET RESERVOIR MODEL

Larson *et al.* (2006) refined the inlet reservoir model by Kraus (2000, 2002) through the introduction of the flood shoal and associated coupling coefficients, which analytically describe the transfer of sediment between the morphological units. The inlet morphology is schematically divided into distinct morphological units including the ebb shoal, bypassing bars, attachment bars, and flood shoal. Each morphological unit is assumed to have a certain equilibrium volume for fixed hydrodynamic and sediment conditions. Sediment is assumed to be transferred through a specific unit at a rate proportional to the ratio between actual and equilibrium volumes.

Assuming that Q_{LST} is transported towards the inlet, sediment bypasses the inlet through the ebb shoal complex at a rate Q_b, to be further transported alongshore downdrift the inlet, (Larson *et al.*, 2006),

$$Q_b = \frac{V_a}{V_{aq}}\frac{V_b}{V_{bq}}\frac{V_e}{V_{eq}}\left[\delta + \beta\left(1-\delta\right)\right]Q_{LST} \tag{17}$$

where V_a, V_b and V_e = volume of attachment bar, bypassing bar, and ebb shoal, respectively, at any given time, with the corresponding equilibrium volumes V_{aq}, V_{bq} and V_{eq}, estimated based on the tidal prism; and δ and β = coupling coefficients defined as follows,

$$\delta = \frac{V_e + V_f}{V_{eq} + V_{fq}},\ \beta = \frac{1 - V_e/V_{eq}}{2 - V_e/V_{eq} - V_f/V_{fq}} \tag{18}$$

where V_f, V_{fq} = volume of flood shoal at any given time and at equilibrium, respectively. The coefficient δ specifies the portion of the incoming transport (Q_{LST}) that goes directly to the ebb shoal (1-δ ends up in the channel) and β the portion of the transport deposited in the channel that is eventually transported to the ebb shoal (1-β goes to the flood shoal) (for details, see Larson *et al*., 2006).

STUDY SITE AND MODEL SETUP

Fire Island Inlet is one of several inlets along the south Long Island (LI) coast, New York (Fig. 2). It is located on the western side of about 130-km long stretch of the Atlantic coast that extends west of Mountauk Point, which is at the eastern most tip

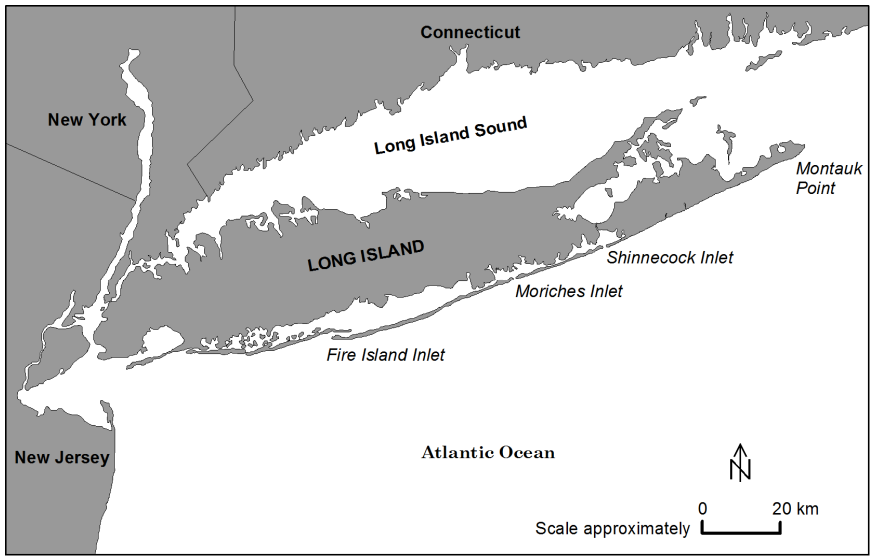


Fig. 2. Study site and locations of the inlets on the south Long Island coast, New York.

of LI. Fire Island inlet has existed continuously since the early 1700's (Smith *et al*., 1999), and from 1825 to 1940, the inlet migrated approximately 8 km to the west (USACE, 1999) (see Fig. 3). The migration of the inlet was temporarily halted by the construction of a jetty on the eastern side of the inlet in 1939 that was given a length of 1525 m (USACE, 1999). However, this jetty did not provide a stable navigation channel, although it was successful in preventing inlet movement for more than a decade (Psuty *et al*., 2005). Fire Island Inlet is the major entrance to the Great South Bay, which has an estimated tidal prism of between $52 \cdot 10^6$ and $62 \cdot 10^6$ m^3, according to different sources (Jarrett 1976).

On the south coast of Long Island there are two other tidal inlets that lie between Montauk Point and Fire Island Inlet, namely Shinnecock and Moriches Inlets. Shinnecock Inlet was formed during a hurricane on the 21st of September 1938, whereas Moriches Inlet was opened during a major storm on the 4th of March 1931 (Smith *et al*., 1999). These tidal inlets together with the Westhampton groin field between Shinnecock and Moriches Inlets have been major sinks for the LST along the south coast of Long Island east of Fire Island inlet (Rosati *et al*., 1999). Inlet formation and migration at Fire Island Inlet has been influenced by the stabilization of Moriches Inlet as well as Shinnecock Inlet (USACE, 1999). These two inlets were therefore included in the modeling of the spit growth at Fire Island Inlet by using the inlet reservoir model. Measurements of inlet cross-sectional areas at Shinnecock and Moriches Inlets were performed at several occasions between 1931 and 1998. The recorded areas were used to calculate the equilibrium volumes of the ebb shoal complexes, from which the equilibrium volumes of the individual morphological

units at the inlets could be estimated (Larson *et al*., 2002). The equilibrium volumes of the flood shoals were set to $4{\cdot}10^6$ m^3 for both inlets (Larson *et al*., 2006).

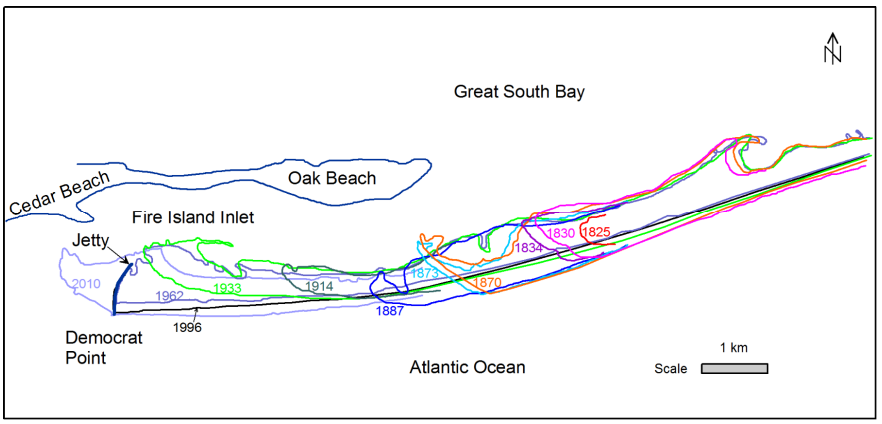


Fig. 3. Historical shoreline and spit growth at Fire Island inlet, New York (after Kana, 1995; Kraus and Seabergh, 2002; and satellite image in 2010).

The calibration parameter values in the empirical predictive formula for the LST rate were taken to be the same as in a previous modeling effort (Hoan *et al*., 2011), with $K_1 = 0.15$ and $K_2 = 0.04$. Following Larson *et al.* (2002), the depth of closure was set to 8 m and the representative median grain size to 0.3 mm. The regional shoreline shape was determined from spatial filtering of the shoreline measured in 1870 when no inlets existed along the modeled stretch using a window length of 7 km (Larson *et al*., 2002).

In order to employ Eqs. (7)-(9) to describe spit growth, the geometrical parameters of the spit must be specified. Based on available maps, Cedar Beach (see Fig. 3) to the west of Fire Island Inlet, which follows the regional shoreline trend of Fire Island, can be regarded as a stable point with respect to the Fire Island barrier elongation. Thus, the Fire Island barrier can be modeled as a spit where growth is restricted by an obstacle. The distance from the initial position to the Cedar Beach along the lengthening regional shoreline trend obtained from the Fire Island shoreline in 1825 (Kana, 1995) is about L = 10500 m. Furthermore, the average width of the Fire Island barrier is taken to be 500 m (W). Based on the measured topography reported by Smith *et al*. (1999), the depth of the entrance from the initial position to the Cedar Beach was taken as linearly decreasing from 8.5 m to 2.5 m. Tidal prism was specified to be $52{\cdot}10^6$ m^3 (Jarrett, 1976) with a semi-diurnal oscillation of about 12 hours tidal period (Psuty *et al*., 2005). The empirical coefficients, ω and C_k, were set to 1.0 and 0.9, respectively, whereas the Manning coefficient m was given a value of 0.025 (Kraus, 1998).

Hindcast wave data (a 20-years time series with waves at an interval of 3 hours from 1976 to 1995) from three WIS Stations along the coast were used as input data for the shoreline change model. The spatial step in the model was set at 100 m, and the input wave parameters were linearly interpolated alongshore based on the three

stations corresponding to this spatial interval. The time step was set at 3 hours, coinciding with the interval of the measured wave data.

The jetty construction on the east side of the Fire Island inlet began in June 1939 and was completed in April 1941 (Bonisteel *et al*., 2004). The jetty intercepted the westward LST and stopped the migration of Fire Island, but by the mid-1950's it had become impounded and sand began bypassing around the tip of the jetty (Kraus *et al*., 2003; Bonisteel *et al*., 2004). This indicates that the jetty was successful to block most of the westward LST transport during the period from 1939 to the mid-1950's. Thus, a boundary condition of no sediment supply for barrier elongation was employed in the model during this period.

Dredged sand volumes were also included in the model. In order to maintain the navigational channel at Fire Island Inlet, approximately 300,000 m^3/yr of sand was dredged from 1954 to 1994 (USACE, 1999). However, the dredging work was carried out along the length of some kilometers of the navigational channel where it is expected to include the deposited sediment coming from both sides of the channel. Roughly half of the dredged sand volume is assumed to come from the east and the other half to come from the west. Thus, in the present study, the dredged sand volume at a rate of 150,000 m^3/yr was modeled as a sink in Eq. (1).

RESULTS AND DISCUSSION

The models were run for a period between 1825 and 2010 to reproduce the barrier elongation at Fire Island Inlet. Simulation results were compared with measured data reported by Kana (1995) and Kraus and Seabergh (2002), and the data based on satellite image in 2010 (see Fig. 4). The measured position of the Fire Island barrier in 1825 was used as the initial condition in the model. Overall, the calculated barrier elongation agreed well with the measured data.

The simulated net transport rate together with derived transport data reported by Rosati *et al.* (1999) are plotted in Fig. 5. The simulated annual net longshore transport rates were in good agreement with the analyzed data, except at Montauk Point where the rate was underestimated. The data from Rosati *et al.* (1999), for Montauk Point, included several important sinks and sources not described in the model, such as offshore losses due to sea level rise (75,000 m^3/yr), beach fill placement (between 0 and 170,000 m^3/yr), and bluff erosion (between 30,000 and 200,000 m^3/yr). These sources will affect the net transport rates and cause a difference between the modeled and analyzed results at Montauk Point.

The net annual LST rate shows an increasing trend from Montauk Point to Fire Island Inlet. Since the tidal inlets act as sinks to the LST when they evolve towards their equilibrium states, the net transport rate decreases significantly across the inlets. The average annual net LST rate obtained in this study is about 108,000 m^3/yr. This value is close to the estimated rate reported by Williams *et al.* (1998) being about 110,000 m^3/yr. The average annual net LST rate at the eastern side of Fire Island Inlet obtained in this study is 220,000 m^3/yr. This value is close to the estimated net

LST rate reported by Rosati *et al.* (1999) being in the range of 160,000 to 230,000 m^3/yr. The fraction of the net LST rate falling into the channel and feeding the spit, estimated from the Eq. (2), is about 165,000 m^3/yr (75% of net LST rate). The

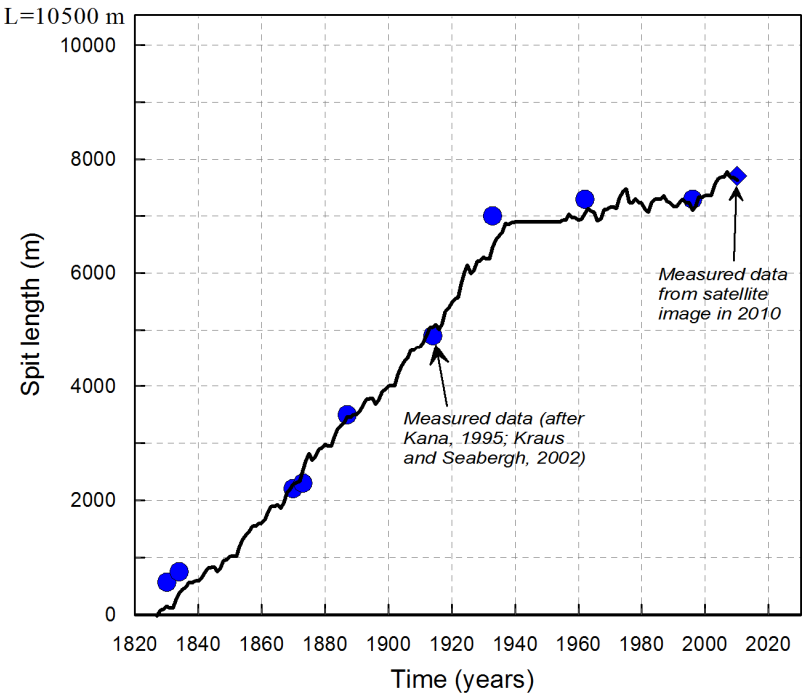


Fig. 4. Comparison between modeled and measured barrier elongation at the Fire Island inlet, New York.

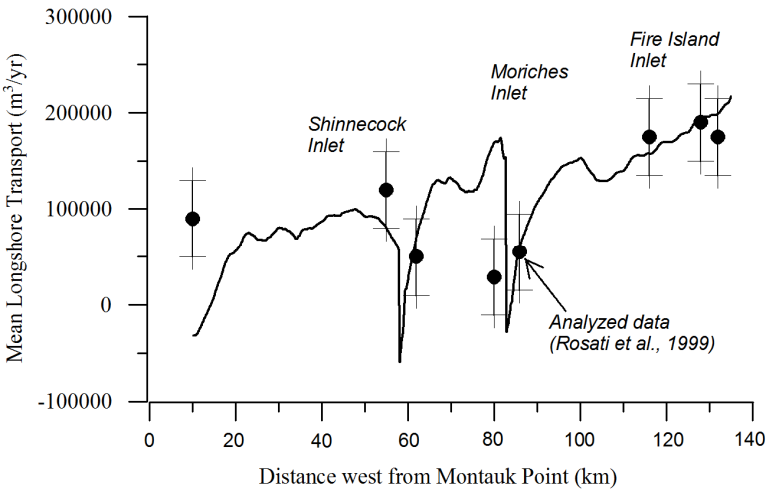


Fig. 5. Comparison between calculated annual net sediment transport rate and estimated data from measurements at Long Island coast, New York.

remaining portion of the net LST (25%) is transferred to the ebb shoal complex and/or lost into deep water.

The westward elongation of the Fire Island barrier was halted by the jetty from 1939 to the mid-1950's, after which the jetty became impounded and sand began bypassing around the tip of the jetty (Kraus *et al*., 2003; Bonisteel *et al.,* 2004). Then, according to measured shorelines at Fire Island Inlet (Kana, 1995; Kraus and Seabergh, 2002), the Fire Island barrier was almost stable until 1996. This period is in close agreement with the period of dredging to maintain channel navigation at Fire Island Inlet reported by Smith *et al.* (1999) and USACE (1999). From 1954 to 1994 a sand volume of about 300,000 m^3/yr was dredged from the channel. However, as discussed above, the dredging work was carried out along the navigational channel where the deposited sediment is expected to come from both sides of the inlet. In this study, half of the dredged sand volume is assumed to come from the westward LST and thus, a dredging sand volume of 150,000 m^3/yr was employed in the model as a sink. This amount of dredging is close to the net LST feeding the spit. This indicates that the dredging at the inlet is the main reason for the stable period experienced at present for the Fire Island barrier.

CONCLUSIONS

A mathematical spit model was introduced for simulating elongation of a restricted or unrestricted spit growth supplied by sediment coming from LST, under the assumptions that spit elongation is in the same direction as the regional shoreline trend, the spit width is constant, and contours of the spit move in parallel. The model requires estimates of the regional shoreline trend and maximum spatial length in which the spit elongates. Inputs for the model are the LST rate together with the breaking wave height at the incoming boundary of the spit. In this study, the ratio between maximum depth at the inlet and depth of active LST, estimated from the breaking wave height at a tip of the spit, is the main parameter governing the portion of the LST rate feeding the spit. The remaining portion of the LST rate is directly transferred to the ebb shoal complex and subsequently bypassed downdrift and/or lost into deep water. For an unrestricted spit growth, the required input of LST for an analytical solution may be the estimated net LST rate. For a restricted spit growth, tidal prism and/or river discharge are required to calculate sediment transport going out from the channel. In addition, other sinks or sources, such as sand removed by dredging or sand supplied by beach fills, are included in the model.

The model was successfully applied to simulate the barrier elongation at Fire Island inlet, New York. The model calculations were compared with measurements of the barrier elongation from 1825 to 2010 and the average annual net LST reported in previous studies. The model result of barrier elongation was in good agreement with the measured data. The calculated annual net LST rates reproduced reported data well, showing an increase in transport rate going west from Montauk Point. The average annual net LST at the eastern side of Fire Island inlet obtained in this study is about 220,000 m^3/yr, of which 165,000 m^3/yr (75% of the entire net LST) is estimated to feed the spit growth. The remaining portion (about 25% of entire net LST) is directly bypassed through the ebb shoal complex. The calculated results

show that the dredging is the main reason for stable period of the spit from 1954 to 1994.

Acknowledgments

This work was partly funded by the Swedish International Development Cooperation Agency (Sida/SAREC) in the framework of the Project VS/RDE/03 "The evolution and sustainable management in the coastal areas of Vietnam" (LXH and PTN), by Coastal Morphology Modeling and Management (Cascade) work unit, System-wide Water Resources Program conducted at the U.S. Army Engineer Research and Development Center (ML and HH), and by Sida/SAREC project SWE-2007-123. Financial support from Japan Society for the Promotion of Science (JSPS) (Postdoctoral Grant, ID No. P10380) and from Vietnam's National Foundation for Science and Technology Development (NAFOSTED), code: 107.03-2010.04, are gratefully acknowledged.

References

Aubrey, D.G. and Gaines, A.G. (1982). Rapid formation and degradation of barrier spits in areas with low rates of littoral drift. *Marine Geology*, 49 (3-4), 257-277.

Bonisteel, J.M.; Peters-Snyder, M. and Zarillo, G.A. (2004). Barrier island migration and morphologic evolution, Fire island Inlet, New York, *Journal of the American Shore and Beach Preservation Association,* 72(1), 21-27.

Bruun, P. and Gerritsen, F. (1959). Natural by-passing of sand at coastal inlets. *Proceedings of the American Society of Civil Engineerings* (New York), Vol. 85, No. WW4, pp. 75-107.

Hanson, H. (1987). GENESIS: A generalized shoreline change numerical model for engineering use. Lund, Sweden: Department of Water Resources Engineering, Lund University, Ph.D. thesis, 206p.

Hanson, H.; Larson, M.; Kraus, N.C. and Gravens, M.B. (2006). Shoreline response to detached breakwaters and tidal current: Comparison of numerical and physical models. *Proceeding of the 30th Coastal Engineering Conference*, World Scientific, pp. 3357-3369.

Hoan, L.X.; Hanson, H.; Larson, M. and Nam, T.P. (2011). Modeling regional sediment transport and shoreline response in the vicinity of tidal inlets on the Long Island coast, United States. *Coastal Engineering,* 58(2011), 554-561.

Jarrett, J.T. (1976). Tidal prism – inlet area relationships. U.S. Army Engineer Waterways Experiment Station, Vickburg, MS, 60p.

Kana, T.W. (1995). A mesoscale sediment budge for Long Island, New York. *Marine Geology,* 126(1), 87-110.

Keulegan, G.H. and Hall, J.V. (1950). A formula for the calculation of tidal discharge through an inlet. *U.S. Army Corps of Engineering, beach Erosion board Bulletin,* vol. 4, 15-29.

Kraus, N.C. (1998). Inlet cross-section area calculated by process-based model. *Proceeding of the 26th Coastal Engineering Conference*, ASCE, pp. 3265-3278.

Kraus, N.C. (1999). Analytical model of spit evolution at inlets. *Proceeding of Coastal Sediments '99*, ASCE, pp. 1739-1754.

Kraus, N.C. (2000). Reservoir model of ebb-tidal shoal evolution and sand bypassing. *Journal of Waterway, Port, Coastal, and Ocean Engineering,* 126(3), 305-313.

Kraus, N.C. and Seabergh, W.C. (2002). Inlet spit and Maintenance of navigation channels. Coastal and Hydraulics Engineering Technical Note ERDC/CHL CHETN-IV-44, U.S. Army Engineering Research and Development Centre, Vicksburg, MS.

Kraus, N.C.; Zarillo, G.A. and Tavolaro, J.F. (2003). Hypothetical relocation of Fire Island inlet, New York. *Proceedings of the 5th International Symposium on Coastal Engineering and Science of Coastal Sediment Processes* (Florida, USA), on CD-ROM.

Larson, M.; Kraus, N.C. and Hanson, H. (2002). Simulation of regional longshore sediment transport and coastal evolution- the Cascade model. *Proceeding of the 28th Coastal Engineering Conference*. World Scientific Press, 2002.

Larson, M.; Kraus, N.C. and Connell, K.J. (2006). Modeling sediment storage and transfer for simulating regional coastal evolution. *Proceeding of the 30th Coastal Engineering Conference* (California, USA), World Scientific, pp. 3924-3936.

Pelnard-Considere, R. (1956). Essai de theorie de l'evolution des forms de rivage en plage de sable et de galets. 4th Journees de l'Hydraulique, Les Energies de la mer, Question III, Rapport No. 1, pp. 289-298 (in French).

Petersen, D.; Deigaard, R. and Fredsoe, J. (2008). Modelling the morphology of sandy spits. *Coastal Engineering,* 55(7-8), 671-684.

Psuty, N.P.; Grace, M. and Pace, J.P. (2005). The coastal geomorphology of Fire Island, A portrait of continuity and change. Technical Report NPS/NER/NRTR-2005/021. U.S. Department of the Interior, National Park Service, Northeast Region, Boston, Massachusetts.

Rosati, J.D.; Gravens, M.B. and Smith, W.G. (1999). Regional sediment budget for Fire Island to Montauk Point, New York, USA. *Proceeding of Coastal Sediment Conference'99,* ASCE, 803-817.

Smith, W.G.; Watson, K.; Rahoy, D.; Rasmussen, C. and Headland, J.R. (1999). Historic geomorphology and dynamics of Fire Island, Moriches and Shinnecock Inlets, New York. *Proceedings of Coastal Sediment'99*, ASCE, 1597-1612.

US Army Corps of Engineers (USACE) (1999). Fire Island Inlet to Montauk Point, Long Island, New York. Main Report and Draft Environmental Impact Statement, Volume I, 1045p.

Soulsby, R. (1998). Dynamics of Marine Sands, Thomas Telford Ltd., London, U.K.

Van Rijn, L.C. (1993). Principles of sediment transport in rivers, estuaries and coastal seas. University of Utrecht, Department of Physical Geography, Aqua Publications.

Williams, G.L.; Morang, A. and Lillycrop, L. (1998). Shinnecock Inlet, New York, site investigation, Report 2, Evaluation of sand bypass options. Technical Report CHL-98-32, U.S. Army Corps of Engineers, Waterways Experiment Station, Vicksburg, MS.

Prediction of the siltation in the intake of nuclear power plant using the water depth monitoring and coupled model

Bum-shick shin[1] and Kyu-han Kim[2]

[1]Assistance Professor, Regional Innovation Center, Kwandong University, 210-701, Gangneung, Gangwon, Korea; PH +82-33-643-3436; FAX +82-33-647-3436; email:sbs114@kd.ac.kr

[2]Professor, Department of Civil Engineering, Kwandong 210-701, Gangneung, Gangwon, Korea; PH +82-33-643-3436; FAX +82-33-647-3436; email:kkhkim@ kd.ac.kr

ABSTRACT

Generally, coastal areas where there are dominant tidal currents and topographic change are maintained in equilibrium by the reciprocating motion of tidal currents. However, artificial action on the current for operating a nuclear plant operation at the intake and the outlet breaks the equilibrium of the tides and this in the end results in disturbing the equilibrium condition of bottom topography.

This research used the variation of siltation pace acquired from monitoring results to formulate coupled model in order to predict the change of water due to artificial construction in the intake in the future more precisely.

As a result of analyzing the water depth change in the intake area according to the survey data of water depth, after dredging work, siltation of 100~140cm/year occurs in the middle of the intake area but siltation of 80~300cm/year is generated at the sides.

Furthermore, we can acknowledge the fact that siltation is generated and then come to the equilibrium for short period after artificial dredging work is executed every 2 years. Therefore, we have to examine these phenomena in prediction of siltation using numerical model test.

In general, the results of sediment transport is expressed by yearly transformation rate based on linear change, but siltation is generated for short time and then come to the equilibrium after artificial dredging work is executed every 2 years in this study area. Therefore, it is necessary to carry out the model tests in same condition with field condition of dredging period (2 years), and it is presented that the numerical modeling results are similar to the field survey data.

In the siltation model test, because a dredging period of 2 years gave an important influence on topography transformation, we eliminated a reappearance error and simulated water depth transformation in intake area using time-dependant coupled model based on survey time in order to represent the topography transformation in the real coast.

INTRODUCTION

It is absolutely required to make practical applications of nuclear power plant technology for supplying energy necessary for industry and life in Korea where natural resources are insufficient. Nuclear power plants in Korea have been

established at Wolsung(4 units, 2,778.7kw), Wooljin(6 units, 5,900kw), Young-gwang(6units, 5,900kw) beginning with the operation of the Gori Nuclear Power Plant(4 units, 3,097kw) in 1978, and this nuclear power corresponds to 38.2% of total power supply. But, nuclear power plants requires seawater in order to cool down waste heat which is discharged at the time of operation, and so all of the nuclear power plants are located near coast areas. As a result of the cooling process, the warm water has been studied to investigate the influence on coastal environments and pattern change of erosion and deposition around the coast. Generally, a reciprocating motion of tidal currents has maintained equilibrium of topography change in coastal areas where tidal current is dominant, but owing to an inflow of seawater for operating the plants, the tidal equilibrium is broken and deposition condition is destroyed, thereby requiring constant dredging to maintain preservation. A siltation charge in Younggwang nuclear power plant the study area has been measured in the field four times a year since 1988 when the second plant began to operate. However, in this study, we have been examining a transformation of erosion and siltation around the intake area since 2006, when dredging work for preservation was carried out after the fifth and sixth plants were completed in 2003 by applying depth-considered coupled model using water depth monitoring data.

STUDY AREA

Study area

The Younggwang nuclear power plant is located on the western coast of Korea, which has a slow bottom slope of 1/100~1/2,000 but a very long tidal interval (spring tide interval: 563.2cm) as compared to water depth.

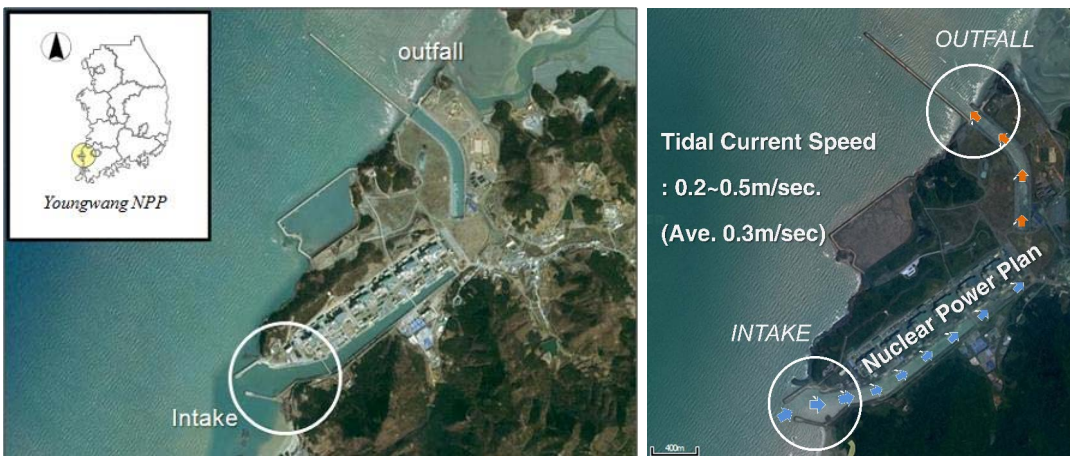


Figure 1. Study Area

The characteristic of Bottom Changes in the study area

According to existing studies, sediment of the study area is transported from offshore, and it is reported that the sediment is moved into the southern and northern parts of the coast by tidal currents, and then drawn into the intake area owing to high current velocity of the intake entrance.

Also, when the 1st and 2nd plants were in operation, sediment transported into the intake area was almost silt clay (below 0.0625mm), but according to the operation of

the 3rd and 4th plants, discharge of cooling seawater had increased, average current velocity of the inside had increased to 0.4m/s from 0.2m/s as well, and a great amount of sediment of silt clay(0.0625~0.25mm) was drawn into the inside of the intake area.

In order to consider the influences of dredging executed every 2 years, we practiced a verification of numerical model tests by analyzing field measurement data of water depth during the period of December, 2005 ~ December, 2007.

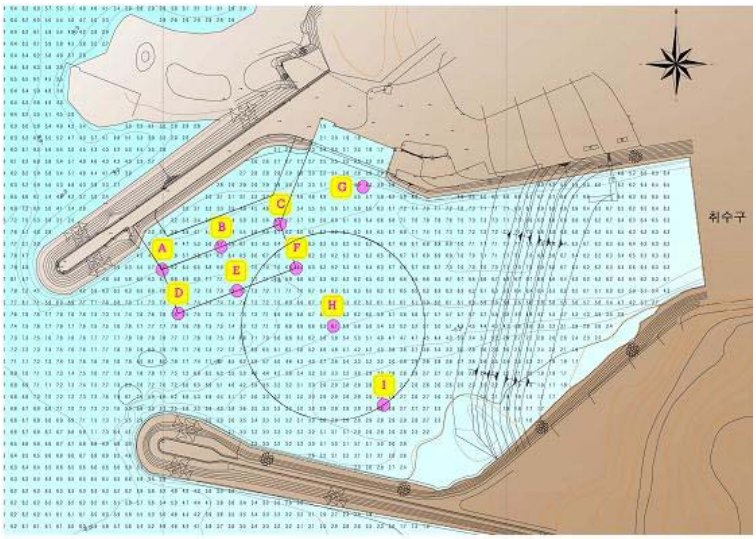


Figure 2. Comparative evaluation points

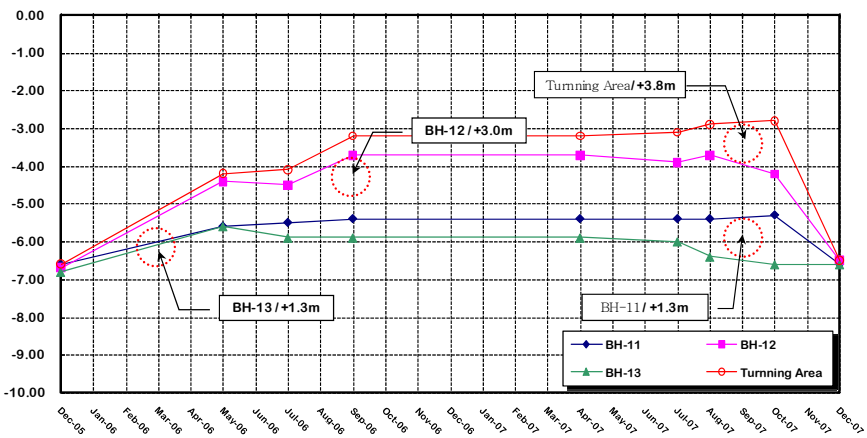


Figure.3 Analysis of topography changes

As a result of analyzing the water depth changes in the intake area through the depth survey data, siltation of 100~140cm/year occurred in the middle(H) of the intake area but siltation of 80~300cm/year was generated at the side points(B, C) after dredging . Furthermore, we can acknowledge the fact that siltation is generated and then come to an equilibrium for a short period after artificial dredging is executed every 2 years. Therefore, we have to examine these phenomena for predicting siltation using numerical model tests.

NUMERICAL SIMULATION

As a process of an establishment of a numerical model, verification of the model and testing the predictions are carried out to investigate an existing situation of the natural environment and predict the changes in the future. We applied two numerical models to predict topography transformation. One is a hydrodynamic model and the other is a siltation model, and the basic flow chart of the numerical model of this study is composed of these two models as shown in Figure.4.

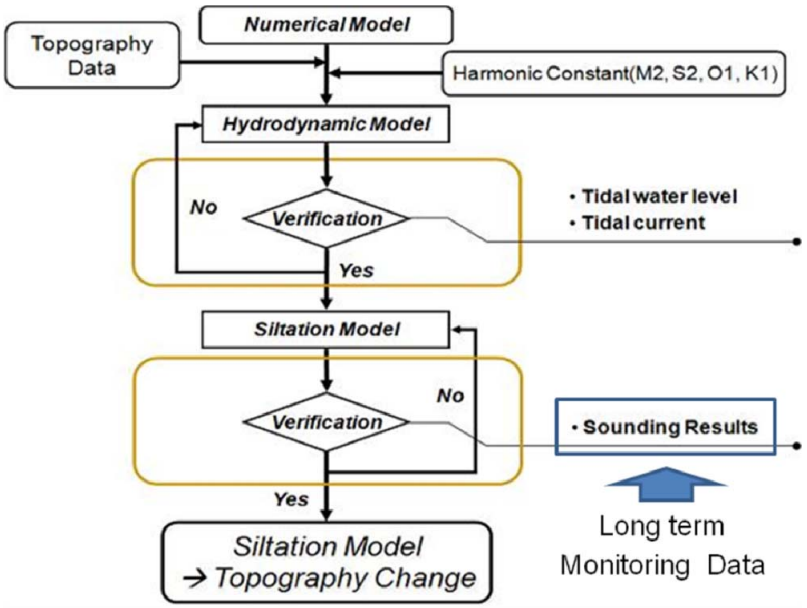


Figure 4. Flow chart of the numerical model

Hydrodynamic model

As current flow in the coast is a 3 dimensional phenomenon, a vertical distribution of currents in horizontal component or currents in vertical direction may work well in some sea areas, but a current's characteristics in the coast can be expressed similarly by means of 2 dimensional currents in general.

In this study, we applied a hydrodynamic model (K-SILT) which is able to reproduce natural environments of a wide area using a 2 dimensional model and calculate advection and diffusion around an intake area. K-SILT is a model to simulate 2-dimensional, non-stationary flows on the assumption that it is homogeneous vertically, and uses the equation of continuity and the equation of motion relating to the depth-integrated bottom and the momentum balance.

▪ Equation of continuity

$$\frac{\partial \eta}{\partial t}+\frac{\partial M}{\partial x}+\frac{\partial N}{\partial y}=0 \qquad (1)$$

▪ Equation of motion

Direction (x)

$$\frac{\partial M}{\partial t}+\frac{\partial}{\partial x}\left(\frac{M^2}{H}\right)+\frac{\partial}{\partial y}\left(\frac{MN}{H}\right)+gH\frac{\partial \eta}{\partial x}+\frac{gn^2M\sqrt{M^2+N^2}}{H^{7,3}}-\frac{\partial}{\partial x}\left(K_H\frac{\partial M}{\partial x}\right)-\frac{\partial}{\partial y}\left(K_H\frac{\partial M}{\partial y}\right)=0 \qquad (2)$$

Direction (y)

$$\frac{\partial N}{\partial t}+\frac{\partial}{\partial x}\left(\frac{M^2}{H}\right)+\frac{\partial}{\partial y}\left(\frac{N^2}{H}\right)+gH\frac{\partial \eta}{\partial y}+\frac{gn^2N\sqrt{M^2+N^2}}{H^{7,3}}-\frac{\partial}{\partial x}\left(K_H\frac{\partial M}{\partial x}\right)-\frac{\partial}{\partial y}\left(K_H\frac{\partial M}{\partial y}\right)=0 \qquad (3)$$

where, x, y, t are coordinates of space, time, η is water elevation, M, N are linear current discharges, g acceleration of gravity, $H(=h+\eta)$ is water depth, elevation below still water level, n is Manning roughness efficient, and K_H is horizontal mixing coefficient. The conditions of the hydrodynamic model test are given in Table 1.

Table 1. Summary of Numerical Simulation

ITEM	Contents
Model	·K-SILT MODEL
Grid	·3.0km × 3.0km = 9.0km²
(Size)	·dx = dy = 10m
(Number)	·90,000 (300×300)
Tide	·S.P. Range : 563.2cm
Cal. Time	·36hr (3 Tides)
Time step	·3sec

Siltation model

The siltation model estimates eroded and deposited sediment discharges by analyzing sediment advection-diffusion equation including a suspension and sedimentation term.

Silt is floated from the bottom according to the change of shear stress due to tidal currents which are generated by tidal interval, while advection and diffusion of sediment are produced again by tidal currents.

In this model, an assumption that silt is transported repeatedly in the process of suspension, advection, diffusion, and sedimentation, the fluid equation of continuity, the fluid equation of motion and advection-diffusion equation relating to concentration of suspended sediment, including a suspension and sedimentation term is applied.

Also, we can estimate topography transportation using the continuity equation of sediment which expresses the relation between suspended and deposited sediment discharges at the bottom and the change of bottom position.

A distribution of suspended sediment concentration is able to be obtained from the following equation.

$$\frac{\partial(HC)}{\partial t}+\frac{\partial(H_uC)}{\partial x}+\frac{\partial(H_vC)}{\partial y}-\frac{\partial}{\partial x}\left(H\varepsilon_x\frac{\partial C}{\partial x}\right)-\frac{\partial}{\partial y}\left(H\varepsilon_y\frac{\partial C}{\partial y}\right)=P-D \qquad (4)$$

in which C is depth-averaged suspended-sediment concentration, u, v are x, y , components of depth-averaged velocity, $H(=h+\eta)$ is water depth, $\varepsilon_x, \varepsilon_y$ is

elevation below still water level, η is water elevation, P is suspended sediment discharge per unit time and unit area, and D is deposited sediment discharge per unit time and unit area.

The explicit difference method is applied in the advection-diffusion equation, where forward difference is used for time, and upwind and center differences are used for space. The continuity equation of sediment is as follows.

$$\frac{\partial}{\partial t}(\rho_b \xi) = P - D \tag{5}$$

SIMULATION RESULTS

Results of hydrodynamic model

In this study area, seawater flows from the south and to the northeast at the time of flood tide, and it flows oppositely at the time of ebb tide. The results of the test indicates that the current velocity of ebb tide is almost the same as that of flood tide, but in the coast, current of flood tide is faster than ebb tidal current. Furthermore, maximum flood tidal current velocity is in the range of 20~50cm/sec, and even maximum ebb tidal current velocity is similar to flood tidal current velocity, right at the entrance of the intake area.

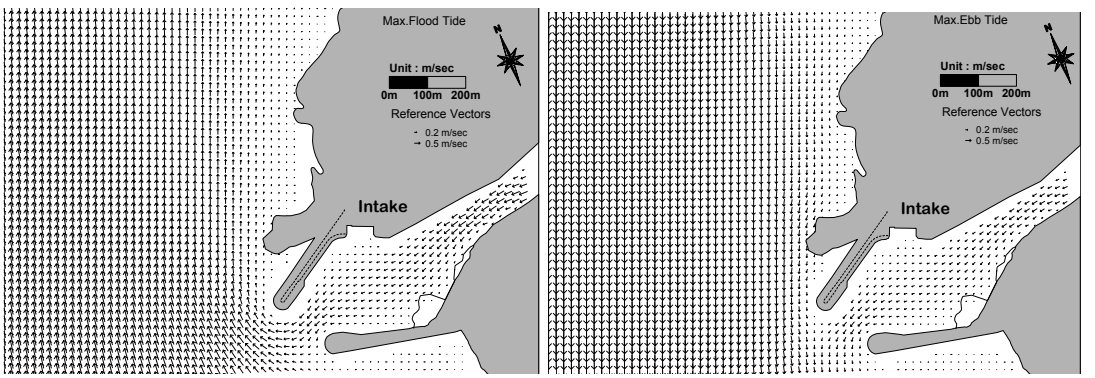


Figure 5. Results of Hydrodynamic model

Verification of bottom topography transformation

In general, the results of sediment transport is expressed by yearly transformation rate based on linear change, but siltation is generated for a short time and then comes to equilibrium after artificial dredging is executed every 2 years in this study area(Figure 6).

Therefore, it is necessary to carry out the model tests in the same conditions as the field conditions of the dredging period (2 years), and it is presented that the verification results of numerical model tests are similar to the field survey data.

Results of siltation model

Given the fact that a dredging period of 2 years gave an important influence on topography transformation, we eliminated a reappearance error and simulated water depth transformation in the intake area using a time-dependent coupled model based

on survey time in order to represent the topography transformation of the real coast in the siltation model test(Figure 7).

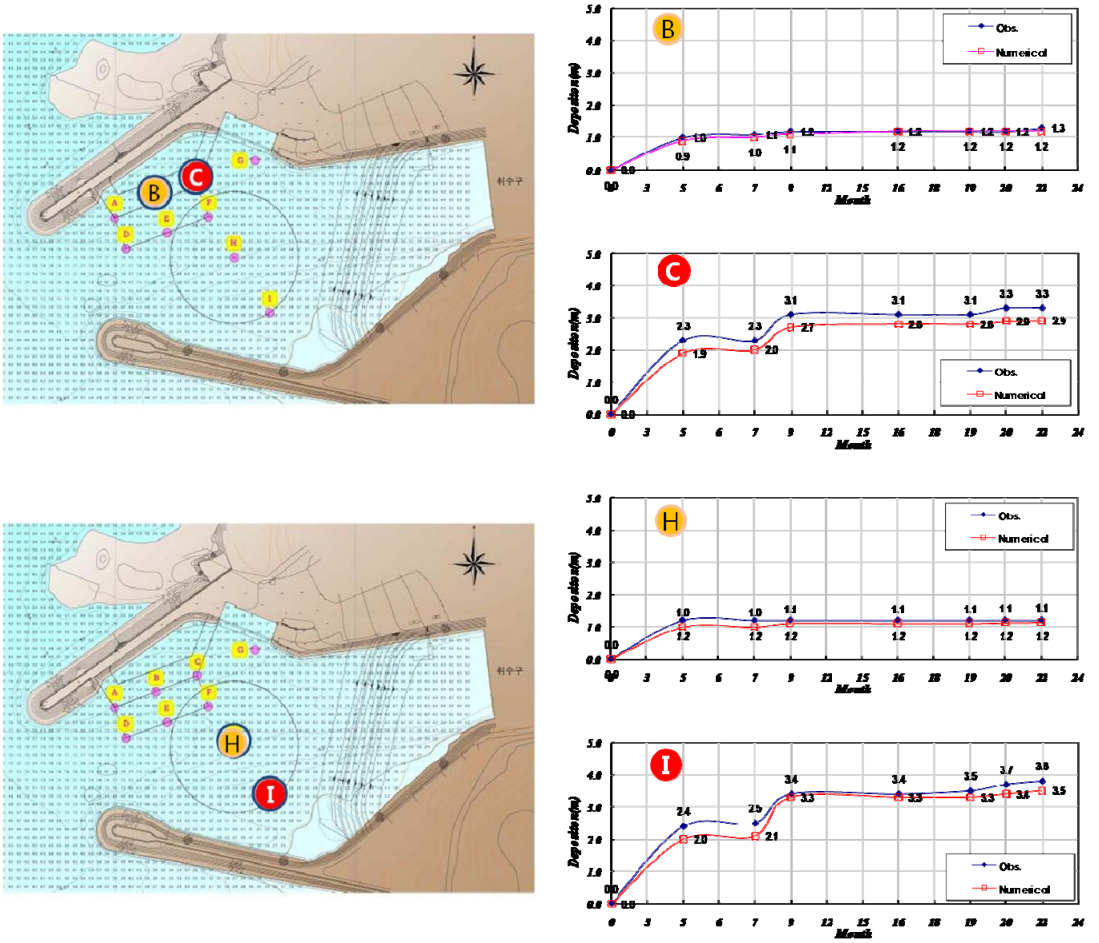


Figure 6. Result of Verification

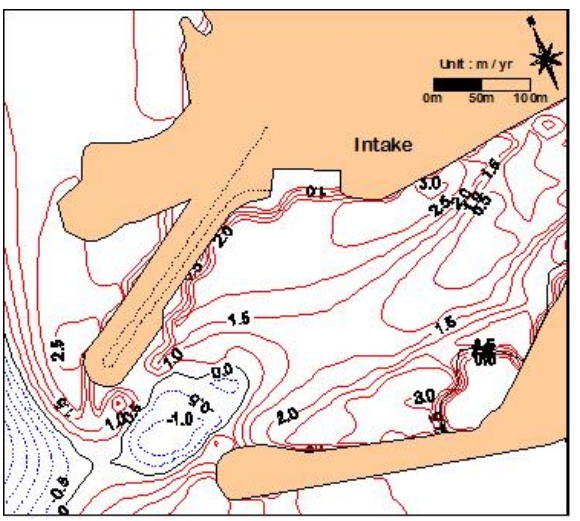


Figure 7. Results of Topography change model

CONCLUSION

As a result of the numerical model test, siltation occurred slightly, to a small degree around the southern and northern structures of the intake area, and siltation was hardly formed in the middle of the intake area. These results have a similar tendency to the field data.

Therefore, in order to predict siltation in this study area where siltation occurs continuously, it is first of all essential to thoroughly examine the selection of location by considering the siltation rate of the period corresponding to the dredging period (2years) in a field condition as well as a yearly siltation rate.

ACKNOWLEDGMENTS

This work was partly supported by the RIC program of MKE(Ministry of Knowledge Economy).

REFERENCES

Shin B. S. and Kim K. H.(2009). “Prediction of the siltation using water depth monitoring in the intake”, The 5st International Conference on Asian Pacific Coasts(APAC), 2009. 10.

Kim K. H. and Bae K. S. (1996). “Applicability Study of Numerical Model for Sedimentation in Navigation Channel, Journal of Korean Society of Coastal and Ocean Engineers”, Vol.8, No.1, pp. 1-9.

Owen M. W. and Odd N. V. M. (1972). “A Two-layer Model of Mud Transport in Thames Estuary”., Proc. of the Institution of Civil Engineering)

Partheniades, E. (1965). “Erosion and deposition of cohesive soils”, Journal of the hydraulic Div., ASCE, 91, No. HY1, 105-139.

Analysis of Morphological changes in the Gold Coast Seaway

M.Sedigh[1], R.Tomlinson[2], A. Golshani[2], Nick Cartwright[3]
[1]School of Engineering & Griffith Centre for Coastal Management, Griffith University
Gold Coast Campus, Qld 4222, AUSTRALIA, (+61)755527608, m.sedigh@griffith.edu.au
[2]Griffith Centre for Coastal Management, Griffith University
Gold Coast Campus, Qld 4222, AUSTRALIA, r.tomlinson@griffith.edu.au (+61)7 55528499, a.golshani@griffith.edu.au (+61)7 55528449
[3]Griffith School of Engineering, Griffith University, Gold Coast Campus, Qld 4222, AUSTRALIA, (+61)755529214 n.cartwright@griffith.edu.au

Abstract

Historical bathymetric data is being collated to map out the trends of morphological changes and ebb-delta growth at the Nerang River entrance which is also known as the Gold Coast Seaway after construction of entrance stabilisation works in 1985. The influences of various environmental and anthropogenic drivers which have impacted on the entrance morphology are investigated using available historical bathymetry, wave, dredging and bypassing data.

Introduction

The Gold Coast Seaway is located on the Australian East coast at a longitude of 27°56'10S and a latitude of 153°25'60E and links an intra-coastal waterway known as The Broadwater with the Pacific Ocean. The Seaway was created when a natural inlet (the Nerang River Entrance) was stabilised in 1986. In the case of Gold Coast Seaway and many other waterways that have channel infilling problems and navigation issues it is crucial to understand the dynamics of the waterways and different variables that affect its morphology.

After construction of the Seaway, although there has been a bypassing system, the growth of the ebb-tidal delta was still one of the main concerns. There have a number of studies that have examined hydrodynamics in the vicinity of the Gold Coast Seaway (eg. Mirfenderesk and Tomlinson, 2008). Moreover, a number of studies have also been carried out on the different factors that influence the morphological changes in the Seaway area and growth of delta (Chapman, 1981; D'Agata and

Tomlinson, 2004; Delft, 1970; Delft, 1976; McCauley, 1997; Munday, 1995; Patterson, 2007; Polglase, 1987; Sennes et al., 2007; Voisey, 2004; WRL and GCCM, 1998), but the dynamics of the Seaway and the development of the ebb-tidal delta are still poorly understood.

Different drivers that influence Gold Coast region morphology

Wave Climate

The Gold Coast Seaway is exposed to several wave conditions during the year. The wave climatology of the Gold Coast can be subdivided into four main categories: Ground swell (GS), wind swell or local wind seas (WS), East Coast Lows (ECL), and tropical cyclones (TC). Ground swell is the dominant offshore wave climate and is typically generated in the mid-latitudes and Southern Ocean. These waves occur year-round and are characterized by long periods and low wave heights with a south-easterly to southerly direction. Wind seas are locally generated, short period waves and wave height and direction can vary depending on the strength, duration, and direction of wind. These conditions are common in the summer months when daytime heating over the mainland causes strong onshore breezes from late morning to early evening. The two most energetic types of waves that affect the Gold Coast are East Coast Lows and tropical cyclones. East Coast Lows are intense low pressure systems typically generated off the south-east tip of Australia in the Tasman Sea. These typically occur in the austral autumn to winter months (April – August), with June being the most common. These storms can last several days and bring large waves, high winds, and rains to the coast. Tropical cyclones are typically generated in Northern Queensland in the Coral Sea and rarely propagate as far south as Southern Queensland. However, their effects are still present as a northerly swell influencing the coast during the late austral summer to autumn (January – March). The predominance of south-easterly waves results in a net longshore transport to the north (Splinter et al., 2010).

Anthropogenic interference

The Gold Coast Broadwater region has been exposed to several human interferences. Rapid development of the canal estates on the Gold Coast which was commencing in the 1960s; the construction of the Gold Coast Seaway and by-passing system in the 1980s with the aims of stabilising the entrance, maintaining a safe navigable channel, preventing shoreline erosion to the north and maintaining an adequate beach width to the south; and dredging several areas in the Broadwater with the aim of nourishing eroded beaches in the Gold Coast region and maintaining a safe navigable channel at the Seaway entrance.

Previous Analysis of Morphological Change

According to an earlier analysis by Munday (1995), the Nerang River Inlet had a history of continual instability before its stabilisation. The inlet moved northwards, due to predominant south-easterly wave direction and the resulting net littoral sand transport to the north. Migration of the entrance has been recorded since early 1800's with rate of movement of up to 60m/year. Since the early 1900's the average inlet migration was 20-40 m/year (Munday, 1995). Between 1900 and 1970 approximately $10x10^6$ m^3 of sand accumulated in the Broadwater, as the inlet migrated northwards, at an average rate of 140000 m^3/year (Delft, 1976). In the early 1980's a decision was made to train the entrance. The Gold Coast Seaway stabilisation was completed in 1986 with two training walls. A new island, known as Wave Break Island, was created in order to reduce wave penetration and protect the western shore of the Broadwater. According to a report from Delft Hydraulics (Delft, 1970), because of the high magnitude of the northerly longshore drift on the Gold Coast any scheme to stabilise the entrance would require commitment to artificial sand bypassing across the entrance. The bypassing plant was also completed in 1986.

In the seven years after the new inlet was opened (November 1985- November 1992), the new ebb-delta grew approximately $3.4x10^6$ m^3. This made the total volume of the ebb-delta system almost $12x10^6$ m^3 above a normal beach the profile (assuming no entrance). During this period the ebb-delta crest deepened to about -6.5 m below sea level, and prograded 550 m offshore and 200 m downdrift (Munday, 1995).

Methods and data

The effects of different variables on morphological changes in the Gold Coast Seaway is being studied over a period of time. Bathymetry measured by Queensland Transport on an approximate annual basis in the Seaway vicinity was obtained and plotted. Changes in bathymetry were then determined between surveys. The quantity and nature of the morphological change is related to the changes that have occurred in the environmental and anthropogenic drivers between surveys.

Offshore wave data

Offshore wave characteristics are estimated every 6 hours using global wind-wave models such as the European Centre for Medium-Range Weather Forecasts (ECMWF) 40 year wave re-analysis (ERA-40) or the National Oceanographic and Atmospheric Administration (NOAA) WaveWatch III (WWIII). ERA-40 wave data is used in this research, since it is the longest, directional wave record available in this area. Caires and Sterl (2005) noted that the original ERA-40 model (1958 –

2001) underestimated large waves compared to measured data and applied a correction factor to the ERA-40 wave heights resulting in a corrected data set known as the C-ERA-40. Here the C-ERA-40 (1958 - 2001) (Caires and Sterl, 2005) and ERA-Interim (1989 - present) data sets which was extracted in Splinter et al. (2010) research from grid point coordinates (154.5,-28.5) located roughly 122 km south east from the Gold Coast Seaway (Figure 1) is used .

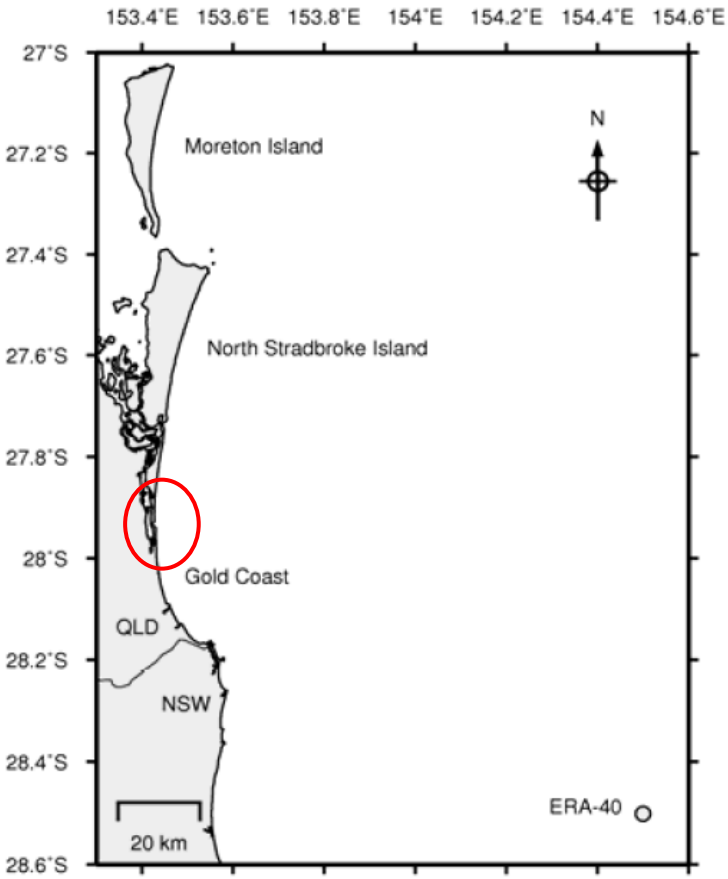


Figure1: Location of study area, Gold Coast. ERA-40 grid point where wave data is extracted from is given at bottom right.

Since the data available from C-ERA-40 and the ERA-Interim in the overlapping period does not completely match together Splinter et al. (2010) used over-lapping time series between the initiation of the ERA-Interim reanalysis to combine data sets and the C-ERA-40 data sets (number of comparison points=18,992) to determine a non-linear correction factor for the ERA-Interim wave heights using a Generalized Additive Model (GAM) technique (Splinter et al., 2010). Therefore, the final wave data that is used in this research was C-ERA-Interim.

Surveying, Volume of sand bypassing and dredging data

Surveying data, dredging and volumes of sand bypassing was provided by Queensland Transport. The survey data is from 2000 up to 2011. The reference datum for various surveys differ as does the aerial extent of the surveys. A full analysis of all surveys will be undertaken in the future, but for the purposes of this preliminary assessment of short-term changes in morphology, along consistent data from 2004 onward will be used.

Bypassing data

Volume of bypassing is available in weekly, monthly and yearly basis. Therefore, from the available data the amount of bypassing for the mentioned time intervals is calculated. The result is as follows:

Table1. Data from Gold Coast Seaway sand bypass based on monthly record (Ref: Gold Coast Region Maritime Safety Queensland | Department of Transport)

Date		Volume Pumped (m^3)
From:	To the end of:	
Jan-04	Jun-04	261,326
Jul-04	Jun-05	659,448
Jul-05	Mar-07	1,184,508
Apr-07	Jul-08	1,033,590
Jul-08	May-09	542,445
Jun-09	Mar-11	1,025,410

Dredging Data

The Dredging data available for this period is shown in Table 2. As can be seen the amount of dredging in the channels is not significant in terms of the morphological evolution of Ebb-tidal delta, so this was neglected in the analysis at this stage.

Table2. Volume of Dredging in The Gold Coast Broadwater since 2004-2009

Financial Year	Channel Name	Volume of Dredging (m^3)
2008/09	North Channel	12,383
2008/09	Canaipa Passage	29,461
2008/09	Coomera River Channel	33,430
2008/09	West Crab Island Channel	21,284
2008/09	North Channel	31,560

Results

Since the surveying has been done at various months of each year, and many of them do not include all the investigated area, the variance of bathymetry between the applicable surveying data was calculated. Therefore, all other effective factors which may influence morphology were calculated for the periods that the variance of surveying data was calculated.

Bathymetric changes

Morphological change can be expressed in terms of volumes of erosion or deposition in a particular area, or in terms of changes in the configuration of the morphological features. In this case the distance offshore to the crest of the delta is chosen as a measure of delta configuration.

In order to calculate the volumes of deposition and erosion the morphological changes of each interval was subdivided to areas of erosion and accretion as you can see in (Figure 2).

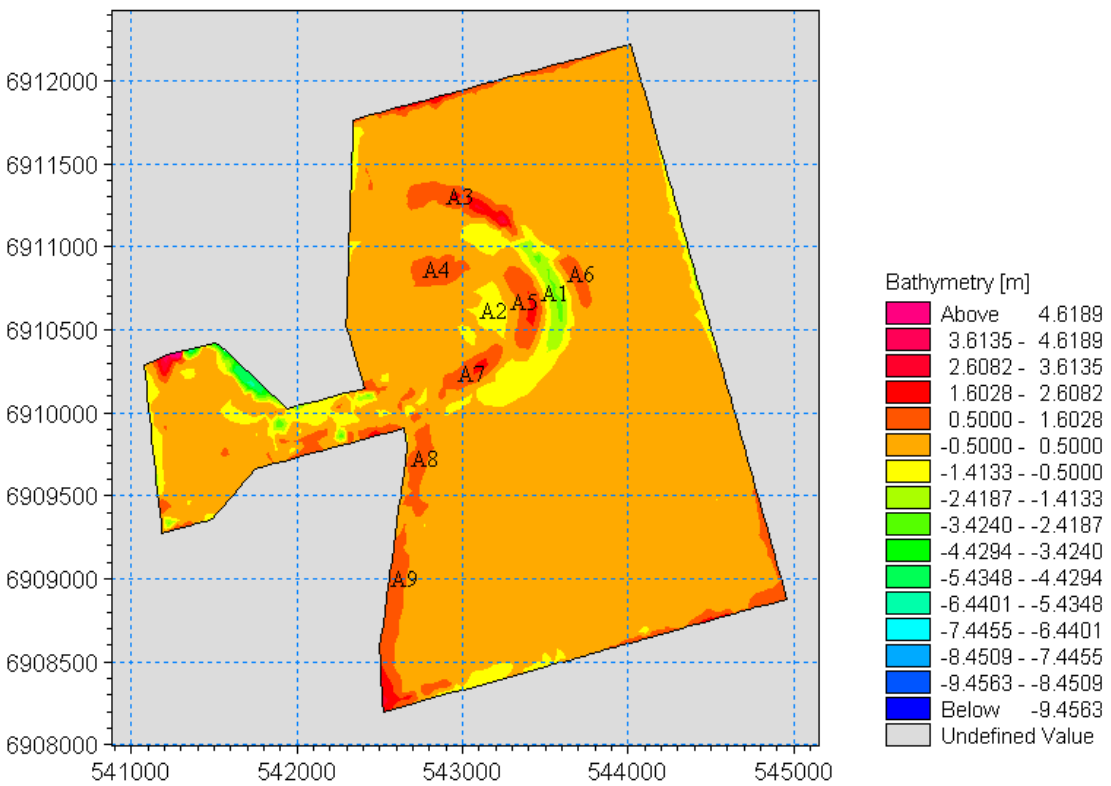


Figure 2: Morphological changes (ΔD) from April 2007 to August 2008 (Positive numbers means accretion and negative numbers means erosion occurred)

The results for the volumetric analysis are indicated in Table3.

Table3. Total volume of sedimentation (deposition/erosion) in the study area

Date Since: / Up to: / Sedimentation	Jan 2004 July 2004	July 2004 July 2005	July 2005 Apr 2007	Apr 2007 Aug 2008	Aug 2008 June 2009	June 2009 March 2011
Total volume of erosion (m^3)	-483,900	-101,612	-142,637	-355,071	-415,106	-902,306
Total volume of deposition (m^3)	1,400,61	319,091	530,558	445,962	1,223,803	510,091
Net volume of sedimentation (m^3)	-343,839	217,480	387,921	90,891	808,698	-392,215
Sedimentation in the seaway Ebb-delta (at the Inlet mouth and to the North)						
Total volume of erosion in delta (m^3)	-294,916	-56,469	-142,637	-355,071	-415,106	-491,561
Total volume of deposition in delta (m^3)	99,410	164,307	500,263	326,524	626,248	510,091
Net volume of sedimentation in delta (m^3)	-195,506	107,838	357,626	-28,547	211,142	18,530

Wave Climate

In order to assess changes in wave climate between surveys wave roses were drawn using MIKE Zero for the wave data sub-sets between morphological changes intervals (Figure 3). As it is shown in Figure 3 which is for one of the intervals, the dominant wave direction in this case and most of other sub-sets is from East and South-East, and wave height is mostly 1-3 meter.

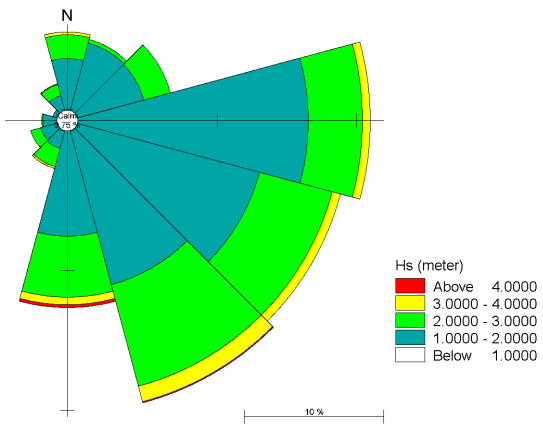
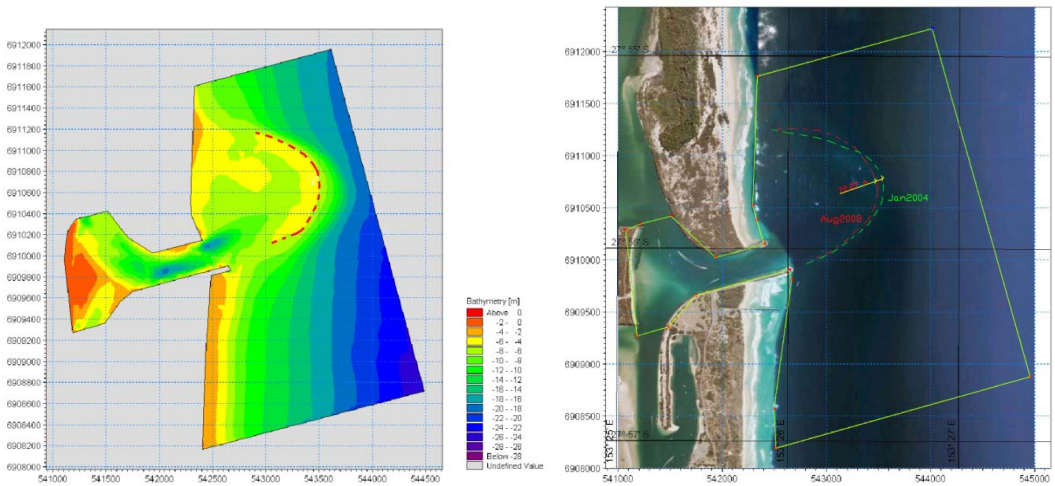


Figure 3: Typical Wave rose from June 2009-January 2011

Delta Crest Movement

As surveying data was not available on an annual basis, analysis was based on the times that surveying were done. Surveying data was imported to MIKE21 to generate a bathymetry map for each survey. The crest of delta seaward edge (at -6 m depth) is chosen as a reference line for analysing the crest of delta movement (Figure 4).



(a) (b)

Figure 4: (a) Bathymetry map established based on surveying data of Queensland Transport in July 2004, Crest movement analysis based on dashed line which is the edge of -6 m depth. (b)Crest movement between Jan 2004 and Aug 2008 (sample)

The result of crest movement (horizontal) analysis is displayed in Table 3, positive numbers indicate seaward/to the east movement.

Table3. Approximate ebb-delta crest movement

Date		Ebb-delta crest movement (to the ocean/horizontal)(m)
From:	To:	
Jan-04	Jul-04	-26
Jul-04	Jul-05	~0
Jul-05	Apr-07	+86
Apr-07	Aug-08	-104
Aug-08	Jul-09	-78
Jul-09	Mar-11	+117

January 2004-July 2004

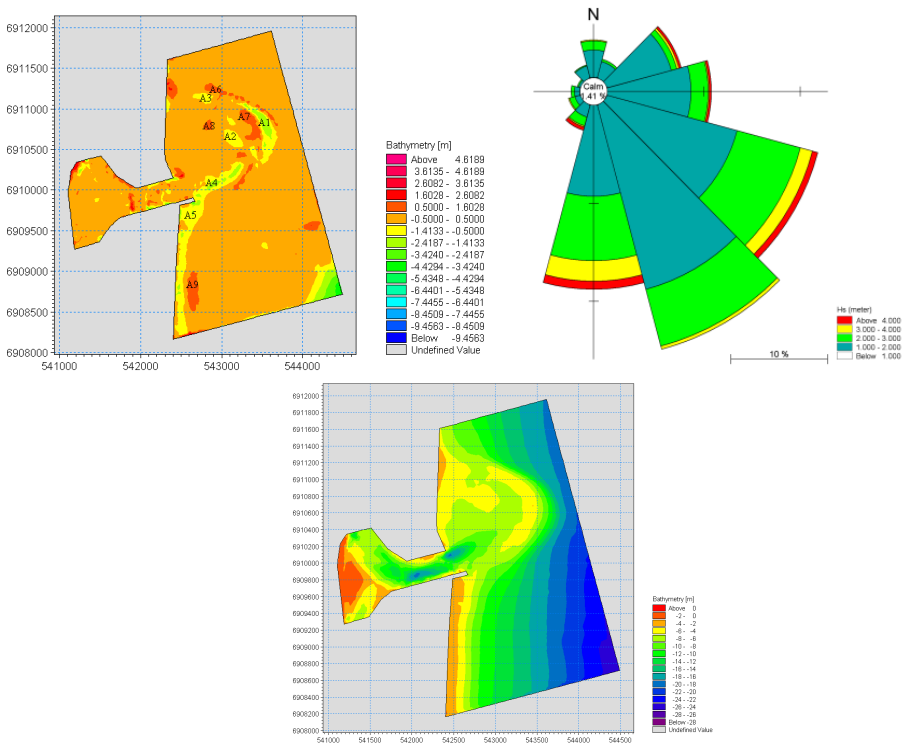


Figure5: (from left to right)-(a)bathymetry changes from Jan2004-July2004,(b)Wave rose in this period, (c)Bathymetry map of Gold coast Seaway in July 2004

Data shows that during this period erosion was dominant, and about 200,000m^3 of the ebb-tidal delta was eroded, and since the crest of delta was eroded, there was about 26 m shoreward movement of the crest (to the west). On the other hand, about 260,000m^3 of sand was pumped through the bypassing system to the North during this period, which would is equivalent to an annual rate of 520,000m^3/year which is close to the assumed average net longshore transport rate.

July 2004- July 2005

It is notable that there is approximately no horizontal movement of the crest of delta from July 2004-July 2005. It could be a sign of equilibrium in the system during a complete yearly cycle of wave climate during which no significant storms occurred. However, some deposition occurred within the delta of about 107,000m^3, with approximately 660,000m^3 of sand pumped. This rate of pumping is close to the average pumping rate monitored until recently.

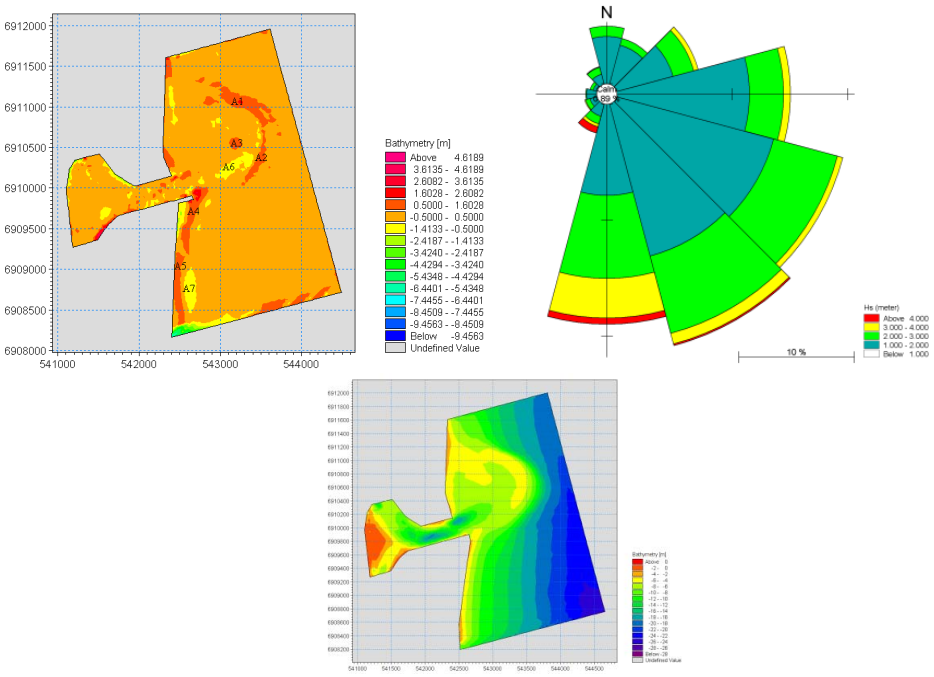


Figure6: (from left to right)-(a)bathymetry changes from July2004-July2005,(b)Wave rose in this period, (c)Bathymetry map of Gold coast Seaway in July 2005

July 2005-Apr 2007

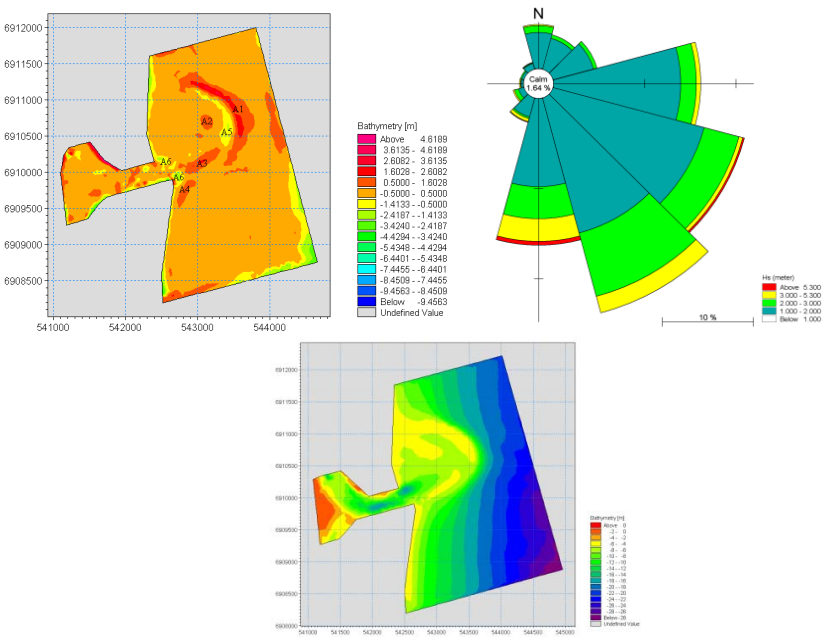


Figure7: (from left to right)-(a)bathymetry changes from July2005-Apr2007,(b)Wave rose in this period, (c)Bathymetry map of Gold coast Seaway in Apr 2007

During this 21 months period a large amount of deposition occurred at the toe of delta which lead to about 86 m progradation of crest farther offshore. The net amount of deposition was about 360,000m^3, while about 1,190,000m^3 sand had been pumped (672,000m^3/year).

Apr 2007-Aug 2008

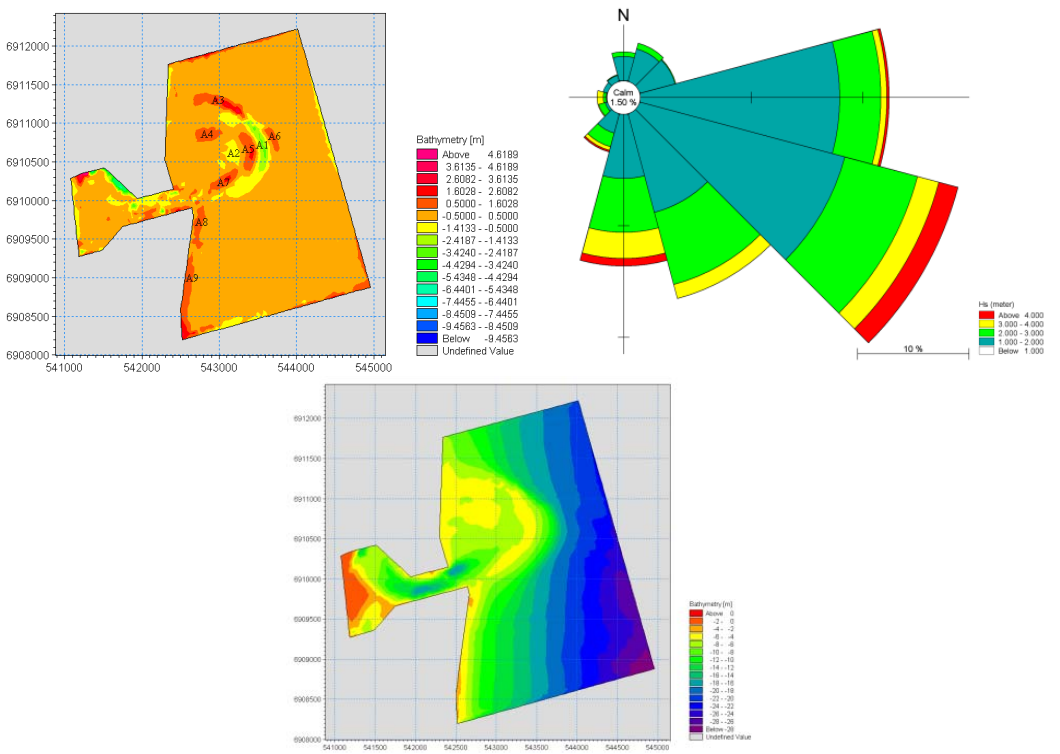


Figure8: (from left to right)-(a)bathymetry changes from Apr2007-Aug2008,(b)Wave rose in this period, (c)Bathymetry map of Gold Coast Seaway in Aug 2008

In this period the deposition that was evident in the toe of delta and caused its progradation in previous time interval is eroded, which result in 104 m movement of the crest shoreward (very close to the place that it had in July 2004 and July 2005) (Figure8). Moreover, it seems that the sand which is eroded from the crest is deposited farther inside the delta, since the approximate net amount of sedimentation in the delta is not large – approximately 29,000m^3 erosion. This change is most likely due to the more easterly wave climate compare with the previous few years. A direct shore perpendicular wave direction would act to restrict the seaward growth of the delta. The amount of sand that pump during this time was 540,000 m^3 which is equal to 648,000 m^3/year, that is approximately equal to the rate of sand pumped during July 2004-July 2005.

Aug 2008- June 2009

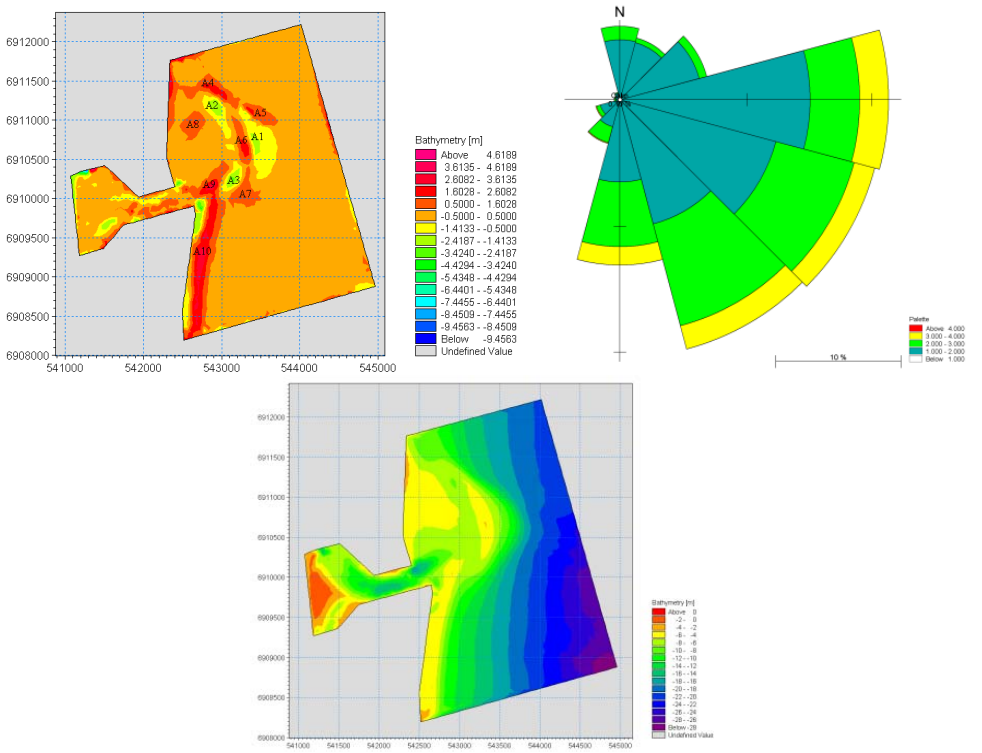


Figure9: (from left to right)-(a)bathymetry changes from Aug2008-June2009,(b)Wave rose in this period, (c)Bathymetry map of Gold Coast Seaway in June 2009

In this period significant storms hit the Gold Coast region including Tropical Cyclone Hamish early in 2009 and the East Coast Low (ECL) in May 2009. The ECL in particular caused significant shoreline erosion in the vicinity of the Seaway, with a large storm bar forming offshore. The storm also scoured the crest of ebb-delta resulting in a shoreward movement of around 80 m, and a longshore elongation of the delta. The amount of sand pumped during this interval was 540,000m^3, while the approximate net volume of sediment added to the delta was about 210,000m^3. As can be seen in Figure 9a and c), it could be also concluded that the erosion in area A2 and A3 (see Fig. 9a) and therefore accretion in area A4 is the influence of both the strong wave induced longshore transport and the cross-shore sand movement due to the dominant easterly wave direction.

June 2009- March 2011

By March 2011 most of the sediment which was deposited by the 2009 storms has eroded back (Figure 10). Analysis of the bathymetry changes shows that the total delta and near shoreline morphology tended to return to the situation that it had

before the 2009 storms, since the crest of delta moved offshore about 117m. The total deposition and erosion within the delta was very low - about 190,000m^3 which could be an indication that the morphology may be reaching an "equilibrium". The volume of sand pumped by the bypassing system was around 103,000m^3 (588,000 m^3/year).

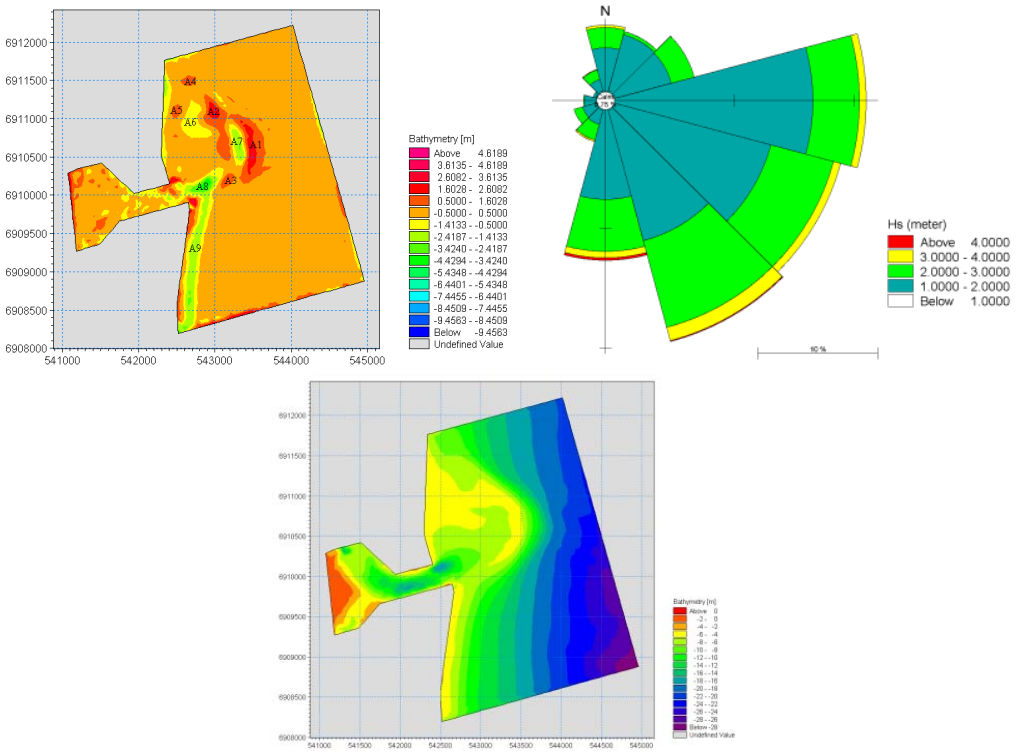


Figure10: (from left to right)-(a)bathymetry changes from June2009-March2011,(b)Wave rose in this period, (c)Bathymetry map of Gold Coast Seaway in March 2011

Conclusion

The bathymetric historical data from 2004 to 2011 was collected and the trend of morphological changes through these years mapped out. According to the analysis it seems that the Seaway ebb-tidal delta may be reaching a point of equilibrium between the amount of longshore and cross-shore sand supply, and volume of bypassing during these years. The major parameter that caused sudden changes in the morphology was large storm activity, with gradual recovery of the ebb-delta volume and configuration.

References

Caires, S. and Sterl, A., 2005. A New Nonparametric method to Correct Model Data: Application to Significant Wave Height from the ERA-40 Re-Analysis. Journal of Atmospheric and Oceanic Technology, 22: 443-459.

Chapman, D.E.M., 1981. Coastal erosion and the sediment budget, with special reference to the Gold Coast, Australia. Coastal Engineering, 4: 207-227.

D'Agata, M. and Tomlinson, R., 2004. Investigation of Ebb Tidal Deltas using a Numerical Model at the Moveable Bed Physical Model Scale, Research Report 27, Griffith Centre for Coastal Management CRC for Coastal Zone Estuary & Waterway Management.

Delft, 1970. Gold Coast, Queensland Australia - Coastal erosion and related problems, Report 257, Delft Hydraulics Laboratory, The Netherlands.

Delft, 1976. Nerang River Entrance Stabilisation, Report on Model Investigation, Delf hydraulic Report M1259.

McCauley, E.K., 1997. The evolution of Jumpinpin Inlet, Griffith University, Gold Coast.

Mirfenderesk, H. and Tomlinson, R., 2008. Observation and Analysis of Hydrodynamic Parameters in Tidal Inlets in a Predominantly Semidiurnal Regime. Journal of Coastal Research, 24(5): 1229–1239.

Munday, D., 1995. Coastal response to the Nerang River inlet stabilisation, Gold Coast, Queensland, Australia, Queensland University of Technology, Brisbane.

Patterson, D.C., 2007. Sand Transport and Shoreline Evolution, Northern Gold Coast, Australia. Journal of Coastal Research, SI 50: 147 - 151.

Polglase, R.H., 1987. The Nerang River Entrance Sand-Bypassing System, 8th Australian Conference on Coastal Ocean Engineering, pp. 222-226.

Sennes, G., Castelle, B., Bertin, X., Mirfenderesk, H. and Tomlinson, R.B., 2007. Modelling of the Gold Coast Seaway tidal inlet, Australia. Journal of Coastal Research, 50: 1086 - 1091.

Splinter, K.D., Golshani, A., Stuart, G. and Tomlinson, R., 2010. Spatial and temporal variability of longshore transport along Gold Coast, Australia, ICCE.

Voisey, C., 2004. Moveable Bed Physical Modelling of Ebb Delta Growth Characteristics, Research Report 25, Griffith Centre for Coastal Management CRC for Coastal Zone Estuary & Waterway Management.

WRL and GCCM, 1998. Numerical Modelling of Sediment Movement and Budget at Seaway, Water Research Laboratory in association with Griffith University for GCCC, Gold Coast

Influence of JONSWAP Wave Spectra Form on Frequency Spectrum of Suspended Sediment Transport Values

I. S. Podymov[1], J. Grüne[2], R. D. Kos'yan[3] and T. M. Podymova[4]

[1]P. P. Shirshov Institute of Oceanology, Southern Branch, RAS, 353467 Gelendzhik-7, RUSSIA; PH (86141) 28281; FAX (86141) 28089; email: podymov@coastdyn.ru

[2]Coastal Research Centre FZK, Merkurstrasse 11, 30419 Hannover, GERMANY; PH (49) 1781841094; email: gruene@fzk.uni-hannover.de

[3]P. P. Shirshov Institute of Oceanology, Southern Branch, RAS, 353467 Gelendzhik-7, RUSSIA; PH (86141) 28281; FAX (86141) 28089; email: rkosyam@hotmail.com

[4]P. P. Shirshov Institute of Oceanology, Southern Branch, RAS, 353467 Gelendzhik-7, RUSSIA; PH (86141) 28281; FAX (86141) 28089; email: podymova@inbox.ru

ABSTRACT

On the base of experimental data the comparison of the suspended sediment concentration fluctuations frequency spectrum with the wave energy spectrum, was fulfilled. It led to some interesting results.

Studies were carried out for different wave conditions, during which γ parameter varied from 1 to 10. Its changes affected the wave energy spectrum. Article examines influence of the wave energy spectrum on frequency spectra of suspended sediment transport.

The paper will provide detailed information about results of this investigation.

INTRODUCTION

In traditional models only the time averaged characteristics of water circulation, sediment and pollutant transport processes are considered. Sometimes the group structure of waves, their transformation within the coastal zone, the contribution of phase shift between sediments and the fluid at different frequencies of an irregular wave spectrum are taking into account. The influence of the form of surface wave spectra, however, has never been considered. First results of the possibility of such dependence were given by (Grüne et al., 2007), where it was shown that the form of wave spectrum could greatly influence on the suspended sediment concentration (SSC) values.

It was noted (first by Phillips in 1958) that at higher frequencies than the

peak frequency, the energy in a given wave-field 'saturated'. This saturation produced relatively equivalent energies for a given frequency regardless of virtually all other parameters.

Hasselmann *et al*., (1973), after analyzing data collected during the Joint North Sea Wave Observation Project (JONSWAP), found that the wave spectrum is never fully developed. It continues to develop through non-linear, wave-wave interactions even for very long times and distances. Considerable data taken off the western shore of Denmark was used to produce a model of the wave spectrum. The model is:

$$S(f) = E(f)\exp\left[-1.25\left(\frac{f_p}{f}\right)^4\right]\gamma^{\Gamma},$$

where

$\Gamma = \exp\left[-\frac{\left(f-f_p\right)^2}{2\beta^2 f_p{}^2}\right]$; $E(f) = \frac{\alpha g^2}{(2\pi)^4 f^5}$; f - is the frequency; f_p – is the peak frequency (frequency at which $S(f)$ is a maximum); α - is the Phillips constant (sometimes called the equilibrium-range parameter); γ - is the peak-enhancement factor (usually taken to be 3.3); and $\beta = 0.07$ for $f < f_p$, or $\beta = 0.09$ for $f > f_p$.

Studies were carried out for different wave conditions, during which γ parameter varied from 1 to 10. Its changes affected the wave energy spectrum. Below are results of investigations of the wave energy spectra influence on frequency spectra of suspended sediment concentration. Results of the studies are important for modeling the processes of suspension and transport of insoluble particles in dynamic sea areas.

EXPERIMENTAL INVESTIGATION

Theoretical base. The JONSWAP spectrum is similar to the Pierson-Moskowitz spectrum except that waves continues to grow with distance (or time) as specified by the α term, and the peak in the spectrum is more pronounced, as specified by the γ term. The latter turns out to be particularly important because it leads to enhanced non-linear interactions and a spectrum that changes in time according to the theory of Hasselmann, (1966).

Wave spectra of a developing sea for different fetches measured at JONSWAP are shown in Figure 1 (Robert H. Stewart, 2006).

Using Hasselmann's wave model we have calculated dependences maximum of wave spectral density and frequency for maximum wave spectral density from the fetch, Figure 2a and Figure 2b. According to the Hasselmann's wave model wave spectral density, peak steep slope of the spectral density (the Peak-Enhancement Factor) and a frequency for the peak depend on fetch of a wave.

In turn value of a maximum of wave spectral density is functionally related to frequency. The dependence of a maximum of wave spectral density on frequency is shown in Figure 3. From drawing it is visible, that to great values of wave spectral density there correspond low values of frequency. That is natural in physical sense. This is one of main differences of Hasselmann's wave model from the model of Moskowitz (1964).

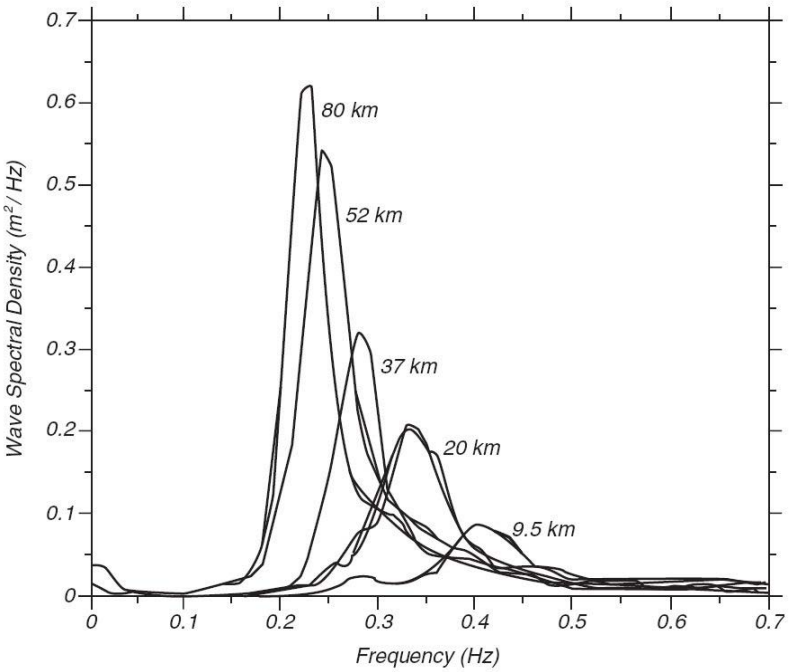


Figure 1. Wave spectra of a developing sea for different fetches measured at JONSWAP.

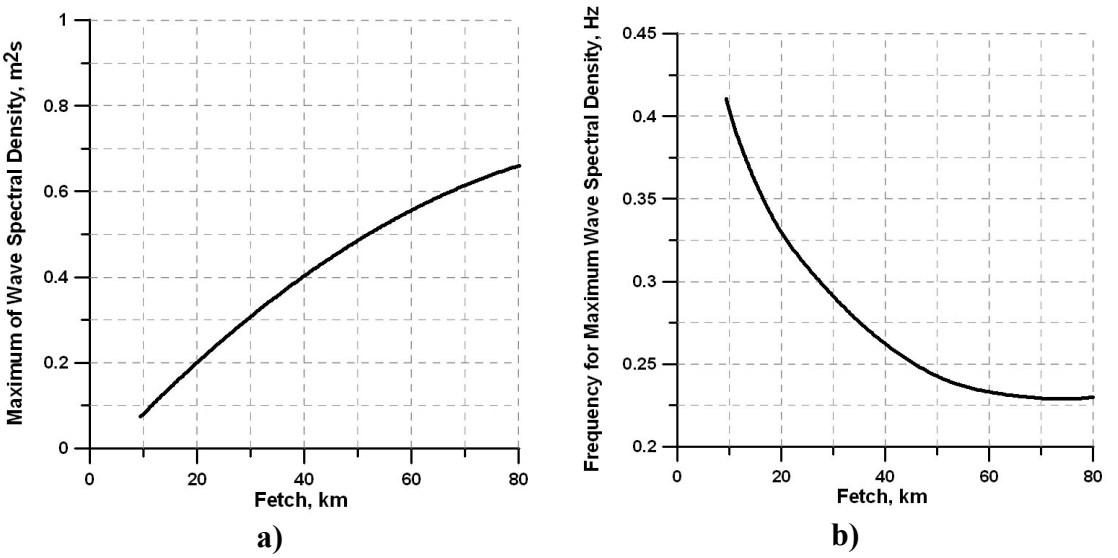


Figure 2. The dependence of wave spectral density maximum (a) and the frequency for wave spectral density maximum (b) from the fetch.

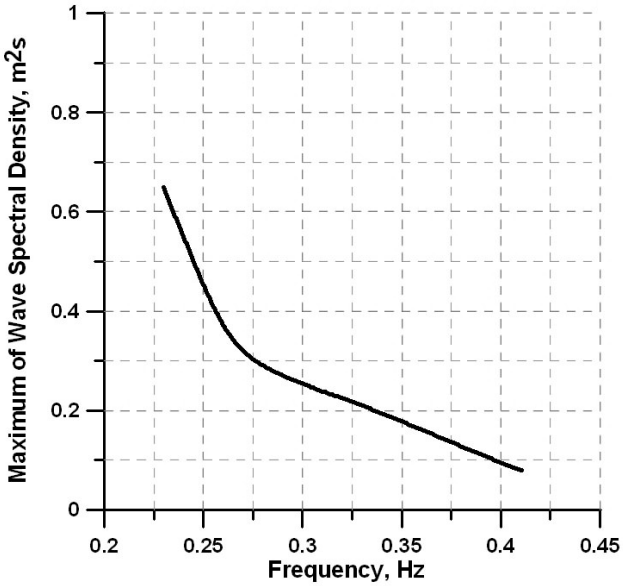


Figure 3. The dependence of wave spectral density maximum on frequency.

EXPERIMENT

Experiment was performed in the large wave channel. For our investigations wave spectra were created by means of a wavemaker. Simultaneous measurements of suspended sediment concentration, free surface elevations and three-component velocities were carried out at several levels above the sea bed. γ- parameter changed in a scale 1-10. $\mathbf{H_{sign}}$ changed between 0.9 – 1.1m. Frequency for the maximum of wave spectral density had a stationary value. Spectra of suspended sediment concentration for different values of γ, for three values of significant waves height $\mathbf{H_{sign}}$ and for two levels are presented in Figure 4 – Figure 9.

In Figure 4 – Figure 9 the linear scales were employed for the clearness. Certainly, used in experiment parameter γ and parameter γ from Hasselmann's wave model are not identical completely. But they are very similar under the performances. Other analogue has not been found in the literature on oceanography. Results of a spectrum analysis are used for build-up of some statistical dependences. Figure 10 shows dependence of maximum of concentration spectral density on values of significant waves height, for six values of γ and for two horizons from the bottom. It is visible from Figure 10b that the greatest influence to fluctuations of suspended sediment concentration near the bottom is initiated by waves with parameter γ=1. Spectrum of such wave is the widest of the considered. It is interesting that increase of $\mathbf{H_{sign}}$ value leads to reduction of suspended sediment concentration near the bottom.

I.e., average value of suspended sediment concentration increases towards the surface. At the same time average value of suspended sediment concentration decreases near the bottom.

Figure 11 shows the dependence of maximum of concentration spectral density on γ values for three values of significant waves height and for two

horizons from the bottom. The wave spectrum with parameters γ=6 and $\mathbf{H_{sign}}$=1.1m is the most interesting (see Figure 11b). It is possible to guess that increase of $\mathbf{H_{sign}}$ will lead to increase of a steepness of a curve for the maximum of concentration spectral density. The analysis of Hasselmann's wave model allows to calculate that parameters γ=6 and $\mathbf{H_{sign}}$=1.1m the wave reaches after distance 80km for fetch (see Figure 1).

In this paper preliminary results of spectral processing for various wave modes are only shown. It is planned that futher working with this subject will make more correct estimations of the presented materials.

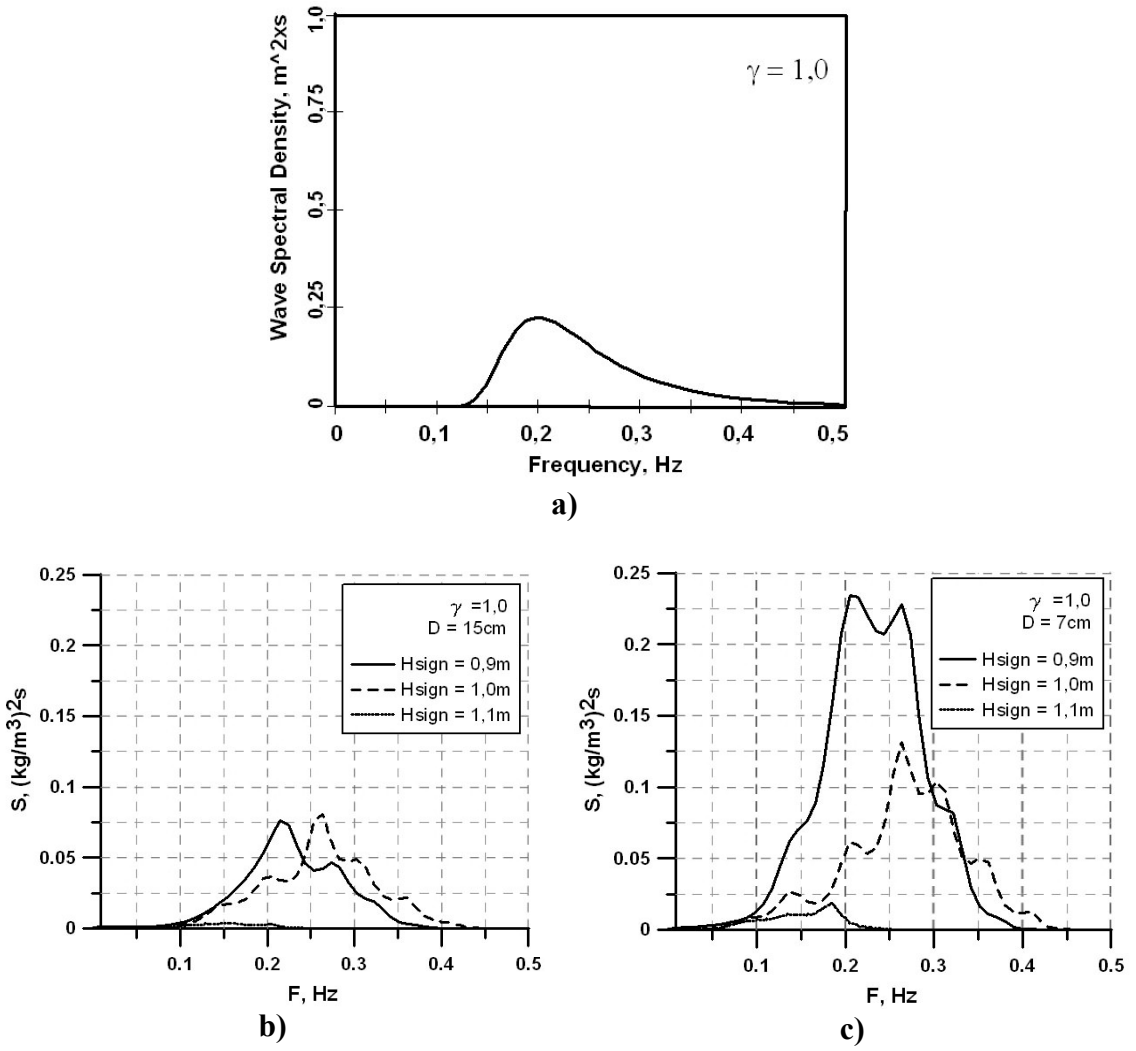


Figure 4. Wave spectral density for γ=1 (a); spectra of suspended sediment concentration (S) for γ=1, for three values of significant waves height $\mathbf{H_{sign}}$, for the distance (D) from the bottom 15cm (b) and 7cm (c).

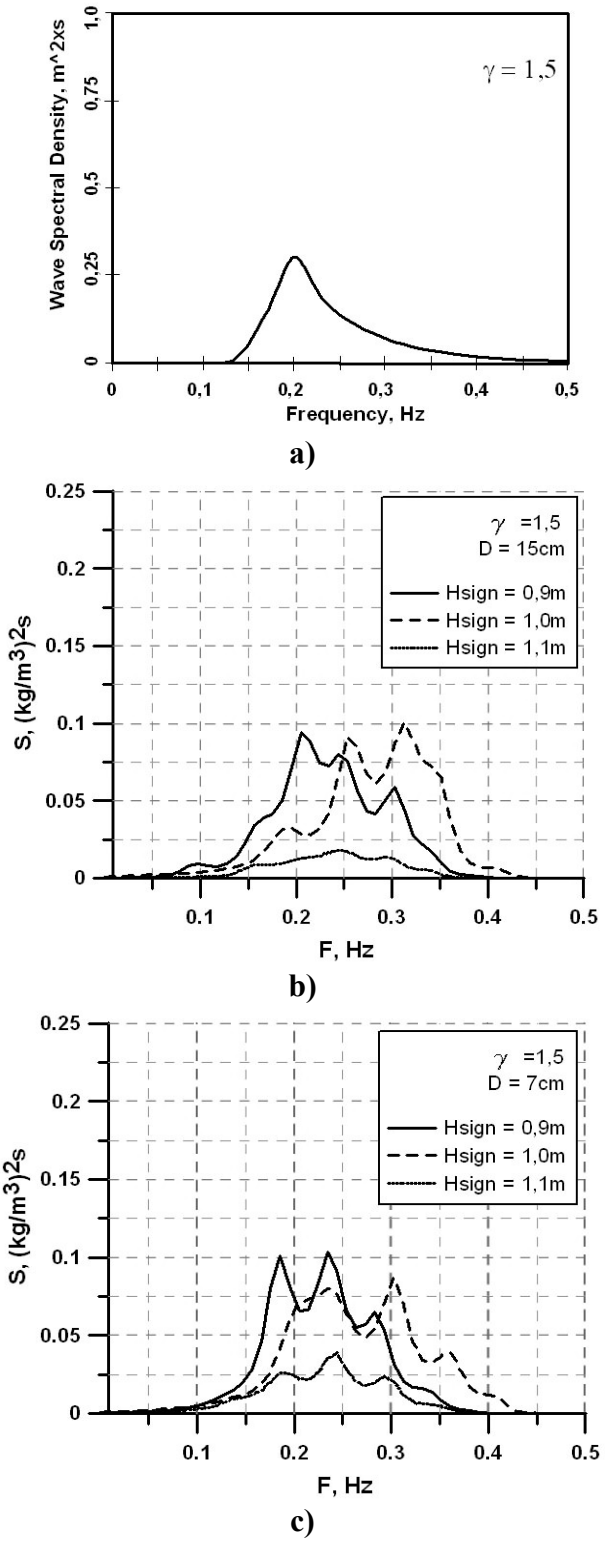


Figure 5. Wave spectral density for γ=1.5 (a); spectra of suspended sediment concentration (S) for γ=1.5, for three values of significant waves height H_{sign}, for the distance (D) from the bottom 15cm (b) and 7cm (c)

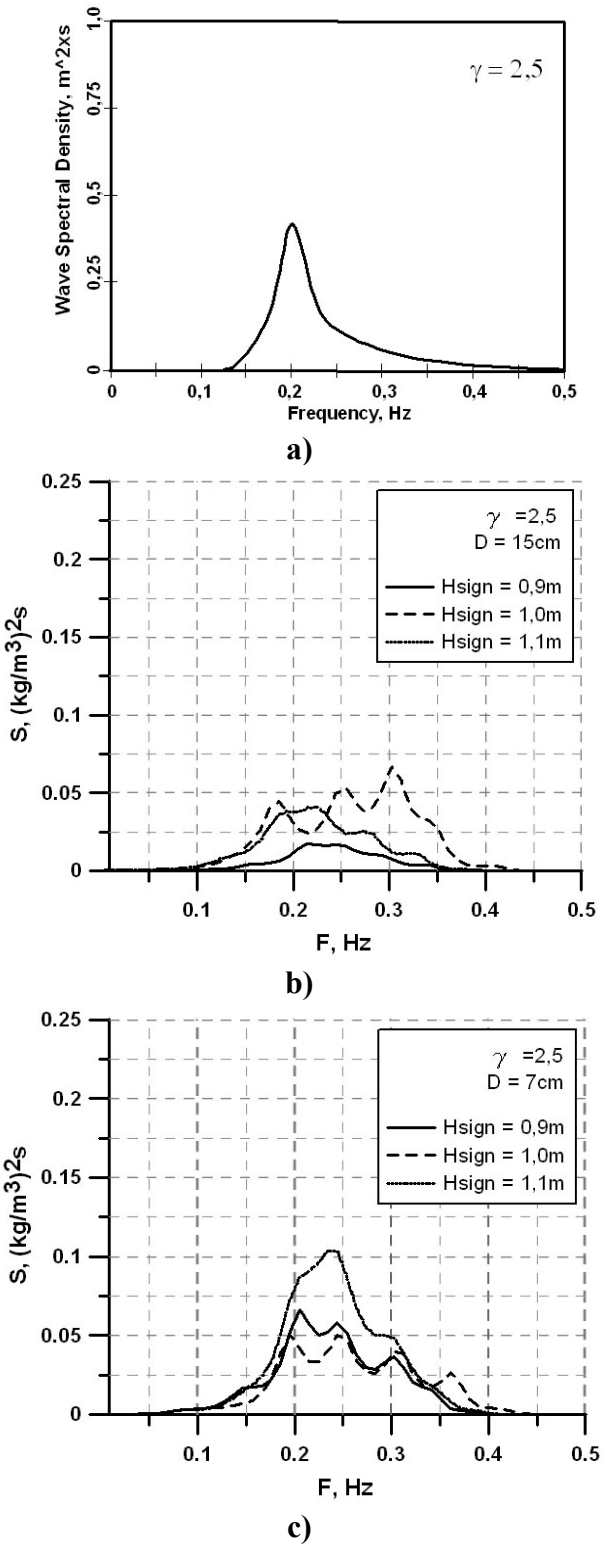


Figure 6. Wave spectral density for γ=2.5 (a); spectra of suspended sediment concentration (S) for γ=2.5, for three values of significant waves height H_{sign}, for the distance (D) from the bottom 15cm (b) and 7cm (c).

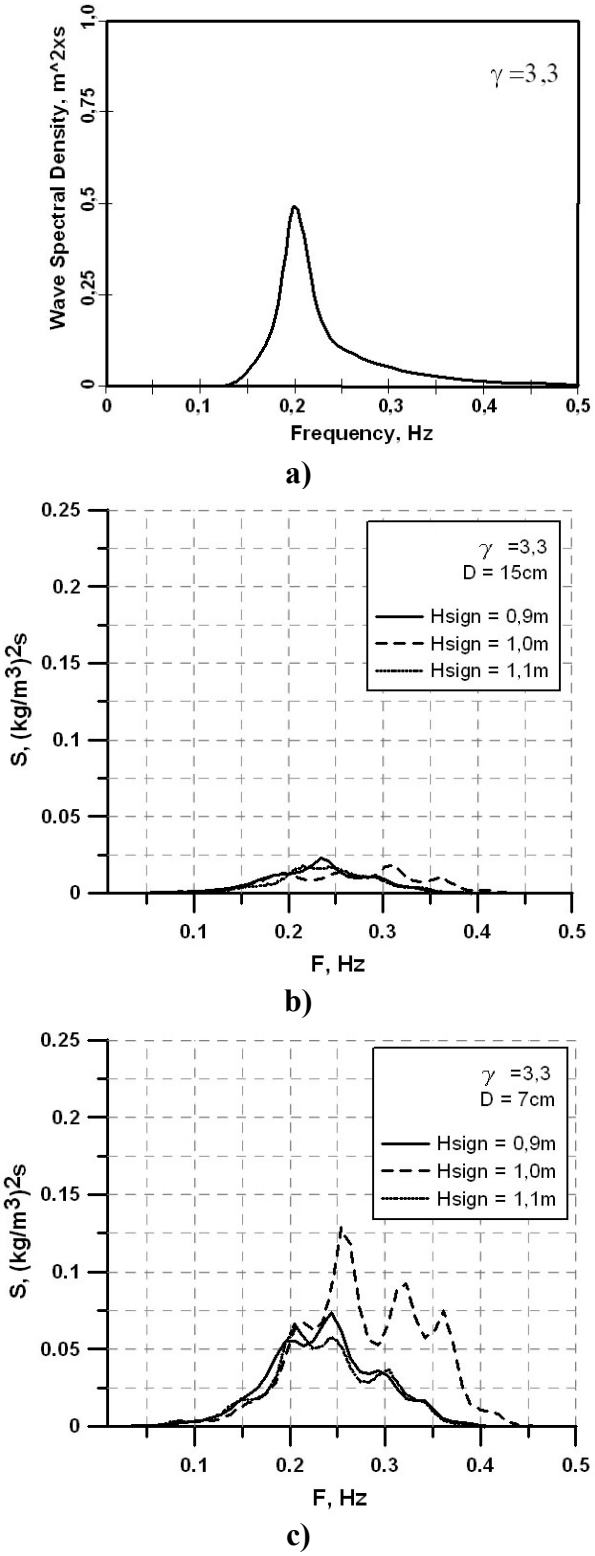


Figure 7. Wave spectral density for γ=3.3 (a); spectra of suspended sediment concentration (S) for γ=3.3, for three values of significant waves height H_{sign}, for the distance (D) from the bottom 15cm (b) and 7cm (c).

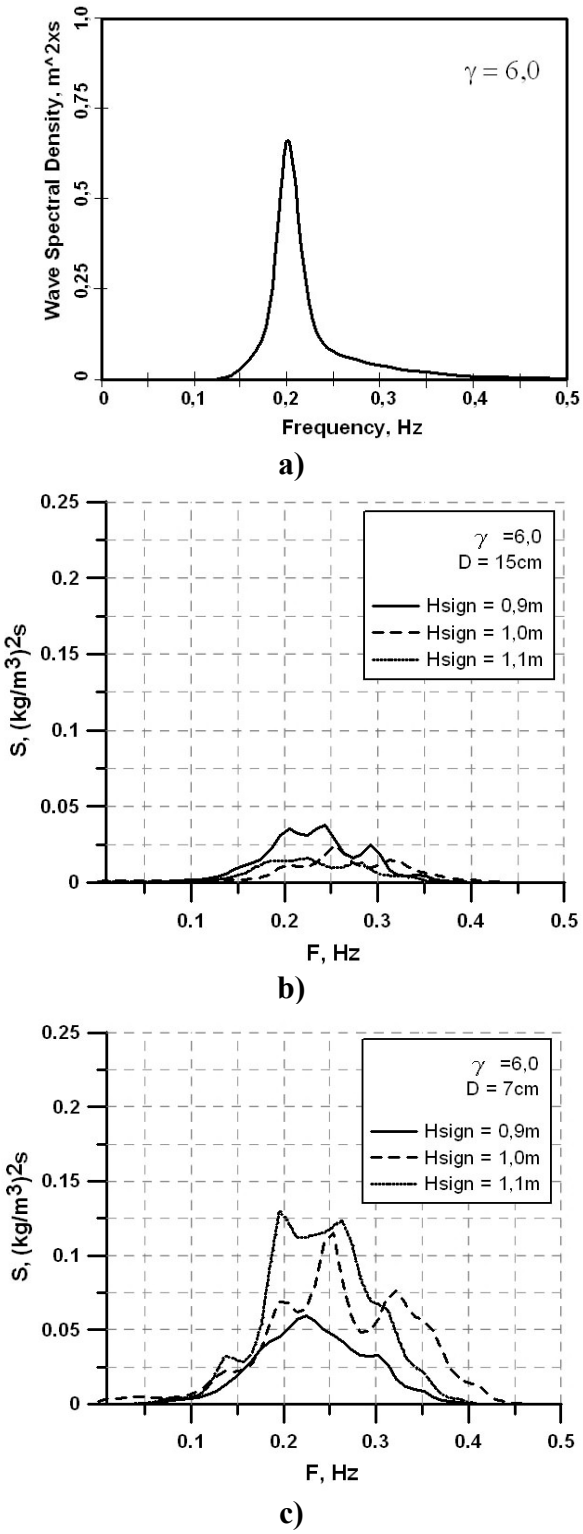


Figure 8. Wave spectral density for γ=6 (a); spectra of suspended sediment concentration (S) for γ=6, for three values of significant waves height H_{sign}, for the distance (D) from the bottom 15cm (b) and 7cm (c).

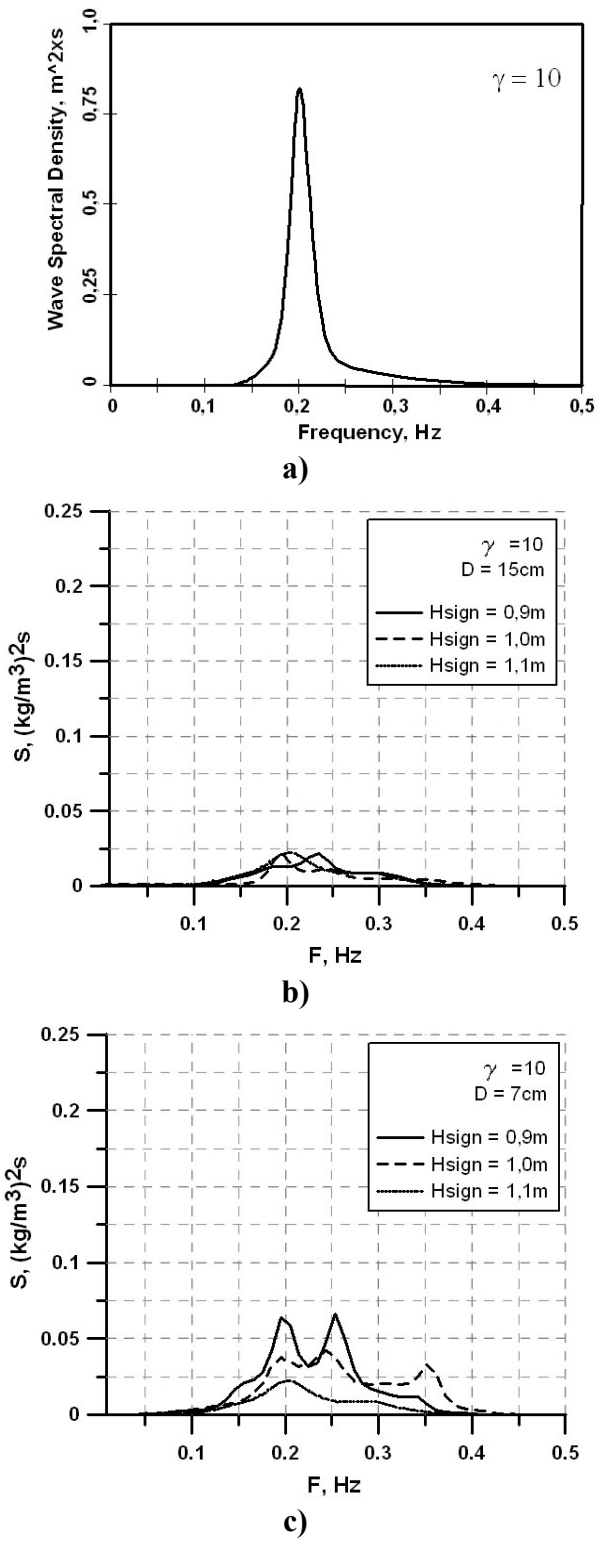
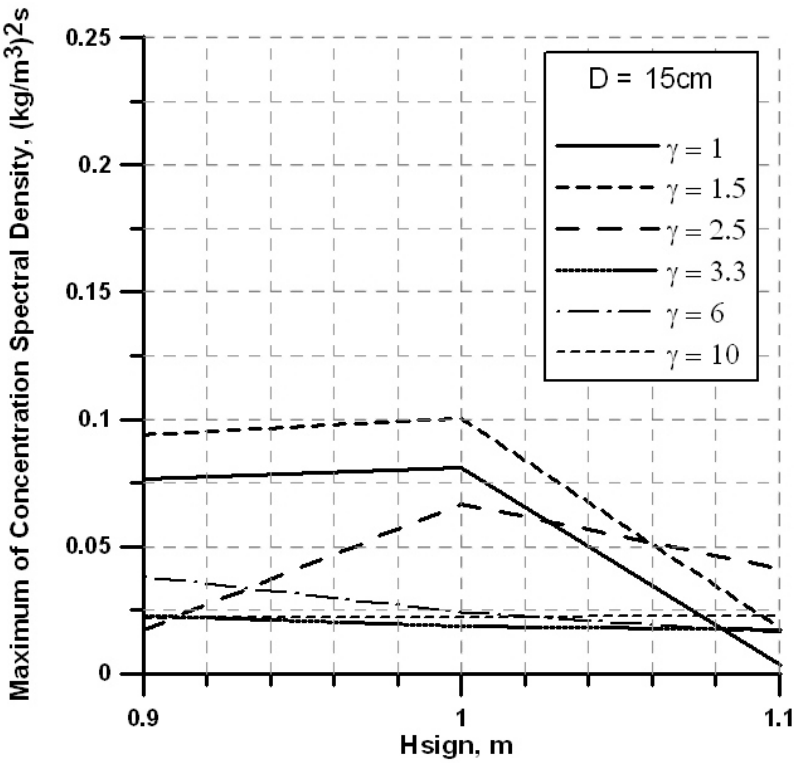
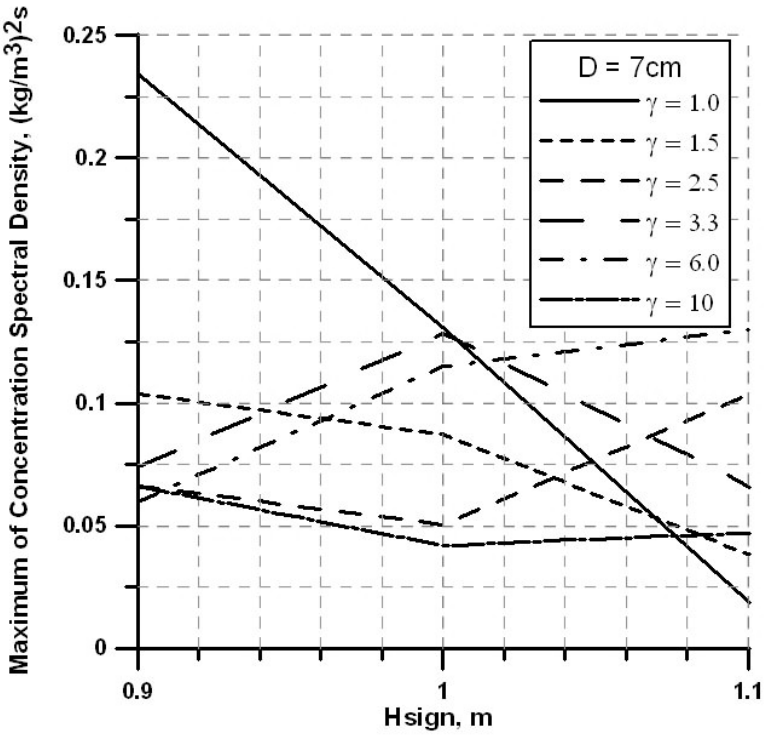


Figure 9. Wave spectral density for γ=10 (a); spectra of suspended sediment concentration (S) for γ=10, for three values of significant waves height H_{sign}, for the distance (D) from the bottom 15cm (b) and 7cm (c).

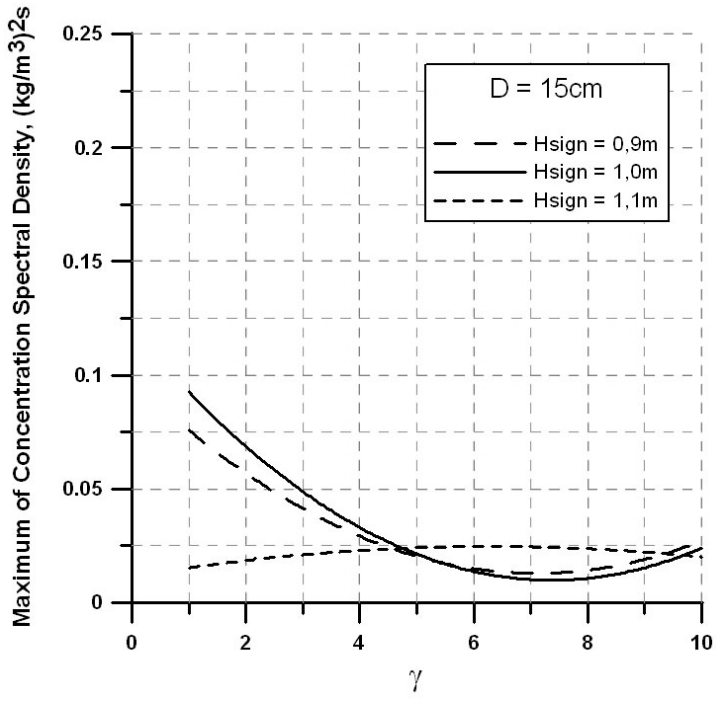


a)

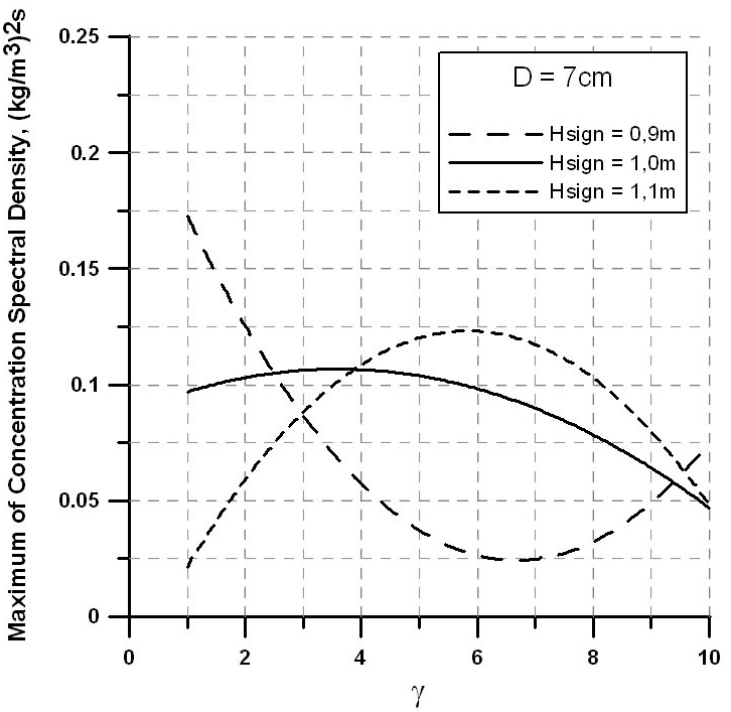


b)

Figure 10. Dependence of maximum of concentration spectral density on values of significant waves height H_{sign}, for six values of γ and for two horizons from the bottom: (a) D=15cm, (b) D=7cm.



a)



b)

Figure 11. Dependence of maximum of concentration spectral density on γ values for three values of significant waves height H_{sign} and for two horizons from the bottom: (a) D=15cm, (b) D=7cm.

CONCLUSION

From the Figure 4 – Figure 9 it is seen that wave spectra forms and wave parameters greatly influence on the suspended sediment concentration values. However functional dependence between these parametres is very complicated.

Waves with the expressed power spectra on peak frequencies possess the most part of kinetic energy. They participate in processes of suspension and carrying over of solid particles more actively. It is possible to presume that for such processes it is possible to describe mechanisms of transport of the suspended sediments by the simplified numerical model (in particular, by one-dimensional diffusion equation for suspended sediment concentration) with enough accuracy.

The preliminary analysis shows that for waves with a wide power spectrum it will not be possible to describe mechanisms of suspended sediment transport by the simplified numerical model. It will be necessary to investigate and describe the reasons forsuspension at each frequency of a spectrum, using methods of the mutual spectral analysis.

Later on, it is planned to investigate the conditions, when the spectral energy is redistributed between peak frequency and the higher frequencies, as well as choose other conditions when degree of influence of wave energy on solid particles is maximum all over the frequencies spectrum.

REFERENCES

Grüne, J., Kosyan, R., Oumeraci, H., Podymov, I., Schmidt-Koppenhagen, R., Vincent, C. (2007). "Large-scale laboratory modelling of suspended sand concentration fluctuations under irregular waves." *Proceedings of the International Conference Coastal Sediments '07*, ASCE, 1801 Alexander Bell Drive, Reston, VA 20191 USA, Vol. 1, 248-259.

Hasselmann, K. (1966). "Feynman diagrams and interaction rules of wave-wave scattering processes", *Rev. Geophysical,* 4 (1), 1-32.

Hasselmann, K., Barnett, T.P., Bouws, E., Carlson, H., Cartwright, D.E., Enke, K., Ewing, J.A., Gienapp, H., Hasselmann, D.E., Krusermann, P., Meerburg, A., Muller, P., Olbers, D.J., Richter, K., Sell, W., and Walden, H. (1973). "Measurements of wind-wave growth and swell decay during the Joint North Sea Wave Project (JONSWAP)", *Ergnzungsheft zur Deutschen Hydrographischen Zeitschrift Reihe A8* (Suppl.), 95 p.

Moskowitz, L. (1964), "Estimates of the power spectrums for fully developed seas for wind speeds of 20 to 40 knots", *J. Geophysical Research 69 (24)*, 5161–5179.

Robert, H. Stewart (2006), "Introduction To Physical Oceanography", *Department of Oceanography, Texas A & M University*, September 2006 Edition, 344 p.

Cohesive Sediment Transport Modeling: Application to the Madura Strait, Indonesia

Nita Yuanita[1)], Muhammad Ali Rini[1)], and Undang Heriawan[2)]

[1)] *Ocean Engineering, Faculty of Civil and Environmental Engineering, Bandung Institute of Technology, Lab. Tek. VI 3rd Floor, Jl. Ganesa No. 10 Bandung 40132-Indonesia; PH (+62)22-2509117 ext 124; FAX (+62)22-2509117; e-mail: nita@ocean.itb.ac.id*

[2)] *Marine Geological Institute, Jl. Dr. Djunjunan No.236 Bandung-Indonesia; email : kerjasama@mgi.esdm.go.id*

ABSTRACT

Madura Strait is located in East Java province, about 800 km east of Jakarta, the capital city of Indonesia. The Madura Strait is subject to ocean waves of less than 1 m height due to its position in semi-enclosed Java Sea in Indonesian archipelago. There are 2 major rivers that carry sediment to Madura strait namely Bengawan Solo River and Brantas River. In the last years sediment transport from Brantas river has been increasing significantly through one of its branch namely Porong River. The development of Suramadu Bridge between Surabaya (at Java Island) and Bangkalan (at Madura Island) contributed to sedimentation pattern in Madura Strait. The shallow bathymetries in major part of Madura Strait threat an environmental problem in the area. Therefore sedimentation model is necessary on attempt to anticipate serious environmental problem in Madura Strait. This study is about mud transport simulation in Madura Strait due to increasing sediment discharge from Porong River.

The analysis was carried out by using MIKE-21 model software developed by DHI Water and Environment. In hydrodynamic simulation, water level boundary conditions were generated using global tide model from MIKE21 Toolbox at the boundary. The simulated water level and velocity were compared with observed data at calibration stations. In the calibration, the bed roughness parameter was adjusted by trial and error until the most satisfactory results were obtained. The root mean square error between computed and observed parameters in calibration was satisfied.

In mud transport simulation, sediment concentration boundary conditions were generated using observation data. The simulated suspended sediment concentration was compared with observed data at calibration stations. Calibration parameters (critical shear stress for deposition, critical shear stress for erosion and erosion coefficient) were adjusted to get satisfaction results. After the calibrated mud transport model was achieved, simulation of several scenarios was applied to predict future behavior of sedimentation in Madura Strait.

I. INTRODUCTION

River cohesive sediment discharge to river mouth plays a significant effect in estuary condition. Especially when waves and tidal in estuary area is not dominant. In many cases river sediment discharge created river mouth sedimentation and later will developed a river mouth. In other cases when estuary hydrodynamic, that is effected by tidal and waves, is relatively active, cohesive sediment discharge will spread over the estuary area.

Estuary that is located in a strait, generally get affected by strait hydrodynamic condition which is active, especially by tidal. When some activities are presence, such as harbor, bridge, fishing port, etc, on that strait, sediment transport will also contribute a signifant effect to those activities.

1.1 Background and Description of Study Area

Madura Strait is located in East Java province, about 1,000 km east of Jakarta (Figure 1), the capital city of Indonesia. The Madura Strait is subject to ocean waves of less than 1 m height due to its position in semi-enclosed Java Sea in Indonesian archipelago. There are 2 major rivers that carry sediment to Madura strait namely Bengawan Solo River and Brantas River. In the last years sediment transport from Brantas river has been increasing significantly through one of its branch namely Porong River.

The development of Suramadu Bridge between Surabaya (at Java Island) and Bangkalan (at Madura Island) contributed to sedimentation pattern in Madura Strait. The shallow bathymetries in major part of Madura Strait threat an environmental problem in the area. Therefore sedimentation model is necessary on attempt to anticipate serious environmental problem in Madura Strait. This study is about mud transport simulation in Madura Strait due to increasing sediment discharge from Porong River. The importance of sedimentation study in this area could be viewed by two reasons. Under the presence of harbour activities on Madura Strait, sedimentation in this area should be studied as the area is surrounded by structures such as turning basin, waterway, and bridge. Another reason is sediment discharge from Porong River that tends to be increased due to mudflow hazard in upstream area.

The Java Sea, where Madura Strait is located, as shown in **Figure 1**, is connected to other seas through the Sunda and Karimata Straits to the west, and Makassar and Flores Sea to the east. The sea is 1,400 km long in the east-west direction and about 400 km wide. The sea is under the influence of two monsoon conditions. In the northern summer months, monsoon winds develop due to airflow from Australia to Asia. The winds over Java Sea are generally northeasterly. This period is referred to as East Monsoon. During the northern winter period winds over Java Sea are generally northwesterly and somewhat stronger than in the east monsoon. The northwest winds period is referred to as the west monsoon and contains the period of high rainfall over Porong catchment and higher wave activity in Java Sea. This area is not subject to

wind fetch in order of thousand, but rather hundreds kilometers. Accordingly under the action of monsoon winds, the north coast of Java is not subject to very large waves.

The study of cohesive sediment (mud) transport and morphology has been carried out since middle of 20th century, e.g Van Straaten and Kuenen (1958), Krone (1962), Waldrop and Farmer (1973). Since that time the process related model to simulate the transport of cohesive sediment and morphology had been studied, e.g Waldrop and Farmer (1973), Christodoulou et.al (1974), Nicholson and O'Connor (1986), and Van Rijn (1987).

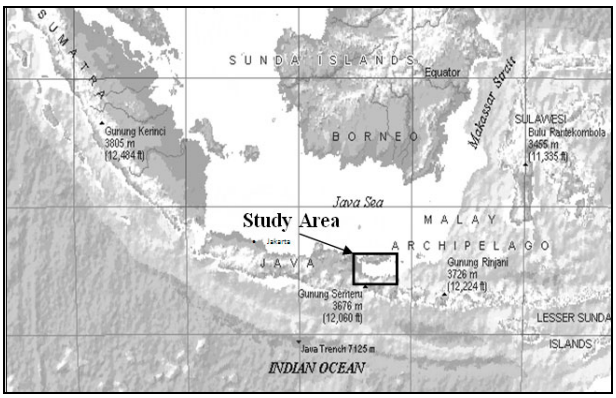


Figure 1 Study area Madura Strait in Java Sea, Indonesia

The publication of sediment transport and morphological simulation using process based models in river mouth areas is few comparing to similar applications in tidal areas, e.g Van Ledden (2003), Lumborg (2004), Ganasut (2005).

In the present study, tidal dynamic process in Madura Strait and sediment pattern around Porong river mouth were analyzed using a mathematical model, MIKE21 HD and MT. In a large extent, the tidal hydrodynamic study of Madura Strait will be useful in management of coastal zone and hazard prevention around the area. The cohesive sediment simulation will be useful for future sedimentation study in Porong river mouth area and would be useful as a reference for similar studies at other locations.

The main objectives of this study were:

a. Perform hydrodynamic and mud transport simulation in Madura Strait area using MIKE-21 HD MT model.
b. Calibration and verification of the hydrodynamics model for water level, velocity and tidal constituents.
c. Calibration and verification of the sediment transport model for suspended sediment concentration and deposition/erosion volume.

1.2 Methodology

Software package MIKE-21 was used in the modeling of Madura Strait. In general, the model were divided to 4 areas due to limited water level data in the boundaries

especially in the offshore area, and limited number of stations with available observed suspended sediment concentration data for calibration and verification of mud transport model. As shown in **Figure 2**, there are three areas for hydrodynamic and mud transport model.

The hydrodynamic simulation was done to provide water level boundary condition in sediment transport simulation in river mouth area. The hydrodynamic model was calibrated for water level and predicted flow velocity.

Given the water level boundaries, the next simulation was for cohesive sediment transport simulation. In this phase, the model results were compared with observed values of suspended sediment concentrations.
The sensitivity analysis was then performed. Several calibration parameters were varied to analyze the effect of each parameter. The significant parameters were identified and used in the analysis of model application results. The model was applied to simulate Porong river mouth development in 2009 - 2010.

II. THEORETICAL CONCEPT

2.1 Hydrodynamics

Using MIKE-21, a software package of 2-Dimensional Horizontal process-based model developed by DHI (2002), the hydrodynamics simulation is done. The Hydrodynamic Module (MIKE-21 HD) is the basic module in the MIKE-21 package. MIKE-21HD Module simulates the water level variations and velocities in response to a variety of forcing functions in lakes, estuaries and coastal areas. The water levels and flows are resolved on rectangular grids covering the area of interest given the bathymetry, bed resistance coefficients, wind field, and hydrographic boundary conditions, etc.

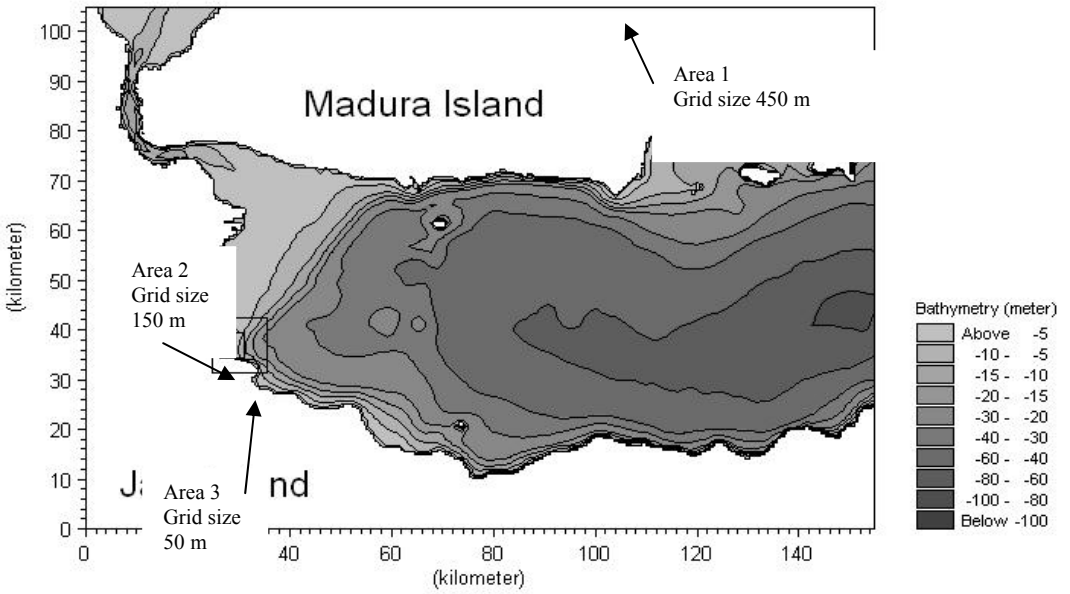


Figure 2 Numerical grid system, bathymetry map and boundaries of model simulation in study area

The hydrodynamic model in MIKE-21 HD is a general numerical modeling system for the simulation of water levels and flows in estuaries, bays and coastal areas. It simulates unsteady 2D flows in one-layer (vertically homogeneous) fluids. Basic principles are conservation of mass and conservation of momentum principles, which lead to continuity, momentum, and advection-dispersion equations. The following equations for the conservation of mass and momentum are integrated over the vertical to describe the flow and water level variations:

Continuity:

$$\frac{\partial \zeta}{\partial t} + \frac{\partial p}{\partial x} + \frac{\partial q}{\partial y} = 0 \tag{1}$$

x-Momentum

$$\frac{\partial p}{\partial t} + \frac{\partial}{\partial x}\left(\frac{p^2}{h}\right) + \frac{\partial}{\partial y}\left(\frac{pq}{h}\right) + gh\frac{\partial \zeta}{\partial x} + \frac{gp\sqrt{p^2+q^2}}{C^2 \cdot h^2} - \frac{1}{\rho_w}\left[\frac{\partial}{\partial x}\left(h\tau_{xx}\right) + \frac{\partial}{\partial y}\left(h\tau_{xy}\right)\right] -$$
$$\Omega p - fVV_x + \frac{h}{\rho_w}\frac{\partial}{\partial x}\left(p_a\right) = 0 \tag{2}$$

y-Momentum

$$\frac{\partial q}{\partial t} + \frac{\partial}{\partial y}\left(\frac{q^2}{h}\right) + \frac{\partial}{\partial x}\left(\frac{pq}{h}\right) + gh\frac{\partial \zeta}{\partial y} + \frac{gq\sqrt{p^2+q^2}}{C^2 \cdot h^2} - \frac{1}{\rho_w}\left[\frac{\partial}{\partial y}\left(h\tau_{yy}\right) + \frac{\partial}{\partial x}\left(h\tau_{xy}\right)\right] +$$
$$\Omega p - fVV_y + \frac{h}{\rho_w}\frac{\partial}{\partial y}\left(p_a\right) = 0 \tag{3}$$

Let denote: x, y = space coordinates (m); t = time (s); h (x,y,t) = water depth (m); ξ (x,y,t) = surface elevation (m); p, q (x,y,t) = flux densities in x-, y-directions (m^3 s^{-1} m^{-1}); p=uh, q = vh; u and v are depth averaged velocities in z- and y-directions; g = acceleration due to gravity (m s^{-2}); f(V) = wind friction factor; V, V_x, V_y, V_y (x,y,t) = wind speed and components in x- and y-directions (m s^{-1}); Ω (x,y) = Corriolis parameter, latitude dependent (s^{-1}); $\Omega = 2\omega\sin(\varphi)$;$\omega$ is angular rotation velocity of the earth and φ is latitude of interested position; p_a (x,y,t) = atmospheric pressure (kg m^{-1} s^{-2}); ρ_w = density of water (kg m^{-3}); τ_{xx}, τ_{xy}, τ_{yy} = components of effective shear stress due to turbulence and viscous effects.

2.2 Sediment Transport

Sediment transport formulations are built into advection-dispersion module, MIKE-21 AD. MIKE-21 solves the so-called advection-dispersion equation:

$$\frac{\partial \bar{c}}{\partial t} + u\frac{\partial \bar{c}}{\partial x} + v\frac{\partial \bar{c}}{\partial y} = \frac{1}{h}\frac{\partial}{\partial x}\left(hD_x\frac{\partial \bar{c}}{\partial x}\right) + \frac{1}{h}\frac{\partial}{\partial y}\left(hD_y\frac{\partial \bar{c}}{\partial y}\right) + Q_L C_L \frac{1}{h} - S \tag{4}$$

Where $\bar{c}$ is depth averaged mass concentration (kg m^{-3}); u, v is depth averaged flow velocities (m s^{-1}); D_x, D_y is dispersion coefficients; h is water depth; S is deposition/erosion term (kg m^{-3} s^{-1}); $Q_L$is source discharge per unit horizontal area (m^3 s^{-1} m^{-2}); and C_L is concentration of source discharge (kg m^{-3}). The bottom shear stress τ_b (N m^{-2}) is calculated with respect to currents and waves using following equation:

$$\tau_c = ½ \rho f_w (U_b^2+U_\delta^2+ 2U_bU_\delta \cos \beta) \quad (5)$$

where ρ is the density of water (kg m^{-3}), f_w is the wave friction factor, U_b is the horizontal mean wave orbital velocity at the bed (m s^{-1}), U_δ is the current velocity at top of water boundary layer (m s^{-1}), and β is the angle between the mean current direction and the direction of propagation (degree).

Formula for sediment deposition was originally proposed by Krone (1962)

$$S_D = w_s C_b p_d \quad (6)$$

Where S_D is deposition rate (kg m^{-3} s^{-1}), w_s is settling velocity (m s^{-1}), C_b is near bed concentration (kg m^{-3}), p_d is probability of deposition which is calculated by

$$p_d = 1-\frac{\tau_b}{\tau_{cd}}, \tau_b \le \tau_{cd} \quad (7)$$

τ_b is bed shear stress (N m^{-2}) and τ_{cd} is critical bed shear stress for deposition (N m^{-2}).

Settling velocity, w_s, described flocculation process. Flocculation is when the concentration of sediment is high enough for the sediment flocs to influence each other settling velocity. The modification of settling velocity also computed due to salinity variation.

$$w_{s,s} = w_s\left(1-C_1 e^{S\cdot C_2}\right) \quad (8)$$

where $w_{s,s}$ is settling velocity due to salinity variation, C_1 and C_2 are calibration parameters and S is salinity. Erosion formula was described as soft partly consolidated sediment (Mehta et al, 1989).

$$S_E = E\exp\left[\alpha(\tau_b-\tau_{ce})^{1/2}\right], \tau_b > \tau_{ce} \quad (9)$$

Where S_E is the erosion rate (g m^{-2}), E is the erosion coefficient, (g m^{-2} s^{-1}), τ_{ce} is critical bed shear stress for erosion (N m^{-2}), and α is coefficient (m $N^{-0.5}$).

III Model Set-up

a. Computational grid and bathymetry

Bathymetrical data of study area was taken from bathymetry data produced by Department of Hydrographic – Indonesia Navy (2003). Bathymetry set-up of model area is shown in **Figure 2**. The largest area (Area 1), that was covered whole Madura Strait, consisted of 344 x 233 cells; each cell is 450 m x 450 m size. The medium-HD area (Area 2) composed by 72 x 72 cells, each cell was 150 m x 150 m size. And the smallest area (Area 3) that covered Porong river area composed by 99 x 99 cells, each cell was 50 m x 50 m.

b. Open sea boundary condition

The water level was prescribed along the open boundary for the model for flow computation. There were 2 open boundaries: Northern and Eastern (**Figure 2**). The Northern and Eastern boundaries were generated using Global Tide Model from MIKE21 Toolbox.

For concentration, the boundary condition, since lack of data it was assumed to be 0.0001 kg m^{-3} (sea water). For the salinity boundary, the boundary condition was taken from MGI data they are equal to 4.0 Practical Salinity Unit.

c. Input Source from river

The river discharge was based on the observed data from the Department of Public Work of Indonesia. The concentration was generated uniformly from MGI data in 2007 1.3 kg m^{-3}. The salinity condition was taken from the data of MGI data it is equal to 0.3 Practical Salinity Unit.

d. Initial Condition

The initial water surface was equal to 0 m MSL. The initial concentration was equal to 0.0 kgm^{-3}

e. Parameter Setting

- Water Column Parameters. The settling velocity depends on flocculation condition with flocculation parameters. The concentration that mud starts flocculation was 0.01 kg m^{-3}. The concentration for hindered settling was 10 kg m^{-3}. The sediment density is 2650 kg m^{-3}.
- Calibration factors. The dispersion coefficient, the critical bed shear stress for deposition, the critical bed shear stress for erosion and the erosion coefficients were initially assumed and adjusted by trial and error.

IV Calibration

In this study, the simulation considers uniform bed resistance (Manning), In this case bed roughness, $k_{s,}$ was calibrated in order to get good agreement between the computed and observed water levels and velocity at the calibration stations. The agreement between the computed and observed water level was presented by the error. Location of calibration stations is presented in Figure 3. There are 5 points namely Karang Jamuang, Surabaya, Karang Kleta, Kali Porong and Pulau Kambing. The best result is obtained in Surabaya station data, as presented in Figures 4 and 5 with error RMS 0.09.

Calibrated model then used to simulate hydrodynamics and mud transport simulation in 1 year period, from July 2008 to July 2009. Results are presented in Figures 6 up to 8. Velocity distribution is presented in Figure 6, figure 6 a) presents velocity distribution for the larger area (area 1) and figure 6 b) presents velocity distribution in Porong river mouth. As presented in Figure 6a), There are 5 study points, P1 and P2

located at the western part of Madura Strait which commonly known as Surabaya Strait, P3 is located nearby Porong river mouth and P3 and P4 are located in the main part of Madura Strait. From visual observation and reference (Tanaka and Ishida, 1999), water movement in Madura Strait have different phase. This phenomenon is due to bathymetry and strait configuration. When water is high in the Java Sea, water enters Madura Strait from P1 and P5, and meet center of Strait, around P3. In this case, water movement is consistently different for western and eastern part of Madura Strait. The other aspect is, type of tidal at the Java Sea near P1 is mixed dominant to diurnal tide, while in the Madura strait mostly affected by semidiurnal tide. Hence the water level movement is not similar. To show this occurrence, computed water level for P3, P4 and P5 are presented in Figure 7.

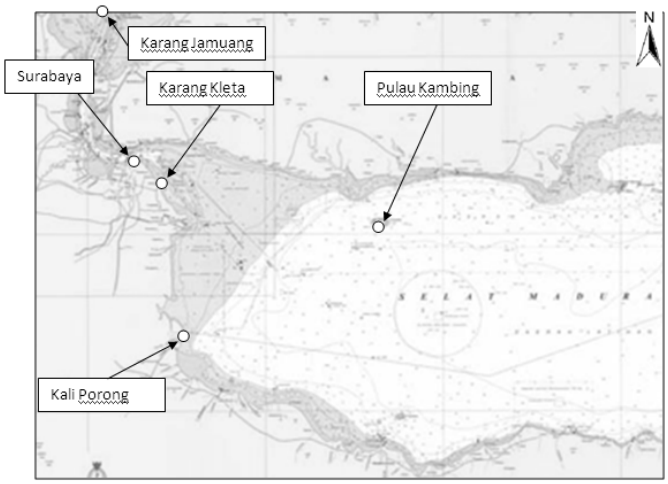


Figure 3 Location of calibration stations

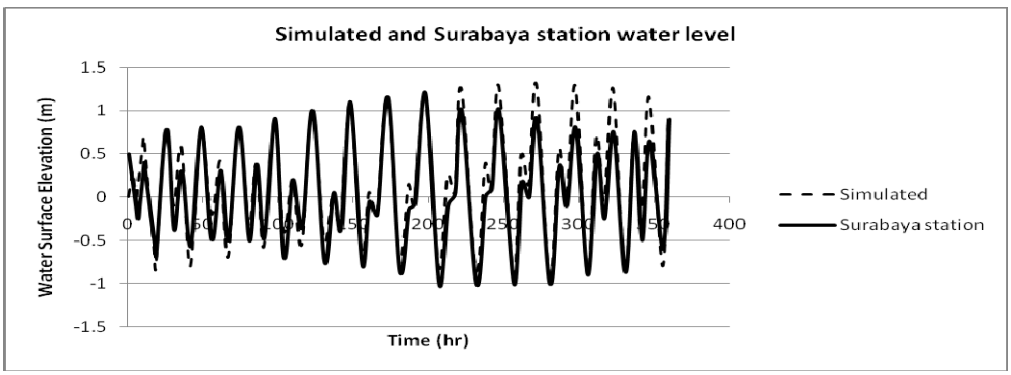


Figure 4 Comparison of observed and simulated water level at Surabaya station

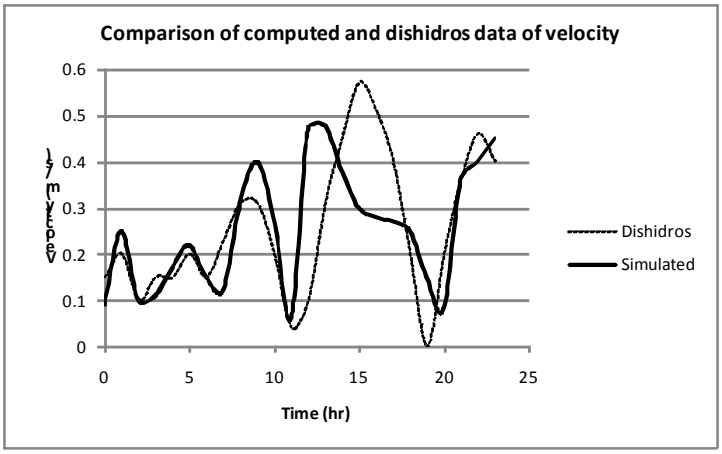


Figure 5 Comparison of observed and simulated flow velocity at Surabaya station

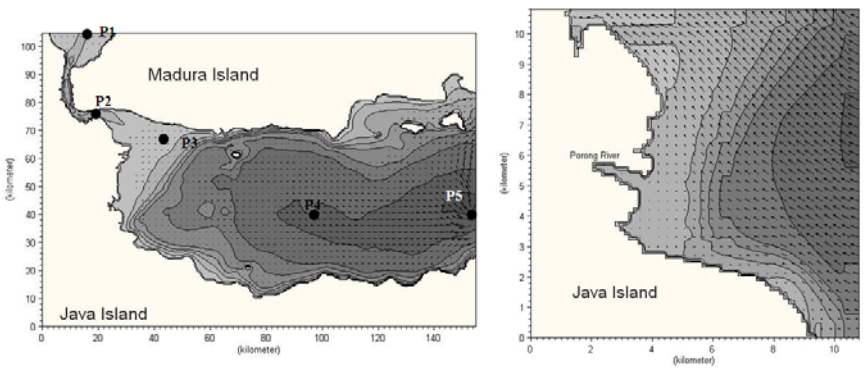


Figure 6 Velocity distribution a) At Madura Strait (area 1), b) At Porong river mouth (area 2)

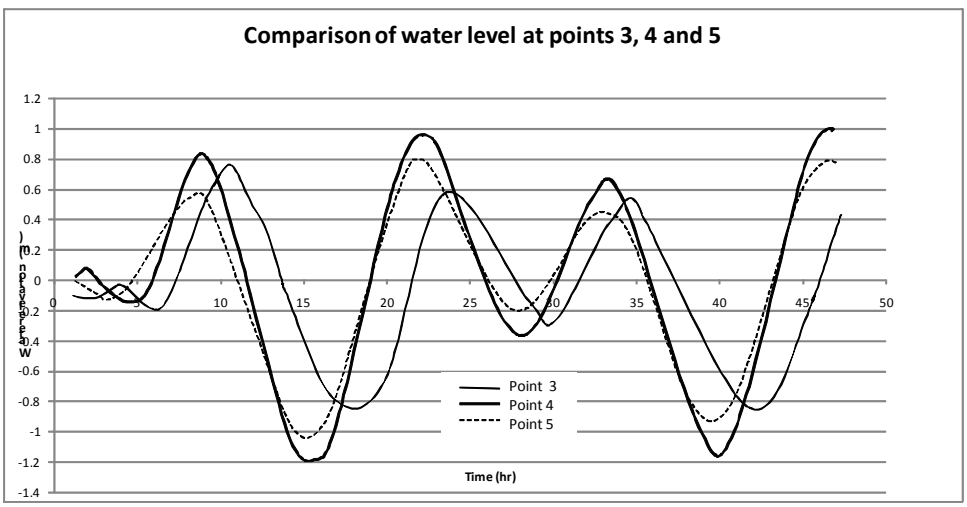


Figure 7 Computed water level at study points P3, P4 and P5

V Sensitivity Analysis

After model calibration step, sensitivity analysis was performed to analyze the sensitivity of several model parameters in particular to their effects on suspended sediment concentration distribution and changes of deposition volume. The period of analysis was 2 months 1 July – 1 September 2009. Results are presented in Figures 8.

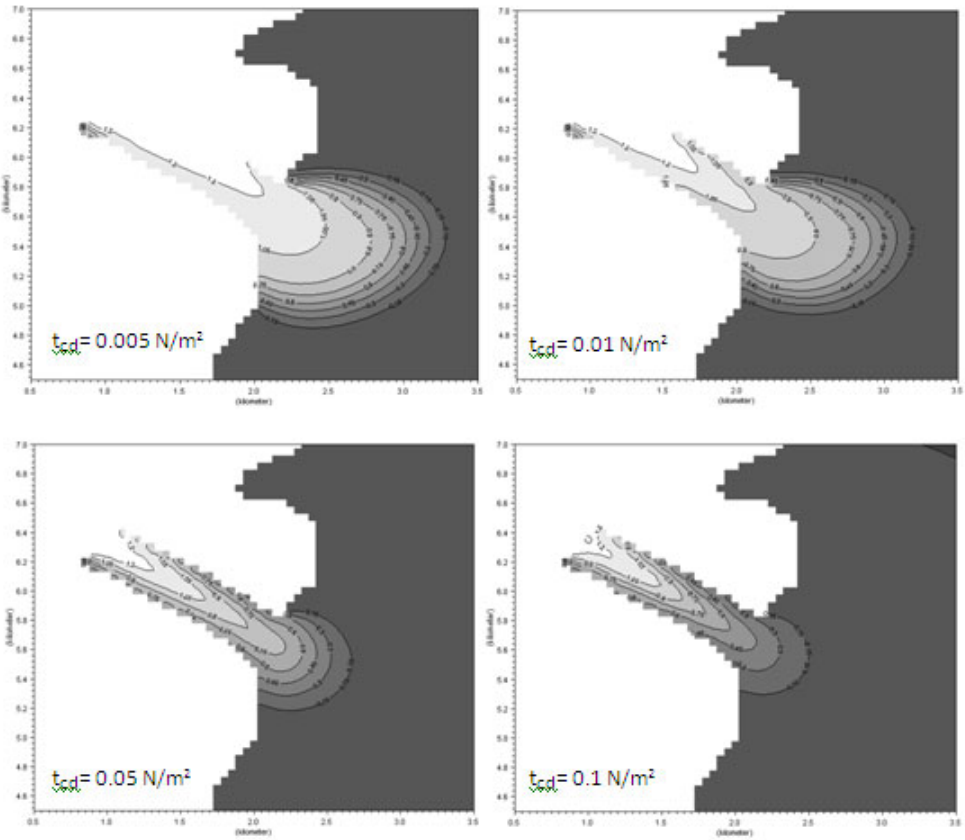


Figure 8 Sensitivity analysis by analyze volume of deposition with various number of critical shear stress of deposition

In sensitivity analysis, the following parameters were varied namely critical bed shear stress for deposition, critical bed shear stress for erosion, erosion coefficient, suspended sediment concentration at river boundary, suspended sediment concentration at sea boundary and initial suspended sediment concentration. The suspended sediment concentration distribution and volume of deposition were compared to analyze their changes. From the analysis, parameters that give significant changes are critical bed shear stress for deposition, critical bed shear stress for erosion and suspended sediment concentration at the river effluent boundary.

Sensitivity analysis on the effects of critical bed shear stress for deposition was done considering τ_{cd} = 0.005 Nm^{-2}; τ_{cd} = 0.01 Nm^{-2}; τ_{cd} = 0.05 Nm^{-2}; and τ_{cd} = 0.1 Nm^{-2}. It was noted that the τ_{cd} = 0.05 Nm^{-2} was the selected parameter value in the

calibrated model. It was found that the critical bed shear stress for deposition had insignificant effect on the computed suspended sediment concentration but it had a significant effect on the deposition volume in the river river.

Sensitivity analysis on the effects of critical bed shear stress for erosion was done considering τ_{ce} = 0.0075 Nm^{-2}; τ_{ce} = 0.015 Nm^{-2}; τ_{ce} = 0.075 Nm^{-2}; and τ_{ce} = 0.15 Nm^{-2}. It was noted that the τ_{ce} = 0.15 Nm^{-2} was the selected parameter value in the calibrated model. It is found that the critical bed shear stress of erosion had insignificant effects on the computed suspended sediment concentration but it had significant effect on the deposition volume in the river mouth.

From sensitivity analysis it was concluded that the most important input model is input from river, especially suspended sediment concentration. Important parameters of model are critical shear stress of deposition and critical shear stress of erosion.

Critical bed shear stress for deposition is physically explained as initial shear stress at the beginning of deposition, this is very important as it is mainly related to deposition. The values of τ_{cd} were found to be in the range of 0.083- 0.11 Nm^{-2} for Bandon Harbour, Surat Thani, Thailand (Lee, 1974), while Mehta (1984) found the value of τ_{cd} for San Francisco Bay mud, USA and Maracaibo estuary mud, Venezuela to be 0.10 Nm^{-2} and 0.08 Nm^{-2} respectively. Winterwep et al. (1991) found the value of τ_{cd} were in the range of 0.03- 0.15 Nm^{-2} for various natural muds from lakes, rivers and estuaries in the Netherlands. Van Ledden (2003) performed the sand-mud simulation in the Friesche Zeegat, a tidal basin in Dutch Wadden Sea, Netherland and found τ_{cd} equal to 0.15 Nm^{-2}. Lumborg (2004) used values of τ_{cd} in the range of 0.02 – 0.04 Nm^{-2} in modeling cohesive sediment transport in Lister Dyb tidal area in Danish Wadden Sea, Denmark. Ganasut (2005) found the similar value with Winterwep et. al (1991) for mud transport simulation in Songkhla Lagoon, Thailand. The value of τ_{cd} in this study is found to be 0.05 Nm^{-2}.

The critical value of bed shear stress for erosion depends on the bed material characteristics such as mineral composition, organic materials, salinity, and density. Erosion of cohesive soil occurs whenever the bed shear stress induced by water flow over the bed is high enough to break the electrochemical inter-particle bonds. The surface erosion takes place by the removal of individual sediment particles. In contrast, mass erosion occurs more or less instantaneously by the removal or entrainment of relatively large pieces of soil, occurring when the flow induced shear stresses on the bed exceeds the soil bulk strength. In the studies covering erosion of natural muds from lakes, rivers and estuaries in the Netherlands, Winterwerp et al. (1991) found that a top layer was eroded by surface erosion at bed shear stresses in the range of 0.15 - 0.30 Nm^{-2}. Ravens (1999) found the value of τ_{ce} in the range of 0.1 ± 0.04 Nm^{-2} in Quincy Bay of Boston Harbor, Massachusetts, USA. Van Ledden (2003) did sand-mud simulation in the Friesche Zeegat, a tidal basin in Dutch Wadden Sea, Netherland and found τ_{ce} equal to 0.5 Nm^{-2}. Lumborg (2004) use values of τ_{cd} in the

range of 0.1 – 0.7 Nm^{-2} in modeling cohesive sediment transport in Lister Dyb tidal area in Danish Wadden Sea, Denmark. Ganasut (2005) applied τ_{ce}, in a range of 0.1 to 0.3 Nm^{-2}.

Selection of critical bed shear stress for deposition and bed erosion is important task in sediment transport modeling. There was a range of critical bed shear stress for deposition and erosion values, which was sensitive in the study area. The bed shear stress distribution and sedimentation condition in the study area was strongly related to hydrodynamic condition e.g. boundary condition and the characteristics of the tides semidiurnal and diurnal.

VI. Results and Discussion

The calibrated model of hydrodynamic and mud transport was used to simulate flow and sediment pattern from July 2009 – July 2010. Results are presented in Figures 11 – 13.

From the simulation, it was found that the amount of deposition and bed thickness was in relation with the value of sediment from river. Hence in time when the sediment source from the river was decreased or increased, the amount of deposition was also decreased or increased in the same order respectively. This result is consistent with the characteristic of river mouths as described by Van Rijn (1998).

From the simulation it was showed that the deposition occurs in most of the river mouth area with bed level changes of not more than 0.25 m. In general, based on the simulation results, the model had successfully simulated sedimentation in the river mouth area. Sediment flux from river into the estuary is fluctuated due to tidal dynamics and river discharge. In the river area where tidal effect is small the sediment is transported as bed and suspended load. The velocity is decreased when the flow enters the estuary and it increases further with respect to tidal condition (from tidal boundary). Coarser sediment deposits near the river mouth when it just enters the estuary. Finer materials are formed in suspension; it may deposit during periods of neap water or transport in suspended form. With effect of salinity, suspended particles tend to bind each other and form heavier flocs particles, which may settle and deposit in the region of low flow velocity. Based on this simulation, sediment discharge from Porong river to Madura Strait affected area about 4 km from river mouth.

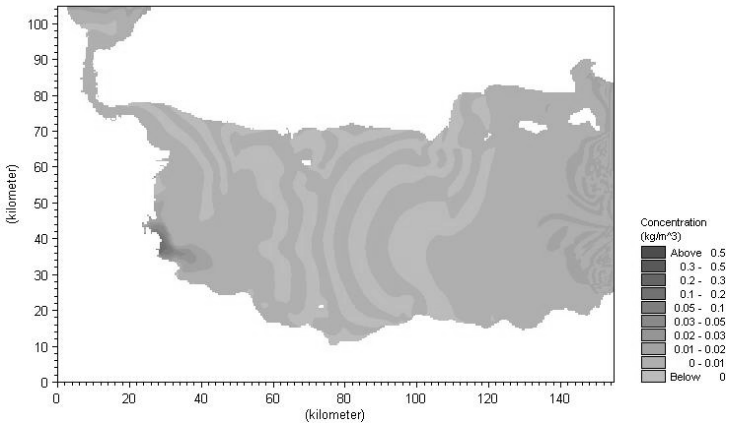


Figure 9 Computed sediment concentration on Madura Strait (area 1) after 1 year period simulation

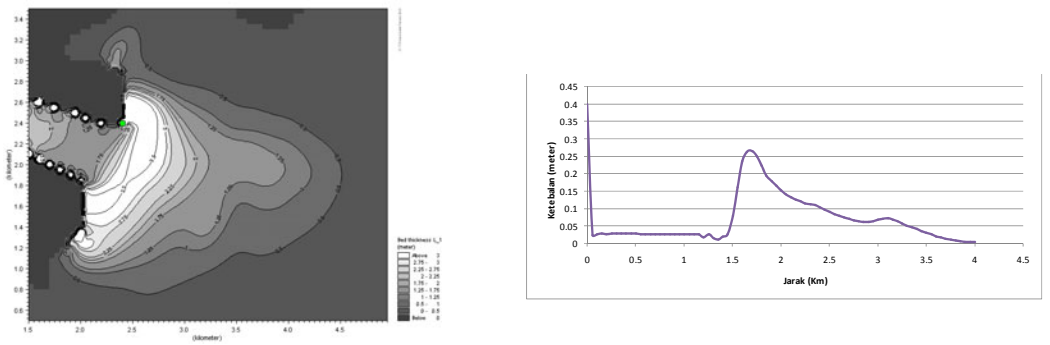


Figure 10 Computed bed thickness changes on Porong river mouth after 1 year period simulation a) plan view b) cross section from river to sea

V. CONCLUSIONS

The numerical model of river mouth development is a considered the most promising approach in river mouth area planning and management. The Porong river mouth was selected as a study case because the catastrophic phenomenon of mudflow from Lapindo area that was discharged to Porong river.

A study on hydrodynamics and morphological simulation in Madura Strait had been done with the main purpose to investigate the hydrodynamic condition in Porong river mouth area and how it affected Madura Strait as general. Calibration of the hydrodynamic model namely the MIKE-21 HD had been done successfully. Sediment transport simulation was performed in the river mouth area using MIKE-21 Mud Transport module, which takes into account sediment flocculation and salinity variation. The model considered only suspended sediment transport, because of most of sediment load in the river that deposited to estuary is fine suspended load. Inputs from the river were discharge and suspended sediment concentration. Boundary conditions at the surrounding sea are water level, suspended sediment concentration and salinity. Sea water levels are generated using Admiralty method with astronomical

constituents based on co-tidal chart in the river mouth area. Calibration and verification parameters were dispersion coefficient, critical bed shear stress for deposition, critical bed shear stress for erosion, and erosion coefficient.

This study presents procedures in modeling sedimentation in river mouth using a 2-dimensional horizontal model that can be used to analyze sediment transport in river mouth areas. From the results it is concluded that current mudflow from Porong river is not give significant effect to sedimentation problem at Madura Strait.

VI. ACKNOWLEDGEMENTS

This study was a part of research that received financial support sponsored by Program Hibah Kompetensi berbasis Institusi – DIKTI (SK 011/PHKI/BT-I/SKP-TG/2010), Ministry of Education Indonesia. The authors would like to express their grateful acknowledgement to Marine Geological Institute who provides numerous data for this research.

REFERENCES

[1] Christodoulou, G.C., Leimkuhler, W.F., and Ippen, A.T. (1974). "Mathematical Model of the Massachusetts Bay Part III, A Mathematical Model for the Dispersion of Suspended Sediments in Coastal Waters", *MIT Report* No. 179.

[2] Danish Hydraulic Institute (DHI). (2002). User Guide and reference manual of MIKE-21 – Coastal Hydraulics and Oceanography hydrodynamic module, Danish Hydraulic Institute.

[3] Danish Hydraulic Institute (DHI). (2002). *Mud transport Module – Scientific Documentation*, Danish Hydraulic Institute.

[4] Department of Hydrographic. (2003). *Tidal Book 2003*, Indonesian Navy.

[5] Ganasut, J. (2005). "Sediment Transport And Morphological Modeling of Songkhla Lagoon, Thailand"*, Dissertation*, Asian Institute of Technology.

[6] Krone, R.B. (1962). "Flume Studies of The Transport of Sediment in Estuarial Processes", Hydraulic Engineering Laboratory and Sanitary Engineering Research Laboratory, Univ. of California, Barkeley, California, *Final Report*.

[7] Lee, P.T. (1974). "Deposition and Scour of Clay Particles due to currents"*, Thesis* no. 650, Asian Institute of Technology, Bangkok, Thailand.

[8] Lumborg, U. (2004) "Cohesive sediment transport modeling – application to the Lister Dyb tidal area in the Danish Wadden Sea"*, Journal of Coastal Research, Special Issue 41*, pp 114-123.

[9] Mehta, A. J., and Joshi, P. B. (1984). *Review of Tidal Inlet Hydraulics, UFL/COEL-TR/054*, Coastal and Oceanographic Engineering Department, University of Florida, Gainesville, FL.

[10] Mehta, A. J., Hayter, E. J. Parker, W. R., Krone, R.B. and Teeter, A. M. (1989). "Cohesive Sediment Transport", *Journal of Hydraulic Engineering*, Vol. 115, No.8, pp. 1076-1112.

[11] Nicholson, J. and O'Connor, B. A. (1986). *"*Cohesive Sediment Transport Model", *Journal of Hydraulic Engineering, ASCE*, Vol. 112, No.7, pp. 621-640.

[12] Ravens, T.M. and Gschwend, P.M. (1999). "Flume Measurements of Sediment Erodibility in Boston Harbor", *Journal of Hydraulic Engineering, ASCE*, Vol. 125, No.10, pp. 998-1085.

[13] Tanaka , S. and Ishida, T. (1999). "Flow Pattern and Sedimentation of Madura Strait Using Remortsensing Sattelite Data", Hydraulic Modeling: Proceedings of the International Conference on Water, Environment, Ecology, Socio-economics and Health Engineering, Korea.

[14] Van Ledden, M. (2003). Sand-mud segregation in estuaries and tidal basins, Communications on Hydraulic and Geotechnical Engineering – Delft University of Technology.

[15] Van Rijn, L.C. (1987). "Mathematical Modeling of Morphological Processes in the Case of Suspended Sediment Transport", *Thesis* approved by the Delft University of Technology, Delft Hydraulics Communication No. 382, Delft, the Netherlands.

[16] Van Straaten, L.M.J.U. and Kuenen, Ph. H. (1958). "Tidal action as a cause of clay accumulation"*, Journal of Sedimentary Petrology*, Vol 28, pp 406-413.

[17] Waldrop, W.R. and Farmer, R.C. (1973). "Three-Dimensional Flow and Sediment Transport at River Mouths", *Technical Report* No. 150, Coastal Studies Institute, Louisiana State University, Baton Rouge, Louisiana.

[18] Winterwerp, J.C., J.M. Cornelisse and C. Kuijper. (1991). "A laboratory study on the behavior of mud from the Western Scheldt under tidal conditions, Nearshore and estuarine cohesive sediment transport", *Workshop*, St. Petersburg, Florida, pp. 295-313.

Numerical modeling of Wind-waves and its Effect on Sediment Transport – An Investigation of Spectral Terms

S. K. Khatri[1] and I.R. Young[2]

[1]Civil Engineering, Santa Clara University, 500 El Camino Real, Santa Clara, CA 95053, U.S.A., PH 408- 554-2334, FAX 408-554-5474, email: skhatri@scu.edu

[2] Vice Chancellor, Australian National University, Canberra ACT 0200, Australia, Swinburne University of Technology, PH +61 2 6125 2510, FAX +61 2 6257 3292, email: vc@anu.edu.au

ABSTRACT:

The interaction between wind waves and sediment movement at shores is a complex process, and its understanding is important. An accurate wave forecasting can result in better estimates of sediment movement along beaches. In addition, it will provide opportunities for improved planning and taking appropriate safety measures against the extreme events.
A number of numerical models for wind-wave prediction are available which use inherent physics for wind-wave evolution. These models perform better for deep water predictions but still lack full understanding of balance of sources terms in finite water depth. An enhanced understanding of these terms will result in better estimation of sediment transport on beaches.
The present study provides increased insight into the variation of two important source terms; non-linear wave-wave interactions and bottom friction which have significant effect on sediment transport. The non-linear wave-wave interactions have positive and negative signature and is the least understood term in wind-wave evolution. The bottom friction is always negative and withdraws energy from the spectrum. Thus, this study has provided better understanding of these two terms, and shows that together these affect the development of peak of the spectrum and hence wave energy. Consequently, because of their importance it will affect sediment balance at the shore.

DESCRIPTION OF THE MODEL:

The understanding of ocean wave dynamics plays an important role in understanding the effects of waves on the processes and structures affected by these; the examples include, design of on-shore and off-shore structures, on-shore and off-shore sediment transport (thus beach dynamics) and extreme events such as hurricanes, coastal flooding and others.

Wind-wave modeling is an important component of such studies. It provides an excellent tool for hindcasting as well as predicting wave conditions as a future event in time and space. The suitable representation of physical processes responsible for wave growth and numerics of the model contribute towards obtaining better

prediction of wave heights. The wind-wave generation being a complex process is difficult to express mathematically due to many uncertainties inherent in the complex nature of these physical processes. The "first and second generation models", normally those developed during 60s and 70s, depend upon adhoc assumptions on the shape of wave spectra and the empirical form of the processes represented. However, this has largely changed because of an increase in the understanding of the processes contributing to wave growth and the computer power that is available today. The development of third generation wave models [WAM (12), WAVEWATCH (18) and SWAN (1)] have contributed towards better understanding of wind-wave development, and are in use since considerable time for wave forecasting and operational purposes.

The above models have been reasonably successful in operational predictions in various parts of the world. However, there has always been a need for the better and sound representation of the physical processes, particularly the nonlinear wave interactions. In the case of WAM, this has been achieved by using Discrete Interaction Approximation (DIA) which is a better representation than the earlier approaches; however, it uses a selected number of wave number combinations. Hence, the need to include more dynamic representation of this term [24]. One of such attempt was done by [9] in the form of EXACT-NL model. The model in its original form was only able to run on CRAY computers and for deep water only. In the present study, the model has been successfully modified to include applications in finite water depth and to run on workstations. The model is applicable for both deep and finite water depth. The essential parts of this model are:

Radiative Transfer Equation:

The wave growth in terms of space and time is often expressed in the form of radiative transfer equation [7, 20]. In this equation the terms on left hand side represent evolution of spectrum which is equated to the summation of all terms that contribute to it. Mathematically, it is written as:

$$\frac{\partial E(f,\theta)}{\partial t} + C_g \frac{\partial E(f,\theta)}{\partial x} = \sum S \qquad (1)$$

where C_g is the group velocity and $E(f,\theta)$ is spectral energy in frequency (f) and direction (θ) domain. "S" represents source terms which include wind input (S_{in}), white cap dissipation (S_{ds}), nonlinear wave interactions (S_{nl}) and bottom friction (S_{bf}) for finite water depth conditions.

Wind Input:

For wind waves, wind blowing over the water surface plays an important role in their growth; it is a positive term and adds energy to the system. A number of parametric forms are used to model wind input term in wave prediction models; these include those proposed by [10, 16, and 17] among others. This term is mostly expressed as a

function of inverse wave age and spectral energy. The modified EXACT-NL model uses the form proposed by [16] and is written as:

$$S_{in} = \max\left[0, 0.025\frac{\rho_a}{\rho_w}\left(\frac{U_{10}}{C_p}\cos\theta - 1\right)\omega E(f,\theta)\right] \qquad (2)$$

where ρ_a and ρ_w are the air and water densities respectively, C_p is the phase speed of waves, U_{10} the wind speed at a height of 10 m and $\omega = 2\pi f$.

White Cap Dissipation:

White cap dissipation represents a negative term that withdraws energy out of the system. Waves loose energy by formation of white caps and it is represented in wave models as a dissipative process. It is normally expressed in a linear form and for the present model a form proposed by [13] is used:

$$S_{ds} = -C\bar{\omega}\left(\frac{\omega}{\bar{\omega}}\right)^n\left(\frac{\alpha}{\alpha_{PM}}\right)^m E(f,\theta) \qquad (3)$$

where *m, n* and *C* are constants; usually a value of 2 is assigned to *m* and *n*, and *C* is equal to $3.33\text{x}10^{-5}$. Further, ω is an integral wave steepness parameter and $\alpha_{PM} = 4.57\text{x}10^{-3}$ which is theoretical value of α for a Pierson-Moskowitz spectrum [14].

Non-linear Wave-Wave Interactions:

It is this source term which is complex in nature and requires considerable mathematical and computer effort for computation. Normally it is expressed in the form of Boltzmann integral given by [6] and is written as:

$$S_{nl} = \omega\iiint \begin{array}{l} G(k_1,k_2,k_3,k_4)\times\delta(k_1+k_2-k_3-k_4) \\ \times\,\delta(\omega_1+\omega_2-\omega_3-\omega_4)\times \\ [n_1n_3(n_4-n_2)n_2n_4(n_3-n_1)]dk_1dk_2dk_3 \end{array} \qquad (4)$$

where $n_i = n(k_i)$ is the action density, k_i represent interacting wave numbers and $G(k_i)$ is the strength of interactions.

Bottom Friction:

In finite water depth, the waves come in contact with the ocean bottom and thus loose energy due to friction. It is this region which is also important for study of sediment transport. The expression proposed by [3] has been used in the model, and is written as:

$$S_{bf} = -\frac{C_f}{g^2}\frac{\omega^2}{\sinh^2 kd}E(f,\theta) \qquad (5)$$

where C_f is a friction coefficient that varies with the bed conditions and d is the water depth.

WAVE MODELING AND SEDIMENT TRANSPORT:

Sediment movement on and off-shore takes place at the beaches and is directly related to the nature of waves and thus the physical processes affecting the wave development in finite water depth. This effect has been modeled through COAWST model developed at USGS [21, 22] which combines atmospheric model, wave prediction model (SWAN) and sediment transport model to study the sediment transport. Although, this model uses complex and well established models currently in use but does not shed any light on the effect of various sources terms that contribute to the wave growth on the sediment transport.
Hence, it is this need that has provided an initiative to carry out the present study. The current study was carried out to investigate the effect of various source terms on the development of wind-wave spectrum. However, it also provides useful insight for the sediment transport in the coastal regions.

EXPERIMENTAL STUDY:

In order to verify the predictions of current wave prediction model, it has been validated against the experimental studies carried out at the Lake George [23, 24, and 25].

The wave growth under fetch limited condition ignoring depth limited conditions has been extensively studied, with well-known measurements reported by [5, 8] among others. Although attempts for such measurements in finite water depth have been made in past, notably those of [2, 4], however, the former was mainly concentrated on finding the depth limited asymptotes rather than providing insight on the evolution along fetch. The latter study although performed with more sophisticated instruments, but was based on measurements at a single location, and hence does not represent true fetch limited conditions.

Hence, an in-depth and well planned wave measurement study in finite water depth was carried out at Lake George [23, 24, and 25]. The purpose of this study was to provide reliable and truly fetch-limited wave growth results.

The above study reported empirical formulae for wave energy and peak frequency. The second part of this experiment has recently been completed with the aim of measuring the source term balance of wind-wave evolution. The formulae suggested in first study for energy and peak frequency growth are applicable both for deep and finite depth wind waves and were found in good agreement with the relationships proposed for deep water in Shore Protection Manual [15]. The non-dimensional relationships used are:

$$\varepsilon = g^2 E / U_{10}^4, \quad \chi = gX / U_{10}^2$$

$$\delta = gd / U_{10}^2, \qquad \nu = f_p U_{10} / g \tag{6}$$

where χ, ε, ν, and δ are non-dimensional fetch, energy, peak frequency and water depth respectively. X is fetch, E spectral energy, d water depth, f_p peak frequency and U_{10} wind speed at a height of 10 m.

According to this study, the non-dimensional energy (ε) is given as:

$$\varepsilon = 3.64\times10^{-3}\left\{\tanh A_1 \tanh\left[\frac{B_1}{\tanh A_1}\right]\right\}^{1.74} \tag{7}$$

where

$$A_1 = 0.493\delta^{0.75}, \quad B_1 = 3.13\times10^{-3}\chi^{0.57} \tag{8}$$

and non-dimensional peak frequency (ν) is expressed as:

$$\nu = 0.133\left\{\tanh A_2 \tanh\left[\frac{B_2}{\tanh A_2}\right]\right\}^{-0.37} \tag{9}$$

where

$$A_2 = 0.331\delta^{1.01}, \quad B_2 = 5.215\times10^{-4}\chi^{0.73} \tag{10}$$

It was shown that when plotted, a family of curves of ε versus χ for different non-dimensional water depths (δ) were obtained. These curves showed a behavior similar to deep water at short non-dimensional fetches, however, they grow as χ increases reaching an asymptotic level for each non-dimensional water depth. A similar behavior was observed for variation of peak frequency i.e. the variation of ν versus χ resulting in different curves for each non-dimensional water depth.

During the same study, the role of bottom friction in development of wind waves was further discussed in detail. It was argued that although the bottom of Lake George consists of mud with no bed movement (no ripple formation), but the results of this study were in close agreement with the previous formulations presented by [4] and [19]. Hence, it was speculated that the active wave generation might not be affected by the bottom conditions and the results could be applicable universally.

COMPARISON BTWEEN MODEL AND EXPERIMENTS

Non-dimensional Energy against Non-dimensional Fetch

Figure 1 shows a plot of non-dimensional energy versus non-dimensional fetch for non-dimensional water depths, δ equal to 1.0, 0.8 and 0.6. The model results are compared with the curves obtained for same parameters from the expressions

proposed in Lake George experimental study [23]. Also shown is the curve for JONSWAP [8] for deep water as well as Pierson-Moskowitz limit [14] for fully developed wave spectrum. The plot shows that both model and experimental studies are in reasonable agreement particularly at short fetch. As the non-dimensional water depth δ increases, the curves progressively reach close to deep water results.

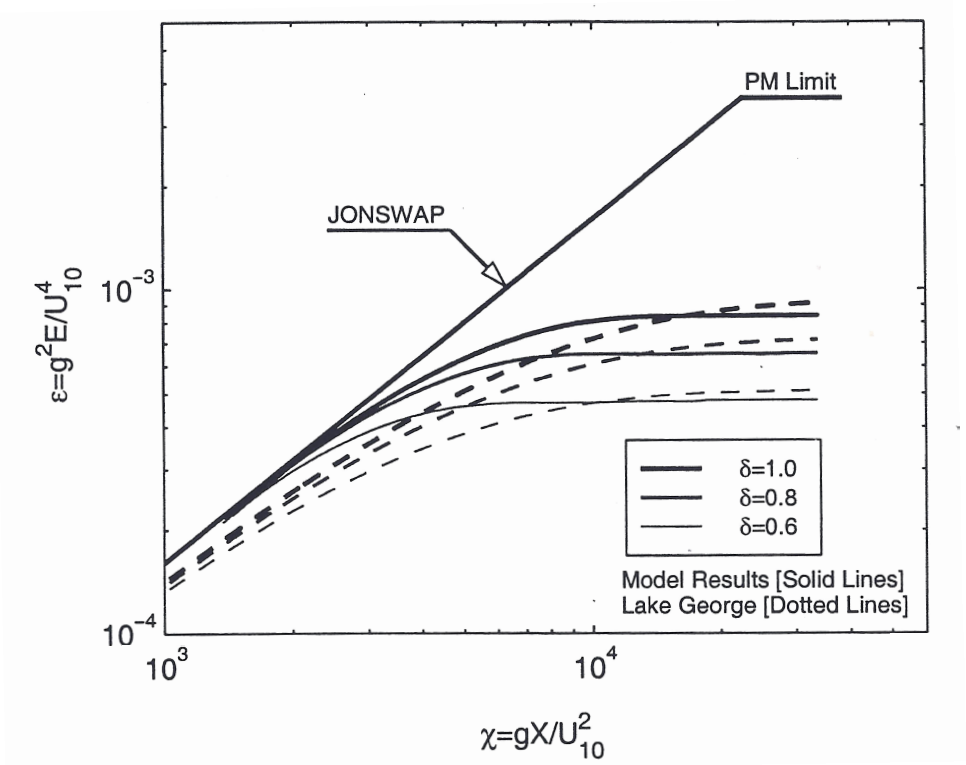


Figure 1: A comparison of non-dimensional growth curves obtained from the model and experimental study of Lake George [Young and Verhagen (1996a)] for different values of non-dimensional water depth, δ. The results for deep water study of JONSWAP [Hasselmaan et al. (1973)] and Pierson-Moskowitz (1964) for a fully developed spectrum are also shown.

Non-dimensional Peak Frequency against Non-dimensional Fetch

Figure 2 shows a plot of non-dimensional frequency ν against non-dimensional fetch χ for various values of non-dimensional water depth, δ. The results from model are compared with the results obtained from the proposed relationship in Lake George experimental study. Also shown is the curve obtained form the relationship proposed by Kahma and Calkeon (1992) together with the Pierson-Moskowitz limit for fully developed spectrum. It can be seen that both model and experimental results are in good consistency and as the non-dimensional water depth δ increases, the curves progressively get closer to the deep water curve of Kahma and Calkeon and towards PM value for fully developed spectrum.

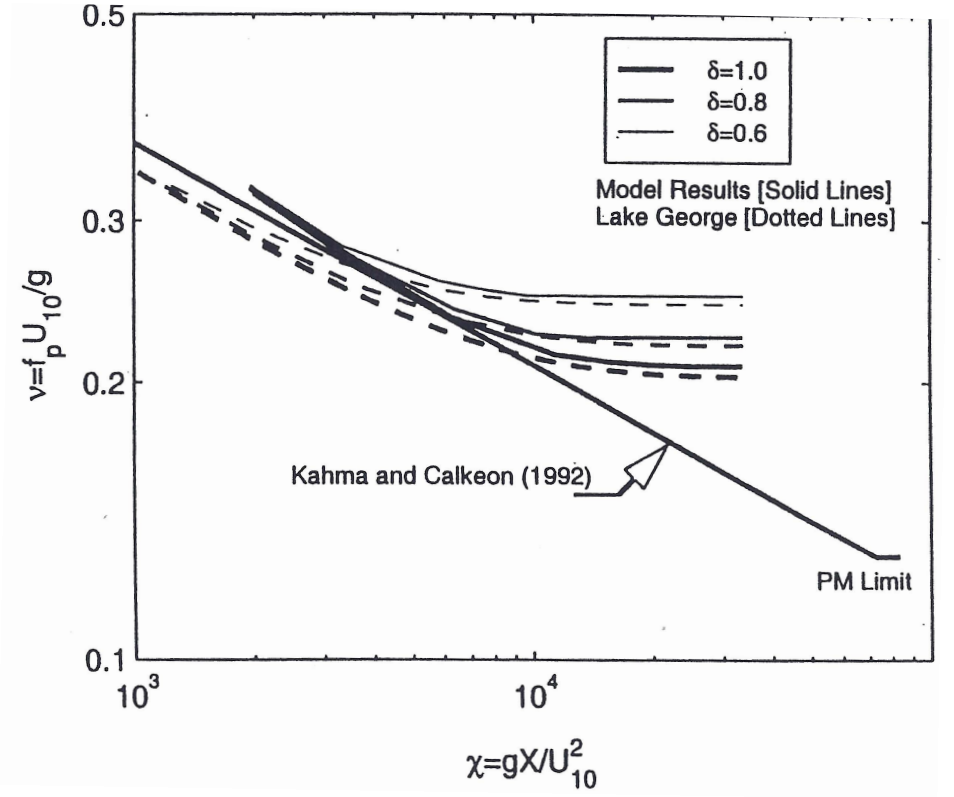


Figure 2: A comparison of peak frequency curves from the model and experimental study at Lake George [Young and Verhagen (1996a)] for different values of non-dimensional water depth, δ. Also are shown the deep water results using Kahma and Calkoen (1992) relationship and the Pierson and Moskowitz (1964) limit for a fully developed wave spectrum.

SOURCE TERM VARIATION AND SEDIMENT TRANSPORT:

Variation of Bottom Friction Term

As the waves enter water of finite depth, orbital velocities increase and energy is lost through bottom friction. The extent of energy loss is dependent upon the type of bed material and the bed geometry. A variation of bottom friction for deep water and different non-dimensional water depths is shown in figure 3. This figure clearly shows that the magnitude of the bottom friction increases with the decrease in non-dimensional water depth, δ which is due to the increased interaction with the bed as the water depth decreases. It is further observed that the bottom friction is mainly concentrated around the peak of the spectrum. The inherent observation form this behavior is that the sediment movement will decrease in water of finite depth. However, the type of bottom material and friction are inter-related and hence amount of sediment transported will be a function of both terms.

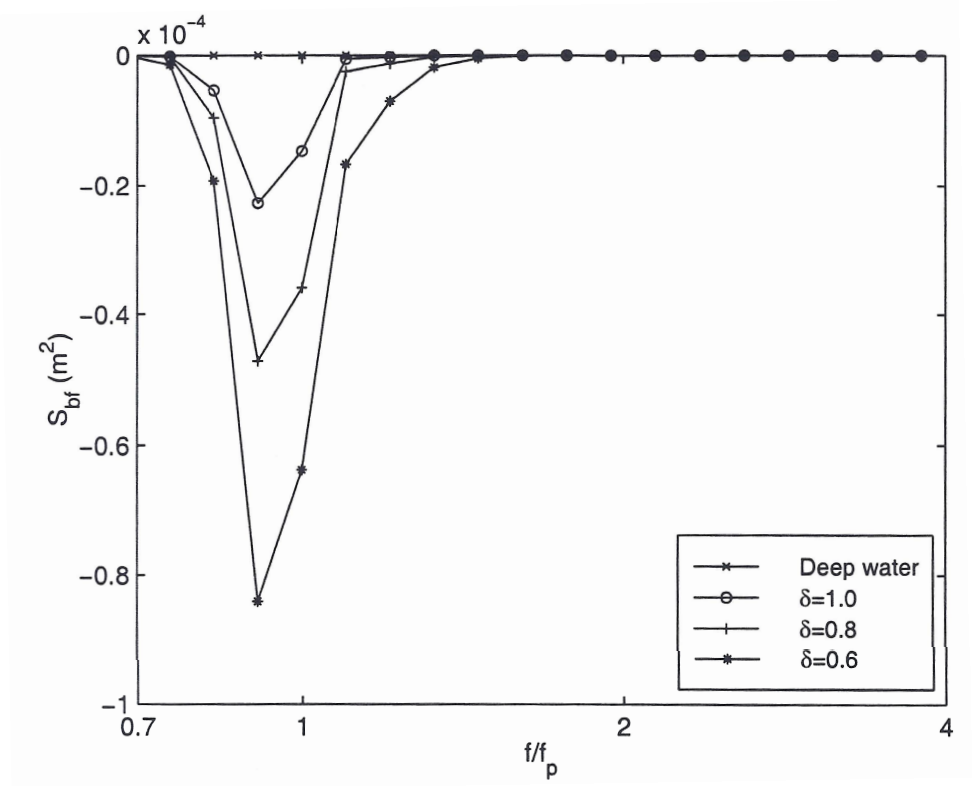


Figure 3: Variation of the bottom friction term, S_{bf} as a function of f/f_p (f_p is the frequency of the peak of the spectrum). A comparison between deep water and different non-dimensional water depths, δ is shown.

Variation of Non-linear Wave Interaction Term

Figure 4 shows the variation of non-linear wave-wave interaction term that plays a significant role in development of wind wave spectrum. The figure clearly shows that S_{nl} has two prominent lobes, one positive and other negative under all water depth conditions. The magnitude of both positive and negative lobes decrease with the decrease in water depth. The position of both lobes remain largely unchanged for $\delta > 0.6$. However, for $\delta = 0.6$, the lobes become broader indicating its effect on broader range of frequencies. This translates into two-dimensional energy growth and the positive lobe indicates clearly that even in finite water, although, other source terms decrease in magnitude but non-linear wave interaction term adds energy to the spectrum and hence can affect the amount of the sediment movement in the coastal regions.

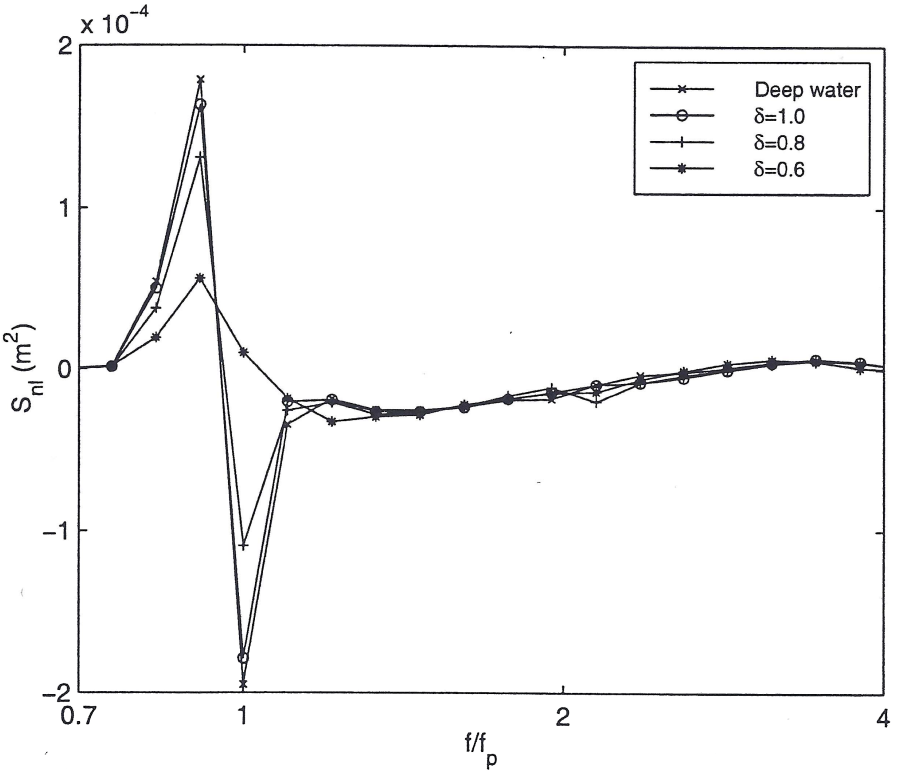


Figure 4: Variation of the non-linear wave interaction term, S_{nl} as a function of f/f_p (f_p is the frequency of the peak of the spectrum). A comparison between deep water and different non-dimensional water depths, δ is shown.

CONCLUSIONS:

The present study has concentrated on using a one-dimensional model for wave forecasting. A useful technique to incorporate full form of non-linear wave-wave interactions has been used which forms an important component of wave prediction models.
Using above two improvements over the other models, the energy and peak frequency curves for different non-dimensional water depths have been obtained. These curves are compared with the fetch limited experimental observations carried to at Lake George, Canberra Australia. It is found that these improvements in the model lead to better agreement between the model and experimental results.

In addition, a study of the source terms that contribute towards the wave growth provide micro level insight into their effect on other related process. The variation of bottom friction and non-linear wave interactions clearly indicate that the effect of these terms in wave development in finite depth. This study also shows that even in shallow water depths, non-linear wave interactions add energy to broad range of frequencies and hence can affect the amount of sediment transport at the beaches.

REFERENCES:

[1] Booij, N., Holthuijsen, L.H. and Ris, R.C. (1996). "The SWAN wave model for shallow water", Int. Conf. Coastal Eng., ASCE, Orlando, 668-676.

[2] Bouws, E. (1986). "Provisional results of a wind wave experiment in a shallow lake (Lake Marken, The Netherlands)", KNMI Afdeling Oceanografisch Onderzoek, OO-86-21, DE Bilt, 15pp.

[3] Bouws, E., Komen, G.J. (1983). "On the balance between growth and dissipation in an extreme depth-limited wind-sea in the southern North sea", J. Phys. Oceanogr., 13, 1653-1658.

[4] Bretschneider, C.L. (1958). "Revised wave forecasting relationships", Proc. 6th Conf. on Coastal Engineering, ASCE, 30-67

[5] Donelan, M.A., Hamilton, J. and Hui, W.J. (1985). "Directional spectra of wind generated waves", Philos. Trans. R. Soc. Lond., A315, 509-562.

[6] Hasselmann, K. (1962). "On the non-linear energy transfer in a gravity-wave spectrum, Part 1. General Theory", J. Fluid Mechanics, 12, 481-500

[7] Hasselmann, K. (1960). "Grundgleichugen der Seegangsvorhersage", Schifftechnik, 7, 191-195.

[8] Hasselmann, K. et al. (1973). "Measurements of wind-wave growth and swell decay during the Joint North Sea Wave Project (JONSWAP)", Dtsch. Hydrogh. Z., Suppl. A, 8, 12, 95pp.

[9] Hasselmann, S. and Hasselmann, K. (1985). "The wave model EXACT-NL", In: Ocean wave Modelling (The SWAMP Group), Plenum Press, New York, 249-251

[10] Janssen, P.A.E.M. (1991). "Quasi-linear theory of wind-wave generation applied to wave forecasting", J. Phys. Oceanogr., 21, 1631-1642

[11] Khatri, S.K. (1997). "In the search of a coastal ocean wave model", Proceedings OCEANS'97 conference, Halifax Canada, 6-9 October 1997

[12] Komen, G.J., Cavaleri, L., Donelan, M., Hasselmann, K., Hasselmann, S. and Janssen, P.A.E.M. (1994). "Dynamics and modelling of ocean waves", Cambridge Univ. Press, 532pp

[13] Komen, G.J., Hasselmann, S. and Hasselmann, K. (1984). "On the existence of a fully developed wind-sea spectrum", J. Phys. Oceanogr., 14, 1271-1285

[14] Pierson, W.J. and Moskowitz, L. (1964). "A proposed spectral form for fully developed wind seas based on the similarity theory of S.A. Kitaigorodskii", J. Geophys. Res., 69, 5181-5190

[15] Shore Protection Manual (1984), U.S. army Coastal Engineering Research Center (CERC), 2 volumes

[16] Snyder, R.L., Dobson, F.W., Elliot, J.A. and Long, R.B. (1981). "Array measurements of atmospheric pressure fluctuations above surface gravity waves", J. Fluid Mechanics, 102, 1-59.

[17] Stewart, R.W. (1974). "The air-sea momentum exchange", Boundary Layer Meteorology, 6, 151-167

[18] Tolman, H.L. (1991). "A third-generation model for wind on slowly varying unsteady and inhomogeneous depths and currents", J. Phys. Oceanogr., 21, 782-797

[19] Vincent, C.L. and Hughes, S.A. (1985). "Wind wave growth in shallow water", J. of waterways, Port, Coastal and Ocean Eng., 111, 765-770.

[20] Willebrand, J. (1975). "Energy transport in a nonlinear and inhomogeneous random gravity field", J. Fluid Mech., 70, 113-126.

[21] Warner, J.C., Sherwood, C.R., Signell, R.P., Harris, C., Arango, H.G., (2008b). "Development of a three-dimensional, regional, coupled wave, current, and sediment-transport model", Computers and Geosciences, 34, 1284-1306.

[22] Warner, J.C., Armstrong, B., He, R., and Zambon, J.B., (2010). "Development of a Coupled Ocean-Atmosphere-Wave-Sediment Transport (COAWST) modeling system" Ocean Modeling, v. 35, no. 3, p. 230-244.

[23] Young, I.R., and Verhagen, L.A. (1996a). "The growth of fetch limited waves in water of finite depth. Part I: Total energy and peak frequency", Coastal Engineering, 28, 47-78.

[24] Young, I.R., and Verhagen, L.A. (1996b). "The growth of fetch limited waves in water of finite depth. Part II: Spectral evolution", Coastal Engineering, 28, 79-100.

[25] Young, I.R., Verhagen, L.A. and Khatri, S.K. (1996). "The growth of fetch limited waves in water of finite depth. Part III: Directional spectra", Coastal Engineering, 28, 101-122

[26] Young, I.R., and Van Vledder, G.Ph. (1993). "The central role of nonlinear wave interactions in wind-wave evolution", Philos. Trans. R. Soc. Lond., A342, 505-524

Enhancement of Cross-Shore Profile Evolution Models for Sustainable Coastal Design

Mohamed A. K. Elsayed 1 and Nabil M. Ismail 2, M.ASCE

1 Assoc. Prof. of Hydraulic Engineering, Mechanical Engineering Department, Maritime Academy (AASTMT), Cairo; formerly, Virginia Tech, Blacksburg, Virginia, USA; email: melsayed_melsayed @yahoo.com
2 Prof. of Coastal Engineering, Department of Construction Engineering, Maritime Academy (AASTMT), Alexandria, Egypt; formerly, Director of Engineering and Technology, Wellstream Int'l Ltd., Panama City, Florida, USA; email: nbismail@usa.net

ABSTRACT

Results obtained from the validation of a cross-shore profile evolution model, Uniform Beach Sediment Transport-Time-Averaged Cross-Shore (UNIBEST-TC), were examined and further analyzed to reveal the reasons for the discrepancy between the model predictions of the field data at the surf zone of the Duck Beach in North Carolina, USA. The UNIBEST model was developed to predict the main cross shore parameters of wave height, direction, cross shore and long shore currents. However, the results of the model predictions are generally satisfactory for wave height and direction but not satisfactory for the remaining parameters.
This research is focused on exploring the discrepancy between the model predictions and the field data of the Duck site, and conducting further analyses to recommend model refinements. The discrepancy is partially attributed due to the fact that the measured values, were taken close to the seabed, while the predicted values are the depth-averaged velocity. Further examination indicated that UNIBEST-TC model runs consider the RMS of the wave height spectrum with a constant gamma-value from the offshore wave spectrum at 8.0m depth. To confirm this argument, a Wavelet Analysis was applied to the time series of wave height and longshore current velocity parameters at the Duck site. The significant wave height ranged between 0.6m and 4.0m while the frequencies ranged between 0.08 to 0.2Hz at 8.0m water depth. Four cases corresponding to events of both high water level and low water level at Duck site were considered in this study. The results show that linear and non-linear interaction between wave height and long-shore current occur over the range of frequencies embracing; the low frequency band of infragravity (0.001- 0.02Hz) waves band and short incident wave band (0.05-0.10Hz). The current results highlight the necessity of incorporating interaction terms between wave - wave and wave- current in the development of cross shore and longshore model formulations.

INTRODUCTION

Understanding nearshore processes is increasingly important because the majority of the world's coastlines are eroding. The increased threat of global warming and the resulting rise in sea level may accelerate erosion problems. Coastal processes

are characterized by complex, nonlinear phenomena as described by Thornton et al. (2000); they also involve patterns covering a wide range of spatial and temporal scales (Figs. 1-a, 1-b).
Many efforts have been underway to develop realistic coupled wave-current-morphologic evolution models. However wave – current interaction not only modifies wave properties but also modifies velocity gradients (Figs.1-c, 1-d) of the longshore and cross shore currents as demonstrated previously by the second author Ismail (1983), (1984) and (2007). Significant progress has been made during the past decade, and the prospects for major advances in the next 10 years are exciting. Even though substantial progress has been achieved in the investigation of physical mechanisms driving coastal morphodynamic processes, present knowledge remains insufficient to correctly understand, model, and forecast the behavior of many coastal systems.

The objective of the current research work is to provide model developers with useful information that can be used for further improvements of the model in areas of poor model performance by applying new theories and expanding the limitation of applicability. Among the available deterministic and probabilistic profile models that have been compared with hydrodynamic and morpho dynamic data of field experiments on the time scale of storms are:

- UNIBEST-TC of Delft Hydraulics (DH);
- COSMOS of HR Wallingford (HR);
- CROSMOR2000 of University of Utrecht (UU);
- BEACH1/3D of University of Liverpool (UL);
- CIIRC of University of Catalunya (UC).

The validation of the above programs was based on the use of hydrodynamic and morpho dynamic data on the LIP experiments in 2D large-scale wave flume of Delft Hydraulics; COAST3D-Storm Experiment at 3D field site of Egmond (The Netherlands) during period of 18 Oct. to 12 Nov. 1998. The general outcome of validation process was as reported by Leo van Rijn et al (2003) and is outlined below.

Profile models can quite accurately (errors smaller than 10%) represent the significant wave height distribution along the surf zone, if the wave breaking model is properly calibrated; the wave breaking coefficient should be a function of local wave steepness and bottom slope for most accurate results. The models can simulate the longshore and cross shore currents in 3D field conditions only in a reasonable way with relative accuracies of 30% to 50%.

Profile models which yield good results for hydrodynamics do not automatically yield good results for morphodynamics; often additional calibration using measured bed profile changes is required to obtain good morpho dynamic results; the calibration coefficients involved are not proven to be site-independent.

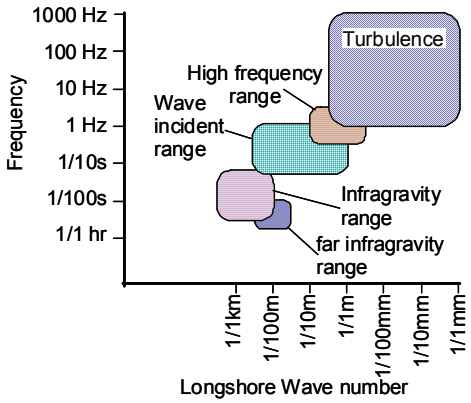


Figure 1-a. Spatial -Time Scales of Waves in the Nearshore

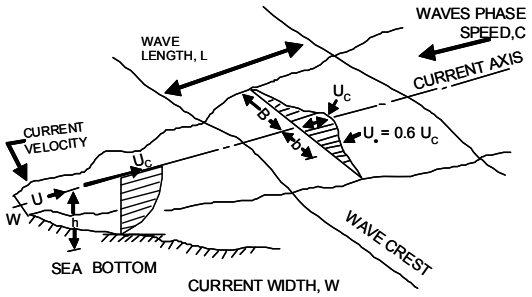


Figure 1-b. Velocity and Length Scales of Waves and Currents (after Ismail & Wiegel, 1983)

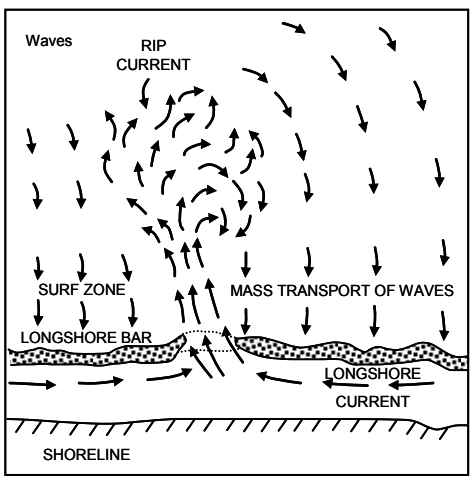


Figure 1-c. Schematic of Nearshore Processes

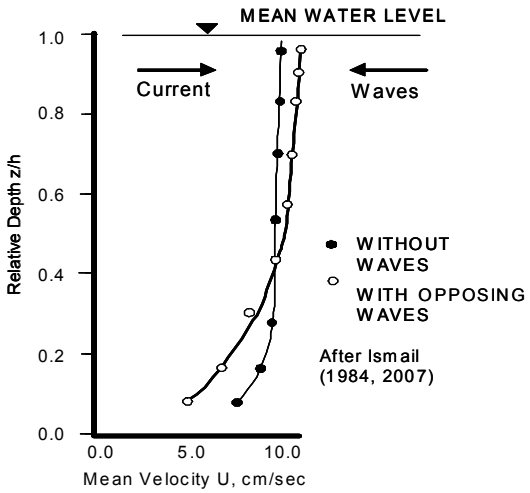


Figure 1-d. Modifications of Current Velocity Profiles

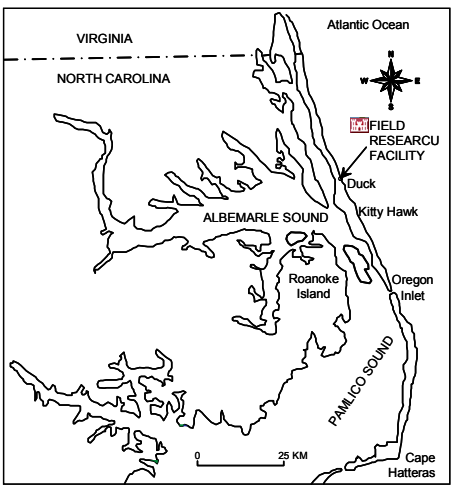


Figure 2-a. Field Research Facilities , US Army Corps, of Engineers, Duck, N.C.

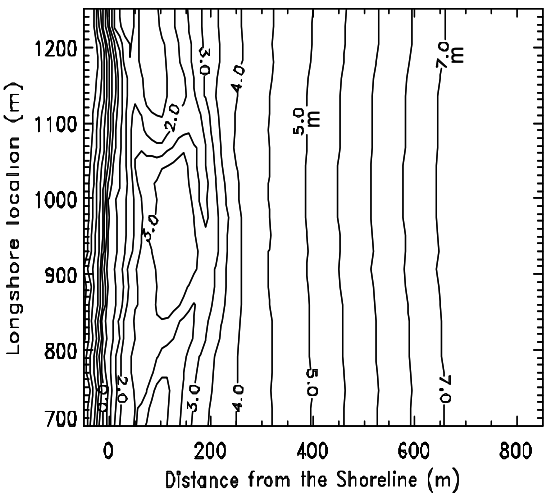


Figure 2-b. Plan View of the Beach Bathymetry at Duck, N.C. (Elsayed, 2006)

Validation of UNIBEST-TC at Duck Coastal Site, NC, USA

The first author of this paper (Elsayed, 2006) has investigated the validity of profile model UNIBEST-TC against the field data of the surf zone of the Duck Beach in North Carolina, USA (Fig.2) for the periods from 22 to 27 September and from 10 to 20 October, 1998. He also tested the model validity at the tidal surf zone of Egmond beach (The Netherlands) for events during the period of April to May1998 (Egmond-Main campaign) within the European COAST3D. The results for the validation were inline with previous results referenced above for the Egmond site in the Netherlands. However, the model prediction for the Duck site in USA is again generally acceptable for wave height and direction but not satisfactory for the longshore and cross current parameters. Further analyses were conducted (Fig. 3) and four cases corresponding to events of both high water level and low water level are considered in this study and listed in Table 1.

Table 1. Wave Conditions for Model Validation Runs at Duck, NC

Case	Water Level	$H_{significant}$	H_{rms}
1	HWL	2.5 m	1.8m
2	LWL	0.6 m	0.4m
3	HWL	0.75m	0.55m
4	LWL	0.67m	0.5m

Motivation for Current Research and Analysis of Coastal Data at Duck Site

The UNISET-TC model has proved to be capable in general of predicting wave height and wave direction for both coastal sites. However the predictions of long-shore current and cross shore currents remain unsatisfactory for the Duck site as well as at Egmond site. The difference between the measured and the predicted values for long-shore current and cross-shore current was attributed partly due to the location of measurements, which are at a certain water depth, and the predicted values which are the depth-averaged velocity. Beside that, the turbulence in the breaker zone leads to errors in the measurements, which could be another factor.

Examination of UNIBEST-TC model indicated that the input to the model was the RMS of the wave height and a constant gamma-value derived from the offshore wave spectrum. Accordingly the model predictions will not take into effect the various wave components within the spectrum (Phillips, 1958). As highlighted by Thornton et al (2000) field observations and models suggest that alongshore currents induced by breaking of wind-waves are often unstable (Longuett-Higgins, 1970). The growing instabilities, called shear waves, have periods of 1-10 minutes. Accordingly, results from fully nonlinear models suggest that shear instabilities might both alter significantly the cross-shore structure of the mean alongshore current and produce energetic eddies. Therefore, it appears that there is a need to examine the wave envelope for short waves and bound long waves and thereby pave the way to improve model predictive capability.

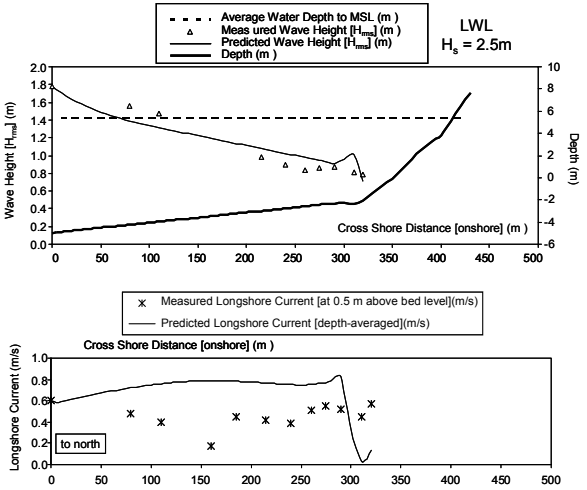


Figure 3-a. Measured and predicted values of wave height and longshore current velocity (case 1)

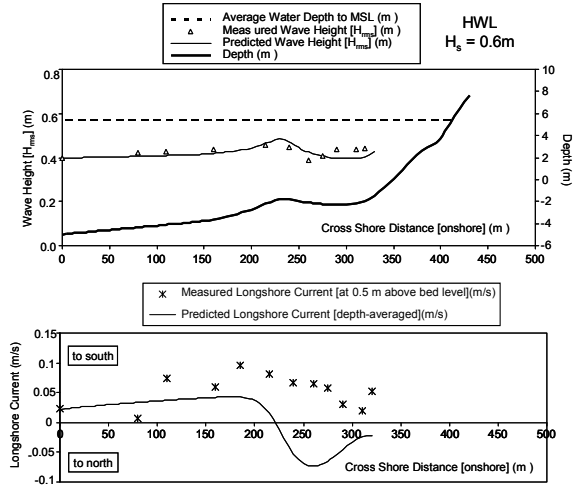


Figure 3-b. Measured and predicted values of wave height and longshore current velocity (case 2)

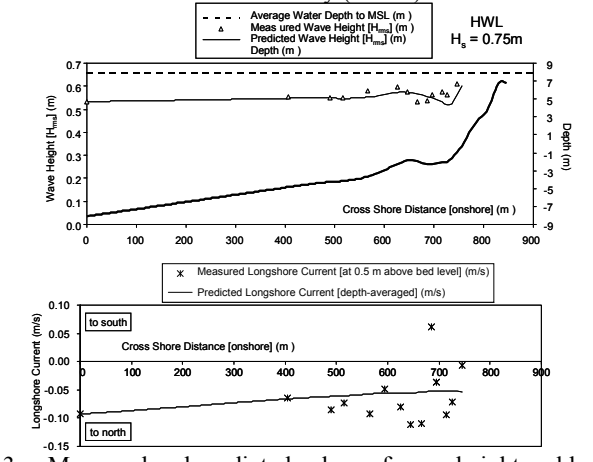


Figure 3-c. Measured and predicted values of wave height and longshore current velocity (case 3)

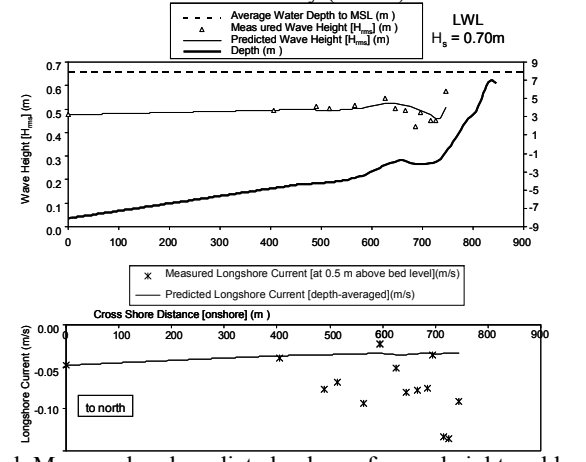


Figure 3-d. Measured and predicted values of wave height and longshore current velocity (case 4)

Duck Coastal Site: Many studies have been carried out in order to interpret the behavior of the bar system in the surf zone of Duck beach in the US. The objective was to study the bar system (consisting of one or two shore-parallel bars) in the surf zone of Duck beach, North Carolina, U.S.A, over long-term periods. As described by Elsayed (2006) the beach and foreshore are rather steep (1:12) and consist of a mixture of medium/coarse sand with median diameters between 0.5 and 1 mm and carbonate shell debris up to 20%. Offshore, the bottom slope approaches to about 1 to 160 at the 8.0m contour, and the median grain size decreases to 0.1 mm. The surf zone at Duck coastal site is characterized by a persistent, very dynamic inner bar, approximately 30 to 120 m offshore of the shoreline with the bar crest between 1.0 and 3.0 m (bar height of 1-2 m) and by a low-amplitude outer bar approximately 300 to 400 m offshore.

Wave Observations: The environmental conditions at the Duck site were described by Fedderson et al (1996) and Elsayed (2006). In 8m water depth, the significant wave height ranged between 0.2 m to 4 m and the mean wave angle between ± 50 degrees. The mean wave frequency ranged from about 0.08 to 0.2 Hz. Maximum mean longshore currents ranged from 0.1 to 1.4m/s. Fluctuations in mean water level were about 1 m at spring tide. Tidal currents in depths less than 8 m are less than 0.03 m/s.

Longshore Current Observations: During the Super Duck field experiment, low frequency alongshore propagating motions were observed by Oltman-Shay et al. *(*1989) that had similar frequencies (0.01 to 0.001 Hz) to but much shorter wave lengths of the order 100m than edge waves. These waves were related to the magnitude and direction of the mean longshore current, and have been related to a shear instability of the longshore current, and thus named shear waves. These waves are vorticity waves, and unlike incident and edge waves are not irrotational. Therefore, to confirm the presence of such spectral variations in wave conditions in 1998 at Duck coastal site its, spectral analysis was conducted to the time series of wave height at 8.0m water depth and the velocities of the long-shore current at the mid point of its profile. These results are shown in Fig. (4-a) through Fig. (4-d) for the four design cases considered in this study at Duck site. The results show patterns of low, medium, and high wave frequency bands.

Fourier and Wavelet Transform: The spectral analysis at a single point by its nature does not show whether if linear or nonlinear interaction does exist. Therefore, Wavelet analysis which is becoming a common tool for analyzing localized variations of power within time series is considered for use. The Wavelet's theory is a powerful alternative to the Fourier analysis and gives more flexible engineering for signal processing particularly for analysis of time series. However this circumstance makes the Fourier transform a poor method for a research of functions with the changeability's characteristics in the time. For example the Fourier transform does not distinguish a signal representing the sum of two sine waves from a signal consisting of the same sine waves but joining sequentially. Accordingly, a Wavelet Analysis was conducted to the obtained time series of wave height and long shore current shown in Fig. (4-a) through Fig.(4-d).

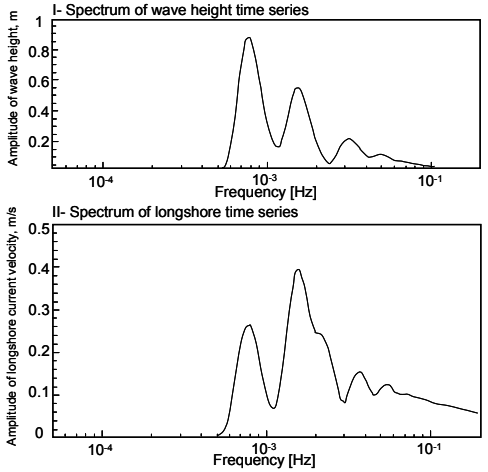


Figure 4-a. (I) Spectrum of the incident wave height
(II) Spectrum of the longshore current (case 1)

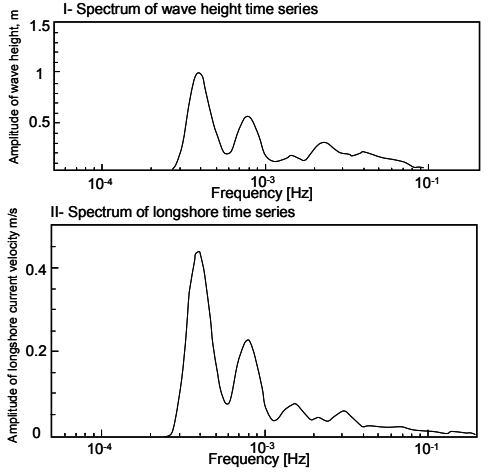


Figure 4-c. (I) Spectrum for the incident wave height
(II) Spectrum of the longshore current (case 3)

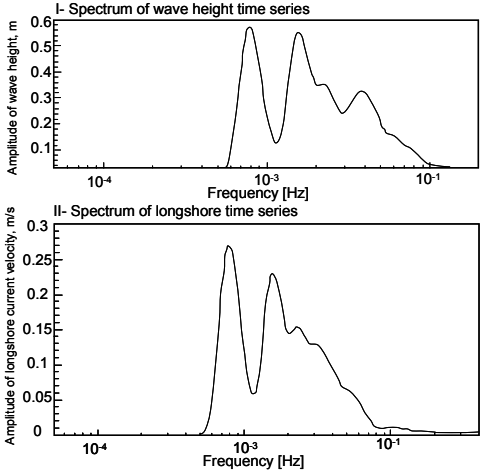


Figure 4-b. (I) Spectrum of the incident wave height
(II) Spectrum of the longshore current (case 2)

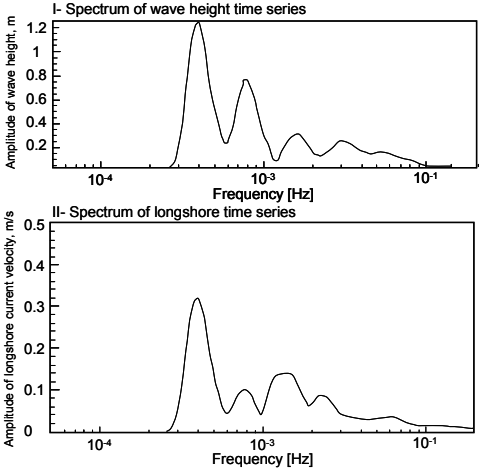


Figure 4-d. (I) Spectrum of the incident wave height
(II) Spectrum of the longshore current (case 4)

In the next section we will give a brief description of wavelet analysis which was applied previously by Elsayed (2008) on the interaction between winds and the induced wind-waves.

Application of Wavelet Analysis to UNISET-TC Predictions

The continuous wavelet transform $W(a,\tau)$ of a function h (t), is defined as:

$$W(a,\tau) = \int_{-\infty}^{+\infty} h(t)\psi^*_{a,\tau}(t)dt \quad (1)$$

where a and τ are scale and time variables respectively, and $\psi_{a,\tau}$ represents the wavelet family generated by continuous translations and dilations of the mother wavelet $\psi(t)$.

These translations and dilations are obtained by

$$\psi_{a,\tau} = \frac{1}{\sqrt{a}}\psi\left(\frac{t-\tau}{a}\right) \quad (2)$$

Following Torrence and Compo (1998) and Addison (2002), the complex Morlet wavelet (Morlet, 1981) to be implemented in this study is defined as:

$$\psi(t) = \Pi^{-1/4} e^{iw_o t} e^{\frac{-t^2}{2}} \quad (3)$$

In this definition, w_o is chosen to be 6.0 to approximately satisfy the wavelet admissibility condition (Farge, 1992).

Torrence and Compo (1998) developed a code for computing the continuous wavelet transform of the time series of the signal. In this work the code was modified to compute the cross–bispectrum and the wavelet cross-bicoherence.

In order to have a statistical stability the wavelet power spectrum is integrated over a finite time interval (Milligen et al., 1995, 1997). Therefore, the wavelet power spectrum becomes:

$$P_{xx} = \int_T W^*_x(a,\tau)W_x(a,\tau)d\tau \quad (4)$$

$W_x(a,\tau)$ wavelet transform of the time series

$W^*_x(a,\tau)$: the complex conjugate of wavelet transform of the time series

T: a finite time interval

The wavelet cross-spectrum is defined as follows:

$$P_{xy} = \int_T W^*_x(a,\tau)W_y(a,\tau)d\tau \quad (5)$$

$W^*_x(a,\tau)$: the complex conjugate of wavelet transform of the first time series

$W_y(a,\tau)$: the wavelet transform of the second time series

It should be noted that the results of the cross-spectrum depend heavily on the fluctuations of the individual signals because if one of the signals is fluctuated less than the other the effect of the more fluctuating signal will dominate in the resultant cross-spectrum (Hajj et al. 1998).

The normalized wavelet cross-spectrum (to have values between 0 and 1) gives the linear coherence as follows:

$$Coh_{xy}(a) = \frac{\left|P_{xy}(a)\right|^2}{P_{xx}(a)P_{yy}(a)} \tag{6}$$

$Coh_{xy}(a)$: linear coherence between two time series

$P_{xx}(a)$: power spectrum of first time series

$P_{yy}(a)$: power spectrum of second time series

$P_{xy}(a)$: cross-spectrum of the first and the second time series

The wavelet cross-bispectrum is defined as follows:

$$B_{yxx}(a1,a2) = \int_T W_y^*(a,\tau)W_x(a1,\tau)W_x(a2,\tau)d\tau \tag{7}$$

where $\frac{1}{a} = \frac{1}{a1} + \frac{1}{a2}$ (frequency sum rule).

The wavelet cross-bispectrum measures the amount of phase coupling in the time interval T that occurs between wavelet components of scale lengths a1 and a2 of x(t) and wavelet component a of y(t) such that the sum rule is satisfied (Milligen et al., 1995).

The normalized squared wavelet cross-bicoherence is defined as

$$[b_{yxx}(a1,a2)]^2 = \frac{|B_{yxx}(a1,a2)|^2}{[\int_T |W_x(a1,\tau)W_x(a2,\tau)|^2 \, d\tau][\int_T |W_y(a,\tau)|^2 \, d\tau]} \tag{8}$$

The wavelet bicoherence is a measure of phase coupling that occurs in a signal or between two signals. Phase coupling is defined to occur when two wave frequencies, f1, f2, are simultaneously present in the signal(s) along with their sum (or difference) frequencies, and the sum of the phases of these frequency components remains constant. The bicoherence measures this quantity and is a function of two frequencies f1 and f2 which is close to 1. When the signal contains three frequencies f1, f2, f that satisfy the relation f=f1±f2, bicoherence does exist. If this relation is not satisfied, then bicoherence is close to zero (Milligen et al., 1995).

The computed linear coherence and quadratic bicoherence represented by Equations (6) and (8) are given in Fig.(5-a) through Fig. (5-d) for the four cases.

SUMMARY OF RESULTS AND DISCUSSION

The results of UNISET-TC model verifications were given in Fig. (3-a) through Fig. (3-d) which illustrate the measured and predicted values for wave height and longshore current. Fig. (3-b) and Fig. (3-d) correspond to the two cases of high water level while Fig. (3-a) and Fig.(3-c) correspond to low water level. Since the field measurements at Duck site do not provide continuous time series required to conduct wavelet analysis, UNISET-TC model was used to obtain the time series of longshore current velocities and wave height.

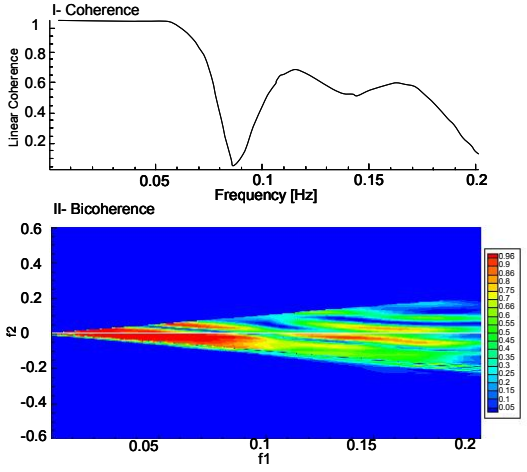


Figure 5-a. (I) Wavelet Coherence (wave height & longshore current) (II) Wavelet bicoherence (wave height f1 & wave height f2 & longshore current f) (case 1)

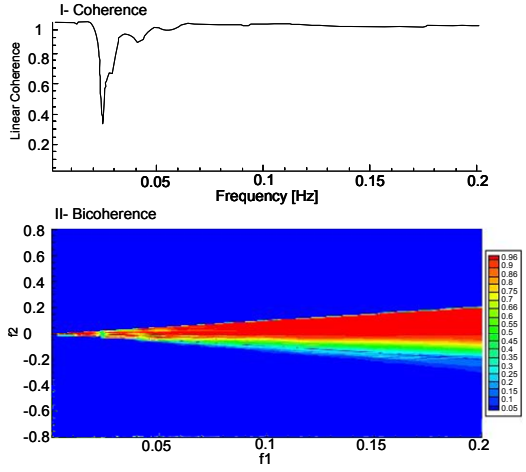


Figure 5-b. (I) Wavelet Coherence (wave height & longshore current) (II) Wavelet bicoherence (wave height f1 & wave height f2 & longshore current f) (case 2)

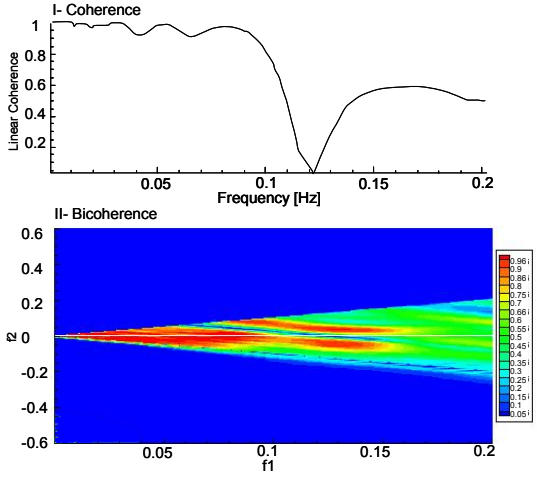


Figure 5-c. (I) Wavelet Coherence (wave height & longshore current) (II) Wavelet bicoherence (wave height f1 & wave height f2 & longshore current f) (case 3)

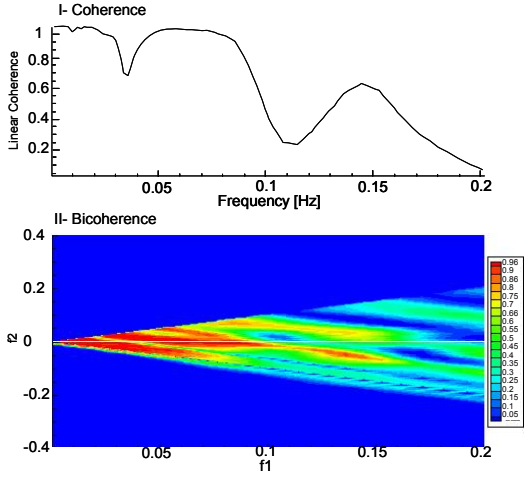


Figure 5-d. (I) Wavelet Coherence (wave height & longshore current) (II) Wavelet bicoherence (wave height f1 & wave height f2 & longshore current f) (case 4)

These time series were shown in Fig. (4-a) through Fig.(4-d) for the four cases of water level. The data in these figures highlight that there are three dominant frequency bands: 0.001-0.01 Hz, 0.01—0.04 Hz and 0.05-0.10 Hz. The first band represents the so-called "shear" which co-exit with bound edge waves and the primary incident waves.

The computed linear coherence and quadratic bicoherence (Equations 6 and 8) which were given in Fig.(5-a) through Fig.(5-d) show that there is both linear and nonlinear interaction between wave height and longshore current for the frequencies that are around or less than 0.1 Hz. The drop in the value of linear coherence at 0.1 and 0.2 is associated with a drop in bicoherence level at the same range of frequencies.

A close inspection of Fig. 5 reveals that there is nearly complete bicoherence for frequencies less than 0.05-0.08 Hz. Such coupled interaction, due to low frequency components, account for the deviations between the model and the prototype. Model deviations, around the offshore bar, are more apparent for the conditions of low water level (Cases 2 and 4). In addition, the presence of the opposing rip currents is more likely to reduce the predicted velocities of longshore currents.

Long Waves (infragravity waves) and Beach Profile Evolutions:

Smith (1998) reports on the observance of these low frequency waves using two "Phased-Array Doppler Sonars" (PADS), which were deployed at Duck, NC, as part of a major near-shore experiment in 1997. Additionally field observations by Senechal, et al (2002) on the French Atlantic coastline showed the presence of a low energy narrow band and long swell but also in the presence of high secondary wave generation due to nonlinear triad interactions. Their work demonstrated the effect of low frequency waves on the beach profile evolution.

The generation of such long period waves can be explained by two different mechanisms. On one hand the breaking is thought to release bound long waves due to wave grouping (Longuett-Higgins, 1970). On the other hand wave grouping produces a break point and set-up oscillation that acts as a piston at the wave group period. In both cases these incident long period waves reflect on the beach face, interfering with the incident waves to produce long period standing waves known as surf-beats (Thornton, 2000). The strong correspondence in field experiments between long wave and morphological features length scales, has suggested that long waves may generate off-shore bars. While strongly depending on the incident wave conditions, these infragravity waves also play an important role on the swash process.

Conclusions

The deviation between the predicted and measured values of long shore currents using UNISET-TC model has been confirmed at Duck coastal site. On the other hand the model prediction is better in cases of high water level compared to the cases of low water level and high amplitude waves. These deviations are due to potential

effects of strong rip currents and subsequent interaction, while high finite amplitude waves give rise to linear and nonlinear interaction.

The current results confirm previous field observations of nearshore processes that waves in the infragravity range, shear and edge waves, play an important role on near shore hydrodynamics and beach morphology.

The results of spectral and wavelet analyses at Duck coastal site highlight the existence of infragravity waves along single or multiple bars and the importance of incorporating the interaction of low frequency waves (less than 0.05 Hz) with the incident wave components (0.08-0.15Hz).

Although many studies using wavelet analysis have suffered from an apparent lack of precise quantitative results, such advanced technique proved to be capable of extracting patterns characteristic of low-, medium- and high-frequency wave bands. The results of wavelet analysis indicate that the linear and non-linear interaction between wave height and longshore current does exist in all cases in the low frequency range which is less than 0.08 Hz.

The main conclusion of this research work is that the UNIBEST- TC and similar models need to take into effect the interaction between waves and longshore currents. Furthermore the models should consider the effects of long waves within the spectrum as well as the generated edge waves. Nevertheless, modeling of this wide range of processes on real beaches needs extensive field data of high spatial and temporal resolutions. Such challenging goal remains to be pursued to enhance state of art prediction of the cross-shore evolution profiles.

REFERENCES

Addison, P.S. (2002). *"The Illustrated Wavelet Transform Handbook, Introductory Theory and Applications in Science"*, 349 p., Bristol, UK, Institute of Physics Publishing.

Elsayed, M.A.K. (2006). “Application of a Cross-Shore Profile Evolution Model to Barred Beaches”, *Journal of Coastal Research*, 22(3), 645-663.

Elsayed, M.A.K. (2006). "A Novel Technique in Analyzing Non-linear Wave-Wave Interaction". *Ocean Engineering*, 33(2), 168-180.

Elsayed, M.A.K. (2007). "Non-linear Wave-Wave Interactions in a Mistral Event". *Journal of Coastal Research,* 23(5), 1318-1323.

Elsayed, M.A.K. (2008). "On the Non-linear Wave-Wave Interactions". *Journal of Coastal Research,* 24(3), 798-803.

Farge, M. (1992). "Wavelet Transforms and Their Application to Turbulence". *Annual Review of Fluid Mechanics*, 24, 395-457.

Feddersen, F., Guza, R. T., Elgar, S. and Herbers, T. C. (1996). "Cross-shore Structure of Longshore Currents during Duck 94", *25th International Conference on Coastal Engineering*, Orlando, Florida, 3666-3679.

Hajj, M.R., Jordan, D.A., and Tieleman, H.W. (1998). "Analysis of Atmospheric Wind and Pressures on a Low Rise Building". *Journal of Fluids and Structures,* 12, 537-547.

Ismail, N. M., and Wiegel, R. L. (1983). "Effect of Opposing Waves on Momentum Jets Spreading Rate", *Journal of Waterway, Port, Coastal and Ocean Division*, ASCE, Vol.109, No.4, 465-483.

Ismail, N.M. (1984). "Wave-Current Models for the Design of Marine Structures", *Journal of Waterway, Port, Coastal and Ocean Engineering*, ASCE, Vol. 110, No. 4, 432-446.

Ismail, N.M. (2007). "Discussion of Reynolds Stresses and Velocity Distributions in a Wave-Current Coexisting Environment", *Journal of Waterway, Port, Coastal and Ocean Engineering*, ASCE, Vol. 133, No. 2, 168-169.

Longuett-Higgins, M.S. (1970). "Longshore Currents Generated by Obliquely Incident Sea Waves". *Journal of Geophys. Res.*, 75, 6790-6801.

Milligen, B.P.V., Hidalgo, C., Sanchez, E., Pedrosa, M.A., Balbin, R., Garcia-Cortes, I., and Tynan, G.R. (1997). "Statistically Robust Linear and Nonlinear Wavelet Analysis Applied to Plasma Edge Turbulence". *Review of Scientific Instruments*, 68(1), 967-970.

Milligen, B.P.V, Sanchez, E., Estrada, T., Hidalgo, C., Branas, B., Carrersa, B., and Garcia, L. (1995). "Wavelet Bicoherence: A new turbulence analysis tool", *Physics of Plasma*, 2(8), 3017-3032.

Morlet, J. (1981). "Sampling Theory and Wave Propagation", *Proceedings of the 51st Annual Meeting of the Society Exploration Geophysics*", Los Angeles, USA.

Oltman-Shay, J., Howd, P. A., and Birkemeier W.A. (1989). "Shear Instabilities of the Mean Longshore Current ", *Journal of Geophys. Res.*, 94(C12), 18031-18042.

Phillips, O.M. (1958). "The Equilibrium Range in the Spectrum of Wind-Generated Waves", *Journal of Fluid Mechanics*, 4, 426-434.

Sénéchal, N., Bonneton, P. and Dupuis, H. (2002). "Infragravity Wave Frequency Structure on a Double-Barred Beach ", *Journal of Coastal Research*, 36, 654-661.

Smith, J.A. (1998). "*Observations of Waves and Currents Near Shore- Duck-1997, NC, USA*", US Army Corps of Engineers; Field Research Facility, http:// www. frf. usace.army.mil/

Thorton, Ed et al. (March 2000). "State of Nearshore Processes Research II", Technical *Report* NPS-OC-00-001, Naval Postgraduate School, Monterey, California 93943.

Torrence C. and Compo, G.P. (1998). "A Practical Guide to Wavelet Analysis", *Bulletin of the American Meteorology*, Society, 79(1), 61-77.

Van Rijn, L.C., Walstra, D.J.R., Grasmeijer, B., Sutherland, J., S. Pan, S., and Sierra, J.P. (2003). "The Predictability of Cross-Shore Bed Evolution of Sandy Beaches at the Time Scale of Storms and Seasons Using Process-Based Profile Models", *Journal of Coastal Engineering*, 47, 295-327.

In the Wet Placement of Articulated Concrete Block Mat by Divers

Eric Thorkildsen[1]

[1]M.ASCE, P.E., Greenman-Pedersen, Inc. 80 Wolf Road, Albany, NY 12205; PH (518) 453-9431; FAX (518) 453-9458; email: ethorkildsen@gpinet.com

The magnitude 9.0 earthquake that struck Japan on March 11th, 2011 highlighted the enormous consequence when cooling mechanisms fail at a nuclear power plant. During this emergency a 'Plan B' scenario was activated that brought sea water into the crippled Fukushima Daiichi Nuclear Power Plant to cool the residual heat. This highlights the importance of having large quantities of water available and the ability to channel that water directly into the reactor.

Another natural disaster, a series of large hurricanes, came through Florida during the 2004 and 2005 seasons creating extensive damage to canals designed to furnish seawater to a nuclear power plant located in Port St. Lucie, Florida. A typical reconstruction project to repair the channel lining might entail dewatering, but that was not an option since as a designated emergency backup mechanism this would shut down the plant. Therefore 'In the Wet' reconstruction made sense and the owners issued a design build proposal mandating no plant shutdowns.

The nuclear facility at Port St. Lucie, Florida is owned and operated by Florida Power and Light (FPL). The facility contains two boiling water reactors. Boiling Water Reactors are similar to a pressure cooker. The nuclear fuel heats water, the water boils and creates steam, the steam then drives turbines that create the electricity, and the steam is then cooled and condensed back to water, and the water sent back to be heated by the nuclear fuel. In the event of a natural disaster, the nuclear reaction that creates heat and steam can be shut down almost instantaneously by inserting control rods, but there is still residual heat that needs to be cooled down over time. Seawater is used to provide cooling to turn the steam back into water. Seawater can also be used as an emergency backup, as it was in the Fukushima nuclear plant disaster.

The canals at the FPL nuclear site are over 5,000 feet long, trapezoidal shaped measuring 150' wide crest to crest, with the volume of 1,000,000 gallons (Figure 1). The water width in the channel is about 100' wide. Removing water from the channels for repairing the hurricane damaged channels was not an option since that would force the shutdown of the plant costing this electricity producing facility millions. A partially dewatered channel alternative was investigated but deemed too costly. In addition, the area is environmentally sensitive, and a breeding ground for loggerhead turtles, which also had to be taken in to consideration. Since loggerhead turtles use the moonlight for navigation, no night work was allowed as the lighting might be misinterpreted by the turtles. Any construction would have to be monitored

for the turbidity it created in the waters. Too much and the project would be temporarily shut down. So there were numerous challenges to any construction team. The winning proposal based on best value was that offered by Greenman-Pedersen, Inc. (GPI) as design engineer with its subsidiary Underwater Engineering Services, Inc. (UESI) as prime contractor, and CONTECH Construction products supplying the embankment repair material.



Figure 1 – Channels at the Port St. Lucie Power Plant

The design solution to future storm surges, wave action and hydraulic stability called for armoring of the channels. Revetment options offered in engineering manuals and an ASCE Task Force devoted to the subject include the use of rip rap, roller compacted concrete, reinforced vegetation, soil cement, cast in place concrete, articulated concrete blocks, geotextile, or gabions. Rip rap was feasible and cost efficient, but the accuracy of underwater placement questionable and the requirement to replenish it made the other options more appealing. The best and winning option was the use of precast articulated concrete block. These blocks are interconnected with cables in the mats allowing flexibility for ease of placement and alignment. The most important aspect of placement was the ability to use divers to ease the blocks into place with minimal turbidity.

Since this reconstruction involved sensitive placement of large precast concrete mats, quality control was paramount. Quality always begins and ends with the staff, in this case the divers. There are thousands of scuba divers in this country; most are

considered ‘recreational divers’. They take a certified course that includes classroom work, pool training, a written exam and finally a ‘checkout’ dive in open water. The whole process can be accomplished in a few weekends. While great training for Caribbean adventures, this by no means prepares the diver for underwater construction. A ‘commercial’ diver is a very different individual. Training, both classroom and water, takes hundreds of hours and many months. Commercial divers must train to a point that their underwater environment becomes a comfortable place to perform construction work. Training includes working with all tools of the trade including underwater welding, drilling, and working with hydraulic and compressed air tools. So what would a diver do underwater? Expectations include placement of formwork, pouring of concrete, welding, cutting cleaning and demolition, just about everything needed to repair or construct a structure out of the water. All divers for this project were commercially trained. But where do you obtain divers familiar with nuclear safety and operations?

Fortunately UESI had divers working in the plant for years, but not on the channel lining. Divers are routinely used in nuclear plant maintenance on all the water supply lines and other elements. A donut shaped structure under the boiling water reactor, called the torus, continually circulates water that could be used as a heat sink in an emergency. Divers used in this maintenance are exposed to low levels of radiation which must be continually monitored. Routine maintenance includes repairs to systems, paint coating and recoating, and other miscellaneous duties. Therefore these divers were already trained in safety operations in and around nuclear power plants, had an intimate knowledge of the facility, and could be made available to repair the channel ling.

All diving operations for the canal reconstruction were carried out using stringent US Army Corps of Engineers specifications. This included the use of ‘surface supplied’ air, meaning the diver relies on compressed air situated on the deck of the vessel. An air compressor was also located on the deck that could be used to provide essentially an unlimited supply of air. See Figure 2. The diver was also outfitted with full communications and video. This allowed manager’s topside to help direct the diver when placing the large mats. Instant Quality Control was provided through the video system as all operations could be viewed on a screen plus tape for post construction review.

Quality is a requirement of all staff, but material quality and selection is equally as important. The use of precast articulate block mats as the primary product for the repair was chosen based on:

- The ability of the product to articulate and to maintain contact with the subgrade
- The quality of the precast concrete blocks
- The ability to install the product without increasing turbidity



Figure 2 - Preparation for Dive, note diver has 'Surface Supplied' air plus full audio and video communication

Many types of articulated block manufacturers exist, and most have proprietary rights to their system. To provide parameters for a hydraulic analysis, tests are conducted on the block systems in large flumes. This can be costly and the expense is paid for by the manufacturer, who then protects their investment through patents. The GPI/UESI team chose CONTECH based on their past experience in similar projects. Figure 3 shows placement of the mat sections by crane. The mats were 38' long by 8' wide.



Figure 3 - Lifting of articulated precast concrete mats by crane

Commercial divers were involved with every phase of the operation. They ensured that the excavation of material was completed to the proper grade. Divers then installed the geotextile filter fabric which required anchorage due to steady channel currents. Installation of geotextile filter fabric by divers is a common repair for channels. Seepage can be dramatically reduced or eliminated by placement of the fabric. Next, the divers guided the precast concrete mats into place with crane signals from the divers utilizing the diver communications system provided in the hard hat dive mode selected by UESI. This was a critical job to assure proper seam alignment. Finally, divers poured special concrete with 'anti-washout' admixtures along the underwater horizontal seams between mats. Portions of the canal water temperatures reached 107 degrees due to the heated water from the plant. UESI upgraded their hot water diving program with updated technologies during the 4 month dive operation in hot water. Chilled water was pumped through the diver's suits to form a cool water barrier. The ability of the diver to work under adverse conditions such as water temperature, current and low visibility is critical to the projects ultimate success.

CONCLUSION

The ability to perform channel and storm control reconstruction underwater is of great benefit to owners by avoiding both facility shutdowns and construction of dewatering systems. The training and experience of commercial divers combined with the advancement in materials like precast articulated concrete block have led to a great increase in 'wet' construction and significant cost savings. Commercial divers can be an integral part of storm control maintenance including condition assessment, rehabilitation and repair.

REFERENCES

Engineering News Record (5/2/2011 Issue) "TEPCO Maps Fukushima Shutdown"

Erosion Control (4/2010 Issue) "Commercial Divers improve quality and efficiency in dam reconstruction"

ASCE Task Force on Overtopping Protection of the Hydraulics Division, "Alternatives for Overtopping Protection of Dams"

Analytic Solution Shoreline at Jetty Under Varying Wave Climate

by Todd L. Walton Jr.[1] and Robert G. Dean[2]

1. *Beaches and Shores Research Center, Institute of Science and Public Affairs, Florida State Univ., 2035 E. Paul Dirac Dr. , Morgan Bldg., Box 5, Tallahassee, FL 32310, E-mail: twalton@fsu.edu (Corresponding Author)*

2. *Civil and Coastal Engineering Dept., Univ. of Florida, Weil Hall, Gainesville, FL, E-mail: dean@coastal.ufl.edu*

Abstract

Future shoreline changes on a sandy beach with a structure such as a jetty or groin can be predicted when wave climate is known. An existing solution for the linearized partial differential equation for shoreline change is presented for the situation where wave climate is not changing and when the angle of the shoreline is small with respect to the waves breaking at the shoreline. The novel solution provided in this paper allows the previous constant wave condition solution to be utilized to be extended to the case where wave climate (i.e. wave direction and wave height) is time varying. Example usage of the method presented shows that shorelines are of different final planform shape for time varying wave conditions even though the sediment transport is the same from time step to time step. Reversals of wave climate time series are shown to provide very different final shoreline shapes even though time series consist of the same wave conditions although in different ordered time.

1. Introduction

When the angle of the shoreline is small with respect to the waves breaking at the shoreline and the wave conditions are not spatially varying, a linearized partial differential equation governing shoreline change can be derived from the longshore sand transport equation coupled with the continuity of sand equation (see for example Walton and Chiu (1979), Dean and Dalrymple (2002)). The solution is a function of time "t" and is given as:

$$\frac{\partial y}{\partial t} = G \cdot \frac{\partial^2 y}{\partial x^2} \tag{1}$$

where x is the alongshore coordinate, and y the offshore coordinate of the shoreline in planform, and G is the "shoreline diffusivity" coefficient which is given by:

$$G = (KH_b^2 C_{gb}/8) \cdot \left(\left(S_g - 1\right)(1-p)(h_c + B)\right)^{-1} \tag{2}$$

where K =dimensionless constant relating immersed weight sand transport to alongshore energy flux, H_b = breaking wave height, C_{gb} = breaking wave celerity, S_g = specific gravity of sediment, p = porosity of sediment, B = berm height of beach above still water, and h_c = limiting depth of appreciable sand transport in the alongshore direction (see for example Dean and Dalrymple (2002)) .

Many investigators have provided analytical solutions for the linearized shoreline change equation (Eq.1) assuming constant wave conditions with varying boundary and initial conditions. Pelnard-Considere (1956) is believed to be the first researcher to take advantage of the linearized shoreline equation to find a planform solution of the shoreline with time at a coastal barrier. Other researchers who have provided solutions include the following: Walton and Chiu (1979) provided non-dimensional solution graphs for numerous solutions; Larson et al.(1987) provided additional solutions for a number of cases (trapezoidal fill area, river point source of sand input to shoreline, river line source of sand input to shoreline, etc.); Walton (1994) provided a solution to a tapered beach fill; Dean (1984, 2003) reviewed analytical solutions of shoreline change applicable to beach nourishment projects along with a new solution for the shoreline change between two groins initially filled with sand; Larson et al. (1997) provided solutions for shoreline evolution in the vicinity of detached breakwaters and seawalls and jetties ; Walton (2005) provided a review of existing bypassing solutions for constant wave conditions; and Walton (2007) addressed extended solutions to beach fills on a barrier island. Further analytical treatments of time-varying wave conditions were considered by Larson et al. (1997) for the case of a single groin/jetty with sinusoidal varying (in time) wave direction using Laplace transforms, while Reeve (2006) and Zacharioudaki and Reeve (2008) present an integral solution to the one-dimensional time varying wave angle and time varying shoreline diffusivity equation for the semi-infinite sand transport case at a groin/jetty with a sediment source/sink term. In the above papers, only unsolved integral solutions are provided and no specific solution cases are considered. The

solutions presented herein differ from the above in that specific computed solutions are provided for the most common engineering problem dealt with in numerical case studies, i.e. that of piecewise constant wave conditions (angle and shoreline diffusivity) in time at a groin/jetty.

2. Pelnard-Considere Solution Background

As previously noted, a widely utilized shoreline solution in practice is the Pelnard-Considere (1956) solution for constant wave conditions represented by a constant shoreline diffusivity coefficient and where the jetty is sufficiently long to prevent all bypassing. The Pelnard-Considere solution is the solution to the field equation (Eq.1) for an initially straight shoreline in a semi-infinite region $0 < x < \infty$ where the boundary condition at the jetty (at $x = 0$) is $-\frac{\partial y}{\partial x}(0,t) = \tan(\alpha_b)$ for the coordinate system provided in Figure 1 where the breaking wave angle has been defined as positive in clockwise direction. The solution provided by Pelnard-Considere (1956) is given herein as:

$$y(x,t) = tan(\alpha_b) \cdot (\frac{2\sqrt{Gt}}{\sqrt{\pi}} \cdot exp\left(-(\frac{x}{2\sqrt{Gt}})^2\right) - x \cdot erfc\left(\frac{x}{2\sqrt{Gt}}\right)) \qquad (3)$$

with $G =$ shoreline diffusivity ($\frac{m^2}{sec}$), and $\alpha_b =$ breaking wave angle $(radians)$, $erfc(\ )$ is the complementary error function, and where the incident breaking wave angle has been assumed small (and constant in time). In view of the small incident breaking wave angle assumption, Eq. (3) can also be written with $\alpha_b \cong tan(\alpha_b)$ for small wave angles which will be utilized herein.

Pelnard-Considere (1956) also considered the situation where the jetty had a finite length and the beach evolution proceeded with the planform at $y(0,t) = L$ and bypassing of beach material was initiated around the end of the jetty. A single solution nomograph of this planform shape is also provided in Walton and Chiu (1979). This extended solution is not considered in the present work.

3. Solution for Piecewise Constant Shoreline Diffusivity at Infinite Jetty

To establish the methodology for the complete solution of piece-wise continuous wave angle and shoreline diffusivity, the somewhat simpler solution of a constant shoreline diffusivity and time varying piece-wise wave angle time series is first presented. As noted in previous paragraphs, the solution for the standard Pelnard-Considere (1956) (P-C) solution is for <u>constant</u> wave angle conditions and cannot be utilized ad hoc for time varying wave angle as seen in nature. At first inspection of the P-C solution, one might intuit that the solution can be extended to the piecewise constant wave conditions that exist in nature for changing wave conditions that are piecewise constant for (typically short) durations of time (3 to 6 hours when dealing with directional wave instruments or wave hindcasting data sources). This intuitive solution approach would be to piece together solutions for the constant wave case

situation where the solution is known at the end of one time step, and change in shoreline position for the piecewise constant wave conditions of the next time step is provided by the P-C solution at beginning and ending times of that time step for the constant wave conditions occurring during the time step. A simple argument will show that this is not the case. If wave angle reduces from one step to the next, it is clear that the corresponding boundary condition at the jetty (of Q=0) requires that sand transport at the jetty must be away from the jetty and the corresponding shoreline change at the jetty during the time step must be negative while the shoreline change at the jetty during the time step from the P-C solution would be positive, thus rendering this approach incorrect.

As the P-C solution is based on the linear partial differential equation (Eq.1), a linear combination of solutions in which both the field equations (Eq.1), and the boundary conditions, and initial conditions combine to the overall field equation, boundary condition, and initial condition is the required solution. Such an equivalent solution is given by utilizing the Heaviside function to turn the required wave conditions at each time step on and off. The easiest way to show such a solution is by example using a three time step solution to the problem.

For utility in explanation, each time step conditions will be represented by the index i where for time step 1 going from $t_0(=0)$ to t_1 is given by $i=1$. The second time step would be similarly represented by the time t_1 to t_2 given by $i=2$, and so on. As the initial condition to all time steps can be $y_i(x)=0$, for $t=t_0=0$, then all additive solutions have the same initial values. Additionally, following the "conservation of *authors* energy" principle, the substitution of α for α_b (i.e. dropping subscript) is used in the following. During the first time step, the boundary condition (b.c.) at the jetty is given by

$$-\frac{\partial y_1}{\partial x}(x=0) = \alpha_1 = \alpha_1 \cdot \mathcal{H}(t-t_0) \tag{4}$$

and the solution $(=y_1)$ valid for any time during the first time step $(t \le t_1)$ is provided by the P-C solution as

$$y_1(x,t) = \alpha_1 \cdot f(G, t-t_0) \cdot \mathcal{H}(t-t_0) \tag{5}$$

which is the P-C solution for wave condition set $\{\alpha_1, G, t-t_0\}$ where

$$f(G,t-t_0) = \left(\frac{2\sqrt{G(t-t_0)}}{\sqrt{\pi}} \cdot exp\left(-\left(\frac{x}{2\sqrt{G(t-t_0)}}\right)^2\right) - x \cdot erfc\left(\frac{x}{2\sqrt{G(t-t_0)}}\right)\right) \tag{6}$$

Proceeding beyond $t \ge t_1$ can be accomplished by utilizing the general solution to the partial differential equation on the semi-infinite plane with boundary condition at the jetty using the following solution (Carslaw and Jaegar (1986)) which is:

$$y(x,t) = \frac{G}{\sqrt{\pi}} \int_{t_0}^{t} \exp\left(-\frac{x^2}{4G(t-\tau)}\right) \frac{\alpha(\tau)}{\sqrt{t-\tau}} d\tau \tag{7}$$

and which can be split into piecewise constant integrals where $\alpha(t) = \alpha_i$ (a constant) for each of the integrals using the boundary condition valid during time step 2 (i.e. $t_1 < t \leq t_2$)

$$-\frac{\partial y_2}{\partial x}(x=0) = \alpha(\tau) = \alpha_1 \cdot \mathcal{H}(t-t_0) - \alpha_1 \cdot \mathcal{H}(t-t_1) + \alpha_2 \cdot \mathcal{H}(t-t_1) \quad (8)$$

with the corresponding P-C solution valid during time step 2 (i.e. $t_1 < t \leq t_2$) as

$$y(x,t) = -\frac{1}{\sqrt{\pi}}\left[\alpha_1 \int_{Gt_0}^{Gt_1} \exp\left(-\frac{x^2}{4G(t-\tau)}\right)\frac{1}{\sqrt{G(t-\tau)}}dG\tau + \alpha_2 \int_{Gt_1}^{Gt} \exp\left(-\frac{x^2}{4G(t-\tau)}\right)\frac{1}{\sqrt{G(t-\tau)}}dG\tau\right] \quad (9)$$

which can be solved in terms of the function $f(G,t)$ as follows for $t_0 < t \leq t_2$.

$$y_2(x,t) = \alpha_1 \cdot f(G,t-t_0)\cdot\mathcal{H}(t-t_0) - \alpha_1 \cdot f(G,t-t_1)\cdot\mathcal{H}(t-t_1) + \alpha_2 \cdot f(G,t-t_1)\cdot\mathcal{H}(t-t_1) \quad (10)$$

Proceeding in a similar fashion, during the third time step (with solution = y_3), the corresponding P-C solution valid up to time step 3 (i.e. $t_0 < t \leq t_3$) is provided by

$$\begin{aligned} y_3(x,t) = {} & \alpha_1 \cdot f(G,t-t_0)\cdot\mathcal{H}(t-t_0) - \alpha_1 \cdot f(G,t-t_1)\cdot\mathcal{H}(t-t_1) \\ & + \alpha_2 \cdot f(G,t-t_1)\cdot\mathcal{H}(t-t_1) - \alpha_2 \cdot f(G,t-t_2)\cdot\mathcal{H}(t-t_2) \\ & + \alpha_3 \cdot f(G,t-t_2)\cdot\mathcal{H}(t-t_2) \end{aligned} \quad (11)$$

and so on. It should be noted that the solution for the case of constant wave angle reduces to the standard Pelnard-Considere solution

$$y(x,t) = \alpha \cdot f(G,t) \quad (12)$$

Representative Wave Climate Time Series Examples where G = constant.

Example 4.1 - constant G, time varying α_b

As a first example, consider an 8 time step series in which one time step (=dt) is equal to 6 $months$ or 15,778,800 sec, and time steps are of equal length, shoreline diffusion is constant ($G = G(i) = 0.14\ \left(\frac{ft^2}{\text{sec}}\right)$ ($\cong 0.013\ \left(\frac{m^2}{sec}\right)$) for $i =$ 1 $thru$ 8) , and only the wave direction angle is changing from step to step. The wave direction angle series is provided as $\alpha_b(i) = \{5, 10, 5, 10, 5, 10, 5, 10\}°$. Although it is clear that wave conditions do not persist in nature for this long, this time step length provides an improved delineation of shoreline changes in graphical form for illustration purposes. The piecewise continuous solution to this P-C case is given in Figure 2 where the numbered shoreline shows the shoreline at the end of the i^{th} time step. Continuing with this example, Figure 3 shows the piecewise

continuous solution to this same P-C case for the scenario where $\alpha_b(i) = \{10, 5, 10, 5, 10, 5, 10, 5\}°$, i.e. the same wave direction angles only in reverse order, and G, dt as before. Note that the storage in the fillet of the jetty is the same due to the same overall transport volume captured by the jetty in both cases although the shorelines at various times are very different and the final shoreline at the end of time step 8 extends to > 650 feet at the jetty in Figure 2 but < 570 feet in Figure 3 showing the importance of wave directional sequencing to the build up of sand at the jetty even though overall sediment volume in the jetty fillet at the end of 8 time steps (= 4 years) is the same.

Example 4.2 – constant G , time varying α_b

As a second example with constant shoreline diffusivity but piece-wise continuous time varying wave angle, consider a 5 time step series in which one time step (=dt) is again equal to 6 $months\ \ or$ 15,778,800 sec, and time steps are of equal length, shoreline diffusion is constant ($G = G(i) = 0.14\ \left(\frac{ft^2}{\text{sec}}\right)$ ($\cong 0.013\ \left(\frac{m^2}{sec}\right)$) for $i = 1\ thru\ 5$) , and only the wave direction angle is changing from step to step. The wave direction angle series is provided as $\alpha_b(i) = \{5, 0, 10, 0, -2.5\}°$. The piecewise continuous solution to this P-C case is given in Figure 4 where the numbered shoreline shows the shoreline at the end of the i^{th} time step. Continuing with this example, Figure 5 shows the piecewise continuous solution to this same P-C case for the scenario where $\alpha_b(i) = \{-2.5, 0\ 10, 0, 5\}°$, i.e. the same wave direction angles only in reverse order, and G, dt as before. Note that the storage in the fillet of the jetty is the same in both examples at the end of 5 time steps due to the same overall transport volume captured by the jetty in both cases although the shorelines and storage volumes at various times are different.

4. Solution for Piece-wise Constant Wave Angle and Shoreline Diffusivity at an Infinite Length Jetty

An extension of the previous solution for the case of constant G and varying α_b can be shown to be the solution for the case of time varying $G(t)$ and $\alpha_b(t)$. The solution follows as before although due to paper size limitations the complete solution is not shown herein. Proceeding in a similar fashion as before, it follows that the solution of the three step case (for $t \le t_3$) is as follows:

$$\begin{aligned} y_3(x,t) = {} & \alpha_1 \cdot f(G_{t_0,t}, t - t_0) \cdot \mathcal{H}(t - t_0) \\ & - \alpha_1 \cdot f(G_{t_1,t}, t - t_1) \cdot \mathcal{H}(t - t_1) \\ & + \alpha_2 \cdot f(G_{t_1,t}, t - t_1) \cdot \mathcal{H}(t - t_1) \\ & - \alpha_2 \cdot f(G_{t_2,t}, t - t_2) \cdot \mathcal{H}(t - t_2) \\ & + \alpha_3 \cdot f(G_{t_2,t}, t - t_2) \cdot \mathcal{H}(t - t_2) \end{aligned} \qquad (13)$$

and so on for additional time steps.

Representative Wave Climate Time Series Examples where G , α_b are variable but piece-wise constant during time step.

Example 5.1- Time Varying G and α_b
As an example of a time varying shoreline diffusion and wave angle situation, a 10 time step series (5 years total duration) is provided in which time steps are again the same duration (6 months) as in Example 4.1 and the piece-wise constant but time varying shoreline diffusion series is given in English $\left(\frac{ft^2}{\text{sec}}\right)$ units as
$G(i) = [0.095, 0.105, 0.115, 0.125, 0.135, 0.145, 0.155, 0.165, 0.175, 0.185]$
or in SI units $\left(\frac{m^2}{\text{sec}}\right)$, as
$G(i) = [0.0088, 0.0098, 0.0107, 0.0116, 0.0125, 0.0135, 0.0144, 0.0153, 0.0163, 0.0172]$
for $i = 1\ thru\ 10$, while the piece-wise constant but time varying wave direction angle series is
$\alpha_b(i) = [\,5.7724, 5.2162, 4.7582, 4.3744, 4.0481, 3.7672, 3.5229, 3.3084, 3.1186, 2.9494]°$.

This shoreline diffusion and wave angle series can be shown to provide a sediment transport equal to $Q(i) = 300{,}000\ \frac{c.y.}{yr}$ $(\cong 230{,}000\ \frac{m^3}{yr})$ (directed toward the jetty) for all i (assuming $h_c + B = 27(ft)$ $(\cong 8.23\ (m))$) where

$$Q(i) = \alpha_b \cdot K \cdot H_b^{5/2} \cdot \sqrt{g/\kappa}\ \cdot (8(S_g - 1)(1-p))^{-1} \qquad (14)$$

is the sediment transport for a shoreline (in linearized case) located along the x axis (i.e. the shoreline initial condition at all x values $[\,\frac{\partial y(x,0)}{\partial x} = 0\,]$, or the shoreline a sufficient distance from the jetty so as not to be influenced by the jetty). On using Eq. 2, the above equation can be show equivalent to the following (i.e. see for example Dean and Dalrymple (2002))

$$Q(i) = \mathrm{G(i)} \cdot (h_c + B) \cdot (\sin(2 \cdot \alpha_b)/2)\ \approx G(\mathrm{i}) \cdot (h_c + B) \cdot \alpha_b \qquad (15)$$

An equivalent constant time G and α_b to produce the same volume of sand storage during total time of sand flow $Q = 300{,}000\ \frac{c.y.}{yr}$ $(\cong 230{,}000\ \frac{m^3}{yr})$ can be found as:
$G = 0.14\ (\frac{ft^2}{sec}) \cong 0.013\ \left(\frac{m^2}{sec}\right)$ and $\alpha_b = 3.9026°$.

Figure 6 provides the shorelines for the time varying $G(i)$ and $\alpha_b(i)$ as shown above while Figure 7 shows the shorelines for the time varying reversed $G(i)$ and $\alpha_b(i)$ series, and Figure 8 gives the shorelines for the equivalent total sediment transport time constant representative G and α_b values above. Note that in all cases the volumes of sand transported to the jetty fillet at the end of the 10 time steps (=5 years) is the same and equal to 1,500,000 c.y. (=1,148,000 m^3) for an assumed closure depth of 27 ft. (= 8.2 meters). Verification of solution volume has been accomplished by integration of the solution $y(x,t)$ along the shoreline

(i.e. $x - axis$) at the end of time step $i = 10$ using Simpson integration.

Example 5.2 Time Varying G and α_b
As a second example of piece-wise continuous but time varying shoreline diffusion and wave angle, the same 10 step shoreline diffusion series as provided in example 5.1 above is utilized with the same magnitude wave angle series, difference being that the wave angle series is now alternating in sign as follows:
$\alpha_b(i) = [\,5.7724, -5.2162, 4.7582, -4.3744, 4.0481, -3.7672, 3.5229, -3.3084, 3.1186, -2.9494]°$
As per previous example, the sediment transport rate in each step is equivalent in magnitude but alternating in direction. As a result, the overall volume of sand in the fillet is now zero, but the shoreline takes a shoreline planform very different from zero. Two figures are presented for this specific example with Figure 9 showing results for the wave angle series provided above with $\alpha_b(1) = 5.7724°$, and with Figure 10 showing results for the same wave angle series only where both the shoreline diffusion time series and wave angle time series are reversed (i.e. $G(1) = 0.185\ (\frac{ft^2}{sec}) \cong 0.0172\ \left(\frac{m^2}{sec}\right)$ and $\alpha_b(1) = -2.9494°$).

5. Summary and Conclusions

In the presented work, simple direct analytic solutions for the case of time varying but piecewise constant wave angle and shoreline diffusivity are presented and applied in a limited number of example cases for related but different time varying series of breaking wave angles and shoreline diffusivities (i.e. wave height, wave period, and wave direction series). In all cases it is clear that the time varying nature of the wave direction is very important to the shoreline shape for this semi-finite region situation, and that a constant wave condition time series of wave parameters which has the same total sediment transport in a given time (i.e. same final groin/jetty fillet volume in a given time) as a time varying wave condition time series of wave parameters may lead to a very different shoreline planform.

6. Acknowledgments

The author would like to thank the Florida Department of Environmental Protection, Bureau of Beaches and Coastal Systems and its Bureau Chief, Mike Barnett for support and the opportunity to do research on beach fill model performance on barrier islands.

7. References

Carslaw, H., Jaeger, J. (1986). *Conduction of Heat in Solids, Second Edition*, Cambridge University Press, Oxford, UK, 510 pp.

Dean, R.G. (1984). Principles of beach nourishment, In: Komar, P. D. (Ed.), *Handbook of Coastal Processes and Erosion*, CRC Press, Boca Raton, FL., pp. 217-232.

Dean, R. G. (2003). *Beach Nourishment: Theory and Practice*, World Scientific, Singapore, 399pp.

Dean, R. G., Dalrymple, R. A. (2002). *Coastal Processes*, Cambridge University Press, Oxford, UK, 475pp.

Larson, M., Hanson, H., Kraus, N.C. (1987). "Analytical solutions of the one line model of shoreline change", *Report TR-CERC-87-15*, Coastal Engineering Research Center, United States Army Waterways Experiment Station, Vicksburg, MS., 95pp.

Larson, M., Hanson, H., Kraus, N.C. (1987). "Analytical solutions of one-line model for shoreline change near coastal structures", *Journal of Waterway, Port, Coastal, and Ocean Engineering*, 123(4), 180-191.

Pelnard-Considere, R. (1956). "Essai de theorie de l'evolution des forms de rivages en plage de sable et de galets", *Fourth Journel de l'Hydralique, les energies de la Mer*, Question III, Rapport No. 1, 289-298 [In French].

Reeve, D.E. (2006). "Explicit expression for beach response to non-stationary forcing near a groyne", *Journal Waterways, Ports, Harbors, Coastal, and Ocean Engineering*, 132(2), 125-132.

U.S. Army Corps of Engineers (1990). *Report - General design memorandum*, Broward County Florida, Shore Protection Project, Jacksonville District Office, Jacksonville, Florida, 129pp.

U.S. Army Corps of Engineers (1991). *Report- General design memorandum*, Palm Beach County, Florida, Shore Protection Project, Jacksonville District Office, Jacksonville, Florida, 198pp.

Walton, T. L. Jr. (1994). "Shoreline solution for tapered beach fill", *Journal Waterways, Ports, Harbors, Coastal, and Ocean Engineering*, 120(6), 651-655.

Walton, T. L. Jr. (2005). "A review of inlet bypassing solutions with nomographs", *Coastal Engineering*, 52, 1127-1132.

Walton, T. L. Jr. (2007). "Storm protection beach fill planning on barrier islands", Shore & Beach, 75(1), 43-48.

Walton, T. L. Jr., Chiu, T. Y. (1979). "A review of analytical techniques to solve the sand transport equation and some simplified solutions", In: *Proceedings Coastal Structures 1979, American Society of Civil Engineers*, New York, N.Y., pp.809-837.

Zacharioudaki, A. and Reeve, D.E. (2008). "Semi-analytical solutions of shoreline response to time-varying wave conditions", *Journal Waterways, Ports, Harbors, Coastal, and Ocean Engineering,* 134(5), 265-274.

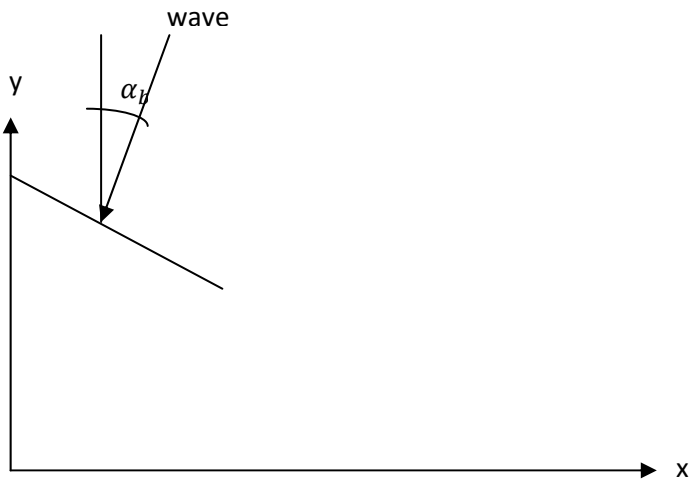


Figure 1. Coordinate System for Pelnard–Considere Solution.

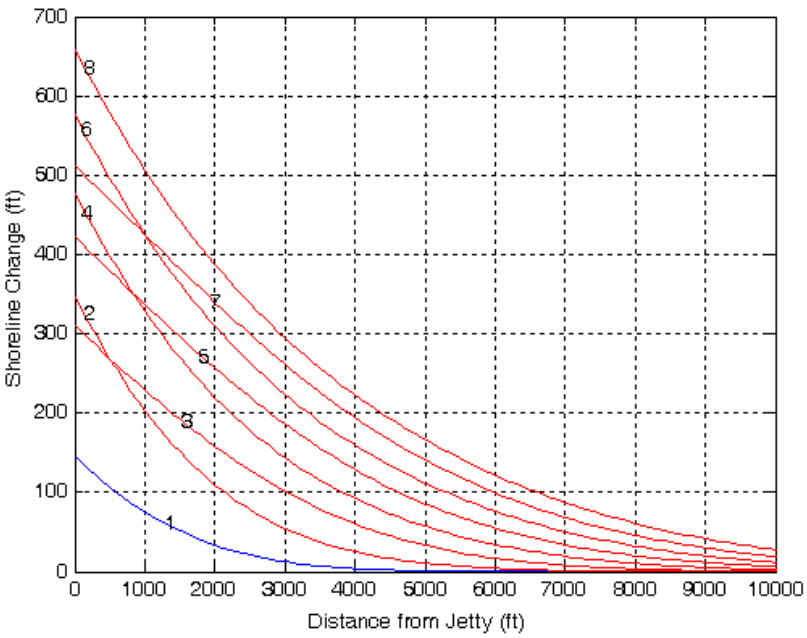


Figure 2. Shorelines from Time Varying Wave Angle Series where $G(i) = 0.14\ \left(\frac{ft^2}{\text{sec}}\right) = 0.013\ \left(\frac{m^2}{sec}\right)$, $and\ \alpha_b(i)\ = \{5, 10, 5, 10, 5, 10, 5, 10\}°$.

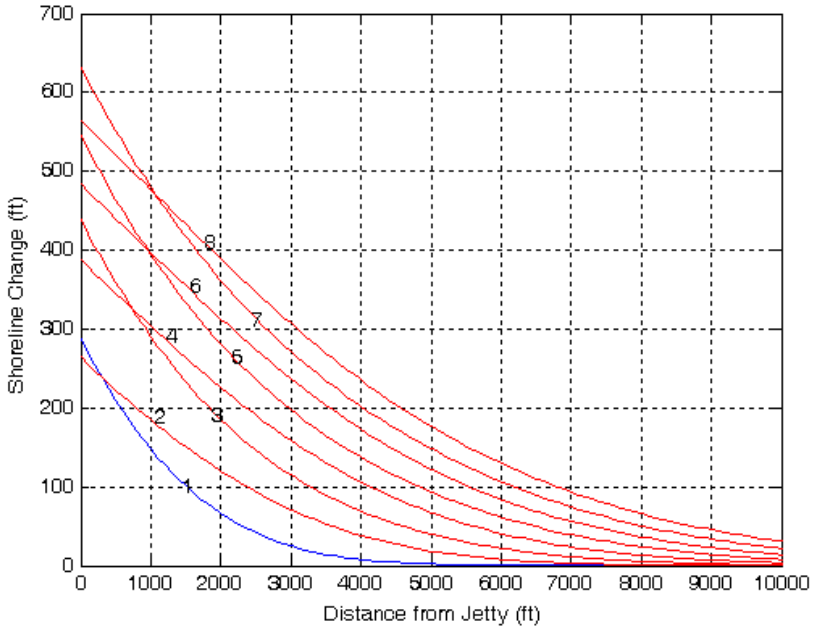


Figure 3. Shorelines from Time Varying Wave Angle Series with same values as Figure 2 only Wave Angle Series is reversed.

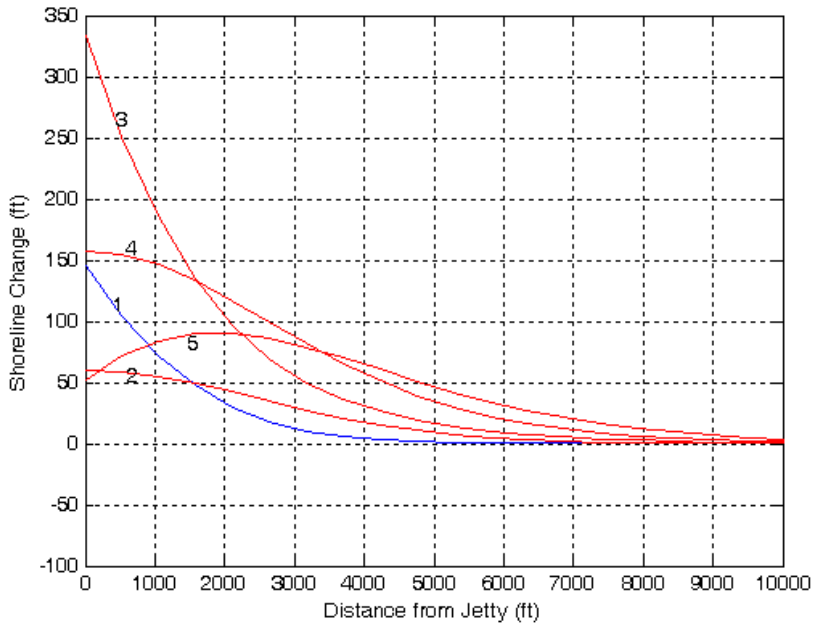


Figure 4. Shorelines from Time Varying Wave Angle Series where $G(i) = 0.14\ \left(\frac{ft^2}{\text{sec}}\right) = 0.013\ \left(\frac{m^2}{sec}\right)$, $and\ \ \alpha_b(i)\ = \{5, 0, 10, 0, \text{-}2.5\}°$.

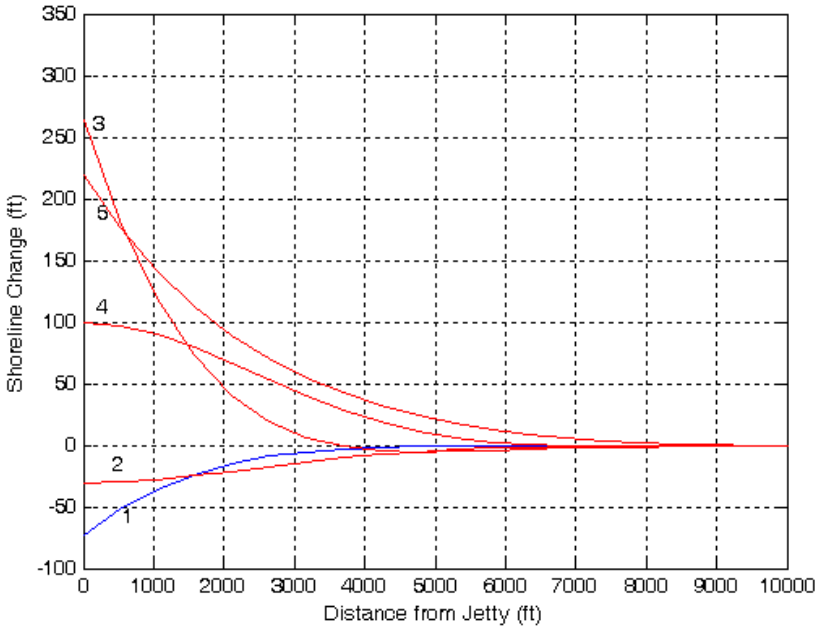


Figure 5. Shorelines from Time Varying Wave Angle Series with same values as Figure 4 only Wave Angle Series is reversed.

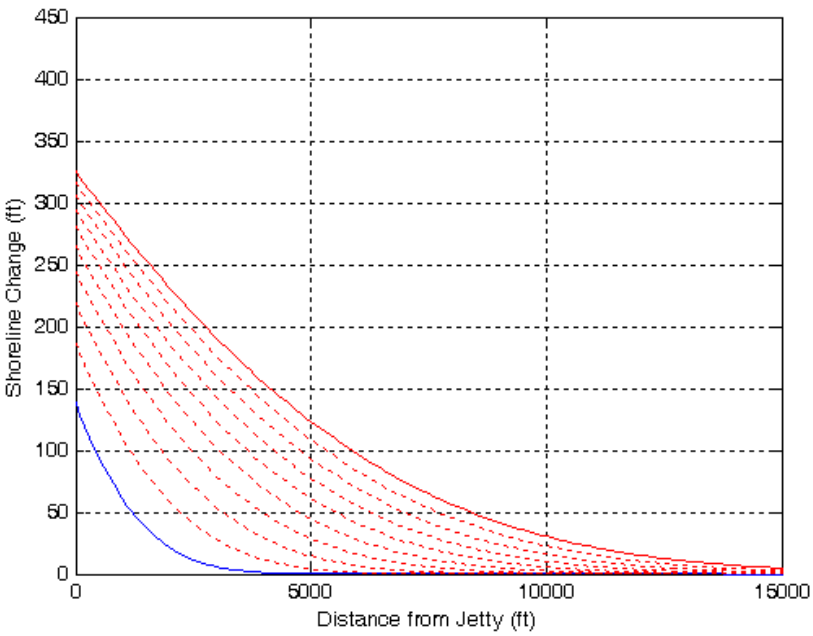


Figure 6. Example 5.1a. Shorelines from Time Varying Shoreline Diffusion Coefficient Series and Time Varying Wave Angle Series where $G(i) = [0.0088, 0.0098, 0.0107, 0.0116, 0.0125, 0.0135, 0.0144, 0.0153, 0.0163, 0.0172]\ \left(\frac{m^2}{\text{sec}}\right)$, $\alpha_b(i) = [\,5.7724, 5.2162, 4.7582, 4.3744, 4.0481, 3.7672, 3.5229, 3.3084, 3.1186, 2.9494]°$.

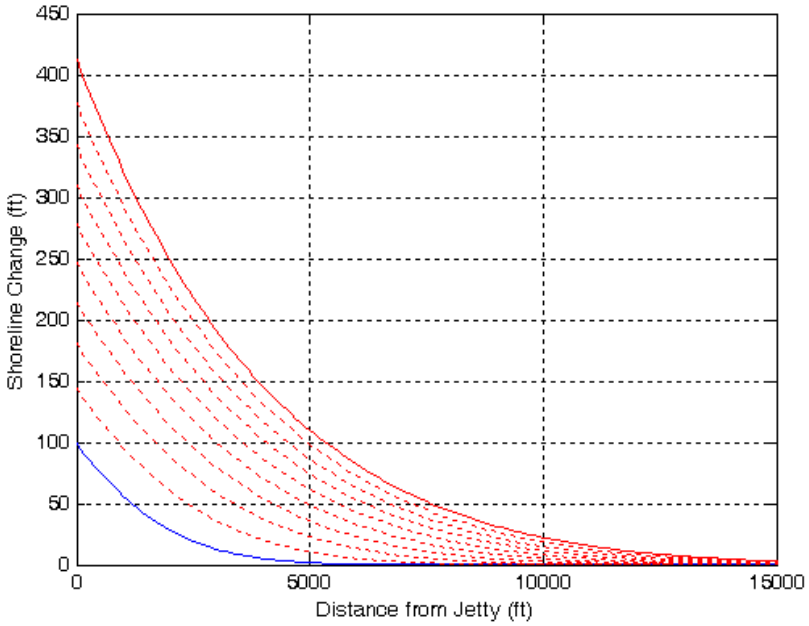


Figure 7. Example 5.1b. Shorelines from Time Varying Shoreline Diffusion Coefficient Series and Time Varying Wave Angle Series where both series have been reversed from those in Figure 6.

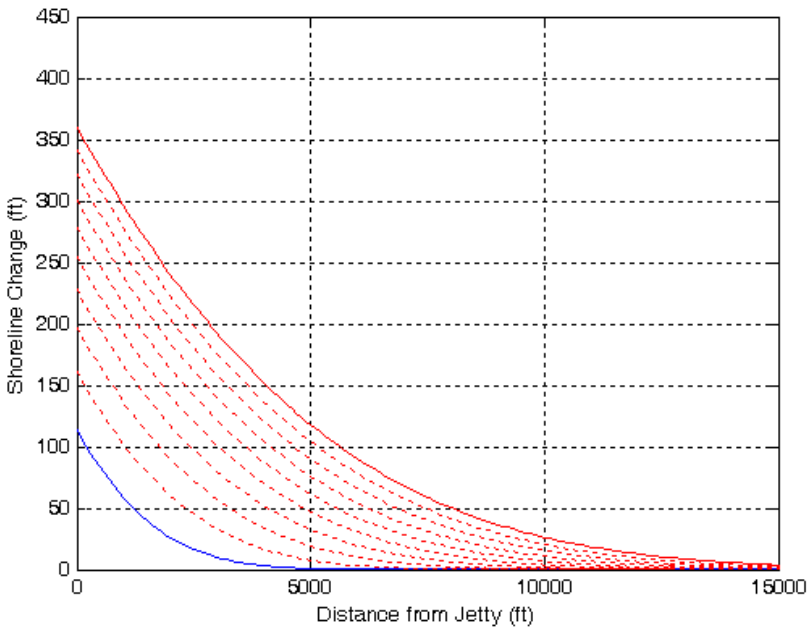


Figure 8. Example 5.1c. Shorelines from Time Constant Shoreline Diffusion Coefficient Series and Time Constant Wave Angle Series where $G = 0.14\ (\frac{ft^2}{sec}) \cong 0.013\ \left(\frac{m^2}{sec}\right)$ and $\alpha_b = 3.9026°$

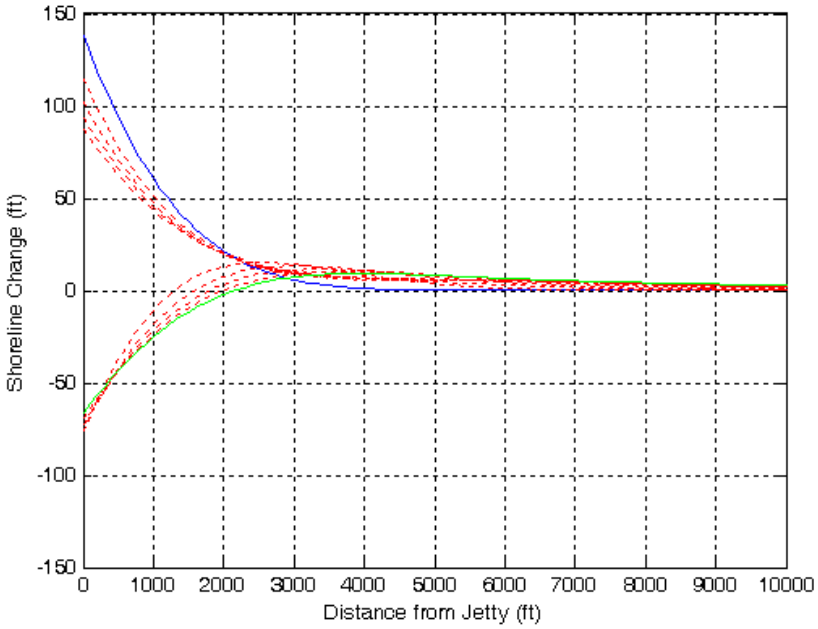


Figure 9. Example 5.2a. Shorelines from Time Varying Shoreline Diffusion Coefficient Series and Time Varying Wave Angle Series where $G(i) = [0.0088, 0.0098, 0.0107, 0.0116, 0.0125, 0.0135, 0.0144, 0.0153, 0.0163, 0.0172]\ \left(\frac{m^2}{\text{sec}}\right)$, $\alpha_b(i) = [\ 5.7724, -5.2162, 4.7582, -4.3744, 4.0481, -3.7672, 3.5229, -3.3084, 3.1186, -2.9494]°$.

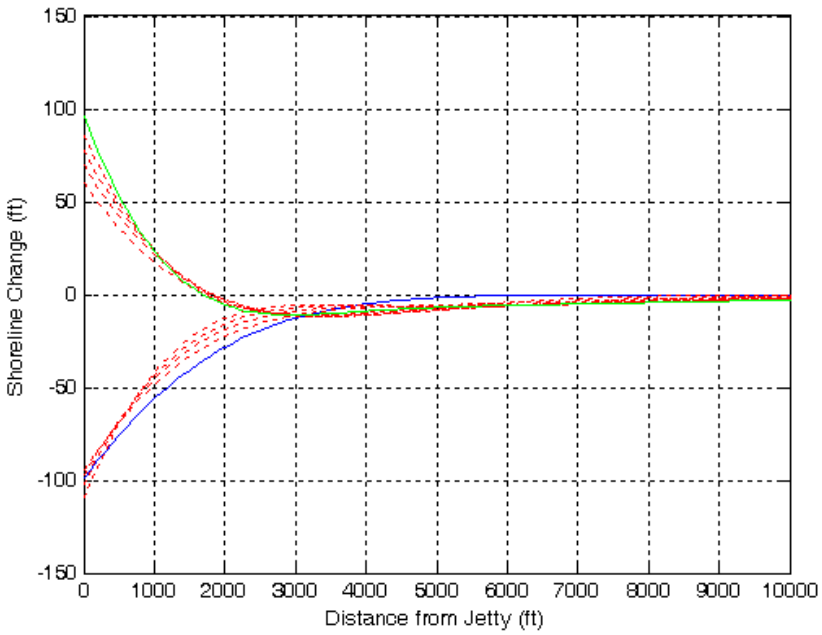


Figure 10. Example 5.2b. Shorelines from Time Varying Shoreline Diffusion Coefficient Series and Time Varying Wave Angle Series where wave angle series has been reversed from that in Figure 9.

EVENT RANKING METHODS FOR CALCULATION OF 100-YEAR WAVE RUNUP ON LEVEES AT OAKLAND INTERNATIONAL AIRPORT, CALIFORNIA

Jeremy Bricker[1], Philip Mineart[1], Sathish Murugaiah[1], John Paxton[1], Rajendram Arulnathan[1], Samuel Won[2], Frank Lobedan[2]

[1]URS Corp., 1333 Broadway, Suite 800, Oakland, CA 94612, USA; phone (510) 893-3600; email bricker@stanfordalumni.org, phillip_mineart@urscorp.com, sathish_murugaiah@urscorp.com, john_paxton@urscorp.com, rajendran_arulnathan@urscorp.com.
[2]Port of Oakland, 530 Water St., Oakland, CA 94607, USA; phone (510) 627-1130; email swon@portoakland.com , flobedan@portoakland.com.

ABSTRACT

In the design of coastal protection structures like levees and seawalls, two important parameters are the design water level and wave height. The design water level determines the required crest height and strength of the structure. The design wave height is used to determine the type of armor necessary to protect the structure from wave attack. Determining the design water level and wave height requires a long time series of water level and wave height data. A rigorous analysis would use hydrodynamic and wave models to determine the hourly water levels and wave heights at the toe of the structure, over a period of many years. However, constraints in budget, time, or computational resources often make this type of analysis impractical. An alternative is to develop an event ranking method to identify the most intense annual storm events, then analyze only those storms in detail. This paper describes two such ranking methods, one of which was applied to Oakland International Airport and shown to work well when compared with results from rigorous hourly two-dimensional wave modeling.

INTRODUCTION

The levees protecting Oakland International Airport (OAK, see Figures 1 and 2) were evaluated for their ability to protect the airport from 100-year flooding due to tides, storm surge, and waves in San Francisco Bay. Historical tidal data, hydrodynamic and wave modeling, and empirical relations were used to determine the levee height and armor type necessary for this level of protection. To determine what level of protection is necessary at OAK, coastal conditions had to be evaluated to determine the 100-year (1% annual chance) still water level (SWL), total water level (TWL), and erosive power. Total water level is equal to the sum of SWL (including both tidal stage and storm surge) and wave runup. Since OAK is located well within shallow San Francisco Bay, ocean swell and tsunami are not items of concern (Borrero et al, 2006). Due to limited computational resources and the limited correlation between observed still water level (including storm surge) and wind velocity, ranking methods were developed to determine which SWL and wind events likely generated the largest annual total water levels, which were then determined accurately via a two-dimensional wave model. These ranking methods were similarly applied to determine the largest annual wave heights, for use in sizing riprap in the levee design.

DETERMINING DESIGN STILL WATER LEVEL

The design SWL was determined through a combination of historical tide data and 2-D hydrodynamic modeling. The NOAA tide gauge at San Francisco's Presidio (23 km northwest of OAK) has recorded hourly data since 1902, while that at the Alameda NOAA gauge (9 km northwest of OAK) has such data available since 1996 (Table 1). In order to estimate the largest SWL events at OAK, a transfer function was developed by using a least squares fit between the maximum daily stages at Presidio and Alameda during Alameda's 13 years of record.

Since this analysis is concerned only with flood water levels, only the daily maximum water levels (not hourly water levels) were used for this procedure. The transfer function was then applied to all 107 years of water level data at the Presidio, to generate a 107-year water level record at Alameda.

During the period of record for the Presidio gauge, a long-term increase in sea level has occurred due to climactic changes. To provide a consistent record of water level (i.e., related to a common sea level), the data were adjusted to the sea level on December 31, 2008. As expected, this trend equals approximately 2 mm/year, which is near global average sea level rise over the past century (Church & White, 2006). However, since the change in water level due to sea level rise was determined only using maximum daily water levels (and not hourly water levels), it also takes into account the historic change in tidal amplitude that may have accompanied the rise in the mean sea level. Since flood water levels are being simulated, this change in tidal amplitude could be important.

After correcting for historic sea level rise (SLR), the Danish Hydraulics Institute (DHI) MIKE-21 two-dimensional hydrodynamic model was used to generate a transfer function relating SWL at Alameda to SWL at OAK. The model boundary conditions were tidal stage outside the Golden Gate and winds recorded at OAK. To limit model simulations only a single year was used to generate a transfer function from the Alameda gauge to OAK. The 1998 water year was chosen for simulation because this was a wet year, so storm surge effects were present in the boundary conditions. The resulting transfer function allowed maximum daily SWL at OAK to be determined based on the Alameda gauge data.

The maximum annual SWL for each of the 107 years of data at OAK were then extracted and fit with a 3-parameter Weibull distribution, allowing the 1% annual chance (100-year) SWL (or any other return period event) to be determined (Figure 3). For planning purposes, the 100-year event for the year 2100 was also evaluated, by considering SLR of 1.4 m (Rahmstorf, 2007).

METHOD 1 RANKING FOR TOTAL WATER LEVEL

Determination of 100-year total water level (TWL) at Oakland Airport (OAK) entailed determining the still water level (SWL) plus wave runup. SWL and runup are not independent but are physically correlated, e.g. a strong onshore wind would generate both large waves (affecting runup) and a storm surge (affecting SWL); even the storm surge itself could result in larger waves in shallow areas by increasing the maximum

wave height before depth-induced breaking occurs. To analyze TWL using a Monte Carlo method would require that the correlation between SWL and wind be known. Instead, to maintain this correlation, the TWL was calculated using a time-series analysis of concurrently observed winds and water levels.

Hourly water level at OAK was determined via the method described above for SWL. That is, the observed 106 year long time series from Presidio, corrected for sea level rise, was transformed to Alameda. Water levels at Alameda were then transformed to OAK using another transfer function. This is the same procedure as above, except that here it's carried out with the full set of hourly data, not just daily maxima.

Hourly wind data were obtained for OAK as shown in the wind roses in Figures 4 and 5. OAK water levels were interpolated onto the same time base as the wind data. However, the entire hourly time series, spanning from 1943-2008, was too long to evaluate with the two-dimensional MIKE21 Nearshore Spectral Wave (NSW) model. Therefore, FEMA guidance (FEMA, 2005) was adhered to, in choosing the 20 largest events each year. In order to determine which winds and water levels would likely generate the 20 largest events each year (still water level plus runup), hourly time series were evaluated for two particular winters: 1987-88 and 1997-1998. The latter winter was chosen because it spanned an El Nino event, during which many storms crossed through the area. The other winter was chosen randomly. TWL was calculated using the MIKE21 NSW results, and then ranked. It was found that most of the top 20 events each year were recognizable by the ranking parameter of Equation (1).

$$\text{Ranking Parameter} = SWL^2 \times \text{sign}(SWL) \times (\text{Wind Speed}) \qquad (1)$$

The dimension of this parameter (m^3/s) is meaningless, as it is used only for ranking events. The validity of equation (1) in predicting the largest TWL events is shown in tables 2 and 3. For both the winter 1997-98 (El Nino) data set and the winter 1987-88 (randomly chosen) data sets, equation (1) correctly predicted 8 of the 10 largest TWL events.

Each water year (October 1 – September 30), all hourly wind and water level data were ranked via Equation (1). The 20 largest events were then extracted to be analyzed with MIKE21 NSW. In choosing the 20 largest events each water year, only events with wind direction between 130° and 310° were considered, as these represent winds onshore to the airport. Winds coming from directions less than 130° or greater than 310° are offshore winds, and do not generate large waves incident on the OAK perimeter dike. In addition, events were required to be spaced at least 12 hours apart; hourly events occurring less than 12 hours apart from each other were considered to be the same event, so only the largest of a group of events occurring within 12 hours of one another was considered. This insured that each storm was counted only once.

Each water year's 20 largest estimated events were then used as input files to MIKE21 NSW, which was used to calculate the significant wave height and period along the OAK perimeter dike for each event. Since the MIKE21 NSW model requires the model grid to be rotated such that all waves are propagating with a positive celerity

component along the x-axis, four different grids were used. These grids were centered such that the negative x-axis (the direction from which the wind blows) pointed 152.5°, 197.5°, 242.5°, and 287.5° clockwise from north. Each grid was then used for winds blowing from within 22.5° of its orientation. Figures 6, 7, and 8 show examples of the wave field hindcast by MIKE21 NSW for the case of a south-southwesterly wind (using the grid with the negative x-axis aligned with direction 197.5°).

For each event, the maximum significant wave height and period were used in the calculation of runup. Runup was determined from procedures found in the Coastal Engineering Manual (USACE, 2006). Runup was determined for the 20 biggest storm events each water year, throughout the 58 year period of record of OAK wind data. TWL for each event was then determined as the sum of SWL and runup for that event. In order to determine the 1% annual chance TWL, each year's highest TWL was identified and fit to a 3-paramter Weibull distribution, as shown in Figure 9, from which the 1% annual TWL was identified. The value was 4.13 m NAVD, for the case in which the mean sea surface elevation remains at its 2008 value. Accounting for a 1.4 m sea level rise by 2100 (Rhamsdorf, 2007), the 1% annual TWL becomes 5.56 m NAVD (Figure 10). The difference between the no-SLR TWL and the 1.4 m SLR TWL is greater than 1.4 m because the higher sea level, in addition to increasing the SWL, also allows waves to grow larger before breaking and to experience less bed friction, resulting in higher runup in addition to the higher SWL.

To validate these TWL results, they were compared to one historical incident. In December 1983, OAK was subjected to a storm that caused significant runup-induced overtopping of the perimeter dike. At the time, the crest of the levee was at an elevation of approximately 3.79 m NAVD (after that storm, the crest of the levee was raised, but the comparison with the event uses the crest elevation at that time). The highest runup event in Figure 10 corresponds to this December 1983 event. The runup hindcasted by the model is 3.91 m NAVD (after correcting for the lower mean sea level in 1983 as compared to 2008), which is high enough to have overtopped the 3.79 m NAVD levee. The model thus agrees with historical observations in hindcasting overtopping during the December 1983 storm.

METHOD 1 RANKING FOR WAVE EROSIVE POWER

Armor layer stability is determined via the Coastal Engineering Manual (USACE, 2006, table VI-5-22), which outlines the data of Hudson (1974). The significant wave height needed for this design is the 100-year H_s. In order to determine this value, an analysis similar to that above for TWL was conducted. However, instead of predicting the maximum 20 TWL events each year, the events resulting in the largest twenty H_s each year were predicted. These were predicted via the relation

$$\text{Ranking Parameter} \sim (\text{Wind Speed}) \qquad (2)$$

Equation (2) was shown to correctly predict the 20 largest wave events during the winters of 1987-88 and 1997-98. Therefore, equation (2) was used to predict the 20 largest events during all years of the wind record. After determining the 20 largest H_s events each year, the annual largest H_s was extracted. Figure 11 shows a histogram of

the largest annual H_s, along with a Weibull fit to these data. The resulting 100-year significant wave height incident on OAK is 1.47 m. Given this 100-year design significant wave height, Hudson (1974) shows that armor stone with median size D_{n50} = 0.64 m is necessary in order that the armor experiences only 0-5% damage in the design storm.

METHOD 2 RANKING FOR TOTAL WATER LEVEL

Method 1 for ranking TWL and wave height events (equations 1 and 2) were sufficient for OAK because the airport's geometry (Figures 1 and 2) and storm wind patterns (Figure 10) result in only southerly to southwesterly winds being of issue. Therefore, most storm winds having significant effect on OAK have similar fetch and incident direction to one another. If winds from many directions (and thus many different fetches) were important, or if ocean swell or other physics needed to be included, then a more sophisticated ranking method would be required. Furthermore, if different locations along the levee were exposed to different waves, or if different sections of the levee had a different geometry (slope or berm width), then runup would be different on these different sections, and again a more sophisticated ranking method would be necessary.

This more sophisticated ranking method replaces the ranking parameter of equation (1) with an estimated TWL based on USACE (2006). For each hourly wind in the available time series, a representative wind wave height H_{m0} near the shoreline is given by the minimum of H_{m0} as determined from USACE (2006) equations (II-2-36), which show how deep-water wave height grows with fetch, and USACE (2006) equations (II-2-37), which show fully-developed deep-water wave height for a given wind speed. For the case of OAK, the representative fetch to the middle of the dike is approximately 10 km for winds incident on the 152.5° grid, 15 km for the 197.5° grid, 15 km for the 242.5° grid, and 12 km for the 197.5° grid. These values are rough approximations, but they are only used for ranking events; events chosen for further analysis will be evaluated in greater detail. For each hour of wind data available, USACE (2006) equations (VI-5-2) and (VI-5-3) are then used to calculate an hourly time series of estimated runup, corresponding to each hour of wind data.

If ocean swell exists as well, the same runup estimation must be carried out for the ocean swell data. The TWL Ranking Parameter for each hour of wind (and ocean swell, if applicable) data is then determined by equation (3).

$$\text{TWL Ranking Parameter} = \text{SWL} + \text{Wind Wave Runup} + \text{Ocean Swell Runup} \quad (3)$$

For each grid octant, the 20 largest ranked events each water year need to be chosen for further analysis. From here on, this method is the same as Method 1. Each chosen event is simulated with MIKE21-NSW. The resulting wave height, period, and direction are then used to calculate accurate runup due to windwaves (and ocean swell, if applicable). A series of the maximum annual TWL is generated for the duration of the wind record. Finally, these events are fit to a Weibull distribution to determine the design frequency TWL.

METHOD 2 RANKING FOR WAVE EROSIVE POWER

Method 2 for ranking erosive power is the same as Method 1, except that the wave height ranking parameter from equation (2) is replaced with the estimated wave height from USACE (2006) equations (II-2-36) or (II-2-37). Method 2 is more accurate than Method 1 in conditions where fetch varies significantly with wave direction.

CONCLUSION

Methods were formulated to determine the design SWL and TWL for the OAK levee. Limited hydrodynamic modeling was used to develop a transfer function, allowing use of a nearby tide gauge in generating a long data record for SWL. Likewise, limited wave modeling was used in developing a ranking system to extract the largest annual TWL events. Further wave modeling was then carried out to determine the TWL resulting from each of these events. Despite limited computational resources, a thorough analysis of coastal conditions was possible.

Two methods of ranking TWL were evaluated for their use in capturing the largest annual TWL event. Similarly, two methods of ranking wave height were evaluated for their use in capturing the largest annual wave height event. Method 1, being the simplest, is only applicable where fetch does not vary significantly with wave incidence direction, and where only wind waves are of importance (i.e. ocean swell is not present). Method 1 worked well for the levee on the west side of Oakland International Airport. Method 2, being more rigorous, is applicable to any general situation. Method 2 must be used where fetch varies significantly with wave direction, or where ocean swell and wind waves are both important.

ACKNOWLEDGEMENTS

We appreciate the staff of Oakland International Airport and the Port of Oakland for funding this work.

REFERENCES

Borrero, J., Dengler, L., Uslu, B., and Synolakis, C., (2006). Numerical modeling of tsunami effects at marine oil terminals in San Francisco Bay. *Report for the Marine Facilities Division of the California State Lands Commission*.

Church, J.A., and White, N.J. (2006). A 20th century acceleration in global sea-level rise. *Geophysical Research Letters*. Volume 33 L01602

FEMA, (2005), Final Draft Guidelines for Coastal Flood Hazard Mapping for the Pacific Coast of the United States.

Hudson, R.Y. (1974). Concrete Armor Units for Protection against Wave Attack; Report of Ad Hoc Committee on Artificial Armor Units for Coastal Structures. Report for the Army Engineer Waterways Experiment Station, Vicksburg, Miss.

Rahmstorf, S., (2007).A Semi-Empirical Approach to Predicting Future Sea-Level Rise.*Science*, 315(5810): 368-370.

USACE, (2006).*Coastal Engineering Manual*.US Army Corps of Engineers.

Table 1 NOAA Tide Gauge Locations Near the Oakland Airport

Site Name	Location (LAT-LON)	Period of Record
San Francisco (Presidio)	37° 48.4'N, 122° 27.9'W	January 1, 1902 – May 31, 2008
Alameda	37° 46.3'N, 122° 17.9'W	January1, 1996 – May 31, 2008

Table 2. Events ranked by Ranking Parameter during the winter of 1997-1998.

TWL rank	TWL (m, NGVD)	SWL (m, NGVD)	Wind speed (m/s)	Wind direction	Ranking Parameter = SWL2 x sign(SWL) x (wind speed)
18	2.03	1.87	12.9	130	45.26
4	2.33	2.09	10.3	130	44.92
2	2.37	1.70	12.9	140	37.39
1	2.41	1.83	10.3	150	34.53
5	2.32	1.76	10.3	140	31.81
8	2.24	1.68	10.3	140	29.05
3	2.36	1.90	7.7	150	27.72
10	2.16	1.59	10.3	150	25.89
6	2.31	1.87	7.2	150	25.29
15	2.10	1.55	10.3	140	24.66

Table 3. Events ranked by Ranking Parameter during the winter of 1987-1988.

TWL rank	TWL (m, NGVD)	SWL (m, NGVD)	Wind speed (m/s)	Wind direction	Ranking Parameter = SWL2 * sign(SWL) * (wind speed)
5	2.08	1.49	10.3	170	22.96
3	2.11	1.70	7.7	230	22.33
1	2.17	1.70	7.7	180	22.16
7	2.04	1.46	10.3	170	22.06
13	1.91	1.28	12.9	140	21.24
4	2.10	1.64	7.7	160	20.60
6	2.05	1.63	7.7	250	20.43
2	2.15	1.75	6.2	180	19.01
8	2.01	1.55	7.7	160	18.52
11	1.99	1.57	7.2	140	17.85

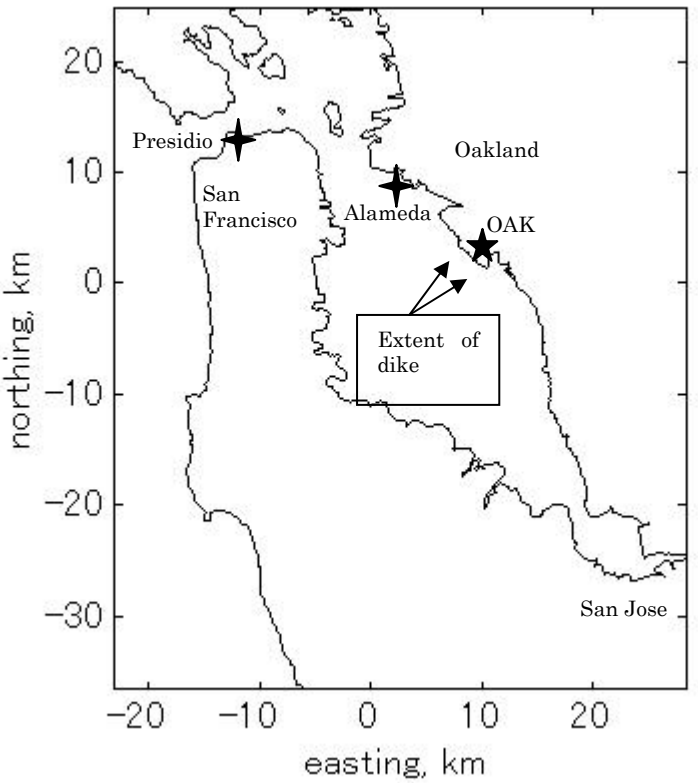


Figure 1. Map of San Francisco Bay and the Oakland Airport. The OAK perimeter dike spans the shoreline between the two arrows shown. The Presidio and Alameda tide gauges are shown as 4-pointed stars, and the Oakland Airport wind gauge is shown as a 5-pointed star.

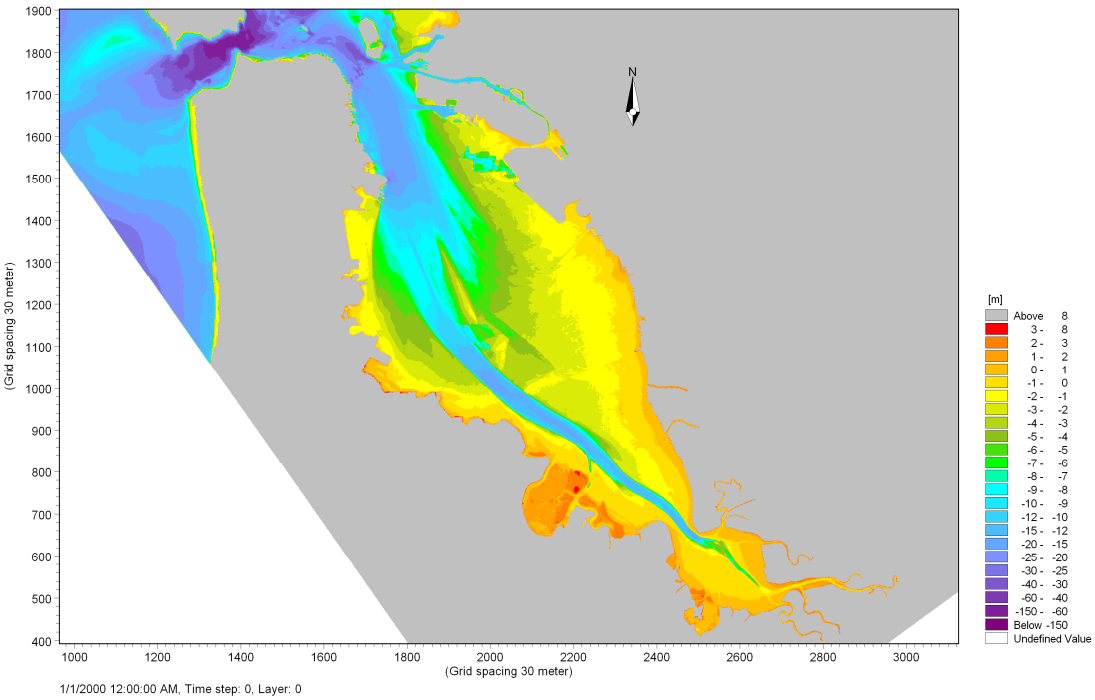


Figure 2. Bathymetry of South San Francisco Bay, in meters NGVD29.

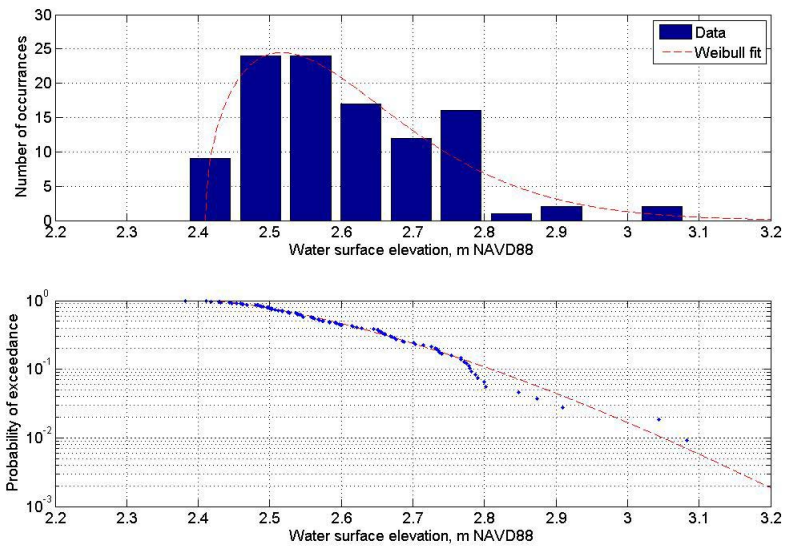


Figure 3. (top) Histogram of maximum annual observed still water levels, and Weibull fit to data. (bottom) Probability of exceedance of water level based on Weibull plotting position, and Weibull fit to data.

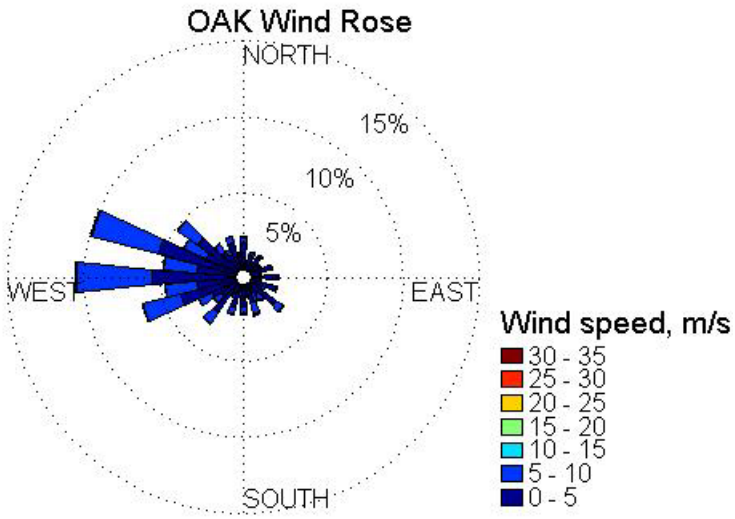


Figure 4. Wind rose at Oakland Airport for all observed winds.

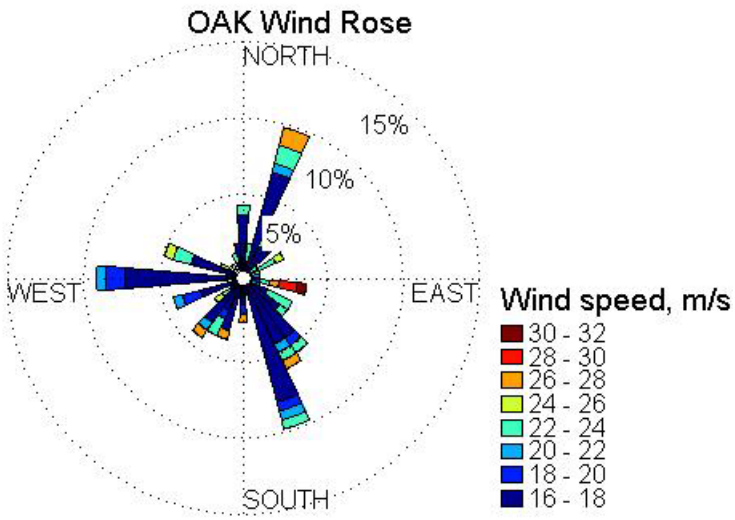


Figure 5. Wind rose at Oakland Airport for winds with speed greater than 15 m/s.

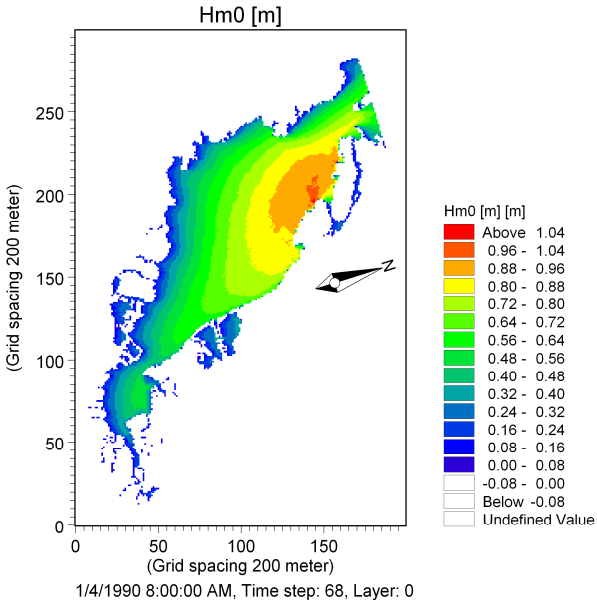


Figure 6. Example significant wave height field output by DHI MIKE21-NSW in South San Francisco Bay, for the case where the grid's –x axis is pointing toward the azimuth 197.5°.

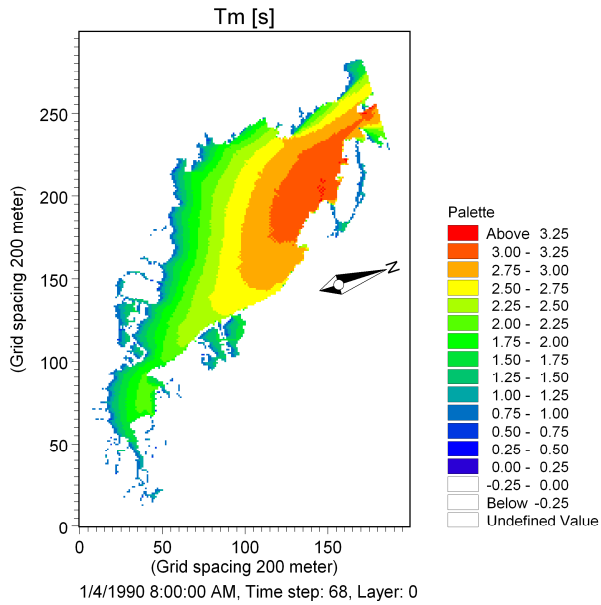


Figure 7. Example peak wave period field output by DHI MIKE21-NSW in South San Francisco Bay, for the case where the grid's –x axis is pointing toward the azimuth 197.5°.

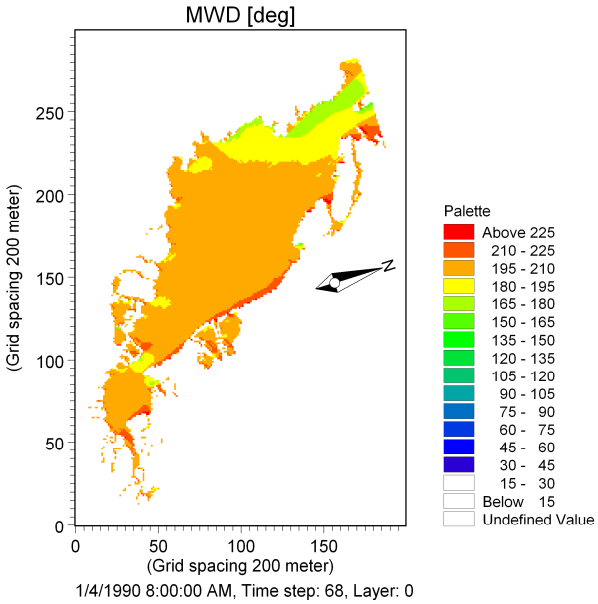


Figure 8. Example mean wave direction field output by DHI MIKE21-NSW in South San Francisco Bay, for the case where the grid's –x axis is pointing toward the azimuth 197.5°.

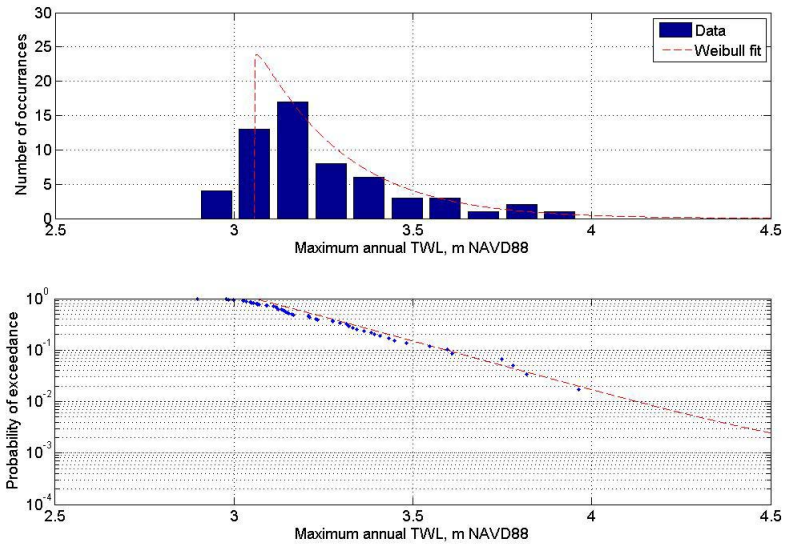


Figure 9. Top: Histogram of maximum annual TWL at OAK. Bottom: Probability of exceedance of TWL.

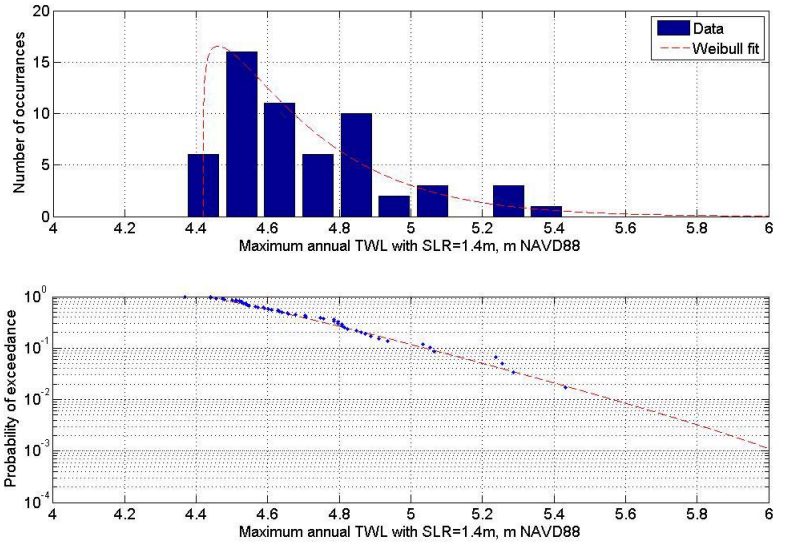


Figure 10. Top: Histogram of maximum annual TWL at OAK for the case with 1.4 m of sea level rise. Bottom: Probability of exceedance of TWL.

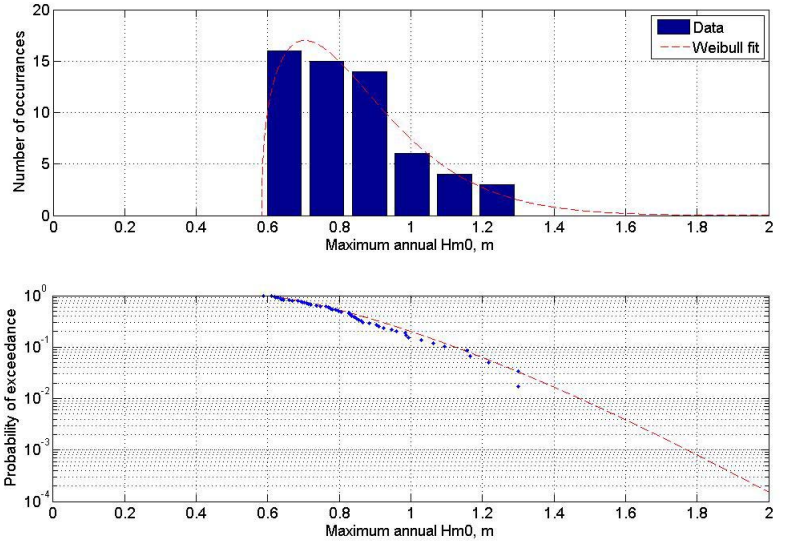


Figure 11. Top: Histogram of maximum annual significant wave height at OAK. Bottom: probability of exceedance of wave height.

SURFABILITY: A PROPOSED SCALE FOR SURFABLE WAVES

Chuck Mesa

U.S. Army Corps of Engineers, Los Angeles District, 915 Wilshire Blvd, Los Angeles, CA, 90017-3401, United States; 213-452-3678; chuck.mesa@usace.army.mil

ABSTRACT

This paper describes a proposed scale for surfability and is field tested with 24 months of visual observations at Imperial Beach, California, USA. At present there is no generally accepted method to classify "surfability", or surf quality, of surfable waves. In this paper surfability is defined by a ten point scale ranging from extremely poor to excellent. Each point on the scale includes a subjective quality rating and an objective percentage representing increasingly higher quality rideable surfing waves. Oceanographic characteristics (height, period, direction, tide, sea surface condition) were simultaneously recorded for cross-comparisons with the surfability rating. Joint distributions delineate which conditions are most conducive to high surfability. Human nature introduces some influences on the visual observations.

INTRODUCTION

High quality surfable waves are an increasingly valuable resource worldwide. Quantitative information of the nearshore surfing climatology is of vital importance to the field of coastal zone management. Coastal engineers and scientists, government, civic planners, and the general public require accurate characterization of the site specific surfing conditions for rational decision making in the coastal zone. Through increasingly widespread dissemination, this information is also vital to promote the responsible use and enjoyment of coastal resources by recreational surfers and all marine enthusiasts.

At present there is no generally accepted method to classify surfable waves. "Surfability", or surf quality, is often expressed by the surfing community in descriptive non-technical terms. These expressions include but are not limited to "hollow", "sick", "barrel", "gnarly", "slab", "soup", and "mush". To experienced surfers, these descriptions convey a vocabulary of surfability, and surfers are able to envision the surfability of waves based on these descriptions. These expressions, however, are of little value to the scientific community. The descriptive based

language of surfing is disconnected from the quantitative based language of the scientific community.

The desire to systematically classify surfability, and thereby bridge the languages of the surfing and scientific communities, established the framework for this study. If surfability can be systematically classified, then surfing conditions at any location can be measured for general condition assessment, or as a method to assess impacts from anthropogenic actions within the coastal zone. However, surfability and surf quality is highly subjective and not easily measured by conventional electronic field data collection methods, i.e. bottom mounted pressure sensors, surface riding buoys, etc. This study employs visual observations which have not traditionally been used as a source of engineering accurate wave climatology information. Visual observations have some human induced influences, but are simple to conduct and are very cost effective relative to other electronic means of field data collection.

This paper describes the results of a field data collection program of visual observations at Imperial Beach, California, USA. Surf zone measurements were obtained by highly trained visual observers. The data was compiled to investigate the efficacy of the surfability concept. It is believed that this represents the first attempt to systematically obtain measured data for the expressed intent to classify surfability

VISUAL OBSERVATIONS

Visual observations of the surf zone conditions at Imperial Beach, California were obtained by Surfline, Inc of Huntington Beach, California. Surfline employs a network of trained personnel who visually estimate and report wave climate twice daily at the shore in a variety of locations along the California coast. The wave climate observations are forwarded to a central office where they are collected and made available to the public through a subscription service.

The wave climate was developed from data collected for a 24 month period from May2009 – Apr2011. A trained observer visually estimated the breaking wave climate at the shoreline twice daily, typically at 0600 (first light) and at 1300; the times were approximate. Waves were observed for a period of 5-10 minutes and physical characteristics measured included surf quality, wave height, wave period, wave direction, sea surface condition, and crowd counts. There were 1,459 measurements over the observation period. Specific details of the observation methodology include:

a. Surfability is a combination subjective/objective rating by the trained observer (who is also an excellent surfer) and is defined by a ten point scale ranging from extremely poor to excellent. Each point on the scale includes a subjective quality rating and an objective percentage representing increasingly higher quality rideable surfing waves. Classifying rideable waves requires a deep understanding of surfing and those aspects of the surf which result in high quality rideable waves. Surfability was reported according to the following scale:
   1. EXTREMELY POOR: Unsurfable or flat conditions.
   2. POOR: Due to lack of surf, very poor wave shape for surfing; poor surf due to other conditions such as wind, tides, or very stormy conditions.
   3. POOR to FAIR: Poor surf with some (30%) fair waves to ride.

4. POOR to FAIR: Generally poor surf with many (50%) fair waves to ride.
5. FAIR: Very average surf with most (70%) waves rideable.
6. FAIR to GOOD: Fair surf with some (30%) good waves.
7. FAIR to GOOD: Generally fair surf with many (50%) good waves.
8. GOOD**:** Generally good surf with most (70%) good waves.
9. GOOD to EXCELLENT: Very good surf with many (50%) excellent waves.
10. EXCELLENT: Extremely good surf with most (70%) waves being excellent to ride and generally some of the best surf all year.

b. Breaking wave heights (crest to trough) were observed and the minimum, average, and maximum were visually estimated to the nearest 1 ft. Visual wave height observations in the surf zone are typically calibrated based on other surfers in the surf zone. The standing body of a person board surfing provides a quasi fixed frame of reference to obtain estimates. It is usual and customary to estimate wave heights based on the following scale: ankle high = 1 ft; knee high = 2 ft; waist high = 3 ft; chest high = 4 ft; shoulder high = 5 ft; head high = 6 ft. Conditions where no surfers are present are dependent on the skill and experience of the observer to obtain an accurate estimate.
c. Wave period is based on an average of 30 waves over the 5-10 minute observation period and was reported to the nearest 1 second.
d. Wave directions were reported relative to the beach normal and estimated to the nearest 5 degrees. Wave directions were recorded as normal (0-10 degrees); slightly from the left (or right) (10-25 degrees); significantly from the left (or right) (greater than 25 degrees).
e. Sea surface condition is an estimate of the smoothness/roughness of the water surface. Sea surface condition was reported according to the following scale: 1=smooth; 2=light bump; 3=bumpy; 4=light chop; 5=choppy; 6=very choppy.
f. Crowd count is an estimate of in-water usage by surfers. Crowd count was reported using the following scale: 1-low; 2-low-medium; 3-medium; 4-medium high; 5-high.
g. Comments from the observer generalizing the overall description of the surfing conditions and highlighting any significant influence on the surfing conditions by any of the specific wave characteristics such as wind, tide, etc.
h. Video monitoring of the surf zone conditions was recorded twice daily coincident with the wave parameter monitoring visual observations. The video format was JPEG loops for a period of 5 minutes to represent an accurate sampling of the surf conditions during the observational process.

SURFABILITY

The histogram of all surfability observations is shown in Figure 1. The histogram is left skewed, ranges between 1-8, a mode and median of 4, and a mean value of 4.1. The distribution is well rounded about the mode.

The absence of ratings with score 9-10 suggests a bias in the observations. The observations include some ratings with score 1, but no ratings with score 9-10. The scale is designed to evaluate the surfability on an annual basis. By definition, during

the course of one year some excellent surfable waves (score 10) should occur. It is theorized the reasons for this bias are rooted in unfamiliarity with and incomplete application of the scale. A wave with surfability score of 10 may occur at any time on any day. It is theorized that the observer might withhold the higher 9-10 scores while waiting for "perfect" conditions. This may be particularly true during the early stages of the observations. This phenomenon is displayed in various competitive human endeavors which require subjective scoring. It is well known that early scoring suffers compared to later scoring as the judges become more familiar with the action that is being scored. Judges a posteriori recognize what action deserves a 10 score with the benefit of retrospective hindsight. While the surf observer clearly and early recognized which conditions were unsurfable (score 1), judgment was restrained on which conditions were excellent (score 10).

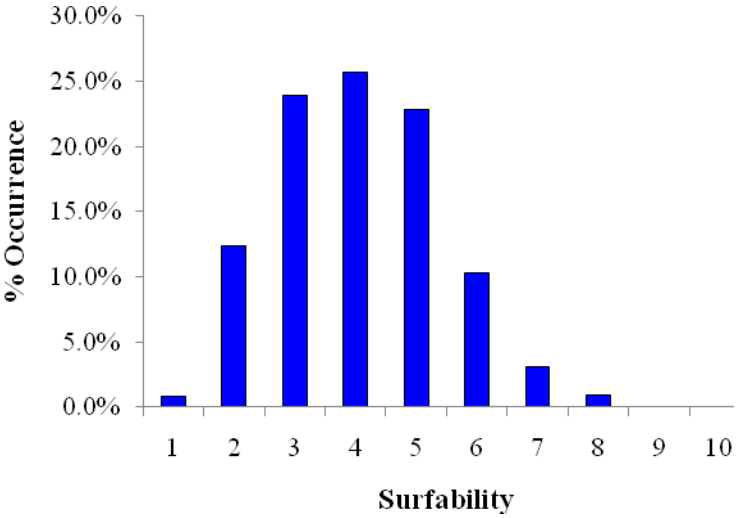


Figure 1 Histogram of Surfability Observations

WAVE HEIGHT

The joint distribution of breaking wave height and surfability is shown in Figure 2. Some general observations can be made regarding the breaking wave height climatology. The observations illustrate a relatively benign wave climate during the 24 month measurement period. The maximum observed wave height is 8 ft which was recorded twice during the 24 month measurement period. The most commonly occurring observed wave height is 2 ft and includes approximately 44% of all observations. This relatively benign wave climate is unexpected given the somewhat severe winter wave climate that can occur in southern California. The highest surfability score occurred with wave heights of 3 ft. Significantly, the highest observed wave heights did not coincide with the highest surfability score. Inspection of the observations indicates the two highest wave height observations coincided with surfability ratings of 3 and 1.

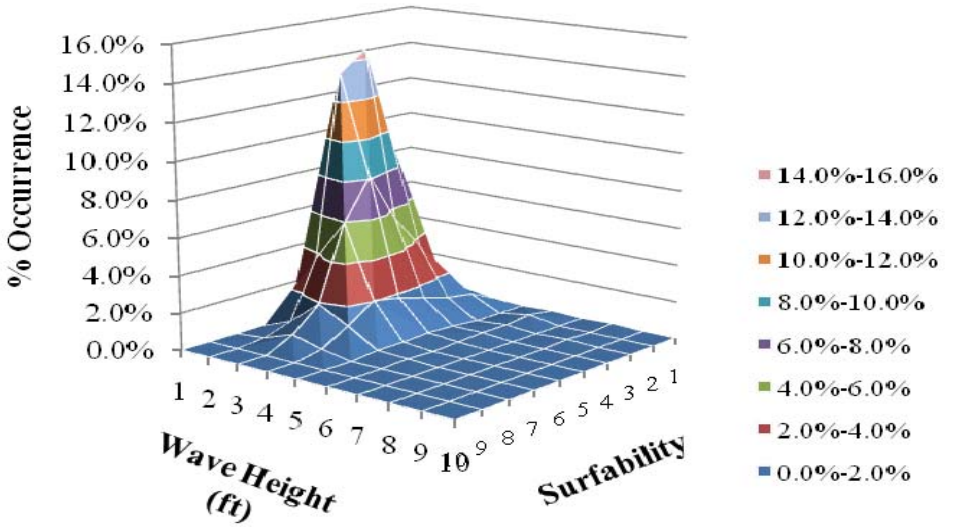


Figure 2 Joint Distribution of Wave Height and Surfability

WAVE PERIOD

The joint distribution of wave period and surfability is shown in Figure 3. There is a very dominant peak at 9 sec (37% of observations) and a secondary peak at 13 sec (3% of observations). The double peaked histogram in this figure illustrates the dual sea/swell nature of the wave climate which is very common in southern California. Shorter period waves are typically associated with sea conditions; longer period waves are typically associated with swell conditions. The cut-off between sea and swell is somewhat subjective but in southern California is generally accepted between 8-10 seconds. The highest surfability score was approximately equally distributed between wave periods 7-12 sec with a slight preference for the 9 sec band coinciding with the dominant wave period.

WAVE DIRECTION

The joint distribution of wave direction and surfability is shown in Figure 4. A majority (44%) of the observations are from shore normal (within 10 deg of normal). The distribution is right skewed with a preponderance (34% versus 19%) for waves arriving from the right (+1) compared to the left (-1). The highest surfability scores very clearly favored the +1 wave direction indicating the west direction. The west direction is most closely associated with the winter season with extratropical storm systems arriving from the west-northwest principal directions.

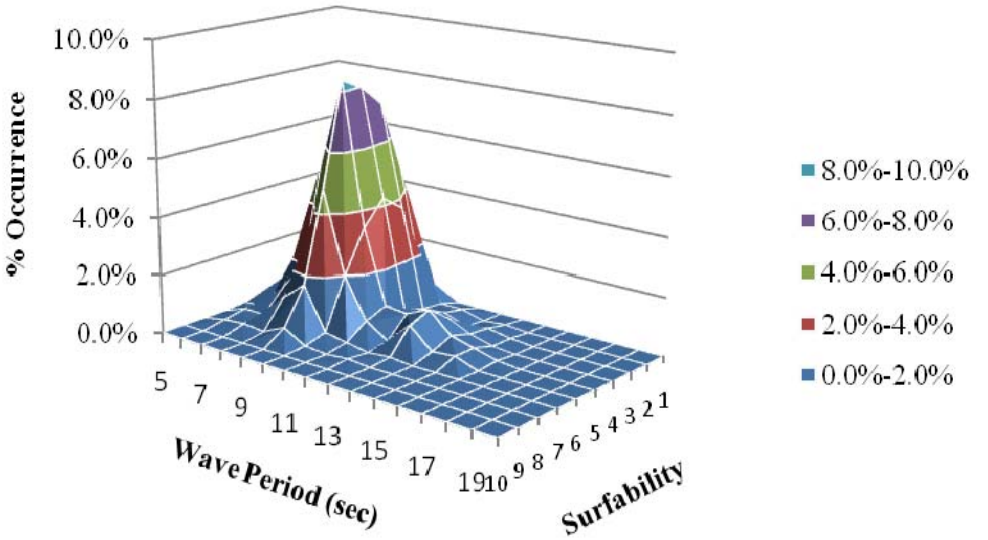


Figure 3 Joint Distribution of Wave Period and Surfability

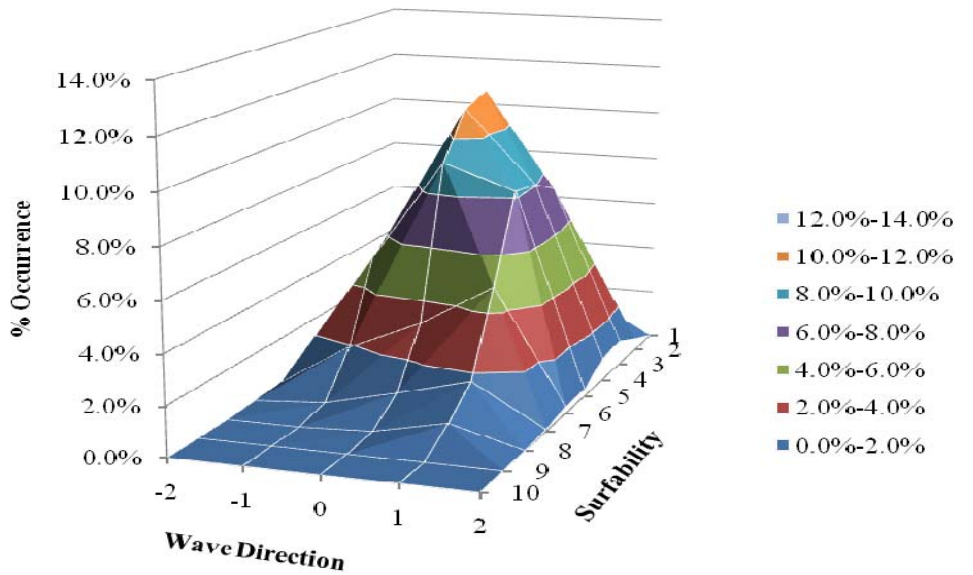


Figure 4 Joint Distribution of Wave Direction and Surfability

TIDE

The joint distribution of tide and surfability is shown in Figure 5. As expected, the distribution is peaked at the mean tidal value (3-4 ft) within the diurnal tidal range (6+ ft). The highest surfability scores are approximately evenly distributed over the tidal range. Although the total number of high surfability scores favors the 4 ft tidal range, the distribution is approximately evenly distributed when adjusted on a

percentage basis. Thus, for tidal values this location indicates no obvious preference for high surfability.

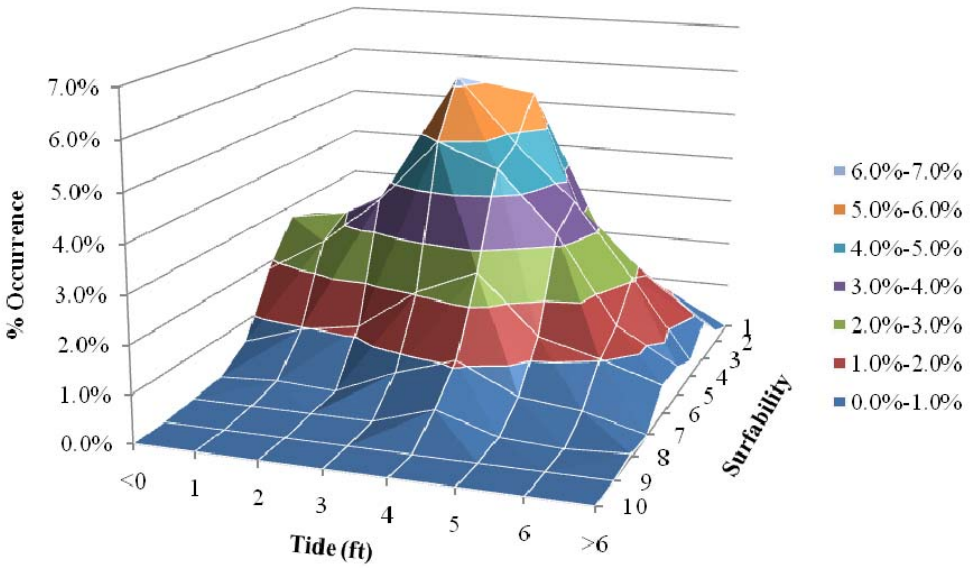


Figure 5 Joint Distribution of Tide and Surfability

SURFACE CONDITION

The joint distribution of surface condition and surfability is shown in Figure 6. The surface condition is significantly left skewed with a significant percentage (79%) of the observations indicating surface condition 1-2. The highest surfability scores very clearly favor surface condition 1, i.e. the calmest surface conditions. The converse is also true; surface condition 6 is clearly associated with the lowest surfability scores. These observations were expected a priori as little or no wind conditions ("glassy" in surfer vocabulary) are the favored surfing conditions; the observations clearly reinforce this statement.

MORNING / AFTERNOON

The measurements indicate a substantial difference between morning and afternoon as shown in Figure 7. All surfability observations were recorded twice daily; typically at 0600 (first light) and at 1300. The results clearly indicate a shift from higher surfability in the morning to lower surfability in the afternoon. The morning histogram has a very pronounced peak at 5 whereas the afternoon peak is 3, indicating degraded surfing conditions. The morning also includes a larger number of observations greater than 6 indicative of more favorable surfing conditions. This result is not unexpected and can be attributed to the wind. In southern California, winds are generally calm and in the offshore direction in the morning while tending to reverse direction to onshore and increase in magnitude steadily thru the afternoon.

Wind magnitude (surface condition) and direction is a substantial contributor to low surfability.

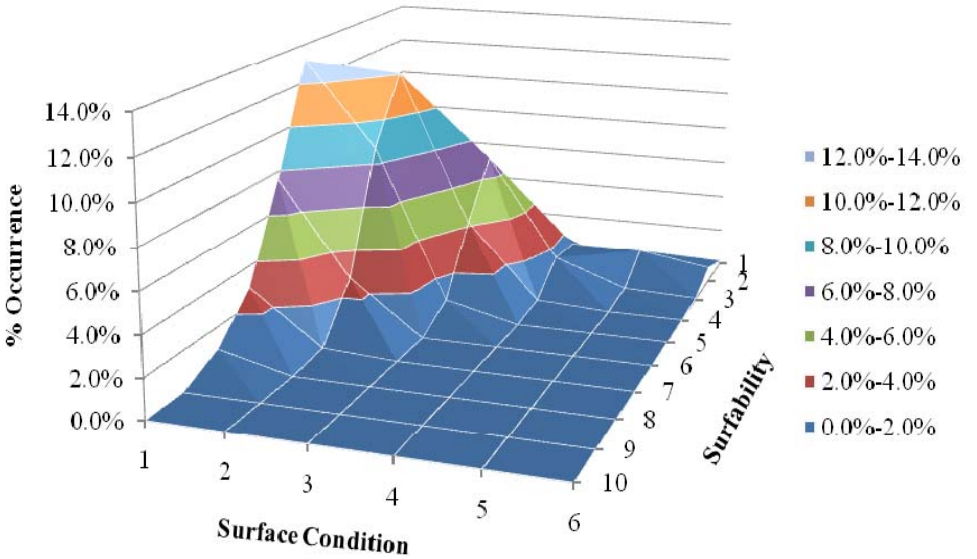


Figure 6 Joint Distribution of Surface Condition and Surfability

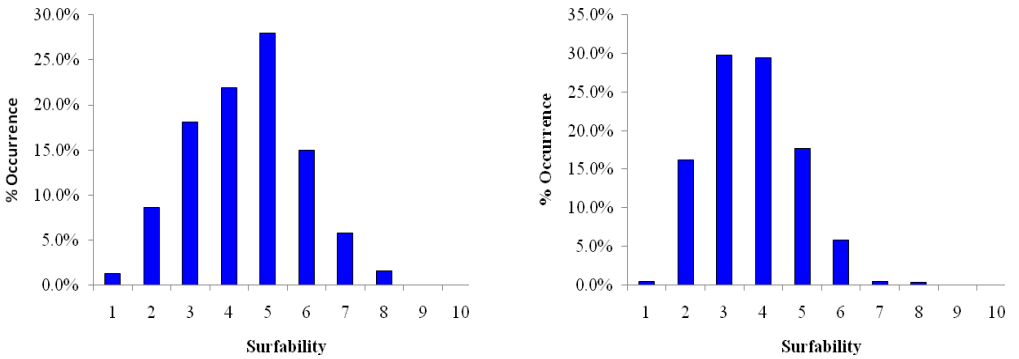


Figure 7 Histogram Comparison of Morning (left) and Afternoon (right)

OTHER

Seasonality: The time series of surfability is a simple indicator of the seasonality of surfability. The measured data indicates the period between Oct-Dec promotes the highest surfability. In southern California, the autumn thru early winter period coincides with the presence of extratropical swell conditions unaccompanied by stormy rainfall events. Stormy rainfall events tend to degrade surfability.

Crowd Counts: Crowd counts are an indicator of usage by surfers. Not surprisingly, high usage is well correlated with high surfability. Additionally, the data indicates the summer months with the most high usage events, a conclusion also not unexpected.

Comments: The descriptive comments reported by the observer for each observation are very informative and useful to further illuminate individual observations. A sampling for a low scoring and high scoring surf condition include:

Score 1: "Hacked-up, blown-out garbage in the 4'-6' range. Very poor overall."
Score 8: "Clean peaks, with lined-up workable walls. Looking really rippable."

The low scoring comment illustrates the point that even though the wave heights were among the larger waves (4-6 ft), the wind is the governing factor creating an unsurfable condition. The high scoring comment includes the term "rippable" which alludes to the condition where the surfer is able to perform many maneuvers on the wave.

DISCUSSION

The original intent of the surfability measurements was to develop a method for systematic classification of the surfing conditions at any location with surfable waves. Using a systematic methodology, measurements obtained before a coastal zone action can be compared to measurements obtained after a coastal zone action in order to assess impacts. The ten point scale is a combination of the objective ("70% waves rideable") and the subjective ("fair"). The objective provides a quantitative measurement of the actual number of surfable waves while the subjective rating is the quality indicator and allows discretion on the part of the expert observer.

The surfability scale was designed with the expectation that the location being evaluated should only be evaluated relative to itself. Every surfing location is unique and a particular surf location cannot and should not be compared with any other location. An average surfable wave at Imperial Beach, CA is in no way comparable to an average surfable wave at the world renowned "Bonzai Pipeline" in Hawaii, USA. Surfability climates vary considerably all over the world and it is not constructive to attempt an absolute comparison of one surfability climate against another surfability climate. Surfability depends on an extensive variety of oceanographic characteristics which renders it pointless to compare surfability among locations. However, it is human nature to unconsciously compare a surf experience against other surf experiences. Thus, it is critically important that the observer performing the subjective evaluation must intrinsically know the criteria for what is considered poor, fair, or excellent for the location under evaluation. This requires an extensive, detailed knowledge of the full range of surfing conditions at the evaluated site in order to objectively make these determinations. Thus, it is best if the observer is a local, long time, and expert surfer with extensive historical background experience so that the objective and subjective determinations can be made.

The surfability scale is designed so that an "average" surfable wave should approximately receive a score of 5. The intent of the scale is to place the most common surfing condition in the middle of the scale and all other surfing conditions, whether more or less favorable, on either side. The scale a priori expects that the majority of the observations will be in the middle with a declining percentage moving away from the most common observations. Thus, the distribution of surfability

observations in most cases will be approximately normally distributed. This feature inherently provides flexibility for the distribution to assume its own characteristic shape incorporating skewness and kurtosis. It is expected that most surfing sites that have surfable waves year round will approximately resemble a normal distribution with some favored skewness and kurtosis. This was clearly shown in this data set. The distribution peak is 4 with nearly equal percentages at 3 and 5 yielding a slightly left skewed but well rounded distribution.

While an approximately normal distribution may be a priori expected for most locations with year round surf, it is likely that some locations could exhibit extreme variations. An example of this potential variation is Pipeline. During the winter season Pipeline breaks with some of the most spectacular plunging surfable waves in the world. These surfing conditions would obviously receive a rating of 10. However, Pipeline can also be completely flat for several summer months and those conditions would receive a rating of 1. Therefore, it is conceivable that the distribution may resemble a "U" shape, with many observations on the low and high ends with fewer observations in the middle.

CONCLUSIONS

Based upon 24 months of visual observation data of the surf zone at Imperial Beach, California, USA, the results contained herein indicate that the proposed method is a reasonable method for describing surfability, or the quality of surfable waves. This analysis provides a quantitative-qualitative scale for describing the surfability at any location. This analysis introduces a ten point scale ranging from extremely poor to excellent. Each point on the scale includes an objective and subjective portion and is expressed in terms of increasingly higher quality rideable surfing waves. Five oceanographic factors (wave height, wave period, wave direction, tide, sea surface condition) were recorded for cross-comparisons with the surfability rating. Joint distributions delineate which conditions are most conducive to high surfability.

The results herein indicate that human nature can induce some bias into the observations. The results suggest the visual observer was "clipping" the highest scoring surfability conditions, i.e. the visual observer was likely reserving the highest scores for "perfect" surfing conditions, which never occurred during the measurement period. The observer is tasked with having expert knowledge of the entire range of surfing conditions at the site, ranging from the very worst to the very best. The observer may have been unconsciously comparing the surfing conditions with other times or locations in his collective surfing experience and thereby introducing a systematic bias. The observer may have been unconsciously reserving the high scores for a similar high scoring "perfect" condition in the past. The preconceived "perfect" conditions may in fact occur only every few years at this location instead of the annual condition as this methodology is designed to measure. Alternatively, the observer may have been unconsciously comparing the high scoring conditions to a high scoring condition at another location. It is incumbent upon the observer to render a completely objective judgment of surfability with no mental comparisons to other places. To do so places an undue burden on the location being measured to

compare to surfing conditions in other locations when in fact those comparisons elsewhere are irrelevant. Thus, it is recognized the utility of the methodology developed herein is directly related to the strengths and frailties of the human observer.

This analysis indicates that visual observations are a reasonable method to obtain engineering accurate information in the surf zone. The data collected in this study suggests that visual observers obtain reasonably accurate wave property information. Recognizing the limitations of the human eye to discern ocean wave properties, visual observations by a trained observer are simple to obtain and have substantial cost advantages over conventional wave measurement methods.

The wave climate measured during this study was not particularly severe. In fact, the measured wave climate was relatively benign. It is acknowledged that the some of the observations made herein may degrade as the sea severity (wave height) increases. The ability of the human eye to accurately estimate very large waves degrades as the wave heights increase, and is substantially muted in the presence of extreme waves. Nonetheless, surfability is still readily definable even in the largest wave conditions. There is no evidence that surfability determination is impacted relative to the other wave properties recorded in this study.

ACKNOWLEDGEMENTS

The author wishes to gratefully acknowledge Messrs. Sean Collins and Kevin Wallis of Surfline, Inc for their assistance in this study.

Landslide Repair and Severe Erosion Mitigation Case Studies in Sensitive Coastal Areas

James Chinchiolo, B.S.[1], Colby Barrett, E.I.T., J.D.[2]

[1]Landslide Solutions, Inc., 9362 Cedarview Way, Elk Grove, California 95758; (916) 698-5133; james@landlslidesolutions.com

[2]Landslide Solutions, Inc., 9362 Cedarview Way, Elk Grove, California 95758; (916) 698-5133; colby@landslidesolutions.com

ABSTRACT

Landslides and severe erosion along our nation's coastlines can present a real challenge to engineers, planners and designers. Not only are the regulatory hurdles associated with construction in sensitive coastal zones significant, many of the common tools available either present a large environmental impact or are not robust enough to handle the corrosion, scour, rapid drawdown, wave action, and other erosion processes associated with coastal sites.

In the context of case studies from three coastal projects across the United States, this paper outlines some of the new and innovative erosion control and landslide mitigation methods available to designers that are both robust enough to survive coastal conditions and specific enough to prevent unnecessary environmental impact. Relevant technologies include traditional soil nailing, high capacity tensioned wire mesh with vegetative inclusions and/or seeded turf reinforcement mats, reinforced architecturally sculpted shotcrete, scour micropiles, and fiberglass composite launched (or ballistic) soil nails/horizontal drains.

The case studies within this paper include a Pacific coastal bluff erosion project using fiberglass ballistic soil nails and architecturally sculpted/stained shotcrete near Crescent City, California; a lakeshore erosion repair using high-strength galvanized steel mesh, launched steel soil nails and native plant impregnated cellular confinement coir on the West Shore of Lake Tahoe in California; and a Pacific coast bluff slide repair using a subsurface combination of horizontal self drilling soil nails and reticulated micro piles along California's scenic Hwy 1.

DEL NORTE COUNTY COASTAL BLUFF EROSION REMEDIATION

Pebble Beach Drive in Crescent City, California, presented a multitude of challenges to Del Norte County Engineer. Shallow landslides along the oceanfront drive were coupled with coastal erosion, confining regulations, archeological concerns, and threats of corrosion. The challenges were particularly evident at two locations along Pebble Beach Drive.
The first, dubbed the south location, fell victim to northern California's heavy winter rains of 2001 and 2002. A 150 linear-foot section of the 36 foot high bluff adjacent to Pebble Beach Drive had failed, leaving an over-steep head scarp. That scarp threatened the stability of Pebble Beach Drive above.

The second, dubbed the north location, consisted of six to eight feet of stiff, high-plasticity clay overlying a siltstone cliff. The clay above fell subject to surface erosion and subsequently exposed the top of the siltstone cliff below. The freshly exposed siltstone, un-capped, was then subjected to erosion and would regress at about the same rate as the clay above. This cycle repeated itself to the edge of Pebble Beach Drive.

Historically, Del Norte County would place large diameter boulders over the side of the bluff to prevent surface erosion and improve slope stability. However, local environmental groups and the California Coastal Commission no longer allow rock revetments for those types of repairs. Furthermore, at the north location, there was concern about disturbing a sacred Native American burial ground. Any drilling in or around the burial ground was strictly prohibited unless it was monitored by an archeologist familiar with the history in that area, adding costly fees to the project. Del Norte County selected launched soil nails with a sculpted and stained shotcrete surface treatment to remediate the bluff erosion.

The British military first developed the launcher apparatus as a part of their chemical weapons program early in the Cold War. It was envisioned that the machine could be used to safely deploy nerve gas canisters up to seven miles away on the battlefield. Upon the discontinuance of the chemical weapons program, the technology was declassified and modified by South African mining engineers to launch soil nails in order to prevent shallow landslides endemic to coal mine tailing piles. In conjunction with the University of Wales and Bernard Myles of Soil Nailing Limited, the launcher was further refined and multiple demonstration projects were completed in the United Kingdom and Western Europe in the late 1980s.

As a result of the success of the Western Europe projects, USDA Forest Service officials organized a series of demonstration projects in the Western United States. A significant portion of maintenance funds for paved roads were being used for shoulder repairs necessitated by slipping and cracking road fills on steep side slopes, and the Forest Service officials determined that the soil nail launcher might be an appropriate solution. The culmination of this demonstration project was a series of landslide repairs in Oregon, California, Colorado, and Washington. A joint publication of the Federal Highways Administration and the USDA Forest service followed, with overviews of the sites' repairs and a preliminary design methodology based on a simplified wedge limit equilibrium analysis (US Forest Service, Application Guide For Launched Soil Nails).

Following these successful demonstrations, thousands of launched soil nails have been installed in approximately 12 states. The preliminary design methodologies have been mostly replaced by commercial limit equilibrium-based slope stability computer programs, and the materials and installation techniques have been refined. In the past six years, New Zealand and Canada have adopted the technique, with further refinements in design methodology coming from groups in New Zealand using finite element analysis to design landslide repairs using launched soil nails (US Forest Service, Application Guide For Launched Soil Nails).

Soil nailing is a reinforcement technique for inserting tensile members into a soil mass. These members provide tensile strength to unstable or potentially unstable soil, and maintain their resisting forces based on the length of the nail inserted past the active or potential slip surface.

The nails resist slope movement by providing bending and shear resistance but provide their largest contribution by acting in tension to increase forces normal to the slip plane.

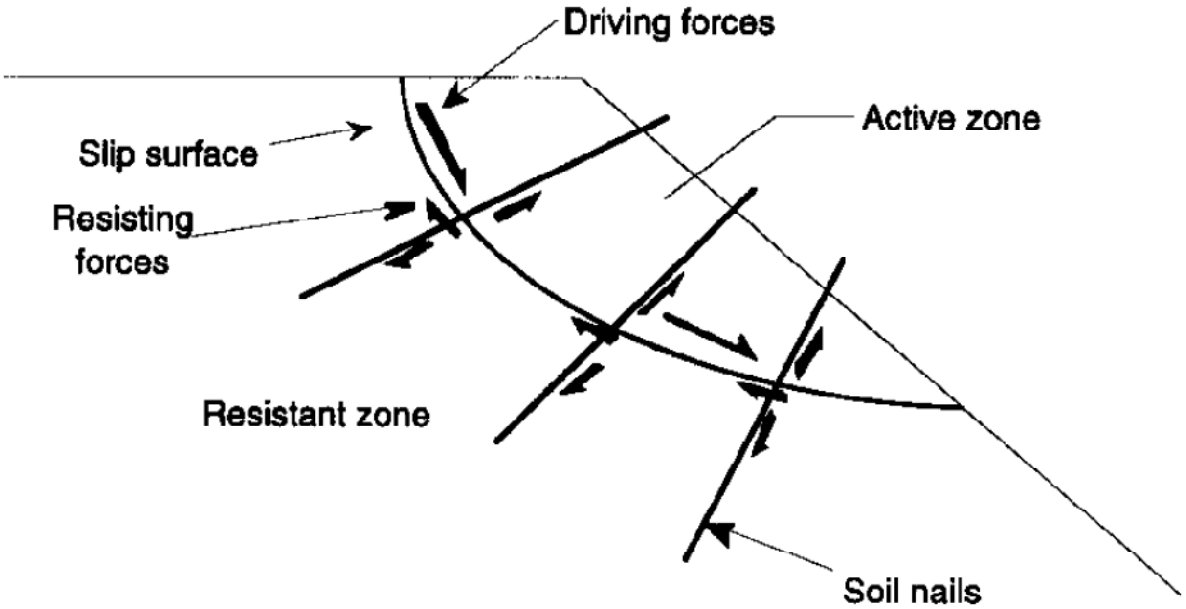


Figure 1: Force Diagram of a Typical Shallow Rotational Landslide Repaired Using Soil Nails (US Forest Service, Application Guide For Launched Soil Nails).

Traditional soil nails are typically installed using a drill which produces an open or cased hole in which a nail is inserted and then filled with cemetitious grout. In landslide materials, caving holes can present difficulties and necessitate drilling with a cased hole, which generally increases cost and project time.



Figure 2: Soil nail launcher installing ballistic nails into sandstone.

Launched soil nails are installed in a single shot at speeds in excess of 200 mph at pressures approaching 3,000 psi. The launcher unit is mounted on a hydraulic excavator and uses high pressure air acting on a collet (plastic collar) attached at the tip of the nail. Compressed air suddenly released against the collet forces the collet and nail through the launcher barrel, much like a dart through a blow-gun. As the nail enters the slope it remains in tension until it comes to rest. Because the forces act on the tip of the nail and simulate "pulling" the nail through the ground, relatively light tensile inclusions can be fired that would bend, buckle, or break if they were installed with forces acting on the rear of the nail. As the nail nears the soil, the collet breaks away and remains in a collector shroud. When the nail enters the soil, the ground around the soil is displaced in elastic compression around the nail tip. This temporary annulus of compression, or "shock wave" is larger than the nail diameter and allows the nail to penetrate relatively unabraded as it travels into the soil, reducing soil drag, damage to nail coatings, and disturbance of surrounding soil. This dynamic shock-wave phenomena produces two distinct benefits to nail launching versus percussion driven nails: first, because the annulus of compression is temporarily larger than nail diameter, drag and abrasion are minimized (during initial demonstrations, nails with stickers applied were fired into gravel piles and exhumed; the stickers were totally in-tact). Second, because the deformation of the soil is elastic, soil disturbance is minimized. It is not uncommon to produce bond strengths equal to the undisturbed shear strength of the soil immediately after firing. In a percussion driven nail, the soil column is disturbed along the nail length, severely limiting nail-soil bond strengths. The annulus of compression surrounding the nail extends 1-3 nail diameters from the outer edge of the nail. The long term effects of this compression annulus are unknown, but "set-up" behavior similar to that seen in driven pile could increase nail-soil bond strength over time.

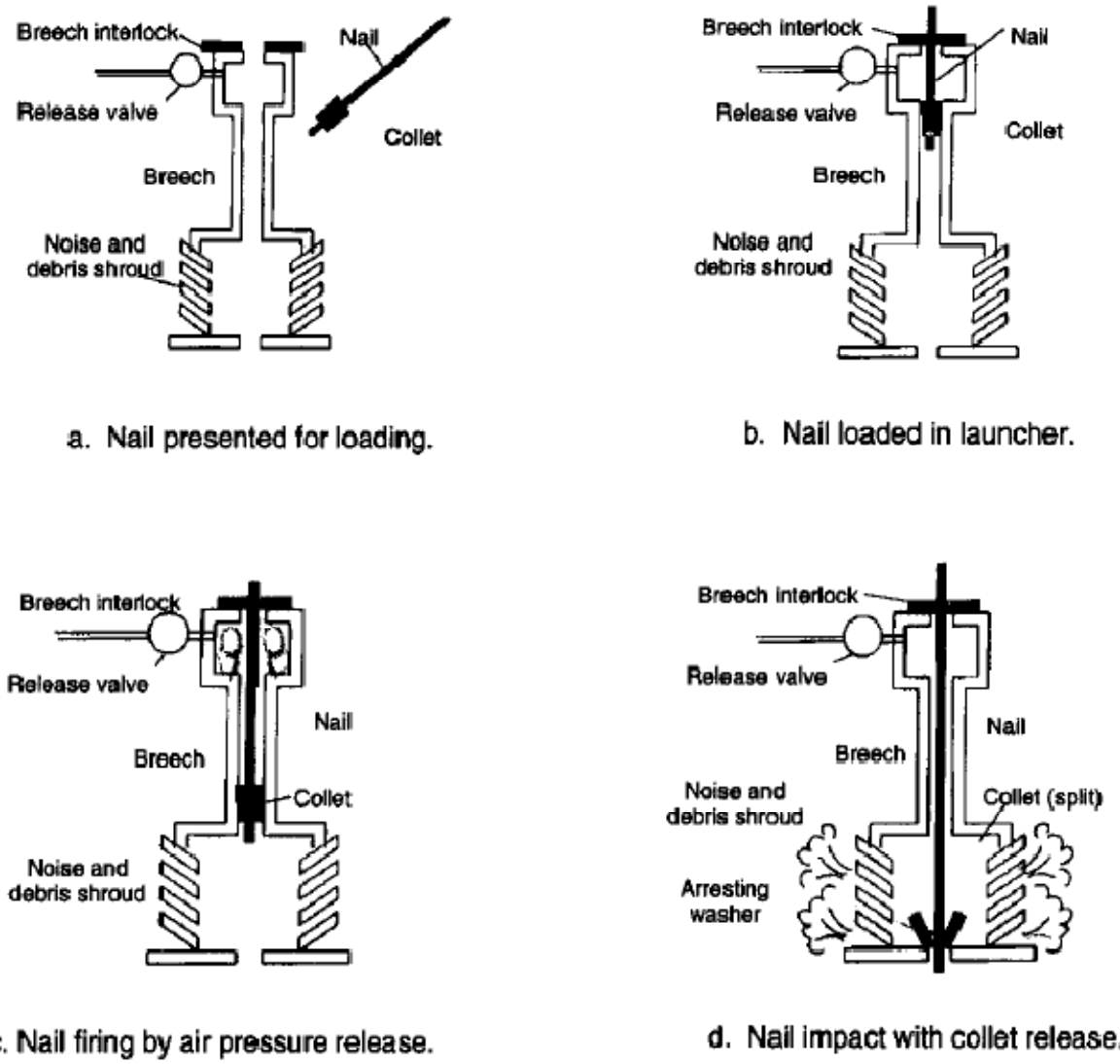


Figure 3: Soil Nail Launcher Firing Sequence (US Forest Service, Application Guide For Launched Soil Nails).

In the initial USDA Forest Service demonstrations, plain or galvanized 1.5 in solid steel nails were installed in a variety of situations, including shallow road failures, cut slopes, and gravel piles. Today, hollow steel or fiberglass tubes are used almost exclusively. With equivalent force, hollow tubes accelerate more rapidly and penetrate into the soil to greater depths. Hollow tubes may also be perforated to act as drains, or pressure grouted to increase apparent bond diameter. Grouted nails may also include a plain or epoxy-coated inner bar to increase tensile and shear capacity and corrosion protection. Assuming a galvanized launched nail was pressure grouted and an epoxy coated inner bar was inserted, the inner steel would be protected by two layers of galvanization, a layer of sacrificial steel, and at least one complete layer of grout and epoxy; exceeding FHWA Class 1 protection for traditional soil nails (FHWA. *2003 Geotechnical Engineering Circular No. 7: "Soil Nailing."*).

LAKE TAHOE BLUFF STABILIZATION AND RESTORATION

Bluff erosion and stability is an ever present problem along the shoreline of pristine Lake Tahoe and one such area presented itself during the planning phase of an estate reconstruction project along the west shore of Lake Tahoe. The inherent problem of an eroding unstable bluff is quite obvious. In this situation the problem was intensified by the desire to build a high end housing structure just feet from the top edge of the bluff while planning to restore the bluff face and construct a walking path to the beach below. In addition, because of tough environmental regulations, most of the work would need to take place from the top of the bluff thus requiring specialized equipment and construction techniques.

These factors were then made even more difficult by stringent Tahoe Regional Planning Agency (TRPA) and local county permit requirements. Permit requirements limited construction from May 1st to October 15th and required a massive amount of BMP's prior to any rains and / or before October 15th. The ultimate goal of the project was to protect, strengthen, support, preserve and provide global stability to the existing bluff surface all without noticeably changing the appearance of bluff.

If bluff surface erosion was not corrected at this site the bluff would have continued to erode back thus reducing usable property at the top of the bluff. If overall global stability of the slope was not corrected the housing structure would have had to be placed on a pilling system sufficient enough to support the house should the bluff continue to fail.

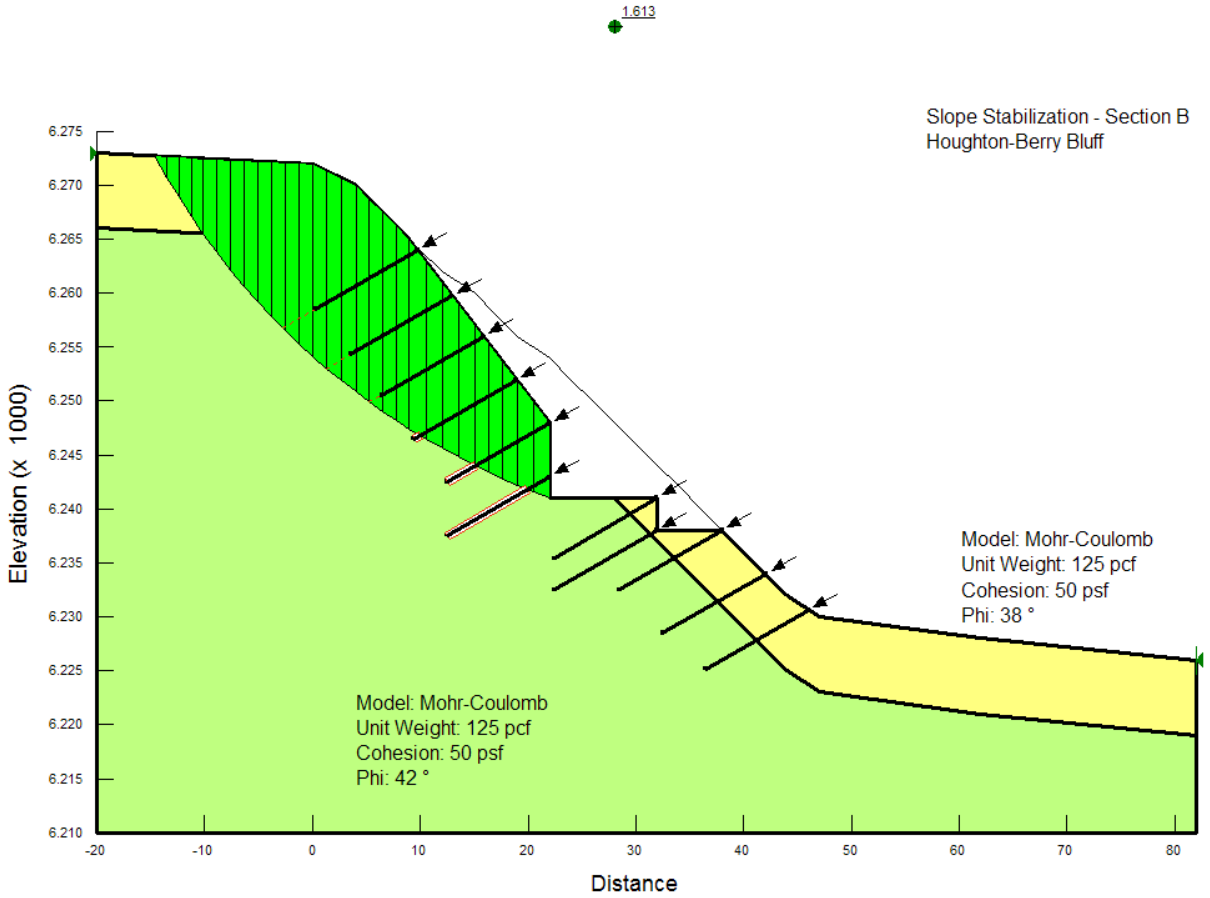
Several stakeholders, agencies and industry professionals all worked in harmony to develop the final bluff erosion and stability plan. Those entities included the owner, project architect, project civil engineer, permit specialist, geologist, landscape design / build contractor and specialty slope stabilization design / build contractor.

After considerable thought and consultation with erosion control vendors and consultants, it was decided that a hybrid biotechnical solution would be required - a smorgasboard of stabilization techniques. Ultimately, a combination of launched soil nails, steel wire mesh and a specialty custom vegetated coir cellular confinement was chosen.

The launched nails were primarily chosen because of the ability to install them with minimal impact to the bluff, faster production rates relative to traditional nails and the ability install the nails from the top of the bluff (no need for equipment on the beach). Cost was also an important factor with regards to the final decision to utilize launched soil nails.

In order to determine the length and spacing of the launched soil nails both a slope survey and a soils report were used. These documents were provided by the project engineering geologist (Jake Hudson of Holdredge & Kull) and information gleaned from them was imported into a commercially available slope stability software tool. The tool then calculated probable slide planes under varying circumstances at a defined Factor of Safety (FoS). An appropriate FoS at this site was determined to be 1.5, effectively meaning that the repair is capable of handling 50%

more than the maximum expected load. Without any stabilization measures the slope was approximated at a FoS 1.0. With the installation of launched nails on 5-ft x 5-ft spacing it was determined the slope could be augmented to reach the targeted FoS 1.5.



Slope W Output Graphic indicating FOS exceeding 1.6.

Galvanized wire mesh was then attached to the tips of the nails with the purpose of providing cohesiveness to the launched soil nail system, a medium to attach the coir cellular confinement and a last defense for erosion in the event of localized coir failure. The mesh was carefully tensioned across the entire slope face. At the bottom of the slope native rocks were hand selected and placed to provide slope buttressing and to protect against high water wave action. The wire mesh was installed prior to the placement of the rocks thus the rocks provided another source of tension as they were set in place.

The success of the entire stabilization system depended in large part on the erosion control and beatification provided by the vegetated surface treatment. The installation of custom vegetated cellular coir surface treatment was installed immediately after the placement of the steel mesh and native rock. Vegetation selected for planting within the cellular coir included; large deeply rooted woody shrubs, forbs, sub-shrubs, ground-cover and grasses that were chosen based on esthetic appeal and ability to retain soil. In order to support these species amended soil was imported and placed within six inch deep honeycomb-configured coir cellular confinement. This biodegradable six inch deep blanket was securely anchored to the steel mehs and stretched in six

foot stripes from top to bottom of slope forming a continuous three dimensional form covering the slope.

Soil sources were tested and a biologically active green-waste composted soil formula was selected. The soil needed to hold and distribute moisture, rapidly germinate seed, grow healthy plants, texture and color to blend with native soil and adhesiveness. Soil was conveyed and packed into the coir layer.

A diverse mix of native plants was specified, ranging in size from 4" native grass plugs to 44" ball and burlap native trees. Larger tree species, Incense Cedar and Jeffery Pine were placed lower on slope to avoid being blown over by the wind. Smaller scale, slower growing native trees such as Mountain hemlock (Tsuga mertensiana) and Subalpine fir (Abies larsiocarpa) and other native shrubs were placed higher on the steepest exposed areas of bluff. The native shrubs provide shade, bird habitat and forage for foul and small mammals. Boulder groupings pinned periodically in the slope with Launched Soil Nails™ also provided an opportunity for small mammal colonization and complimented the boulders throughout the rest of the property. Native ground covers and forbs like Squaw Carpet (Ceanothus prostratus) and Mountain Pride Penstemon (Penstemon newberryi) added color, attracting beneficial insects. Additionally, small burnet (Sangusorbia minor) provided nitrogen fixing.

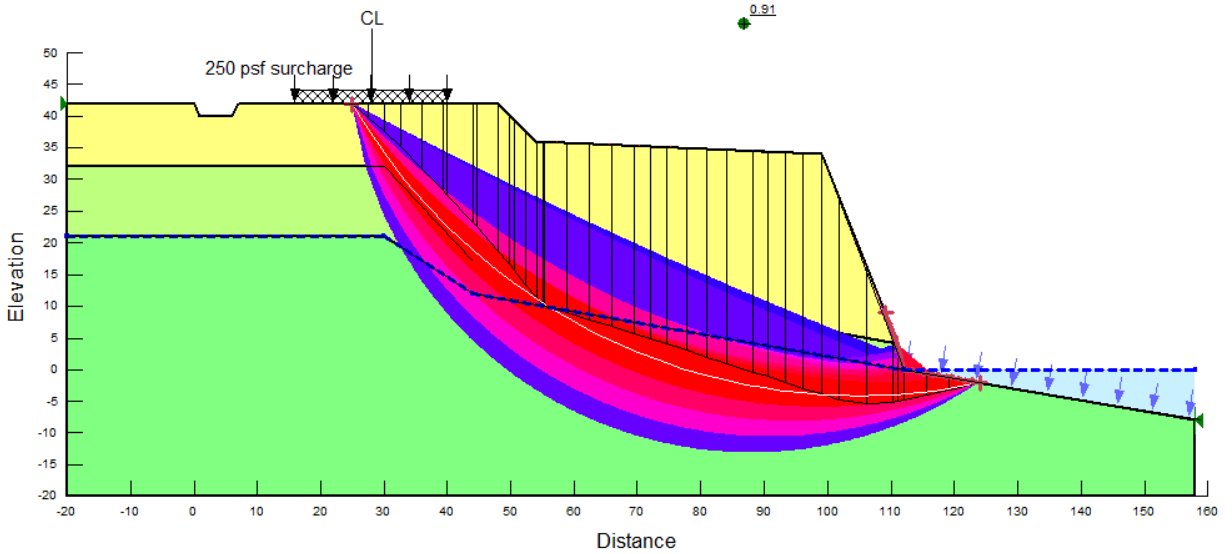
Five gallon and larger plants were installed in small openings cut through the cellular coir and steel mesh. Inserting the root mass of these larger plants into the subsurface soil allowed space for root growth and trunk flare. A final mulch layer formulated with a matrix of long, medium and fine natural fibers was distributed throughout the entire area. The mulch layer was composted with a small amount of formulated soil for one week to activate microbial activity, and then firmly felted on the surface. After mulching a seed mix of shrubs, forbs and native grass was broadcasted evenly over the mulch. A three foot wide path was constructed and surfaced with recycled rubber composite pavers. The construction process was completed by September 15, 2010. By October seed had begun to germinate and plant materials already exhibited growth. The entire planted area is now irrigated and controlled by a sophisticated irrigation controller that automatically turns the entire irrigation system off if any irrigation line breach is detected. The system controls an in-line drip irrigation system providing low volume, low impact supplemental irrigation for the first three growing seasons.

Late October 2010 brought an unusually strong rain event (4-inches within 24 hours). The stabilized area weathered the storm without an issue. Project monitoring and maintenance will continue through October 2015.

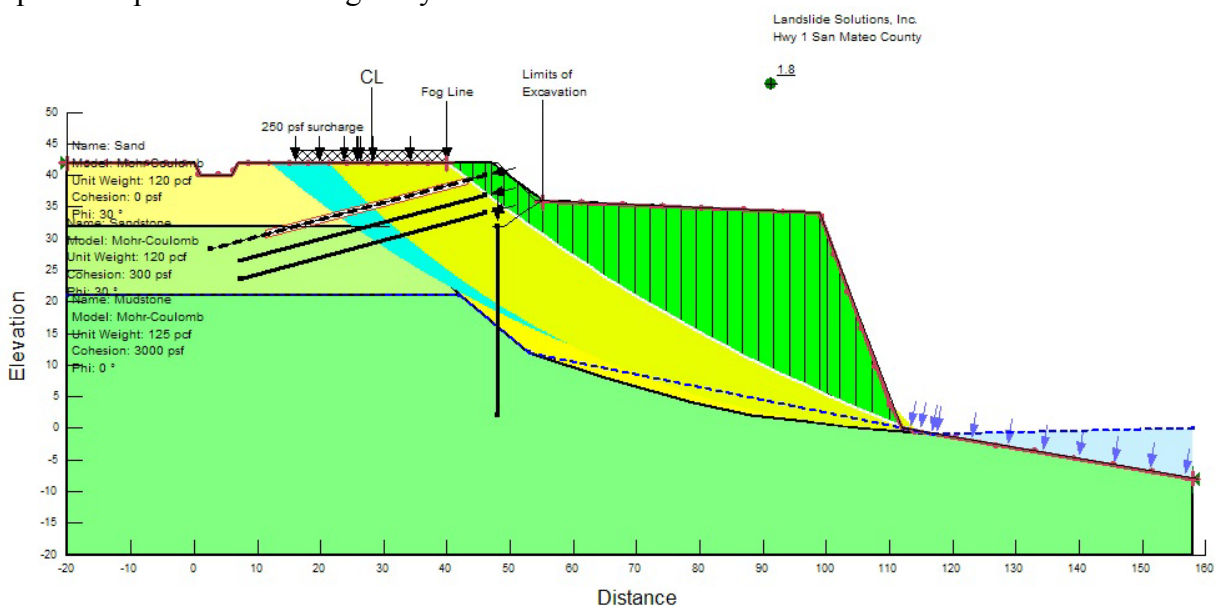
From conception to completion this project took more than three years. Construction took two and one half months with more than two years in planning and permitting negotiations. The project has met the expectation of all entities involved and provides an attractive natural looking foot path to the beach, stabilized slope suitable for a building above and a restored view from land and water.

PACIFIC COAST LANDSLIDE REPAIR

Highway 1 at Pescadero Creek Road in San Mateo County California, presented a multitude of challenges to CalTrans Geotechnical Design West. A large 140 linear foot portion of bluff supporting Highway 1 was simply sliding out to sea, the highway needed to be stabilized immediately, CalTrans environmental department required that the repair stay within the departments current right of way and the coastal commission required little or no impact to the shoreline. Together with CalTrans supplied geotechnical soils data a repair scheme was devised that required minor excavation just outside of the edge of pavement, self drilling soil nails and self drilling micropiles and 1,400 SF of shotcrete. The excavated soil was then placed back over the repair then hydro seeded with a native seed mix.



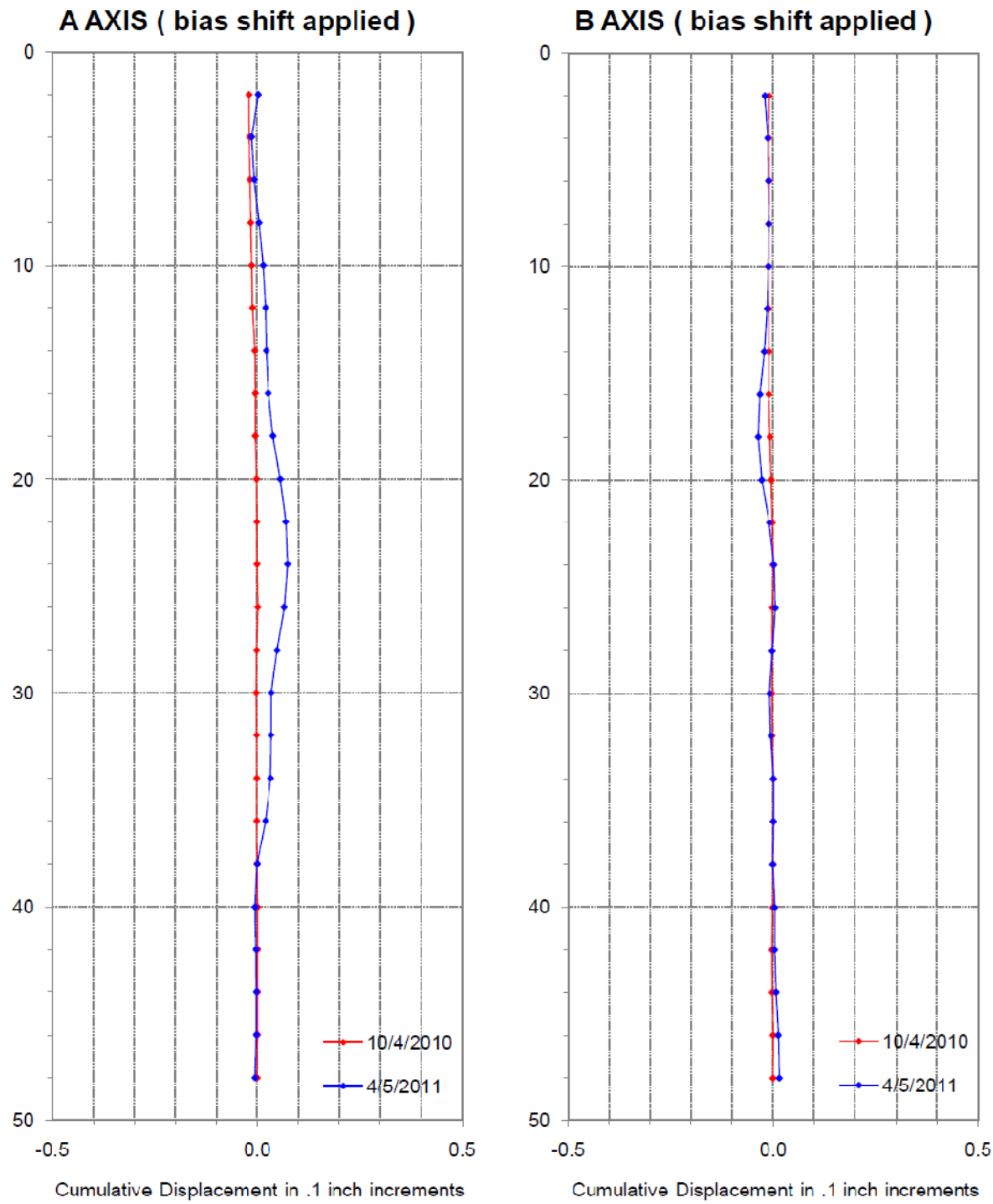
Slope W output file indicating unity.



Slope W output file indicating repaired slope above 1.8 FOS.

CalTrans reported a cost savings of over 2 million dollars when compared to the capitol improvement project planned for the site. Inclinometer casing was installed to verify performance and to date readings indicate that the site is stable and the slide has been mitigated

Commutative Displacement (Inches)



Data supplied by CalTrans District 4

REFERENCES

GeoSlope International, Inc. Slope/W 2007.

Unites States Forest Service. 1994. *Application Guide for Launched Soil Nails*. Vol. 1, FHWAFPL-99-003, U.S. Government Printing Office, Washington, D.C.

O'Sullivan, A. and Grant, M. 2007. "Aspects for Consideration in the Design of Soil Structures Reinforced with Inclusion." *New Zealand Geomechanics News* 74: 76-81

FHWA. *2003 Geotechnical Engineering Circular No. 7: "Soil Nailing."*

Wave Effects on Bathymetric Depressions

Luce Bassetti[1], Sean O'Neil[2]

[1]HALCROW, 1101 Channelside Drive, Suite 200 S, Tampa, FL 33602, USA;
PH (813) 386-1990;FAX (813) 386-1991; lbassetti@halcrow.com

[2]HALCROW, 22 Cortlandt Street, 31st Floor, NY 10007, USA; PH (212) 608- 3990; FAX (212) 566-5059; oneilst@halcrow.com

Abstract

Wave refraction and diffraction effects resulting from bathymetric depressions (a dredged borrow pit and a dredged entrance channel to a port) were investigated for a major port expansion project. Due to the complex bathymetry and port configuration, a combination of physical and numerical modeling was developed. A third generation, phase-averaged, spectral wind-wave model was developed for this study using an unstructured mesh. The model was used to transform offshore wave conditions to provide the extreme nearshore wave design conditions of significant wave height, peak period, and mean wave direction (H_{m0}, T_p, MWD). A time-domain, Boussinesq-type wave model was also established to simulate the propagation of waves traveling from deep water to shallow water involving the primary wave motion as well as the bound and free long waves. This model is capable of reproducing the combined effects of most of the wave phenomena of interest to the harbor engineer, including shoaling, refraction, diffraction and partial reflection of irregular, finite amplitude waves propagating over complex bathymetry (i.e., borrow pits, dredged channel). The results of the study indicate that the surface interactions with the deep-draft and wide navigation channels significantly influence the incident waves and manifest themselves into both amplification and attenuation of the incident wave field. Both of these effects in-turn critically influence inputs to design, planning of port infrastructure, as well as assessment of harbor agitation and vessel downtime. While in recent years port designers have typically relied upon numerical wave models to perform most of the initial studies, in our study a combination of physical and numerical modeling was used. Based on the combined observations from the physical and numerical modeling results, conclusions and recommendations from this work show that both models compared well. Wave heights observed in the physical model were similar to or slightly higher than the numerical predictions.

1. Introduction

Multiple projects in recent years have consistently shown that the presence of a deep draft navigation channel or a borrow pit, a) alters the wave field approaching a harbor over a considerable spatial scale to the point of significantly affecting the design wave conditions outside the harbor and wave impacts to adjacent shorelines, and b) significantly alters the amount of wave energy penetrating into a harbor. The physical process of wave refraction, reflection/scattering and transmission, all of which are dependent on the interactions of waves with the side slopes of the channel, determine the design (amplified) wave heights for the breakwater/revetment as well as the (attenuated) energy penetrating into the harbor basin.

Such interaction can play a significant role during port master planning, shoreline protection and channel sedimentation. It is clear that the interaction of surface gravity waves with the side slopes of navigation channels and dredging (borrow) pits is of critical importance. Our study presents the numerical and physical modeling steps taken to insure a thorough understanding of the changes to the wave field due to the borrow pit and the dredged channel. Waves approach from offshore of our major port from 8 main directions: SW, WSW, W, WNW, NW, NNW, N and NNE. The extension of the port was designed so that:

- the least amount of wave energy penetrates into the harbor area,
- the wave disturbance at the berths is minimized to avoid downtime,
- the approach, entrance, and inner basins are navigable.

2. Numerical and Physical Model

Due to the complex bathymetry and port configuration, a combination of physical and numerical modeling was developed. Both models compare rather well to observations and measured data for all cases, with the wave heights for the physical model similar to or slightly higher than the numerical predictions.

A third generation, phase-averaged, spectral wind-wave model based on DHI's MIKE 21 SW FM model using an unstructured mesh was used during this study. The model was used to transform the offshore wave conditions to provide the extreme nearshore wave design conditions of significant wave height, peak period, and mean wave direction (H_{m0}, T_p, MWD) which were necessary for the design of breakwater protection structures around the port. The structures include a main breakwater extension, an east breakwater and a lee breakwater. These structures are shown in Figure 1 below.

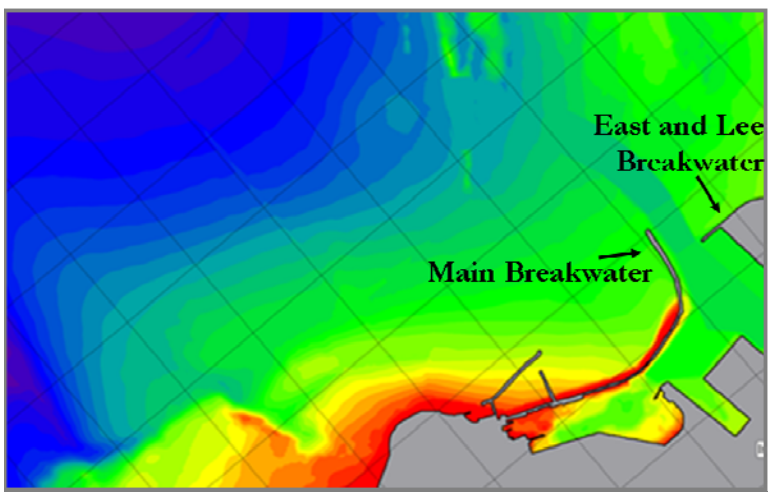


Figure 1. Location of the main breakwater extension, the east and the lee breakwaters designed for the major port expansion.

The wave transformation modeling was carried out using univariate, directional extreme conditions based on OWI GROW hindcast winds and waves form a deepwater location offshore of the port. The wave conditions have been combined with extreme water

level conditions, including long-term sea level rise due to climate change, for the 50-year design life of the project. Offshore wave conditions used in the wave transformation model are presented in Table 1.

A time-domain, Boussinesq-type, wave model utilizing DHI's MIKE 21 BW model was also established to simulate the propagation of wave propagating from deep water to shallow water involving the primary wave motion as well as the bound and free long waves. This model is capable of reproducing the combined effects of most of the wave phenomena of interest to the harbor engineer. The phenomena most important for this study include shoaling, refraction, diffraction and partial reflection of irregular, finite amplitude wave propagating over complex bathymetry (i.e., borrow pits, dredged channel). Table 2 presents the offshore wave conditions used in this wave penetration and agitation model using unit (1m) wave height boundary conditions, and the resulting nearshore wave heights are given as a scaling of 1m. Thus, if the offshore boundary condition is 3.5m from a particular direction, and the wave model computes a wave height scaling of 1.2 at a nearshore point, then the actual wave height at the nearshore point should be read as 3.5*1.2=4.2m.

Wave Direction	Wind Direction	H_{m0} (m)		T_p (sec)		Wind Speed (m/s)	
		100-year	1-year	100-year	1-year	100-year	1-year
225 (SW)		5.3	3.3	11.7	9.3	22.7	16.2
247.5 (WSW)		7.9	4.9	14.2	11.3	21.3	15.2
270 (W)		8.2	5.1	14.5	11.5	20.3	14.5
292.5 (WNW)		7.4	4.6	13.8	10.9	19.0	13.6
315 (NW)		5.5	3.4	11.9	9.5	16.7	11.9
337.5 (NNW)		4.8	3.0	11.2	8.9	15.8	11.2
360 (N)		4.3	2.7	10.6	8.5	16.3	11.6
22.5 (NNE)		3.8	2.4	10.0	8.0	14.7	10.5

Table 1. Offshore wave conditions used in the wave transformation model.

Wave Direction	H_{m0} (m)	T_p (sec)
W	1	8, 10, 12
WNW	1	8, 10, 12
NW	1	8, 10, 12
NNW	1	8, 10, 12
NW	1	6, 8, 10

Table 2. Offshore wave conditions used in the wave penetration and agitation model.

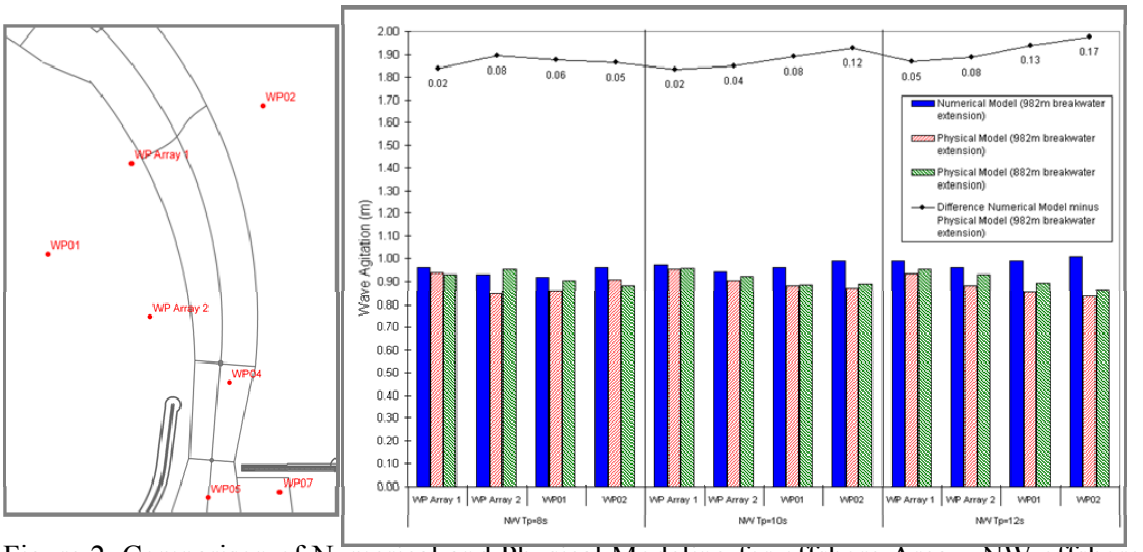


Figure 2. Comparison of Numerical and Physical Modeling for offshore Area – NW offshore unit wave height (H_{m0} = 1m).

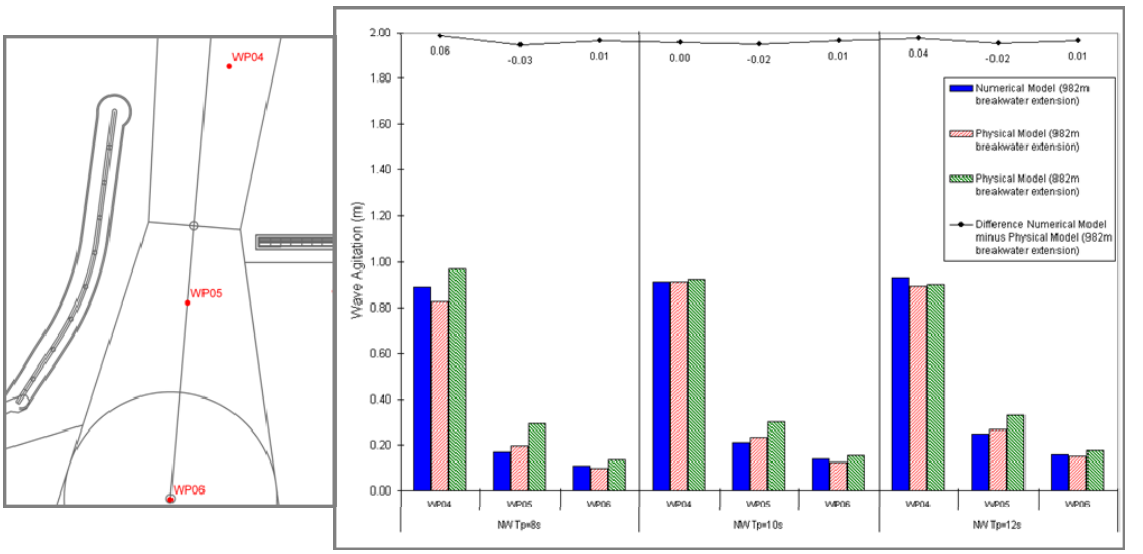


Figure 3. Comparison of Numerical and Physical Modeling for the entrance channel – NW offshore unit wave height (H_{m0} = 1m).

The physical processes of wave refraction, reflection/scattering, and transmission, all of which are dependent on the interactions of waves with the side slopes of the dredged areas, determine the design (amplified) wave heights for the breakwater/revetment as well as the (attenuated) energy penetrating into the harbor basin. Waves heights observed in the physical model were similar to or slightly higher than the numerical predictions (Figure 2 and Figure 3).

The results show a very good match between the two models allowing high confidence that the numerical model was very well calibrated.

3. Port Expansion and dredging channel impact

The main physical processes that encompass the interaction of surface gravity waves with the depth transition between two regions with a noticeable change in depth are refraction, scattering/reflection, diffraction, and transmission. For the general problem of oblique waves propagating over a submerged trench, the relative depth difference at the up-wave edge of the trench acts as a refractive barrier which can lead to large reduction in transmission and the accompanying increase in reflection coefficient. Unit wave heights (1m) were used at the model boundary for the 4 critical directions and tested with three wave periods for each direction: WNW (8,10,12s); NW (8,10,12s); NNW (6,8,10s); N (6,8,10s).

It was observed that the rubble mound structures for the main breakwater extension enable the wave energy to be absorbed efficiently. Consequently, the main breakwater extension does significantly protect the port entrance and also significantly reduces the wave energy within the port.

Three layout scenarios were considered to study the impact of the port expansion and dredging channel on the existing port:

- Case A: Existing condition with half-reclamation in place,
- Case B: Port expansion with half-reclamation,
- Case C: Port expansion with full-reclamation.

Figure 4 presents the numerical model result from the worst-case direction and period combination, comprised of waves approaching from the NNW with a peak period of T_p=10s. Figure 1 also shows that the presence of the port expansion does protect the inner port by reducing the wave energy up to 40%. The main breakwater extension also shelters the existing port, and especially the Quay A and Quay B area (Figure 4 black rectangles). This is seen by the cooler (blue to purple) contours corresponding to reduced significant wave height.

The numerical model results indicate that the port expansion does not have any significant impacts on wave agitation within the port despite showing slight increases at some locations. As expected, port expansion and modification of the port configuration, as well as the dredged entrance channel, all have opposing effects on wave agitation conditions within the port:

- The port expansion provides further protection for the Port and results in less wave energy approaching the southern part of the port; but by changing the shape and size of key breakwaters, the wave agitation at some location is slightly worse than with the original breakwater,
- On the other hand, the modified breakwater allows more penetration of waves at the entrance to other important areas. However, these waves will not significantly impact vessel operation through the entrance.

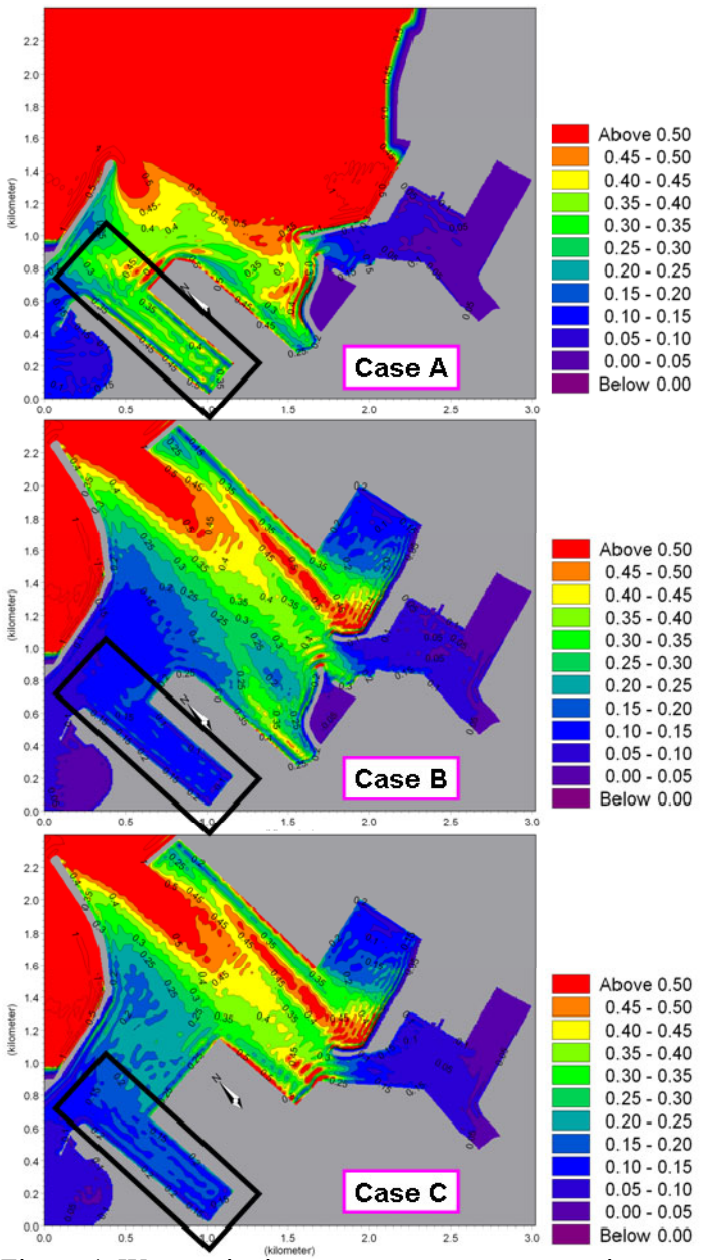


Figure 4. Wave agitation map – worst case scenario waves from NNW, Tp=10s. The BLACK rectangle shows locations of Quay A and Quay B areas.

During this part of the study, the borrow pits were not included. Based on the borrow pit study, it has been shown that wave agitation is slightly reduced at the different inner port Quays with the borrow pits in place, which implies that the total wave energy penetrating into the Port is decreased. Consequently, it is believed that with the borrow pit in place, the localized increases in wave agitation at some locations would be reduced.

A closer look at the different key directions (NNW, WNW, NW, and N) shows that waves are typically small regardless of the layout scenarios studied:

- For the WNW waves, the new layout has a small positive impact on wave agitation, with a decrease of approximately 0.01 to 0.04m in wave agitation coefficient,
- For NW waves, the new layout has a small negative (increase of approximately 0.01 to 0.03m) impact for some areas, and a small positive or negligible impact for other areas,
- For NNW waves, the new layout has a negative impact at several locations with an increase of approximately 0.05m in wave agitation coefficient in some areas,
- For the North condition, the new layout has a negligible impact.

For the worst case direction (NNW) the wave agitation coefficient increases by about 0.05m compared to the existing port layout.

The port expansion and dredged entrance channel will cause more impacts in the vicinity of the southern part of the port), which is mainly due to the modifications of the breakwater to allow bigger ships to enter this specific location.

4. Short waves and borrow pits' influence

Two different borrow pit were studied and compared to the Base Case (see Figure 5). Case D with an area of 12.7 million m^2 and case E with 5.1 million m^2 (see Figure 6). The irregular polygon for Case D has a constant depth -2.5m everywhere, whereas the smaller but deeper area Case E is a rectangle but with and irregular pattern of sand harvesting given by the contours.

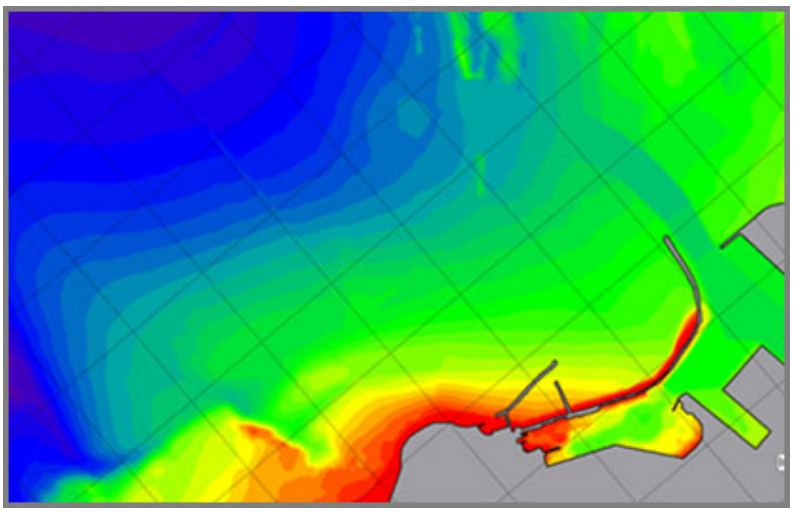


Figure 5. Base Case – Study area bathymetry without borrow pit

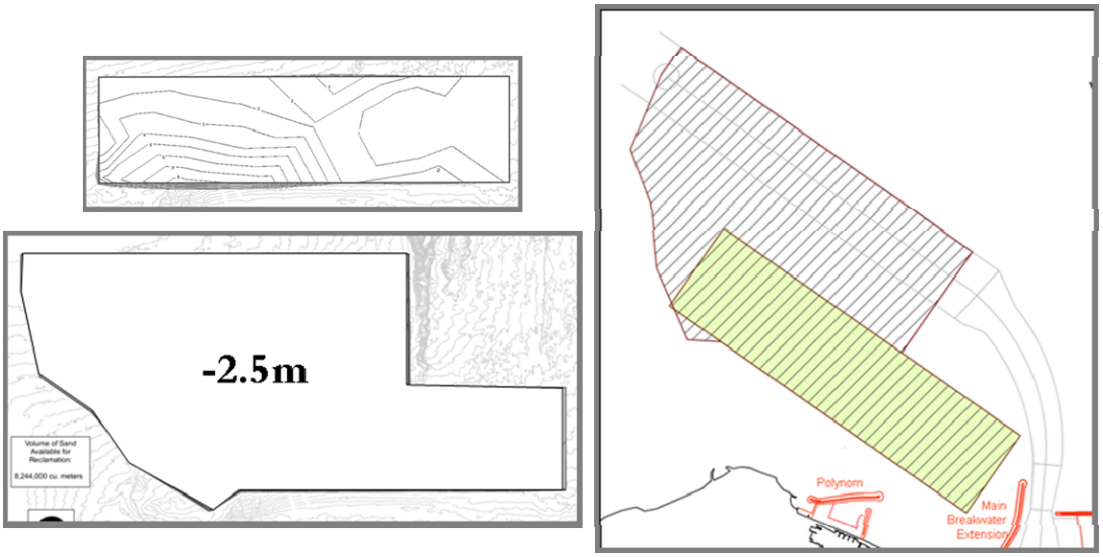


Figure 6. Borrow Pit Areas. Case D (upper left) and Case E (upper right).

Four directions (worst cases) were studied with short waves to determine the impact of the borrow pits on the Area A, namely: NNW (Tp=6, 8, 10s), NW (Tp=8, 10, 12s), WNW (Tp=8, 10, 12s) and W (Tp=8, 10, 12s).

Model results showed that the change in wave energy and the different wave refraction patterns that will occur due to the borrow pits will vary with incident wave direction, wave period, and bathymetry changes. The study presents local wave height reduction and enhancement, and also revealed that the impact of waves on adjacent structures resulting from a borrow pit dredged to 2.5 m below the existing bottom depth, and the new smaller-deeper borrow pit, is relatively small.

The following conclusions were drawn from the borrow pits study:

- The borrow pit with smaller area and deeper dredge spots yields waves at adjacent structures with relatively small changes compared to the Base Case,
- For the smaller and deeper borrow pit, there is a positive impact (i.e., decrease in wave height) for Points 8, 10 and 11 (Figure 7); but a decrease was already seen for the larger borrow pit with -2.5 m dredged from the existing bottom,
- For the smaller and deeper borrow pit, wave heights increase outside the port compared to the Base Case and also compared to the case of the larger borrow pit with -2.5 m maximum dredged depth.

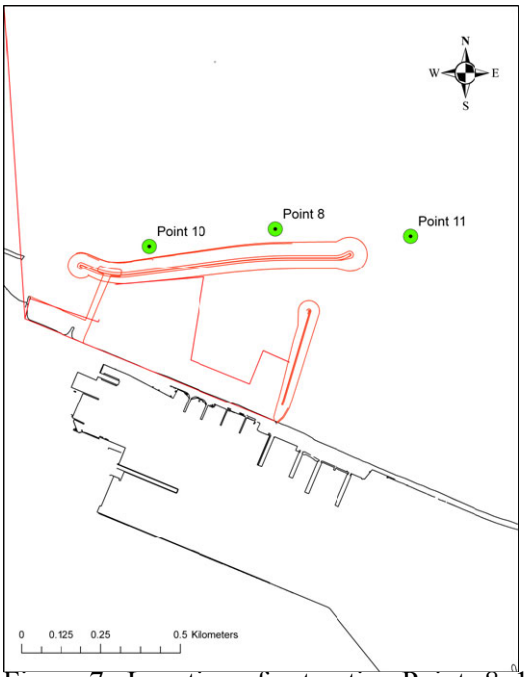


Figure 7. Location of extraction Points 8, 10 and 11.

Comparison at some key locations (Figure 8) of the Base Case model (with dredging pit) versus Case D (Larger – constant -2.5m borrow pit) and Case E (Smaller – deeper borrow pit) are presented in Figure 9 and 10 for the worse incoming wave conditions.

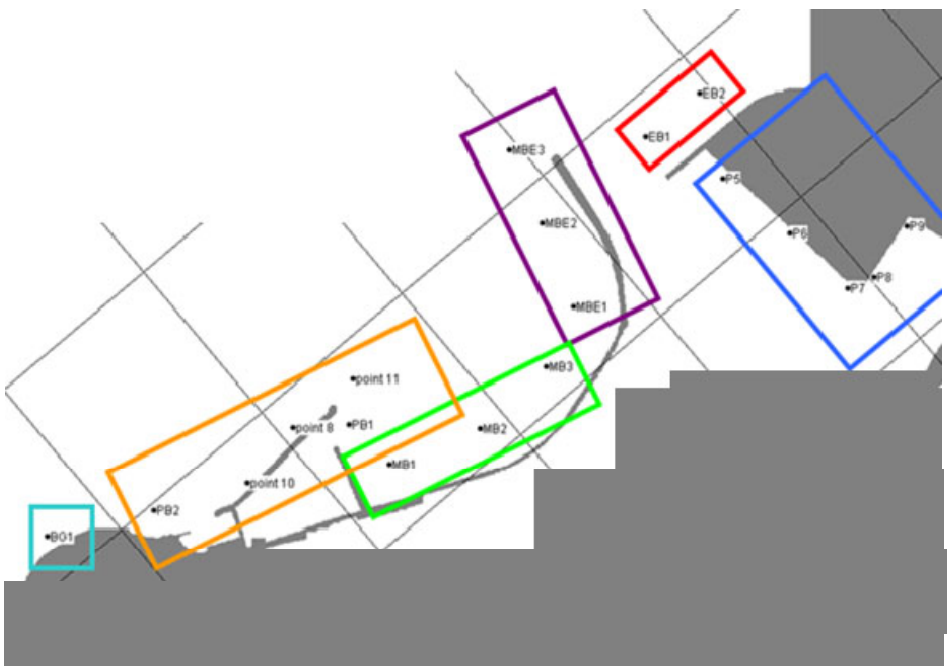


Figure 8. Extraction points used in borrow pit study.

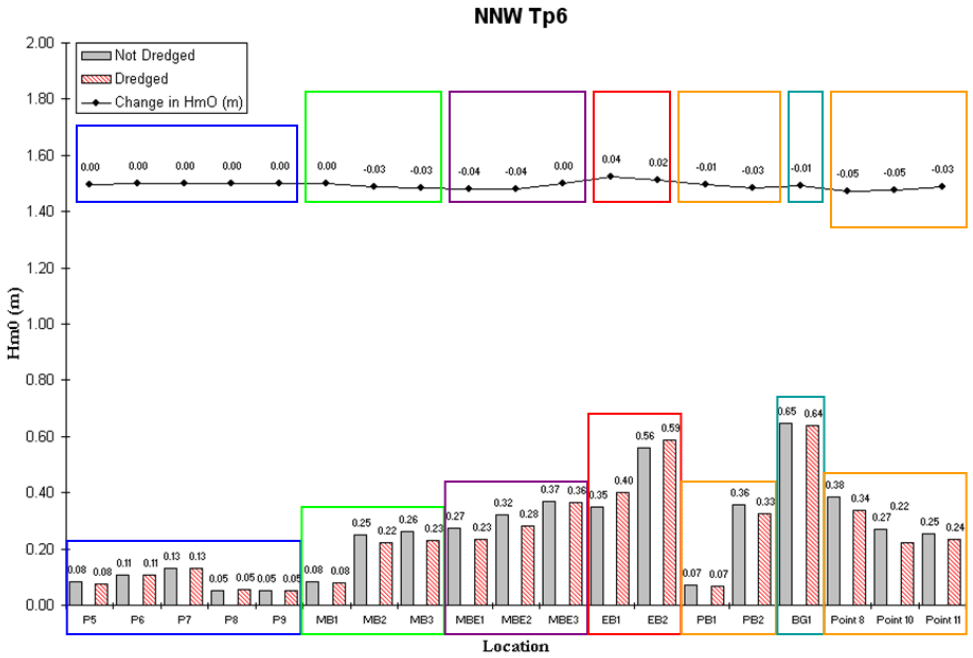


Figure 9. Comparison of Base Case versus Case D for NNW, T_p=6s, H_{m0}=1m.

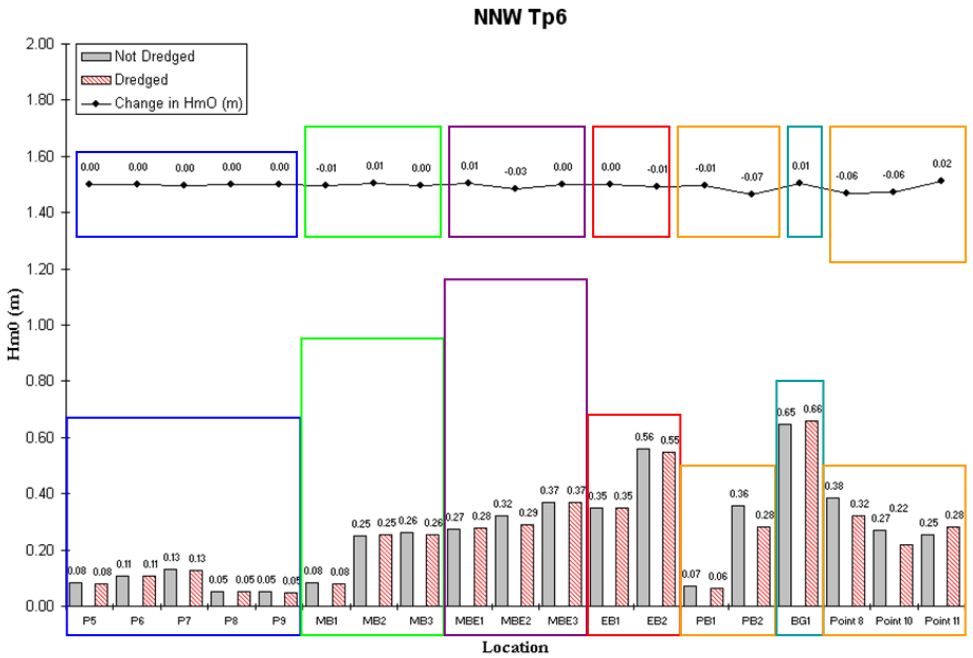


Figure 10. Comparison of Base Case versus Case E for NNW, T_p=6s, H_{m0}=1m.

5. Conclusions

Five main conclusions can be highlighted from the study of this major port.

- The numerical and physical models provide similarity in wave height outside and inside the port hence validate our numerical model,

- The change in wave energy and the different wave refraction patterns that will occur due to the borrow pits will vary with incident wave direction, wave period and bathymetry changes. Local reduction and enhancement can be seen in different locations,

- The study revealed that the impact of waves on adjacent structures resulting from a borrow pit dredged to -2.5 m below the existing bottom depth, as well as a smaller-deeper borrow pit, is relatively small,

- The borrow pit with smaller area and deeper dredged spots yields waves at adjacent structures with relatively small changes compared to the Base Case,

- Because the minimum water depth when the short waves are shoaling (feeling the bottom) is approximately 4 m and the ambient water depth varies from approximately15-30 m, only relatively longer period waves are affected by the borrow pit geometries.

PROPELLER WASH ON A SLOPE

Ayşe YÜKSEL OZAN[1], Kubilay CİHAN[2], Yalçın YÜKSEL[3]

Department of Civil Engineering, Yildiz Technical University, 34210, Esenler/Istanbul, Turkey.

[1] Corresponding author, Ph.D., ayuksel@yildiz.edu.tr, Tel: +90 212 3832931, Fax: +90 212 3835133

[2] Ph.D., kcihan@yildiz.edu.tr Tel: +90 212 3832932, Fax: +90 212 3835133

[3] Prof. Dr., yuksel@yildiz.edu.tr, Tel: +90 212 3832924, Fax: +90 212 3835133

ABSTRACT

Erosion protection for quay structures has big importance due to propeller jet damage. Because of economic reasons a great number of large ships can berth with their own power today. During berthing and unberthing, propeller jet may cause serious scour on sloping rip rap banks, around pile or quay walls. Thus, occurrence of ship propeller-induced damages has became very common problem nowadays. In this research, propeller wash on a slope was studied. The experiments were performed in a laboratory flume in Yıldız Technical University, Hydraulic and Coastal Engineering Laboratory. Two different slope angles which were m=2.5 and m=3 were considered. The propeller has 0.1 m diameter and 625 rpm, 690 rpm and 820 rpm in the experiments. The velocity distrubition and scour on the slope were obtained. The propeller jet velocity distrubution was obtained with Acoustic Doppler Velocimeter (ADV) along the propeller axis. The damaged slope profile and the scour and accummulation behaviour at the toe along the spanwise direction were obtained.

Key Words: Propeller jet, quay structures, erosion, ADV.

1. INTRODUCTION

Incredible increases in Serious damage by propeller erosion has occurred around harbour structures in many ports in the world. One of the reasons for the increase is due to the installation of higher-powered engines and bow thrusters in recent years. The attack on bed and banks of navigation channels and harbor basins, leads to serious erosion (Figure 1). Velocities at propeller jets at the exits of propellers, as well as at side thrusters can easily be 11 to 12 m/s with resulting bed velocities from 3 to 4 m/s (Long et al., 1987). Scour protection for underwater structures are genarally designed with riprap which are built with different size of gravels.

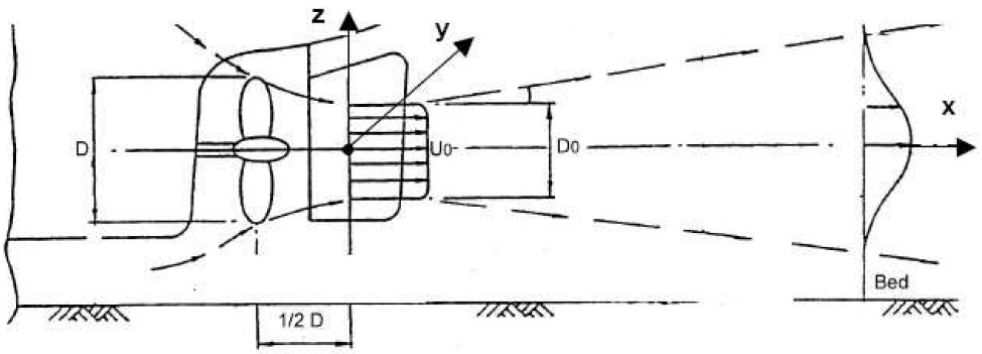


Figure 1. Propeller jet, definition sketch (Roubus and Verhagen, 2007)

Verhagen (2001) studied bowthrusters and the stability of a riprap revetment. Schokking (2002) investigated the stability of stones in propeller-induced jet wash on a slope using an experimental model. Schokking (2002) considered ducted and non-ducted propeller and 1/3 slope ratio in his study. Schokking (2002) defined that the damage on a slope occurs at the lowest part of the slope. Moreover, Schokking (2002) conducted a field study in the Amsterdam-Rijnkanaal to see the effect of bowthrusters in inland waterways. He stated that the scour tends to be shallow and widespread at long- straight quays. Yuksel et.al. (2005) studied on propeller jet scour around pile and pile groups on a sand bed. They used submerged round jet flow to simulate propeller jet flow. Ozan and Yuksel (2010) studied on simulaton of a 3D submerged jet flow around a pile to investigate propeller jet effect around a pile on a sand bed. They also used submerged round jet flow to simulate propeller jet flow.
PIANC (1997) published a guideline for the designed armoured slopes under open quay walls. However, there are still unclear problems on the design of these structures and needs extensive studies for the pile type quays under propeller jets. In this study, the propeller jet velocity distrubution was obtained with Acoustic Doppler Velocimeter (ADV) along the propeller axis. The damaged slope profile and the scour and accummulation behaviour at the toe along the spanwise direction were obtained.

2. EXPERIMENTAL SET-UP

The study was performed in a laboratory flume in Hydraulic and Coastal Engineering Laboratory, Yıldız Technical University. Both sides of flume were made of glass. It includes a propeller system. Propeller rotation was controlled with an automation panel. The experimental set-up was constructed in view of Schokking (2003)'s model (Figure 2 and Figure 3).

Characteristics of the propeller used in the experiments are presented in Table 1. The propeller was placed 19 cm above the bed to illustrate the ship propeller above the bed.

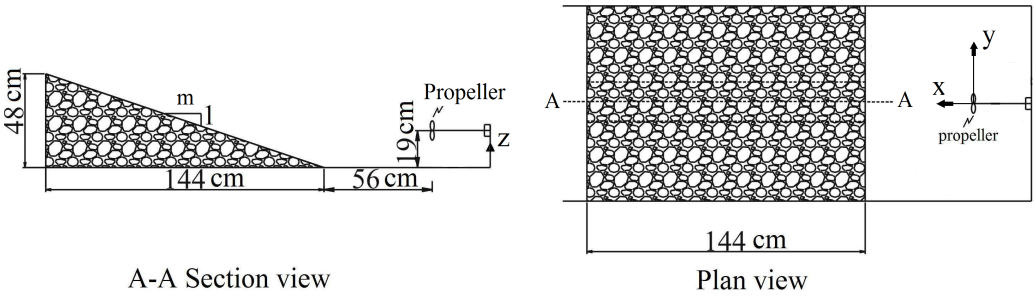


Figure 2. Experimental set up



Figure 3. Experimental set up photos

Table 1. Propeller characteristics

Propeller diemater, D_p	10 cm
Blade number, N	4
Pitch ratio, P'	1.4
Blade area ratio, β	0.4
Thrust coefficient, C_t	0.51

In the experiments, 1/2.5 (m=2.5) and 1/3 (m=3) slope angles were considered. The constant water depth was 48 cm above the bed which corresponds to the top of the slope.

The eroded area (A) is the function of the following variables:

$$A = f_1\left(U_0, D_p, D_{n50}, X, Z, \rho, g, \mu, \rho_s, h\right) = 0$$

where U_0 is efflux velocity, D_p is propeller diameter, D_{n50} is median gravel size, X is horizontal distance between propeller and slope, Z is vertical distance between propeller axis and bed, ρ is density of fluid, g is acceleration of gravity, μ is dynamic

viscosity of fluid, ρ_s is density of gravel and h is water depth. Efflux velocity is calculated from the following equation given by Blaauw et al. (1978):

$$U_0 = nD_p\sqrt{C_t}$$

where n is number of propeller revolutions per second and C_t is propeller thrust coefficient. By dimensional analysis, the non-dimensional parameters were obtained as follows;

$$F\left(\mathrm{Re}, h/D_{n50}, D/D_{n50}, X/D_{n50}, Z/D_{n50}, A/D_{n50}^2, Fr_d^2, D_p/D_{n50}, \rho_s/\rho\right) = 0$$

Rajaratnam (1981) obtained that if $Re>10^4$, the effect of viscosity could be neglected. In this study, the Reynolds number was $Re>10^5$. Therefore, the effect of viscosity could be neglected. Additionally, water depth, propeller diameter, propeller distance to the slope and bed, gravel median diameter were considered constant. Additionally, ρ_s/ρ non-dimensional parameter was considered inside of the Froude number to consider submerged jet flow. As a result the erosion area could be written as follows:

$$S = A/D_{n50}^2 = f_2\left(Fr_d\right)$$

Densimetric Froude nember was defined as

$$Fr_d = U_0/\sqrt{gD_{n50}\left(\rho_s - \rho/\rho\right)}$$

where, U_0 jet exit velocity, d_{50} mean sediment diameter, ρ_s sediment density, ρ water density. Three different Froude Number were considered between 4.1 and 5.3 in the experiments. Slope was formed with gravel and its characteristics were given in Table 2.

Table 2 Characteristics of the gravel

	D_{n50} (mm)	D_{n60} (mm)	D_{n90} (mm)
Coarse gravel	D_{cn50}=8.62	9.53	12.54

Velocity measurements were performed with ADV Acoustic Doppler Velocimeter. For the velocity measurements, gravel used in the experiments were glued up on a plexiglas plate. The suspended material (10-50 grams per cubic meter) supplied by NORTEK was used in the experiments. 3D down-looking ADV probe was used in this study. The acoustic sensor comprised one transmitting and three receiving

transducers. The transmitting transducers emitted acoustic beams with a frequency of 25 Hz. The interception of these four beams, including the width of the transmitting pulse, defines the sampling volume. This volume is 3-9 mm long and approximately 6 mm in diameter (Nortek web).
In order to get the erosion areas, the scour profiles were measured with electronically indicating point gauge. Potassium permanganate was injected for flow visualization in order to determine the sidewall effects in the flume. In the all plots shown here, the streamwise, vertical and spanwise directions were presented by x, z and y respectively and the corresponding velocity components were given by u, w and v.

3. RESULTS AND DISCUSSION

3.1 Velocity profiles

Velocity measurements were performed for both slope angles for 690 rpm. Here, only one slope angle (m=3) results were presented since there is no significant difference between the velocity distributions for different slope angles. Non-dimensional streamwise velocity (u/U_{eff}) distributions along the propeller axis ($0.5 \leq x/D_p \leq 6$) were presented in Figure 4. The influence of the propeller axis is obviously seen close to the propeller ($2 \leq x/D_p$) and this influence disappears after $x/D_p \geq 3$. The maximum axial velocities situated almost at the same points which are $z/D_p \sim \pm 0.3$. Non-dimensional spanwise (v/U_{eff}) and vertical velocity (w/U_{eff}) distributions along the propeller axis ($0.5 \leq x/D_p \leq 6$) were presented in Figure 5. The spanwise velocity is effective until $x > 5D_p$. Despite streamwise and spanwise velocity, vertical velocity is almost zero. Vertical velocity is effective only close to the propeller which correspons to $x/D_p \geq 1$. This results have a good aggreement with Schokking (2003)'s results.

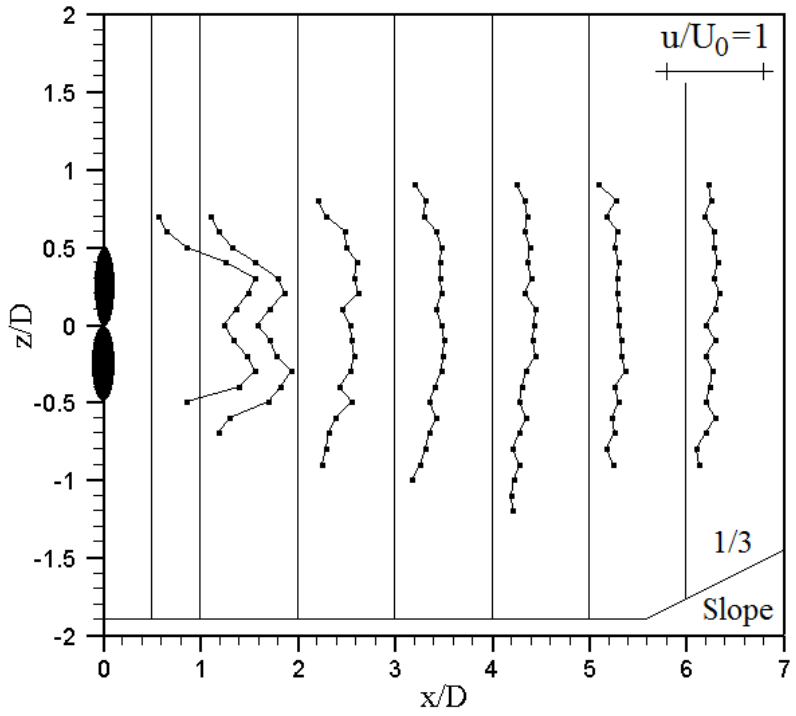


Figure 4. Non-dimensional streamwise velocity distributions along the propeller axis

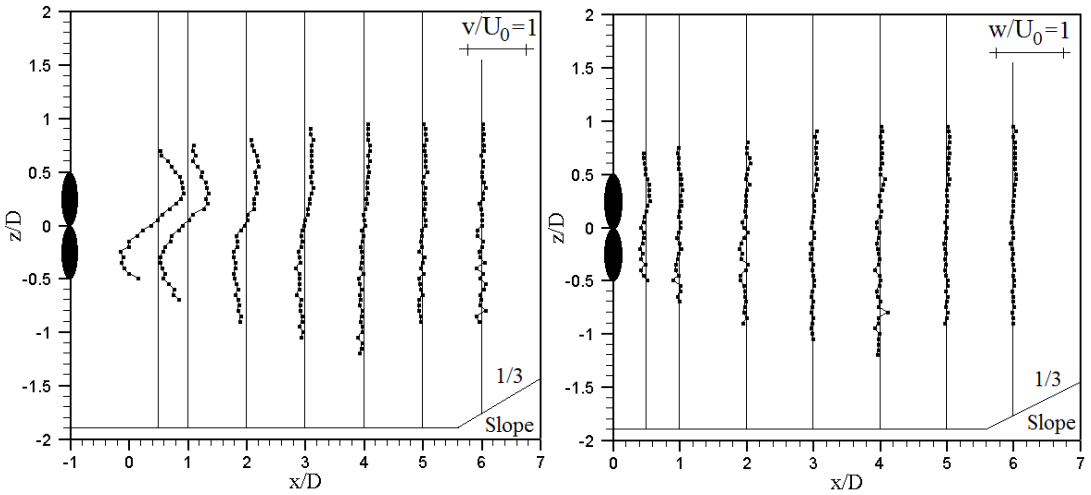


Figure 5. Non-dimensional spanwise and vertical velocity distributions along the propeller axis

3.2 Scour profiles

3.2.1 Slope angle, m=2.5

Typical damage profiles of the slope are shown in Figure 6. It was seen that the gravel on the slope moves in three directions under the propeller jet effect. Stones closer to the toe moved downward, however they also moved in spanwise direction (y-axis) on both sides of the jet axis. As a result, an eroded area occurred at the center of the toe. The height of the scoured area is almost 0.5Z. Furthermore, the stones on the upper part of the slope moved downward and upward. The scouring and accumulation areas occurred beneath the propeller axis.

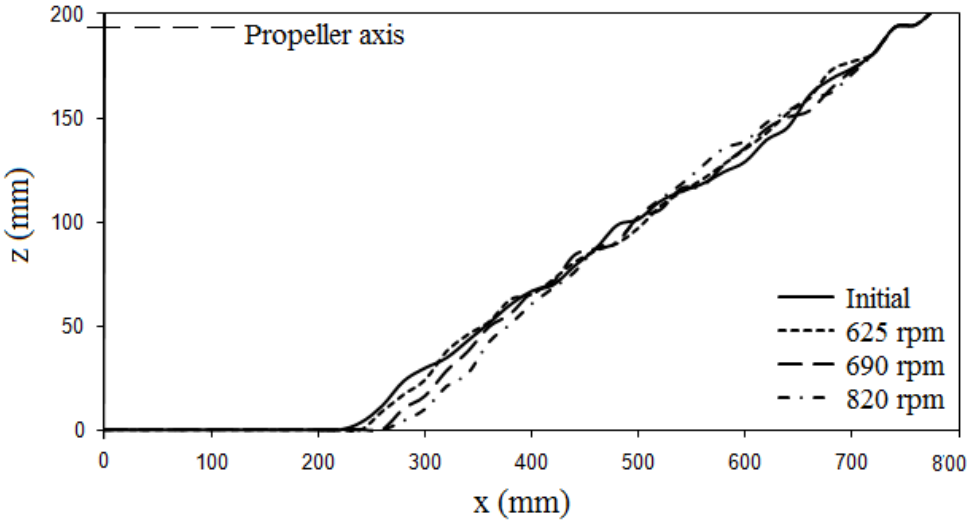


Figure 6. Typical damage profiles for m=2.5

The cumulative variations of the non-dimensional scour and accumulation along the slope are presented in Figure 7. $\Delta z=z_f-z_i$ is the difference in vertical elevation at a point measured on the model, where z_i is the initial elevation, and z_f is the final elevation after the damage under the propeller jet effect. An eroded area developed at the toe and scour depth increases with increasing rpm values. Meanwhile, the accumulation area was established at the upper part of the eroded area and its height also increases with increasing rpm values.

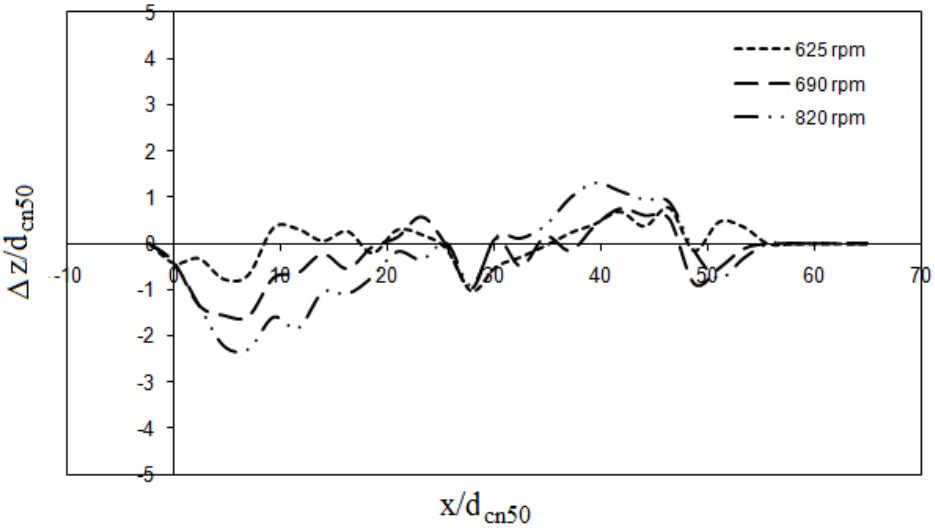


Figure 7. The cumulative variations of the scour and accumulation along the slope for m=2.5

Cumulative accumulation profiles along the transversal line of the toe for different propeller velocities were given in Figure 8. The profile at the right side of the propeller axis was given here since the scoured and accumulated areas are symmetrical according to the propeller axis. Accumulation area enlarges and its height also increases with increasing rpm values. The accumulated area reached its maximum value at 2Dp far from the propeller axis.

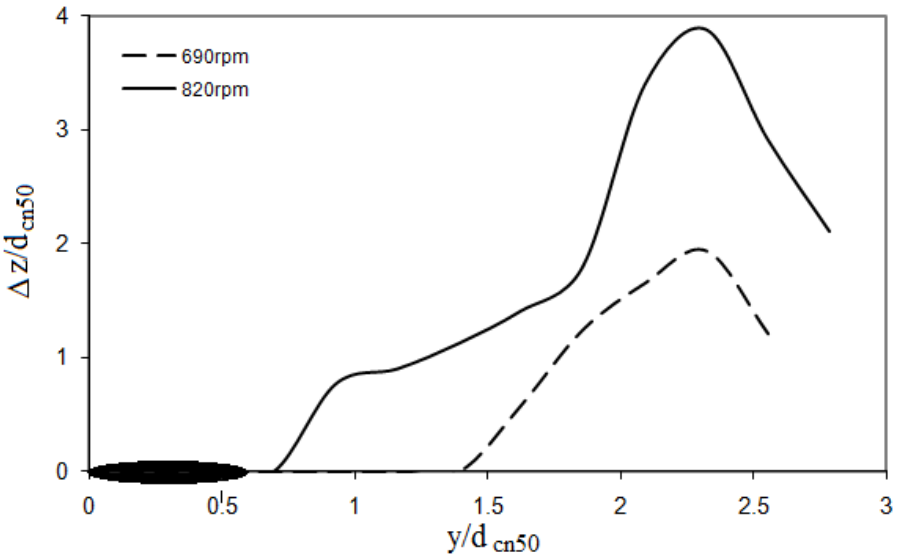


Figure 8. The cumulative variations of the accumulation along the toe at the beginning of the slope for m=2.5 (y=0 refers to the propeller axis)

3.2.1 Slope angle, m=3

Typical damage profiles of the slope are shown in Figure 9. The behavior of the gravels on the slope same with the slope of m=2.5. Stones closer to the toe moved downward and they also moved in spanwise direction (y-axis) on both sides of the jet axis. The scouring and accumulation areas occurred beneath the propeller axis again. However, the height of the scoured area is less than 0.5Z which means lower slope angle leads to the establishment of the scouring area closer to the toe.

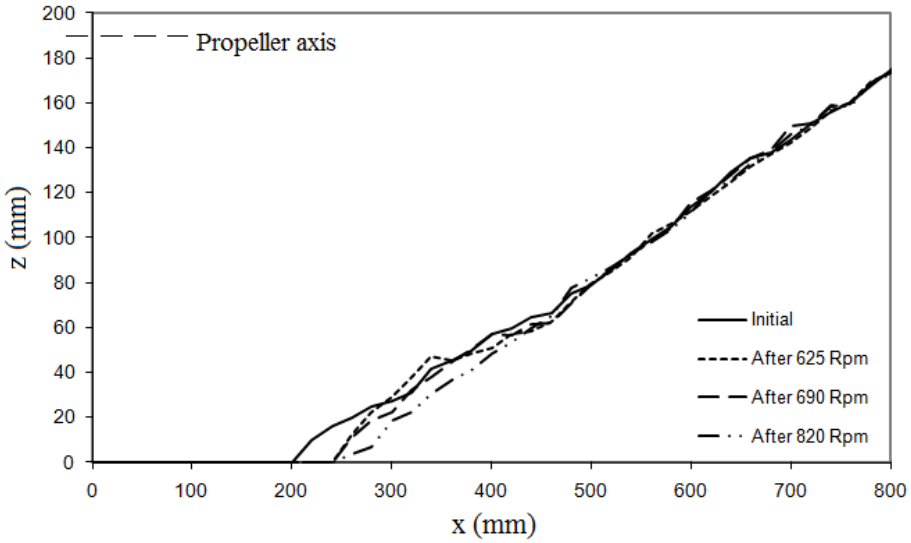


Figure 9. Typical damage profiles for m=3

The cumulative variations of the non-dimensional scour and accumulation along the slope are presented in Figure 10. Scour depth increases with increasing rpm values and the accumulation area was established at the upper part of the eroded area. Apart from this the depth of eroded area and the height of accumulated area are smaller for lower slope.

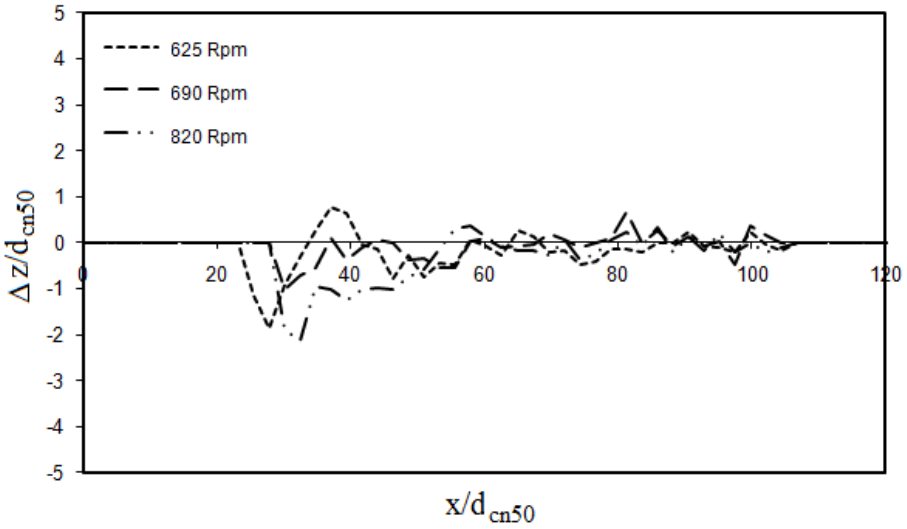


Figure 10. The cumulative variations of the scour and accumulation along the slope for m=3

Cumulative scour profiles along the transversal line of the toe for different propeller rotations were given in Figure 11. The profile at the right side of the propeller axis was given here since the scoured and accumulated areas are symmetrical according to the propeller axis. Scour area enlarges and accumulation area spreads with increasing rpm. Moreover, the width of the scoured area is $1D_p$ at the beginning of the damage and it enlarges with increasing rpm. However, the maximum height of the accumulated area was almost same for 690 rpm and 820 rpm values.

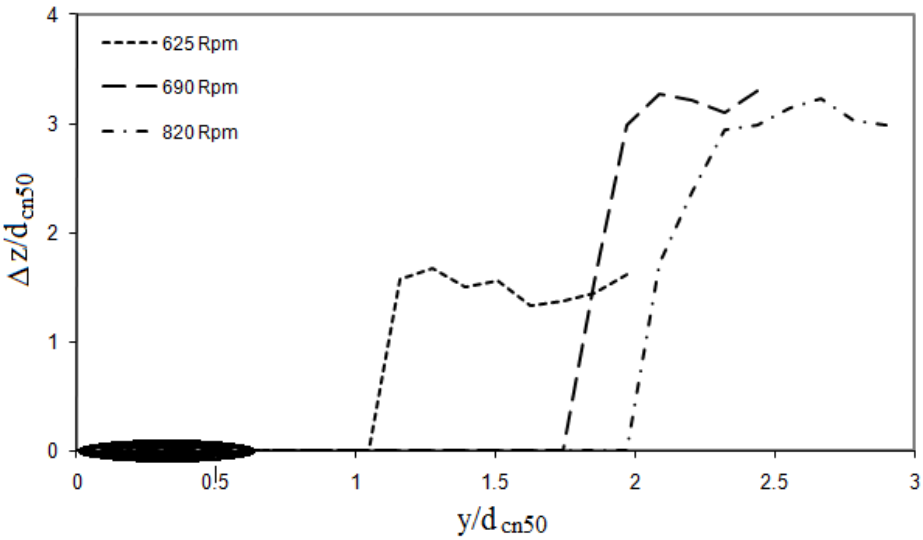


Figure 11. The cumulative variations of the accumulation along the toe at the beginning of the slope for m=3 (x=0 refers to the propeller axis)

The comparison of cumulative accumulation profiles along the transversal line of the toe for different slope angles at 690 rpm value were given in Figure 12. The height of the accumulation area increases with decreasing slope angle. Apart from this the beginning of the accumulation was occurred far from the propeller axis for lower slope angle.

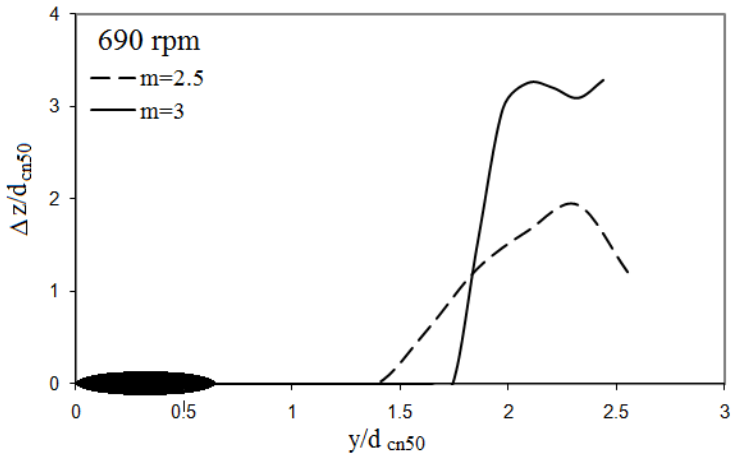


Figure 12. The comparison of cumulative variations of accumulation along the toe at the beginning of the slope for 690 rpm (x=0 refers to the propeller axis)

The comparison of cumulative accumulation profiles along the transversal line of the toe for different slope angles at 820 rpm value were given in Figure 13. The height of the accumulation area increases with increasing slope angle which is different from 690 rpm. The increase of the propeller velocity causes serious erosion along the slope. And also, increasing slope leads to rise on the accumulation at the toe. Furthermore, the beginning of the accumulation area is almost at the edge of the propeller.

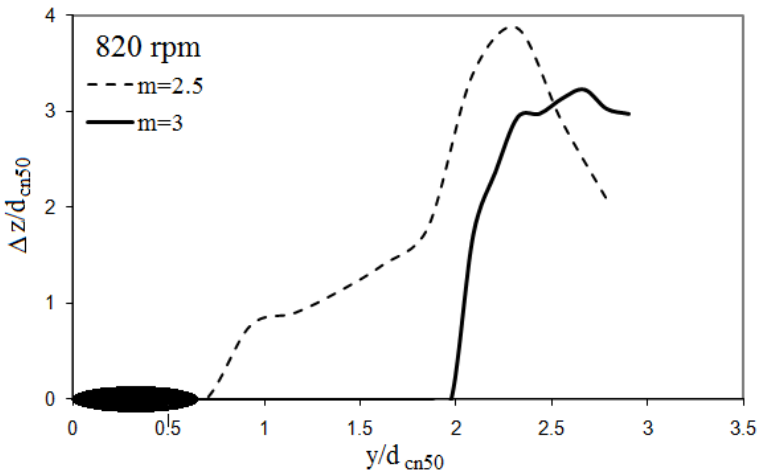


Figure 13. The comparison of cumulative variations of accumulation along the toe at the beginning of the slope for 820 rpm (x=0 refers to the propeller axis)

4. CONCLUSION

In this study, the effect of propeller jet flow on the armoured slope under berthing structures was investigated. Velocity and scour measurements were performed. The damaged slope profile and the scour and accummulation behaviour at the toe along the spanwise direction were obtained.

In the velocity measurements,it is obtained that the maximum streamwise velocities situated almost at the same points which are $z/D_p \sim \pm 0.3$. The spanwise velocity is effective until $x=5D_p$. Despite streamwise and spanwise velocity, vertical velocity is almost zero and effective only close to the propeller ($x/D_p \geq 1$).

Propeller jet effect is dominant from the toe of the slope to $2D_p$ height which almost corresponds to the axis of the propeller for all cases. Moreover, the length of the eroded area decreases with decreasing slope angle.

Scour depth and accumulation height increases with increasing propeller velocity for both slope angles.

The behavior of scour and accumulation along the toe in spanwise direction was obtained. Accumulation area enlarges and its height also increases with increasing rpm values. The height of the accumulation area increases with decreasing slope angle for steep slope angle where it increases with increasing slope angle for higher propeller velocity. And also, increasing slope leads to rise on the accumulation at the toe. Furthermore, the beginning of the accumulation area is almost at the edge of the propeller.

ACKNOWLEDGEMENTS

The authors are thankful for the financial support of The Research Fund of Yildiz Technical University.

REFERENCES

Blaauw, H. G., and Kaa, E. J. Van de (1978), “Erosion of bottom and sloping banks caused by the screw race of the manoeuvering ships”, Publ. No. 202, Delft Hydraulics Laboratory, Delft, The Netherlands.

Longe, M. J. P., Hergert, M. P. And Bylk, M. R., 1987. “Problems d’erosion aux ouvrages de quai existants causes par les propulseurs d’etrave et les helices principles des novires lors de leurs acostages aou appareillages.”, PIANC, Bulletin No. 58.

PIANC, 1997, “Guidelines for the design of armoured slopes under open piled quay walls”, Report of working group 22, supplement to Bulletin 96, 38 pp.

Rajaratnam, N. (1981). “Erosion by plane turbulent jets.” J. Hydr. Res., 19 (4), 339-358.

Roubos, A., Verhagen, H.J., (2007) “Uncertainties in the Design of Bed Protections Near Quay Walls”, 4th Conference on Port Development and Coastal Engineering (PDCE), Varna, Bulgaria.

Schokking, L.A., 2002, “Bowthruster-induced Damage”, MSc Thesis, Delft University of Technology.

Verhagen, H.J., "Bowthrusters and the Stability of a Riprap Revetment", 22nd International Conference on Hydrodynamics and Aerodynamics in Marine Engineering, 1-4 October, 2001, Varna, Bulgaria.
Yuksel, A., Celikoglu, Y., Cevik, E., Yuksel, Y., 2005, "Jet Scour around Vertical piles and pile groups", Ocean Engineering, v. 32, Issue 3-4, pp 349-362.
Yuksel Ozan, A., Yuksel, Y., 2010, "Simulation of a 3D submerged jet flow around a pile", Ocean Engineering, v. 37, Issue 8-9, pp 819-832.

Geotextile Tube solution for Dos Bocas PEMEX marine facilities beach erosion problem at Tabasco, Mexico

Felix Tseng [1] , Zoe Lin [1], Alfonso Solis [2] , Marco Sánchez [3]

[1] ACE Geosynthetics, No.33 Jing 3 Rd., C.E.P.Z. Wuchi, Taichung Hsien, Taiwan, R.O.C.;
Email : sales@geoace.com
[2] Axis Ingenieria S.A. de C.V., c25 #528C x 60 y 62 Alcalá Martín CP 97050 Mérida, Yuc., México;
Email : info@axisingenieria.com.mx
[3] ML Ingenieria, Sagredo 237, Col. Guadalupe Inn C.P. 01020, Del. Alvaro Obregon, Mexico, D.F.;
Email : ml@mlingenieria.com

Keywords: *Geotextile tube, beach erosion, oil conduction pipes*

ABSTRACT

Mexico is located in the subtropical region. Due to the concentration of strong tropical cyclones, numbers of hurricanes batters the territory all year round. Recent years, with the phenomenon of global warming, hurricanes increase year by year, not only in the quantity but also in the power, and indirectly cause the coastline to fall back, eventually the coastal erosion issue threatens the alongshore structures. PEMEX (Petróleos Mexicanos) is the major oil corporation in Mexico; built along the coastline, its installations are also invaded by hurricanes.

In 1982, PEMEX built up a private port in the Gulf of Mexico south of Dos Bocas port, Tabasco State. The construction of this port blocked the drift sand. After many years of the wave and longshore current effect, the seashore at east side of the port where many oil pipelines were located, turned out in lack of sand source arising the erosion problem and lost its protection. Thus, Dos Bocas coastline was facing severe challenges, how to solve the problem of coastal erosion and oil pipeline protection became the top priority for PEMEX.

PROJECT DESCRIPTION

Mexico is one of the world's top three oil suppliers; oil is the largest source of foreign exchange in Mexico. To maintain the normal production and pipeline operations becomes essential. The case is about oil pipeline protection program for PEMEX Marine facilities (DBPM) in Dos Bocas seashore, State of Tabasco (Fig. 1).



Figure 1. Project site location.

In the east side of Dos Bocas port, the groyne area is divided in seven intervals (Fig. 2), the fourth interval includes three oil pipelines which they are responsible for transmission of the oil onshore to the marine for sale. In addition, the seventh interval contains four oil pipelines of 36 inches each where they transfer the oil from marine oilwell to the in-land storage tank (Fig. 3).



Figure 2. Project coastal area.

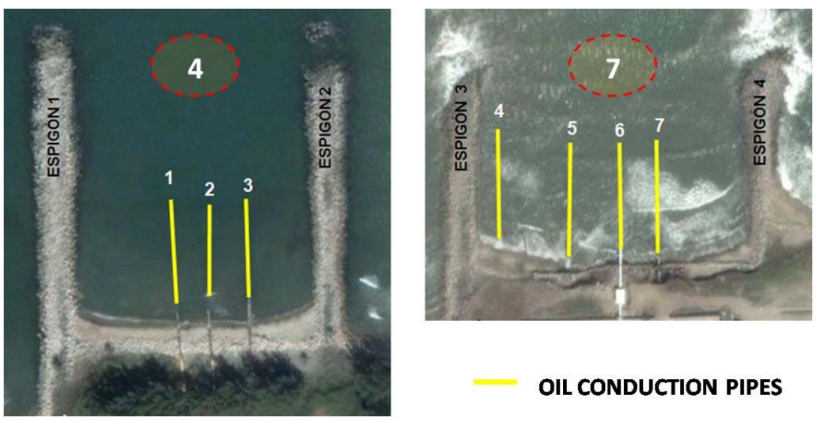


Figure 3. Oil conduction pipes plan view.

Two decades ago, PEMEX used groynes and stones as protecting purpose of the area; however these stacked stone and groynes were seriously damaged by long-term wave

action, and these structures loose 30% of their original length and 40 % of their height. For this reason, not only the coastline is not stabilized, but also faces greater risk for the gradual beach erosion problem. Consequently, these serious problems already threaten the foundation of pipeline and in-land storage tank security.

The main issue is pipeline based on the surf zone, where drift sand activity is very frequent. Prolonged exposure to wave action, the sand foundation of oil pipeline is tragically undermined, and there is risk of pipeline fracture at any time. Once the pipeline stop its operation, besides of bringing impact to the Mexican economy, the greater the problem will result in marine oil pollution disaster.

Therefore, the case is divided into two parts. Firstly, protection of the pipeline base against risk of being emptied out, and secondly the construction of submerged breakwaters, using an artificial beach nourishment way to restore eroded coastline, the length of the breakwaters is approximately 1.9km.

DESIGN CONCEPT

Traditional stone protection construction methods have high maintenance cost, and difficulties in the obtainment of its sources; furthermore, they require large hanging equipments to carry on the installation. Although this is an alternative to construct submerged breakwaters, it cannot become the basis for pipeline protection.

Taking into consideration the efficiency of installation and easy maintenance, ACETube® requires simple equipment (just sand pump and small boat), so it can acquire the in-situ sand to fulfill its structure, and bring the least impact to the local environment.

ACETube® demonstrates the application in a flexible manner, while solving the beach nourishment problem, reducing the wave energy, and giving support to the oil pipelines, ACETube® providing diverse solutions to these three major problems is found in the case.
In this coastal erosion protection project, ACETube® plays role of two main effects, one of it, as submerged breakwater, it can break the waves and reducing wave energy delivered to the shore, diminishing the disturbance and sand drift phenomenon, even less to cut down the use of sand for beach nourishment.
Besides the above mentioned, another effect of ACETube® is to perform as the protection of pipeline base, by giving support to the pipeline with undermined base, and preventing the uneven subsidence causing danger in security.

Therefore, PEMEX has considered the Economy, Ecology and Function to decide the best alternative for the problem solution, and ACETube® has become the only selection among millions of candidates.

ACETube®: Pipeline support component

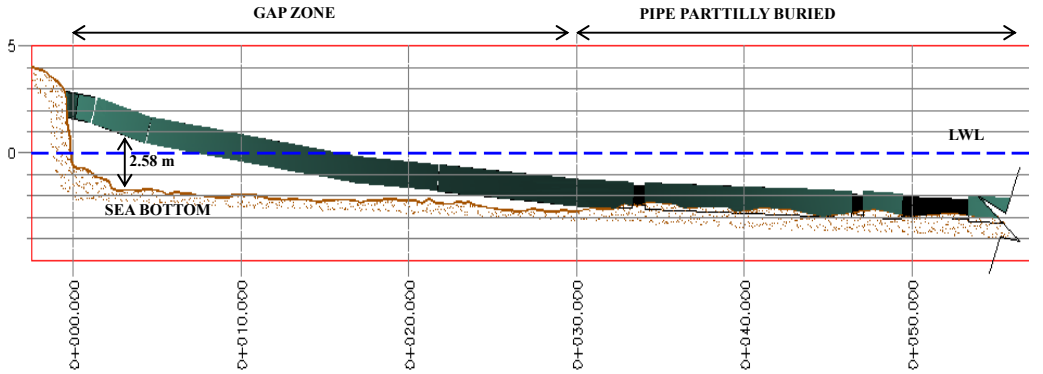


Figure 4. Profile for pipe 7.

The oil pipelines of PEMEX located in the shoreline of Dos Bocas, preliminary studies of the seventh interval show that the pipelines number 5 to 7 are found with serious erosion problems, the most critical parts are the pipelines number 6 and 7. The gap between the base and the pipeline is up to 2.5m high (Fig. 4). To fill this undermined vacancy, it must adapt to the changes in seabed topography. Then, the gap underneath of pipeline has adopted two section designs (Fig. 5), with the variable sized of ACETube® fabricated by ACE Geosynthetics. The engineering applies pilling method of ACETube®s to fill up the emptiness between the base and pipeline. Through the flexible characteristics of the geotextile tube, it could help to overcome the sea-bed changes, and adequately support loading effect.

The perfect performance of flexible geotextile tubes, successfully defeats the problems that traditional RC or stone cannot solve, and it becomes the precedent application of pipeline base protection.

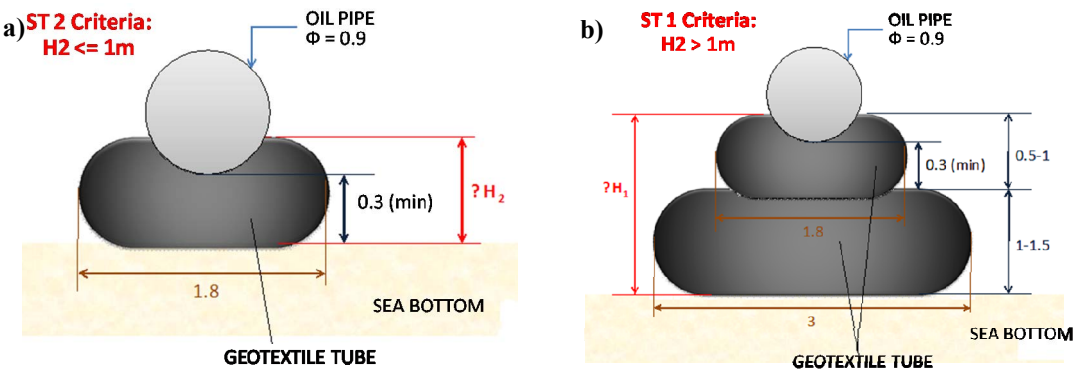


Figure 5. Designed sections; a) gap < 1m), b) gap >1m.

Submerged Breakwater

The project is planned to construct submerged breakwater at 30-40m far from the coastline. The major function is to reduce the incident wave energy, effectively control the breaking wave position, so that the passing wave will not disturb the sand beach, but still it can deliver steady drift sand retained on the rear of submerged breakwater.

Then, the design concept of ACETube® filling height, taking into account the distance with open sea of 30-40m at an average low tide water level surface (LWL), it is set to be 1-1.25m. Also considering this height demand and the base undermining danger, ACETube® submerged breakwater design includes following three components: main tube with circumference of 7.8m, antiscour apron to prevent undermining, and at seaward side a small tube to anchor and fix the scour apron. These three components are stitched together in the manufacturing plant to facilitate the construction convenience. See Figure 6.

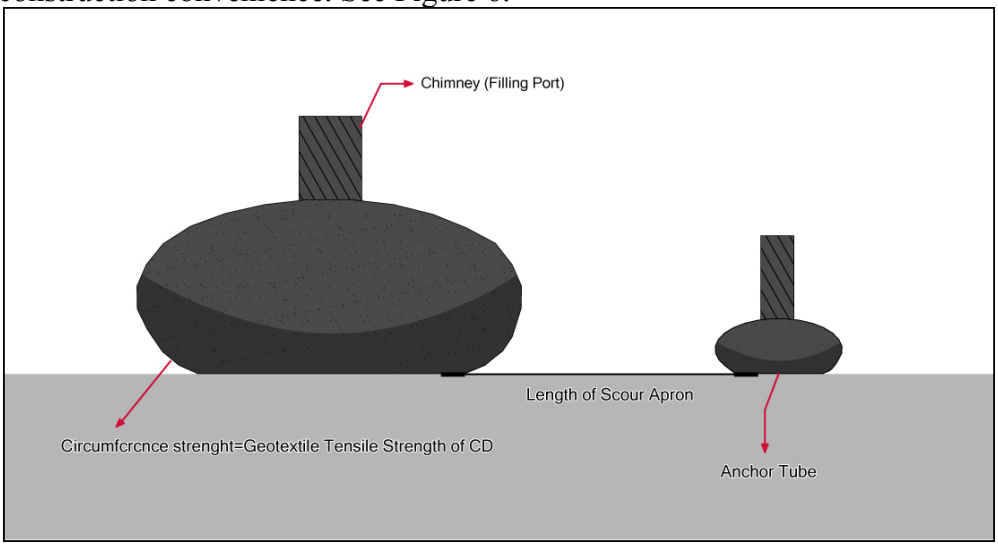
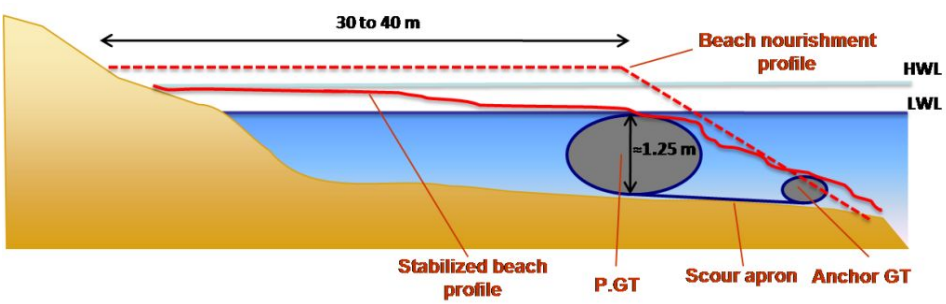


Figure 6. Breakwater cross section

Beach Nourishment

The success factor of beach nourishment was the size of filling particles. Through numbered of underwater specimen extraction and particle size analysis, the decision was made on adopting the submerged sandbank source from 400m offshore. Thanks to the advantage of borrowed material with median diameter larger than the native beach sand, it saved a lot of quantity of filling material applied for backfilling. The design of beach elevation is greater than high tide water level (HWL) 0.1m, after filling it reclaim of 30-40m (Fig 7.) width of steep beach in order to protect the in-land storage tanks.



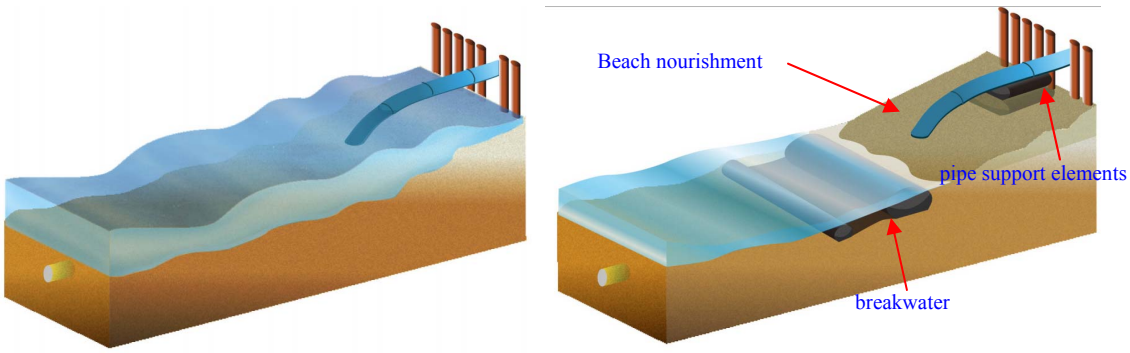


Figure 7. Beach nourishment designed profile

CONSTRUCTION PROCESS

This is a case about underwater construction with ACETube®. Before construction, any harmful material that can damage the geotextile must be removed from the seabed. Prior to the filling, the ACETube® must be anchored in the right position. Then, initiate the filling, the appropriate anchor of ACETube® will determine the success or failure of the filling job. During filling, the stress of geosynthetic material will vary depending on the filling pressure; thus, the excess pressure will cause damage to geotextile tube, therefore the control of pumping pressure becomes the key of the installation process.



Figure 8. Filling ACETube® tasks. a) pipe support elements, b) breakwater

ACETube®'s features are: high tensile strength, high sewing efficiency, high permeability, low aperture size and light weight. These characteristics can not only accelerate the construction speed, ensure the complete success of filling, but also the lightweight ACETube® provides handling convenience to whole operation.
The equipments applied for the case are: 4 inched diameter of pipeline and pump capacity of 40-50m^3/hr. Water and sand ratio is approximately 10 to 30%, all the filling sand source is obtained from 50-70m offshore.

When ACETube® filling is complete, we've continued to use 12 inches pipeline and dredge boat capacity of 250m^3/hr to conduct the beach nourishment job, the obtained sand source is transported with 10 inch rubber hose to the beach nourishment area (Fig 9.). As a result, the seventh interval has reached the total filling volume of 62,000m^{3}of sand source.



Figure 9. Beach nourishment activities

EFFECTIVENESS

The pipeline support project completed in July 2009, the following charts shows before and after construction (Fig. 10 & 11). As early mentioned, the flexibility of ACETube® which characteristic allows conforming the geographical shape and structural changes, not only solved the 2.5m gap between the oil pipeline and base, but also it prevented the risk of pipeline fissure at any time. Finally, it brought the effect of support, transferring the pipeline weight through the ACETube® components towards the seabed, then becoming the key success of the project.



Figure 10. Before-after comparison for pipes 3



Figure 11. Before-after comparison for pipes 6 and 7.

During the construction period, ACETube® offers the perfect performance of the energy dissipation, as shown in Figure 12. ACETube® submerged breakwater anticipatively reduces the wave energy, leaving the remained waves energy across it and taking the drift sand to the energy dissipation zone. Gradually, the drift sand is accumulated at back of the submerged breakwater. By the observation of beach section data, there were initial positive results although the beach nourishment construction has not yet started (Fig 13.).

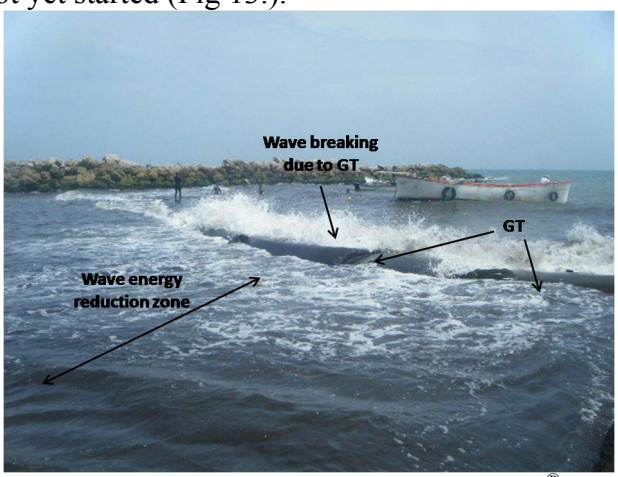


Figure 12. Wave breaking due to ACETube®

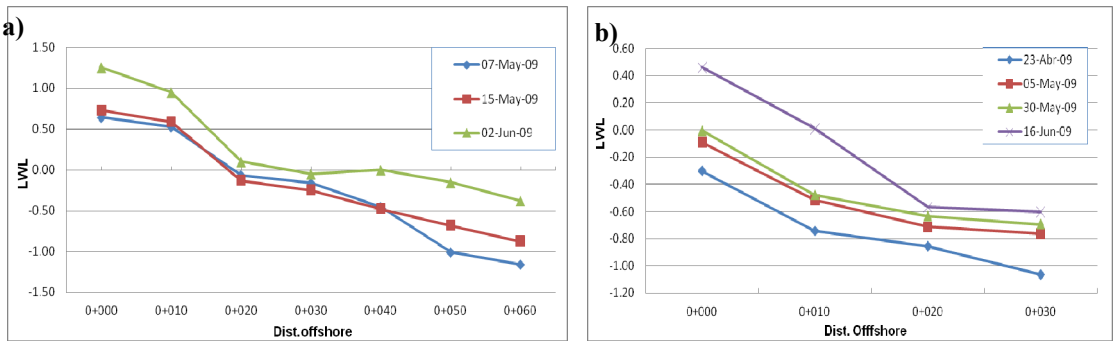


Figure 13. Beach profile evolution after breakwater installation; a)Section 1, b)Section 7.

The engineering method of submerged breakwater technology makes the beach shoaled, preventing the direct impact of the long-wave energy on coastal structures, also securing the safety of the in-land storage tank (Fig 14.). In addition, the nourished beach extends the serving life of the ACETube® supporting components. Moreover, found in the installation process, many algae soon after the construction has been attached to ACETube® surface (Fig 15.), demonstrating that ACETube® submerged breakwater design has low impact effect on the ecological environment.



Figure 14. Final situation for section 4



Figure 15. algae has been attached to ACETube® surface

CONCLUSION

The construction method with flexible ACETube®, demonstrated wide range applications using tube structure, following are the advantages of flexible tube structure against the traditional engineering methods:

- The installation of flexible tube structure can adopt the local materials by

minimizing the damage of local environment.
- ACETube® used in pipeline protection, replaced the traditional construction method, providing innovation and economic application, by becoming as good alternative of engineering method.
- ACETube® has high tensile strength, high permeability and lightweight by offering economical, convenient and efficient solution.
- As in the case, the installation of ACETube® only needs small and easy-to-handle equipments, which it can be beneficial to the construction and future maintenance.
- As the other cases in Mexico (Alvarez et al., 2006; Alvarez and Espinoza, 2008; and Escalante and Solis, 2008), protection of marine structure with ACETube® offers an efficient and environment-friendly construction method.
- Dos Bocas coastline protection project proves that ACETube® can extend the rebuilding life of the beach.

ACETube® not only solved the Dos Bocas coastline erosion risk and pipeline protection issue, but also beautified the shoreline by nourishing the beach.

ACKNOWLEDGEMENTS
Project was recruited and executed by MARSA S.A de C.V. Supervision and engineering developed by AXIS INGENIERIA. Geotextile Tube supplier and manufacturer were ML INGENIERIA and ACE GEOSYNTHETICS respectively, both giving fully technical support during project construction. Authors whish to thank Petroleos Mexicanos (PEMEX) for providing economical resources for project construction, and MARSA S.A de C.V. for conducting the project.

REFERANCE
Alvarez, E., Rubio, R., & Ricalde, H. (2005). “Beach Restoration with Geotextile Tubes as Submerged Breakwaters in Yucatan, Mexico”. Proceedings of the International Symposium on Tsunami Reconstruction with Geosynthetics–Protection, Mitigation and Rehabilitation of Coastal and Waterway Erosion Control. Bangkok, Thailand, pp. 123-135.

Alvarez, E., & Espinosa, B. (2008). “The role of the Geotextile Tubes in coastal protection and beach restoration. The experience in Yucatan, Mexico”. First Pan American Geosynthetics Conference, Cancun, Mexico

Escalante, S., & Solis, A. (2008). “Coastal dune stabilization using geotextile tubes at Las Coloradas”. Gesoynthetics magazine, Vol. 26(1), pp. 16-24.

Leshchinsky, D., Leshchinsky, O., Ling, H.I., & Gilbert, P.A. (1996). “Geosynthetic tubes for confining pressurized slurry: some design aspects”, Journal of Geotechnical Engineering, ASCE, Vol. 122(8), pp. 682-690.

U.S. Army Corps of Engineers. (2004). “Coastal Engineering Manual”. Coastal Engineering Research Center, Vicksburg, Miss. US

THE HUB EFFECT on a PROPELLER SCOUR AROUND a PİLE

Kubilay Cihan[1], Ayşe Yüksel Ozan[2] , Yalçın Yüksel[3]
Department of Civil Engineering, Yildiz Technical University, 34210,
Esenler/Istanbul, Turkey.
[1] Dr., kubilaycihan@gmail.com, Tel: +90 212 3832932, Fax: +90 212 3835133
[2] Dr., ayuksel@yildiz.edu.tr, Tel: +90 212 3832931, Fax: +90 212 3835133
[3] Prof. Dr., yuksel@yildiz.edu.tr, Tel: +90 212 3832924, Fax: +90 212 3835133

ABSTRACT
Propeller induced scour has been taken big attention in last three decades. Erosion caused by propeller jets around berting structures has been an important research subject in engineering area for years. In this study, the hub effect on a propeller scour around a pile was searched. The experiments were performed in a laboratory flume in Yıldız Technical University, Hydraulics and Coastal Engineering Laboratory. A 1/1.5 slope with coarse gravel and rip-rap layer with fine gravel were considered. Pile was constructed at the toe of the slope. Firstly experiments were performed for free propeller jet and then for hub jet. The propeller has 0.1 m diameter and the hub has 0.104 m diameter and 0.3 m length. The experiments were conducted for 560 rpm, 690 rpm and 820 rpm. The results of free and hub propeller jet were compared and it is found that hub causes decrease in scour.

KEYWORDS: Scour, Propeller, Pile, Armoured slope

1. INTRODUCTION
Incredible increases in ship dimensions and installed engine power, introduction of new types of ships with bow thrusters in recent years yield very important local scour problems at the seabed, the sloping banks of navigation channels, quay structures (e.g. walls and piles) which in many cases threatens to undermine berth structures and sloping banks. Scour protection for underwater structures and pipelines, quay piles and walls are genarally designed with riprap. This riprap sturucture are built with different size of gravels.
In general, scour is dangerous to any kind of marine structures.Verhey (1983) studied on the stability of bottom and banks subjected to the velocities caused by propeller jet. He presented a method to predict, approximately the velocities behind a propeller of manoeuvring ships. Verhagen (2001) achieved a study on bowthrusters and the stability of a riprap revetment. Verhagen (2001) made an analyse to simulate propeller jet and studied on Shields and Izbash methods which can be used for stability of riprap on a slope attacked by propeller flow.
Schokking (2002) investigated the stability of stones in propeller-induced jet wash on a slope using an experimental model. Schokking (2002) considered ducted and non-ducted propeller and 1/3 slope ratio in his study. Schokking (2002) found out that the damage on a slope occurs at the lowest part of the slope. Additionally, Schokking (2002) performed a field study in the Amsterdam-Rijnkanaal to see the effect of bowthrusters in inland waterways. He stated that the scour tends to be shallow and widespread at long- straight quays. Beside this, short quays or quays with geometric

anomalies lead to consistent berthing vessels, which leads to the development of deeper, concentrated scour holes.
Yuksel et.al. (2005) studied on propeller jet scour around pile and pile groups on a sand bed. They used submerged round jet flow to simulate propeller jet flow. Roubos and Verhagen (2007) investigated design formulas for bed protections in the port of Rotterdam. They made a risk based analysis to evaluate the different strategies and their consequences. Raikar and Dey (2009) performed a study on maximum scour depth at piers in armor-beds. They presented a design method to determine the maximum equilibrium scour depth at piers embedded in a sand-bed overlain by a thin armor-layer of gravels. Ozan and Yuksel (2010) studied on simulaton of a 3D submerged jet flow around a pile to investigate propeller jet effect around a pile on a sand bed. They also used submerged round jet flow to simulate propeller jet flow.
PIANC (1997) presented a guideline for the designed armoured slopes under open quay walls. However, there are still unclear problems on the design of these structures and needs extensive studies for the pile type quays under propeller jets. In this study, the propeller induced scour around the pile type berth structures was investigated. The aim of this study is to find out the effect of propeller (in a hub and without a hube) jet flow on the stability armoured slopes under berth structures. To achieve this, scour measurements were conducted in the experiments. Armour layer damages on the slope were defined using a damage level parameter which is given by Van der Meer (1988).

2. EXPERIMENTAL SET-UP

The study was conducted in a laboratory flume in Hydraulic and Coastal Engineering Laboratory, Yıldız Technical University. Both sides of flume were made of glass. It includes a propeller system. Propeller rotation was controlled with an automation panel. Experimental set-up is shown in Fig. 1.

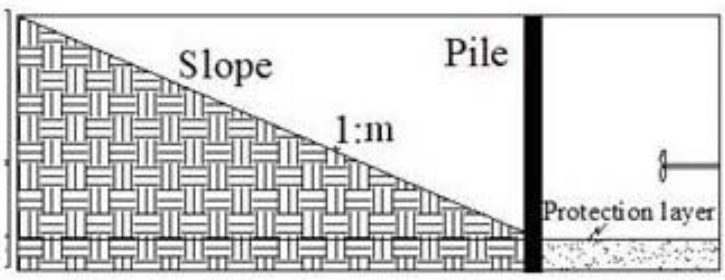


Figure 1. Experimental set up

Characteristics of the propeller used in the experiments are presented in Table 1. The propeller was replaced 19 cm above the bed.

Table 1. Propeller characteristics

Propeller diameter, D_p	10 cm
Blade number, N	4
Pitch ratio, P’	1.4
Blade area ratio, β	0.4
Thrust coefficient, C_t	0.51

The cylindrical pile was made of plexiglass and placed at the begining of the slope and on the propeller axis. The fixed water depth was 48 cm above the bed which corresponds to the top of the slope.
The eroded area (A) is the function of the following variables:

$$A = f_1\left(U_0, D_p, D_{n50}, D, X, Z, \rho, g, \mu, \rho_s, h\right) = 0 \quad (1)$$

where U_0 is efflux velocity, D_p is propeller diameter, D_{n50} is median gravel size, D is pile dimater, X is horizontal distance between propeller and slope, Z is vertical distance between propeller axis and bed, ρ is density of fluid, g is acceleration of gravity, μ is dynamic viscosity of fluid, ρ_s is density of gravel and h is water depth. Efflux velocity is calculated from the following equation given by Blaauw et al. (1978):

$$U_0 = nD_p\sqrt{C_t} \quad (2)$$

where n is number of propeller revolutions per second and C_t is propeller thrust coefficient. By dimensional analysis, the non-dimensional parameters were obtained as follows;

$$F\left(\mathrm{Re}, h/D_{n50}, D/D_{n50}, X/D_{n50}, Z/D_{n50}, A/D_{n50}^2, Fr_d^2, D_p/D_{n50}, \rho_s/\rho\right) = 0 \quad (3)$$

Rajaratnam (1981) studied on the erosion produced by a plain jet and defined that if $\mathrm{Re}>10^4$, the effect of viscosity could be neglected. In this study, the values of Reynolds number were calculated between 1.2×10^4 and 2.2×10^4. Therefore, the effect of viscosity could be neglected. Moreover, water depth, propeller diameter, propeller distance to the slope and bed, pile diameter, gravel median diameter were considered constant.
Densimetric Froude nember was defined as

$$Fr_d = U_0 \Big/ \sqrt{gD_{n50}\left(\rho_s - \rho/\rho\right)} \quad (4)$$

where, U_0 jet exit velocity, d_{50} mean sediment diameter, ρ_s sediment density, ρ water density.
Slope was composed with coarse gravel and protection layer was composed with fine gravel. The dimension ratio of coarse gravel to fine gravel was chosen as 2.1 in the experiments. The characteristics of the gravels were given in Table 2.

Table 2 Characteristics of the gravels

	d_{n50} (mm)	d_{n60} (mm)	d_{n90} (mm)
Coarse gravel	d_{cn50}=8.62	9.53	12.54
Fine gravel	d_{fn50}=4.00	4.50	6.05

In order to get the erosion areas, the scour profiles were measured with electronically indicating point gauge before and after tests.

RESULTS AND DISCUSSION

Case 1: propeller rotates freely in a body of water

The variations of the cumulative scour and accumulation along the slope at the propeller axis are presented in Figure 2. Here, $\Delta z = z_f - z_i$ and z_f is final elevation and z_i is initial elevation. Accumulated area at downstream of pile was clearly seen in Figure 2. Gravels on slope replaced due to propeller jet and they moved down on slope becaues of gravity. Therefore, eroded area developed towards crest. While profiles occured for 690 rpm and 820 rpm are almost same, profile for 560 rpm is different. The accumulation and erosion areas increases with increasing rpm.

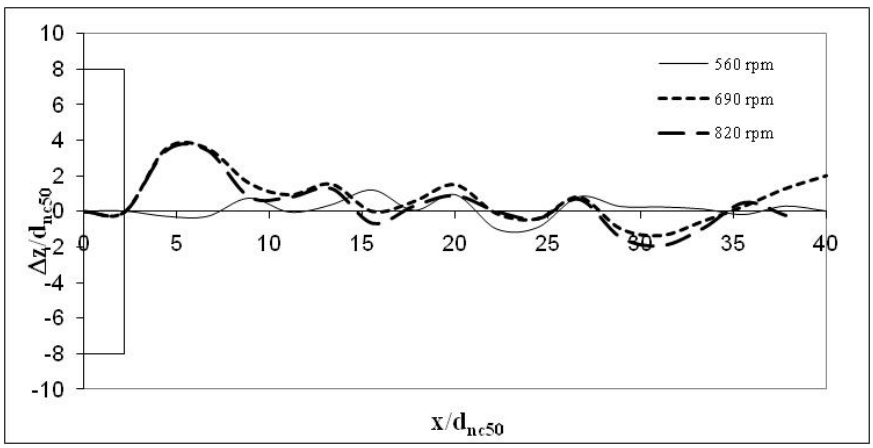


Figure 2 The variation of the scour and accumulation along the slope

Case 2: propeller rotates in a hub

The variations of the cumulative scour and accumulation along the slope at the propeller axis are presented in Figure 3. Accumulated area at downstream of pile was clearly seen in Figure 3. Eroded area developed towards crest. The profiles occured for 690 rpm and 820 rpm are similar like Case 1, the profile for 560 rpm is different. The accumulation and erosion areas increases with increasing rpm.

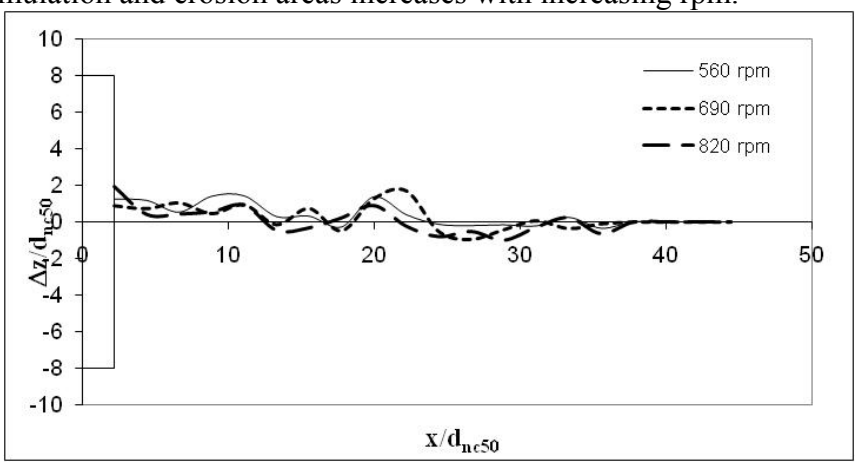
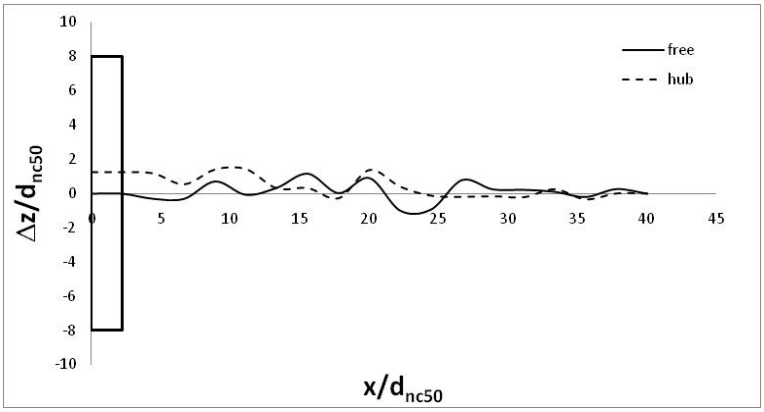
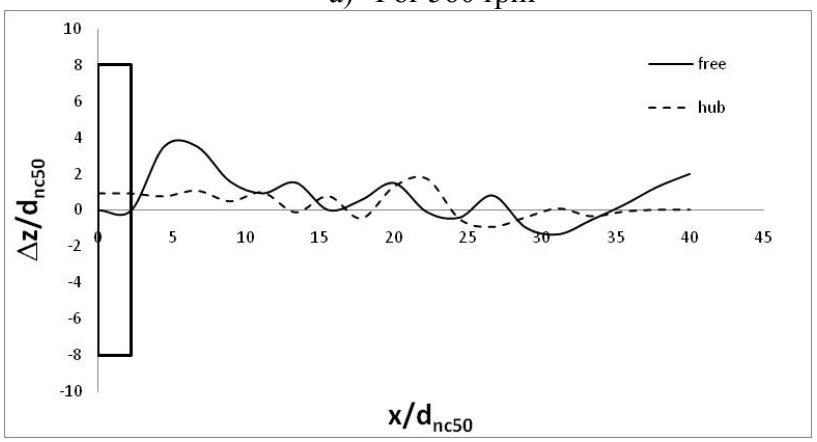


Figure 3 Profiles of the slope for different propeller rotations

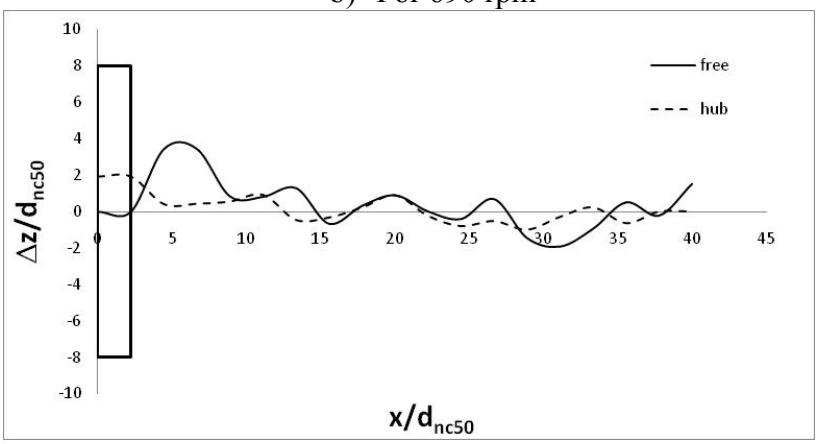
The variations of the cumulative scour and accumulation along the slope at the propeller axis for Case 1 and Case 2 are presented together in Figure 4. It is seen that deformations on slope for Case 1 are larger than Case 2.
Schokking (2002) declared that the free-propeller jet carried almost %40 higher relative turbulance. And also he said that the velocity decrease for the ducted propeller was a lot smaller than the free one. So results of differences between deformations on slope for Case 1 and Case 2 can be differences on velocity and relative turbulance.



a) For 560 rpm



b) For 690 rpm



c) For 820 rpm

Figure 4 Profiles of the slope for Case 1 and Case 2

Armoured materials on slope resists to environmental loading with its weight individually. Its response against external forces is different from other type material like sand. Therefore, instead of scour depth, damage parameter (S) was used to determine effect of propeller jet on pile groups placed armoured slope.The damage parameter is defined by using Van der Meer's (1988) formula. This damage level is defined by

$$S=\frac{-A}{D_{n50}^2} \tag{5}$$

where S is the damage level, -A is the erosion area, and D_{n50} is the nominal diameter for the rock. According to Van der Meer (1988) the level of the start of the damage, S=2-3, is equal to the definition of "no damage" and "failure" is equivalent to S=8 for a two-diameter-thick armor layer on a filter layer and for a slope of 1:1.5. Damage levels on the slope for Case 1 and Case 2 are shown in Figure 5. The damage level increases with increasing the densimetric Froude Number and also damage level is higher for Case 1

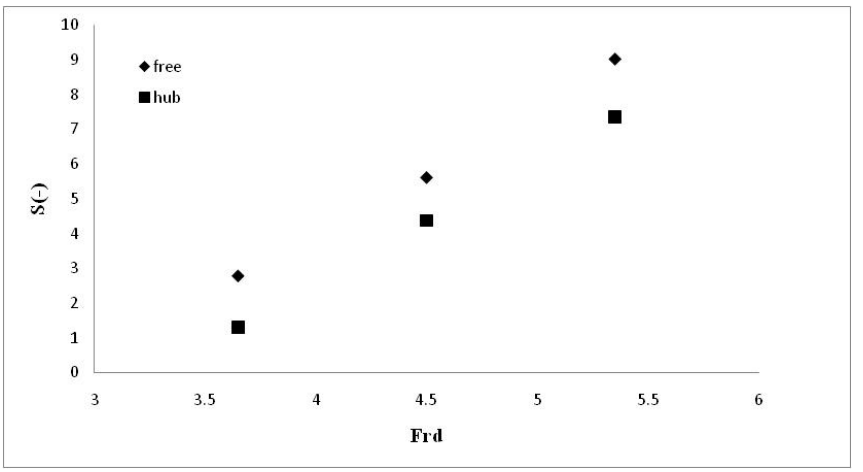
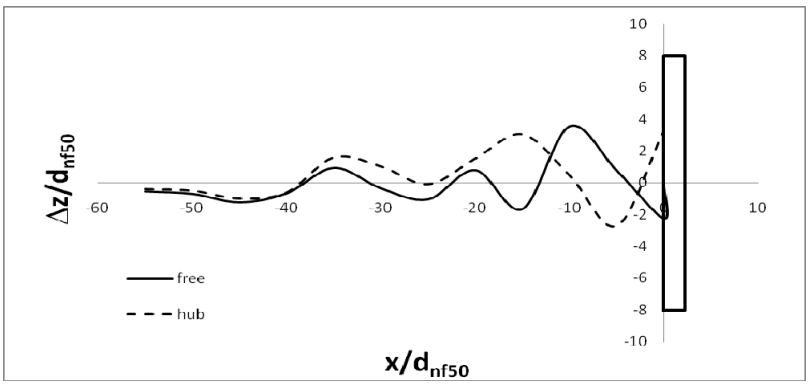
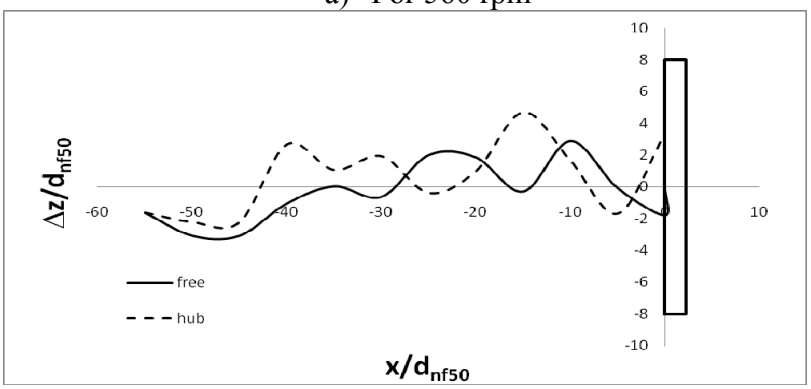


Figure 5 Damage levels on the slope

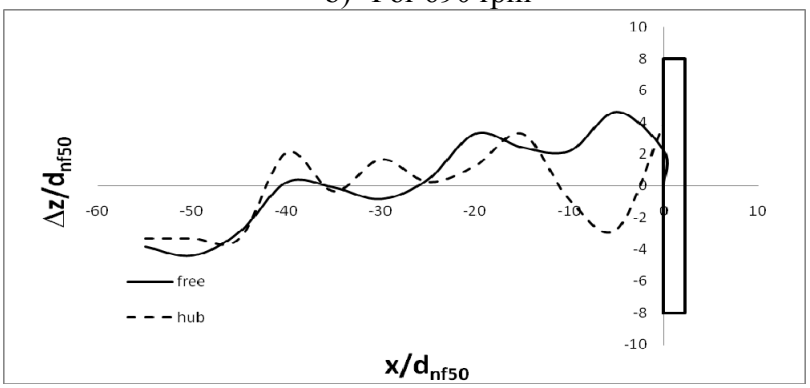
The cumulative variations of the scour along the protection layer in front of the pile at different rpm values for Case 1 and Case 2 were also presented together in Figure 6. On the apron, generally the propeller jet mechanism is active and eroded area increases with increasing rpm. Therefore, in a distance at the upstream of the pile, there are accumulation areas. In this zone, pile mechanism is active and downflow due to the pile obstruction acts on protection material. But the pile obstruction causes the decrease on the jet energy. And also gravels moves down on the slope due to propeller jet and they develops accumulation areas.



a) For 560 rpm



b) For 690 rpm



c) 820 rpm

Figure 6 The cumulative variations of the scour along the protection layer in front of the pile for Case 1 and Case 2

CONCLUSION

In this study, the propeller induced scour around the pile type berth structures was investigated. The aim of this study is to find out the effect of propeller (in a hub and without a hube) jet flow on the stability armoured slopes under berth structures.

The damage level increases with increasing the densimetric Froude Number and also damage level is higher for Case 1.

Deformations on slope for Case 1 are larger than Case 2.

On the apron, generally the propeller jet mechanism is active and eroded area increases with increasing rpm. On the other hand, gravels moves down on the slope

due to propeller jet and they develops accumulation areas at upstream of the pile for all cases.

ACKNOWLEDGEMENT
The authors are thankful for the financial support of The Research Fund of Yildiz Technical University.

References

Blaauw, H. G., and Kaa, E. J. Van de (1978), "Erosion of bottom and sloping banks caused by the screw race of the manoeuvering ships", Publ. No. 202, Delft Hydraulics Laboratory, Delft, The Netherlands.

Longe, M. J. P., Hergert, M. P. And Bylk, M. R., 1987. "Problems d'erosion aux ouvrages de quai existants causes par les propulseurs d'etrave et les helices principles des novires lors de leurs acostages aou appareillages.", PIANC, Bulletin No. 58.

PIANC, 1997, "Guidelines for the design of armoured slopes under open piled quay walls", Report of working group 22, supplement to Bulletin 96, 38 pp.

Roubos, A., Verhagen, H.J., (2007) "Uncertainties in the Design of Bed Protections Near Quay Walls", 4th Conference on Port Development and Coastal Engineering (PDCE), Varna, Bulgaria.

Schokking, L.A., 2002, "Bowthruster-induced Damage", MSc Thesis, Delft University of Technology.

Tsinker, G. P., 1995. "Marine Structures Engineering, Specialized Applications", ISBN 0-412-98571-3, Chapman&Hall.

Verhagen, H.J., "Bowthrusters and the Stability of a Riprap Revetment", 22nd International Conference on Hydrodynamics and Aerodynamics in Marine Engineering, 1-4 October, 2001, Varna, Bulgaria.

Van der Meer, J.W., 1988, "Rock Slopes and Gravel Beaches under Wave Attack" PhD Thesis, Delft Hydraulics Communication No: 396.

Verhey, H.J., 1983, "The Stability of Bottom and Banks Subjected to the Velocities in the Propeller Jet Behind Ships", Publication No:303, 8th International Harbour Congress, Antwerp, Belgium, June 13-17.

Yuksel, A., Celikoglu, Y., Cevik, E., Yuksel, Y., 2005, "Jet Scour around Vertical piles and pile groups", Ocean Engineering, v. 32, Issue 3-4, pp 349-362.

Yuksel Ozan, A., Yuksel, Y., 2010, "Simulation of a 3D submerged jet flow around a pile", Ocean Engineering, v. 37, Issue 8-9, pp 819-832.

ROCKEFELLER REFUGE GULF SHORELINE PROTECTION DEMONSTRATION

Brett L. Geesey, P.E.[1], Daniel J. Heilman, P.E.[2], and Ronald L. McPherson[3]

[1] HDR Engineering Inc., 600 Jefferson St., Suite 850, Lafayette, LA 70501; (337) 266-2342; Brett.Geesey@hdrinc.com

[2] HDR Engineering Inc., 555 N. Carancahua, Suite 1650, Corpus Christi, TX 78401; (361) 696-3344; Daniel.Heilman@hdrinc.com

[3] HDR Engineering Inc., 555 N. Carancahua, Suite 1650, Corpus Christi, TX 78401; (361) 696-3350; Ronald.McPherson@hdrinc.com

ABSTRACT

Currently, 25 to 35 square miles of wetlands are lost each year along coastal Louisiana. The shoreline along the Rockefeller Wildlife Refuge in Cameron Parish is experiencing some of the highest rates of loss, with estimates of long-term shoreline retreat ranging from 30 to 40 ft/year (Byrnes *et al*. 1995). To combat the direct loss of wetlands at Rockefeller Refuge, the Louisiana Office of Coastal Protection and Restoration (OCPR) teamed with the National Marine Fisheries Service (NMFS) and Louisiana Department of Wildlife and Fisheries (LDWF) to implement the Rockefeller Refuge Gulf Shoreline Stabilization Project. The project intent is to halt erosion along the 9.2 mile portion of the Refuge west of Joseph Harbor Bayou. Due to the challenges presented by extremely soft soils, requirement to protect the marsh shoreline for up to hurricane conditions, and limited construction budget, a smaller demonstration project utilizing three alternative designs was proposed and constructed in Fall/Winter of 2009. The alternatives constructed include: gravel beach fill, light-weight aggregate core breakwater, and a low crested "reef" breakwater. Following construction, a monitoring plan was implemented to assess the ability of the three alternatives to combat erosion along the shoreline.

The monitoring plan was designed to collect a comprehensive set of data to document the performance of the alternatives for one year following construction. A metocean data station was installed at the project site to collect wave, wind, and tide data for 6 months. Concurrent measurements of waves offshore and leeward of the breakwaters were conducted to assess wave transmission. In addition, the project area was surveyed approximately every four months to document the structure geometry, shoreline and nearshore profile changes, and structure settlement. The later was performed by surveying settlement plates that were installed during construction. In addition, a separate control area near the project location was surveyed to assess shoreline retreat with no shoreline protection. Aerial photography was obtained during each survey to visually document the conditions during the surveys.

INTRODUCTION AND PURPOSE

To combat the loss of wetlands at the Rockefeller Wildlife Refuge, OCPR teamed with NMFS and LDWF to implement the Rockefeller Refuge Gulf Shoreline Stabilization Project. The project intent is to halt erosion along the 9.2 mile portion of the Refuge west of Joseph Harbor Bayou ("Joseph Harbor"). Due to the extremely soft soil and other challenging site conditions, a smaller demonstration project utilizing several alternative shoreline protection designs was constructed in late 2009. Funding for construction of the demonstration project was provided through the Coastal Impact Assistance Program (CIAP).

The overall project location is the western 9.2 miles of Gulf shoreline along the Refuge from Joseph Harbor to Beach Prong (Figure 1); the demonstration portion of the project is located just west of Joseph Harbor. The beach along the project area is predominantly composed of soft marine clays with a veneer of crushed shell perched along the crest of an escarpment that defines the shoreface. The beach is backed by extensive marsh. The area is directly exposed to waves and currents from the open Gulf of Mexico, and high tides and/or storms, especially during tropical cyclones, contribute to erosion that averages over 30 ft/yr (Byrnes *et al*. 1995).

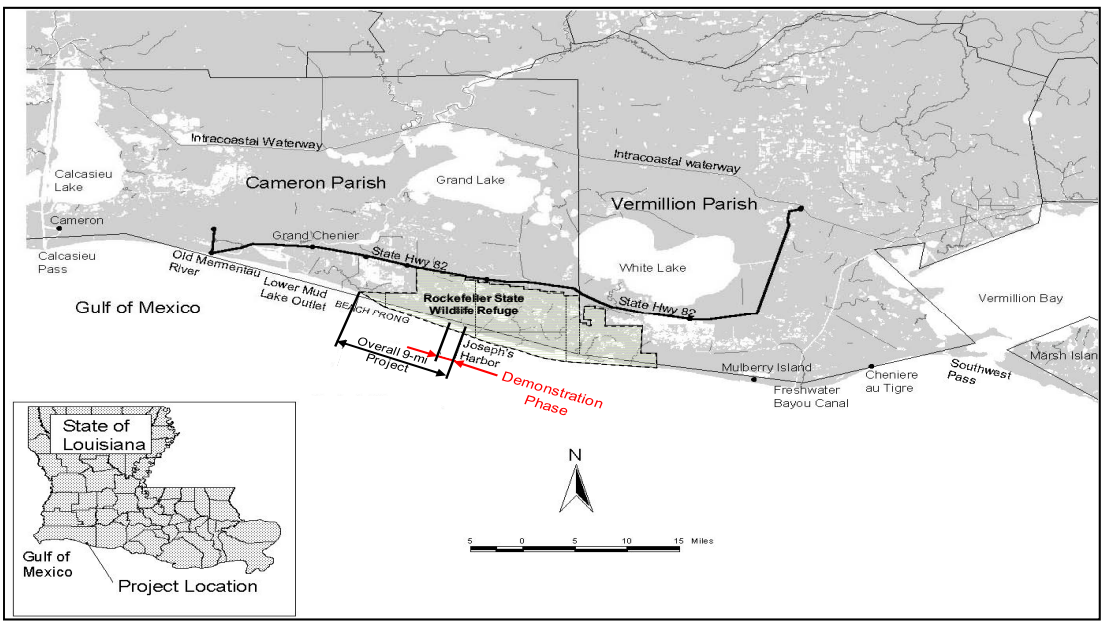


Figure 1. Project Location.

For the relatively unique alternatives considered for protection of the Refuge shoreline, limited or lacking available design guidance posed a challenge in predicting wave dissipation and transmission and soil/structure interaction. In addition, coastal processes along mud coasts are not well understood, and the innovative designs proposed likely had some redundancy or limitations based on the assumptions made. For the current demonstration project, two reef breakwater alternatives and a gravel beach fill alternative were constructed at a cost of $5,638,500. To address some of the unknowns and better understand the performance

characteristics of the constructed alternatives, a monitoring plan was developed and implemented. During 14 months following completion of construction in December 2009, the three constructed alternatives were monitored through collection of field data. Subsequent performance analysis as well as evaluation of cost, constructability, and other parameters will be applied to develop recommendations for final design and implementation of the full 9.2 mile project.

SITE CONDITIONS

A detailed characterization of site conditions was provided in Shiner Moseley (2006). A summary of key site conditions that are of particular relevance to the monitoring program is provided below.

Geotechnical Conditions

Subsurface conditions are relatively uniform alongshore and across-shore within the project area. Between approximate elevations +5 feet and 0, the soil is a loose to medium-dense shell with shell fragments. Below this stratum to an approximate depth of 40 feet is a very-soft to soft under-consolidated, very erodible clay that was reported during the geotechnical field investigation to have a consistency "similar to drilling mud." Below the stratum of very-soft to soft clay to a depth of at least 100 feet is a stiff to very stiff clay. Grab sampling performed during the geotechnical investigation did not reveal any significant surface deposits of sand or shell across the submerged portion of the beach profile. Surface sediments are relatively uniform across-shore and alongshore, although there is an abrupt change across-shore at the waterline where the surface sediments change from shell particles to silt and clay.

Nearshore Profile

The back beach and upper beach consist of a veneer of shell hash overlying marsh sediment; this shell hash is transported landward by waves during higher tides and storms. The lower berm is predominantly exposed clays with some remnant plant stems and roots; this berm, where it exists, is typically much flatter than the upper and lower beach and forms a terrace. Figure 2 shows the lower berm submerged with waves directly attacking the marsh fringe. The profile continuing offshore consists of a relatively shallow, gently-sloping seafloor along the project shoreline.



Figure 2. Waves directly attacking marsh fringe.

Geomorphology

Byrnes *et al.* (1995) documented that modern rates of shoreline recession within Louisiana's Chenier Plain are generally increasing with time, and that the long-term average rate along the Rockefeller Refuge is about 35 ft per year. In Figure 3, recent surveys of the nearshore profile illustrate the high rates of erosion typical of the project area. Although higher rates of erosion have recently occurred near Joseph Harbor, these may be due to readjustment of the shoreline associated with the loss of a small island at the mouth of the channel (Figure 4). Longer-term records do not appear to indicate a higher erosion rate near Joseph Harbor.

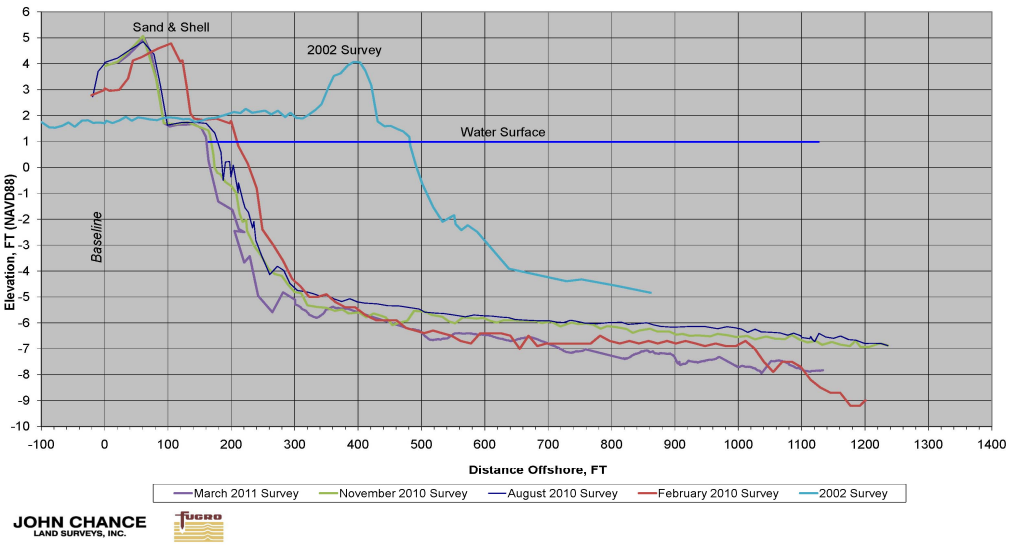


Figure 3. Surveyed profile displaying extent of shoreline recession (Sta. 425+00).



Figure 4. Rapid erosion at Joseph Harbor between 1968 and 1998 (photographs courtesy of Mr. Guthrie Perry, LDWF).

Tropical cyclones play a significant role in erosion along the Rockefeller Refuge shoreline. During storms, deposits of shell that are perched atop the beach along the Refuge shoreline are typically transported landward by waves as washover deposits onto the marsh. This process results in an exposed zone of fragmented marsh seaward of the beach to be reworked during and/or after the storm.

Depending on storm duration, the stronger storms that generate a large surge may not necessarily produce the most severe erosion since the beachface and marsh become submerged and are somewhat protected by a cushion of water as waves pass overhead. However, storms with a large surge can still produce severe erosion. For example, in September 2005, Hurricane Rita produced a surge of approximately 15 ft at Calcasieu Pass and, based on comparison of pre- and post-storm aerial photographs, caused over 150 ft of erosion along portions of the project reach.

Waves

During project design, wave modeling was performed to estimate nearshore wave height for various storm return periods. Results indicated that, during storms, nearshore wave heights have a much stronger dependency on surge elevation than offshore wave height or windspeed. Storm waves are primarily controlled by the broad, shallow shelf offshore of the Refuge that attenuates waves as they travel landward. Therefore, because surge elevation directly controls nearshore wave heights, surge elevation, as opposed to windspeed or offshore wave height, was the key factor in defining the project design waves. Although attenuation by fluid mud was also recognized as a potentially important factor in controlling nearshore wave heights, methodology for confident estimates of the dampening influence of mud was not available.

Tides

The tide along the Louisiana coast is mixed, meaning that both semi-diurnal and diurnal signals are present, but the diurnal component is typically dominant. Although no long-term tide statistics are available for the immediate project area, long-term records and published tidal statistics are available through NOAA for Grand Isle, which is approximately 170 miles to the east, and Sabine Pass, which is approximately 60 miles to the west. The diurnal tide ranges at Grand Isle and Sabine Pass are 1.1 ft and 1.6 ft, respectively. Note that, because the tide range is defined as the difference between daily high and low waters, on the Louisiana coast the tide range does not reflect the much larger range in water elevation that occurs seasonally due to meteorological and other factors.

Subsidence and Sea-Level Rise

The combination of vertical land motion (such as subsidence) and eustatic (i.e., global) sea-level rise is termed "relative sea-level rise." Relative sea-level rise at Rockefeller Refuge was projected to be five to ten inches over the desired 20-year design life of the project. Future increases in relative sea level rise could gradually decrease the ability of the shoreline protection structure(s) to attenuate waves.

PROTECTION ALTERNATIVES

The demonstration project was constructed along the Gulf shoreline of the Rockefeller Refuge just west of Joseph Harbor. Two breakwater sections, each having an approximate length of 500 ft, and a beach fill section approximately 650 ft in length were constructed for the demonstration project. A fourth alternative, a concrete panel breakwater, was included as an "additive alternate" item in the construction bidding documents but not constructed due to cost. The breakwater sections consisted of a reef breakwater and a reef breakwater with lightweight aggregate core (LWAC). Figure 5 shows the constructed location for each alternative.



Figure 5. Locations of Constructed Test Sections (photo date: 2/16/10).

Project Design Criteria

The primary challenge for this project is design and construction of a cost-feasible structure that will be both hydraulically stable under open-coast wave conditions and geotechnically stable despite very soft foundation soils. Potential project alternatives were evaluated based on their ability to: 1) prevent beach erosion for up to Category 1 hurricane conditions (approximate return period of 10 years), 2) be designed, constructed, monitored, and maintained over a 20-year design life for $42,000,000 with a construction cost of about $38,000,000 or $785/ft, and 3) where practicable, the structure should remain stable for up to a 100-year return period storm event. Modified design criteria were considered for a hypothetical increase of the construction budget by 50% (i.e., from $38,000,000 to $57,000,000) and relaxation of the "no erosion under a Category 1 hurricane" requirement.

Reef Breakwater

Reef breakwaters are rubble mound structures that typically have a rock size similar to that found in the armor and/or first underlayer of conventional breakwaters. Reef breakwaters are typically constructed without underlayers or a core of smaller stone, are broad crested in comparison to conventional breakwaters, and have a crest height near the still water surface (barely emergent and/or submerged). By traditional definition, reef breakwaters are designed to adjust in cross-section in response to the waves and currents at the site, a characteristic not considered here.

Although reef breakwaters are lower than conventional breakwaters, their much broader crest helps promote breaking and attenuation of waves that may otherwise pass over and through the structure with minimal energy reduction, although still allowing some wave transmission under day-to-day conditions. For this project, the key benefit is reduced bearing pressure on the soil. The original design included construction of crushed stone beach fill landward of the breakwater to absorb remaining smaller waves that are transmitted across the breakwater. However, during construction it was decided to exclude the beach fill behind the breakwater for two reasons: (1) measured settlement of the breakwater during construction was substantially less than anticipated, allowing the breakwater crest to be higher than planned and (2) the extremely soft soils prevented efficient operation of land-based equipment required for placement of beach fill landward of the breakwater.

A typical section of the reef breakwater is shown in Figure 6. The design (pre-settlement) crest elevation and width are shown along with the constructed nominal dimensions. Based on the design crest elevation of +1.0 ft NAVD88, Fugro estimated total settlement to be approximately 1.2 ft. The specified riprap gradation required a minimum W_{50} of 1,000 lb and W_{max} of 5,000 lb. A photograph of the constructed breakwater is shown in Figure 7.

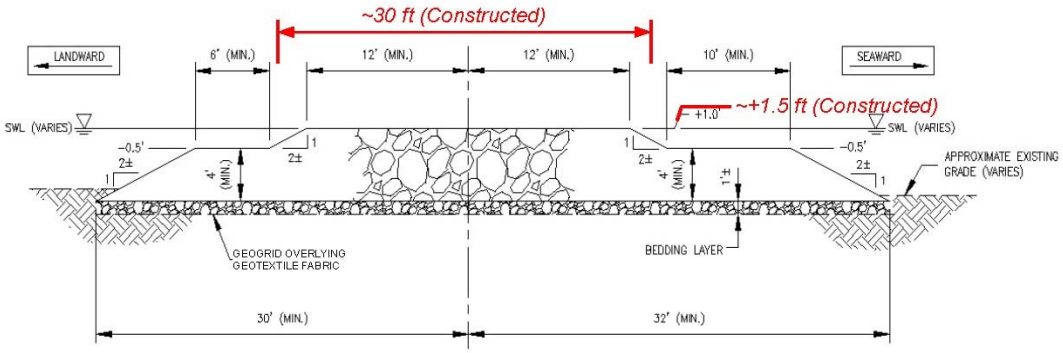


Figure 6. Design Section for Reef Breakwater. Constructed nominal dimensions are shown in red italics.



Figure 7. Reef Breakwater (7/23/09).

Reef Breakwater with Lightweight Aggregate Core

For the reef breakwater with LWAC, the stone within the core of the breakwater was replaced with an encapsulated lightweight aggregate that is almost neutrally buoyant, in effect decreasing the bearing pressure and allowing greater crest elevation and increased wave attenuation. A typical section of the reef breakwater with LWAC is shown in Figure 8. The design (pre-settlement) crest elevation and width are shown along with the constructed nominal dimensions. Based on the design crest elevation of +3.25 ft, Fugro estimated total settlement to be approximately 1.3 ft. The specified riprap gradation was the same as for the reef breakwater.

The lightweight aggregate was contained within geotextile bags that are shown in Figure 9. An important element of the monitoring program is to assess the potential for damage to the bags and/or decreased hydraulic stability caused by the LWAC and greater crest elevation.

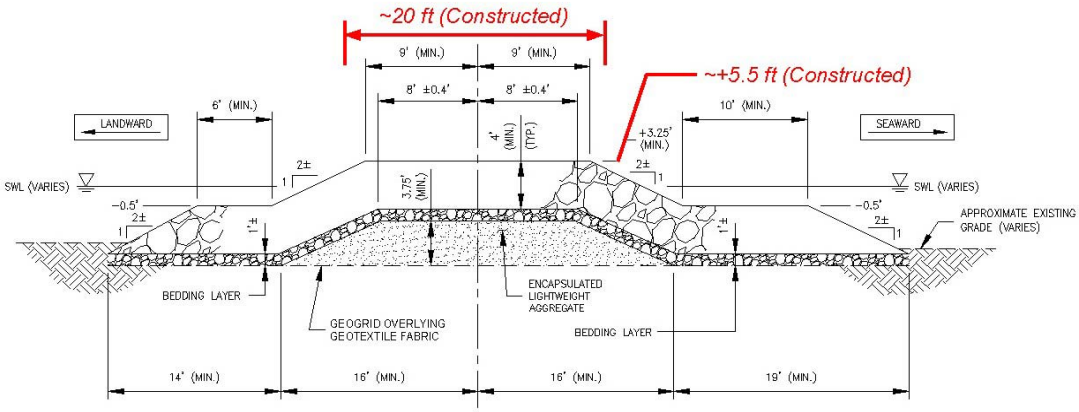


Figure 8. Design Section for Reef Breakwater with LWAC. Constructed nominal dimensions are shown in red italics.



Figure 9. Geotextile Containers being placed for LWAC.

Beach Fill

In addition to the two reef breakwater approaches, the demonstration project included beach fill constructed with crushed stone. Although both stand-alone beach fill and beach fill landward of the reef breakwater were originally planned, the beach fill landward of the breakwater was not constructed for reasons discussed above.

Although gravel (and cobble) beach fills have been successful at several locations around the world, no previous projects were identified where the material was placed on soft clay. Figure 10 shows a typical section of the beach fill constructed for the demonstration project. Including settlement, the placement density was about 20 yd^3/ft.

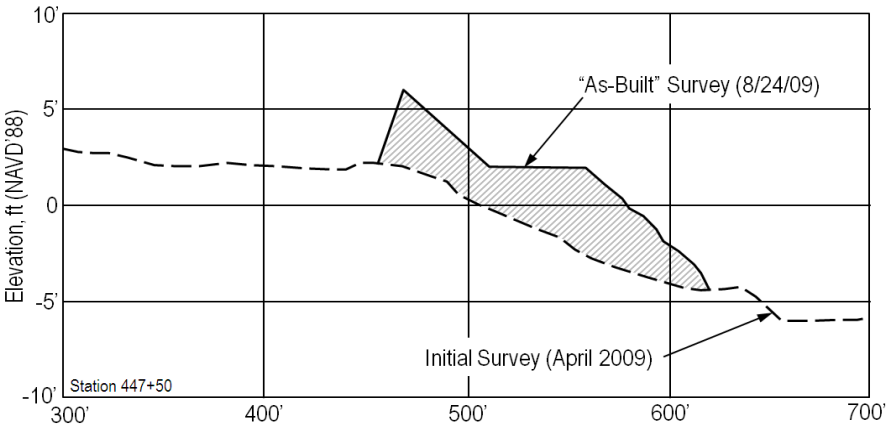


Figure 10. Typical "As-Built" Section for Crushed-Stone Beach Fill.

During design, wave-induced longshore transport and spreading, particularly "end losses" at each lateral end of the fill, were identified as forcing mechanisms that would influence the test installation. Although methods of predicting rates of longshore transport for coarse-grained materials are relatively limited, the known dependence of beach fill longevity on initial length was generally expected to present a considerable challenge in representing a full 9.2 mile beach fill with a much shorter test installation. Because performance of the test section was expected to be influenced significantly more by end losses than a longer project, terminal groins were planned at each end of the fill to reduce lateral spreading. The focus of the monitoring program was thus intended to be evaluation of cross-shore, not longshore, performance.

Construction-sequencing requirements resulted in installation of the terminal groins prior to the beach fill. As already discussed, construction of the portion of the beach fill behind the reef breakwater was deducted from the work; this deduction occurred after both groins had already been constructed. Figure 11 shows photographs of the constructed beach fill and terminal groins.



Figure 11. Beach Fill and Terminal Groin.

MONITORING OVERVIEW

Although formal monitoring of the demonstration project did not commence until completion of construction, survey data and aerial photography collected prior to and during construction were included in this performance assessment. Figure 12 shows locations for the collected data.

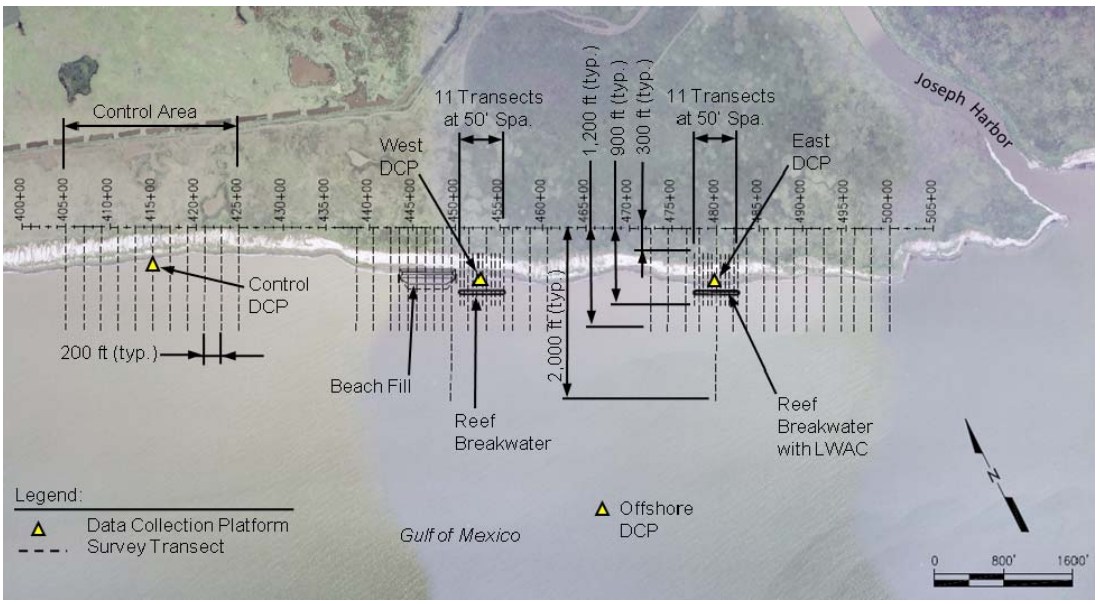


Figure 12. Data Collection Locations.

Topographic/Bathymetric Survey

Baseline survey conditions for the post-construction monitoring were established during the final survey performed by the construction contractor. After construction, topographic and bathymetric surveys were performed by John Chance Land Surveys, Inc. in August 2010, November 2010, and March 2011. Compared to the control area, shoreline recession during the monitoring period was significantly reduced leeward of the breakwaters (see Table 1).

Table 1. Measured Shoreline Change.

Location	Average Recession, ft
Reef Breakwater with LWAC	3
Reef Breakwater	12
Control Area	41

*Based on survey data (Feb '10 to March '11) along approximate +1' contour

Along with the transects shown in Figure 12, settlement plates installed during construction within each breakwater were surveyed to measure actual settlement of each test section. As shown in Figure 13, both breakwaters remain well above target elevations.

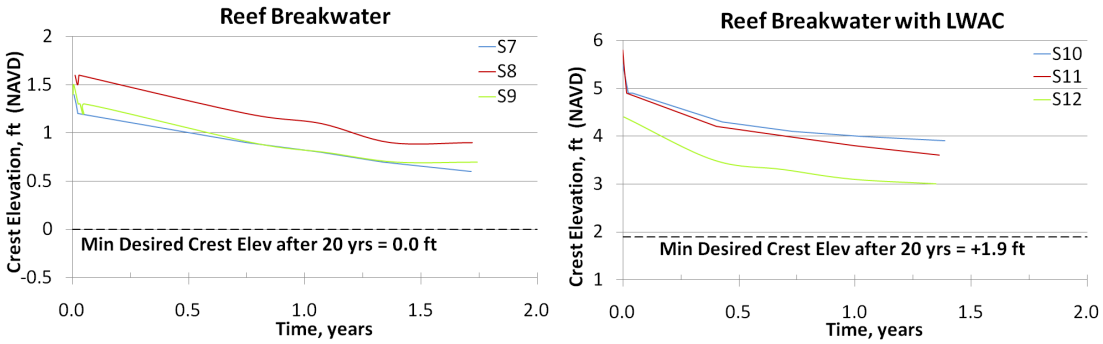


Figure 13. Settlement versus Time.

Aerial Photography

Aerial photographs, both oblique and vertical, were obtained by Gulf Coast Aerial Mapping Co., Inc at the time of each survey. The aerial photography was used as a visual aid in reviewing the general integrity of each test section as well as to provide a qualitative comparison of shoreline response along the project site. An example of the aerial photography for the reef breakwater with LWAC is shown in Figure 14. Note the decreased shoreline recession leeward of the breakwater.

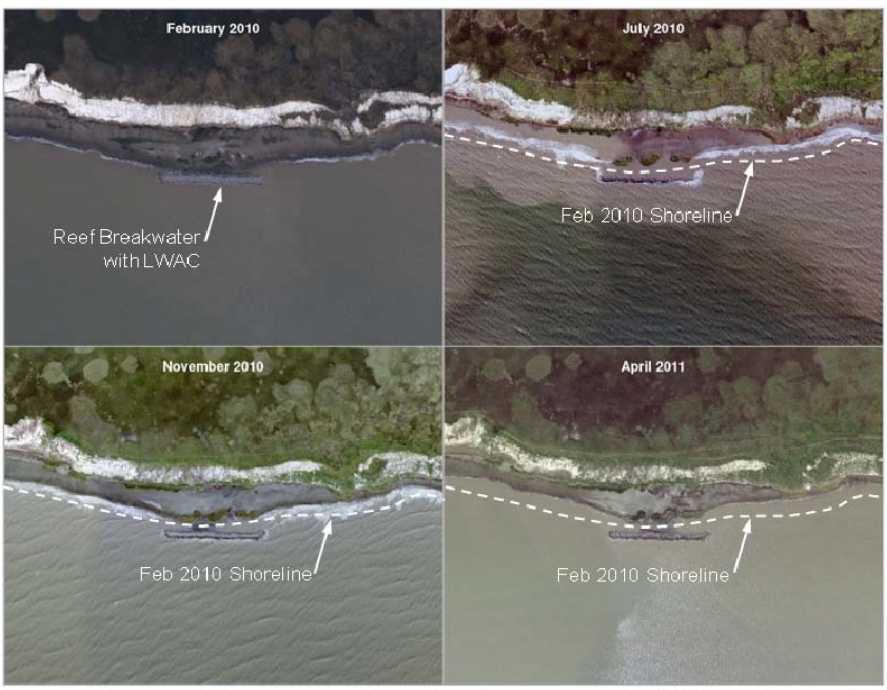


Figure 14. Aerial Photography of Reef Breakwater with LWAC.

Wave and Tide Data

Wave and tide data were collected by ENCOS, Inc. for approximately six months following the end of construction. As shown in Figure 12, wave and tide data were collected at four locations: (1) landward the reef breakwater with LWAC ("East DCP"), (2) landward the reef breakwater ("West DCP"), (3) at the control area ("Control DCP"), and (4) offshore of the test sections. Along with collecting wave

and tide data, meteorological data were collected at the West DCP and included wind speed and direction, daily precipitation, relative humidity, barometric pressure, and air temperature. Wave data obtained at the Offshore DCP are being applied with wave data obtained at the East DCP and West DCP to determine actual transmission of waves under varying conditions. The data will be compared to approximate baseline conditions measured at the Control DCP. Wave data at the Control DCP will also be applied to assess the relationship between shoreline response in an unprotected area and measured wave characteristics. Full details will be provided in HDR (2011, in prep.).

SUMMARY AND INITIAL RESULTS

The Rockefeller Wildlife Refuge in southwest Louisiana is experiencing extremely high rates of erosion along the Gulf coast resulting in a loss of valuable habitat and natural resources. Challenging site conditions along with specific design requirements and a limited budget prompted construction of a demonstration project of several shore protection alternatives in an effort to assess the most viable option for 9 miles of protection along the Refuge shoreline.

Three alternative test sections were designed, constructed, and monitored. Although analysis of the data collected during the monitoring phase is still ongoing, preliminary analyses have led to some key initial findings:

- Both the reef breakwater and the reef breakwater with LWAC appear to have provided an increased level of protection to the shoreline directly landward of the structures.
- Because of its higher crest, the reef breakwater with LWAC appears to be providing better protection, allowing less wave energy to pass to the shore.
- The shoreline in a "control" area has continued to erode at rates similar to that previously observed along the project area.
- Instantaneous settlements during construction averaged 0 to 4 inches, much less than the 6 to 24 inches predicted during design. Subsequent consolidation settlements (after construction) averaged approximately 50% of the total settlement expected over the 20 year project life.
- Excessive lateral spreading of the beach fill limited quantitative monitoring of the test section. However, based on construction bids received for the demonstration project, this alternative is unlikely to be feasible from a cost standpoint.
- Collection of wave, tide, and meteorological data has provided a greater overall understanding of the environmental conditions present at the site.

The information collected through the construction and monitoring of this demonstration project will be applied to refine the design of the full 9.2 mile project. Remaining work in assessing the project alternatives includes a detailed analysis and comparison of surveyed shoreline and nearshore profile change, a comparison of wave transmission at each breakwater for various wave and water level conditions, and a comparison of measured and calculated wave transmission coefficients. Final results will be presented, along with recommendations, in a report to be provided to

the State of Louisiana Office of Coastal Protection and Restoration (see HDR 2011, in prep.).

REFERENCES

Byrnes, M.R., McBride, R.A., Tao, Q., and Duvic, L. (1995). Historical Shoreline Dynamics Along the Chenier Plain of Southwestern Louisiana. *Gulf Coast Assoc. of Geol. Soc. Trans.*, Vol. 95, pp. 113 – 122.

Fugro Consultants LP. (2004). Geotechnical Study, Test Sections, Rockefeller Refuge Gulf Shoreline Stabilization Project. Report No. 0604-1370, Houston, Texas.

Fugro Consultants LP. (2002). Geotechnical Study (Part I of II), Gulf Shoreline Stabilization Project, Rockefeller Refuge, Cameron Parish, Louisiana. Report No. 0602-1316, Houston, Texas.

HDR Engineering, Inc. (2010). Rockefeller Refuge Gulf Shoreline Stabilization (ME-18), Project Completion Report. Prepared for Louisiana Office of Coastal Protection and Restoration, HDR Project No. 124452 (PW69815), Corpus Christi, Texas.

HDR Engineering, Inc. (2011, in prep). Rockefeller Refuge Gulf Shoreline Stabilization (ME-18), Post Construction Monitoring Report. Prepared for Louisiana Office of Coastal Protection and Restoration, HDR Project No. 125250 (PW69815), Lafayette, Louisiana.

LaCoast.gov. (2003). ME-18 General Project Fact Sheet, "Rockefeller Refuge Gulf Shoreline Stabilization (ME-18)," Coastal Wetlands Planning, Protection and Restoration Act, http://lacoast.gov/reports/gpfs/ME-18.pdf.

Shiner Moseley and Associates, Inc. (2006). Rockefeller Refuge Gulf Shoreline Stabilization (ME-18), Final Design Report. Prepared for Louisiana Department of Natural Resources, SMA Project No. J200.10108.04, Corpus Christi, Texas.

The 2012 San Diego Regional Beach Sand Project

Chris Webb[1] and Shelby Tucker[2]

[1]Senior Coastal Engineer, cwebb@moffattnichol.com; Moffatt & Nichol, 3780 Kilroy Airport Way, Suite 600, Long Beach, CA 90806; PH 562-426-9551; FAX 562-424-7489
[2]Senior Regional Planner, stu@sandag.org; San Diego Association of Governments, 401 B Street, Suite 800, San Diego, CA 92101-1900; PH 619-699-1916; FAX 619-699-1905

ABSTRACT

The San Diego Association of Governments (SANDAG) is embarking on a second Regional Beach Sand Project (RBSP II) since adoption of their Shoreline Preservation Strategy (SANDAG 1993). The Shoreline Preservation Strategy (SPS) called for beach nourishment to offset regional sand losses and beach narrowing. The first RBSP (RBSP I) was a success, in that it widened beaches for up to seven years in some areas as reported by monitoring (Coastal Frontiers Corporation 2010), while not adversely impacting the environment (AMEC 2005). This second RBSP (II) is intended to replicate and potentially improve on the benefits of RBSP I, while still not causing environmental impacts. Several alternatives were analyzed for shoreline position, change to recreational beach area, and impacts to lagoons. Two alternatives appear to perform successfully, and the region selected one for implementation. This paper presents results of analyses for the proposed alternative.

INTRODUCTION

The San Diego Association of Governments (SANDAG) approved a Coastal Regional Sediment Management (RSM) Plan in 2009 that calls for large- and small-scale nourishment over time. Regional sediment management is necessary to counteract effects of an existing coastal sediment deficit, sea level rise, and occurrence of El Nino events in the face of increasing demand for beach recreation and need for shore protection. SANDAG is committed to large-scale nourishment in the future as an element of RSM, while local agencies implement small-scale nourishment.

As a big step toward large-scale nourishment, SANDAG plans to implement a second Regional Beach Sand Project (RBSP) within the San Diego region. This is the second in a series of efforts to nourish multiple littoral cells with sand. The first RBSP (RBSP I) was the first of its kind effort on the west coast and provided a successful opportunity to perform large-scale nourishment with minimal adverse effects. This second RBSP (RBSP II) may include more and better sand, greater longevity, shifted beach footprints, and greater economic return. The intent of RBSP II is to implement SANDAG's long-term vision of maintaining and restoring the region's beaches through application of lessons learned from the first project to maximize benefits, minimize impacts, and optimize the long-term sediment management process. SANDAG is continuing preliminary engineering of this project and has initiated final

engineering for construction, scheduled for 2012. The status of this project, modifications from the initial project, and problems and solutions associated with implementation are presented to demonstrate lessons, challenges, and benefits.

PROJECT DESIGN

Preliminary project design was completed in 2009 and included three alternatives for analyses. Sand placement is proposed at up to 11 sites throughout the County from dredging of up to three offshore borrow sites. A map of the project area is shown in Figures 1 and 2. The alternatives consist of: 1) 1.8 Million Cubic Yard (MCY) Near-Repeat of RBSP I; 2) 2.7 MCY Additional Receiver Sites; and 3) 2.9 MCY Increased Quantities. Beach-fill footprints range in quantity from a maximum of 650,000 cubic yards to a minimum of 101,000 cubic yards. Designs were conceived to maximize environmental sensitivity and avoid causing adverse impacts to sensitive marine habitat. Existing habitat constraints include nearshore reefs, offshore reefs, and lagoons. Alternative 3 will not move forward due to a lack of funding and to potential risks to habitat.

After evaluation of all alternatives, the region identified Alternative 2 (with revisions and therefore designated as Alternative 2R) as the preferred project alternative. Alternative 2R includes the placement sites, sand quantities, and sand borrow sites shown in Table 1 below. Data presented in this paper are relative to Alternative 2R.

Receiver Site	Probable Borrow Site	Alternative 2R Sand Quantities
Oceanside	SO-6 and/or SO-5	420,000
North Carlsbad		225,000
South Carlsbad North	SO-5	158,000
South Carlsbad South		0
Batiquitos		118,000
Leucadia		117,000
Moonlight Beach		105,000
Cardiff		101,000
Solana Beach		360,000
Torrey Pines		245,000
Imperial Beach	MB-1	650,000
	TOTAL	2,499,000

Table 1 – Proposed Project Sites and Sand Quantities



Figure 1 - Vicinity Map of Beach Placement and Offshore Borrow Sites in North County

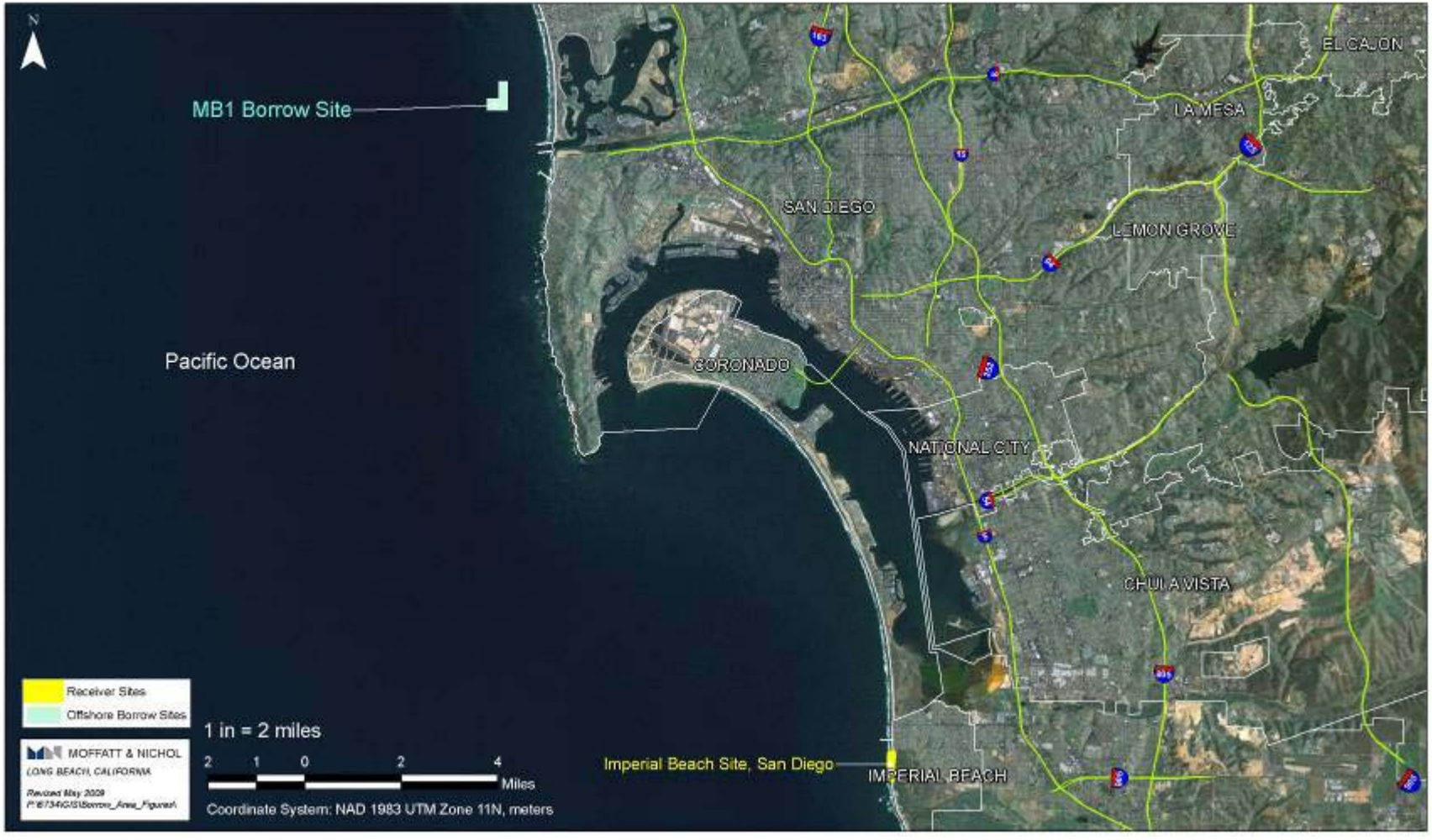


Figure 2 - Vicinity Map of Beach Placement and Offshore Borrow Sites in South County

ANALYSES

Extensive analyses were performed as part of preliminary engineering to quantify beach widening, sand dispersion, and sedimentation to identify potential beneficial effects and impacts. Data are presented below primarily for Alternative 2R.

Shoreline Position and Recreational Beach Area. Numerical modeling of the fate of beach fills was performed using GENESIS for North County (by Everest International Consultants) where multiple fills will be placed along an irregular coastline, and a diffusion method at South County where one fill will be placed along a relative straight coast. A 5-year project lifespan was assumed based on monitoring results of RBSP I. A full discussion of model set-up, calibration, and verification are provided in the SANDAG Shoreline Morphology Study (Moffatt & Nichol 2011).

GENESIS results show significant beach widening over the short-term at the placement sites, with rapid lateral sand dispersion. Longer-term widening (up to 5 years post-project) is predicted at areas where two or more fills will occur in close proximity, and at areas with large placement volumes. Examples are South Oceanside, South Carlsbad, North Encinitas, and Solana Beach. Model results are shown in Figures 3, 4 and 5. Table 2 also shows long-term beach changes from all alternatives for comparison.

SITES	LONG-TERM (5 YEAR) WIDENING OF BEACHES FOR ALL ALTERNATIVES (In Feet)		
	Alternative 1	Alternative 2R	Alternative 3
South Oceanside	50	50	55
North Carlsbad	35	35	45
South Carlsbad North	15	25	25
South Carlsbad South	15	25	25
Batiquitos Beach	-5	-5	0
Leucadia	15	15	15
Moonlight Beach	0	0	0
Cardiff	15	20	30
Solana Beach	20	35	45
Torrey Pines	40	40	40

Table 2 – Long-Term Beach Widening Predicted at North County Beaches

Recreational beach area is an important parameter to estimate economic return from the project. State funds are the primary source used for the project and economic benefits to the State from the project serve to justify its participation. Recreational beach areas were estimated by calculating the total area of the beach berm throughout the region after the project. Recreational beach areas increase at the end of 5 years for each alternative as follows: 10% for Alternative 1; 15% for Alternative 2R, and 20% for Alternative 3. Table 3 below shows the increase in recreational beach area by year.

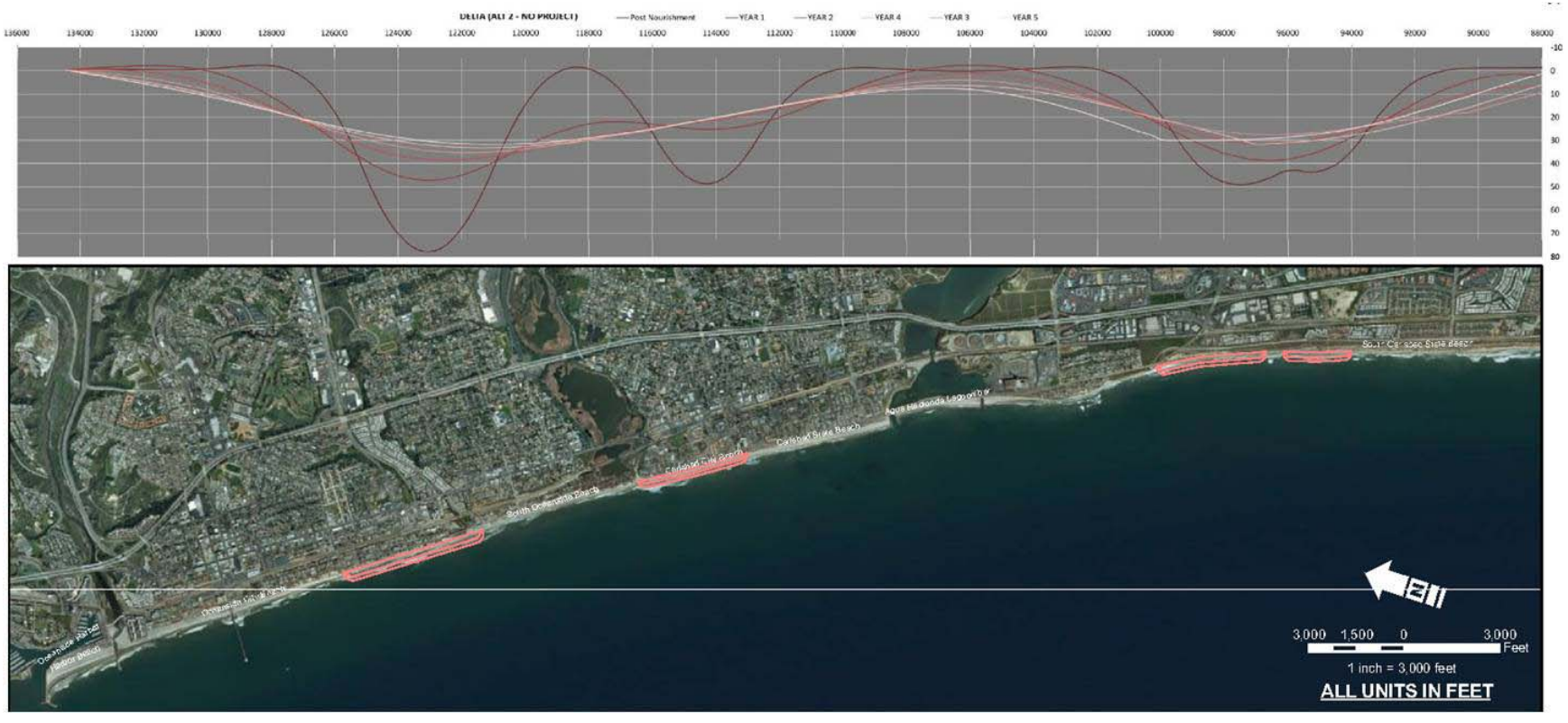


Figure 3 – GENESIS Results for Alternative 2, Northern Reach



Figure 4 – GENESIS Results for Alternative 2R, Central Reach

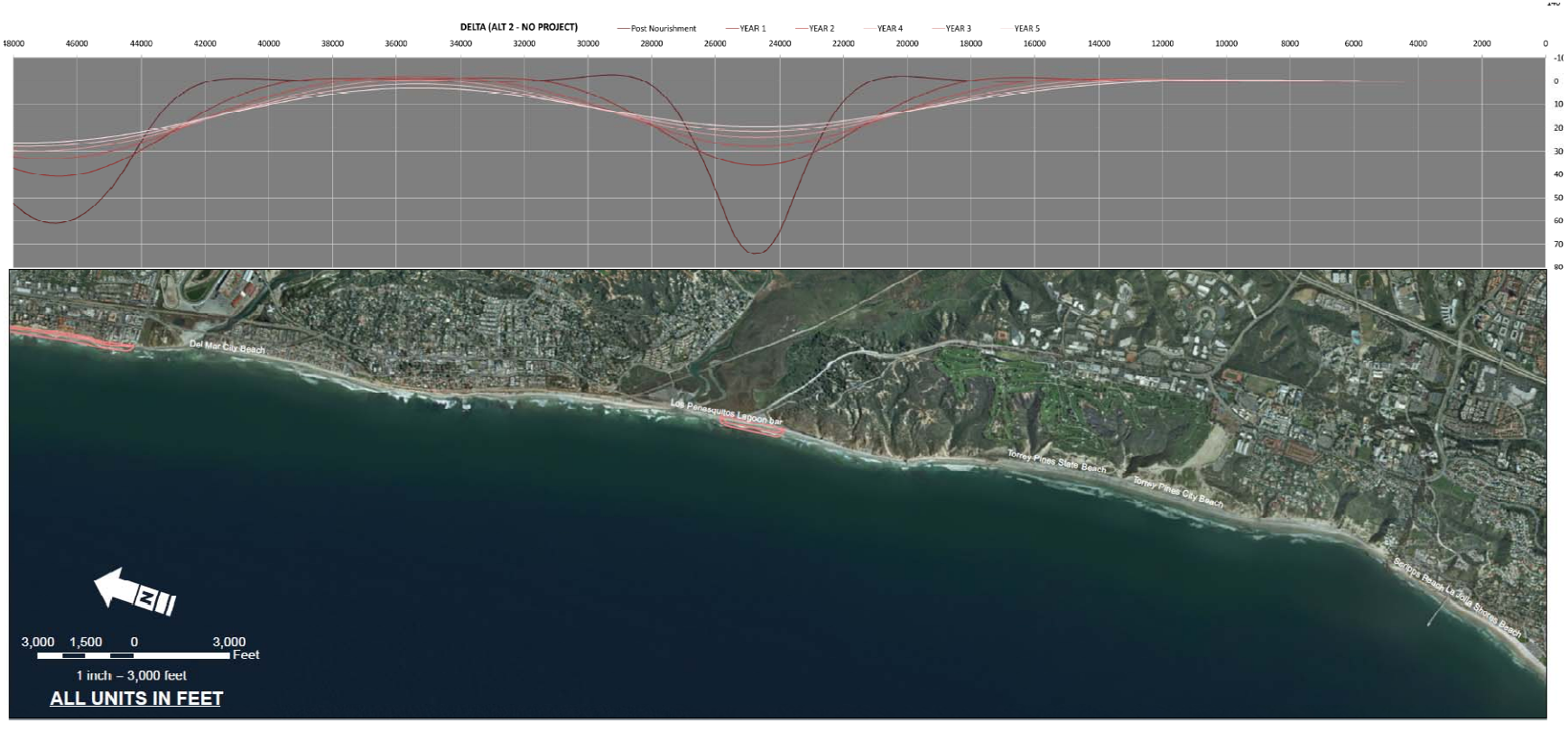


Figure 5 – GENESIS Results for Alternative 2R, Southern Reach

Item	Existing Total Area	Immediately Post-Construction	New Area Remaining After Each Year				
			Year 1	Year 2	Year 3	Year 4	Year 5
TOTALS	187	57	46	40	35	32	29
% Change	No Change	30%	25%	21%	19%	17%	15%

Table 3 – Recreational Beach Area Created by Alternative 2R

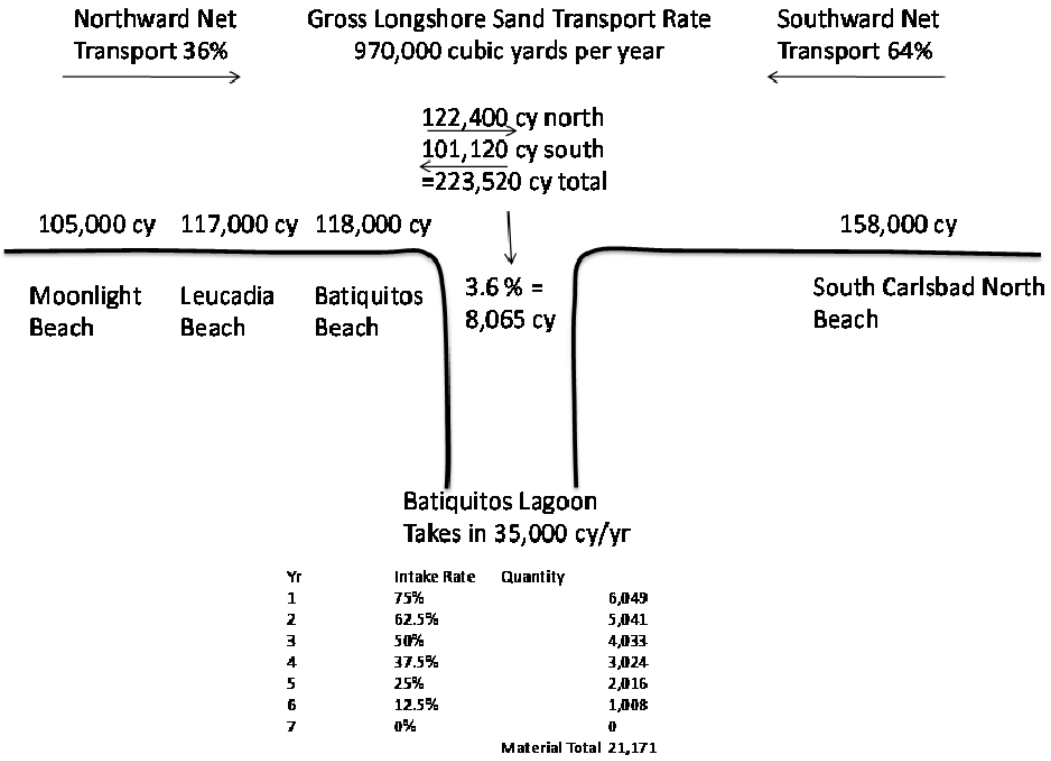
Lagoon Shoaling for North County Lagoons. Coastal lagoons are evaluated for potential sedimentation from the project. A total of six lagoons exist along North County San Diego and one lagoon exists at South County. The lone South County lagoon is estimated to not experience effects from this project because the predominant longshore drift direction transports sand from the beach fill away from lagoon, rather than toward the lagoon (USACE 1987). The analysis presented below applies to lagoons in North County and is presented in the Final Environmental Impact Report for the project (AECOM 2011). Sedimentation predicted at each North County lagoon was estimated using the existing lagoon shoaling rate determined from historic records, and increasing the sand supply alongshore from effects of RBSP II.

Determining the existing shoaling rate involved review of existing maintenance dredging records at each lagoon as presented in the annual shoreline monitoring reports prepared for SANDAG by Coastal Frontiers Corporation (2010). Maintenance dredging volumes are generally assumed to be a surrogate value for sand shoaling at lagoons, with certain exceptions. Comparing maintenance dredging records before and after RBSP I indicate any project-related effects caused by that project, which is similar to RBSP II in North County with the exception of Solana Beach.

The existing shoaling rate was then estimated to be a proportion of the existing gross longshore sand transport rate in North County San Diego. The existing longshore sand transport rate in North County was determined by taking the average of previous estimates from the literature (USACE 1991). The gross longshore sand transport rate value used in the analysis is 970,000 cubic yards per year. The net values of longshore sand transport to the south and to the north are 64% and 36%, respectively, as provided by the literature (Moffatt & Nichol 2011, and USACE 1991).

Once the existing shoaling rate at each lagoon was calculated, SANDAG estimated the possible increase in sand supply to each lagoon with sand placement proposed under RBSP II. This was done by summing the sand quantity to be placed within a certain distance of each lagoon, and within the coastal reach or compartment considered to be of potential influence to the lagoon. Such reaches or compartments exist between natural partial-barriers to longshore transport, such as headlands or major reefs (e.g., Terramar Point, Swami's, Tabletop Reef) and contain at least one lagoon entrance. The sand quantity within the compartment was subdivided into the proportion predicted to travel north and the proportion predicted to travel south from the receiver sites. This calculation provided sand quantities that have the potential to be transported across individual lagoon mouths and be eligible to enter the lagoon mouth during incoming tides. Figure 6 shows an example of this analysis for Batiquitos Lagoon.

Figure 6 – Method Applied to Batiquitos Lagoon



The sand volume eligible to enter the lagoon mouth is multiplied by the sand trapping rate (previously estimated) to represent a total sand volume able to enter the lagoon at any given time after project construction. Not all of that sand would necessarily remain in the lagoon, as some of the sand may return to the ocean during out-going tides or stormflow events. This effect of the project is assumed to extend over time rather than being instantaneous. A seven year period of potential sedimentation is assumed based on SANDAG monitoring results of RBSP I (Coastal Frontiers 2010). It is further assumed that the project effect is greatest in year 1, and linearly decreases to reach no effect at year 7.

The sand quantity estimated to enter the lagoon mouth is multiplied by a factor representing the assumed level of effect for each year. For example, based on the engineer's judgment it assumed that 75% of the inflowing sand may remain in the lagoon after year 1, 62.5% may remain after year 2, 50% may remain after year 3, and so on. The sand volume remaining after each year is summed to reach a total sand quantity estimated to remain in the lagoon from RBSP II after 7 years. This sand quantity represents a conservative estimate of sand that could potentially enter an individual lagoon mouth and served as the basis of discussion with each lagoon management entity. Estimated sand quantities contributed to each lagoon and the record of negotiations is presented in Table 4.

Lagoon	Sand Shoaling Volume From RBSP II, Alternative 1 (cubic yards)	Sand Shoaling Volume From RBSP II, Alternative 2 (cubic yards)	Lagoon Owner With Maintenance Responsibility	Negotiation Dates
Agua Hedionda	0	0	NRG Cabrillo Power Operations	Jan. 14, 2011
Batiquitos	25,700	40,700	Batiquitos Lagoon Steering Committee	Jan. 6, 2011
San Elijo	10,000	10,000	San Elijo Lagoon Conservancy	Jan. 7, 2011 and Jan. 20, 2011
San Dieguito	4,200	10,300	Southern California Edison	Jan. 7, 2011
Los Penasquitos	10,200	10,200	Los Penasquitos Lagoon Conservancy	Jan. 7, 2011, and Jan. 14, 2011

Table 4 - Estimated Lagoon Shoaling Rates

RESULTS

Project analyses indicate that Alternative 2R would generate greater benefits to the region than RBSP I (Alternative 1). Therefore, two cities propose the larger volumes of Alternative 2R to demonstrate that progressively larger sand volumes can be strategically placed within the region while not causing adverse impacts to marine habitat. Alternative 2R is not anticipated to cause adverse impacts, however a slightly increased risk of impacts exists over RBSP II so this project will require monitoring of biology for verification.

Other modifications to RBSP II from RBSP I include moving two footprints slightly farther north from their initial placement locations, and using coarser sand for beach fill material. Each modification is discussed below.

Beach fill footprints at Oceanside and Imperial Beach were shifted slightly north toward their respective recreational piers to capitalize on possible increased public beach use associated with the public amenities such more available parking and park space. Shifting of the footprints did not substantially change results, other than causing beach widening closer to the piers. Shifts of these two fills also moved them farther from sensitive resources and therefore decreased risks of habitat impacts.

Coarser sand is proposed for use in RBSP II to increase longevity of the fills. Several fills for RBSP I were short-lived and dispersed rapidly due to relatively fine median sand grain sizes. The region desires to maximize benefits by using coarser sand if possible. Coarser sand material is available in nearby offshore borrow sites. Modeling incorporated this project component by specifying the mean gradation of the receiver beaches after construction. Model results indicate fairly extensive fill lives, given wave conditions assumed for the modeling. These parameters are discussed in more detail in the SANDAG Shoreline Morphology Study (Moffatt & Nichol 2011).

SANDAG recently completed environmental review and permitting, with construction planned in spring of 2012. Monitoring will occur after construction for a period of 4 years to quantify project benefits and any adverse effects.

ACKNOWLEDGEMENTS

Project funding is provided by the California State Department of Boating and Waterways and the participating coastal cities. Technical support was provided by the firms of Everest International Consultants, Coastal Frontiers Corporation, Science Applications International Corporation, Merkel & Associates, AECOM, URS Corporation, Alpine Ocean Surveys, and Fugro Pelagos, Inc.

REFERENCES

AECOM. 2011. Final Environmental Impact Report/Environmental Assessment. San Diego Regional Beach Sand Project II. May 2011.

AMEC Earth & Environmental, Inc. (AMEC). 2005. Regional Beach Sand Project, Year 4 (2004-2005) Post-Construction Monitoring Report for Intertidal, Shallow Subtidal, and Kelp Forest Resources and Comprehensive Analysis Report (2001-2005).

Coastal Frontiers Corporation. 2010. SANDAG 2008 Regional Beach Monitoring Report, Annual Report. Prepared for SANDAG, May 2009.

Moffatt & Nichol. 2011. Final Shoreline Morphology Study, Regional Beach Sand Project II. May 2011.

SANDAG. 1993. Shoreline Preservation Strategy for the San Diego Region. San Diego, CA, 43 pp.

USACE. 1987. Coast of California Storm and Tidal Wave Study, Silver Strand Littoral Cell Preliminary Sediment Budget Report. U.S. Army Corps of Engineers Los Angeles Distinct, Los Angeles, CA.

———. 1991. Coast of California Storm and Tidal Wave Study, San Diego Region, Final Report. U.S. Army Corps of Engineers Los Angeles Distinct, Los Angeles, CA.

Determination of Wave Transmission Coefficients for Oyster Shell Bag Breakwaters

Richard J. Allen[1] and Bret M. Webb[2]

[1]Student, Department of Civil Engineering, University of South Alabama, 6021 USA Drive South, Mobile, Alabama 36688; PH (251) 460-6174; FAX (251) 461-1400; email: rja801@jaguar1.usouthal.edu

[2]Assistant Professor, Department of Civil Engineering, University of South Alabama, 6021 USA Drive South, Suite 280, Mobile, Alabama 36688; PH (251) 460-6174; FAX (251) 461-1400; email: bwebb@usouthal.edu

ABSTRACT

Problems are inevitable in the use of oyster shell bag breakwaters. Oyster shell bag breakwaters have been used in many locations throughout the USA to quantify their ecological benefits, but little research has been conducted regarding their wave attenuating properties. Quantitative information has been produced for traditional structures, but nothing has been published to describe the attenuating properties of an oyster shell bag breakwater. Currently, projects employing oyster shell bag breakwaters would need to adopt published methodologies for determining the transmissive properties of traditional materials or conduct individualized experimentation for their project to determine the adequate dimensions necessary to handle the hydrodynamic loads applied to them. Projects using this methodology could over design or under design the oyster shell bag breakwaters. The objective is to resolve this issue by conducting laboratory experiments in a controlled setting and comparing those results to existing methodologies available in the published literature.

The results obtained in this report are a substantial finding in terms of constructing oyster shell bag breakwaters. The data obtained from testing is compared to published methodologies for measuring the wave transmission coefficient of low crested breakwaters (Van der Meer et al., 2005), which produces a distinguishable resemblance based on the 43 tests conducted during this study. However, additional testing should be conducted to enhance the initial findings by including practical application variables such as wave variability and structure placement in relation to the shoreline.

INTRODUCTION

The nation's wetlands, which have naturally protected the shoreline for centuries are disappearing. Preventing this loss of wetlands along the coastlines has become a top priority. Previous research has shown that coastal wetlands can only survive when

wave heights are below 0.14 m on average (Shafer, 2003). In some cases, increased wave energy along estuarine shorelines has risen above this threshold destroying the natural wetlands (Zalewski, 2002). The wave energy has been increasing as a result of global warming, increased boat activity, and excessive implementation of man-made structures (Davis J. E., 1998). Historically when the wetlands began to recede, hardened structures such as bulkheads and seawalls were implemented. Now, these hardened structures along the nation's shoreline have begun to stir debate amongst ecologists: they claim hardened structures eliminate vital habitat for marine life (Swann, 2008). In an effort to eliminate these structures, alternatives such as living shorelines are gaining popularity.

The key component of many living shoreline protection projects along high wave energy shorelines is a breakwater. These breakwaters are used in an attempt to protect wetlands from the damaging wave energy propagating towards shore. The breakwater is typically placed offshore leaving an aquatic zone between it and the shoreline. While energy dissipation is the primary goal of a breakwater, research has shown that they provide additional ecological habitat for aqueous as well as terrestrial biology. An evaluation performed on the Chesapeake Bay showed the installation of breakwaters created relatively instant habitat for various aquatic biology on the surface and within the pores of the breakwater structure (Davis, Takacs, & Schnabel, 2006).

Breakwaters are composed of various types of material and constructed in all sorts of shapes. While the materials vary, the most popular shape is a trapezoidal profile oriented parallel to the shoreline. Breakwaters are not a continuous length along the shoreline, which would create a dead zone between it and the shoreline during the ebb tide (Duhring, 2006). Instead, gaps are provided along the length of the breakwater to allow some portion of the wave energy to propagate through as well as provide an escape to aquatic life that would become trapped during ebb tide.

Common materials used in breakwaters are concrete, rock, and more recently oyster shells. In the past, breakwaters were constructed of durable, high-density rock, which was readily available. Examples of rock or rubble mound construction are ubiquitous in coastal defense and armament even today. The design and placement of these structures can be reviewed in the Coastal Engineering Manual (2002) which references Seelig (1980) for the estimation of the hydrodynamic properties relating to rubble mound breakwaters. Some of the other factors affecting the use of rock in breakwaters are the size, density, shape, and gradation (Poole, 1991).

Precast concrete armor units are another popular choice when constructing a breakwater. Precast concrete allows the designer to modify the shape of the breakwater to a level that he/she feels is the most effective. One concept has remained the same; the stability of the unit is provided by its self-weight. The units can be arranged in random patterns, a double row, or a single row. The double row arrangement allowed the rows to be staggered to give full protection to the shoreline while maintaining the necessary openings required for the ecology (Duhring, 2006). Finally, since the stability of the unit is controlled by its weight these structures are extremely large and require heavy equipment to install. The stress of the heavy

equipment impedes the already fragile ecosystem the breakwater is trying to protect or restore (Bakker, Berge, Hakenberg, & Klabbers, 2003).

Oyster shell substrate used in the creation of breakwaters is becoming more popular. Natural oyster reefs have historically protected coastal shorelines. Society's encroachment on the coastline has destroyed many of theses natural defense structures. The degradation is caused, in part, by the constant manipulation of the coastline to satisfy the needs of society (Coen, et al., 2007). The benefits of oyster shell bag breakwaters significantly outweigh the traditional materials. Oyster shell substrate is a natural, renewable material that is inert and has been shown to enhance settlement of juvenile bivalves (Henderson & O'Neil, 2003). The use of oyster shell substrate in living shorelines also removes the material from the waste stream. When used to create a composite breakwater structure, oyster shell substrate is commonly placed in tubular mesh bags. These 'oyster shell bags' are then stacked or placed, often by hand, to create the composite breakwater. Finally, the most significant benefit associated with using oyster shells as a breakwater media is the sustainability. The oyster shells used in breakwaters do not have to be produced; it is a recycled product that would otherwise be discarded as waste from restaurants. The cost of oyster shells is also a product of sustainability. The cost of an oyster shell bag breakwater placement is \$60-\$70/m^3 as compared to a Wave Attenuation Device (WAD) at \$600-800/m or a rock breakwater at \$400-650/m (Boyd, 2007).

Oyster shell bag breakwaters have an added benefit of producing oysters. In a study conducted on the east coast, the production of oysters on multiple restoration projects was weighted against the initial cost of the respective project. The findings revealed that the cost of a restoration project would be recovered in a maximum of 14 years, if no maintenance was conducted on the reef. If the reef was "seeded" with juvenile oysters the recovery of the initial costs could be achieved in 5 years (Henderson & O'Neil, 2003).

Problems still remain in the use of oyster shells. Oyster shell bag breakwaters have been used in many locations throughout the USA to quantify their ecological benefits, but little research has been conducted regarding their attenuating properties. Quantitative information has been produced for traditional structures containing rock, and concrete armor units, but nothing has been published to describe the attenuating properties of an oyster shell bag breakwater. Currently, projects employing oyster shell bag breakwaters would need to adopt published methodologies for determining the transmissive properties of traditional materials or conduct individualized experimentation for their project to determine the adequate dimensions necessary to handle the hydrodynamic loads applied to them. Projects using this methodology could be over or under designing the oyster shell bag breakwaters. The remainder of this article is an attempt to resolve this issue by conducting laboratory experiments in a controlled setting and comparing those results to existing methodologies available in the published literature.

OBJECTIVE

Sufficient tests are conducted to determine transmission coefficients of waves attenuated by various dimensions of oyster shell bag breakwaters. The data from the testing is used to develop a non-dimensional graph that relates the wave characteristics to the breakwater dimensions. The transmission coefficient is also equated using the equations developed by Van der Meer (2005). The transmission coefficient obtained from Van der Meer (2005) and the coefficient determined through testing is compared in a one-to-one graph. This graph is then used to answer the question of the Van der Meer (2005) equations' validity when applied to oyster shell bag breakwaters.

METHODOLOGY

Definitions. The testing conducted in the study is designed to measure the transmitted wave height, H_t, which is attenuated by the structure. The incident wave height, H_i, is the wave height measured before the interaction of the structure. To simplify testing and analysis, and to minimize experimental errors, the incident wave height is measured as the wave height produced by the wave generator prior to the placement of any oyster shell bags in the testing area. All wave heights are measured as the difference in water level from the crest of a wave to the trough of the wave. The transmission coefficient, K_t, is measured by the ratio of the transmitted wave height to the incident wave height and is reported as a dimensionless parameter. The depth of the water, d, is measured as the still water level within the basin. The wave period, T, is defined as the time elapsed between the crest of two waves passing a stationary point; in this study that point is defined by the wave gage location. The wavelength, L, is defined as the horizontal distance between two wave crests. The structure crest width, B, is defined as the average width across the top of the structure measured by averaging the width measurement at three locations. The structure height, h_c, is defined as the height of the structure measured from the basin floor. The freeboard, R_c, is measured as the difference of the structure height and the depth of the still water level (U.S. Army Corps of Engineers, 2002). Most of the parameters are shown below in Figure 1.

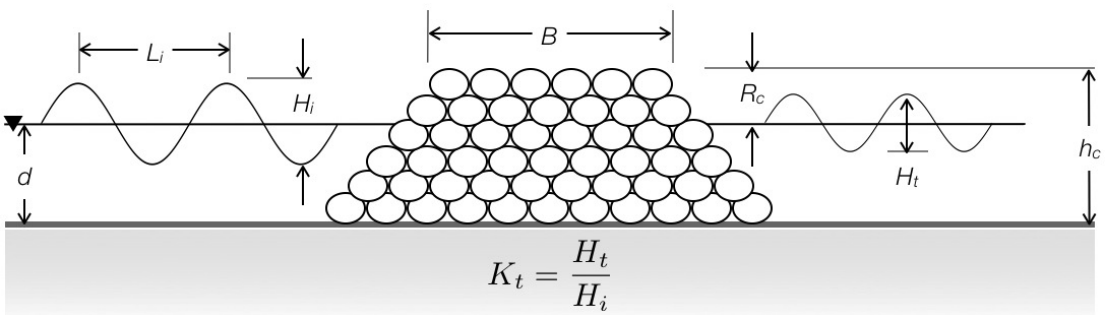


Figure 1: Definition sketch.

Experimental Setup. The tests performed in this study are conducted in the University of South Alabama's wave basin. The wave basin is 6.09 m (20 ft) wide

and 9.14 m (30 ft) long. Waves are generated in the basin by a unidirectional bulkhead capable of producing monochromatic waves, which propagate across the basin to a sloping sand beach. For the tests conducted in this study, a splitter wall is built 0.76 m (2.5 ft) from the side of the basin, 4.88 m (16 ft) in length, beginning 0.61 m (2.0 ft) from the bulkhead's maximum stroke. The splitter wall built within the basin served to minimize the effects of refraction around the oyster shell bag breakwater being tested. The wall is constructed from timber and held in place using high-density armor stone. The upright portion of the wall is supported by triangular stanchions which are placed 0.61 m (2.0 ft) on center along the outboard side as shown in Figure 2.



Figure 2: Photo of the basin at the University of South Alabama after installing the splitter wall and re-slopping the beach face.

Wave Gages. The wave height measurements obtained during testing are determined using a two-wire capacitance gage. The gage is placed on the leeward side of the testing area. The gage is calibrated using the incident wave height prior to the placement of any material in the testing area. By doing so, the effects of the splitter wall could be eliminated since the baseline incident wave height and the transmitted wave height are both recorded with the partition wall in place and the only difference in the two recordings is due to the placement of the oyster shell bags in the testing area. The sampling rate of the gage is set at 10 Hz; the data is digitally recorded using a program created by National Instruments called LabView. This program records the data then exports it to a Microsoft Excel file for use in analysis.

Oyster Shell Bags. The composite breakwater structure is made up of oyster shell bags 0.75 m (2.5 ft) in length having a nominal diameter of 0.076 m (3 in). The bags are constructed using a 0.76 m (2.5 ft) section of 0.10 m (4 in) PVC pipe. An empty bag is placed in the pipe and tied on one end. Oyster shells are then scooped into the assemblage and shaken/compacted until full, then the open end is closed using a cable tie, Figure 3 shows a completed bag. The oyster shells and the netting material used in the project are obtained from the Alabama Department of Conservation and Natural Resources (ALDCNR)-Coastal Section. The netting material used in the study is distributed by Atlantic Aquaculture Supply, LLC. It is described as "Oyster Setting Bag Net" with openings of 0.017 m (5/8 in) and manufactured as a tube with a diameter of 0.123 m (4.5 in) (Atlantic Aquaculture).



Figure 3: Photo of a completed oyster shell bag that is used in testing. The bags are nominally 0.076 m (3 in) in diameter and 0.82 m (30 in) long. A total of 120 bags are produced for the testing.

The oyster shells obtained from ALDCNR are mature eastern oyster, *Crassostrea virginica* shells that were recovered from the extinct reefs located along the shores of Mobile Bay in Alabama. A sample of the oyster shells are supplied to Southern Earth Sciences to determine its grain size distribution using ASTM standards for aggregate. A summary of the findings is provided in Figure 4.

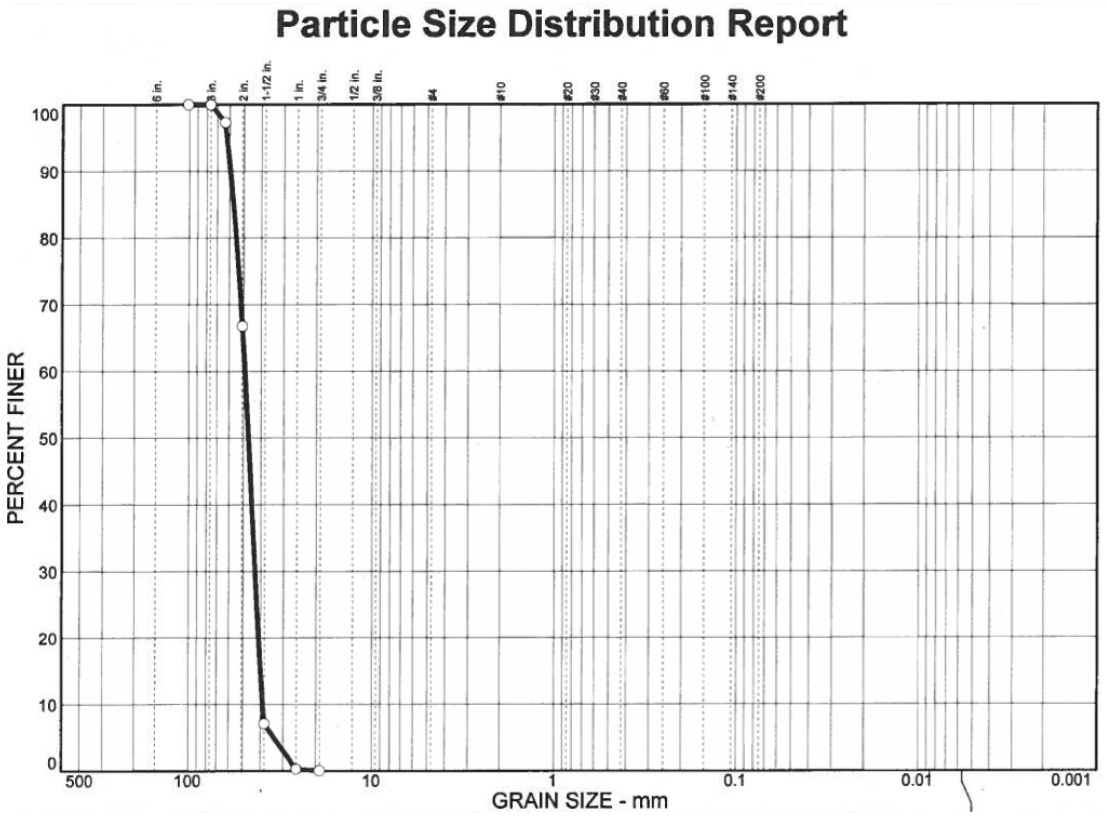


Figure 4: Grain Size Distribution Graph Supplied by Southern Earth Sciences

Scaling. The testing performed in this study did not follow a specific scale, although a Froude scaling with respect to a project on Mon Louis Island in Alabama produced almost a 1:1 scale. Since the results are dimensionless and only a function of the wave height and the structure size no further scaling is considered. The only portion of the testing that could be scaled is the size of the oyster shells. Scaling the oyster shells is not possible since the scaling would need to be controlled by both Froude and Reynolds number scaling. Scaling effects could have been reduced if oyster shells of a smaller size were available in a large enough quantity, but acquiring oyster shells of the proper size was not feasible within the scope of the study. In addition, smaller shells tend to escape through the mesh of bagging material. Furthermore, reducing the size of the shells, either by obtaining smaller shells, which are difficult to find, or by mechanical means, may introduce a strong bias in the results due to a corresponding decrease in structure porosity.

Experimental Procedure. A matrix is constructed to produce a range of values, which would be adequate to describe the attenuation of wave height and period by bagged oyster shells. The matrix contains 36 unique combinations of structure height and crest width. Seven additional tests are conducted using different wave characteristics, resulting in a total of 43 unique experiments. The height of the structure is varied from 1 bag high to 6 bags high, which yields a structure height 1.5 times greater than the still water depth. The crest width is also varied for each structure height. Structure crest widths vary from 4 bags to 19 bags, yielding a total

of six unique crest widths. The largest crest width is proportional to the incident wavelength.

A structure side slope of 1:1.5 (H:V) is kept constant throughout testing. The water depth remains constant throughout the experiment as well. For selected experiments where the freeboard is greater than zero, three additional trials are run using a larger wave height and longer wave period to produce overtopping. The larger wave provides additional data of the variation between wave heights for a similar structure. To reduce the contamination of reflection of the wave energy from the shoreline, the trials are conducted in "bursts." After each trial the basin is allowed to return to rest. The data used from each "burst" consists of the first three or four waves, which reach the wave gage and before the first wave transmitted is able to reach the shore and return to the wave gage. An average root-mean-square transmitted wave height, H_t, is obtained for each experiment by averaging the RMS wave height in each burst. The graphs provided are in terms of dimensionless parameters of the relationship between the structure and the incident wave characteristics.

RESULTS

The objective of the testing is to produce the measured transmission coefficients of various oyster shell bag breakwater dimensions for a single wave height which is shown below in Table 1. The RMS incident wave height used in this testing was 0.10 m (0.301 ft) with a period of 1.34 sec and wavelength of 2.17 m (6.60 ft).

Table 1: Transmission coefficients for an incident wave height of 0.10 m (0.301ft). Physical dimensions are in meters.

Crest Width, B	Structure Height, h_c	Transmission Coefficient, K_t	Crest Width, B	Structure Height, h_c	Transmission Coefficient, K_t
0.38	0.08	0.97	0.41	0.29	0.46
0.84	0.09	0.92	0.89	0.31	0.11
1.30	0.08	0.89	1.30	0.30	0.05
1.62	0.09	0.84	1.61	0.29	0.02
1.89	0.09	0.78	1.96	0.30	0.11
0.60	0.09	0.91	0.61	0.30	0.16
0.41	0.17	0.87	0.43	0.36	0.15
0.83	0.16	0.85	0.89	0.37	0.06
1.30	0.16	0.78	1.30	0.36	0.39
1.62	0.17	0.72	1.60	0.37	0.24
1.93	0.16	0.61	1.96	0.37	0.01
0.61	0.17	0.88	0.61	0.36	0.09
0.41	0.24	0.78	0.42	0.43	0.12
0.84	0.24	0.59	0.89	0.45	0.05
1.30	0.23	0.60	1.32	0.42	0.31
1.60	0.23	0.47	1.62	0.42	0.14
1.93	0.23	0.34	1.96	0.45	0.06
0.61	0.23	0.63	0.61	0.43	0.08

In addition to the original testing a second incident wave height of 0.17 m (0.524 ft) is used when the freeboard of the breakwater is greater than zero. The corresponding wave period is 2.03 sec with a wavelength of 3.51 m (10.7 ft). A summary of these values is provided in Table 2.

Table 2: Transmission coefficients for larger incident wave height of 0.17 m (0.524 ft). Physical dimensions are in meters.

Crest Width, B	Structure Height, h_c	Transmission Coefficient, K_t
1.96	0.30	0.09
0.61	0.30	0.36
1.96	0.37	0.02
0.61	0.36	0.14
1.62	0.42	0.06
1.96	0.45	0.03
0.61	0.43	0.10

From the data in Table 1 the following non-dimensional relationship, shown in Figure 5, is developed between the ratio of the structure height and water depth (h_c/d) versus the measured transmission coefficient (K_t), for the testing conducted using the smaller wave. The variation of measured K_t in a two-dimensional parameter space is provided in Figure 6, which demonstrates the wave attenuation characteristics as a function of non-dimensional structure height and length.

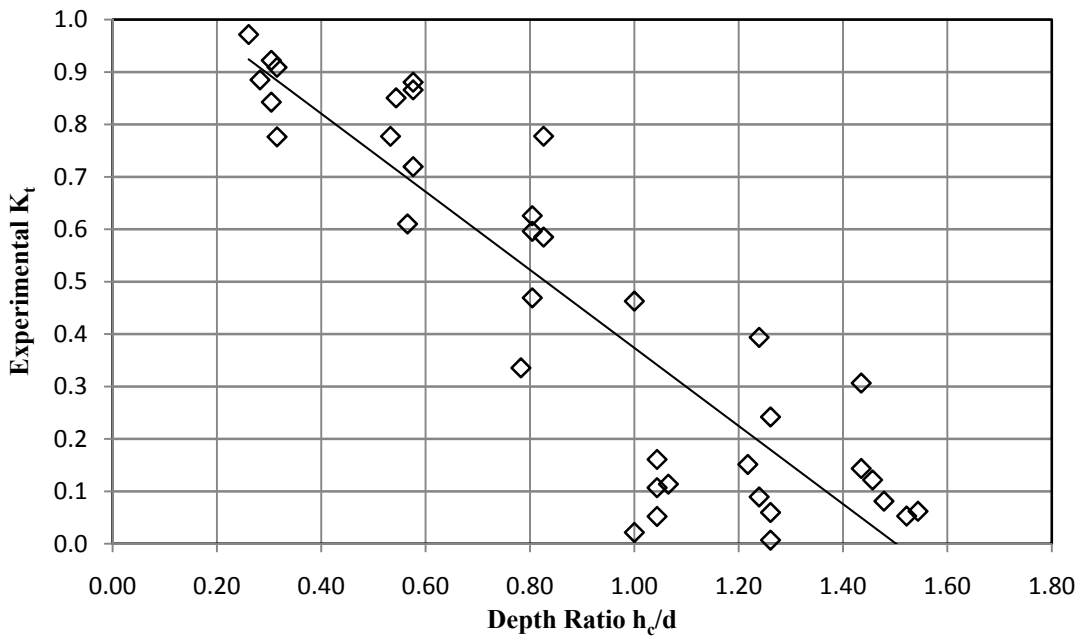


Figure 5: Graph of the relationship of the structure height and water depth vs. the measured transmission coefficient of the small wave used during the tests.

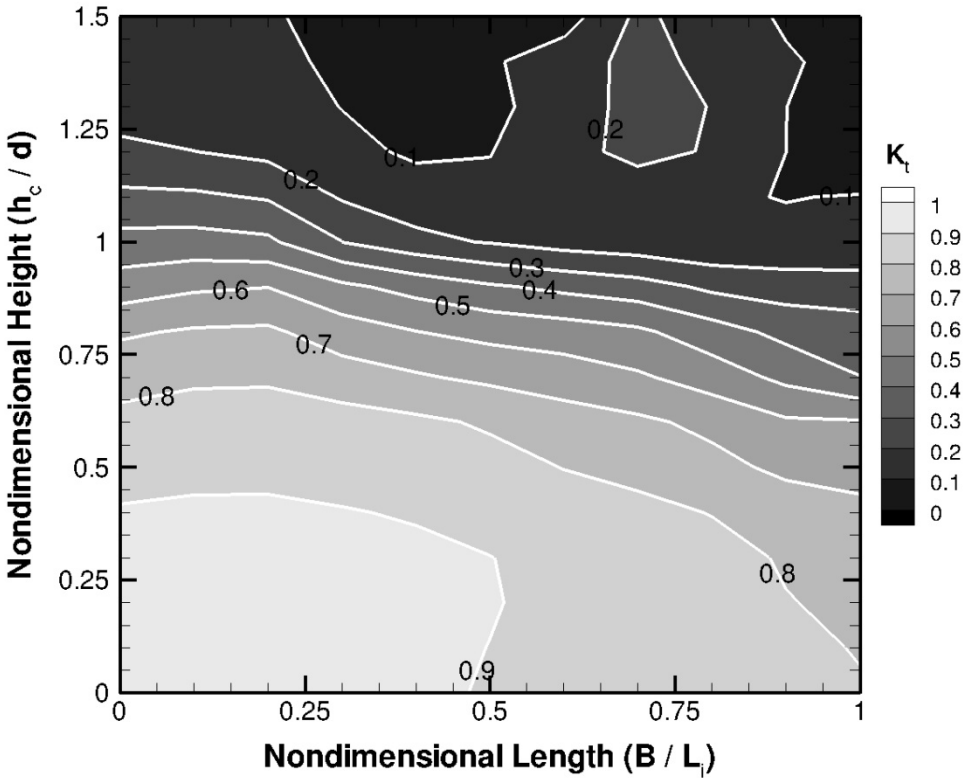


Figure 6: Variation of K_t as a function of non-dimensional structure length and height.

DISCUSSION

The results obtained from the testing are compared to published methodologies for estimating transmission coefficients. The Coastal Engineering Manual (2002) provides information on how to calculate the transmission coefficient using equations formulated by Van der Meer (U.S. Army Corps of Engineers, 2002). The equations given by Van der Meer et al. (2005) are a continuation of previous literature published by d'Angremond et al. (1996) and Van der Meer and d'Angremond (1992). The formulae depend primarily upon non-dimensional relationships between the incident wave height and the physical characteristics of the structure. The final equations published in Van der Meer et al. (2005) are shown below.

$$\text{For } \frac{B}{H_i} < 8 \qquad K_t = -0.40\frac{R_c}{H_i} + 0.64\left(\frac{B}{H_i}\right)^{-0.31}(1 - e^{-0.50\xi})$$

$$\text{For } \frac{B}{H_i} > 12 \qquad K_t = -0.35\frac{R_c}{H_i} + 0.51\left(\frac{B}{H_i}\right)^{-0.65}(1 - e^{-0.41\xi})$$

Note that a gap exists in the range $8 < B/H_i < 12$, where the Van der Meer et al. (2005) equations give a discontinuity in this range and it is suggested that linear interpolation is used for values of B/H_i that fall within this range. Additionally, Van

der Meer et al. (2005) suggests limits for the maximum and minimum values of K_t. The lower limit, K_{tl}, is defined as a constant 0.05. The upper limit K_{tu}, is given a linear dependency on B/H_i and is determined by the equation given below.

$$K_{tu} = -0.006\frac{B}{H_i} + 0.93$$

The transmission coefficients of the structures tested are calculated using the parameters described by Van der Meer et al. (2005). These coefficients are then compared to the transmission coefficients determined from the test data from Table 1 and Table 2 by using a one-to-one graph shown in Figure 7.

From Figure 7, one can see the similarities in the two determinations of the transmission coefficient. With a slope of approximately one, the Van der Meer et al. (2005) equation is shown to be adequate in estimating the wave height attenuation of an oyster shell bag breakwater. However, Figure 7 shows the predicted K_t values from Van der Meer et al. (2005) are an under estimate from the measured values obtained through testing. This could be a result of the porosity of the oyster shell bag breakwaters being different than the rubble breakwaters used in the Van der Meer et al. (2005) tests.

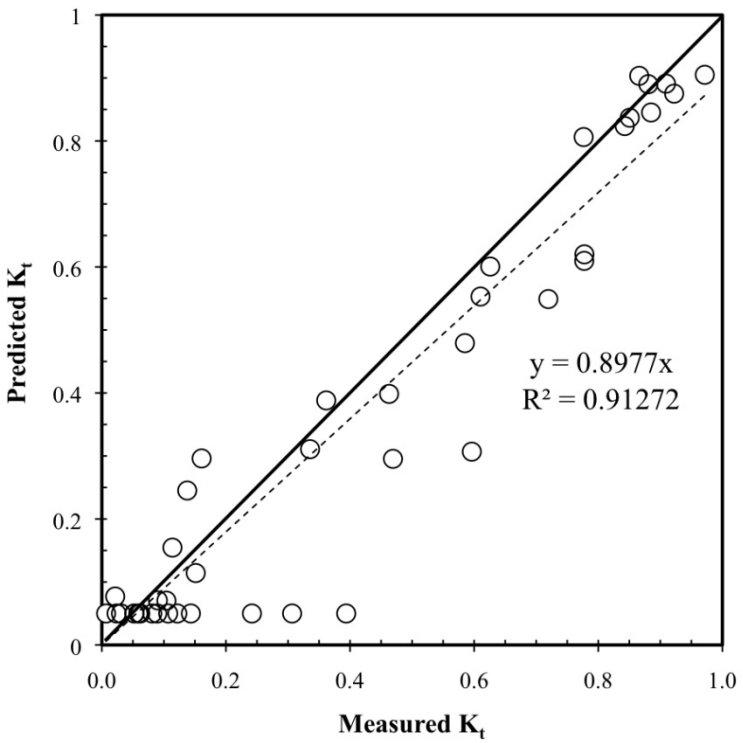


Figure 7: A comparison of measured and predicted transmission coefficients using the predictive equations of Van der Meer et al. (2005). Open symbols (o) represent measured data, the dashed line is a linear regression with a zero intercept, and the dark solid line represents perfect agreement.

Also shown in the graph is the product of the forced lower limit of the Van der Meer et al. (2005) equations. Based on the research performed by Van der Meer et al. (2005), the equations are no longer valid for predicting K_t, once the freeboard of the structure becomes positive. Through the limited testing performed during this research it is also obvious that predicting K_t becomes difficult once the freeboard becomes positive. This is shown in Figure 7 from the results. As the dimensionless freeboard becomes larger the data become skewed. The skew is likely due to outside variables affecting the transmissive properties of the structure. As the freeboard becomes larger, the transmissive properties of the structure become more reliant on factors such as run up and overtopping which are not accounted for in the predictive equations given by Van der Meer et al. (2005).

CONCLUSIONS

The results obtained in this report are a substantial finding in terms of constructing oyster shell bag breakwaters. The resulting data obtained from testing is compared to published methodologies for measuring the wave transmission coefficient for low crested breakwaters (Van der Meer et al., 2005), which produces a distinguishable resemblance based on the 43 tests conducted during this study. In general, experimental testing suggests that:

1) The transmission coefficient increases with dimensionless freeboard.

2) The K_t increases with dimensionless crest width.

3) The methodology of Van der Meer et al. (2005) provides realistic values of K_t within the range of tested parameters.

However, additional testing should be continued, even though the overall data presented from the testing is similar to the predictive equations. The additional testing should focus on the areas within the results where the comparison with Van der Meer et al. (2005) was not in agreement. More specifically, the variation of wave characteristics over a single structure dimension should be examined. Using this data, one could obtain a better understanding of the relationship between the wave characteristics (i.e. wave period, length, and height) and the structure dimensions associated in the transmissive properties, which could ultimately lead to more predictive formulae. Furthermore, testing should be extended outside the "ideal setting" to include more realistic applications, where irregular wave, reflection, and other non-pure transmissive characteristics are included in the predictive formulae.

ACKNOWLEDGEMENTS

The authors would like to thank Carl Ferraro from the Alabama Department of Conservation and Natural Resources – Coastal Division for the acquisition of oyster shells and bagging material. Thanks should also be given to Lewis Copeland, Vice President, Southern Earth Sciences for providing geotechnical descriptions of the oyster shells. Additionally, the parents of Richard Allen should also be acknowledged

for their contribution to the production of the oyster shell bags. Finally, a special thanks to the Department of Civil Engineering at the University of South Alabama for the use of the wave basin, and to Caren Reid Dixon for her assistance in the laboratory testing.

REFERENCES

Alabama Department of Environmental Management . (1995). Coastal Area Management Program Division 335-8. Alabama Administrative Code .

Atlantic Aquaculture. (n.d.). Soft Mesh Polyethylene Netting. Retrieved November 19, 2010, from Atlantic Aquaculture: http://www.atlanticaquaculture.com/soft_mesh_polyethylene_netting.htm

Bakker, P., Berge, A., Hakenberg, R., & Klabbers, M. (2003). Development of Concrete Breakwater Armour units. Coastal, Estuary and Offshore Engineering Specialty Conference. Moncton, Nouveau-Brunswick, Canada: Canadian Society for Civil Engineering.

Boyd, C. (2007). Living Shorelines 101. Mississippi Alabama Sea Grant Consortium.

Coen, L. D., Brumbaugh, R. D., Bushek, D., Grizzle, R., Luckenbach, M. W., Posey, M. H., et al. (2007). Ecosystem Services Related to Oyster Restoration. 341 (July 4).

d'Angremond, K. V., & de Jong, R. (1996). Wave Transmission at Low Crested Stuctures. 25th Int. Conf. on Coastal Engineering (pp. 3305-3318). ASCE.

Davis, J. E. (1998). Wetland Shoreline Protection and Erosion Control: Design Considerations. U.S. Army Corps of Engineers.

Davis, J. L., Takacs, R. L., & Schnabel, R. (2006). Evaluating Ecological Impacts of Living Shorelines and Shoreline Habitat Elements: An Example From the Upper Western Chesapeake Bay. Management, Policy, Science, and Engineering of Nonstructural Erosion Control in the Chespeake Bay, (pp. 55-61). Williamsburg, VA.

Duhring, K. A. (2006). Overview of Living Shoreline Design Options for Erosion Protection on Tidal Shorelines. Management, Policy, Science, and Engineering of Nonstructural Erosion Control in the Chespeake Bay. Williamsburg, VA.

Henderson, J., & O'Neil, J. (2003). Economic Values Associated with Construction of Oyster Reefs by the Corps of Engineers. ERDC TN-EMRRP-ER-01.

Poole, A. B. (1991). Rock Quality in Coastal Engineering. 24.

Seelig, W. (1980). Two-Dimensional Tests of Wave Transmission and Reflection Characteristics of Laboratory Breakwaters. Vicksburg, MS: Army Engineer Waterways Experiment Station.

Shafer, D. R. (2003). Preliminary Evaluation of Critical Wave Energy Thresholds ot Natural and Created Coastal Wetlands. Vicksburg, MS: TN-WRP-HS-CP-2.2. Engineering Research and Development Center.

Swann, L. (2008). The Use of Living Shorelines to Mitigate the Effects of Strom Events on Dauphin Island, Alabama, USA. American Fisheries Society Symposium. 64. American Fisheries Society.

U.S. Army Corps of Engineers. (2002). Coastal Engineering Manual (Vols. 1110-2-1100). Washington D.C.: U.S. Army Corps of Engineers.

Van der Meer, J. W., Briganti, R., Zanuttigh, B., & Wang, B. (2005). Wave Transmission and Reflection at Low-Crested Structures: Design Formulae, Oblique Wave Attack, and Spectral Change. Coastal Engineering , 52, 915-929.

Van der Meer, J., & d'Angremond, K. (1992). Wave Transmission at Low Crested Stuctures. Costal Stuctures and Brakwaters (pp. 25-41). London: Institution of Civil Engineers.

Zalewski, M. (2002). Ecohydrology-the use of ecological and hyrological processes for sustainable management of water resources. Warsaw, Poland: Hydrological Sciences.

SHORE PROTECTIVE REVETMENT CROWNED WITH PEDESTRIAN WALKWAY AT STRAND BEACH, CALIFORNIA

Chia-Chi Lu[1], Thomas J. Fischetti[2] & Ronald M. Noble[3]

[1] Noble Consultants Inc., 2201 Dupont Drive, Suite 620, Irvine, CA 92612, USA.
cclu@nobleconsultants.com.
[2] Noble Consultants Inc., 2201 Dupont Drive, Suite 620, Irvine, CA 92612, USA.
tfischetti@nobleconsultants.com.
[3] Noble Consultants Inc., 2201 Dupont Drive, Suite 620, Irvine, CA 92612, USA.
rnoble@nobleconsultants.com.

ABSTRACT

To provide adequate protection against storm wave attack, minimize terrace slope erosion, enhance public safety, and maintain lateral beach access, the 2,100-foot aged riprap revetment was repaired under the site's development plan at Strand Beach, California. Furthermore, to promote public use of the project beach area and enhance the aesthetic scenic view, an 8-foot wide pedestrian walkway with a 3-foot high retaining wall was built atop the revetment. The integrated walkway/retaining wall structure provides additional protection against storm wave impingement. A 3-year post-construction beach monitoring program was implemented to document any potential revetment construction impact on coastal processes at Strand Beach after the revetment repair. It was found that the coastal processes impact on Strand Beach as a result of the revetment repair is inconsequential.

BACKGROUND

A planned oceanfront development site located at Strand Beach, Dana Point, California, shown in Figure 1, was historically protected by an aged riprap revetment against storm wave attack. Years of service had left the under-engineered riprap revetment with dislodged stones and incapable of its shore protective function. Figure 2 illustrates the pre-project revetment condition at Strand Beach. The engineering task primarily involved repair of the aged, under-designed riprap revetment with larger stones to provide shore protection against increasing occurrence of severe storm wave attack resulting potentially from meteorological change owing to the global warming effect. The repair, however, would need to satisfy requirements related to land use, aesthetic, biological, ecological, recreational and water quality issues.

PERMIT PROCESS

A coastal engineering assessment for the proposed development plan was prepared to characterize local and regional coastal processes (Noble Consultants Inc, 2001 & 2002). Comparison of various shore protective alternatives was performed to identify potential project impacts related to wave characteristics in the surf zone as well as

cross-shore and alongshore sediment transport. Four shorefront protective measures along with the "no action" alternative were analyzed. Each measure was assessed to determine its overall engineering design merits, its function in protecting the shorefront slope against wave attack, and the potential for any adverse coastal processes and environmental impacts. It was concluded that repair of the aged revetment structure topped with a new pedestrian walkway to enhance recreational activity is the preferred alternative. Subsequently, a development permit was secured for the preferred alternative from regulatory agencies.



Figure 1. Project Vicinity and Location



Figure 2. Pre-Project Revetment Condition

INTEGRATED STRUCTURE DESIGN

An engineering analysis of oceanographic design criteria and a coastal process assessment of potential project-induced impacts formed the basis from which permit

compliant and structurally sound design criteria were established for the shore-front protective revetment. A wave runup analysis was performed to determine the height of the repaired revetment. Wave runups were computed from a depleted beach profile eroded down to the bedrock layer. The top of the revetment at +22.7 feet, MLLW would prevent wave overtopping under most storm events. Minor wave overtopping may occur only under an extremely rare occasion during which waves break near the toe of the revetment coincident with an extreme high water level. Occurrence of such an event, simultaneously including the eroded profile to the bedrock, breaking waves and the selected highest water level, would be similar to or even rarer than those storm events observed in the 1983 El Nino year.

Aesthetic and regulatory constraints dictated the crest of the revetment structure three (3) feet below the elevation necessary for wave uprush protection. Exposing the upper 3-foot terrace slope to potential wave-induced overtopping would unacceptably compromise the effectiveness of the repaired revetment. Therefore, an integrated revetment/walkway structure providing dual purposes of both erosion control and recreational enhancement along the terrace slope was designed.

The designed revetment structure includes 1) a class No. 2 bedding layer with filter fabric between the slope face and 2) two layers of riprap stones. The revetment begins at bedrock elevation of +2.7 feet, MLLW and ends at +19.7 feet, MLLW. A riprap toe is not necessary since the bedrock where armor stones were directly placed on is not erodible. The revetment is approximately 7-feet thick with 4- to 5-ton stones used for the two base levels to provide more resistance to wave attack. The upper levels to the height of +19.7 feet, MLLW is tapered down to 2-ton stones. Allowing for seasonal variance, approximately 40 percent of the revetment structure will be buried by sand in the summer months, based upon an average sand elevation at +10 to +11 feet, MLLW.

The walkway equipped with a retaining wall located atop of the repaired revetment was designed to not only provide public recreational enhancement within the beach area but also serve as a buffer for the lowered revetment structure against wave uprush. It is not often that a subject architectural amenity, such as a sidewalk, is required to satisfy the harsh demands of shoreline slope protection in a highly corrosive environment. For the sustained beauty of the revetment walkway, a design process critical to crack control and utilizing material enhancements that prevent the onset of corrosion is necessary.

The structural design of the pedestrian walkway began with a finite element model for the monolithic framework of the combined walkway and revetment structure consisting of the walkway slab, a retaining wall and footing. Figure 3 shows the graphic display of the model simulation. The seaward portion of the walkway, beyond the stem wall and footing, cantilevers over the riprap revetment beneath it. The shifting rock would not provide a reliable foundation critical to minimize cracks and prevent corrosion. Geotechnical recommendations for the sit included lateral soil pressure, hydrostatic and surcharge loading criteria. These recommendations were

implemented and the resulting service loading conditions were modeled. Live loading patterns were developed and combined in a variety of ways to account for critical stress conditions.

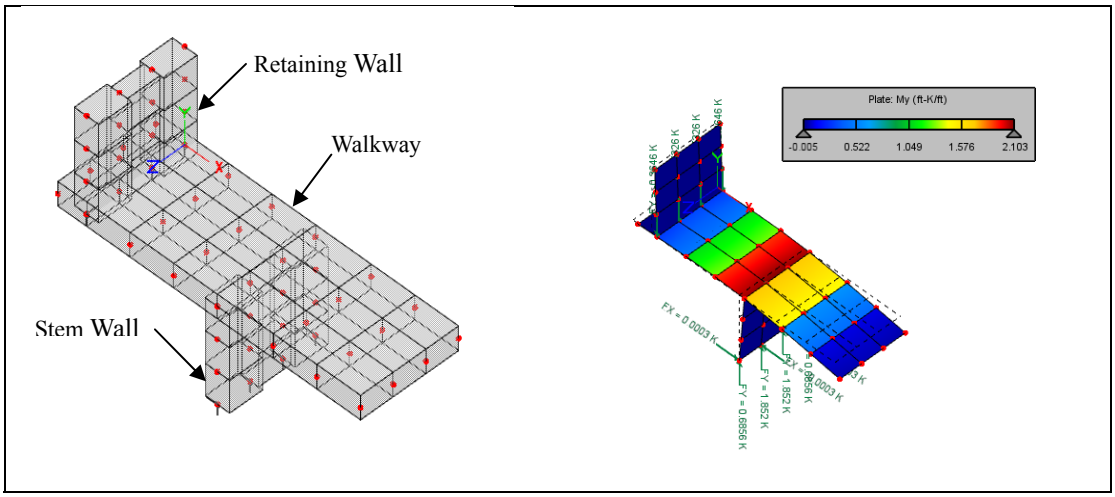


Figure 3. Graphic Display of Finite Element Model and bending Stress Analysis for the integrated Structure

Code-specified loading combinations were considered in the analysis. Concrete reinforcement was selected to satisfy all cases. Bending stresses were reviewed and held to limits where tension zone cracking would be minimized (see Figure 3). Corrosion inhibitors, a 5,000 psi compressive strength, a maximum 0.45 water cement ratio, epoxy coated reinforcement and three-inches of concrete cover over reinforcement were the additional measure that was taken to improve durability of the concrete structure in the harsh marine environment. Reinforcement was selected for each group of plate elements, and stress levels confirmed to be within Code limitations. Figure 4 illustrates the design cross section of the proposed revetment structure and the walkway with the retaining wall (Noble Consultants Inc., 2005).

CONSTRUCTION PHASE

Construction of the integrated structure began at the revetment section. The riprap revetment was repaired via initial excavation of the structure footprint down to the bedrock layer and subsequent stone placement in sequential layers from the bottom to the top. A temporary steel-plate shoring wall was individually erected for each construction section of approximately 100 feet in length to prevent ocean water inundating the excavated construction site that was below the high tide line. As shown in Figure 5, filter fabric was wrapped around riprap stones in the bottom layer and was continuously laid across the terrace slope before placement of riprap stones to the design height. Bedding stone material was also used to stabilize the filter fabric laid on the terrace slope.

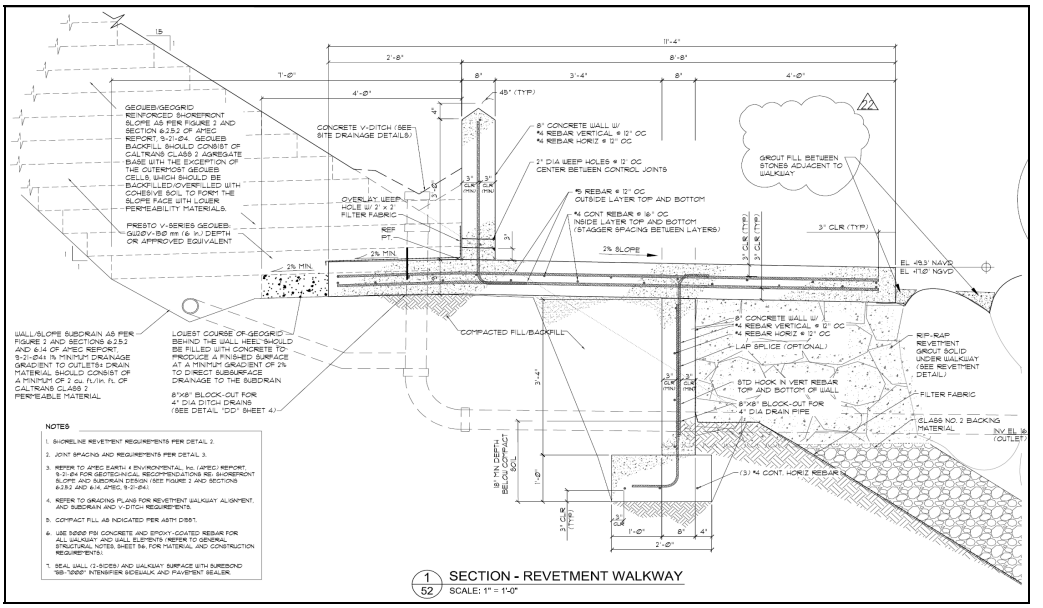


Figure 4. Typical Cross-Section of the Integrated Revetment Walkway



Figure 5: Riprap Stone Placement

Proper implementation of the revetment walkway needed to satisfy the aesthetic and durability objectives of the design requirement with equal weight and high priority. The line and grade of the walkway was required to be true and flawless to the naked eye. The concrete was free of cracks outside the control and expansion joints with consistent finished surfaces. Beneath the surface, concrete was placed solidly into forms with a 3-inch cover over reinforcement.

Following good design practices, proper material selections and effective placement, a specific curing process was required to ensure high-quality concrete. To minimize residual stresses in newly placed concrete that would result in uncontrolled cracking, the temperature and humidity of the environment surrounding the newly placed concrete was controlled. Curing required more than an occasional drive-by watering

from the water truck. The temperature and humidity were monitored, adjusted, and recorded to the same degree of concern as each of the previous steps to realize the concrete's full potential. Figure 6 displays the construction process of the walkway/wall structures, while Figure 7 illustrates the completed revetment/walkway structure including the retaining wall as well as the overall post-project site conditions.



Figure 6. Construction of Walkway and Retaining Wall



Figure 7. Post-project Site Conditions

POST-CONSTRUCTION BEACH MONITORING

A beach monitoring program, as required by the California Coastal Commission and the City of Dana Point, was implemented to document any potential revetment

construction impacts on coastal processes at Strand Beach during and after the revetment repair (Noble Consultants Inc., 2010). The required monitoring program included monthly visual inspections to identify any abnormal changes of sand level at Strand Beach during the construction period, which was completed in June 2007. Subsequently, a 3-year post-construction beach monitoring program consisted of quarterly beach profile surveys at six locations from the day-lighted toe of the repaired revetment structure to the approximate Mean Lower Low Water (MLLW) line.

Strand Beach in the past 5 years from 2005 to 2010, spanning the pre-, during-, and post- construction period, exhibited a general cyclic trend of beach advance in the summer months, shoreline retreat in the winter season, and subsequent recovery in the spring. Sands were carried offshore in the winter and stored in a bar formation. The beach widened and reformed as sands from the offshore bar returned during the following summer months. The offshore sand movements were induced by the stormy high waves in the winter, while the reverse trend resulted from the low longer-period swells commonly observed in the summer.

The typical seasonal variation at Strand Beach is also evident from a comparison of the photographs taken during the monitoring period. Figures 8 and 9 show the photographs taken at one location looking toward both the upcoast directions in the winter (March photos) and in the summer (September photos), respectively. Wide beach conditions with a berm formation occurred in the summer months, while depleted beach conditions without a berm formation were observed in the winter.

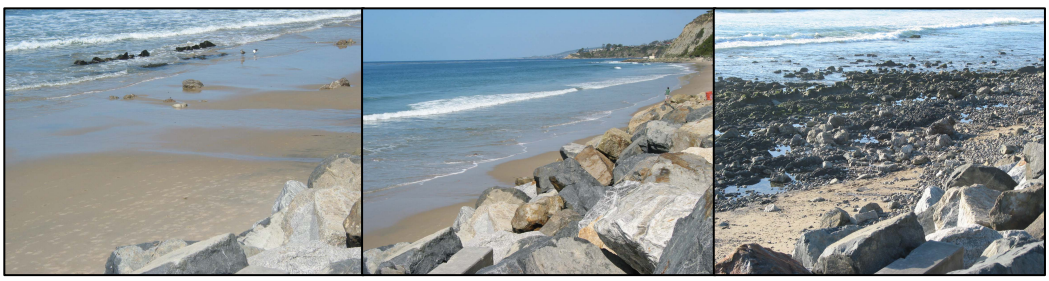


Figure 8. Strand Beach Conditions Observed in March of 2008, 2009 & 2010

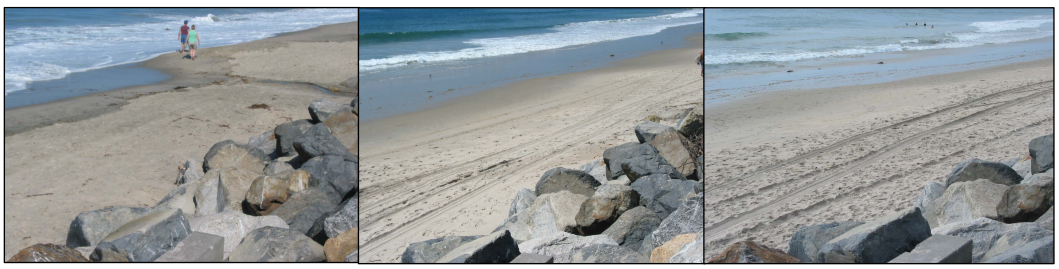


Figure 9. Strand Beach Conditions Observed in September of 2008, 2009 & 2010

During the 2009-2010 El Nino season, Beaches in southern California including Strand Beach were severely eroded after an occurrence of sequential storms in January 2010. The entire northwestern segment of Strand Beach was eroded and stripped down to the bedrock layer similar to the conditions observed in the 1983 El Nino season. Figure 10 illustrates the Strand Beach condition within the upcoast shoreline segment in February, March & September, respectively. The depleted beach observed in February was partially recovered in March; and by September the entire beach was naturally restored to its typical widened condition similar to those observed in the previous years. The presence of the reconstructed revetment induced little impact on the coastal processes within Strand Beach even during the El Nino season.

Figure 11 shows the surveyed distances from the pre-set baseline to the Mean Sea Level (MSL) position for all surveyed profiles at each station. It is noted that the MSL line is at an elevation of +2.77 feet, MLLW. The average distance of six stations at Strand Beach (i.e. 0+00, 4+00, 8+00, 12+20, 18+60 and 24+00) is also plotted for each individual survey. It can be seen that the average MSL position seasonally advanced and retreated in response to the variation of the predominant wave pattern in different seasons. Neither an upward (accretion) nor downward (erosion) trend of beach behavior was deduced from the surveys since 2005 including the pre-, during- and the post-construction.



Figure 10. Strand Beach Conditions in February, March & September 2010

SUMMARY

An integrated shore protective structure of a concrete walkway with a retaining wall atop a repaired revetment was designed and built to serve dual purposes of storm wave protection and recreational enhancement. Hidden below the surface of this unique concrete structure are the engineered solutions to optimize aesthetic quality of the walkway improvements while withstanding abrasive environmental demands of this shorefront protective revetment.

The 5-year beach monitoring program indicates that similar seasonal variations of sand gain and loss at Strand Beach were documented during various project periods (i.e., pre-construction, during-construction or post-construction). No distinguished long-term trend of shoreline retreat or advance can be projected from the past 22 monitoring surveys. Temporary short-term beach depletion was observed during the

past El Nino season in 2009-2010. However, Strand Beach had recovered by September 2010 and exhibited a typical summer beach condition. Thus, the coastal processes impact on Strand Beach as a result of the revetment repair is inconsequential. It is anticipated that beach behavior at Strand Beach in the future will be similar to those observed in the previous years.

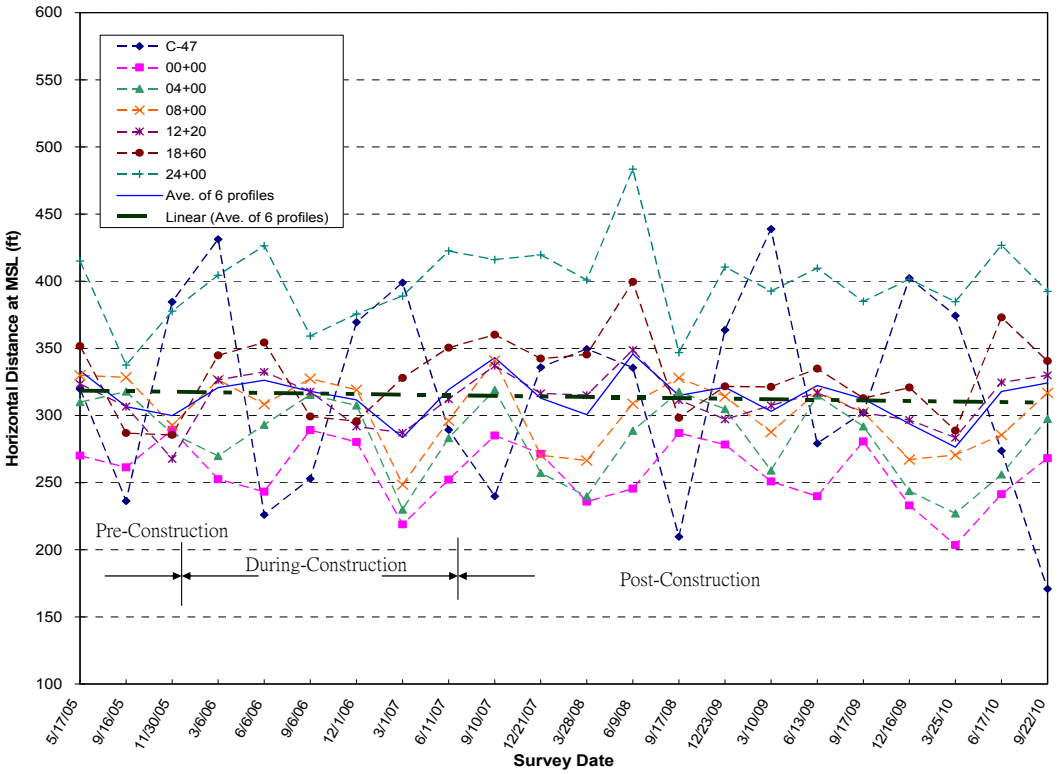


Figure 11. Temporal and Spatial Variation of MSL Positions

REFERENCES

Noble Consultants Inc., 2001. "Coastal Processes Assessment for Headlands Development and Conversation Plan", Prepared for Headlands Reserve LLC, September 2001.

Noble Consultants Inc. 2002. "Supplemental Assessment for Shorefront Protection Alternatives, Headlands Development and Conversation Plan, Dana Point, California", Prepared for Headlands Reserve LLC, May 2002.

Noble Consultants Inc., 2005. " Plans and Specifications of Revetment, Walkway & Retaining Wall Details", permitted by the City of Dana Point for Headlands Reserve LLC, June 2005.

Noble Consultants Inc., 2010. " Strand Beach Monitoring Program, Orange County, California", Final Report, Prepared for Headlands Reserve LLC, December 2010.

Extreme Total Water Levels for Twin Lakes Beach, Santa Cruz, CA

C. Fassardi[1], L. Bassetti[2] Ph.D. and J. Davies[3]

[1]Halcrow, Inc., 5740 Fleet Street, Suite 120, Carlsbad, CA 92009; PH (760) 444-1130; FAX (760) 444-1131; email: fassardiCD@halcrow.com

[2]Halcrow, Inc., 1101 Channelside Drive, Suite 200 S, Tampa, FL 33602; PH (813) 386 1990; FAX (813) 386 1991; email: bassettiL@halcrow.com

[3]County of Santa Cruz, 701 Ocean Street, Room 510, Santa Cruz, CA 95060; PH (831) 454-2280; FAX (831) 454-3420; email: RED026@co.santa-cruz.ca.us.

ABSTRACT

A coastal engineering study was performed to compute extreme Total Water Levels (TWL's) for three different global warming scenarios to assist in the selection of realistic scenarios for analysis, and in the development of corresponding realistic coastal protection solutions for the Twin Lakes Beachfront Improvements Project in Santa Cruz, CA. The study involved, among others, the development of a 39-year long wave hindcast in shallow water, the development of TWL hindcasts, and calculation and mapping of 100-year TWL's along the coast where the improvement project is being planned by the County of Santa Cruz. The 100-year TWL contours for a 50-year project lifetime were used in the conceptual design of the architectural plans and coastal protection structures.

INTRODUCTION

The County of Santa Cruz (County) is in the process of developing conceptual designs for the Twin Lakes Beachfront (TLB) Improvements Project. The project consists of a roadway realignment, and the inclusion of bicycle lanes, pedestrian walkways, improved parking and beach access on the stretch of coastline along East Cliff Drive from 5th Avenue to 9th Avenue at Schwan Lake; and a pedestrian pathway from 9th Avenue to 11th Avenue along the beach fronting the lake.

The project area, shown in Figure 1, is fronted by the Twin Lakes State Beach which is bounded to the west by the Santa Cruz Harbor and to the east by 11th Avenue on the east side of Schwan Lake. The construction of the Santa Cruz Harbor in the early 1960s disrupted the littoral drift reducing the supply of sand to the beaches to the east of the harbor entrance. The existing sandy Twin Lakes State Beach is the result of annual beach nourishment which has been performed since 1986. Sediment shoaling the harbor entrance channel is removed and deposited on the beach at a rate of approximately 200,000 cubic yards per year.

Anecdotal evidence and investigations conducted on behalf of the County have shown that during years of severe winter storms or less than planned beach

nourishment, the beach could be depleted of sand due to the erosive action of the waves; exposing the bluffs, the adjacent roadway and the planned improvement to potential damage due to wave erosion, overtopping and flooding. Considering:

- that in the absence of the beach storm waves would reach further landward,
- the current projected trends in sea level rise due to global warming,
- that much of the planned improvements would be constructed seaward of the existing alignment of East Cliff Drive, and
- the exposed location of the project to ocean waves,

coastal protection structures would be necessary to stabilize the exposed bluffs and protect the planned beachfront improvements.



Figure 1. Twin Lakes State Beach.

However, the various combinations of projected sea level rise scenarios due to global warming, severe storms and possible disruption of beach nourishment would lead to a variety of scenarios for which different coastal protection solutions could be developed in a compromise between the impacts of the marine environment and the requirements of the project.

In order to conceive realistic scenarios for analysis and to develop corresponding realistic coastal protection solutions, a coastal engineering study was performed to characterize the site, to define design conditions and, fundamentally, to compute Total Water Levels (TWL's) for three different global warming scenarios. Using this information, the architectural plans of the planned improvements, wave conditions and overtopping analysis, alternatives of coastal protection structures and structural systems were developed and evaluated for the different stretches of the project coastline.

CHARACTERIZATION OF THE SITE

BATHYMETRY

Offshore and local bathymetry were obtained from the Digital Elevation Model (DEM) developed by the National Geophysical Data Center (NGDC) for Monterey, CA. Bathymetric datasets used in the compilation of the Monterey DEM include 42 NOS hydrographic surveys, 17 California State Sea Floor Mapping Lab multi-beam sonar surveys located along the southern coast, 6 USGS multi-beam sonar surveys that cover the deeper areas within the bay, and extracted ENC/RNC sounding data. Coastline datasets for the Monterey DEM were obtained from NOAA's Office of Coast Survey (OCS) and the National Marine Fisheries Service, Southwest Fisheries Science Center/Moss Landing Marine Laboratory (NMFS,SWFSC/MLML); the California State Land Commission (CSLC); the California Dept. of Fish and Game, Marine Region GIS Unit (CDFG); and the U.S. Geological Survey (USGS).

WAVES

Site-specific, long-term wave data at Santa Cruz was not available for this study. Therefore, a wave hindcast just offshore TLB was synthesized from Oceanweather's GROW's point 39170 deep water long-term wave hindcast. The GROW hindcast consisted of wind speed and direction, and wave height, period and direction every 3 hours, partitioned in seas and swell, from January 1, 1970 to December 31, 2008. In addition, wave measurements made by Scripp's Coastal Data Information Program (CDIP) offshore Santa Cruz were collected for calibration of the wave hindcast at TLB. The CDIP data set consisted of wave heights, periods and directions measured with a pressure sensor array from 1981 to 1999 (with a few gaps).

Given the computational expense of transforming from deep water to shallow water the 39-year long deep water wave hindcast, the wave hindcast at TLB was computed using transfer functions that related the wave conditions at TLB with the corresponding conditions in deep water. The transfer functions were computed using the wave conditions that resulted from transforming from deep water to the locations of interest in shallow water a matrix of unit seas and swell heights for a range of periods, directions and water levels. Use was made of MIKE 21 Spectral Wave (SW), a numerical model developed by the Danish Hydraulic Institute (DHI) to perform the seas and swell transformation simulations.

The wave transfer functions and hindcasts were computed at two locations. A wave hindcast considered to be representative of wave conditions at TLB was computed in a water depth of approximately 9.55 m (MLLW). In addition, given the availability of measurements at CDIP Station 006, wave conditions at this location were also computed to perform a calibration and verification of the wave predictions. Figure 2 shows the locations of CDIP Station 006 and the location at which the TLB wave hindcast was computed.

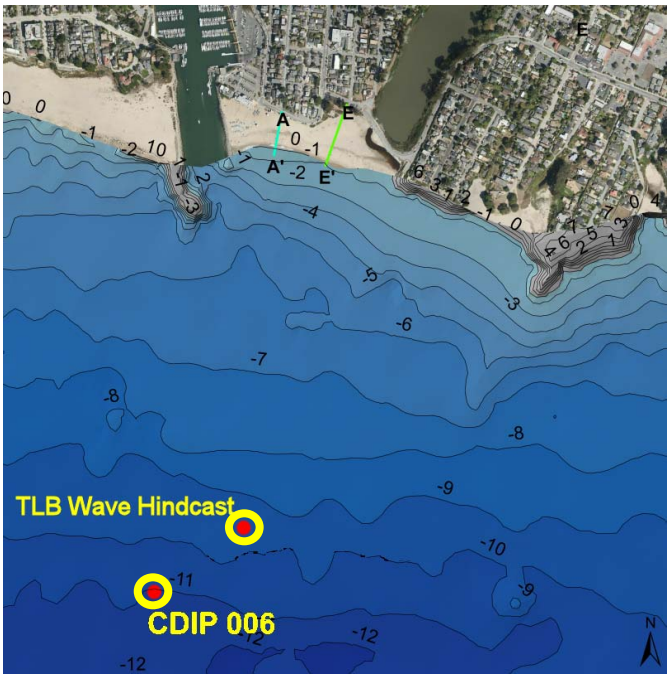


Figure 2. Wave hindcast locations, depths in m (MLLW).

An initial comparison between the hindcast and measurements at CDIP 006 showed discrepancies that where adjusted by means of scale and offset coefficients derived from a Q-Q plot analysis. Figure 3 shows a Q-Q plot of the measured and predicted (hindcast adjusted) wave heights at the CDIP 006 location from 1993 to 2001. The agreement is very good, however a slight under-prediction of waves heights is noted.

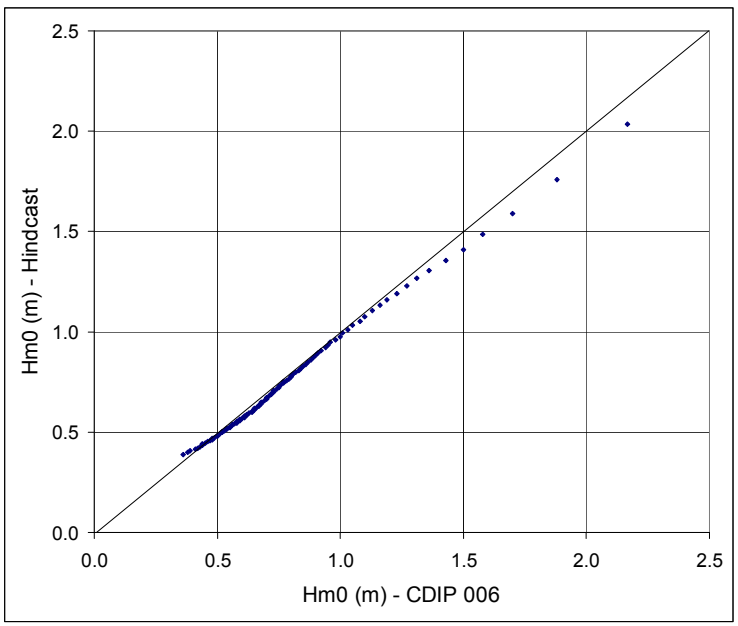


Figure 3. Q-Q plot of predicted (hindcast adjusted) versus measured wave heights at the CDIP 006 location from 1993 to 2001.

TIDAL DATUMS AND SEA LEVEL RISE SCENARIOS

Tidal datums for Santa Cruz were obtained from the NOAA nautical chart 18685. Tidal datums such as the Highest Astronomical Tide (HAT), Lowest Astronomical Tide (LAT), Mean Sea Level (MSL) and most importantly the offset between the MLLW and the National Geodetic Vertical Datum of 1929 (NGVD 29, Santa Cruz vertical topographic datum) were not available and were derived using data from nearby Monterey and Moss Landing tide stations. HAT and LAT were computed using the harmonic constituents available for Santa Cruz at NOAA's Tide and Currents website (http://tidesandcurrents.noaa.gov). Table 1 shows the tidal datums for Santa Cruz. Note in Table 1 that the difference between MSL and NGVD 29 is small (0.06 m) and therefore for the purposes of this study the MSL was considered coincident with the NGVD 29.

The time history of long-term still water levels at Santa Cruz (levels due to the astronomical tide, barometric and wind setup, El Niño/La Niña) were not available. Therefore, these were synthesized generating the astronomical tide using the harmonic constituents available for Santa Cruz and adding the water level anomaly (difference between measured and predicted) for Monterey to account for effects other than the astronomical tide. Given its close proximity to Santa Cruz, the water level anomaly for Monterey was considered representative for Santa Cruz.

Table 1. Tidal datums for Santa Cruz.

		re MLLW[1] (m)	re MLLW[1] (feet)	re NAVD 88 (m)	re NGVD 29 (m)	re NGVD 29 (feet)
Highest Astronomical Tide	HAT[2]	2.16	7.07	2.23	1.38	4.54
Mean Higher-High Water	MHHW	1.63	5.35	1.70	0.86	2.82
Mean High Water	MHW	1.42	4.65	1.49	0.64	2.12
Mean Sea Level	**MSL[3]**	*0.83*	2.73	*0.905*	0.06	0.20
Mean Low Water	MLW	0.34	1.11	0.41	-0.43	-1.42
Mean Lower-Low Water	MLLW	0.00	0.00	0.07	-0.77	-2.53
Lowest Astronomical Tide	LAT[2]	-0.49	-1.60	-0.42	-1.26	-4.13
North American Vertical Datum	NAVD 88	*-0.07*	-0.24	0.00	-0.84	-2.77
National Geodetic Vertical Datum	NGVD 29[4]	*0.77*	2.53	0.84	0.00	0.00

1. tidal datums per NOAA nautical chart 18685
2. HAT = M2 + S2 + N2 + K1 + O1, (LAT = - HAT)
3. MSL - MLLW = 0.833 m, and MSL - NAVD 88 = 0.905 m as in Moss Landing
4. NGVD 29 - NAVD 88 = 0.843 m

The following sea level rise scenarios were considered in this study:

- sea level rise with no global warming, year 2110 (100 years from 2010)
- sea level rise due to global warming, year 2060 (50 years from 2010)
- sea level rise due to global warming, year 2100 (90 years from 2010)

Due to the absence of long-term water level measurements at Santa Cruz, the sea level rise with no global warming for the year 2110 was computed extrapolating the linear trend of the historical measurements at nearby Monterey.

Sea level rise due to global warming 50 and 90 years from 2010 were selected from Heberger et al. (2009). The A2 medium-high greenhouse-gas scenario, characterized by *"self-reliance and preservation of local identities (IPCC, 2000), and population expected to continuously increase, but economic growth and technological development are expected to be slow"* was selected, between the more and less conservative scenarios A1-F1 and B1. Table 2 lists the three sea level rise scenarios selected for this study.

Table 2. Sea level rise scenarios.

Scenario	Sea Level Rise m (feet)
No Global Warming, year 2110	0.13 (0.44)
Global Warming, year 2060 (50 years from 2010)	0.60 (2.00)
Global Warming, year 2100 (90 years from 2010)	1.40 (4.60)

TOPOGRAPHY AND BEACH PROFILES

Figure 4 shows the topography referred to NGVD 29 at 1-foot intervals, and the location of representative beach transects at which TWL's were computed.



Figure 4. TLB topography and aerial photo (elevations in feet, NGVD 29).

APPROACH AND DEFINITION OF TOTAL WATER LEVELS (TWL'S)

Generated by infrequent storms, extreme water levels are events of relatively short duration that can cause significant damage. The increase of water levels along the

coast above the astronomical tide, hereinafter referred to as the TWL, is mainly due to four distinct effects: barometric pressure, wind and wave setup, and wave runup. At exposed US Pacific Coast locations such as Santa Cruz, the increase of water level due to barometric pressure and wind setup, often referred to as "storm surge", could be a component of relatively minor effect when compared to the potential increase of water level due to wave setup and runup.

The TWL, referred to a datum of choice, is composed of water levels forced by different mechanisms and with different time scales. At one end of the time scale, the MSL exhibits variations in a time scale of years. The Still Water Level (SWL), which oscillates about the MSL, is forced by the astronomical tide and storm surge (wind setup and atmospheric pressure changes), both of which have time scales of hours. Locations on the US Pacific Coast such as Santa Cruz are affected by changes due to El Niño/La Niña which have an intra-annual time scale. Waves breaking on the beach will induce a time varying elevation of the SWL. The static (mean) elevation is often referred to as the wave setup while the swash, with a time scale of seconds, is the amplitude of the time varying elevation. Finally, the wave runup is defined as the set of discrete water-level elevation maxima measured on the foreshore, with respect to the SWL (Stockdon et al., 2006). Figure 5 shows a schematic of these various water levels.

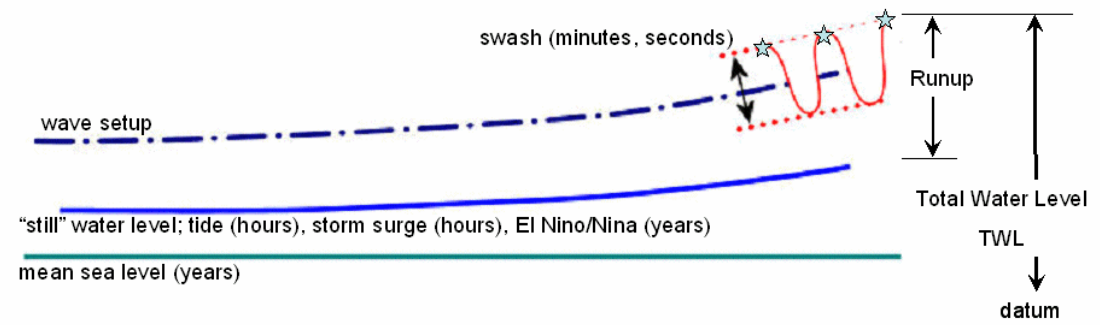


Figure 5. Water levels.

Traditionally, extreme water levels and corresponding flooding risks have been computed using an "event" based approach. At exposed locations on the US Atlantic and Gulf Coasts, where continental shelves are wide and hurricanes deliver strong winds, the risk of extreme water levels can be associated to the risk of the forcing event, a hurricane, given the dominant contribution of the event-induced effects to the total water level. At exposed locations on the US Pacific Coast no single effect is dominant; relatively lower wind velocities, narrow continental shelf widths and narrow wave spectra all combine to make wave setup and runup to be effects of the same order of magnitude as the astronomical tide. Furthermore, all these are statistically independent and their statistical relationships are not well defined. Consequently, the application of joint probabilities, Monte Carlo simulations or empirical methods are difficult and often inaccurate, given the somewhat subjective and simplified definition of the probabilities of the joint effects.

Following FEMA guidelines (FEMA, 2004), a response based approach was used in this study to compute the extreme TWL's, for the three sea level rise scenarios listed in Table 2. A response based approach offers the principal advantage that assumptions concerning the joint probabilities of the astronomical tide, storm surge, swell and seas setup/runup do not need to be addressed, as in an event based approach, since the risk of extreme water levels can be determined from the analysis of the long-term TWL (the response) that result from the combination of these processes, which are obtained from measurements and/or numerical predictions. In many ways, this is a more objective approach since any joint probability assumptions of events and simplifications do not have to be made.

Accordingly, and for each of these scenarios, the wave hindcast computed in shallow water just offshore TLB, was used to force a wave runup model to derive the corresponding long-term runup time histories at selected locations along the project site. The wave runup was added to the predicted still water levels to obtain the TWL time histories. Finally, extreme value analyses were performed to compute the 1% annual extreme TWL (100-year return period) for each sea level rise scenario, and at each selected location.

The SWL was computed adding the tide levels at Santa Cruz and the sea level anomaly at Monterey. Wind setup was computed using the formulation of Kamphius (2000) and wind conditions at the GROW hindcast location. The resulting elevation of the water level due to this effect was added to the SWL. Due to its simplicity and sound experimental background, the parametric model developed by Stockdon et al. (2006) was used to compute the wave runup time histories.

For each sea level rise scenario, TWL's were computed for transects (see Figure 4) A-A', E-E' and FGH. At transect B-B's TWL's were computed by averaging the A-A' and E-E' TWL's. Slopes for these transects were computed from the summer (nourished beach) profiles made available by the County from topographic surveys. The following slopes were considered representative of a typical nourished beach condition.

- slope of profile A-A' = 0.065
- slope of profile E-E' = 0.030
- slope of profile FGH = 0.036

Due to the lack of historical measured beach profiles and the uncertainty in the accuracy of the winter (eroded beach) profiles, slopes for this condition were assumed to be the same as those of the summer (nourished beach) profiles. However, because for the selected sea level rise scenarios the winter (eroded beach) profiles would be mostly submerged, the TWL's computed for these accounted only for wave setup.

For each sea level rise scenario, 100-year TWL's at beach transects A-A', E-E' and FGH were computed by fitting the corresponding 39 annual TWL maxima for the summer (nourished beach) and winter (eroded beach) profiles to the Weibull

distribution. Table 3 lists the 100-year TWL's at TLB for transects A-A', B-B', E-E' and FGH in the summer (nourished beach) and winter (eroded beach) beach conditions, where the TWL at B-B' was computed averaging the A-A' and E-E' TWL's.

Table 3. 100-year TWL's at TLB for transects A-A', B-B', E-E' and FGH.

	TWL (NGVD 29) m (feet)							
	Transects							
	A-A'		B-B' *		E-E'		FGH	
	Summer (nourished)	Winter (eroded)	Summer (nourished)	Winter (eroded)	Summer (nourished)	Winter (eroded)	Summer (nourished)	Winter (eroded)
No Global Warming, Year 2110	4.37 (14.3)	3.99 (13.1)	3.95 (13.)	3.72 (12.2)	3.53 (11.6)	3.45 (11.3)	3.68 (12.1)	3.55 (11.6)
Global Warming, Year 2060	4.87 (16.)	4.48 (14.7)	4.44 (14.6)	4.21 (13.8)	4.01 (13.2)	3.93 (12.9)	4.16 (13.6)	4.03 (13.2)
Global Warming, Year 2100	5.73 (18.8)	5.33 (17.5)	5.29 (17.4)	5.05 (16.6)	4.85 (15.9)	4.76 (15.6)	4.99 (16.4)	4.86 (15.9)

* average of transects A-A' and E-E'

Note in Table 3 that TWL's are higher when there is sand on the beach (summer, nourished) and that TWL's are higher along the A-A' transect than along the E-E' transect. When there is sand on the beach, the runup is composed of the wave setup and the swash (see Figure 5) while during the winter, when the beach is eroded and water levels are anywhere higher than MSL (or in sea level rise scenario due to global warming) the super-elevation of the water level due to waves would consist mainly of wave setup because the beach would be submerged and waves would be reaching the bluffs. Because transect E-E' is milder than transect A-A', runup at E-E' is less than along A-A' because waves loose momentum and dissipate faster on horizontal than on vertical travel. Figure 6 shows estimates of 100-year TWL contours for the three sea level rise scenarios selected, and for the summer (nourished beach) condition. TWL contours between transects A-A' and E-E' were interpolated to provide a smooth transition in the area between the transects.

The TWL's presented in Table 3 can be considered representative, but they must also be considered as preliminary estimates given that:

- the beach topography and slopes used to derive the TWL predictions represent just one of the several configurations that these could adopt after beach nourishment; and
- the computation of TWL's is very sensitive to beach slopes.

More accurate TWL estimates in the project area would require detailed beach topographic surveys for both summer (nourished beach) and winter (eroded beach) conditions and analysis using a wave/hydrodynamic model. No contours were produced for the winter (eroded) condition because no beach topography was available for this condition.



Figure 6. 100-year TWL's (m) for the three selected sea level rise scenarios, summer (nourished beach) condition.

PREDICTED AND OBSERVED TWL'S

A qualitative comparison between a TWL prediction and observation of the storm of February 24, 2008 is presented in this section. The comparison is qualitative because: a) the beach topography at the time of the storm was likely different than the one available for this study and used to plot the TWL contours, b) the beach would erode as the storm develops and slopes change, and c) observations are based on photographs for which time is unknown.

Figure 7 shows a photograph of high water levels at the east end of TLB by Schwan Lake and Figure 8 shows the predicted TWL contour during the peak TWL at transect FGH; the dashed line shows an estimate of the location of local TWL contour after the likely erosion of the berm to the southeast. The comparison is good as the TWL prediction shows water along most of the revetment and the photograph shows a water level slightly below the top of the road, with some rocks exposed, in the culverts area of the lake. The predicted TWL in the Schwan Lake area is +8.95 feet NGVD 29, and the top of the road at the culvert outfall structure has an elevation of +10.11 feet NGVD 29. The water flooding East Cliff Drive is likely due to wave overtopping. However, to the west of the inlet the photograph shows a flooded area larger than predicted. It is noted that the exact topography of the beach during the day of the storm is not known and that the beach may have eroded during the development of the storm providing for a larger floodable area. Figure 9 shows the significant wave height (Hm0) offshore TLB, the SWL and TWL time histories

during the storm. Note that if the storm would have arrived a couple of days earlier the maximum TWL could have reached 100-year levels as the storm would have coincided with a spring tide.

Estimated conditions during the peak TWL at transect FGH were: peak TWL at 2/24/08 9:00 (GMT); significant wave height = 3.05 m (10.02 feet) (offshore TLB); peak period = 17.7 seconds; mean wave direction = 209 degrees; SWL = 0.78 m (2.57 feet) NGVD 29; TWL (summer beach profile) = 3.32 m (10.9 feet) at transect A-A', 2.60 m (8.53 feet) at E-E', and 2.73 m (8.95 feet) at FGH.



Figure 7. Water levels at the Schwan Lake inlet during the storm of 2/24/08.

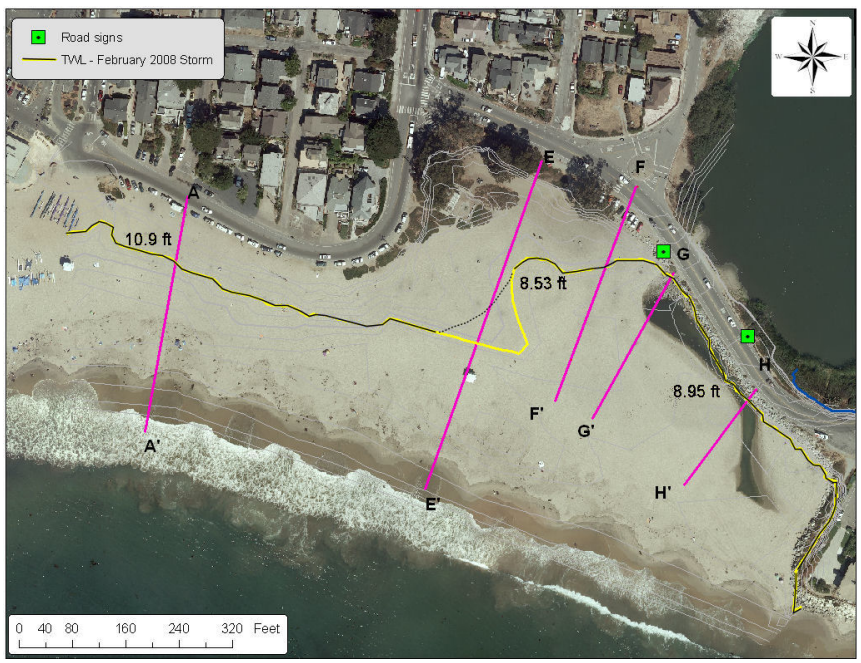


Figure 8. Predicted TWL during the peak of the storm of 2/24/08.

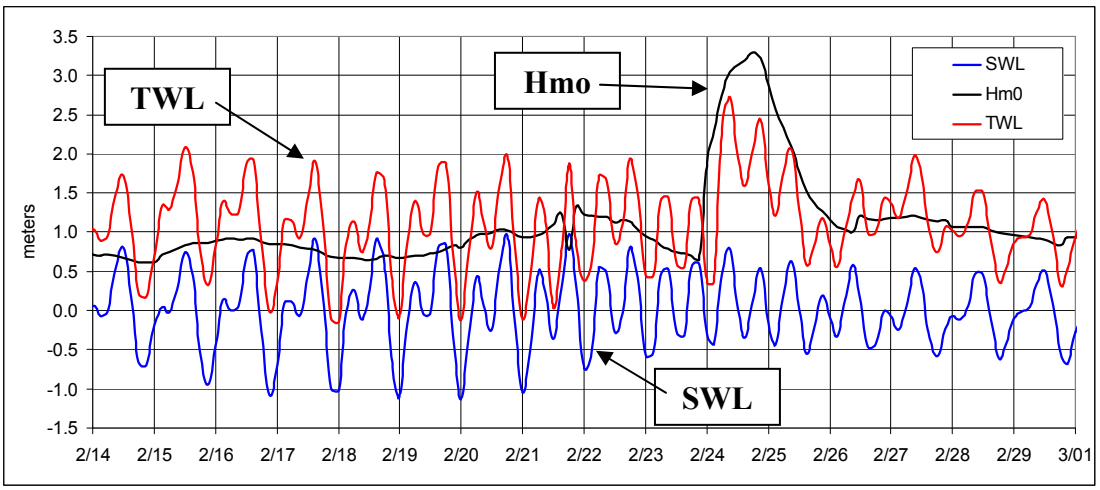


Figure 9. Offshore significant wave height (Hm0), SWL and TWL at transect FGH around 2/24/08 (GMT).

WAVE OVERTOPPING

Mean overtopping discharges at various locations along the TLB were computed to estimate appropriate elevations to minimize damage due to overtopping for the type of coastal protection structures selected. Use was made of NN_OVERTOPPING, a neural network-based prediction tool developed by Delft Hydraulics as part of the CLASH project. NN_OVERTOPPING predicts mean discharges based on 8,372 input-output combinations obtained from measurements performed in hydraulic scale models.

As opposed to the simplified representation of the structures used by empirical formulations, the representation of the structure and wave conditions in NN_OVERTOPPING is achieved by means of a set of 15 parameters. Figure 10 shows an example of parametrization for one of the seawall types considered along various locations of the TLB coastline, shown in Figure 11. Sections 1 to 9 feature various types of seawalls, while section 10 to 13 features a rock revetment.

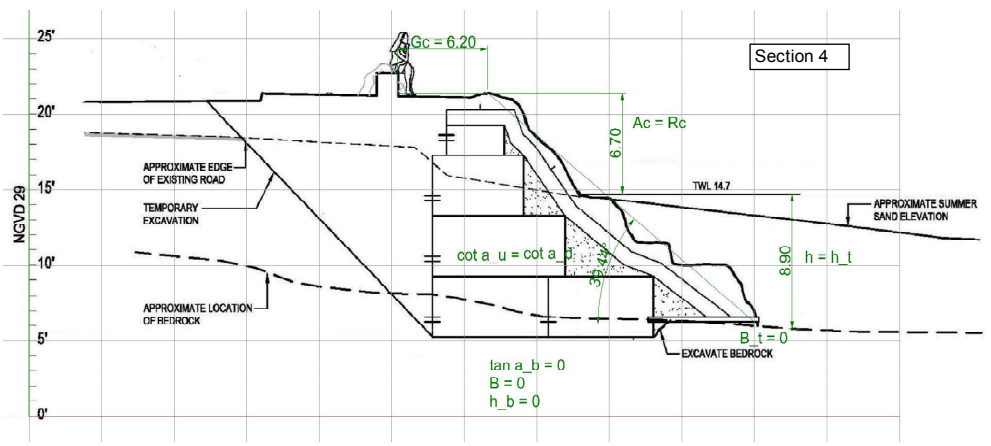


Figure 10. Parametrization of a seawall for NN_OVERTOPPING.

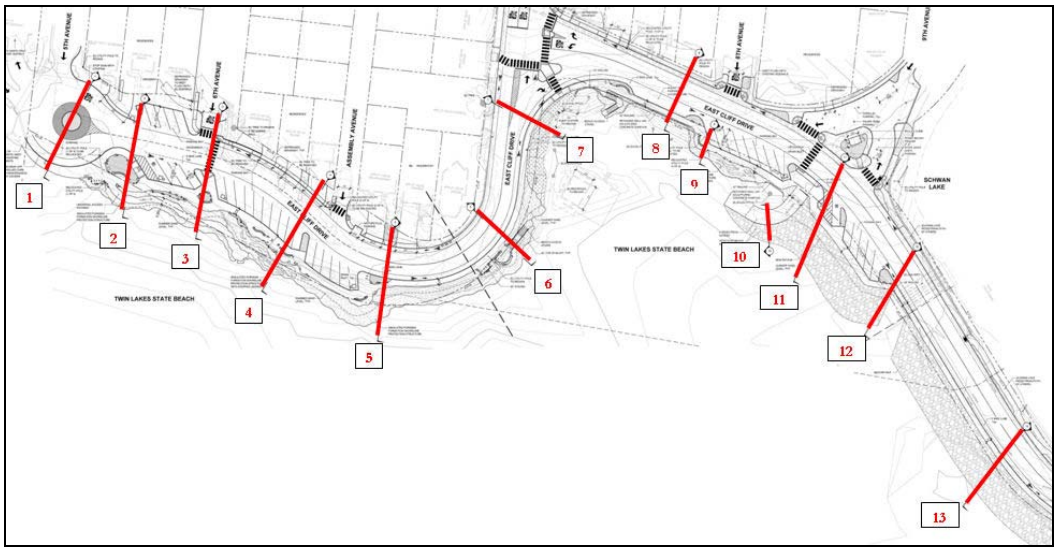


Figure 11. Location of wave overtopping calculations.

Table 4 shows the mean overtopping discharges at the locations (sections) shown in Figure 11, and for the elevations selected for the improvements. These ranged from 18 to 20 feet on the western end of the beach, and 19 to 13 feet (NGVD 29) in the area fronting Schwan Lake. The 50-year sea level rise prediction due to global warming was used in the analysis for sections 1 to 9, given the selected estimated lifetime of the improvements of 50 years in that area. From section 10 to 13 the existing road would require a significant change in elevation and therefore calculations were performed for a sea level rise scenario with no global warming. Highlighted sections indicate locations were the 200 l/s/m mean discharge level, used as damage criteria, would be exceeded. As expected, in the event of high water level and waves, the causeway at sections 12 and 13 will experience severe overtopping. At section 1, overtopping should be expected in the event the beach is eroded (winter profile) in that area. However, it must be pointed out that a winter profile at section 1 is hypothetical, and it is a scenario that has not been observed in the recent past.

Table 4. Mean overtopping discharges (Q) at various sections.

Section	Scenario	TWL (feet NGVD 29)	*Wave Angle (deg)	Water Depth (feet)	**Wave Height (feet)	***Wave Period (sec)	Q (l/m/sec)
1	Global Warming Year 2060, Winter Beach Profile	14.7	0	8.3	5.8	14.3	341
2	Global Warming Year 2060, Winter Beach Profile	14.7	0	7.4	5.2	14.3	219
3	Global Warming Year 2060, Winter Beach Profile	14.7	0	5.1	3.6	12.1	40
4	Global Warming Year 2060, Winter Beach Profile	14.7	0	8.9	6.2	14.3	88
5	Global Warming Year 2060, Winter Beach Profile	13.8	0	13.8	9.7	15.4	218
6	Global Warming Year 2060, Winter Beach Profile	13.8	45	13.6	8.4	15.4	167
7							
8	Global Warming Year 2060, Winter Beach Profile	12.9	0	6.2	3.8	14.3	0
9	Global Warming Year 2060, Winter Beach Profile	12.9	0	11.9	7.4	14.3	70
10	No Global Warming Year 2110, Summer Beach Profile	11.6	0	10.6	6.7	14.3	127
11	No Global Warming Year 2110, Summer Beach Profile	11.6	0	10.6	6.7	14.3	116
12	No Global Warming Year 2110, Summer Beach Profile	11.6	0	10.6	6.7	14.3	626
13	No Global Warming Year 2110, Summer Beach Profile	11.6	0	10.6	6.7	14.3	299

* wave angle relative to normal of the structure
** depth-limited wave height
*** mean period Tm1-0 = Tpeak / 1.1

The wave overtopping predictions presented in this study are preliminary and were used only as a initial guidance for determining the adequacy of the selected elevations of the proposed structures. They are not recommended to be used for detailed design, where the assessment of the performance of the proposed structures, from an overtopping perspective, should be done on the basis of hydraulic model tests.

REFERENCES

EUROTOP, 2007. Wave Overtopping of Sea Defences and Related Structures: Assessment Manual. http://www.overtopping-manual.com

FEMA, 2004. Final Draft Guidelines for Coastal Flood Hazard Analysis and Mapping for the Pacific Coast of the United States, Appendix D.4.2. November 2004.

Herberger, M., H. Cooley, P. Herrera, P. Gleick, and E. Moore. 2009. The Impacts of Sea-Level Rise on the California Coast. Sacramento. California Climate Change Center.

Intergovernmental Panel on Climate Change. 2000. Special Report on Emissions Scenarios. Cambridge University Press, UK.

Kamphuis, J. W., 2000. Introduction to Coastal Engineering and Management. World Scientific Publishing.

NOAA Technical Memorandum NESDIS NGDC-20 (2009). Digital Elevation Model of Monterey, California: Procedures, Data Sources and Analysis. http://www.ngdc.noaa.gov/mgg/inundation/tsunami/data/monterey_ca/monterey_ca.pdf

Stockdon, H.F., Holman, R.A., Howd, P.A., and A.H. Sallenger, Jr. 2006. Empirical Parameterization of Setup, Swash, and Runup. Coastal Engineering, 53(7), pp. 573-588.

Determination of Shoreline Evolution: A Case Study

H. Anıl Arı Güner[1], Yalçın Yüksel[2] and Esin Özkan Çevik[3]

[1] Hydraulic and Coastal Engineering Laboratory, Department of Civil Engineering, Yıldız Technical University, P.O. Box 34349, PH +90 212 3832933; FAX +90 212 3835133; email: aari@yildiz.edu.tr

[2] Hydraulic and Coastal Engineering Laboratory, Department of Civil Engineering, Yıldız Technical University, P.O. Box 34349, PH +90 212 3832924; FAX +90 212 3835133; email: yuksel@yildiz.edu.tr

[3] Hydraulic and Coastal Engineering Laboratory, Department of Civil Engineering, Yıldız Technical University, P.O. Box 34349, PH +90 212 3832925; FAX +90 212 3835133; email: cevik@yildiz.edu.tr

ABSTRACT

In the present work, the shoreline changes of a sandy beach in Karaburun, Turkey, are studied by using a numerical simulation model (LITPACK). The work is motivated by the considerable erosion and siltation problems caused a sediment deposition near and inside the harbor entrance which prevented the boat traffic and caused a vital problem for the harbor operations. The study's scope is two-fold: to help in understanding the dynamics of the beach based on results of the field work and to study the responses of this beach by numerical simulation, utilizing the topographic and sediment field data and measured wave data. The validation and verification of the numerical model was perfomed by RTK-GPS measurements. The results of the numerical simulation concerning the coastline evolution are found to be in agreement with the measurements.

1. INTRODUCTION

The coastal zone is a physically dynamic and ecologically sensitive environment which is subject to a variety of anthropogenic pressures (urban growth, industrial development, tourism) and natural (climatic induced) events resulting in significant coastal erosion. It is often densely populated and is a region of commercial, industrial and recreational activity. It is an important environment to be monitored and managed effectively for sustainable use.

The site of the field study is Karaburun coastal village located at the south west coast of the Black Sea at 41°21'05"N and 28°41'01"E, which is Northwest of Istanbul (Figure 1). It has a WNW-ESE general orientation and an extension of approximately 4 km. There is a fishery harbor at the western end of the 4 km sandy beach. The harbor operations are effected by the sedimentation problem due to noncontrollable

sediment transport towards the harbor entrance (Figure 2). Mainly two problems exist in the site; these are (1) shoreline erosion at the updrift and (2) accretion at the mouth of the harbor (downdrift). Since there was not any measure to control the longshore sediment transport in the region, a considerable volume of sediment deposition near the secondary breakwater was observed. Its extension towards the harbor entrance caused a decrease in water depth at the entrance and inside the harbor. In order to develop proper engineering methods, determination of the shoreline change and control of the longshore sediment transport became important.

The sedimentation increased through the harbor after the existing groyne was removed which was close to the secondary breakwater (350 m away from the breakwater). The groyne was removed before September 1996. The other problem for the region is the shoreline erosion. Therefore considerable rate of shoreline change was observed in the site.

Enormous erosion occurred along the beach between 1996 and 2000. However the shoreline reached almost its equilibrium stage between 2000 and 2004. On the date of 16 June 2005, the sand was dredged which accumulated at the entrance of the harbor and near the secondary breakwater.

In this study, the parameters effecting sediment transport in the region were carefully examined. The shoreline change was determined by using both measurement data and the numerical model results.

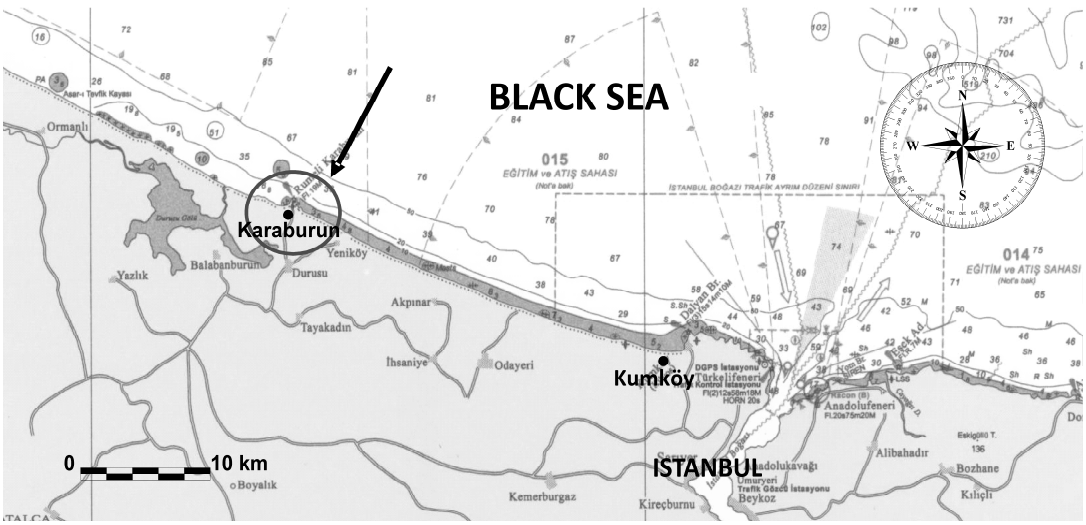


Figure 1. Location of Karaburun Coastal Village



Figure 2. Karaburun Fishery Harbor and the shoreline (looking towards south east direction)

2. METHODOLOGY

2.1 Model Description

Determination of the shoreline change was performed with a widely known numerical modeling system called LITLINE which is a module of LITPACK software package. The model is based on one-line theory for shoreline change modeling.

LITPACK, developed by DHI (Danish Hydraulic Institution), is a software package for simulating non-cohesive sediment transport in wave and currents, littoral drift, coastline evolution and profile development along quasi uniform beaches (DHI, 2008a). The main modules of the LITPACK are: Non-cohesive sediment transport (LST); Longshore current and littoral drift (LITDRIFT); Coastline evolution (LITLINE); Cross-shore profile evolution (LITPROF) and Sedimentation in trenches (LITTREN).

The LITLINE module

LITLINE is the module that computes the changes of a shoreline over a period of time using spatially and temporally varying longshore transport. LITLINE calculates the coastline position based on the input of the wave climate as a time series. The model is, with minor modifications, based on one-line theory, in which the cross-shore profile is assumed to remain unchanged during erosion/accretion.

The coastal morphology is solely described by the coastline position (crossshore direction) and the coastal profile at a given longshore position. LITLINE is applied

in this research on shoreline changes due to natural conditions, protected constructions and research on shoreline recovering measures by artificial beach nourishment. The application of LITLINE is underpinned by the equation of the continuity for sediment volumes $Q(x)$ (DHI, 2008b):

$$\frac{\partial y_c(x)}{\partial t} = -\frac{1}{h_{act}(x)}\frac{\partial Q(x)}{\partial x} + \frac{Q_s(x)}{h_{act}(x)\Delta x} \quad (1)$$

where, $y_c(x)$ is the shoreline position; t is the time; $Q(x)$ is the longshore sediment transport expressed in volume; x is the longshore position; $h_{act}(x)$ is the height of the active cross-shore profiles; Δx is the longshore discretization step; $Q_s(x)$ is the source/sink term expressed in volume.

$h_{act}(x)$ and $Q_s(x)$ are calculated based on user specifications, in which $Q(x)$ derived from the table of sediment transport rate in surf zone. From an initial shoreline position $y_{initial}(x)$, the evolution in time is determined by solving the above equation (DHI, 2008b).

The continuity equation for sediment volumes is solved using an implicit Crank-Nicholson scheme, giving the development of the shoreline position in time.

Input data for the module comprise topography conditions including position of the shoreline, the dune properties, offshore contours and the appearance of the cross-shore profile along the beach, the roughness coefficient of the bed. These parameters are specified based on a coordinate system in which x-axis is baseline quasi-parallel to the initial coastline, and y is perpendicular to x and oriented sea (Figure 3).

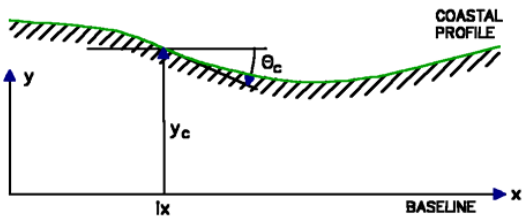


Figure 3. Coordinate system in LITLINE (DHI, 2008b)

Other input data for LITLINE are: sediment characteristics (mean diameter of sediment D_{50}, geometrical spreading); hydrologic conditions, (that is medium sea level consisting of storm surge and tide); wave conditions (wave field depicted into 2D wave table, consisting of parameter of wave height, wave directions and periods). Current conditions: beside the wave-induced current automatically calculated, other factors are also mentioned and directly entered into the program with currents parameters such as speed, direction and other parameters of structure conditions (number, position, apparent dimensions and factors for active dimensions of coastal structures such as: groynes, jetties, revetments, breakwater). Results are the output data of the model shown in graphic and tabular forms, consisting of: (1) Shoreline position in time series (m); (2) Depth of the topographic bed (m); (3) Sediment transport rate (m^3/day); (4) Accumulation of sediment transport rate (m^3); (5) Sediment transport rate unit (m^3/m).

2.2 Model Application

The direction of the longshore sediment transport was determined towards west-north-west (WNW) (towards the fishery harbor) from the field studies and measurements. A considerable amount of sediment deposition in and nearby the Karaburun fishery harbor occurred because of noncontrollable sediment transport.

In the first step of the study, the shoreline evolution between the years of 1996-2000 was investigated. The shoreline measured with RTK-GPS technique on the date of 18 September 1996 was used as the initial shoreline. The RTK-GPS measurements provided an accuracy of 2-3 cm horizontally. Figure 4 shows the shoreline evolution between the years of 1996 and 2000. The shorelines were obtained from RTK-GPS measurements. As seen from the figure, a considerable amount of accretion occurred near the secondary breakwater after the removal of the groyne located 350 m away from the harbor. Maximum accretion of 92 m was observed. In addition, the erosion on the updrift of the beach increased. Maximum shoreline recession length was 45 m.

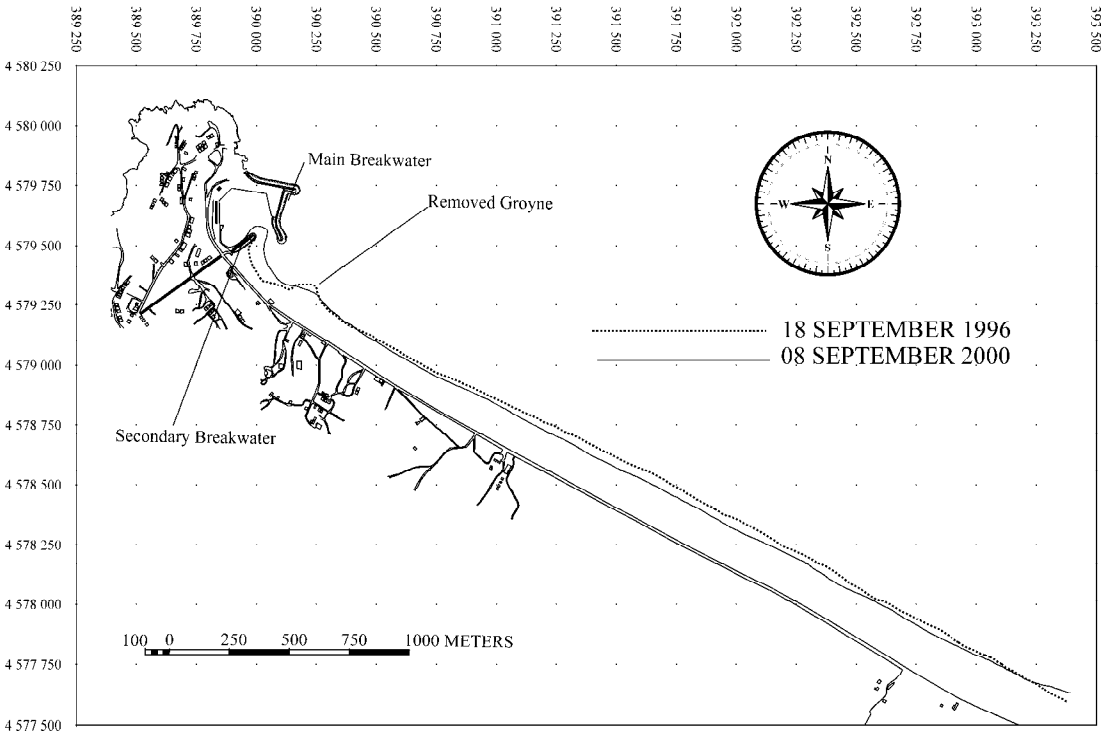


Figure 4. The shoreline evolution between 1996-2000

In the area of study, beach profiling was carried out (September 1996) in order to produce the characteristic profiles and their morphodynamic features. The cross-shore profile bathymetry with the values of bed roughness and grain properties (size, fall velocity and gradation) at each grid point were employed as input for the LITLINE model. Four profiles located at 1000 m intervals were used. Figure 5 reveals the location of the profiles.

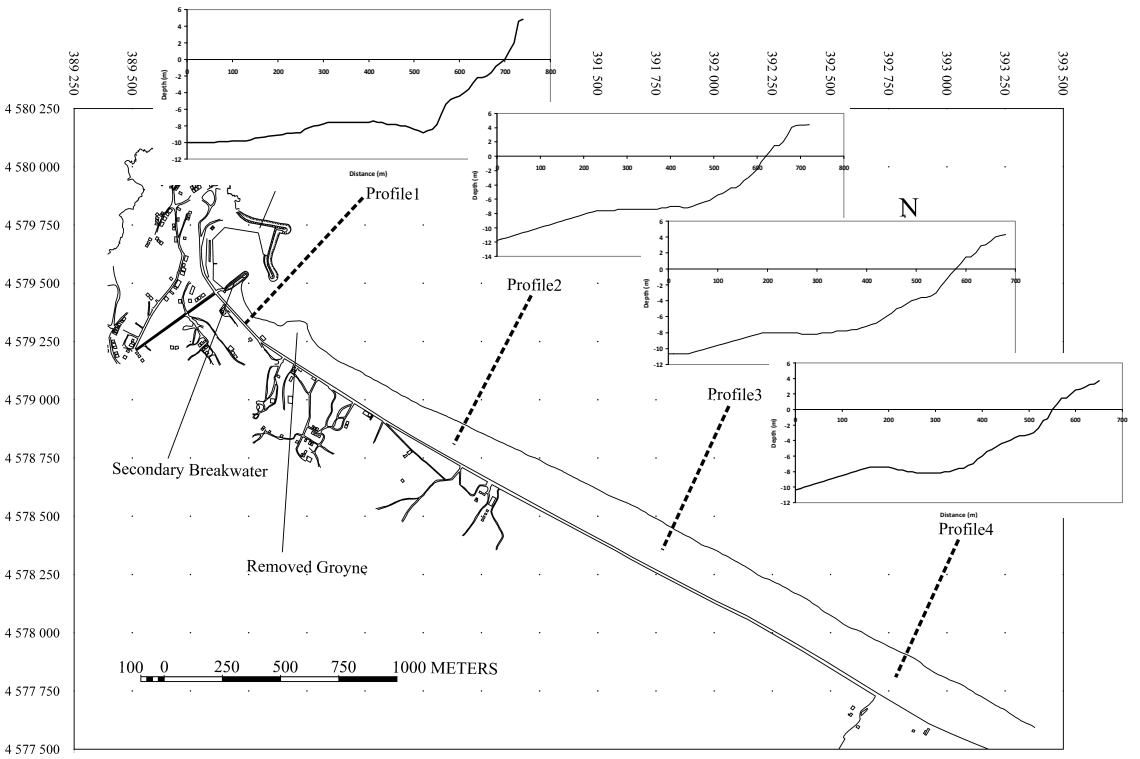


Figure 5. Cross-shore profiles

The input data for the LITLINE module are:

Wave data: It was obtained from a numerical model called MIKE 21 SW (DHI, 2008c) which was developed by DHI. The numerical wave model was calibrated against measured wave data (between the years of 2003-2005) and successfully simulated the wave field of the research area. The wave climates which are extracted from the numerical model are given in Figure 6. Positions for wave climate extractions correspond to the cross-shore profile locations at the depths of -9 m, -11.8 m, -10.6 m and -8.4 m, respectively. The dominant wave directions for both swell and wind waves are north-north-east (NNE), north-east (NE), east-north-east (ENE) and north (N).

Bottom profiles at different coordinates: The cross-shore profiles in LITPACK are described by a line series (one dimensional grid) of the cross-shore bathymetry perpendicular to the coastline in a number of equidistant grid-points, measured from the offshore depth. The first grid point should be at a position where the wave generated shore-parallel currents are negligible (approx. 8-15 m water depth, depending on wave climate) (DHI, 2008b).
The values of the parameters used for all bottom profiles given in Figure 5 are:

- Bed roughness: 0.01 m;
- Median grain size (D_{50}): 1.5 mm
- Fall velocity: 0.12 m/s
- Spreading factor for grain sizes (σ_g) ($\sqrt{d_{84}/d_{16}}$): 1.4

Initial shoreline: Measured shoreline of 1996 was digitized from survey and transformed to the model coordinate system (Figure 4). The modeled region covered 3.85 kilometers of beach. This shoreline reach was modeled by 385 grid-cells 10 m long each. The angle between the shoreline normal and North is 27°.

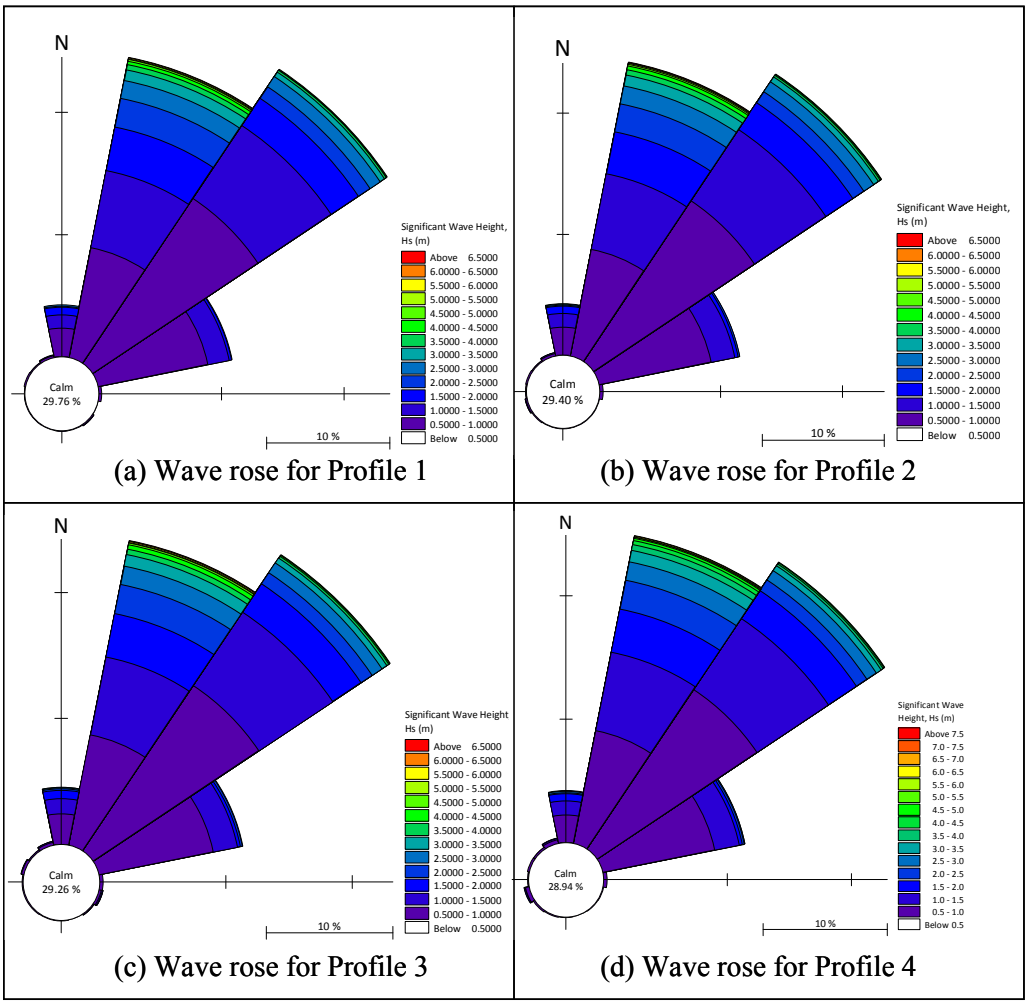


Figure 6. Wave climates at given profiles

Sediment characteristics: Karaburun beach is composed of very coarse sand with an average median diameter of 1.5 mm. The grain size distribution of these samples were determined by sieving. It is well-sorted sand according to the ratio of $D_{84}/D_{16}=2$.

Besides it is necessary to put other data when having constructions such as revetment, groyne, emerged breakwater, submerged breakwater and jetty. The number of construction types and the coordinates depicting the location of each construction are required. In the current work one type of construction namely breakwater at the western end of the beach was used. However the shape of the harbor is not suitable for defining a construction type in LITLINE. Therefore, the

breakwaters of the harbor were idealized as a representative breakwater. This means that the downdrift boundary was assumed as complete barrier.

The simulations were carried out in two phases for the period from September 1996 to September 2000 using 1-hour step generating a total of 34,067 time steps. The first simulation phase from 1996 to 1998 was used for model calibration. Following calibration, the second simulation phase from October 1998 to September 2000 was used to verify the calibrated model.

The first major calibration factor is the net annual drift. Before beginning to calculate the shoreline evolution it must be ensured that the input wave climate provides the sediment transport rates as expected. It is advisable to compute and verify the annual net littoral transport budget before entering LITLINE (DHI, 2008b). This is done by the LITPACK littoral transport module LITDRIFT (DHI,2008d). In the current work, the net annual drift obtained from LITDRIFT was compared with the survey data. The percent error between the measured and the calculated net LST rate (m^3/year) obtained from LITDRIFT was 18.1%.

In LITLINE the "active height" of the profile is a main calibration parameter. The active height $h_{act}(x)$ of the cross-shore profile is composed of two components (DHI, 2008b):

$$h_{act}(x) = D_{act}\langle x \rangle + h_{beach} \tag{2}$$

D_{act} is the active depth, which, as a function of the longshore position, is kept constant in time regardless of the contemporary water level, wave conditions etc. h_{beach} is the height of the "front beach" or berm.

By altering the active depth in shoreline file, the final calibration can be performed. According to the surveys h_{beach} was found to be 6 m. The active depth (D_{act}) varied between the values of 6 m-12 m. The calibration perfomed against the measured shoreline data showed that the most fitting active depth was 10 m for Karaburun coastal region.

Calibration involved determining the sediment transport calibration parameters, appropriately representing the lateral boundary conditions and the cross-shore profile parameters.

4. RESULTS and DISCUSSION

The calibration of the LITLINE was performed using the field measurements. The shoreline change between the years of 1996-2000 was simulated using LITLINE module and compared with the RTK-GPS measurements.

LITLINE simulated the shoreline change between the years of 1996 and 1998. The root mean square percentage error (RMSPE) and normalized root mean square error (NRMSE) were 1.6% and 7.1%, respectively (Figure 7). Following this simulation,

the second simulation phase from October 1998 to September 2000 was used to verify the calibrated model. The root mean square percentage error (RMSPE) and normalized root mean square error (NRMSE) were found to be 1.9% and 5.7%, respectively for this case (Figure 8).

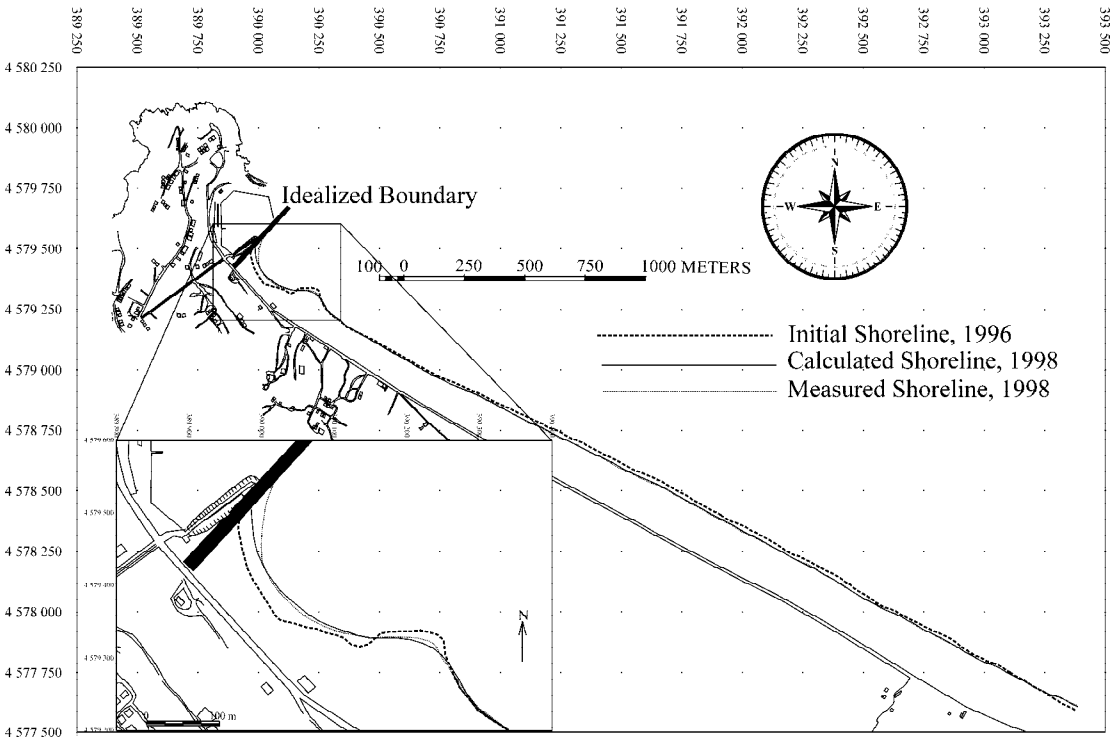


Figure 7. Calibration results (measured vs. model output)

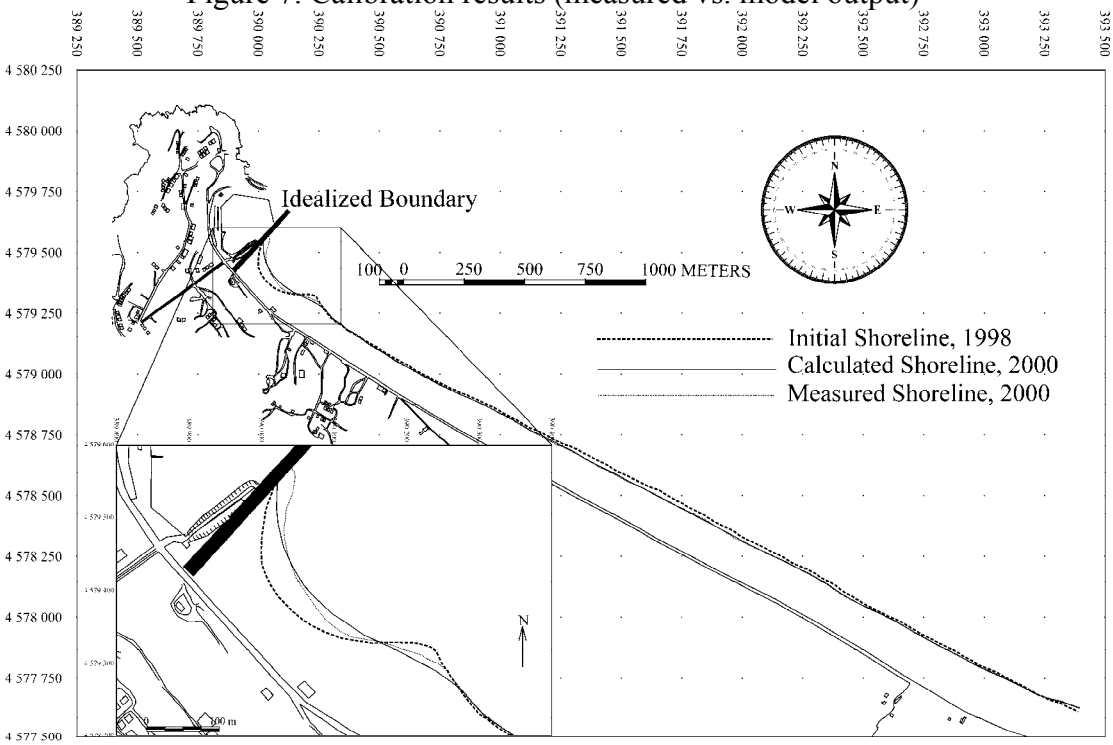


Figure 8. Verification results (measured vs. model output)

The main observations at the study area are summarized as follows.

- The study area is an active beach with an annual net drift amount of 72,000 m^3/year.
- The coastal area was covered with dunes at different heights ranging between 4 m-6 m.
- The removal of the groin after 1996 accelerated the accretion near the second breakwater and entrance of the harbor.
- The Karaburun shoreline reached its equilibrium shape between 2000 and 2004.
- On the date of 16 June 2005, the sand accumulated at the entrance of the harbor and near the secondary breakwater was dredged. This provided safely navigation to and from the harbor.
- The annual net sediment transport direction is towards the harbor from east-north-east (ENE) to west-north-west (WNW).
- The maximum shoreline retreat was 24 m at the updrift of the beach, whereas the maximum accretion was 60 m near the secondary breakwater between the years of 1996-1998.
- The maximum shoreline retreat was 22 m at the updrift of the beach, while the maximum accretion was found to be 32 m near the secondary breakwater between 1998-2000.

The main findings obtained from LITLINE are summarized as follows.

- The most important calibration factor is the net annual drift. The numerical model must be tuned according to the actual sediment transport and its calibration parameters.

- The other calibration factor is the active depth. In the current work, the active depth of the research area was found to be 10 m by altering the values.

- Lateral boundary conditions are also very important. In this study one boundary condition was employed. The geometry of the fishery harbor was not compatible with the LITLINE model. However, representing the harbor as a single breakwater gave reasonable results. But, the active length of the breakwater had a significant influence on the shoreline change. The most fitting length of the breakwater was found to be 350 m. This corresponds to the active depth location.

5. CONCLUSIONS

In the current work, a section of a sandy beach of Karaburun, Turkey, was studied with the use of in-situ measurements and topographic profiles, laboratory sediment analysis and the software package LITPACK, which simulates the sediment transport and shoreline evolution under the action of waves and currents.

The LITPACK model can be successfully applied for simulating, calculating and forecasting orientation of shoreline changes due to erosion and sedimentation process.

The study shows that the prediction of long-term shoreline variation needs field work, analysis, observations and reliable and continuous wind and wave data.

References:

DHI, 2008a. LITPACK-Noncohesive Sediment Transport in Currents and Waves, User Guide, DHI Water and Environment.

DHI, 2008b. LITLINE Coastline Evolution, User Guide, DHI Water and Environment.

DHI, 2008c. MIKE 21-Wave Modelling, User Guide, DHI Water and Environment.

DHI, 2008d. LITDRIFT Longshore Current and Littoral Drift, User Guide, DHI Water and Environment.

Efficacy of Stone Filled Marine Mattresses for Cable Protection in a Nearshore Mixed Sediment Environment

M. Dalon[1], R. Muñoz[2], D. Gaffney, P.E., M. ASCE[3] and J. Fiske[4]

[1]Ocean & Coastal Consultants, Inc., 20 E. Clementon Rd, Gibbsboro, NJ 08026; PH (856) 248-1200; Email: MaDn@COWI.Com
[2]Ocean & Coastal Consultants, Inc., 20 E. Clementon Rd, Gibbsboro, NJ 08026; PH (856) 248-1200; Email: RoMu@COWI.Com
[3]Ocean & Coastal Consultants, Inc., 20 E. Clementon Rd, Gibbsboro, NJ 08026; PH (856) 248-1200; Email: DoGa@COWI.Com
[4]Tensar International Corporation, 2500 Northwinds Pkwy, Alpharetta, GA 30009, PH (770) 344-2090; Email: JFiske@TensarCorp.Com

ABSTRACT

Stone filled polymeric marine mattresses were utilized for the protection of solid core submarine conductor cables. The large diameter cables were found partially or fully exposed, and in a few locations were suspended above the seafloor, extending from the shoreline to approximately 305 meters offshore. The mixed sediment shoreline, where the cables make landfall, is highly dynamic and is exposed to storm energy.

Multiple alternatives were evaluated for post lay protective burial of the cables. Stone filled polymeric marine mattresses were selected because of their low cost and quick implementation to reduce operational and safety concerns. The stone filled polymeric marine mattresses were designed to prevent uplift and slip during local storm events.

A total of 146 stone filled polymeric marine mattresses, measuring 6 meters by 2 meters by 15 centimeters, were used to cover approximately 915 meters of cable. Installation of the mattresses took 11 days. In areas of suspension, stone backfill was utilized to support the cables and the marine mattresses were oriented with lengths perpendicular to the direction of a cable to provide additional scour protection.

Post monitoring of the project includes annual surveys. Initial monitoring efforts have observed marine growth on the structures and localized areas of deposition and erosion surrounding the flexible marine mattresses. These changes are expected and ongoing project monitoring continues to demonstrate that the project is successful.

INTRODUCTION

Large diameter solid core submarine conductor cables were found exposed in the inter-tidal zone of a mixed sediment shoreline. Following an underwater exploratory survey to detect the limits of exposure, discrete areas of various degrees of cable exposure were identified across the inter-tidal zone and into the

sub-tidal zone, approximately 305 meters from the shoreline. The exposure of these submarine cables at the project site creates an operational and safety risk. The nearshore environment is utilized by boats, vehicles, humans, and wildlife. Direct contact with the exposed cable could damage the cable and the object of contact. Furthermore, the loss of supporting sediment allows movement of the cables that could also cause damage. In order to reduce the risk of potential contact and movement of the cables, they must be covered and protected.

The goal of the project was to develop a provisional solution to protect the cables, while a long term solution to the cable exposure was explored and defined. Various environmental and operational concerns dictated that the provisional solution needed to be rapidly deployed and removable. Multiple options were considered. The project team defined the preferred provisional solutions to be a series of marine mattresses placed continuously throughout the limits of exposure. The series of marine mattresses were designed, constructed, and installed to create a single monolithic structure to protect the individual cables from contact and movement. The structure also restricts scour of the surrounding sediment to prevent additional exposure areas. Efforts have followed construction to determine the effectiveness of the marine mattress solution and its efficacy as a long term solution.

SITE CONDITIONS

The exposed submarine cables are located along an open shoreline that is exposed to local wind and wave energy. The shoreline is part of the back side of a terminal moraine that was created during last glacial activity and is characterized by mixed sediments. Although the shoreline is relatively stable, the nearshore environment is dynamic.

The nearshore profile of the project site at the time of exposure is shown in Figure 1. The slope of the beach at the shoreline is relatively steep with a slope of 1:10. The inter-tidal zone is relatively flat with a slope of 1:100 and extends approximately 125 meters from the shoreline. At the edge of the inter-tidal zone there is an offshore shoal that is partially exposed at low tide. This shoal has been documented in historical records and is known to move offshore and onshore. The sub-tidal area beyond the shoal has a slope of 1:60.

Sediment through the area of exposure is mixed in both the horizontal and vertical extents. Surface sediment along the shoreline is predominately sand with area of gravel and cobble. Within the inter-tidal zone the sediment is mainly gravel and cobbles with sand and shells filling the voids. The surface sediment along the shoal and the sub-tidal zone is predominately sand. Sediment borings taken at the shoreline, inter-tidal zone, and shoal indicate subsurface stratification of sediment. These layers of sand, gravel, and cobble can be seen in erosional scarps along the shoreline as shown in Figure 2.

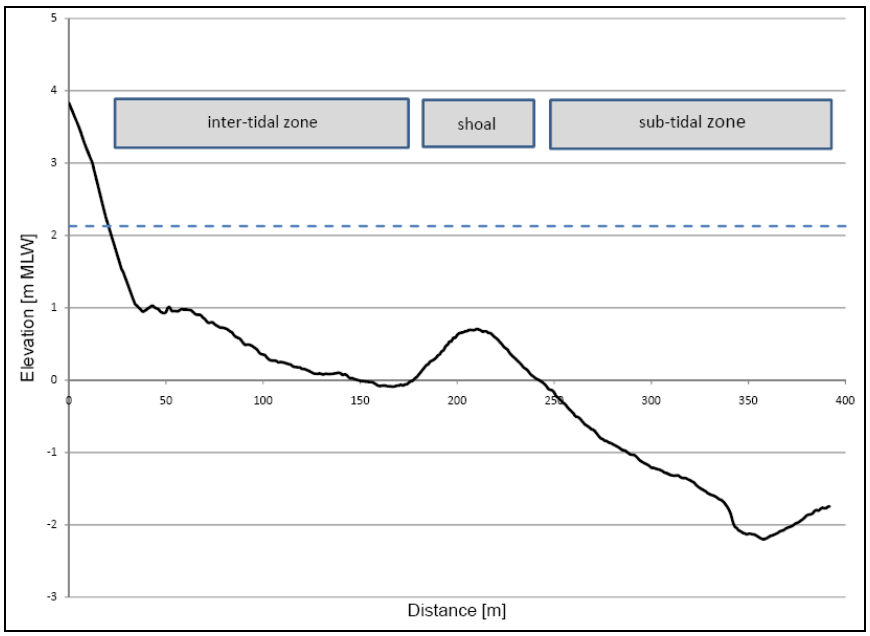


Figure 1 - Nearshore profile in area of exposure



Figure 2 - Mixed sediment at erosional scarp

The shoreline in this area is relatively stable with no longterm erosion or accretion however the nearshore sediment environment is highly dynamic. Sediment transport is predominately alongshore and is caused by periodic local storm events and nearby dredging events. A study of historical bathymetric surveys indicated that there is a sediment envelope of 1.5 meters than can flux on an order of months within the vicinity of the shoal.

Wind, wave and water level data are available through a local wave buoy that records wind and wave measurements and a tide gauge that records water level. The area is dominated by local wind generated waves. The extreme winds in the area are from the west-northwest and east with a 50 years design wind speed of 35

m/s. Records indicate that wave heights greater than 1 meter occur 4%. Wave periods range from 1-7 seconds. There are wind, wave, and tidal currents. The tides in this region are semi-diurnal with a range of 2 meter resulting in tidal currents up to 2 m/s.

CABLE EXPOSURE SURVEY

Following the discovery of the exposed cable in the inter-tidal zone, the limits of offshore exposure needed to be defined. The cables location and level of exposure was identified using sonar, seismic, magnetic, and visual means. Side scan sonar was used to measure underwater cable exposure on the seafloor. Sub-bottom acoustic seismology was used to locate the position and level of existing cover of the underwater buried cables. Magnetic methods identified the location of the buried cables in the tidal zone. Visual methods identified the location of the exposed cables in the tidal zone.

The investigations identified a multiple cables that had a total of six discrete areas of exposure at elevations that ranged from -1 to 2 meters below MLW. The continuous length of exposure cable ranged from 3 to 84 meters. The level of exposure for all but one section was partial exposure. A single location was found where approximately 6 meters of cable was fully exposed and suspended above the seafloor. This area of full exposure was located offshore the shoal in the sub-tidal zone.

DESIGN

Due to the dynamic nature of the seafloor in the nearshore zone it was determined that the cables be continuously protected between the limits of exposure to ensure the immediate safety and operability of the cables. The design team decided that an armor or cover layer be used to provide provisional protection to the cable while a long term solution was explored and defined. The armor layer needed to be durable, stable, flexible, rapidly deployed, removable, cost-effective, proven, and able to be permitted. The project team evaluated multiple cover methods including: split concrete pipe, Seabed Scour Control System (SSCS), Sarmac Mattress, and Marine Mattress. The marine mattress was selected as the preferred provisional solution.

The marine mattress utilized in this project was the Triton Marine Mattress System by Tensar International Corporation (Tensar). The Triton Marine Mattress is fabricated with Tensar geogrid, braiding, and stone. The Tensar polymeric geogrid is the back-bone of the marine mattress. It is manufactured using polypropylene resins with 2% (minimum) carbon block for UV protection resulting in a durable material that is highly resistant to environmental, chemical, and UV degradation. The estimated service life of the geogrid is greater than 50 years (Tensar 2010). A UV stabilized braid composed of high density polyethylene (HDPE) was used to secure the components of the geogrid to form the mattress. The stone used to fill the mattress was specified to have a minimum and maximum dimension to be 4 and 15 cm, respectively. This size stone alone would be mobile in the project environment, however when contained within the marine mattress the stones and the structure are stable. A 60 cm wide nonwoven geotextile was attached along the bottom of the mattress to provide an abrasion buffer between the cable and the marine mattress.

Each mattress measured 2 meters wide by 6 meters long by 0.15 meters thick. Baffles every two feet along the mattress were designed to restrict the redistribution of stone along the length of the mattress. Lifting hoops were designed into each end of the mattress to facilitate the placement of the mattresses. To construct the monolithic structure at the project site, the mattresses were designed to be connected using bodkin type mechanical connectors.

The layout design was based on the type of exposure. In areas of partial exposure, the marine mattresses were designed to be installed lengthwise, centered along the cable. This was done to minimize the structure footprint for environmental restrictions and to reduce material and installation costs. In areas of full cable exposure and suspension, the marine mattresses were designed to be placed lengthwise, centered across the cable. This orientation provides additional scour protection to the cable. Small aggregate fill was designed to be placed between the suspended cable and the seafloor to support the cable and the marine mattress. Gaps between adjacent marine mattresses were designed to be no more than 20 cm so they could be connected to create a monolithic structure.

INSTALLATION

In 11 days, a total of 146 stone filled polymeric marine mattresses were used to cover approximately 915 meters of cable. The mattresses were pre-fabricated off site, transported, and installed using marine construction techniques in water depths of 0 to 3 meters. Both the design of the marine mattress and the skilled labor of the contractor allowed for the rapid and effective installation without incident

Each marine mattress was prefabricated off-site by the contractor. The mattresses were individually assembled on a custom platform as shown in Figure 3. Stones meeting the required specifications were placed into the marine mattress structure. Once filled with stone, the geogrid was folded lengthwise over each end of the mattress to form lifting loops and secured with braiding. The completed mattresses were stockpiled and prepared for transportation. Shipments of marine mattresses arrived at the project site daily on flatbed trailers. The mattresses were relocated onto the construction barge with a land based crane and prepared for placement.

The marine mattresses were installed in the nearshore environment utilizing a crane mounted barge and installation crew (Figure 4). The location of each marine mattress was staked (adjacent to the cable) by a survey crew according to the layout design plan. The crane lifted each mattress with a custom built spreader bar that attached to the lifting hoops at each end of the mattress. As the crane slowly lowered the mattress, an installation team guided the mattress to its final placement. Land based crew wading in the inter-tidal zone and underwater divers in the sub-tidal zone were utilized during installation. Adjacent mattresses were then mechanically connected. The ends of adjacent mattresses were to be no more than 15 cm from each other and 95% of the marine mattresses met this specification.



Figure 3 - Off-site fabrication of the marine mattress



Figure 4 - Installation of marine mattress

An as-built survey of the marine mattress was conducted to provide a baseline to future monitoring following the construction of the marine mattress system an. At this time, it was observed that the nearshore environment had begun to adapt to the marine mattresses. Local sediment and shell fragments began to fill the stone voids of the marine mattress as shown in Figure 5 below. Marine wildlife was found to occupy the gaps between mattresses. The long term movement of sediment and the cables as well as the marine environment will be evaluated through a monitoring plan.



Figure 5 - Marine mattress post-installation

MONITORING

To ensure the protection of the cables and the surrounding environment an approved monitoring plan was initiated and approved by the local regulatory authorities to occur over three years. The monitoring plan consists of visual observations following major storm events and annual environmental assessments and surveys of the marine mattresses and cables. During this time it will be determined whether or not the marine mattresses are performing in such a manner to provide a permanent solution, or if additional work will be required to secure the cables and ensure public safety.

The first annual survey was conducted four months after the installation of the marine mattress. Visual observations indicate that the marine mattresses have naturalized to their marine environment. Sediment and shells have migrated within the voids of the stone. Marine growth was apparent on the marine mattresses. Crustaceans were observed to be utilizing the areas in and around the marine mattresses as habitat.

A survey of the marine mattresses discovered sediment erosion and deposition around the marine mattress and the resulting adjustment of the marine mattresses. A summary of the measured horizontal and vertical change of the marine mattresses is shown in Figure 6 and Figure 7. The marine mattresses had an average horizontal and vertical change of 3 and 8 cm, respectively. In the sub-tidal zone the elevation and location of the marine mattress and the cable experience more movement than the inter-tidal zone. Changes in the elevation and location of the marine mattress were measured up to 80 cm. The movement is the result of sediment transport surrounding the mattresses. Multiple marine mattresses were partially and fully covered by local sediment. The flexible nature of the marine mattress allows them to adapt to the local sediment changes without

exposing the submarine cable or suspending the marine mattress above the seafloor. The limits of the marine mattresses movement will be tracked with future monitoring to ensure protection of the cables.

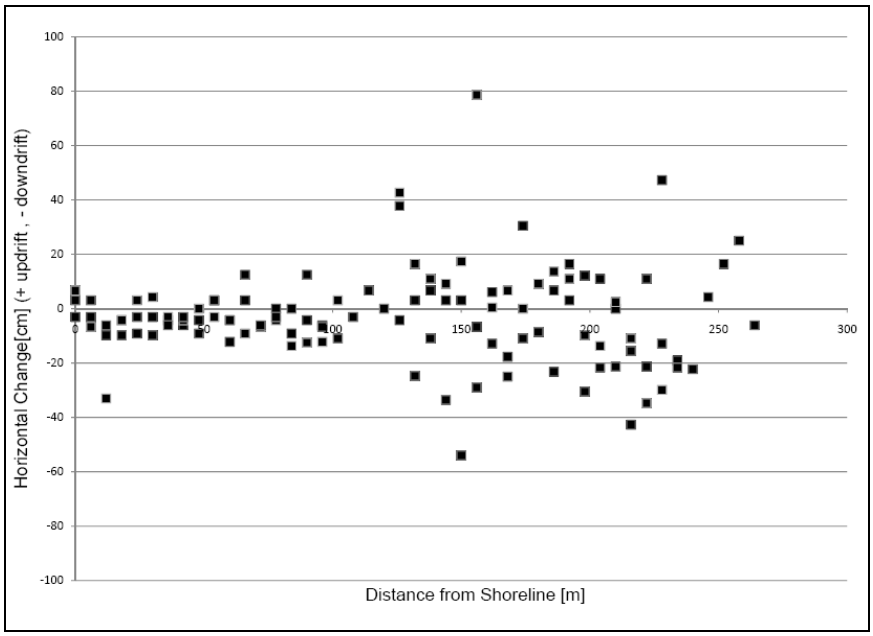


Figure 6 - Horizontal Change of Marine Mattresses

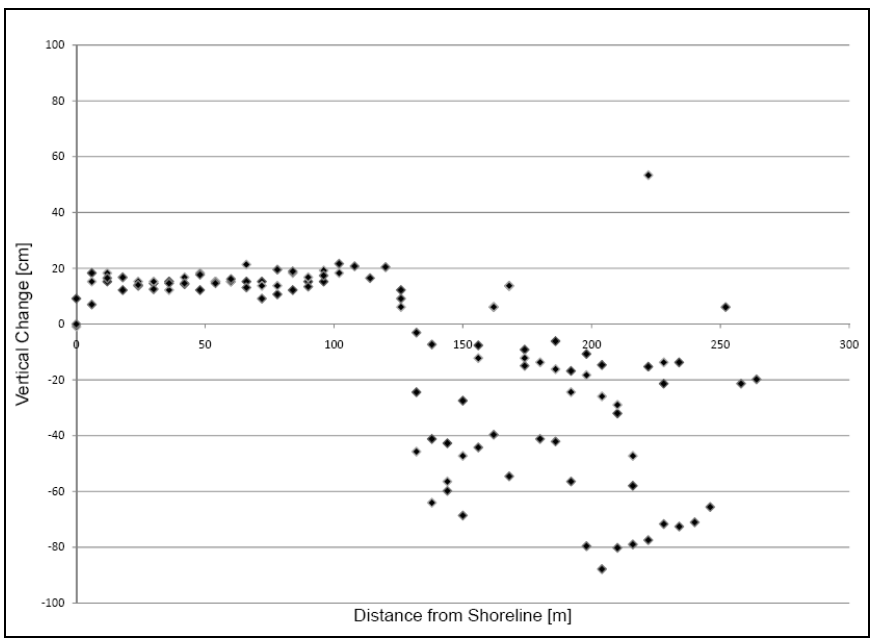


Figure 7 - Vertical Change of Marine Mattresses

Small sections of the marine mattresses in the intertidal zone experienced erosion along the edges of the marine mattresses causing a cross slope or hump to form over the cable as shown in Figure 8 below. The elevation difference between the center of the marine mattress and the edge ranged 6 to 9 cm on the downdrift side and 24 to 60 cm on the updrift side of the marine mattress. The marine mattress was not observed to be suspended above the seafloor. The flexibility of the marine mattress allows the structure to adjust to the changing environment and

will be monitored in the future. To reduce scour along the edge of the marine mattress and the resulting hump, a geotextile scour apron extending beyond the edge of the marine mattress could be used in future applications.



Figure 8 - Marine mattress hump

A redistribution of stone within a single marine mattress was observed in the area of the marine mattress hump. The stones shifted towards the lower elevation at the edge of the mattress leaving a void of stone over the cable and exposing the nonwoven geotextile abrasion buffer attached to the bottom of the marine mattress. The void did not affect the ability of the marine mattress to inhibit scour of the underlying sand and no voids were detected below the marine mattress. To reduce the redistribution of stone across uneven surfaces the spacing on the transverse baffles could be reduced or a series of lengthwise baffles could be added in future applications.

The need for protection was emphasized by the discovery of a small tear on the surface of the marine mattress. The tear was in the vicinity of entangled fishing tackle and is likely the result of a direct strike from a boat. This area was patched with a piece of geo-grid and braiding and will be monitored in the future.

CONCLUSION

To provide provisional protection to an area of exposed submarine conductor cables a total of 146 polymeric marine mattresses were easily constructed and installed by a local contractor over 11 days. The results of the post-construction monitoring show that the flexible nature of the marine mattress is needed to protect the submarine cables in a dynamic, mixed sediment, nearshore environment. Continuing monitoring is in place to evaluate the marine mattress and determine if they can provide a permanent solution to the cable exposure or if alternate means need to be explored and implemented. Future application could utilize a grid of baffles within the mattress to prevent stone redistribution along the length and width of the structure and a scour apron to reduce local scour.

REFERENCES

Hughes, Steven A. (2006). "Uses for Marine Mattresses in Coastal Engineering," ERDC/CHL CHETN-III-72, US Army Corps of Engineers.

NOAA (2010a). Tide Data, National Oceanic and Atmospheric Administration, http://tidesandcurrents.noaa.gov.

NOAA (2010b). Wave Data, National Oceanic and Atmospheric Administration, http://www.ndbc.noaa.gov.

NOAA (2010c). Wind Data, National Oceanic and Atmospheric Administration, http://www.ndbc.noaa.gov.

Tensar (2010). Durability of Tensar Geogrids in Marine Applications, Letter to the Author.

Monitoring Shore Protection Projects along the Florida Panhandle using Three-Dimensional Spatial Data

Lauren M. Dunkin[1], John McCormick[2]

1. USACE ERDC, 7225 Stennis Airport Rd., Suite 100, Kiln, MS 39556, USA. lauren.m.dunkin@usace.army.mil
2. USACE ERDC, 69 Darlington Ave, Wilmington, NC 28403, USA. john.w.mccormick@usace.army.mil

Abstract: Shore protection projects are designed to improve the resiliency of the coastal area, particularly for areas that are vulnerable to extreme storm events. Having multiple surveys for the area allows for change detection of geomorphic features and the condition of the nourishment project to be identified. Methods to identify geomorphic features for change detection have been developed using three-dimensional spatial data to assist in the monitoring efforts of shore protection projects. The spatial variation for the beach system, including the dune peak elevations, beach width, and volume, are monitored for several surveys for change detection and to identify areas of vulnerability, since having dunes and a wide beach increases the resiliency of a coastal region.

INTRODUCTION

Shore protection projects are designed to mitigate erosion effects and improve the resiliency of the coastal area during extreme storm events. Beach nourishment is the most common type of shore protection project because it provides less intrusive impacts compared to structures while providing storm protection and additional benefits for recreation (Dean and Dalrymple, 2002). Having dunes and a wide beach protects upland infrastructure during extreme storm events by reducing the wave energy and allowing sediment to be eroded. The sacrificial sediment is eroded to the nearshore environment, but is not lost from the system and can return during periods of quiescence.

Assessing the morphology of geomorphic features is important for routine monitoring as well as evaluating the impact to the shore protection project after a storm event. Pre- and post-storm surveys are vital to the assessment of damage caused by extreme storm events. The use of airborne lidar (light detection and ranging) to collect topographic and bathymetric data has greatly improved the efficiency and accuracy of monitoring morphological changes as compared to traditional survey methods.

Several studies have shown that lidar data can be used to extract features, such as

dunes, to assess the vulnerability of the region (Houser et al., 2008; Saye et al., 2005; Stockdon et al., 2009), monitor beach nourishment projects (Gares, et al., 2006), and identify the shoreline and change rates (Stockdon et al., 2006).

Engineering projects that are constructed in the coastal environment must perform to the design specification while being resilient to extreme storm events. Shore protection projects are designed to provide improved protection under normal conditions as well as maintain resiliency during storm events. Mapping the spatial variation for a coastal region is invaluable for monitoring coastal engineering projects. High-resolution elevation and imagery data is collected along the U.S. coastline as part of the National Coastal Mapping Program (NCMP) which is funded by the U.S. Army Corps of Engineers (USACE) Headquarters. The NCMP is executed by the Joint Airborne Lidar Bathymetry Technical Center of Expertise (JABLTCX) and the data products are intended to support the coastal engineering and research needs within USACE. Three-dimensional spatial data can be used to enhance the assessment of projects, which are typically monitored using two-dimensional profiles.

The objective of this research is to utilize the three-dimensional spatial data for the development of methods to efficiently monitor geomorphic morphology at a shore protection project site. To show the applicability of using lidar data for change detection and monitoring coastal projects, a 30 km stretch of Bay County, Florida is used to demonstrate the procedure.

METHODS

Study Area

The study area along the Florida panhandle is considered to be critically eroded from the Walton County and Bay County line to St. Andrews Inlet which provides access to Panama City, FL (FDEP, 2007). The narrow beach width of this coastal region makes the area vulnerable to erosion and overwash. The study area is shown in Figure 1 for the 30 km stretch of coast in Bay County, FL. Efforts to slow or mitigate the erosion of sand were initiated by bypassing sand from the inlet to the downdrift beach and constructing a beach nourishment project. The beach nourishment project was constructed after Hurricane Katrina in 2005 due to the severity of erosion caused by the hurricanes of 2004 and 2005. The hurricane seasons of 2004 and 2005 were extremely active with Hurricane Ivan (2004), Hurricane Dennis (2005) and Hurricane Katrina (2005) impacting the area and causing erosion. The beach nourishment project extended the width of the beach which in conjunction with the dunes will provide a natural defense to the upland area.

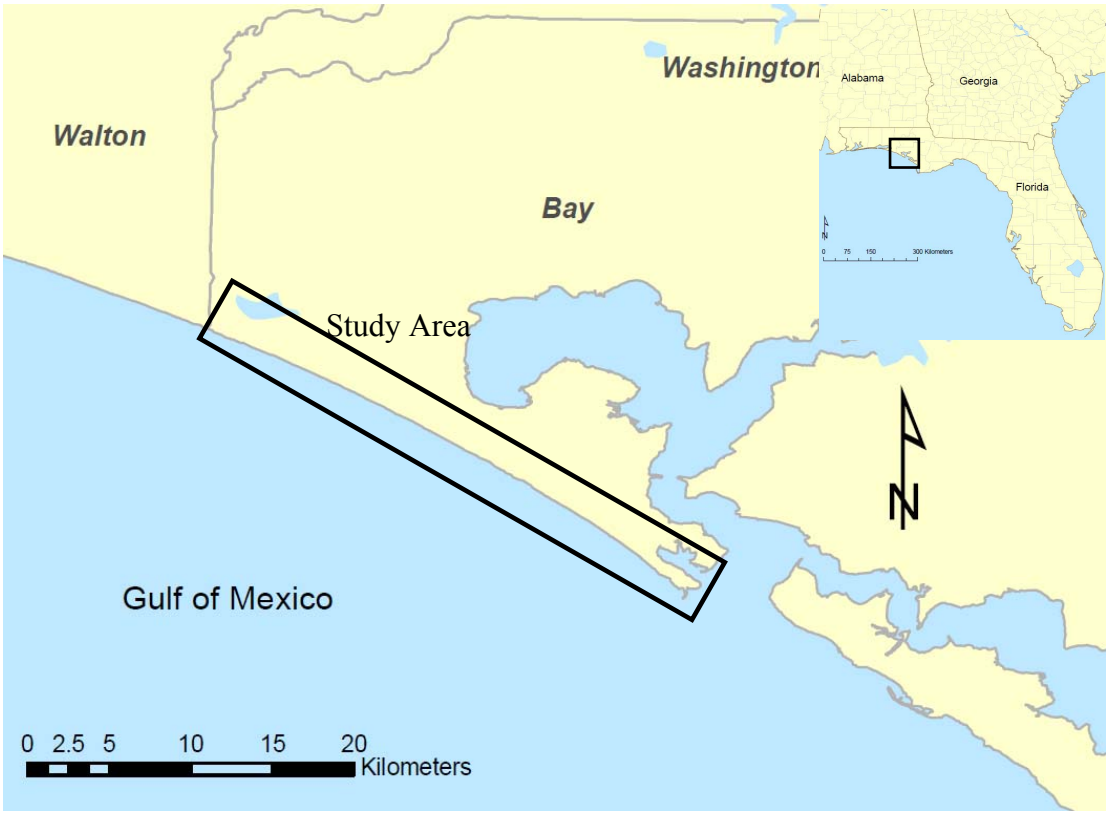


Figure 1. Study area in Bay County, FL

Data

The surveys conducted as part of the NCMP provide complete coverage of the coastal zone on a recurring basis and therefore are ideally suited for monitoring changes to geomorphic and bathymetric features. The data used for this analysis was collected by the Compact Hydrographic Airborne Rapid Total Survey (CHARTS) system which is shared between the USACE and U.S. Naval Oceanographic Office (NAVOCEANO). The CHARTS system includes a 3 kHz bathymetric laser, a 20 kHz topographic laser, an Itres Compact Airborne Spectrographic Imager (CASI)-1500, and DuncanTech-4000 RGB digital camera (Wozencraft and Lillycrop, 2006). The lidar and imagery data collected by the CHARTS system is processed into Geographic Information System products and include bathymetric and topographic Digital Elevation Models (DEMs), RGB orthomosaics, North Atlantic Vertical Datum 88 (NAVD88) shorelines, building footprints, and bare earth grids (Wozencraft et al., 2007). The data is divided into 5km stretches of the coast. This data is uniquely available to address the need for three-dimensional analysis of shore protection projects.

The surveys of Bay County, FL used for this analysis were flown for 1) April-May 2004 (Pre-Ivan), 2) November-December 2004 (Post-Ivan), 3) November-December 2005 (Post-Katrina), and 5) April-May 2006 (Post-Nourishment). This data is uniquely available to assist in storm event assessment when pre- and post-storm surveys exist as well as aid in change detection to identify trends for a complete

understanding of the impacts to the coastal zone due to storm events and assist with monitoring beach nourishment projects.

Data Analysis

Lidar elevation data can be used to monitor morphological changes at shore protection projects when multiple surveys of the area exist. Geomorphologic metrics that are important for monitoring include the seaward dune and the mean high water (MHW) line. The MHW was considered to be a constant elevation of 0.22m which is the MHW relative to the North Atlantic Vertical Datum 1988 (NAVD88). For this analysis, the beach width is considered to be the distance from the seaward boundary at the MHW line to the 2m contour which is considered to be the average elevation for the seaward dune toe. Although the dune toe elevation can vary in elevation and location, a constant value was used for the entire length of the study area. The volume of the beach width can be used to identify areas of vulnerability since having dunes and a wide beach provides protection to upland infrastructure in addition to providing recreational benefits. The assessment of volumetric change from multiple surveys lends insight into the movement of sediment.

The analysis for the study area was divided into 5km sections (Figure 2). Transects were extracted from the bathymetric and topographic DEMs with the resolution of the spot elevation at 1 m with 30 meter spacing interval between profiles. The MHW and dune feature were extracted from these transects using a series of MATLAB codes. The transects were analyzed profile-wise to find the MHW line, 2m contour, peak of the dune, width of the beach, and volumetric changes for the beach width. The data was not smoothed since the raw lidar data was processed before the grids were generated to remove noise. The peaks were found by using the MATLAB signal processing function, “findpeaks” which compares neighboring data points and classifies the local maxima. The volumetric change was determined for each transect for the length of the study area using trapezoidal integration for the beach width. The multiple surveys were analyzed to show the impact from Hurricane Ivan in 2004 and the condition of the nourishment project compared to the survey in 2005 Post-Katrina.

The methods developed for this study could be applied at any shore protection project that has sufficient lidar coverage. The volumetric change of the beach width for individual transect and the total volume change for the entire section were determined to assess the impacts of extreme storm events to the coast and to monitor the beach nourishment project. Having multiple surveys for the area allows for change detection of geomorphic features and the condition of the nourishment project to be identified to assist with recovery efforts and understanding of the movement of sediment.

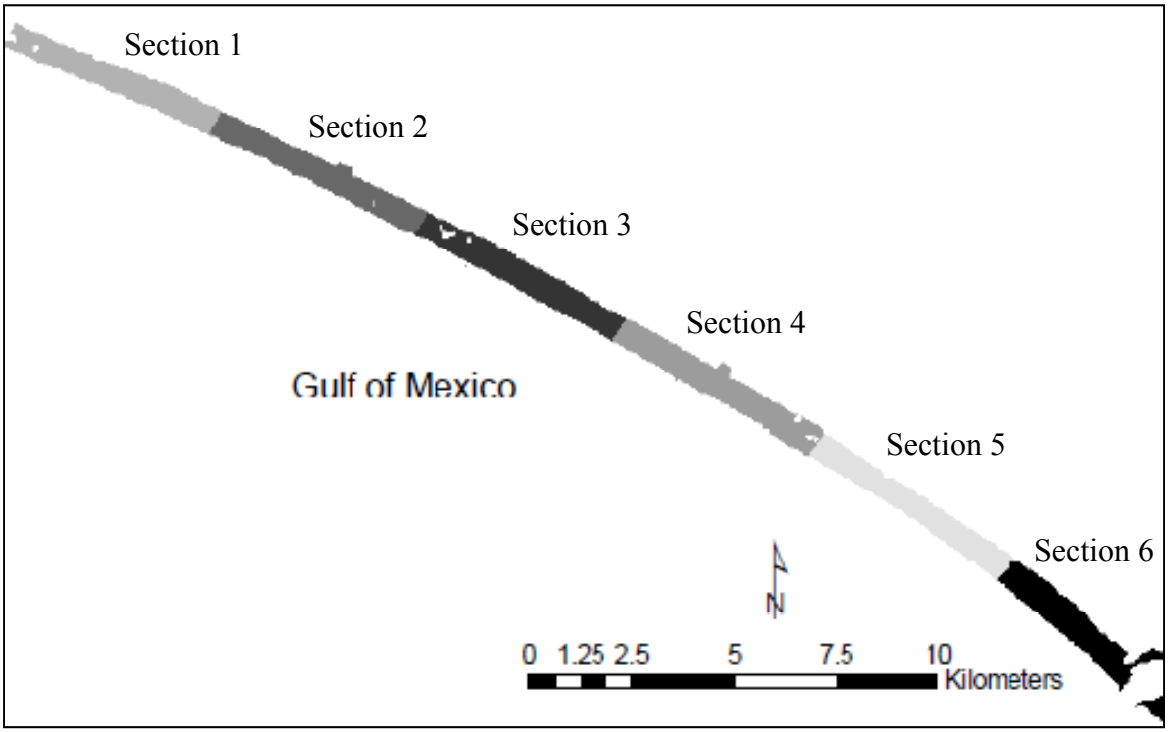


Figure 2. Sections of the study area

RESULTS

Geomorphic Metrics

As mentioned previously, having dunes and a wide beach can provide increased protection during a storm event, so being able to assess these geomorphic metrics and compare the results for multiple surveys is invaluable to understanding the condition of the nourishment project and vulnerability of the region. Dunes with the highest elevation also typically have a wider beach which is measured as the distance from the MHW to the dune toe. The 2004 Pre-Ivan NCMP survey was used as the base survey to compare the 2004 Post-Ivan. Table 1 gives the average dune peak elevation and the average beach width for the sections of the 30km stretch of coast starting at the Walton and Bay County line going east towards St. Andrews Inlet (Figure 1). The average dune peak elevation ranges from 2.5 to 3.5 for the 2004 Pre-Ivan survey. The dune peak elevation location comparison is shown in Figure 3 left. The 2004 Pre-Ivan dune line is seaward of the 2004 Post-Ivan dune line. This is likely a result of erosion to the seaward most dunes caused by the increased wave action during the hurricane. Since the seaward most dunes would provide the first line of defense during a storm event, the increase in the average dune height for the 2004 Post-Ivan survey correlates to having erosion of the seaward dune due to the methodology of the analysis. This is further evidenced by the substantial loss of the beach width for the majority of the sections from the 2004 Pre-Ivan survey to the 2004 Post-Ivan survey. The beach width for the 2004 Pre-Ivan survey is wider for sections 1, 2, and 6. These sections are about 30m wider than the middle sections. However, the 2004 Post-Ivan beach widths are narrower for sections 1 and 2 with the other sections gaining beach

width compared to the 2004 Pre-Ivan survey. The cause of the beach width gain is likely due to the landward shift of the 2m contour location as a result of erosion to the seaward dune. The MHW line for the 2004 Pre-Ivan survey is seaward of the 2004 Post-Ivan MHW line in section 3 (Figure 3 right) as a result of erosion. Since this section experiences beach width gain, the cause is determined to be related to the landward shift of the 2m contour. After Hurricane Ivan in 2004 and Hurricane Katrina in 2005, it was apparent that the area would continue to experience erosion and a beach nourishment project was initiated.

The seaward most dunes from the 2005 Post-Katrina survey and 2006 NCMP are very similar and more consistent with the 2004 Pre-Ivan survey signifying recovery of the seaward dune. In addition, the beach width is the narrowest for the 2005 Post-Katrina survey for all section except section 6 that is adjacent to St. Andrews Inlet. After the beach nourishment project, the beach width increases substantially for the 2006 NCMP survey. The total average beach width for the entire study area increases by about 97m from the 2005 Post-Katrina survey to the 2006 NCMP survey. The beach nourishment project adds sediment to the beach system and thus can influence the location of the 2m contour which is used for the landward extent of the beach width.

Table 1. Geomorphic metrics (m) for each section and survey period

	2004 Pre-Ivan	2004 Post-Ivan	2005 Post-Katrina	2006 NCMP
Dune Height				
Section 1	3.5	4.2	3.4	3.7
Section 2	3.5	4.0	3.3	3.0
Section 3	2.9	3.8	3.0	2.7
Section 4	2.5	3.8	2.7	2.3
Section 5	3.1	3.9	2.7	2.7
Section 6	3.3	4.0	3.5	3.7
Beach Width				
Section 1	138.0	115.5	96.6	112.2
Section 2	137.7	117.5	84.3	107.8
Section 3	103.6	128.1	67.2	104.4
Section 4	103.5	139.7	70.6	99.3
Section 5	120.5	130.2	113.6	115.6
Section 6	143.3	143.8	147.8	138.6

An example of the dune peak line is shown in figure 4 left. The dune peak for 2005 Post-Katrina is landward of the dune peak from the 2006 NCMP survey. The 2006 NCMP survey dune line is likely seaward of the 2005 Post-Katrina survey dune line since the beach nourishment project added additional sediment to the beach system, thereby altering the location of the seaward most dune peak.

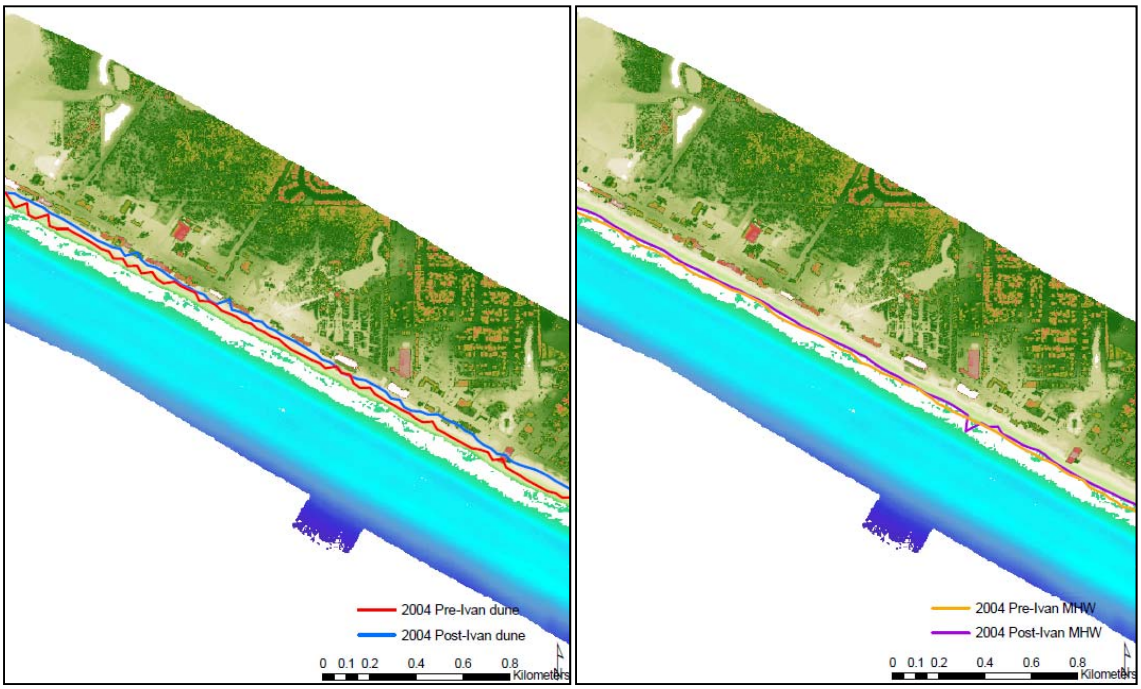


Figure 3. Dune peak and MHW location for the 2004 Pre-Ivan and 2004 Post-Ivan surveys

The MHW line for the 2005 Post-Katrina and 2006 NCMP survey is shown in figure 4 right. As expected, the MHW line for the 2006 NCMP survey is seaward of the 2005 Post-Katrina survey. Interesting to note is that the MHW line from the 2006 NCMP survey is fairly linear where as the MHW line from the 2005 Post-Katrina survey has more of a cuspate trend which is likely a result of the increased waves from the hurricane.

The sums of the volumetric change for each section from the 2004 Pre-Ivan survey and 2004 Post-Ivan survey and the 2005 Post-Katrina and 2006 NCMP surveys are provided in Table 2. The beach width volume change is predominately erosional for the 2004 Pre-Ivan to the 2004 Post-Ivan survey. Figure 5 shows the results for the volumetric changes in beach width for the 2004 Pre-Ivan survey and the 2004 Post-Ivan survey. The accretional areas of the beach volume change occurred in locations where the elevation is higher. The beach volume change for Sections 3and 4 was accretional for this time period as was seen in the beach width change and is likely a methodological response. The blue line is the volumetric change per profile. The red line is smoothed using a local regression using weighted linear least squares and a 2nd degree polynomial model that assigns lower weight to outliers in the regression. The method assigns zero weight to data outside six mean absolute deviations.

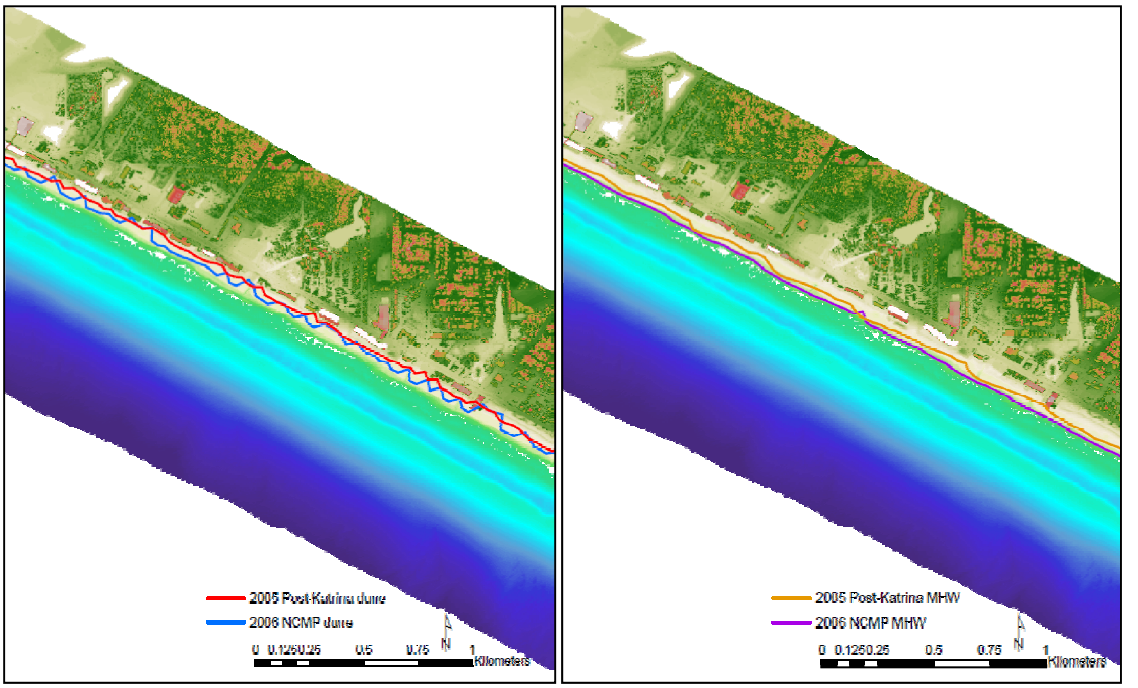


Figure 4. Dune peak and MHW location for the 2005 Post-Katrina and 2006 NCMP (post-nourishment) survey

The volume change of the beach width was predominately accretional for the 2005 Post-Katrina and 2006 NCMP survey except at section 5 where there was slight erosion. As mentioned previously, the location of the landward and seaward extent of the beach width was not fixed; therefore, the volume change could vary and was meant to be an indicator of vulnerability. Figure 6 shows the results for the volumetric changes in beach width for the 2005 Post-Katrina survey and the 2006 NCMP survey that is post-nourishment. As expected, the volume change for the area is predominately accretional. The blue line is the volume change per transect and the red line has been smoothed to remove the peaks associated with the high resolution of the transects.

The width of the beach from the MHW to the dune toe is an important geomorphic metric to consider since having a wide beach can provide increased protection during a storm event. The elevation of the dune is also important because the dunes act as a barrier during a storm event helping to protect upland portions of the coast. The beach widths as well as the elevations of the dune peak are important geomorphic metrics that can be used to assess the condition of the region and the vulnerability to extreme storm events. Retreat and dune loss were the primary results for the post-storm surveys; however, the area gains sediment during a beach nourishment project constructed before the 2006 NCMP survey.

Table 2. Volume change of beach width for various sections

Period	Sections	Sum (m^3)
May 2004 - Nov. 2004	Section 1	-2042
	Section 2	-2042
	Section 3	1617
	Section 4	1885
	Section 5	-533
	Section 6	-1565
	Total	-2681
2005 - May 2006	Section 1	1855
	Section 2	2073
	Section 3	3330
	Section 4	2228
	Section 5	-32
	Section 6	453
	Total	9908

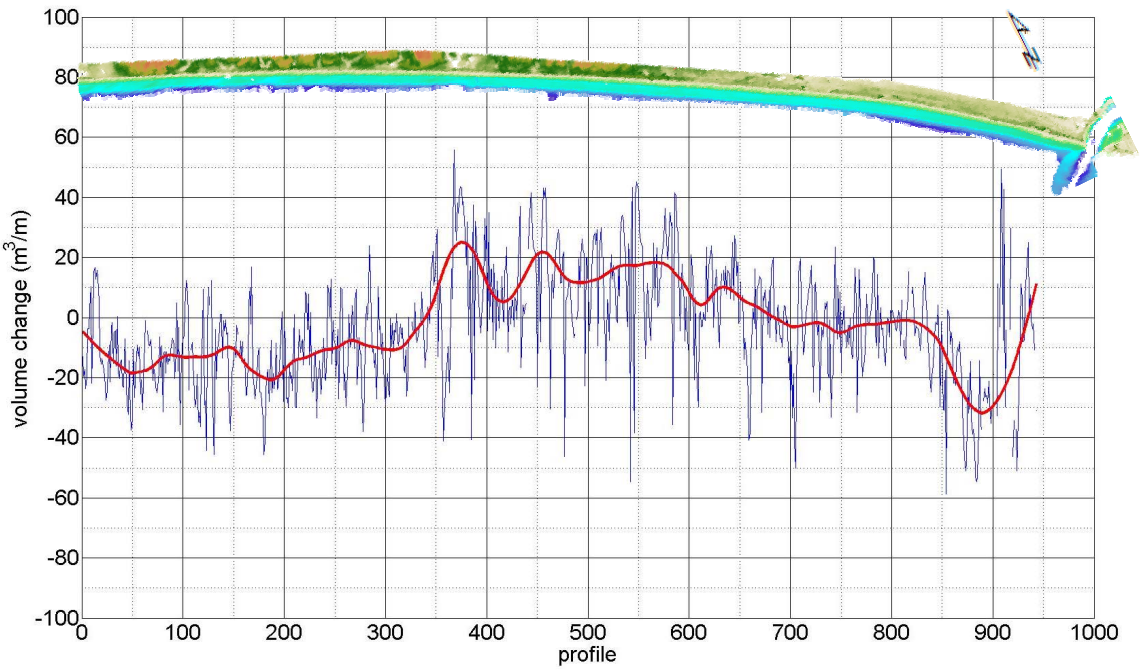


Figure 5. Beach width volume change per profile (blue line) and smoothed value (red line) for the 2004 Pre-Ivan and 2004 Post-Ivan

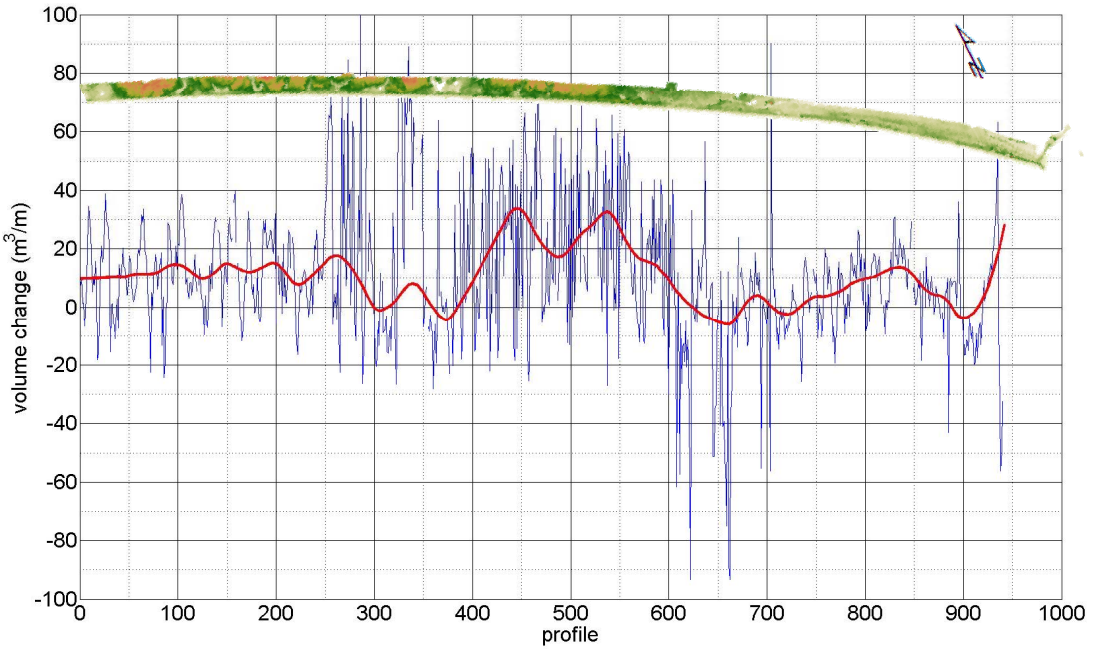


Figure 6. Beach width volume change per profile (blue line) and smoothed value (red line) for the 2005 Post-Katrina and 2006 NCMP (post-nourishment) survey

The use of lidar derived elevation data can be used to assess the condition of a beach before and after nourishment. The lidar data is a valuable asset to coastal planners and managers for storm damage assessment and monitoring beach nourishment projects.

CONCLUSIONS

The geomorphologic features were quantified for several surveys to show the change in areas after extreme storm events and a constructed beach nourishment project. Lidar derived elevation products were used to assess the area after the extreme storm events and the improvements from the beach nourishment project. The 2006 NCMP survey will provide a base post-nourishment survey for subsequent monitoring efforts. The trend for the beach width and dune system was erosional for the 2004 Pre-Ivan and 2004 Post-Ivan surveys. As expected, the beach nourishment project added additional sediment to the system which resulted in net volume gain for the beach width metric for the 2006 NCMP survey. The methods developed using three-dimensional data will enable planners and engineers to efficiently assess the condition of the coastal region and navigation projects, evaluate the vulnerability of these areas and projects to extreme storm events, and predict future conditions for the project life-time. Future goals to improve the procedures and applicability of these methods include defining fixed landward extent for the beach width analysis and performing the study at several shore protection project sites.

ACKNOWLEDGEMENTS

Information presented herein, unless otherwise noted, is based on work funded by Headquarters, USACE, Operations, Construction, and Readiness Division. The use of trade names does not constitute an endorsement in the use of these products by the US government. Permission was granted by the Chief of Engineers to publish this work.

REFERENCES

Dean, R.G and Dalrymple, R.A. (2002). "Coastal Processes with Engineering Applications," Cambridge, UK.

Florida Department of Environmental Protection (FDEP) (2007). "Critically eroded beaches in Florida," Bureau of beaches and coastal systems.

Gares, P.A., Wang, Y., and White, S.A. (2006). "Using LIDAR to monitor beach nourishment project at Wrightsville Beach, North Carolina, USA," Journal of Coastal Research, 22(5), 1206-1219.

Houser, C., Hapke, C., Hamilton, S. (2008). "Controls on coastal dune morphology, shoreline erosion and barrier island response to extreme storms," Geomorphology, 100, 223-240.

Saye, S.E., van der Wal, D., Pye, K., and Blott, S.J. (2005). "Beach-dune morphological relationships and erosion/accretion: An investigation at five sites in England and Wales using LIDAR data," Geomorphology 72, 128-155.

Stockdon, H.F., Doran, K.S., and Sallenger, A.H., Jr. (2009). "Extraction of lidar-based dune-crest elevations for use in examining the vulnerability of beaches to inundation during hurricanes," Journal of Coastal Research, 53,

Stockdon, H.F., Holman, R.A., Howd, P.A., and Sallenger, A.H., Jr. (2006). "Empirical parameterization of setup, swash, and runup," Coastal Engineering, 53 (7), 573-588.

Wozencraft, J.M. and Lillycrop, W.J. (2006). "JALBTCX Coastal Mapping for the USACE," International Hydrographic Review, 7(2), 28-37.

Wozencraft, J.M.; Macon, C.L., and Lillycrop, W.J. (2007). "CHARTS-Enabled Data Fusion for Coastal Zone Characterization," Proceedings of the Sixth International Symposium on Coastal Engineering and Science of Coastal Sediment Processes 2007 (Reston, Virginia, USA, ASCE), 1827-1836.

Myrtle Beach (2001-2010) – Another Decade of Beach Monitoring Surveys after the 1997 Federal Shore-Protection Project

Timothy W. Kana, PhD, Haiqing Liu Kaczkowski, PhD, PE, and Philip A. McKee

Coastal Science & Engineering Inc, PO Box 8056, Columbia, SC 29209-8056; PH (803) 799-8949; FAX (803) 799-9481; email: tkana@coastalscience.com, hkaczkowski@coastalscience.com, pmckee@coastalscience.com

ABSTRACT

Situated in the center of a 25-mile (40-km) arcuate shoreline between Little River Inlet and Murrells Inlet, Myrtle Beach, South Carolina, is the heart of a booming tourist area. However, Myrtle Beach suffered beach degradation in the 1980s. As recently as 1985, much of Myrtle Beach was armored by seawalls and there was little or no high-tide beach. Myrtle Beach was also found to have lost sand between the 1950s and 1980s at rates of 0.5–2.5 cubic yards per foot per year (cy/ft/yr) (1–6 m3/m/yr). Despite the poor natural condition of the beach and constant loss of sand year after year, Myrtle Beach has become one of the best beaches in the United States due to the nourishment efforts by the City of Myrtle Beach (1986-1989) and the federal government (1997 and 2008).

The federal nourishment project was constructed by hydraulic dredge in 1997 using an offshore deposit. Approximately 2.2 million cubic yards (1.7 million cubic meters – m3) were placed along the 9.23-mile-long (14.85 kilometers) shoreline of Myrtle Beach. The average fill density was ~45 cy/ft (113 m3/m). Annual surveys have been performed by the authors since 2001 using a network of 70 profile lines, most of which extend beyond 15-ft (4.6-m) depths (the estimated Depth of Closure) in this setting. In 2008, as planned by the federal government, an additional 1.5 million cubic yards (1.15 million cubic meters) were added to Myrtle Beach, further advancing the shoreline. The average fill density of the 2008 project was ~33 cy/ft (83 m3/m). Survey results show that the net gain between January 1997 and May 2010 represents 83 percent of the nourishment volume placed. Therefore, nourishment losses have been moderate, totaling ~17 percent of the federal fill. The average annual loss rate since 1997 has been ~1.15 cy/ft/yr (2.9 m3/m/yr), which is below the loss rate for the 1986-1989 project (measured within the visible beach to low-tide wading depth). The lower rate partly reflects an incrementally coarser sediment placed in 1997 (~0.3 mm versus ~0.25 mm mean grain size) and no major storms.

PROJECT HISTORY

Like many eroding beach communities in the U.S., the City of Myrtle Beach requested federal assistance to restore and maintain the beach in 1977. The vicinity map of Myrtle Beach is shown in Figure 1. To bridge the typical 20-year period between federal authorization and construction, the City of Myrtle Beach completed an interim beach nourishment project between 1986 and 1987 via trucks hauling sand from inland borrow sources. At the end of the project, a total of 853,350 cubic yards (cy) (652,433 m3) of sand were placed along Myrtle Beach's 8.5-mile-long (13.7 kilometers – km) shoreline at a cost of (~)$4.5 million. At that time, it was the second largest nourishment project ever performed in the United States using trucks and an inland source of sand (CERC, 1984). The interim project was impacted by Hurricane *Hugo* (1989) and a severe northeaster storm in March 1993. The City qualified for FEMA post-storm renourishment funds. Thus, between 1986 and 1990, a total of 1.25 million cubic yards (~1 million cubic meters) were placed on the beach at a cost of (~)$7 million. The average fill density for the two nourishment events combined was ~28 cubic yards per foot (cy/ft) (~70 m^3/m). Annual monitoring for ten years (1986 to 1996) confirmed average annual volumetric losses of ~1.6 cy/ft/yr (~4 $m^3/m/yr$), closely matching the predicted loss rate to low-tide wading depth. Approximately 25 percent of the nourishment remained in place on the visible beach by 1996. Kana et al (1997) summarized the ten-year performance (1986-1995) of the interim beach nourishment project.

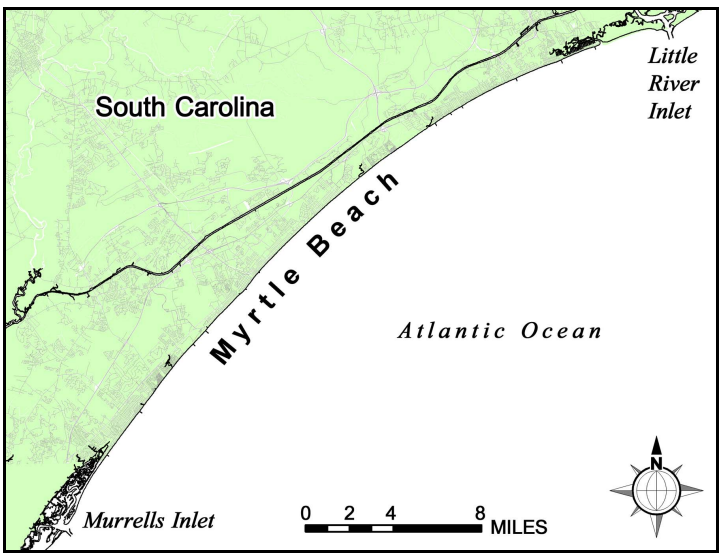


FIGURE 1. Vicinity map of Myrtle Beach (SC).

After the 1986-1987 Myrtle Beach interim nourishment project reached its tenth anniversary, the U.S. Army Corps of Engineers implemented a 22-mile-long (35 km) federal project which encompassed North Myrtle Beach (Reach 1), Myrtle Beach (Reach 2), and Garden City/Surfside Beach (Reach 3) (USACE, 1993). Reach 2 is a 9.23-mile (14.85 km) length of ocean shoreline between 82nd Avenue North and 29th Avenue South (Figure 2). This paper will focus on the 1997 federal project and its performance at Reach 2 (i.e., Myrtle Beach).

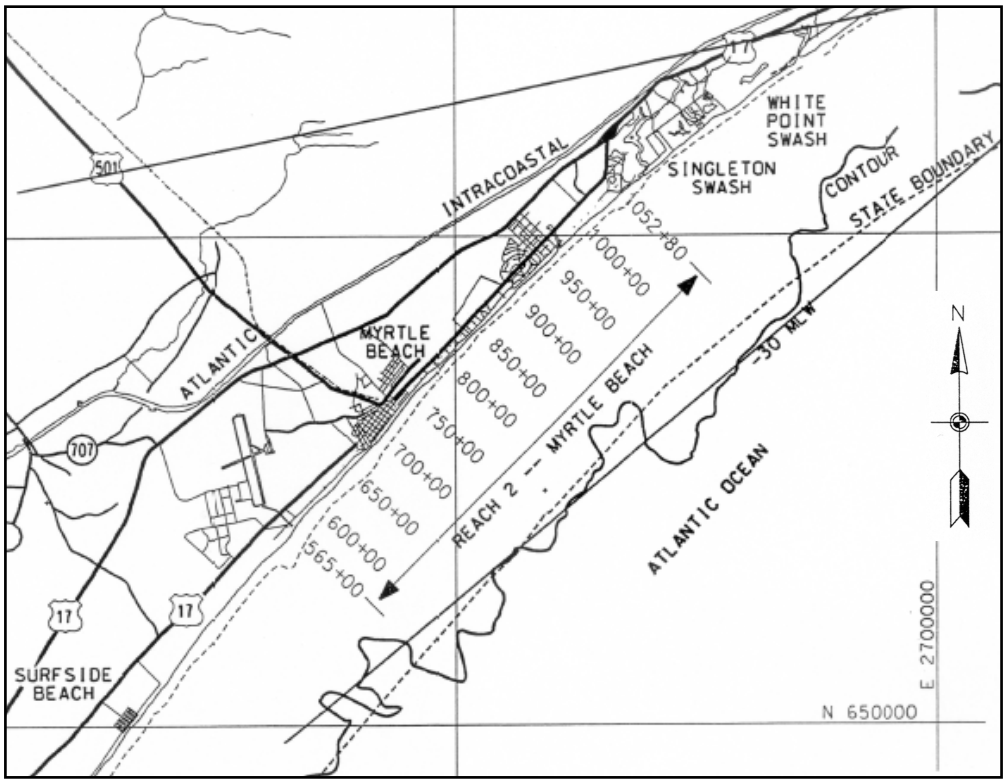


Figure 2. Federal project limits for Reach 2 – Myrtle Beach Shore Protection Project (from USACE 1993).

The federal project was constructed under the authority of the Water Resources Development Act (WRDA) of 1990 (Public Law 101-640). Section 934 of the WRDA of 1986 (Public Law 99-662) authorized federal participation in a 50-year Myrtle Beach shore-protection project, which includes periodic beach nourishment along Myrtle Beach until the year 2046. The first nourishment under this authorization was initiated on 29 January 1997 and was completed 31 December 1997. The 1997 federal project was constructed by hydraulic dredge using an offshore borrow area. Approximately 2.2 million cubic yards (~1.7 million cubic meters) were placed at a cost of (~)$17 million. The average fill density was ~45 cy/ft (113 m3/m).

PROJECT MONITORING REQUIREMENT

The Project Cooperation Agreement (PCA) between the federal government and the City of Myrtle Beach governs construction and maintenance responsibilities. In accordance with the PCA, annual monitoring of the nourishment project is required. The USACE is responsible for the first three annual observations, the City of Myrtle Beach thereafter. The City has retained Coastal Science & Engineering (CSE) since 2001 to complete the annual monitoring. Annual monitoring reports are submitted to the City and the USACE regulatory and listed in the reference section (e.g., CSE 2002,

2010). The present paper is a summary of the project performance between 2001 and 2010 based on the annual surveys.

Project monitoring is performed to track the fate of beach nourishment and document the movement of sand out of the nourishment area. Monitoring provides estimates of shoreline movement trends and identifies areas of erosion and accretion after nourishment, providing important design guidance for future beach projects. Beach monitoring aids in documenting the condition of the protective storm berm and the enhancement of the dune habitat.

The goal of annual monitoring activities is as follows:

- Satisfy USACE requirements under the PCA so that the City remains eligible for federal cost-sharing of nourishment projects.
- Quantify the beach-fill volume and berm width to determine whether the threshold for a renourishment project has been met.
- Evaluate the beach condition and performance of the 1997 nourishment project.

PROJECT SETTING

Annual surveys have been performed by the authors since 2001 using a network of 70 profile lines, most of which extend beyond 15-ft (4.6 m) depths (the estimated Depth of Closure) in this setting. Four reaches (phases) are referenced from north to south following an earlier division of the shoreline (Siah et al 1985) for the 1986–87 nourishment project. Survey stations are shown in Table 1 and Figure 3 along with reach divisions.

Table 1. Project setting.

Reaches	Federal Names	Reach Length		Boundaries
		ft	m	
North	Phase IIN	12,950	3,947	82nd Avenue N to 52nd Avenue N
Residential	Residential	7,762	2,366	52nd Avenue N to 31st Avenue N
Central	Phase IIS	12,257	3,736	31st Avenue N to 2nd Avenue N
South	Phase I	12,314	3,753	2nd Avenue N to ~29th Avenue S
Totals		45,283	13,802	82nd Avenue N to 29th Avenue S

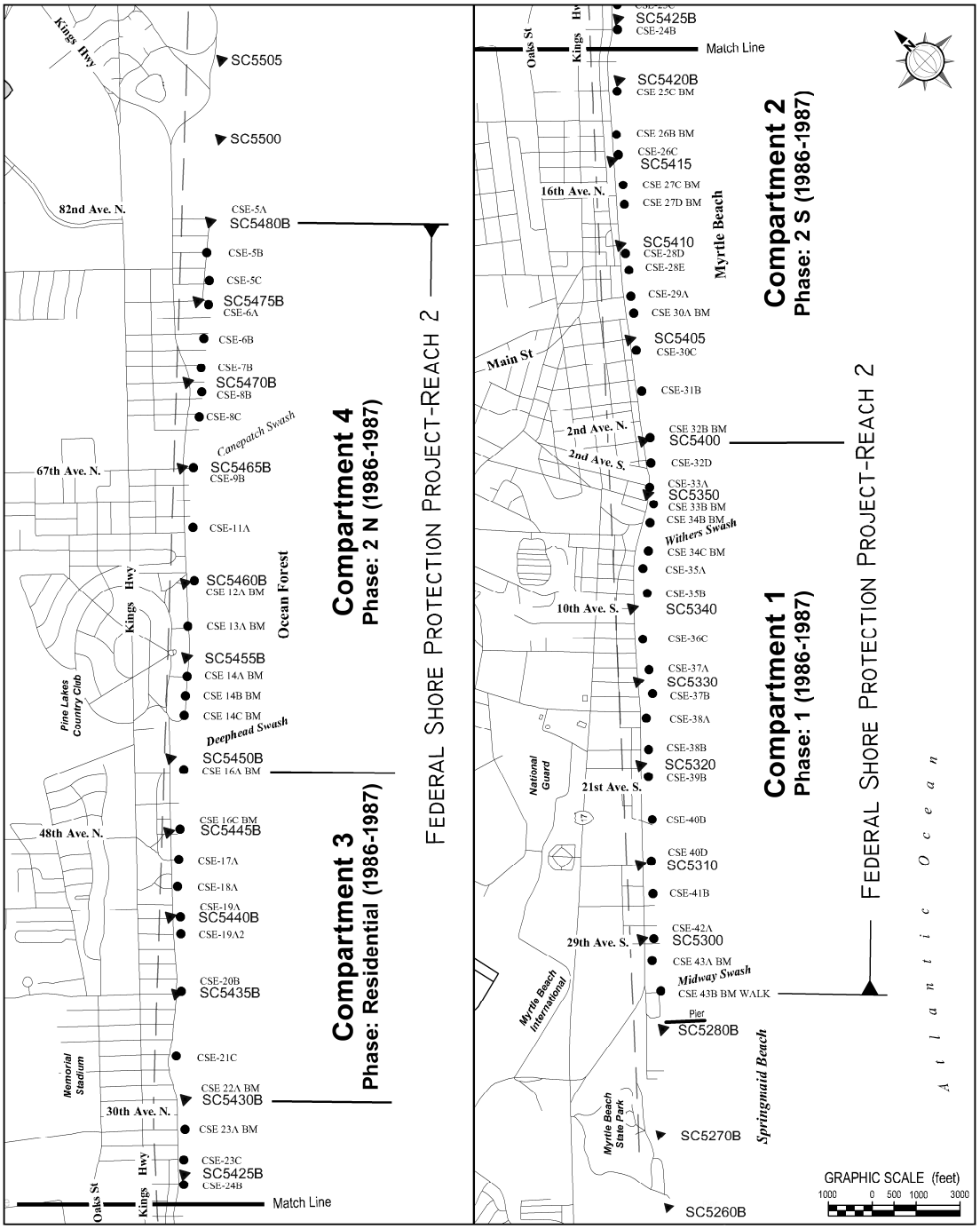


Figure 3. Vicinity map showing the location of permanent state profile stations (5200-5500 series), CSE profiles, and project compartments and reaches.

PERFORMANCE STANDARDS

Standard 1 — Storm-Berm Width

The renourishment criteria of the federal project contains the following:

- Storm protection consists of a berm with a minimum top width of 15 ft (4.6 m) at +9 ft (+2.7 m) NGVD elevation.
- Renourishment is deemed necessary when 25 percent of the berm length is reduced to 15 ft (4.6 m) of width at the +9 ft (+2.7 m) NGVD elevation.

The reason for the above-noted renourishment criteria is historical. Many federal projects were in states that did not have systematic programs for monitoring the coastline with topographic surveys. The storm-berm width can be determined using a one-person set of observations that does not require volumetric topographic surveys. Therefore, in the Project Cooperation Agreement (PCA), the Corps of Engineers established the criteria of storm berm width to estimate remaining protection from storms.

The average storm-berm widths at the state stations are listed in Table 2. Deficit berm widths are defined with respect to the 15-ft (4.6-m) width criteria; therefore, estimated shoreline lengths lacking storm-berm protection can be calculated.

Table 2. Storm-berm widths.

	May-01	Dec-02	Jun-03	Jun-04	May-05	Jun-06	May-07	Jun-08	Jun-09	May-10
Average (ft)	41.6	45.6	40.4	36.1	43.5	47.5	39.7	40.7	62.0	63.6
Average (m)	12.6	13.8	12.2	10.9	13.2	14.4	12.0	12.3	18.8	19.3
Deficit (m)	2,107	780	673	2,551	1,341	629	3,171	3,171	1,908	1,304
Deficit (%)	15.4	5.7	4.9	18.6	9.8	4.6	23.2	23.2	13.9	9.5

For the 2007 and 2008 monitoring seasons, 10,403 ft (3,171 m) of beach failed to meet the minimum 15-ft (4.6-m) storm-berm width requirement, which in this case is 23.2 percent of the entire beach. As stated in the PCA, a failure of 25 percent would trigger renourishment under federal guidelines. As planned by the federal government, an additional 1.5 million cubic yards (1.15 million cubic meters) were added to Myrtle Beach between November 2008 and January 2009. The 2008 renourishment project further advanced the shoreline. The average storm-berm width in June 2009 increased 22 ft (6.7 m) compared to the condition in the previous survey season before the renourishment project. The two federal nourishment events have placed a

total of 3.76 million cubic yards (2.83 million m3) of sand along the Myrtle Beach shoreline, which is about four times the volume placed during the interim projects (1980s).

Standard 2 — Profile Volumes

A more accurate and reliable measure of beach nourishment performance is the computation of remaining sand volume on the beach within certain depth limits. Unit volume (often given in cubic yards per linear foot) is a measure of the amount of sand contained in a unit length of beach. Sand volumes are computed within this one-foot-wide wedge of sand extending from the dune line or seawall to a particular depth offshore.

Unit volumes for each survey date and unit volume changes between selected dates were calculated to determine the quantity of sand in one linear foot of beach at each survey station. These unit volumes were used to calculate the station-to-station net volumes, the subreach net volumes, and finally the net volume for the entire project area. The calculated station-to-station net volumes are proportional to the distance between stations and represent the alongshore distribution of sand volume. These net volumes by reach were subsequently divided by the applicable reach lengths to yield weighted average unit volumes, where the weighting takes into account the variations in applicable shoreline distances from station to station.

Myrtle Beach served as a prototype for applying the concept of profile volumes as a measure of beach conditions (Kana 1993). The methodology was adopted into law under the 1988/1990 South Carolina Beach Management Act.

Volume Computation Boundaries

The calculation limits for volume computations at Myrtle Beach are defined by horizontal lenses. The upper lens is from +10 ft to −5 ft (+3 m to −1.5 m) NGVD and the lower lens is from −5 ft to −15 ft (−1.5 m to −4.6 m) NGVD. The upper lens encompasses the active beach to low-tide wading depth. The majority of the nourishment sand volume was placed in the upper lens, which is the recreational portion of the beach. The lower lens represents the outer surf zone extending to the estimated closure depth which is defined as the theoretical water depth below which there is little measureable change in the seabed elevation due to waves and currents. The estimated closure depth of Myrtle Beach is −15 ft (−4.6 m) NGVD (Kana 1997).

Volume Changes and Volume Remaining

The unit volumes of the two lenses were calculated and compared, and the sum of the volumes of the two lenses was also calculated yielding the total sand volume present in the entire survey zone [+10 ft to −15 ft (+3 m to −4.6 m) NGVD] as shown in Figures 4 to 6. The effect of the federal nourishments can be clearly seen in the increase in volume between January and December 1997 and June 2008 and 2009 in Figure 4. Figure 5 shows the trends in underwater volume between −5 ft and −15 ft (−1.5 m and −4.6 m) NGVD for the four reaches. In this lens, the profile volumes

remained relatively stable in the ten-year period between 2001 and 2010. The volume changes in the underwater region due to nourishment are not as pronounced as in the upper beach region (compare those shown in Figure 4) because a majority of the volume was placed above the low-tide wading depth.

Figure 6 combines the wading depth and underwater unit volumes. These data tend to show smoother trends because they integrate changes over most of the littoral zone. Thus, gains occurring above low water offset losses occurring below low water and vice versa. Between December 1997 and June 2008, there was a net project-wide reduction of 11.5 cy/ft (28.75 m3/m) in unit volume; equating to an average annual loss of ~1.1 cy/ft/yr (~2.7 m3/m/yr) over the ~10.5-year time span. In June 2008, the estimated unit volume calculated from the upper lens was ~305 cy/ft (~762.5 m3/m). In June 2009, the unit volume for the entire survey zone was ~338 cy/ft (~845 m3/m). The 2008 renourishment of Myrtle Beach increased the unit volume by 33 cy/ft (83 m3/m) as made evident by the June 2009 survey. The May 2010 survey found that the unit volume was ~336 cy/ft (~840 m3/m) which indicates 2.6 cy/ft (6.5 m3/m) in unit volume were lost since the previous survey (June 2009). Such faster than average volume loss rate may have been the result of the continuous sand adjustments after the 2008 nourishment project.

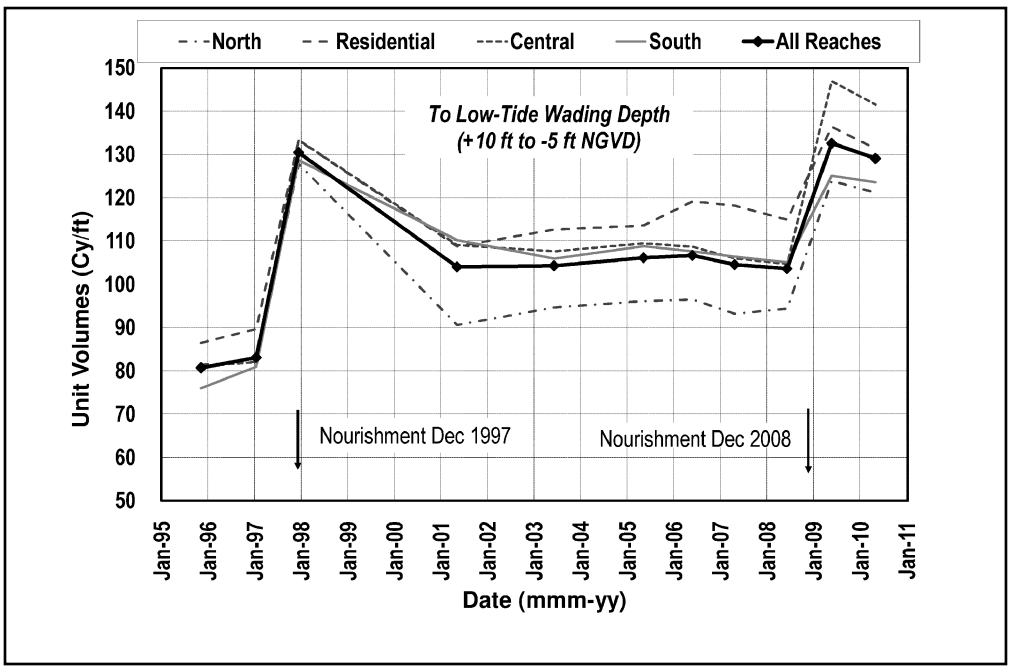


Figure 4. Unit volumes by reach measured between +10 ft and −5 ft (+3 m and −1.5 m) NGVD. [1 cy/ft equals ~ 2.5 m3/m]

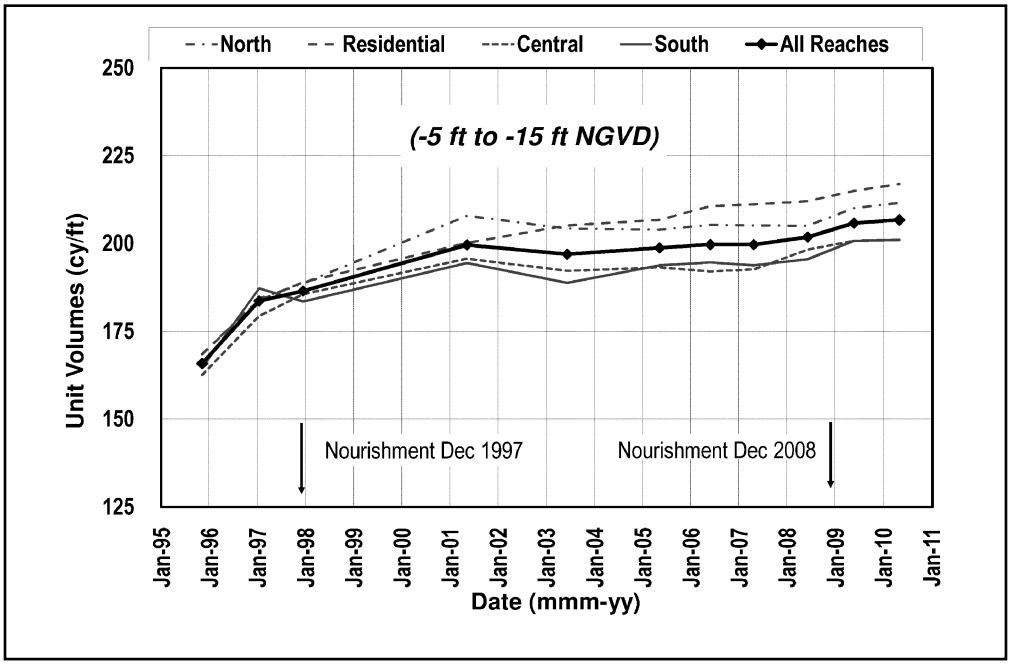


Figure 5. Unit volumes by reach measured between −5 ft and −15 ft (−1.5 m and −4.6 m) NGVD. [1 cy/ft equals ~2.5 m3/m]

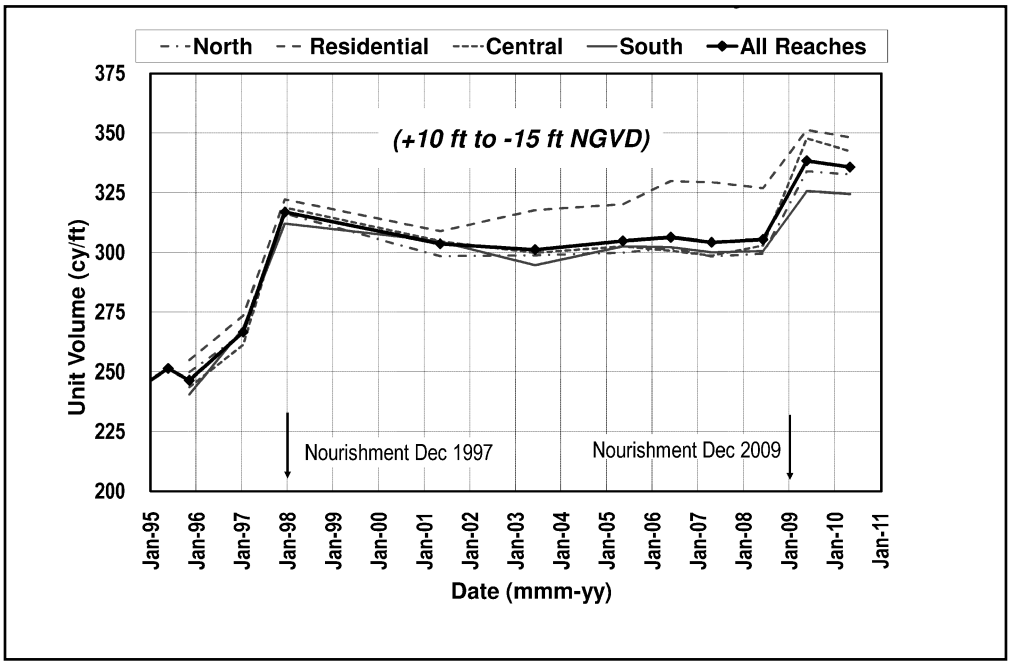


Figure 6. Unit volumes by reach measured in entire survey zone between +10 ft and −15 ft (+3 m and −4.6 m) NGVD. [1 cy/ft equals ~2.5 m3/m]

The net volume of sand remaining was estimated by applying the unit volume calculated at each measured profile over an applicable shoreline distance. The method (known as the average-end-area-method) uses the average unit volume of two adjacent profiles multiplied by the distance between the profile stations to estimate

the volume of sand remaining between the two profiles. The total volume of sand remaining in the project area is simply the sum of the individual section volumes measured to a common vertical datum.

The total sand volumes remaining on the beach in the entire survey zone between +10 ft to −15 ft (+3 m to −4.6 m) NGVD are shown in Figures 7 and 8. Results indicate there has been a net gain of ~1.46 million cubic yards or 3.57 cy/ft/yr of sand (~1.12 million cubic yards or 8.9 m3/m/yr) between May 2001 and May 2010. From the 3.57 cy/ft/yr (8.9 m3/m/yr) net gain, the authors estimate that an average gain in sand volume of 2.78 cy/ft/yr (~7 m3/m/yr) occurred on the recreational beach above low-tide wading depth, while only 0.79 cy/ft/yr occurred in the underwater lens from low-tide wading depth to the closure depth.

It should be observed that before the 2008 renourishment project, the average loss of sand on the recreational beach above low-tide wading depth was only −0.06 cy/ft/yr (−1.5 m3/m/yr) between May 2001 and June 2008. Low rates of change during this period left Myrtle Beach with a relatively healthy sand supply prior to this renourishment.

If the December 1997 post-nourishment condition is used as a reference point, then between December 1997 and June 2008, there was a total loss of 518,685 cy (396,563 m3) over the entire project area, which is equivalent to an average loss of −1.1 cy/ft/yr (−2.7 m3/m/yr) over the 10.5-year period. The Residential Reach performed better than average with a net gain of +0.45 cy/ft/yr (+1.1 m3/m/yr), while the remaining three reaches showed a net loss of sand with the North Reach performing the poorest at −1.6 cy/ft/yr (−4 m3/m/yr). Between May 2007 and June 2008, the North, Central, and South Reaches accumulated sand while the Residential Reach lost sand. Between June 2008 and June 2009, all four reaches gained sand due to the renourishment project, and one year after the renourishment project in May 2010, there was an average loss of −2.88 cy/ft/yr (−7.2 m3/m/yr) in all reaches as illustrated in Figure 7.

Using the January 1997 condition as a reference point, Figure 8 details the nourishment volumes remaining for the project area relative to this pre-nourishment condition for the respective survey dates. Myrtle Beach had an estimated net gain of 3,127,181 cy (2,391,666 m3) of sand in the littoral zone out to the closure depth between January 1997 and May 2010 [measured between +10 ft and −15 ft (+3 m and 4.6 m) NGVD]. Pre- and post-nourishment surveys indicate that the actual sand volume placed during the two most recent projects (1997 and 2008) was closer to 3.76 million cubic yards (2.87 million m3). The net volume remaining in May 2010 represents ~83 percent of the total nourishment volume. Because of the relative coarseness of the remaining sand (compared to pre-nourishment conditions), the lost material is believed to be mostly the fine to medium sand placed during nourishment projects. The lost sand likely migrated downdrift of the project limits, while very fine sand and silt would have migrated offshore beyond the −15 ft (−4.6 m) closure depth.

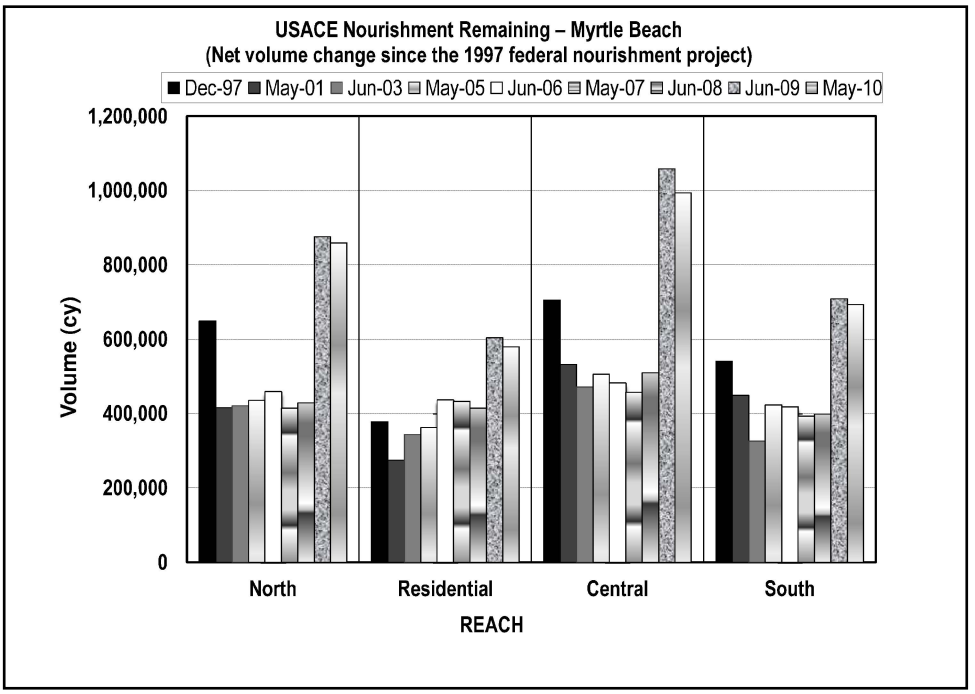


Figure 7. Nourishment volume remaining by reach between the foredune/seawall at +10 ft (+3 m) to closure depth at −15 ft (−4.6 m) NGVD compared with January 1997 conditions (with total volume of ~12.1 million cubic yards) along Myrtle Beach. [1 cy equals ~0.75 m3]

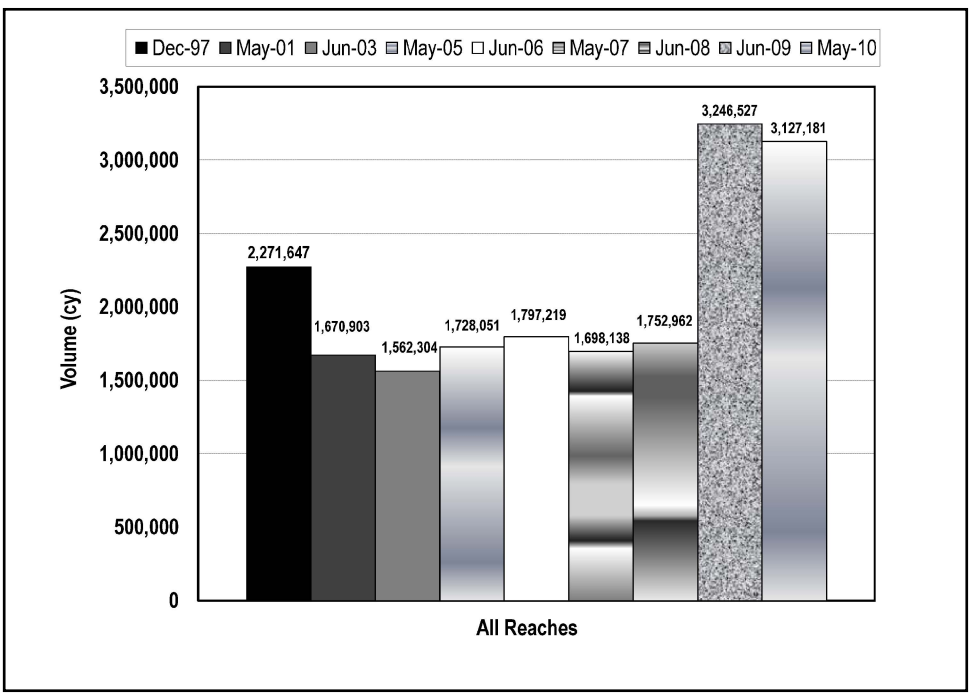


Figure 8. Total nourishment volume remaining between the fore-dune/seawall at +10 ft (+3 m) to closure depth at −15 ft (−4.6 m) NGVD compared with January 1997 conditions (with total volume of ~12.1 million cubic yards) along Myrtle Beach. [1 cy equals ~ 0.75 m3]

OTHER PERFORMANCE STANDARDS

Another requirement under the PCA is a yearly visual observation of the beach along with submission of standard USACE inspection forms. These observations and inspections document the general conditions along the beach. Evidence of erosion or accretion and occurrence of escarpments in the fill, beach cleanliness, public access, and dune vegetation conditions are noted.

Sediment samples at representative stations and several cross-shore positions have also been collected during each yearly survey. The composite texture and grain size at the beach are determined and compared with corresponding values from the previous year. More details can be found in annual survey reports (e.g., CSE 2002, 2010).

CONCLUSION

Survey results show that Myrtle Beach had an estimated net gain of 1.46 million cubic yards or 3.57 cy/ft/yr of sand (1.12 million m3 or 8.9 m3/m/yr) between May 2001 and May 2010. There has been a net gain of 3,127,181 cy (2,391,666 m3) of sand in the littoral zone out to the closure depth between January 1997 and May 2010. The net gain between January 1997 and May 2010 represents 83 percent of the nourishment volume placed. Therefore, nourishment losses have been lower than projected in the USACE (1993) planning documents, totaling ~17 percent of the federal fill. Overall, the beach condition is healthy, and the dune and vegetative cover have matured over this period. Twenty five years after its first nourishment and thirteen years after the 1997 federal project began, the condition of Myrtle Beach is considerably better than pre-project conditions with a wider dry beach, restored protective dune, and buried seawalls (Figure 9). The cost of these improvements has totaled (~)$40 million (2010 adjusted value). This equates to (~)$33/ft/yr ($110/m/yr). The typical oceanfront property value along Myrtle Beach is presently in the range $25,000–$50,000 per linear foot.

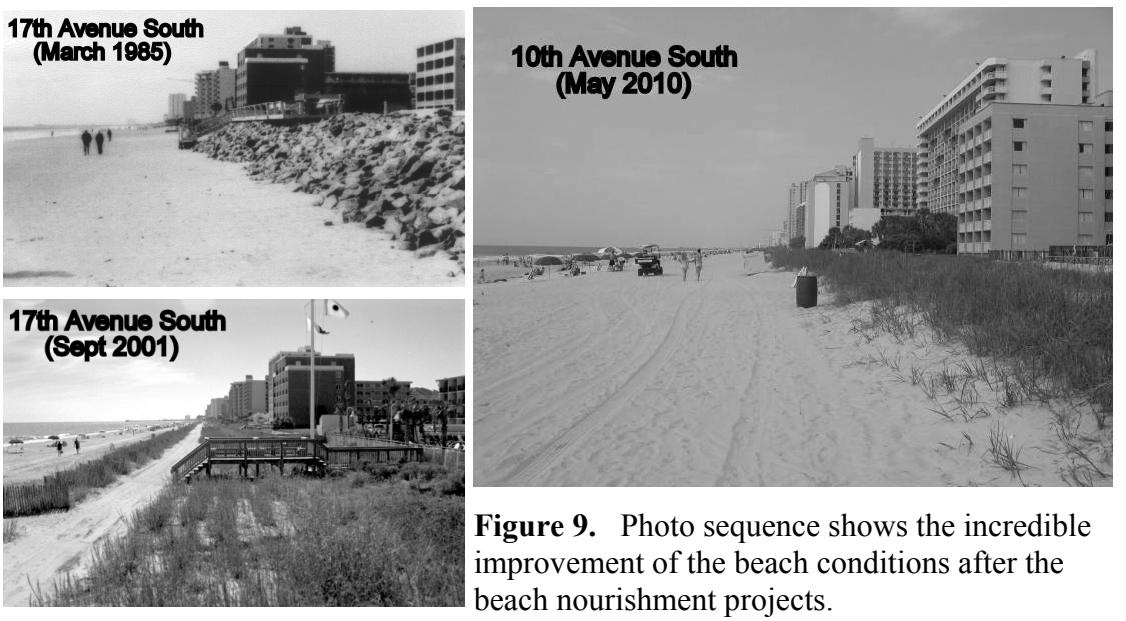


Figure 9. Photo sequence shows the incredible improvement of the beach conditions after the beach nourishment projects.

REFERENCES

CERC. (1984). *Shore Protection Manual*. Fourth Edition, U.S. Army Corps of Engineers, Coastal Engineering Research Center, Ft. Belvoir, VA; U.S. Government Printing Office, Washington, D.C., 2 vols.

CSE. (2002). "Monitoring and analyses of the 1997 Myrtle Beach–Reach 2 shore protection project – 2002 beach monitoring report." Final Report for City of Myrtle Beach; Coastal Science & Engineering, Columbia, SC, 38 pp + appendices.

CSE. (2010). "Monitoring and analyses of the 1997 Myrtle Beach–Reach 2 shore protection project – 2010 beach monitoring report." Final Report for City of Myrtle Beach; CSE, Columbia, SC, 65 pp + appendices.

Kana, T.W. (1993). "The profile volume approach to beach nourishment." In D.K. Stauble and N.C. Kraus (eds.), *Beach Nourishment Engineering and Management Considerations*, ASCE, New York, NY, pp. 176-190.

Kana, T.W., R.E. Katmarian, and P.A. McKee. (1997). "The 1986-1995 Myrtle Beach nourishment project ten-year performance summary." *Shore & Beach*, Vol 65(1), pp. 8-23.

Siah, S.J., E.J. Olsen, and T.W. Kana. (1985). "Myrtle Beach nourishment project." Engineering Report for City of Myrtle Beach. CSE (Columbia, SC), and Olsen Associates, Inc. (Jacksonville, FL), 160 pp. + appendices.

USACE. (1993). Myrtle Beach, South Carolina, shore protection project. *Draft General Design Memorandum*, US Army Corps of Engineers, Charleston District, SC, 46 pp. + appendices.

What's Left of the Malibu Coastline and a Method to Replenish the Beaches

Reinard T. Knur, G.E., C.E.G.

Geotechnologies, Inc., 439 Western Avenue, Glendale, California 91207;
Ph (818) 240-9600, Fax (818) 240-9675; email: rknur@geoteq.com

California State University, College of Engineering and Computer Science, Civil Engineering Department, 5151 State University Drive, Los Angeles, California;
Ph (323) 343-4450, Fax (323) 343-6316

ABSTRACT

Erosion and sand loss from the Malibu coastline has been reported for several decades, but minimal effort has occurred to widen or restore the beaches. The primary focus has been to harden the coastline with seawalls and bulkheads, resulting in poor laterally-accessible beaches with limited recreation or protection value. A comparison of current conditions to those observed over a decade ago revealed that most sections of the coastline have eroded. A few beaches have remained relatively unchanged, and even fewer beaches have accreted.

This paper proposes a long term and sustainable sediment nourishment method by utilizing the multiple, steeply-sloped, ephemeral creeks that discharge to the Malibu coastline. This method requires grading a portion of selected creeks near their ocean outlet to create a flat-bottomed channel to store sediment placed there. When flowing, the creek would then mobilize and discharge the sediment to the coast where natural processes of separation and distribution can occur.

INTRODUCTION

A thesis prepared by the author in 2000 presented a historical sediment budget model for the 56.02 km-long Malibu coastline from Point Mugu to Santa Monica Canyon. The coastline and sand-supplying watersheds within the study area are illustrated on Figure 1. The sediment budget model was created using the Debris Production Area Method by the County of Los Angeles (LACDPW, 1991) and tailoring it for this study. The model was calibrated to the study area by using local debris basin sediment accumulation rates, sediment grain size curves, fire-flood sequences, and dam construction history. The result was an estimate of the average annual sediment yield rate along the entire coast for both pre-development and current conditions. The thesis demonstrated that the sediment yield to the coast was reduced largely due to capture by several debris basins located along the southern slope of the Santa Monica Mountains and by the Malibu Creek watershed, as well as due to the loss of erosion caused by coastal armoring and coastal development (Knur, 2000).

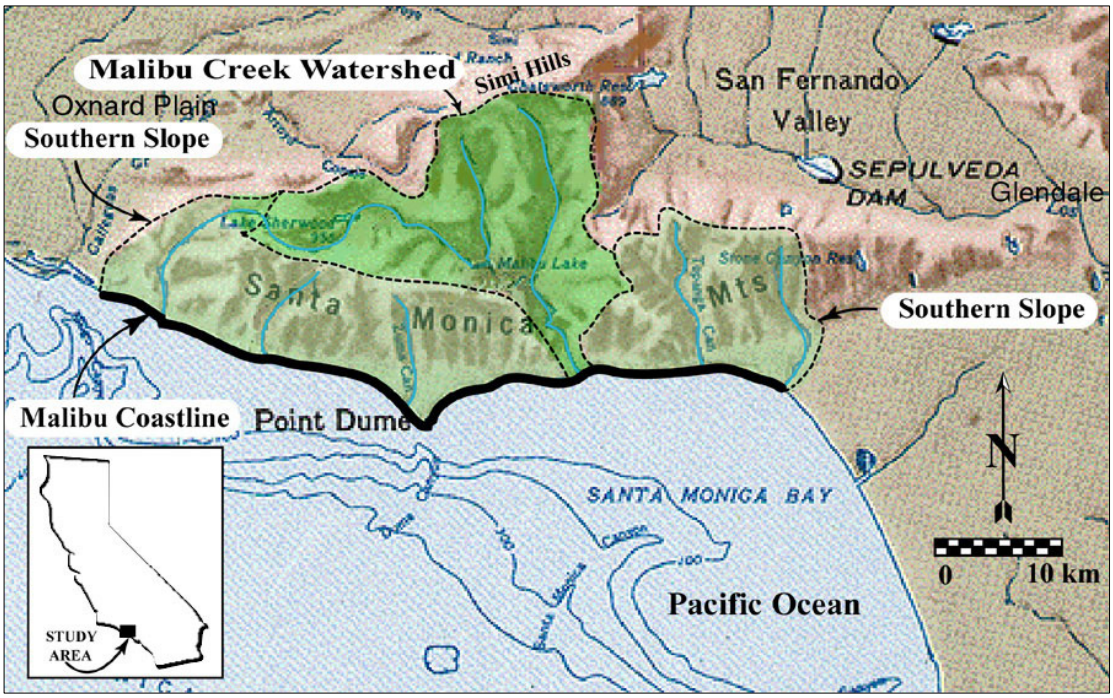


Figure 1. Location Map.

The thesis suggested that there is a general misconception of the original, natural beach widths along the coast. Several unintended artificial recharge episodes occurred during the early years of Malibu development, from the 1920's through the 1940's, due to initial construction and subsequent widening efforts of the Pacific Coast Highway (PCH). In the ensuing years, the littoral current carried the artificial recharge down the coast and natural recharge was reduced by development. The thesis concluded that the beaches along the Malibu coastline would continue to erode. Portions of the coastline were already noticeably eroded in 2000 when comparing historical aerial photos to then-current conditions. Also, anecdotal evidence such as coastal armoring and misaligned beach access hardscape suggested a formerly higher sand elevation.

An update to the observations made by the author in 2000 as part of the original thesis was included as part of this paper. Several of the same locations were also photographed to compare to earlier photos. Comparison of these photographs reveals a loss of sediment at almost all beaches, with a few isolated beaches showing sediment accumulation.

Unless efforts to artificially recharge sediment to the coast is initiated, sand losses will continue to occur to the detriment of the residents and the beach-going public. It is the author's opinion that a baseline amount of sand will remain due to the capturing effects from the rock point and natural jetties, but not enough to permit recreation activities they previously supported. The only planned beach recharge project is the Broad Beach Restoration Project (Moffatt and Nichol, 2011). A comprehensive plan for the restoration of the Malibu Lagoon is planned but it does not include artificial beach recharge efforts (Moffatt and Nichol, 2005).

This paper proposes a method to artificially recharge sediment to the coast by creating a sediment sluice. This involves modifying a portion of the bottom of many of the coastal canyons for use as a sediment storage site. When sufficient runoff occurs, the sediment will be conveyed to the beaches where it can be naturally graded and distributed along the coast. This method would avoid many of the regulatory objections to conventional "beach dumping." A return of the sediment yield to pre-development conditions is not anticipated. However, at a minimum, 1,600 m^3/yr could be sustainably recharged. With improved design and efficiency this estimated quantity could increase several-fold.

COAST MORPHOLOGY

The Malibu coastline has multiple steeply descending canyons draining to the coast making it uniquely suited for the sediment sluicing approach. Additionally, the canyons are not extensively developed, and easily accessible by PCH. A short description of the coast morphology follows.

The Coastline. The Malibu coastline is composed of a series of east-west and northwest-southeast trending pocket beaches. The coastline defined in this paper extends from Point Mugu to Santa Monica Canyon for a distance of 56.02 km. (Figure 1). The pocket beaches are generally no more than a few hundred meters in length, with the exception of Zuma/Westward Beach which measures almost 7 km long. The pocket beaches are bounded by rocky headlands such as Sequit Point, Point Dume, and Latigo Point. Boulder and cobble mounds at creek mouths form natural jetties that also define pocket beaches. Much of the coastline was formerly bounded by cliffs up to 30 m high.

The offshore topography of the Malibu coastline gradually slopes to the south at a gradient of 50:1 (horizontal to vertical). However, offshore from Point Dume lies the Dume Submarine Canyon (Figure 1). The mouth of this canyon extends within 245 m of the mean high tide line and descends to a depth of almost 690 m level at a 6:1 gradient. This submarine canyon represents the largest sediment sink on the coastline with an estimated 70% of the sediment lost.

To mitigate beach erosion problems, several jetties were constructed from the 1920's to the 1940's from Las Flores Canyon and Santa Monica Canyon to capture sediment and minimize sand losses from. Today, most of the coastline is developed and armored with bulkheads or seawalls. Many homes are suspended above the surf zone on piles.

The Watersheds. The study area is located at the southern edge of the western Santa Monica Mountains where they meet the Pacific Ocean. The Santa Monica Mountains are characterized by an elongated, central ridge that is eroded by transverse-oriented and steeply inclined, V-shaped canyons. The southern slope watersheds measure 407.0 km^2 in area. The sediment supplying watersheds are subdivided into the Malibu Creek watershed and a collective group of watersheds that drain the southern slope of the mountains. The Malibu Creek watershed is the largest single watershed that drains

to the Malibu coast, measuring 288.7 km^2. Several dams and debris basins have been constructed within this watershed since the 1880's, and each has accumulated varying amounts of sediment. The Rindge Dam, built in 1926, is filled to capacity with sediment.

Delineation of the Malibu Coastline. A station line was established for this study to assign locations to each canyon outlet and to each sediment source along the coast. The station line is equivalent to the mean high tide line. The station line begins at Point Mugu on the west at station km0.00 and ends at Santa Monica Canyon at station km56.02, increasing in the direction of the littoral current flow. Figure 2 shows the location of the five largest canyons, Point Dume, and the origin and terminus with their station numbers.

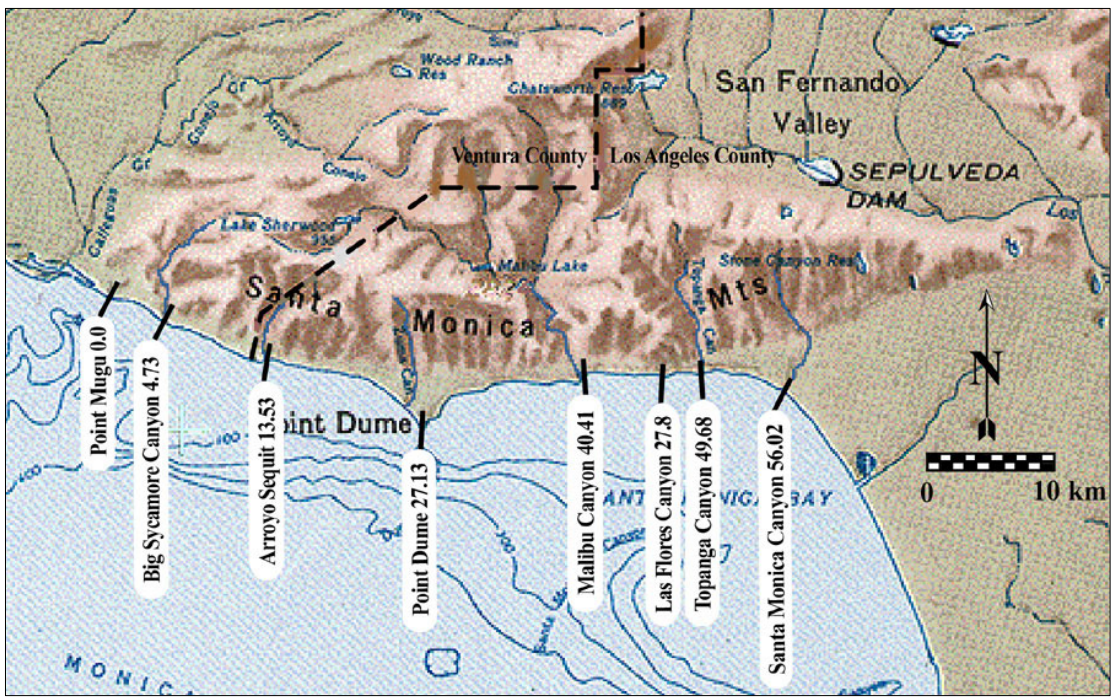


Figure 2. Malibu Coastline Stationing.

COASTAL SAND YIELD (PRE-DEVELOPMENT)

The value of any sediment recharge effort cannot be determined without first understanding the spatial relationships of the sand sources and sinks, as well as determining the historical yield to current sediment yields. The methodology and results of the study are summarized below.

Creek Sources. To determine creek sand yields, the author tailored the existing method used by the Los Angeles County Department of Public Works, Hydraulic/Water Conservation Division (LACDPW, 1991). Calculating Debris Potential Areas using the LACDPW approach does not require a large number of input variables as required by other deterministic models. By calibrating this method

with existing sedimentation data, grain size curves, hydrologic data, and fire histories, a first-order, sediment yield estimate was obtained. This method also incorporates spatial relationships that some other sedimentation models lack.

Bluff Sources. Bluff erosion sand yield rates were estimated by measuring lengths of erodible coastline and taking into consideration geology, bluff profiles, and published erosion rates.

Findings. The average annual sand yield for sand sized particles from creek and bluff sources during pre-development conditions is presented in Figure 3. This graph shows the cumulative quantity of sand that was annually discharged to the coastline, on average, during pre-development conditions. The graph also illustrates that the quantity of available sand increases in the direction of net littoral drift, with the exception of the loss at Dume Submarine Canyon. Littoral drift into the subject area from upcoast of Point Mugu was not considered in this analysis due to the observable difference in upcurrent and downcurrent beach widths (BEACON (2009).

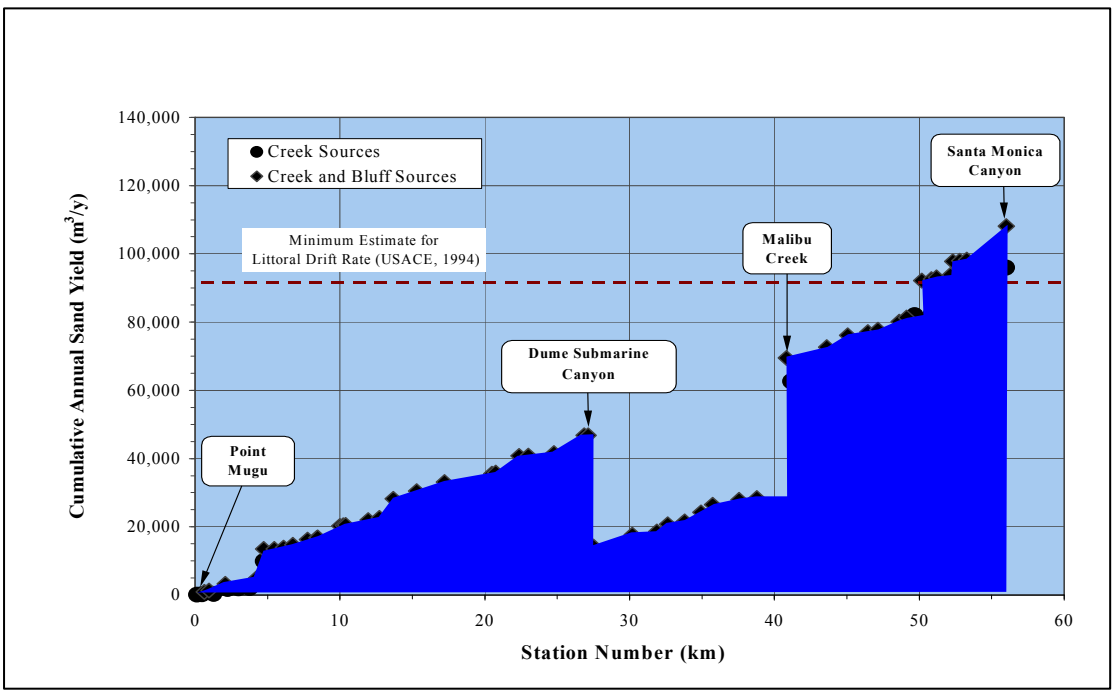


Figure 3. Cumulative Annual Sand Yield, Pre-Development.

The station numbers shown on the horizontal axis correlate to those in Figure 2. Each circle on the graph represents the incremental contribution from a creek source to the sand budget. Each diamond represents the combined incremental contribution from stream sources and section of applicable bluff erosion. Loss of sand into the Dume Submarine Canyon is shown as a precipitous decrease in the sand budget. The sand added from Malibu Creek is shown as a precipitous gain. The total volume of sand delivered to the coastline from creek and bluff sources at Santa

Monica Canyon is approximately 108,000 m^3/yr during natural (pre-development) conditions. This quantity closely approximates the estimate for annual littoral drift in the area, estimated at 92,000 m^3/yr by the USACE (1994).

COASTAL SAND YIELD (CURRENT)

Figure 4 shows the average annual sand budget for the same portion of the coastline after construction of dams in the Malibu Creek watershed, the addition of debris basins on the south slope of the Santa Monica Mountains, and coastline armoring. The graph illustrates current (year 2000) conditions where the sand yield from the creek and bluff erosion is reduced to 70,000 m^3/yr.

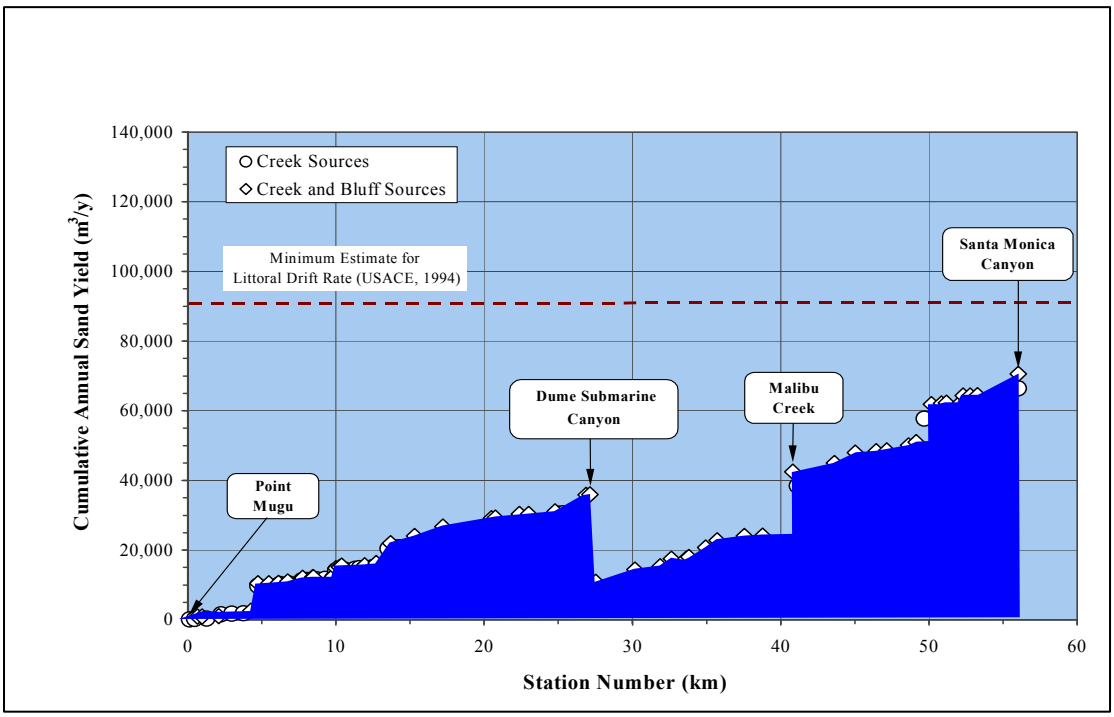


Figure 4. Cumulative Annual Sand Yield, Current

Artificial Recharge. Artificial recharge locations and sand volume were determined by comparing coast topographic profiles obtained from the State of California Department of Public Works and the Los Angeles County Surveyor. Artificial recharge as reported by various other sources was also included. Sand sized material was estimated to be 50% of the total eroded sediment for bluff and creek sources (OWEN, 1994). Episodic recharge of sediment by construction and maintenance of PCH from the 1910's to the 1940's added approximately 579,000 m^3 of sand sized sediment to the coast. This quantity equates to approximately 15 years worth of sediment lost at the eastern end of the study area. The impact of artificial recharge due to PCH construction was greater near the origin of the study area.

Observations. The episodic artificial recharge represents a total of 15 years worth of sand loss due to damming and reduced bluff erosion (38,000 m^3/yr at Santa Monica Canyon). Local impacts of this sand loss are far greater at locations further upcoast

where the sand supply is less. Since it takes many years for the sand to be carried along the coastline, the artificial recharge probably influenced the beach widths for a greater period of time. This amount of sand undoubtedly delayed the consequences of the reduced annual sand budget.

The upper graph on Figure 5 shows the volumes and locations of fill placed in the 1920's to 1940's due to PCH construction and widening. Superimposed on the graph are also fills placed in the 1950's through 1994 as a result of debris basin cleanouts and highway maintenance. Most the artificial recharge was upcoast of Malibu Creek (31,000 m^3 between 1979 and 1994, 328,000 m^3 between 1926 and 1940).

The lower graph of Figure 5 illustrates the difference between average annual sand yields along the coast for pre-development (Figure 3) and present (Figure 4) conditions. The shaded area below the graph represents the accumulated incremental loss of sand to the coast. At Santa Monica Canyon, the accumulated loss of sand is 38,000 m^3/yr (35% of the total).

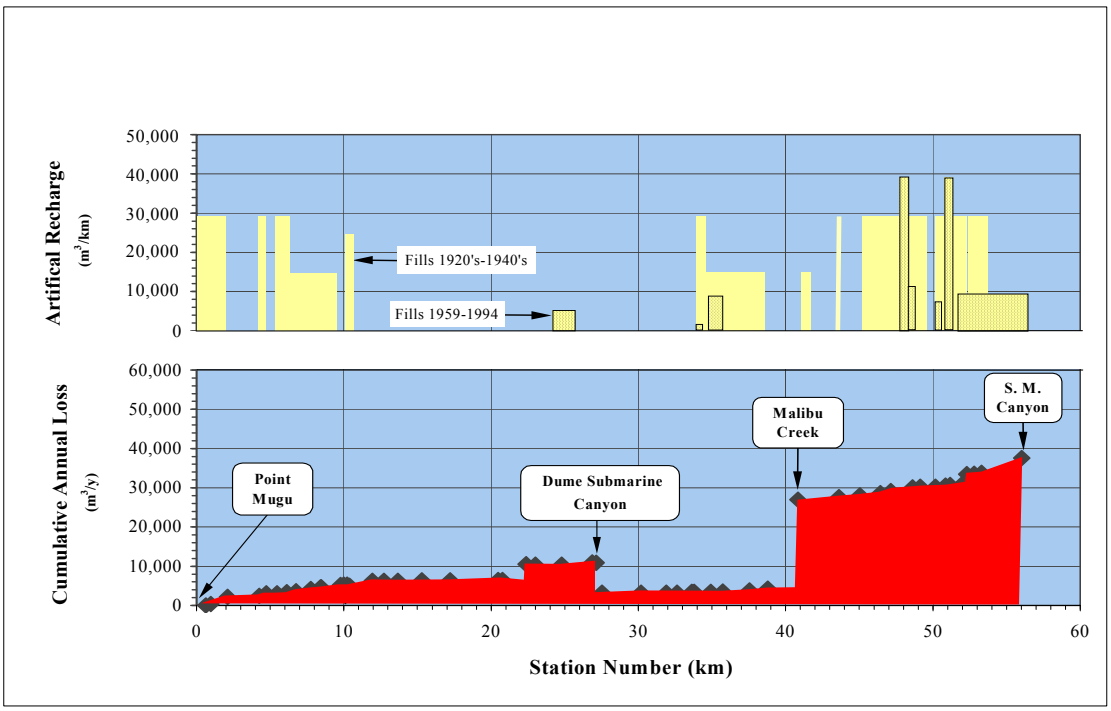


Figure 5. Difference Between Pre-Development and Present Sand Yields Also Showing Location and Quantity of Artificial Recharge.

The loss of sediment yield from the Malibu Creek watershed is the greatest of any canyon along the coast, with a reduction of 25,712 m^3 (55% of the total canyon sediment yield). Trancas Canyon has a reduction of 3,205 m^3 loss per year. However, due to the smaller average annual sediment yield, this sediment yield reduction

represents a 69% loss from this canyon. Interestingly, this large percentage loss may be the reason for the significant beach erosion that has been reported at Broad Beach located immediately west of the canyon mouth (Moffatt and Nichol, 2010).

PHOTO COMPARISONS AND OBSERVATIONS

From 1997 to 1999, ground-based photographs were taken along the entire study area to document existing conditions and for comparing to historical aerial photographs. In 2011, the same photo locations were revisited to note changes to the coastline. A few photos are compared below. Station numbers identifying their location are provided. Significant sand losses were noted at County Line Beach (Figure 6) and at Broad Beach (Figure 7) between 1999 and 2011. Some sand accumulation was noted at Colony Beach (Figure 8). Figure 9 shows a lot-specific, lateral access-restricting seawall placed at Carbon Beach sometime since 1997.

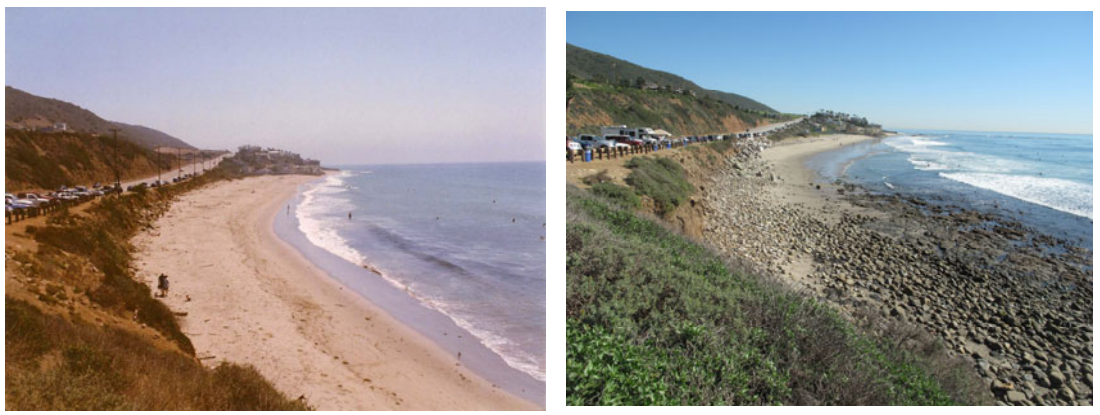


Figure 6. County Line-km10.24, Photos Dated 8/23/99 and 1/28/11



Figure 7. Broad Beach-km20.92, Photos Dated 8/23/99 and 1/28/11



Figure 8. Colony Beach-km39.43, Photos Dated 12/14/99 and 4/22/11

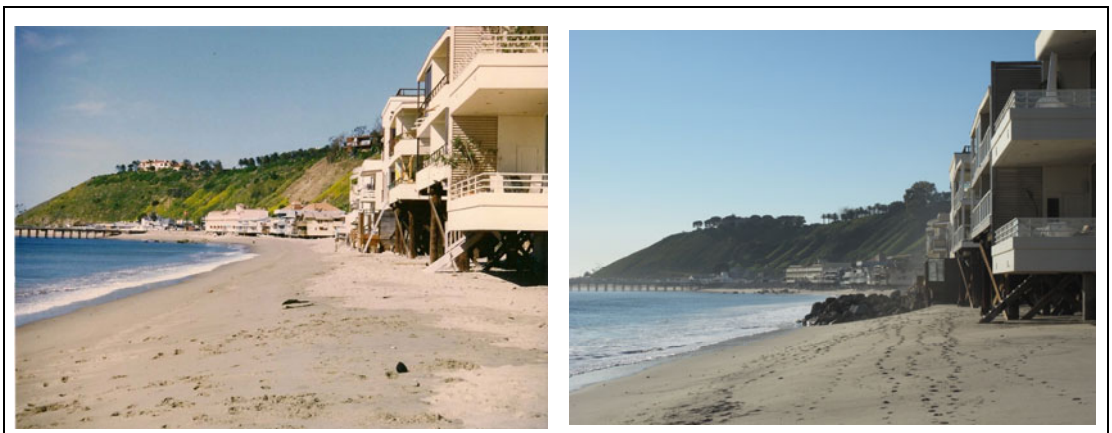


Figure 9. Carbon Beach-km41.81, Photos Dated 3/5/97 and 1/28/11

Currently, Malibu does not have a comprehensive sediment management plan. Most coastal protection has been performed under emergency conditions to save specific developments. Hence, coastal protection has been synonymous with coastal armoring, resulting in a coastline with poor recreation or protection value. Due to the presence of beach armoring or to exposed, naturally-occurring boulders, passive erosion may occur in the future (Griggs, 2010).

The limited sand restoration efforts that have occurred in Malibu were summarized in a report by the OWEN Group (OWEN, 1997). The sand restoration resulted from "emergency" highway and debris basin cleanouts performed by CalTrans and the U.S. Army Corps of Engineers. The study recommended five beaches that were considered favorable for sediment disposal. Despite the findings of the report, sand replenishment did not occur, to the knowledge of the author. Only recently, an unrelated sand replenishment and restoration project (460,000 m^3) has been proposed for the Broad Beach area east of Trancas Point (Moffatt and Nichol, 2011).

A PROPOSED RECHARGE SOLUTION-THE SEDIMENT SLUICE

Function. The proposed sediment sluice method requires mechanically placing loose sediment in a pregraded creek bottom. A storm of sufficient magnitude and intensity would mobilize the sediment and carry it into the foreshore where natural sorting will occur. After the storm, the sluice would have to be evaluated for additional sediment filling. Several episodes of filling and mobilization can occur through the wet season. Cobble to sand sized material would be sorted by dynamic beach processes; silt and clay would be deposited offshore in a natural manner. It is assumed that the sand sized material would eventually be deposited in the foreshore or in an offshore berm. Wave and wind energy would then provide the energy to distribute the sand along the beach.

Design. The sluice should be designed for small sediment volumes and comply with current grading codes. Later as the canyon specific fluvial dynamics are better understood, the sluice could be modified for the site conditions. It must be recognized that each site will have different fluvial and coastal dynamics which must be considered.

The sluice should be trapezoidal in cross section with a flat bottom at least 2.5 m wide to allow for construction equipment to distribute the sediment. The sides should be sloped at a 2:1 (horizontal to vertical) gradient. The depth can be no greater than the existing creek depth. An average depth would be approximately 1.6 m. The length of the sluice can be as great the site allows, however, it should be at least 30 m long to permit efficient sediment filling with efficient belly-dump trucks. Assuming a 1.6 m bank depth, the minimum sized sediment sluice considered could be 8.5 m wide. A schematic diagram showing minimum sluice dimensions is presented on Figure 10.

The sluice may extend across the entire creek bottom, however, there may be a need for a separate sluice from the main channel. For example, Malibu Creek is a migration route for state-protected steelhead trout. A separate side channel used for sediment sluicing could permit a bypass to the main channel. Such a bypass would allow native species, such as steelhead, to thrive unaffected by the sluice .

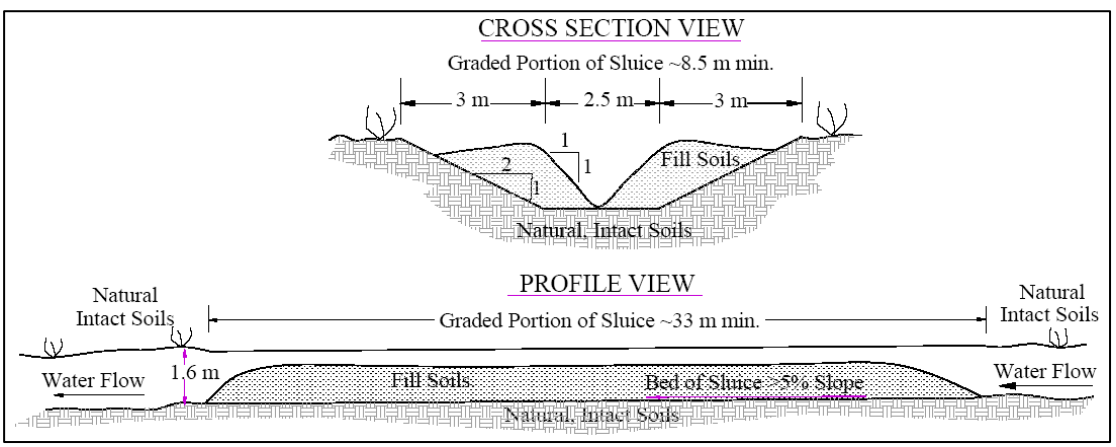


Figure 10. Cross Section and Profile of Proposed Sediment Sluice

The sides and bottom of the sluice should not be lined in order to maintain a natural appearance. Typical riparian growth in the channel is acceptable but would have to be trimmed to keep the channel open.

Location. The sediment sluice methodology takes advantage of the many undeveloped steep gradient canyons located in the subject area. Also, the sluices can be located near the creek mouth resulting in a short transport distance. Based on the earlier work by the author, 21 canyons were identified as having an average annual sediment yield rate of 750 m^3/yr or more. A list of the potential locations is provided in Table 1. With few exceptions, these canyons have high flows during rainfall events, and only flow for a few days to a couple of weeks after a major rainfall. Many of the identified creek watersheds have not been significantly developed or dammed, and therefore, do not have a sediment deficit. However, these canyons should not be eliminated from consideration since they represent significant sediment delivery capacity and they are located upcurrent of the eroded beaches.

Two of the identified canyons are shown on Figure 11, Trancas Creek and Malibu Creek. Both of these locations have suffered large reductions in sediment delivery, and both are the focus of large, future public works projects (Moffatt and Nichol, 2005 and 2011). Implementation of the proposed sluice may garner larger local support as a result.



Trancas Canyon-km22.39



Malibu Canyon-km40.42

Copyright © 2002-2010 Kenneth & Gabrielle Adelman, California Coastal Records Project,

Figure 11. Photos of Selected Sediment Sluice Locations.

Table 1. List of Potential Canyons for Sediment Sluices.

Canyon Name	Outlet Coastal Station (km)	Watershed Area (km^2)	Annual Sediment Yield, Pre-development (m^3/yr)	Annual Sediment Deficit, Current (m^3/yr)
La Jolla Canyon	2.25	9.50	1,443	191
Big Sycamore Canyon	4.73	55.14	7,901	5
Deer Canyon	7.68	5.00	937	0
Little Sycamore Canyon	10.00	12.61	2,395	0
Arroyo Sequit	13.53	28.55	5428	0
Encinal Canyon	19.57	5.21	866	28
Trancas Canyon	22.37	22.61	4,626	3,205
Zuma Canyon	24.99	23.49	4,550	476
Ramirez Canyon	30.17	8.86	1,773	0
Escondido Canyon	32.31	8.50	1,689	0
Solstice Canyon	34.69	11.65	2,268	0
Corral Canyon	35.49	9.25	2,080	0
Malibu Canyon	40.42	197.80	57,563	25,712
Carbon Canyon	43.52	5.67	1270	0
Las Flores Canyon	44.74	10.67	2491	106
Tuna Canyon	49.13	3.86	1,023	86
Topanga Canyon	49.68	51.62	10,758	0
Santa Ynez (Sunset) Canyon	52.24	18.31	4,037	2,045
La Pulga Canyon	53.49	3.81	895	284
Temescal Canyon	54.20	7.41	1,570	217
Santa Monica Canyon	56.02	34.34	6,406	1,745
			Total	34,100

Sediment Sources. Sediment for the sluice would be drawn mostly from opportunistic sources, such as debris basin cleanouts, highway maintenance, local grading projects. Sediment from the Rindge Dam in Malibu Creek would be considered an excellent source. Local sediment is preferred so as to mimic the density, grain size, and shape already presentalong the beaches. The size fraction should be skewed toward the sand sized fraction and not include soils that are primarily clay. Also any sediment should be screened to remove boulder-sized rocks, since they may not be mobilized in the smaller creeks.

Anticipated Recharge Volumes. To roughly estimate the minimal recharge volume, all 21 of the canyons cited in Table 1 were considered and minimal sluice dimensions proposed in Figure 10 used. The sluice should be maintained at half capacity and the fill sediment can have only 50% of sand sized material. If only one storm per year moblized the sediment, a total of 1,600 m^3/yr could be added. Depending on the grain size distribution, the amount would be greater if gravel and cobbles were considered. In addition, if the sluices could be refilled multiple times or increased in size, the sediment volumes would be greater.

Costs. Initial upfront costs would include feasibility studies, permitting, land acquisition and sluice grading. Recurring costs would include sluice maintenance and fill importing. Other recurring costs would be for fluvial and coastal studies, and project management. When considering only the cost of fill import, Patsch and Griggs (2006) cite a range of \$6.50 to \$10.00/yd^3 equivalent to \$8.50 to \$13.00/m^3. Using the median value, the minimum annual fill cost would be \$35,000/yr.

CONCLUSIONS

The Malibu coastline has eroded further since the presentation of the author's original work in 2000. Very little sand replenishment has been accomplished because development along the coastline has restricted most access points. This has limited the locations where direct sediment placement can occur. Beach protection has been constrained to armoring projects, as observed during the recent site visits.

The coastline is geographically well suited for sediment sluicing, due to the multiple steeply descending canyons and seasonal flows. This method would be a more holistic approach for sand delivery, circumventing many of the arguments typically cited against artificial recharge (Patsch and Griggs, 2006 and CDBWSCC, 2002).

The sediment sluice method would, at a minimum, recharge about 1,600 m^3 of sand to the Malibu coast. This value represents about 5% of the total annual sediment deficit for the 56.02 km study area, but will have a greater impact further upcoast where the sediment volumes are smaller. The sediment could be recharged simlutaneously at several locations, affecting a large area of the coast. With time, each sluice could be modified to accommodate the largest sediment volume possible.

Physical constraints such as land availability, proximity to neighbors, road access, and vegetation would affect the feasibility, location, and design of the sluice. The sluices should be closely managed. Eventually, the sediment sluices could be included as part of the Local Coastal Plan, and implemented as part of regular civic maintenance work.

REFERENCES

Beach Erosion Authority for Clean Beaches and Nourishment (BEACON), (2009), *Coastal Regional Sediment Management Plan, Central Coast from Pt. Conception to Pt. Mugu, Final Report.*

California Department of Boating and Waterways and State Coastal Conservancy, (CDBWSCC), (2002), *California Beach Restoration Study*, Sacramento California.

City of Malibu, (September 13, 2002), *Local Coastal Program, Local Implementation Plan*, 313 pages.

Griggs, G.B. (2010), "The effects of armoring shorelines-The California experience", *in* Shipman,H., Dethier, M.N. Gelfenbaum, G.,Fresh, K.L., and Dinocola, R.S. eds., 2010*, Puget Sound Shorelines and the Impacts of Armoring-Proceedings of a State of the Service Workshop*, May 2009, U.S. Geological Survey Scientific Investigations Report 2010-5254, p77-84.

Knur, R.T., (2000), "The Effect of Dam Construction in the Malibu Creek Watershed on the Malibu Coastline Sediment Budget, California"*, A thesis presented to the Faculty of the Department of Civil Engineering and Geology, California State University, Los Angeles,* 135 pages.

Los Angeles County Department of Public Works (LACDPW), (1991), *Hydrology/Sedimentation Manual with Appendix.*

Moffatt and Nichol, (June 17, 2005), *Final Malibu Lagoon Restoration and Enhancement Plan Prepared for the California State Coastal Conservancy and California Department of Parks and Recreation,* Job No. M&N File 5381.

Moffatt and Nichol, (June 2010, *Broad Beach Restoration Project Sand Source Investigation Report*", Prepared for Trancas Property Owners Association, Job No. 6935, 25pages.

Moffatt and Nichol, (January 2011) *Broad Beach Restoration Project, Coastal Development Permit Project Description – Final*, Prepared for Trancas Property Owners Association, Job No 6935, 27 pages.

Owen Group, Inc., (October 1997), *Evaluation of Sediment from Malibu/Santa Monica Mountains Debris Structures and Evaluation of Malibu Area Beach Disposal Sites*, Prepared for Los Angeles County Department of Public Works, 60 pages.

Patsch, K. and Griggs, G, (2006), "Littoral Cells, Sand Budgets and Beaches: Understanding California's Coastline", *California Department of Boating and Waterways, California Coastal Sediment Management Workgroup*.

U.S. Army Corps of Engineers (USACE), (April 1994), *Reconnaissance Report-Malibu/Los Angeles County Coastline, Los Angeles County, California*, 193 pages.

Behavior of Shore Protection Structures at Alexandria, Egypt, during the Storm of December 2010

B. El-Sharnouby[1] and A. Soliman[2]

[1] Professor of Ports and Marine Structures, Faculty of Engineering, Alexandria University, Alexandria, Egypt, email: bahaa.elsharnouby@yahoo.com
[2] Associate Professor of Ports and Coastal Engineering, Dean of Port Training Institute, Arab Academy for Science and Technology and Maritime Transport, P.O. Box 123, Alexandria, Egypt; PH (002) (0)10 170-8865, FAX (002) 03 482-9930; email: akram.soliman@pti-aast.org

ABSTRACT:

Recently, December 2010, a severe storm hit Alexandria city, Egypt, and directly attacked its shoreline. Wind gusting to 65 kilometer per hour lasted for about two days creating a deep water wave of a height of 7.5 meter for the first time in the last 100 years. This paper documents the different types of shore protection structures and methods (sand nourishment, revetment, groins, sea walls, emerged and submerged breakwaters) used to protect Alexandria coastline at the area of study and their behavior during this storm.

This study concluded that the submerged breakwater used to protect Miami to Montaza beach, east of Alexandria, showed good efficiency concerning wave transmission and shore protection at storm times. It is recommended to apply the submerged offshore rubble mound breakwater and / or submerged offshore artificial reefs, to induce wave breaking and energy dissipation and to limit the wave heights to protect Alexandria coastline.

I- INTRODUCTION

Alexandria is the second largest city in Egypt, contains more than one third of the national industries and is considered as Egypt's principal seaside summer resort on the Mediterranean Sea. Alexandria's beaches are the main summer resort of the country and is considered one of the most notable summer resorts in the middle east, for, in addition to its temperate winters, its beaches, with white sands and magnificent scenery, stretch for 140 km along the Mediterranean Sea, from Abu Qir, in the east to Al-Alamein and Sidi Abdul Rahman, in the west. These attributes make Alexandria a favourite tourist spot; more than one million local summer visitors together with about 4.5 million residents enjoy the summer season at Alexandria every year (Frihy et al. , 1996). During summer of 2006, Alexandria received about 63 cruise ships containing 70,000 tourists and its hotels provided the equivalent of 47,000 visitor nights. During the same summer, Alexandria beaches received 3 million local visitors and 250,000 day trip visitors (Soliman & Reeve, 2007). A satellite image for Miami to Montaza beach west of Alexandria is shown in Figure 1.

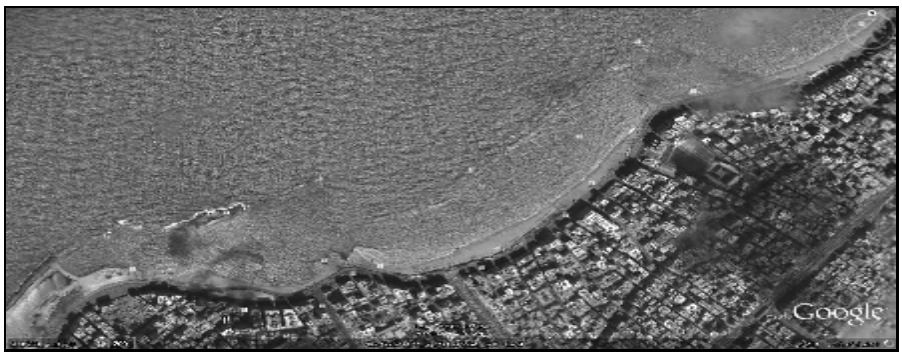


Figure 1. A satellite image for Miami to Montaza beach west of Alexandrian, (Google Earth, 2011).

In the last few years, Alexandria coastline suffers from many erosion problems along its coastline which result from natural and human activities in the coastal zone. The beach width gradually decreased due to the action of the waves and currents. With the time, some beaches have disappeared totally and the wave action has attacked the toe of seawalls. Figure 2 shows example of erosion and flooding occurring at Alexandrian coastline during storm of winter 2006.



Figure 2. Erosion and flooding occurring at Alexandrian coastline.

Flooding problems appeared also in these eroded areas affecting the traffic flow. In winter 2003 to 2006, the shore line of Mandara beach at Alexandria, Egypt, had suffered serious flooding and erosion problems. The sand beach was vanished with wave scouring underneath the road seawall. Waves and sea sand jumped over the broken seawall to the Cornish road as can be shown in Figure 3.



Figure 3. Example of flooding at the Alexandrian coastline.

Recently, December 2010, a storm attacked Alexandria city and its beaches. The storm winds generated deep wave height of 7.5 meter for the first time in the last 100 years. As a result of this surge storms, water and sand overtopped the seawall and destroyed many parts of it. Figure 4 shows one example of this serious problem.



Figure 4. Wave attacks Alexandria coastline during the storm of winter 2010.

Due to the continuity of coming wave and speedy winds, the sea level has been raised for about one meter causing a serious flooding problem as shown in Figure 5.



Figure 5. Wave flooding due the sea level rise at Alexandria coastline, 2010.

Factors distributing to the erosion problems at Alexandria coastline can be summarized as follows:

- Incident waves, storm events, and sea level rise.
- Instability of Egyptian north delta coast due to lack of Nile River sedimentation and decreasing water flow into the sea.
- Loss of a considerable part of the sand beach due to extending the shore road towards the sea.
- Elimination of sources of organic sediments as result of water pollution
- Noticeable rise of temperature, sequent increase of wave height, and longer time of seasonable storms as features of climate changes.

Conventional beach protection structures such as groins and revetments are becoming increasingly unpopular, principally due to their adverse impact on beach amenity and aesthetic considerations. In contrast, submerged structures are widely perceived to be capable of providing the necessary beach protection without a loss of beach amenity or negative aesthetic impact (Ranasinghe & Turner, 2006).

The submerged breakwaters have only recently been adopted for beach protection. Black and Andrews (2001) mention that there are relatively few reported investigations of shoreline response to submerged structures.

During the past 20 years, alternative solutions were adopted for shore protections of Alexandria city. There was no clear strategic plan for the protection of Alexandria coastline and for that each zone of Alexandria shoreline has been protected by different type of structure. In the following section, summary of theses shore protection structures is presented and illustrated.

II- ALEXANDRIA SHORE PROTECTION STRUCTURES

In this study, fifteen kilometer of Alexandria coastline extended from Chatby beach in the west to Montaza beach in the east is selected. This area is divided into ten zones according to the type of shore protection structure used as follows**:**

- **ZONE 1**

The first zone at Chatby area has been protected by a high sea vertical wall since this area is 3-5 meter above sea water level. Small sand beach is in the lea ward of that wall as shown in Figure 6.



Figure 6: The vertical sea wall with the sandy beach at Chatby beach.

- **ZONE 2**

The second zone extended after Chatby to Cleopatra beaches for almost 3500 meters. This area has been strengthened by strong revetment. 20 to 30 meter width of 10 ton concrete cubic blocks have been installed for a height up to 5 meter as shown in Figure 7.



Figure 7: Shore protection by concrete cubic blocks at Sporting beach.

- **ZONE 3**

This zone is located at Cleopatra beach which is protected by offshore detached narrow and low crest breakwater.

- **ZONE 4**

The fourth zone is Mostafa Kamel with almost 1500 meters length. This area consists of three marine clubs built offshore and have been protected by a combination of low and high crest rouble mound breakwaters and revetment.

- **ZONE 5**

Zone 5 is the beautiful historical Stanly bay which has depended through the years on sand nourishment.

- **ZONE 6**

Groins have been selected for the protection of Gleem area as can be shown in Figure 8.



Figure 8: A satellite image for groins for Geleem Area, (Google Earth, 2009).

- **ZONE 7**

The private beach and the boat marina at San Stefano area have been surrounded with strongly armored quite elevated breakwaters.

- **Zone 8**

Next to San Stefano area, revetment has been adopted to Loran and Mahroosa areas. Figure 9 present this solution. As can see from Figures 7and 9, the revetment protected the shore line against further erosion but the beach profile was completely reinforced.



Figure 9: Reinforcement of beach profile by concrete revetment at Loran.

- **ZONE 9**

Sidi Besher area is an almost 3000 meter long beautiful beach which has no artificial protection yet. There is a natural submerged reef offshore this area. Figure 10 shows the beautiful sandy beach of Sidi Besher area.



Figure 10: View of Sidi Besher beach shows beautiful sandy beach with high visitor density in summer.

- **ZONE 10**

The zone is 3500 meters long from Miami to Montaza beach. This area has suffered severe erosion in 2003 storm. With time, the beach width decreased and vanished in some locations. The waves attacked the road itself after washing all the sand as can be notice from Figure 11.



Figure 11: Damage at Mandra beach during winter 2003.

In order to stabilize the eroded beach, a long, wide crest, and deep submerged breakwater has been constructed. The breakwater system consists of one main parallel breakwater and two overlapping parts as shown in Figure 12.

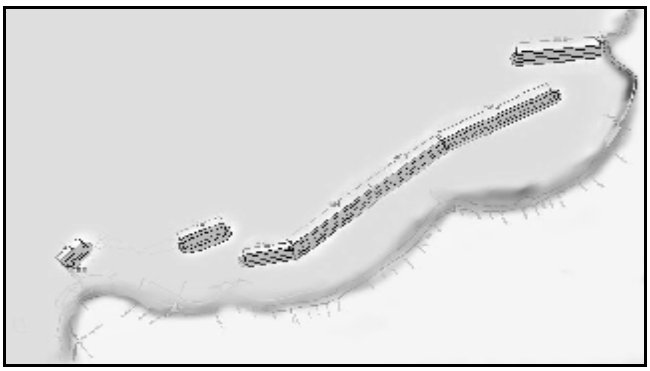


Figure 12: Layout of submerged breakwater applied at Miamy-Montaza area.

Total length of the breakwater segments is almost 3000 meter, 150 to 350 meter offshore, and 2.5 to 8.5 meter depth. Width of the breakwater crest ranges from 36 to 46 meters which is equal to the incident wave length. The construction of the breakwater started 2006 and was completed in the beginning of 2009 except for a 100 meter long end part. The part across Beir Masood area has not been completed yet due to lack of finance.

The submerged breakwater was attacked by 7.0 meter deep wave height in December 27th, 2006. Figure 13 shows the good efficiency of the breakwater in storm-condition. The shore line and sea-wall remained safe along the breakwater with noticeable good quality of water in the leeside in summer.

More details of the coastal structures which had been used to protect Alexandria coastline can be found at El-Sharnouby & Soliman (2010). In the following section, the efficiency of the different types of shore protection structures, used in the study area during the December 2010 storm, is discussed.



Figure 13: Efficiency of the submerged breakwater at 7.0 meter depth in storm time.

III- BEHAVIOUR OF SHORE PROTECTION STRUCTURES DURING DECEMBER 2010 STORM:

The performance of these different types of shore protection structures, which has been shown in the previous section, at storm of winter 2010 is as follows:

III-1 Sea vertical wall:

The vertical sea wall in Chatpy area (Zone 1) completely prevented the waves from attacking the road, but caused severe erosion at the front of the structure. The narrow beach disappeared and erosion reached the foundation of the sea wall.

III-2 Concrete blocks revetment:

Along the shore line, between Chatpi and Cleopatra (Zone 2), the several rows of concrete blocks were effective as a line of defence against wave attack .Only wave splash could pass over the revetment to the road. However, beach profile was completely reinforced and sand beach vanished without any comeback any time of the year. Due to wave flooding over the revetment several times during storms, many of the blocks, with steel hanging bars, cracked.

III-3 Detached breakwater:

The narrow low crest detached breakwater used to protect Cleopatra beach (Zone 3) was a complete failure as presented in Figure 14. Most of the breakwater disappeared and what left is good only for sea birds to rest on. Waves crossed the breakwater easily, and the relatively short distance between the breakwater and shore line did not do any good for energy absorption.



Figure 14: Failure of the detached breakwater at Cleopatra beach.

III-4 Low and high crest rouble mound breakwater:

The three marine clubs at Mostafa Kamel area (Zone 4) suffered water flooding over the breakwaters and through the openings. The different types of shore protection structures acted negatively against each other. A comprehensive rehabilitation program was adopted for this area to establish only one joined protection structure.

III-5 Sand nourishment:

Sand nourishment was particularly good enough at Stanly beach (Zone 5). Offshore this area a marine bridge supported on piles was instructed. The pile foundations at sea level and the base layer at sea bed level played a good role in dissipating wave energy.

III-6 Groins:

Gleem area (Zone 6) suffered severe wave attack during the storm. Groins added no good to protect beach and on shore buildings against wave action. Even, the very little accumulated sand within years has been disappeared during the storm. Figure 15 shows the low efficiency of the groins when waves attacked Gleem area during the storm of winter 2010.



Figure 15. Waves attacked Gleem area during the storm of winter 2010.

III-7 Elevated strongly armored rouble mound breakwater:

As it might be expected, the quite high level heavy armor stones group of breakwaters 200 meter long each could protect the shore line at the private sector of San Stefano (Zone 7). Unfortunately, the negative side effect of the perpendicular and parallel breakwaters was quite pronounced at the shadow area of the breakwaters. Loran and Mahroosa areas (Zone 8) nearby San Stefano experienced the worst storm effect in Alexandria. In spite of the concrete revetment, the concentration of wave energy caused a considerable destruction. Waves took off side walk concrete slabs out of the side walk after jumping over the revetment. Shore road was flooded with water and small aggregates and concrete fences were destroyed and through away. Figure 16 shows the damages of the concrete slabs and fences.



Figure 16: Damages of the side walk and concrete fences at Loran area.

III-8 Sand nourishment at Sidi Besher beach:

The natural submerged reef offshore at Sidi Besher beach (Zone 9) could not help this time neither the sand nourishment. Waves covered the whole beach, attacked and destroyed fences and wood houses, and crossed over to the street as explained in Figure 17.



Figure 17: Damages of Sidi Besher beach due to waves attacks during 2010 storm.

III-9 Submerged breakwater:

Two years after the construction of the submerged breakwater at zone 10, the beach width behind it varied from 50 to 150 meter compared to 0.0 to 20.0 meters before installation without any nourishment. Figure 18 present a comparison between the beach width after and before the construction of the submerged breakwater.



Figure 18: Comparison between the beach width after and before the construction of the submerged breakwater at Mandra beach (El-Sharnouby & Soliman, 2010)

Details about the submerged breakwater design procedures in attached with a monitoring program which has been applied for the last two years to measure the performance of the submerged breakwater can be found at El-Sharnouby & Soliman (2010). The submerged breakwater showed tremendous efficiency concerning wave transmission and shore protection at storm times.

During this storm, the breakwater showed the same trend. Approaching high waves were broken over the submerged breakwater with transmission efficiency more than 75% as can be seen from Figure 19. The adequate water area behind the breakwater contributed well in dissipating the transmitted energy.



Figure 19: Waves breaking over the submerged breakwater as Mandara beach during the storm of winter 2010.

The wide sand beach took care of any left sweeping water. Figure 20 shows the good effect of submerged breakwater in the protection of Miami beach during the storm of winter 2010.



Figure 20: Effect of submerged breakwater in the protection of Miami beach during the storm of winter 2010.

The sea shore remained untouched in most locations along Miami-Montaza zone. Only few spots suffered gentle movement of water and sand to the street without any sort of destruction. After the storm, the breakwater itself was examined and no loss of his stone layers was recorded. The sand beach did not lose that much

and regained its beach lines within weeks. The good performance of the submerged breakwater may be due to the followings:

- Minimum value of the freeboard (f), and maximum value of breakwater crest width (B=incident wave length) regardless of incident wave height, height of the structure, and water depth.
- Continuity of the 3000 meters long submerged breakwater without direct openings.
- Breakwater and site layout.
- Attenuation of transmitted wave over an adequate water area.
- The accretion of wide sand beach.
- Method of construction (end land method)
- Strong breakwater foot.

IV-CONCLUSION

During the last few years, significant erosion occurs along most of Alexandria's beaches as a result of sediment starvation, coastal processes and sea level rise. In winter of 2003 to 2006, many surge storms struck the Alexandrian coastline, water and sand overtopped the seawall and destroyed many parts of it. In December 2010 Alexandria was hit by the strongest storm ever recorded in recent history. These kinds of storms are expected to increase in the coming years, due to phenomena of sea level rise.

Along its long shoreline, various shore protection structures and methods were tested during the storm of December 2010. Sea vertical wall protected the shore road, but erosion took place at the front of the structure down to the sea wall foundation. Detached narrow and low crest breakwater was a complete failure with adverse results. Elevated rouble mound breakwater was effective, but had a quite severe negative impact on areas at its shadow. Concrete revetment acted fine, but the sand beach sand completely disappeared and many blocks cracked after the flooding. Sand nourishment temporally protected against flooding, but did not do much good during the storm. Without any impact on beach amenity and aesthetics, the long, wide, and deep submerged breakwater could amazingly protect the shore line from destructive waves. The efficiency of the submerged breakwater was by far better than theoretically predicted concerning both transmission and erosion**.**

Other alternative which can be used is the submerged artificial reefs. More recently, submerged artificial reefs applications have varied widely, including: aquaculture production; coastal protection (Seaman and Jensen, 2000); and habitat protection (Baine, 2001). Artificial reef materials must last a minimum of 30 years to provide ecological services economically, and also be non-toxic to the marine environment (Grove et al., 1991).

REFERENCE

Baine, M. (2001). "Artificial reefs: a review of their design, application, management and performance." *Journal of Ocean and coastal management,* 44, 241-259.

Black, K., and Andrews, C. (2001). "Sandy shoreline response to offshore obstacles: Part 1. Salient and tombolo geometry and shape." *Journal of Coastal Research,* Special Issue 29 Natural and Artificial Reefs for Surfing and Coastal Protection, 82– 93.

El-Sharnouby, B., and Soliman, A. (2010). "*Shoreline Response for Long Wide and Deep Submerged Breakwater of Alexandria City, Egypt*". Proceeding of 26th International Conference on Seaports and Maritime Transport, Arab Academy for Science, Technology & Maritime Transport, Alexandria, Egypt.

Frihy, O.E., Dewidar, K.M., and El-Raey, M. (1996). "Evaluation of coastal problems at Alexandria, Egypt." *Journal of Ocean and coastal management*, 30 (2-3), 281-295.

Grove, R.S., Sonu, C.J. and Nakamura, M. (1991). "Design and Engineering of Manufactured Habitats for Fisheries Enhancement." *Artificial Habitats for Marine and Freshwater Fisheries,* W.J. Seaman and L.M.E. Sprague, Academic Press, Inc., San Diego, California. 109 – 149.

Seaman, W.J. and Jensen, A.C. (2000), "Purposes and Practices of Artificial Reef Evaluation." *Artificial reef evaluation: with application to natural marine habitats*, W.J. Seaman, CRC Marine Science Series, CRC Press LLC, Boca Raton, Florida, USA, 1 – 20.

Soliman, A., and Reeve, D. (2007). *"Artificial Submerged Reefs: A solution for Erosion Problems along Alexandria Coastline, Egypt?."* Proceeding of the IMA 2nd Conference on Flood Risk Assessment, Plymouth, UK, 41-50.

Soliman, A., and Reeve, D. (2009). *"Applying the Artificial Submerged Reefs techniques to reduce the Flooding Problems along the Alexandria Coastline"* Proceeding of the Institution of Civil Engineers Conference "Coasts, Marine Structures and Breakwaters", Edinburgh, Scotland, UK, 1-12.

Ranasinghe, R., and Turner, I. L. (2006). "Shoreline response to submerged structures: A review." *Coastal Engineering,* 53, 65-79.

Predictability of Beach Nourishment Project Performance in Florida

Robert G. Dean[1] and Luciano Absalonsen[1]

Abstract

Beach nourishment provides a near-natural approach to shoreline maintenance. Beach nourishment design and evaluation aids are described and demonstrated for predicting the performance of projects. These entail broad scale quantification of closure depth and wave conditions coupled with a relatively simple one-line numerical model. The applicability of these aids is demonstrated by comparison with two well-monitored projects in which the proportion of nourishment material remaining in the placement area obtained through monitoring is compared with the predicted proportion versus time. It is concluded that overall performance can be predicted within approximately $\pm 25\%$.

Introduction

Beach nourishment comprises the placement of large quantities of good quality material on the beach or within the nearshore to advance the shoreline seaward. The need for beach nourishment can be due to natural or human induced erosion or could simply be the desire to have more land; however, the need is usually due to erosion. In the following, design and evaluation aids for beach nourishment will be presented with simple tools that have been developed for the State of Florida. It is noted that a number of numerical models are available for this purpose ranging from the simple (discussed herein) to the much more elaborate. The advantage of simple models is the capability to focus on the physics, interrelationships and causes of the performance of a particular design. As shown in Figure 1, sand can be added either as "Beach Nourishment" discussed here or in the shallow offshore waters as "Profile or Berm Nourishment" with the anticipation of the sand moving onshore and/or reducing wave energy.

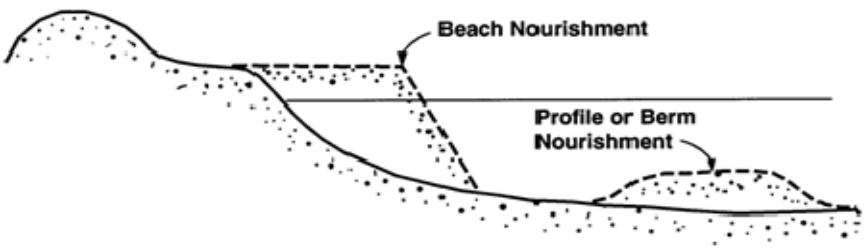


Figure 1. Two Different Types of Nourishment

[1] Dept. Civil and Coastal Eng'g. Univ. Florida, Gainesville, FL 32611.

Settings for Beach Nourishment

Three general settings for beach nourishment are considered.

The simplest setting is that of a long unencumbered shoreline such as shown in Figure 2a. It can be shown that if the nourishment sediment is compatible with the native sediment, the evolution of the project depends strongly on wave height and project length, but is quite insensitive to the wave direction. This is a considerable advantage in design as wave height characteristics are generally much better understood than are wave direction characteristics.

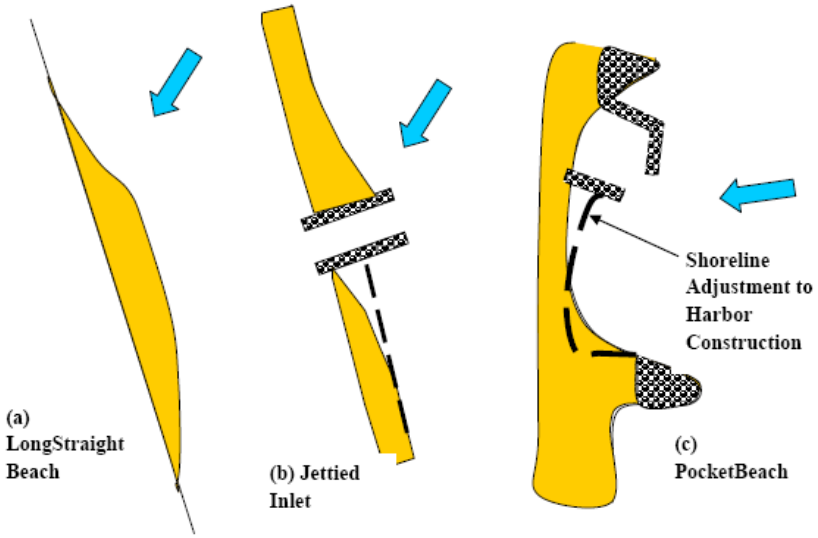


Figure 2. Three Beach Nourishment Settings Considered.

The case of a nourishment project downdrift of a littoral barrier, shown in Figure 2b is somewhat common as structures such as a jetty interrupt the net longshore sediment transport and without bypassing of the net longshore sediment transport, will cause an erosional zone that will progress downdrift. The performance of a nourishment project downdrift of a littoral barrier thus depends rather strongly on the wave direction.

Often a harbor or some other structure placed in a pocket beach as shown in Figure 2c will cause a redistribution of sand within that system and the need for beach nourishment. In other cases the response to sea level rise or construction of a seawall which encroaches on the beach system may be the impetus for nourishment. The post-nourished equilibrium planform in such a case can be approximated by a uniform advancement throughout the pocket beach. The possibility of sand "leaking" out of the system around the containing headlands due to this advancement must be considered.

Aids for Design and Evaluation of Beach Nourishment Projects Performance

In the simple treatment presented here, beach nourishment design can be idealized in terms of profile and planform considerations. Beach nourishment material is usually placed at slopes

steeper than equilibrium and represents a "bulge" in the shoreline. Waves act to equilibrate the beach profile and smooth out the bulge in the beach planform, see Figure 3. Usually the time scale of profile equilibration is considerably shorter than that of planform response which allows consideration of an instantaneous profile equilibration. Once the profile is equilibrated, we assume it stays in equilibrium and moves in the cross-shore direction without change of form. We also assume that the vertical dimension of the active profile is constant. This is usually taken from the berm height, B, to the depth of closure, h_*, discussed in the following section.

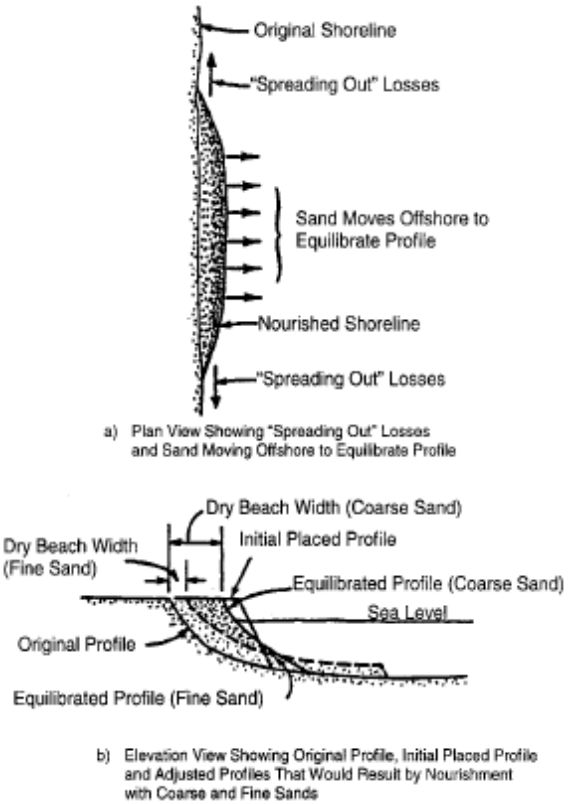


Figure 3. Sand Transport "Losses" and Beach Nourishment Profiles Associated With Beach Nourishment Projects.

Profile Considerations

Depth of Closure: It is clear that the depth to which the profile is active depends on the particular wave and, possibly to a lesser extent, the current characteristics at a particular time. However, in order to carry out beach nourishment design (and many other types of coastal engineering designs), it is convenient to have a definite offshore limit of profile equilibration. This is the so-called "depth of closure" and has been formalized by Hallermeier (1981) as the depth to which the significant wave would cause a certain bottom agitation 12 hours per year. This closure depth will be referred to here as h_*. Figure 4 presents estimates of the closure depth around the sandy beaches of the State of Florida.

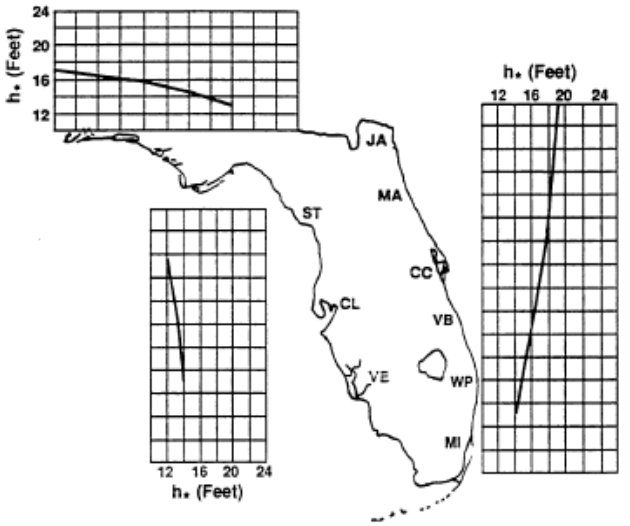


Figure 4. Estimates of Closure Depth Around the State of Florida.

Equilibrium Beach Profiles: Profiles in nature are quite variable. The concept of Equilibrium Beach Profiles (EBPs) is quite valuable providing a means for dealing in the design realm with this complex issue. For beach nourishment purposes, ideally sand can be located that is compatible with the native and thus the equilibrated beach profile will be more or less the same as the native. In such case, the profile response is simplified substantially. However, it may be necessary to consider sands that are finer or coarser than the native.

Compatible Sediments: If the nourishment sediment is the same size as the native, it is generally assumed that the nourished profile will be of the same form as the native profile and it is not necessary to be concerned with the form of the profile. In this case, the profile is considered to translate a uniform cross-shore distance, Δy_0, without change of form over the vertical dimension ($h_* + B$) in response to a change in unit volume, V per unit beach length as shown in Figure 5 and by the equation

$$\Delta y_0 = \frac{V}{h_* + B} \qquad (1)$$

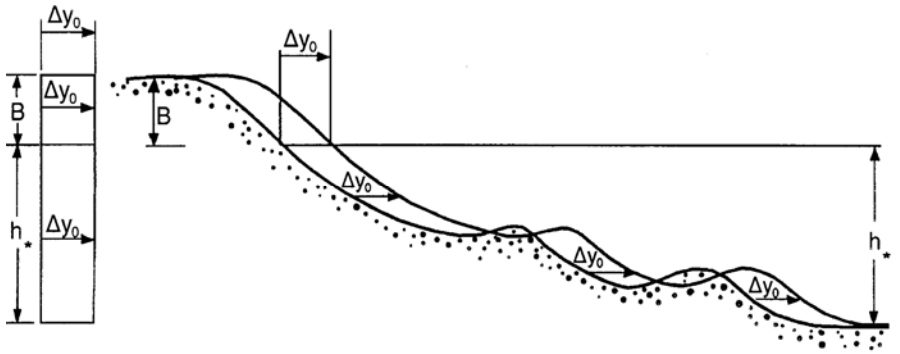


Figure 5. Profile Translation, Δy_0 , Associated With Volume Density Addition, V, Compatible Sands.

Nourishment Sediments Larger or Smaller Than the Native: It is well known that beaches composed of coarser sediments will be steeper than fine grained beaches and that beach profiles tend to be concave upwards. This profile shape has been formalized by Bruun as

$$h(y) = Ay^{2/3} \qquad (2)$$

In which $h(y)$ is the depth at a distance y seaward and A is a "Profile Scale Parameter". Moore (referenced in Dean, 2002) examined many profiles and found the relationship between A and sediment diameter, D shown in Figure 6.The effect of a nourishment grain size different than the native results in the possibility of three classes of nourished profiles: "submerged", "non-intersecting" and "intersecting" as shown in Figure 7. Here we will not be concerned with the detailed methods of calculating the equilibrated dry beach width, but simply note that as shown in Figure 8, there are substantial advantages in nourishing with coarser material which results in more dry (visible) beach for a given quantity of sediment. Figure 9 presents the additional dry beach width versus nourishment sediment volume for three sediment sizes.

It is noted that methods are available, but not presented here, for dealing with the more realistic problem of nourishment sediments represented by a range of sizes.

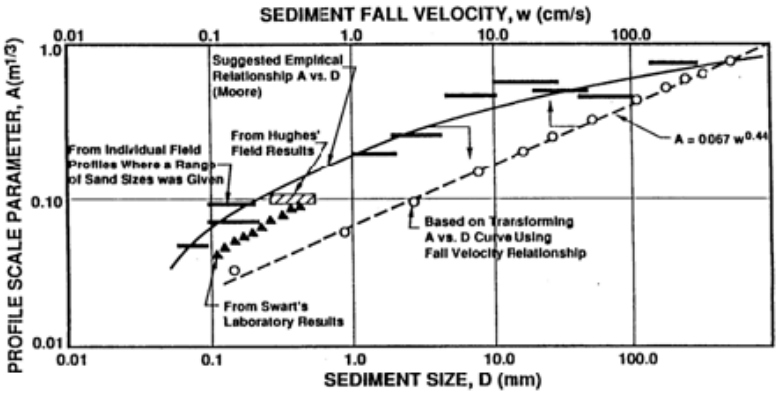


Figure 6. Variation of Profile Scale Parameter, A ,With Sediment Diameter, D, and Fall Velocity, W.

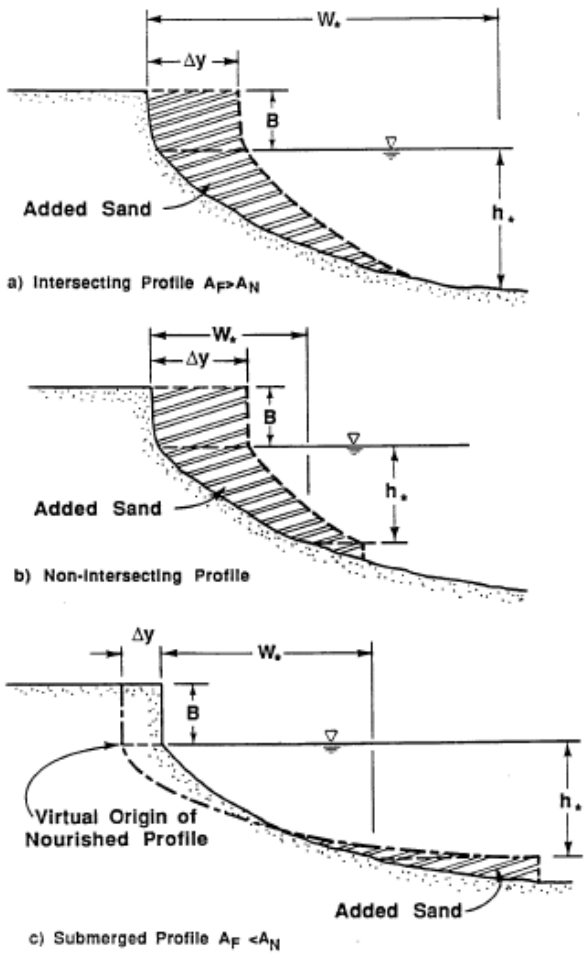


Figure 7.Three Generic Types of Nourished Profiles.

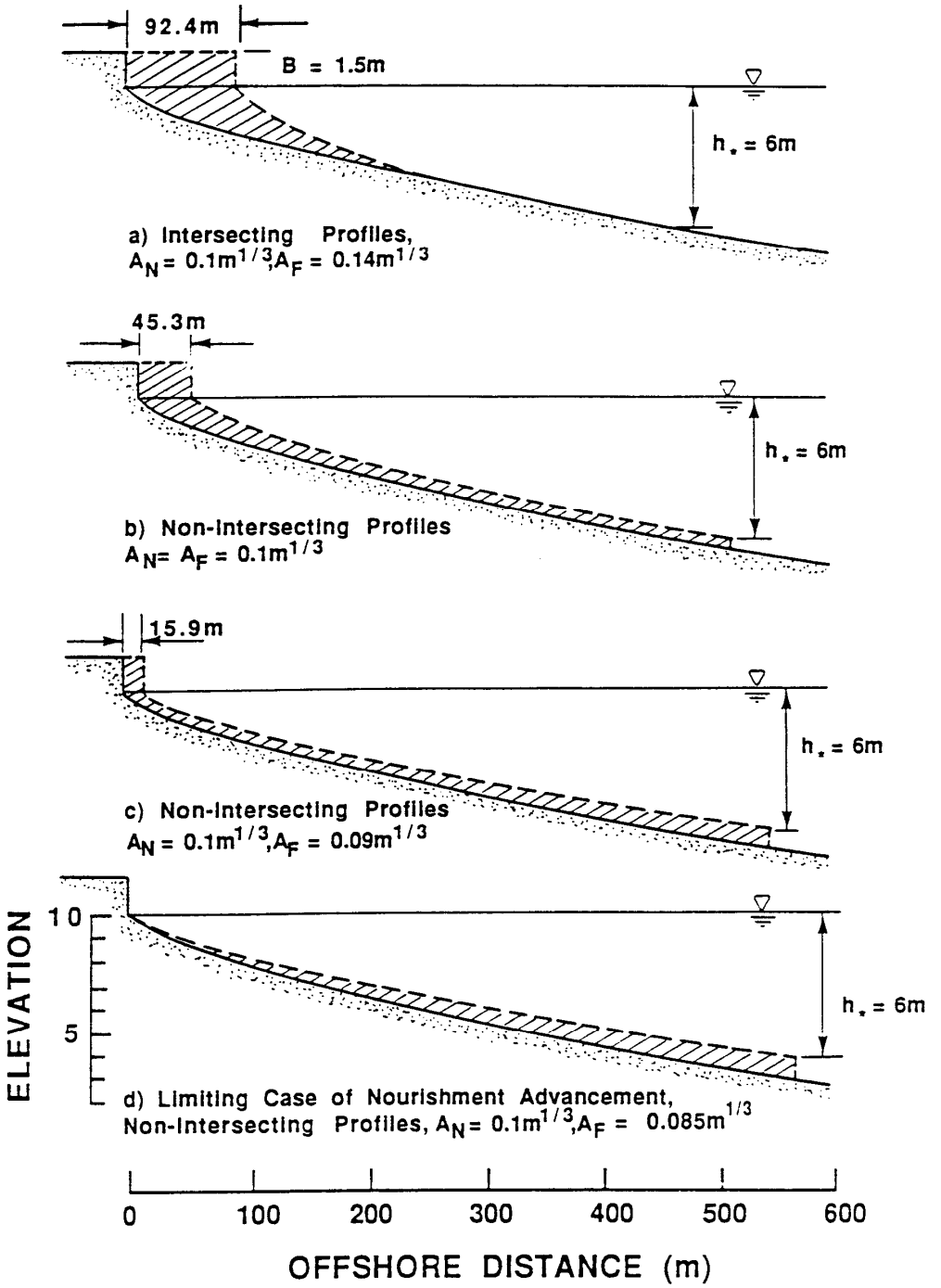


Figure 8.Effect of Nourishment Material Profile Scale Parameter, A_F on Equilibrated Dry Beach Width, Four A_F Values. Same Nourishment Density of 340 m^3/m (135 yd^3/ft) for All Four Cases. Nourishment Profile Scale Parameter = 0.1 $m^{1/3}$.

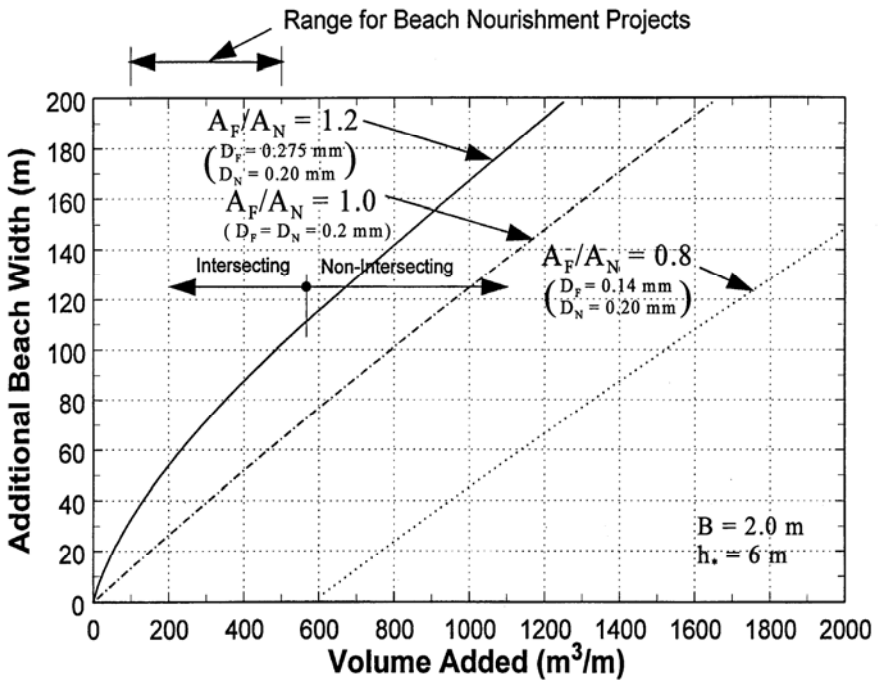


Figure 9. Additional Dry Beach Width Versus Volume of Sand Added per Unit Beach Length. h_* = 6 m, B = 2.0 m.

Planform Considerations

The two equations that are applied for nourishment planform predictions are the sediment transport equation and the continuity equation. These two equations are incorporated into a fairly simple one-line numerical model that allows for the representation of groins as well as beach nourishment projects. This Fortran program and a Users Manual are available upon request from dean@coastal.ufl.edu. The transport equation depends on the wave height and wave direction and the continuity equation simply keeps us honest requiring that sediment eroded from one area is deposited in another. Stated differently, in our accounting of sediment volumes, we do not create or destroy sand. The numerical model considers the profile to remain in equilibrium and can account for longshore variation of background erosion simply by superposition.

Based on wave gages that the Department of Coastal Engineering maintained along Florida's shorelines for a number of years, a number of aids have been developed. These include the closure depth based on Hallermeier's formulation (1981) shown in Figure 4 and an effective wave height (Figure 11) and wave period (Figure 12).

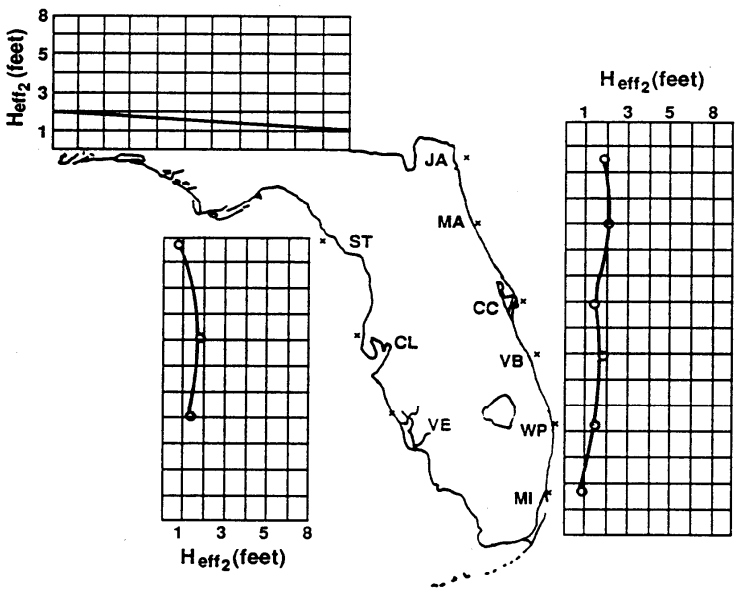


Figure 11. Estimates of Effective Deep Water Wave Height Around the Florida Peninsula.

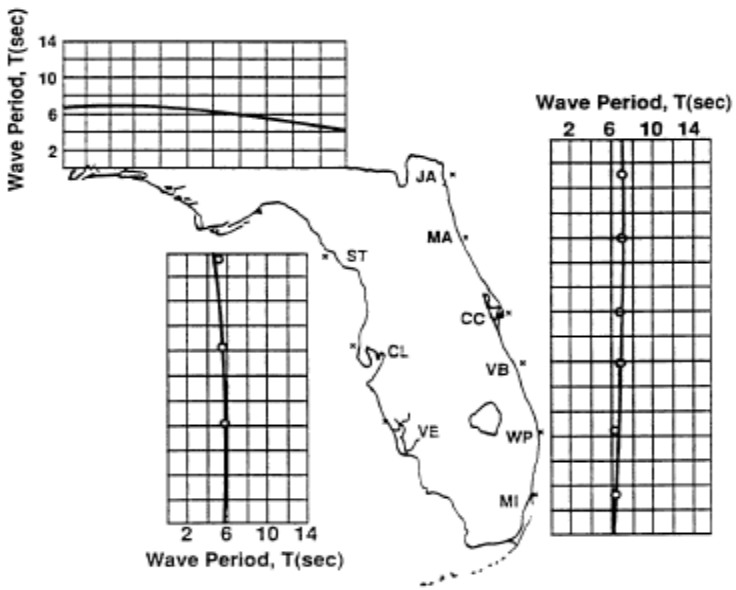


Figure 12. Estimates of Effective Wave Period Around the Florida Peninsula.

Examples of the Monitored vs Predicted Performance of Two Beach Nourishment Projects

The documented and predicted performances of two representative well-monitored beach nourishment projects in Florida will be examined.

Delray Beach, FL: Delray Beach, FL is located on the Florida southeast coast, has been nourished since 1973 and yearly monitoring of this 2.65 mile long project has been conducted. This project setting is the most simple being located on a long straight beach (see Figure 2a). Table 1 summarizes the nourishment history. Through 2002, a total of 5.75 million cubic yards had been placed and it has been shown that in addition to providing a wide beach over the 2.65 mile project length, this project has acted as an effective "feeder beach" for the adjacent shorelines. Figure 12 presents a pre-project photograph in the 1960's and shows that the coastal highway which serves as an evacuation route had been threatened. The revetment in Figure 12 is composed of interlocking concrete blocks and was constructed and failed, then reconstructed and failed a second time followed by beach nourishment. Figure 13 presents a 2010 Google photograph of the Delray Beach project area in which the beach is approximately 250 to 300 feet wide. Additionally, as noted, the beaches to the north and south of the project area are now much wider that prior to the first nourishment.

Figure 14 presents the results of a "blind-folded" comparison of the monitored and predicted performance in terms of total sand volume remaining within the placement area. The terminology "blind-folded" means that there were no adjustable parameters applied in the prediction methodology.

Table 1

Delray Beach Nourishment History

Nourishment Date	Nourishment Volume (Millions of Cubic Yards)
1973	1.63
1978	0.70
1984	1.3
1992	1.02
2002	1.10



Figure 12. Portion of Delray Beach, FL Shoreline in the Early 1970's. Failed Interlocking Revetment.

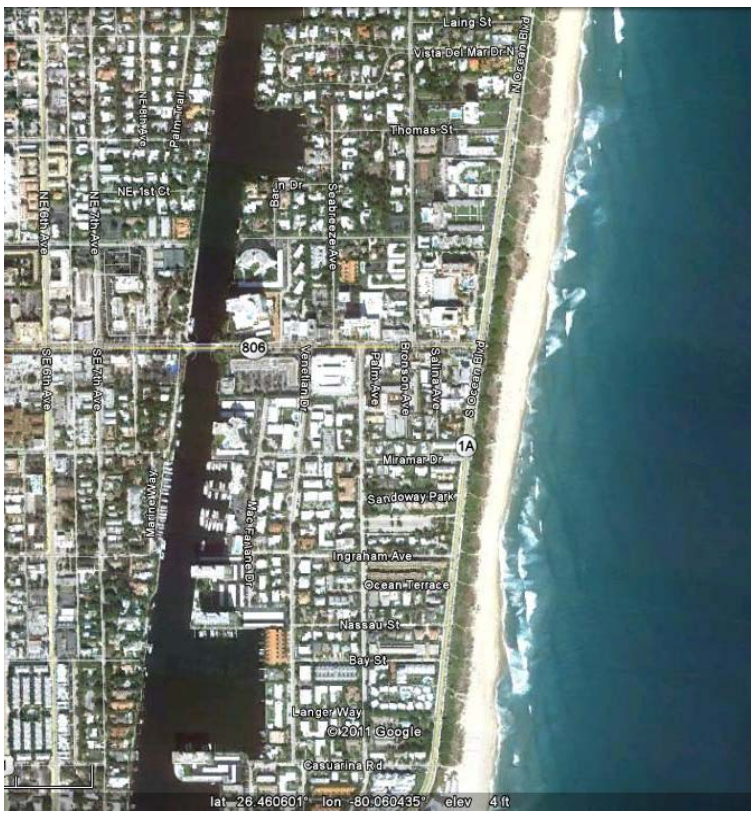


Figure 13. 2010 Google Photograph of Delray Beach, FL in Which the Beach is 250 to 300 ft Wide.

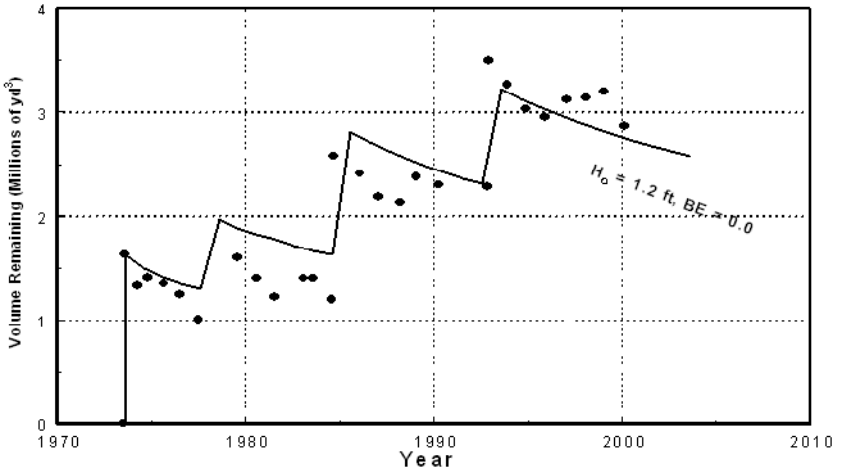


Figure 14. Blind-folded" Comparison of Monitored and Predicted Delray Beach, FL Project Performance. Note: "BE is "Background Erosion".

Perdido Key, FL Beach Nourishment Project: Perdido Key is part of the Gulf Islands National Seashore administered by the National Park Service. It is located in western Florida immediately west (downdrift) of Pensacola Pass which has been dredged for more than a century, see Figure 15. This project was somewhat unique in the sense that the sand was free! The Navy was considering locating a Homeport in Pensacola Harbor which required deepening of the Entrance Channel and Harbor. Most of the sand was of high quality and provided a very good match to the white silica sands comprising the native beach. It was less expensive to place this sand on the beach than in an offshore disposal site. This project setting is one of the more difficult as the appropriate boundary condition on the eastern end next to Pensacola Pass is not obvious. In nature, the nourished shoreline at this end is affected by waves and currents. For purposes here, a "pinned" boundary condition was considered at the eastern end. The western boundary condition is represented by simply extending the numerical model a sufficient distance west such that the model limits do not affect the model performance. The project was constructed in 1989 – 1991 and comprised the placement of 5.4 million cubic yards of beach nourishment over a beach length of 4.4 miles and 3.9 million cubic yards as an underwater berm in water depths of 6 m over a length of 2.2 miles. Figure 16 shows the project under construction in 1989.

The project was monitored for a total period of approximately 8 years including 33 profiles, two directional wave gages, a tide gage and a meteorological station.

A blind-folded comparison of the predicted and monitored performance is presented in Figure 17. It is seen that both the monitoring and predictions indicate greater loss rates at the eastern end of the project. Also of interest in Figure 17 are the more rapid loss rates associated with the incidence of hurricanes affecting the area (Browder and Dean, 2000)

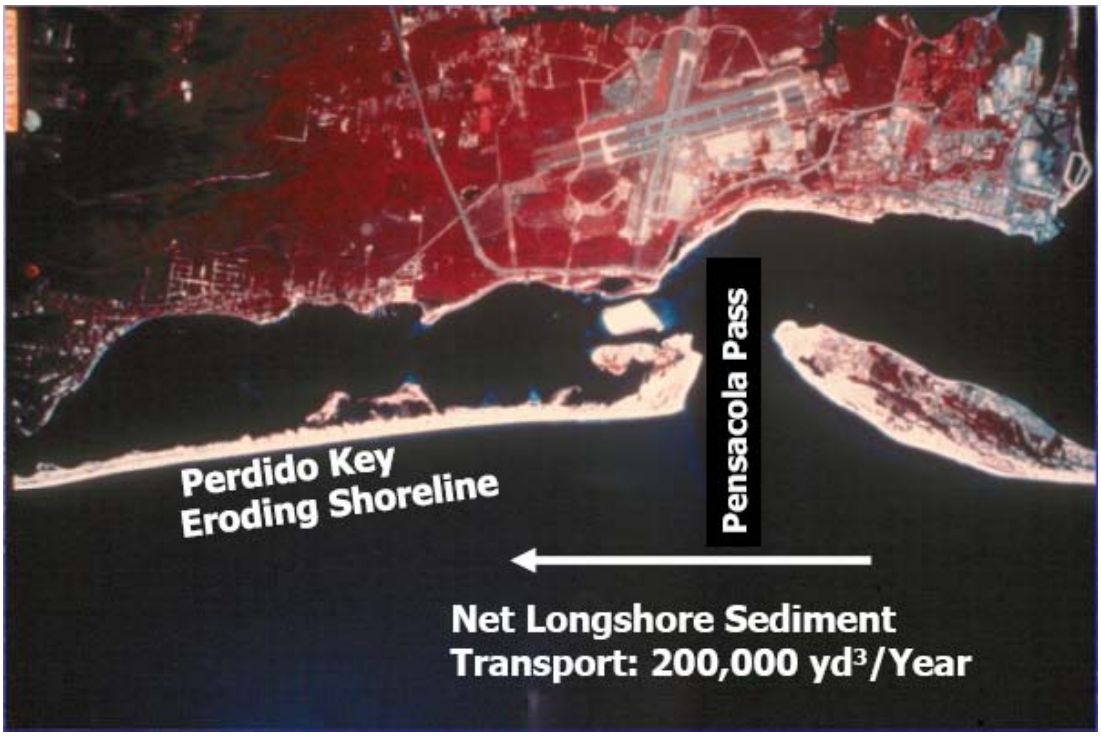


Figure 15. Perdido Key, FL Project Location.



Figure 16. Perdido Key During the 1989 Nourishment.

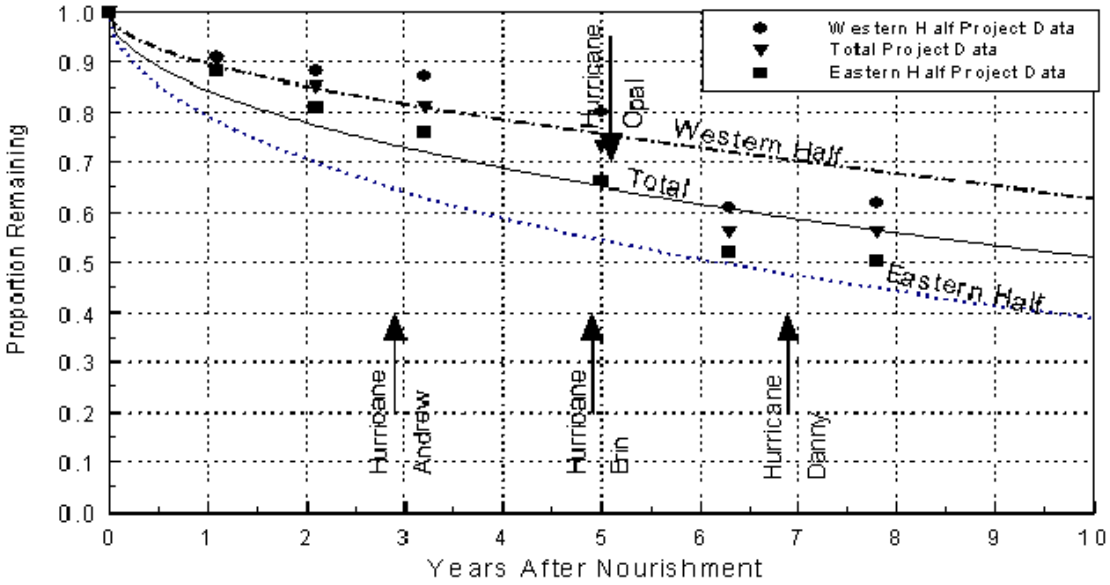


Figure 17. “Blind-folded” Comparison of Monitored and Predicted Perdido Key, FL Project Performance.

Conclusions

Development and application of quite simple beach nourishment design and evaluation aids has proven effective for Florida beach nourishment projects. Of greatest importance are estimates of the depth of closure and effective wave heights around the sandy beach portions of the state. These quantities and local variables including berm height and background erosion serve as input to a simple one-line numerical model that has proven effective in predicting overall performance to within $\pm$ 25%. This design aids provide a structure against which monitoring results can be compared, thereby improving the design aids. Similar design and evaluation beach nourishment aids are encouraged for other locations.

References

Browder, A. B. and R. G. Dean (2000) “Monitoring and Comparison to Predictive Models of the Perdido Key Beach Nourishment Project, Florida, USA”, Coastal Engineering, Vol. 39, pp. 173-191.

Coastal Planning and Engineering, Inc. Personal Communication Regarding Delray Beach, FL Nourishment Porject.

Dean, R. G. (2002) “Beach Nourishment: Theory and Practice”, World Scientific, Inc., 399 Pages.

Hallermeier, R. J. (1981) “A Profile Zonation for Seasonal Sand Beaches From Wave Climate”, Coastal Engineering, Vol. 4, No. 3, pp. 253-277.

Applying the Design/Build Project Delivery Method to Shore Protection and Other Coastal Works Projects

James E. Spady, PE, M.ASCE [1]

[1] Clark Nexsen, 6160 Kempsville Circle, Suite 200A, Norfolk, VA 23502; PH (757) 455-5800; FAX (757) 455-5638, email: jspady@clarknexsen.com

ABSTRACT

The design/build method of procurement is now a major source of project administration for the Owner and has been successfully employed through a broad spectrum of construction. Recent history indicates that building and bridge construction has been the primary beneficiary of the design/build procurement method but there has been a movement to deploy this contracting method to other project types including shore protection and other coastal works. As this project delivery method migrates into these specific areas, the design/build team will be faced with a set of challenges not typically experienced within the traditional design/build project. These challenges may include lengthy regulatory reviews that influence the design and construction schedule, adjusting project goals and requirements as existing physical features change during the design and construction process, modifying design solutions to address the unknown conditions inherent to construction along the shoreline, and adapting construction activity to address the local fauna and flora regulatory requirements. Conversely, the benefits that can be derived from the design/build project delivery method can be substantial relative to the overall project costs. These benefits can include better design solutions resulting from the collaboration between designer and contractor, reducing the owner's administrative time and expense by consolidating the contract into a single design/build entity, potential to reduce the project delivery time, and a coordinated effort between designer and contractor to quickly address field issues that arise during construction.

Understanding the opportunities and challenges presented to the design/build team is essential to ensuring a successful result from the collaboration between owner, designer, and contractor. Owners, Designers, and Contractors who function within the shore protection and coastal works field should be particularly aware of these opportunities and challenges as the traditional project delivery methods are replaced by the design/build project delivery method.

INTRODUCTION

The design/build procurement method is not a recently discovered contracting method rather it is a return to the "master builder" concept of construction. The "master builder" would bear the responsibility of designing, procuring materials, and

overseeing all aspects of construction from conception to final completion. The "master builder" method of construction has been employed throughout the world over many centuries and examples can be found when visiting many countries. These examples would include cathedrals, pyramids, roads, henges and monuments, breakwaters, ports, harbors, navigation channels, irrigation systems, and virtually any type of project or structure that could be conceived and constructed by the "master builder". Design/build procurement has become relevant in today's construction environment through the re-joining of the Designer and the Contractor to create the design/build entity.

The design/build procurement method is rapidly becoming the procurement method of choice for contracting agencies with limited budgets and pressing infrastructure needs. The design/build procurement method, which merges the design and construction responsibility into a single entity, allows the designers and builders to collaborate to make sound decisions that result in better value solutions for the Owner. The design/build procurement method also serves to reduce the demands on the Owner's manpower resources since multiple contracts can be consolidated into one contract between the Owner and the design/build entity. This consolidation of contracts allows the Owner to reduce the time and effort expended for project coordination and contract administration.

The design/build procurement method has grown to become a substantial portion of the contracting method employed by contracting agencies. According to the Design-Build Institute of America (DBIA 2011), non-residential design/build procurement has steadily increased from 1985 to the present. The Design-Build Institute of America (DBIA 2011) projects that by 2015 design-build procurement will capture approximately 50% of the non-residential market, design-bid-build projects will capture approximately 40% of the non-residential market, and the remaining 10% of non-residential projects will be accomplished employing the construction management at risk procurement method. This growth trend is expected to continue into the less traditional design-build markets including shore protection and other coastal works projects as contracting agencies continue to pursue more effective contracting methods.

With the growing trend of design/build procurement it becomes important, regardless of project type, size, or location, for the Owner to be able to employ this contracting method when applicable. Further, it is incumbent upon the Designer and Contractor to understand the intricacies of design/build procurement to determine whether their business organization and business plan can support participating in this method of project procurement.

DESIGN/BID/BUILD AND DESIGN/BUILD COMPARISION

The design/bid/build organizational relationships require each entity, i.e., Owner, Designer, Contractor, etc., to participate within the project framework as dictated by the various contractual agreements. Figure 1. characterizes the interaction

between the design/bid/build parties when executing a project by means of the design/bid/build method. The solid arrows in Figure 1. indicate not only the contractual commitments but also the communication hierarchy anticipated in a design/bid/build contract. The dashed arrows in Figure 1. indicate the communications conduit between the Designer and the Contractor which occurs when the Designer intends to convey design intent or additional information by means of the Request For Information protocol. It is readily apparent that the Design/Bid/Build procurement method requires extensive effort to build and maintain records of communication between the various parties.

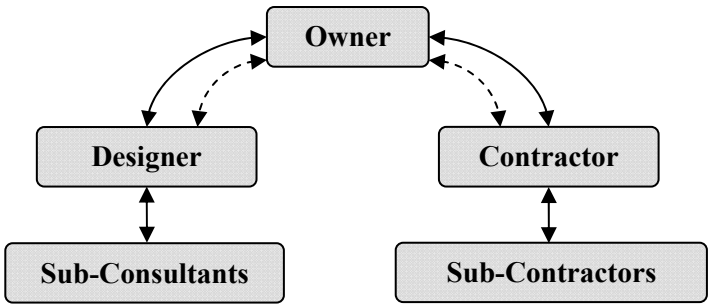


Figure 1. Typical Design/Bid/Build Relationship Diagram

Figure 2. illustrates a typical project procurement flowchart for the design/bid/build process. This flowchart indicates the various steps that an Owner, Designer, and Contractor will execute to provide the various services or activities needed to develop, design, bid, and construct a design/bid/build project.

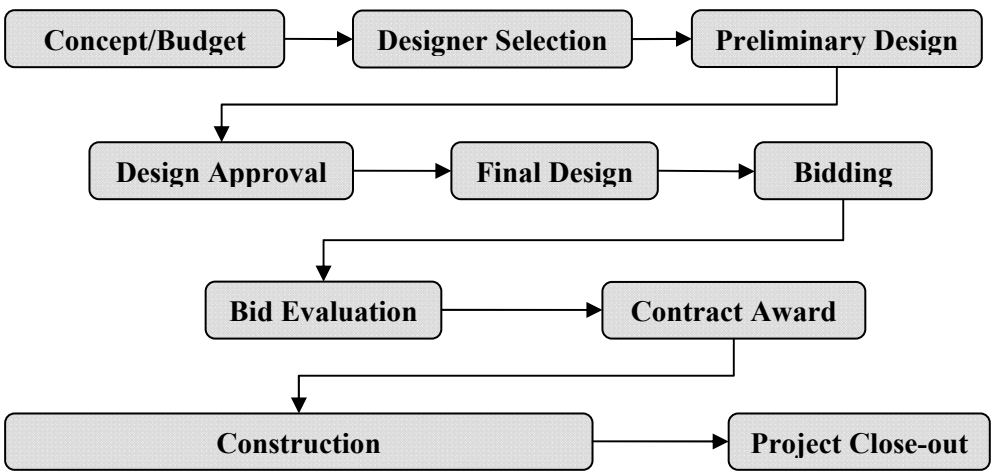


Figure 2. Typical Design/Bid/Build Procurement Flowchart

The Concept/Budget, Designer Selection, Design Approval, and Contract Award phases are typically the responsibility of the Owner. The Preliminary Design and Final Design phases are typically the responsibility of the Designer. The Construction phase is the responsibility of the Contractor. The Bidding, Bid

Evaluation, and Project Close-out phases are typically shared responsibilities between the Owner and the Designer. It is worth noting that each step in the design/bid/build process must be effectively completed before the subsequent step can be initiated. Another condition of the design/bid/build process demonstrated by the flowchart is the disjointed involvement by each participant during the process, i.e., the Owner, Designer, and Contractor alternate responsibilities and assignments throughout the design/bid/build process. These two circumstances frequently result in "dead time" or "waiting time" that inhibits the parties from completing their assignments and responsibilities in a timely fashion.

The design/build organizational relationships allow the Owner to designate responsibility for the design and construction of the project to the design/build entity. Figure 3. demonstrates the interactions between the various parties within the design/build process. The solid arrows in Figure 3. indicate the contractual commitments and the communication hierarchy expected in a design/build project and the dashed arrows represent the communications conduit within the design/build team. The design/build team concept reduces the number of separate entities participating in the process thus reducing the administrative time associated with contract administration, record keeping and communications.

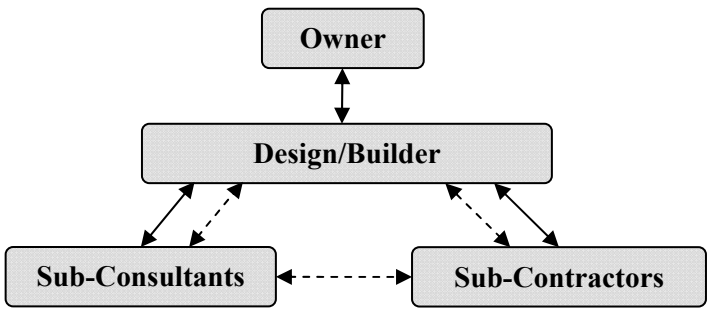


Figure 3. Typical Design/Build Relationship Diagram

Figure 4. represents a typical project procurement flowchart for the design/build process. Similar to Figure 1., this flowchart indicates the various steps that an Owner, Designer, and Contractor will perform to provide the various services or activities needed to develop, design, bid, and construct a design/build project.

In the design/build procurement method the Concept/Budget, Design/Builder Selection, and Design Approval phases are typically the responsibility of the Owner. The Preliminary Design, Final Design, and Construction phases are typically tasked to the design/build team. The Project Close-out phase is typically a shared responsibility between the Owner and the Design/Builder. By combining the design and construction entities into a single team, the process consolidates many of the tasks identified in the design/bid/build methodology. Consolidating tasks and assignments normally performed by separate entities in the design/bid/build allows the design/build team to streamline activities and improve the overall project schedule performance. Further, the "dead time" or "waiting time" experienced in the

design/bid/build process is minimized in the design/build process and the parties can more effectively complete their assignments and responsibilities to meet the project schedule.

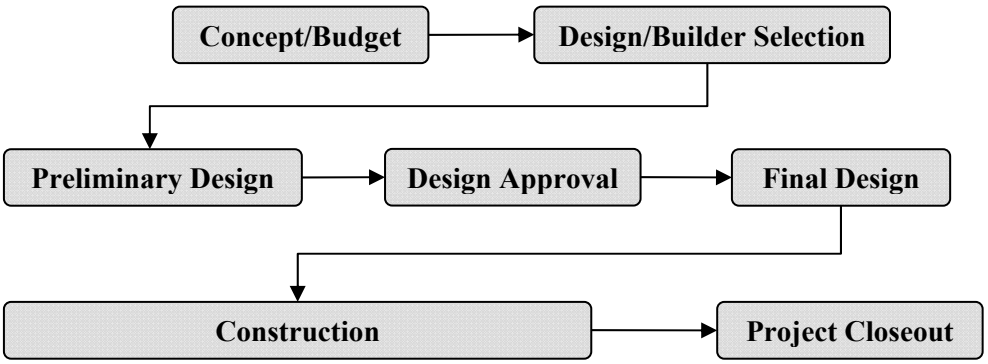


Figure 4. Typical Design/Build Procurement Flowchart

A comparison between the design/bid/build procurement and the design/build procurement Relationship Diagrams and Procurement Flowcharts illustrates three of the key advantages of the design/build procurement method. First, the design/build procurement method consolidates the design and construction effort into a single entity thus reducing the amount of time and effort expended by the contracting agencies' staff to administer the project. Second, the design/build procurement method delegates the tasks and responsibilities associated with the design and construction process to the design/build team thus streamlining the effort expended to procure the project. And third, the design/build procurement process allows the Designer and the Contractor to collaborate during the design/build process to utilize the experience and capabilities of each party to achieve a best value solution for the Owner.

DESIGN/BUILD APPLIED TO SHORE AND COASTAL WORKS PROJECTS

The design/build procurement, when applied to shore protection and other coastal works projects, is very similar to the process employed to perform building and bridge construction. The Owner will develop a conceptual design, provide the conceptual design along with any other specified criteria to each design/build team for pricing, and solicit proposals. The design/build team collaborates to perform the technical effort to prepare a design solution, develops the cost proposal, and submits the proposed design and cost proposal. The Owner receives and reviews the bids and proposed designs and awards the project to the design/build team based on the Owner's specified criteria. The successful design/build team will collaborate to develop the final design which is submitted for approval by the Owner, and then commences construction based on the approved plan. At the completion of construction the Owner performs the project close-out effort and releases any final payments to the design/build team.

This procedure is essentially identical to the procedures required to accomplish the design/build procurement for a building or bridge structure. The variations generally arise during the Concept/Budget phase when initial design considerations begin, during the Final Design phase when alterations to the plan are considered to address Owner and Regulatory Agency input, and during the Construction phase when the Designer and the Contractor work collaboratively to address construction issues.

During the Concept/Budget phase the Owner may elect to have the preliminary design developed to an advanced stage that dictates specific limitations for the design solution and these dictates may impact the construction methods or techniques employed by the Contractor. These limitations may derive from the requirements stipulated by the appropriate regulatory authority, limitations on the accessibility or availability of the project site, or from present and future needs of the Owner. The Owner should be aware that design conceptual plans developed during the Concept/Budget phase may create artificial limitations or restrictions that impact the final design and construction effort and associated project costs.

The Design phase is that period when the design/build team may need to address conditions or requirements stipulated by regulatory agencies. Frequently, the design development will need to be advanced sufficiently to allow accurate analysis and mitigation of environmental impacts. The Designer, Contractor and Owner should be cognizant that the proposed design solution may require adjustments and additional design effort to satisfy the requirements of the regulatory agency.

Changes to the design solution or construction method may result from conditions encountered during the Construction phase. These conditions may result from damage arising from storm events occurring during the construction period, changes to the coastal processes affecting the project site, discovery of unknown utilities or sub-surface structures within the construction area, discovery of items of historical context that may require further investigation by agencies or localities with jurisdictional oversight, or changes to the Owner's operational procedures. The Owner, Designer, and Contractor may need to include these topics in discussions during the initial phases of work to determine appropriate and effective protocols for the various issues which may arise during construction.

SHORE AND COASTAL WORKS DESIGN/BUILD CHALLENGES

Shore protection and other coastal works projects may be subjected to unique project constraints and impacts that building and bridge construction would not normally experience. Building and bridge structures constructed through the design/build process will have reasonably well defined project goals and objectives as dictated by the Owner's requirements. Criteria for building projects related to location, size, orientation, occupancy, loading requirements, architectural context, and sustainability goals can be well defined during the Concept/Budget phase and related to the design/build team for competitive pricing. These criteria can be applied

by the design/build entity to prepare a competitively priced product that satisfies the Owner's requirements. Similarly, criteria for bridge projects can be well described by the Owner during the Concept/Budget phase and conveyed to the design/build team for competitive pricing.

Shore protection and other civil works projects may have less well defined objectives and goals because of changes to existing physical features arising from ongoing coastal processes, interpretation of best practices for the design of shore protection and coastal structures, continued degradation of the existing structure(s) arising from prolonged exposure to the processes causing the damage, implementation of a local design solution that complies with the regional requirements, and requirements to perform long term studies and modeling to validate design solutions. Similarly, goals and objectives that can be well defined during the Concept/Budget phase can change rapidly based on input from the permitting authority, impacts of meteorological events such as storms and hurricanes, resolution of legal conflicts arising from riparian rights disputes, changes in regulatory requirements related to local flora and fauna, and changes to local or regional economies that impact the need for the project.

A list of challenges that may arise when applying the design/build procurement method to a shore protection or coastal works project follows. This list gives a broad spectrum of considerations for projects that may be constructed adjacent to or near the shoreline.

Data Acquisition for the Conceptual Plan. An effective Concept/Budget plan will require that accurate and up-to-date data be acquired to accurately depict the project requirements for the design/build team. This data should include topographic and physical survey, bathymetric survey, subsurface investigations, identification and location of existing utilities, and research of existing contract documents. Often, many parts of these data are not readily available during the Concept/Budget phase and cause the conceptual or preliminary design to be incomplete, overly conservative, or inappropriate for the actual conditions.

The Owner can address the concerns arising from inadequate or incomplete data by providing all documentation used to develop the conceptual plan to the design/build team during the Bidding phase. Providing this data for use by the design/build team during the Bidding phase will convey the limitations of available data and will afford the design/build team the opportunity to consider appropriate contingencies for the price proposal and scheduling proposal. The design/build team may also use this data to determine the level of effort and cost implications that may be required to acquire the needed data. The Owner should also consider providing any future developments or improvements that may impact the project site so that due consideration may be given by the design/build team during the preparation of the proposed design and pricing.

The Owner should use the Concept/Budget phase to prepare sufficiently detailed design requirements so that the design/build team can prepare an accurate design and price proposal. The Owner may require the services of a consultant to assist during the Concept/Budget phase if the development of the conceptual plan goes beyond the technical capability of the Owner's personnel. Because of familiarity with the project and technical requirements the consultant that is retained during the Concept/Budget consultant may also be contracted to assist during the Bid Evaluation phase.

Overly Restrictive Design and Submittal Requirements. The Owner or contracting agency with limited design/build procurement experience frequently reverts to the requirements normally associated with design/bid/build procurement. Thus, the Owner or contracting agency may define "preferences" as requirements, require more submittals then is actually needed, or place artificial constraints on the design and construction process.

One of the benefits of the design/build procurement method is that the Designer and Contractor develop the level of information required to perform the necessary construction effort. There is no significant benefit to require information beyond that needed by the Contractor to perform the work. The Owner and Designer should exercise care during the preparation of the contract documents to avoid including extraneous or superficial information that is not required in the performance of the construction activity.

Similarly, the delegation of the design and construction to the design/build team could result in the reduction of the necessary design submittals. Many contracting agencies employ methods that require submittals throughout the course of design development that may no longer be needed when using the design/build procurement method. In many cases, elimination of unneeded design submittals may result in a reduction of administration time and effort expended by the Owner to review unnecessary design submittals.

Changes to Existing Conditions. Changes to existing conditions result from ongoing coastal processes acting at the project site, impacts of storm events, discovery of items of historical context, discovery of unforeseen sub-surface features, and discovery of flora and fauna that may require mitigation or avoidance. These changed conditions may impact the ability of the Designer and Contractor to accomplish the required work in the allotted schedule.

The Owner, Designer, and Contractor may consider early discussion to determine what contingencies should be included to address conditions that are subject to change during the design and construction process. The time and effort to address changed conditions may be substantial since this may involve acquisition of additional data to validate the original design, design effort associated with validation of the original design, procurement of additional or different construction materials, and addressing environmental concerns through mitigation or avoidance.

Permitting Requirements. The permitting process that is typically required for projects at or near the shoreline can be extensive and time consuming. Flora, fauna, and benthic life forms can be found to have a significant impact upon the design solution, construction methods, and environmental protection requirements employed during the Construction phase. In many cases, the Owner will obtain environmental permits based on the Concept/Budget plan and provide this permit to the design/build team. The design/build team would then bear the responsibility of incorporating the stipulations attached to the environmental permits into the design and construction process.

The Owner may consider assigning the responsibility to obtain the necessary environmental permits to the design/build team in lieu of obtaining and providing permits based on the Concept/Budget plan. Assigning the responsibility to obtain environmental permits to the design/build team allows the Designer and Contractor to have more involvement in and exercise more control over the process to obtain the necessary environmental permits.

The Owner and the design/build team may also consider early coordination with the jurisdictional regulatory agencies to address concerns and requirements that may impact the design solution. If "pre-meetings" with the jurisdictional regulatory agency are permitted then data collected from this meeting may give the design/build team better insights how to adjust or revise the proposed design solution to satisfy the concerns of the appropriate authorities.

Restrictions to Construction Activity. There are often limitations placed on construction activity and scheduling related to Owner requirements, regulations related to local flora and fauna, regulations related to work within environmentally sensitive areas, and regulations related to sound or light emissions. These limitations placed on the effort to perform the construction activity may have a direct impact on project costs since these conditions may require the Contractor to perform work outside of typical working hours, impact project scheduling because of work is limited to a specific seasonal duration, or install physical controls to protect existing flora, fauna, and benthic life forms.

Discussion to review the appropriate protocol related to construction activity limitations may be beneficial to the Owner and the design/build team. These discussion will serve to review the requirements, determine what specific controls will be required to comply with specific construction activity limitations, review the enforcement methods required for each construction activity limitation, and determine how each construction activity limitation affects the ability of the Contractor to perform the work.

Appropriate Project Size. The project size may have an influence on the interest level of Designers and Contractors to collaborate as a design/build entity. Further, the Owner may have reservations to attempt a design/build solution for

smaller projects because there may be little interest from the larger Designer and Contractor and the smaller Designer and Contractor may be reluctant to pursue this opportunity. It is of little value to the Owner to develop a Concept/Budget plan based upon the design/build procurement method and then discover that there is insufficient interest by design/build teams to pursue the project.

The Owner can reduce, or eliminate, this project challenge by conducting a market research to gage the interest of prospective Designers and Contractors. The Design-Build Institute of America (DBIA 2009) contains a Market Research and Acquisition Plan concept which an Owner could use as a tool during the Concept/Budget phase. These types of tools would allow the Owner to gage interest in the project, develop a list of interested Designers and Contractors, and research the expertise and capabilities of the interested Designer and Contractors prior to advertising the design/build project.

Perceived Bias of the Design/Build Process by the Owner and Design/Builder. For Owners, Designers and Contractors who are new to or not participating in the design/build procurement method there is a general perception that the design/build procedures are biased for the other parties. These biases generally derive from the adversarial roles frequently taken by the Owner, Designer, and Contractor during the traditional design/bid/build procurement process. The design/build procurement process often can reduce or eliminate these adversarial roles because the Designer and the Contractor collaborate as a team to develop a best value solution for the Owner who is a de facto member of the design/build team.

A statistical study of a broad spectrum of projects submitted to the Construction Industry Institute was performed for the National Institute of Standards and Technology (Thomas et al 2002) which compared a number of parameters including cost, schedule, safety, change, rework, and practice use. The findings of this study indicate that, in general, there appears to be a performance advantage to the Owner when using the design/build project delivery method but there does not appear to be a clear performance advantage for the Contractor between design/build and design/bid/build project delivery. In general, these findings appear to indicate that design/build procurement could be a suitable project delivery method that does not give an unfair performance advantage to either the Owner or the Contractor. Although the design/build procurement method may not necessarily be suitable for each project type, there does not appear to be evidence that this procurement method is unduly biased toward the Owner, Designer, or Contractor.

DESIGN/BUILD OPPORTUNITIES AND BENEFITS

In a general sense, design/build procurement affords the Owner, Designer, and Contractor with opportunities to improve the outcome of any type of construction project. The benefits accrued through the use of the design/build procurement method typically originate from the potential for schedule reductions, the exposure that staff members receive to the other parties involved in the design/build process,

the opportunity for the Owner to use the Best Value Selection in lieu of the Low Bid Selection, opportunities to deploy the design/build procurement process to smaller projects, and development of relationships between the Owner, Designer, and Contractor.

Potential for Schedule Reductions. A report prepared for the USDOT-Federal Highway Administration (FHWA 2006) to evaluate the effectiveness of the design/build procurement method stated,

> *"The greatest motivation and realized benefit to a project contracting agency of using design-build instead of design-bid-build contacting is the ability to reduce the overall duration of the project development process by eliminating a second procurement process for the construction, reducing the potential for design errors and omissions, and allowing for more concurrent processing of design and constructing activities for different portions of the same project.*"

Reduction of time obligations, whether in regards to eliminating time to administer additional contracts or to reduce project schedules, is a significant contribution to the efficiency of the design/build procurement method. The Owner, the Designer, and the Contractor will benefit from the opportunities afforded when schedules are reduced through the design/build procurement method. In a similar fashion, the potential to reduce contract claims and subsequent schedule impacts is a significant benefit to each participating party since this will reduce the risk of financial loss resulting from litigation or arbitration.

Designer-Builder Collaboration. The opportunity for the Designer and Contractor to collaborate on the design solutions for design/build projects enhances the design product and allows the Designer and Contractor to capitalize on the strengths of each party. Better design solutions afford the Owner with the opportunity to maximize the available budget while receiving the best value solution.

Another benefit of the collaboration between the Designer and the Contractor is the opportunity for each party to learn new aspects about the design and construction of projects. Younger, less experienced design staff members can learn valuable aspects of the construction industry when they are afforded the opportunity to interact with more experienced construction staff members. Conversely, the younger, less experienced construction staff members can be exposed to good design practices through their interaction with more experienced design staff members. Similarly, members of the Owner's staff who participate in design/build procurements can receive valuable experience that enhances their understanding of good design practices, good construction practices, and a better understanding of how to incorporate this knowledge into other projects.

Use of Best Value Selection. The Owner retains specific options rendering decisions to award projects by way of the design/build procurement process. Typically, the Owner may choose to award based on low bid or best value. Low bid

is awarded to the design/build entity that offers the lowest price to perform the work. Best value is the award based on the Owner's interpretation of the total value offered by the design/build entity in conjunction with the specified price. The Owner will include the award method in the project solicitation and, if best value is the selection method, the Owner will identify the specific items that contribute to the perceived value of the project.

In many cases, the Owner will opt to award based on best value because this affords the design/build entity to prepare a design solution and price proposal that is targeted to the specific needs of the Owner. Award based on best value also encourages the design/build entity to seek to achieve a higher level of quality for the proposed design solution but remain within the Owner's budget. A higher quality design solution may result in a more robust and durable structure or system, an extended service life, delivery of the project employing a reduced schedule, or any other specific item that may have relevance to the Owner.

Opportunities to Use the Design/Build Procurement Process for Smaller Projects. The design/build process is typically viewed as applicable to projects with large scope and construction budgets. Owners, Designers, and Contractors are becoming more familiar with the overall design/build procurement process because of the increased use of this contracting method. Owners are becoming less reluctant to use the design/build procurement method for projects with smaller construction budgets as the design/build procurement gains more exposure and demonstrates more successful results. As Owners are challenged to achieve better results with shrinking budgets the use of design/build procurement will become more integral to projects of varying size and complexity.

Development of Relationships Between Owner, Designer and Contractor. One important aspect for the Owner, Designer, and Contractor resulting from the use of the design/build process is the opportunity to develop relationships outside of the normal practice or operating segment. The use of the design/build procurement method encourages individuals to work more closely with and learn more about the business practices of the other parties within the design/build team. These newfound relationships encourage cross-germination of ideas, opportunities, and concerns across the full spectrum of the design/build team and allow the design/team members to increase their knowledge of the overall design and construction process. The result of this interaction between design/build team members is an increased awareness of how those individual's contributions affect the design/build process, improvement of the skills for the design/build team members, and the opportunities to extend these relationships through the increased use of the design/build process.

CONCLUSIONS

The increased use of the design/build procurement method is having a significant impact for Owners, Designers, and Contractors and is expected to become more fully ingrained in the construction industry in the coming years. The growth of

the design/build procurement method is expected to have a positive effect for Owners as they are required to achieve more effective results with shrinking budgets. The design/build procurement method is also expected to have a positive influence with Designers and Contractors as they expand their markets through the integration of the design and construction process.

Although shore protection and other coastal works projects offer a different set of challenges then building and bridge construction, the design/build procurement method can offer opportunities which result in design solutions that better satisfy the Owner's requirements and increase the profitability of the Designer and Contractor. The Owner, Designer, and Contractor should be fully cognizant of the techniques and organizational relationships associated with the design/build procurement method to maximize the value and returns for each participating party.

ACKNOWLEDGEMENTS

Support for this paper has been graciously provided by Clark Nexsen, Architecture & Engineering. Edward C. Westerman, PE, SE, Clark Nexsen Director of Structural Engineering, provided the necessary resources to research several of the topics discussed within this paper. Permission to publish was granted by Clark Nexsen, Architecture & Engineering.

REFERENCES

Design-Build Institute of America (DBIA). (2009). *Manual of Practice*, DBIA, Washington, DC.

Design-Build Institute of America (DBIA). (2011). "What is Design-Build?" http://www.dbia.org/about/designbuild/

Thomas, Stephen R., Macken, Candace L., Chung, Tae Hwan, and Kim, Inho (2002). *Measuring the Impacts of the Delivery System on Project Performance – Design-Build and Design-Bid-Build*. Construction Industry Institute, Austin, Texas.

USDOT-Federal Highway Administration (FHWA) (2006). *Design-Build Effectiveness Study –As Required by TEA-21 Section 1307(f)*. FHWA, Washington, DC. http://www.fhwa.dot.gov/reports/designbuild/designbuild.pdf.

The Challenges of Permitting Coastal Projects in the 21st Century

Walter F. Crampton[1]

[1]TerraCosta Consulting Group, Inc., 3890 Murphy Canyon Road, Suite 200, San Diego, CA 92123-4450; PH (858) 573-6900; email: wcrampton@terracosta.com

ABSTRACT

This paper provides a Southern California perspective on the competing societal interests that coastal property owners, both public and private, must face when dealing with coastal erosion. From the owner's perspective, accelerated coastal erosion creates an urgent need to protect their property; while many others simply view this as a natural process that delivers sand to the beach and can most simply be solved by removing the threatened property. As we enter into the 21st century, there is increasing pressure for the government to regulate and require mitigation for any impacts to the state's shoreline. Moreover, mitigation measures for this impact may result in costs approaching or exceeding the cost of the proposed shoreline stabilization. This paper discusses the challenges of permitting coastal engineering projects and possible measures/solutions for permitting coastal engineering projects in the 21st century.

INTRODUCTION

Upland urbanization has deprived the shoreline of littoral sediment. Implementation of the Clean Water Act has further limited the supply of coastal sediments, essentially making all erosion illegal, including all riverine sands that feed most coastlines. Coastal property owners are dealing with accelerated coastal erosion and the increased need/urgency to protect their properties. Agencies have concluded that coastal erosion is a natural process that delivers sand to the beach, not an emergency that requires shoreline stabilization.

Any proposed shoreline stabilization measures must be mitigated, essentially reimbursing the public for depriving them of the sand that would have otherwise naturally fallen onto and renourished the public's beach. Much debate continues regarding sand rights, who owns the beach, and for that matter, the sand in the coastal bluffs that will some day fall onto the beach.

A corollary question: Does the upland property owner even have a right to use a downslope property to protect his/her property? For shoreline stabilization measures constructed on the sandy beach, or for that matter, any construction below the mean high tide line, is deemed to be on public property, or on the state's sovereign tidelands and requires permission and specific lease arrangements for the "temporary" use of those properties.

Sea-level rise will further accelerate coastal erosion, particularly when considering passive erosion, and must be incorporated into the evaluation of whether to allow the proposed shoreline stabilization. Environmental groups often oppose these projects and can significantly slow down or often stop the project.

Mitigation measures usually result in fees, occasionally exceeding the project's construction costs and can exceed the per foot costs of a comprehensive mitigation program by an order of magnitude or more. Additionally, mitigation fees might never be used to mitigate the impact. Moreover, the ultimate permits may be limited to a finite life or contain rolling easements.

In this paper, we discuss the challenges of the permitting component of coastal engineering projects and possible measures/solutions for permitting coastal engineering projects in the 21st century.

BACKGROUND

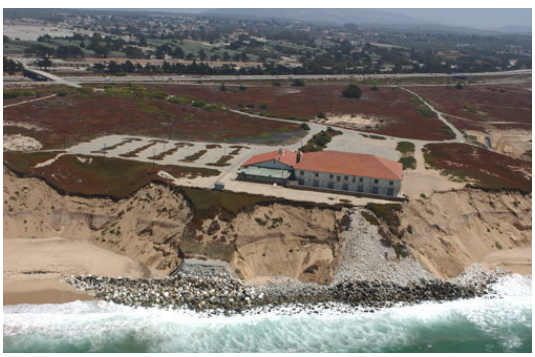
California's beaches define our quality of life and they generate over $15 billion annually in tax revenue. In 1998, the California Department of Boating and Waterways commissioned Dr. Philip King of the Public Research Institute at San Francisco State University to study the economic benefits of California's beaches. In addition to generating over $15 billion annually in tax revenue, California's beaches generated 883,000 jobs across the United States, and when the indirect and induced benefits of spending were added to direct revenue, California's beaches total contribution to the national economy was $73 billion in 1998.

In 1999, the State of California created the Public Beach Restoration Program through Assembly Bill 64, providing $10 million for grants to be administered by the California Department of Boating and Waterways, with one of their products being the California Beach Restoration Study published in January 2002. A motivating factor behind AB 64 was the continued loss of public beaches and a clear recognition of the need to protect this important and valuable state resource. In the Executive Summary of the study report, it was noted that visitors to California beaches spent over $61 billion in 2001, providing significant motivation to protect and restore this economic resource, with the report concluding that beach nourishment is by far the most effective way to restore and enhance California's beaches. The report also concluded that 70 to 90 percent of beach sand originates from California's rivers, but coastal dams currently prevent over one-quarter of the average annual volume of sand supplied by streams from reaching the beaches. The report went on to conclude that removing dams or bypassing sediment around dams could significantly reduce the sediment deficit along much of California's coastline.

The study report's conclusions regarding removal of dams was in part influenced by major efforts from environmental groups, the U.S. Army Corps of Engineers, and the U.S. Bureau of Reclamation to remove two dams built in the 1920s and 1940s within

southern California that have since completely filled in with sediments originally destined for southern California beaches. The Matilija Dam in Ventura County is located about 18 miles upland from the coast, with 5 to 7 million yards of sediment impounded behind the dam, while the Rindge Dam on Malibu Creek in Los Angeles County, located about 2 miles upland from the coast, impounds somewhere between 0.8 and 1.6 million cubic yards of sediment. Notably, the downcoast beaches from both of these watersheds are in critical need of this trapped upland sediment.

The concept of passive erosion was popularized by Professor Gary Griggs from U.C. Santa Cruz using Stilwell Hall at Fort Ord in Monterey Bay as the poster child for passive erosion, graphically showing how coastal armoring destroys coastal access and the loss of the beach (Fig. 1a). The Stilwell Hall example is also noteworthy in that the rock revetment protecting the bluff-top military facility was removed in 2004, thereby enabling the natural coastal processes, within a few years, to reclaim this artificial anthropogenic headland, creating a new natural linear shoreline with a healthy back beach (Fig. 1b).

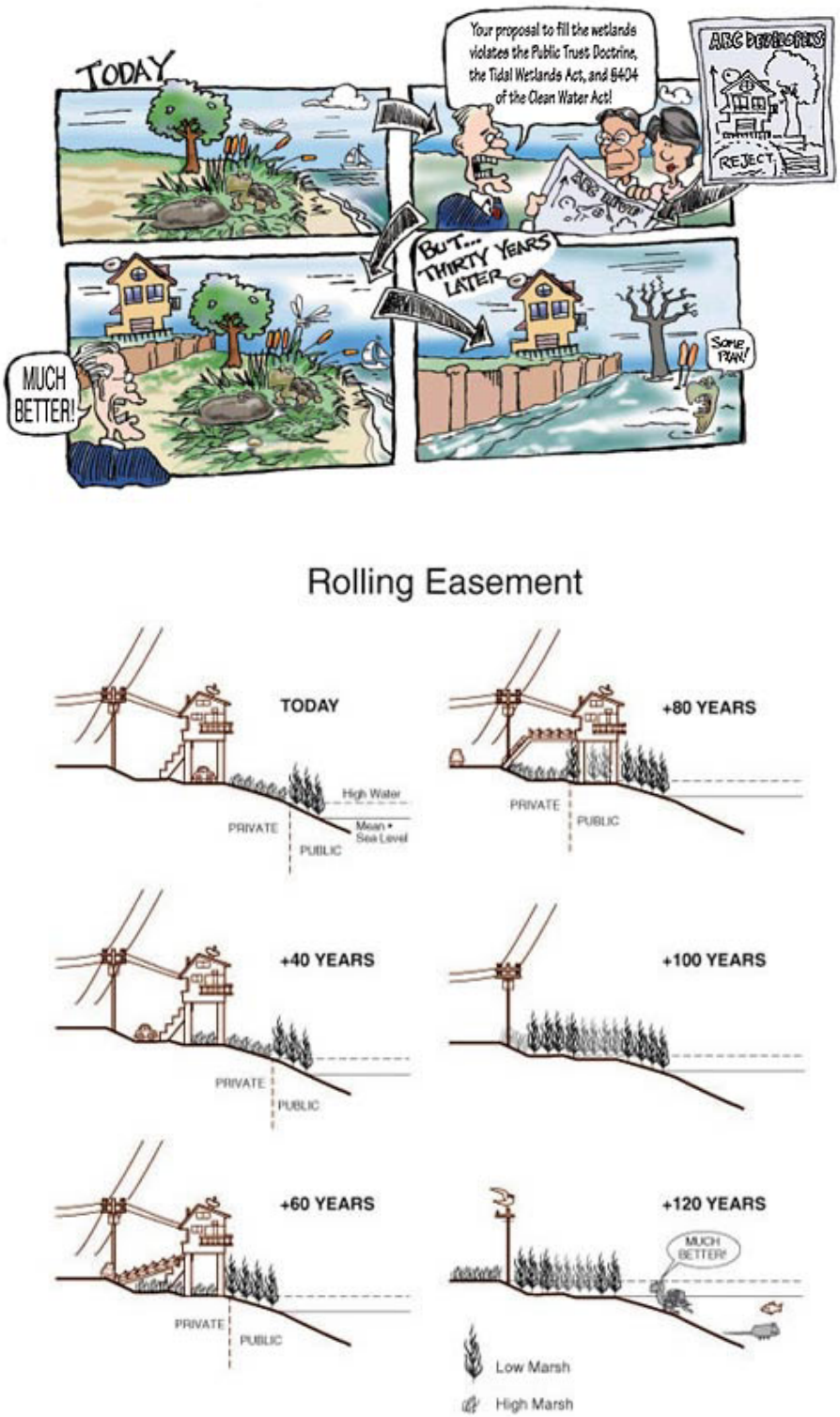




Copyright © 2002-2010 Kenneth & Gabrielle Adelman, California Coastal Records Project
www.californiacoastline.org

Figure 1a. Stilwell Hall-2003 **Figure 1b. Stilwell Hall since removed-2010**

The concept of rolling easements was popularized in 1998 by James Titus of the EPA with his paper titled, "Rising Seas, Coastal Erosion, and the Takings Clause: How to Save Wetlands and Beaches Without Hurting Property Owners." Titus argued that absent policy changes within the next century, the majority of America's publicly owned tidal shorelines could be replaced by a wall, not because anyone decided that this should happen, but because no one decided that it should not. The most common response to coastal erosion has been to build a wall near the boundary between the private dry land and the public tidelands, saving the former but allowing the latter to erode away and this trend would only accelerate with sea level rise. Titus presented a compelling argument for rolling easements, allowing construction near the shore, but requiring the property owner to recognize nature's right to advance inland as sea level rises. The following cartoons (Fig. 2) nicely illustrate the problem with not properly planning for ongoing coastal erosion and the concept of a rolling easement.



Source: James G. Titus, Rising Seas, Coastal Erosion, and the Takings Clause: How to Save Wetlands and Beaches Without Hurting Property Owners. Maryland Law Review (1998), Volume 57, 1279-1399.

Figure 2. The problem with not properly planning for ongoing coastal erosion and the concept of a rolling easement.

In 1999, the Sand Rights '99 – Bringing Back the Beaches Conference focused on the many conflicts and problems that California and other coastal states face as coastal erosion encroaches upon private improvements, addressing both management programs, planning and public policy issues, the value of beaches for the public, and several discussions on sand rights and the rights of private property owners motivated to protect their property weighed against the rights of the public and the public good derived from the public's use and enjoyment of these beaches. Attorney Katherine Stone presented a very thought-provoking series of arguments that sand rights should be incorporated into the state's Public Trust Doctrine, thereby empowering the government to regulate and require mitigation for any impacts to "one of our nation's most important resources."

In 2007, Meg Caldwell, Director of the Environmental and Natural Resources Law and Policy Program at Stanford Law School and who, from 2004 through 2006, served as Chair of the California Coastal Commission, wrote a compelling article for the Regents of the University of California Ecology Law Quarterly titled, "No Day at the Beach: Sea Level Rise, Ecosystem Loss, and Public Access Along the California Coast." In this lengthy article, Caldwell first summarizes the anticipated effects of sea level rise along the California Coast and the attendant pressure to armor the coast as sea level rises, the impacts associated with passive erosion decreasing the quality of the coastal experience for the many visitors to this state's coastline, and the need to reshape local coastal programs, suggesting implementation of rolling easements in California, and the use of the Public Trust Doctrine to fulfill its public trust duties in protecting and preserving the state's tidelands and through extension, the state's shorelines. As past Chair of the California Coastal Commission, there was also considerable discussion covering the five basic policy objectives for coastal use, ranging from protecting and enhancing coastal resources, ensuring balanced resource use, maximizing public access, ensuring priority of coastal dependent uses, and encouraging coordinated planning. When charged with responsibility for sustainability and stewardship, particularly in view of the potential for future sea level rise, she expresses the grave concern that coastal armoring that will accompany rising waters will likely destabilize coastal planning, limit public access, threaten coastal uses, and damage coastal resources. Caldwell argues that it is incumbent upon the state to begin to plan and prepare for sea level impacts now while early action can still be effective. Although owners of existing structures are permitted to armor under certain conditions, the Commission and other state agencies continue to explore management options that respect property owners' rights while still fulfilling their stewardship responsibilities.

In 2008, the Public Policy Institute of California published their study, "Preparing California for a Changing Climate," with a section on Coastal Management addressing the tradeoffs of coastal armoring, beach nourishment, and retreat/relocation, along with possible policy modifications, including the "no further armoring" policy, along with the policy of Rolling Easements.

Given these evolving coastal management considerations, in 1993, the California Coastal Commission began a program for mitigating the quantifiable impacts of seawalls on beach width and sand supply. The Commission developed a three-part formula to derive the dollar amount of the mitigation fee to be levied for each proposed seawall. It is based on three proven and quantifiable effects of seawalls on beach width and sand supply: encroachment, decreased beach width on a retreating shoreline, and reduction of sand supply from cliff armoring. The formula calculates the cost of the sand that would be needed during the life of the structure to offset these effects. The methodology used to derive the formula is technically sound and appropriate. Simplifying assumptions have been made to facilitate its application and to provide consistency. However, it is the applicant's responsibility to provide the numerical values of the variables in the formula, such as the shoreline retreat rate.

Although the Commission can condition a project to require payment of a mitigation fee, the Commission cannot, for example, establish a shoreline property assessment program that could address shoreline management on a more comprehensive basis, and thus the existing sand mitigation fee program, which assesses only those properties that are before the Commission for a particular project, cannot generate sufficient fees to offset the coastwide erosion that continues to plague California and other coastal states. In recent years, the Commission has sought additional ways to quantify the adverse impacts to public access and recreation that result from shoreline armoring in order to develop more appropriate mitigation for those impacts.

In 2005, the Commission contracted with Dr. Philip King to perform an economic analysis of the loss of recreational values associated with a proposed seawall to be located in North County San Diego; however, it was concluded that these types of studies cannot be easily extrapolated to a different project site. Currently, the Commission requires that as part of any Coastal Development Permit application for coastal armoring, applicants address the adverse impacts of shoreline devices on public access and recreation opportunities and to consider ways those impacts could be mitigated. Mitigation might be in the form of a particular public access or recreational improvement to be located in close proximity to the project, or might involve an in-lieu fee to be used some time in the future for a public access/recreation improvement.

In 2007, the City of Solana Beach adopted an interim in-lieu fee program to mitigate the adverse impacts associated with coastal armoring. Until the City completes and the Commission certifies an economic study that more precisely determines the economic cost, the ultimate costs to the property owner remain unknown. As such, the City's program currently requires a $1,000 per lineal foot fee paid as a deposit and an agreement from the applicant that the applicant will pay any additional fees once the economic study is complete and certified by the Coastal Commission.

In October 2010, the Coastal Commission instituted a new program to address the unknown effects of sea level rise by authorizing permits for coastal armoring for only 20 years. "Such authorization for a limited period of time acknowledges the seawall

is not necessarily a permanent structure and allows for a reassessment of site conditions in the future. After 20 years, an Amendment to this Permit will be required to allow the Commission to reevaluate the seawall's efficiency and the impacts it causes to public resources. Any reauthorization of the seawall will be based on the conditions at that time, taking into consideration the status of the existing development requiring protection, impacts and mitigation, and when the seawall might be removed." The wording in recent staff reports is particularly noteworthy: "To ensure that this project does not prejudice future shoreline planning options, including with respect to changing and uncertain circumstances that may ultimately change policy and other coastal development decisions (including not only climate change and sea level rise, but also due to legislative change, judicial determinations, etc.), staff recommends that this approval be conditioned for a twenty-year period. …. The intent of the twenty-year authorization is to recognize this time-frame reality, and also to allow for an appropriate reassessment of continued armoring at that time in light of what may be differing circumstances than are present today. Of course it is possible that physical circumstances as well as local and/or statewide policies and priorities regarding shoreline armoring are significantly unchanged from today, but it is perhaps more likely that the baseline context for considering armoring will be different – much as the Commission's direction on armoring has changed over the past twenty years as more information and better understanding has been gained regarding such projects, including their affect on the California coastline."

PERMITTING COASTAL PROJECTS IN A CHANGING CLIMATE

The economic value of this state's beaches is undisputed, particularly in urban areas, and given the specter of a potential one, to worst case two meter rise in sea level by the end of the 21st century, coastal regulators are taking a more aggressive approach to the permitting of coastal armoring. When considering new coastal armoring projects, the development team must be able to stand in the shoes of the regulators and to understand and address their very real concerns over the sustainability and their responsibility for stewardship of the coastline.

As engineers, we should always strongly endorse the removal of any impediments to upland sediments from reaching the littoral zone to replenish the state's beaches, including when appropriate the removal of no-longer functioning dams or, for that matter, flood control facilities. As engineers, we should speak against the unintended collateral consequences of legislation like the Clean Water Act that precludes sediment from leaving upland sources that were previously destined for the littoral zone.

As coastal engineers, we should discourage those prospective clients that live atop coastal bluffs comprised of unconsolidated sediments on eroding shorelines similar to Stilwell Hall from attempting to obtain coastal permits for armoring their shoreline. As coastal engineers, when conducting an alternatives analysis for a proposed project, we should honestly and objectively consider the viability of a rolling easement as

proposed by Titus and others. In short, as coastal engineers, we must take a holistic approach to every proposed project. A prospective client/property owner faced with accelerated erosion threatening his/her improvements might, upon objective reflection, prefer a softer solution when objectively weighing the long-term consequences and cost of any imposed mitigation on a coastal armoring project.

Given these many challenges, one must also consider the geomorphology of the California coastline. While this state's geology contributes to its spectacular coastal scenery, it also raises some interesting challenges and opportunities for coastal management, where the shoreline is backed by erosion-resistant rocky coastlines, coastal plains, and marine terraces. In all instances, the bedrock sea floor continues seaward of the sea cliff, and it is on top of this bedrock substrate that the transient beach sands reside. Thus, in addition to the rocky coastline, we are also trying to protect this fairly thin ribbon of sand that has, over the geologic millennia, fairly persistently fronted many of our coastal bluffs; that is, until man's habitation of this state's coastal watershed. This is an important concept, as the elevation of the bedrock sea floor at the base of the sea cliffs typically ranges from a few feet above mean sea level to about 5 feet below sea level, and in the absence of a transient sand beach, this bedrock sea floor has relatively little recreational value; it is simply so low in elevation that it is almost always inundated within the coastal surf zone or, in the case of more erosion-resistant bedrock, deep water often exists at the base of the coastal bluff.

It is the transient sand beach fueled by the upland watershed that maintains this thin ribbon of sand that we, as a state and a nation, have come to embrace. The Southern California coastal wave environment is such that the waves build the back beach berm up to about elevation +10 to +12 feet, and it is this beach berm, occasionally several hundred feet wide, that represents the resource that we are all trying to protect.

Many lose sight of the true impact of over 80 percent of southern California's residents living on the west side of the coastal range, with all of this urban development clearly impacting the sediment supply to the state's beaches. These conflicting societal interests, presumably for the benefit of the citizens of Southern California, have proven to be to the detriment of Southern California's coastal resources.

A fundamental problem along many areas of southern California backed by coastal bluffs is that today, there is an almost total absence of sand, exposing the underlying bedrock sea floor and exposing the sea cliffs to significantly more coastal erosion. Along most of California, this has occurred in the almost total absence of seawalls, and in those areas of the coastline comprised of relatively erosion-resistant sea cliffs, the removal of seawalls that currently protect these sea cliffs will not fix the problem. Once this fundamental fact is understood, it should become obvious that planned retreat, managed retreat, or rolling easements will likewise not fix the problem for those beaches backed by erosion-resistant sea cliffs. This should in no way diminish

the importance of removing coastal armoring protecting this state's unconsolidated coastal bluffs like those at Stilwell Hall, but in other areas along the state shoreline, where coastal erosion is advancing at such a slow rate, often at less than an inch per year, passive erosion is simply not a problem. Within an otherwise massive erosion-resistant geologic unit, faulting may create a localized zone of increased erosion, necessitating the construction of a seawall to protect bluff-top improvements. Clearly in these areas, passive erosion is not a concern, but that said, a rolling easement based on the erosion of the adjacent non-fractured bedrock should also be acceptable to the property owner.

As a practicing coastal engineer, I will represent that bluff-top property owners today recognize the severity of coastal erosion along the California coast and the regulatory challenges that they will face to protect their property. It is also fair to say that not one property owner relishes the thought of spending over half a million dollars to protect their home from the significantly increased erosion resulting from the urbanization of the upland watershed. However, they too recognize that, by their proximity to the top of the coastal bluff, they are also part of the bigger problem. Given the realities of climate change and the mandate placed on the regulatory agencies charged with the stewardship of this state's coastline, the piece-mealing of shoreline armoring projects on a lot-by-lot basis will become more difficult, if not impossible, in most instances to permit. Coastal engineers must take a holistic approach, addressing the coastal geomorphology contributing to the problem and the entire suite of viable engineering alternatives for addressing, and possibly mitigating, what many view as a natural coastal process.

In many instances, where the lower sea cliff is comprised of a modestly erosion-resistant geologic unit, say with unconfined compressive strengths ranging from 10 to 50 kg/cm^2 and previously protected by a modest back beach width of say 100 to 200 feet, little if any marine erosion will occur, with annualized erosion rates of less than 1 inch per year, given the southern California wave environment.

Fast forward several decades, urbanize the upland watershed, and sever the riverine sediments that at one time supplied the beaches; add to that sand mining within the lower reaches of the coastal rivers and we see the loss of the one-time persistent back beach (previously around elevation +10 to +12 feet) now regularly exposing the bedrock shore platform near mean sea level, with the sea cliffs now subjected to wave attack on a daily basis. Given this environment, the annualized erosion rate may increase to something on the order of 0.5 to 1 foot per year, creating the need for upslope property owners to protect their properties. Given this scenario, one must recognize that this beach did not disappear because seawalls were built. The opposite is true: seawalls were needed because the beach disappeared. Assume now for a moment that no seawalls are allowed in the hopes that some modest transient beach will develop; however, the simple reality is that, in this example, the coastal bluffs possess sufficient erosion resistance so as to release coastal bluff sediments at such a slow rate that the available littoral transport capacity of southern California's wave environment simply sweeps these sands out of the system. Planned retreat or rolling

easements cannot and will not measurably replace the 10+ feet of sand loss that previously comprised the persistent back beach solely due to the urbanization of the upland watershed.

Depending upon the net seasonal littoral transport volumes, these coastal segments may also lend themselves to beach nourishment projects intended to replace the relatively narrow recreational beach to again provide sufficient protection to the relatively erosion-resistant sea cliff that backs the beach. When necessary, a relatively narrow nourished beach can be augmented by coastal armoring, typically a seawall, with the federal benefit cost (bc) ratio of such a project generally exceeding the bc ratio of a wider nourished beach sufficiently wide to preclude any future erosion of the sea cliffs backing the beach. This is the case with the proposed U.S. Army Corps of Engineers Encinitas-Solana Beach Shoreline Protection Project in North County San Diego, with the bc ratio of a narrow beach backed by limited coastal armoring of 1.46, while the wider beach nourishment alternative, absent any sea cliff protection, had a bc ratio of less than 1.

While California's Beach Restoration Study and the Public Policy Institute Study both recommend beach nourishment as a viable alternative given the proper wave and shoreline environment, project funding is often problematic, particularly now given the economic conditions of both the state and federal government. That said, the Coastal Commission's current proposed mitigation fee structure, coupled with a 20-year permit life, makes privately funding even relatively large coastwide beach nourishment projects an attractive alternative to simply paying mitigation fees that may never result in a substantial beach nourishment project, with its attendant increase in property values.

Coastal communities throughout the state are starting to consider the benefits of pursuing the formation of a Geologic Hazard Abatement District (GHAD) as a political subdivision of the state for the prevention, mitigation, abatement, and control of geologic hazards, including coastal erosion, as authorized under Division 17 of the Public Resources Code. When formed, the GHAD is a state agency governed locally either by the property owners within the boundary of the agency or, if desired, by the local city council. The GHAD can issue bonds at tax exempt rates to fund planning, design, and construction. Assessments levied on GHAD property owners pay for the bonds and maintenance of improvements. Assessments are directly related to the amount of benefit each property receives. The listed benefits of a recent San Diego County GHAD include:

- A comprehensive plan for both the rebuilding of the beach and the protection of the bluffs along this section of shoreline
- A plan that delivers increased beach access and improves safety for everyone using the beach
- A means to finance sand retention systems with a combination of private seed money and funding from various public sources
- A uniform and aesthetically pleasing solution for the entire project area

- Economies of scale, providing significantly lower costs, simplified procedures, and fast results compared to pursuing a series of individual projects
- A vehicle to assure ongoing maintenance and renewal of existing protective systems
- A means to finance seawall and infill projects with private funding
- A financing vehicle for owners who otherwise could not afford the cost of improvements
- Provides a proactive and positive demonstration model of coastal management for the California Coastal Commission

Two GHADs currently exist in San Diego County, both providing coastal protection, with another GHAD in the planning stages specifically intended as a coastwide program for beach nourishment as mitigation for the construction of those shoreline armoring projects considered necessary, with the permit duration concurrent with the GHADs commitment to maintain a prescribed renourished beach. This program meets the objectives of the Public Policy Institute's program for California coastal management with a changing climate, and similarly achieves the objectives of saving the beach by James Titus.

As we proceed into the 21st century, the permitting of coastal protection projects will require a coastwide perspective with the needs of the public likely driving many of these projects. As coastal engineers, we must pursue project alternatives that address the needs of all interested stakeholders; truly a challenging undertaking.

SKAGWAY SMALL BOAT HARBOR - VERTICAL WAVE BARRIER

Nels Sultan[1], Ph.D, PE, Steve Spencer[2], PE, Todd Nottingham[1], PE and Lisa Dale[1], PE

[1]PND Engineers, Inc., 811 First Avenue, Suite 570, Seattle, Washington, 98104;
p. 206.624.1387; e-mail: nsultan@pndengineers.com

[2]Pacific Pile & Marine, 582 S Riverside Drive, Seattle, Washington, 98108;
p. 206.331.3873; e-mail: steves@pacificpile.org

ABSTRACT

This paper describes the design and construction of a partially penetrating vertical wall breakwater in Skagway, Alaska. The breakwater was constructed using ½-inch thick steel galvanized pipe pile with flat sheet pile welded to either side to form a "combi-wall". A steel waler along the top transfers lateral wave impact loads to pile clusters with vertical and batter pipe piles. The wave barrier blocks waves, while allowing fish passage and water circulation through the gap between the bottom of wall and seafloor. The entire 330 feet long structure was transported on one barge, requiring careful load-out and planning. The wave barrier was designed by PND Engineers, Inc. and installed by Pacific Pile and Marine, LP. The project was completed with no injuries and received the 2010 Project of the Year Award from the Pile Driving Contractor's Association (PDCA).

INTRODUCTION

The City of Skagway became the first incorporated city in the Alaska Territory in 1900. Skagway was the "Gateway to the Klondike" during the gold rush of 1898, which brought waves of prospectors in search of gold. For the past 20 years Skagway has been a tourist destination, drawing people from around the world to experience the breathtaking Alaskan landscape.

Today the Skagway port area provides berths for five cruise ships up to 1000 feet in length. During the cruise season, these ships deliver nearly 10,000 visitors each day to the community. A popular destination is the inner harbor where tour boats, fishing charters and local fisherman moor their vessels. The Municipality of Skagway has long planned to expand this popular area, but the plans were frustrated due to the wind and waves which the surrounding fjord funnels towards the harbor. Expansion of the inner basin required a breakwater to protect expanded facilities.

The project site is located immediately south of the entrance to the Skagway Small Boat Harbor (Figure 1). The breakwater (Figure 2 and 3) is adjacent to the Alaska Marine Highway Ferry Terminal float to the west. The ferry terminal and nearby cruise ship docks were a factor for design and construction. During the summer, as many as four cruise ships dock along the small Skagway waterfront. Harbor boat traffic is also at its maximum during the summer. Traffic in and out of the harbor significantly decreases near the end of September at the end of the cruise ship season.



Figure 1. Aerial Photo – Skagway Small Boat Harbor – Before Construction

Working in Alaska is not for the faint of heart, and Skagway is no exception. Although the summer months boast beautiful, mild weather with long days of sunlight, these prime months are unavailable for construction due to the influx of seasonal tourism. The winter months are quite different. Although still a beautiful place, Skagway, sitting in a valley between the mountains, acts as a wind tunnel for very cold Northerly winds or strong Southerly winds that cause disruptive waves on the waterfront. The wind in combination with short days makes it a challenging environment for construction.

Construction was done in late 2009. The early spring was unavailable due to in-water permit restrictions. Construction began when Pacific Pile and Marine (PPM) arrived

onsite in late September, after the cruise ship season. The crews worked long hours in the harsh Alaskan fall conditions to avoid the even harsher winter weather in December. PPM was able to complete construction of the breakwater by late December by staying focused and diligent.



Figure 2. Skagway Small Boat Harbor Wave Barrier

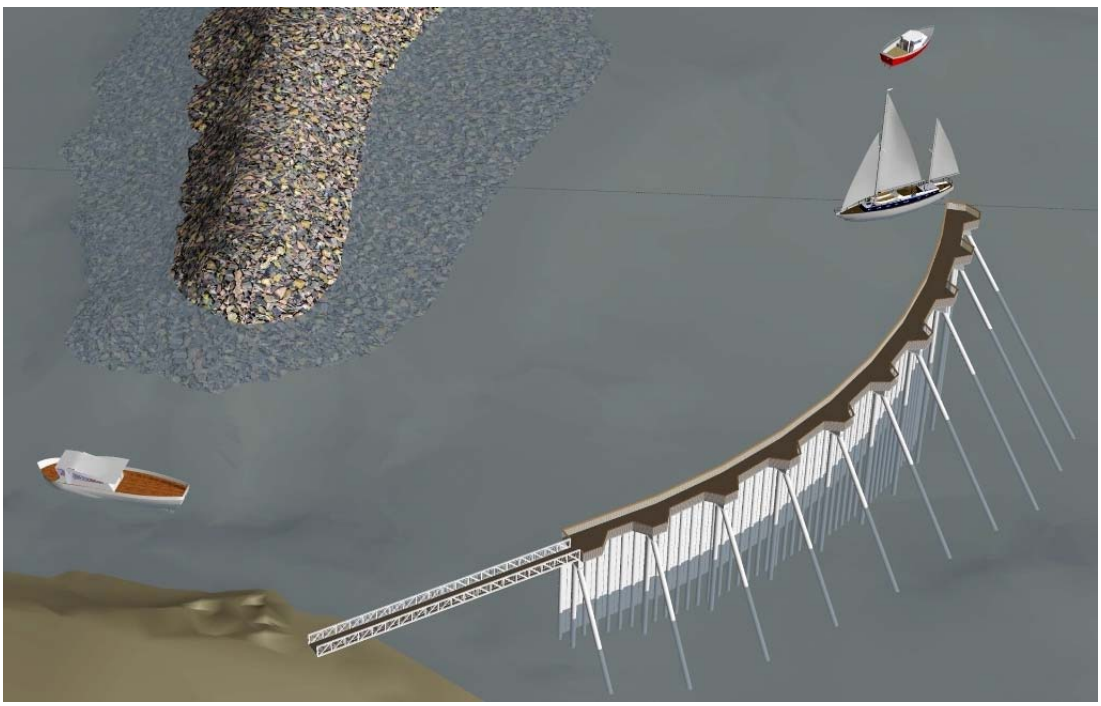


Figure 3. Skagway Wave Barrier – Oblique View (Rendering)

PROJECT NEED

The Municipality of Skagway accepted the transfer of the Skagway Small Boat Harbor from the State of Alaska approximately 10 years ago and has periodically commissioned improvement projects in the harbor area. The projects have focused on uplands improvements, and pedestrian accessibility. The Municipality's plans for inner harbor improvements were stalled due to the southerly wave surge that entered the partially protected harbor. To protect the marina, and the boats moored in the harbor, the Municipality considered various breakwater concepts which would serve to improve the harbor's security without affecting operations. The breakwater concepts were discarded as undesirable or impractical until the partially penetrating breakwater was shown to be viable in the water depth outside the harbor

With the strong public and tourist presence in the region, the Municipality also required a structure which was aesthetically pleasing, as well as pedestrian accessible. Typically, a breakwater wall stands alone, providing an important functional role for a harbor area. To this end, a public access, timber promenade on top of the breakwater was created. This is the first structure of its kind in the area and has attracted much use.

DESIGN FEATURES

The partially penetrating breakwater design is an ideal application for the Skagway harbor entrance, considering the unique site conditions, water depth and wave environment. The breakwater was designed to protect from southerly waves in waters up to 70 feet deep, while providing an adequate entrance channel width. The technology and its development are described in a number of references including PND (1998), Gilman and Kriebel (2000), BC Research Corporation (1991) and USACE (2007). Vertical wave barriers are an area of active research, with recent results reported in Kriebel (2007) and Rao, et al (2009), among others.

The partial penetrating breakwater includes a steel wall composed of steel pile and flat sheet pile with supporting bearing pile. The wall is formed is a series of 20-inch diameter steel pipe piles (half-inch wall thickness) with flat sheet pile welded to either side. The pile/sheet pile combinations are installed by threading the sheet pile interlocks together to provide a continuous wall. The galvanized pipe pile and flat sheets form a "combi-wall". A steel waler along the top of wall transfers lateral wave impact loads to pile clusters formed from vertical and batter pipe piles. Each pile cluster is attached to the waler with a pinned connection. Figures 4 and 5 show the typical barrier pile and a typical section. Figure 6 shows a photo of the pile cluster box cap, pinned connection and waler, without the promenade.

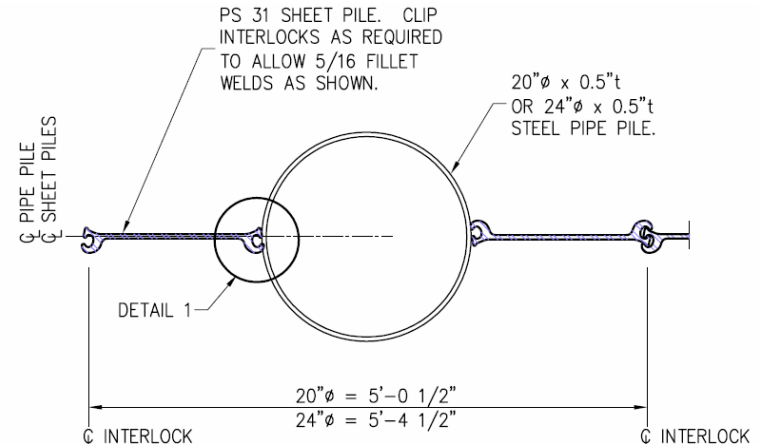


Figure 4. Typical Barrier Pile

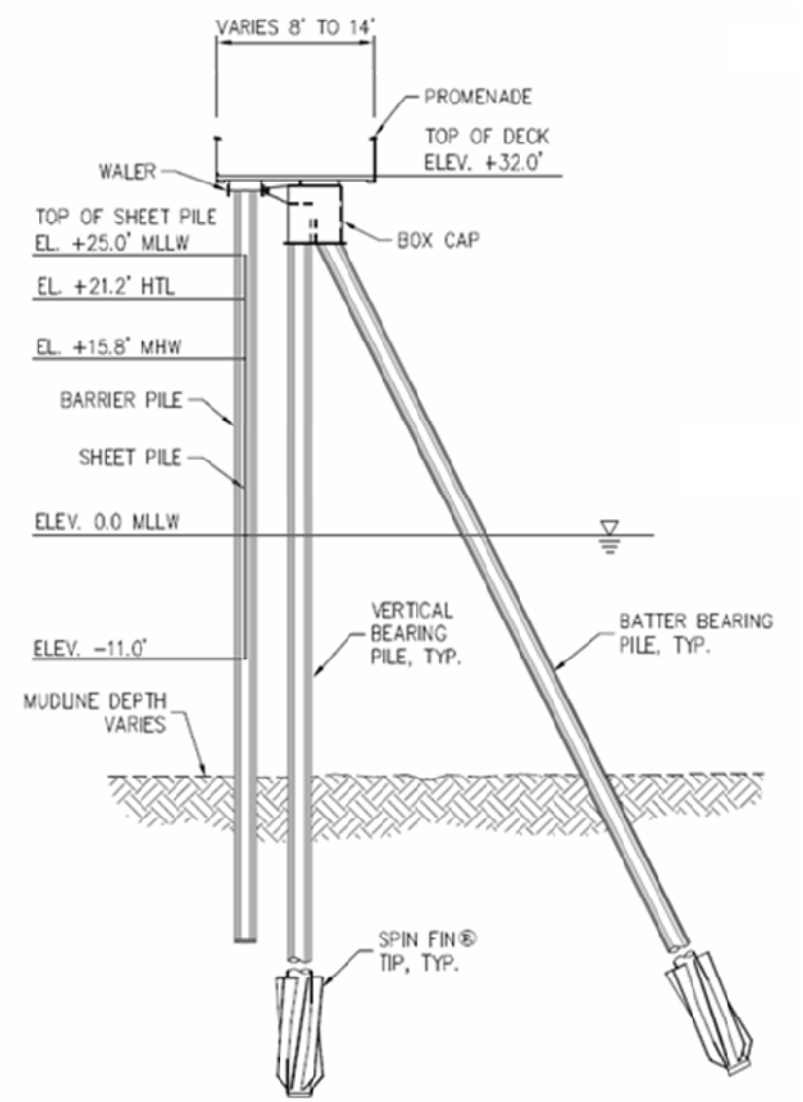


Figure 5. Wave Barrier Section with SPIN FIN® Pile Dolphin



Figure 6. Wave Barrier Pile Cluster, Box Cap and Waler (without Promenade)

The sheet pile wall bottom terminates at elevation -11-feet MLLW, above the seabed. The 20-inch diameter piles are driven into the ground for support, but the sheet pile does not touch bottom. The partial penetration reduces horizontal wave impact loads and significantly reduces material quantities. Most of the wave energy is in the upper part of the water column. The partial penetration also allows fish passage and water circulation through the gap between the bottom of wall and seafloor.

The vertical wall is supported by pile clusters, composed of 24-inch diameter (half inch wall thickness) bearing piles. Each of the bearing piles are fitted with SPIN FIN® pile tips, an innovation developed by PND. These modified tips are composed of several angled steel plates welded to the bottom of the piles which cause the piles to spin when driven. The SPIN FIN pile tips increase compression and tension capacity of the piles, which in turn provides cost savings to the owner through shorter pile lengths. The angled plates provide more bearing and pulling area once the piles are locked off by welding to their caps. The pile tip is shown in Figure 10 later in a later section of this article.

The design is capped by a promenade (walkway), accessed by a 100 feet long catwalk from shore. The timber deck and a perimeter handrail is supported by the waler and bearing pile box caps. This public access feature is a popular attraction for cruise ship visitors and others viewing the spectacular natural scenery, and for fishing and shrimping. The promenade structure added much value to the project for relatively small added cost.

For this project, the partially penetrating vertical wave barrier was the best breakwater choice, providing effective protection while minimizing the footprint of the structure. The Skagway wave barrier includes batter piles to resist the horizontal wave load. However, in shallow water with smaller wave loads the batter piles are sometimes not necessary and a vertical cantilever wave barrier is sufficient.

BREAKWATER TYPES

Vertical wall wave barriers offer a number of advantages that are sometimes overlooked relative to rubble-mound rock breakwaters and floating breakwater alternatives. The choice of breakwater type is largely dependent on wave height and period. The largest waves require rubble-mound structures that are able to absorb wave energy. Floating breakwaters can be used for smaller wave heights and periods, and allow for transient moorage space. Vertical structural wall types address the range falling between that of rubble-mound and floating breakwaters. Figure 7 shows the typical range of application for different breakwater types as a function of wave height and period. Vertical walls are also an advantage where space is limited, and where environmental considerations require a minimal structure footprint.

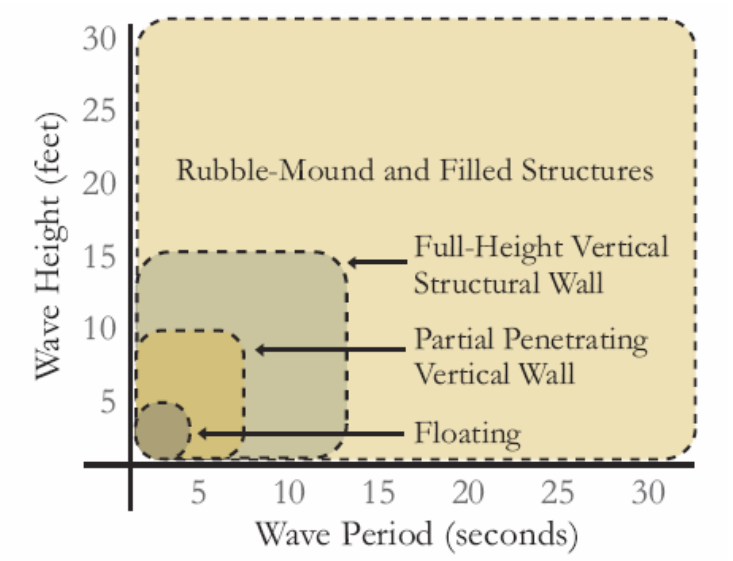


Figure 7. Breakwater Alternatives – Typical Environmental Conditions

WAVE NUMERICAL MODEL

Wave conditions for alternative breakwater alignments were evaluated with the CGWAVE numerical model. CGWAVE is a phase resolving wave model that solves depth averaged equations of wave motion on a finite element mesh. The model is well suited to modeling complex bathymetry and waves in harbors. The model results were compared to desktop calculations to assess whether the model results were reasonable.

Figure 8 shows CGWAVE model output with the breakwater in place. Without the breakwater there is a clear path into the marina for waves. Wave diffraction around the tip of the existing rock breakwater resulted in large, unacceptable wave heights throughout most of the basin. The new breakwater prevents a straight path for waves into the harbor and greatly reduces the wave height. The initial design provided a single curved breakwater. However, after further analysis, a stem wall was included to reduce potentially adverse wave reflections at the adjacent Alaska Marine Highway Ferry Terminal float. After construction only minimal reflected waves were observed moving towards the adjacent ferry float.

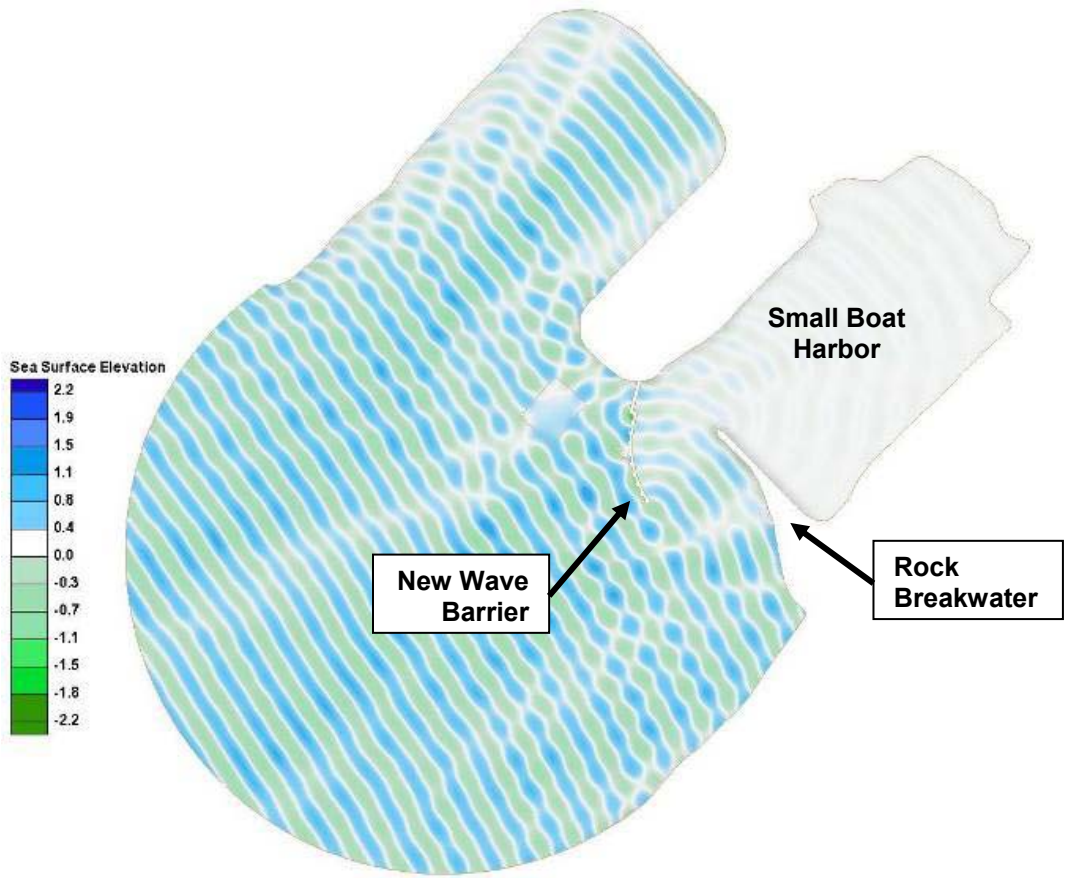


Figure 8. CGWAVE Numerical Model Output – Plan View of Sea Surface

The wave barrier alignment was evaluated considering all factors. The original harbor entrance allowed boats to access the harbor directly from the south. Unfortunately, this also allowed the strong southerly wind storm surges to easily enter the harbor and wreak havoc on the existing float system. The breakwater needed to block the strong southerly wind storm wave surges but also allow clear access into the harbor. The curved breakwater alignment was developed which shields the harbor entrance from southerly storms, while allowing harbor access along a channel from the east.

METOCEAN CRITERIA

Input wave conditions and metocean criteria were determined based in part on measured wind data from the Skagway airport. Wave calculation methods were applied to determine the wave height and period associated with wind speeds and fetch lengths. The hindcast significant wave height, peak period, and maximum wave height were calculated using methods in the US Army Corps of Engineers Coastal Engineering Manual (USACE, 2007).

The design wave for the breakwater has a significant wave height of 5.0 feet, peak period 4.5 seconds. Water depths at the tip of the new breakwater are about 55 feet below Mean Lower Low Water (MLLW) datum. However, the tide range is large, with the highest observed tide in 2006 equal to +24 feet, MLLW. Therefore the total water depth at highest tide can be 80 feet.

Average daytime temperatures in December range from 22°F to 31°F, but feel much colder in fall and winter because of the near constant wind. Daylight was very limited during construction, with only four hours of daylight during December and overcast conditions further limiting ambient light.

DESIGN AND CONSTRUCTION CHALLENGES

Because the only entrance into the harbor was also the project site, construction had to allow harbor boat traffic to enter and exit. The construction location also meant barges and floating equipment would be exposed to strong southerly storms, requiring robust anchoring/mooring systems. Barge anchor systems also had to work around potential conflicts with harbor traffic, adjacent dock traffic and ferry traffic.

Pacific Pile and Marine tackled the project by planning the construction using only two barges. One barge was the designated working crane barge, and the other was a materials barge piled high with steel pile and pre-fabricated items (Figure 9). PPM used their planned construction sequence to guide loading the materials barge in the appropriate order. For this project, the larger bearing piles were among the last to be loaded on the materials barge because they would be the first to be driven into the ground in Skagway. With the exception of a couple items, all the steel pile

and fabricated materials were placed on one barge for the sealift from Seattle, Washington to Skagway, Alaska.

Care was taken in both fabrication and design to minimize work in the field. The tight work window offered little time for field welds and site assembly. Bearing pile box caps were shop fabricated in one piece, wall pile cap beam was fabricated in approximately 30 feet long sections. Handrails were fabricated in sections. The catwalk was completely assembled (except for timber deck) prior to arrival in Skagway.



Figure 9. Barge Transport

CONSTRUCTION MEANS – CHALLENGES AND SOLUTIONS

The project was installed in one season, September-December, 2009. The short construction schedule was a consequence of working around in-water work permit windows, avoiding work during the busy summer cruise ship season, while also avoiding severe winter weather. The project was substantially complete 3 months after mobilization to site. Severe environmental conditions included cold temperatures, wind, snow, limited daylight, rough seas, water depths over 75 feet, and a 20+ feet tide range.

Work scheduling included adaptive management to deal with adverse weather conditions. PPM crews tried to average six twelve hour shifts a week. Rather than scheduling a specific day of the week to take off, the PPM construction supervisors would watch the weather forecast and pick a poor weather day for the day off. If the weather held the crews would work more than six consecutive days. Work would shut down as needed due to bad weather to ensure the crew's safety. Balancing the need to work long hours and a continued commitment to safety allowed Pacific Pile and Marine to complete the project without a single recordable injury.

The pile driving crew was faced with many challenges, including driving 140 to 160 feet long by 24 inch diameter battered bearing piles in high winds, a rough sea state, and 25 foot tides. Figure 10 shows one 24-inch pile lofting into position for driving.

To minimize pile splices in the unfavorable conditions most of the pile were driven full length. Even with water depths approaching 70 feet at high tide, over half of the pile extended above the practical template elevation making them top heavy and unstable in the batter position. To stabilize the pile without extending the template height, PPM offset the pile from the template the necessary distance and vibrated it several feet into the soft marine sediments before laying it over to the batter position. After confirming the pile was correctly positioned and at the correct batter it was vibrated an additional 40 to 60 feet with an ICE 44B vibratory hammer before being impacted to the required tip elevation with an I-36 diesel impact hammer.

Driving the bearing pile in one piece reduced the workers exposure to the elements and decreased their time spent staged on over-water templates. By reducing the need to access the work on icy template beams in windy, dark conditions the risk of falls and accidents was decreased. Figure 11 shows various construction activities, including welding the pile cap to the pile clusters, and threaded barrier piles prior to driving.



Figure 10. 140 to 160 Feet Long Spin Fin Bearing Pile, 24 inch Diameter

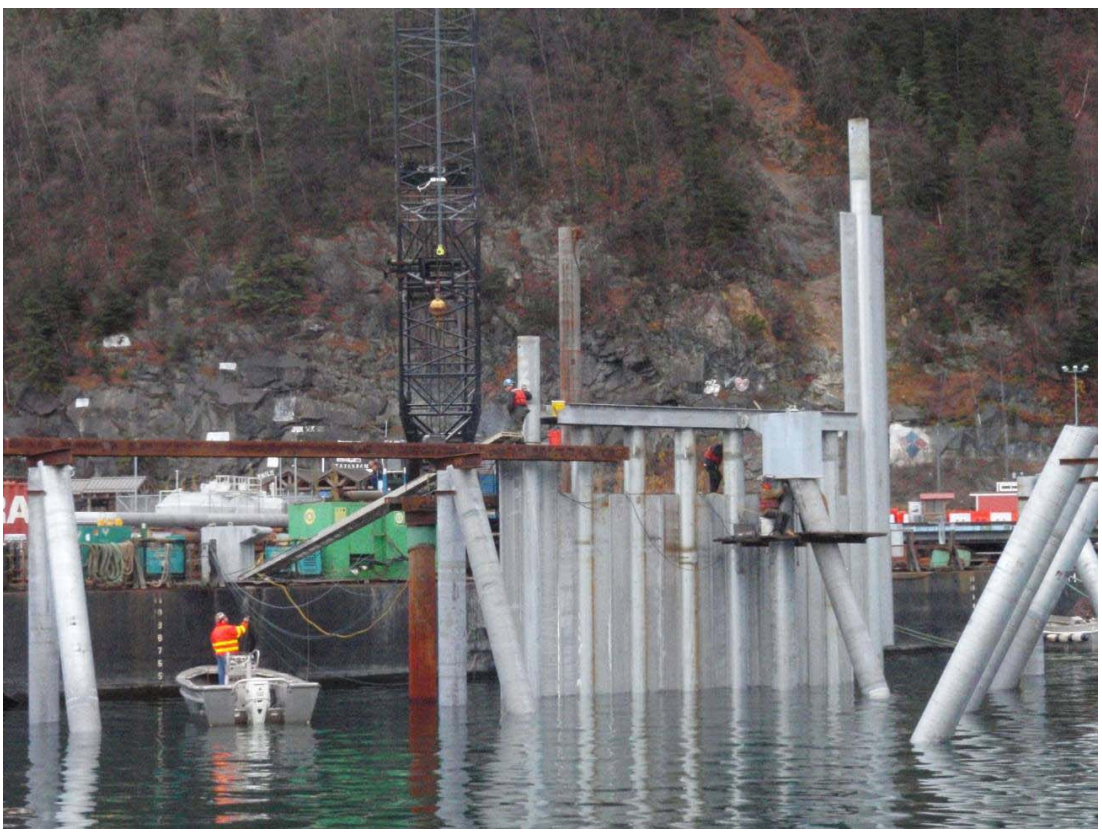


Figure 11. Construction

Installation of the interconnected barrier pile was performed without any significant issues largely due to the pile installation crew's methodical execution combined with the engineer's careful design of the barrier pile lengths in relation to the anticipated mud line elevations. In order to properly function as a wave attenuator the sheet sections of the combination barrier pile had to reach a required depth. Often this required that the pipe section of the barrier pile be set into the marine sediments several feet before the sheets could be threaded. Any misalignment by the pile driving crew made threading the sheets impossible or if threaded would result in a steel bind. PND successfully designed the pile lengths to minimize the length of pipe pile imbedded in the marine sediments prior to threading the attached flat sheets. Had the importance of minimizing pile penetration prior to threading the sheets been unrecognized in the design phase, the contractor would have had a more difficult time constructing the interlocked barrier pile wall.

COST SAVINGS

To construct the partially penetrating wave barrier using the shortest possible pile, the barrier pile were designed with a flat closed end. The two inch thick solid end cap allowed the pile to be terminated at a shallower depth than open ended pile. However, this had the potential of making the pile installation difficult if hard layers were encountered at shallower depths than anticipated.

Achieving the planned pile tip elevations for the barrier piles was critical to ensuring that the flat sheets welded to the pipe sections were all at the same elevation, with an even top-of-wall alignment visible. PPM's installation sequence, generally based on the TESPA (1995) sheet pile installation guidelines, required a stepped installation approach to ensure proper alignment and to avoid steel binding; for these reasons the contractor was reluctant to impact drive the barrier pile if they reached practical refusal with a vibratory hammer prior to achieving the required sheet elevations.

PPM field crews worked closely with the PND field engineer to apply driving criteria that allowed various size holes to be cut in the pile end plate that insured the required tip/sheet elevations were met just before the pile would reach practical vibratory refusal. Through close coordination the contractor's pre-bid planned means and methods did not have to change as a result of variations in the actual subsurface conditions that were encountered, nor did the engineer need to modify the design. As-built pile capacities met the designed pile capacities based on the driving logs and blow counts.

CONCLUSIONS

The new breakwater has worked as intended, successfully blocking waves and greatly improving conditions in the harbor (Figure 13). The owners report a number of storm events after construction that included large waves. This project is a good example of steel vertical wave barrier technology. It is a practical and efficient design that can be installed rapidly. The project also demonstrates that marine based remote construction requires careful load-out and planning. Public access and walkways can be added easily to vertical wave barriers, relative to rock breakwaters, which typically restrict access. The promenade is a valuable feature at relatively low added cost (Figure 12).

With the breakwater improvements located outside the harbor the Municipality is now free to expand their harbor to accommodate increased small boat traffic from the local community as well as the neighboring land locked Yukon Territory. Standard float configurations can now be used that do not have to withstand harbor entrance waves over three feet that had commonly entered the harbor previously. Phased improvements are planned over the next several years including full build out per a harbor master plan that uses the entire basin.



Figure 12. Promenade



Figure 13. **Skagway Vertical Wave Barrier**

REFERENCES

British Columbia Research Corporation (1991). "Physical Model Study of the PN&D Wave Barrier with Evaluation in a Proposed Harbour Expansion at Seward, Alaska" (report), Vancouver, Canada.

Gilman, J.F. and Kriebal, D.L. (2000). "Partial Depth Pile Supported Wave Barriers: A Design Procedure", in Proceedings of Coastal Structures '99 Conference, Losada (Ed.), ISBN No. 9058090922, pp. 549-557.

Kriebal, D. (2007). "Experiments on Oblique Wave Interaction with Vertical Wave Barriers", Coastal Structures 2007, Proceedings of the 5th Coastal Structures International Conference, pp. 259-270.

Peratrovich, Nottingham and Drage, Inc. (1998). "Wave Barrier Design Procedure", report to the Alaska Science and Technology Foundation, ASTF Project 95-3-110.

Raoa, S., Shirlala, K.G., Varghese, R.V. and Govindaraja, K.R. (2009). "Physical model studies on wave transmission of a submerged inclined plate breakwater", Ocean Engineering, V. 26, pp. 1199-1207.

TESPA (1995). "Installation of Steel Sheet Piles", Technical European Sheet Piling Association, L-2930 Luxembourg.

US Army Corps of Engineers (2007). "Coastal Engineering Manual, Part VI-5", Engineer Manual - EM 1110-2-1100.

Passing Vessel Hydrodynamic Model Validations in Complex Waterways

S. Fenical[1] and F. Salcedo[2]

[1]Principal, Author, ASCE Mooring Subcommittee, Coast & Harbor Engineering, Inc., 155 Montgomery Street, Suite 301, San Francisco, CA 94104; PH (415) 773-2164; FAX (415) 276-3784; Email: scott@coastharboreng.com
[2]Coastal Engineer, Coast & Harbor Engineering, Inc, 155 Montgomery Street, Suite 301, San Francisco, CA 94104; PH. (415) 773-2154; FAX (415) 276-3784; Email: frank@coastharboreng.com

ABSTRACT

Passing deep-draft vessels in confined navigation channels generate significant hydrodynamic forces on berthed vessels and affect mooring systems and shoreside structures. Accurate prediction of these forces is essential for design of waterways and navigation channels, improvement of navigation safety, and optimizing port operations.

There are several methods for predicting passing vessel impacts (hydrodynamics, forces) that are well known in the industry. Many of these methods produce reasonable estimates for pressure fields, particularly in open water, and have been used successfully in the past for various port and waterway projects. The present paper is intended to provide improvements to these predictions for complex waterways, increase the reliability of engineering design, and in turn reduce risk for navigation in confined waterways and improve port operations.

The Vessel Hydrodynamics Longwave Unsteady (VH-LU) modeling system original development was described in Fenical *et al.* (2006) and has been under continual development as part of a comprehensive hydrodynamic modeling system, incorporating ambient hydrodynamic processes present in realistic port settings. The modeling system has been previously validated (Fenical *et al.* 2007) using field water level and velocity measurements, laboratory water level measurements, and laboratory berthed vessel loading measurements for all 12 test results reported by Remery (1974).

The present paper describes validations of the modeling system using recent laboratory vessel hydrodynamic data, as well as recent large-scale laboratory berthed vessel loading data with the presence of a quay wall reported by van Wijhe *et al.* (2008). The results of the comparison between the quay wall tests of van Wijhe *et al.* (2008) are believed to be the most accurate published to date. Finally, the present paper describes recent real-world application of the modeling system to wharf design projects.

HYDRODYNAMICS VALIDATIONS

Vessel hydrodynamic patterns become altered by shallow, irregular banks near deep-draft navigation channels. The following section describes validation of water level fluctuations in complex waterways using laboratory data. The laboratory data used for validation in the present paper are those reported by LaTaire *et al.* (2009) and van Wijhe *et al*. (2008), both for containerships. Water level measurements from LaTaire *et al.* (2009) included shallow, submerged banks and pressure field wave transformation including hydraulic jump formation. Figure 1 shows a comparison between measurements by LaTaire *et al.* (2009) and water surface elevation predictions by VH-LU. VH-LU modeling was performed at full scale and laboratory tests were conducted with scale approximately 80:1. The comparison is considered excellent considering the complex hydrodynamics present in the shallows (farthest gauge) and relatively small scale of the measurements.

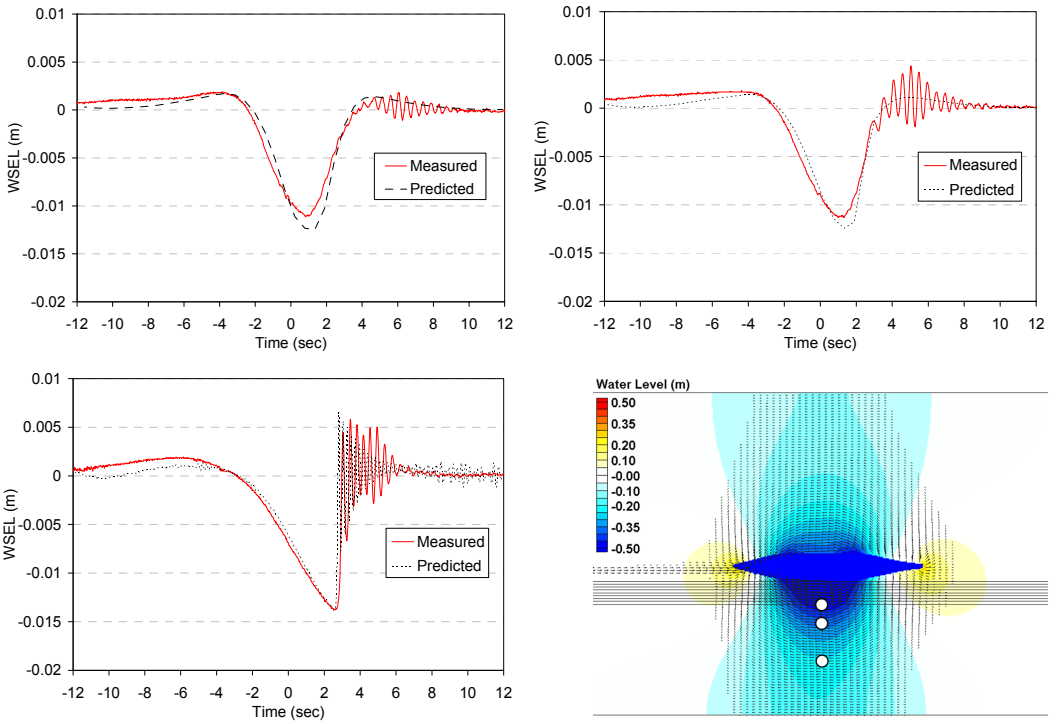


Figure 1. Comparison of measured and predicted water levels (top left is gauge nearest the vessel, bottom left is gauge farthest from the vessel). Bottom right shows plan view of water levels and locations of gauges.

Measurements from a recent passing vessel study for the Port of Rotterdam reported by van Wijhe *et al*. (2008) included the presence of a berthed vessel moored 1.4m from a vertical quay wall. The tests consisted of a 12,500 TEU containership passing a Panamax containership. Hydrodynamics and berthed vessel loads were reported for passing vessel distances of 75m and 150m and a passing speed of 5.5 knots. Since the study reported by van Wijhe *et al*. (2008) included a vertical quay wall and relatively large scale (38.2:1), it is considered an important set of

laboratory results for validation of passing vessel-induced hydrodynamics and berthed vessel loading.

Figure 2 shows the experimental setup reported by van Wijhe *et al*. (2008), including the locations of water level gauges and current meters. Figure 3 shows water levels (color contours) and velocities (vectors) predicted by the VH-LU model for the 75-m passing distance case with vessels approximately amidships. Water level and velocity data were extracted from the modeling results at the gauge locations shown in Figure 2 for comparison with measurements. Figure 4 shows a comparison between measured water levels (top) and velocities (bottom) and those predicted by the VH-LU model for the 75-m passing distance case, and Figure 5 shows the comparison for the 150-m passing distance case. The comparisons demonstrate that the VH-LU model accurately reproduces the measured values, and that the VH-LU model represents advancement in the accurate prediction of pressure field hydrodynamics in complex waterways, such as those with a vertical quay wall.

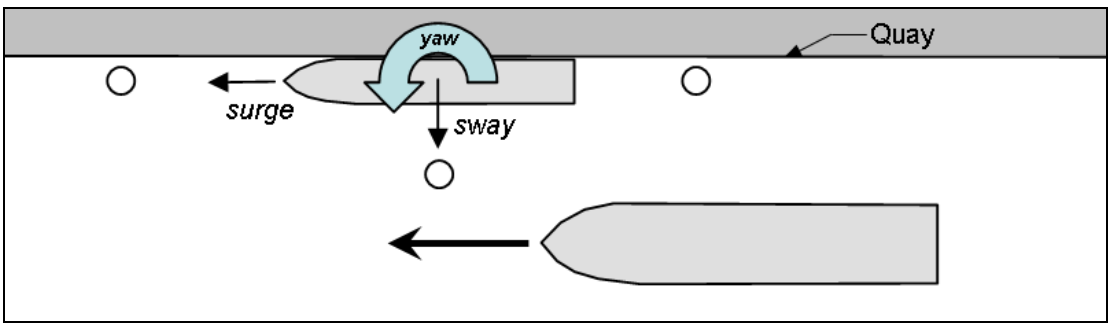


*Figure 2. Experimental setup reported by v*an Wijhe *et al. (2008). Open circles represent water level/velocity gauges.*

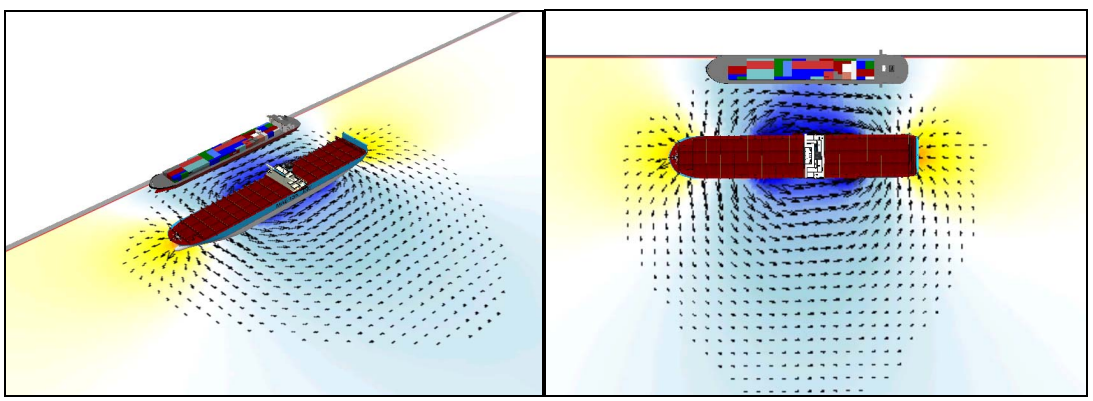


Figure 3. VH-LU predicted water levels (color contours) and velocities (vectors) for 75-m passing distance case with vessels amidships; oblique (left) and plan view (right).

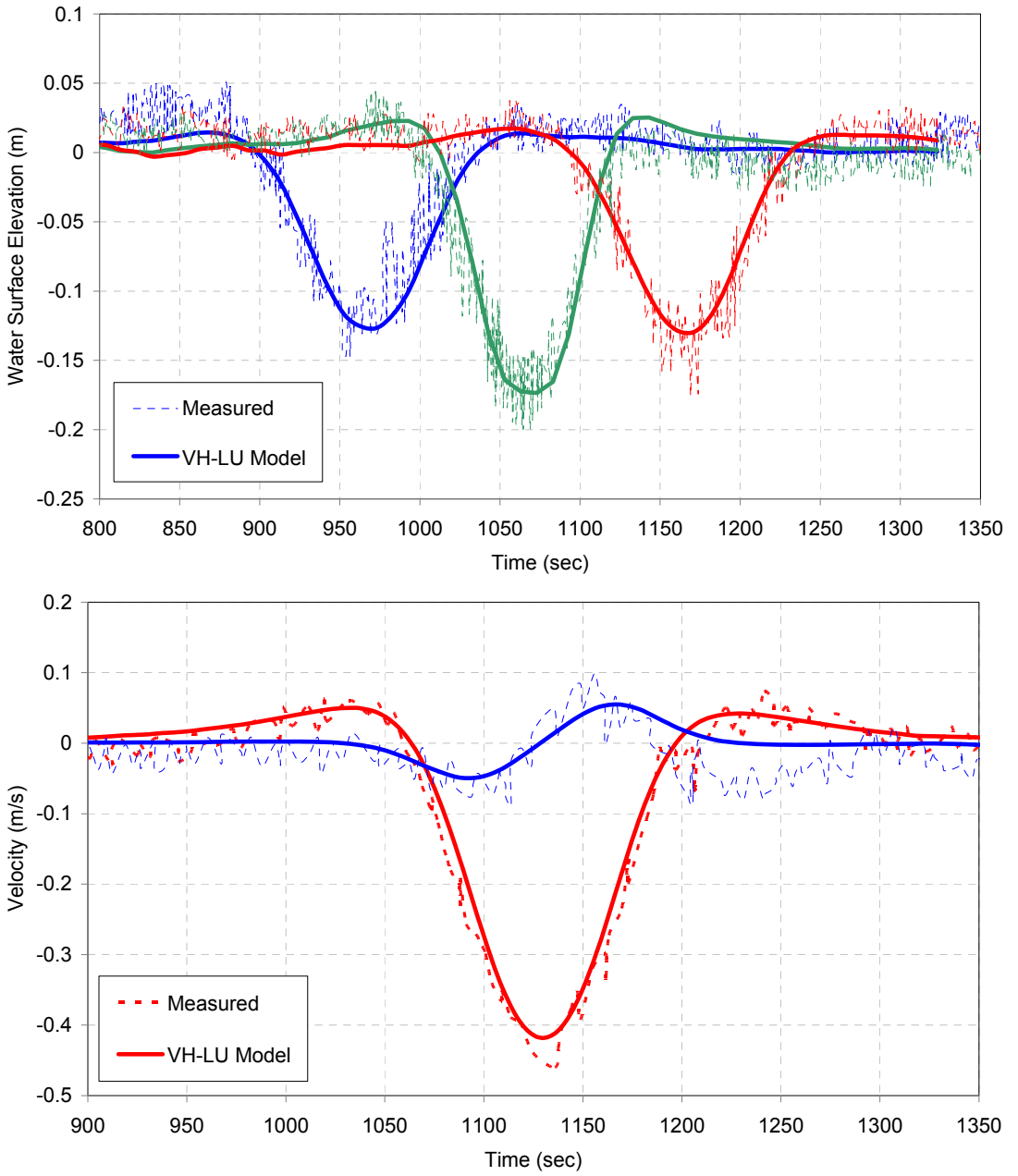


Figure 4. Comparison of measured and VH-LU predicted water levels (top) and velocities (bottom) for 75-m passing distance case.

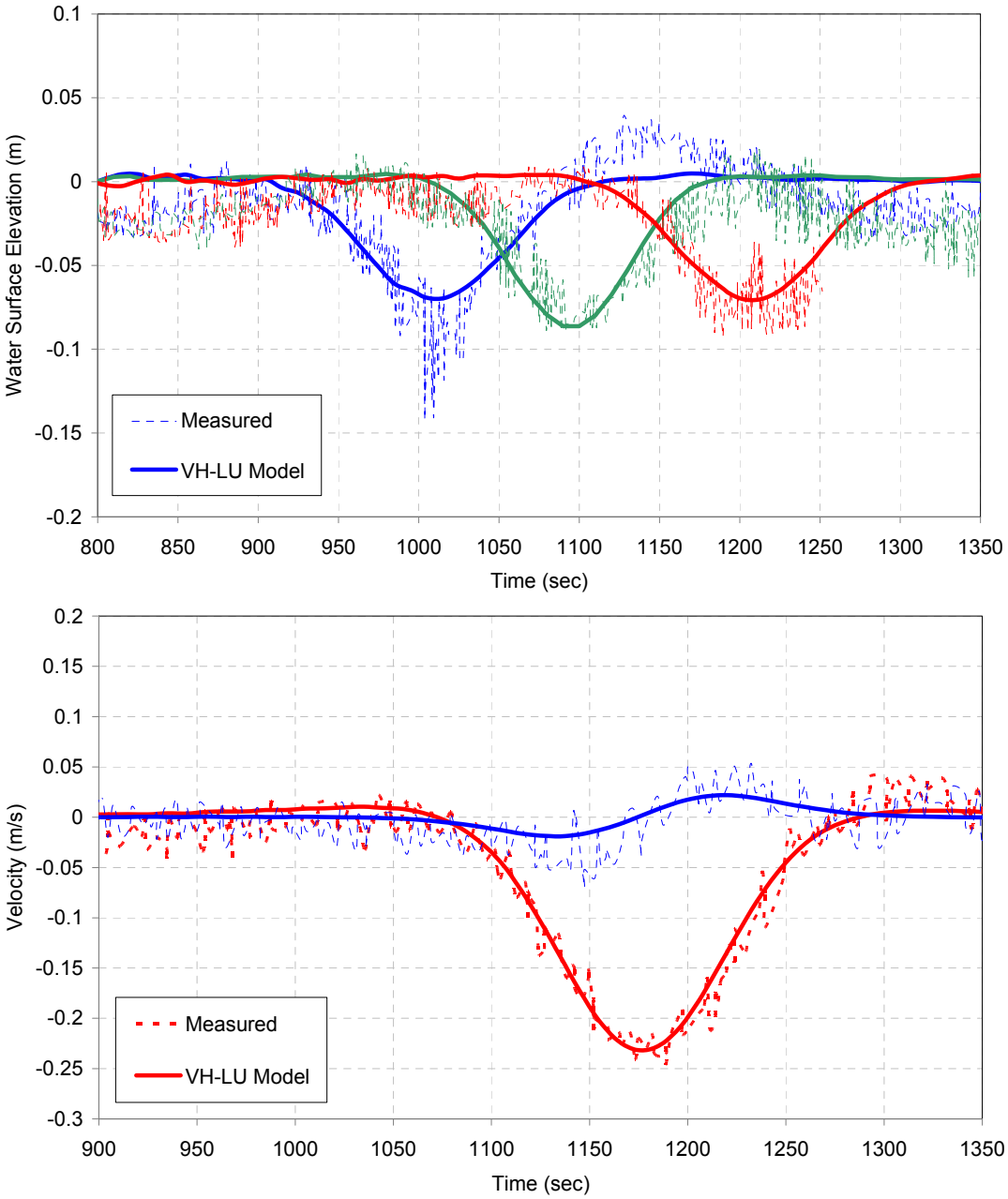


Figure 5. Comparison of measured and VH-LU predicted water levels (top) and velocities (bottom) for 150-m passing distance case.

BERTHED VESSEL LOADING VALIDATIONS

The VH-LU model has been previously validated with all 12 berthed vessel loading cases reported by Remery (1974), as described in Fenical (2007). The tests reported by Remery, while believed to be of the highest quality, were all for open water conditions. Therefore, additional validation was performed for the passing

vessel loads reported in van Wijhe *et al.* (2008), which included the presence of a vertical quay wall adjacent to the berthed vessel.

Figure 6 shows a comparison between measured and VH-LU predicted surge and sway forces (top) and yaw moments (bottom) for the captive model test with 75-m passing distance reported in van Wijhe *et al*. (2008). The VH-LU model generates accurate predictions of loads and moments for this complex waterway situation. Therefore, the VH-LU model represents an improvement in computational procedure accuracy for pressure field forces and moments on the berthed vessels in complex waterways.

Figure 7 shows the results of comparison for the 150-m passing distance case. As with the 75-m passing distance case, the VH-LU model accurately represents the measured loads and moments for the 150-m passing distance case.

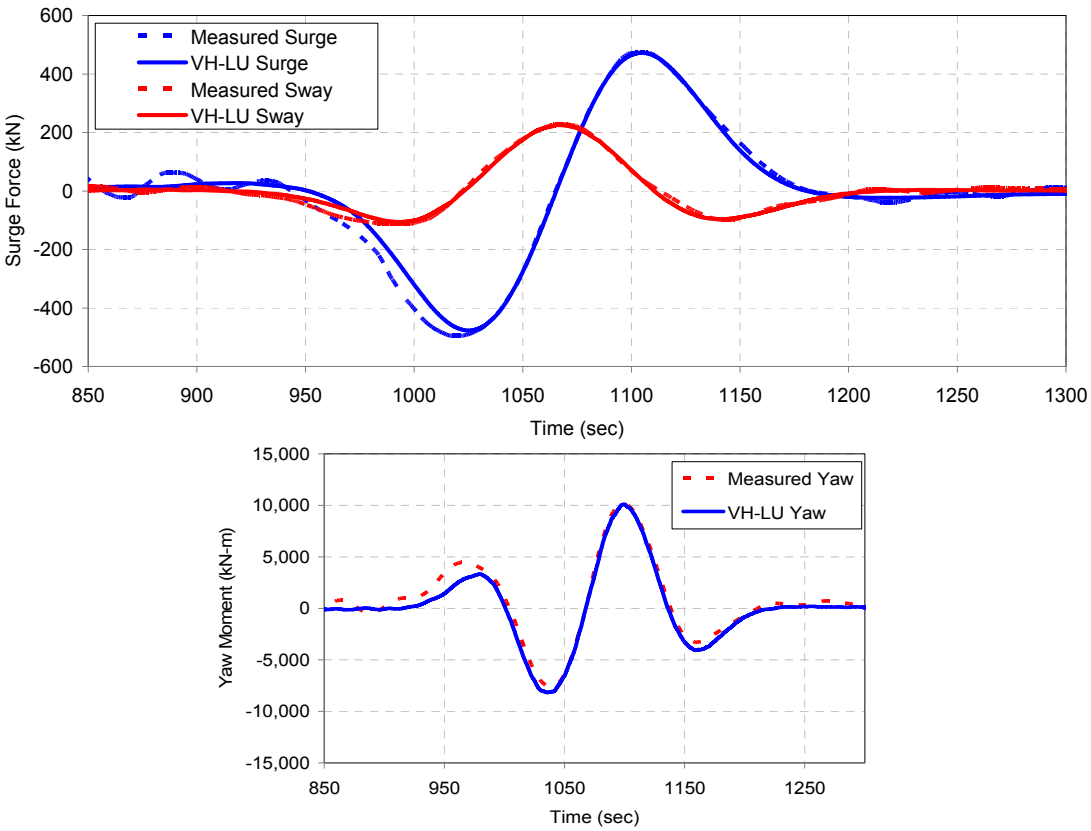


Figure 6. Comparison of measured and VH-LU predicted surge and sway forces (top) and yaw moment (bottom), 75-m passing distance at speed 5.5 knots.

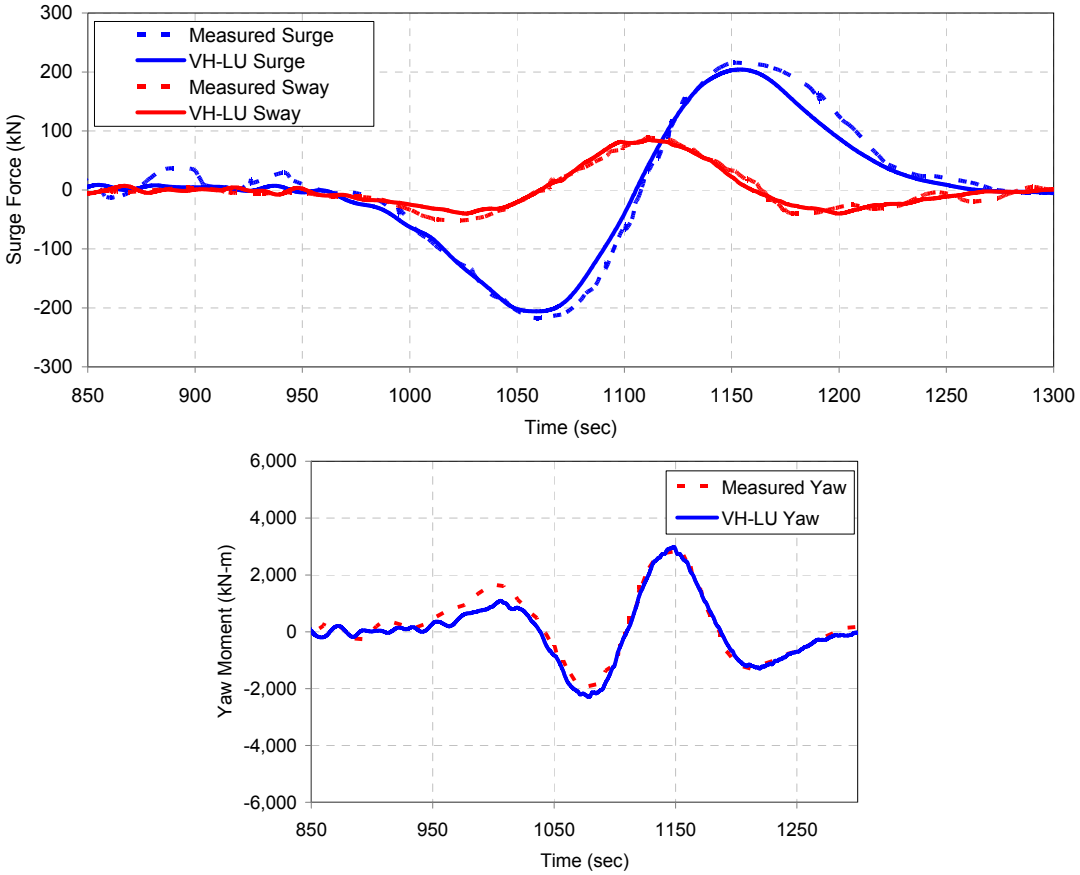


Figure 7. Comparison of measured and VH-LU predicted surge and sway forces (top) and yaw moment (bottom), 150-m passing distance at speed 5.5 knots.

CASE STUDIES

Passing vessel hydrodynamic modeling was performed as part of mooring and berthing analysis for the Pier 27 Cruise Terminal, Port of San Francisco. The VH-LU system was used to evaluate hydrodynamic loads on the berthed Queen Mary 2 cruise ship generated by the passing containership Emma Maersk. Figure 8 shows the cruise terminal layout and berthed and passing vessel locations. Simulations were performed for constant passing speeds but with different ambient ebb and flood currents, which reach 4 knots and greater near the terminal. Peak load magnitudes were similar for surge and sway because the berthed vessel is moored at an approximately 45-degree angle to the passing vessel. In this particular case, results indicated that the loads on the berthed vessels for even the most extreme cases are smaller than wind loads and did not govern mooring system design.

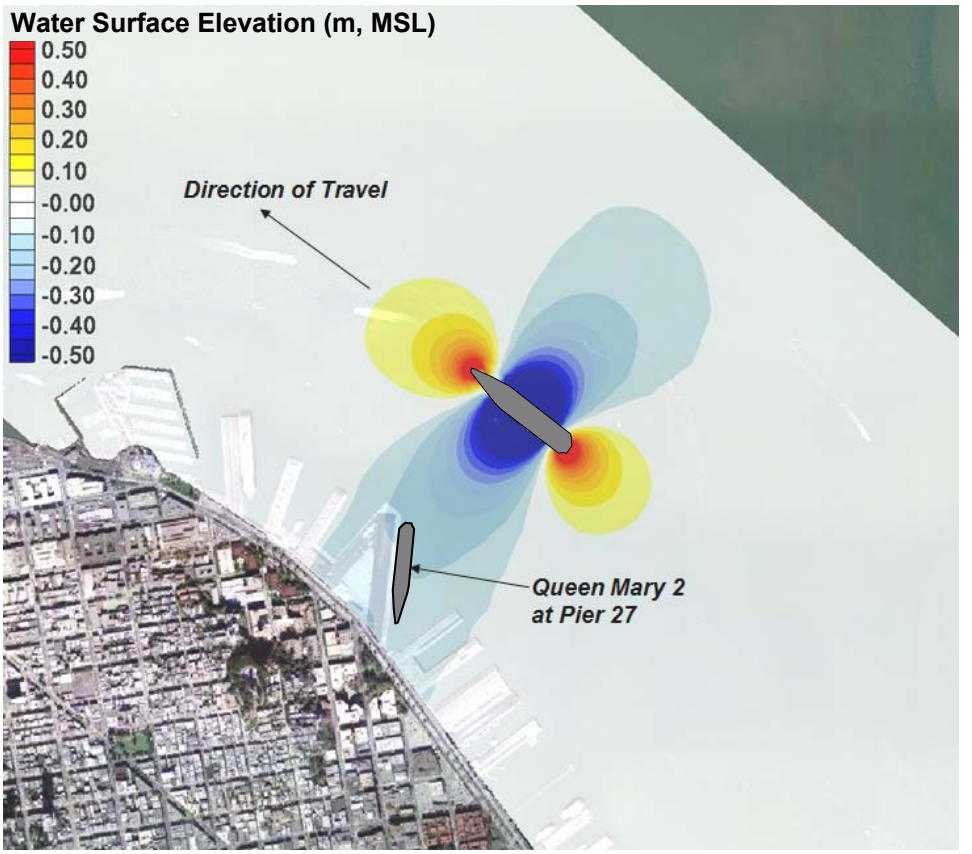


Figure 8. Water level fluctuations generated by passing Emma Maersk near cruise ship Queen Mary 2 berthed at Pier 27 Cruise Terminal.

Passing vessel hydrodynamic modeling was performed to evaluate mooring conditions for the REK Pier, Port of Tampa, Florida. The analysis required hydrodynamic modeling due to the complex channel and passing vessel conditions. The berth was oriented at nearly a 90-degree angle to the main channel, and cruise ships were known to accelerate through the area with drift angles to compensate for strong cross-winds. Figure 9 shows the REK Pier layout and berthed and passing vessel locations. Surge loads were the largest and of most interest due to reduced mooring capacity in the surge direction. Results were used further to evaluate impacts to the mooring system and design improvements.

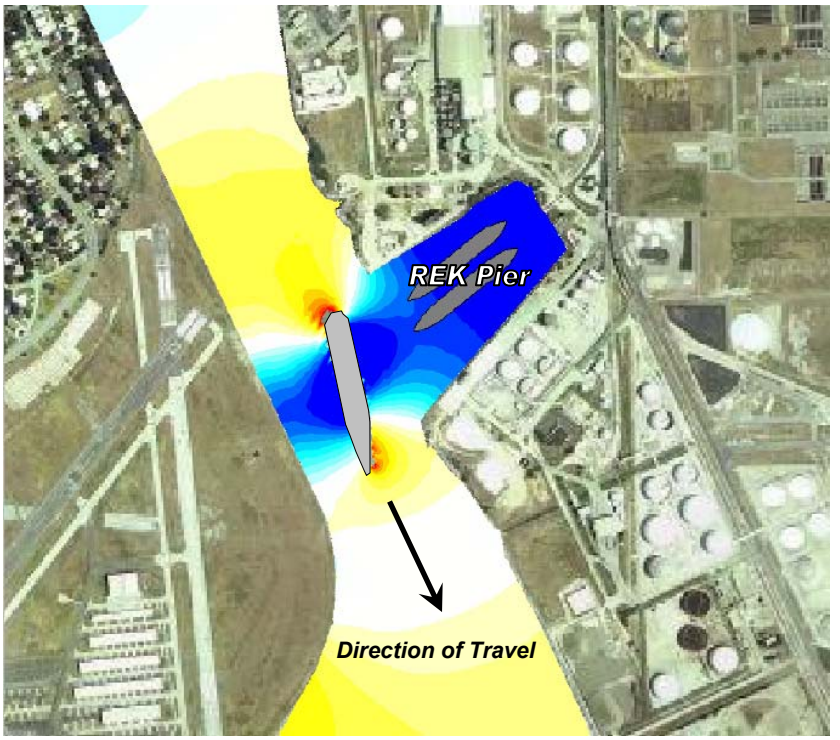


Figure 9. Water level fluctuations generated by passing cruise ship near tankers berthed at REK Pier.

REFERENCES

Fenical, S., Kolomiets, P., Kivva, S. and Zheleznyak, M. 2006. "Numerical Modeling of Passing Vessel Impacts on Berthed Vessels and Shoreline," ICCE 2006.

Fenical, S. 2007. "Vessel Hydrodynamics and Berthed Vessel Loading Model Verification with Field Data and Laboratory Data," Ports 2007.

LaTaire E., Vantorre, M., Eloot, K. 2009. "Systematic Model Tests on Ship - Bank Interaction Effects," International Conference on Ship Manoeuvring in Shallow and Confined Water: Bank Effects, Antwerp, Belgium.

Remery, G.F.M. 1974. "Moving Forces Induced by Passing Ships," Offshore Technology Conference, Paper Number OTC 2066.

van Wijhe, H.J. and Pinkster, J.A. 2008. "The effects of ships passing moored container vessels in the Yangtzehaven, Port of Rotterdam." Operations in Canals and Waterways (SOCW).

Cruise Ship Maneuvering and Berthing at Pier 27 Cruise Terminal, San Francisco, CA

K. Von Blohn[1], J. Davey[2], M. Tirindelli[3], S. Fenical[4]

[1] Port of San Francisco, Pier 1, San Francisco, CA 94111; Email: kim.vonblohn@sfport.com
[2] Port of San Francisco, Pier 1, San Francisco, CA 94111; Email: john.davey@sfport.com
[3] Coast & Harbor Engineering, 155 Montgomery St., Ste 301, San Francisco, CA 94104; PH (415) 773-2089; Email: matteo@coastharboreng.com
[4] Coast & Harbor Engineering, 155 Montgomery St., Ste 301, San Francisco, CA 94104; PH (415) 773-2164; Email: scott@coastharboreng.com

ABSTRACT

The Port of San Francisco (POSF) is planning to improve maneuvering and berthing conditions at Pier 27 Cruise Ship Terminal in San Francisco, CA. Pier 27 has been an operational cruise terminal since May 2006, with 27 cruise ships visiting since that time. Pier 27 is located in an area of strong tidal currents, crossing the berth at an approximately 45-degree angle. Maneuvering and berthing at Pier 27 is more challenging than at other POSF berths, because it extends further seaward than any of the other piers and exposes the vessels to stronger currents during the berthing process. The tidal currents at the site, combined with the relatively narrow existing berth configuration, presently results in arrival/departure times being adjusted to avoid the stronger current conditions. Maneuvering and berthing analyses were performed with the objective of reducing the frequency of these arrival/departure time adjustments. The analysis included evaluation of coastal conditions, ship maneuvering simulations and evaluation of mitigation measures to improve maneuverability and berthing.

COASTAL CONDITIONS AT PIER 27

Pier 27 is located on the eastern waterfront of the City of San Francisco, has a berth approximately 1,300 ft long and 200 ft wide (at the inner one-third), and is maintained to a depth of 35 ft (MLLW), as shown in Figure 1. Coastal conditions at the terminal were evaluated as part of the maneuvering and berthing studies at Pier 27, including tidal currents, tides, winds and wind-waves. Wind data were extracted from Alameda Naval Air Station and it was observed that winds at the project site were primarily from the west. Analysis indicates that forces of concern for maneuvering are primarily tidal currents with a smaller contribution from winds. Numerical modeling was performed using a Bay-wide hydrodynamic model (MORPHO, Kivva *et al.*, 2006), which was validated previously using measured currents (NOAA) and at Pier 27 using recent observations.

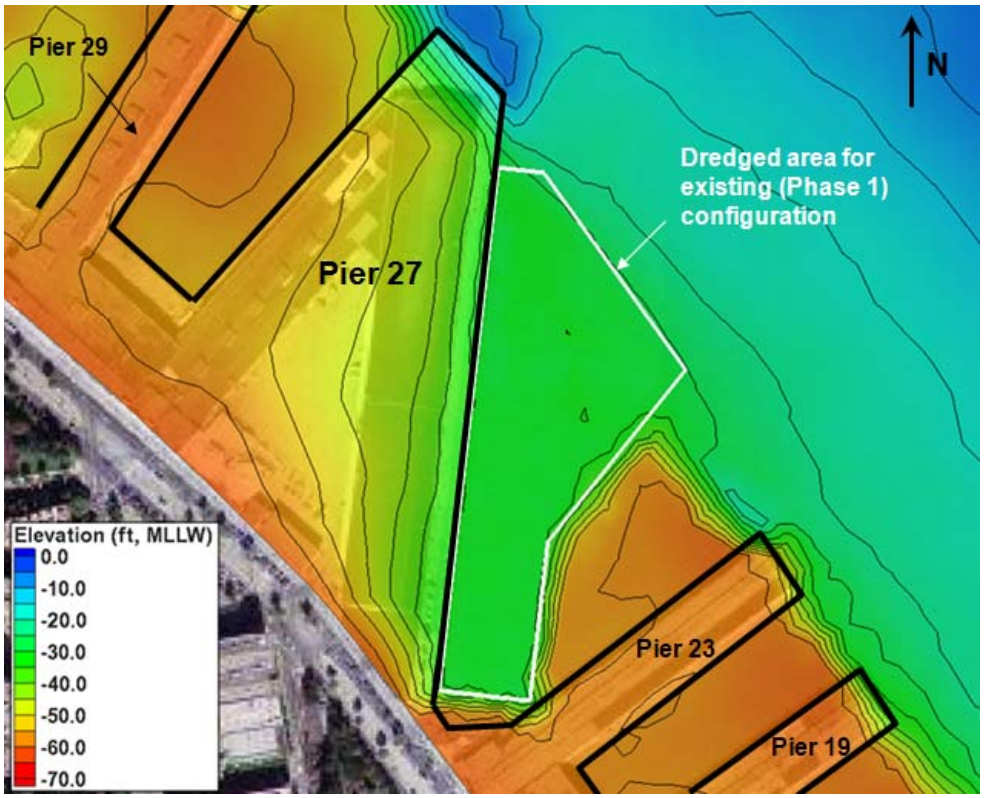


Figure 1. Pier 27 Cruise Terminal location and existing (Phase 1) berth configuration shown as a white line.

Figure 2 shows peak ebb and peak flood currents simulated by MORPHO in the vicinity of Pier 27. Analysis of the modeling results and site observations indicate that at the seaward edge of Pier 27, currents are moving offshore (in the ebb direction) more than 65 percent of the time due to eddying near the shoreline generated by the Pier 39 breakwaters. The results of tidal current simulations were analyzed and nine representative current conditions were extracted, ranging from 0.5 to 2.5 knots for ebb currents, and 0.5 to 2.0 knots for flood currents. These currents were predicted at the seaward tip of the pier, and much higher currents were observed directly seaward. Statistical occurrence of winds was also evaluated for inclusion into the ship simulations and analysis, and west winds with speeds between 10 and 30 knots were used.

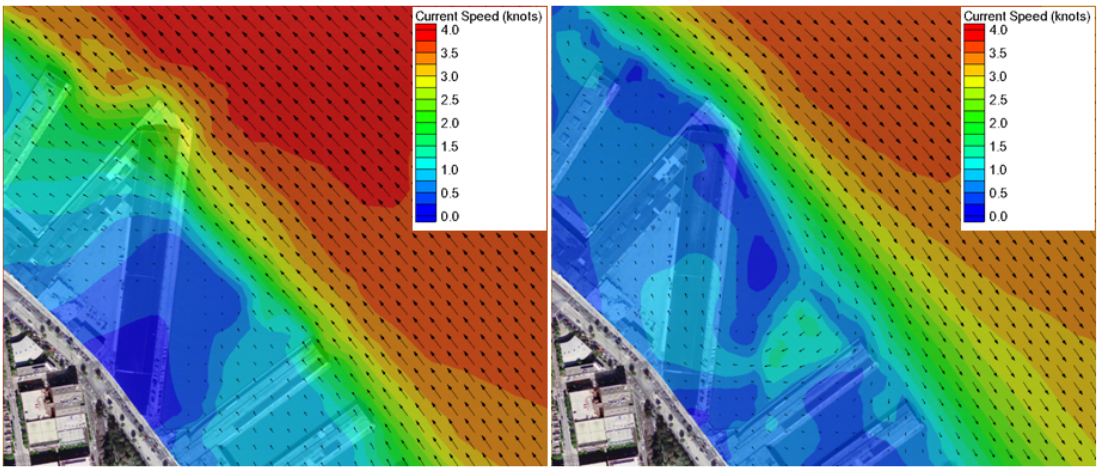


Figure 2. Peak ebb (left) and flood (right) currents simulated in vicinity of Pier 27.

HISTORICAL BERTHING EVALUATION

Historical and existing arrival/departure time adjustments were estimated for all previous arrivals/departures (2006 to end of 2010). A total of 34 cruise ship arrivals and departures were on POSF's schedule between May 2006 and the end of 2010. The percentage of possible historical arrival/departure time adjustments was estimated using the frequency of occurrence of all tidal currents stronger than those present during the berthings/unberthings. Tidal currents were estimated at the time of each arrival and departure from 2006 to present using a neural network-based correlation between predicted tides at nearby NOAA stations (Alcatraz, Treasure Island and Rincon Point) and current velocity/directions at the project site developed based on shorter-term numerical modeling. Historical data show that in the past several years (and for typical vessels), *arrivals* have occurred during ebb current speeds less than approximately 0.6 to 0.7 knots and during flood current speeds less than approximately 1.2 to 1.3 knots. *Departures* have occurred during a much wider range of conditions. These conditions (0.6 to 0.7 knots for ebb arrivals and 1.2 to 1.3 knots for flood arrivals) are assumed to be conditions for which no time adjustments are required. For all other cases when current velocities exceed these values, it is assumed that arrival/departure time adjustments (1 to 4 hours in duration) were required. Based on this approach, it was estimated that the historical occurrence (probability) of arrival/departure time adjustments at the existing berth was approximately 50 to 60 percent.

REAL-TIME MANEUVERING AND BERTHING SIMULATIONS

Cruise ship maneuvering and berthing simulations were performed with members of the San Francisco Bar Pilots (Bar Pilots) at Coast & Harbor Engineering's (CHE) offices on June 1-2 and 7-9, 2010 using the PC Rembrandt system (BMT Seatech, 2010). CHE utilized the Rembrandt ship maneuvering software, with models of the Sapphire Princess (LOA 946 ft) and Sun Princess (LOA 856 ft) obtained by permission from Princess Cruise Lines (see Figure 3). Tug assistance during the simulations was provided by up to two 80-ton bollard pull tugs.

Three-dimensional display of the berth and surrounding areas were provided on multiple HDTVs for better pilot visual reference during the berthing process. Example snapshots from the simulations are shown in Figure 4.



Figure 3. Sapphire Princess (left) and Sun Princess (right).

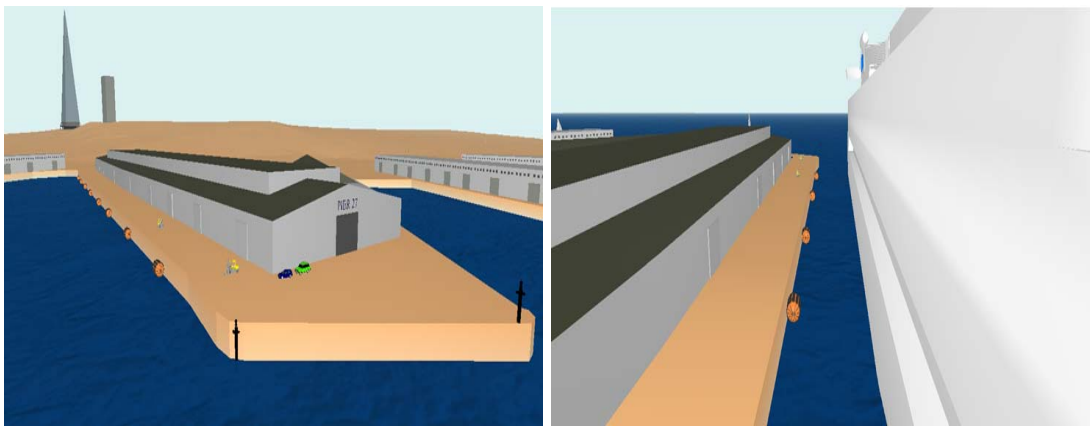


Figure 4. View of Pier 27 from Sapphire Princess starboard bridge wing looking to the side (left) and starboard bridge wing looking aft (right).

76 real-time simulations were performed during the five-day period. Berthing maneuvers were performed by 14 members of the Bar Pilots, providing realistic variability in the approach to berthing and pilot experience. Berthing maneuvers represented starboard-side-to and port-side-to berthings, as well as a limited number of departures under strong current conditions. The simulations included 27 different combinations of tidal current conditions and berth configurations, with current speeds ranging from 0.5 to 2.5 knots on ebb, and 0.5 to 2.0 knots on flood. The existing berth (Phase 1) and two berth widening scenarios (Phase 2 and Phase 3) were included for all tidal current conditions. Winds were also included in a limited number of simulations; however, it was decided that the effects of wind were relatively predictable and would be included in an approximate manner later to reduce the number of simulations.

EVALUATION OF BERTHING AT THE EXISTING (PHASE 1) BERTH

The existing (Phase 1) berth has a minimum width of approximately 200 ft and a maximum width at the seaward end of approximately 530 ft, as shown below in Figure 5. In this example from the simulations, the vessel Sapphire Princess was used. Figure 6 shows two real-life photos of the berthing process on May 10, 2010 taken looking aft from the starboard bridge wing of the Sapphire Princess as she turned past the corner of the wharf into the berth, arriving starboard-side-to. The environmental conditions during the berthing included approximately 0.5-knot flood currents with winds approximately 10-12 knots near the terminal.

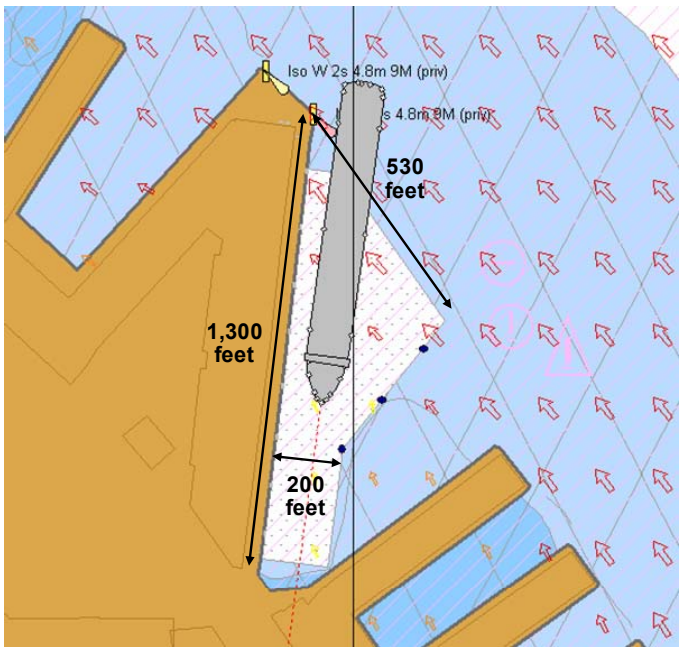


Figure 5. Pier 27 existing berth with Sapphire Princess.

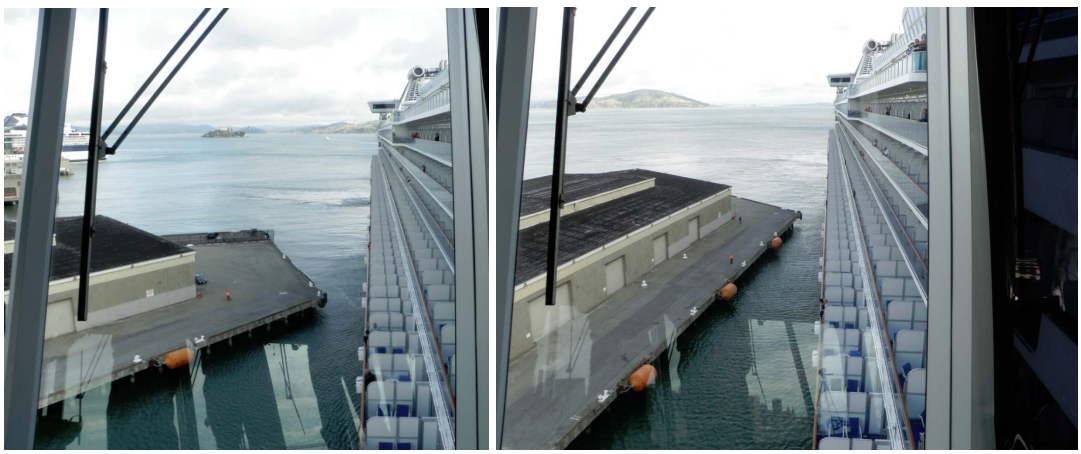


Figure 6. Sapphire Princess berthing on May 10, 2010 looking aft from starboard bridge wing.

Typical berthing maneuvers for the existing (Phase 1) berth taken from the real-time maneuvering simulations are shown in track plots in Figures 7-9. Figure 7 shows example starboard-side-to berthing maneuvers observed in the simulations during relatively mild ebb (left) and mild flood (right) currents. Generally, a large portion of the berth is used even during mild current conditions. Figure 8 shows example starboard-side-to berthing maneuvers observed in the simulations during relatively strong ebb (left) and strong flood (right) currents. Figure 9 shows example port-side-to berthing maneuvers observed in the simulations during ebb (left) and flood (right) currents. The majority of the simulations performed during the strongest ebb and flood current conditions required either significant tug assistance or were not successful.

Results of the real-time simulations were highly variable, particularly for stronger currents, due to significant variability in pilot experience and approach to berthing at the terminal. Many of the pilots had not performed these maneuvers in real life during stronger current conditions. However, the simulations were useful in describing the feasible berthing approaches, which for the existing (Phase 1) berth conditions and large conventional cruise ships, are more or less limited to the types of maneuvers shown here.

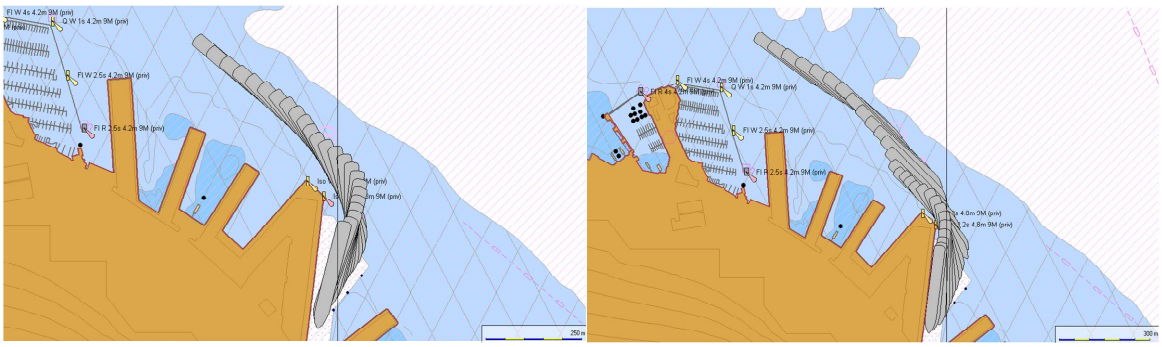


Figure 7. Starboard-side-to approaches observed in the simulations during mild ebb (left) and mild flood (right) currents for the existing (Phase 1) berth.



Figure 8. Starboard-side-to approaches observed in the simulations during strong ebb (left) and strong flood (right) currents for the existing (Phase 1) berth.

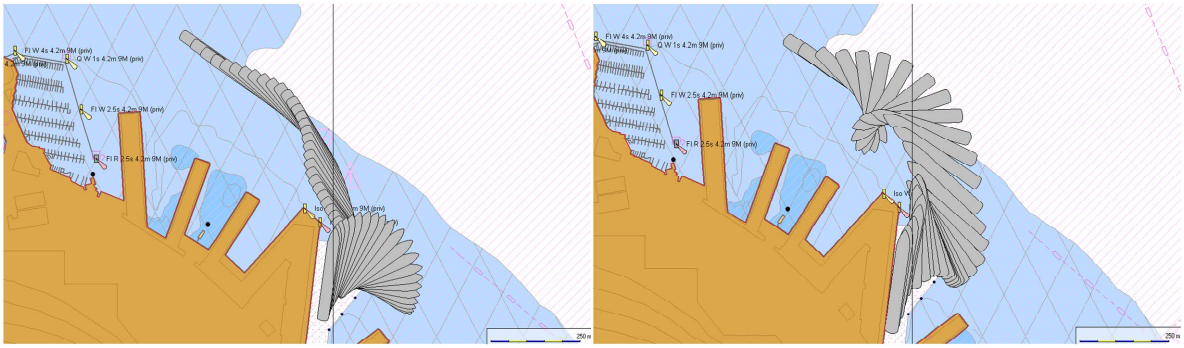


Figure 9. Port-side-to approaches observed in the simulations during ebb (left) and flood (right) currents for the existing (Phase 1) berth.

In order to provide another means of quantifying berthing requirements for the existing (Phase 1) berth, detailed maneuvering force data were extracted from the simulations, and compared with cruise ship power capabilities. In particular, the forces able to be applied by the cruise ship engines and thrusters were compared with environmental forces applied to the vessel during a typical berthing maneuver. Figure 10 shows Sapphire Princess during a typical ebb current berthing, with the two snapshots representing two instances in time during the berthing. During this approach, the maximum practical forward speed into the berth is approximately in the range of 2.0 knots. Once the bow has entered the berth, the vessel must maintain its stern position while the current acting on the vessel tends to push the stern either towards the dock (during ebb currents) or towards the southern shallows (during flood currents). The duration between these two ship positions (left and right) is 90 seconds at 2.0 knots forward speed. Forces required to maintain the ship's lateral position in the current must be reliably sustained for extended periods of time.

Figure 11 shows the range of forces acting on the stern half of the Sapphire Princess as a function of ebb and flood current speed (as measured at the seaward end of Pier 27) during the starboard-side-to berthing process. The higher end of the filled range represents forces when the vessel is more exposed (Figure 10, left), while the lower end of the range represents forces when the vessel is farther inside the berth area (Figure 10, right). For example, when Sapphire Princess is in its more exposed position, at a time when ebb currents at the end of Pier 27 are 1.5 knots, the total lateral load on the stern half of the vessel is approximately 80 tons.

Analysis of these lateral loads on the stern of the vessel indicates that even when operating at 100 percent for several minutes without interruption, the stern thrusters on the Sapphire Princess (which have 2.3 times more total horsepower than those on board the Sun Princess) are not capable of maintaining the ship's position when ebb currents exceed approximately 1.3 knots, and when flood currents exceed approximately 1.6 knots. Engine power (use of independent engines and rudders) can only be used on a limited basis during this time because bow position and forward speed must be maintained to get the stern out of the current.

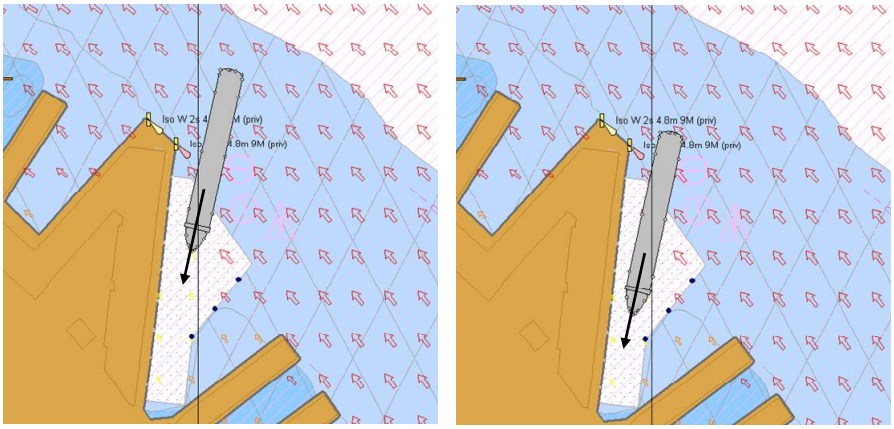


Figure 10. Typical starboard-side-to approach during ebb currents. Time between vessel positions is approximately 90 seconds at forward speed 2 knots.

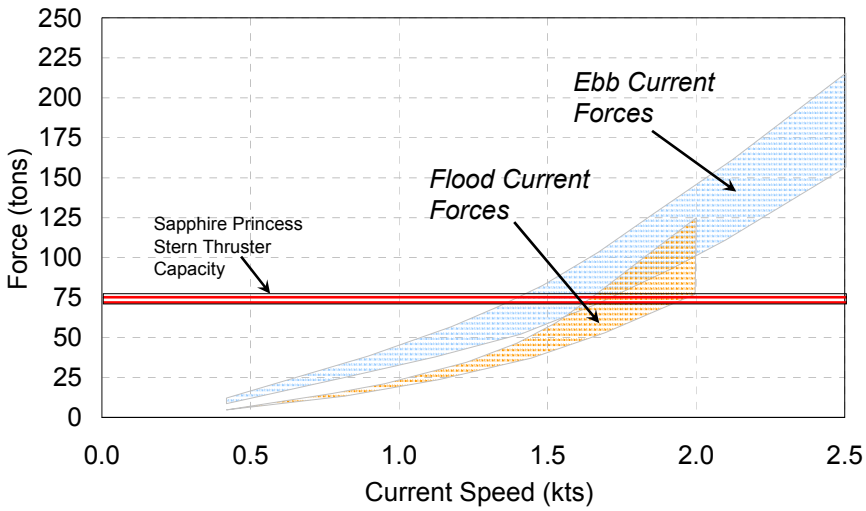


Figure 11. Lateral current loads on stern half of Sapphire Princess during starboard-side-to berthing on ebb and flood currents.

SUMMARY FOR EXISTING (PHASE 1) BERTH

Upon completion of simulations for the existing (Phase 1) berth it was concluded that the coastal conditions and ship handling in the simulator were overall a good representation of reality. Pilots also remarked that the berth marker buoys (already in place at the time of this paper) are helpful as visual aids in the berthing process. The evaluation of existing (Phase 1) berth arrival/departure time adjustments and development of operational recommendations was performed using 1) observations from the simulations; 2) power requirements during berthing maneuvers; and 3) consideration of the significant variability inherent in the berthing process. This variability requires that some factor of safety be added to account for pilot experience at the terminal and approaches to berthing, changing wind conditions, and

the possibility of thruster power failure during berthing maneuvers (which has occurred several times at the POSF).

It was estimated based on the schedule that throughout the history of major cruise ship operations at Pier 27 (since 2006), arrival/departure time adjustment frequency was up to approximately 50 to 60 percent. Providing detailed environmental data at the site (model or measured) can be expected to assist in reducing the frequency of these arrival/departure time adjustments at the existing (Phase 1) berth. It is important to note that in many cases, the existing (Phase 1) berth arrival/departure time adjustments are between approximately 1 and 4 hours in duration and many of these time differences may not significantly affect operations. Based on the results of the simulations, detailed recommendations for berthing and unberthing typical vessels (similar to Sapphire Princess and Sun Princess) at the existing (Phase 1) berth were developed. These recommendations included safe current speeds for berthing on both ebb and flood currents, and recommendations for tug usage during these currents. It was also recommended that on-site environmental data should be provided, either using enhanced computer model data or on-site measurements. If measured data are desired, it is recommended to install a P.O.R.T.S (NOAA)-type reporting station (or equivalent) which would enable access to wind, tide, and current data by Vessel Master and Pilots via phone and internet connections.

MEASURES TO MITIGATE ARRIVAL/DEPARTURE TIME ADJUSTMENTS

Prior to initiation of maneuvering simulations, CHE evaluated potential measures for mitigating the present adjustments in arrival/departure times. Mitigation measures were developed in coordination with the POSF and the Bar Pilots. These measures were intended to either 1) reduce current speeds at the seaward end of the berth (flow diversion structures); or 2) increase maneuvering room (berth widening alternatives).

Numerical modeling and analysis indicated that flow diversion structures (solid walls) greater than 200-300 ft in length were required at the end of Pier 27 to provide any significant change in currents and must also endure impacts of large storm waves from the southeast, making them cost-prohibitive. In addition, these structures would likely alter sediment transport in the area and may impact ongoing maintenance dredging requirements at the project site and other nearby facilities. Therefore, only berth widening alternatives were developed for testing during real-time maneuvering simulations. CHE developed two berth widening alternatives, as shown in Figure 12:

- Phase 2 berth would require approximately 40,000 cubic yards of initial dredging at depth 35 ft (MLLW). The berth area would be increased by approximately 35 percent; however, the effective berth width (the width useful for maneuvering) would only be increased by approximately 25 percent.
- Phase 3 berth would require approximately 90,000 cubic yards of initial dredging at depth 35 ft (MLLW). The berth area would be increased by approximately 55

percent and the effective berth width would be increased by approximately 100 percent.

Numerical modeling and analysis indicated that neither berth widening alternative significantly affected the overall tidal current speeds or directions at the wharf. All three berth configurations, including existing (Phase 1), Phase 2 and Phase 3 berths, were carried forward for evaluation in the real-time maneuvering simulations.

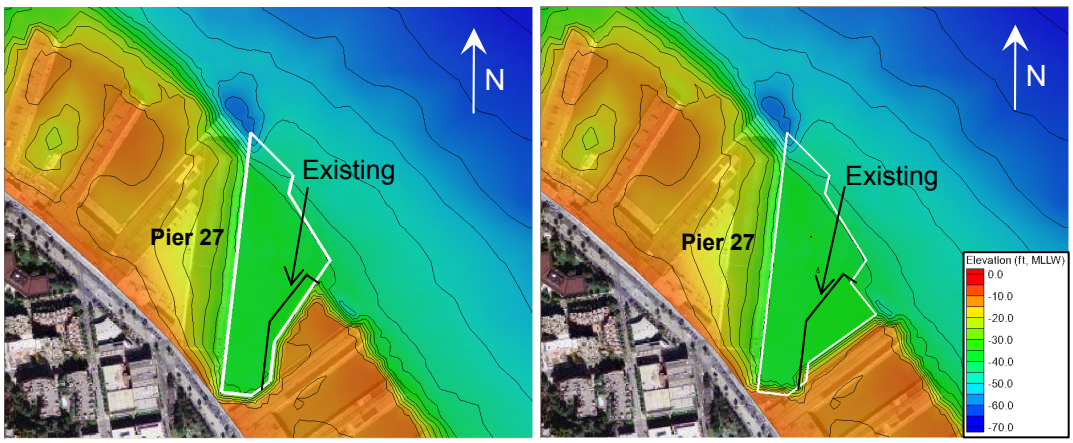


Figure 12. Berth widening schemes Phase 2 (left) and Phase 3 (right), shown as white lines. Existing (Phase 1) berth boundary is also shown as a black line on both plots.

The primary goal of the real-time simulations for Phase 2 and Phase 3 berths was to identify the potential benefit to terminal operations posed by the dredging work. In particular, the goal was to evaluate the potential mitigation of arrival/departure time adjustments that is feasible following construction of the two alternatives. As for the existing (Phase 1) berth, the evaluation of future likely Phase 2 and Phase 3 arrival/departure time adjustments was performed using 1) observations from the simulations; 2) power requirements during berthing maneuvers; and 3) consideration of the significantly variability inherent in the berthing process.

Figure 13 shows track plots from two typical berthing maneuvers into the existing berth (Phase 1, top) and Phase 3 berth (bottom) during strong flood tidal currents. The approach to berthing is significantly different. For the existing (Phase 1) berth, the vessel is required to navigate very close to Pier 27 and turn into the berth (broadside to the current) much sooner, all while maintaining significant forward speed so as to quickly get the stern out of the current. For Phase 3, the vessel can pass Pier 27 at a much more comfortable distance, come to a nearly dead stop when the stern is aligned with the corner of the pier, and rotate the bow into the berth. The berthing time for Phase 3 is reduced by half, and the average force required to be exerted by the vessel is 2.5 times lower than for the existing (Phase 1) berth. These trends were generally observed, however not being always evident, in every simulation.

Figure 14 shows track plots from two typical berthing maneuvers into the existing berth (Phase 1, top) and Phase 3 berth (bottom) during strong ebb tidal currents. The primary concern during arrivals on ebb currents is keeping the stern from being pushed onto the corner of the wharf. The existing (Phase 1) berth requires that the vessel stern moves much closer to the corner of the wharf, leaving little room for error and requiring significant forward speed be maintained while moving into the berth. The Phase 3 berth allows the vessel stern to maintain a much larger distance from the wharf during the berthing process.

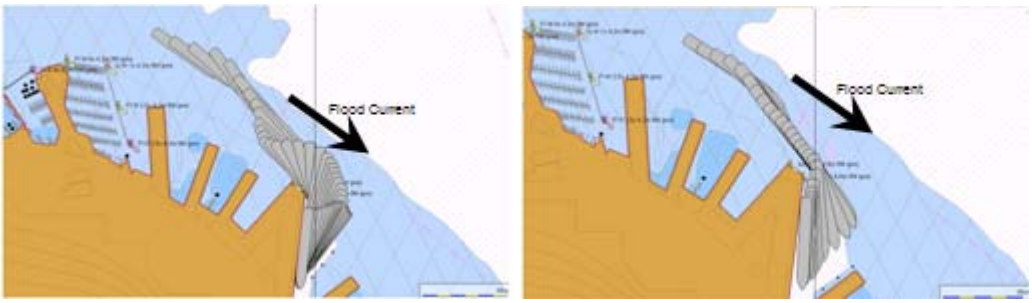


Figure 13. Typical maneuver into existing berth (Phase 1, left) and Phase 3 berth (right) during strong flood tidal currents.



Figure 14. Typical maneuvers into existing berth (Phase 1, left) and Phase 3 berth (right) during strong ebb tidal currents.

SUMMARY FOR PHASE 2 AND PHASE 3 DREDGING ALTERNATIVES

The following observations were made based on the results of the analysis for Phase 2 and Phase 3 dredging alternatives:

- Overall, differences between existing (Phase 1) and Phase 2 berth maneuvering are relatively minor.
- The Phase 2 berth does not allow alternate berthing approaches that would allow pilots to bring the vessels to a near-stop prior to swinging into the berth, which significantly enhances berthing safety.
- Phase 3 dredging creates opportunities for these safer berthing maneuvers for the majority of cruise ships visiting the terminal.

- During departures, both Phase 2 and Phase 3 berth dredging alternatives would provide more room to pull the vessel off the seaward end of the dock and safely exit the terminal (obviously much more so for Phase 3 dredging). Typical vessels would likely be able to safely exit both the Phase 2 and Phase 3 berths during all flood and most ebb current conditions.
- The Phase 2 berth does not allow vessels to safely exit the berth during arrivals in case of an emergency because the effective width is only 25 percent greater than the existing (Phase 1) berth. Phase 3 dredging is expected to provide the opportunity for quickly maneuvering out of the berth in case of an emergency.

These observations and analysis results were further used to determine the following regarding future arrival/departure time adjustments at Pier 27:

- Phase 2 Berth: The reduction in arrival/departure time adjustments for the Phase 2 berth compared to the existing (Phase 1) berth is only evident during a small number of tidal conditions (particularly mid-range ebb currents and large flood currents). The arrival/departure time adjustments for the Phase 2 berth are estimated to occur approximately 25 to 35 percent of the time, and are therefore slightly better than for the existing (Phase 1) berth. However, the arrival/departure time adjustment estimate for the Phase 2 berth is lower than the historical arrival/departure time adjustment frequency determined based on past berthings (50 to 60 percent), indicating that the additional dredging, as well providing more detailed environmental data, can be expected to assist in minimizing future arrival/departure time adjustments.
- Phase 3 Berth: Simulations clearly indicate that the Phase 3 berth alternative provides significantly enhanced berthing safety, room for error and has significantly lower power requirements and fuel consumption than the Phase 2 or existing (Phase 1) berth. While some larger vessels are still likely to adjust arrival/departure times to avoid the strongest of ebb currents, the future arrival/departure time adjustments for the Phase 3 berth are projected to be approximately in the range of 10 percent, significantly lower than the existing (Phase 1) and Phase 2 berths. The Phase 3 berth arrival/departure time adjustment frequency is also significantly lower than the historical arrival/departure time adjustment frequency (50 to 60 percent), indicating that the Phase 3 dredging, as well providing detailed environmental data, can be expected to minimize and potentially eliminate berthing arrival/departure time adjustments at Pier 27.

BERTH WIDENING UPDATE

Between submittal of the abstract and the time of this paper, the Pier 27 berth has already been widened to the Phase 2 dimensions, and multiple cruise ship arrivals and departures have taken place. Communication with Bar Pilots has indicated, as predicted during the study, that the widened (Phase 2 only) berth has already enhanced berthing and unberthing safety at the terminal. Also, the study conclusion that Phase 2 dredging would allow departures during any current conditions has been confirmed by the Bar Pilots.

REFERENCES

BMT Seatech. 2010. "PC Rembrandt Ship Maneuvering and Navigation Simulation System." User Guide.

Kivva, S.L., P. Kolomiets, T. Shepeleva, and M. Zheleznyak. 2006. "CHEWPCE-MORPH. A Numerical Simulator for Depth-Averaged Surface Water Flow, Sediment Transport and Morphodynamics in Nearshore Zone. Version 2.0." User guide.

Elastic Buckling Capacities of Piles Subject to Partial Section Loss

Breanna Bailey[1], Prashant Deopurkar[2], L. U. Sankar Samudrala[3], and Lakshmana Rao Upputuri[4]

[1]Department of Civil and Architectural Engineering, Texas A&M University-Kingsville, MSC 194, 700 University Blvd, Kingsville, TX 78363; PH (361) 593-2369; FAX (361) 593-2069; email: breanna.bailey@tamuk.edu

[2]Thomas and Betts, 3590 Eagle Trace Drive, Apt#301, Memphis, TN 38125; PH (361) 406-7364; email: Prashant.Deopurkar@tnb.com

[3]1100 W Corral Ave, Apt#59, Kingsville, TX 78363; PH (361) 355-1802; email: sankar_civil_engg@yahoo.co.in

[4]1100 W Corral Ave, Apt#79, Kingsville, TX 78363; PH (210) 542-4932; email: upputurilakshmanarao@yahoo.co.in

ABSTRACT

Finite element analyses were conducted to determine critical buckling loads for rectangular, hollow pipe, and I-shaped piles subject to corrosion losses in the splash zone. Elastic buckling analyses generated Euler buckling loads for models with partial section loss in the splash zone as well as section loss across the entire pile length. Cross-sections were subjected to 25%, 50%, and 75% material loss. Rectangular and hollow pipe piles retained more than 70% of their capacity even when 75% of the material was lost in the splash zone. The I-shaped pile, however, became unstable for material loss exceeding 25% because lost flange material significantly reduced the moment of inertia. Results for hollow pipe piles indicate that they are likely to experience inelastic yield prior to buckling. For all three cross-sections, critical buckling loads were higher when loss was limited to the splash zone versus the full pile length.

INTRODUCTION AND MOTIVATION

Coastal infrastructure systems experience the load and fatigue demands of their on-shore counterparts but are also subject to additional stresses from the marine environments in which they exist. Coastal structures, such as piers, bridges, and off-shore oil platforms, frequently contain exposed steel components. Over time, steel components are subject to material loss due to corrosion. Issues of economy and long-term sustainability drive the need for a rigorous understanding of the resiliency of existing coastal infrastructure systems.

The economic effects of corrosion are substantial, with as many as 55% of offshore pipeline failures attributed to corrosion damage; some of this damage was due to internal corrosion from fluids passing through the pipe, but approximately 70% was due to external corrosion (Lozev et al. 2005). The city of Corpus Christi, located approximately 40 miles from Texas A&M University-Kingsville where the current

research program was conducted, is significantly affected by corrosion. A recent remediation of the 4-mile seawall revealed a 7% material loss in the webs and flanges of steel piles used as part of the city's defense against storm surges (Massengill et al. 2008). This 7% material loss was estimated to reduce the bending capacity of the steel piles by 36% (Massengill et al. 2008).

As in the case of the Corpus Christi seawall, coastal structures are supported by piles, with steel piles being commonly in use (Harris and Lorenz 1993). The most frequently selected steel pile cross-sections are hollow circular pipes and HP-sections (Prakash and Sharma 1990; Hopkins and Monahan 1990). Pipe piles are particularly attractive for marine applications, as their round cross-section reduces drag forces from waves (Prakash and Sharma 1990).

The pile's splash zone lies between the highest and lowest tide levels, as illustrated in Figure 1. This zone is exposed to frequent wet-dry cycles, constant turbulence, and winds, all of which make it particularly susceptible to corrosion (Apicella et al. 1996). The splash zone is almost universally recognized as the most critical region for corrosion damage (Escalante et al. 1977; Zen 2005; Thaesler et al. 2005; Harris and Lorenz 1993; and Lozev et al. 2005).

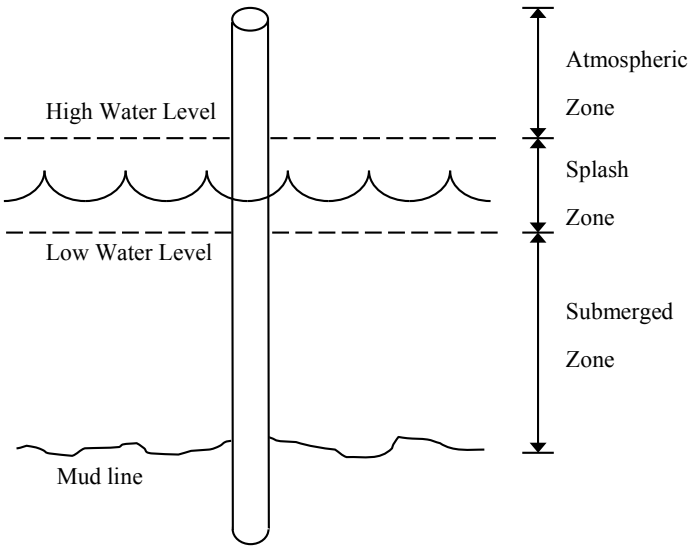


Figure 1. Schematic of a hollow pipe pile illustrating atmospheric, splash, and submerged zones. High and low water levels depend upon tidal action. The continuous wet/dry cycle in the splash zone makes it a highly corrosive region.

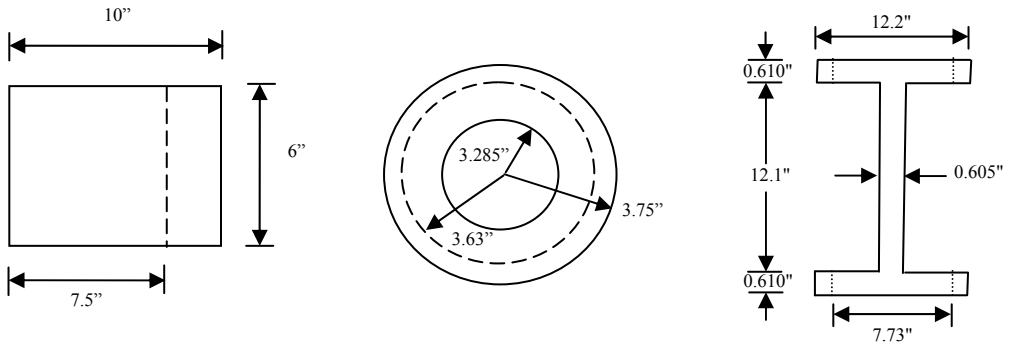
While considerable research efforts have been devoted to developing effective methods for corrosion protection, research to understand the capacity of members affected by corrosion is fairly limited. The purpose of the current work is to examine the critical buckling capacities of steel piles subject to partial section loss in the region of the splash zone. This research provides the first step towards creating a harmonized set of equations for predicting residual pile capacity as a function of section loss, similar to the design equations for columns found in the AISC *Steel Construction Manual* (AISC manual). The focus of this paper is to (1) determine how differently shaped piles are affected by section loss; and (2) determine the usefulness of conservatively estimating section loss in the splash zone as occurring

throughout the entire length of the pile.

METHODOLOGY

Finite element analyses were conducted on representative examples of rectangular, hollow pipe, and I-shaped steel piles. The basic pile geometry was suggested by an engineer working in the Corpus Christi Branch of HDR Engineering, Inc. Steel piles investigated in this study were 30 feet (9.1 m) long with a 5-foot (1.5-m) splash zone and a 15-foot (4.6-m) submerged zone (refer to Figure 1). The piles were driven into the mud line to the extent that fixity could be assumed, while the tops of the piles were free to translate but not rotate.

Finite element analyses calculated critical buckling loads for all three cross-section types when the piles were subject to partial section loss in the region of the splash zone as well as along the full length of the pile. The cross-sections were subject to 25%, 50%, and 75% section loss both in the splash zone and along the full length, for a total of seven analyses per geometry when full section capacity was included. Figure 2 illustrates how the cross-sections were reduced to account for section loss. The original cross-sections were a rectangle measuring 6”x10” (15.2 cm x 25.4 cm); a HSS 7.5x0.5 pipe; and a HP 12x74.



(a) (b) (c)

Figure 2. The three cross-sections represented in this study with dashed lines showing how cross-sectional area was reduced for 25% section loss. (a) The 10” dimension was reduced for the rectangular section; (b) the outer radius was reduced for the HSS 7.5x0.5; and (c) the flanges were reduced for the HP 12x74.

A local rehabilitation project provided the motivation for this study and the selection of the HP 12x74 cross-section. The rectangular cross-section was included because it possessed a similar moment of inertia to the HP 12x74. Initially, a hollow pipe with a similar moment of inertia was selected, since pipe shapes are so prevalent in pile construction. As will be discussed later, the HSS 7.5x0.5 geometry was eventually selected to reduce the degree of non-linear behavior in this study.

Moment of inertia was considered a critical parameter in the selection of pile geometries because of its role in determining the critical buckling load of a compression member. The AISC manual calculates nominal compressive strength (P_n) as a function of the member’s gross section area (A_g) and critical stress (F_{cr}), as illustrated in Equation (1) (AISC 2006). Equations for critical stress vary for linear versus nonlinear buckling behavior, but in both instances critical stress is a function

of Euler buckling stress. Therefore, a first step towards providing an estimate of compressive strength for instances of partial section loss must be to understand the relationship between Euler buckling and partial section loss. As can be seen in Equation (2), Euler buckling stress (F_e) is a function of modulus of elasticity (E), effective length (KL), and the radius of gyration (r) (AISC 2006). Clearly, area, moment of inertia, and radius of gyration are critical parameters in this investigation. Tables 1 to 3 summarize these parameters for the selected cross-sections. Values are given for full capacity sections as well as sections subject to 25%, 50%, and 75% loss due to corrosion.

$$P_n = F_{cr} A_g \tag{1}$$

$$F_e = \frac{\pi^2 E}{\left(\frac{KL}{r}\right)^2} \tag{2}$$

Table 1. Rectangular Cross-Sectional Properties

Cross-Sectional Property	Full Section	25% Section Loss	50% Section Loss	75% Section Loss
Area (in^2, cm^2)	60 *(387.1)*	45 *(290.3)*	30 *(193.5)*	15 *(96.8)*
Moment of Inertia (in^4, cm^4)	180 *(7492)*	135 *(5619)*	62.5 *(2601)*	7.81 *(325)*
Radius of Gyration (in, *cm*)	1.73 *(4.39)*	1.73 *(4.39)*	1.44 *(3.66)*	0.72 *(1.83)*

Table 2. Hollow Pipe (HSS 7.5x0.5) Cross-Sectional Properties

Cross-Sectional Property	Full Section	25% Section Loss	50% Section Loss	75% Section Loss
Area (in^2, cm^2)	10.3 *(66.5)*	7.73 *(49.9)*	5.15 *(33.2)*	2.58 *(16.6)*
Moment of Inertia (in^4, cm^4)	63.9 *(2660)*	44.9 *(1869)*	29.1 *(1211)*	13.5 *(562)*
Radius of Gyration (in, *cm*)	2.49 *(6.32)*	2.41 *(6.12)*	2.38 *(6.05)*	2.29 *(5.82)*

Table 3. I-Shaped (HP 12x74) Cross-Sectional Properties

Cross-Sectional Property	Full Section	25% Section Loss	50% Section Loss	75% Section Loss
Area (in^2, cm^2)	21.8 *(141)*	16.4 *(106)*	10.9 *(70.3)*	5.46 *(35.2)*
Moment of Inertia (in^4, cm^4)	186 *(7742)*	47.2 *(1965)*	3.71 *(154.4)*	0.212 *(8.82)*
Radius of Gyration (in, *cm*)	2.92 *(7.42)*	1.70 *(4.32)*	1.71 *(4.34)*	0.197 *(0.50)*

Critical buckling loads were calculated using an elastic Euler buckling analysis. The analyses were conducted using ABAQUS finite element software. The ABAQUS solution procedure is an iterative one in which an initial load is gradually increased until a specified number of buckling modes have been discovered. Euler buckling corresponds to a sudden deformation of the structural member. The eigenvalues discovered during an Euler buckling analysis are multiplied by the initial load to calculate the critical buckling load for the pile. The rectangular and hollow pipe cross-sections were modeled with one-dimensional beam elements, and the I-shaped cross-section was modeled using shell elements. The modulus of elasticity was 29000 ksi (approximately 200,000 MPa), and the theoretical effective length factor was 1.

RECTANGULAR PILE RESULTS

Based on Euler buckling, the theoretical buckling load for the rectangular cross-section is 397.5 kips (approximately 1768 kN). A finite element model of the cross-section at full section capacity replicated this buckling load and showed a maximum von Mises stress of 6.61 ksi (45.6 MPa). Since a typical structural steel has a yield stress of 50 ksi (345 MPa), this low von Mises stress indicates that the rectangular pile will buckle well in advance of inelastic behavior.

Figure 2 presents the critical buckling loads determined by finite element analyses for the 6”x10” (15.2 cm x 25.4 cm) solid, rectangular cross-section. These results are summarized in Table 4 along with the decrease in performance compared to a full-capacity pile. The rectangular cross-section was subject to 25%, 50%, and 75% section loss across the entire pile as well as local loss in the splash zone.

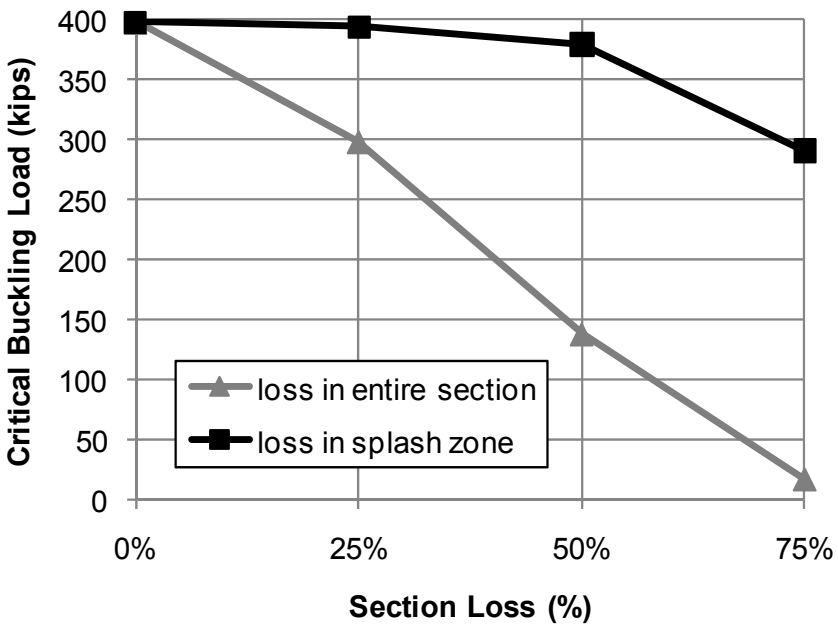


Figure 2. Critical buckling loads for a rectangular pile subject to section loss across the entire pile length and local loss in the splash zone only.

Table 4. Critical Buckling Loads for Rectangular Pile

Percentage of Section Loss	Section Loss Across Entire Pile		Section Loss in Splash Zone	
	Critical Buckling Load (kips / *kN*)	Decrease from Full Section Capacity	Critical Buckling Load (kips / *kN*)	Decrease from Full Section Capacity
25 %	298 *(1326)*	25%	394 *(1753)*	1%
50 %	138 *(614)*	65%	379 *(1686)*	5%
75 %	17.3 *(77.0)*	96%	291 *(1294)*	27%

Clearly, the rectangular cross-section possesses significantly more residual strength when section loss is limited to the splash zone than when the pile is subjected to uniform section loss. At 75% section loss, the pile's strength would be effectively depleted if the pile were modeled as having section loss along its full length, while a model of partial section loss reveals that over 70% of the pile's capacity is remaining. These results suggest that piles subject to only partial section loss maintain resiliency that should be considered in the repair process. Moreover, the results indicate that estimating a pile as having lost section across its entire length, when damage is actually located in the splash zone, is dramatically over-conservative.

Von Mises stresses at the critical buckling loads for the pile indicate that elastic buckling is likely to occur before inelastic material yield. Models with section loss in the splash zone experienced highest von Mises stresses in the reduced section. The peak von Mises stress observed for the rectangular pile was 25.3 ksi (174 MPa) for the 75% section loss, splash zone model.

HOLLOW PIPE PILE RESULTS

While results for the rectangular pile indicated elastic buckling as the dominant failure mechanism, the need for an inelastic analysis to gain a complete understanding of pile behavior becomes evident when examining hollow pipe cross-sections. Several finite element analyses of hollow steel shape (HSS) pipe cross-sections were performed to determine the critical buckling loads, as summarized in Table 5. The pipes were subjected to a 75% section loss in the splash zone.

Table 5. Summary of critical buckling loads and von Mises stresses for various HSS pipes subject to 75% section loss in the splash zone.

HSS Pipe Cross-Section	Critical Bucking Load (kips / *kN*)	Von Mises Stress at Buckling Load (ksi / *MPa*)
HSS 14 X 0.625	1109.5 *(4945)*	180.1 *(1242)*
HSS 16 X 0.625	1671.2 *(7434)*	237.9 *(1640)*
HSS 10 X 0.625	383.0 *(1704)*	89.0 *(614)*
HSS 8.625 X 0.625	240.4 *(1069)*	65.4 *(451)*
HSS 7.5 X 0.5	128.4 *(571)*	52.7 *(363)*

Table 5 includes the von Mises stress values experienced by the pipes at the

critical buckling load. Most cross-sections examined in this work had von Mises stresses in excess of 50 ksi (345 MPa), the yield strength of standard grade 50 steel. This behavior indicates that pipe piles are more likely to yield inelastically before buckling. The HSS 7.5x0.5 pipe was selected for further study because it experienced the lowest von Mises stresses at 75% section loss, although the 52.7 ksi (363 MPa) stress would still exceed elastic limits. Figure 3 and Table 6 summarize the critical buckling loads determined for the HSS 7.5x0.5 pile due to section loss across the entire pile as well as localized loss in the splash zone. The critical buckling load for the full-section HSS 7.5x0.5 pile was 140.1 kips (623 kN).

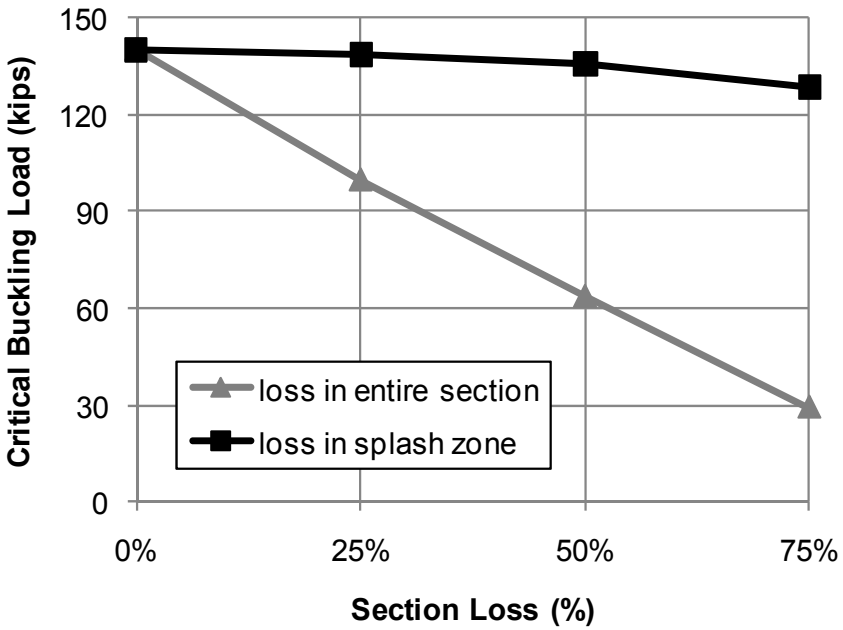


Figure 3. Critical buckling loads for a hollow pipe pile (HSS 7.5x0.5) subject to section loss across the entire pile length and local loss in the splash zone only.

Table 6. Critical Buckling Loads for Hollow Pipe Pile

Percentage of Section Loss	Section Loss Across Entire Pile		Section Loss in Splash Zone	
	Critical Buckling Load (kips / *kN*)	Decrease from Full Section Capacity	Critical Buckling Load (kips / *kN*)	Decrease from Full Section Capacity
25 %	99.7 *(444)*	29%	138.5 *(616)*	1%
50 %	63.6 *(283)*	55%	135.6 *(603)*	3%
75 %	29.3 *(130)*	79%	128.4 *(571)*	8%

As with the rectangular pile, results for the hollow pipe show significant residual strength when section loss is localized to the splash zone, as opposed to loss along the full pile length. Even at 75% section loss in the splash zone, the pile retains over 90% of its original capacity.

I-SHAPED PILE RESULTS

Figure 4 presents the critical buckling loads for the HP12x74 cross-section when subjected to cross-sectional losses of 25%, 50%, and 75% across the entire pile as well as local loss in the splash zone. These results are also presented in Table 7. The full-capacity buckling load for the HP 12x74 was 297.5 kips (1323 kN).

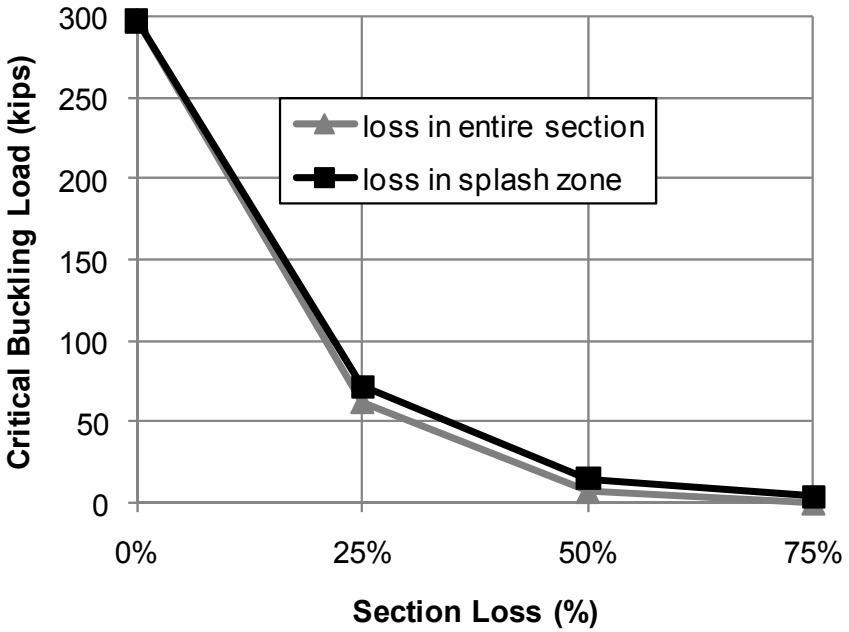


Figure 4. Critical buckling loads for an I-shaped pile (HP 12x74) subject to section loss across the entire pile length and local loss in the splash zone only.

Table 7. Critical Buckling Loads for I-Shaped Pile

Percentage of Section Loss	Section Loss Across Entire Pile		Section Loss in Splash Zone	
	Critical Buckling Load (kips / *kN*)	Decrease from Full Section Capacity	Critical Buckling Load (kips / *kN*)	Decrease from Full Section Capacity
25 %	62.5 *(278)*	79%	71.8 *(319)*	76%
50 %	7.23 *(32)*	98%	15.1 *(67)*	95%
75 %	0.11 *(0.5)*	100%	4.16 *(19)*	99%

As with the rectangular and hollow pipe cross-sections, the HP 12x74 buckling capacity for section loss in the splash zone is consistently higher than when the pile is modeled as having section loss across the entire pile length. However, the advantage of modeling section loss in the splash zone only is significantly smaller with the I-shaped cross-section. From Tables 1 to 3, it is apparent that the moments of inertia and radii of gyration for the I-shaped cross-section decrease at a more rapid rate than for the other geometries considered in this study. This rapid decrease occurs because section loss is modeled by first removing area from the flanges of the HP

12x74. In any I-shaped cross-section, the flanges dominate the calculation for moment of inertia, with web contributions being almost negligible. Therefore, as the flanges are eroded by corrosion, the compressive capacity decreases dramatically. This model of section loss was selected for the current study because it best matched the observed field conditions.

The HP 12x74 experienced very low stresses at the critical buckling load. The stresses at failure decreased rapidly as the degree of section loss increased, and von Mises stresses for the 75% section loss model were less than 1 ksi (6.9 MPa). The cross-section buckled almost immediately once material loss exceeded 50%. Figure 5 illustrates the deflected shape of the 75% section loss model; the model has a clear inflection point in the reduced-section splash zone. It can be seen that in order to model this degree of loss, the entire flange and a portion of the web had to be removed.

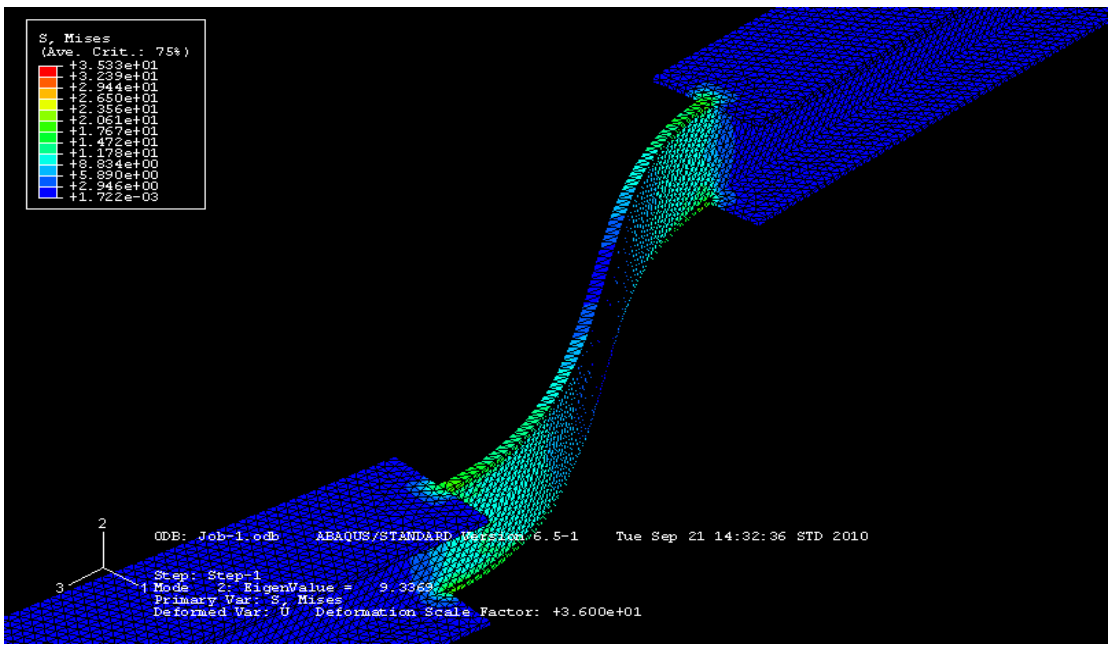


Figure 5. Deflected shape of splash zone region for HP 12x74 subjected to 75% section loss in splash zone.

CONCLUSIONS

This paper presented details of elastic buckling analyses conducted on representative examples of rectangular, hollow pipe, and I-shaped piles. While significantly more work must be completed before a set of predictive design equations can be proposed, the following conclusions may be reached:

- For all three geometries, estimating section loss throughout the entire length of the pile was conservative. For the rectangular and hollow pipe piles, this estimate did not reflect the degree of residual capacity remaining in the pile and should be avoided. The difference between buckling capacities for splash

zone versus full length cross-section reductions for the HP 12x74 pile, however, was almost negligible. These results suggest that estimating section loss across the full length of an I-shaped pile could provide a quick rule of thumb to determine remaining capacity. Additional geometries should be explored, as should size effects.

- The rectangular and I-shaped piles both exhibited elastic behavior and are expected to buckle well before the onset of material yield. The hollow pipe piles, however, appear to be highly nonlinear. An elastic analysis is insufficient to accurately predict behavior for this type of pile.
- Both the rectangular and hollow pipe piles possess significant residual strength that could be considered in remediation plans. The I-shaped pile results, however, indicate that this cross-section becomes unstable above 50% section loss.

The next generation of pile models will consider both shell and solid geometries to improve overall modeling accuracy. In addition, inelastic material behavior will be considered, and post-buckling analyses will be conducted.

REFERENCES

American Institute of Steel Construction (AISC). (2006). *Steel Construction Manual*, 13th Ed., AISC, Chicago, IL.

Apicella, Frank, Glen Nickelsen, and Frank Wang. (1996). "Repair of Marine Structures Using an All-Polymer Encapsulation Process." *Materials Performance,* 35(9), 28-32.

Escalante, E., W. P. Iverson, W. F. Gerhold, B. T. Sanderson, and R. L. Alumbaugh. (1977). *Corrosion and Protection of Steel Piles in a Natural Seawater Environment*: *NBS Monograph 158.* U.S. Department of Commerce, National Bureau of Standards, Washington, D.C.

Harris, George M. and Alan Lorenz. (1993). "New Coatings for the Corrosion Protection of Steel Pipelines and Pilings in Severely Aggressive Environments." *Corrosion Science*, 35, 1417-1423.

Hopkins, Robert M. and Craig C. Monahan. (1990). "Corrosion Survey of Steel H-Piles Supporting a Small Craft Harbours Wharf in Trepassey, Newfoundland." *Corrosion in the Marine Industry Bulletin*, 83 (935), 155-161.

Lozev, M. G., R. W. Smith, and B. B. Grimmett. (2005). "Evaluation of Methods for Detecting and Monitoring of Corrosion Damage in Risers." *Journal of Pressure Vessel Technology*, 127, 244-254.

Massengill, Jeff, Brent Moore, Dan Garza, and Allan Hayes. (2008). "Defending Corpus Christi." *Civil Engineering*, 78(6), 48-53, 80-81.

Thaesler, Patricia, Lawrence Kahn, Rita Oberle, and Cornelia Demers. (2005). "Durable Repairs on Marine Bridge Piles." *Journal of Performance of Constructed Facilities,* 19(1), 88-92.

Zen, Kazuaki. (2005). "Corrosion and Life Cycle Management of Port Structures." *Corrosion Science*, 47, 2353-2360.

Field Observations and Numerical Modeling of Infragravity Waves

Yang Zhang[1], Hemming Schäffer[2], Chris Carr[3], Sean O'Neil[4]

[1]Halcrow, Inc., 1101 Channelside Drive, Suite 200 S, Tampa, FL 33602, USA; PH (813) 386-1990; Fax (813) 386-1991; ZhangY@halcrow.com

[2]SchäfferWaves, Sortedam Dossering 59D st. DK-2100 Copenhagen Ø, Denmark, Hemming@SchafferWaves.dk

[3]Halcrow, Inc., 22 Cortlandt Street, 31st Floor, New York, NY 10007, USA, CarrCM@halcrow.com

[4]Halcrow, Inc., 22 Cortlandt Street, 31st Floor, New York, NY 10007, USA, ONeilST@halcrow.com

Abstract

Field observations and numerical modeling of infragravity (IG) waves were conducted in support of the expansion of a major seaport. Measurements show that the overall energy level of IG waves is similar between stations deployed outside and inside the port, while spectra of IG waves show a clear peak of ~0.01 Hz at the inside-port stations and IG spectra at the outside-port stations are very broad-banded and somewhat white-noise-like, without a predominant peak frequency. Roughly linear dependence of long-wave amplitude on short-wave amplitude is observed from the field data. Long waves are also observed to be very directionally scattered, with seaward-propagating components dominant over contributions from the shoreward propagating components. In the numerical model, a non-standard approach, by employing a customized filter layer in the surf zone to mimic the short-wave breaking and run-up processes, is used to reduce the resolution requirement and thus the computational burden by an order of magnitude. Numerical model results are in good agreement with measured long-wave amplitude and compare favorably with the measured long-wave spectra. Furthermore, the directional properties of long waves from the numerical model are also confirmed by the analysis of measurement data.

1. Introduction

Ocean-facing ports are usually well protected against sea and swell (i.e. short waves) by using breakwaters and/or other defensive measures. However, protection against infragravity (IG) waves can at times be much more difficult. Infragravity waves, also known as long waves, have periods ranging from 30 s to several minutes, and may be in the same range of as the natural resonant periods of port basins and/or moored vessels. Therefore, IG waves can induce low-frequency resonance in harbors (e.g., Bowers, 1977) and may lead to accidents such as excessive vessel motions and mooring line breakages. Prediction of long wave response is important for development and expansion of a port.

Munk (1949) first observed low-frequency (lf) wave motion outside the surf zone and termed it as 'surf beat' (also referred as IG waves in the literature) as these lf waves were believed to be generated in the surf zone as a result of a beat (subharmonic) phenomenon induced by the short wave groups. Tucker (1950) cross-related the short-wave envelope with the local lf

wave motion and found that seaward-propagating long waves appeared to be negatively correlated with the shoreward-propagating short wave groups. Subsequent field observations have demonstrated that in the surf zone and swash zone the surface elevations and velocity spectra are very often dominated by lf energy (Huntley et al., 1977; Guza and Thornton 1982; Wright et al., 1982).

Two main generation mechanisms have been recognized in the literature for IG waves due to short waves. One is quadratic interactions among frequency pairs of sea/swell waves (short waves), resulting in group-bound long waves (Biésel, 1952; Longuet-Higgins and Stewart, 1962). The other mechanism is the generation of free long waves by temporal-spatial variation of the breakpoint of the short waves, also known as 'dynamic wave set-up' (Symonds et al., 1982; Symonds and Bowen, 1984). Schäffer (1993) developed a theoretical model that accounts for both generation mechanisms based on linear shallow water equations with a forcing term (which represents the short-wave radiation stresses), and compared the model predictions with laboratory experiments of Kostense (1984) with good qualitative agreement.

Laboratory experiments on a plane beach (1:10 slope) by Baldock et al. (2000) suggested that the breakpoint variation is the dominant forcing mechanism for steep incident wave conditions. Battjes et al. (2004) performed an analysis of Boers (1996) laboratory data and found that shoaling of the incoming lf wave depends on the normalized bed slope parameter (i.e., relative depth change per wave length). For small normalized bed slopes, the breakpoint generation mechanism is insignificant, whereas the incident bound lf waves are the dominant contributor, and for steep regime the opposite is expected. Van Dongeren et al. (2007) found that the normalized bed slope also controls the reflection coefficient and dissipation due to breaking of the long waves at the shoreline. In the mild-slope regime the dissipation due to breaking of the long waves in the vicinity of the shoreline is much higher than the dissipation due to bottom friction. Numerical models for simulating IG waves have developed including Hibberd and Peregrine (1979), Roelvink (1993) and Van Dongeren et al. (1994), among many others. More recently, numerical model results by Madsen et al. (1997), based on Boussinesq equations including wave breaking and run-up, show good agreement with the bi-chromatic wave group data from Kostense (1984). The Boussinesq model has been successfully applied in various harbor studies, while computational limits have typically only allowed for inclusion of wave breaking for areas of the order of a few square kilometers (Kofoed-Hansen et al., 2005).

The understanding of IG waves has been well advanced in the past fifty years due to their theoretical and practical importance. However, numerical modeling of IG waves remains non-trivial and often very challenging for realistic, complex three-dimensional bathymetries. In this paper, long wave studies were performed in support of the proposed expansion of a major seaport, including both field observations and numerical modeling. Appreciable long wave phenomena were measured at the port in the past, and long waves appear to be one of the primary sources of port downtime. The field measurement and analysis approach are described in Section 2. The numerical model is described in Section 3. Measurement results, as well as model-data comparisons, are shown in Section 4. Conclusions are summarized in Section 5.

2. Field Measurement and Analysis

The port under consideration is situated at the southern end of a natural crenulate bay. A field data acquisition campaign was conducted from January to March, 2010 with emphasis on IG waves. Six measurement stations were installed, including two directional wave (PUV) gauges (ST01 and ST03) and a high-resolution ADCP gauge (ST02) at the port entrance, and two pressure transducers (ST04 and ST05) being affixed to quay walls within the port. At the port entrance, stations ST01, ST02 and ST03 were deployed in approximately 13m water depth, and were arranged to be close to each other. The primary purpose of the ST01 and ST03 (bottom-mounted PUV gauges) are to measure the long waves including their directional properties. Measurements from these two gauges can be compared against each other and be used for quality assessment. To more accurately measure short waves, a high-resolution ADCP was also deployed at the same area.

The PUV gauges were set up to collect bursts of 8192 samples of pressure and velocities at a rate of 1 Hz, occurring every 6 hours. The ADCP was configured to obtain three-dimensional current data within 0.5 m depth bins throughout the water column based on 200 samples taken every 10 minutes. Wave data was also obtained in bursts where a burst measured 2400 samples of wave data with a sampling rate of 2 Hz, and with burst duration of 20 minutes occurring every 3 hours. The pressure gauges (ST04 and ST05) inside the port were set up to record bursts of 8192 samples of pressure data at the rate of 1 Hz, and measurements were taken every 3 hours.

Pressure data were converted to surface elevation data using the appropriate linear-wave transfer function. Wave spectra were obtained using the Fourier transform of 50% overlapping data segments of the surface elevation fluctuations with a Hamming window applied to each segment. With 20s being used as the threshold period value for discriminating between short and long waves, characteristic heights of short and long waves were calculated by integrating the frequency spectrum over the short-wave frequency band (>0.05 Hz) and over the long-wave frequency band (0-0.05 Hz), respectively. For the PUV measurements, the concurrent wave horizontal particle velocities (U,V) with the surface elevations enable analysis of the directional characteristics of waves, in particular of the long-wave field. This directional information is essential for assessing the nature of the origin of the long waves at the project site, so as to recognize various sources of the long waves and evaluate the relative importance of these sources. The maximum entropy method (Nwogu et al., 1987) was employed for the directional wave analysis. As it was most interesting to investigate the directional characteristics of waves during storm sea states, directional wave analysis was conducted only for selected storms. All data recorded from the ADCP station were processed and analyzed to obtain heights and spectra of short waves using the instrument manufacturer-provided software.

3. Numerical Model

The numerical model simulations of IG waves were set up based on DHI's MIKE21 BW model solving the Boussinesq wave equations. The model is a time-domain, phase-resolving model for directional, irregular waves. The model captures both short and long waves in the same model, and inherently includes nonlinear wave-wave interaction effects, which are

essential for the long-wave generation by short-wave grouping. In addition, surf zone wave dynamics, including the generation of free long waves associated with the breaking processes of short waves, are also accounted for in the Boussinesq model. In principle, the model describes all the various generation mechanisms and transformations of long waves. On the other hand, since the detailed model resolves the short-wave breaking and run-up processes, it requires a very fine resolution in both space (typically 1-2m grid size required for the surf zone) and time. Consequently, it is often computationally prohibitive for engineering practice when a relatively large area is involved. Thus, Kofoed-Hansen et al. (2005) included breaking in the modeling of a small fishing harbor, while it was excluded in their modeling of a huge seaport.

The distance between the two headlands at both ends of the embayment (the port is situated at its southern end) is approximately 12km. The predominant incoming wave directions offshore of the project site are from west-north-west to north-north-west, and the bay faces approximately west-north-west. Thus, the more northerly waves will schematically tend to generate long waves that travel along the bay shoreline towards the port. Due to the potential growth of such edge-wave-like trapped modes along the coast, it is desirable to model the coastal stretch of the entire bay. Based on these considerations, the model domain was selected to cover the port and the entire bay, which is an area of roughly 13km by 6km. For such a large domain, it is computationally prohibitive to use the full modeling approach (i.e., including wave breaking and run-up and the associated requirement of a fine spatial and temporal resolution).

A non-standard, reduced approach was thus taken in the present study of a large port to reduce the computational burden by an order of magnitude. The fundamental concept of this approach is to carefully tune numerical schemes in the surf zone to mimic the short-wave breaking and run-up processes, while retaining the main features of the full approach everywhere else. Specifically, a customized filter layer was employed in the surf zone to provide a frequency-dependent response with high absorption of the short waves while allowing long waves to pass through. To test and validate this underlying idea of using a customized filter layer in the surf zone, a range of numerical wave flume tests were conducted including both a synthetic constant depth case and a representative bottom profile at the project site. More details of these tests are provided in the following section.

Numerical flume Tests

A filter layer in the numerical model provides an overall frequency-dependent damping function. These spatial filters are applied a number of times during each time step of the time integration procedure within the model. Each spatial filtering process corresponds to a damping function in wave-number space and it can be converted into a frequency-dependent function by using the dispersion relation. The overall response of the reflection function versus frequency can be assessed theoretically by considering how many times the filtering takes place while waves pass through the filter layer.

The first set of numerical experiments was conducted in a 1200m long numerical flume with a constant water depth of 4m, see Figure 1. A filter layer was placed adjacent to the vertical wall (fully reflecting boundary) at the down-wave end of the flume. The filter coefficients were obtained by smoothing a layer of constant coefficients. The purpose of the smoothing is

to minimize undesired local reflections that could arise from abrupt changes. The integral property of the filter is theoretically unaffected by the smoothing, and it was also verified numerically that the modeled results were not sensitive to the specific choice of smoothing.

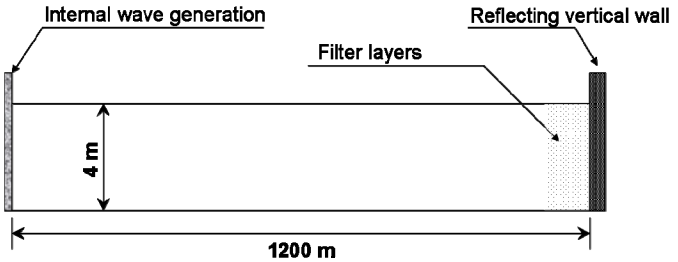


Figure 1. Schematic drawing of the numerical wave flume of a constant water depth of 4m with filter layers adjacent to a fully reflecting vertical wall at the down-wave end.

The numerical experiments were conducted using the incident-wave time-series from a white-noise spectrum with a very small significant wave height. The use of the white-noise wave signals is convenient for investigating the frequency-dependent function provided by the filter layer over the frequency range of both long and short waves in one single test. Very small significant wave heights were applied to avoid any nonlinear effects, as the purpose of this experiment was to examine the linear processes. The input wave time-series were selected to have exactly 2^N steps, where N is an integer, and only the second half of modeled time-series of surface elevations was used for the reflection analysis.

The overall reflection characteristics of the filter layer backed by a reflective boundary were obtained by a linear reflection analysis of the simulated surface elevation time-series. Following Schäffer (2009), a two-point wave separation procedure is used, which involves the surface elevation time-series at the point of interest and its immediate down-wave neighbor.

Figure 2 shows comparisons of the overall response regarding to the reflection characteristics versus frequency between theoretical predictions and numerical model results for two different time intervals. It is shown that overall there is a good agreement between the theoretical predictions and the results obtained by analyzing the numerical model simulations. Consequently, the theory is suitable for indicating how the filter parameters can be adjusted to obtain a certain decay of the reflection function vs frequency.

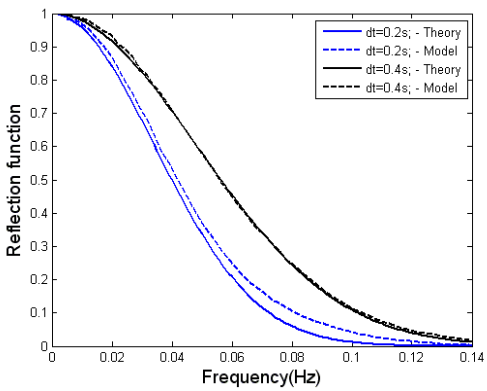


Figure 2. Overall reflection function versus frequency for a filter layer backed up by a reflective boundary. Solid lines: theoretical prediction; dashed lines: numerical model.

The use of customized filter layer in the surf zone was further examined by performing numerical tests using a representative cross-shore bottom profile of the bay. A range of simulations of the non-standard approach were examined and compared to the reference simulation results which were obtained by using the full modeling approach including wave breaking and run-up. The non-standard approach with a filter layer placed at 1.5m water depth (where is roughly the offshore limit of the surf zone for 1m incident waves), provided the best results as compared with the full approach. Note that this approach allows for breaking and run-up of the long waves that passed through the filter layer, and thus the potential dissipation of long waves at shoreline were taken into account. A similar analysis approach as for the constant depth experiments was used, and results from the tuned non-standard approach are in good agreement with the full approach, see Figure 3. The tuned filter layers were subsequently applied in the 2D simulations.

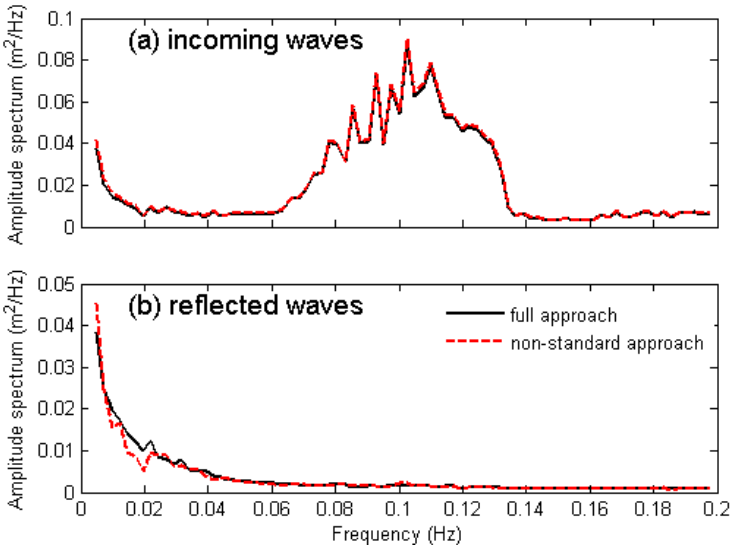


Figure 3. Amplitude spectra of the modeled (a) incoming waves, and (b) reflected waves using the tuned non-standard approach in comparison with results from the full approach. The JONSWAP wave spectra with Hm0=1m and Tp=10s were used in these simulations. The wave separation analysis was conducted at a location offshore the surf zone.

4. Results

The measured significant heights of short waves over the entire measurement period are shown in Figure 4a. Six storms were recorded during this field campaign with the maximum significant short-wave heights exceeding 1.5 m from ST02. It can be seen from Figure 4a that the short-wave heights are close between the 3 stations at the port entrance. Measured short-wave height is nearly identical at ST01 and ST03, whereas measurements from ADCP (ST02) are consistently higher. This is understandable because a bottom-mounted pressure sensor deployed at water depth of approximately 13 m may not even sense the surface waves of relatively short periods, and therefore will not fully capture the wave energy. This is especially obvious for calm sea states, during which the wave periods tend to be small. It also can be seen that short wave height is dramatically reduced at stations inside the port as compared to that at the port entrance, owing to the breakwater which provides effective protection against short waves.

Relationship between long waves and short waves

The significant heights of long waves during these storms were observed in the range of 20 to 30 cm (see Figure 4b), and there is a high correlation between the long- and short-wave height. It is interesting to note that long waves appear to have similar energy levels at all the measurement stations with slightly higher long-wave heights at stations inside the port, although short waves are significantly reduced inside the port.

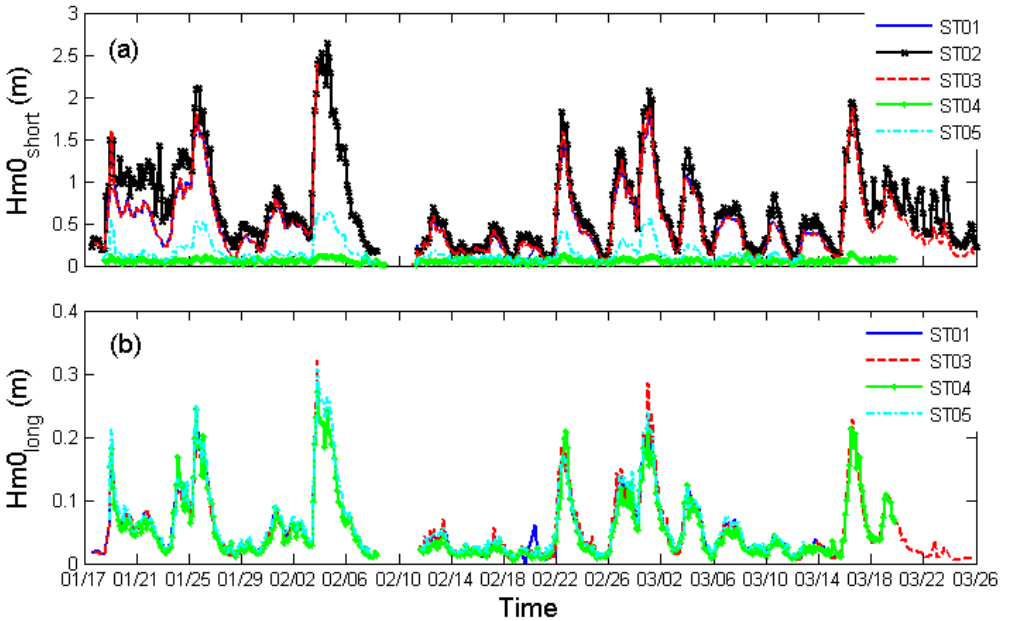


Figure 4. Measured significant height of (a) short waves and (b) long waves at measurement stations for the entire measurement period.

As discussed previously, one of the main generation mechanisms for long waves is by non-linear interactions between short waves. Further analysis has been performed to investigate the relationship between short waves and long waves using scatter plots of wave height data at measurement stations (Figure 5). It appears that the relationship between long- and short-wave heights is much closer to linear than quadratic. This observation agrees with previous long-wave field measurements (Guza and Thornton, 1982; Elgar et al., 1992, among others), in which observed long waves had a roughly linear dependence on short-wave amplitude, although the incident-bound-long-wave theory (Longuet-Higgins and Stewart, 1962) predicts that long-wave amplitude is proportional to the square of the short-wave amplitude. This implies that long waves at the project site are not dominated by the incident bound long waves.

According to theory, the amplitudes of long waves generated by short wave grouping also depend on wave periods and directionality, in addition to the amplitude, of the offshore incident waves. It was noted that during the measurement period, all 6 storms are more or less coming from the same direction. It was also noted that during storms wave periods tend to be larger (in the range of 8 to 12s). Considering the limited measurement period and that only a limited number of storms were recorded, no attempt was made to examine the detailed dependence of the long-wave amplitude on the directionality and wave periods of the offshore incident waves. Based on numerical sensitivity tests, it was shown that the offshore incident waves with higher wave periods tend to lead to larger long waves.

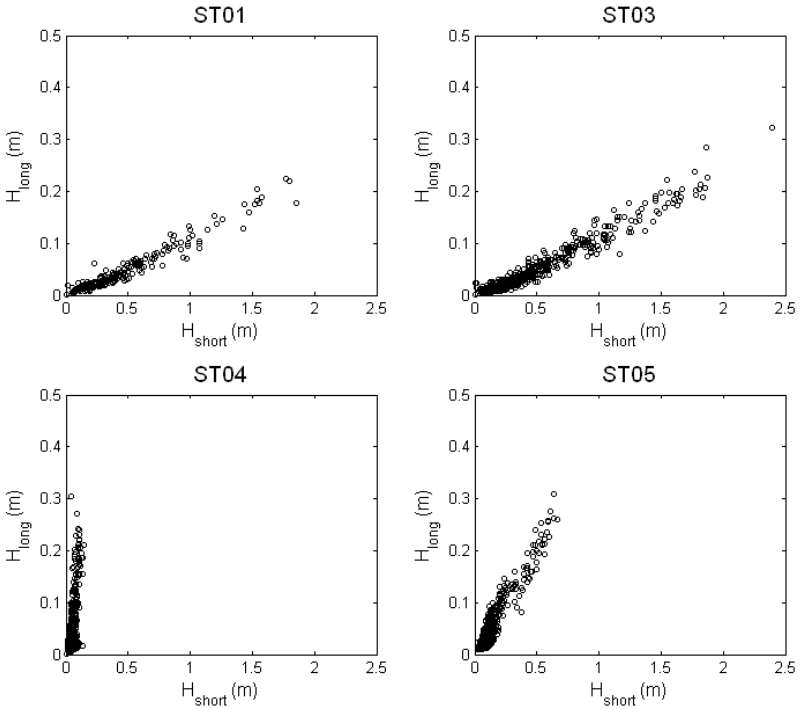


Figure 5. Scatter plots of short-wave height vs. long-wave height at the measurement stations.

Directionality of long waves

To establish a more complete understanding of the long wave characteristics at the project site, the directional properties of the long waves were investigated. In previous numerical studies by others the directional properties of long waves were assumed to be similar to those of the short waves. In contrast, it was proposed in this study that long waves generated/amplified in the surf zone and reflected off the shoreline are significant components at the project site, if not the dominant component. To verify this hypothesis, directional spectral analysis were performed using the time-series of wave particle velocity data for selected individual measurement bursts during storm sea states. Figure 6 shows the estimated main wave direction and directional spreading varying with frequencies from measurements at ST01 for burst January 25, 1400-1600 Hrs. The significant heights of short and long waves from the same burst are about 2 m and 20 cm, respectively. From Figure 6, it can be seen that there is a distinct change in wave direction and directional spreading occurred at about 0.065 Hz, which is close to the frequency of 0.05 Hz adopted in this study as threshold separating long waves from short waves. It is evident that the short waves (0.07 – 0.2 Hz) travel towards shore with a fairly uniform direction of 330 degrees, which is roughly perpendicular to the shoreline. The directional spreading of short waves is quite small, approximately 20 degrees, with some appreciable variations with frequencies. In contrast, directions of the long waves are very scattered and generally away from the coast towards offshore. Directional spreading of long waves is very large, in the range of 60 to 81 degrees. The directional spreading was computed using circular moments (Kuik et al. 1988) and has a theoretical maximum of ($\sqrt{2}$ *180/π)=81.0 degrees. This maximum appears for a uniform directional distribution for which the concept of a mean direction in no longer meaningful. This observation verifies our conceptualization of long wave characteristics at project site: long waves are not just an incident phenomenon; free long waves originating from the upper portion of the adjacent

crenulated bay and emitted through reflection from the coastline are significant contributors and likely the dominant components. Similar plots for other measurement bursts are consistent with Figure 6, and will not presented here for brevity.

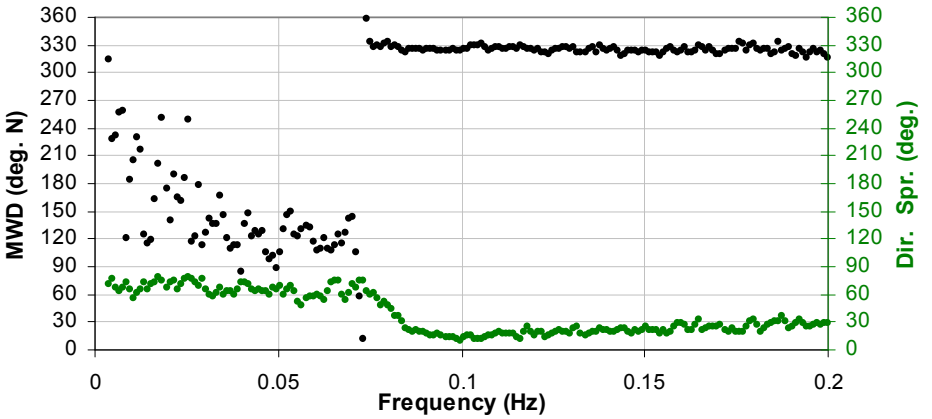


Figure 6. Estimated wave direction (left axis) and directional spreading (right axis) as a function of frequency, from measurements at ST01 for burst January 25, 1400-1600 Hrs.

Directional properties of waves were also examined qualitatively by plotting the instantaneous wave horizontal orbital velocity components, particularly the long-wave particle velocities. Figures 7 shows the scatter plots of the particle velocities associated with short waves and long waves (In the plot, U_{IG} and V_{IG} are used to present the long-wave particle velocities, respectively), from the same measurement burst as in Figure 6. As expected, a clear trend can be observed from the scatter plot for short waves, which suggests that short waves have a predominant propagation direction (in this case, approximately 330 degrees) and are directionally narrow-banded. In contrast to short waves, the 'cloud' of long-wave particle velocity plot is highly scattered, without any obvious trend. This confirms the directional analysis results as shown in Figure 6, i.e., that long waves are very directionally scattered and very dissimilar to the short waves.

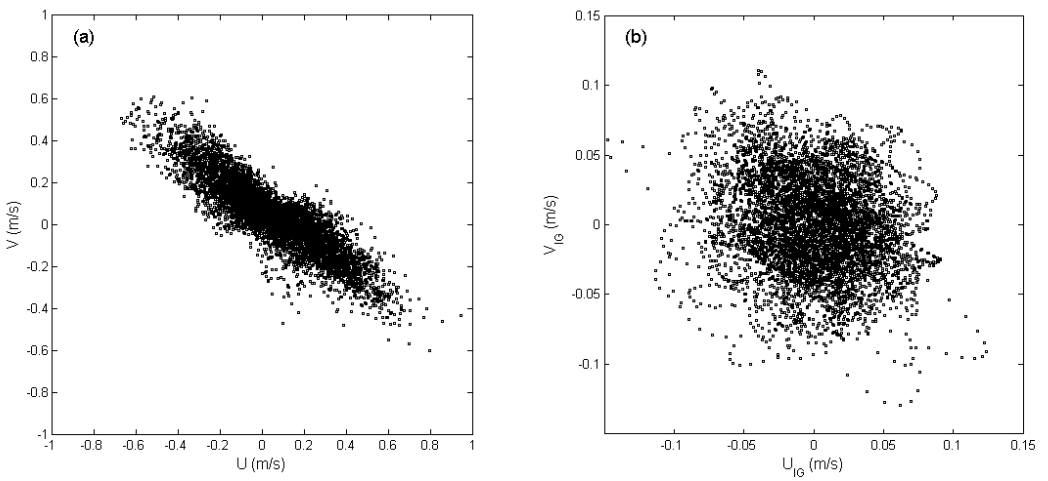


Figure 7. Scatter plot of instantaneous (a) short-wave and (b) long-wave particle velocity component (U, U_{IG}) versus (V, V_{IG}). The measurements at ST01 for burst Jan-25 1400-1600 Hrs were used. The time-series of long-wave particle velocities are obtained by applying a low-pass filter to the raw velocity data.

Comparisons with model results

For each of the selected storms, numerical simulations were performed using stationary offshore boundary conditions determined by transforming the wave conditions measured at the offshore wave buoy to the offshore boundary of the model. For each simulation case, the model was run for 2.5 hours, and only the last 2-hr of simulation results were used for analysis. Modeled significant heights of long waves compare favorably with observations at all measurement stations for selected storms (see Figure 8). The average absolute error of the modeled long-wave heights is only about 3 cm as compared with observations, which is quite satisfactory considering the complex nature of long waves and the various difficulties and uncertainties in long wave modeling (especially for such a large domain and complex geometry as in this study). It may also be worthwhile to point out that the model predicts the long-wave heights at the inside stations fairly well, while the previous studies, which assumed that long waves are mainly an incident-wave phenomenon, considerably underestimated the long-wave heights inside the port.

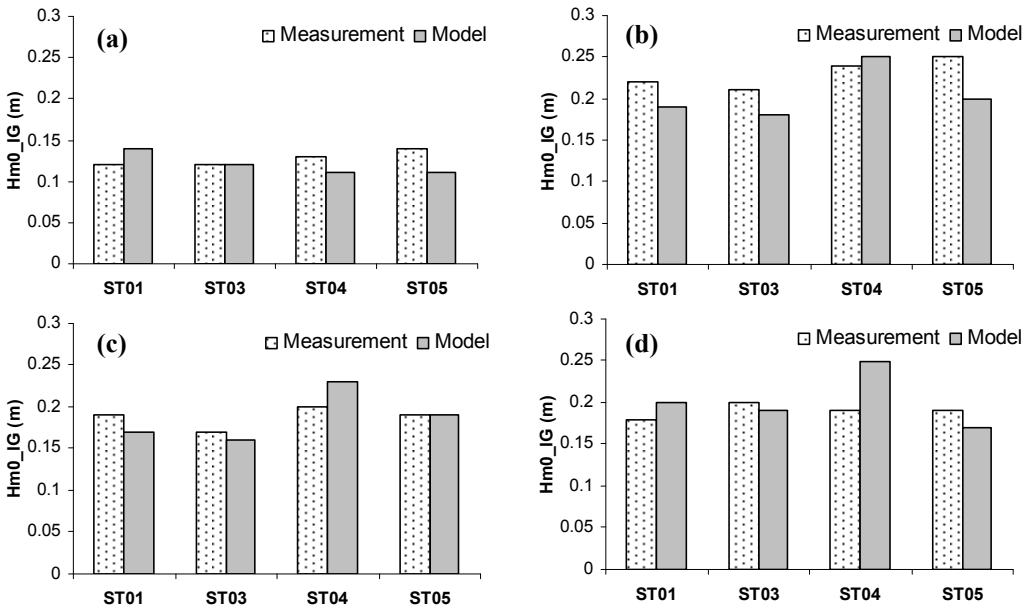


Figure 8. Comparison between measured and modeled long-wave height at measurement stations during storms. (a) January 25, 0800-1000 Hrs; (b) January 25, 1400-1600 Hrs; (c) January 26, 0200-0400 Hrs; (d) February 03, 1400-1600 Hrs.

Figure 9 shows the measured and modeled energy density spectra of long waves at all the 4 measurement stations. The measurement burst period on January 26, from 0200 to 0400 hours, was used for the spectral analysis. The model results agree well with the measurements in terms of the general shapes of long-wave spectra at the stations both outside and inside the port. At stations at the port entrance, the spectra of long waves are relatively flat with a decreasing trend through most o the long-wave frequency band. At the inside stations, clear spectral peaks can be observed, with a primary peak of approximately 0.01 Hz (100 s) and secondary peaks at both the lower and higher portion of the long-wave frequency band. The numerical model predicted the measured spectral peaks of long waves well. A similar comparison plot for the February 03 storm is given in Figure 10. The most striking difference between model results and measurements in these two figures seems to be the model under-

predicting the energy in the upper part (i.e., 0.03 - 0.05 Hz) of the long-wave frequency band, especially for the inside stations. However, it should be noted that the energy level in that frequency band is quite small for both measurements and numerical model.

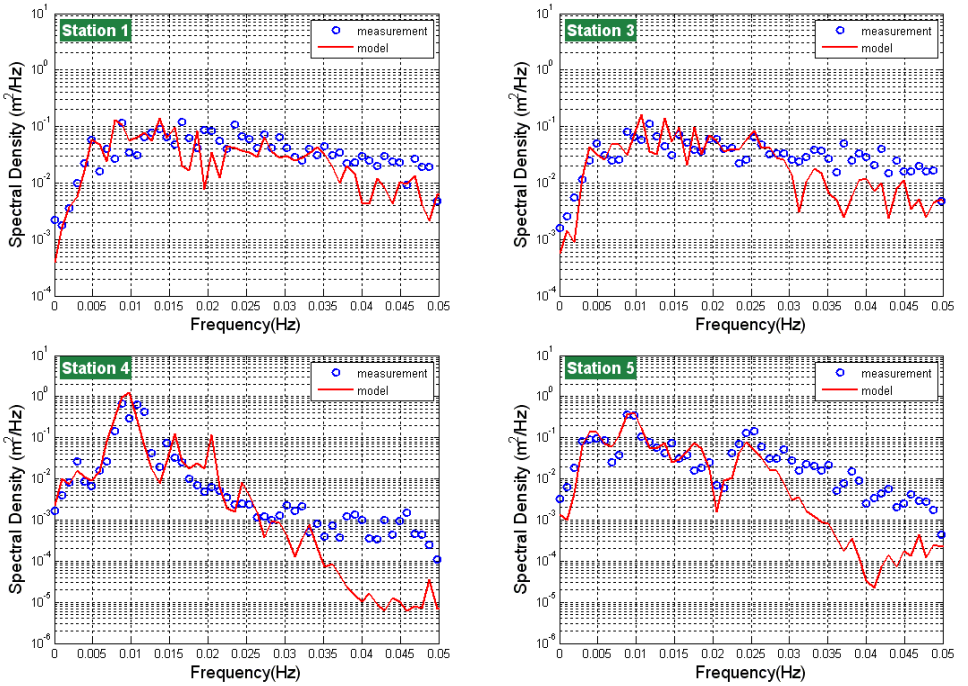


Figure 9. Comparison of spectra of IG waves between measurements and model results (January 26, 0200 to 0400 Hrs)

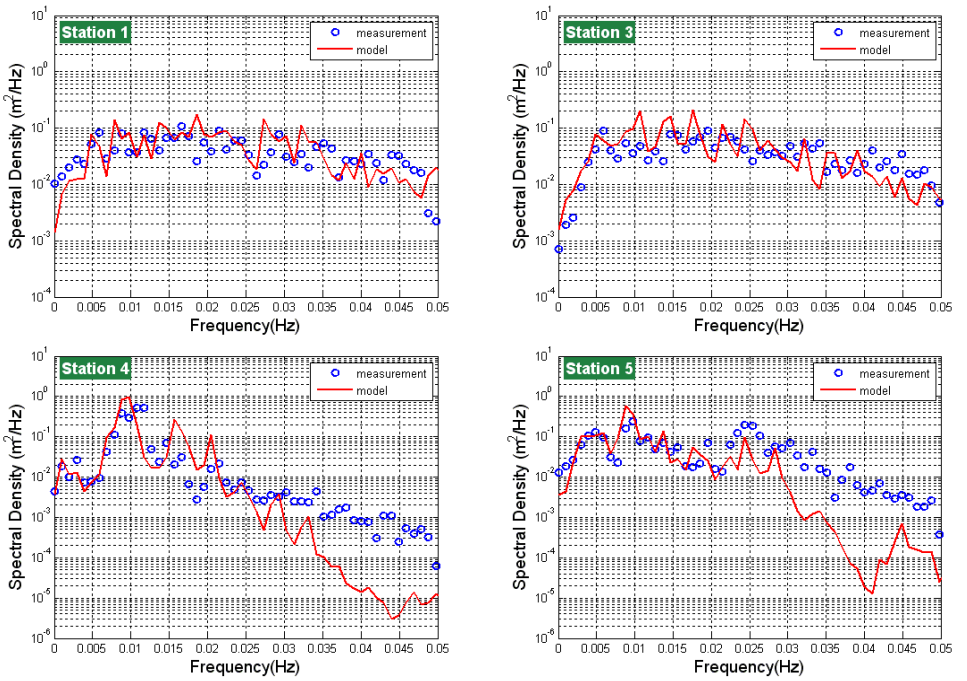


Figure 10. Comparison of spectra of IG waves between measurements and model results (February 03, 1400 to 1600 Hrs)

As discussed previously, a reasonable comparison of the directional characteristics of long

waves between measurements and model is important, as this would allow us to have further confidence in the numerical model as a predictive tool. Comparisons of the directional properties of long waves between measurements and model results are shown through scatter plots of long-wave particle velocity components as shown in Figure 11. The numerical model results are seen to show reasonably similar 'clouds' as measurements. The model results also suggest that long waves are very directionally scattered, which is in good agreement with measurements.

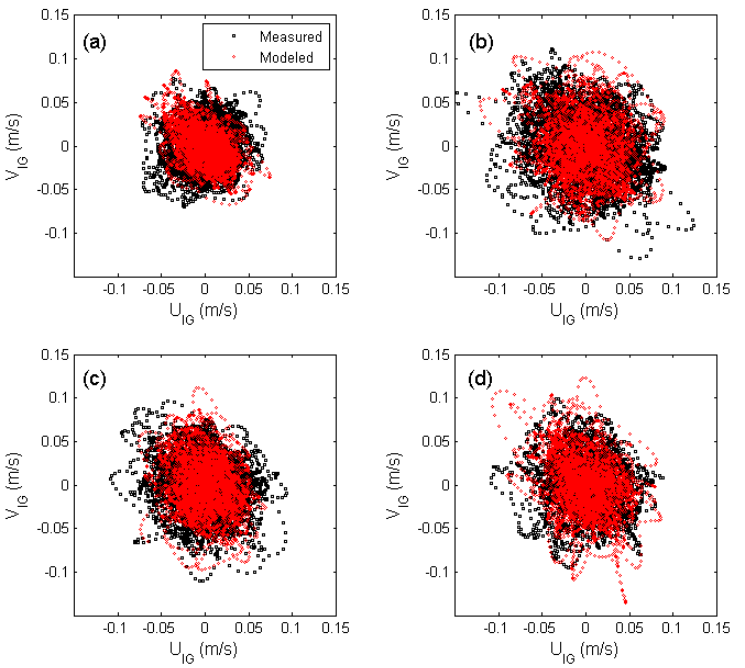


Figure 11. Scatter plots of the instantaneous particle velocities of IG waves from measurements (black dots) and model results (red dots). (a) January 25, 0800-1000 Hrs; (b) January 25, 1400-1600 Hrs; (c) January 26, 0200-0400 Hrs; (d) February 03, 1400-1600 Hrs.

5. Conclusions

Field observations and numerical modeling of IG waves were conducted in support of the expansion of a major seaport. IG waves with heights of 20-30 cm were measured both at the entrance to and inside the port during storms that occurred during the field measurement campaign. It was found that the overall IG wave energy level is similar between the outside and inside stations, while the peak periods and the spectral shapes of the measured IG waves are very different at inside stations from those outside the port. Spectra of IG waves show a clear peak at approximately 0.01 Hz (i.e., 100 s) at inside stations, whereas the spectra at outside stations are very broad-banded without a predominant peak frequency, which may suggest the amplification of energy occurs at frequency of approximately 0.01 Hz as a result of the long wave response to the port geometry. Field data shows that the long-wave height is roughly linearly dependent on short wave height, although the dependence appears to be slightly stronger than linear (much weaker than quadratic). Directional analysis of field data shows that long waves are very directionally scattered, with seaward-propagating components dominant over contributions from the shoreward propagating components. Directional

spreading of long waves is observed to be very large, in the range of 60 to 81 degrees, where 81 degrees is the theoretical maximum.

Based on the Boussinesq model, a non-standard, reduced approach was taken in the present study of a large port to reduce the computational burden by an order of magnitude, by employing a customized frequency-dependent filter layer in the surf zone to mimic the short-wave breaking and run-up processes. This eliminates the need for a very fine spatial and temporal resolution as required when using the full approach including wave breaking and run-up. The approach was tested and validated using numerical flume experiments and then implemented into the 2DH numerical model. Observed long-wave heights during storms were reproduced well by the numerical model both at the outside and inside stations. The model results agree reasonably well with measurements that long-wave spectra are very broad-banded at the outside stations, and are much narrower at the inside stations, with peak frequencies of approximately 0.01 Hz. Comparisons of the directional properties of long waves between measurements and model results are shown via scatter plots of long-wave particle velocity components. The numerical model results are seen to show reasonably similar 'clouds' as measurements. These comparisons provide confidence in the model as a predictive tool to evaluate the proposed port expansion and to provide the long-wave forcing for ship motion modeling.

References

Baldock, T. E., and D. A. Huntley (2002), Long-wave forcing by the breaking of random gravity waves on a beach, *Proc. R. Soc. London, Ser. A*, 458, 2177– 2201.

Baldock, T. E., D. A. Huntley, P. A. D. Bird, T. O'Hare, and G. N. Bullock (2000), Breakpoint generated surfbeat induced by bichromatic wave groups, *Coastal Eng.*, 39, 213– 242.

Battjes, J. A., H. J. Bakkenes, T. T. Janssen, and A. R. van Dongeren (2004), Shoaling of subharmonic gravity waves, *J. Geophys. Res.*, 109, C02009, doi:10.1029/2003JC001863

Biésel, F., Équations générales au second ordre de la houle irréguliére, *Houille Blanche*, 7, 372– 376, 1952.

Bowers, E. C. (1977), Harbour resonance due to set-down beneath wave groups. *J. Fluid Mech.* 79, 71-93.

Elgar, S., Herbers, T. H. C., Okihiro, M., Oltman-Shay, J., and Guza, R. T. (1992), Observations of infragravity waves. *J. Geophys. Res.,* 97, 15 573-15 577.

Guza, R. T. and Thornton, E. B. (1982), Swash oscillations on a natural beach. *J. Geophys. Res.*, 87, 483-491.

Hibberd, S. and Peregrine, D. H. (1979), Surf and run-up on a beach: a uniform bore. *J. Fluid Mech.*, 95, 323-345.

Huntley, D. A., Guza, R. T., and Bowen, A. J. (1977), A universal form for shoreline run-up spectra? *J. Geophys. Res.*, 82, 2577-2581.

Kofoed-Hansen, H., Kerper, D.R., Sørensen, O.R., and Kirkegaard, J. (2005), Simulation of

Long Wave Agitation in Ports and Harbours using a Time-domain Boussinesq Model. *In Proceedings of the 5th International Symposium on Ocean Wave Measurement and Analysis - WAVES 2005, Madrid, Spain.*

Kostense, J. K. (1984), Measurements of surf beat and setdown beneath wave groups, paper presented at *19th International Conference on Coastal Engineering*, ASCE., Houston, Tex.

Kuik, A. J., van Vledder, G. P. and Holthuijsen, L. H. (1988). A method for the routine analysis of pitch-and-roll buoy wave data. *J. Phys. Oceanography*, 18, 1020-1034.

List, J. H. (1992), A model for the generation of two-dimensional surf beat. *J. Geophys. Res.*, 97, 5623-5635.

Longuet-Higgins, M. S. and Stewart, R. W. (1962), Radiation stress and mass transport in gravity waves, with application to 'surf beats'. *J. Fluid Mech.,* 13, 481-504.

Madsen, P. A., Sorensen, O. R., and Schäffer, H. A. (1997), Surf zone dynamics simulated by a Boussinesq type model. Part 2. Surf beat and swash oscillations for wave groups and irregular waves. *Coastal Eng.*, 32, 289-319.

Munk, W. H. (1949), Surf beats. *Trans. Am. Geophys. Union,* 30, 849-854.

Nwogu, O., Mansard, E.P.D., Miles, M. and Isaacson, M. (1987), Estimation of directional wave spectra by the Maximum Entropy Method. *Proc. IAHR Seminar on Wave Analysis and Generation in Laboratory Basins,* XXII IAHR Congress, Lausanne, Switzerland, 363-376.

Roelvink, J. A. (1993), Surf beat and its effect on cross-shore profiles. PhD. thesis, Technical University of Delft.

Schäffer, H. A. (1993), Infragravity waves induced by short wave groups. *J. Fluid Mech.*, 247, 551-588.

Schäffer, H. A. (2009), A fast convolution approach to the transformation of surface gravity waves: Linear waves in 1DH. *Coastal Eng.*, 56, 517-533.

Symonds, G., and A. J. Bowen (1984), Interactions of nearshore bars with incoming wave groups, *J. Geophys. Res.*, 89, 1953– 1959.

Symonds, G., Huntley, D. A., and Bowen, A. J. (1982), Two-dimensional surf beat: long wave generation by a time-varying breakpoint. *J. Geophys. Res.*, 87, 492-498.

Tucker, M. J. (1950), Surf beats: sea waves of 1 to 5 min period. *Proc. R. Soc. Lond.*, A 202, 565-573.

Van Dongeren, A., J. Battjes, T. Janssen, J. van Noorloos, K. Steenhauer, G. Steenbergen, and A. Reniers (2007), Shoaling and shoreline dissipation of low-frequency waves, *J. Geophys. Res.*, 112, C02011, doi:10.1029/2006JC003701.

Van Dongeren, A. R., Sancho, F. E., Svendsen, I. A., and Putrevu, U. (1994), SHORECIRC: a quasi- 3D nearshore model. *In Proc. 24th Int. Conf. Coastal Engineering*, pp. 1321-1334. New York: American Society of Civil Engineers.

Wright, L. D., Guza, R. T., and Short, A. D. (1982), Dynamics of a high energy dissipative surf zone. *Mar. Geol.,* 45, 41-62.

Coastal Engineering for Renovation of San Francisco Marina West Yacht Harbor

M. Hobson[1], F. Filice[2], S. Fenical[3], M. Tirindelli[4]

[1] San Francisco Department of Recreation and Parks, 30 Van Ness Ave. 5th Floor, San Francisco, CA 94102; PH (415) 581-2575; Email: Mary.Hobson@sfgov.org
[2] San Francisco Department of Public Works, 30 Van Ness Ave. 5th Floor, San Francisco, CA 94102; PH (415) 558-4011; Email: frank_filice@ci.sf.ca.us
[3] Coast & Harbor Engineering, 155 Montgomery St., Ste 301, San Francisco, CA 94104; PH (415) 773-2164; Email: scott@coastharboreng.com
[4] Coast & Harbor Engineering, 155 Montgomery St., Ste 301, San Francisco, CA 94104; PH (415) 773-2089; Email: matteo@coastharboreng.com

ABSTRACT

Coastal engineering analysis and numerical modeling were performed for the San Francisco Marina West Yacht Harbor Renovation to develop engineering solutions for improving wave conditions in the marina and reducing sedimentation in the entrance channel. Analysis was performed using hydrographic survey data sets to quantify and locate sedimentation patterns in the entrance channel, and alternative mechanisms for reducing sedimentation were evaluated. The wave systems at the West Harbor are complex and formed of three main components: Pacific Ocean swell arriving through the Golden Gate, harbor seiche generated by the swell, and wind-waves from the north and northeast. To maximize wave protection in the harbor, breakwater designs were evaluated considering all three wave systems. Numerical modeling and analysis was also performed to evaluate changes in currents caused by the project, including entrance channel flow changes that impact navigation safety, and changes in marina water quality.

DEVELOPMENT OF NEW BREAKWATER ALTERNATIVES

In developing the alternatives, CHE accounted for the results of wave modeling at the project area existing conditions and also the findings and recommendations from previous studies. Three different types of breakwaters were evaluated: rock (rubble-mound), steel/concrete sheetpile and floating breakwaters.

Breakwater alternatives for each of these types were developed to provide the required wave protection. Overall, more than 25 different breakwater alignments and locations were evaluated, including attached and detached breakwaters. These alternatives were screened using the evaluation criteria (cost, navigability and water quality) and the preferred alternative for detailed analysis was selected. Upon evaluation of many different alternatives, the preferred alternative breakwater was selected and is shown in Figure 1.

The preferred alternative breakwater consists of a solid sheetpile wall near the marina green and a floating breakwater offshore of the entrance. The preferred configuration provides an approximately 100-ft wide northern navigation channel

between the floating breakwater and the -12 ft (MLLW) bottom elevation contour defined by April 2009 bathymetry (maximum sedimentation) at the North Jetty. A 300-ft wide southern navigation area would exist between the floating breakwater and the seawall. These navigation areas are shown in Figure 1.

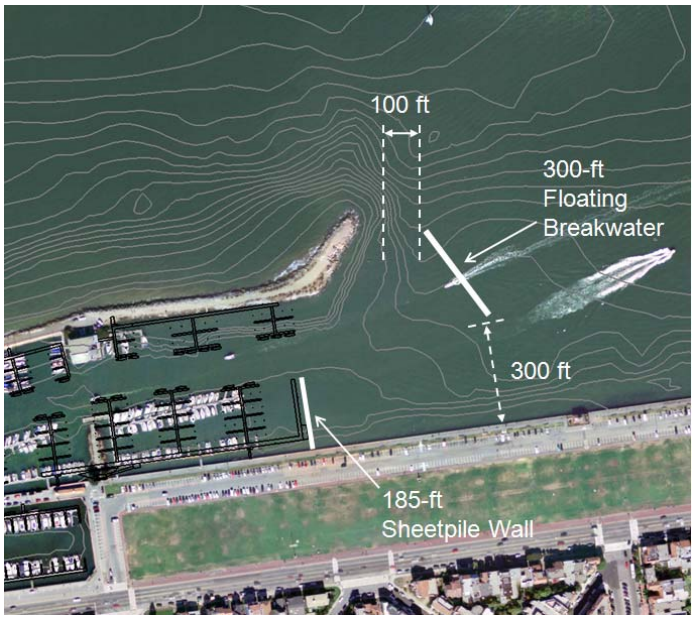


Figure 1. Proposed (optimized) sheetpile-floating breakwater combination. Note: bathymetry contours represent pre-construction conditions.

The proposed breakwater sections (south and outer) are described in further detail below.

- South Sheetpile Wall. The south sheetpile wall is located adjacent to the James Fair Seawall. The sheetpile wall is preliminarily offset 15 ft from the seawall to avoid construction impacts and enhance current circulation. The preliminary length of this sheetpile wall is approximately 185 ft. The preliminary crest elevation of the sheetpile wall is +10 ft (MLLW).
- Outer Breakwater. The outer breakwater is a 300-ft floating breakwater, anchored by stake piles or helical anchors with anchor chain or Seaflex-type anchor lines. The beam, draft, and freeboard of the concrete pontoon floating breakwater are 15, 6 and 3 ft, respectively. The specific location of the outer breakwater was selected to provide excellent wave protection for the floats and minimize risk for sedimentation precluding effective navigation (i.e., to avoid narrow channel locations where sedimentation will affect navigability).

The benefits of the preferred alternative configuration are the following:

- Optimum Navigation. The proposed configuration does not constrict navigation to a narrow location where sedimentation will quickly deteriorate navigation conditions and require excessive maintenance dredging. The

preferred outer breakwater alternative has a 100-ft wide entrance channel at the north end, and a 300-ft navigation area to the south.

- Reasonable Cost. The south sheetpile wall location is shallow and has relatively mild wave conditions (and hence, forces on the structure), and should allow efficient design.
- Transient Moorage. Floating breakwaters can easily be equipped with utilities if required, and used for transient moorage, or even permanent moorage following addition of finger floats.

WAVE PROTECTION PERFORMANCE EVALUATION

The preferred alternative described above was evaluated to verify it meets the project wave protection criteria. Wave protection performance criteria were developed based on multiple sources including PIANC (1995) and project experience with other similar marinas. The minimum performance criteria chosen were significant wave height limits at the proposed floats of 1.0 ft during the 1-year event, and 2.0 ft during the 50-year event (both assuming vessels moored in head seas). If feasible, wave conditions less than 1.0 ft in height during the 50-year event are desirable.

Three different wave analyses were performed: 1) NE wind-waves were evaluated using phase-averaged spectral tools on a Bay-wide scale, followed by nearshore refraction-diffraction-reflection-transmission modeling with full 2D spectral coupling; 2) Boussinesq wave transformation modeling was performed to evaluate swell penetration for all breakwater alternatives; and 3) results from the Boussinesq modeling were extracted at locations throughout the harbor and seiche was evaluated using low-frequency filtering.

Wind-wave breakwater performance was evaluated using a combination of the phase-averaged wind-wave growth and transformation model SWAN, spectrally coupled for nearshore modeling using the 2D wave transformation model HWAVE-S (Zheleznyak *et al.*, 2009). The HWAVE-S model simulates all relevant wave transformation processes, including wave transmission through floating structures using transmission parameters pre-determined from empirical (laboratory) studies. The evaluation was conducted for the 50-year event, which was determined based on sensitivity tests to be the governing condition.

Figure 2 (left) shows wave patterns under existing conditions for the 50-year event from the worst-case direction from a float protection perspective (60 degrees True North). Wave heights during the 50-year event (as well as 1-year event) are above the breakwater performance criteria and mooring float design criteria (also significant wave height of 2.0 ft in the 50-year event), confirming the requirement for wave protection. The HWAVE-S model reproduces the wave reflection off the seawall reported by marina users, and demonstrates the need for good wave protection near the south breakwater location. Figure 2 (right) shows wave conditions (significant wave heights) for the preferred alternative during the 50-year

storm. The transparent areas in Figure 2 are locations where wave heights are below a significant wave height of 1.0 ft. The preferred alternative provides excellent wave protection during the design storm event at the proposed float locations. 50-year storms from all directions were tested and this particular condition resulted in the most conservative design.

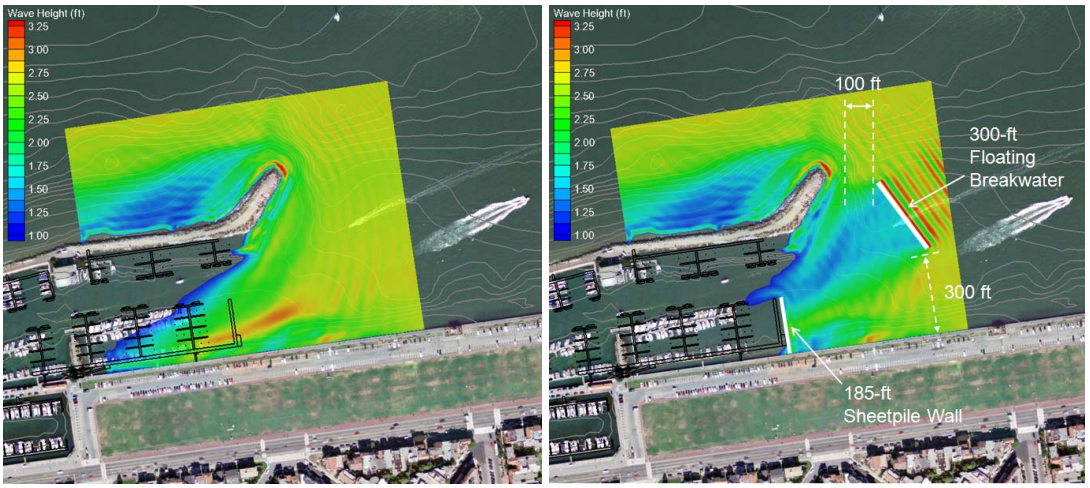


Figure 2. Existing conditions (left) and post-project conditions (right) wave patterns during the 50-year storm event (waves from the ENE).

Figure 3 shows a normalized incident swell time history (left) and normalized swell heights in the harbor for the preferred alternative (right). The results indicate that the swell penetration into the harbor is similar to that for existing conditions. The wave protection provided by the south sheetpile breakwater compensates for removal of the interior moles and does not exacerbate swell transmission inside. The floating breakwater was not included in the swell and seiche analysis because it is not expected to provide any measurable protection from those wave systems.

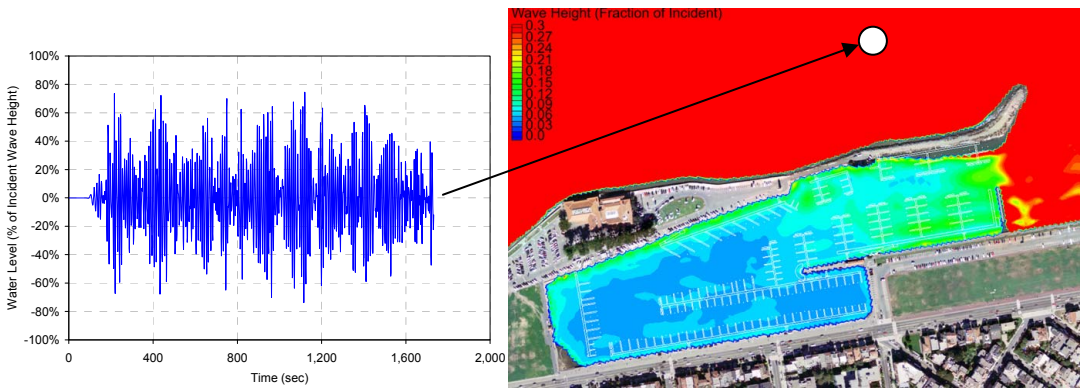


Figure 3. Normalized swell height pattern for preferred alternative sheetpile breakwater.

Seiche is a very long-period oscillation within harbors that can be caused by a variety of long-period forcing, including ocean swell and swell groups, current eddy fluctuations, wind, and other atmospheric fluctuations. Theoretical formulations indicate that the fundamental period and first harmonic mode of oscillation of the West Yacht Harbor are approximately 470 and 160 seconds, respectively, at mean sea level. Observations of the seiche were made on November 18, 2009 at 13:00 (PST), a time when tidal currents were slack and significant wave heights at the San Francisco Bar Buoy were approximately 14 ft with period 15-16 seconds. Observations made at the Scott St. Mole culvert indicated a strong, consistent flow through the culvert for approximately 80 seconds in each direction, representing 160-second period seiche-induced oscillations in the harbor.

Since these natural periods of the harbor are very long, it is not likely that the breakwater alternatives will affect seiche generation or transformation. However, in order to validate this assertion, harbor seiche was independently evaluated to determine the magnitude to which seiche would be mitigated. Figure 4 shows locations in the harbor where wave time histories were extracted for seiche analysis. Figure 3 (left) shows the time history of swell waves and swell groups present in the incoming waves at Point 1 offshore of the site.



Figure 4. Locations of wave/seiche time history extraction.

Time histories extracted at Points 2-7 were processed with various moving averages to filter out the individual swell waves and isolate the longer-period seiche oscillations predicted by the model. Figure 5 clearly indicates harbor seiche generated by the numerical model with a fairly regular period of approximately 160 seconds, matching both the theoretical first harmonic mode of oscillation and the observations of November 18, 2009. The seiche height is approximately 4-5 percent of the incident swell height. Results indicate that at most of the locations in the harbor, the seiche is largely unaffected by the breakwater alternatives. However, seiche conditions do appear to be improved due to removal of the Scott St. Mole,

since reflections in this area are removed. Also, the Scott St. Mole culvert (not included in the model) causes some impacts with regard to seiche because relatively strong currents were observed pushing against the floats on the east side during the seiche.

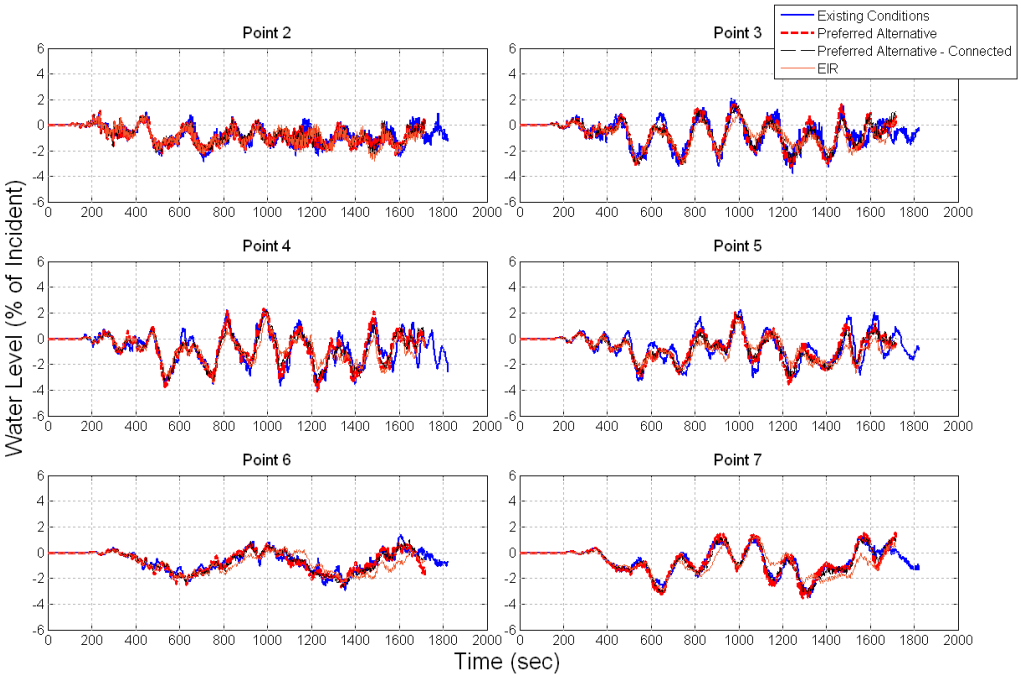


Figure 5. Time histories of harbor seiche (normalized by incident significant wave height) at various locations for all breakwater alternatives.

The following conclusions can be drawn from the results of harbor seiche modeling and analysis:

- Seiche cannot be effectively mitigated at any location inside the harbor by any of the breakwater alternatives.
- Removal of internal land features (such as the Scott St. Mole) and areas of restricted flow (such as the Scott St. Mole culvert) are expected to lessen the impacts of the harbor seiche on floats, vessels, and navigation conditions.
- Deepening of the harbor by dredging, although not evaluated here, will slightly increase the seiche period and is likely to result in slightly less seiche impacts.

CIRCULATION ANALYSIS

The project and preferred breakwater alternative were also evaluated in terms of their impact on circulation patterns for the purpose of evaluating navigation and water quality changes within the marina. Circulation was evaluated using the MORPHO model (Kivva *et al.*, 2004). Since the floating breakwater draft is less than roughly 15-20 percent of the total depth at low tide (and less at high tide), the effects of the

floating breakwater on circulation are not expected to be significant and were neglected.

Circulation conditions were evaluated during a 21-day period with a typical range of tidal current speeds. The Bay-wide circulation model was used to force a nested domain covering the marina and adjacent areas. Figure 6 shows circulation patterns during a typical peak ebb (left) and flood (right) current. Modeling results show the gyre within the entrance to the harbor that is generated by the North Jetty extension. A similar but opposite-direction gyre is present during both peak flood and peak ebb currents.

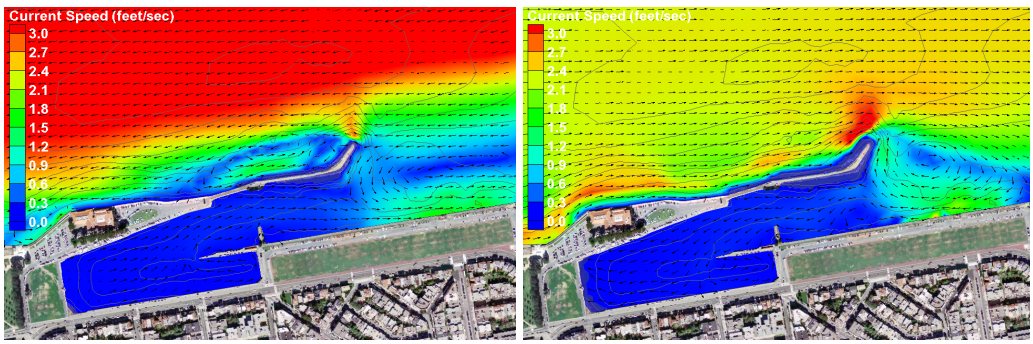


Figure 6. Typical peak ebb (left) and flood (right) tidal current patterns for existing conditions.

Figure 7 shows typical ebb (left) and flood (right) current patterns after the sheetpile wall construction, removal of the Scott Street mole, and shortening of the west mole. Current patterns shown in Figure 7 indicate that navigation conditions are likely to be similar to existing conditions, and no significant problems are anticipated. Water quality within the marina after construction was evaluated by calculation of the change in residence time using flushing of a conservative tracer. Although residence time after construction was slightly larger than for existing conditions, turnover was still considered to be good and other factors such as consistent west winds are known to enhance flushing. Therefore, no water quality issues were anticipated.

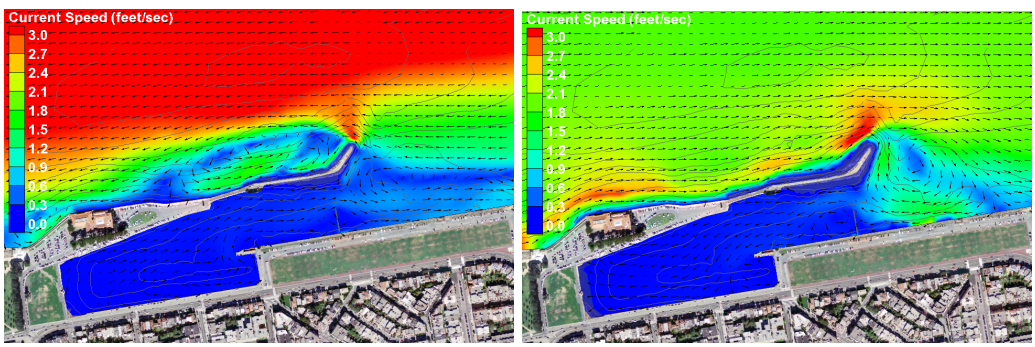


Figure 7. Typical peak ebb (left) and flood (right) tidal current patterns after construction.

SEDIMENTATION ANALYSIS

Sedimentation analysis was conducted to determine typical entrance channel infill rates and evaluate sediment management alternatives. Sedimentation rates were evaluated in areas adjacent to the entrance channel, solely based on measured sedimentation for periods during which dredging was not performed. Bathymetry data from 15 different hydrographic surveys performed within West Harbor between 1992 and the present were collected, processed, and analyzed. Figure 8 shows example hydrographic surveys from May 2002 and June 2005.

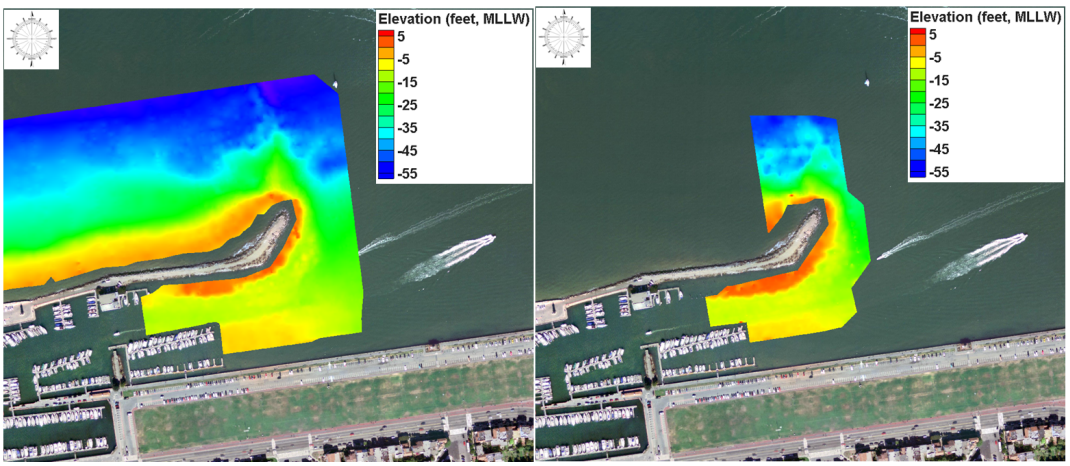


Figure 8. Bathymetry data from May 2002 (left) and June 2005 (right) as an example.

The total volume of sediment present within the denoted areas (EC1, EC2 and Channel Area) was computed for every available hydrographic survey from 1994 to present. Figure 9 shows the change in sediment volume in the denoted areas (all three areas combined) above elevation -20 ft (MLLW) between 1994 and 2009. In Figure 9, the solid line segments indicate periods of sedimentation where no dredging occurred, and dashed lines are periods where the volume of sediment was affected by dredging.

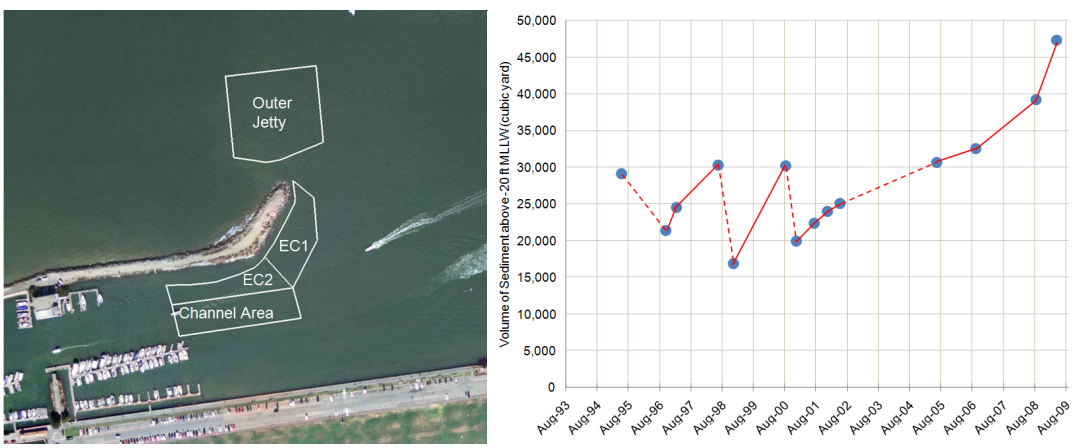


Figure 9. Locations of sedimentation calculation (left) and volume of sediment in San Francisco Marina entrance channel (EC1, EC2 and Channel Area) above -20 ft MLLW in the period 1995 to 2009 (right).

SEDIMENT MANAGEMENT ALTERNATIVES ANALYSIS

Two types of sedimentation control alternatives were considered: 1) control structures that would direct sedimentation to areas of little or lesser impact; and 2) sediment traps that would capture and allow dredging of sediment prior to entering the marina entrance channel. Upon completion of sedimentation analysis and development of a better understanding of sedimentation processes at the marina, installation of permanent, costly structural alternatives was dismissed, and only sediment trap alternatives were further considered.

Sediment trap alternatives consist of over-excavation of the bottom slope upstream (in terms of net transport) of the entrance channel to provide capacity for sediment settling, and maintaining (dredging) the trap prior to when it becomes filled. The size and location of the sediment trap were selected to: 1) minimize maintenance costs; and 2) ensure sufficient time before the entrance channel depths are significantly compromised to comply with environmental permit conditions such as dredge windows, sampling and testing, reporting, surveying, and to achieve economy of scale with fixed costs and to ensure availability of cost-effective disposal options.

In the past, sediment trap dredging was performed at the "Outer Jetty" site (see Figure 9), with relatively large dredging volumes. This area is located north of the proposed breakwater in relatively deep water. The Outer Jetty sediment trap location encounters sediment transport rates that are many times larger than the sedimentation rate in the entrance channel areas. Sedimentation analysis indicates that the 2005 Outer Jetty sediment trap dredging episode (approximately 25,000 cu yd) was somewhat effective in reducing the marina entrance channel sedimentation for a short period of time. However, this sediment trap was filled quickly by sediment from the large ambient sediment transport in the offshore locations, and sediment bypassed the trap in shallower areas; therefore, it appears to have been relatively inefficient from a total cost perspective. Due to significant dredging efforts required to maintain an effective Outer Jetty sediment trap, sediment traps in this location (north of the jetty) were not recommended.

The preferred sediment trap location was found to be south of the north jetty tip where sediment transport is already bound for the entrance channel or berthing areas. Sediment traps were evaluated that had at least 2 to 3 years of sedimentation capacity between maintenance dredging episodes. The preferred sediment trap alternative is shown in Figure 10. This figure shows the trap with April 2009 bathymetry (left) and bathymetry after trap dredging (right). The April 2009 condition represents a relatively large amount of accretion and the largest amount of sediment on record (1994 to present) in the entrance channel areas. Therefore, the trap boundary was designed to encompass the majority of observed sedimentation area in the April 2009 bathymetry.

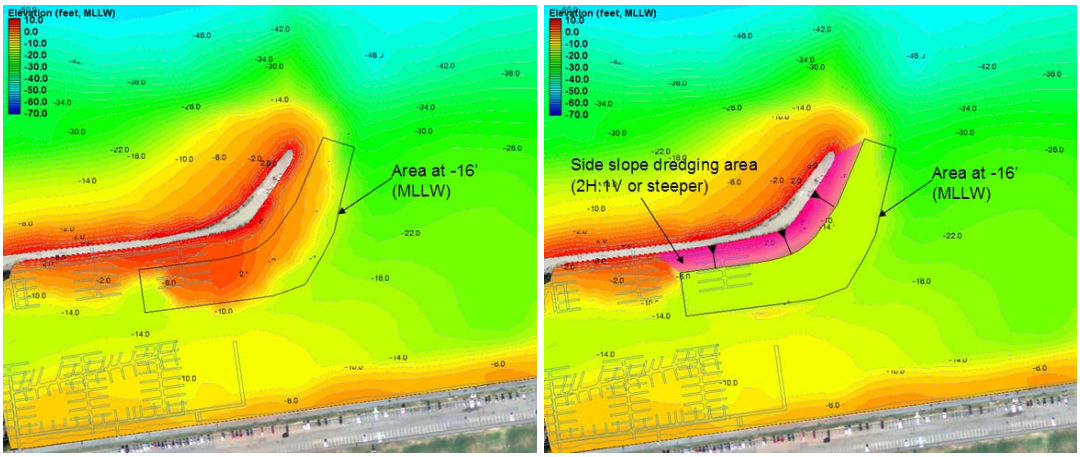


Figure 10. Location of proposed sediment trap with April 2009 bathymetry (left) and after trap dredging (right).

The trap capacity, i.e., the volume of sediment that can enter the trap area before the navigation channel would begin to experience significant sedimentation, is roughly 15,000 to 20,000 cu yd (i.e., approximately 2 to 3 years of capacity). The trap capacity depends on the required depths under the floats, which is likely to trigger maintenance dredging faster than sediment encroachment into the navigation channel. The present sediment trap design is expected to allow sufficient time to plan maintenance dredging activities and avoid channel sedimentation problems.

CONCLUSIONS

Coastal engineering analysis and numerical modeling were performed as part of the San Francisco Marina West Yacht Harbor Renovation project. The objectives of the analysis were to develop engineering solutions for improving wave conditions in the marina and mitigating the occurrence of entrance closures resulting from excessive sedimentation in the entrance channel.

Based on the results of the analysis, an effective breakwater concept and practical sediment management recommendations were developed to minimize cost and risk, while providing safe and reliable navigation conditions. The preferred breakwater alternative consists of a 185-ft sheetpile wall near the marina green and 300-ft concrete pontoon floating breakwater offshore of the entrance. The preferred alternative resulted in an effective, low-risk breakwater alternative with good long-term wave protection for the berthed vessels and infrastructure. A low-risk and cost-effective approach of maintaining a sediment trap inside the entrance channel was proposed to reduce further risk of entrance channel closure. Sedimentation processes are expected to be well understood under this approach, and no unforeseen conditions are likely to occur.

REFERENCES

Kivva, S., Kolomiets, P., Shepeleva, T. and Zheleznyak, M. 2004. "A Numerical Simulator for Depth-Averaged Surface Water Flow, Sediment Transport and Morphodynamics in Nearshore Zone, Version 2.0." User's Manual.

Permanent International Association of Navigation Congresses (PIANC). 2004. "Criteria for Movements of Moored Vessels in Harbours – A Practical Guide."

Zheleznyak, M., Demchenko, R. and Kolomiets, P. 2009. "Spectral Hyperbolic Wave Transformation Model, Version 1.0." User's Manual.

Floating Breakwater Modeling and Design for Oyster Point Marina

David Dykstra[1], Xiuying Xing[2], and Christopher Devick[3]

[1]Moffatt & Nichol, 3780 Kilroy Airport Way, Suite 600, Long Beach, CA 90806; PH (562) 426-9551; FAX (562) 424-7489; email: ddykstra@moffattnichol.com
[2]Moffatt & Nichol, 3780 Kilroy Airport Way, Suite 600, Long Beach, CA 90806; PH (562) 426-9551; FAX (562) 424-7489; email: xxing@moffattnichol.com
[3]Moffatt & Nichol, 2185 N. California Blvd., Suite 500, Walnut Creek, CA 94596; PH (925) 944-5411; FAX (925) 944-4732; email: cdevick@moffattnichol.com

ABSTRACT

Oyster Point Marina in San Francisco Bay, California has recently been modified to allow ferry service within the marina basin. The modifications included reconfiguring the entrance channel which resulted in increased wave activity within the marina basin and subsequent damage to vessels and docks. A numerical model study of wave penetration into the marina basin and potential mitigating measures was conducted and concluded that floating breakwaters within the marina basin could be used effectively to reduce the wave energy to acceptable levels.

One unique aspect of the floating breakwaters within the basin is that the wave reflection had to be minimized in order to maintain acceptable wave heights in the main marina fairway. Most applications of floating breakwaters to protect small craft harbors are not concerned with the reflected wave energy as it would normally propagate into open water and not typically interfere with navigation.

A large scale physical model study was undertaken to evaluate various floating breakwaters. The model study included monitoring the reflected wave conditions as well as the transmitted waves. Modifications to standard floating breakwaters were tested to evaluate the energy dissipation which would result in reduced wave reflection and the transmitted waves.

The results of the physical model study were used in a Boussinesq model of wave penetration into the marina basin simulating the measured wave transmission and reflection as porous boundaries at the multiple floating breakwater locations.

INTRODUCTION

Oyster Point Marina is a 589 berth commercial and recreational small boat harbor located on San Francisco Bay approximately ten miles south of San Francisco and 2 miles north of San Francisco International Airport (Figure 1). In 2008, the San Francisco District of the US Army Corps of Engineers (Corps) completed the design and constructed a modification to the existing breakwater system at the Oyster Point Marina. The modification allowed ferry vessels to enter the harbor to accommodate the San Francisco Bay Water Emergency Transportation Authority's Oyster Point Ferry Terminal. The design intended to maintain the wave climate in the harbor close to the pre-construction condition, and in any case compatible with the small boat harbor operation.

Since construction of the breakwater modification, a distinct change in wave energy transmitted into the harbor via the entrance channel has been noted. New wave patterns and an increase in wave energy have been observed during storm events involving southerly winds. A numerical model study of wave penetration into the marina basin to provide an explanation for the change that apparently occurred as a result of the modification (Moffatt & Nichol, 2009).

The results of this investigation suggested an in-basin floating breakwater plan (Figure 2) as likely to be the most cost effective and least environmentally intrusive design solution from amongst the various alternatives considered. Since there was relatively little quantitative information on the performance characteristics of the specific L-shaped floating breakwater configuration proposed, the numerical model of harbor wave conditions used in the study of alternatives (BOUSS2D) could not be fully calibrated for the floating breakwater.

A physical model study was conducted at the Canadian Hydraulic Center (CHC) of the National Research Council of Canada. The results of the physical model tests included the transmitted wave, reflected wave, and energy dissipation. These results were used to accurately characterize the performance of the floating breakwaters in a Boussinesq numerical wave model of the marina basin and entrance channel by applying variable porosity in model grid points in the vicinity of the proposed floating breakwaters.

FLOATING BREAKWATER PHYSICAL MODEL TESTING

The model tests were conducted in the CHC Coastal Wave Basin. The basin is 206 ft (63 m) long by 46 ft (14 m) wide by up to 4.5 ft (1.35 m) deep. The size of this basin allowed for a relatively large scale setup to minimize scale effects. A geometric scale of 1:8 was selected based on the available water depth and the constraints related to the available equipment and instrumentation. The scaling of other parameters such as velocity, force, and mass were based on Froude scaling relationships.

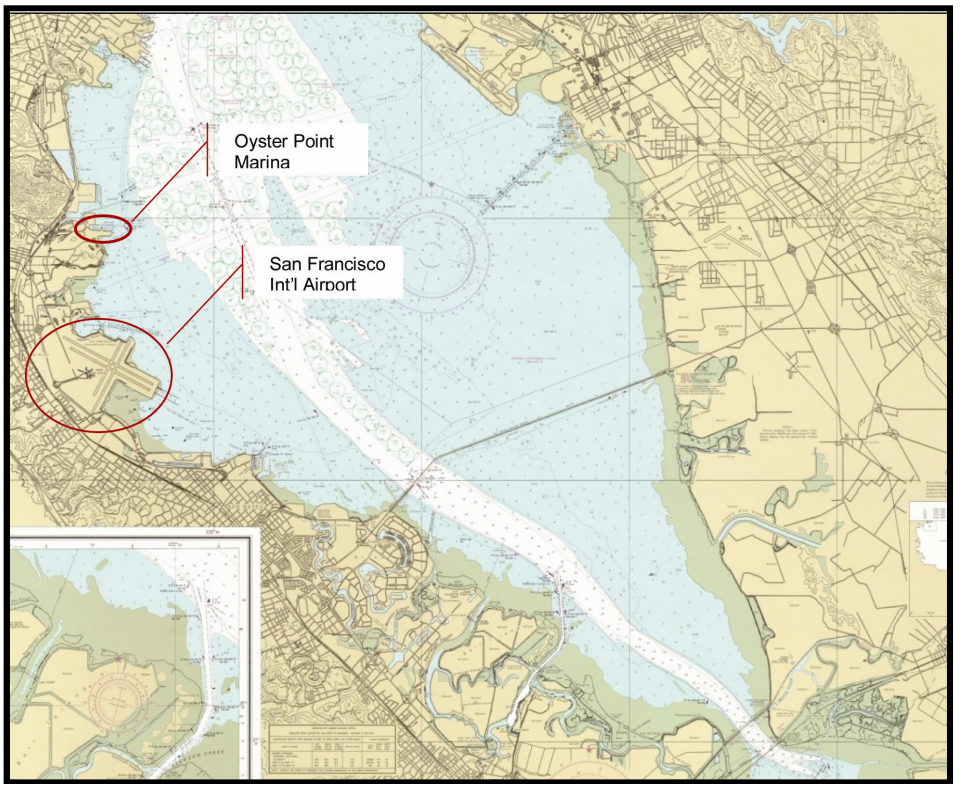


Figure 1. Location of Oyster Point Marina in San Francisco Bay. (Image source: NOAA Nautical Chart, 18651 San Francisco Bay, Southern Part).

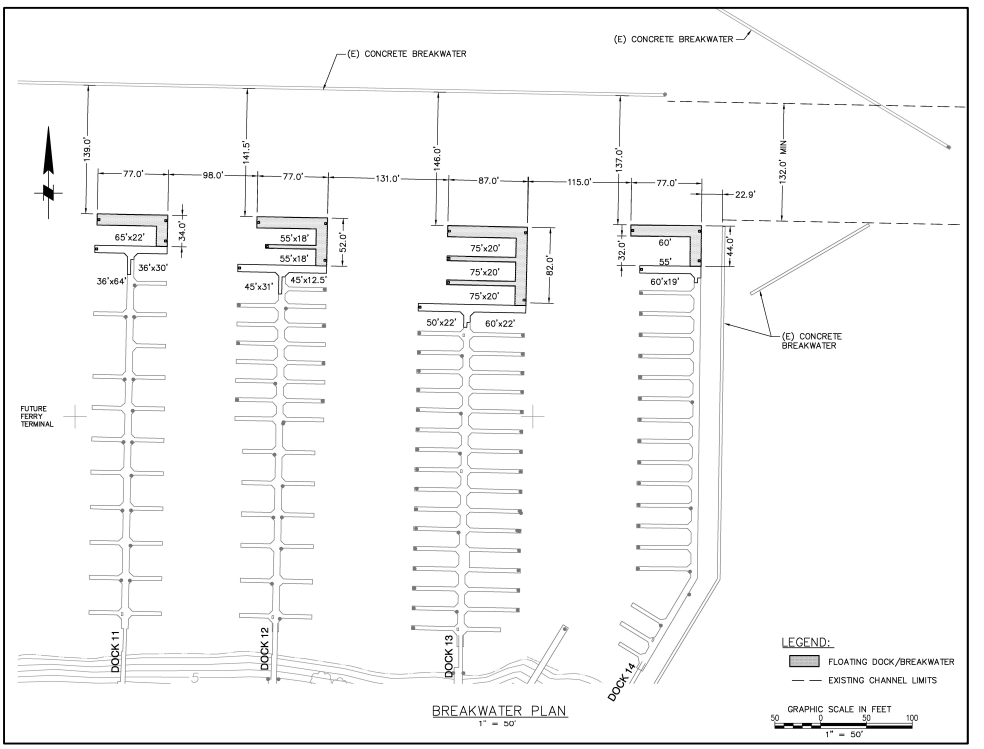


Figure 2. In-Basin Floating Breakwater Plan for Oyster Point Marina.

The physical model layout was designed and constructed to evaluate the performance of a single L-shaped floating breakwater unit in waves approaching from a single direction. The single wave direction was based on the preliminary Boussinesq wave modeling which showed very little variation in wave direction within the marina regardless of the incident wave in San Francisco Bay. The physical model layout is illustrated in Figure 3. The plan form of the floating breakwater consisted of two segments in an L-shape with a longer segment of 26.5 m prototype scale and a slightly shorter segment at 22.9 m and each segment being 3.7 m wide.

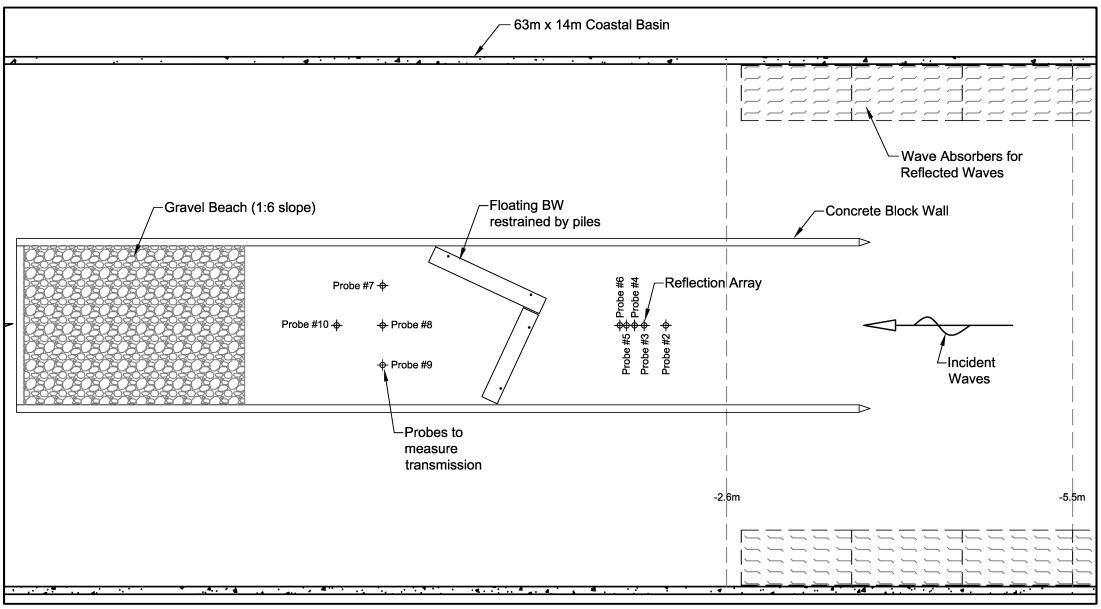


Figure 3. Physical Model Layout for Floating Breakwater Tests.

A temporary test channel with walls made of concrete blocks lined with a flexible plastic barrier was constructed within the wave basin. The test channel was only very slightly wider than the outer dimensions of the floating breakwater, so that very little wave energy could propagate around the floating breakwater thereby only allowing wave energy due to wave transmission through the breakwater in this area of the basin. A gently sloping (1:6) porous gravel spending beach with low wave reflection was installed at the end of the test channel opposite the wave machine. This beach effectively dissipated most of the incident wave energy. Additional wave absorbers were also installed along the basin side walls perpendicular to the wave machine in order to dampen any cross-waves that might arise around the entrance to the test channel.

Five different breakwater configurations were investigated in this study. Configuration A consisted of a rigid connection between both segments of the floating breakwater with a freeboard of approximately 0.3 m with a solid skirt extending 0.76 m below the bottom of the rectangular float for a total breakwater height of 1.98 m. Configuration B consisted of the same breakwater section, but with the segments detached to allow for independent motion of the two breakwater segments. Configuration C consisted of the detached breakwater segments and a solid

skirt, but with the freeboard increased to approximately 0.6 m in an effort to reduce observed overtopping. Configuration D consisted of the detached segments, 0.6 m freeboard, with slatted skirts along the upwave side of the segments instead of the solid skirt. The depth of the skirt below the rectangular float remained the same at 1.98 m. Configuration E is similar to configuration D with the addition of a 0.3 m high parapet at the top of the upwave edge of the breakwater segments to further reduce wave overtopping. The floating breakwater configurations are summarized in Table 1.

Table 1. Summary of Physical Model Breakwater Configurations.

Configuration	Segment Connection	Freeboard (ft)	Draft (ft)	Skirt Height (ft)	Skirt Type	Parapet
A	Rigid	1.0	5.5	2.5	Solid	No
B	Detached	1.0	5.5	2.5	Solid	No
C	Detached	2.0	4.5	2.5	Solid	No
D	Detached	2.0	4.5	2.5	Slatted	No
E	Detached	2.0	4.5	2.5	Slatted	Yes

Prior to conducting the model tests of the floating breakwater configurations, the model basin wave generator was calibrated to reproduce 22 different combinations of water levels, wave heights, and wave periods in the absence of the floating breakwater. The water levels for the wave generator calibration were based on various return interval tides. The water levels consisted of MLLW (0.00m), MSL (1.15m), MHHW (2.19m), and 5 year return period (2.81m). The wave heights and periods were derived from the preliminary numerical modeling results. All wave conditions consisted of irregular wave spectra with uniform wave direction over a one-hour prototype time period. The calibration conditions are summarized in Table 2.

Wave gauges were placed in the basin as illustrated in Figure 3. Wave gages 2 through 6 were placed along the centerline of the basin upwave of the floating breakwater to measure the reflected wave energy. These gauges are also capable of measuring the incident wave height and period, but as previously discussed, the incident wave characteristics were always taken to be the calibrated values as these were the most accurate. Wave gauges 7 through 10 were placed on the leeward side of the floating breakwater to measure the transmitted wave energy, two gages along the centerline and two towards sides of the wave channel. Only centerline wave gages 8 and 10 were used for further analysis due to the apparent influence of wave reflection along the basin walls. Along with the various breakwater alternatives, the water level, wave height, and wave periods were varied over a total of 67 separate breakwater tests. These tests included some repeat tests to confirm repeatability of tests results. The bulk of the testing was conducted for the higher freeboard with

decoupled breakwater segments since this configuration appeared to be the most effective during the testing program.

Table 2. Specified Water Level and Wave Conditions for the Physical Model Tests (Prototype Scale).

#	Name	Water Level (m MLLW))	Water Level Description	Calibrated Hmo (m)	Calibrated Tp (sec)
1	A1	0.00	MLLW	0.95	3.51
2	A2	0.00	MLLW	1.01	4.13
3	A3	0.00	MLLW	1.04	5.05
4	B1	1.15	MSL	0.68	2.80
5	B2	1.15	MSL	0.81	3.10
6	B3	1.15	MSL	0.83	3.50
7	B4	1.15	MSL	0.77	4.44
8	C1	2.19	MHHW	0.67	2.81
9	C2	2.19	MHHW	0.80	3.08
10	C3	2.19	MHHW	0.84	3.50
11	C4	2.19	MHHW	0.78	4.41
12	C5	2.19	MHHW	0.40	2.49
13	D1	2.81	5-year	0.80	3.17
14	D2	2.81	5-year	0.83	3.49
15	D3	2.81	5-year	0.76	4.39
16	D4	2.81	5-year	1.01	3.50
17	D5	2.81	5-year	1.01	3.98
18	D6	2.81	5-year	0.96	5.03
19	D7	2.81	5-year	1.33	3.54
20	D8	2.81	5-year	1.43	4.05
21	D9	2.81	5-year	1.45	5.09
22	D10	2.81	5-year	0.47	2.49

PHYSICAL MODEL TEST RESULTS

The wave transmission is computed as the ratio of the average of the two centerline gages behind the floating breakwater divided by the incident wave height as determined by the wave generator calibration tests. The results are plotted as a function of the wave period based on previous investigations which have related the wave transmission to the relative breakwater width which is the breakwater width divided by the incident wave length.

The results for the higher freeboard with shallower draft breakwater for varying water levels are illustrated in Figure 4. These results are for all skirt configurations as there

appeared to be little variation of the wave transmission with skirt configuration. The wave transmission is only slightly greater for the highest water level when compared to the other water levels; there is not a significant reduction in wave transmission with lower water levels until MLLW, where the wave transmission is substantially less than the other water levels, particularly at longer wave periods. This substantial reduction in transmission at the lowest water level suggests maximizing the breakwater draft to optimize the performance. However, the breakwater should remain off the seafloor for all tide levels to minimize potential for damage to the structure.

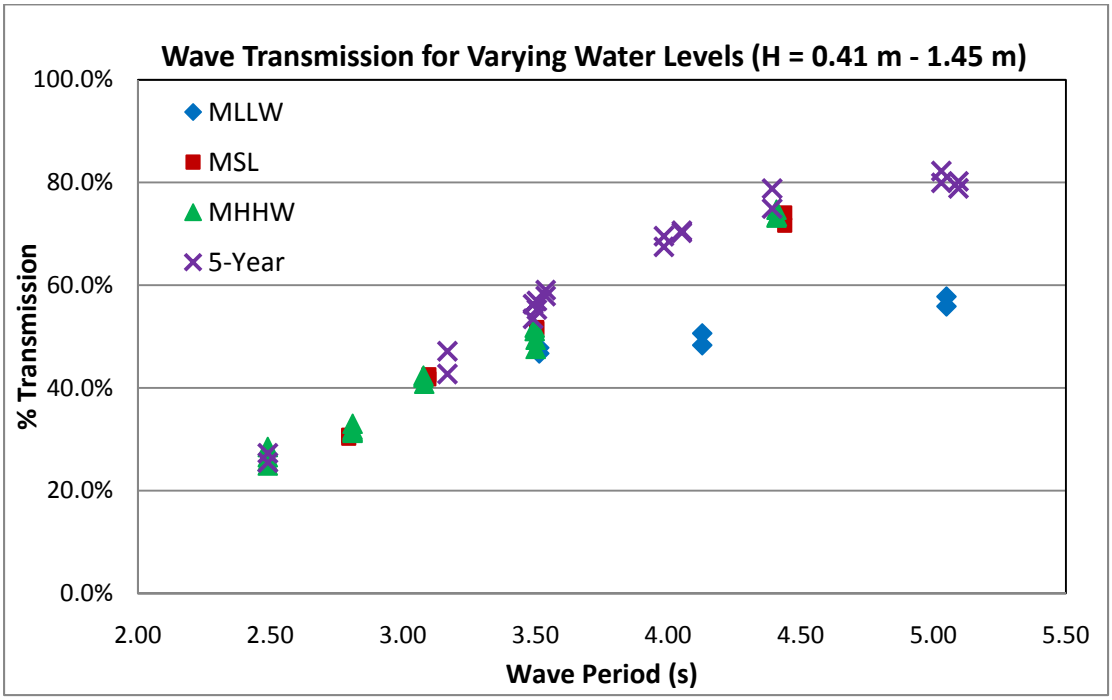


Figure 4. Wave Transmission vs Water Level for Higher Freeboard Floating Breakwater.

The wave reflection coefficient as a function of the water level is illustrated in Figure 5. The reflection coefficients range from approximately 8% to 34%. There appears to be little relationship between the wave period and the reflection coefficient. There also appears to be a great deal of variation within each wave period. The variability is likely due to the complex wave reflection resulting from the oblique angle of the floating breakwater segments. This oblique angle does not result in the reflected wave propagating directly down the channelized model area. Instead, the waves reflect towards the side of the model basin and then reflect off the model basin walls. This three dimensional effect could not be avoided given the layout of the model test program. Since the reflected wave energy is computed from the wave gage array which separates the incident wave energy from the reflected wave energy, there is also some loss of accuracy due to the fact that the wave gage spacing is not optimal for all wave periods. However, identical wave gage locations and reflection computations were used in both the physical model and the numerical model for the calibration.

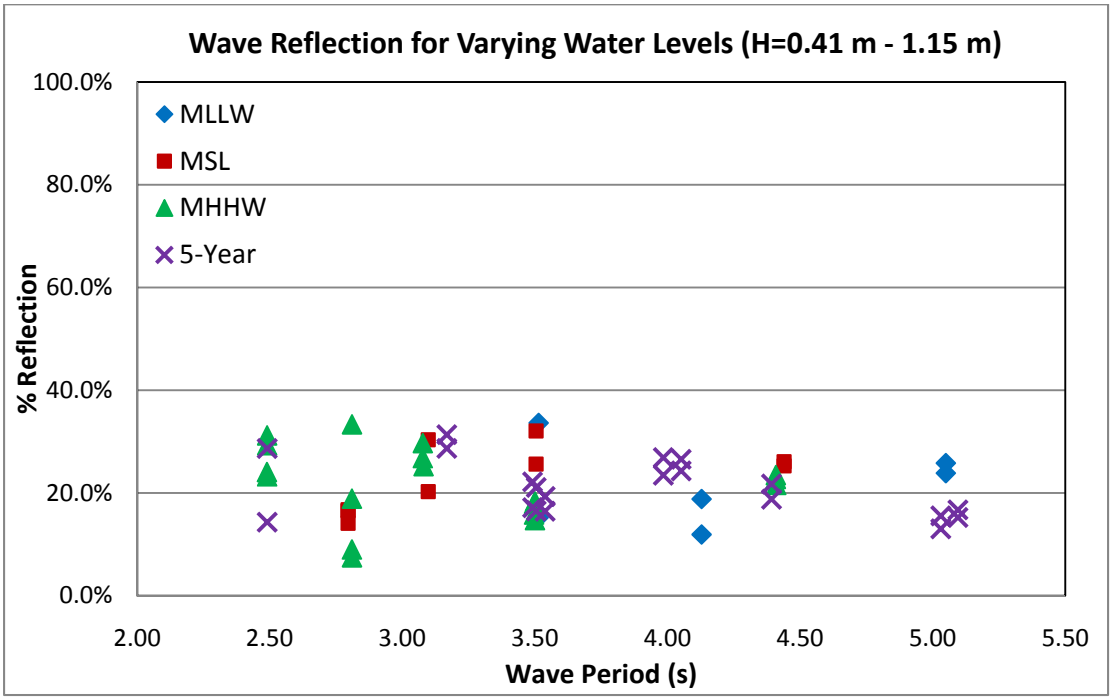


Figure 5. Wave Reflection for Varying Water Levels for Higher Freeboard Floating Breakwater.

A comparison between the wave transmission results for the higher freeboard breakwater with the performance curve of the Coastal Engineering Manual (CEM 2008) is illustrated in Figure 6 along with the physical model test results from Cox, et al (2007). The results of the current model tests are consistently less than suggested by the CEM. This is likely due to the fact that the wave transmission suggested in the CEM is based on physical model tests using regular waves as opposed to this model test program which used irregular wave spectra. This observation is consistent with the results of Cox, et al where both regular and irregular wave tests were performed. Although the regular wave transmission from Cox is slightly lower than the CEM performance curve, the results for irregular waves are significantly less than the regular wave results. Overall, the results of the irregular wave tests in this physical model study are similar to the work of Cox, et al.

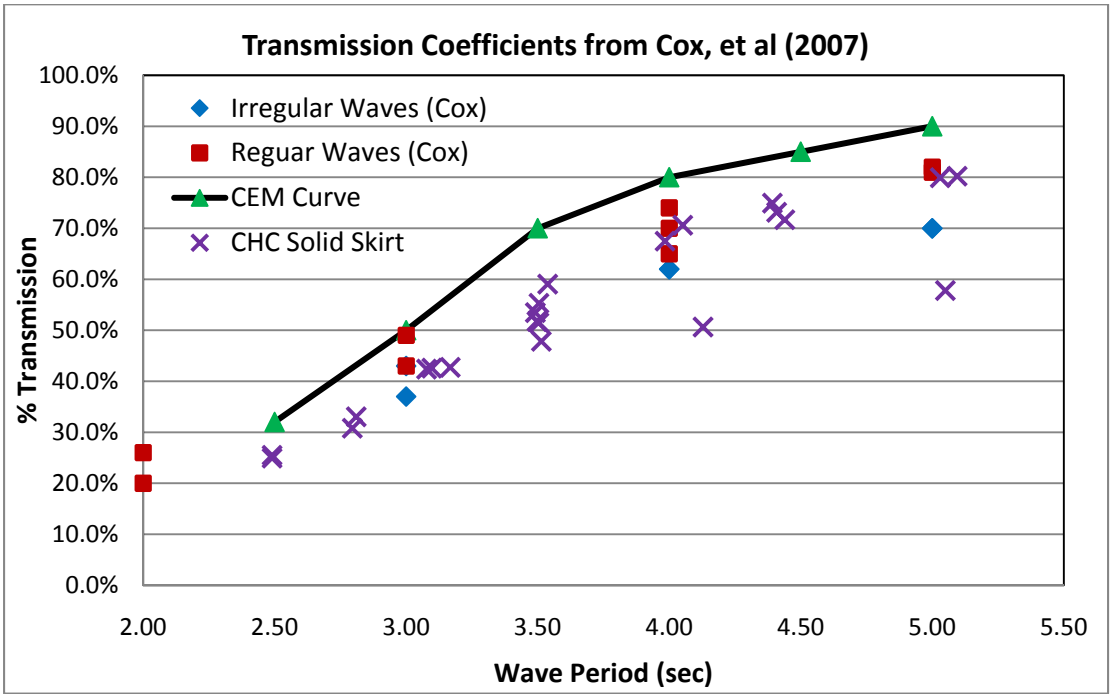


Figure 6. Wave Transmission Results for Regular and Irregular Waves from Cox, et al (2007)

NUMERICAL MODELING OF THE FLOATING BREAKWATER

The wave penetration into the marina is investigated using the BOUSS-2D model, which was developed by the U.S. Army Corps of Engineers. BOUSS-2D is valid from deep to shallow water and simulates wave transformation mechanisms including shoaling and refraction over variable bathymetry, reflection and diffraction around structures, energy dissipation due to wave breaking and bottom friction, cross-spectral energy transfer due to nonlinear wave-wave breaking and bottom friction, cross-spectral energy transfer due to nonlinear wave-wave interactions, breaking induced longshore and rip currents, wave-current interaction and wave interaction with porous structures.

BOUSS-2D does not directly simulate floating structures, but with proper application of damping and porosity layers it can reasonably represent the energy transmission, dissipation and reflection phenomena of floating structures, as long as the transmission and reflection is properly calibrated.

The transmission and reflection coefficients related to the floating breakwater are calibrated for different wave periods using a combination of porous layers and damping layers. The calibration modeling layout is illustrated in Figure 7 for the numerical model, which reproduces the conditions in the physical model. Gage locations that are used in transmission and reflection calculations are the same as in the physical model.

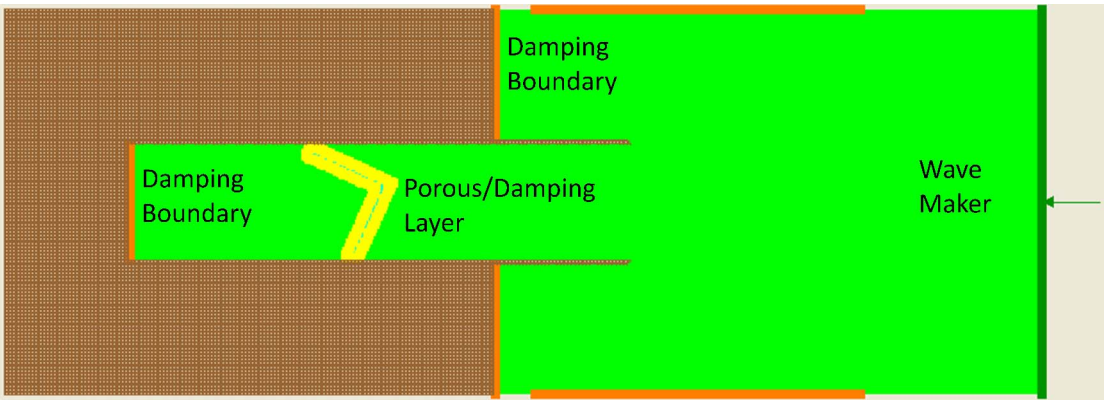


Figure 7. Layout of Numerical Model Calibration for Floating Breakwater Test.

The calibration results for the wave transmission and reflection coefficients are illustrated in Figure 8 and Figure 9 for various selected water levels. As shown in Figure 8, the transmission coefficient is well calibrated. As expected, longer waves transmit more energy through the floating breakwater. Longer period waves have higher transmission coefficients, and for same wave period, higher water levels (longer wave length) results in relatively greater transmission.

Unlike the transmission coefficients, the reflection coefficients from the physical model tests do not exhibit a trend with wave period but generally range from 15% to 30%. Because of the complex three dimensional wave transmission and dissipation, the physical model reflection coefficients appear to vary randomly, even for the same wave period and same water level in some cases. The calibrated numerical model reflection coefficients generally fall within in the same range, 15% to 30%, which makes the calibration reasonable.

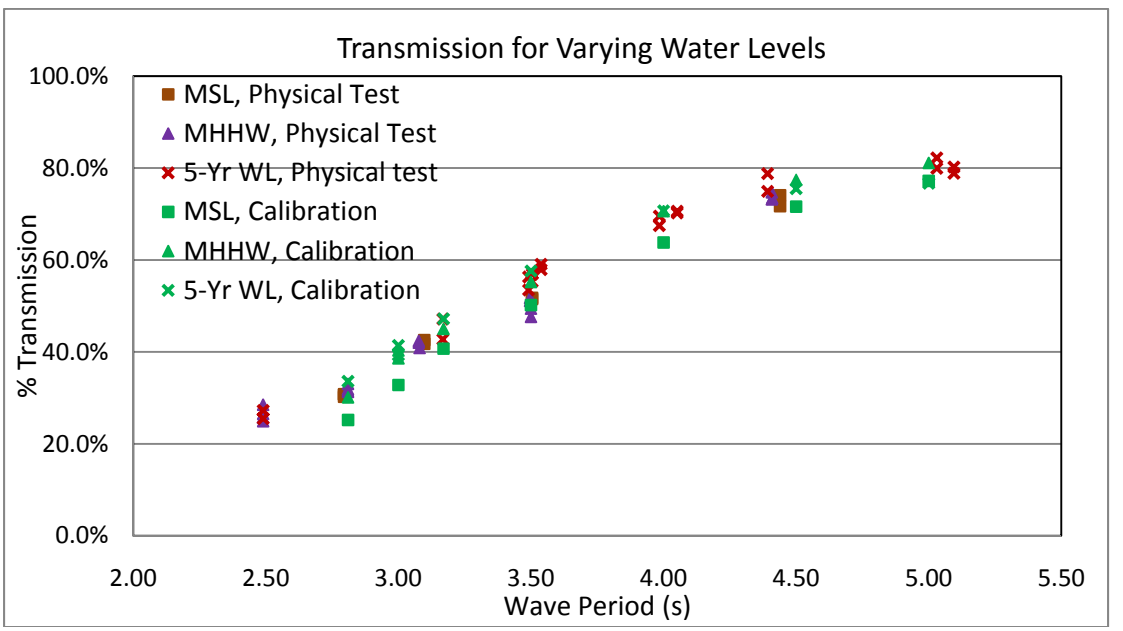


Figure 8. Transmission Coefficients Calibration for the Floating Breakwater.

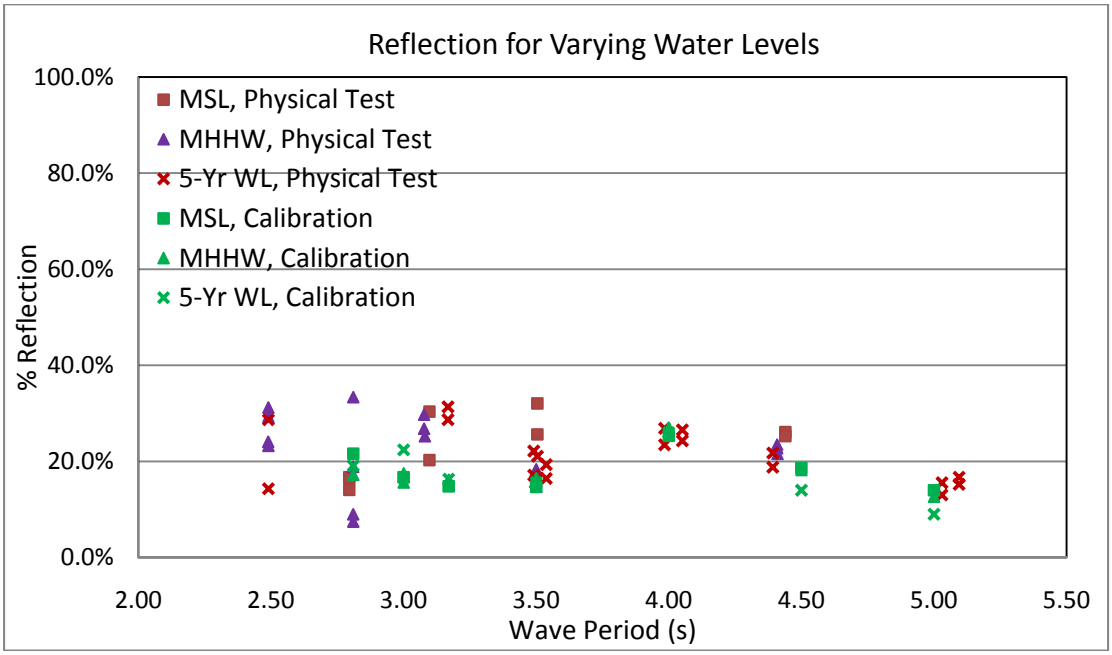


Figure 9. Reflection Coefficient Calibration for the Floating Breakwater.

The performance of the floating breakwater in the marina basin was modeled and evaluated by numerical simulation. For comparison both pre-construction and existing conditions were simulated. The outside breakwater differences between the existing case and the pre-construction case are located at the marina entrance. In the preconstruction case, the entrance is narrower, with two short sheet pile breakwater legs extending from the south jetty of the marina, one toward the west and the other one toward the northeast. In the existing case, the two short breakwater legs and a portion of the south jetty have been removed and the opening of the marina is wider to meet the ferry navigation requirements. The floating breakwaters provide protection for the berthing area through the use of floating breakwaters at the end of the finger slips. In order to maintain the main channel width within the harbor and provide room for breakwater installation, a number of existing slips will be removed.

Due to the performance requirements for both short term and long term wind events, the floating breakwater was evaluated with 2-yr, 50-yr and 100-yr waves for six wind directions (ENE, E, ESE, SE, SSE, S), and varying water levels. Due to space limitation, only 2-yr wave events generated by an ESE direction wind are presented here for illustration purposes. The simulated wave conditions generated by 2-year ESE wind for the in-basin floating breakwaters, existing and pre-construction cases are shown in Figure 10 through Figure 12.

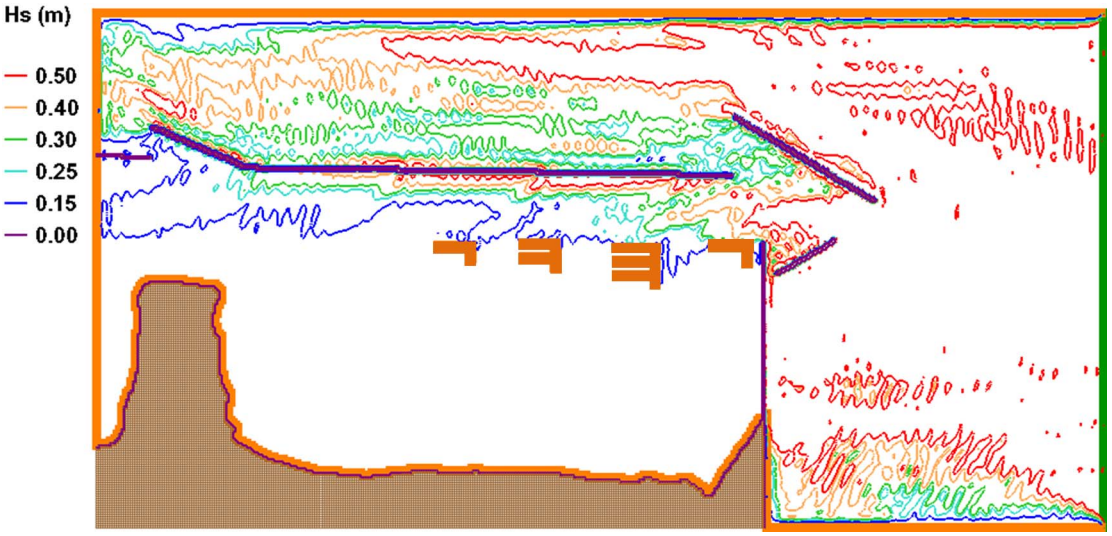


Figure 10. Simulated Wave Condition Generated by 2-Year ESE Wind for the In-Basin Floating Breakwater Case.

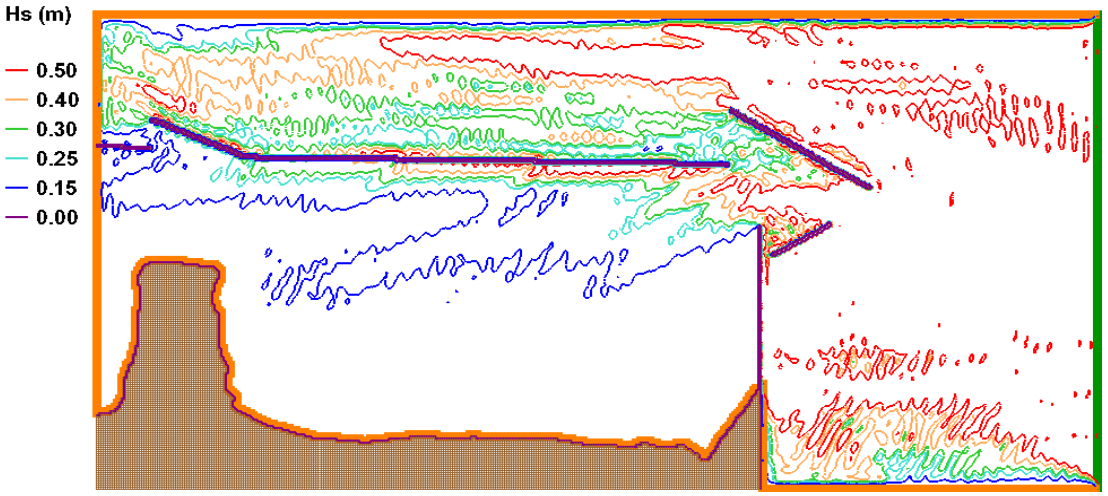


Figure 11. Simulated Wave Condition Generated by 2-Year ESE Wind for Existing Case.

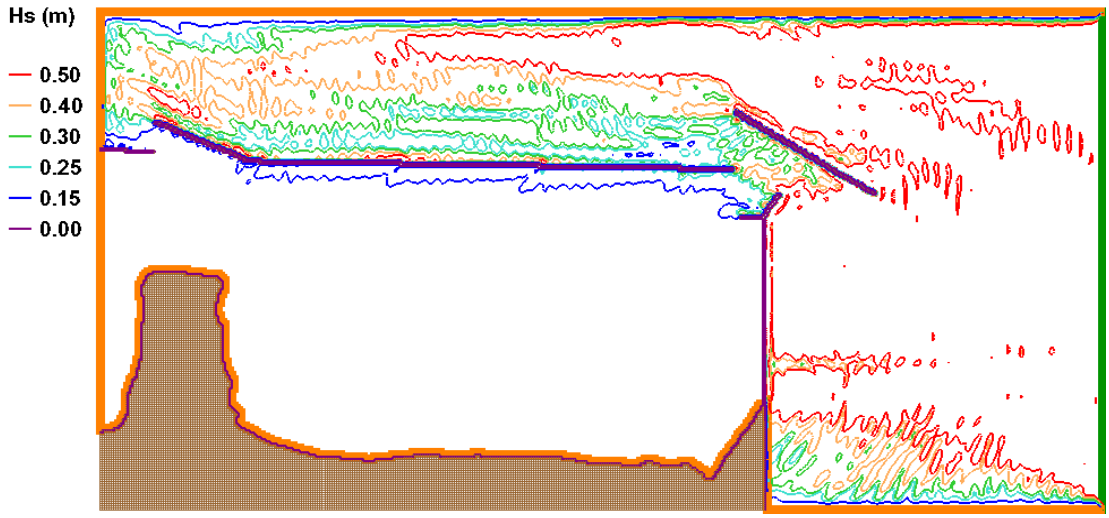


Figure 12. Simulated Wave Condition Generated by 2-Year ESE Wind for the Pre-Construction Case.

Generally the wave conditions are more severe under existing case compared with the other cases. For the existing case, the waves approach the marina at about 115 degrees and can propagate directly through the entrance.

With the in-basin floating breakwater case, waves in the berthing area are generally reduced compared with existing wave conditions. These 2-yr wind generated waves have periods between 3 sec and 4 sec. It's seen from Figure 8 that the transmission coefficient ranges from 40% to 70% for waves of 3 to 4 seconds. For the ESE wind, waves inside the berthing area (on the lee side of the floating breakwaters) are generally less than 0.15m (0.5ft) with the floating breakwaters in place.

CONCLUSIONS

While floating breakwaters have historically been shown to be somewhat limited in their effectiveness, there are applications where short period, low amplitude waves are of concern and the potential for a floating breakwater to provide adequate protection is practical. For Oyster Point Marina, the limited space for a breakwater and the requirement for limiting wave reflection within the marina basin, the floating breakwater alternative is attractive. The possibility of utilizing the breakwaters as components for slip fingers is also attractive for limiting loss of berthing space.

The physical model testing of the floating breakwater configuration for Oyster Point Marina provided evidence that the performance of the floating breakwaters was adequate to address the increased wave heights due to the recent entrance channel modifications. However, additional evidence that the wave climate within the marina basin was adequate for berthing small craft had to be demonstrated. This was accomplished with a Boussinesq numerical model of wave penetration into the marina basin that could simulate the performance of the floating breakwaters. The numerical model results suggest that adequate marina wave protection could be achieved.

REFERENCES

Moffatt & Nichol (2009). "Oyster Point Marina Coastal Reassessment and Plan for Improvement". Report prepared for the U.S. Army Corps of Engineers, San Francisco District.

Cox, R., I. Coghlan and K. Colette (2007). "Floating Breakwater Performance in Irregular Waves With Particular Emphasis On Wave Transmission and Reflection, Energy Dissipation, Motions and Restraining Forces". *Coastal Structures 2007*.

USACE. (2008). *Coastal Engineering Manual*. EM-1110-2-1100 Part II-7 Harbor Hydrodynamics. Pg.II-7-23 – II-7-25.

Final Monitoring Results for Kaumalapau Harbor Breakwater, Lanai, Hawaii

Jessica H. Podoski[1], Thomas D. Smith[2], and Lyndell Hales[3]

[1]US Army Corps of Engineers, Honolulu District, Civil Works Technical Branch, Bldg. T-223, Ft. Shafter, Hawaii 96858; PH (808) 438-1680; email: Jessica.H.Podoski@usace.army.mil

[2]US Army Corps of Engineers, Honolulu District, Civil Works Technical Branch, Bldg. T-223, Ft. Shafter, Hawaii 96858; PH (808) 438-0581; email: Thomas.D.Smith@usace.army.mil

[3]US Army Corps of Engineers, Engineering Research and Development Center, Coastal and Hydraulics Laboratory, 3909 Halls Ferry Road, Vicksburg, Mississippi 39180; PH (601) 634-3207; email: Lyndell.Z.Hales@usace.army.mil

Abstract

The Kaumalapau Harbor Breakwater Repair Project has been monitored since late 2006 as part of the US Army Corps of Engineers' (USACE) Monitoring of Completed Navigation Projects (MCNP) Program. Various aspects of the structure's post-construction performance have been investigated in order to gather information that will improve the knowledge available in planning the design, construction, and overall effectiveness of future coastal navigation structures. Goals of the monitoring program for this project include monitoring armor layer and cap settlement in the years following completion, evaluating the structure toe stability, gathering strength data for the Core-Loc armor unit used on the breakwater, and determining the effectiveness of the breakwater in reducing wave energy inside the harbor.

Data collected in support of the above goals included: deepwater and shallow water wave measurements, underwater and above water visual inspection, underwater multi-beam survey, above water Tripod-LiDAR (Light Detection and Ranging) surveys, and concrete strength measurements. In addition, wave transformation modeling has been completed in order to evaluate the wave climate at the harbor, and all data have been included into the USACE Enterprise Coastal Inventory GIS Database. A summary of the data and findings are presented, with a discussion of lessons learned as well as areas where further research is needed.

1. Introduction and General Description

Repair of the Kaumalapau Harbor breakwater on the island of Lanai, Hawaii was completed in July 2007 by the USACE Honolulu District and the State of Hawaii (Figure 1). The breakwater design includes the use of 31.75 metric-ton (m-ton) CORE-LOC™ (Core-Loc) concrete armor units, some of the largest armor units of this type to be constructed to date, with the toe of the structure located in 21.3 meters

(m) of water (Sea Engineering, Inc., and Group 70 International, 2008). The breakwater is approximately 97 m in overall length, with a "dogleg" shape in order to maximize the use of the existing rubblemound structure foundation. A cast-in-place monolithic concrete cap encloses the crest of the breakwater, and acts as a buttress for the armor units at the crest in case of wave overtopping. The purpose of the breakwater is to reduce wave energy at the barge pier within Kaumalapau Harbor, where all fuel and supplies for the Island of Lanai are offloaded on a regular basis.



Figure 1. Kaumalapau Harbor and repaired breakwater.

The USACE MCNP Program has been implemented to determine the extent to which the USACE's navigation projects are fulfilling their intended purposes and to assess how well they perform when subjected to design-level environmental conditions. The objective of the program is that these determinations, combined with concepts and understanding already available, will lead to the development of more effective and economical engineering solutions to coastal and hydraulic problems, strengthened and improved design criteria and methodology, improved construction practices and cost-effectiveness, and advanced operation and maintenance techniques. Additionally, the program aids in identifying where current technology is inadequate or where additional research is required.

The Kaumalapau Breakwater Repair Project was chosen for inclusion in the program due to its state-of-the-art design elements, its exposure to extreme wave conditions, and the unique construction methods that were required to build it. Goals of the program for this project include monitoring armor layer and cap settlement in the years following completion, evaluating the structure toe stability, gathering strength data for the Core-Loc armor unit used on the breakwater, and determining the effectiveness of the breakwater to reduce wave energy inside the harbor. Data collected in support of the above goals includes: deep and shallow water wave measurements, underwater and above water visual inspection, underwater multibeam survey, above water Tripod-Mounted Light Detection and Ranging (T-LiDAR)

surveys, and concrete strength measurements. In addition, wave transformation modeling has been completed in order to evaluate the wave climate at the harbor, and all data has been included into the USACE Enterprise Coastal Inventory GIS Database.

2. Wave Measurements and Wave Transformation Modeling

A Datawell Waverider buoy, located approximately 1 mile west of the harbor in 200 meters depth, was deployed in May 2007 as part of this program under the Scripps Coastal Data Information Program (CDIP). The buoy data, including both spectral and parameterized wave height, period and direction, is available on the web in real-time. The wave data recorded since deployment of the buoy includes waves from the northwest (315 True North (TN)) counter-clockwise through south-southeast (158 TN), with the majority of waves arriving from south-southwest (32%) and south (30%). The largest wave event recorded occurred in December 2007 with a significant wave height of 4.3 m, wave period of 8.3 seconds, and wave direction from 224 TN. This event was a "kona storm", an upper level subtropical cyclone that forms near the islands and causes high winds and waves to approach from the southeast through southwest. In this case, waves approached from the southwest which allowed for direct propagation to the harbor, located on the southwest coast of the island. In addition, the University of Hawaii's Department of Oceanography deployed a pressure sensor wave gage in the lee of the breakwater adjacent to the barge pier for one year immediately following construction, between July 2007 and June 2008. This data was available after recovery of the instrument and was used to evaluate post-repair wave conditions at the barge pier, as well as to validate the wave modeling described in the following.

Wave modeling completed as part of the program includes transformation of deep water waves to the CDIP buoy and locations directly adjacent to the harbor using Simulating Waves Nearshore (SWAN) (Delft University of Technology, 2010) and Refraction/Diffraction (REF/DIF) (Kirby, 1994), quantification of extreme events that might damage the breakwater using long-term Wave Information Study (WIS) wave hindcast data, and development of a lookup table for extreme and common events that correlates conditions at the CDIP buoy to 8 locations inside and outside the harbor in a "lookup table". The lookup table results were validated and improved with wave data collected inside the harbor with a pressure sensor, as well as data collected with a roving wave buoy deployed at various locations inside the harbor over the course of a single day.

In addition, a computer program was developed to automate the lookup table, and allow conversion of long-term buoy wave data into estimated wave parameters at several selected locations inside and outside the harbor (Figure 2). The program, known as KPWAVE (Sea Engineering, Inc., and Group 70 International, 2009), uses predictive algorithms to estimate the wave transmission coefficient in each output location based on wave direction and period. A three-dimensional (wave period, wave direction, and wave transmission coefficient) predictive "surface" developed for each output location allows for interpolation and some extrapolation of the discrete

wave data collected, enabling a wider database of wave transformation information to be used to estimate long-term wave climate within the harbor.

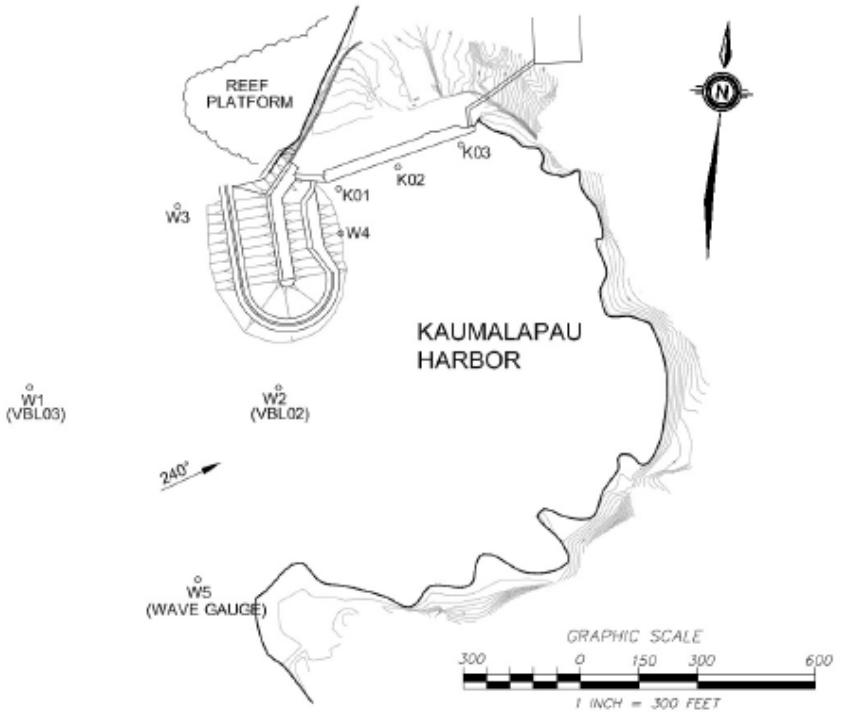


Figure 2. KPWAVE Output Data Locations (W2, W3, W4, W5, K01, K02, K03)

This program was used to develop a 3.5 year time series of wave parameters at the selected harbor output locations for May 2007 through December 2010. Comparison of KPWAVE output wave height at the location coincident with the pressure gage with the measured data from the gage indicates that the accuracy of the program in predicting wave height is closely correlated to deep water wave direction. During summer months, when waves are typically from southwest through south, KPWAVE compares well with measured data. During winter months, when wave direction is more variable and from south through northwest, the program tends to overpredict the actual wave height in the lee of the breakwater, sometimes drastically so. Figure 3 shows a comparative time series plot of predicted vs. measured wave height plotted on the primary y-axis, with wave direction at the deep water CDIP buoy plotted on the secondary y-axis. This comparison suggests that although the program and its predictive algorithms need further refinement for waves from the west and northwest (predicted values are significantly greater than measured in December 2007), it is generally a reasonable estimate of conditions within the harbor as correlated to the offshore buoy.

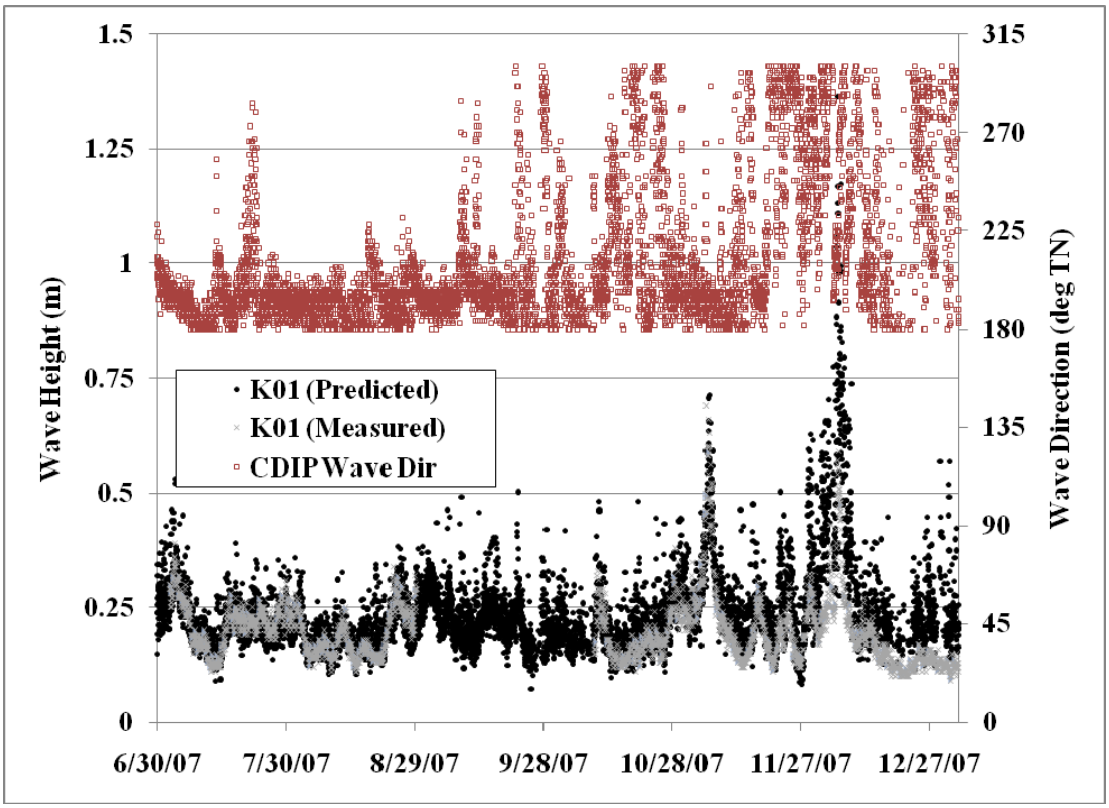


Figure 3. Measured vs. Predicted wave height at Station K01 (primary y-axis) and Deep Water Buoy Wave Direction (secondary y-axis)

Analysis of the entire 3.5 year time series output at all output locations within the harbor indicates that the largest response in terms of wave height (and thereby wave energy) is experienced during long-period waves from the south and short period waves generated by Kona storms and coming from southwest. However, none of the recorded waves have approached the design wave height of the project (10.7 m), which would likely only occur during a hurricane passing close to the island.

Finally, although pre-project wave data within the harbor does exist (approximately one year of wave height and period data were collected near the barge pier in January – December 1994), it is difficult to make a direct pre- vs. post-project comparison between this and the more recent wave data inside the harbor to determine whether the repaired breakwater is significantly reducing wave energy at the barge pier. Because of the relatively short duration of each dataset, the lack of offshore buoy data during the pre-project data collection, and year to year variability of the wave climate, an attempt to draw meaningful conclusions from even a seasonally adjusted comparison of wave height data and/or period would be conjecture at best. However, informal discussions with regular harbor users have revealed that the transit through the harbor entrance and ease of mooring at the barge pier following the breakwater repair is much improved, especially during moderate northwest swells. In addition, the users have noted that the availabilty of real-time wave data from the offshore CDIP buoy has significantly aided in the determination of whether the vessels

(particularly the fuel barge owned by Lanai Oil Company, Inc. which travels bi-monthly from Maui to Kaumalapau Harbor for delivery) will be able to safely enter and tie up within the harbor, and therefore has reduced costs and delays due to inter-island transits that would previously be terminated either in progress or upon arrival to Lanai.

3. Structure Inspections

Periodic above-water inspections of the breakwater have documented the stability of armor units, the armor unit/concrete cap interface, and qualitative performance of the concrete cap through photographs, hand measurements, and GPS recordings. The baseline above water inspection conducted in November 2007 identified several apparent voids in the armor layer and significant quantities of undersized underlayer stone visible through these voids. These issues were documented for future investigation under the MCNP program, but were not considered deficiencies during administration of the construction contract.

An underwater inspection was also conducted in November 2007 with a Remotely Operated Vehicle (ROV) to document with video the conditions of the below water armor units and underlayer, specifically at the structure toe. Inspection of the underwater portion of the breakwater identified areas of the oceanside toe trench and harborside toe berm where large variations in stone size and berm slope may exist. Orientation and entrenchment of toe armor units appeared mostly uniform and satisfactory. Some variation in spacing between toe armor units was noted. Interlocking and density of armor units along the sideslope of the structure appeared satisfactory; however, comprehensive visual coverage of the entire sideslope was not possible with the ROV.

A follow up above-water inspection was completed in August 2009. The inspection noted that overall the breakwater condition appeared satisfactory, with some areas of concern due to loose spacing of armor units, slight settling/movement of units near the concrete cap evident by increasing gaps between the armor units and cap interface, as well as minor wear and tear of armor unit edges. At the time of the inspection, the concrete cap appeared in satisfactory condition with no cracking or spalling evident; however, as noted in the 2007 inspection some stone smaller than the underlayer specified size were visible in spaces between crest armor units. None of the visual inspections to date have noted broken or significantly damaged armor units, nor has there been any documentation of dislodged underlayer stone or any other evidence to suggest concern with the performance of the structure since its construction.

4. Multibeam Survey and T-LiDAR Surveys

In 2008, a high-resolution multibeam underwater survey was conducted to provide a baseline for measurement and monitoring of any future changes to the breakwater due to settling or other movement of the Core-Loc concrete armor units (Sea Engineering, Inc., 2009). Point cloud images from the survey clearly show the individual armor units, including the two bottom rows of Core-Loc units that comprise the trenched toe

of the breakwater. Estimated vertical accuracy of the survey (calculated using a root mean square summation of both bias errors and random errors) is +/- 8.5 centimeters (cm). A follow up underwater survey was not possible as part of the current MCNP program; however, if a repeat survey is completed by the Honolulu District or the program at a later time with a similar spatial density and level of accuracy, it is reasonable to assume that significant changes in the position or orientation of the armor units may be detectable upon detailed comparison of the surveys. Multibeam backscatter intensity was also collected as part of the 2008 survey and was analyzed for identification of bottom sediment types in the project area, which range from coarse sand and gravel to fine and/or silty sand.

As noted, one of the primary goals of the monitoring program at this project was to examine and measure the above water armor layer and cap settlement in the first years following construction. In order to accomplish this goal, it was desired that a method that could quantify the overall structure and armor layer movement as a function of both time and spatial location be used. In addition, it was hoped that this monitoring method would aid in determining how the overall settlement of the structure affected both the stability of the armor layer as a whole, as well as the concrete cap. Finally, the method used to monitor the above water structure needed to be able to identify any breakage of concrete armor units and possibly determine whether this breakage was due to armor layer movement, or some other cause. Based on these criteria, high-resolution and extremely precise T-LiDAR data surveys were conducted in June 2007 (just prior to construction completion), July 2008 (1 year post-construction), and 2010 (3 years post-construction) on the above water portion of the breakwater, including the armor units and cap. Table 1 shows the number of tripod setup locations, the total number of T-LiDAR scans, and the total number of data points collected for each survey. The estimated single point positional accuracy for this technology is +/- 4mm, with point spacing typically in the centimeter to sub-centimeter range. The technology requires line-of-sight visibility of the intended target, and the target distance can range from 3 to 800 m, with some variation in positional accuracy with this distance.

Table 1. T-LiDAR Survey Information.

Survey Date	# of setup locations	# of scans	Data Points
June 2007	7	115	66 million
July 2008	17	312	128 million
August 2010	26	151	86 million

One of the challenges of land-based data collection on an ocean-surrounded structure was to ensure that sufficient data coverage on the ocean side of the breakwater was collected such that movement of individual armor units in this area could be measured. A two step approach was utilized to solve this problem. First, the T-LiDAR instrument was mounted 4.25 m above the breakwater cap with an elevated tripod to obtain an aerial view of the structure for several scans during each survey.

Second, the instrument was set up at low tide on rock outcrops on the side of the harbor opposite from the breakwater. Multiple elevated tripod setup locations on the ocean side of the breakwater cap timed to coincide with low tide allowed the laser scanner to look down on Core-Loc units close to the waterline. This technique provided data for approximately 70% of the visible Core-Loc units on the ocean side of the breakwater. Data collected from the small rock outcrops (reached by boat) on the southern side of the harbor and from the dock provided close to 100% coverage of the breakwater head and harbor side of the breakwater (Podoski et al., 2009).

Comparison of these ultra-dense georeferenced positional data (in point cloud form) has enabled the detection of armor unit movement (measured as maximum observed displacement at any point on an individual unit) as small as 5 centimeters, and in excess of one meter, as shown by the comparison of 2007 and 2007 point cloud images in Figure 4. The comprehensive coverage area and high positional accuracy of these data sets results in the ability to visualize and compare movement of almost every armor unit visible above the waterline as well as the concrete cap, allowing for an overall analysis of the breakwater's above water stability in the three years following construction. This analysis has revealed several interesting characteristics of the movement that has occurred during this time.

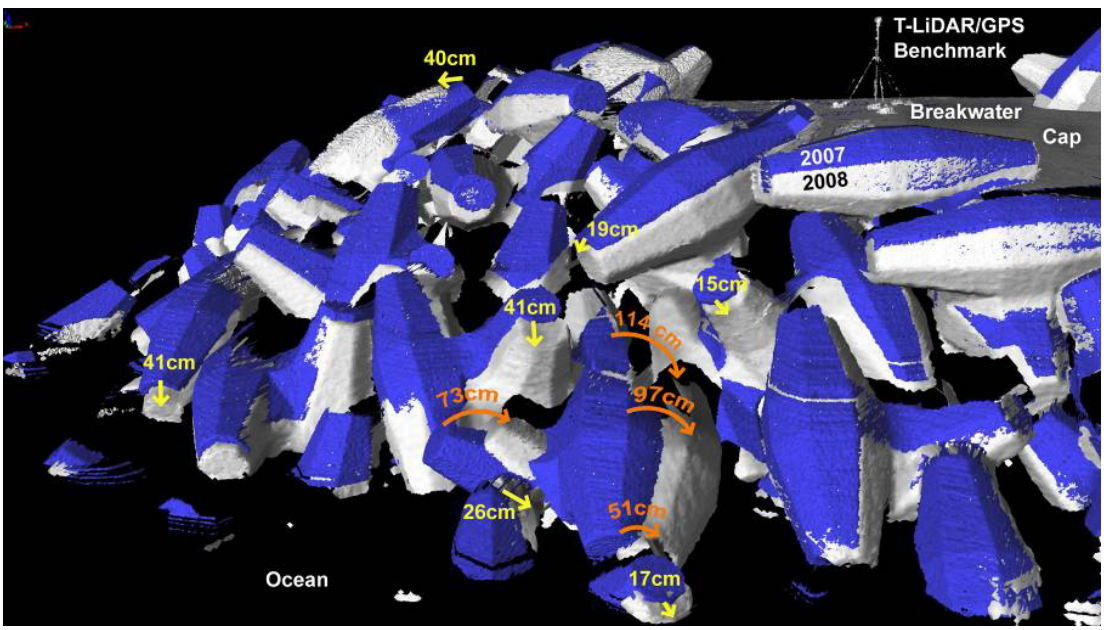


Figure 4. Point cloud data showing measured armor unit displacement between 2007 data (dark) and 2008 data (light) on the ocean side of the breakwater head. The arrow-arcs show rotational displacement and straight line arrows show translational displacement.

First, the visible movement of individual armor units has been both rotational and translational, but has been primarily toward the structure (rather than being pulled away or "off" the breakwater) and/or lower in elevation (also shown in Figure 4).

This appears to indicate that the units are indeed settling and "nesting" into a tighter matrix, rather than being loosened or pulled apart. Secondly, the movement has typically been observed to occur in groups of several adjacent armor units, illustrating the interdependence of each armor unit on those surrounding it and in direct contact with it, whether above, below, or alongside.

Next, and possibly the most significant result from this data collection, is the relatively dramatic variation in both the quantity and magnitude of armor unit movement when comparing the first year following construction (June 2007 – July 2008) to the two following years (July 2008 – August 2010). Side by side evaluation of color-coded change detection maps for these two time periods clearly shows that the majority of significant armor unit movement (defined here as movement greater than 10 cm in an individual unit) occurred within the first year post-construction, with comparatively much less discernable change in armor unit position occurring between the second and third T-LiDAR surveys in 2008 and 2010, respectively. This result is in agreement with previously undocumented suppositions that the majority of armor layer settling and nesting occurs within approximately the first year after placement.

In addition, the change measurements over the various time segments (as well as for the entire monitoring period) have shown that the largest movements of individual armor units, on the order of 20 cm to over 1 m, are in units located in two locations: the ocean side head and ocean side "dogleg" of the structure (Figure 5, Locations A and B). This concentration of armor unit displacement may be explained by one or more of the following factors:

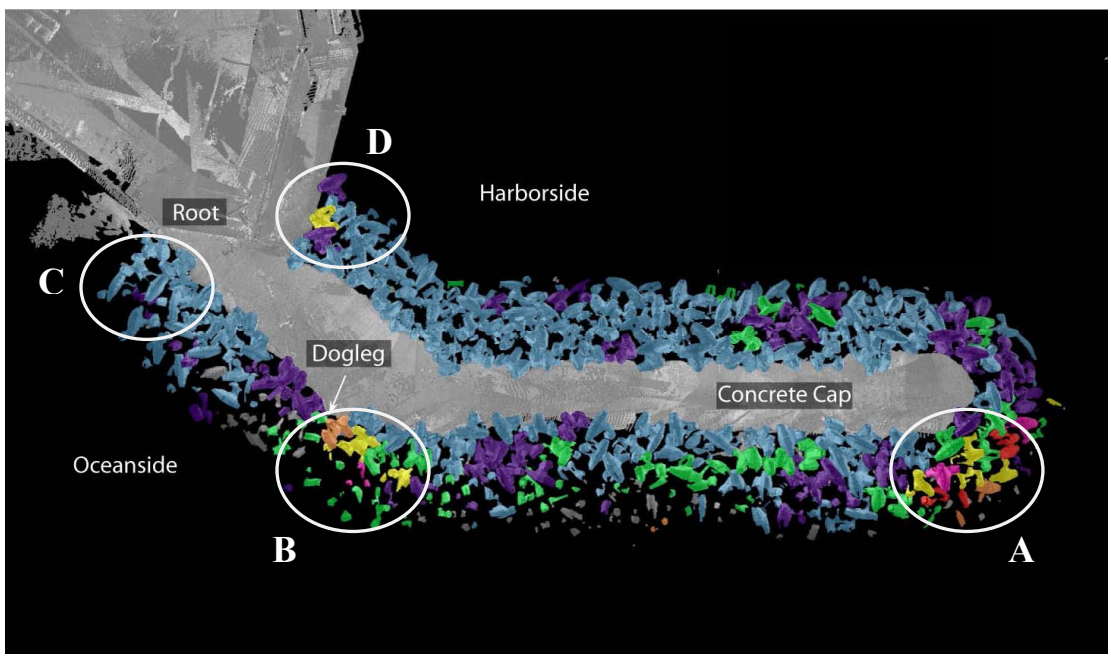


Figure 5. Plan view of T-LiDAR Point Cloud (A. Ocean side Head, B. Ocean side Dogleg, C. Ocean side Root, D. Harbor side Root)

1) The constructed packing density of armor units is likely lower in these areas in comparison to other areas on the breakwater, due to the change in structure orientation and thereby armor layer shape in these areas (i.e. – armor units become more spread out during construction when being placed around a bend or curve).

2) Interlocking and contact of adjacent armor units at these locations is possibly less optimal than that in other locations, due to the above mentioned increases in the breakwater curvature.

3) Wave impact and wave surge forces are greatest along the ocean side of the breakwater due to its increased exposure to incoming waves, which in combination with either or both of the above factors, could initiate movement of armor units.

4) The lack of significant armor unit displacement seen on the harbor side may be a result of the fact that the structure has not been overtopped by any major wave events.

Other observations that have been made through analysis and comparison of the T-LiDAR data sets have provided information on specific areas that were of concern during the design phase and also the construction phase. There has been minimal (less than 10 cm) displacement of armor units at the ocean side root of the structure (Figure 5, Location C). This was an area of concern during the design phase of the project due to a large submerged rock platform that exists adjacent to this part of the structure. Physical model tests showed that there could be armor unit stability issues due to the surge action caused by this feature, so the design of the structure incorporated the use of tremie-placed concrete to secure toe armor units along the structure root.

The harbor side of the structure at the root, adjacent to the barge pier (Figure 5, Location D), became an area of concern during construction when a modification was made by using a partial armor unit (breakage occurred during placement at the head, so the unit was removed) to abut the existing bulkhead wall, due to the fact that a complete armor unit would not fit into this area. The displacement measured in this unit between the 2007 and 2008 surveys was between 21 and 30 cm, and in two adjacent armor units, displacement was measured between 6 and 10 cm. However, the displacement measured between the 2008 and 2010 surveys shows that the partial armor unit has not experienced additional movement, and only one of the adjacent units experienced detectible movement, less than 10 cm.

Finally, the analysis of the T-LiDAR survey data has shown that there has been no breakage of any above water armor unit to date, which indicates that the scale of armor layer settlement has not been significant enough to cause significant stress on the individual armor units. The data analysis also shows that there has not been a detectable settling of the elevation of the concrete structure cap since its construction. This suggests that the concrete cap has remained intact and is functioning correctly despite the armor layer settlement and movement that has been observed. All of these observations, which answer key questions that were posed at the outset of the monitoring plan, would have been very difficult or impossible to obtain by solely

visible inspection or even traditional survey techniques. This comprehensive and precise data set has enabled the thorough evaluation of the settling and movement of the above water components of the breakwater both spatially and temporally, and has reinforced the qualitative evaluation that the structure is performing as anticipated in the years immediately following construction.

5. Concrete Strength Measurements

Another primary objective of the monitoring program was to gather strength data on the relatively new Core-Loc concrete armor unit. Limited knowledge exists on Core-Loc material strength distribution over the unit, material strength increases with aging, and the relationship between Core-Loc strength, movement, and breakage. The monitoring plan intended for examination of individual armor unit strength to potentially lead to improved concrete mixture designs that provide more robust armor units capable of tolerating an expected amount of movement during settlement.

In an effort to accomplish this goal, non-destructive and destructive testing of one Core-Loc concrete armor unit procured through MCNP funding from the normal production run of armor units being cast for the Kaumalapau Harbor breakwater was performed during the casting process, in September 2006. The objective of the testing was to gather non-destructive material property data on the armor unit, and to determine the tensile load needed to break one of the legs of the unit from the rest of the body. It was also anticipated that the testing would provide further information on the relationship between the compressive and tensile flexural strength of the concrete (as determined by standardized testing practices and dictated in the contract specifications). This testing was completed by the USACE Engineering Research and Development Center (ERDC) Geotechnical and Structures Laboratory, and Bevilacqua Research Corporation (O'Neil, 2008).

Non-destructive testing carried out included pulse-velocity measurements, which are a record of the length of time required for a sound wave to travel through the concrete at various chosen locations where a separation distance has been pre-measured. This speed is an indicator of the quality and material properties of the concrete, and can be correlated to concrete strength through accompanying compressive strength tests on cores taken from the same armor unit. Pulse velocity data can also be used to show material variations such as paste density and aggregate distribution within a given concrete specimen. Due to the complex geometry of the Core-Loc unit, efforts to estimate the separation distances proved unsatisfactory. As an alternative method, pulse-velocities from core samples taken after breaking of the unit (described in the following paragraphs) were used to verify concrete condition and statistical variation. The pulse-velocity measurements collected from core samples were within acceptable ranges according to estimation guidelines and indicated that the material properties were consistent throughout the specimens. Visual observation of cut cross sections from the collected cores also confirmed consistency from the top to bottom in terms of aggregate distribution.

Destructive testing of the armor unit was conducted by static loading of the armor unit until failure, and by laboratory testing of core samples taken from the unit following breakage. The failure of the armor unit was completed at the concrete casting yard where it was formed. The loading mechanism consisted of a ganged matrix of six 50-kip hydraulic rams placed between two legs of the unit, each with a 100-kip load cell attached to its piston arm for monitoring the load of each ram and the overall load of the system (Figure 6). A total of eight strain rosettes were bonded to the armor unit at various locations where compressive and tensile loads were expected to be highest. The load was increased uniformly until the Core-Loc broke just above the saddle in the upper half of the leg (a tensile surface), at an applied load of 418 kilonewtons (kN). This was a lower failure load than expected, based on the contract specified tensile stress of 4.83 megapascals (MPa), and the theoretical failure plane geometry. In addition, observation of the failure surface of the Core-Loc revealed that a large percentage of the aggregate was pulled out of the concrete rather than fracturing, indicating a poor bond between the aggregate and cement paste. This condition can be caused by a high water to cement ratio or by silty aggregate; however no indication of either of these problems was documented during the concrete batching by either the concrete supplier or the government construction officers monitoring the adherence to contract specifications.



Figure 6. Photo of Static Loading of Core-Loc Unit

Results of compressive and tensile-split testing of the core samples from the armor unit done in the ERDC laboratory indicated that all samples exceeded the contract requirements for strength (31.03 MPa compressive strength and 4.83 MPa tensile strength). Malfunctions in three of the eight strain rosettes during field testing to failure (including the rosette at the failure location) caused a loss of pertinent data necessary for full analysis of the principal strains and stresses experienced during the failure testing. However, derived stress data from the incomplete strain measurements imply that the tensile stresses at and near critical failure locations in this particular

armor unit were at or slightly above the minimum flexural tensile stress required by concrete contract acceptance criteria.

The results of this testing indicated that the concrete used in the tested armor unit had adequate material properties, however the flexural tensile breaking strength of the unit was lower than expected, based on standard calculations incorporating a theoretical failure plane. This suggests that the tensile stress capacity of an armor unit with complex geometry is significantly different than that of a simple beam used to establish concrete requirements through standardized testing methods. This data, though somewhat incomplete, is an indication that the relationship between actual strength of Core-Loc armor units in the field and specified concrete strength in contract documents is not well understood, and that further testing should be done in order to improve these criteria.

6. Conclusions

An extensive amount of varied data has been collected between 2006 and 2010 in support of the monitoring of the repaired Kaumalapau breakwater. In summary, the following conclusions have been drawn by the data analysis:

- Wave measurements in the years following construction and wave modeling have documented the wave climate near the structure and within the harbor. Long-period south swell and kona storms appear to cause the highest wave response in the harbor on a typical basis. The breakwater has improved mooring conditions within the harbor. No wave events have approached the design wave for the structure.
- Visual and remote inspections have shown that the toe of the structure has remained intact and appears to be functioning as intended, and that no breakage or significant damage has been observed in the armor units or in the concrete cap.
- The T-LiDAR and multibeam survey data collected indicate that the breakwater armor units and cap have experienced settling and movement, but most movement occurred in the first year after construction and both the armor layer and the cap have functioned as an integrated unit and the overall structure has remained stable.
- The majority of movement noted in the armor layer has occurred in areas where the structure orientation changes (dogleg and head). This may be a result of reduced armor unit packing density or interlocking, and/or additional wave energy in these areas.
- Concrete strength measurements indicated potential weakness in armor unit durability, however, no related issues such as armor unit breakage have been observed.
- The relationship between specified concrete strength according to standardized testing methods and concrete strength of a geometrically complex armor unit is not well understood, further data collection in this area would help to improve design criteria.

7. References

Delft University of Technology. (2003-2010). *User Manual, SWAN Cycle III, version 40.81,* The Netherlands.

Kirby, J. T. and Dalrymple, R. A. (1994). "Combined Refraction/Diffraction Model REF/DIF 1, Version 2.5. Documentation and User's Manual", Research Report No. CACR-94-22, Center for Applied Coastal Research, Department of Civil Engineering, University of Delaware, Newark.

O'Neil, E. (2008). *Testing and analysis of a concrete core-loc armor unit, Kaumalapau breakwater rehabilitation, Lanai, Hawaii.* Concrete Consulting, Vicksburg, MS. Report prepared for U.S. Army Engineer District, Honolulu, HI.

Podoski, J. H., Bawden, G., Bond, S., Smith, T.D. and Foster, J. (2009). "Post-construction monitoring of a core-loc breakwater using tripod-based LiDAR." *Proceedings of Coasts, Marine Structures, and Breakwaters 2009.* Institution of Civil Engineers, Edinburgh, Scotland, United Kingdom.

Sea Engineering, Inc. (2009). *Kaumalapau harbor: Multibeam sonar survey investigations.* Report prepared for U.S. Army Engineer District, Honolulu, HI.

Sea Engineering, Inc., and Group 70 International. (2008). *Kaumalapau breakwater repair: design and construction summary, with emphasis on core-loc armor units*. Report prepared for U.S. Army Engineer District, Honolulu, HI.

Sea Engineering, Inc., and Group 70 International. (2009). *Wave transmission modeling: Kaumalapau harbor, Island of Lanai, Hawaii.* Report prepared for U.S. Army Engineer District, Honolulu, HI.

Modeling Support of the St. Johns River Project, Jacksonville, FL

Dennis W. Webb[1] and Philip T. Sylvester[2]

[1]U.S. Army Corps of Engineers, Engineer and Development Center, CEERD-HN-N, 3909 Halls Ferry Road, Vicksburg, MS; PH (601) 634-2455; FAX (601) 634-3218; email: Dennis.W.Webb@usace.army.mil

[2] U.S. Army Corps of Engineers District, Jacksonville, CESAJ-EN-WM , 701 San Marco Blvd, Jacksonville, FL 32207; PH (904) 232-1142; email: Philip.T.Sylvester@usace.army.mil

ABSTRACT

The U.S. Army Corps of Engineers District, Jacksonville (SAJ) and the U.S. Army Corps of Engineers, Engineer and Development Center (ERDC) performed three model studies of St. Johns River, Jacksonville FL during the period of 2005 – 2010. The model studies included two- and three-dimensional hydrodynamic modeling of currents and a real-time ship simulator study. The first two model studies focused upon the Mile Point area where the St. Johns Bar Pilots Association restricts the movement of larger vessels during ebb tide due to strong crosscurrents. The crosscurrents occur from Pablo Creek on the south and Sisters Creek on the north. The third model study was to evaluate SAJ's GRR-2 plan to deepen and widen the entire deep-draft Federal project. The final result was a channel design allowing larger ships access to JAXPORT docks and reduce or eliminate tidal delays.

INTRODUCTION

Jacksonville, FL is located on the northeast corner of the state (Figure 1). The ships calling at the port of Jacksonville (JAXPORT) must transit St. Johns River, which links Jacksonville to the Atlantic Ocean. The SAJ and the ERDC conducted three modeling efforts to improve navigation in St. Johns River reducing or eliminating tidal delays at Mile Point and deepening and widening the entire deep-draft navigation channel.

Each of the modeling efforts consisted of a hydrodynamic model and real-time ship simulation. The hydrodynamic model was used to calculate currents, which were input into the ship simulation database. Real-time means that ship movements on the simulator require the same amount of time as they would in real life. This allows mariners to quickly get accustomed to the simulator and begin making productive simulation runs. The ship simulator calculates vessel response to a variety of forces as the simulation vessel being piloted (ownship) transits the project area. These forces include currents, bank effects, rudder, engine speed, ship-to-ship interaction,

wind, bottom effects and waves. The environmental conditions (current, wind, and bathymetry) are stored in a database and read into the simulation software at the beginning of the exercise.

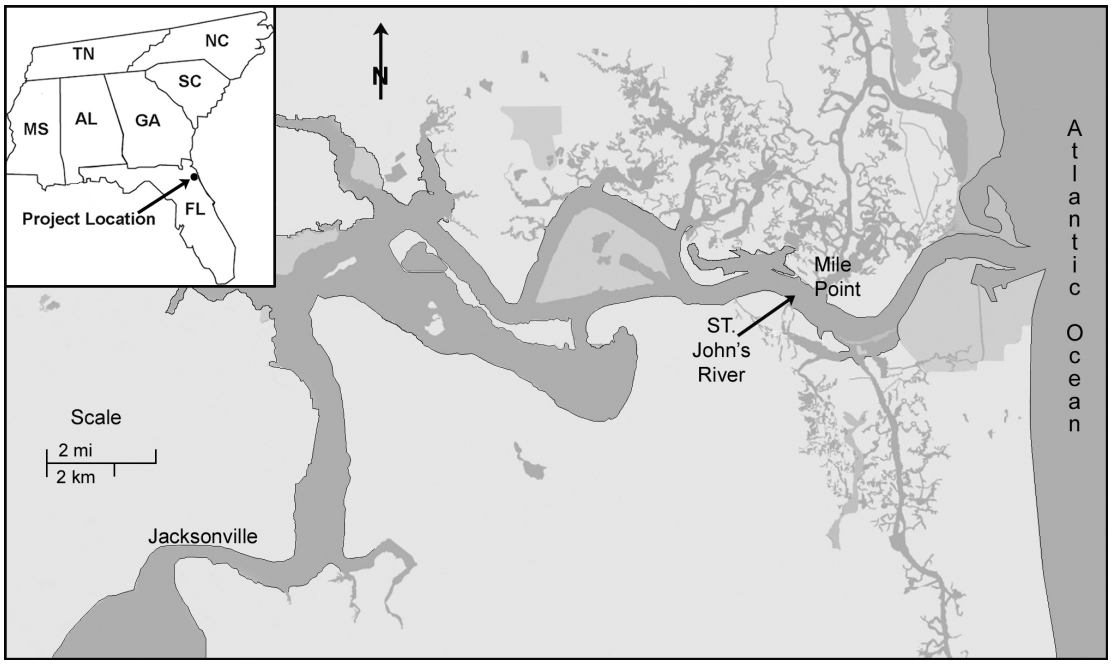


Figure 1. Project Location

In addition to the environment conditions, the simulator also requires visual databases. These include the visual scene, radar, and electronic chart display and information systems (ECDIS). Figure 2 shows a St. Johns Bar pilot operating the simulator for the GRR-2 study. The visual scene is displayed on the five screens that are visible in the same figure. The ECDIS is to the pilot's left and the radar is to his right. The radar is partially obscured by the pilot's head. The center display, between the ECDIS and radar, provides information to the pilot, such as; speed, rate of turn, engine speed, rudder angle, bow and stern lateral velocities, and wind speed and direction. The photo in Figure 2 is taken from the view of an inbound ship meeting an outbound ship in Brills Cut. The ERDC has two simulators which can function independently or be coupled for two-way traffic. The outbound ship was also piloted by a St. Johns Bar pilot.

Simulator studies typically begin with a reconnaissance trip. Two reconnaissance trips were taken for the St. Johns River studies. The first was taken in May, 2005 and the second was taken February 2009. The primary purpose of a reconnaissance trip is to experience vessel transits first hand, from the vessel bridge, and observe the pilot during a full range of pilot-command vessel-response events. Equally important during transits is the observation of local navigation conditions and the collection of

digital photographic data that will later be used to develop the visual scene. Representatives of ERDC and SAJ were able to ride total of five ships.



Figure 2. ERDC Ship Simulator - St. Johns River

MILE POINT CROSSCURRENT REDUCTION STUDY

Presently, the St. Johns Bar Pilots Association restricts the movement of larger vessels during ebb tide due to strong crosscurrents at a section of St. Johns River known as Mile Point (Figure 3). The restrictions are keyed to vessel draft and known vessel handling quality. Mile Point Lower Range and Turn and Training Wall Reach are crossed by the Atlantic IntraCoastal Waterway (ICW). The crosscurrents occur from Pablo Creek on the south and Sisters Creek on the north.

In an attempt to reduce or eliminate tidal restrictions, SAJ proposed to increase the cross-sectional area for flow into and out of Pablo Creek, Webb and Sylvester (2001). The increase in cross-sectional area is designed to reduce the current magnitude and ease the angle at which the current enters the St. Johns River. This proposal is shown in Figure 4. SAJ also proposed widening Training Wall Reach by 100 ft on the southwest side to allow two-way traffic (Figure 5).

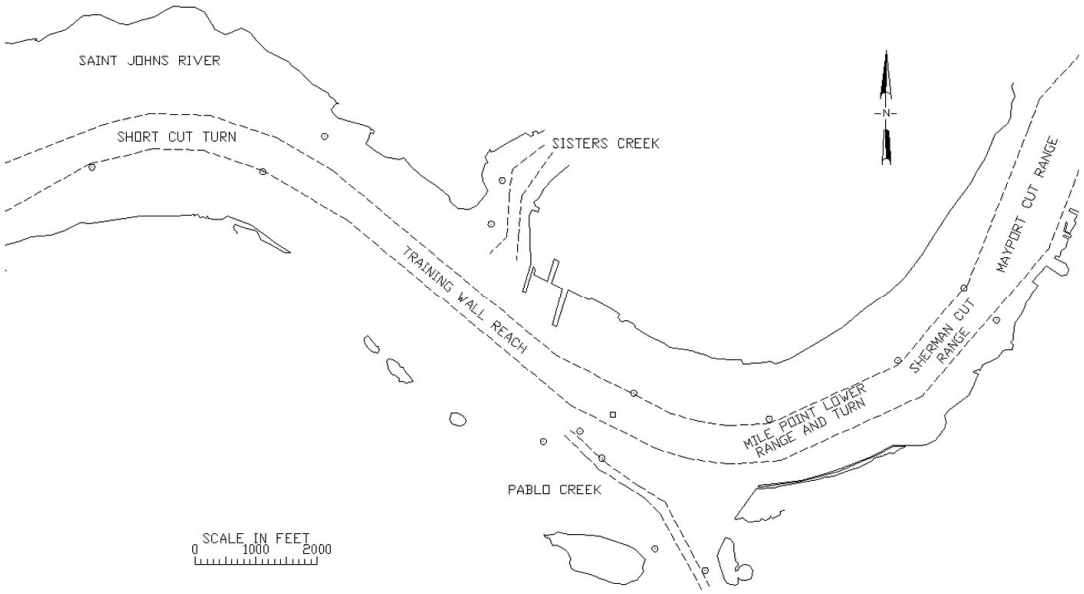


Figure 3. Mile Point

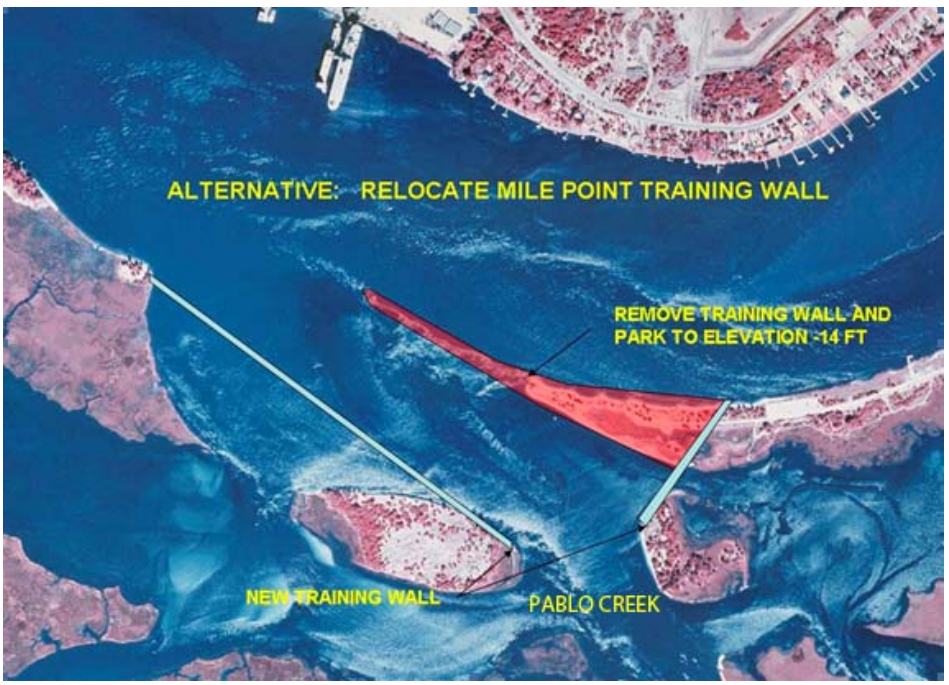


Figure 4. Widening Mouth of Pablo Creek

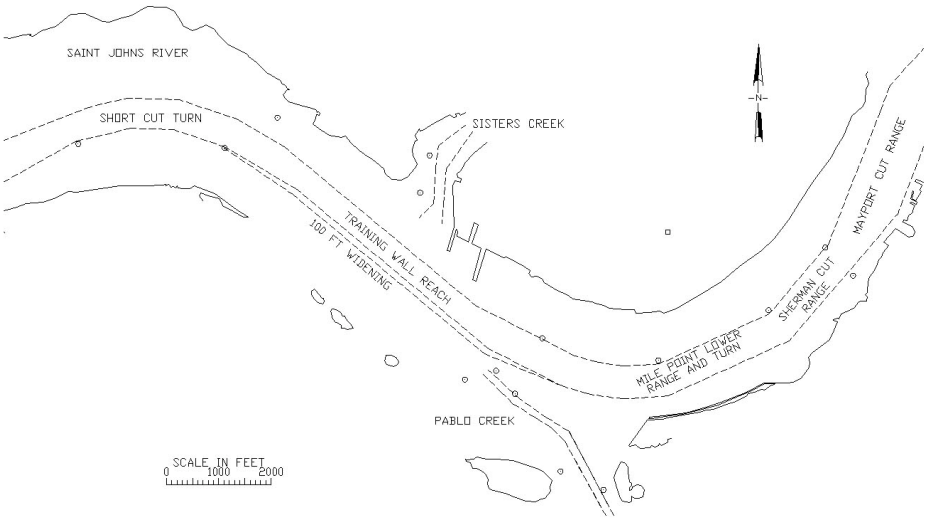


Figure 5. 100 FT Widening for Training Wall Reach

Database Development. Currents for both the existing and proposed channels were calculated by SAJ. Initially, a two-dimensional depth-averaged model was used. However, that model was converted to three-dimensional later in the study. Current data for the maximum strength of both the ebb and flood tides in St. Johns River and the maximum strength of ebb tide at Pablo Creek were extracted and converted into the format required by the ERDC Ship/Tow Simulator. Figure 6 shows the existing condition current field for maximum ebb at Mile Point. Figure 7 shows the current field for maximum ebb at Mile Point with the mouth of Pablo Creek widened.

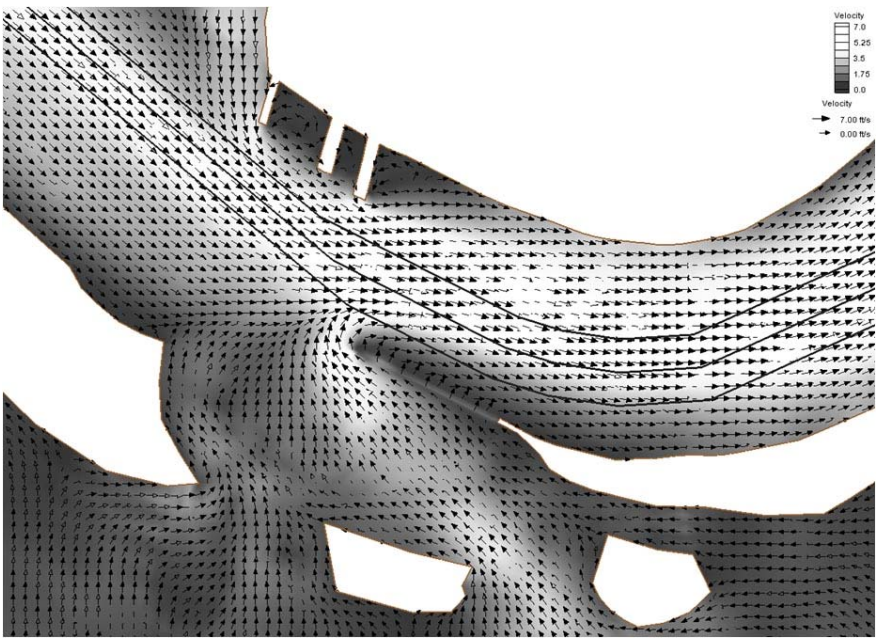


Figure 6. Existing Conditions, Maximum Ebb Tide

Two ship models were used for the Mile Point Navigation Study. The *Sibohelle* is a 797- x 106- x 38-ft tanker. The *Susan Maersk* is a 1140- x 140- x 47.5 ft containership. The Mile Point portion of St. Johns River is presently 3 ft deep, mean lower low water (MLLW). The depth portion of the simulator database was overridden to a depth of 52 ft MLLW to allow the *Susan Maersk* to transit. This is done to simulate a worst case scenario. Two two-way runs were also simulated. For those scenarios, the *Sibohelle* met the *SL Pride*. The *SL Pride* is a 865- x 106- x 30-ft containership. In addition, a two-barge tow transiting the ICW and crossing St. Johns River was simulated to ensure that the proposed improvements did not adversely affect barge traffic.

The ERDC Ship/Tow Simulator provides an ECDIS for the pilots. The ECDIS was modified to reflect proposed improvements.

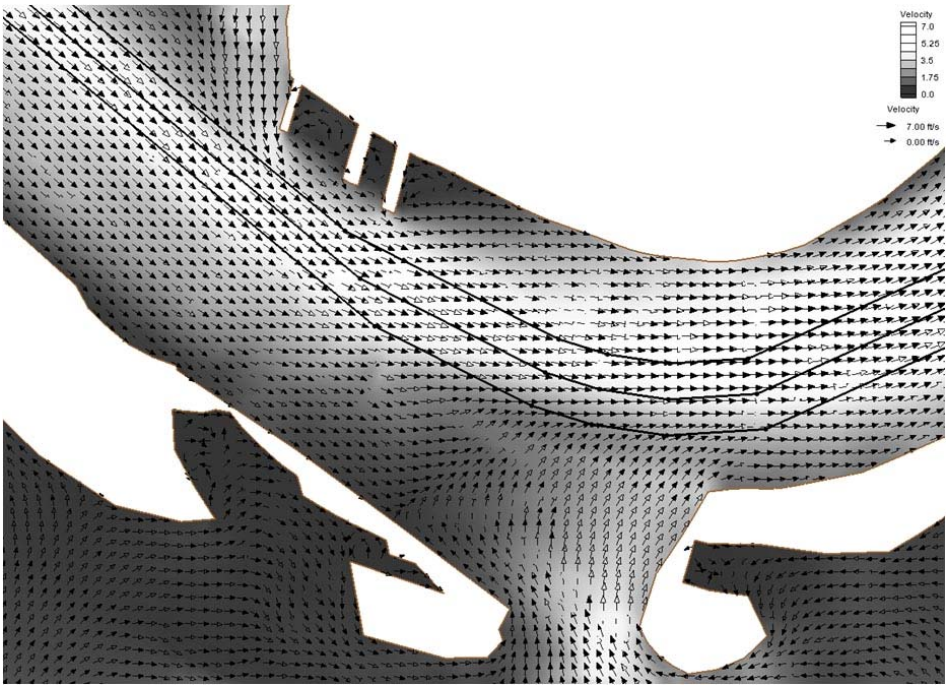


Figure 7. Maximum Ebb Currents, Mouth of Pablo Creek Widened

Validation. Validation for Mile Point was conducted September 27-30, 2005. Validation is a checkout of the existing condition simulation databases. An existing condition model must be successfully validated before it can be modified to reflect proposed conditions. Two St. Johns River pilots participated in validation. The visual scene, bank effects, ship models, radar and ECDIS were all successfully validated. However, the current database was not successfully validated. The initial model verification resulted in the conclusion that the simulated water current vector fields provided by the District did not accurately reflect conditions in the river near

Mile Point and those simulated vector fields would not be adequate for conducting a testing program of project alternatives.

The District developed revised water current vector fields from additional three-dimensional model study. The three-dimensional model did not cover the entire St. Johns River, but rather the Mile Point area only. The revised currents were reviewed by the pilots in Jacksonville and determined to be suitable for validation on the simulator. The May 2006 simulation testing runs were preceded by a successful validation of the revised water current vector fields.

Results. Testing with ship pilots was conducted May 15-18, July 11-13 and July 17-19, 2006. Two pilots participated in the May session. One pilot attended each of the July sessions. Simulation of towboat traffic was conducted Sept 18-20, 2006. At the end of each week of testing, the pilots were given a final questionnaire to complete.

Tests were conducted for ships heading both inbound and outbound. Three tidal conditions were tested. They were; maximum flood on St. Johns River, maximum ebb on St. Johns River, and maximum ebb from Pablo Creek. Maximum ebb from Pablo Creek occurs shortly after the start of ebb tide in St. Johns River. This is regarded as the worst case since the river currents aren't strong enough to dampen the crosscurrents coming out of Pablo Creek. Results were presented in the form of composite track plots. It is beyond the scope of this paper to discuss all results from the simulation program. However, results will be presented for one scenario each for ships and tows.

Ship Inbound, Maximum Ebb from Pablo Creek. Results of inbound simulations with the maximum ebb tide leaving Pablo Creek are shown in Figure 8. This figure contains the track plots for the *Sibohelle* transiting the St. Johns River with the mouth of Pablo Creek widened. Five runs were completed under this condition because one pilot wanted to try it a second time.

Towboat Northbound, Maximum Ebb from Pablo Creek. Results of northbound tow simulations with the maximum ebb tide leaving Pablo Creek are shown in Figure 9. The captains felt widening the mouth of Pablo Creek improved navigation under all conditions tested. Towboat simulations were not included in the future studies.

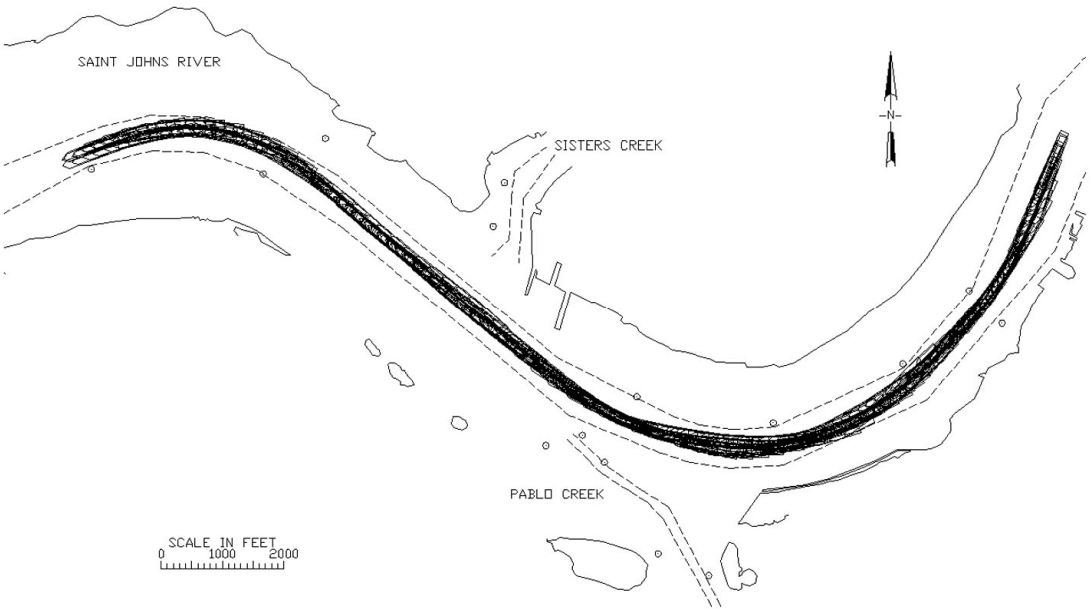


Figure 8. Track Plot Sibohelle, Maximum Ebb Tide Leaving Pablo Creek

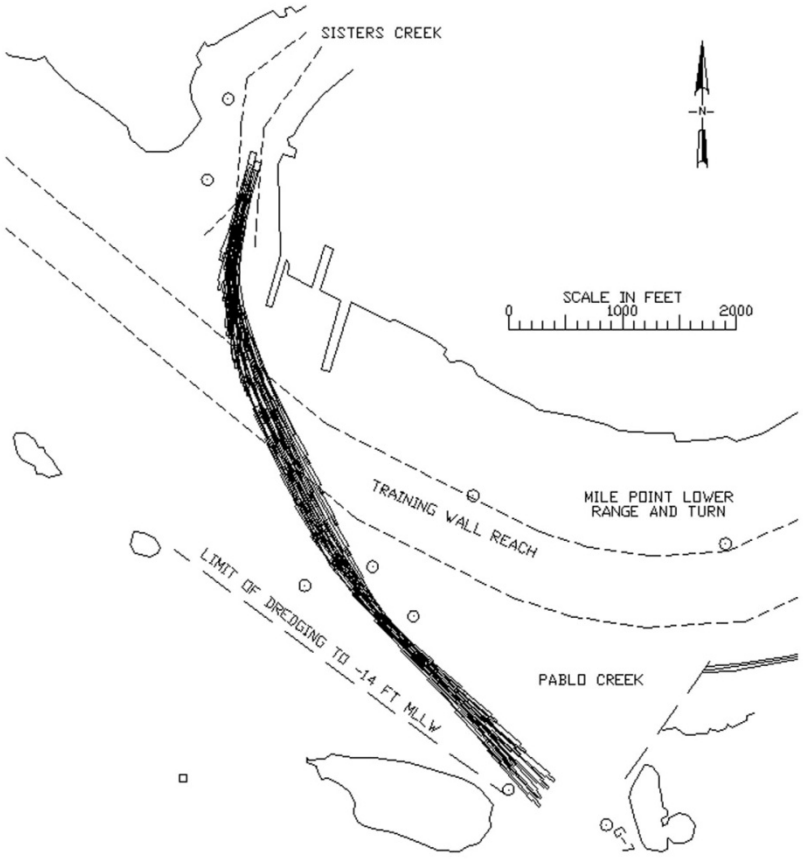


Figure 9. Northbound Tows, Maximum Ebb from Pablo Creek

CONCLUSIONS Based upon the simulator results and the pilot's final questionnaires, the following conclusions are made for the Mile Point improvements.

1. Widening the mouth of Pablo Creek improved navigation for the maximum ebb, maximum ebb from Pablo Creek, and maximum flood.
2. Three of the four ship pilots felt that tidal restriction would be lifted or greatly reduced. Captain James P. Winegeart, President of the St. Johns Bar Pilot Association wrote a letter dated September 3, 2010 supporting widening the mouth of Pablo Creek.
3. The pilots felt that widening Training Wall Reach would not improve two-way traffic beyond what they are already doing.
4. Widening the mouth of Pablo Creek improved navigation for tow traffic on the ICW.

RECOMMENDATIONS

1. Based upon the simulation results and pilot comments, we recommend that the mouth of Pablo Creek be widened to reduce or eliminate tidal restrictions.

MILE POINT CHANNEL WIDENERS

In 2009 SAJ wanted to evaluate three wideners on the west side of Training Wall Reach to determine if a widener variation could be designed and tested that would reduce or eliminate the tidal restrictions, Webb and Sylvester (2001). Three wideners of 300 ft, 400 ft, and 525 ft width were proposed (Figure 10). The wideners are referred to as Plan 1, Plan 2, and Plan 3, respectively. To assist SAJ in this determination, the ERDC conducted a proof-of-concept navigation study utilizing real-time ship simulation modeling to evaluate the proposed Mile Point wideners. Model development and online testing occurred at the ERDC in Vicksburg, MS during the period from June 2009 to September 2009.

To quickly provide SAJ with input as to the effectiveness of the wideners, a proof-of-concept study was undertaken. If the wideners appear to be effective, a more robust study could be conducted.

Several assumptions were made to meet the time requirements of this effort. The existing condition currents from the 2004 study were used for all three plans. The same current directions and magnitudes from the 2004 study were used for Plans 1, 2, and 3. The bathymetry within the wideners was deepened. The water in the area for widening is fairly deep, so this seemed a reasonable assumption. Subsequent analysis of SAJ's three-dimensional hydrodynamic modeling effort indicates that use of the water currents from the 2004 study was reasonable. Results from the three-

dimensional hydrodynamic modeling effort were not available for simulator database conversion and quality assurance inspection prior to real-time testing.

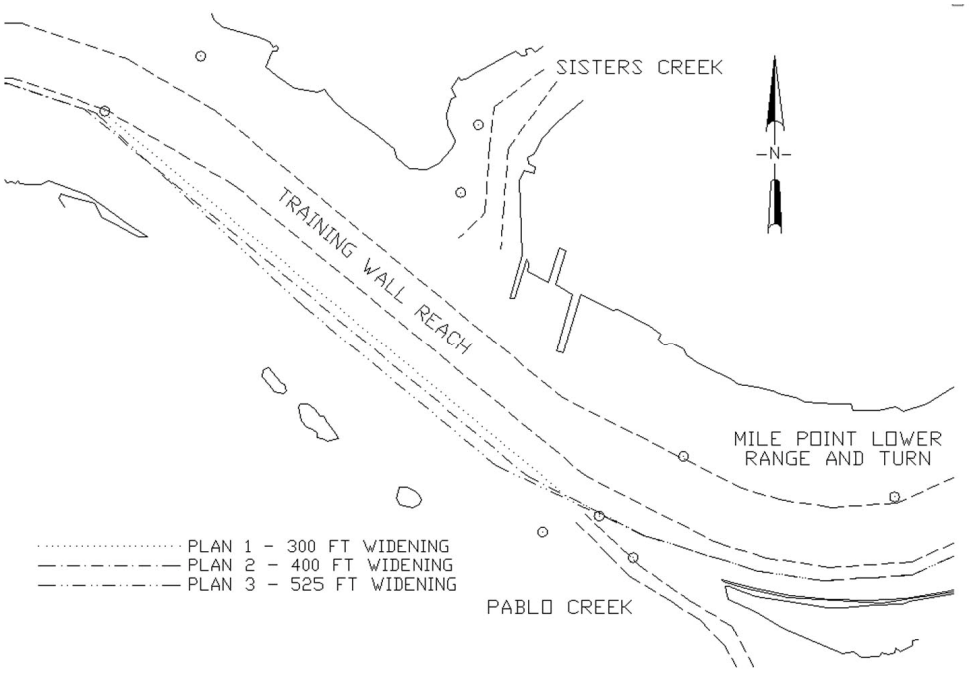


Figure 10. Plans 1, 2, and 3

Three pilots participated in the real-time simulation study over a three day period. All three are members of the St. Johns Bar Pilots Association. For many full navigation studies, six pilots participate for one week each. However, for this proof-of-concept study, an adequate amount of transit testing data was collected in the shortened testing period to evaluate the wideners.

CONCLUSIONS. Based upon the simulator results and the pilots' comments, the following conclusions are made for the Mile Point wideners.

1. The pilots, as observed by ERDC and SAJ personnel, attempted to use the wideners to make the turn and avoid getting set toward Atlantic Marine.
2. The pilots felt that using the wideners put their vessels in harm's way and would not use them unless they were 100% certain about currents.
3. The pilots, after using the wideners in the simulation, stated that they felt the wideners would not reduce tidal restrictions for Mile Point.
4. Based upon the simulator runs, the pilots felt that widening the mouth of Pablo Creek, as tested in the earlier study, could reduce or eliminate tidal restrictions for Mile Point.

SAINT JOHNS RIVER GRR-2 IMPROVEMENT PROJECT

The US Army Corps of Engineers District, Jacksonville (SAJ) is evaluating proposals to deepen the entire St. Johns River to up to 50 ft and possibly widen portions of the

channel, Webb and Sylvester (in preparation). The project limits are shown in Figures 11 and 12. There were three original proposed alternative channels. Alternative 1 (Alt 1) deepened to 50 ft on the existing channel footprint. Alternative 2 (Alt 2) deepened to 50 ft and included some widening and turning basins. Alternative 3 (Alt 3) deepened to 50 ft and included some widening and turning basins. It is beyond the scope of this report to provide details of the widening for Alternatives 2 and 3.

The study to evaluate the GRR-2 proposals to deepen and widen St. Johns River assumes that the Mile Point Alternative 1 will be constructed. The three dimensional model used to calculate currents from Mayport Cut to White Shells Cut was operated with Mile Point Alternative 1 in place. If the Mile Point Alternative 1 is not to be constructed, the results of the GRR-2 simulator study will be invalid.

Ships used during the simulation test program were as follows:

1. Susan Maersk, 1140- x 140- x 47.5-ft containership
2. Hanjin Miami, 980- x 141- x 47.5-ft containership
3. Generic Panamax, 965- x 106- x 44.- ft conainterhip
4. H. A. Sklenar, 797- x 106- x 47.5-ft bulk carrier

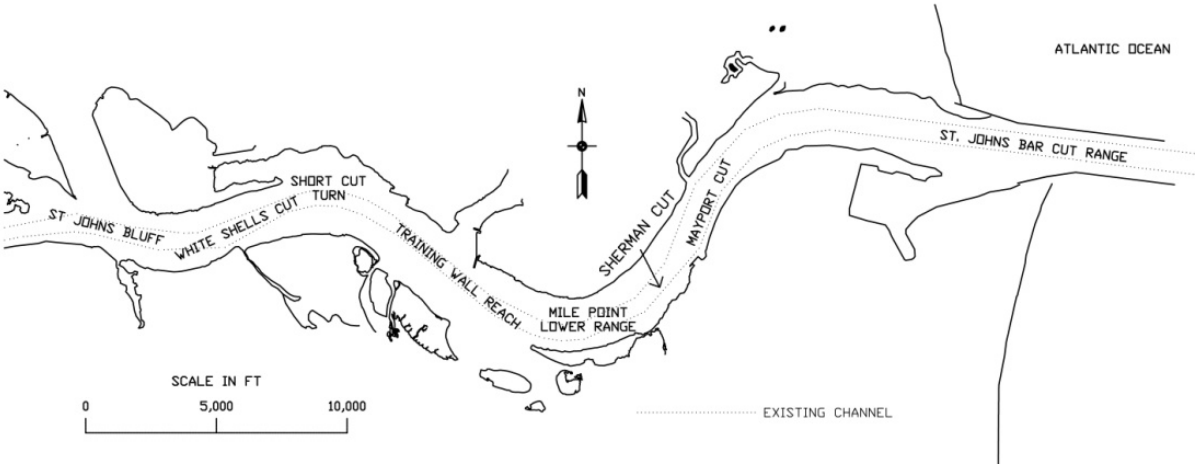


Figure 11. St. Johns River, Eastern Half

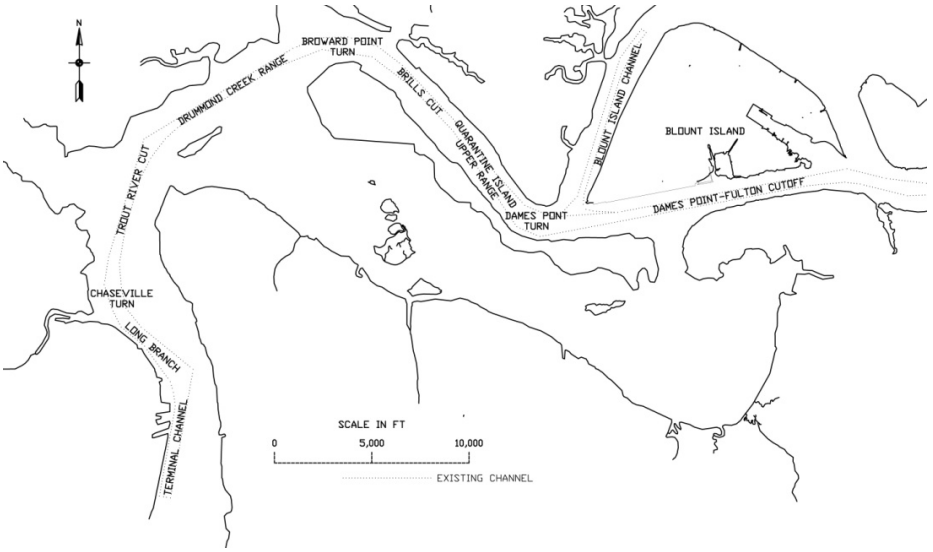


Figure 12. St. Johns River, Western Half

FIRST ROUND OF TESTING. Evaluation of the results from the first round of testing was accomplished through a series of meetings attended by the pilots, SAJ, and ERDC.

On September 16th, 2010 a working group was held at the St. Johns Bar Pilots office in Mayport, FL. The US Army Corps of Engineers was represented by Steve Conger, Phil Sylvester, Laurel Reichold (all of SAJ), and Dennis Webb (ERDC). St. Johns Bar Pilots were represented by Captains Chris Mons, Bill Brauer, Jay Winegeart, and Joe Heath. The objective of the working group was to evaluate the three channel improvement alternatives (Alt 1, Alt 2, and Alt 3) for each channel segment of the waterway. These three alternatives had been examined during a real-time ship simulation effort conducted at the ERDC Ship Simulator in Vicksburg, MS. The four pilots present at the working group had participated in the simulations.

The group examined vessel track plots of the simulation and notes taken during the simulation. Personal observations were also recalled. This took approximately four hours and resulted in a consensus opinion on a new alternative channel. This new channel, Alt 4, is a combination of the most appropriate of Alt 1, Alt 2, and Alt 3 for each channel segment. In addition, two minor modifications not included in the three previous alternatives were added to Alt 4. Two-way traffic for the design ships is provided for in Training Wall Area, Brills Cut, and Drummond Creek.

An additional Alternative, Alt 5 was also developed. The only change from Alt 4 was additional widening on the northwest side of St. Johns Bluff reach. Alt 5 will only be simulated for St. Johns Bluff reach and its approaches since the remainder of Alt 5 is identical to Alt 4.

TESTING. One week of real-time pilot testing was undertaken for the Alt 4 and Alt 5 channels. Captains Chris Mons and Bill Brauer S. Johns Bar Pilots Association operated the simulator November 9 - 12, 2010. Captains Steve Harvey, Dan Ramsey, and Tony Hogg, docking pilots for the Port of Jacksonville, participated in the turning basin simulations December 6 – 10. The scenarios shown in Table 1 were tested with the harbor pilots.

Table 1. GRR-2 Simulation Tests With Harbor Pilots	
Test Reach	Meeting Location
Mayport Cut to Dames Pt Fulton Cutoff.	Training Wall Reach
Mayport Cut to Dames Pt Fulton Cutoff	St. Johns Bluff
Drummond Creek Range to Dames Pt Fulton Cutoff	Brills Cut
Tallyrand to Dames Point Turn	Drummond Creek

A sample track plot is shown in Figure 13.

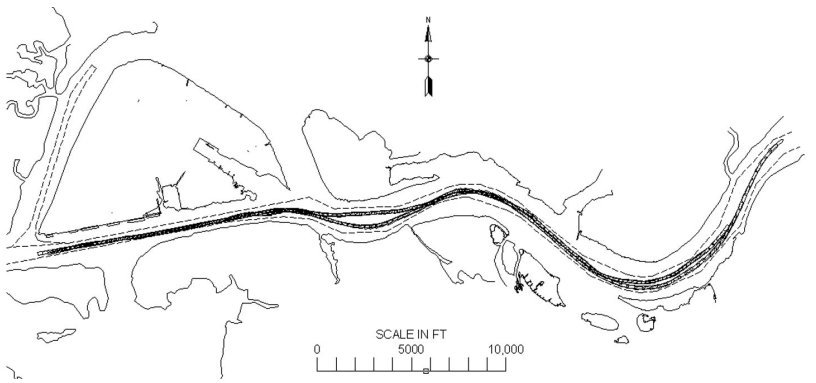


Figure 13. Hanjin Miami Meeting Hanjin Miami in St. Johns Bluff, Ebb Tide

The following turning basins were tested with the docking pilots: Blount Island Basin, Brills Cut Basin, Broward Point Basin, and Talleyrand Basin. A sample track plot is shown in Figure 14.

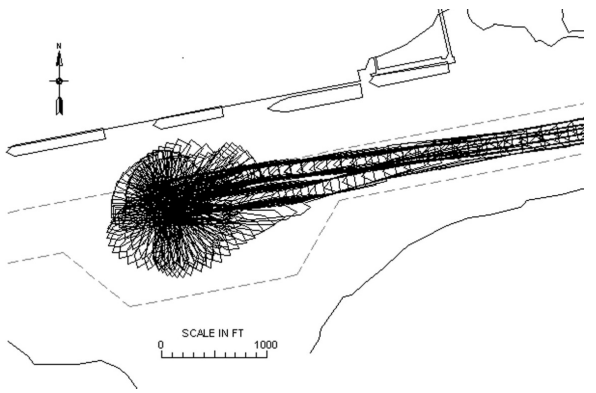


Figure 14. Turning Basin Test, Blount Island, Susan Maersk, Ebb Tide

RESULTS The following are recommendations based upon the results of the simulator study. With the exceptions of St. Johns Bluff Reach and Short Cut Turn Alt 4 is recommended. Note: Alt 4 and Alt 5 are identical everywhere but St. Johns Bluff Reach. In St. Johns Bluff Reach Alt 5 was too restrictive on the north east end and Alt 4 was wider than necessary on the north west end. The widening shown in Figure 14 is recommended.

The following recommendations are made for the turning basins.

1. At Blount Island, as tested, 2500 ft length and 1700 ft total, including berth,.
2. At Brills Cut the 2500 ft by 1700 ft (including berthing area) is adequate. The final location will depend upon the terminal to be constructed.
3. At Broward Point the location is inappropriate for a turning basin.
4. At Talleyrand Alts 5 and 7 were adequate. Since Alt 7 is smaller, it should be selected.

CONCLUSIONS

SAJ and ERDC successfully used real-time ship simulation to design a navigation improvement project which appears will result in navigation improvements on St. Johns River when constructed. Tidal delays at Mile Point will likely be reduced or eliminated. There will be several locations for meeting of large ships to allow the container traffic to function efficiently. Three turning basin designs were successfully tested that would allow for safe and efficient vessel traffic management contributing to the elimination of transit delays and dockside labor cost wastefulness.

REFERENCES

Webb, D. W. and Sylvester P. T. (2011). *Navigation Study for Mile Point Channel Improvements Data Report,* Vicksburg, MS.

Webb, D. W. and Sylvester P. T. (2011). *Proof-of-Concept Study for Mile Point Channel Wideners Data Report,* Vicksburg, MS.

Webb, D. W. and Sylvester P. T. (In Preparation). *Navigation Study for Saint Johns River GRR-2 Improvement Project Data Report - Draft,* Vicksburg, MS.

Wave Amplification at Harbor Entrance due to Submerged Shoal

Hyung Seok Yoo[1], Byung Guk Min[1], Kyu Han Kim[2], Sungwon Shin[2]

[1]Department of Commercial Diving, Korea Polytechnics, 779, Noam, Gangneung, Gangwon, 210-932, Korea, PH +82-33-610-6131; FAX +82-33-610-6131; email: soma0226@gmail.com

[2]Regional Innovation Center, Kwandong University, 522, Naegok, Gangneung, Gangwon, 210-701, Korea, PH +82-33-643-3436, FAX +82-33-647-3436; email: kdocean@chol.com

ABSTRACT

In this study, we identified the cause of the wave height amplification in the channel entrance and modified the configuration of the breakwater to improve the docking system in Daepo Harbor.
We investigated the cause of the wave height amplification in the vicinity of channel entrance and obstruction elements in the channel entrance through a bathymetric survey of precision using a multi beam echo sounding (MBES), side scan sonar (SSS), sub marine photography and wave observation together with numerical simulation.
In the field observation, wave heights were amplified due to the submerged shoal area and it was measured by pressure-type wave gauges. Moreover, the numerical simulation also indicates the wave height amplification on the submerged shoal. In addition, the verified numerical model was used to suggest a countermeasure to minimize the wave height amplification by rearranging the breakwater configuration.
Currently, we are monitoring wave height amplification continuously. Moreover, hydraulic model tests for various cases are being carried out to elucidate the characteristics of the wave height amplification around the submerged shoal area and to develop a new support system for ship movement in the harbor. The results of this study are expected to contribute to the safety of ship movement in the vicinity of submerged shoal.

ADDITIONAL INDEX WORKS; wave height amplification, submerged shoal, bathymetric survey of precision, wave observation, docking system

INTRODUCTION

Daepo Harbor is located on the east coast of South Korea as shown in Figure 1. A harbor extension project has been underway since 2003, which is to expand the existing small fishery harbor into a large-scale, multipurpose harbor. The project is estimated to be completed by 2010 and the construction of a seawall and a breakwater has almost been completed for ships to use the harbor during the project as shown in Figure 2.



Figure 1. Korean peninsula (left) and Daepo Harbor (right) on east coast of Korea.



(a) (b)

Figure 2. Extension of Daepo harbor since 2003. (a) before extension; (b) after extension(2009.07)

However, in the process of construction, difficulty in ship maneuverability occurred in Daepo Harbor. As the east breakwater was extended, the wave height in the channel entrance increased and small ships using the existing harbor encountered danger near the harbor entrance. Therefore a ship was flipped over near the harbor entrance in March 2009 due to the high amplitude of waves. Since the accident, construction was suspended, prompted by the local fishermen's demands to solve the problem to prevent future accidents. Therefore, the breakwater construction was remained incomplete as shown in Figure 2 (b); solid lines are completed and dotted lines are planned.

In this study, we identified the cause of the wave height amplification in the channel entrance and modified the configuration of the breakwater to improve the docking system in Daepo Harbor. First, we investigated the cause of the wave height amplification in the vicinity of the channel entrance through a precision survey of bathymetry using a multi beam echo sounding (MBES) system in accompanied with numerical simulation. Furthermore, we investigated the detail bottom topography of the sea bottom using side scan sonar (SSS). Also, we found out obstruction elements in the channel entrance through submarine photography by divers.

WAVE CHARACTERISTICS IN THE STUDY AREA

The study area is located in the northern part of the east coast of South Korea. The mean tidal range is less than 0.3 m. Wave characteristics are obviously different in between winter and summer. Waves from the northeast are dominant in winter season and those from between the northeast and the southeast are evenly distributed. This is because the Korean peninsula is located in monsoon area. In the winter season, the climate in Korea is influenced by continent and mostly affected by the ocean in summer season. Therefore, wind comes from the northwest in winter season and comes from southeast in summer season.
In spite of different wind directions in both seasons, waves in shallow water depth come from the northeast ($\pm 20^{o}$) due to the refraction by the topography since the shore line faces to the northeast (Kato, et al., 2001).

PRECISION SURVEY OF BATHYMETRY

In the current study, the bathymetric survey was conducted precisely to investigate the cause and range of wave height amplification in channel entrance. The survey included multi beam echo sounding (MBES), side scan sonar (SSS), and submarine photographing. Obstructive factors can also be found through this survey. Figure 3 shows the survey area, the location of wave height measurement, and the area of numerical simulation. Survey area was designated as the area of 1km×1km from the southeast part of channel entrance.

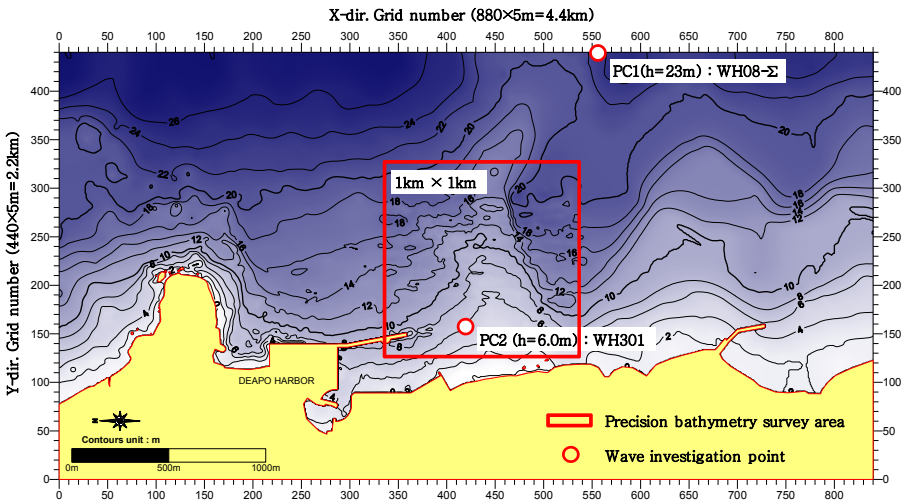


Figure 3. Range of field observation and numerical modeling.

It is known that MBES provides the high quality digital information of ocean bottom topography. Therefore, International Hydrographic Organization (IHO) suggests that MBES be used for bathymetric survey with high resolution in the area where the safe navigation of ship is important (IHO, 1998)

Figure 4 shows an example of 3D bottom topography surveyed by MBES. This figure indicates that there is a large submerged shoal in the southern side of the breakwater in Daepo harbor. In Figure 5, the survey results using MBES were compared to those using Single Beam Echo Sounding (SBES) in 2006. The differences between two measurements were up to 5m cross-sectional data, as shown in the figure. This difference between two results is caused by the method of survey. The method of SBES has much lower resolution compared with MBES.
So the effects of submerged shoal had not been considered enough when the Daepo harbor was planned for construction. Therefore, the bathymetric survey using MBES is highly recommended to design and construct harbors. Moreover, bottom bathymetry should be surveyed wide enough compared with the area of harbor development.

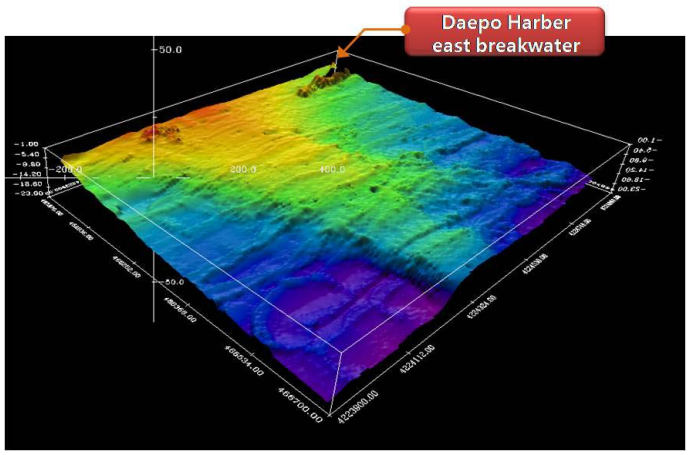
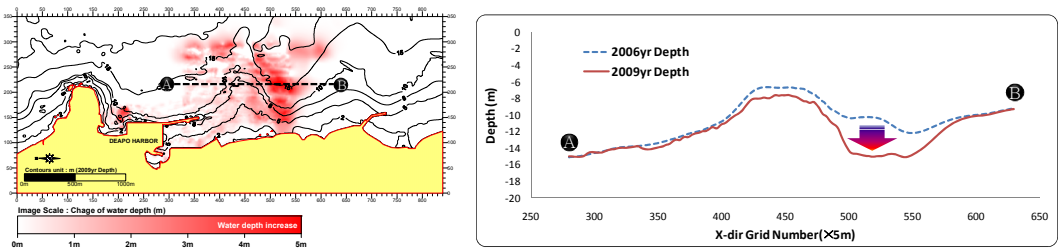


Figure 4. Precision bathymetric survey using MBES



(a) (b)

Figure 5. Differences of survey results between 2006yr and 2009yr. (a) plan view; (b) cross-sectional view of dotted line in (a)

Furthermore, we investigated the detail bottom topography of the sea bottom using side scan sonar (SSS). Also, we found out inhibitory factors in the channel entrance through submarine photography by divers. Side scan sonar and submarine photography are typical methods for the bottom topographic survey and underwater exploration.
Figure 6 shows the image data of the bottom, the distribution of sediment, algae, and

the rapid slope area near the southeast part of Daepo harbor from SSS and submarine photography. Through these methods, it is found that there was a larger submerged shoal composed of rocks near the southeast part of the harbor entrance and sands were distributed in other area. Especially, rapid slop area was located between rocky area and sandy area. Moreover, it was found that algae habitat was located in the middle of the submerged shoal. Algae almost reached to the water surface and can be an inhibitory factor of ship navigation.

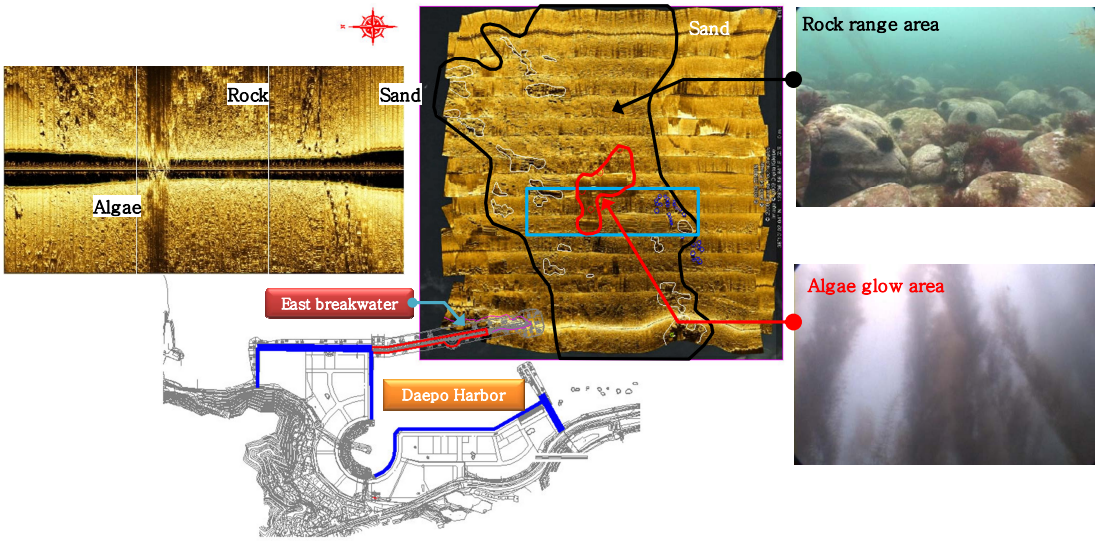


Figure 6. Detail bottom topography using SSS and submarine photography

FIELD OBSERVATIONS

Wave heights and directions were measured simultaneously in shoreward and landward of the submerged shoal to investigate the effect of wave direction on wave height amplification in channel entrance and to estimate the amount of wave height amplification quantitatively.

Wave gages were mounted at PC1 with 23m and PC2 with 6m of water depth in Figure 3. Field observations were conducted from November 22 to December 14, 2009.

Pressure type wave gages (WH-301) were used to measure wave heights correctly in surf zone. The advantage of the pressure type wave gage is that its structure is simple and it is applicable to the surf zone (Draper, 1966). Moreover, there is no limitation of ship navigation since the wave gage is installed at the bottom.

The wave heights during the period of observation were measured continuously every 0.5 seconds. The wave gages were anchored with bolts on the rocks firmly as shown in Figure 7.

The method of data analysis suggested by Sasaki, et al. (1987) was used. This method converts pressure fluctuation data to surface elevation. The time domain of pressure data is transformed to the data in the frequency domain through FFT, first. Secondly, the pressure transfer function to estimate water surface elevation is

multiplied by the pressure data in the frequency domain. Then, the data is transformed to the time domain data through IFFT.
Wave heights were calculated using zero-up crossing method. Wave directions were estimated using covariance method based on the covariance between three components; water surface elevation, and horizontal fluid particle velocities with x, y directions.



Figure 7. A photograph of wave gage anchoring at the bottom.

Figure 8 shows the time series of significant wave heights ($H_{1/3(PC1)}$, $H_{1/3(PC2)}$), wave direction at PC1 and PC2, and $H_{1/3(PC2)}/H_{1/3(PC1)}$. $H_{1/3(PC2)}/H_{1/3(PC1)}$ values are lower than 1.0 mostly during the period of observation. However, in E~ESE direction, as wave direction approaches ESE (December 3~5; December 11~12), $H_{1/3(PC2)}/H_{1/3(PC1)}$ tends to be greater than 1.0.
Especially, $H_{1/3(PC2)}/H_{1/3(PC1)}$ increases as wave steepness $H_{1/3(PC1)}/L_{1/3(PC1)}$ decreases as shown in Figure 9. Maximum wave height amplification was 1.36 when the wave steepness was 0.016. $H_{1/3(PC1)}$ at that time was 1.5m, $T_{1/3(PC1)}$ was 8.2sec, and the direction was S76°E while $H_{1/3(PC2)}$ was amplified up to 2.04m. Figure 9 shows the $H_{1/3(PC2)}/H_{1/3(PC1)}$ as a function of $H_{1/3(PC1)}/L_{1/3(PC1)}$ from 4 pm, December 11 to 1 pm, December 12. From this result, we found that the wave with ESE direction effects on the wave height amplification in harbor entrance since the waves from this direction pass through the submerged shoal. Wave amplification phenomena behind the submerged shoal were already proven by both laboratory experiments (Vincent and Briggs, 1989) and numerical simulations (Chawla et al., 1998) using elliptical submerged shoal.
Therefore, we can assume that more severe wave heights amplifications will possibly be occurred during storm season in summer because high waves come with storm from SE.

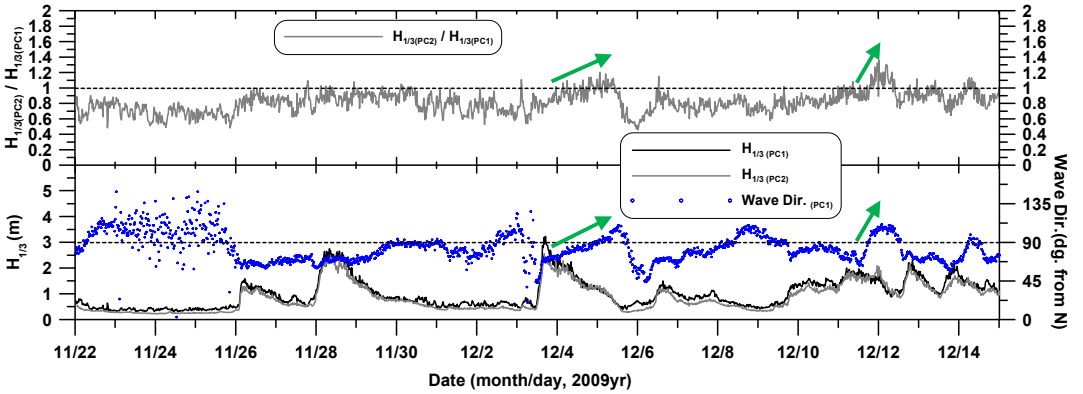


Figure 8. Variations of $H_{1/3(PC1)}$, $H_{1/3(PC2)}$, $H_{1/3(PC2)} / H_{1/3(PC1)}$ and Wave direction as a function of time.

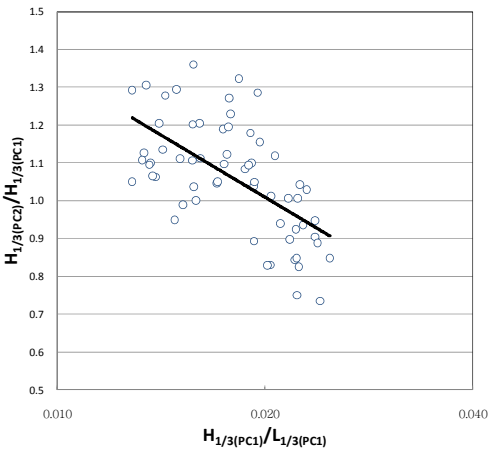


Figure 9. Relationship between $H_{1/3(PC2)} / H_{1/3(PC1)}$ and $H_{1/3(PC1)} / L_{1/3(PC1)}$ (12/11 16h~12/12 13h)

NUMERICAL MODEL

Numerical simulations were performed to find and improve the problems of current ship entrance system.

First, the results of numerical simulations were compared with the data from the field observations to verify model reliability. Second, the numerical model was used to find the problem of ship entrance system in abnormal wave condition. Third, we assured that it is necessary to improve the current ship entrance system.

Table 1 summarized input wave conditions for numerical simulations. The governing equation of the numerical model is time-dependent mild-slope irregular wave equations (Isobe, et al., 1992). The detail description of the model can be found in the reference.

The model simply verified for wave height amplification using the wave height data with the direction of E~ESE from the field observation (4pm, December 11 ~ 1pm,

December 12).
Computational domain is 4.4km×2.2km and grid size is 5m for dx and dy as shown in Figure 3. The model results in terms of wave height amplification as a function of wave steepness predicted well in comparison with the results from the field observation as shown in Figure 10.

Table 1. Input wave conditions for numerical simulations.

Conditions	Wave dir.	$H_{1/3}$ ($(H_{1/3})_o$) (m)	$T_{1/3}$ (sec)
For model verification	ESE	1.5	6, 7, 8, 9
		2.0	7, 8, 9
	E	1.5	6, 7, 8, 9
		2.0	7, 8, 9
Abnormal wave conditions	N58.0°E(NE)	3.5 (4.0)	11
	N71.7°E(ENE)	3.3 (3.6)	10
	N85.2°E(E)	2.6 (2.9)	9
	S81.8°E(ESE)	2.3(2.7)	8
	S69.4°E(SE)	1.6(2.2)	8.
Design wave conditions	N57.8°E(NE)	5.31(6.11)	11.16
	N75.1°E(SE)	4.68(6.84)	11.01

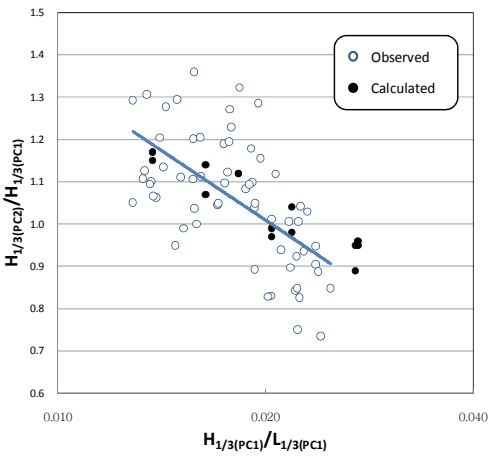


Figure 10. Comparison of wave investigation result and Numerical model result

The wave conditions for numerical model input to find the problems of ship entrance system are also in Table 1. The abnormal wave conditions were referred from the report of long term wave estimates published by Korean government, MOMAF (Ministry of Maritime Affairs and Fisheries).
Figure 11 shows the typical wave height distribution with the direction of SE and we

can easily find wave amplification phenomena using this figure. Figure 12 shows the alongshore variation of wave height ratio in line A-B indicated by Figure 11.
In these figures, planned harbor entrance will mostly be affected by the submerged shoal as incident waves come from SE direction. Figure 11 indicates that the largest wave amplification appeared in planned ship route when the waves from SE.

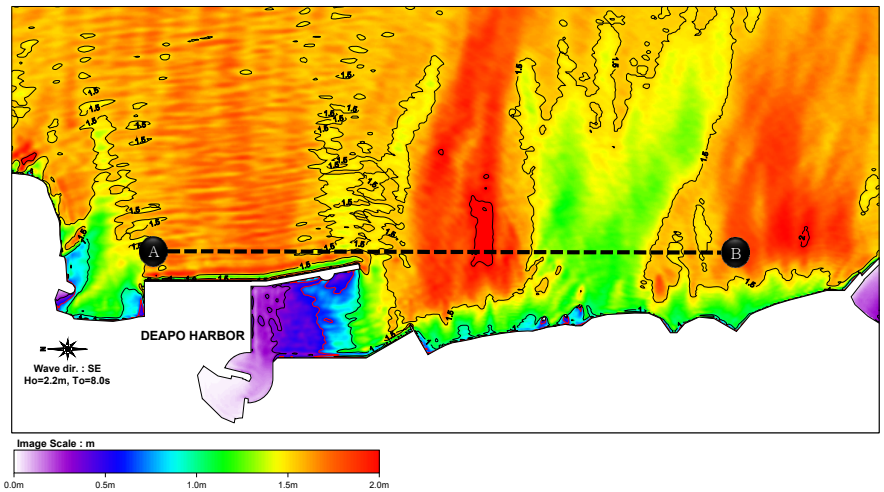
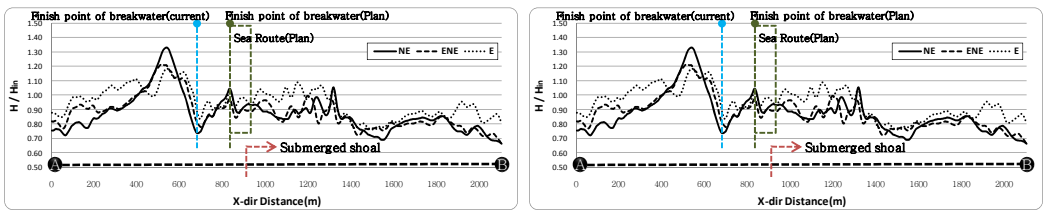


Figure. 11 Computed result of wave transformation

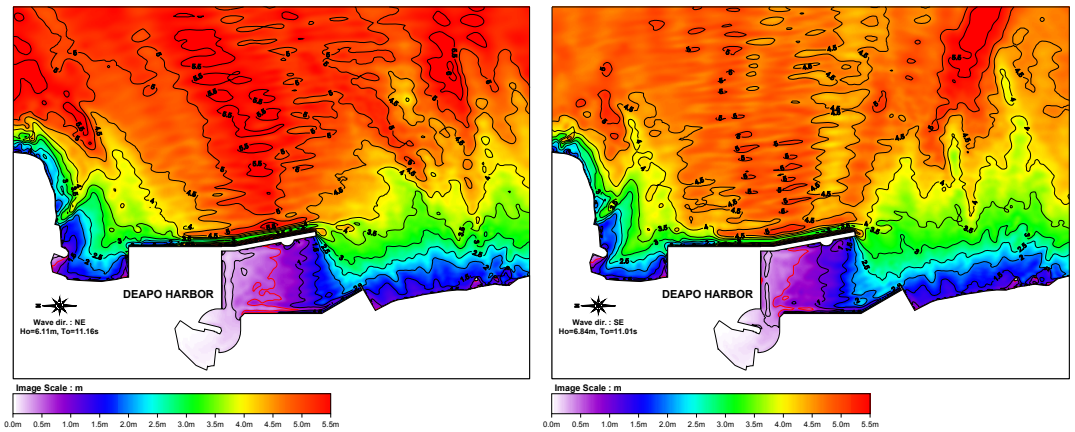


(a) (b)

Figure. 12 Computed spatial variation of wave height over submerged shoal.
(a) NE~E; (b) E~SE

Based on the field observation and numerical simulation results, it is found that the planned harbor entrance is affected by wave amplification due to the submerged shoal. Therefore, it is suggested as an alternative that the extension of the breakwater should be minimized. In addition, harbor tranquility should also be considered carefully. For this reason, numerical simulations were conducted to investigate harbor tranquility under the existing harbor condition using the design waves of 50yr return period. The waves with NE and SE directions in the simulations were considered.
Figure 13 shows the results of harbor tranquility from the experiments. As a result, waves of 0.6m heights were widely distributed inside harbor area, which is the maximum wave height for loading limitation. The wave height in some places near the harbor entrance was more than 1.5m. Therefore, it is necessary that the breakwater should be extended in terms of harbor tranquility. Also, the extension of

east breakwater should be minimized to enhance safe navigation and a plan for harbor construction needs to be improved in harbor tranquility point of view.



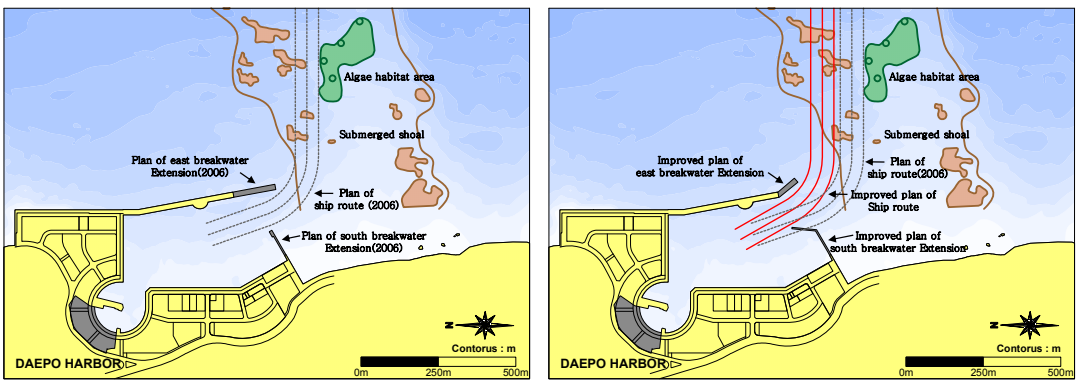
(a) (b)

Figure. 13 Numerical simulations of harbor tranquility. Wave direction: (a)NE; (b)SE

IMPROVEMENT OF SHIP ENTRANCE SYSTEM

The length of breakwater was supposed to be increased by 140m based on the construction plan that was set in 2006. If the east breakwater were elongated as the original plan, the harbor entrance and the ship route were supposed to be located within the area of submerged shoal and near the algae habitat. Therefore, ships have difficulties in navigation in this region.

In this study, we suggested that the plan of harbor construction plan be changed in order to improve ship entrance system. It was proposed that the harbor entrance should be far enough from the submerged shoal and that the harbor tranquility be maintained. Therefore, the east breakwater was elongated by 75m and the angle was changed into 30° offshore ward. In order to keep harbor tranquility, the extension length of south breakwater was changed from 90 m to 170m. The detailed plan is described in Figure 14.



(a) (b)

Figure 14. The improvement of harbor construction plan: (a) Original (b) Changed.

CONCLUSIONS

In this study, we analyzed the wave amplification phenomena due to the submerged shoal through the precision survey of bathymetry and the field observation of wave characteristics. These results can contribute the accumulation of field data about the wave amplification due to the submerged shoal and the understanding of hydrodynamics. It was also found that the resolution of bathymetric survey is very important to set a plan for harbor construction.

Numerical simulations of wave transformation were performed to find and improve the problems of current ship entrance system. The results showed that the harbor entrance was largely affected by the submerged shoal as incident waves come from SE direction. The largest wave amplification appeared in planned ship route when the waves from SE. It was also found that the extending breakwater is inevitable to keep harbor tranquility.

Therefore, it was proposed that the harbor entrance should be far enough from the submerged shoal and that the harbor tranquility be maintained. The applicability and reliability of this proposal were proved by the results and comparisons of numerical simulations and the field observations.

Through this study, we learned the importance of the bottom topographic survey and the field observation of wave climates in terms of the plan for harbor construction. The monitoring of wave height amplification is currently being conducted. Hydraulic model tests are also being conducted in several different cases. The results of this study are expected to contribute to set a plan of harbor construction in terms of the safety of ship movement in the vicinity of submerged shoal. However, the relationship between the wave height amplification due to the submerged shoal and Bragg reflection (Hara and Mei, 1987; Liu and Cho, 1993) is remained as a future study.

ACKNOWLEDGMENT

This study was supported partly by the RIC program of the Ministry of Knowledge Economy of Korea.

REFERENCES

Chawla, A., Ozkan, H.T. and Kirby, J.T. (1998). "Spectral model for wave transformation and breaking over irregular bathymetry." *Jour. Waterways, Port, Coastal, and Ocean Eng.*, ASCE, 124(4), 189-198.

Draper, L. (1966). "The analysis and presentation of wave data-A plat for uniformity." *10th Coastal Eng. Conf.*, ASCE, 1966, pp.1-11.

Hara, T. and Mei, C.C. (1987). "Bragg scattering of surface waves by periodic bars : Theory and experiment" *J. Fluid Mech.*, 178, 221-241.

IHO (1998). "IHO standards for hydrographic surveys." *4th edition, special publication No.44, International Hydrographic Bureau*, Monaco.

Kato, S., Park, J.W., Kim, K.H., Choi, B.H., Kim, K., and Yamashita, T. (2001). "Coastal current and sediment circulation system in the East(Japan) sea", *11th PAMS/JECCS Proceedings*., 149-150.

Kubo, Y., Kotake, Y., Isobe, M., Watanabe, A. (1992). "Time-dependent mild slope equation for random waves." *Proc. 23rd Int. Conf. on Coastal Eng.*, ASCE, pp. 419– 431.

Liu, P.L-F. and Cho, Y.S. (1993). "Bragg reflection of infragravity waves by sandbars." *J. Geophy Res.*, 98(C12), 22733-22741.

Ministry of Maritime Affairs and Fisheries (MOMAF). (1998). *An annual report of long term wave estimates.*, Korea.

Sasaki, H., Goda, Y., Koangai, T. (1987). "Development of an on-line wave data processing unit for field observation." *Technical note of the Port and Harbor Research Institute, ministry of transport*, Japan, No.580.

Vincent, C.L., and Briggs, M.J. (1989). "Refraction-diffraction of irregular waves over a mound." *Jour. Waterway, Port, Coastal and, Ocean Eng.*, ASCE, Vol.115, No.2, pp.269-284.

Utilizing Vessel Based Mobile Laser and Bathymetry Survey Techniques for Survey of Four Southern California Breakwaters

T. J. Mitchell[1] and M. N. Chang[2]

[1]Fugro Consultants, Inc., Offshore Survey Division, 4820 McGrath Street #100, Ventura, CA, 93003-7778; PH (805) 650-7000; FAX (805) 658-6679; tmitchell@fugro.com

[2]US Army Corps of Engineers, Los Angeles District, Navigation Section, P.O. Box 532711, CESPL-CO-ON, Los Angeles, CA, 90053-2325; PH (213) 452-3405; FAX (213) 452-4195; mohammed.n.chang@usace.army.mil

ABSTRACT

Traditionally, breakwater surveying is especially challenging and often dangerous due to weather conditions and the need to deploy personnel physically on the breakwater and generally lacking in terms of detail, especially spanning the water line.

Utilization of mobile laser scanning and integrating with multibeam echosounder bathymetry allow the opportunity to produce models of the breakwater both above and below the water surface with very low health and safety exposure to personnel. These models are more accurate, more complete and more reliable than performing visual inspections, GPS surveys or using bathymetric methods alone. The comprehensive nature of the data products allows for vast improvements in the characterization of the breakwater condition and allow for better engineering decisions and design. Fugro and the US Army Corps of Engineers carried out surveys of four breakwaters in Southern California in 2009 and 2010 providing a detailed model for identifying damage, erosion and investigating required remediation.

INTRODUCTION

The Los Angeles District Corps of Engineers is responsible for the maintenance of many of the coastal and navigation structures in California, from Morro Bay to San Diego. In 2009, the District was successful in obtaining some funding from the American Recovery and Reinvestment Act (ARRA) to be used to conduct a Comprehensive Condition Survey for the San Pedro and Dana Point Harbor breakwaters. The use of vessel-based multibeam and mobile laser scanning survey technologies was determined to be able to respond quickly to the contracting needs as well as being able to provide data to the District rapidly. After the successful completion of the San Pedro breakwater, it was determined that this technology should be employed on an additional projects, such as the Long Beach breakwater.

CORPS OF ENGINEERS REQUIREMENTS

In order to determine the condition of the coastal and navigation structures under its jurisdiction, the District has developed a three stage, progressive method of determining the condition of these structures.

The principal method is to perform Visual Walk-Through Inspections. The method consists of a team of 2-3 Corps personnel, mostly coastal engineers, physically walking on the structures and inspecting for any damage or movement of units. The cost of this method is minimal, and is ideally performed on an annual basis. However data collected is not measurable and comparison between inspections is anecdotal rather than quantitative.

The next method is the Structural Survey which deploys a team of 2-4 surveyors to measure and obtain data on the structures. This method is more costly than the visual walk-through inspection but some data can be obtained and compared to data collected in the past. It also provides empirical and measureable data for evaluation, however the extent and detail of the data is generally limited to that of several cross-sections.

The most thorough method is to perform a Comprehensive Condition Survey (CCS) of the structure. This involves a full survey of the structure, from both above and below water. In some cases, samples of the structure are taken to determine the geotechnical conditions. The cost of this type of survey can be extensive.

The inspection method(s) selected depends upon the condition of the structure or funds available. If the conditions warrant an aggressive examination of the structure, the Comprehensive Condition Survey can be performed without the other types of survey.

In all three cases, the methodologies require several personnel to be physically on the breakwater, which has increased safety risk due to the difficult and dangerous walking surface, exposure to open water and in cases where the breakwater does not extend to shore it is necessary for the personnel to embark and disembark from a vessel. If these risks to Corps staff can be mitigated, that is of significant importance.

PROJECT BACKGROUND

The four breakwaters that utilized the technology described in this paper are: San Pedro Breakwater, Middle Breakwater, and Dana Point's East and West Breakwaters.

The San Pedro and Middle Breakwaters are part of the Los Angeles-Long Beach Harbor's three breakwaters. The third breakwater is the Long Beach Breakwater. These breakwaters were constructed during the period 1898-1949. The San Pedro Breakwater is approximately 2.1 miles in length and +14' in height elevation. It is the western-most component of the three breakwater system. The breakwater extends from Point Fermin to Angel's Gate, the 2,100 feet wide opening which forms the main navigational channel to Port of Los Angeles. The original breakwater (STA

0+05 –STA 92+64) is a complex section consisting of rubblemound substructure core and a superstructure consisting of cut and fitted stone blocks.

The last Comprehensive Condition Survey performed on this structure was in 1996. The results from that survey showed that the structure is structurally stable, but an elevation deficiency was observed. The measured elevation differences ranged from 1 to 3.5 feet. It was recommended that an investigation and rehabilitation study be initiated and that the study should involve risk assessment and cost analysis to determine the most cost effective method for structural repair.

The Middle Breakwater is approximately 3.5 miles in length with a +14' crest elevation. The detached breakwater is in between Angel's Gate and Queens Gate, the 2,000 feet wide opening which forms the main navigational channel to the Port of Long Beach. The breakwater is also a rubblemound structure. The last Comprehensive Condition Survey performed on the structure was in 1985. The observation from that survey is that the structure is structurally stable, with no patterns of slope or bearing failure. Both the San Pedro and Middle Breakwaters have had frequently visual walk through inspections since their comprehensive condition surveys were completed.

Dana Point Harbor is located approximately 40 miles southwest of Los Angeles and Long Beach Harbor. The harbor is protected by the East and West Breakwaters, constructed in 1968, it was the last harbor built in the Los Angeles District. The East Breakwater is approximately 0.4 miles in length with a crest elevation of +14'. The West Breakwater is approximately 1.0 miles in length with a crest elevation of +18'. Both breakwaters were designed as semi-permeable rubblemound structures. The last Comprehensive Condition Survey was performed in 1991. In that survey the East Breakwater was evaluated in excellent condition while the West Breakwater had two areas showing some displacement in the armor stones. It was recommended that annual walk through inspections be maintained and the next Comprehensive Condition Survey be performed in 5-10 years. Since the breakwater was designed as semi-permeable, sediment has been seeping through the West Breakwater since the 1980's, causing navigation difficulties in the Main Channel. In addition, the local agencies have reported the poor water quality in an area called "Baby Beach", located on the northwest corner of the harbor. A Comprehensive Condition Survey was due for each of these structures when considering when the last surveys were performed.

SELECTION OF TECHNOLOGY

In 2009, the Los Angeles District was awarded funding from the American Recovery and Reinvestment Act (ARRA) to perform Comprehensive Condition Surveys for San Pedro Breakwater and the two breakwaters at Dana Point. Due to the nature of the funding, which was designated to quickly jumpstart the economy and creating jobs, the District recognized that the contract needed to be award as quickly as possible. The idea of utilizing a vessel based mobile laser and bathymetry survey became the best option given the lessened risk to personnel, the requirement for prompt issuance of contracts and in order to obtain data as quickly as possible to complete the

comprehensive condition survey. It would also provide good baseline information on these two structures for any future studies when needed.

Upon reviewing the initial results of the San Pedro Breakwater survey, the District decided to allocate funding from its Operations and Maintenance budget in order to perform a similar survey for the Los Angeles-Long Beach Harbor Middle Breakwater.

MULTIBEAM BATHYMETRY

Topography and features below the waterline have been surveyed for decades using sonar based technology. Sound pulses are fired from a sensor through the water column and the return time of the pulse to the sensor is used to calculate the range between the sensor and the bottom of the water body. More recently, multibeam sensors have been introduced which collect an array of pulses perpendicular to the vessel's direction of travel many times per second. This technique collects a swath of range observations to map in a push-broom manner. There are several variants of this technology on the market today using either an array of discrete beam observations or interferometric pulses that are continuous across the swath. Accuracies, range capabilities, swath width and distance between observations (and thus observation density) are all variable depending on the sensor and water depth.

In all cases, multibeam bathymetry requires observation of position and orientation of the sensor in order to produce real-world coordinates to each point. In high accuracy applications, which are the subject of this paper, this is typically done using an integrated Global Navigation Sensor System (GNSS – also commonly known as GPS) and Inertial Measuring Unit (IMU – also commonly referred to as Inertial Navigation System (INS)). The GNSS system is used for tracking the precise location of the system and assisting the IMU in tracking the orientation of the system. When tightly-coupling the processing of these two systems, the resulting trajectory of the sensor is typically very accurate and robust in working in most environments.

The final trajectory created using data collected with the GNSS and IMU sensors is processed in conjunction with the range and angle data from the multibeam sensor to create numerous discrete observations typically expressed as XYZ coordinates in the appropriate coordinate system and units for the project.

Because water is heterogeneous in terms of its environmental factors, the speed that sound waves travel through the medium is inconsistent. This is largely caused by variations in density, temperature, pressure and salinity. Observation of the velocity of sound through the water column is required in order to properly model the time required for the sonar pulses to travel through the water and correct for scaling error. Observations very close to the water surface are often subject to random reflection and noise making observations close to the water surface elevation unreliable.

SIDESCAN SONAR (SSS)

For the first two programs (Dana Point and San Pedro Breakwater), backscatter (equivalent to intensity) imagery was collected using the GeoAcoustics GeoSwath system. Effectively, the intensity of the signal's backscatter is observed at the sensor and this is used to produce a panchromatic image of the subsurface. For the Los Angeles Middle Breakwater survey, since the appropriate utilities have not yet been developed to read this information from the R2Sonic system, it was necessary to deploy a separate side-scan sonar device to capture this information for the Middle Breakwater survey. In this case, an Edgetech 272-TD SSS was used recording at 500 kHz. In all cases, the imagery data was mosaiced as the final product for the client.

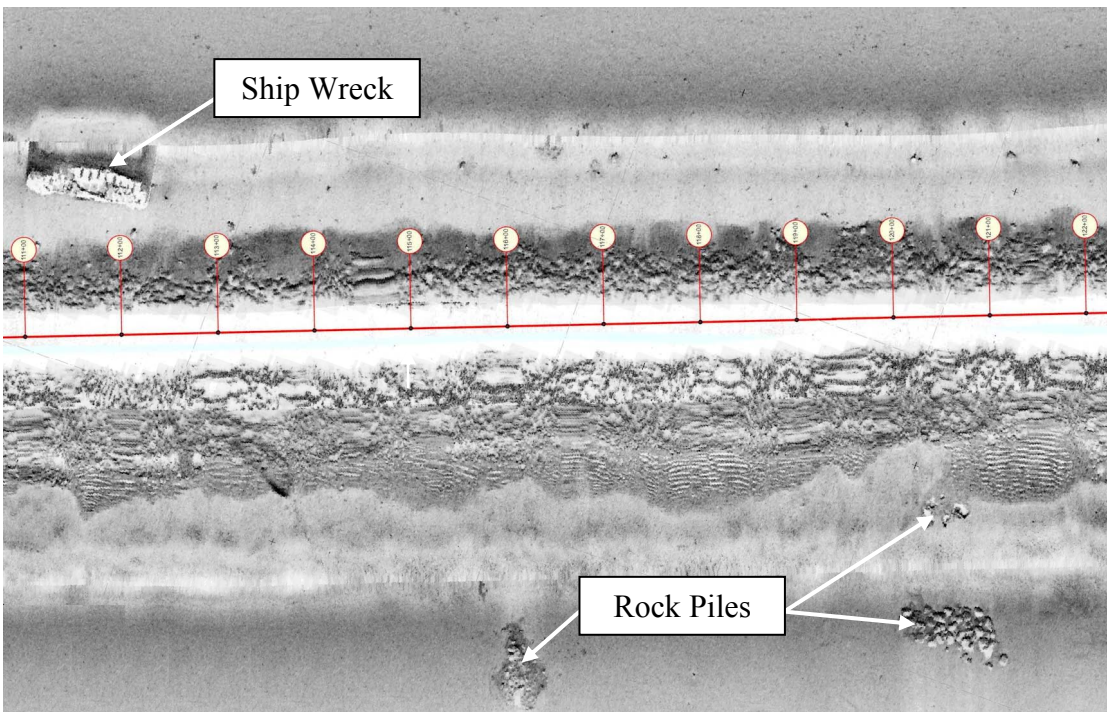


Figure 1. San Pedro Middle Breakwater – Sidescan Sonar Data

MOBILE LASER SCANNING

Laser scanning technology is analogous to multibeam technology although it uses light waves (typically in the near infrared spectrum between 1000 um and 1600 um) for surveying above water. Commercial laser scanners employ oscillating or rotating mirrors to project the ranging beams either in a fan-shaped array or else in a 360 degree circular pattern. Installations of the sensor generally have the scan pattern projected either perpendicular to the direction of travel or else at roughly 45 degrees to the direction of travel. In the later case, the vehicle is often equipped with two scanners. In all scenarios, the scan pattern moves through the area of survey by the motion of the survey platform in the same fashion as a multibeam survey. Near-infrared light is absorbed or reflected by water, therefore it is not possible for mobile laser scanning units to perform observations below the water surface.

Also like with multibeam surveys, position and orientation are critical to producing real-world coordinates for the observations, therefore mobile laser scanning systems are effectively always coupled with GNSS/IMU sensors.

Most laser scanning sensors also capture back-scatter information (referred to as intensity). This can be used in a similar manner as sidescan sonar to produce black and white imagery. When paired with a metric digital camera, color values (red/green/blue) can be extracted as attributes for the laser point cloud as well.

INTEGRATION

Since the respective technologies are limited in their field of view on the opposite side of the water medium, they are well suited to be employed together when projects require information spanning the waterline. Many applications deploy these technologies from the same vessel platform although in some cases, moving the laser scanner to a ground based vehicle can offer additional perspective views for capturing data that is not visible from the vessel. This might commonly include features such as the back side of a levee or building, downstream face of a dam where water conditions might prevent vessel access or the upper deck features of a bridge or pier structure. For water based surveys, the choice of vessel platform is largely contingent on water depth and the draft of the vessel and/or seaworthiness. Vessels with significant draft are not suitable for shallow water operations; however a small vessel may not be sufficiently seaworthy to carryout survey work in the open ocean. Most projects will have specific requirements that will dictate the appropriate platform.

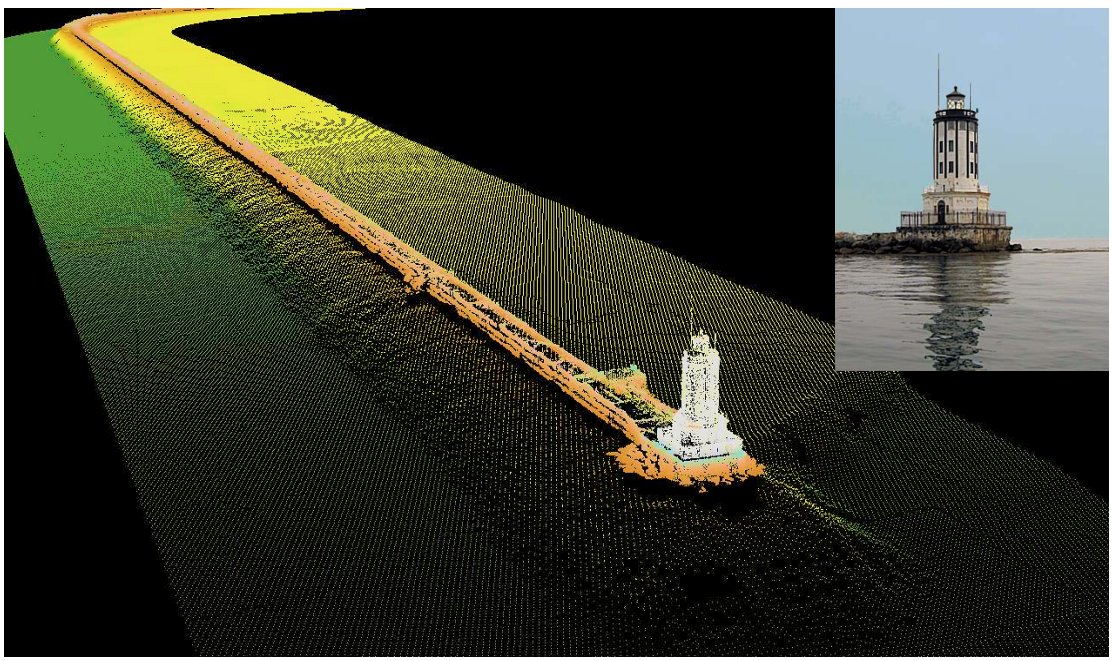


Figure 2. San Pedro Breakwater: Angel's Gate Lighthouse – point cloud data.

DATA COLLECTION

Four breakwaters in three sites were surveyed during three separate mobilizations:

Table 1. Project Information.

Site	Date of Survey	Multibeam	Mobile Laser	Sidescan Sonar
San Pedro	Aug. 13-15/2009	GeoSwath Plus	Optech ILRIS	GeoSwath Plus
Dana Point	Oct. 20-24/2009	GeoSwath Plus	Optech ILRIS	GeoSwath Plus
LA-LB Middle Breakwater	Oct. 7-10/2010	R2Sonic 2024	Optech ILRIS	EdgeTech 272-TD



Figure 3. San Pedro and Middle Breakwaters.



Figure 4. Dana Point Harbor – Area of survey identified in yellow.



Figure 5. Fugro Survey Vessel *Julie Ann* with mobile laser scanner.

In all three projects, data was collected using Fugro's small survey vessel, the *Julie Ann*. All sensors can be deployed from the vessel yet it is small enough to be transported to the necessary sites on a standard vehicle trailer. In all cases, the multibeam data collection was carried out during high tide to maximize the coverage of the breakwater below water while the laser scanning surveys were conducted during low tide to maximize the coverage above the waterline. This methodology allowed for overlap between the two point cloud data sets.

All data surveyed was referenced to Mean Lower Low Water elevations local to each site and surveys were tied to local benchmarks using either Real-Time Kinematic or Post-Processed Kinematic GNSS processing methods. This ensured positional accuracy of the vessel to within a few centimeters and was necessary to achieve the required accuracy and for harmonizing the point cloud data sets.

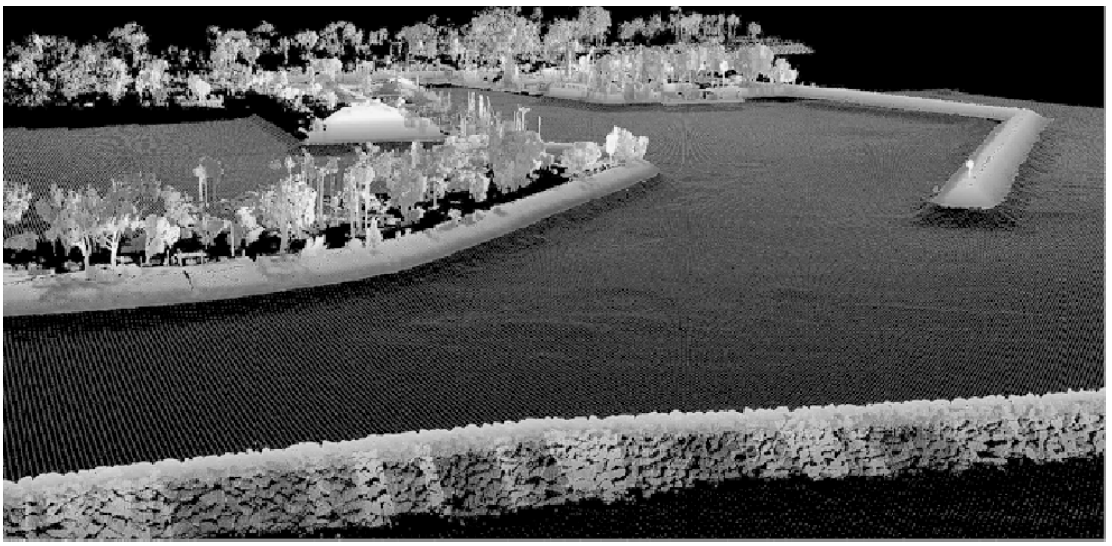


Figure 6. Dana Point – integrated multibeam and laser data.

DATA PROCESSING

Although the laser scanner and multibeam bathymetric sensor both produce point cloud data, initially data processing is done with separate workflows using software that is designed to work with the point cloud data specific to the sensor. In the case of the multibeam data, CARIS was used for generating the point cloud data, editing noise from the point cloud and exporting a cleaned, gridded surface. Sonar sensors can often collect observation data that is erroneous or irrelevant. This could include noise in the water column, vegetation or even fish. In breakwater surveys, the most challenging and prevalent issue is caused by vegetation such as seaweed and kelp. Also, as discussed previously, multibeam data collected above the sensor head has much more uncertainty introduced by the steep angle of the sensor, motion of the water at the surface and the reduced reliability of the sound velocity model. Therefore, some data immediately below the water surface is often trimmed.

For the mobile laser scanning data, it was edited in early projects using Fledermaus and QT Modeler. Later projects used TerraSolid's TerraScan and proprietary point cloud editing software created by Fugro. For laser scanning data, the first step is to remove reflection data caused by multipath of the laser signal being reflected off of the water surface. Infrared light acts in many ways like the visible light spectrum and a high proportion of laser observations that strike the water surface will be reflected and create a multipath signal showing a reflection of the above water topography below the water line. However, there is no significant characteristic that clearly identifies these points as being in error. Intensity (or backscatter) is not sufficiently dampened during multipath to be used for classification of many erroneous points. All laser data below the water line is by nature erroneous since infrared light does not effectively penetrate water or is highly refracted, rendering it very inaccurate. Since water levels change constantly during data collection – from wave action to tidal flux – removal of this data is typically conservative and it is common to sacrifice some good data in order to ensure the absence of erroneous data.

Both data processing methods require trimming back data near the waterline, which would result in a gap in the collected data sets of several inches on either side of the waterline. However because the breakwater projects are all in tidal areas, this was mitigated by collection of the multibeam data at high tide and laser scanner data at low tide and thus having overlapping data. This was also valuable in quality assurance by demonstrating that the data from the laser and multibeam sensors was aligned.

The data from the multibeam and laser sensors was combined in TerraScan, at which time the fit between data sets was verified. Then features that did not represent the breakwater or the seafloor were removed. This largely included data that was again vegetation (seaweed), infrastructure (such as light houses or signage) but the most complex issue was removing birds (pelicans) that were on top of the breakwater. This aspect was the most time consuming and manual aspect of the data processing.

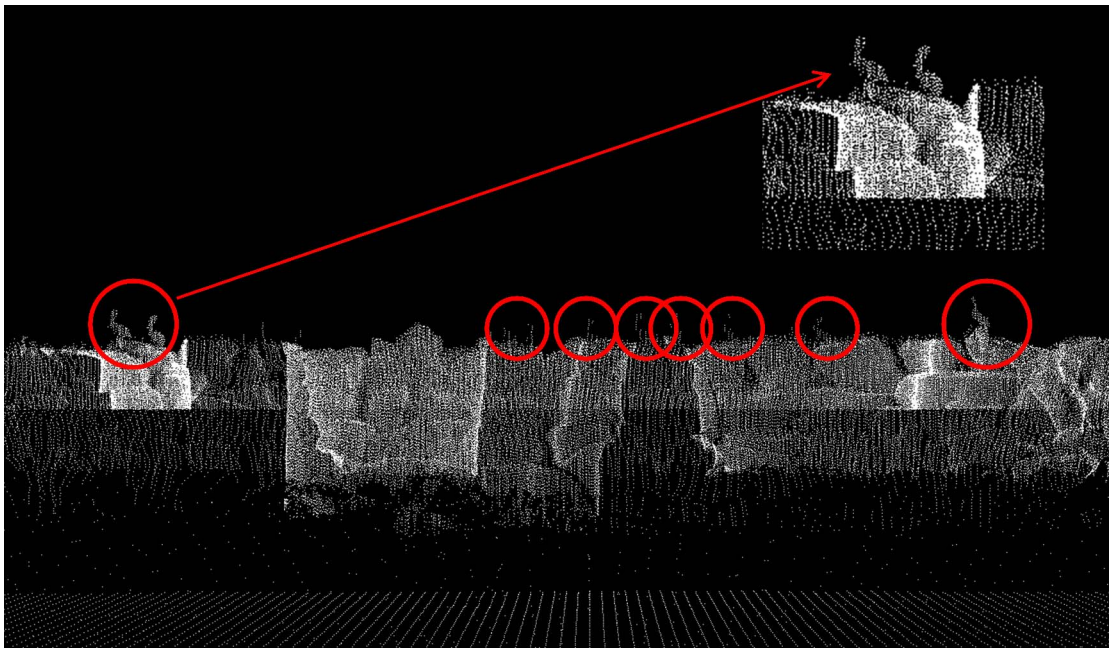


Figure 7. Manual editing of point cloud was required to remove unwanted features such as pelicans and kelp.

Once the point cloud data cleaning was completed, ESRI ArcGIS was used to produce a triangulated irregular network (TIN) and then for creating cross-sections of the breakwater from the TIN. The TIN was also an intermediate step in producing contours for planimetric maps of the sites.

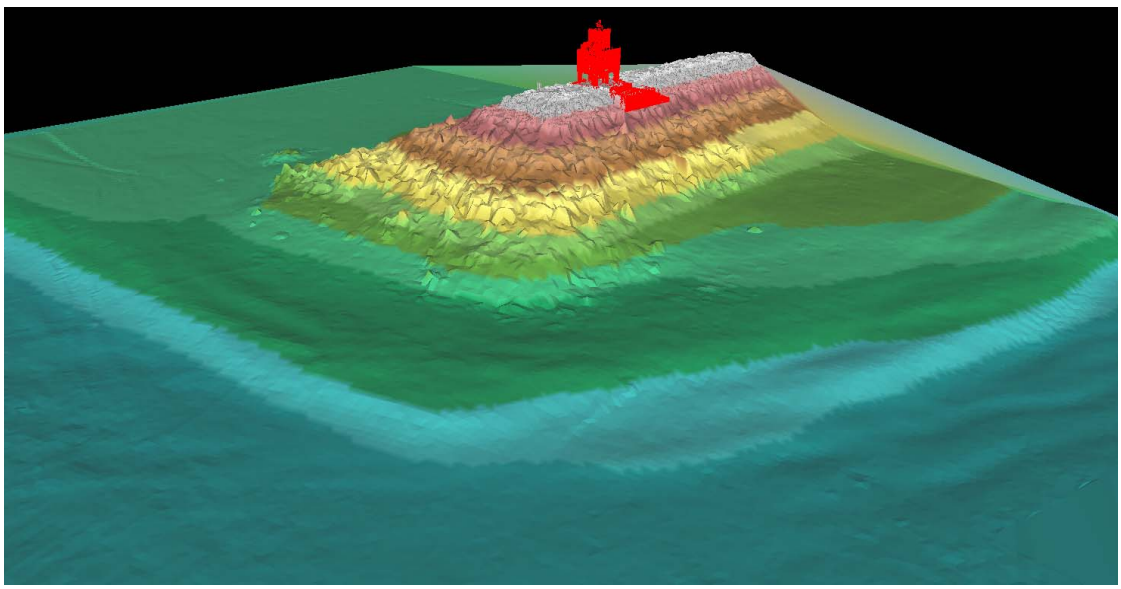


Figure 8. San Pedro Middle Breakwater – 3D TIN Surface. Light house point cloud in red.

APPLICATION OF DATA

The survey data provided a full coverage of the present-day conditions for the San Pedro Breakwater Comprehensive Condition Survey. Also for the CCS, one of the goals was to determine the risk associated with subsidence of the structure. The data collected from the survey has been used to accurately model the breakwater and can be used to predict the subsidence risks. The data collect for the Middle Breakwater have been used to fill in any data gap for the San Pedro Breakwater CCS. The data can also be used as a baseline conditions for the breakwaters for any future studies.

Survey data collected from Dana Point Harbor East and West breakwaters provided an excellent empirical description of the present-day physical conditions of the structures. As mentioned earlier, the additional issues identified at Dana Point Harbor (sediment accumulation in the Main Channel and poor circulation at Baby Beach) prompted the District to subsequently fund a storm Waves, Circulation and Sediment Study. The Coastal Modeling System (CMS), which was part of this study, was modified to address the circulation issue. Survey data collected using this technique was a critical input element for the CMS model.

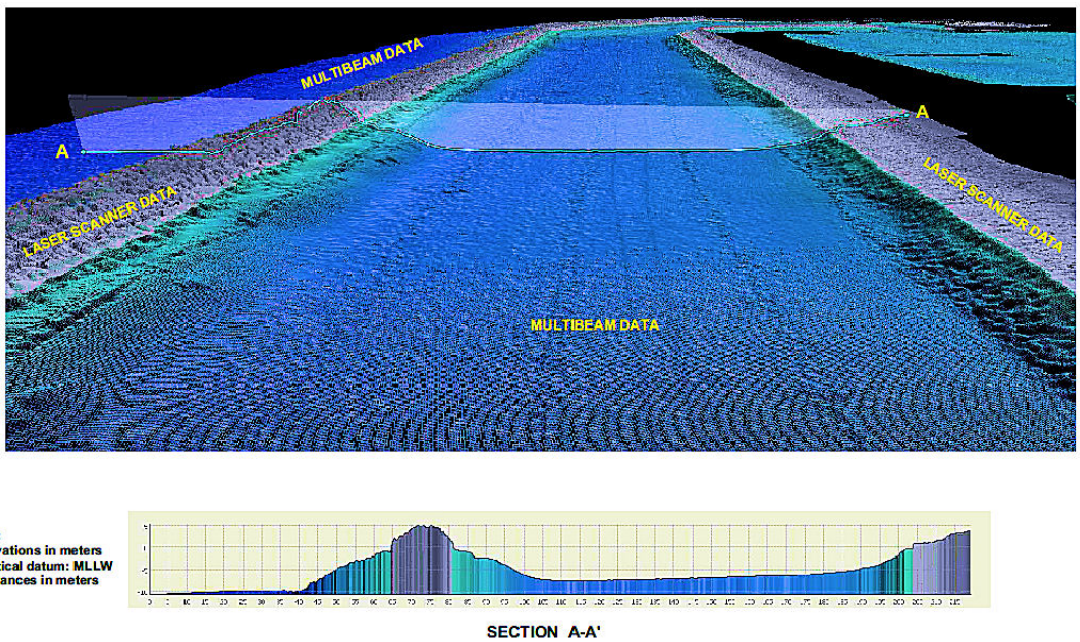


Figure 9. Dana Point – Cross-Sections Through Main Channel and West Breakwater.

FUTURE APPLICATIONS/DEVELOPMENTS/LESSONS LEARNED

The key advantages realized in the use of this system were its reduced exposure risk for personnel, rapid timeline and better coverage in comparison from the previous labor intensive surveys. With the ease of collecting data both above water and below water in couple of passes by the vessel, this application can be utilized on a wider basis. Additionally, the technology could also be applied to other navigational and water retention structures, such as locks and dams, as well as for environmental and ecosystem restoration projects.

As these projects were carried out over the span of more than a year, many lessons were learned and several developments took place. Key among these was upgrading the multibeam technology from the GeoSwath to the R2Sonic system. This was primarily done to achieve higher accuracies and resolution of the underwater data. However another advantage is the R2Sonic's ability to collect back-scatter snippet data which in the near future will be useable for producing imagery essentially equivalent to that provided by the side-scan sonar used on these projects. Integration of a digital metric camera has also been completed, allowing for better interpretation of point cloud data where features (such as birds) can be more readily identified.

Operationally, collection of the bathymetry and laser sensor data both simultaneously at high tide was discovered to provide an additional look angle at the top of the breakwater, which was determined to be valuable when the break water elevation is relatively high. Techniques were developed to keep processing efficiency at a minimum while introducing additional data.

Many iterative developments in the data processing methods and employment of the TerraSolid and Fugro software for point cloud editing. Additional refinement in quality assurance was also developed over the course of the projects. Alternative methods to creating a TIN are being explored to look at ways to possibly better model the breakwater and thus the resulting cross-section and contour data.

REFERENCES

Christenson, G.E., & Ashland, F.X., Assessing the stability of landslides – overview of lessons learned from historical landslides in Utah, *Proceedings for the 16 40th Symposium on Engineering Geology and Geotechnical Engineering*, Logan, Utah State University, 17 p., 2006.

International Hydrographic Organization (IHO), *IHO Standards for Hydrographic Surveys*, Special Publication No. 44, 5th Edition, International Hydrographic Bureau, 2008.

Jaboyedoff, M., Oppikofer, T., Abellán, Derron, M., Loye, A., Metzger, R. & Pedrazzini, A. Use of LiDAR in landslide investigations: a review, *Natural Hazards*, **DOI 10.1007**/s11069-010-9634-2, 2010

Mettenleiter M., Obertreiber N., Hrtl F., Ehm M., Baur, J., Fröhlich, C. (2008), "3D Laser Scanner as Part of Kinematic Measurement Systems", 1st International Conference on Machine Control & Guidance 2008, June 24-26, 2008, Zurich, Switzerland

Mitchell, T., Suarez, G. and Hogan P., 2010. "Integrated Remote Sensing of Bathymetry and Onshore Topography for Asset Inspection, Hydrology Modelling and Hazard Assessment", Remote Sensing and Hydrology 2010 Proceedings and International Association of Hydrological Sciences Red Book (In Print)

Schultz, W. H. (2007). Landslide susceptibility revealed by LIDAR imagery and historical records, Seattle, Washington *Engineering Geology* **89**, Issues 1-2, pp. 67-87, 2007

U.S. Army Corps of Engineers (USACE), *EM 1110-2-1003 Change 1* Engineering and Design - Hydrographic Surveying. Department of the Army, 2004.

U.S. Army Corps of Engineers (USACE), *EM 1110-1-1005* Engineering and Design - Control and Topographic Surveying. Department of the Army, 2007.

Site Planning and Hydraulic Design of a Cargo Seaport Exposed to Typhoons and Tsunamis – A Project Case in the Philippines

E.C. Cruz[1]

[1]Institute of Civil Engineering, University of the Philippines, Diliman, Quezon City 1101, Philippines; PH (632) 927-7149; FAX (632) 4343635; email: eric.cruz@up.edu.ph

ABSTRACT

A methodology for selecting the most suitable seaport site from two or more prospective sites is presented. Hydraulic analyses of the wave climate under prevailing and typhoon conditions are based on simulations using a nearshore wave model. The inland incursion of tsunamis is computed based on prognostic equations of long waves. The selection method is based on the overall rating using a site suitability matrix. The hydraulic analyses are also used in preliminary engineering design of the port dock and in determining the wave conditions for the engineering design of the port structure.

INTRODUCTION

For an archipelagic country like the Philippines, seaports are a vital infrastructure. They are indispensable in the movement of passengers and cargo between the various islands of the country. The bigger ports also serve international cargo and passenger traffic between major islands. Because water transport is more economical than air transport, goods and merchandise that move between various parts of the archipelago and from overseas are handled and distributed primarily via the country's seaports.

Identifying a general location of a seaport site is a critical step in the pre-engineering phase of a new port facility for the distribution of goods and other cargo. Various criteria are usually taken into account at this stage, including business issues, port operations, technical issues, and even those related to political jurisdictions. This step typically identifies two or more prospective sites that meet the determinative criteria. The port facility may include landside components, such as terminal facilities and supply and distribution structures, but it is generally the seaport structure, such as the docking area, that is critical in the overall operations of the port facility.

The judicious choice of the port site is the necessary first step in the planning, design and construction of the port facility. The choice of the best site for the port is an important decision on which the overall economic cost of port construction. In actual cases of erroneous site selection, engineering measures intended to rectify the

pre-planning mistake resulted in undesirably jacking up the costs of engineering design. In worse cases, post-construction retrofitting necessitated by unaccounted forces and hazards present at the site offered temporary alleviation, but finally end up being ineffective. In some other cases, the facility had to be abandoned altogether. One known case of ill port siting is the oil-loading wharf of Standard Oil Company in El Segundo, California, which was unwittingly located along a stretch of the coastline which is a wave concentration zone (Dunham, 1951). For certain wave approach directions and periods, high breaking waves formed at the side of the oil wharf, closing the facility for extended durations.

Identifying the proper port location or selecting the best one from several prospective sites requires correctly evaluating both technical and economic data. On the technical side, information on the physical environment of the prospective sites must be evaluated by carrying out hydraulic analyses to identify the most suitable site. These analyses also determine most of the data needed to undertake the subsequent engineering design for the selected port site.

This paper aims to present a methodology of carrying out the seaport site selection based on quantitative analyses of various technical data and an overall rating of subjective criteria in seaport site selection. The methodology applies to the site planning phase of port development.

SEAPORT SITING – ENGINEERING CONSIDERATIONS

Seaports are perpetually exposed to the action of waves and tides. A reasonably tranquil sea condition is necessary to allow for unhampered loading and unloading of cargo and passengers at the docks. As these operations are performed during normal times, the ambient conditions of the sea must be known under the prevailing waves and tides. It is not enough that waves are low during these times; the waters around the docks must also be not agitated. Sea agitation is caused not only by uneven distribution of wave heights around the port, but also by the interaction of approaching waves with those reflected by marine vessels, seabed features and shore structures. Turbulent agitation can also be caused by approaching waves that break very close to the docks and/or by interaction with nearshore currents generated by these approaching waves. Local wave agitation can also be induced by wave interaction with discharges from river outfalls and sea-bound drainage outflows.

Typhoons and other meteorological disturbances including translating low-pressure areas must be accounted for, as they can cause cargo operations to cease and require special mooring systems for docking. Where such measures are not adequate, a harbor will be necessary to provide protection to all docked and moored vessels.

In sites along coastlines that are susceptible to seismic events, the hazards posed by tsunamis must also be assessed. While proximate tsunamigenic sources are the immediate concern, tsunamis generated even by distant sources can cause critical damage to a prospective site. The spatial extent of tsunami incursion must be determined prior to site development planning.

Plan-form areas of adequate navigable depth must be available in the prospective site to allow for the safe passage of ships into and out of the port. A navigable basin area must also be available for safe maneuvering of vessels around the docks of a harbor. For docks that are not contiguous with the shore, the required access pier must not be overly long as to become a cost-prohibitive component of the port facility.

Prior to port site selection, an overall characterization of prospective sites is undertaken to short-list those meeting critical technical criteria discussed above. In a siting study for a cargo port in the Philippines, two prospective sites shown in Figure 1 were identified. Site 1 is along an undeveloped mildly sloping coast, while Site 2 is close to an existing port facility area that has been damaged by tropical storms.



Figure 1. Photos of prospective sites: (left) Site 1, and (right) Site 2.

Figure 2 shows the mean depth distributions obtained from bathymetric surveys commissioned for the two sites. In conjunction with secondary data, these primary data provide the necessary input to the technical evaluation of the sites' port-hosting suitability, discussed below.

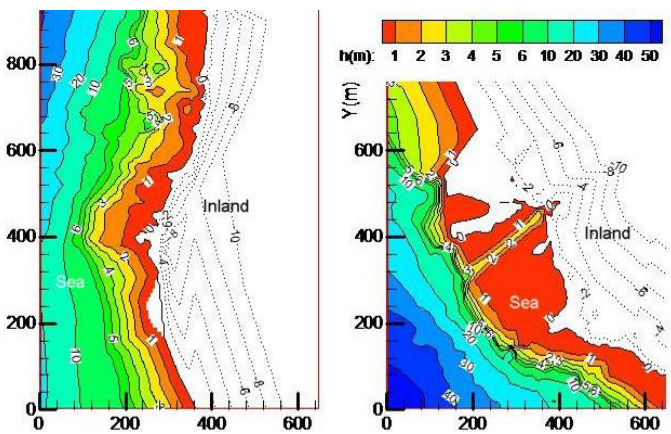


Figure 2. Nearshore bathymetry of candidate sites: (left) Site 1, (right) Site 2.

HYDRAULIC ANALYSIS OF WAVE CLIMATE

In the port's pre-engineering phase, knowledge of the prevailing wave climate around the prospective sites is crucial to the site suitability assessment. Such knowledge is

needed in identifying the location of the loading area and the zones in the nearshore that are tranquil most of the time, which can be used for the mooring of small vessels. Wave climate information is also used to estimate the durations of loading and unloading of cargo in the docks. In order to predict the prevailing wave height distribution around the port, a model of wave transformation is usually applied together with estimates of offshore wave conditions. A Boussinesq-type model of wide frequency dispersion range applicable to impermeable seabed (Cruz et al., 1997) is used for this purpose, which can be written as:

$$\frac{\partial \eta}{\partial t} + \nabla \cdot [\mathbf{u}(h+\eta)] = 0 \tag{1}$$

$$\frac{\partial \mathbf{u}}{\partial t} + (\mathbf{u}\cdot\nabla)\mathbf{u} + g\nabla\eta + \frac{h^2}{6}\left(\nabla\cdot\frac{\partial \mathbf{u}}{\partial t}\right) - (\tfrac{1}{2}+\gamma)h\nabla\left(h\nabla\cdot\frac{\partial \mathbf{u}}{\partial t}\right) - \gamma g h\nabla[\nabla\cdot(h\nabla\eta)] + \mathbf{F}_b + \mathbf{F}_s + \mathbf{F}_w = 0 \tag{2}$$

where $\eta(x,y,t)$ is the water surface displacement from still water level, $\mathbf{u} = (u,v)$ the depth-averaged fluid particle horizontal velocity vector, (x,y) the horizontal coordinates, t time, $\nabla = (\partial/\partial x, \partial/\partial y)$ the horizontal gradient operator, γ the frequency dispersivity extension factor, g the gravity acceleration, $\boldsymbol{F_b}$ the wave-breaking energy-dissipation term, $\boldsymbol{F_s}$ the structure-induced damping term, and $\boldsymbol{F_w}$ the bottom friction term. Equations (1) and (2) express the mass continuity law and the principle of momentum conservation for wave motion. The model is valid from relative depths (h/L) ranging from deep water to the shallow waters typically found around sea ports.

The input to the model includes the still-water depths $h(x,y)$, initial values of the water surface elevations and velocities, wave conditions at the offshore boundary, and parameters of spatial and time discretization. The model solves for the unknown η and $\mathbf{u}$ at all grid points and time steps, from which the wave heights and other hydrodynamic parameters, such as breaking location and wave-induced currents, are determined. The numerical implementation of the wave model above and its verification are discussed in Cruz et al. (1997), and applications to harbor wave studies are discussed in Cruz (2007b).

The wave conditions needed to compute the nearshore wave fields are the height, period, and direction of the incident waves at the offshore boundary of the computational domain, which is typically located in deep water. These offshore wave conditions are hindcast based on data of surface wind speeds and directions, effective fetch and wind duration. The conditions are associated with a statistical offshore wave, which is then parameterized in terms of wave frequency and directional distribution depending on the type of wave input, i.e. regular or irregular waves with various frequency components, and directional distribution (Horikawa, 1988).

Figure 3 shows the wind rose diagram for a typical year of the project sites in Figure 1. This summarizes the frequency occurrence and directional distribution of surface winds from a long record at a wind station closest to the sites. These location- and elevation-specific wind data are converted to offshore surface wind data based on

certain hydraulic and geodetic information of the wind station, including distance from the coast, and wind vertical distribution profile (PPA, 1995). After an analysis of the wave effective fetches of the site, a hindcast of the prevailing offshore waves in deep water is undertaken, some results of which are shown in Table 1. The table shows the height and period of the significant wave in deep water. The significant wave is a statistical wave that represents the average of the highest one-third of all waves expected to pass the deep water location (Dean and Dalrymple, 1992).

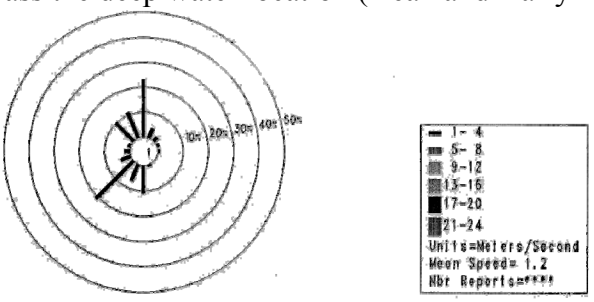


Figure 3. Windrose diagram.

Table 1. Offshore wave hindcast

Surface wind		Significant Wave	
Direction	Speed (m/s)	Height (m)	Period (s)
NW	1-4	0.52	3.06
WNW	1-4	0.76	3.60
W	1-4	0.72	3.47
WSW	1-4	0.63	3.15

Figures 4 and 5 show the local wave climate around the port sites simulated using the wave model above under prevailing wave conditions for a potentially critical offshore wave approach from the west northwest, simultaneously with a mean high tide. In this case, the height and period of the deep water wave are 76 cm and 3.6 seconds (see Table 1). In both figures, the first plot provides an image of the transient water surface configuration, revealing the wave transformation patterns around the seaport site. The second plot shows the post-processed wave height distribution.

Figure 4 reveals the wave transformation patterns close to the shore, consisting largely of wave refraction and breaking. The wave height distribution reveals that along the coastline of the seaport site, wave energy concentrations (red zones) appear at certain areas for this approach direction.

Figure 5 shows the corresponding nearshore wave field of Site 2 when offshore waves approach from the same direction. The snapshot of the transient water surface reveals the refraction and diffraction patterns caused by that site's seabed and coastal plan-form. The resulting wave heights indicate the wave breaking zones on the steep-sloped convex-shaped seabed and the relatively sparse energy focusing (red zones) in the foreshore (region between breaking points and the shoreline). The zones of calm waters, i.e. low waves (blue zones), are also revealed.

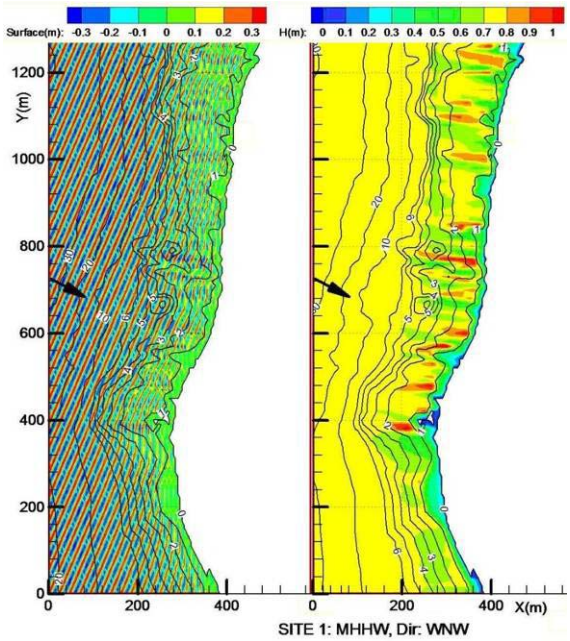


Figure 4. Simulated wave climate at Site 1.

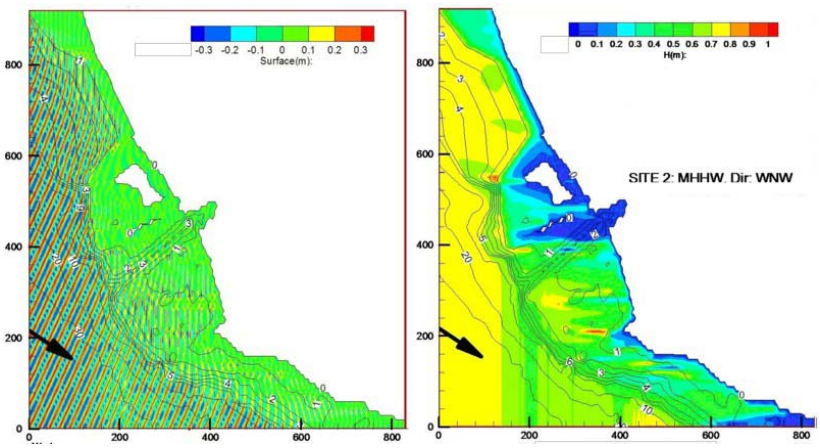


Figure 5. Simulated wave climate at Site 2.

ACCOUNTING FOR TROPICAL STORMS

Astronomic tides, caused by the forces of attraction between the moon and earth, are important forcing not only in the wave climate around port sites, but also in the vertical siting of the port docks. Records of mean sea surface movement at tidal stations at several coastal locations around the country are routinely synthesized and published annually (Namria, 2007). This tide table also provides a forecast of the tidal fluctuations at the same stations. A one-week window of such tide fluctuations in January is shown in Figure 5, plotted against time in days. This shows the typical tidal characteristic of most coastal locations in the Philippines, which consists mostly of semi-diurnal patterns, when two high tide peaks and two low peaks occur within a day, and diurnal patterns, when a single high and low tide occur daily.

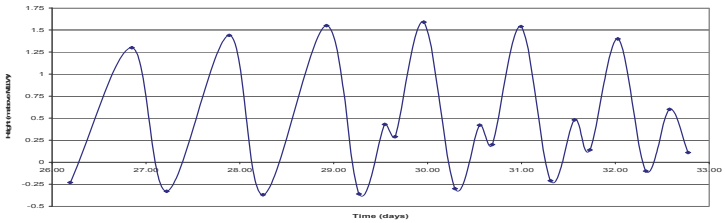


Fig.6 Tide fluctuations (one week)

The syntheses of recorded tide fluctuations are also published in the tide table. These include tide statistics and extremes, such as MHW (mean high water), MTL (mean tide level), HWL (high water level), etc. Due to the semi-diurnal characteristic of Philippine tides, statistics such as MHHW (mean higher high water) and MLLW (mean lower low water) are more important in wave climate analyses and port design.

Tide-associated water level movements are accounted for in wave climate analyses by adding the corresponding tide fluctuation to the mean depths shown in Figure 2. It is thus important to correctly tie the survey with the Namria datum. Figure 7 shows the simulated wave field for Site 1under the same conditions as those in Figure 4, except that the water level is at the lower tide level of MLLW. It is seen that, in addition to a seaward migration of the shoreline, a low tide level also results in substantially difference wave height distribution around the port site. In general, wave heights fronting the shore are smaller. This low wave height is attributed to the early onset of wave breaking resulting from smaller effective depths during low tide. It must be noted however that tide fluctuation effects on wave climate vary from site to site because the slopes, depth distribution, and shoreline shape are very location-specific. The tide levels also affect the vertical siting of the pier docks which is part of the hydraulic design of the port facility.

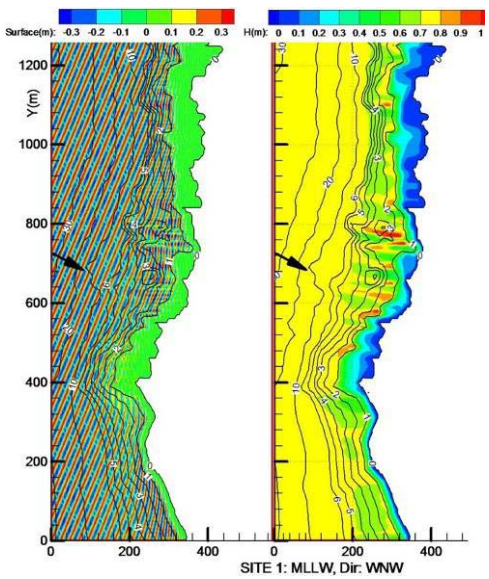


Fig.7 Prevailing wave climate at Site 1 at low tide MMLW

The strong winds of tropical storms generate large surface waves that approach a distant coastline without being dissipated until they break. Depending on the slope of the seabed and the "steepness" of the approaching wave, this breaking point can be very close to the shore. In addition, the translating low-pressure area in the middle of the storm can track very close to a prospective site and cause considerable increase of water level, called "storm surge", especially near the coast where the waters are shallow and are thus prone to the wind's sucking action. This may lead to coastal flooding and further increase the potential damage to a seaport by the already huge approaching waves.

When storms turn into typhoons with maximum gust speeds exceeding about 32 m/s, the potential damage can be catastrophic. It is generally difficult to predict the track of a typhoon, so that a realistic accounting of such storms can be made by hindcasting the local waves probably induced by one or more historical storms that tracked the prospective sites. The maximum gust speed of such historical storms, available from published data of climatological extremes of PAGASA can be used as basis of offshore wave conditions to simulate the typhoon-induced local wave field. The storm surge for open marine locations such as port sites can be estimated from the historical water levels in tide tables.

Figure 8 shows results of simulation of the wave field induced in Site 1 due to a historical typhoon that generated winds from WNW. The storm surge is accounted for as an input elevated water surface throughout the domain. The transformation of the approaching high waves (left plot) is prominent in the shallow waters of the port site, which results in conspicuous wave energy concentrations (right plot) along the coast. Hydrodynamic effects of offshore features, like the circular shoal at 30-meter depth which causes wave scattering leeward, are also revealed. Wave breaking is also prominent but does not seem to be depth-controlled, resulting in relatively calm waters shoreward of the breaking point. This simulation results reveal the unsuitable areas for the prospective port, i.e. where waves are largest, mainly in front of the submerged headlands.

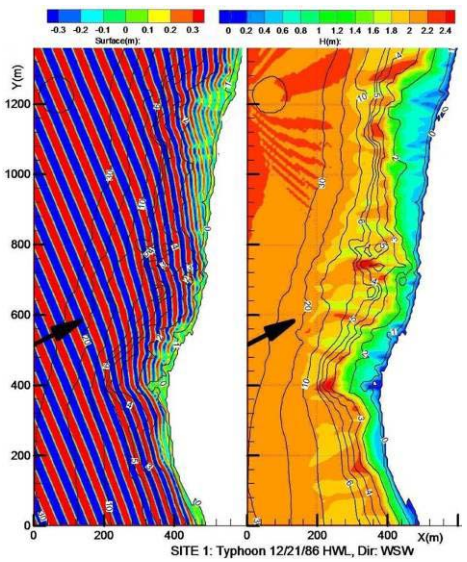


Figure 8. Typhoon-induced wave field at Site 1.

Figure 9 shows the corresponding results under the same typhoon for Site 2, which appears to host smaller and less intense wave concentration zones, and yields wider calm waters in its foreshore area.

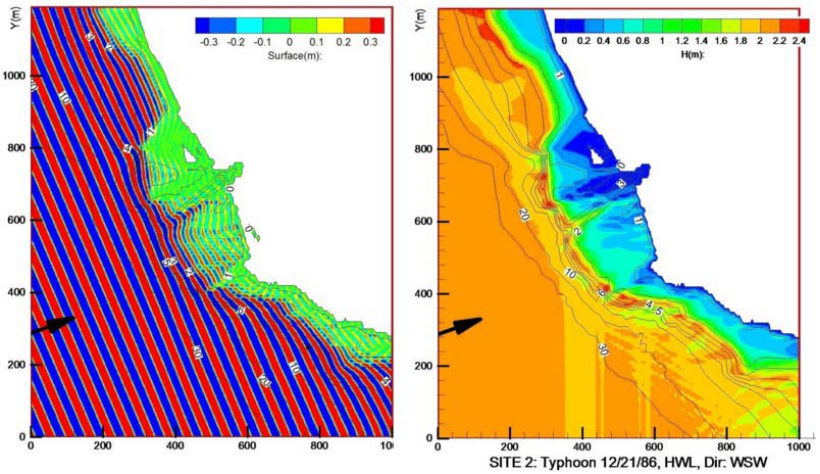


Figure 9. Typhoon-induced wave field at Site 2.

ACCOUNTING FOR OCEAN HAZARDS – TSUNAMIS

Seaports are exposed to the hazards of the oceans. Sites near seismically active seas have to be assessed for their susceptibility to incursion by tsunamis that may be generated by submarine earthquakes from both near and far sources. The South Asian tsunami of December 2004 and the March 2011 Japan tsunami disasters, for example, highlight the importance of accounting for such unusual but potentially catastrophic event.

Being situated along the seismically active Pacific Ring of Fire, the country has most coastlines exposed to tsunami hazard. Following a tsunami susceptibility analysis of the project coast, which established the existence of both near-source and far-source tsunami generators, a quantification of tsunami incursion into the prospective sites is performed to assess the inland extents of the highest historical tsunamis as well as of potential tsunami events. To estimate the tsunami parameters offshore, historical data of tsunamigenic seismic events and tsunami-induced runup observations along proximate coastlines are obtained from a tsunami event database (USNGDC). For the prospective sites of this project, Table 2 lists 4 pertinent tsunamigenic events from among those returned by the NGDC database search. The following additional data are used to estimate the offshore conditions of the strongest historical tsunami: (a) location of the source trench of the tsunami event; (b) target coast; (c) seabed topography between source and target including shoals, ridges, etc.; and (d) ground elevation and location of observed tsunami runup.

Tsunami incursion analysis applies the following equations:

- Wave runup equation for long waves based on Miche formula, for partial standing waves whose surf-similarity parameter extends beyond the upper limit for the usual wind waves

- Wave breaking criterion of Le Mehaute and Kho (1967) based on bed slope and deep water wave steepness. This criterion may indicate breaking or non-breaking wave condition prior to runup. This criterion is used to locate the point of breaking seaward of the effective shoreline.
- Breaking height of tsunami wave based on Weggel (1972) which also depends on both the seabed slope as well as the breaking wave steepness.

Table 2. Tsunamigenic events near the project site

Tsunami Event	Year/Mo/Day	Earthquake Magnitude
1	1910/12/30	6.2
5	1922/03/01	6.0
6	1923/07/18	5.5
9	1952/03/19	7.7

A computer code is applied to implement the procedure using offshore-to-land profiles along selected transects (see Figure 10) as primary data. In summary, the incursion computations account for the following input data: (a) tsunami conditions offshore including height, period and approach direction; (b) tide levels; (c) nearshore bathymetry; and (d) surface topography. For a potential tsunami case, the tsunami offshore conditions are estimated from the potential earthquake intensity associated with the tsunamigenic trench, which is part of the geologic study for the sites.

Figure 10 shows tsunami incursion maps for Site 2. The left plot is for a historical tsunami height of 11 cm, while the right plot is for a potential tsunami height of 5 cm. Two incursion limits are marked for each: one for a low-tide scenario, the other for a high-tide. It is seen that a higher tsunami induces a stronger penetration inland of tsunami. However, contrary to expectation, a high tide does not necessarily lead to more inland movement of a tsunami wave. Details of the theory and numerical implementation of the incursion analysis are found in Cruz (2007a).

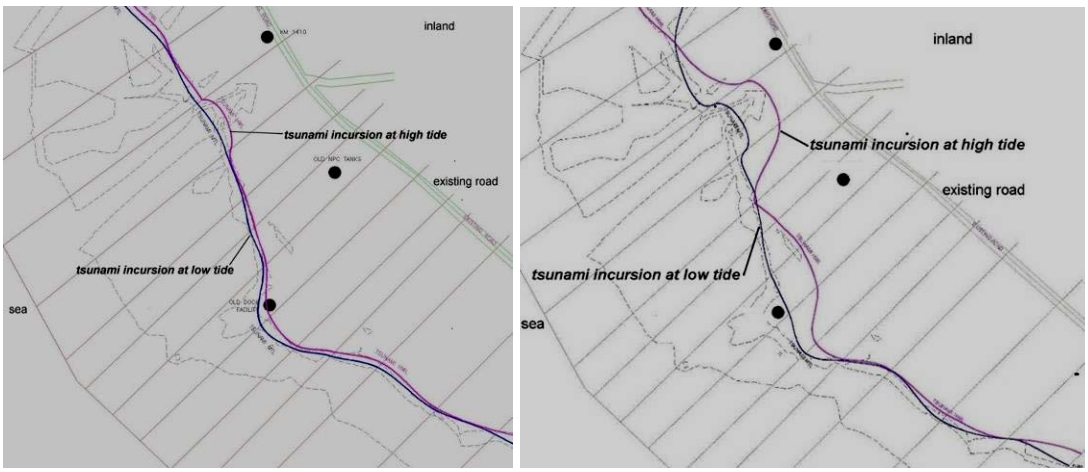


Figure 10. Incursion map for (left) historical, and (right) potential, tsunamis for Site 2

Information on tsunami susceptibility and the incursion map are both useful not only in port site suitability analysis but also in the development planning of the selected site. For example, permanent structures and those designed with low risk exceedance limit should be located outside the tsunami-prone areas. In the disaster response strategy of port operations, the incursion map is useful in locating a suitable evacuation area for personnel and sensitive port facilities. This is particularly important for port sites with limited backshores, such as those near coastal bluffs.

SITE SUITABILITY EVALUATION

To select the most suitable seaport site among prospective ones, a port-hosting suitability matrix is completed (Table 3). This matrix incorporates the results of the various technical analyses above and allows for subjective weighting of the relative importance of other considerations including, for example, proximity to existing transport network, the suitability to port operations of existing adjacent topography, the long-term viability of port operations as limited by siltation, and the presence of coastal structures that may affect the port water tranquility.

Table 3. Seaport site suitability matrix.

Criterion	Subjective Weight	Site 1	Site 2
1. Local prevailing wave climate	1.0	1	3
2. Typhoon-generated local waves	1.0	2	3
3. Bathymetric location	0.75	2	3
4. Length of access pier(s)	0.75	3	2
5. Tsunami Incursion	0.50	3	1
6. Other considerations			
• Transport network	0.25	2	1
• Existing coastal structures, etc.	0.25	3	1
	Overall rating	2.0	2.35

Paramount issues are indicated by higher weights, and the suitability of each prospective site is quantified by objective ratings (increasing scale) based on the foregoing technical analyses. The prospective site with the highest weighted overall rating should come out as the most suitable seaport site. For this project, Site 2 is the more suitable with a qualified rating of 2.35 on a scale of 1 to 3, 3 being the highest.

HYDRAULIC DEISGN OF SEAPORTS

Bathymetric Siting. The siting of the docks depends mainly on the existence of an adequate marine area that can accommodate the required minimum draft of vessels to use the port. The design ship metrics, including its dead-weight tonnage, and the bathymetric profile of the site are hence necessary information in the cross-shore siting of the dock. Where several possible locations are available along the prospective property, the necessary longshore siting must be based on the results of

wave climate analyses for both prevailing offshore wind and typhoon conditions. Extreme tide levels, including the recorded lowest and highest values, must also be considered in both cross-shore and longshore siting. The lowest tide normally governs the cross-shore siting of large-draft ships.

Figure 11 shows a possible scheme of siting and layout of the pier for Site 1 based on these factors. In this case, two design ships are specified with metrics. The sea-side of the pier serves as a cargo dock and the shallower shore-side will host a smaller tanker. Once identified, the location of the pier is used to layout the required access pier to obtain information for comparing the indicative costs of the docks and for landside facility planning. Ship metrics and the other data above can be integrated with the results of wave field analyses to determine hydraulic design parameters for the piers, such as required minimum deck elevation.

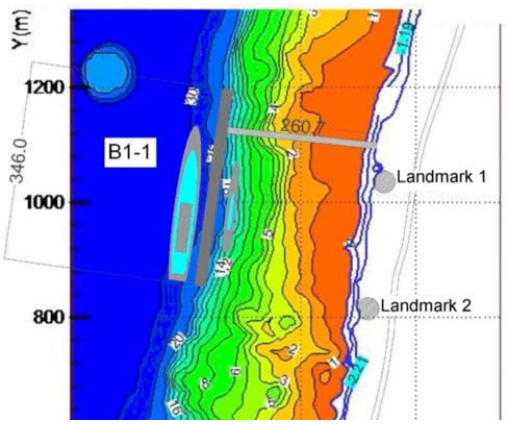


Figure 11. Bathymetric siting and layout of pier, Site 1.

Deck elevation. The vertical location of the pier docks is an important input to the structural design of the dock superstructure and substructure (foundation). Minimum elevation requirements of docks are prescribed in engineering design of ports and other similar facilities (eg, PPA, 1995). These requirements must be complemented by the results of quantitative analyses for typhoon-induced storm surges and the maximum wave heights around the port site. The vertical location of the dock will additionally depend on the acceptable risk for wave overtopping, if it is allowed at all. Design requirements may also exist for certain types of seaports, such as those used for Ro-ro vessels or those that need to allow passage of smaller vessels (USACE, 2004; OCDIJ, 1991)

Dock alignment. Berthing areas for standard vessels are required to meet certain geometric requirements depending on the type and dead-weight tonnage of the ship. These requirements are used to determine the minimum length of the pier dock(s). Based on the syntheses of wave climate analyses, one or more schemes of satisfying these dock requirements can be laid out. One such scheme is shown in Figure 11 for an open dock layout, that is, docking on either side of the pier is allowed. The

minimum length of the access pier is determined based on the tide-induced water levels at the site. Typically, the access pier is tied to a ground area at the MHHW level. In some cases where short docking time is allowed, the docks are located in shallower water to save on the cost of the access pier.

Table 4 shows the lengths of the piers for two plan-form alignments of the port docks, one of which is shown in Figure 11. The access piers are tied to ground at MHHW. Economic considerations may govern the selection of the suitable alignment.

Table 4. Pier lengths.

	Docking Pier Length (m)	Access PierLength (m)
Scheme B1-1	201	173.3
Scheme B1-2	201	162.0

Design wave conditions. Data of wave conditions for the structural design of the port structures can be synthesized from the wave climate analyses. These include the wave period and wave heights for each of the critical approach directions of incident waves. The critical wave conditions are usually governed by typhoon or tropical storm conditions.

Unlike other types of civil engineering structures, the conditions for the structural design of coastal structures depend on the type of structural material. Structures made up of flexible material such as timber marine piles or rubble-mound gravity structures are designed with lower design wave heights. In comparison, structures that are considered rigid, such as steel piles or reinforced-concrete bulkheads of wharf docks, are designed with higher wave heights (CERC, 1984).

Table 5 summarizes the design wave conditions for the plan-form alignment in Figure 11. Since the wave height (H_D) is the most critical design parameter for the dock structure, an accurate numerical determination based on the foregoing hydraulic analyses is thus warranted.

Table 5. Design wave conditions.

Direction	Wave Period (s)	H_D (m), Flexible type	H_D (m), Rigid type
W	4.4	2.9	3.8
WNW	6.7	3.0	4.0

CONCLUSIONS

Hydraulic analyses are necessary for the siting of seaports. These are facilitated by the use of a wave model for seaports which allows the quantitative assessment wave heights around the site. The analyses must consider the prevailing wave conditions as well as those under typhoons or tropical storms. Various water levels corresponding

to site-specific tide characteristics must also be accounted for. For areas susceptible to seismic events, tsunami hazard must also be assessed.

Where two or more sites are involved, the selection of the most suitable location must be based on an overall rating of the sites based on the results of the hydraulic analyses and a subjective weighting of the criteria appropriate for the port use and operations. The site with the highest overall rating is the most suitable seaport-hosting site.

Together with design ship dimensions and other requirements, the results of wave climate analyses are also used in the engineering design of the selected port site.

REFERENCES

Coastal Engineering Research Center (CERC). (1984*). Shore Protection Manual, Volumes I and II, 4th Ed.,* U.S. Government Printing Office.

Cruz, E.C. (2007a). "Computation of tsunami incursion on coastal terrains." *Proceedings, 2007 Phil. Inst. Civil Engineers. National Midyear Convention,* PICE. WRE 1-16.

Cruz, E.C. (2007b). "Wave climate studies in coastal harbors." *Proceedings, 33rd Phil. Inst. Civil Engrs. National Convention, Cebu City.* WRE 1-9.

Cruz, E.C. (2008). "Seaport site selection based on coastal engineering analyses." *Proceedings, 6th Regional Symposium on Infrastructure Development, Bangkok, Thailand*, 96-101.

Cruz, E.C., M. Isobe, and A. Watanabe (1997). "Boussinesq equations for wave transformation over porous beds." *Coastal Eng.*, Vol.30, Nos.1-2, 125-156.

Dean, R. and Dalrymple, R. (1992). *Water Wave Mechanics for Engineers and Scientists*, World Scientific Publishing, Singapore

Dunham. J.W. (1951). "Refraction and diffraction diagrams". *Proceedings, 1st Conference Coastal Engineering*, ASCE, 33-49.

Horikawa, K., ed., (1988). *Nearshore Dynamics and Coastal Processes.* University of Tokyo Press.

Le Mehaute, B. and R.C.Y. Kho (1967) "On the breaking of waves arriving at an angle to the Shore", *Jour. Hydraulic Research*, Vol. 5, No.1, 67-88.

National Mapping and Resource Information Authority (2007). *2007 Tide and Current Tables, Philippines Coast and Geodetic Survey Department.*

Overseas Coastal Area Development Institute of Japan (OCDIJ). (1991). *Technical Standards for Port and Harbour Facilities in Japan, New Edition.*

Philippine Ports Authority (PPA). (1995). Design Manual for Port and Harbor Facilities in the Philippine Ports Authority.

United States Army Corps of Engineers (USACE). (2004). *Coastal Engineering Manual*

United States National Geophysical Data Center (USNGDC). http://www.ngdc.noaa.gov

Weggel, J.R. (1972) "Maximum breaker height", *Jour. Waterways, Harbors, Coastal Eng. Div.*, ASCE, Vol.98, No. WW4

Measurement of Structure Response to Ferry Berthing Loads

Jonathan Hutchinson, M.S., E.I.T.
Alaska Department of Transportation
& Public Facilities

Andrew T. Metzger, Ph.D., P.E.
Assistant Professor
University of Alaska Fairbanks
College of Engineering and Mines
(primary author)

Abstract

The load environment from side-berthing ferry landings is not well understood. This is due, primarily, to a lack of information for loads from ferry-class vessels. As a result, a great deal of uncertainty exists when designing such structures for vessel impacts. The intent of this study is to fill, at least in part, existing knowledge gaps related to load demands on ferry landing structures from vessel impact. This manuscript will focus specifically on a means for acquiring strain, displacement and approach velocity measurements at active ferry landings. This is accomplished using traditional instruments for measuring strain and deformation; coupled with modern data acquisition equipment. The result is a system that monitors structural response metrics that are useful to engineers tasked with analyzing and designing ferry landing structures. The automated system is a practical approach to studying multiple berthing events and allows collection of a statistically-significant sample - providing a pathway to reliability-based design criteria. Preliminary results of approach velocity and elastic potential energy of the structure due to berthing action will also be presented to demonstrate the utility of the automated data acquisition system.

INTRODUCTION

The Alaska Marine Highway System (AMHS) is a vital part of the transportation system in Southeast Alaska; connecting over 33 ports, many of which are only accessible by air or sea. The Auke Bay ferry terminal facility in Juneau operates year round and over 150,000 passengers and 30,000 vehicles pass through this terminal each year.

Measurements from berthing events at the Auke Bay ferry landing are being collected and recorded using an automated system consisting of motion sensors, strain gauges, tide gauges and linear motion transducers (LMT's) all connected to on-site dataloggers. This system allows us to acquire statistical samples of berthing parameters during regular operation of the terminal. The parameters studied included berthing energy and approach velocity.

A goal of this project is to collect a statically significant sample of vessel berthing parameters. This information would then be used to develop reliability-base berthing velocity and energy design criteria with an acceptably low probability of exceedance. Ideally, this information will be calibrated with existing design standards; like the AISC steel manual and ACI 318. Is so doing, design engineers could apply current standards with confidence and without the need for assumptions required by current approaches used to design vessel landing structures.

To demonstrate the utility of the automated system, we will present preliminary results from velocity measurements. We will also be demonstrated how the elastic potential energy in the structure, due to the action of the vessel, is extrapolated from fender displacement measurements.

LITERATURE REVIEW

The typical design methodology for vessel berthing structures is based on a quasi-static kinetic energy method. In this method, the apparent kinetic energy of the vessel is equated to the elastic potential energy of a deformed structure.

In the kinetic energy method, berthing energy is estimated based on the vessel's apparent kinetic energy and a number of berthing coefficients. Berthing energy is taken to depend on the approach velocity of the vessel, the displacement of the vessel, and a series of coefficients that compensate for a number of factors that can affect the magnitude of the energy.

The general kinetic energy design equation is as follows (Gaythwaite):

$$E_f = \frac{W}{2g} V_n^2 C_e C_m C_c C_s$$

Where:

C_e= Eccentricity coefficient, which accounts for the vessel's rotation (i.e., angle of approach), typical values range from 0.5 to .8

C_m= Virtual mass coefficient, which accounts for added mass due to entrained water, typical values range from 1.3 to 1.8

C_c= Configuration coefficient, which accounts for pier type and geometry, typical values range from 0.8 to 1

C_s = Softness coefficient, which accounts for the relative stiffness of the vessel hull and fender, typical values range from 0.9 to 1

W = Displacement of the vessel

V_n = Component of vessel's velocity normal to the pier.

E_f = Kinetic energy transferred from the berthing vessel to the structure

While the kinetic energy method is readily used in design, its accuracy is also highly dependent on the selection of suitable berthing coefficients and approach velocity. The results of the analysis must often be coupled with past experience to develop an effective design.

The state of practice for ferry landing design has, in general, lagged behind other fields of structural engineering. This is apparent as there is no generally accepted design standard for vessel berthing structures, and berthing demand information is very limited. Most available information on this topic is for military or large cargo vessels such as oil tankers and container ships. Improved understanding of vessel loads on ferry landings will reduce uncertainty when designing such structures and likely lead to more cost effective and reliable designs.

Statistical Approach

One approach to the vessel berthing problem is the use of statistical data, typically consisting of a set of physically measured parameters such as fender deflections, environmental conditions, and vessel approach velocities. Berthing energies are deduced from these measurements and described statistically.

The statistical approach considers the relationship between berthing frequency and probability of exceedence of a design energy threshold. With this philosophy, the structure may be proportioned so that the probability of experiencing berthing energies in excess of a structure's design energy is acceptably low. This will imply that the structure is designed for an acceptable level of risk.

(I.A. Svendsen, 1970) conducted a study on the impact energies of a wide range of ships ranging from a few hundred DWT to 90,000 DWT. The energies from 750 total maneuvers were recorded and measured at three different harbor sites in Denmark, then graphed against probability of exceedence. This was accomplished using a mechanical device attached to a tape measure.

(B.F. Saurin, 1963) conducted a similar study on impact forces of large tankers berthing to a jetty. Statistical data was collected for approach velocities as well as impact forces on two fenders spaced 300' apart. Echo sounders were used to estimate approach velocity, while displacement gauges were used to measure the compression in each fender during impact.

The data in this study was statistically analyzed based on Gumbel's method shown in Figure 1, indicating the probability of any particular energy value not being exceeded on the next occasion. This method is useful in predicting the maximum impact

load to be expected over a given number of berths or design life. The design life at the location of study, Finnart, UK, was 30 years for a total of 3,000 berths. While the data from this study is site specific, it can be generally applied to structures/locations of a similar nature.

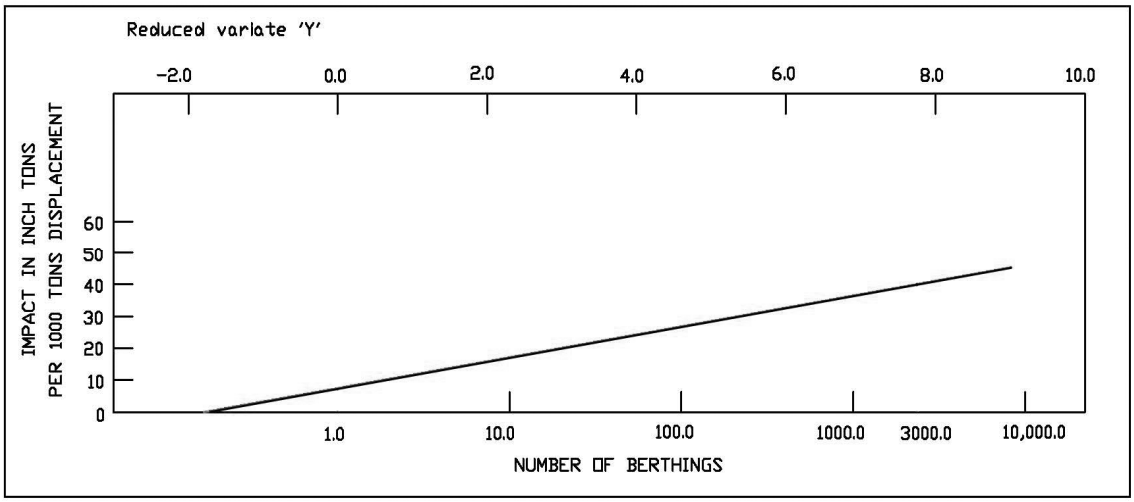


Figure 1: Design Energy, Produced with data from (B.F. Saurin, 1963)

(Dent and Saurin, 1969) produced the following recommendations based on numerous tests:

For design of berths of average exposure to laden vessels:

1. 90 in-tons per 1,000 DWT of design ship at yield stress in the fenders (16.8 kip ft/1,000 DWT)
2. 60 in-tons per 1,000 DWT as a normal maximum related to approximately maximum working stresses in the breasting structures and fenders (11.2 kip-ft/1000 DWT)

For berths located in protected harbors, a value of 5/8 of the above values are recommended

(Toppler and Weersma, 1973) presented a similar statistical approach that accounted for varying berthing frequency and size. They came up with the following:

Ultimate energy for fully laden vessels at normal exposure:

1. For low frequency berthing, 2,000 kip ft/100,000 DWT (275 meter tons/100,000 DWT)
2. For high-frequency berthing, 1.25 times the low-frequency value.

It was recommended that for loading terminals and ballasted vessels, 85 percent of the above values should be applied. For very exposed locations a factor of 1.10 and for sheltered harbors a factor of .85 should be applied (Figure 2).

These studies all involved ocean-going cargo vessels and tankers.

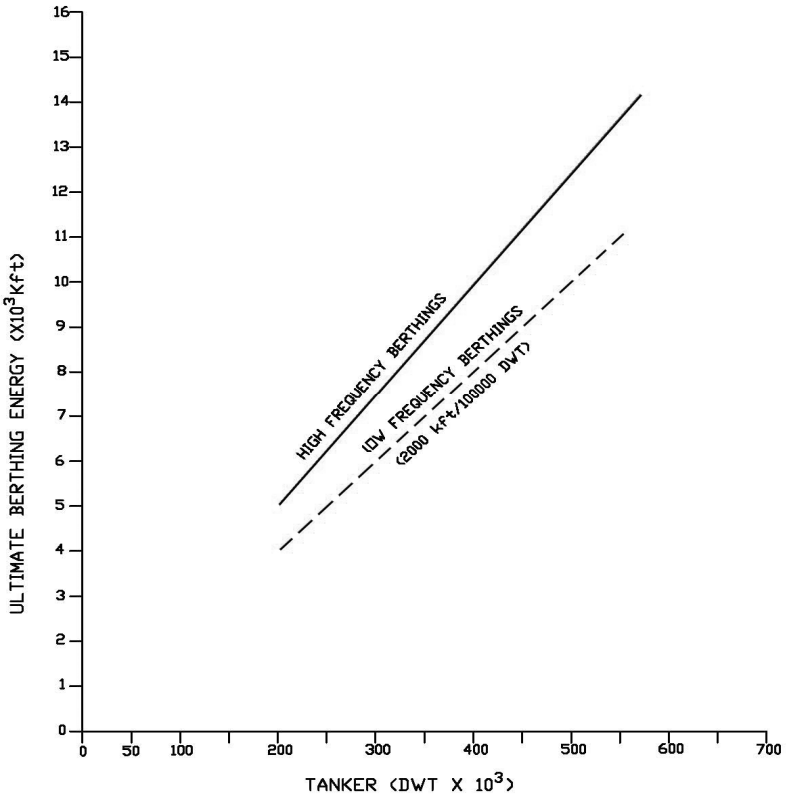


Figure 2: Ultimate Energy, After (Toppler and Weersma, 1973)

A study by (Jahren and Jones) conducted in 1993 for the Washington State DOT involved the development of design criteria for berthing energies from ferries on end berthing type structures (wingwalls). The criteria were derived from a velocity histogram from 568 landing events collected using CCTV (closed circuit television) and a video recorder. A general berthing coefficient to be used with the kinetic energy method was then derived by comparing the apparent kinetic energy of the vessel to the energy absorbed by the wing walls for 18 berthing events. The study also discusses design recommendations based on the tradeoff between acceptable structure damage and long term maintenance costs (Figure 3).

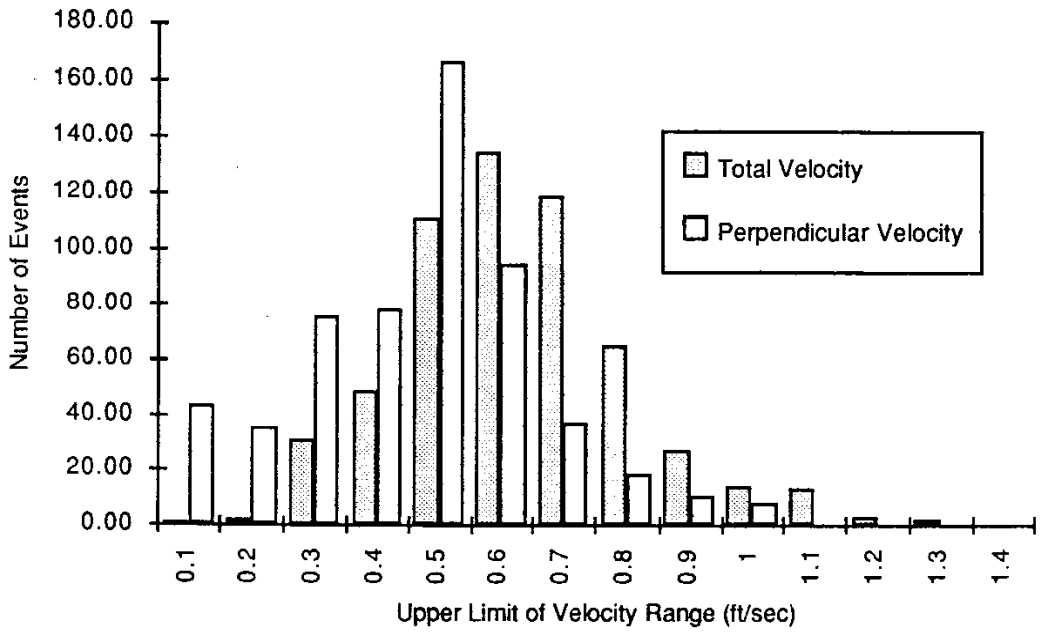


Figure 3: Velocity Histogram, After Jahren and Jones (1993)

Another study, conducted by (Ueda et al. 2002) involved developing a method to determine the factor of safety of current fender design methods in Japan, based on exceedence probabilities. The probability of failure of fenders designed in accordance with the 1999 Japanese Design Standard was calculated using statistical methods which determined the probability of berthing energy exceeding the effective fender capacity. A fender could then be designed for a known factor of safety for any desired reliability. The study focused primarily on cargo and container ships of DWT ranging from 5,000 to 35,000, but gives general insight into designing fenders from a statistical approach.

METHODS AND PROCEDURE

The load environment on ferry landings is not well quantified, and remains largely based on assumptions and historical knowledge developed over a number of operation/failure cycles. Previous literature has focused primarily on tanker-sized vessels and cargo ships of a magnitude much greater than the ferries used by the AMHS. The limited amount of information, specifically for Alaska, has led to the design of structures with an unknown reliability.

This manuscript will discuss a means to acquire information needed to improve upon our understanding of the load environment on ferry landing structures. The study will focus on the Auke Bay facility with the following goals:

- Formulating risk-based design criteria consistent with reliability engineering methods, using measurements from the Auke Bay landing.
- Providing a broad set of statistical design parameters that can be readily applied to current AMHS design methods.

Presented here, will be the instrumentation scheme used to monitor metrics of berthing demands during actual events. We will also present preliminary findings on the in- situ monitoring of 112 berthing events from 4 vessels at the Auke Bay ferry landing in Juneau, Alaska . Vessel displacements range from 5552 to 7683 long tons. The field testing was designed to measure berthing parameters simultaneously in order to develop a time history of the vessel-structure interaction before, during, and after vessel impact. Specifically, the following parameters were measured:

- Vessel position vs. time

- Fender displacements during impact
- Strains in piling
- Tide levels
- Strains in bollards during and after tie-up.

For brevity, this paper will focus on approach velocity and impact energy.

Site Description

The Auke Bay ferry terminal is located in the panhandle of Alaska in Juneau, and is naturally protected by a series of islands and fjords. The landing features both side and stern berths and can accommodate a total of three ferries at any time. The side berthing portion of the landing consists of 14 dolphins and two transfer bridges divided into the east and west berths (Figure 4). The stern berth is for a catamaran ferry (the Fairweather) and was not included in this study. This investigation focuses on side berthing dolphins most affected by the vessels: the east berth dolphins, labeled W2, E1, E2, E3, and E4 in Figure 5.

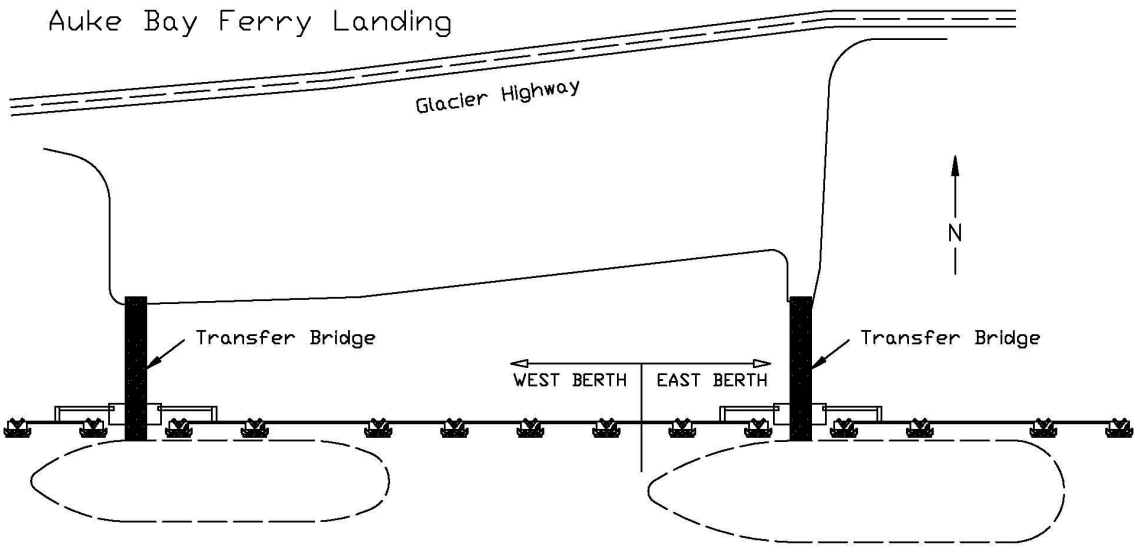


Figure 4: Auke Bay Side Berth

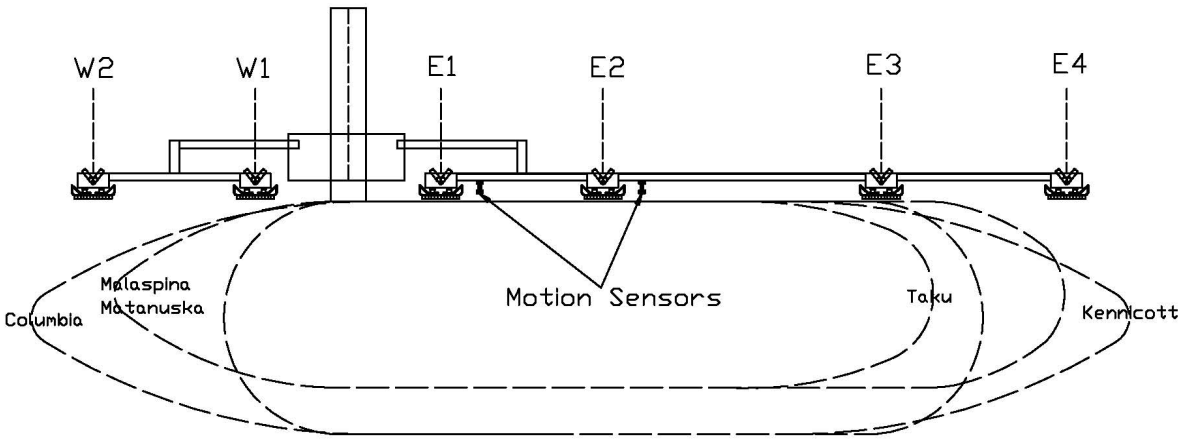


Figure 5: Auke Bay East Berth

Berthing Structure Description

Each mooring dolphin consists of two separate components, a fender system and a tripod system. The fender system consists of two 40” side-loaded cylindrical fenders, and four 18” diameter vertical fender piles supporting a timber facing. The tripod system consists of three 18” diameter steel piles; a single vertical pile and two piles battered at approximately 3:1. (See Figure 6 for details).

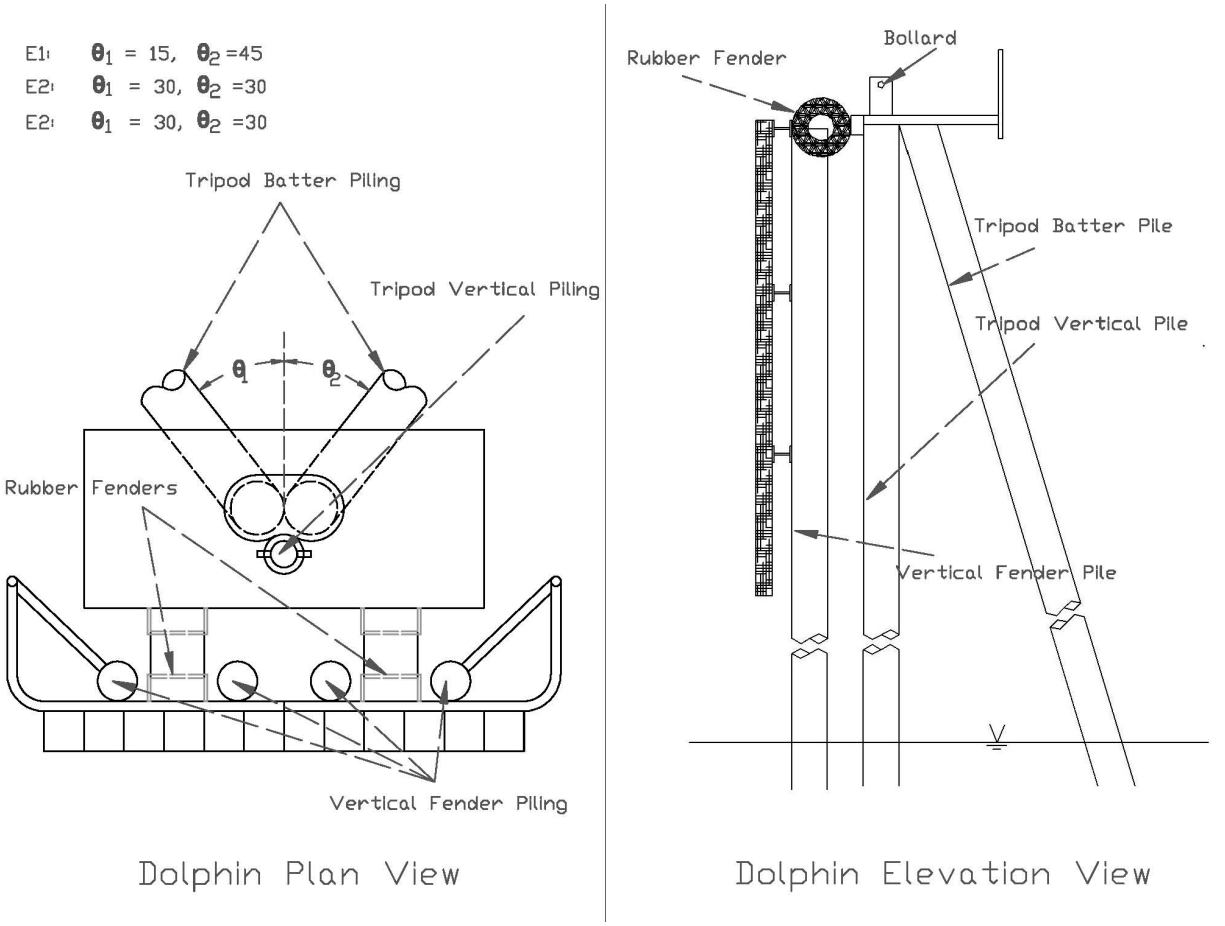


Figure 6: Typical Berthing Dolphin

Vessel Descriptions

Berthing events from the four different vessels that land on the east berth were monitored. The vessels range from 5550 to 7690 displacement (long tons). Table 1 has general vessel information. Figure 7 shows each vessel clockwise from the top left: Columbia, Matanuska, Malaspina, and Kennicott.

Table 1: Vessel Specifications

Vessel Information				
Vessel Specs	Matanuska	Malaspina	Columbia	Kennicott
Length (ft)	408	408	418	382
Beam(ft)	74	74	85	85
Displacement (long tons)	5569	5552	7683	7503
Loaded Draft (ft-in)	16' -11 5/8"	16' -11 3/8"	17' -6 1/8"	17' -6"



Figure 7: Vessels in this study

Instrumentation

In order to measure the desired berthing parameters, an automated instrumentation system was designed and installed at the Auke Bay terminal along the east berth, labeled W2, E1, E2, E3 and E4 in Figure 5. During deployment, it was observed that dolphins E1, E2, and E3 were experiencing berthing action. Impacts were not observed at dolphins E4 or W2 or W1.

The complete Auke Bay instrumentation system consisted of:

- Two Campbell Scientific CR5000 dataloggers

- Three Senix TSPC motion sensors
- six linear motion transducers (LMT's or string pots)
- Twenty six 90 degree chevron strain gages (two 1/4 bridges per gauge)
- One field computer running RTDAQ ® (Real Time Data Acquisition) software developed by Campbell Scientific Inc.

Other additional hardware included; Environmental protection boxes for the dataloggers, Belden instrumentation wire, two RavenXTG digital cellular modems, and two modem antennas.

The system was designed to monitor all the instrumentation installed on dolphins W2, E1, E2, E3, and E4 simultaneously during any given berthing event. The instrumentation components were hard wired into the two dataloggers, with (W2 and E1), and (E2, E3, and E4) wired into dataloggers one and two respectively. The dataloggers operated and received instructions via an internal program written in *CRBasic* using RTDAQ. The system was set to read and collect at 5 Hz in order to adequately capture the events. Each berthing event was captured and recorded for ten minutes in order to obtain a time history of each event both during impact and tie up.

The data acquisition system was designed to measure the approach distance vs. time of an incoming vessel, fender displacement, axial force in the tripod piling, and tide level during the event. To accomplish this, the following hardware was installed.

- Four ¼ bridge (2 chevron) strain gages mounted 180 degrees apart around the surface of each tripod pile on dolphins E1, E2, and E3. Figure 11

- Two *Senix TSPC* motion sensors mounted on the catwalk (walkway between dolphins) 10’ from dolphins E1 and E2. Figure 8
- Two LMT’s per dolphin mounted adjacent to each rubber cylindrical fender on E1, E2, and E3. Figure 10
- One Senix TSPC motion sensor mounted on E1 and oriented perpendicular to the water surface. Figure 9

The strain gages were used to obtain the response of the tripod systems to vessel impact by measuring axial strain. The two rosette gages were wired into a full bridge to measure axial strain only, negating any bending effects in the piling. The gages, mounted on stainless steel shims, were welded to the surface of each pile and coated in a sensor-safe silicone sealant to protect them from the harsh environment. Figure 12 illustrates placement of the instrumentation on the dolphins.

The LMT’s were used to measure the linear displacement in the rubber cylindrical fenders (of known stiffness) on each dolphin during an event. LMT’s were mounted adjacent to each cylindrical fender. While the LMTs measured the deflection of the side-loaded cylinder fenders, the strain gages were installed to capture events that fully compressed the fenders. Evidence of this having occurred previous to the project is evident on the dolphins.

Motion sensors mounted on the catwalk were used as data collection triggers. When the vessel was at a predefined distance from the motion sensors, the datalogger would begin saving data. The motion sensors were set to trigger the program ‘on’ to begin recording at a vessel distance of 200 inches from the face of the sensor, and

trigger ‘off’ after ten minutes. Data was collected at 5 Hz over the ten minute period, resulting in a time-history for each instrument of approximately 3000 measurement records.

A motion sensor mounted on E1 was used as a tide gage.



Figure 8: Position Sensors



Figure 9: Tide Gauge

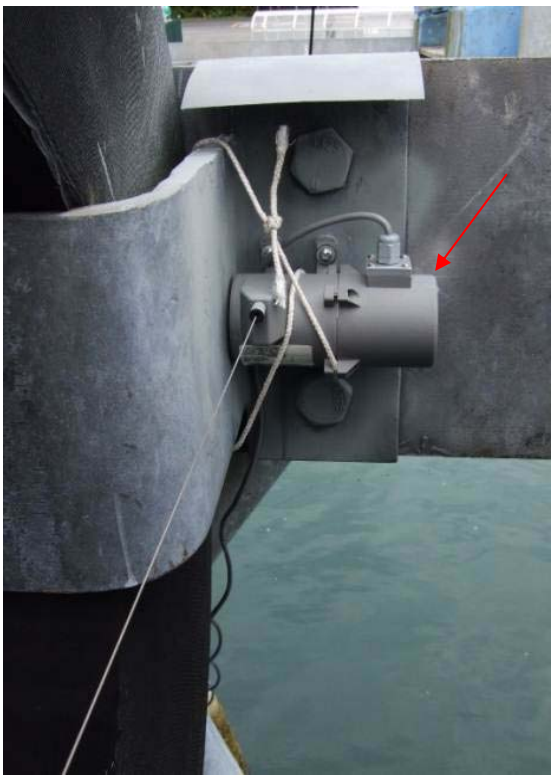


Figure 10: Linear Measurement Transducer (LMT)



Figure 11: Strain Gauge instrumented piles

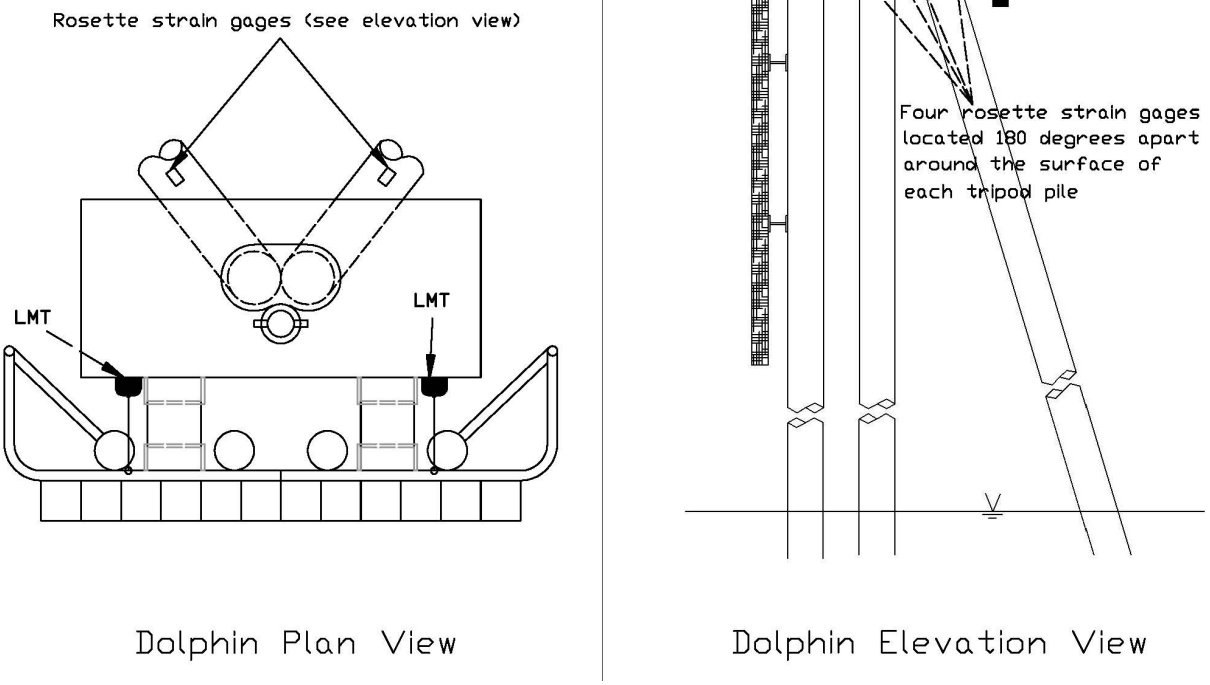


Figure 12: Instrumentation Placemen

Vessel Position Measurements

In this study, the time histories of 199 measurements were used to estimate approach velocities just prior to impact on dolphins E1 and E2. Fender displacement data, recorded simultaneously with vessel motion, was used to ascertain the time of impact. Approach velocities were determined from the vessel motion vs. time graphs and averaged over approximately one second just prior to impact.

Fender displacement and vessel position are graphed together in Figure 13. The raw position vs. time graphs provide valuable insight into many aspects of a berthing maneuver; showing how the maneuver and approach can vary significantly on a vessel and event basis. The sharp peaks in the graphs generally indicate the use of bow thrusters or mooring lines/winches used to move the vessel closer to the berthing structure. The sharp valleys in the graphs generally represent either impact/ rebound off the fenders, or the use of bow thrusters which reverse the vessel's direction normal to the fender face.

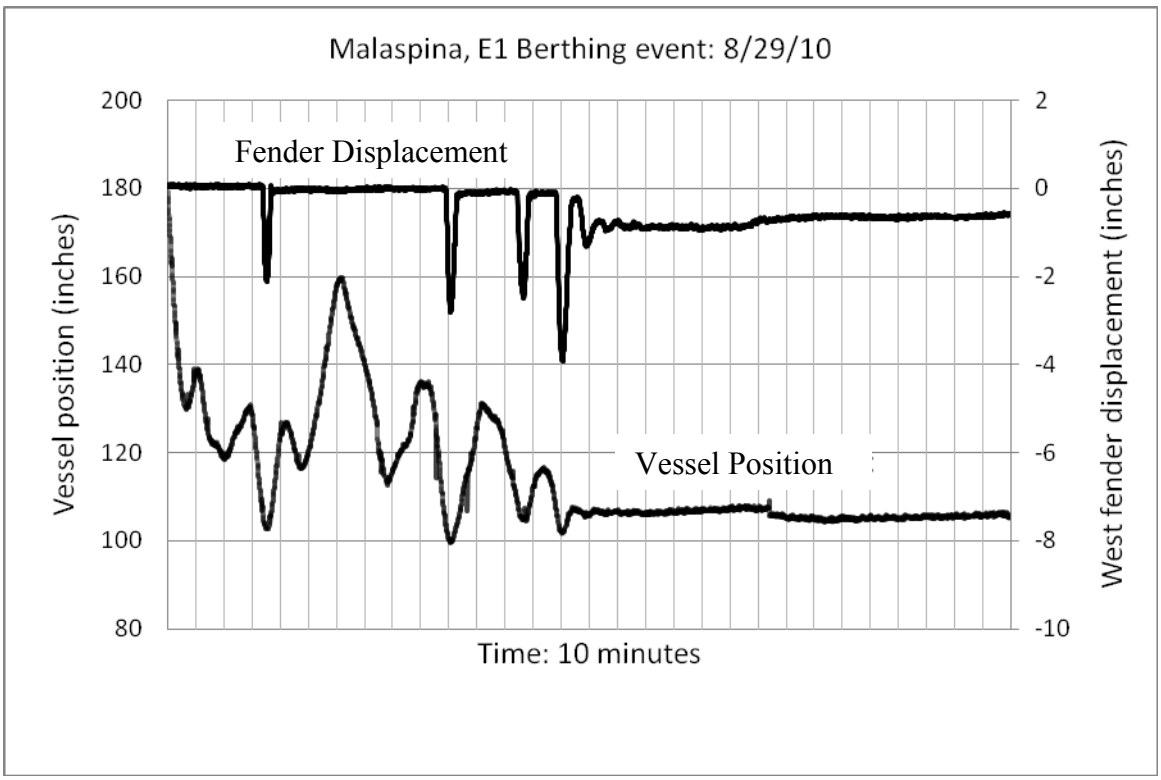


Figure 13: Vessel Position vs. Fender Displacement

Impact events can be easily determined when the position vs. time and fender displacement vs. time graphs are compared (Figure 13). The static offset from the zero position indicates the displacement of the fenders after the vessel has been tied-up.

The time histories have shown that multiple impacts are frequent. In addition, the maximum approach velocity per berthing event is often not the result of initial approach and impact; but rather the result of maneuvers used to position the vessel after initial contact. Such maneuvers typically result from sources such as bow thrusters, environmental effects, and mooring lines/winching activity used to position the vessel.

Berthing Energy

Berthing energy is the most common parameter used by engineers when designing berthing structures. When a vessel impacts the structure, a portion of the kinetic energy of the vessel must be absorbed by the structure being impacted. A previous study has shown that energy absorbed by the supporting structure may be as much as 10-25% of the total berthing energy (Gaythwaite).

Previous literature has also typically used only fender deflections as a basis for determining berthing energy. While this assumption is valid in many cases, elastic energy absorbed by the tripod structures at Auke Bay will be included in this study.

The fender system on each dolphin consists of two side loaded cylindrical fenders (40” diameter). designed to deflect approximately 13.25 inches and resist a 15-kip load, and four vertical fender piles covered in a timber facing (Figure 6). The four piles are assumed to have a lateral stiffness of zero and thus do not contribute to the overall stiffness of the fender system. This assumption was made based on pile driving logs provided by the AKDOT&PF; which indicated the presence of extremely soft material with low lateral stiffness up until the last couple feet. Engineers with the AMHS

concurred with this assumption. All hydrodynamic, inertial, and damping effects are also considered to be insignificant.

In order to determine the overall energy absorbed by the dolphins during a berthing event, the overall stiffness and deflection of both the fender system and the tripod for each dolphin needed to be quantified. The stiffness of each tripod system was estimated separately for dolphins (E1, E2, and E3) using a structural analysis software (SAP2000). With details from the working drawings, the geometry and mechanical behavior of each dolphin was modeled as accurately as possible. Pile driving logs were used to roughly estimate the depth of fixity for each vertical pile. The rubber cylindrical fenders were modeled as springs separating the fender face from the tripod. The stiffness of the tripods, as well as the combined tripod and fender systems were determined by applying a unit load to the fender faces of each model, from which the deflection was recorded. Stiff nesses were obtained from the load/deflection structural analysis results using a commercial structural analysis software(Figure 18).

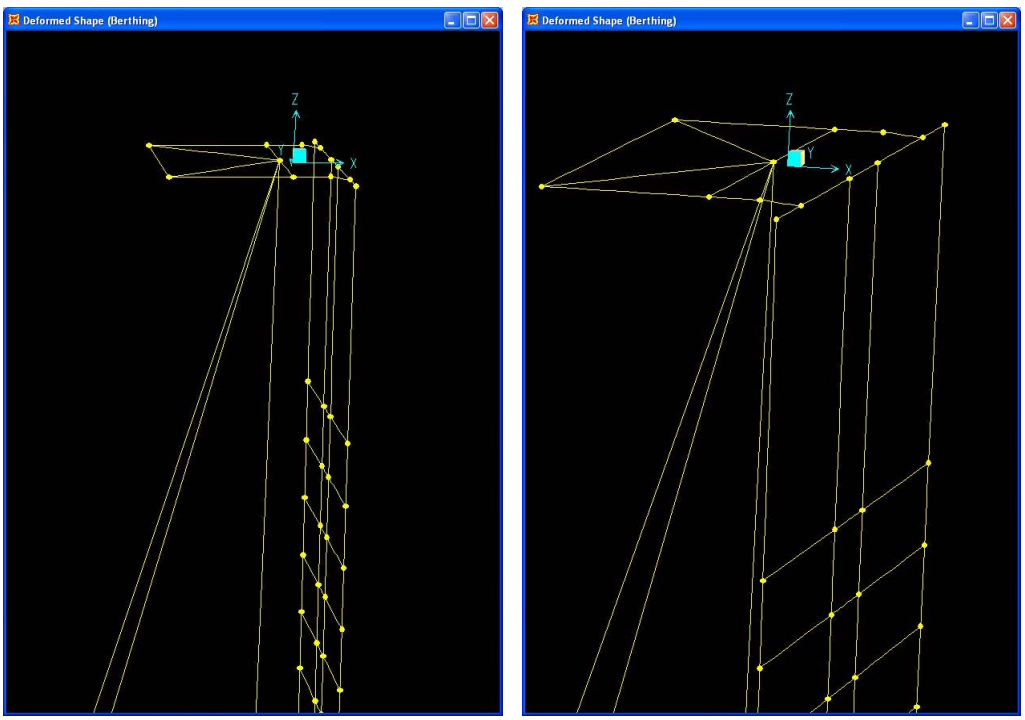


Figure 14: Sap2000 Structural Model of Dolphin E2

Three dolphins (E1, E2, and E3) were instrumented with LMT's adjacent to each cylindrical fender in order to monitor the displacement of each fender during a berthing event. Using a known stiffness for the cylindrical rubber fenders, the maximum displacements (measured by the two LMT's) from each event were then used to determine the energy absorbed by the fender system using Equation 3.1.

Equation 3.1

Where E_F = *Energy absorbed by the fender system* $(Kip * ft)$

K_f = *stiffness of each rubber fender* $(\frac{Kips}{inch})$

x_{wf} = *Displacement of the west fender* $(inches)$

x_{ef} = *Displacement of the east fender* $(inches)$

K_f = 2.046 kips/inch per rubber fender, or 4.091 kips/inch total (two fenders per dolphin) for dolphins E1, E2, and E3. Fender system stiffness was extrapolated from fender manufacturer specifications.

The equation for the total combined energy absorption of the fender and tripod system is described by the equation below, and schematized as a series of springs in figure 19.

$$E_T = \frac{1}{2} K_f (x_{wf}{}^2 + x_{ef}{}^2) + \frac{1}{2} K_t x_t{}^2$$

Where E_T = Total energy absorbed by the fender + tripod system ($Kip * ft$)

K_t = Stiffness of the tripod system ($\frac{kips}{inch}$)

x_t = Displacement of the tripod system ($inches$)

x_T = Total displacement of the dolphin ($x_t + x_f$)($inches$)

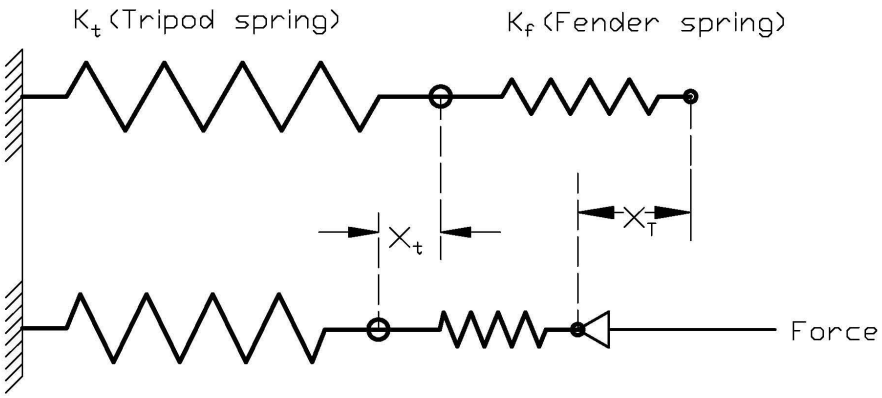


Figure 3.15: Dolphin Spring Schematic

Figures 16 and 17 show the force vs. deflection (stiffness) and elastic-potential energy- vs. displacement curves for the tripod, fender, and combined system for Dolphin E1.

The stiffness of the tripods (K_t) on E1, E2, and E3 were found to be 27.661, 23.419, and 25.696 kips/inch respectively from the SAP models. The total potential energy of dolphins E1, E2, and E3 (fender +tripod) were determined in terms of fender energy to be:

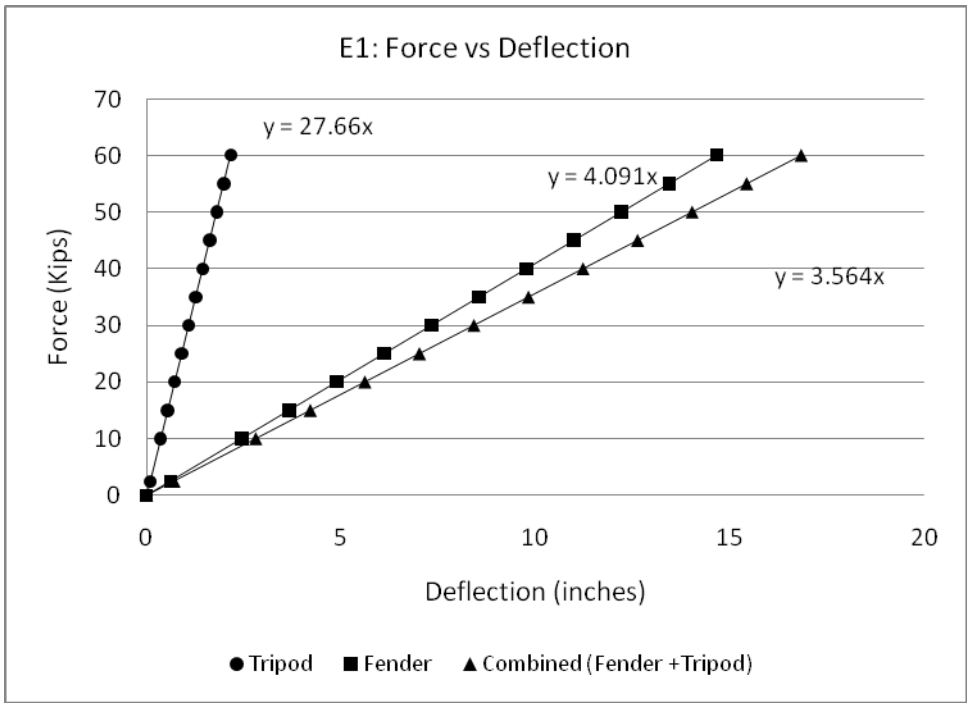


Figure 16: Dolphin E1 Stiffness

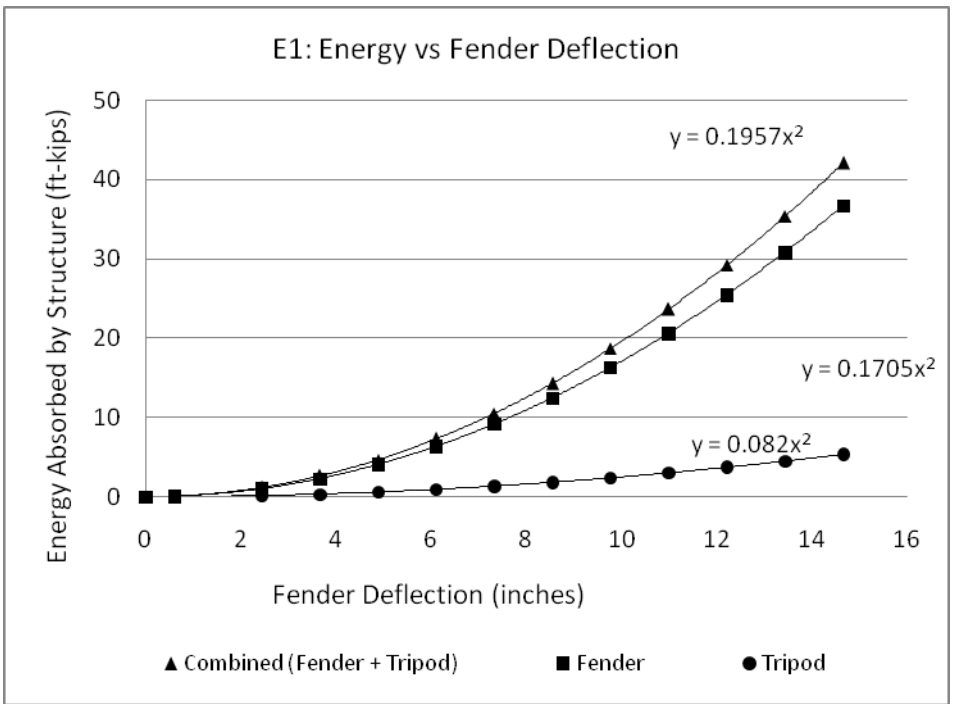


Figure 17: Dolphin E1 Elastic Potential Energy

RESULTS

Results for kinetic energy and approach velocity are presented in this section. Results are displayed in the form of histograms, probability distribution fits, cumulative probability curves, probability of non-exceedence curves.

The histograms provide a graphical representation of the frequency distribution of each parameter observed over a range of measurements. The purpose of the histograms is to evaluate the relative frequencies of each parameter by displaying the number of times various measurements occurred over 112 total berthing events. Probability distributions were fitted to their respective histograms, and provide a continuous load distribution based on measurement frequencies. Probability distributions associate measurements or experimental results with their respective probabilities of occurrence. Cumulative probability distributions are derived from the sum of probability distribution curves, associating measurements with their respective probabilities of not being exceeded or equaled (percentiles). Probability of non-exceedence curves provide the same information as the cumulative probability distributions, however they are particularly useful for analyzing occurrence probabilities at extreme values. They also graphically depict the ‘goodness of fit’ of the probability distribution to the empirical data. The degree of linearity is reflective of how well a distribution matches the empirical data.

Velocity

Approach velocity was determined from the position vs. time data and is displayed in the form of histograms, statistical distribution fits, cumulative probability curves, and probability of non-exceedence curves.

While multiple approaches and impacts frequently occur during a vessel berth, these figures only reflect the approach velocity and impact corresponding to the largest fender deflection on each dolphin for each berthing event.

Velocity for all vessels on dolphins E1 and E2:

The combined vessel histogram (Figure 18) lumps the approach velocity measurements from all the vessels berthing to dolphins E1 and E2. The combined data includes all of the velocity measurements taken at Auke Bay over the entire measurement cycle (9 months). The lumped velocity data consists of 199 total measurements, with a maximum measured approach velocity of 0.50 ft/s. The mean approach velocity for all vessels is 0.164 ft/s. The 'cumulative probability' plot (Figure 20) and the 'probability of non-exceedence' plot (Figure 21) show the percentile velocities, representing the probability that a particular velocity will not be exceeded per berthing event.

- The values for the 99.99%, 99.995%, 99.999% and 99.9998% percentile velocities for a berthing event are: 0.74 ft/s, 0.78 ft/s, 0.850 ft/s, and 0.905 ft/s respectively.

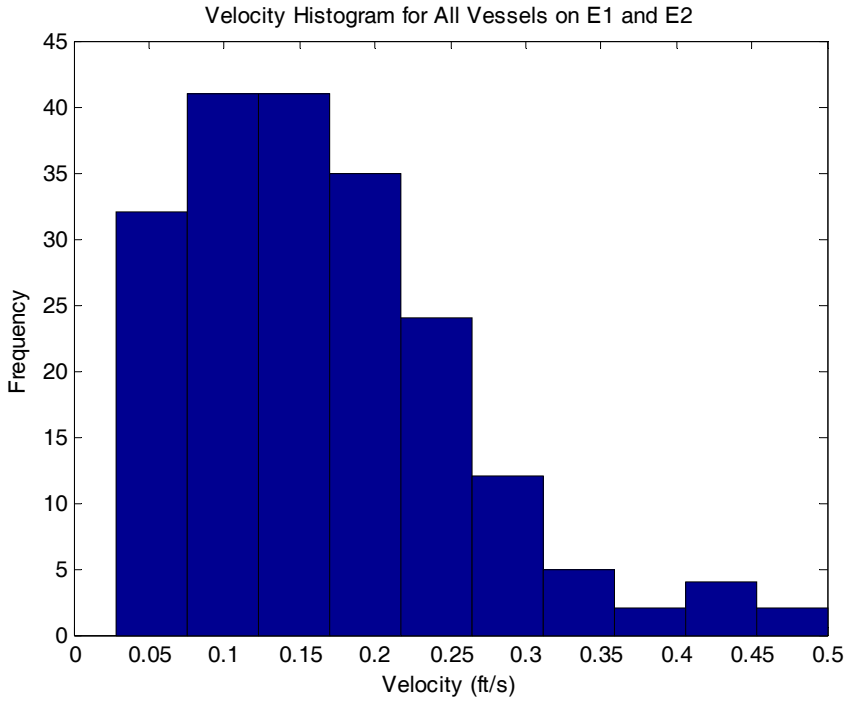


Figure 18: Velocity Histogram for All Vessels on E1 and E2

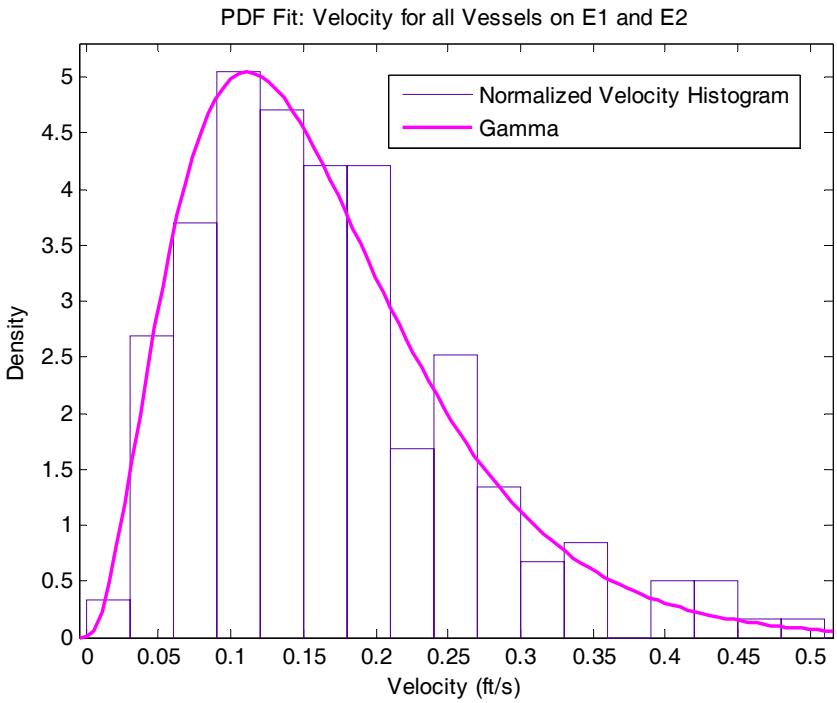


Figure 19: PDF Fit - Velocity for all Vessels on E1 and E2

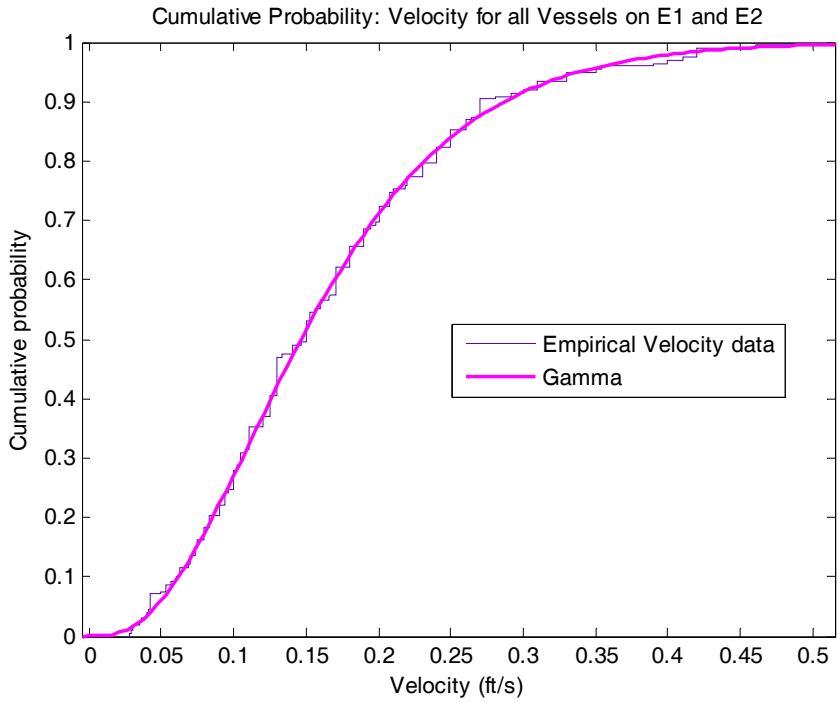


Figure 20: Cumulative Probability – Velocity for all Vessels on E1 and E2

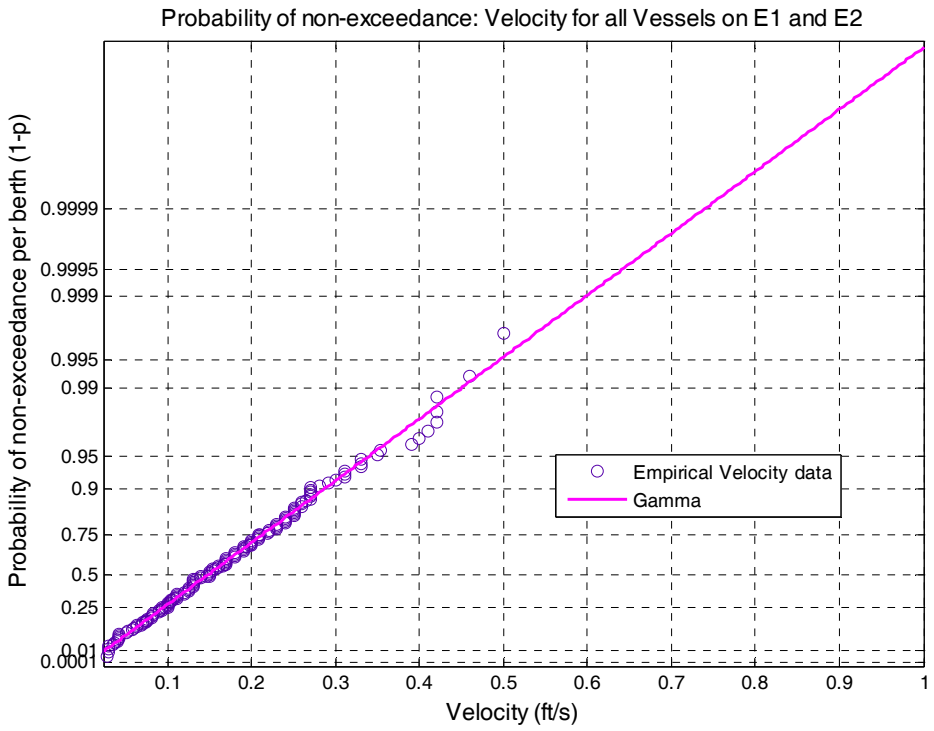


Figure 21: Percentile Plot – Velocity for all Vessels on E1 and E2

Energy

Energy results are presented in the form of histograms, statistical distribution fits, and probability curves in Figures 22 through 25. The energy data represents the elastic potential energy for all vessels studied on dolphins E1, E2 and E3. That is, the total energy absorbed by the berthing structure, which takes into consideration the fender system as well as the backing structure (tripod).

A variety of distributions were fit to the elastic energy data. The distribution found to fit the berthing energy histograms most accurately appeared to be the Weibull distribution, which is commonly used in lifetime modeling. The Weibull distribution was

chosen particularly for its closeness of fit to the energy data, and its ability to predict extreme berthing energy values.

The maximum berthing energy recorded was 33.33 ft-kips, with a mean of 4.41 ft-kips.

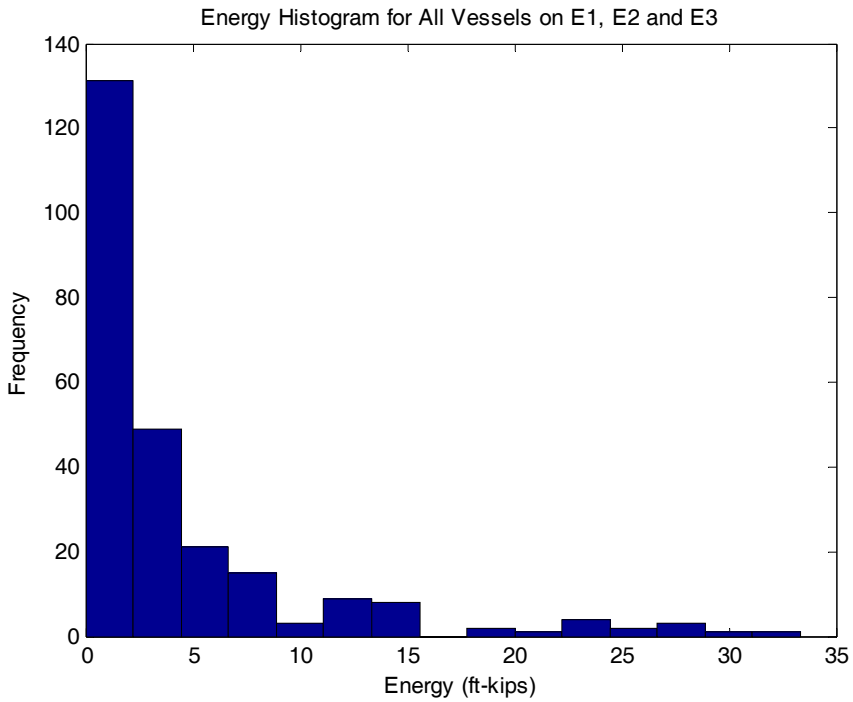


Figure 22: Energy Histogram for All Vessels on E1, E2 and E3

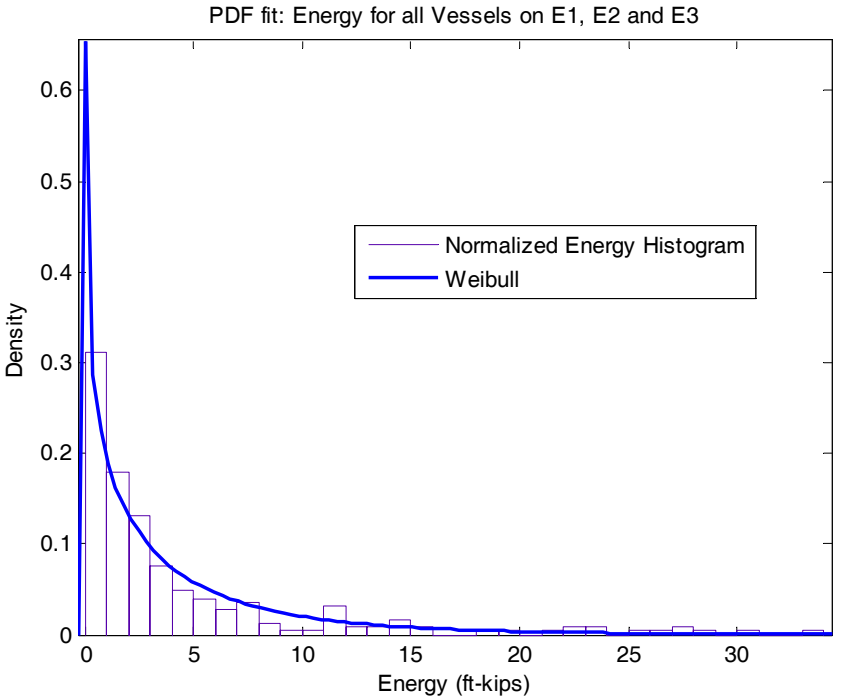


Figure 23: PDF Fit – Energy for all Vessels on E1, E2 and E3

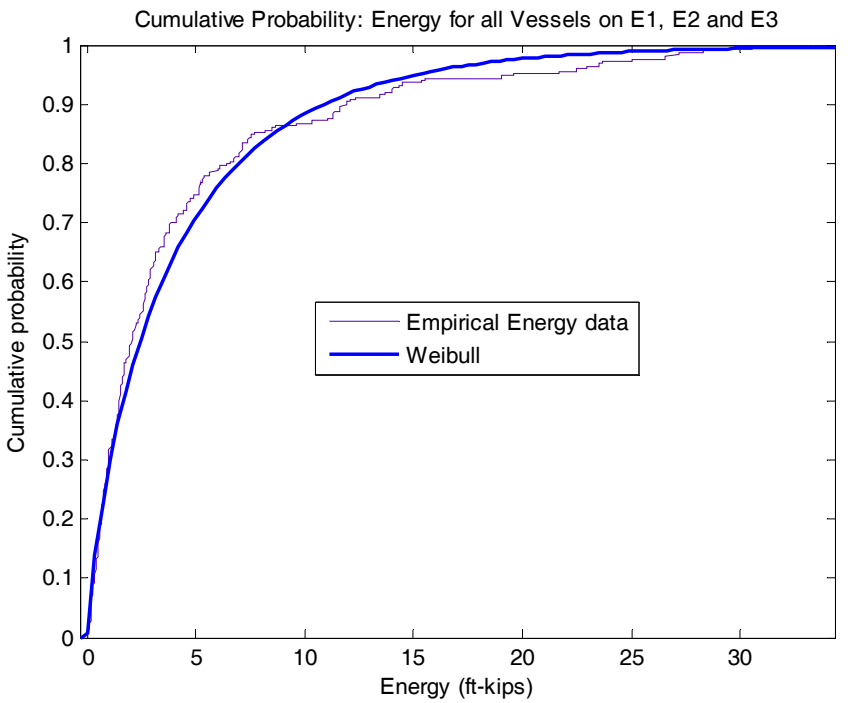


Figure 24: Cumulative Probability – Energy for all Vessels on E1, E2 and E3

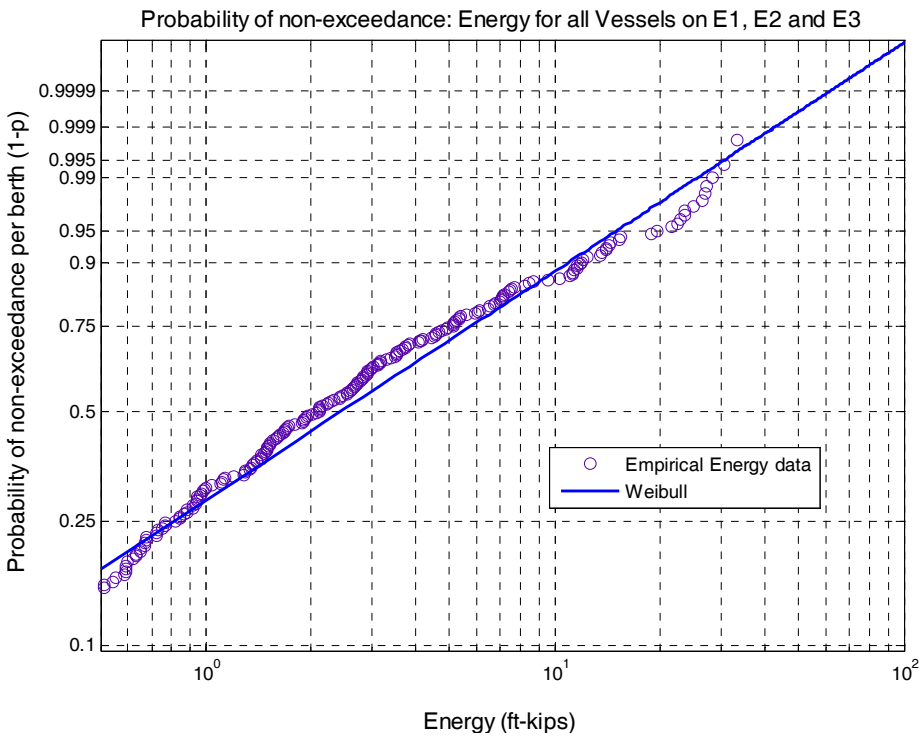


Figure 25: Percentile Plot – Energy for all Vessels on E1, E2 and E3

CONCLUSION

Understanding vessel berthing parameters, like velocity and impact energy, is critical to the design of cost effective and reliable berthing structures. When a berthing structure is designed, a certain level of uncertainty exists that is typically accounted for using a factor of safety or reduction in allowable stress. However, even with these measures, there is the possibility that actual demands may exceed design berthing parameters at some point in the life of the structure. It is often the case that engineers have developed their own design guidelines through trial and error over many operation/failure cycles, and developed factors of safety that compensate for assumptions in design values. The result is that many berthing structures are design and constructed with limited information, leading to designs rooted in assumptions and with discretion.

This study analyzed the berthing events of four different vessels at the Auke Bay ferry landing in Juneau, Alaska. The data acquisition system used for this project demonstrated the utility of modern equipment for monitoring structural response to berthing impacts. Data acquired in this study resulted in a set of statistics for approach velocity and energy. This information provides a basis for reliability based design of future structures.

Overall, the complex and variable load environment on berthing structures implies the advantage of a reliability approach, in which fenders and backing structures can be rationally designed for exceptional events. This study demostrates the feasibility

of acquiring a statstically significant sample of berthing paramters using traditional measuring instruments driven by modern data achisition systems. In this, industry-wide adoption of relaibility-based design philosophy (e.g., the LRFD method) may be feasible as well as practical.

REFERENCES

Toppler, J.F., and Weersma J., (1973), “Planning and Design of Fixed-Berth structures for 300,000 to 500,000 DWT Tankers,” Journal of Petroleum Technology

Saurin, B.F., (1963), “Berthing forces of large tankers,” Proc. Of the Sixth World Petroleum Congress, Frankfurt, Section VII, Paper 10

Svendsen, I.A., (1970), “Measurement of impact energies on fenders,” The Dock and Harbour Authority, Vol. 51, no. 599 & 600

Gaythwaite, John W., (1990). “Design of Marine Facilities for the Berthing, Mooring, and repair of Vessels.” Van Nostrand Reinhold, New York.

Port of Long Beach Sustainable Design and Construction Guidelines

Renée Yarmy[1] and Doug Sereno[2]

[1]Renée Yarmy, Bachelor of Architecture, California State Polytechnic State University, Pomona, Master of the Built Environment in Sustainable Development, University of New South Wales, Sydney, Australia, Lead Sustainability Planner, TEC Inc., 514 Via De La Valle, Suite 308, Solana Beach, CA 92075; PH (858) 509-3157 ext. 8426; FAX: (858) 509-3158; email: rdyarmy@tecinc.com.

[2]Doug Sereno, Director of Program Management, Port of Long Beach, 3rd Floor, 925 Harbor Plaza, Long Beach, CA 90802; PH (562) 590-4146 ext. 3276; FAX: (56) 901-1730 ; email: sereno@polb.com.

ABSTRACT:

The Port of Long Beach (Port) has systematically moved forward in developing tools, mechanisms, and decision-making frameworks to further Port sustainability by developing the *Port of Long Beach Sustainable Design and Construction Guidelines (Sustainability Guidelines)*. Developed out of the *Port of Long Beach Green Port Policy (Green Port Policy)* mandates, the *Sustainability Guidelines* promote projects that are designed, constructed, and operated utilizing the triple bottom line approach to sustainability: community integrity, environmental *stewardship*, and economic vitality. The *Sustainability Guidelines* also emphasize sustainable marine, site, infrastructure, and building-related construction projects, operational procedures, and management processes with the aim of "going beyond" traditional project design. The Port is evaluating the *Sustainability Guidelines* for their ability to improve the Engineering Bureau's project management processes while contributing to the goals of the *Green Port Policy* and Port Engineering as a whole. Concurrent to this examination, the implementation of the *Sustainability Guidelines* brings to light additional benefits to the Port and surrounding community. The Port is testing the *Sustainability Guidelines* on pilot projects to measure their effectiveness and the level of effort required to implement them.

Introduction: Sustainability Drivers at the Port of Long Beach

The Port of Long Beach (Port) has defined sustainability as an understanding that economic vitality and community integrity are tied to the preservation of natural resources for present and future generations. As a part of its strategic mission, the Port has a responsibility to consider and address the effects on the environment and community in order to continue its "license to operate." Each Port employee recognizes this responsibility and strives to ensure that decision making at every level considers the "triple bottom line" of sustainability by encouraging environmental stewardship, fiscal responsibility, and community health and well-being. Sustainability is integrated into the Port's business practices through the goals of the *Port of Long Beach Green Port Policy (Green Port Policy)* (Port of Long Beach 2005). Consistent with this philosophy, the Port's Engineering Bureau developed the *Port of Long Beach Sustainable Design and Construction Guidelines (Sustainability*

Guidelines). The *Sustainability Guidelines* emphasize the development of marine, site, infrastructure, and building-related construction projects and operations that integrate sustainable practices into the Port's planning, design, construction, operations, and management processes. The *Sustainability Guidelines* contain recommendations that align with the goals of the *Green Port Policy* and identify opportunities to "go beyond" the traditional way of approaching design, construction, and operations.

The *Sustainability Guidelines* focus on the peculiarities and specificities that exist in a wide range of Port engineering project types and take into consideration existing Port processes, work flow requirements, and the Port's organizational structure. Additionally, the *Sustainability Guidelines* provide information on sustainable attributes to Port program managers, engineers, and planners as they develop, design, and construct their projects. The *Sustainability Guidelines* include applicable, truth-tested sustainability attributes that can provide a better return on investment and promote trade growth while ensuring sound environmental and community stewardship. The *Sustainability Guidelines* address a broad range of sustainability initiatives, including:

- Minimizing material, energy, and water intensity associated with all phases of Port projects;
- Capturing efficiency improvements in planning, design, construction, and operations;
- Promoting the use of best available technology and construction processes to minimize environmental impacts;
- Protecting the health of the adjacent communities and preventing potential harmful side effects of Port operations; and
- Improving biodiversity, air quality, water quality, and alternative/renewable energy infrastructure, the use of recycled/recyclable/rapidly renewable content materials, and extending material and product service life and durability.

To ensure consistency with federal, state, municipal, and Port directives and guidance, the *Sustainability Guidelines* have referenced the following plans, programs, and manuals:

- *Green Port Policy*
- San Pedro Bay Ports (SPBP) Clean Air Action Plan (CAAP)
- Water Resources Action Plan (WRAP)
- California Air Resources Board (CARB)
- Energy Policy Act of 1992 (EPAct) and subsequent amendments
- American Association of Port Authorities (AAPA) Sustainability Guiding Principles
- California Green Building Standards Code, California Code of Regulations Title 24, Part 11 (CALGreen Code)

In particular, the *Green Port Policy* and the AAPA Strategic Sustainability Initiative have served as key drivers in the Engineering Bureau's expansion of sustainable design, construction, and management practices (AAPA 2007).

Green Port Policy

The *Green Port Policy* mandates the Port to "integrate sustainable practices into Port development and operations by actively promoting an organizational culture of environmental enhancement, fiscal responsibility, and community integrity." The *Green Port Policy* services the environment and the community by considering all Port related operations and aims to avoid or minimize negative impacts. The *Green Port Policy* incorporates the following five guiding principles:

1. Protect the community from harmful environmental impacts of Port operations.
2. Distinguish the Port as a leader in environmental stewardship and compliance.
3. Promote sustainability.
4. Employ best available technology to avoid or reduce environmental impacts.
5. Engage and educate the community.

To facilitate the planning, implementation, and reporting of Green Port programs and projects, six program elements are established in the *Green Port Policy*:

1. Wildlife – Protect, maintain, or restore aquatic ecosystems and marine habitats.
2. Air – Reduce harmful air emissions from Port activities.
3. Water – Improve the quality of Long Beach Harbor waters.
4. Soils/Sediments – Remove, treat, or render suitable for beneficial reuse any contaminated soils and sediments in the Harbor District.
5. Community Engagement – Interact with and educate the community regarding Port operations and environmental programs.
6. Sustainability – Implement sustainable practices in design and construction, operations, and administrative practices throughout the Port.

The *Green Port Policy* has significantly reduced the Port's impact on the environment and community through programs and initiatives such as the Green Flag vessel speed reduction program for air quality, Green Leases that promote environmental covenants, and the SPBP CAAP. The implementation of the *Sustainability Guidelines* continues the programs and initiatives developed under the *Green Port Policy*.

American Association of Port Authorities Strategic Sustainability Initiative

The Port of Long Beach was instrumental in the development of the AAPA Sustainability Task Force and promulgation of AAPA's Sustainability Guiding Principles. The Port has acknowledged the following Sustainability Standard Business Practices within the *Sustainability Guidelines*:

- Sustainability involves the simultaneous pursuit of economic prosperity, environmental quality, and social responsibility.
- Ports hold a unique role in transportation, logistics, and infrastructure development.
- Ports must be financially viable in order to achieve their missions and

contribute to the economic prosperity of their regions and nations.
- Ports recognize that their activities may impact the environment and natural resources.
- Ports recognize that they have responsibilities as members of the communities in which they operate.
- Ports recognize that a long-term balanced approach is required.

In addition, the *Sustainability Guidelines* facilitate the implementation of the AAPA Sustainability Guiding Principles:

1. Communicate the goals of sustainability across the organization and allocate resource requirements for implementation.
2. Integrate sustainability throughout port activities and in both near-term and long-term planning processes.
3. Build upon and share existing sustainability best practices, keys to success, lessons learned, and approaches for implementation.
4. Communicate and engage with internal and external stakeholders to encourage open dialogue, accountability, and collaboration.
5. To the extent possible, use appropriate data and metrics as part of the process for implementing sustainability.
6. Evaluate the total life cycle costs of projects and decisions.
7. Recognize that sustainability is a dynamic effort requiring flexibility and continuous improvement.

Port of Long Beach Program Management Division – Sustainability Vision

As a leader in sustainable port practices, the Port's Program Management Division aims to develop innovative and successful approaches to environmental stewardship. The potential for localized impacts on the environment and need to protect community health and well-being drive the improvement of Port project management practices. Technological and operational advances have allowed the Port to effectively address and mitigate environmental and health-related impacts in new and innovative ways. The Port has extended this philosophy into the development of the *Sustainability Guidelines*. The Program Management vision for the *Sustainability Guidelines* is to improve upon existing and traditional port design, construction, and management processes by aligning sustainability opportunities with the Program Management Division Project Delivery Manual. In addition, the *Sustainability Guidelines* strive to go beyond the requirements of the SPBP CAAP, WRAP, CARB, and EPAct by integrating the following processes:

- Life Cycle Cost Analysis;
- Advancement of sustainable stormwater practices;
- Development of shallow marine habitats;
- Encouraging the reuse (rather than disposal) of contaminated material;
- Contract-directed restrictions on idling construction vehicles/equipment;
- Waste diversion beyond mandated quantities;
- Noise abatement improvements;
- Training and educational outreach;

- Public meetings beyond the permitting and regulatory requirements;
- Additional mitigation strategies; and
- Adaptive management.

The *Sustainability Guidelines* recognize that local, regional, and federal environmental regulations continually evolve. Thus, the language of the *Sustainability Guidelines* has been formatted to be flexible in adapting to regulatory changes.

Tools Developed for Analyzing Sustainability Guideline Components

In developing the *Sustainability Guidelines*, existing national and international sustainability tools and frameworks were analyzed. Following this initial analysis, a Sustainability Attributes Definition List and Matrix were developed to identify applicable sustainability elements associated with Port project types. The Sustainability Matrix became a valuable tool in the facilitation of cross-divisional coordination meetings among the Port's Engineering and Environmental Divisions. These meetings engage representatives with responsibilities in environmental program management, project design, construction management, contracting, program management, and operations to discuss, review, and assess the applicability of sustainability approaches and opportunities for improvement in project management practices. The matrix also serves as a framework and summary for the Strategic Sustainability Checklists.

Components of the Sustainability Guidelines

Implementation Process Flow Chart

The Implementation Process Flow Chart illustrates existing Engineering Project Management processes at the Port (as defined by the Program Management Division's Project Delivery Manual) and identifies where specific tasks associated with sustainability implementation are integrated into existing processes. The flow chart illustrates the integration of sustainability meetings, reviews, and documentation associated with sustainably managed projects. The flow chart illustrates how the implementation processes for sustainable projects are aligned with existing Port processes (see Figure 1).

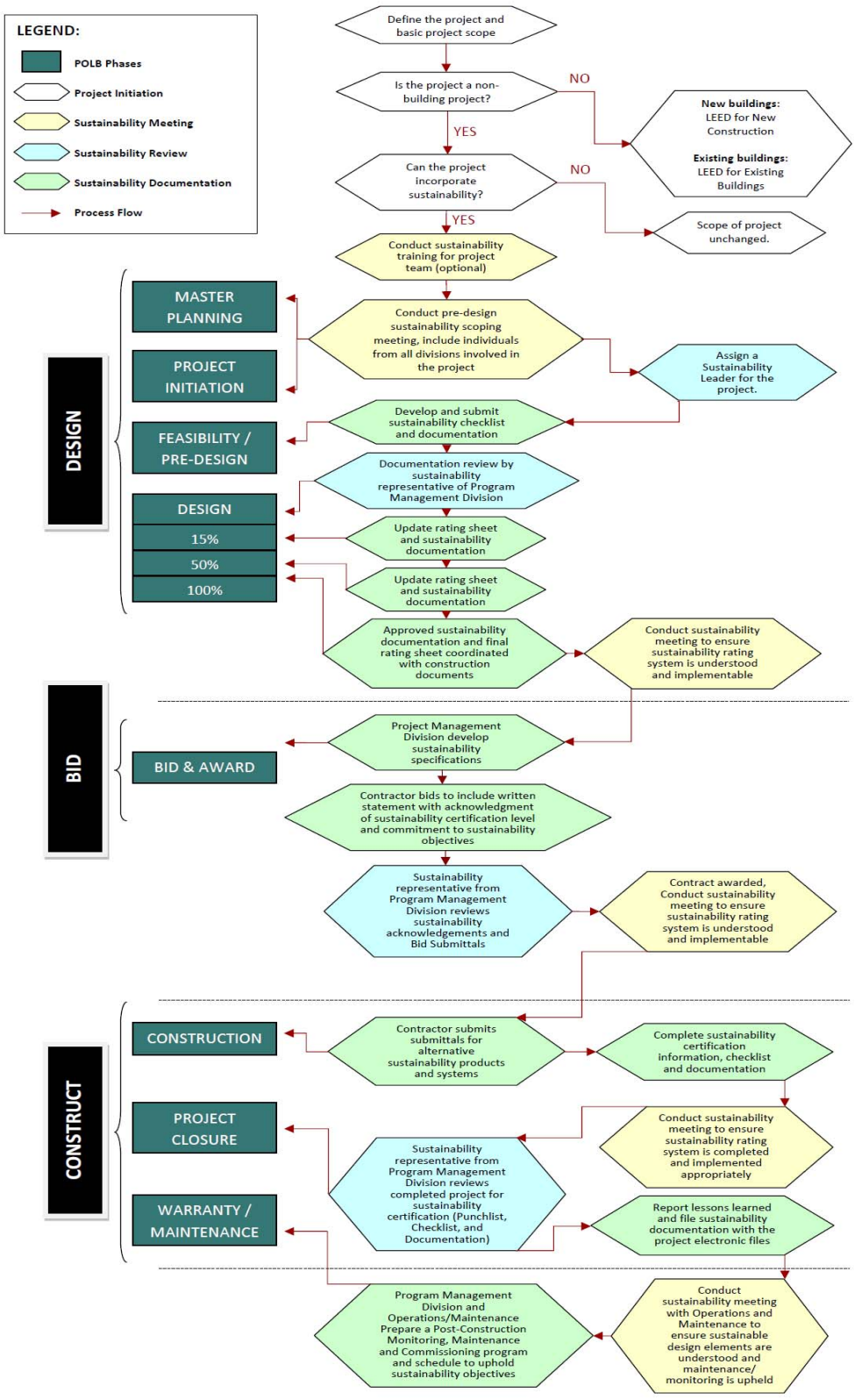


Figure 1. Implementation Process Flow Chart.

Implementation Process Checklists

The success of a sustainably designed and constructed project relies heavily on cross-divisional communication. The Implementation Process Checklists encourage communication and interactive management processes throughout a project's development and are aligned with the phases outlined in the Program Management Division's Project Delivery Manual (Port of Long Beach 2009):

- Master Planning
- Project Initiation
- Feasibility Pre-Design
- Design 15/50/100%
- Bid and Award
- Construction
- Project Closure
- Warranty/Maintenance

To improve project coordination and communication, the Implementation Process Checklists are consulted at the beginning of each phase of project development to identify additional management tasks, meetings, and documentation (see Figure 2). As the project transitions between phases, the project file is updated to reflect a project's current scope and applicable sustainability strategies. In addition, the Implementation Process Checklists identify recommended documentation to assist in the tracking of sustainable projects. The Program Management Division at the Port is responsible for tracking the execution of projects and through this document, ensuring:

- The project's sustainability attributes are communicated and understood by all Divisions involved in the project; and
- The construction documents and specifications clearly identify the sustainability attributes of the project prior to bid.

Strategic Sustainability Checklists

The Strategic Sustainability Checklists are a significant component of the *Sustainability Guidelines*. The checklists reflect the intrinsic qualities of typical Port projects and address decisions like design attributes, construction processes, appropriate material selection, equipment requirements, and efficiencies in construction equipment operation. During the project's initiation, the applicable sustainability checklist for the appropriate project type is used to identify opportunities where sustainable attributes can be integrated into that project. The goal of the sustainability strategies is not only to provide project guidance, but to also educate the project team on sustainable strategies and encourage innovation. The *Sustainability Guidelines* contain the following 13 project types:

1. Group A: Dredging
2. Group B: Wharves
3. Group C: Roadways, Railways and Bridges

4. Group D: Stormwater Management
5. Group E: Landscaping
6. Group F: Utilities Systems
7. Group G: Demolition of Existing Facilities
8. Group H: Revetment
9. Group I: Terminals
10. Group J: Remediation Projects
11. Group K: Geotechnical Soil Improvement
12. Group L: Traffic Management
13. Group M: Technology Projects



2.3.3 Feasibility Pre-Design: Process Checklist

Consider:

- ☐ Reviewing the selected sustainability strategies and their feasibility (e.g., LCCA, cost, scheduling, stakeholder issues), including:
  - ☐ Making any needed changes to the scope of work, design criteria or management plan;
  - ☐ Identifying if additional sustainability data, documentation, and stakeholder input is needed;
  - ☐ Determining who will gather the data and assemble information; and
  - ☐ Consider if the Board needs training, data, or information about the selected sustainability strategies in advance of their project approval process.
- ☐ Ensure that information about the sustainability strategies is included in the Design Criteria, Preliminary Costs, and Basis of Design Documents.
- ☐ Consider Sustainability Status Meeting with appropriate team members and internal/external stakeholders.
- ☐ Document the Board's approval of the project and the associated sustainability strategies.
- ☐ Confirming that the documentation is up-to-date with new information (approvals, lessons learned, barriers, keys to success, updates, etc.) as it emerges.
- ☐ Updating the Responsibility Assignment Matrix with sustainability tasks.

Possible Documentation:

- ☐ Project documentation updated and current.
- ☐ Training materials for the Board.
- ☐ Internal Team meeting minutes regarding sustainability discussions.

Approval Signature: _____ (Digital Signature) MM/DD/YYYY (Date)

Figure 2. Sample Implementation Process Checklist.

The Strategic Sustainability Checklists are formatted to identify sustainability considerations across a broad range of topics specific to the Port project groupings.

The Strategic Sustainability Checklists are divided into sections focusing on the triple bottom line approach to sustainability: economic benefit, environmental stewardship, and community integrity. Each strategy contains information on the **intent**, **target**, and **benefit** of the identified sustainability attribute (see Figure 3). The Strategic Sustainability Checklists are divided into the following sections:

- Economic Considerations and Documentation
- Site/Marine Restoration and Integrated Vegetation
- Improve Transportation Efficiency
- Waste Management
- Materials and Resource Efficiency
- Energy Management and Efficiency
- Air Emissions and Atmosphere
- Water Management and Efficiency
- Public Outreach and Community Relations
- Innovation in Design
- Port Priorities
- Maintenance, Monitoring and Reporting

As the project moves through the planning, design, and construction phases, the Strategic Sustainability Checklists are re-evaluated as necessary. When major changes are made to the sustainability aspects of the project, changes are documented and contribute to "lessons learned" on the project. The sustainability strategies also provide a methodology for identifying the project's maximum impact on environmental stewardship, community integrity, and economic value. Projects and approaches can be compared using these criteria and evaluated based upon the Port's overall strategic goals.

The incorporation of sustainability strategies into a project may include additional requirements in the construction drawings and specifications, the development of a community educational program, or a life cycle cost analysis report generated to outline economic benefits and return on investment. Additionally, in an effort to promote community integration and economic development, the sustainability strategies also consider further outreach and coordination with other divisions across the Port including Communications and Community Relations, Trade Relations and Port Operations, Maintenance, Real Estate, and Environmental Planning.



3.2.1 Group A: Dredging

Strategic Sustainability Checklist

SUSTAINABILITY STRATEGIES	Environmental	Social	Economic	Total Strategies

GROUP A Dredging/Disposal and Landfill
- Dredging Operations and Management
- Disposal Management
- Landfill Management

Intent:
Reduce the impacts dredging and the disposal/landfill management of dredged material has on site and marine environments. Consider impacts dredging has on air emissions, energy consumption, noise pollution, biodiversity and water quality.

Targets:
Identify opportunities for the use of dredged material for concurrent Port projects. Utilize equipment that minimizes impacts on energy consumption, water quality and air emissions. Maximize shallow marine habitat restoration projects.

Benefits:
Considering sustainable actions improves trade growth (channel navigation), promotes material reuse in Port projects (dredge material for site projects), and is in line with the Port's commitment to sustainability.

"✓" Indicates a Benefit to the Triple Bottom Line Approach to Sustainability
Note: These are shown for illustrative purposes.

Economic Considerations and Documentation:

Intent:
Develop a Life Cycle Cost Analysis (LCCA) for the project to identify the advantages and disadvantages of sustainable project attributes, determine the most cost effective approach, and recognize ongoing versus capital costs. Encourage materials that are extracted and manufactured within the local and regional area to stimulate the regional economy and reduce GHG emission through the reduced demand for long distance transportation.

Targets:
Define a sustainable project scope through the process of LCCA to determine which project has the most environmental, economic and social benefits. Establish a goal for the use of materials and suppliers sourced locally and/or regionally based on a percentage of the overall amount or cost of materials.

Benefits:
A LCCA fosters awareness of the triple bottom line approach and return on investment (ROI) when comparing project alternatives, design features, and systems. Using local and regional materials reduces fossil fuel usage and transportation costs whilst stimulating local and regional economies and fostering community trust and integration.

			2	2	2	
		Life Cycle Cost Analysis (LCCA) - **Ongoing Costs (Maintenance/Operational Costs)** - **Capital Costs (Construction Costs)** - **Return on Investment - Triple Bottom Line** - **Energy Reduction/Optimization** - **Water Reduction** - **Waste Reduction** - **Non-Renewable Material Reduction** - **Sustainable Technologies, etc.**				
		Consider:				
1.1	☐	A Life Cycle Cost Analysis to document all associated economic, social and environmental benefits or disadvantages to the project.	✓	✓	✓	0
		Local/Regional Materials and Suppliers				
		Consider:				
1.2	☐	Using the dredge material locally at the Port or within the community, where appropriate, recognizing the economic value of healthy dredge material as construction materials.	✓	✓	✓	0
					Summary	0

Figure 3. Sample Strategic Sustainability Checklist.

Sustainability Summary Sheet

The *Green Port Policy* requires annual evaluation of the goals and objectives for each Green Port Element. Determining the level of success on implementation of the *Green Port Policy* requires monitoring, measuring, and accounting of contributing projects and initiatives. The *Sustainability Guidelines* provide the framework for the Port's Engineering Bureau to track and account for those projects where sustainability attributes have been implemented and thereby contribute to the goals of the *Green Port Policy*. Every project that goes "beyond the standard approach" (i.e., a project that includes sustainability attributes where none were previously considered) is deemed a sustainable port project. Through use of the *Sustainability Guidelines* reporting process, Program Managers can monitor and measure implementation using the Sustainability Summary Sheet. It is important to recognize that timely, detailed record-keeping is essential to sustainable projects.

The Sustainability Summary Sheet takes into account the practical considerations faced by Program Managers at the Port and functions as a "report card" to assess the project's sustainability performance against similar project types (see Figure 4). Altogether, the Sustainability Summary Sheet documents the project's attributes including:

- Project information;
- Applied sustainability strategies and application;
- A list of the Port staff members responsible for reviewing the project;
- An overview of the total sustainability strategies applied to the project with a breakdown of the project's benefits to the triple bottom line approach; and
- Lessons Learned.

The Sustainability Summary Sheet also serves as a tool to engage stakeholders in the process of evaluating sustainable projects. As Port and community priorities change over time, so too will the application of the *Sustainability Guidelines* and the content of the Sustainability Summary Sheet. However, the reporting process should aim for consistency to allow internal and external stakeholders to benchmark project performance and assess the progress of Port projects moving towards sustainability.

As comparisons between Port projects are established, sensitivities to the varying factors influencing the project are important. These variables include project size, geographical influences, economic conditions, and environmental mitigation measures. To ensure that comparisons between similar Port projects are reliable and meaningful, these variables are documented throughout the project's development. The Lessons Learned section of the Sustainability Summary Sheet should reflect successful and unsuccessful aspects of the project's capability to implement sustainability. This section also enables Port decision makers to understand the opportunities and obstacles that exist in implementing sustainability.

Total Sustainability Strategies	Environmental	Social	Economic	Total Strategies
	0	0	0	0



		How has this strategy been addressed? Or, why was this strategy not addressed?	Provide details of supporting documentation/reference material.
1.1	A Life Cycle Cost Analysis to document all associated economic, social and environmental benefits or disadvantages to the project.	0	0
1.2	Using the dredge material locally at the Port or within the community, where appropriate, recognizing the economic value of healthy dredge material as construction materials.	0	0
2.1	Demonstrating in the LCCA that trade growth opportunities due to sustainably managed projects are beneficial.	0	0
2.2	Documenting how the sustainability of the project supports and/or is beneficial to real estate services and tenant leases.	0	0
3.1	Re-use of non-contaminated dredge material for wharf and terminal construction projects, bankside protection from soil erosion, or identify other site rehabilitation opportunities at the Port where the reuse of dredge material is appropriate.	0	0

Figure 4. Sample Section of Sustainability Summary Sheet.

A transparent documentation process is essential to stakeholder collaboration and is critical to the successful use of the Sustainability Summary Sheet. Supporting documentation processes include references to specific sheets in the construction documents, specification section numbers and product information, Life Cycle Cost Analysis documentation, and other identifiable processes. The supporting documentation should be accurate and detailed so that environmental, social, and economic benefits or disadvantages are acknowledged. Innovative strategies applied to projects utilize the Innovation Documentation Form to justify beneficial attributes. Program Managers using the *Sustainability Guidelines* should be able to compare past projects against future projects, and to the degree possible, against emerging global sustainability goals and metrics.

Sustainability Guidelines Current Implementation and Way Forward

Implementation of the *Sustainability Guidelines* is currently in process at the Port. The *Sustainability Guidelines* have been submitted in final form to the other internal engineering divisions, as well as several external organizations for review on an informal basis. Three levels of training and testing are planned at this time. Training for engineering management will occur first to ensure buy-in and support. Additional management training will be offered to other senior and executive management to generate support for the *Sustainability Guidelines*. Once this support is solidified, presentation of the *Sustainability Guidelines* to the Board of Harbor Commissioners will request formal adoption as policy. Board adoption has the weight of policy and will incorporate the *Sustainability Guidelines* as an element of the *Green Port Policy*.

Concurrent with training and adoption as policy, the Program Management Division is finalizing pilot testing of the *Sustainability Guidelines* on past and current projects. The first phase is to apply the *Sustainability Guidelines* to three past projects to test their relevance and performance on projects executed under standard Project Delivery Manual methodology. Three projects currently in progress will also be targeted for application of the guidelines to compare results against the completed projects. In addition, several new projects will be initiated using the *Sustainability Guidelines* to determine the level of effort required to implement and document compliance.

Final implementation and testing of the system is expected to take up to one year to complete. Meanwhile, the Port has engaged with other West Coast ports to develop sustainability guidance that will use the Port's *Sustainability Guidelines* as a starting point. This additional review is expected to further refine the *Sustainability Guidelines* through focused discussions by the most current and knowledgeable practitioners of Port engineering.

In its final form, application of the *Sustainability Guidelines* will be formally implemented as a project of the Port's Green Port Integration Initiative. Each division in the Port is required to implement one sustainability project whose performance can be objectively measured to support annual progress and reporting on sustainability. In the long term, the *Sustainability Guidelines* will be applied to every project that Program Management delivers and will be refined as lessons are learned.

The *Sustainability Guidelines* were not designed to become a universal standard against which all port projects could be measured. Instead, the explicit goal is to develop a system against which Port Engineering could benchmark and optimize internal project execution. As these *Sustainability Guidelines* mature and the number of project implementations grow, the Port will have an objective database to measure its level of incorporation of the basic tenets of sustainability into its every day processes.

REFERENCES

American Association of Port Authorities (AAPA). (2007) "AAPA Sustainability Resolution." http://aapa.files.cms-plus.com/PDFs/sustainability_resolutions.pdf. (March 29, 2011).

Port of Long Beach. (2011). "Sustainability." http://www.polb.com/environment/sustainability/default.asp. (April 14, 2011).

Port of Long Beach. (2009). *Program Management Division's Project Delivery Manual*, Long Beach, California.

Port of Long Beach. (2005). "Green Port Policy." http://www.polb.com/environment/green_port_policy/default.asp. (April 14, 2011).

Boat-wake Observations at Jensen Beach, Florida

A. Sheremet[1], U. Gravois[1], M. Tian[1], and T.K. Blankenship, P.E., M. ASCE[2]

[1]Civil & Coastal Engineering, 365 Weil Hall, University of Florida, Gainesville, FL 32611; PH: (352) 392-9537x1429; email: alex@coastal.ufl.edu

[2]Coastal Systems International, Inc. 464 South Dixie Highway Coral Gables, FL 33146; PH: (305) 661-3655; FAX: (305) 661-1914; email: tblankenship@coastalsystemsint.com

ABSTRACT

A field experiment was conducted in October-December 2011 to measure wave activity at Jensen Beach, Florida, at a projected mooring field. The goal of the experiment was to observe the wind-wave climate, and also understand the contribution of boat traffic to wave agitation. Time-frequency analysis (wavelet transform, and instantaneous frequency, e.g., Mallat, 1998) was used to identify boat wakes in the wind-wave background. The method allows for detecting boat wakes and studying their statistics, even in the presence of a relatively strong broad-banded wind-wave background (in this case the wind-wave spectrum is approximately 0.2-Hz wide, with the peak at 0.5 Hz).

INTRODUCTION

Martin County has retained Coastal Systems International, Inc. to design a managed mooring field at Jensen Beach, Florida. In order to assess the necessity of including a wave attenuator in the design for the facility, Martin County has authorized a field study at the site to observe wave characteristics. In addition to wind-generated waves, disturbances by boat traffic are an important source of wave variance at Jensen Beach. The goal of the project was to detect and characterize both components of the wave field at the site.

In contrast to wind-waves, comparatively spatially homogeneous and stationary over a time scale of the order of 1 day, boat-wakes are transient pulses, non-homogeneous and strongly directional, with a typical duration of 1 minute. Following early theoretical investigations (Froude, 1877; Kelvin, 1887), the study of the generation and propagation of ship wake intensified toward the end of the last century (Ursell, 1960; Peregrine, 1971; Sorensen, 1973; Mei, 1986; Ertekin et al., 1986; Gourlay, 2001; Torsvik et al., 2006 and many others (reviews of prior work by Wehausen, 1973; Sorensen, 1973; Newman, 1978; Soomere, 2003). Historically, ship wake research focused on optimizing ship performance (Newman, 1978). Recently, however, they have also received attention for their impact on the environment (Bauer et al., 2002; Parnell and Kofoed-Hansen, 2001; McConchie and Toleman, 2003; Stevens and Ekermo, 2003; Soomere and Kask, 2003), and have even

been proposed as models for the generation and propagation of freak waves Kharif and Pelinovski (2003); Trulsen and Dysthe (1997); Soomere (2003) Although the process of generation and propagation of boat wakes is well understood, we are not aware of any attempt to study the longer term statistics of boat-wake activity. Previous discussions of boat-wake observations (Sorensen, 1973; Soomere and Kask, 2003) have been largely based on idealized wake shapes.

One of the main goals of this project was to detect and characterize boat wake activity in the Jensen Beach area. This posed two challenges: identifying all the wake events recorded by the instruments, and developing a consistent approach to the statistical description of boat wakes. Wake detection requires separating a transient, localized signal from the ambient stationary signal. Here, we employ time-frequency analysis to detect the characteristic time-frequency shift that differentiates wakes from the stationary wind-wave background. The method also suggests a natural, unifying approach to the statistical description of the boat-wake "climate", regardless of random distortions due to propagation processes (e.g., reflection, dissipation, etc).

FIELD EXPERIMENT

The University of Florida collected wave measurements at Jensen Beach from Sept. 15th to Dec. 10th 2010, using a 1228.8-kHz WorkHorse ADCP (Acoustic Doppler Current Profiler, Teledyne RD Instruments) with directional wave measurement capability, and a Vector ADV (Acoustic Doppler Velocimeter, Nortek AS). Both instrument locations are in approximately 2.5-m water depth. The location of the sensors is shown in Figure 1.

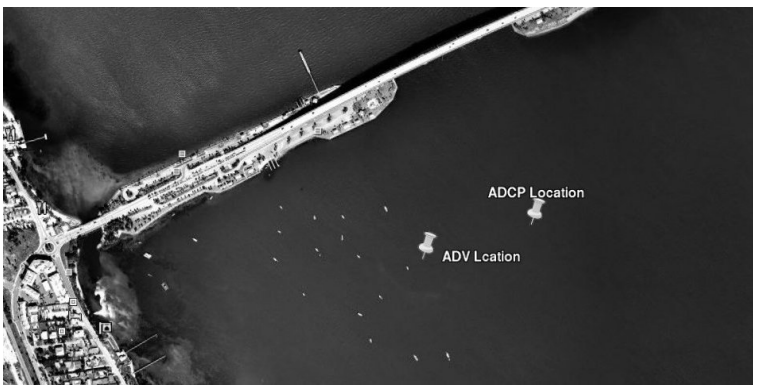


Figure 1: Experiment site. ADCP : Lat. 27°14.994', Lon. 80° 13.070. ADV: Lat. 27° 14.972; Lon: 80° 13.214.

The ADCP provided estimates of the mean currents and directional wave spectrum. The transducer was placed 0.7 m above the bed, with a blanking distance of 0.72 m. Pressure and the vertical structure of flow velocity were sampled at 2 Hz, in 20-min measurement bursts every hour. The sampling scheme used and the power requirements of the instrument allowed it to function for the entire duration of the deployment. All directional data collected was projected onto a reference frame with the x-axis pointing to East, y-axis toward North, and z-axis upward.

The ADV was located at approximately 0.5 m above the bed, and sampled pressure and the three-dimensional flow velocity at 4 Hz. Measurement bursts spanning several hours of continuous sampling are necessary to capture these transient trains (order of a minute) of short waves (period of about 2-2.5 s). Due to battery capacity constraints, the ADV observations were scheduled in 3-hour measurement bursts alternating with 3 hours of inactivity. The instrument recorded for 48 days.

DATA ANALYSIS AND RESULTS

Wind waves. The methods for the analysis of wind waves are well established. Directional wave spectra were estimated using the RD Instruments software, with a frequency resolution of 0.0078 Hz and angular resolution of 4 degrees. Wind-wave spectra were also estimated from ADV pressure observations, using standard Welch estimates (Welch, 1967). ADV pressure series of 15-min length were divided into 50% overlap (64-s segments, 256 samples) that Hanning-windowed, and Fourier transformed yielding an approximately 26-DOF spectrum estimate. The spectra were corrected for depth using the linear amplification factor

$$K^2(f,d) = \left(\frac{\cosh kd}{\cosh kh}\right)^2, \quad (1)$$

where the wave number k and the radian frequency $\omega = 2\pi f$ satisfy the dispersion relationship $\omega^2 = gk\tanh kd$, with h is the height of the instrument above the bed (0.5 m) and d is the 15-min average of the observed water level. To avoid amplifying noise in the high-frequency tail of the spectrum, the depth correction was applied only for the frequencies with $K^2(f,d) < 10$. The frequency range cut off in the depth-corrected spectral shape was replaced with a f^{-5} tail.

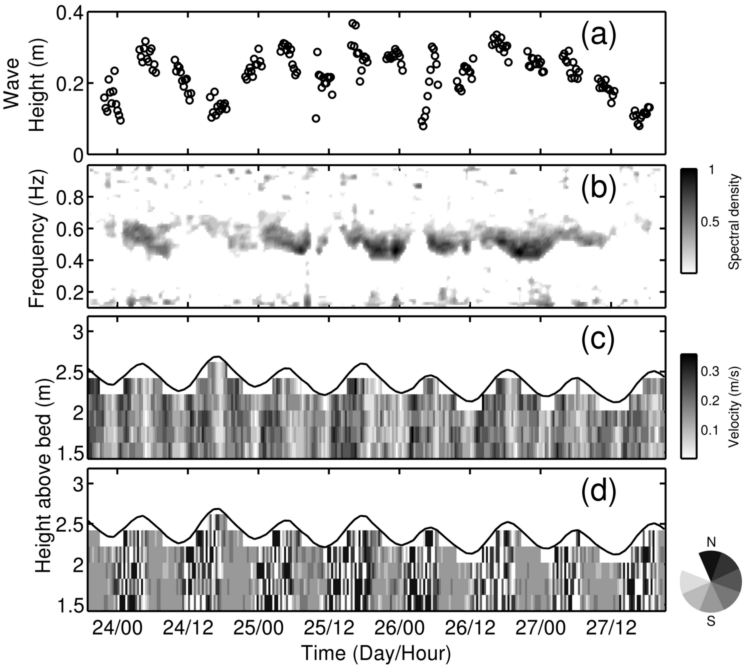


Figure 2: Waves and mean currents, Sept 26th - 30th, 2010.: a) Significant wave height (ADCP – line, ADV – circles); b) wave frequency spectrum (ADCP); c) mean water level and current velocity (ADCP); d) current direction (ADCP).

Wind-wave conditions are illustrated in Figure 2 for a 3-day period of relatively high (for the area) wave activity. In general, significant heights of wind-waves (Figure 2a) rarely exceeded 0.4 m, with peak periods typically between 2 and 2.5 s (Figure 2b). The propagation direction of wind-waves was largely aligned with the NNW-SSE axis of the intracoastal water. Because the area is partially protected from the north by the bridge (Figure 1), the higher wave events are typically associated with southeasterly wind. This is the case of the pulses seen in Figure 2b, which also propagate against the tidal current.

Maximum mean surface currents are typically less than 0.5 m/s, with tidal flood currents flowing northward, and ebb currents southward.

Boat wakes. At a fixed location, boat wakes can be characterized as short wave-trains (order of 10 waves), with a leading group of long waves followed by increasingly high frequency waves. This characteristic time-frequency shift can be used to separate wakes from the wind wave background, using time-frequency analysis tools such as the windowed Fourier transform, the wavelet transform, and/or estimates of instantaneous frequency (e.g., Mallat, 1998).

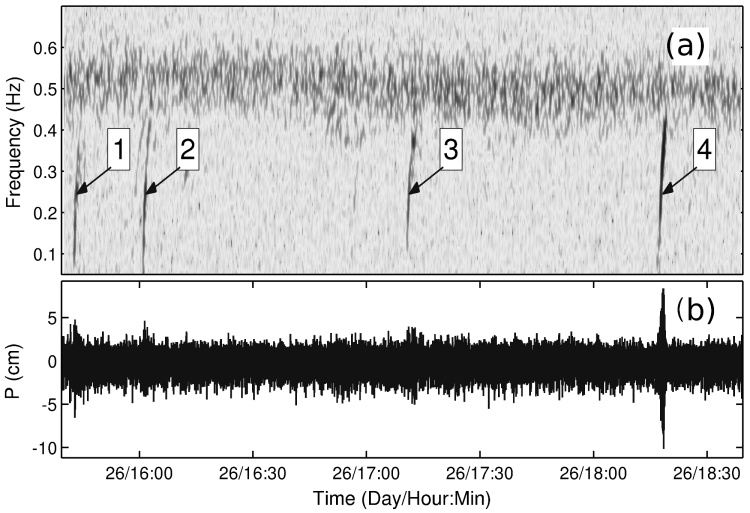


Figure 3: Wakes embedded in the wind-wave background (Oct. 26, 2010, 15:00 hours). a) spectrogram; b) corresponding pressure time series. Identified wakes are marked by numbers.

Like the Fourier analysis, the windowed Fourier and wavelet transforms decompose the signal in a set of "elementary" localized oscillations. A common such elementary function is the Morlet wavelet, a Gaussian windowed complex exponential. The contribution of each elementary function is represented by modulus squared of the complex coefficients of the decomposition – called spectrogram for the windowed Fourier transform, and scalogram in the case of the the wavelet transform. Because the decomposition is local, the spectrum is a function of both the frequency and time. For the purposes of this study the two methods produced equivalent results.

Figure 3 illustrates the use of the windowed Fourier transform for wake detection. Large amplitude wakes are clearly identifiable in the ADV pressure record as intermittent "spikes" (Figure 3b). Weaker wakes, which can still pose risks due to the low-frequency leading waves, are harder to detect, because their amplitudes might not emerge above the ambient wave variance. For time-frequency spectral analysis, 3-hour ADV measurement burst (pressure, Figure 3b) was divided into 95%-overlapping windows of 256 points (approx. 1 min). The resulting spectrogram (Figure 3a) shows a continuous wind-wave band in the frequency range of $f \simeq 0.5$ Hz, but also exhibits clearly visible "streaks" across the lower frequency band $f < 0.4$Hz. Comparing Figures 3a and3b, some streaks correspond to spikes in the time pressure series (e.g. event 4), but some do not (e.g., events 1-3).

The relation between these streaks and the wake structure is apparent when looking at the details of the spectrogram. Figure 4 shows the structure of the spectral time-frequency shift associated pressure signal for a typical, well defined wake (recorded on Nov 18th, 15:39 hours). The change in the time-frequency position of the spectral peak is associated with the frequency increase toward the tail of the wake. Any method used to estimate the free surface elevation using a depth correction (e.g., coefficient K in equation 1 depends on frequency) should account for this frequency shift. Linear corrections have been shown to work well for wakes (Ellis et al., 2006). Here, the correction given by equation 1 is applied using the instantaneous frequency of the wake, defined as (e.g.,

Mallat, 1998)

$$f(t) = \frac{1}{2\pi}\frac{d\arg p_a(t)}{dt}$$

where $p_a(t) = p(t) + i\mathsf{H}\{p(t)\}\}$ is the analytic signal associated with the measured signal $p(t)$ (e.g., pressure), with H the Hilbert transform.

In this study, wakes were identified based on a number of typical wake properties.

Large amplitudes: strong wakes have larger amplitudes than the background waves (they appear as spikes in the record). This criterion is not useful if the ambient waves and wakes have similar amplitudes.

Low-frequency leading waves: as illustrated in Figure 3, the leading wave group in a wake has frequencies lower than the background wind waves.

Time-frequency shift: the low-frequency leading wave is typically followed by increasingly high-frequency waves. In a spectrogram (scalogram), this appears as a streak.

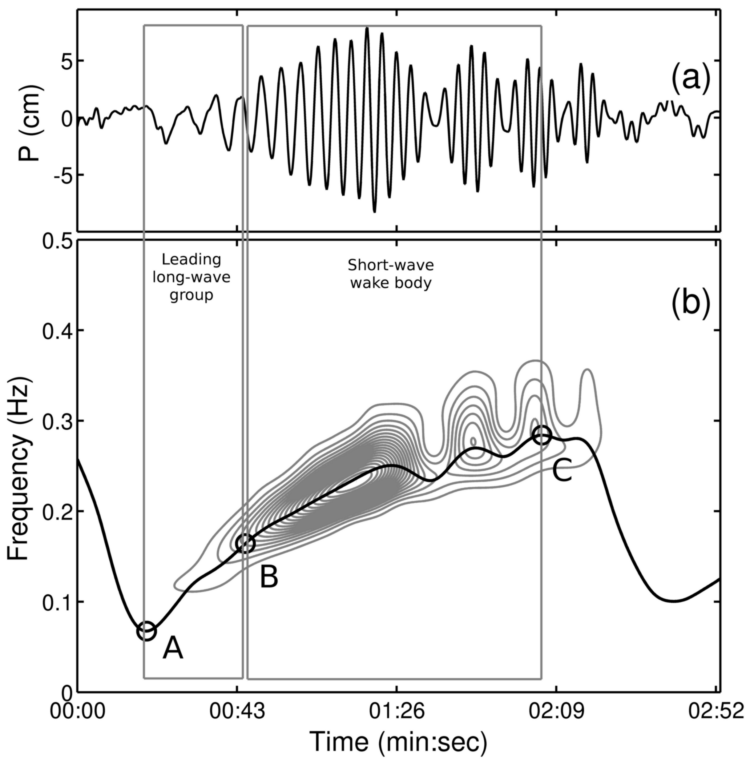


Figure 4: Typical wake: a) Depth-corrected free surface elevation; b) Spectrogram contours and instantaneous frequency (thick line).

Correlated pressure and velocity fields: in general, at Jensen Beach, because wind-waves are typically short (weak depth penetration), and the velocity contains significant non-wave components (e.g., turbulent eddies), bottom pressure and velocity observations are weakly correlated. In contrast, the low-frequency leading group of waves in a wake reaches deep into the water column, resulting in temporary strongly correlated pressure and velocities.

Statistics. Methods suggested previously for characterizing wakes (e.g., Sorensen, 1973) represent in essence efforts to address the difficulty posed by the time-frequency shift of the wake. In reality, idealized wake shapes are seldom seen; wake fragments from remote sources, reflected wakes, overlapping wakes, and other distortions are much more common than well developed/defined wake.

However, if the wake is defined as a chirp, its time-frequency shift characteristics provide a natural way to classify and analyze the statistics of wakes. While, in our experience, the time-frequency shift is always smooth, for simplicity, we propose to break the wake signal into two distinct families of waves (Figure 4b):

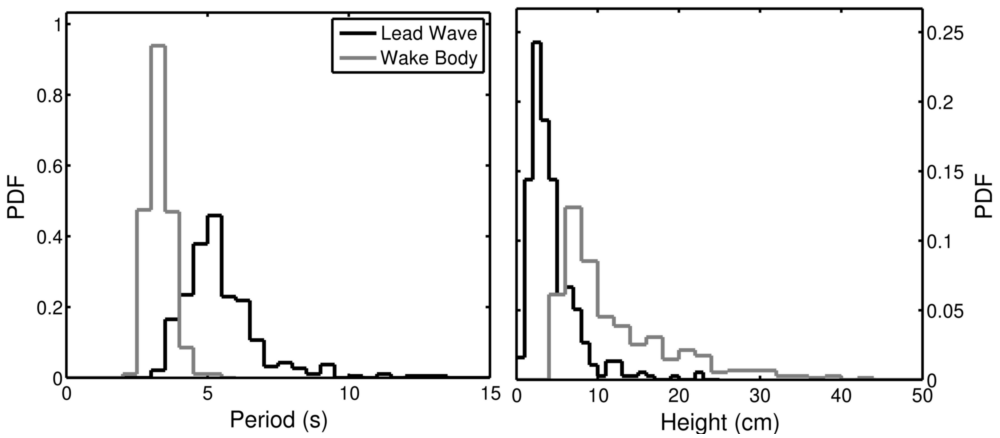


Figure 5: Estimates of the probability density functions for Left: mean leading-group and wake-body periods; Right: mean height of leading group, and *maximum* height of wake body.

The leading group: this contains the low-frequency waves that first arrive at the location of the sensor. These are typically low amplitude waves. In Figure 4b, this is the time segment between points A and B. For application purposes, this segment was defined here as the first 1/4 of wake duration.

The wake body: the remainder of the wake, containing higher-frequency waves chasing the leading group. The wake body has typically larger amplitudes, and sometimes also exhibits some groupiness (e.g., Figure 4a). In Figure 4b, this is the time segment between points B and C, and represents the remainder 3/4 of the wake duration.

The wake duration is defined here as the span in time of the scalogram "streak" (Figure 4b). Using the instantaneous frequency estimate, this is the time interval between the minimum and maximum frequency points that bracket a wake. In Figure 4b, this is the time interval between the minimum (point A) and the next maximum (point C) of the instantaneous frequency. Note that the definition of the wake duration is robust (derives directly from its instantaneous frequency characteristics) whereas the choice of the position of point B (separation between the leading group and wake body) is arbitrary.

Using these definitions, boat wakes were identified in this study following a procedure that took into account the characteristics of the 4-Hz ADV time-series, as well as the time-frequency phase-lag distributions of pressure and horizontal velocities. Because the record is dominated by weak wakes, to avoid skewing wake statistics toward low numbers, the total wake population (approximately 620 possible wake events) was screened for unambiguously identifiable wakes. The resulting population (375 events) was used for the statistics. Figure 5 illustrates the application of the above definitions to the statistical description of boat wakes observed at the Jensen Beach site. The probability density functions (PDF) are given for the period and height averaged over the leading group and wake body. As expected, the leading group is characterized by larger periods and smaller amplitudes. The distribution of maximum height is given for the wake body because the maximum height is more relevant for design purposes.

CONCLUSIONS

Characterizing the contribution of boat traffic to wave agitation at Jensen Beach, Florida, posed two challenges – separating the wakes from the wind-wave background, and formulating a statistic description of wake events. The main conceptual difficulty, the transient character of a wake and the associated time-frequency shift, is also the key element that allow for formulating an efficient approach. In a time-frequency spectrogram (or scalogram), the wakes appear as "streaks", chirps, spanning a wide frequency range and are clearly defined against the narrower-band stationary wind wave signal. The time-frequency shift is also essential for wake classification and statistics, generating a natural, comprehensive set of selection criteria to identify unequivocally individual wake events. Based on the wake chirp characteristics, the statistics of heights and periods of the wake can be readily derived.

While in this study wakes were identified manually, the method is robust enough to allow the implementation of an automatic detection algorithm (under development). This study demonstrates the usefulness of the approach and suggests a wider range of applications, from statistical studies of boat-induced erosion to boat-traffic monitoring and control.

The experiment discussed here represents in some sense a minimum-resource (due to time and scope constraints) field approach to separating wakes from the wind-wave background. The approach can be considerably improved, for example, by using spatially-distributed (horizontally and vertically, e.g., current profilers) arrays of sensors (see, e.g., Sheremet et al., 2005, for an example of directional analysis based on spatial arrays). Spatial arrays can provide additional information about the wind-wave/wake field, such as propagation direction, wake type (e.g., sub/super-critical), and possibly even elements of boat identification, such as cruise speed, boat class etc.

From a more practical perspective, this project is an example of a relatively small investment in a field study that resulted in significant cost savings to the project. The field investigation provided insight into the full range of waves that might be experienced at the project site, and showed that additional, costly, protective structures were unnecessary.

Acknowledgments. Vic Adams (Coastal and Oceanographic Engineering Laboratory, University of Florida) was in charge of the field-operation logistics, and contributed significantly to the success of the field experiment. This study was sponsored by Martin County, Florida, USA.

References

Akylas, T. R., Kung, T. J., and Hall, R. E. (1988): "Nonlinear Groups in Ship Wakes," Proc. 17th Symposium in Naval Hydrodynamics, The Hague, The Netherlands, August 29–September 2, National Academy Press, Washington, D.C.

Bauer, B. O., Lorang, M. S., and Sherman, D. J. (2002): "Estimating Boat Wake-Induced Levee Erosion Using Sediment Suspension Measurements," J. Waterway, Port, Coastal, Ocean Eng., 128, pp. 152–162.

Ellis, J. T., D. J. Sherman, and B. O. Bauer, (2006): "Depth compensation for pressure transducer measurements of boat wakes", Journal of Coastal Research, SI 39 (Proceedings of the 8th International Coastal Symposium), 488 - 492. Itajaí, SC, Brazil.

Ertekin R. C., W. C. Webster, and J. V. Wehausen, (1986): "Waves caused by a moving disturbance in a shallow channel of finite width", J . Fluid Mech. 169, p. 275-292.

Froude, W., (1877): "Experiments Upon the Effect Produced on the Wave-Making Resistance of Ships by Length of Parallel Middle Body," Trans. Inst. Naval Architects, 18, pp. 77–87.

Gourlay, T. P., (2001): "The Supercritical Bore Produced by a High-speed Ship in a Channel," J. Fluid Mech., 434, pp. 399–409.

Thomson, W. Lord Kelvin, (1887): "On Ship Waves," Trans. Inst. Mech. Eng., 8, pp. 409–433.

Kharif, C., and Pelinovsky, E., (2003): "Physical Mechanisms of the Rogue Wave Phenomenon," Eur. J. Mech. B/Fluids, 22, pp. 603–634.

Mallat, S. (1998): "A wavelet tour of signal processing", Academic Press.

McConchie, J. A., and Toleman, I. E. J., (2003): "Boat Wakes as a Cause of Riverbank Erosion: A Case Study from the Waikato River, New Zealand," Journal of Hydrology New Zealand, 42, pp. 163–179.

Mei, C. C., (1986): "Radiation of Solitons by Slender Bodies Advancing in a Shallow Channel," J. Fluid Mech., 162, pp. 53–67.

Newman J.N., (1978): "The theory of ship motions," Advances in Applied Mechanics, 18, 221-283.

Peregrine, D. H., (1971): "A Ship's Waves and its Wake," J. Fluid Mech., 492, pp. 353–360.

Parnell, K. E., and Kofoed-Hansen, H., (2001): "Wakes From Large High-speed Ferries in Confined Coastal Waters: Management Approaches With Examples From New Zealand and Denmark," Coastal Manage., 29, pp. 217–237.

Sheremet, A., R. T. Guza, and T. H. C. Herbers (2005): "A new estimator for directional properties of nearshore waves", J. Geophys. Res., 110, C01001, doi:10.1029/2003JC002236.

Soomere, T., and Kask, J., (2003): "A Specific Impact of Waves of Fast Ferries on Sediment Transport Processes of Tallinn Bay," Proc. Est. Acad. Sci. Biol. Ecol., 52, pp. 319–331.

Soomere, T., (2007): "Nonlinear components of ship wake waves", Appl. Mech. Rev. 60.

Sorensen, R. M., (1973): "Ship-Generated Waves," Adv. Hydrosci., 9, pp. 49– 83.

Stevens, R. L., and Ekermo, S., (2003): "Sedimentation and Erosion in Connection with Ship Traffic, Göteborg Harbour, Sweden," Environ. Geol., 43, pp. 466–475.

Torsvik, T., Dysthe, K., and Pedersen, K., (2006): "Influence of Variable Froude Number on Waves Generated by Ships in Shallow Water," Phys. Fluids, 18, p. 062102.

Trulsen, K., and Dysthe, K., (1997): "Freak Waves-A Three-Dimensional Wave Simulation," 21st Symposium. on Naval Hydrodynamics, Trondheim, Nor- way, June 24–28, National Academy Press, Washington, D.C., pp. 550–560.

Ursell, F., (1960): "On Kelvin's Ship-Wave Pattern," J. Fluid Mech., 8, pp. 418–431.

Wehausen, J. V., (1973): "The Wave Resistance of Ships," Adv. Appl. Mech., 13, pp. 93–244.

Welch, P.D., (1967): The Use of Fast Fourier Transform for the Estimation of Power Spectra: A Method Based on Time Averaging Over Short, Modified Periodograms", IEEE Transactions on Audio Electroacoustics, Volume AU-15, pages 70–73.

Wyatt, D. C., (1988): "Analysis of Ship-Generated Surface Waves Using a Method Based Upon the Local Fourier Transform," J. Geophys. Res.,93 C11, pp. 14133–14164.

Sustainable coastal development in response to natural and anthropogenic impacts as well as to climate change

I. Brøker[1] and K. Mangor[2]

[1] DHI, Agern Allé 5, DK 2970 Horsholm, Denmark; PH: +45 4516 9174; FAX: +45 4516 9292; e-mail: ibh@dhigroup.com

[2] DHI, Agern Allé 5, DK 2970 Horsholm, Denmark; PH: +45 4516 9170; FAX: +45 4516 9292; e-mail: km@dhigroup.com

INTRODUCTION

There is huge pressure on the world's coasts due to development demands from coastal societies. The coastal area is special, because it defines the transition from land to sea. The coastal area thus offers access to the sea but on the other hand the sea also constitutes a severe restriction on the coastal area. Furthermore, the coastal area is a morphological active zone under the influence of the following "forces", processes and climate changes:

- Natural "forces" such as tides, surges and waves, and extreme events such as tropical cyclones (typhoons/hurricanes) and tsunamis
- Natural processes, such as sediment transport, coastal erosion, sand accumulation, sedimentation and location for river mouths and tidal inlets
- Climate change manifesting itself in the form of Sea Level Rise (SLR) and changed wind patterns

The increasing pressure on the shorelines and the coastal landscape from the above mentioned factors in combination with the anthropogenic activities (ports, coastal protection/sea defence, reclamations, coastal and offshore waterfront developments, cooling water intakes and outlets, infrastructure projects, wind farms, etc.) highlight the need for sustainable development in order to meet future demands in this region, while also taking into consideration the impacts associated with climate change. The concept of "Working with Nature" is important when the goal is to obtain an overall sustainable development.

HOW TO OBTAIN A SUSTAINABLE COASTAL DEVELOPMENT

Sustainable development is a pattern of resource use that aims to meet human needs while preserving the environment so that these needs can be met not only in the present, but also for future generations. (Bruntland Commission). With other words,

sustainable and holistic development serves the requirements of our society in terms of development needs and economic growth so that we get most possible out of the resources at the same time as we respect the environment or even rehabilitate past environmental damages. A holistic approach builds on the idea that the value of a given system (development) is more than the sum of the individual properties (physical, environmental, social, economic etc.) of which it is composed. This type of development requires the following initiatives and activities:

- The society must define its development goals in the form of **coastal zone management plans** and a series of **shoreline management plans**. It is important that only activities which, in one or the other way, require access to the sea are planned for in the coastal area due to the scarcity of space and due to the special threats and opportunities which characterises the proximity to the coast. Examples of such activities are the following:
    - Fishery and industrial ports need access to (deep) water
    - Tidal inlets need to be kept open and deep to provide the possibility for navigation
    - Various types of industry and public utilities need access to cooling water
    - "Offshore" wind turbines need sea area some distance from the coast
    - Various types of public infrastructure need access over the beach, such as bridges, tunnels and cables
    - Sand extraction activities on coasts and in rivers introduce coastal erosion and should consequently be regulated/restricted
    - Coral mining and coral reef destruction introduce coastal instability and environmental damage
    - Coastal recreational activities (hotels, apartment blocks, chalets and public beaches) need good beaches and good water quality
    - Aquaculture needs good water quality

  These plans reflect the needs of the society and shall respect the following coastal characteristics:
    - The coast is morphological active due to the impact of waves, tides and surges, which express themselves in terms of sediment transport, coastal erosion/accretion and sedimentation
    - Low lying coastal areas and hinterland may be exposed to coastal flooding due to storm surges (storms and tropical cyclones), sea level rise and tsunamis
    - Rivers discharge sediments to the coast in the form of sand and fine suspended sediments
    - Tidal inlets need to be open to provide water exchange to coastal lagoons
    - The coastal area, and especially river mouths and tidal inlets, tend to be very morphological active

The challenge for development in the coastal area is consequently to fulfil the needs of the society by utilising the unique opportunities provided by the coastal area but also taking into consideration the threats of coastal erosion/flooding and climate changes and at the same time securing that the various development items are neither disturbing each other nor having severe environmental impact.

TYPES OF COASTAL SCHEMES

There are many types of schemes being constructed along the coasts. The main types of schemes, which will be described in the present context, are:

1. Waterfront Development Schemes (WDS)
2. Shoreline Management Schemes (SMS)
3. Coast Protection Schemes (CPS)
4. Sea Defence Schemes (SDS)
5. Combined Sustainable Schemes (CSS)

There are also other types of schemes being constructed in coastal areas such as: Offshore Development Schemes (ODS) (refer the major schemes in the Arabian Gulf), ports, harbours, intake structures, etc. However, these schemes are not anticipated in the present context.

The objectives of the various schemes are different: Some schemes are development schemes which are built mainly for housing, tourism development and recreational reasons (WDS), whereas other schemes are built to mitigate different types of problems (SMS, CPS, SDC). A summary describing the problems leading to implementation of a scheme, the objective/characteristics of the scheme, the hydraulic issues within the scheme, and the impacts of the new scheme is presented in Table 1.

The most important technical aspect in the planning and development of any coastal section is that the natural conditions in the development area are understood and form the basis for any development in this area.

The following practical guidelines in terms of physical functionality and minimum impact of the different types of schemes can be provided.

Waterfront Development Scheme. A waterfront development scheme typically consists of the following marine elements:

- Artificial beaches, typically by building new beaches
- Reclaimed area for development
- Terminal structures to prevent loss from the artificial beaches, possibly combined with marinas or lagoon openings
- Artificial lagoons, either built into the sea in connection with beach reclamations or excavated into the mainland
- Lagoon openings, possibly navigable
- Marinas possibly combined with a lagoon

The Dubai Marina area (Marsa Dubai) can be characterised as a typical waterfront development scheme which is built for development reasons and not as a reaction to coastal instability, see Figure 1. It consists of the above mentioned elements.

Table 1. Summary of types of schemes and their relation to problems, objectives, characteristics, hydraulic issues, land use, coastal classification and impact of the scheme.

Type of scheme	Reason for implementation of scheme	Objective of scheme	Key characteristics of scheme	Hydraulic and environmental issues within the scheme	Permanent impact of scheme
Waterfront Development Schemes (WDS),	Lack of development area Lack of beach space and lagoon areas for private development	Economic development Enhancement of landscape quality in private development area	Land reclamation New beaches Excavation of new lagoons New marinas	Beach quality Flushing Water quality	Impact of scheme within the sediment cell
Shoreline Management Schemes (SMS), this includes Beach Parks (BP)	Mainly coastal erosion in coastal cell, natural or caused by other interventions	Mitigation of erosion problem Development of recreational public beach	Beach fill for new equilibrium beach Coastal structures to support new beach and lagoon opening	Beach stability and quality Flushing Water quality	Scheme is built to compensate coastal erosion but may cause erosion along adjacent sections
Coast Protection Schemes (CPS)	Coastal erosion risk	Only coast protection, not beach preservation	Typically rubble revetment	Exposure to waves and tide/surges	The scheme protects coastal facilities, however, the beach will be lost
Sea Defence Schemes (SDS)	Flooding risk	Protection against coastal flooding	Seawall, dike or reinforced dune	Exposure to tide/surges and waves	May impact on coastal conditions
Combined Sustainable Scheme	Deterioriated natural coastal environment	Rehabilitation and protection in general	Combines all elements of above schemes	Secures protection and sustainable development	Mainly positive impact as protection and rehabilitation are the main purposes of the scheme

Shoreline Management Scheme. A shoreline management scheme (SMS) is very similar to a waterfront development scheme; however, it is typically a public scheme built to compensate coastal instability and to rehabilitate and expand the beach and marine elements in an area. A SMS consists typically of the following marine elements:

- Artificial beaches and beach reclamations, typically by realigning/expending an existing beach to fit the equilibrium orientation
- Terminal structures to prevent loss from the artificial beaches, maybe combined with marinas or lagoon openings
- Artificial lagoons, either built into the sea in connection with beach reclamations or excavated into the mainland
- Lagoon openings



Figure 1. Examples of WDC and SMS. Upper: WDC example:Marsa Dubai. Lower: SMS or Beach Park example: Amager Beach Park, Copenhagen.

Amager Beach Park in Copenhagen is an example of a public beach park, where the themes are beaches, park areas and a recreational lagoon whereas there is no space for housing and similar private facilities, see Figure 1 lower panel. Further description can be found in Mangor et al., 2008.

Coast Protection Schemes. Historically, many coast protection schemes have caused severe damages to beaches as these are typically lost in connection with a hard coast protection scheme. If a protection scheme is constructed with the sole purpose of protecting the coast (the coast is the land landwards of the coastline) and coastal facilities against a receding coastline without eliminating the cause of the erosion, then the result will be that the erosion process continues until there is no more sand available. This typically happens if an eroding section is protected by a revetment. This type of protection is mainly used in areas where natural qualities of the coastal area are already eliminated by different kinds of development, such as industry, public utilities and private housing areas, and where the presence of a beach has no importance for the land owner. If the goal is to protect the coastal landscape including the beaches and access along the coast, in contrast to the simple goal of only protecting the coastal installations, then coastal protection shall be put into a broader context as described under shoreline management schemes.

It is therefore relevant to outline which types of coast protection are applicable if the goal is not only to protect the coast, but also to support a sustainable coastal development. The following types of coast protection are applicable when the objective is also to preserve or rehabilitate sandy beaches or beach sections:

- Management solution: The best way to secure a natural coast is to avoid the situation where protection becomes necessary by introducing a setback line which secures sufficient space for the natural development to take place. This is too late at many developed stretches but is should be implemented at all non-developed coasts
- Beach nourishment is best suited for controlling shoreline evolution along long sections of coast, where the cause of erosion is a deficit in the littoral budget, for one or the other reason. Beach nourishment is not suitable for small sections of eroding coast. Furthermore, beach nourishment requires regular repetition
- Mixed protection provided by coastal structures supporting sections of stable beaches. This kind of protection is especially suitable if the equilibrium orientation of the coast is not too different from the general alignment of the coastline in the considered section

Sea Defence Schemes. A sea defence structure has the purpose of protecting low-lying land against coastal flooding. The level of flooding shall be established by performing analyses taking the following contributions into account:

- Tides
- Meteorologically generated storm surges caused by major depressions and tropical storms (hurricanes and typhoons)

- Wave run-up
- Sea level rise caused by climate changes
- Tsunamis (see comments below)

It is normal practice to design coastal facilities without taking tsunamis into account as this would require unrealistic high sea walls or very wide no-build areas; however, very sensitive installations shall be secured against the impact of tsunamis, such as nuclear power plants. Information campaigns and warning systems are the most used precautions against the impact of tsunamis.

The risk of flooding can be evaluated by comparing the flooding levels for different return periods with the level of the coastal area, taking different life times and the acceptable percentage of risk during the life time for various schemes into consideration. The design life time is important for the assessment of the influence of the sea level rise. The great uncertainty in forecasting the sea level rise shall also be taken into account.

Seawalls, dikes, artificial dunes and raising the level of a specific activity area are the traditional sea defence elements normally used to protect an area against the risk of flooding. New reclaimed areas shall be designed with sufficient top level to take the flooding risk into account.

If the goal is to protect and enhance the quality of a low lying coastal landscape, in contrast to the simple goal of only protecting the coastal installations against flooding, then sea defence measures shall be put into a broader context as described under combined sustainable schemes.

Combined Sustainable Schemes

The above mentioned high pressure on the coastal zone combined with the impacts of climate changes indicate that it is necessary to think in more broad and flexible solutions in relation to coastal protection and sea defence techniques in order to obtain sustainable solutions. Traditional solutions (revetments, seawalls and dikes) are very inflexible and often counteract natural mechanisms, such as gradual retreat of the coastline and associated shoreward movement of the dune system. Furthermore, traditional protection solutions have often been introduced as remedial measures to compensate for negative impacts of other interventions, which is a reactive approach. But now, with the increasing impact of climate changes in the coastal zone, there is a good reason for shifting to a more proactive approach to obtain a sustainable development by taking into account all the needs and requirements in the coastal zone in integrated projects where present and future (climate changes) protection needs are combined with needs for development and rehabilitation of coastal resources. An example of an integrated coastal project could be a scheme which rehabilitates a coastal section by removing hard protection measures, providing new beaches for recreation and for local fishing activities, providing protection against erosion and flooding including the impacts of climate

changes and providing new space for development. Such a scheme will typically consist of artificial beaches and lagoons, reclaimed areas and coastal structures.

GENERAL CONSIDERATIONS FOR COASTAL SCHEMES

The main challenge in developing successful WDS, SMS and CSS along a coastal section is to understand the natural environmental conditions in the area and utilise the possibilities they provide as outlined in the following:

- Coastal instability problems are permanently solved, e.g. by building new beaches in the equilibrium orientation. More soft solutions, such as nourishment, are not applicable at such locations as regular maintenance is required. Classification of the coast relative to the wave conditions in terms of: a) the angle between the orientation of the coast and the equilibrium orientation is therefore important for the layout of a stable scheme and b) in terms of the exposure to waves is similarly important in order to design a good quality and safe beach
- Combining the requirements for terminal structures with meeting other demands in the area such as plans for expanding marinas, the need for new lagoon openings or the need for viewing and promenading facilities, etc. It is generally important to use the concept of multi-functional facilities for the development of new coastal structures due to the very limited space in coastal areas and due to the high demand for recreational facilities
- Lagoons shall only be considered in areas with a good water quality as the ambient water quality will govern the water quality in the lagoon and in areas where the amount of suspended sediments is small as high concentrations of suspended sediments will cause severe siltation in the lagoon
- Consider the presence of waves along a section as an opportunity for building good recreational beaches as the requirement for a good quality and safe beach is moderate wave exposure. An unstable coastal section shall therefore neither be protected by a revetment, as this will lead to loss of the beach nor by building sheltering structures for the beach, as this will lead to poor quality beaches due to lack of wave exposure. Use the concept of "Building with Nature", i.e. use the wave exposure to provide stable and good quality beaches by dividing the beach into sections turned up against the prevailing waves by the use of supporting coastal structures.

Internal functionality of the Scheme. The functionality of the artificial nature elements of the scheme is important to build into the layout of the scheme from the beginning as these are decided by the natural conditions, which cannot be changed. The functionality is especially related to the artificial beaches and lagoons.

Artificial Beaches

- The beach shall be exposed to waves to secure a good beach quality ($H_{S,12h/y}$ > 0.5 to 1.0 m) but for safety reasons the wave exposure shall not be too large during the bathing season (H_S < 0.8 m during the bathing season)
- Thus, avoid building beaches where the waves are not big enough and protect the beach partially if the waves during the bathing season are too large
- The orientation of the beach shall be the equilibrium orientation, i.e. the beach shall face the predominant waves
- Introduce few multi-functional terminal structures to secure against loss of sand thereby providing relatively long beach sections. There must not be sheltered corners behind the structures as these may introduce dangerous rip currents and trapping of sand, seaweed and debris. The structures shall have a streamlined form and the angle between the structure and the beach shall be concave to avoid corners, which may otherwise trap seaweed and debris
- Use only high quality clean marine sand

Artificial Lagoons

Good water quality in the lagoon is of paramount importance for the recreational value of the lagoon. This leads to the following requirements:

- The water quality in the adjacent water areas shall be excellent, which means that it shall be clean and clear (low content of suspended fine sediments)
- Good flushing of the lagoon shall be secured. This may require several openings to the sea and maybe forcing of circulation
- Discharge of pollutants and nutrients shall be avoided or limited
- The waterfront perimeters inside the lagoon shall be selected to provide the best possible recreational functionality, whereas protection is only a secondary requirement inside the lagoon. There are in principal the following types of perimeter structures:
    - Rubble mound slopes or revetments which, however, may not be attractive from a recreational and visual point of view
    - Vertical walls and bulkheads, which are suitable along promenades and in marinas, etc.
    - Stepped slopes, which are suitable along promenades and park areas
    - Piled decks and piers in concrete or wood, which are suitable along promenades, at private property and in marinas
    - Floating piers, which are suitable along promenades, at private property and in marinas
    - Sandy beaches are normally only advisable in very large or semi open lagoons as a wave exposure is required to maintain a good quality beach.

The above issues concern the internal functionality of the scheme, which shall by secured through early “work with nature” input in the planning process. However, it is also important to secure the requirement for minimum impact and sustainable development of the scheme.

Securing sustainability of WDS, SMS and CSS. Securing sustainability of a development scheme requires integration of horizontal (sector) and vertical (spatial) requirements. This highlights the importance of sufficient coordination between all involved authorities and stakeholders.

The general marine requirements for obtaining sustainability of a WDS, a SMS or a CSS are:

- Secure that the scheme does not impact the flushing and water quality in the adjacent area, neither during construction nor during the operation phase. Optimise and propose mitigating measures as required
- Secure that the scheme has a minimum impact on coastal conditions on the adjacent coast in respect to coastal stability and beach degradation. Optimize the layout for minimising the impact. If this is not enough propose and implement mitigating measures as required. This especially relates to the possible impact of major coastal structures such as expanded marinas and lagoon openings, as they may have impacts in the cell at both sides of the structure and not only to the side, where it is part of the actual scheme

EXAMPLES OF SUSTAINABLE SCHEMES

Koge Bay Beach Park: An old example of a sustainable project, which has proved to work very well, is the Koge Bay Beach Park located south of Copenhagen. This site was before the implementation of the project characterised by a shallow shoreface with some barrier islands and a low lying hinterland, which suffered from frequent flooding. The shallow coast was not suitable for recreation for which there was a huge demand as the backland is heavily populated. An integrated scheme was developed, combining construction of artificial beaches on top of the barrier islands for recreation, construction of 4 new marinas, excavation of new lagoons between the beach islands and the coast and introduction of a dike throughout the entire stretch, which secured the low lying backland against flooding. The project is show in Figure 2 below.

New landscaping in connection with the Fehmarnbelt Link project: The Danish and the German governments have decided to build a fixed link over the Fehmarnbelt connecting Denmark and Germany. The presently preferred type of link is an immersed tunnel comprising combined motorway and rail facilities between Rødby in Denmark and Puttgarden in Germany. The alignment is presented in Figure 3.

The conceptual design of the tunnel is performed by an international joint venture (RAT JV) composed of Rambøll (Denmark), Arup (UK) and Tunnel Engineering Consultants (Holland), with DHI and Schønherr A/S as sub-consultants for the layout of the landscaping adjacent to the tunnel portals.

In the process of excavating the trench for the tunnel there will be a surplus volume of excavated soil in the order of magnitude of 16 million m^3. This surplus volume of soil is planned to be used for creating a large new coastal landscape along the Danish Coast. The new landscape will consist of sections of beaches, armoured sections, a recreational lagoon and a coastal lagoon with wetlands, and a cliff section, which by erosion will supply the downstream coast with sediments.



Figure 2. Koge Bay Beach Park South of Copenhagen, inaugurated in 1980. Left: Natural conditions. Right Upper: Aerial photo. Right Lower: Satellite image with the alignment of the dike shown as a red line.

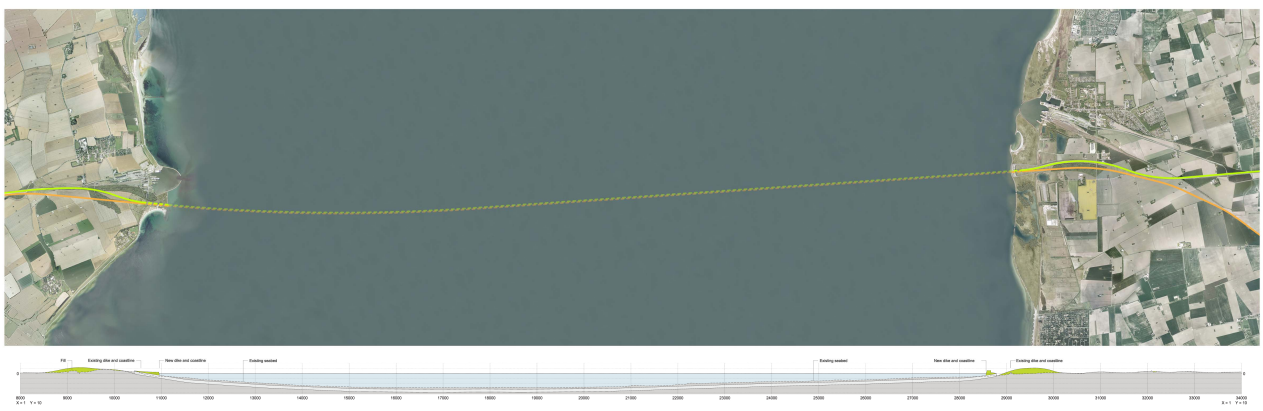


Figure 3. Tunnel alignment between Puttgarden (left) and Rødby (Right) (North to the right).

The objective of the reclamation works is to utilise the surplus volume of soil from the dredging of the tunnel trench for building of new artificial landscapes which add

new nature as well as environmental and recreational values to the area. Furthermore, the objective is also to re-establish some of the environmental values, which were lost in connection with the construction of a major dike along the coast in the area following a major flooding event in 1872. Finally, another objective was to mitigate the blocking of the littoral transport in the area by Rødby harbour, which was constructed more than 100 years ago, which resulted in disappearance of the beach in front of the dike east of the harbour. The mitigation of this cutting off of the littoral transport is done by introducing an unprotected cliff in the eastern part of the reclamation, which by erosion will supply sediments to the downstream coast.

The new landscape has been formed as a streamlined area along the existing coast with an extension into the sea similar to that of the existing Rødby Ferry Harbour whereby it is secured that there will be no additional blocking of the flow through the strait. The eastern part of the reclamation accommodates the tunnel portal and terminates towards east near the natural beach, see Figure 4.

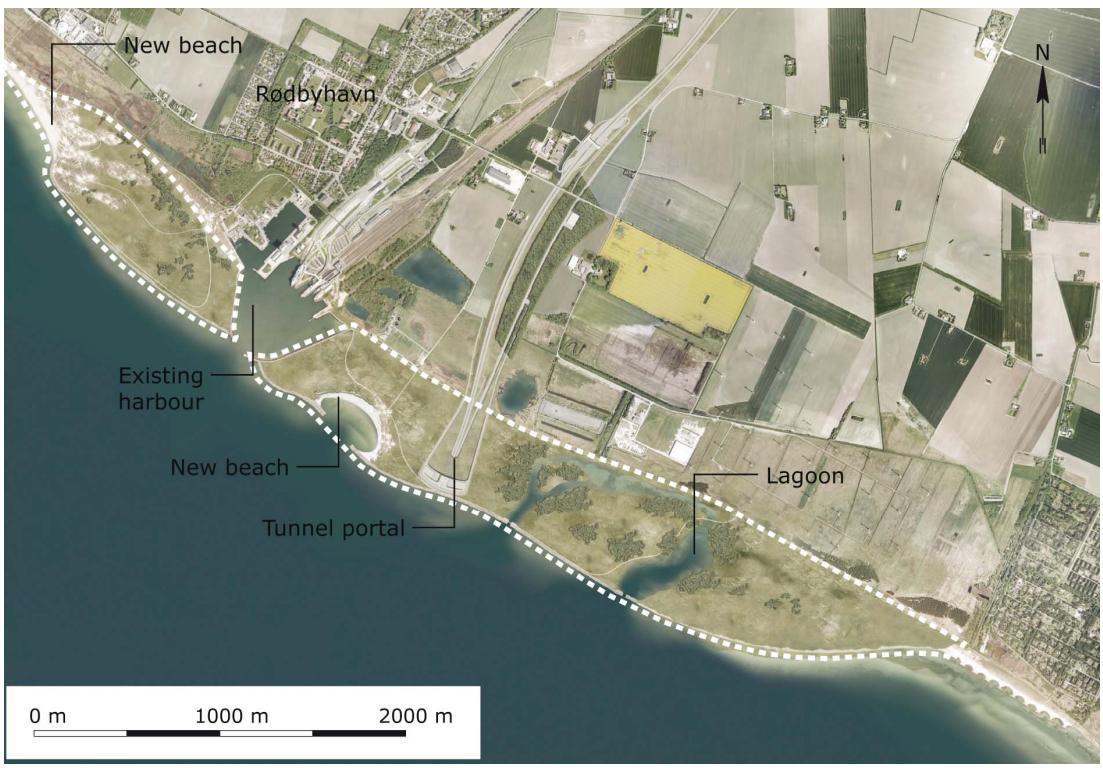


Figure 4. Overview over the planned reclaimed area along the Danish coast.

The existing dike, which runs along the stretch, is not influenced by the reclamation and the dike will consequently still protect the low lying hinterland. The reclaimed area will be designed with different perimeter types dependent of the different technical and environmental functions of the specific stretches as follows:

- The stretch off the portal will be protected by a rubble mound seawall
- Adjacent stretches will be protected by rubble mound revetments
- An artificial beach in the western end of the reclaimed area

- An environmental lagoon with wetlands etc. in the eastern part of the reclamation; also a recreational lagoon is being considered
- The reclaimed area is terminated towards east with a 1.5 km long unprotected area, where a "natural" cliff will develop thereby supplying sand to the downstream coast

The proposed landscaping is considered as a "win-win" situation. A nearby disposal area for the surplus 16 million m^3 of dredged material from dredging of the tunnel trench is created and the landscaping introduces a positive impact in the form of supplying artificial "natural" landscape elements. These will add new "nature", environmental and recreational values to the area and will partially rehabilitate an area, which has suffered severely from engineering projects of the past. This is an ideal example of a "Working with Nature" approach to a large infrastructure project.

New artificial beach in Alexandria. A new artificial beach has been constructed off the Alexandria Corniche at a stretch which was completely depleted for sand, see Figure 5. This project provides protection of the hinterland at the same time as the beach is rehabilitated and expanded.



Figure 5. Example of a stable artificial beach at a starved exposed coast, Alexandria, Egypt (November 09, under construction).

Rehabilitation of the beach at Marataizes, Brazil. An example of a shoreline management scheme is presented in **Error! Reference source not found.**6. This scheme protects and restores a beach section lost due to coastal erosion combined with pressure from land. The scheme consists of a major beach fill supported by rounded detached headlands, which provide optimal support for the beach fill and minimum visual impact. The rounded headlands have the additional advantage that

they do not provide any semi-sheltered areas, which may generate rip currents that could be a risk for bathers. The headland concept is described in Mangor 2004.



Figure 6. Example of beach rehabilitation using headland structures in combination with beach fill, Marataizes, Brazil. Left: Under construction. Right: Finalised project.

REFERENCES:

Unpublished project reports for the various referenced projects

Mangor, K. (2004). *Shoreline Management Guidelines.* Book published by DHI.

Mangor, K., Brøker, I. and Hasløv, D. (2008). *Waterfront developments in harmony with nature.* Published in TERRA et AQUA, Number 111, June 2008.

Renewable Ocean Energy

Billy L. Edge[1], Ph.D, P.E., D.CE, Dist.M. ASCE and Nancy M White[2], MLA PhD

[1]Director Ocean Energy Program, UNC - Coastal Studies Institute, and Professor, Civil, Construction, and Environmental Engineering Dept., North Carolina State University, Raleigh, NC 27695-7908, Ph: 919-515-7387, email: bledge@ncsu.edu.

[2]Director UNC Coastal Studies Institute, PO Box 699, 217 Budleigh St., Manteo, NC 27954, Ph: 252-475-3663, email: nmwhite@csi.northcarolina.edu.

ABSTRACT

The oceans' systems offer significant potential for electrical power generation for hydrokinetic, ocean current and ocean thermal energy. Currently, the technologic readiness is premature for implementation on a grid scale. There has been limited testing of tidal and wave devices in the US on the east and west coasts. However no full-scale field tests for ocean current have been conducted. There is ample opportunity for crosscutting, multidisciplinary research and development to bring ocean energy to the grid. The North Carolina Legislature has taken the initiative to create the opportunity for exploring renewable ocean energy for the mid-Atlantic region and specifically for the State by funding a significant research program primarily directed at the technology.

INTRODUCTION

Around the world, there is a renewed interest in ocean energy and this is being expressed in large-scale investments in research, development and installations. As these installations become production grade systems, the costs will be driven to compete as a logical supplement to more traditional power systems thereby reducing dependence on non-renewable energy sources. The complex regulatory framework is evolving as agencies adapt to the new technology. The important and significant interest in siting and environmental concerns will create opportunities for stakeholders to learn more about these emerging technologies, participate in the development of ocean energy, and explore interdependencies among systems.

The Electric Power Research Institute found that for the entire U.S. coast about 2,100 TWh/yr (TerraWatt-hour per year) exists. This amount of power is sufficient to satisfy the needs of the US if it could be harnessed. However, it is not distributed evenly and the east coast has noticeably less than Alaska and the Pacific Northwest. New England and the Mid Atlantic offer about 110 TWh/yr of wave energy. In reality however, if one could extract about 15% of the wave energy and the net output would be further reduced by 90% due to power train efficiencies

and a plant availability of 90%, the expected production would be about 13.3 TWh/y. Dividing the total power by the length of the coast will show what could be available to North Carolina. Suffice it to say there is significant energy off the coast of North Carolina if it could be economically captured.

North Carolina's Research Program

In pursuit of renewable energy for the State of North Carolina, the UNC Coastal Studies Institute is leading a program to focus on ocean-based sources of energy from tides, currents and waves. Initial efforts are focused on the quantification of wave energy and testing of near shore prototype devices at or near Jeannette's pier that is located on the Atlantic Ocean in Nags Head, North Carolina. Jeannette's pier, shown in Figure 1, has been constructed as a multiuse facility including a platform to support experiments in the ocean. Considering its distance from deep water and major currents, it is most suitable for wave energy research. Although this is a multiuse facility, provisions have been made on the pier for insertion of equipment and cables, electronic measuring, sensing and control equipment both on the pier end and in the IT room of the aquarium at the root of the pier. The ocean energy program has also invested in educational opportunities at the site with touch screens and content which are installed adjacent to the aquarium at the Pier. This will allow the facility to serve as an excellent outreach platform for visitors and educational groups. The pier will fit within the framework of Technology Readiness Level (TRL) 7, open water system test and validation, and with the availability of floating plant, divers, instrumentation and data collection it should be very desirable for a variety of tests. The TRL's were initially defined by NASA and subsequently modified for energy research and development by DOE's National Renewable Energy Laboratory (NREL).

The research program includes coastal, electrical, and industrial engineering needed for the R&D required to harness various forms of ocean energy and develop a strategy for future integration into the energy needs of the State. Research will include discrete as well as integrated system studies in the near shore, coastal shelf and deep ocean areas. The presentation will include a detailed description of the status of the research program, types of devices being explored and developments in hydrodynamics and pressure systems. It will also highlight the environmental studies required to evaluate the effects of a wave energy conversion (WEC) device.



Figure 1. Jennette's Pier at Nags Head, North Carolina, supports ocean energy research, an aquarium, education exhibits and marine related teaching.

WAVE ENERGY

The wave energy resource assessment is the first major study for the program. The USACE WIS study was very helpful in defining a twenty-year hindcast of wave conditions off the North Carolina coast. Many of the nearshore points are within twelve miles of the shoreline which is likely within an economical distance for transporting energy to the grid and providing maintenance from a shore base. Figure 2 illustrates the gross energy available at the WIS stations with levels as high as 0.213 GW-hr/year/meter of shoreline. Efficiency of wave energy converters (WECs) is likely to be from 10 to 30 per cent yielding produced energy likely to be no more than a tenth of the identified gross amounts.

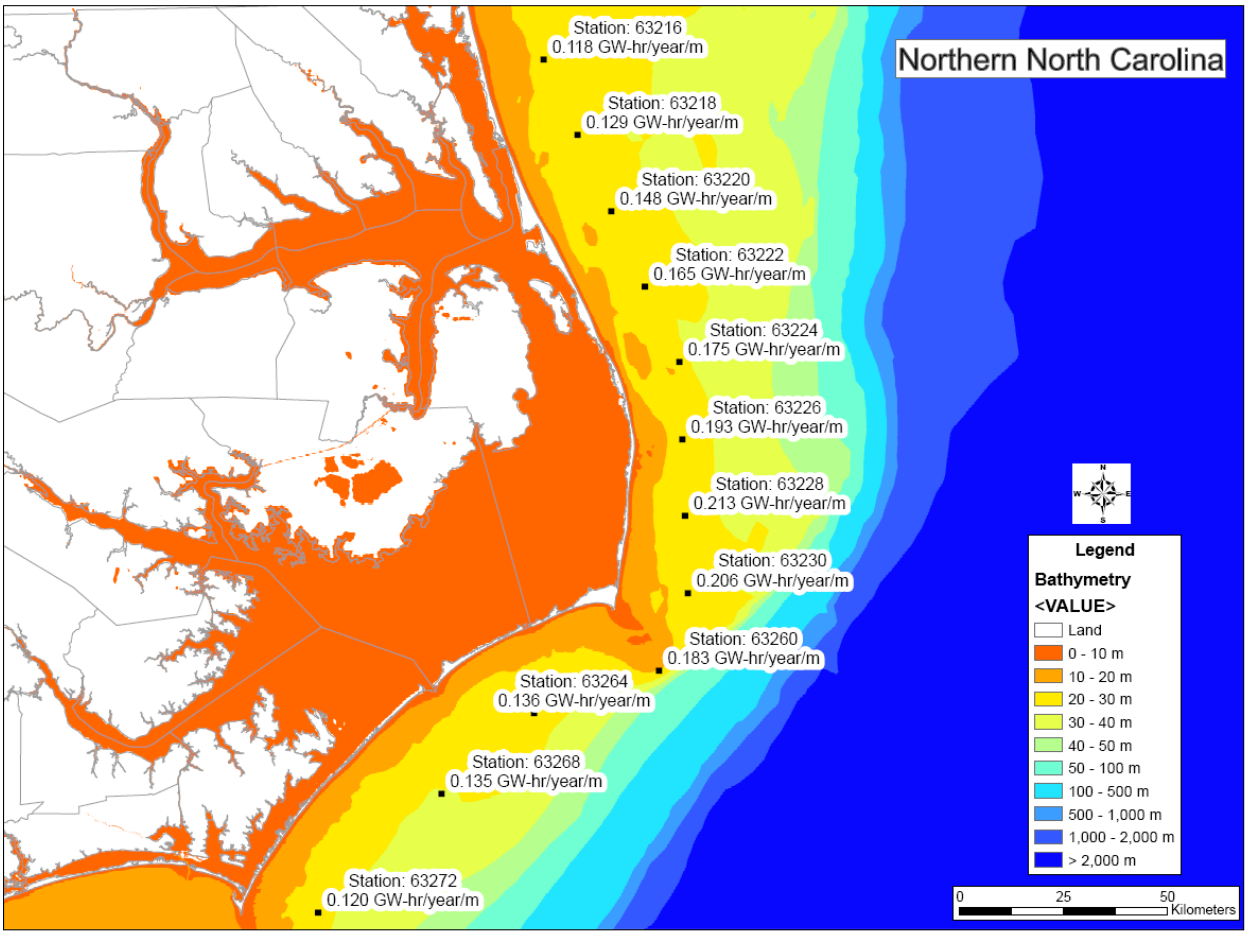


Figure 2. Gross wave energy developed from USACE WIS wave study.

To support the WIS wave estimates, a more detailed study is now underway. It covers the entire state coastline and carries the energy to the shoreline. The study is using ADCIRC and UNSWAN (Dietrich et al., 2010) with a coastline resolved at less than one kilometer for both model applications. Both grids extend to the middle of the Atlantic, approximately 60 degrees west latitude, avoiding boundary issues. The WIS study has produced a long-term wave hindcast at discrete output locations for the Atlantic coast. This long-term hindcast (1980-1999) was generated using a 2-G wave model in a multi-grid nested mode taking advantage of high quality wind fields. The wind fields are a combination of the AES-40 (Cox and Swail, 2001), defining the wind fields for the North Atlantic (the WIS Level 1 domain); Level 2 defining the winds for the domain found in Figure 1; and value added winds for two distinct regions called L3N and L3S. The latter three sets of winds contain tropical systems carefully embedded in each of the time and spatially varying domains. These winds were also carefully evaluated for quality and consistency required for all long-term wave hindcast efforts. In addition to providing the Basin-scale level 1 winds, regional winds with enhanced storm information will be provided from the Level 2/Level 3 products (Figure 3).

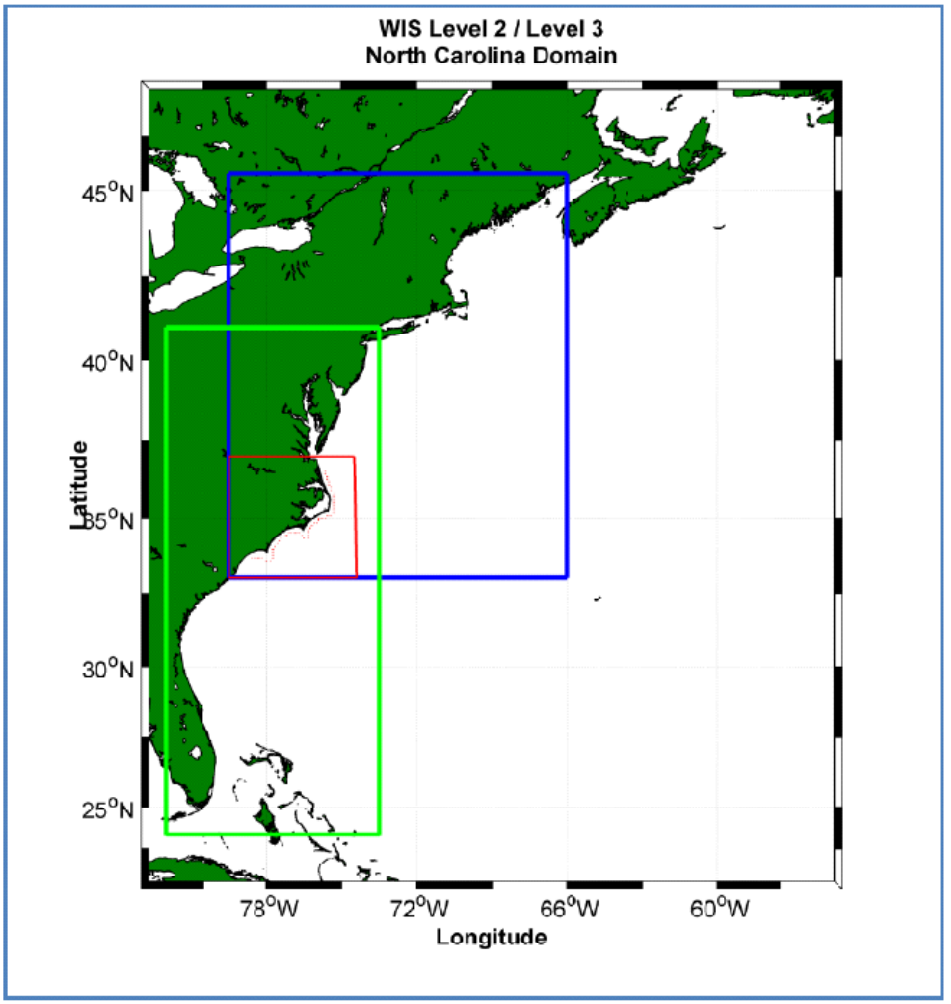


Figure 3. Wave Information Study Level 2, Level 3N, Level 3S, and North Carolina target study area.

The wind fields will be used throughout the Figure 3 Level 1 domain to hindcast waves in the system. The process will employ the combined ADCIRC – SWAN numerical tools throughout the entire domain. The North Carolina Renaissance Computing Institute (RENCI) will provide expertise and guidance in the design of a simulation system for computing the 20-year hindcast of wind-driven waves using the high resolution model grid for wave propagation as described below. RENCI will also provide expertise in high-performance and high-throughput computing to complete the required simulations. The computations will occur using existing RENCI infrastructure. Individual compute jobs will be distributed across the Open Science Grid (OSG), which includes internal RENCI resources when available.

The grid used in computation varies in horizontal resolution from typically 5 km at the shoreline to approximately 800 kilometers in the open ocean. For the North Carolina coastline, the grid

has been refined to provide resolution to less than 1 km at the coast and decreasing in resolution offshore as shown in Figure 2.

ADDITIONAL RESEARCH

Because UNC-CSI is a system wide program administered under UNC System the program is able to bring in the best and most relevant talent including those from out of state. For example we have an established partnership with Florida Atlantic University -- one of the National DOE centers to work with us to assess Gulf Stream energy and how it may be tapped. While the Gulf Stream may be a difficult resource to assess and utilize--it can deliver substantial base load power. We need to know offshore conditions for any technological development; so while we are assessing offshore power and conditions, we will be also developing the potential for two big breakthroughs: the Gulf Stream base load power delivery potential and technology developed by one of our partners at Scripps for deep water offshore energy storage which can be used for both discrete applications and grid delivery for any renewable.

Much of the baseline work has already been started such as the offshore environmental assessment, stakeholder education, economic and marketing studies as well as the deployment of monitoring equipment. These studies serve all state interests for offshore energy whether it is gas or wind or hydrokinetics.

During the first year, we established a short term and long term research plan for the State of North Carolina. Early in the program we brought in expert advisors, started the baseline research that is being done by UNC CH, NCSU, RENCI, the USACE, John Hopkins and Scripps. Field equipment has been obtained such as a new Datawell Waverider monitoring buoy needed for testing new devices and monitoring ocean conditions, signed contracts for construction needed for deployment and the monitoring work, as well as cabling brought in from offshore from an existing AWAC (Doppler monitoring buoy) CSI has been managing for the last 8 years. Since the AWAC is owned by the USACE, CSI is working with them for refurbishment and planned redeployment.

The Technical Advisory Committee (TAC) consisting of recognized national and international experts in the field of ocean renewable energy was formed to help guide the Project. The TAC will work with CSI to help guide the research and position North Carolina as a leader in this industry.

CSI conducted a Research Symposium on March 2-3, 2011, in Raleigh, North Carolina, to present national and international activities in renewable ocean energy and to develop a research agenda to position NC as a leader in this industry. The symposium was attended by more than 70 North Carolina University researchers, partners such as the State's Department of Commerce, and members of the TAC. The results of the symposium guided the development of a request for research proposals, which was released to the Partners on March 17, 2011.

A Strategic Relationship with Resolute Marine Energy ("RME") has been initiated. RME is a developer of wave energy technology that is currently being funded by the US Department of Energy ("DOE") for a demonstration project. Subject to this appropriations request, the RME demonstration project will be located at Jennette's pier at Nags Head.

Pacific Energy Ventures ("PEV") was retained to assist CSI in developing a strategic plan that leverages North Carolina's unique resources and is integrated with other national and international efforts. PEV is also working with the Oregon Wave Energy Trust, DOE, and the Bureau of Ocean Energy Management ("BOEM") to help accelerate the testing and appointment of wave and tidal energy throughout the United States. They will work with the research teams to help prepare and submit proposals to DOE and BOEM later this year.

Research Proposals were received from all of the Partners on May 6, 2011 and are currently being evaluated by members of the TAC. Fourteen proposals were received spanning a variety of topic areas including wave energy testing, resource assessment, stakeholder engagement, and a highly novel deep water ocean energy storage system. Final selections will be made by the end of May, and all funds will be encumbered by the end of June 2011.

CONCLUSION

Renewable ocean energy is one of the largest sources of energy on the earth but it remains difficult to develop. Many efforts are ongoing in Europe, the Pacific Northwest, and the Northeast pushing the development. There are still many issues to resolve – particularly in bringing this energy ashore where there is a smaller wave climate as well as design issues for production and survivability in tropical storms. Nonetheless, since research is needed to support the development of any offshore infrastructure and energy sources, it is logical to investigate all sources of power, potential for their integration, and for delivery to the grid. North Carolina has made an investment in ocean energy in order to reap the benefits of a new economy that builds upon the intellectual talent in the State universities, as well as be unique to and will serve the interests of North Carolinians.

REFERENCES

Cox, A. T. and V. R. Swail, 2001: A global wave hindcast over the period 1958-1997: Validation and climate assessment. *J. Geophys. Res*., **106**, 2313-2329.

Dietrich, J. C., and Coauthors, 2010: A high-resolution coupled riverine flow, tide, wind, wind wave, and storm surge model for southern Louisiana and Mississippi. Part II: Synoptic description and analysis of Hurricanes Katrina and Rita. *Mon. Wea. Rev*., 138, 378–404.

Defining Engineering Guidance for Living Shoreline Projects

Rob Walker, P.E.[1], Bonnie Bendell[2], and Louise Wallendorf, P.E.[3]

[1]Anchor QEA, LLC, 26300 La Alameda, Suite 240, Mission Viejo, CA 92691, rwalker@anchorqea.com
[2] North Carolina Division of Coastal Management, 1638 Mail Service Center, Raleigh, NC 27699-1638, bonnie.bendell@ncdenr.gov
[3]United States Naval Academy, 590 Holloway Road, Annapolis, MD 21402, lou@usna.edu

ABSTRACT

The concept of "living shorelines" involves the use of native vegetation and low-lying structures to provide shoreline stabilization, while attempting to mimic the natural landscape. Living shorelines are frequently a desirable alternative to hard engineering structures, such as bulkheads and rock revetments, which have the potential to dramatically change shoreline conditions and can lead to a complete loss of intertidal area, as well as associated habitat, recreational, and aesthetic benefits.

The Coastal Zone Management (CZM) technical committee of the Coasts, Oceans, Ports and Rivers Institute (COPRI) has a vested interest in the research of sustainable alternatives for shoreline protection and coastal management. As the concept of living shorelines comes to the forefront in the search for alternative coastal management strategies in our ever-evolving coastal areas, the CZM committee has set out to further develop the fundamentals of living shoreline design based on a comprehensive review of living shoreline case studies.

INTRODUCTION

Shoreline erosion within the estuarine environment is a concern to nearly every coastal state. The erosion is typically caused by moving water, either from wind-generated waves or as a result of boat wakes. A variety of alternatives exist to combat such erosive forces, including shoreline hardening through bulkheads and rock revetments, coastal management through setbacks and appropriate development practices, and beach nourishment. The use of shoreline armoring structures to stabilize the shoreline edge in a fixed location has long been the standard for protecting eroding shorelines of sheltered coasts. The use of such structures, however, can have an impact on the surrounding ecosystem by accelerating the loss of valuable habitat, and on adjacent shorelines caused by interactions with sediment transport and supply mechanisms.

"Living shorelines" have been defined as shoreline stabilization methods that employ as many natural habitat elements as appropriate for site conditions to protect shorelines from erosion (Erdle et al., 2006). For low- to medium-energy environments that are prone to shoreline erosion, living shorelines have the ability to provide needed protection while also enhancing habitat and ecological function. In a high-energy or headland site in an estuary, more classical structures are necessary if shoreline stabilization is required. Design practices for both living shorelines and more classical coastal structures for low-, medium-, or high-energy estuarine environments are discussed by Hardaway and Byrne (1999). Living shoreline projects can be very broadly defined. Projects will always need to include the use of coastal vegetation and usually, but not always, a low-lying structure. The structure can be in the form of a shore-parallel breakwater or sill, or even shore-perpendicular groins. The type of material that can be used for these structures can vary greatly as well, and includes rock, oyster bags or other shellfish, broken concrete, sheet pile, coir logs, or even old trees and woody debris. Often thought of as a "hybrid" alternative, the concept of living shorelines involves low-lying structures constructed to protect an area of newly planted wetland vegetation until it can be established or re-established and, in turn, provide opportunities for habitat restoration while simultaneously serving as shoreline protection.

For decades Mid-Atlantic states such as Maryland, Virginia, and North Carolina have investigated the use of living shorelines to counteract the habitat loss of shoreline armoring. An overview of some previous investigations is provided in this paper. However, the coastal engineering challenge has been how to design a sustainable living shoreline to stabilize the coast, while also allowing the rehabilitation of marsh habitat. To assist in refining the coastal engineering design guidance on living shorelines, the CZM committee has been formulating a database of parameters to be used to compile the design details from living shorelines projects nationwide. By establishing a system of documentation and implementing a large-scale case study evaluation, the CZM committee aspires to establish a comprehensive database of information that may be applied to science-based guidance on the planning, design, and implementation of living shoreline projects.

BACKGROUND

In 1969 a marsh development research program began at North Carolina State University under the sponsorship of the U.S. Army Corps of Engineers (USACE) Coastal Engineering Research Center (CERC). This led to extensive baseline techniques summarizing how to replant marshes for shoreline protection and dredge spoil stabilization. This work is listed extensively in Knutson et al. (1981).

Knutson et al. (1981) report the results of a national survey of 89 replanted marshes, at least one year after replanting and without any rubble or manmade structures. For each site, a variety of characteristics are identified as specific indicators of shoreline wave climate. Of these parameters, sediment grain size within the swash zone, fetch, and shoreline configuration correlate with the success of a marsh replanting project.

In general, fine grain size (less than 4 mm), coves (compared to straight shoreline or headlands), and reduced fetch (.5 to 1.0 miles) correlate with the highest percentage of success. The concept of classifying low-, medium-, and high-energy shorelines using ranges of grain size, shoreline type, and fetch was introduced. The use of fetch ranges to classify low-, medium-, or high-wave-energy shorelines has persisted over time.

Rogers (1989) describes how the early development of low-cost sills placed just offshore of planting areas can improve the success rate of the marsh grass growth by reducing the effects of the wave climate. Two sites in North Carolina were created by accident, one near Ocracoke Island in 1962 and one near the Pamlico River in 1978. In each case a sill was constructed offshore without backfill due to missteps in scheduling and paperwork and, during a 1-3-year period, marsh grasses grew in the lee. Two additional test sites were constructed later as test cases in Currituck and Croatan Sound; in each case, a free standing timber wall or sill was constructed offshore of an eroding shoreline and marsh grasses were planted in the lee. At each site, a successful marsh was slowly re-established.

THE LIVING SHORELINE APPROACH TO SHORE PROTECTION

Vegetation

When appropriately sited, a planted marsh can be a cost-effective solution to shoreline erosion. The vegetation serves to protect upland areas in two ways. First, the stems of the grasses act like a porous breakwater, gradually dissipating the energy before reaching upland. Second, the marsh species builds a tough root mat less prone to erosion than sediment alone, and are capable of absorbing the force of breaking waves (Shafer et al., 2003). Broome et al. (1992) note that previous studies have shown that 50 percent of wave energy is dissipated in the first 8 feet of marsh, and 100% is dissipated in 100 feet of marsh. Roberts (1991) evaluated the habitat value of 22 created coastal marshes in northern and central Florida, concluding that the basic habitat requirements of fish, bird, and mammal species were being met by the man-made features.

The success of planted marshes for shore protection is a function of the nearshore wave environment. Shafer et al. (2003) estimate that marsh planting with no structural component can be successful if the fetch is less than one mile and boat wakes are not a significant contributor to coastal erosion. They go on to recommend that a marsh fringe at least 10 feet wide is necessary for erosion control, but 20 feet or more is preferred. Sharp et al. (1980) also contend that a width of marsh less than 10 feet will not be effective at reducing erosion, and Hardaway and Byrne (1999) recommend a maximum slope of 10:1 to ensure site stabilization. Broome et al. (1992) note that if marsh vegetation exists naturally within close proximity to the site of interest, the planting of coastal vegetation for erosion control has a high rate of success.

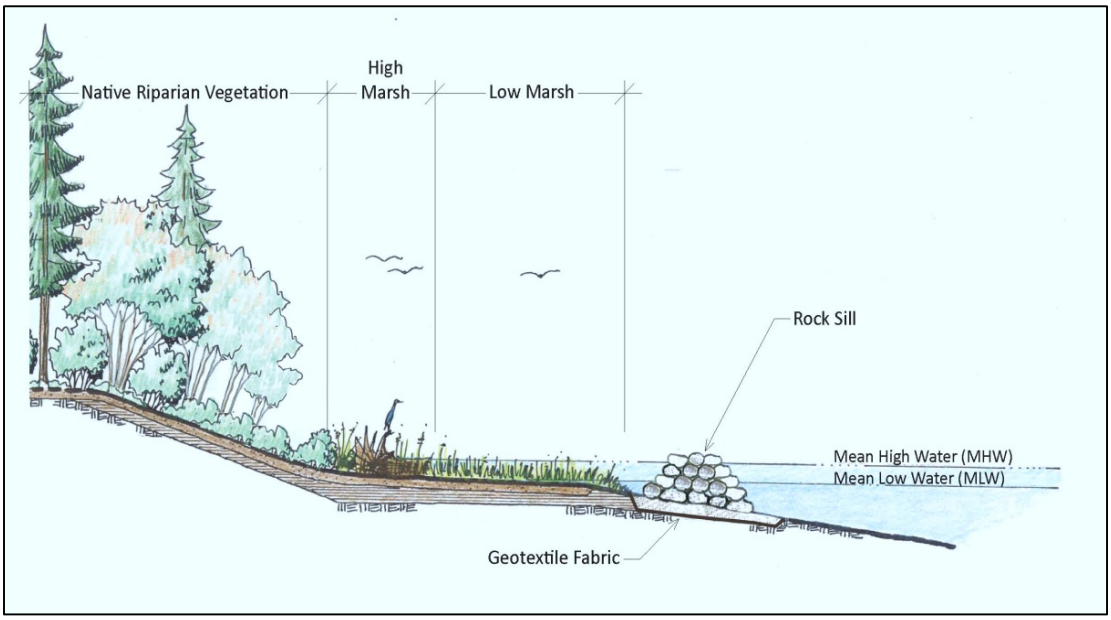


Figure 1. Cross-section representation of living shoreline project with rock sill and marsh planting.

Structural Elements

Most living shorelines are made up of two distinct elements—an offshore low relief structure usually referred to as a sill, and an intertidal area between the offshore sill and the upland containing emergent marsh vegetation. Figure 1 provides a conceptual cross-section of the typical living shoreline design. The sill can be constructed of a number of materials including rock, oyster shells, and treated wood, and typically protrudes above the normal high water level by no more than six to 12 inches.

For areas subject to greater fetches or significant boat wakes, the sill is used to provide an initial absorbance of wave energy and allow the establishment of marsh vegetation. In such a scenario, the sill and coastal vegetation work in harmony to dissipate the energy and protect the upland shoreline. Based on a review of case studies along the coasts of Texas and Alabama, Shafer el al. (2003) determined that sill and wetland combinations can be effective for fetches of more than 10 miles and in areas of serious boat-wake problems.

Sills are usually designed with overlaps, gaps, or dropdowns to promote water circulation that allows water, fish, and nekton access to the marsh area. Figure 2 provides a visual depiction of such design techniques. The overlap design presented in panel A provides an opening by splitting the offshore sill into two sections. In the area where the two sections meet, they overlap for a few feet in a parallel offset manner. The gap design presented in panel B provides an opening by splitting the offshore sill into two sections. In this design the two ends do not fully meet, leaving a gap in the offshore sill. The dropdown design presented in panel C provides access by periodically lowering the height of the offshore sill.

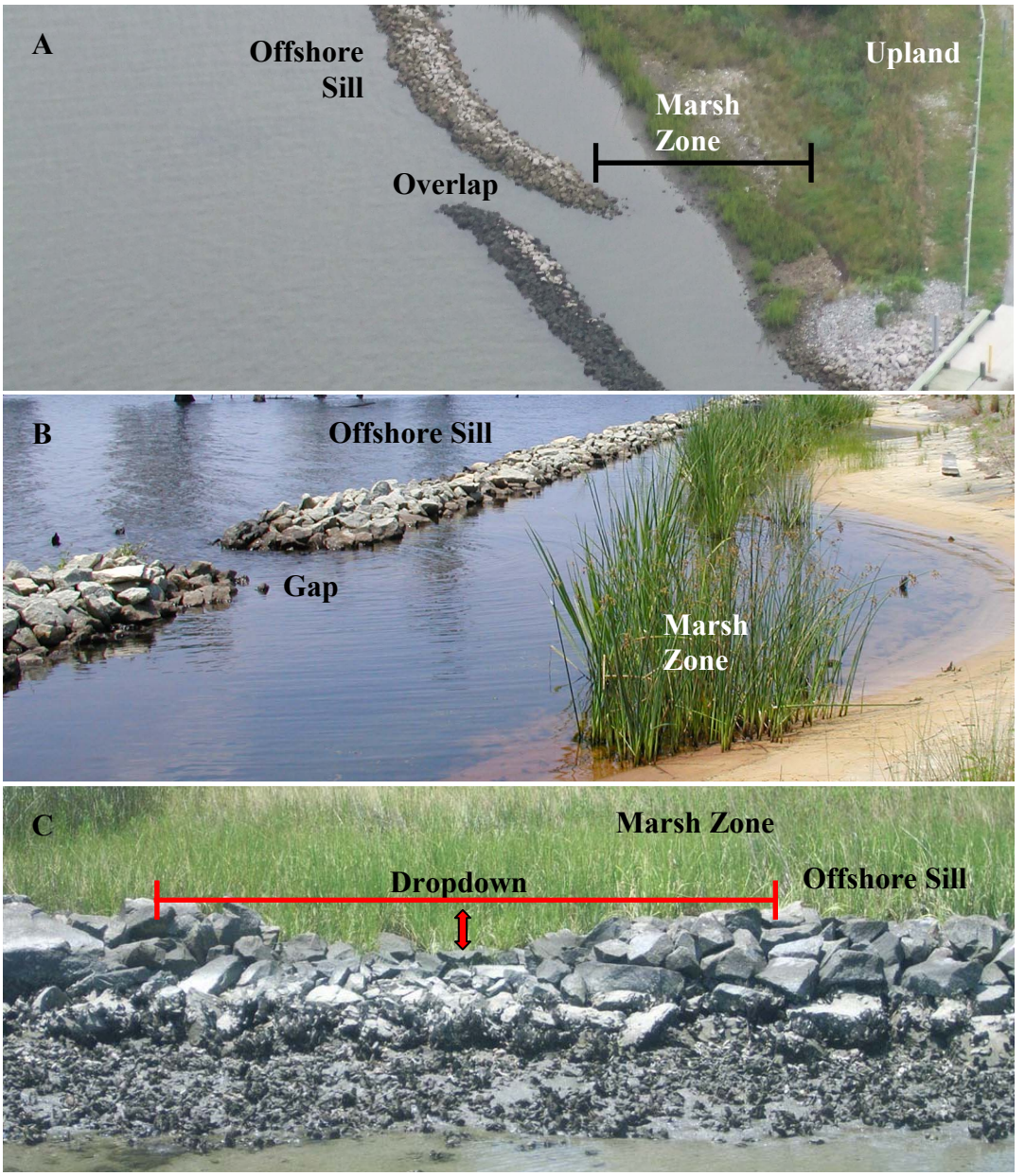


Figure 2. Overview of three techniques used to promote the exchange of water and marine organisms throughout the living shoreline system (Fear and Bendell, 2011).

While every site is different and the design criteria is in great part a function of the site use, a publication by the Maryland Department of the Environment (MDE) recommends that sill structures be designed to withstand the forces of a storm that would occur once every 20 to 30 years on average (MDE, 2008). An adequately designed structure provides protection for most storm events without the higher costs of a more elaborate structure. This is achieved by maintaining a low crest elevation, which reduces costs and also creates a submerged condition during elevated water levels caused by storm surge. The location of the structure with respect to water level greatly reduces the impact the structure receives due to wave energy.

Benefits of Living Shorelines

When properly installed, living shorelines provide many benefits in addition to shoreline stabilization. Acting as natural buffers to wave energy, marsh vegetation also filters pollutants and improves water quality and clarity in surrounding waters. Oyster reefs used as sills also provide similar functions in regard to water quality. Habitat provided by living shorelines allows the establishment of additional foraging and nesting areas for native species. Often a less costly alternative to typical shore protection methods, living shorelines also provide aesthetic value by creating natural landscapes and opportunities for viewing marine wildlife (Thomas-Blate, 2010).

In New York, a state task force on sea level rise recommended that state permitting regulations be modified to encourage the use of living shorelines over traditional armoring structures in areas requiring protection because of the environmental benefits they provide (New York State Sea Level Rise Task Force, 2010). In addition to the immediate environmental benefits, living shorelines were also thought to be more "adaptable" to increased sea level rise by stabilizing and enhancing marshes and potentially minimizing disruptions of long-term shoreline migration.

Potential disadvantages of living shoreline projects are summarized by Currin et al. (2010), and include the replacement of shallow-water habitat with sill and, consequently, an alteration in ecosystem services of the site, as well as filling of intertidal lands with potential for loss of public trust resources. Care must be taken during design to minimize impacts to adjacent shorelines, and provide adequate wave protection to allow for marsh establishment. Given the multiple advantages of living shorelines and overall contributions to the aquatic ecosystem, these types of tradeoffs are often thought to be acceptable when compared with other forms of shore protection (Rogers and Skrabal, 2001).

Regulatory Permitting of Living Shorelines

Based, in part, on a lack of published guidance and reference documentation regarding design and performance of living shoreline projects, gaining the approval of regulatory agencies of such alternatives has a history of being a challenge. Currently in North Carolina, the permit process for obtaining a bulkhead, riprap revetment or timber sill is obtained via a general permit, an expedited permit process. A rock sill style living shoreline takes longer to completely permit due to additional oversight required by various regulatory agencies on every project. This is ironic since some of the first investigations for using planted marsh as shore protection occurred in North Carolina. However, collaborative efforts by the North Carolina Division of Coastal Management (NCDCM), North Carolina Coastal Federation, and North Carolina Sea Grant have managed to make good progress in moving the regulatory framework forward towards the allowance of living shorelines as a means for shore protection.

In contrast to North Carolina, states such as Maryland and Virginia have made significant progress in supporting living shorelines as an alternative to hard shore protection options. In 2007, 14 percent of the 7,100-mile Chesapeake Bay shoreline

in Maryland was stabilized artificially (USACE, 2010). Shortly after The Living Shorelines Summit in 2006 (Erdle et al., 2006), the Maryland legislature took the proactive step of passing the Living Shorelines Bill of 2008, requiring Maryland property owners to use living shorelines for shore protection. Exceptions to the policy can only be granted by the MDE. Guidance on living shorelines designs for homeowners has been created (MDE, 2008) and additional shore protection technical guidance for engineers and contractors in Chesapeake Bay is being prepared (USACE, 2011). This guidance is designed to be an update to the 1981 low-cost shore protection guide (GAI Consultants, 1981), deleting many of the outdated practices and incorporating information on living shorelines. While the practices in this upcoming document should be applicable throughout the Chesapeake Bay, there is a focus on the upper Chesapeake Bay and Maryland's regulatory environment.

While the Virginia Institute of Marine Science (VIMS) has extensive recent publications on living shorelines (Hardaway et al., 2009; Hardaway, Mulligan and Duhring, 2010), the state of Virginia does not have an official position on the use of living shorelines for erosion protection. The state provides guidelines for permitting in the various regions of the shoreline, while the fifteen coastal counties are responsible for issuing permits. They each use different procedures to approve the permits, resulting in complicated regulatory environment for designers, contractors, and property owners. VIMS (2010) studied the shore protection regulatory framework of Maryland, North Carolina, and Massachusetts and presents techniques used by other states to encourage living shorelines designs. They recommend the use of a living shorelines general permit, with a more streamlined procedure for obtaining project approval.

North Carolina Case Study

In 2009, NCDCM began the Marsh Sill Evaluation Project as part of an effort to develop alternatives to vertical structures. The project was a qualitative technical assessment of 27 marsh sills constructed in North Carolina with the purpose of determining if these structures are functioning as they were originally intended.

The recent study by NCDCM was able to conclude ten findings as a result of a statistical analysis of the field data sheets:

- Marsh sills were not found by the field team to present a hazard to navigation.
- Marsh sills were observed to provide erosion protection to the property upon which they were installed.
- Marsh sills were often built in combination with other structures.
- Marsh sills that utilized the gap or overlap design were observed to provide better water, fish, and other nekton access to the area behind the sill compared to ones utilizing the dropdown design.
- It was unclear whether marsh sills cause erosional impacts on adjacent property.

- After completion of the field aspects of this project, the resource agencies in North Carolina still prefer to review and comment on marsh sill permits on a case-by-case basis.
- The mound material used in the marsh sills are often colonized with oysters.
- The marsh sills visited supported marsh grass and do not appear to be creating new uplands.
- Marsh sills were observed to be free from damage.
- No marsh sill related impacts to water quality were observed.

In summary, the North Carolina study concluded that sills are providing erosion protection to the property on which they were constructed, are not causing adverse impacts to water quality, are not a hazard to navigation, but may be causing some erosional impacts on adjacent properties. NCDCM has stated that it intends to re-evaluate and revise its policies as more information on living shorelines becomes available.

DESIGN CONSIDERATIONS

Living shoreline projects are usually only appropriate for low-to-medium energy coastal environments. Open coast beaches and shorelines with large exposed fetches produce too much energy for successful establishment of a marsh community. Factors that contribute to the success or failure of a living shoreline project can vary from fetch to water depth, and are in much part a reflection of the amount of natural or man-made wave energy present at the site. Knutson et al. (1981) evaluated the wave climate at planted salt marshes throughout the U.S. based on a suite of coastal parameters presented below in Table 1.

Table 1. Indicators of shoreline wave climate based on Knutson et al. (1981).

Fetch	Width and Slope of Intertidal Zone
Offshore Depth	Median Grain Size of Intertidal / Swash Zone
Orientation with respect to Prevailing Winds	Bank Height
Proximity to Navigation	Shore Configuration (straight, meandering, headland, cove)
Tide Range	

Knutson et al. (1981) developed a subjective index of the probability of "success" that incorporated estimates of wind fetch distance, sediment grain size, and shoreline geometry. The relative exposure index (REI) developed by Keddy (1982) has been used to investigate relationships between wave energy, sediment type, and survival of coastal vegetation. By evaluating a variety of shoreline variables such as fetch, shoreline orientation, nearshore slope, and depth, Sharp et al. (1980) developed the Vegetative Treatment Potential (VTP) for the applicability of marsh vegetation for shoreline protection. Based on the list of criteria, a site that receives a VTP value of

23 or more is assumed to have good potential to be stabilized by vegetation. Using a modified version of the REI, Shafer and Streever (2000) found evidence to suggest a maximum wave energy threshold for the existence of natural marshes in Galveston Bay, Texas. Shafer et al. (2003) investigated the existence of critical wave energy thresholds for long-term marsh stability by reviewing case studies located in Texas and Alabama.

Roland and Douglass (2005) correlated site-specific wave statistics with the existence of coastal vegetation to develop a quantitative estimate of the upper level of tolerance to wave energy for one common, native species (*S. alterniflora*, smooth cordgrass) in coastal Alabama. The upper limit of wave energy for (noneroding) salt marsh existence was a median significant wave height of about H = 0.3 feet and a corresponding 80th percentile (less than this level 80 percent of the time) significant wave height of H= 0.7 feet. Sites with less wave energy had vegetation along the shoreline. These values generally correspond with a an old rule-of-thumb that extends at least back to Knutson (1981) that marshes can exist where the storm waves are less than one foot high.

CZM CASE STUDY EVALUATION

Shoreline restoration and stabilization following the living shoreline concept is an evolving science, and lessons learned from project case studies are actively being assessed to aid in the development of sound engineering guidance for the most appropriate site-specific designs. Similar to other works of coastal engineering, living shoreline designs would ideally be a collaborative effort among biologists, engineers, and other scientists; however, in many cases living shoreline projects have been designed and built with little or no basis of design. This has led to a suite of lessons learned, including marsh or structure failure due to inadequate designs or inappropriate siting. Project case studies have also demonstrated how overly conservative construction can actually inhibit the establishment of living coastal marsh and marine organisms.



Figure 4. (Left) 2002 photo of Duke Marine Lab site, prior to construction. (Right) 2008 photo of Duke Marine Lab living shoreline 5.5 yrs after construction.

Table 2: Evaluation of the Duke University Marine Lab 300-foot-long Sill at +34°43'2.88", -76°40'23.36"

Evaluation Criteria		Duke University Sill
A.	**Pre-Project Conditions at Site**	
A.1	Vegetated wetlands present?	Not near the sills site
A.2	Submerged Aquatic Vegetation (SAVs)?	No
A.3	Major plant species present	None – bulkheaded
A.4	Bank elevation above MHW	1.8'= ft
A.5	Pre-construction erosion present?	No - bulkheaded
A.6	Pre-construction erosion rate	Unknown
A.7	Pre-construction erosion at adjacent parcels?	No – bulkheaded
A.8	Nearshore slope below MHW	Unknown
A.9	Existing structures or debris	Asbestos sheet bulkhead with pier pilings & offshore fish pen
B.	**Coastal and Environmental Considerations**	
B.1	Adjacent water body	Gallant's Channel
B.2	Open shellfish water?	No
B.3	Maximum exposed fetch	0.66 miles
B.4	Orientation relationship between project and max. exposed fetch	From the southwest
B.5	Adjacent to navigation channel?	Yes
B.6	Tidal range	3 feet
B.7	Water Depth 30 ft from MHW	-3 to -5.5 ft
B.8	Water Depth 100 ft from MHW	Unknown
B.9	Max depth limited wave height	Unknown
B.10	Max estimated wave period	Unknown
B.11	Boat wake exposure	Medium
B.12	In a No-Wake zone?	No
B.13	Description of nearby structures impacting coastal processes or creating end effects.	Island is mostly bulkheaded with a bridge & causeway to the north.
B.14	Salinity	High
C.	**Design Considerations**	
C.1	Was fill brought in?	Yes
C.2	Type of fill (silt, sand, gravel)?	Sand
C.3	Approx. amount of fill	800 CY placed in the water
C.4	Includes a sill structure?	Yes
C.5	Proposed nearshore slope below MHW	Suitable for marsh plants
C.6	Shallow bottom conversion to marsh	9100 sq ft
C.7	Upland conversion to marsh	7500 sq ft
C.8	Shallow bottom conversion to structure	3750 sq ft for sill
C.9	Total project cross-section width	85 feet

Table 2 (continued): Evaluation of the Duke University Marine Lab 300-foot-long Sill at +34°43'2.88", -76°40'23.36"

Evaluation Criteria		Duke University Sill
D.	**Evaluation of Structural Elements**	
D.1	Type of structure(s)	Rock sill
D.2	Structure type and materials	Class II granite
D.3	Average distance of structure offshore (from MHW)	70 ft max, ~50 ft avg
D.4	Average distance of structure offshore (from MLW)	Unknown
D.5	Structure base width	12.5 ft
D.6	Length of structure	300 ft for sill
D.7	Structure crest width	2 ft
D.8	Structure side slope	1.5 H:1V
D.9	Monolithic or layered?	Monolithic
D.10	Height of structure	3.5 ft max
D.11	Max depth seaward of structure	Unknown
D.12	Max depth landward of structure	Unknown
D.13	Drop-downs, gaps, or overlaps?	Drop-downs
D.14	Width of drop-downs or gaps	11 feet
D.15	Spacing btw gaps/drop-downs	~100 feet
D.16	Original design criteria (*e.g.*, designed for 50-year storm event?)	Unknown
D.17	Type of foundation	Geotextile Fabric
D.18	Was geotextile used in foundation?	Yes
D.19	Porosity of structure	Unknown
E.	**Evaluation of "Soft" Elements**	
E.1	Percent vegetative cover between structure and MHW	90%
E.2	Was geotextile fabric used?	No
E.3	Primary vegetation below MHW	Spartina Alterniflora
E.4	Type of substrate below MHW	Sand
E.5	Primary vegetation above MHW	Spartina Patens
E.6	Type of substrate above MHW	Sand
E.7	Root mat developed by vegetation?	Yes
E.8	Planted area cross-section width	72.5 ft
E.9	Additional ecological benefits from project?	Oyster growth on sill structure
F.	**Project Performance**	
F.1	Overall performance of Living Shoreline for erosion protection	Medium
F.2	Overall performance of Living Shoreline for habitat enhancement	Medium
F.3	Unforeseen benefits from project	Unknown

The goal of collaborative research by the science and engineering community is to determine a middle ground that promotes habitat restoration while providing adequate shoreline protection. To assist in developing the knowledge base on the engineering design considerations for living shoreline projects, the CZM has been gathering information on case study sites. Beginning with the 27 living shoreline case studies recently investigated by NCDCM with a biological and regulatory focus, the committee will evaluate the sites based on a determined set of evaluation criteria (see Table 2). Additional study sites will be from Maryland, Virginia, Georgia, Washington, and the Gulf Coast.

To demonstrate the committee's approach, Table 2 provides an example tabulation of site-specific information that is being collected for the case study sites. Herein, the living shoreline project constructed at the Duke Marine Lab in Beaufort, North Carolina, in 2002 is presented as an example. Figure 4 provides images of the Beaufort site prior to and after construction of the living shoreline.

With organized data on a large number of living shoreline sites, the committee will investigate the relationships among site and design parameters. Similar to previous work by USACE (1980), Shafer et al. (2003), and Sharp et al. (1980), the combination of site characteristics that is specific to each project will be evaluated independently and collectively in an effort to better understand factors controlling success and failure of living shoreline projects.

LOOKING AHEAD

Living shorelines have proved to be a successful alternative method of shore protection for low- to medium-energy environments, while also providing extensive benefits to habitat and water quality. Although the majority of projects have been focused on the U.S. Mid-Atlantic coast, the living shoreline concept is applicable to other areas around the country. Every project site is different and there are tradeoffs in the installation of any form of shoreline stabilization. Similar to any form of activity that impacts the complex coastal environments created by tidal bays and estuaries, the planning and design of living shoreline projects require a site-specific analysis of conditions. Designs should be based on wind and wave climate, shoreline type and orientation, and in accordance with surrounding natural coastal features.

The placement and structural design of the coastal sill, which holds/protects the intertidal marsh in living shorelines, is optimally designed on the fine line between structural success and failure. If the sill is under designed or placed in the incorrect location, the marsh is washed away; if it is overdesigned, a true intertidal marsh is not created. The CZM committee of COPRI is in the process of developing a comprehensive database of quantitative information on living shoreline case studies. The committee hopes to provide scientists and engineers with a valuable tool to further investigate the relationships, thresholds, and correlations between design parameters influencing project success on a national scale.

The CZM committee asks the coastal community for additional examples of living shoreline projects for inclusion to the project database. Interested parties that have case studies (ideally with decent to good record keeping), please contact the authors.

ACKNOWLEDGMENTS

Sincere appreciation is given to Scott Douglass, Spencer Rogers, and Peter Hummel for reviewing this paper in draft form and providing valuable thoughts and recommendations.

REFERENCES

Broome, S.W., Rogers, S.M., and Seneca, E.D. (1992). *Shoreline Erosion Control using Marsh Vegetation and Low-Cost Structures*. North Carolina Sea Grant.

Currin, C.A., Chappell, W.S., and Deaton, A. (2010). "Developing Alternative Shoreline Armoring Strategies: The living shoreline Approach in North Carolina", *in* Shipman, H., Dethier, M., Gelfenbaum, G., Fresh, K. L., and Dinicola, R. S., eds., 2010 Puget Sound Shorelines and the Impacts of Armoring- Proceedings of a State of the Science Workshop, May 2009: U.S. Geological Survey Scientific Investigations Report 2010-5254, pp. 91-102.

Erdle, S. Y., Davis, J. L., Sellner, K. G. (2006). *Management Policy, Science, and Engineering of Nonstructural Erosion Control in the Chesapeake Bay – Proceedings of the 2006 Living Shorelines Summit.* CRC Publication No. 08-164, 136 p.

Fear, J. and Bendell, B. (2011). *Assessment of 27 Marsh Sills in North Carolina*. Final Report. North Carolina Division of Coastal Management. April 2011.

GAI Consultants, Inc. (1981). *Low-Cost Shore Protection: a guide for property owners*, Washington D.C, US Army Corps of Engineers (USACE), 155 p.

Hardaway Jr., C. S. and Byrne, R.J., (1999) *Shoreline Management in Chesapeake Bay*, Virginia Institute of Marine Sciences, College of William & Mary, Special Report in Applied Marine Science & Ocean Engineering No. 356, 54 p.

Hardaway Jr., C. S, Milligan, D., and Duhring, K. (2010). *Living Shorelines Design Guidelines for Shore Protection in Virginia's Estuarine Environments*, Virginia Institute of Marine Sciences, College of William & Mary, Special Report in Applied Marine Science & Ocean Engineering No. 421, 123 p.

Hardaway Jr., C. S., Milligan, D. A., O'Brien, Kevin P., Wilcox, C. A., Shen, J. and Hobbs, C. H. (2009). Encroachment of Sills onto State-Owned Bottom: Design Guidelines for Chesapeake Bay, Virginia Institute of Marine Science, March 2009, 54 p.

Keddy, P.A. (1982). "Quantifying within-lake gradients of wave energy: Interrelationships of wave energy, substrate particle size, and shoreline plants in Axe Lake, Ontario," Aquatic Botany 14, 41-58.

Knutson, P.L., Ford, J.C., and Inskeep, M.R. (1981). "National survey of planted salt marshes," Wetlands 1, pp. 129-157.

Maryland Department of the Environment (MDE). (2008). *Shore Erosion Control Guidelines for Waterfront Property Owners*. Water Management Administration. December 2008.

New York State Sea Level Rise Task Force. (2010). *Report to the Legislature.* New York State Department of Environmental Conservation, Albany, NY. 103 p.

Roberts, T.H. (1991). "Habitat Value of Man-Made Coastal Marshes in Florida", Technical Report WRP-RE-2, US Army Engineer Waterways Experiment Station, Vicksburg, MS.

Rogers, S.M. (1989). "Erosion Control: Marsh and Low-cost Breakwaters", Coastal Zone '89, American Society of Civil Engineers, New York, NY, pp. 751-764.

Rogers, S.M. and T.E. Skrabal. (2001). *Managing Erosion on Estuarine Shorelines*. *The Soundfront Series.* Publication # UNC-SG-01-12. 32p. North Carolina Sea Grant, N.C. State University, Box 8605, Raleigh, NC 27695-8605.

Roland, R. M. and Douglass, S. L. (2005). Estimating Wave Tolerance of *Spartina alterniflora* in Coastal Alabama. Journal of Coastal Research, 21(3), pp. 453-463. West Palm Beach, Florida.

Shafer, D.J., Roland, R., and Douglass, S.L. (2003). Preliminary Evaluation of Critical Wave Energy Thresholds at Natural and Created Coastal Wetlands. US Army Engineer Research and Development Center (ERDC). Wetlands Research Program. ERDC-TN-WRP-HS-CP-2.2, 12 p.

Shafer, D.J. and Streever, W.J. (2000). "A Comparison of 28 Natural and Dredged Material Salt Marshes in Texas with an Emphasis on Geomorphological Variables". *Wetlands Ecology and Management 8*, pp. 353-366.

Sharp, W.C., Belcher, C.R., and Oyler, J. (1980). Vegetation for Tidal Stabilization in the Mid-Atlantic States. US Department of Agriculture, Soil Conservation Service, Bromall, PA, 19 p.

Thomas-Blate, J.C. (2010). *Living Shorelines: Impacts of Erosion Control Strategies on Coastal Habitats.* Atlantic States Marine Fisheries Commission (ASMFC). Habitat Management Series No. 10, February 2010.

US Army Corps of Engineers (USACE). (2010). *Chesapeake Bay Shoreline Erosion in Maryland: A Management Guide*, USACE, 136 p.

US Army Corps of Engineers (USACE). (2011) Shore Protection: A Guide for Engineers and Contractors in the Chesapeake Bay Region, Baltimore, MD, USACE (in preparation)

Virginia Institute of Marine Sciences (VIMS), Study of Tidal Shoreline Management in Virginia: Recommendations for Living Shorelines and Tidal Resources Sustainability SJR35 December 17, 2010

DEMAND FORECASTING FOR YACHT TOURISM PLANNING IN TURKEY

A.Karanci[1], I.Guler[2], A.Ergin[1] , A.C. Yalciner[1]

[1]Department of Civil Engineering, Middle East Technical University, Ankara,Turkey

[2]Yuksel Proje Uluslararasi A.Ş., Ankara, Turkey

ABSTRACT

Integration of forecasts to the strategic planning is necessary for sustainable and use of the coastal resources. In this study two different quantitative forecasting techniques - Exponential smoothing and Auto Regressive Integrated Moving Average (ARIMA) methods - were used to estimate the demand for yacht berthing capacity demand till 2030 in Turkey. Forecast results suggested that yacht tourism will continue to intensify increasing the demand on infrastructure.

Aiming a dynamic plan which is responsive to both national and international developments in yacht tourism, potential investments were determined by using multi-criteria decision making processes. This study provides a multi dimensioned point of view to planning problem. The paper highlights the need for sustainable and dynamic planning at delicate and high demand areas such as coasts.

INTRODUCTION

Turkey, with its climate, protected bays, cultural and environmental resources is an ideal place for yachting. Subsequently, yacht tourism is developing consistently. Yacht tourism can cause unmitigated development and environmental concerns when aiming to achieve tourist satisfaction. As the demand for yacht tourism intensifies, sustainable development strategies are needed to maximize natural, cultural and economic benefits.

Forecasting plays a crucial role in tourism planning. Demand forecasts of yacht tourism will be the fundamental input for national regional and local development plans to reduce the risk of future shortages or surpluses in goods and services.

In this study, two time-series forecasting techniques - exponential smoothing and ARIMA - were utilized to forecast the 2030 yacht berthing space demand for Turkey.

YACHT TOURISM IN TURKEY

Yacht tourism in Turkey has come up with the revival of domestic and especially foreign demand in the second half of 1980's. The first motion of yachting in Turkey has been provided by appropriate foundation of Aegean and Mediterranean coasts for yacht tourism and in addition by being estranged of world yachters from other yachting regions in terms of hygiene, intensity and habits.

As seen from Table 1, marinas and berthing facilities in Turkey are mostly located at Aegean and Mediterranean Regions. There are no marinas or related facilities that are in operation in Eastern Mediterranean and Black Sea Coasts.

Table 1: Capacities of Marinas and Berthing Facilities in Turkey (DLHI, 2010)

Province	No	Marina	Sea	Land
Antalya	1	Kaleiçi Marina	65	0
	2	Çelebi Marina	235	300
	3	Setur Finike Marina	300	150
	4	Kemer Türkiz Marina	240	140
	5	Kaş Marina	450	150
Aydın	6	D-Marin Didim	580	600
	7	Setur Kuşadası Marina	350	175
Muğla	8	Ece Saray Marina	400	0
	9	Fethiye Municipality Marina	150	0
	11	My Marina Berthing Place	75	0
	12	Göcek Municipality Marina	150	0
	13	Port Göcek	385	150
	14	Skopea Marina	67	0
	15	Göcek Club Marina	205	0
	16	Marina Turk Göcek Village Port	185	240
	17	Marina Turk Exclusive	100	0
	18	Bodrum Milta Marina	455	50
	19	Bodrum Belediye Marina	300	0
	20	D-Marin Turgutreis	550	100
	22	Port Bodrum Yalıkavak	350	100
	23	Yat Lift	0	100
	24	Ağanlar	0	200
	26	Albatros Marina	150	240
	27	Netsel Marmaris Marina	676	120
	28	Martı Marina	350	100
	29	Marmaris Yacht Marina	460	575
İzmir	31	Levent İzmir Marina	70	60
	32	Setur Altınyunus Çeşme Marina	180	60
	33	Alaçatı Marina	250	70
	34	Dalyanköy Berthing Place	100	0
	35	IC Çeşme Marina	400	100
	36	Sığacık Marina	400	200
	37	Old Foça Berthing Place	75	0
İstanbul	38	Kumburgaz Güzelce Marina	250	100
	39	B. Çekmece Marina	150	0
	40	Ataköy Marina	700	100
	41	Kalamış and Fenerbahçe Marina	1,010	220
	42	Atabay Marina	0	100
Balıkesir	43	Ayvalık Setur Marina	200	150
Çanakkale	44	Çanakkale Marina	65	0
TOTAL			**11,075**	**4,650**

Total yacht mooring capacity of marinas and yacht mooring facilities in Mediterranean Basin is about 500 thousand and the capacity of Turkey constitutes approximately 4% of total capacity in Mediterranean Basin (see Figure 1).

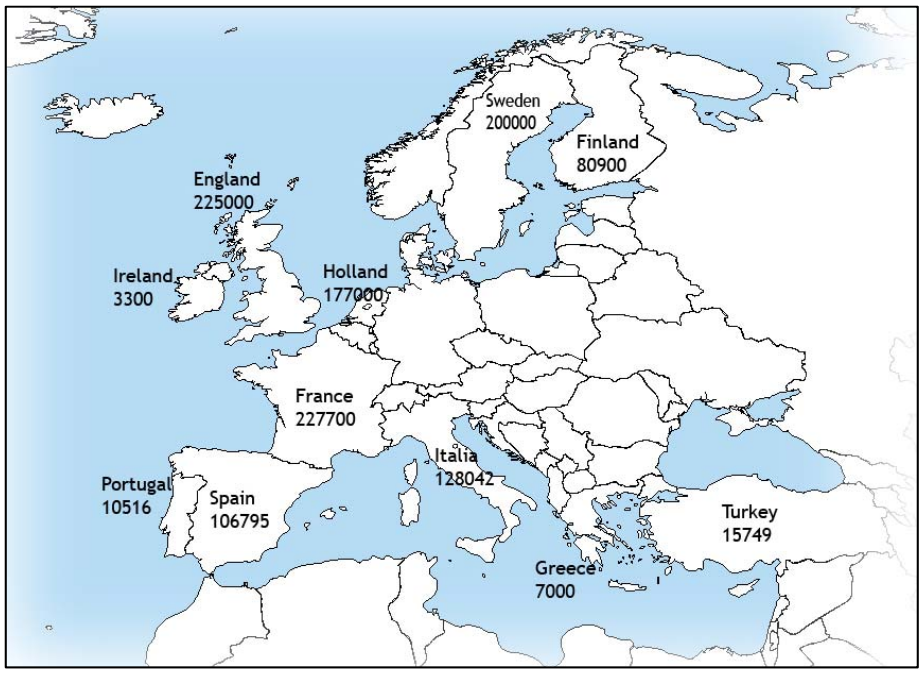


Figure 1. Yacht Berthing Capacities in Mediterranean

In recent years due to sea pollution occurred in Western Mediterranean Sea and increases in prices, Eastern Mediterranean Sea has become an indispensable place for yachters. Taxes imposed for yachts in European Union countries caused yachters to visit Eastern Mediterranean Sea; and this has constituted a good opportunity for Turkey for yacht tourism. Yachters' demand for discovering new places result in new yachting places in Eastern Mediterranean Sea. In addition, especially Mediterranean, Aegean Sea and Marmara Sea have a great economic potential with their natural and historical wealth, geographical properties and mild climate conditions.

METHODOLOGY and ANALYSIS

In general tourism demand forecasting is generally categorized into two-categories: quantitative and qualitative(Song & Li, 2008). Qualitative methods use expert judgments to organize the past information of the variable. Qualitative forecasts are used when historical information about the variable is not available.

Quantitative methods employ mathematical rules to identify the patterns and relationships of the phenemonon to predict future patterns. Quantitative methods can be used when the past information of variable exists and can be quantified. These methods also assume past patterns will continue into the future.(Makridakis, Wheelwright, & Hyndman, 1998)

In this study exponential smoothing and non-seasonal ARIMA were used in forecasting the future yacht berthing demand. Demand forecasting methods are given below, briefly.

Exponential Smoothing

Exponential smoothing method produces smoothed time series by assigning exponentially decreasing weights to older observations. In this method as the weight of the data will decrease exponentially as data get older (Touran & Lopez, 2006). Since seasonality is not expected in annual data single exponential smoothing was adopted.

ARIMA

The abbreviation ARIMA stands for "autoregressive integrated moving average." ARIMA approach is designated to design the simplest model for describing the past patterns of observed data forecasting that are based on linear functions of observations. Forecasts produced by ARIMA models are based on linear functions of the sample data.

ARIMA processes which are sometimes called as Box-Jenkins models consists of three parts. The model is often denoted as ARIMA(p,d,q) where p is the order of autoregressive component, d describes the order of differencing needed in order to achieve stationary time series and q describes the order of moving average component. The three components of the ARIMA method are described below.

DATA and VARIABLES

In this study future demand study for berthing spaces is carried out for the next 20 years. Thus, historical data is needed to extrapolate up to 2030 within the scope of the design phase.

Available Yacht Tourism Data

In Turkey, the most difficult challenge for forecasting is inadequacy of the available yacht tourism data. Data presented in Yacht Statistics Yearbooks (Ministry of Culture and Tourism, 1992 - 2009) only relays yacht movements in Turkey, not berthing space demand.

In order to acquire the lacking historical data for yacht berthing space demand, surveys have been performed in Coastal Tourism Structures Master Plan Studies (DLHI, 2010). In scope of the Master Plan Studies, a questionnaire inquiring information about capacity, infrastructure, yacht berthing trends, environment protection measures and demographic information about the employees of the yacht harbor was prepared and sent to 35 yacht harbors located at Turkey shores. The response rate was %63; 22 of the questionnaires were returned. The berthing capacity provided by the marinas which responded to questionnaires corresponded to %81 of the capacity of Turkey.

The yacht berthing historical data gathered from the questionnaires had not accounted for the yachts moored freely at the protected bays. These yachts over-crowd the bays and cause environmental threats to the marine environment due to anchoring and waste disposal. In order to prevent these social an environmental problems, yachts mooring freely at the protected bays should be encouraged to use organized berthing spaces by creating adequate capacity and enforcing legal obstacles. In order to create adequate capacity these yachts should also be accounted for in future demand. An index which calculates the free yacht/mooring space density is produced in order to include these yachts into the forecasts. For the calculations, data was taken from;

- Göcek capacity assessment study (METU, 2007)
- Bay Assessment Study (Chamber of Shipping Bodrum Branch, 2006)
- Bodrum Bay Assessment Study (Chamber of Shipping, 2006)

Mentioned studies (Göcek Capacity assessment study and bay assessment studies) all provide number of yachts moored freely at Aegean Sea Bays. Incorporating these data with the yacht numbers found from Google Earth images yacht numbers moored freely at protected bays were found. The free yacht/mooring space proportion of the regions was then calculated to attain a connection between the existing infrastructure and free yachts.

The free yacht/mooring space proportion defined as densities are given in Figure 2 where four different areas were categorized. The least dense area is Marmara Region with a density of 0.17. The most crowded area is the coastline between Bodrum and Göcek. Density for this area is calculated as 0.34. The density between Bodrum to Çanakkale and Kaş to Anamur are found as 0.25 and 0.22 respectively.

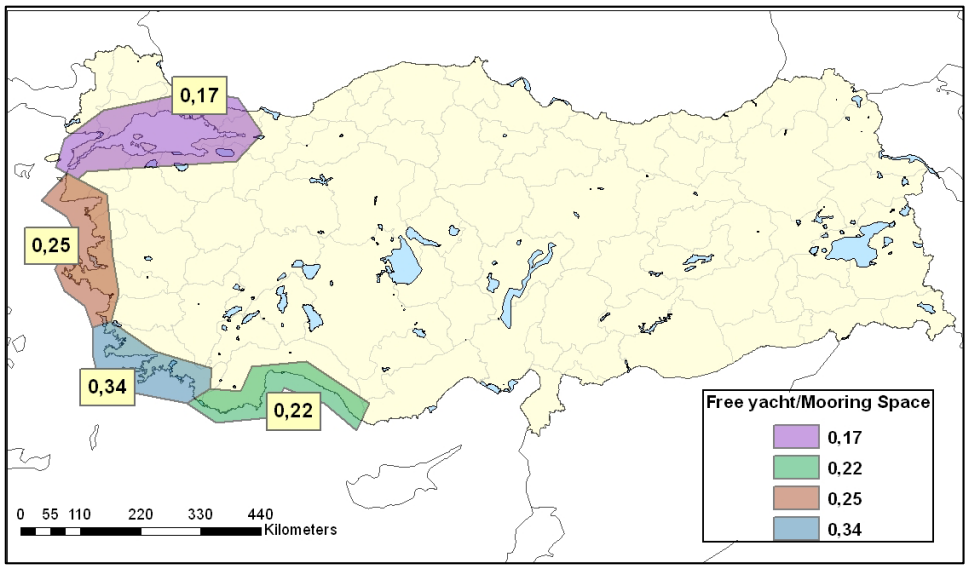


Figure 2. Yacht Densities at Turkey Shores

Combining the data from Coastal Tourism Structures Master Plan Study (DLHI, 2010), with the calculated index values historical yacht berthing space demand from 1998 to 2008 for Turkey is gathered. Demand for berthing space is given in Figure 3.

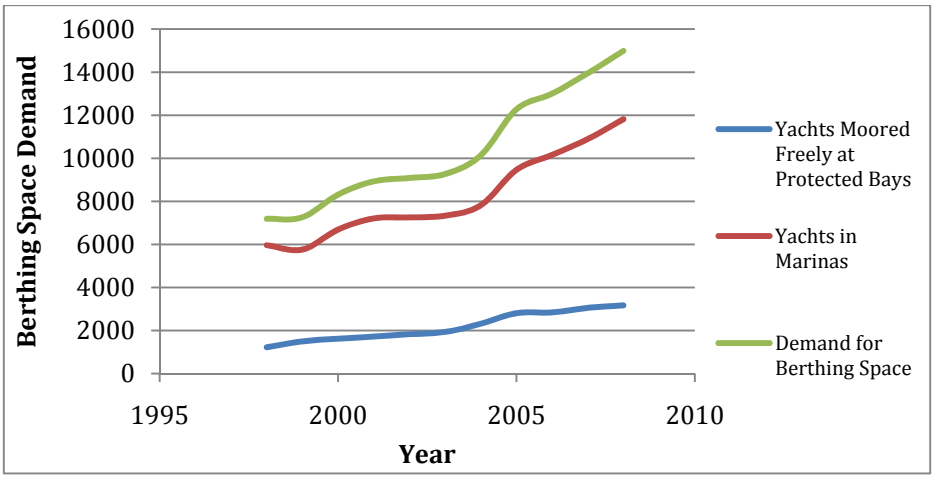


Figure 3. Berthing Space Demand Trends in Turkey

RESULTS AND ANALYSIS

The accuracy of the models discussed was analyzed according to the mean absolute percentage error (MAPE) and the Pearson product moment correlation coefficient (r).

Mean absolute percentage error (MAPE) is a sum of the absolute errors for each time period divided by the actual value for the period, divided by the number of periods. Then, by convention, this value is multiplied by 100. This is a simple measure allowing the comparison of different forecasting models with different time periods and numbers of observations, and weighting all percentage error magnitudes the same (Song & Witt, 2000). Lower MAPE values are preferred to higher ones since they indicate a forecasting model with smaller percentage errors (Frechtling, 2001). MAPE can be denoted as:

$$MAPE = \frac{1}{n} \times \left(\frac{|e_t|}{D_t} \right) \times 100$$

Where n is number of periods, e is the forecast error and D is the actual demand value.

Table 2 shows the results of the different forecasting models. ARIMA (0,1,0) model show similar results and outperform the naïve and exponential smoothing models.

Table 2. Accuracy Comparison of Forecasting Models Used

	r	MAPE
Naive	0.905	6.783
Single Exponential Smoothing	0.813	5.294
ARIMA (0,1,0)	0.947	3.143

According to the analysis, ARIMA seems to be the best forecasting method for berthing space demand. Accordingly, the results using ARIMA is presented.

YACHT DEMAND ESTIMATIONS USING ARIMA METHOD

Using SPSS software seasonal ARIMA models were analyzed using 95% confidence interval. Annual berthing space data from 1998 to 2008 was entered in to the model. The best fitting forecasting model was chosen according to MAPE values.

SPSS analysis estimated that ARIMA (0,1,0) model gives the best fit when MAPE is used as the measure of accuracy. MAPE for ARIMA (0,1,0) model is calculated as 3.143 which indicates a suitable fit. The predicted berthing space demand data and confidence intervals for ARIMA (0,1,0) is given in Table 3 and Figure 4.

Table 3. Yacht Demand Estimations with ARIMA Method

Year	Lower %95	Predicted Demand	Upper %95
2011	16,004	17,891	19,423
2012	16,549	18,708	20,497
2013	17,126	19,526	21,539
2014	17,725	20,343	22,559
2015	**18,341**	**21,162**	**23,562**
2016	18,970	21,979	24,552
2017	19,610	22,797	25,531
2018	20,259	23,614	26,501
2019	20,917	24,432	27,462
2020	**21,581**	**25,249**	**28,417**
2021	22,250	26,067	29,367
2022	22,926	26,884	30,310
2023	23,606	27,702	31,249
2024	24,290	28,519	32,184
2025	**24,978**	**29,337**	**33,115**
2026	25,669	30,155	34,043
2027	26,364	30,973	34,967
2028	27,062	31,790	35,888
2029	27,762	32,608	36,807
2030	**28,465**	**33,425**	**37,723**

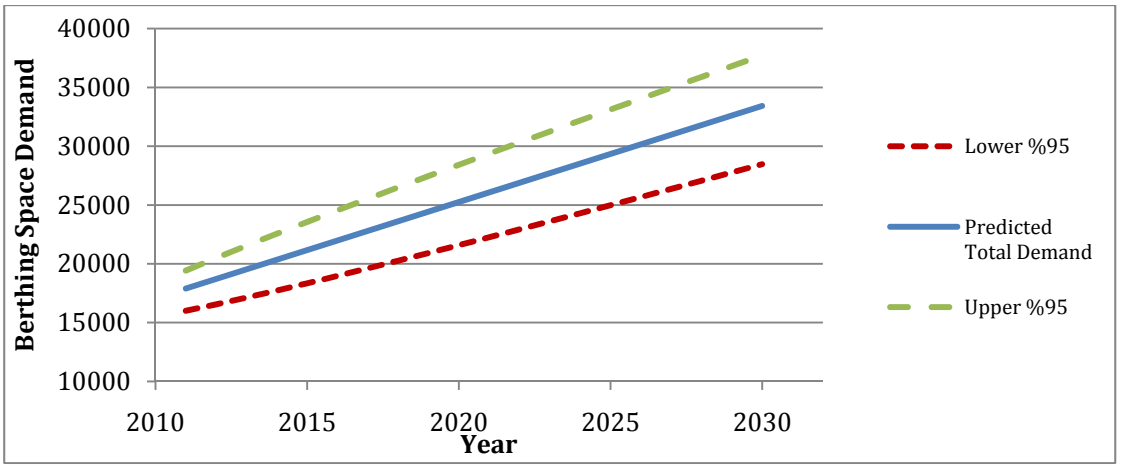


Figure 4. Berthing Space Demand Trends in Turkey Estimated by ARIMA (2010 – 2030)

Distribution of the berthing capacity along the Turkish coastal areas was done using the estimations (see Table 3) produced by ARIMA forecasting method.

BERTHING SPACE DEMAND DISTRIBUTION FOR TURKEY (2010-2030)

Based on environmental, socio-economic and geographic data and the opinions gathered from stakeholders such as marina operators, local communities and government officials an allocation model was developed for the successful allocation of the predicted demand seeking social and economical growth while preserving the coastal environment. Therefore new marina investments were proposed in view of the above given sustainable development principals. In Turkey, existing marinas are mostly located in the most attractive and often the most fragile environments. However, because of the highly fragile nature of coastal environments over exploitation of these areas may have severe consequences on the environment. The uneven utilization of Turkey coasts also causes unequal distribution of investments and tourism expenditures. While popular areas benefit significantly from tourism, remaining areas are mostly neglected. In order to overcome the regional disparities and protect the ecological integrity of the coasts when planning for spatial development of marinas social, economic and ecological development effects were considered. According to these properties, 8 different regions were formed (see Figure 5).

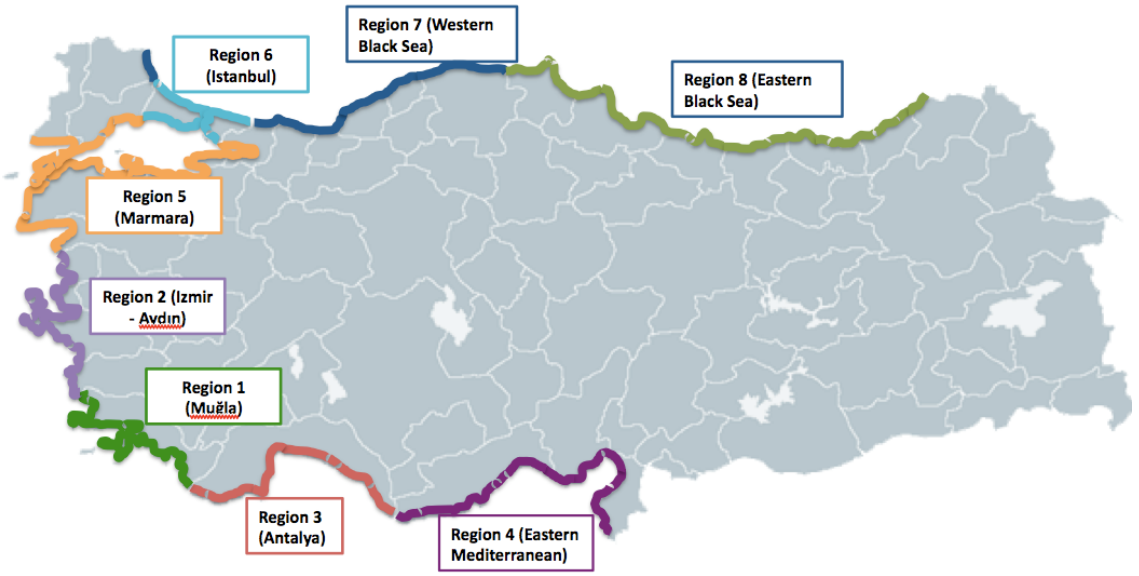


Figure 5. 8 Different Coastal Regions of Turkey

Distribution of the forecasted demand amongst the proposed 8 regions at 2030 was carried out by AHP (Analytic Hierarchy Process) decision making model (Karanci, 2011) (see Table 4). AHP was used to prioritize the coastal regions in order to distribute the berthing space demand aiming sustainable development.

Table 4. New Berthing Spaces Proposed in view of Sustainable Development (2010-2030)

Regions	**Proposed Berthing Spaces**	**Total Berthing Spaces**
Region 1 (Muğla)	1,600	9,904
Region 2 (İzmir – Aydın)	2,000	5,670
Region 3 (Antalya)	1,600	4,930
Region 4 (Eastern Mediterranean)	1,200	2,300
Region 5 (Marmara)	900	1,750
Region 6 (İstanbul)	1,200	3,830
Region 7 (Western Black Sea)	2,400	2,400
Region 8 (Eastern Black Sea)	3,000	3,225
Total	**13,900**	**34,009**

As can be seen from the Table 4, the total yacht berthing space at 2030 for Turkey is proposed to be approximately 34,000.

CONCLUSIONS

In this study forecasts were done by very limited data. So it is especially crucial that the results of the forecasting should be monitored and evaluated at 5 year periods. There is not only lack of crucial data, but most existing data are not readily processed for yacht tourism forecasting and planning. Therefore, there is not only a need for data collection studies also need for useable data for the coastal tourism at Turkey.

For the future studies, sustainable development plans should be integrated with GIS for a spatial recognition of the coasts and uses. It is also recommended to re-design the prioritization process with the opinions gathered from the users of the yacht tourism system.

REFERENCES

Chamber of Shipping. (2006). *Bay Assessment Study*. Bodrum

Chamber of Shipping. (2006). *Bodrum Bay Assessment Study*. Bodrum

DLHI. (2010). *Coastal Tourism Structures Master Plan Study*. Ankara.

Frechtling, D. C. (2001). *Forecasting tourism demand: methods and strategies*. Oxford: Butterworth-Heinemann.

Karanci, A. (2011). *Statistical and Spatial Approaches to Marina Master Plan for Turkey.* M.Sc, Middle East Technical University, Ankara.

Makridakis, S. G., Wheelwright, S. C., & Hyndman, R. J. (1998). *Forecasting: Methods and Applications* (3 ed.). NY: Wiley.

Ministry of Culture and Tourism. (1992-2008). *Yacht Statistics Yearbook*. Ankara

METU. (2007). *Determination of Yacht Carrying Capacity in Gocek Bay*. Ministry of Environmnet and Forest.

Song, H., & Li, G. (2008). Tourism Demand Modelling and Forecasting - A review of Recent Research. *Tourism Management, 29*(2), 203 - 220.

Song, H., & Witt, S. F. (2000). *Tourism Demand Modelling and Forecasting: Modern Econometric Approaches*. Oxford: Elsevier.

Touran, A., & Lopez, R. (2006). Modeling Cost Escalation in Large Infrastructure Projects. *Journal of Construction Engineering and Management, 132*(8), 853 - 860.

Current challenges in coastal management in the Netherlands; examples of pilot projects

J.P.M. Mulder [1,2,3], and J.A. van Dalfsen[1]

[1] Deltares, Unit Marine and Coastal Systems, P.O. Box 177, 2600 MH Delft, The Netherlands; PH (+31-88-3358464); FAX (+31-88-3358582); email: jan.mulder@deltares.nl ; jan.vandalfsen@deltares.nl

[2] University of Twente, Water Engineering and Management, P.O. Box 217, 7500AE Enschede, The Netherlands

[3] Netherlands Centre for Coastal Research / NCK, P.O. Box 177, 2600 MH Delft, The Netherlands

ABSTRACT

A need for upscaling of sand nourishments to guarantee sustainable conditions for safety against flooding and preservation of coastal functions, combined with the need to enhance an integrated coastal zone management in the Netherlands, has initiated a number of pilot experiments.
The management background and the approach leading to the pilots are illustrated. Central to the approach is a connection between large scale requirements and small scale needs, applying a concept of Building-with-Nature. The three pilots illustrate different applications; two for mega-scale nourishments and one for sand mining.
Monitoring of the pilots must reveal the effectiveness of the designs; evaluation of the approach to connect large- and small scales, must indicate its wider applicability.

INTRODUCTION

North Sea coast of the Netherlands

The Dutch coastline along the SE part of the North Sea (Fig. 1) is about 350 km long. Some 15% of the coast consists of sea dykes and other man made sea barriers, some 10% are beach flats along the tips of the northern Wadden islands, 75% are dune areas of varying widths from less than 100 metres to several kilometres (Fig.4). The primary function of the coast is protection of the low-lying hinterland against flooding. The sandy coast however represents important values to other functions as well: ecological values, drinking water supply, recreation, residential and industrial functions. Coastal erosion, dominant along half of the Dutch coast, is endangering these functions.

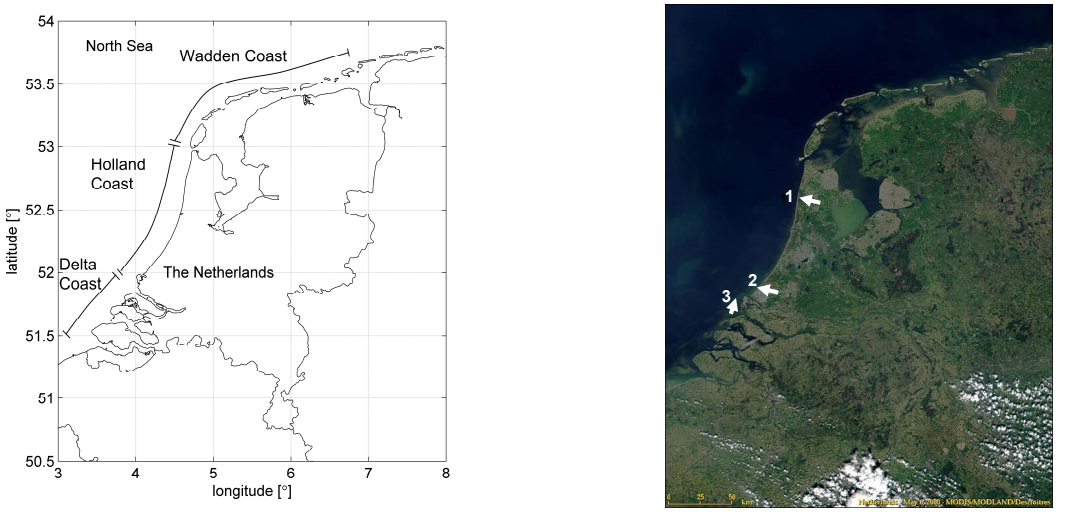


Figure 1. The Netherlands; (1) Hondsbossche- and Pettemer Zeewering; (2) Pilot Sand Engine; (3) ecological landscaping pit

Coastal management in the Netherlands

To ensure safety against flooding, safety standards for all flood defenses in the Netherlands, including the dunes, have been established by law (Flood Defense Act, 1996; Water Act, 2009). The standard for sandy dunes is related to a critical residual dune volume, that is being tested in a 6-yearly test procedure. In addition to that, the Acts define the need to preserve the coastline.

The latter has been a management objective since 1990, when the policy of "Dynamic Preservation" has been adopted by the government in order to stop structural erosion of the coast. Defining the 1990 coastline position as the reference coastline and sand nourishments as the preferred intervention procedure, the main objective of the policy is sustainable preservation of safety against flooding and of functions in the dune area. From 1990 the yearly available total nourishment volume has been 6 Million cubic meter. In 2000 it was decided that in order to achieve *sustainable* preservation, it was necessary to extend the policy to a larger scale; the yearly nourishment volume was raised from 6 to 12 Million cubic meter.

This has resulted in a coastal policy with objectives at three different scales (see e.g. Van Koningsveld and Mulder, 2004; Mulder et al., 2011):

- at the small scale, preserving a critical residual dune volume in order to guarantee *momentaneous* safety against flooding;
- at the medium scale, maintaining the coastline in order to guarantee a s*ustainable* preservation of safety and functions; and since 2001
- at the large scale, maintaining the sand volume in the coastal foundation i.e. the active sand volume in the area between the -20 m depth contour and the landward boundary of the dune massive.

Preservation of flood defenses of the sandy coast involves three governance levels: a) the national level, Ministry of Infrastructure & Environment; b) regional level, four coastal Provinces and seven coastal Water Boards; and c) local level, several municipalities. The role of the State is threefold: overall supervision, flood defense management at Wadden islands and of the Delta dams, and coastline management. As overall supervisor the State also bears responsibility for (strategic) policy. Daily management of flood defenses of the sandy Holland- and Delta coast is the task of the Water Boards. The role of Provinces is supervision of Water Boards and coordination and integration of coastal policy. For implementation of coastline management, e.g. the design of annual nourishment schemes, the State seeks advice from Provinces, Water Boards and municipalities and stakeholder organizations.

It is noticable that flood defense management – responsible for momentaneous safety against flooding –, and coastline management – responsible for sustainable safety – at the ministerial level, until now have been organised along two separate lines including separate organisations and finances.

CURRENT CHALLENGES

Upscaling of nourishments

The present policy nourishing a yearly averaged volume of 12 million cubic meter has succesfully contributed to achieve objectives at the small – and medium scale levels: preserving (and enhancing) dune strength and maintaining of the coastline (Mulder and Tonnon, 2010). However, the contribution to the third and largest scale level (i.e. maintaining of the active sand volume of the coastal foundation) appears to be insufficient. A latest update of the sediment balance of the coastal foundation (De Ronde, 2008) shows a negative total of ca. 20 million cubic meter per year. The conclusion is that - in order to achieve the large scale objective of maintaining the active sand volume of the coastal foundation - nourishments would need upscaling from 12 to 20 million cubic meter per year (NWP, 2009).
However, it is good to realize that this accounts for an estimated sea level rise of 2 mm/ year. An higher rate of sea level rise, would require an equivalently higher amount. In this respect, in a study on future adaptation options to climate change in the Netherlands, the authoritive Deltacommissie (2008) suggests a raise of nourishment budgets up to 85 million cubic meter per year until the year 2050.

Enhancing *Integrated* Coastal Zone Management

The latest evaluation of the Dynamic Preservation policy (Lubbers et al., (2007) shows that specifically the goal to stimulate "coherence between different parts of the coast, i.e. Wadden sea, estuaries and Holland coast" – i.e. spatial integration –, and the objective of "maintaining the coastal foundation", have not sufficiently been operationalized. The need for a better elaboration of these aspects is further stressed by the future raise in nourishment demand.
Another important conclusion from the policy evaluation is that the objective to sustainably preserve not only safety, but also boundary conditions for all other

functions in the coastal system, is only partly achieved. It appears there is a societal need – expressed by provinces, municipalities and private parties – to explicitly execute sand nourishments for other coastal functions than coastal safety alone. In practice, however, nourishment claims for these other user functions (e.g. in coastal towns) often imply relatively expensive beach nourishments, whereas long term safety issues can be served by cheaper shoreface nourishment. This shows that at present, functional integration in Dutch coastal management still is limited.
In this respect, another issue which arises is that responsibilities (and finances) for coastal functions are fragmented over different Ministries, whereas actually different Ministries should be involved together. A similar observation claims that one of the bottlenecks in Dutch public administration is fragmentation, where each ministry is focusing on different sub-aspects of societal issues. Furthermore, political culture even prescribes that one minister does not interfere with the field of another (non-intervention principle). These findings underpin that integration and coherence of policy and governance, guiding principles of sustainable development, need serious improvement. It underlines the recommendation to raise the profile of Integrated Coastal Zone Management and enhance its integration with sectoral policies.

CONNECTION OF SCALES, CONNECTION OF STAKES

Large scale requirements and small scale needs

An answer to the challenges may be found in combining the two. This translates the challenges into the question: "how can the nourishment volume optimally serve stakes at different levels?'
The need for upscaling of nourishments is related to the governments (large scale) responsibility for sustainable preservation of safety and functions. Considering "sand as the carrier of functions" (NSS, 2006), sustainable boundary conditions for all functions require maintaining the active sand volume in the coastal foundation; a large scale, long term requirement expressed in terms of a total nourishment *volume*. Preservation of this volume is primarily the governments stake.
The *distribution* of the volume - both allocation in space (where) and in time (when, how often), and the method (how) -, will determine its effects on smaller scale- and short term needs. Thus the distribution of nourishment sand affects stakes at all levels, both national, provincial, regional and local.
Taking the large scale requirement for upscaling of the nourishment volume as a starting point, active involvement of all stakes in the design proces of the distribution scheme, may enhance sectoral integration. The challenge is to find possible combinations of large scale, long term requirements with small scale, short term needs.

Building with Nature

Taking a long term perspective as a starting point, introduces "time" as an important aspect in the design of nourishments. Sustainable strategies for nourishments and (related) sand mining imply building-with-time. A suitable concept that is consistent with this approach is Building with Nature, which originates from the Czech

hydraulic engineer J.N. Svasek and was further explored and linked to the field of Integral Coastal Zone Management by Waterman (2008). Building with Nature type solutions aim to create added value through integral consideration of all functions and values of a coastal system (Aarninkhof et al., 2010). We adhere to the concept of Building with Nature by adopting three guiding principles towards the design of sustainable strategies for sand mining and coastal nourishments (www.ecoshape.nl):

1. Make optimal use of natural processes.
2. Explore opportunities for nature development as an integral component of project design.
3. Reserve space to accommodate for natural system dynamics

Pilot examples

Although coastal management practice in the Netherlands over the last two decades represents a first example of a multi-scale, Building with Nature-like approach, the current challenges have initiated a number of pilots exploring optimal ways of upscaling nourishments and integration of different functions at different scales. Three of the pilot projects illustrating the approach will be discussed below.

The first two relate to sand nourishments: the Pilot Sand Engine illustrates a mega nourishment of 20 million cubic meter (~10,000 cubic meter/meter) serving multiple purposes; the Pilot Sandy Sea Dike illustrates an application of a sand nourishment to a hard stucture. A third example relates to sand mining in which opportunities for habitat development are studied.

PILOT SAND ENGINE

Background

Under responsibility of the Ministry of Infrastructure and Environment (formerly known as Verkeer en Waterstaat) between 1990 and 2010 a total of 180 million cubic meter of sand has been nourished on the Dutch coast, with a yearly frequency. Typical sizes of individual nourishments have varied between 0,2 and 1 million cubic meter (200 – 500 cubic meter / meter). Main arguments behind the distribution of nourishments have been maintaining the reference coastline (BKL), regarding safety against flooding as the primary function. Around 2003 the question was raised whether a lower frequency of larger nourishment volumes might be more efficient. At the same time the Ministry became more open to intensify the involvement of stakeholders. In parallel, coastal provinces were developing a long term vision on development of the coast (www.kustvisie.nl; www.kustvisiezuidholland.nl), showing a need for additional space for recreation and nature development, especially in the province of Zuid Holland.

Combination of the efficiency question by the ministry and the spatial need of the province eventually has led to the initiative by the Province of South Holland, together with the Ministry of Infrastructure and Environment, local municipalities and Water Board, NGO's and business, to define a Pilot Project "Zandmotor / Sand Engine".

Mega nourishment with multiple objectives

The pilot implies a mega-nourishment of approximately 20 million cubic meter (~ 10,000 cubic meter / meter) on the coast of Holland, between Hook of Holland and The Hague (Fig. 1). Integrated objectives of the pilot are:

- at the large scale i.e. at the level of the ministry, to create long term safety conditions and realize a reduction in cost of coastal maintenance;
- at medium and small scales i.e at the level of the province and municipality, the creation of extra space for nature and recreation,
- overall, in an innovative manner.

After a planning period of two years and an Environmental Impact Assessment procedure, implementation has started in March 2011 (Fig. 3). The work must be completed October 2011. The project will be closely monitored for a period of 10 years on its geomorphological, ecological and social-economical consequences.

Designs

Numerous different locations and designs ranging from shore face nourishments, detached islands, peninsula's, shore-attached bars, bell and hook-shaped designs were modeled over periods ranging from 20 to 50 years (Mulder and Tonnon, 2010; Figure 2.-right). Based on costs, safety, ecological and recreational aspects the hook-shaped design was selected as the so-called preferred alternative in the EIA (Figure 2-left). The initial dimensions are 2 km longshore at the beach and 1,5 km cross shore.

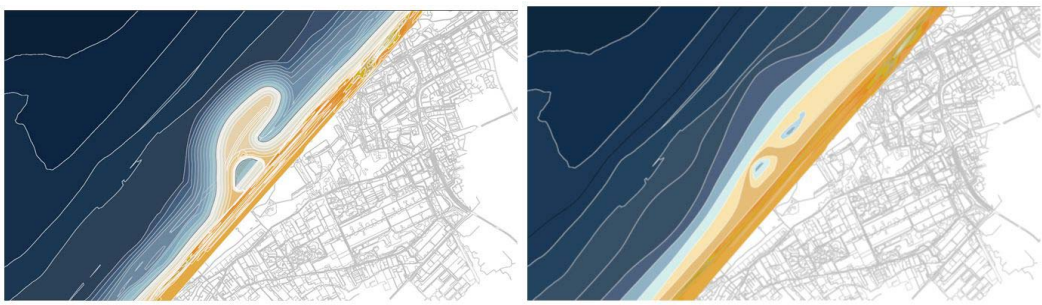


Figure 2. Final design of Pilot Sand Engine Delfland (left); computed morphological development after 15 years (right) (courtesy: Deltares / DHV)

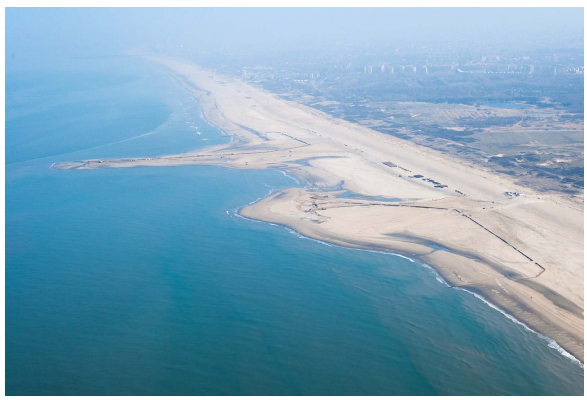


Figure 3. Construction phase of Sand Engine March 22, 2011 (photo courtesy Rijkswaterstaat)

The final design reflects the input of stakeholders at various levels. The artificial 'dune lake' at the base of the hook was introduced in a later design stage, to mitigate adverse hydrological effects on the drinking water station in the existing dune area.

PILOT SANDY SEA DIKE

Background

Safety against flooding today is, and traditionally always has been of primary concern in the low-lying Netherlands. In the past this has led to the construction of sea dikes along the weakest stretches of our sandy coast (Figure 4). One example represents the Hondsbossche en Pettemerzeewering (Figure 1, 4 and 5).

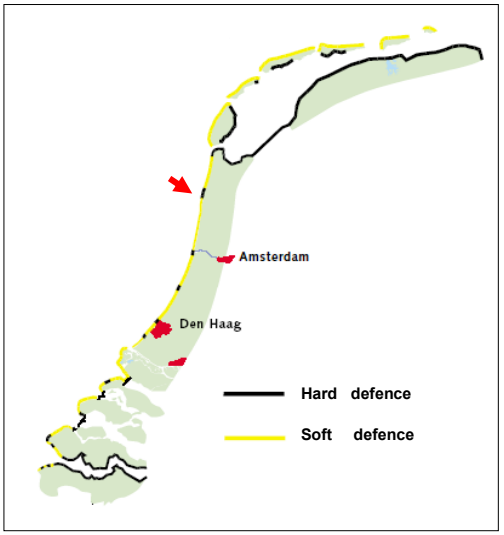


Figure 4. Overview of hard and soft sea defences in the Netherlands. Arrow indicates location of the sea dike Hondsbossche en Pettemerzeewering.



Figure 5. Hondsbossche- and Pettemer Zeewering (courtesy Rijkswaterstaat).

In 1990, at the start of the Dynamic Preservation policy (see introduction) all attention was focused on stopping structural erosion along the sandy parts of the coast. Along the sea dikes, no reference coastline has been defined. As a consequence no direct compensation by nourishments of structural erosion at sea dikes took place. Structural erosion and the resulting maintenance efforts at sea dikes came on the account of the flood defense management, not of coastline management (see introduction).
Basically this situation has continued also after 2001, when an additional large scale objective of maintaining the sand volume of the coastal foundation was adopted. The opportunity of compensating structural erosion in the coastal foundation of the sea dikes by nourishments has hardly been used sofar. One cause is the the lack of a distinct nourishment distribution criterion for sea dikes comparable to the reference coastline for the dunes. Another, is the strict separation between flood management - and coastal maintenance departments (see introduction). The potential of the pro-active approach of the latter, is hardly being recognized by the former.
However, recent reconfirmation of the importance of the overall sandy character of the coast (Deltacommissie, 2008; NWP, 2009) and discussions on maintenance of the coastal foundation, gradually are introducing a change. A first shore face nourishment of the sea dike Hondsbossche en Pettemerzeewering was implemented in 2008. In present plans for reinforcement of the sea dike, sandy solutions are prominent.

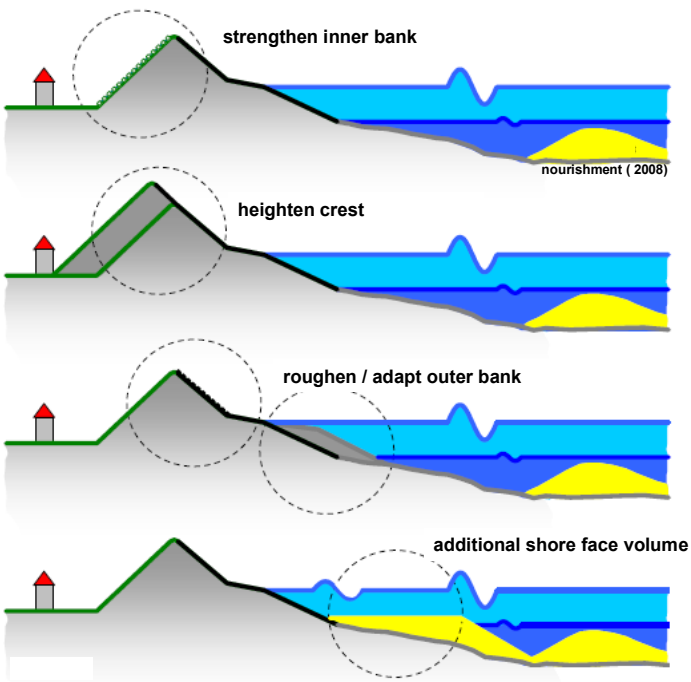


Figure 6. Variants of dike reinforcements (Arcadis, 2010).

Dike reinforcement
Based on the prospective of more adverse hydraulic design conditions, the Hondsbossche en Pettemer Zeewering formally has been earmarked a Weak Link in

in coastal defence of the Netherlands (Beleidsagenda, 2002). Commisioned by the government and under direction of the province and water board, over the last years several plans have been developed for reinforcement of the sea dike and improvement of spatial quality of the area. Local stakeholders were intensively involved in the proces.

Designs

Environmental Impact Assessment studies (Arcadis, 2010) have investigated several variants of dike reinforcements (Figure 6). Based on the EIA, the province and water board supported by the local community, decided on a sandy reinforcement of the sea dike as the favorable variant. In October 2010 the decision has been confirmed by the ministry, pointing at the long term advantages of sand nourishments for safety. Province and water board have been commisioned to elaborate a detailed design. Special attention wil be given to the long term effects on maintenance of the sandy reinforcement, taking account of the large scale coherence in the coastal foundation of the sea dike and adjacent sandy dunes. Preliminary estimates of the required sand amount involved in the reinforcement, indicate a volume of ca. 20 million cubic meter. Implementation is expected to start in 2012.

PILOT ECOLOGICAL LANDSCAPING OF BORROW PITS

Background

Unlike other coastal seas where sand resources commonly are limited, the North Sea is characterized by abundant sand resources. In discussions on upscaling of nourishments, availability of sand is not an issue. Related to sand mining, discussions concentrate on integral consideration of all functions of the coastal system, more specifically ecological optimization.

Traditionally, the environmental impacts of sand mining are considered negative resulting in environmental policies that set restrictions and limitations to the mining operations. The potential postdredging value of the borrow area is rarely considered as a result of which opportunities that could improve or add to the overall sustainability of the dredging project are missed. Ecological landscaping aims to make a dredging pit attractive to a variety of benthos and flora that in turn attract fish, sea mammals and birds. This through creating different habitats by way of bed forms and/or combinations of sediment characteristics. This is expected to lead to an increase of biodiversity in the borrow area.

Ecological landscaping

Ecological landscaping in sand mining areas involves the realisation of bed level gradients and other morphological features in newly dredged pits (Van Dalfsen and Aarninkhof, 2009). Whereas present mining policies aim at rapid recovery and restoration of the original habitat on a flat sea bed, the concept of ecological landscaping aims to promote opportunities for nature and economy through development of new, enriched habitats in landscaped mining pits. The feasibility of this concept is derived from recent measurements on the North Sea which reveal a relation between local habitat characteristics and the geomorphology of the sea bed (Baptist et al. 2006). Results show that tidal ridges accommodate different benthic

habitats, which are important to both benthic and pelagic organisms (Figure 5). More generally, a zoning exists within geomorphological features (such as tidal ridges), where the crests give home to relatively poor benthic communities and the adjacent slopes and troughs host benthic communities of higher density and diversity. On the basis of these observations, the application of ecological landscaping in sand mining pits is expected to promote the development of valuable habitats at places where these would naturally not occur, or only on the very long term.

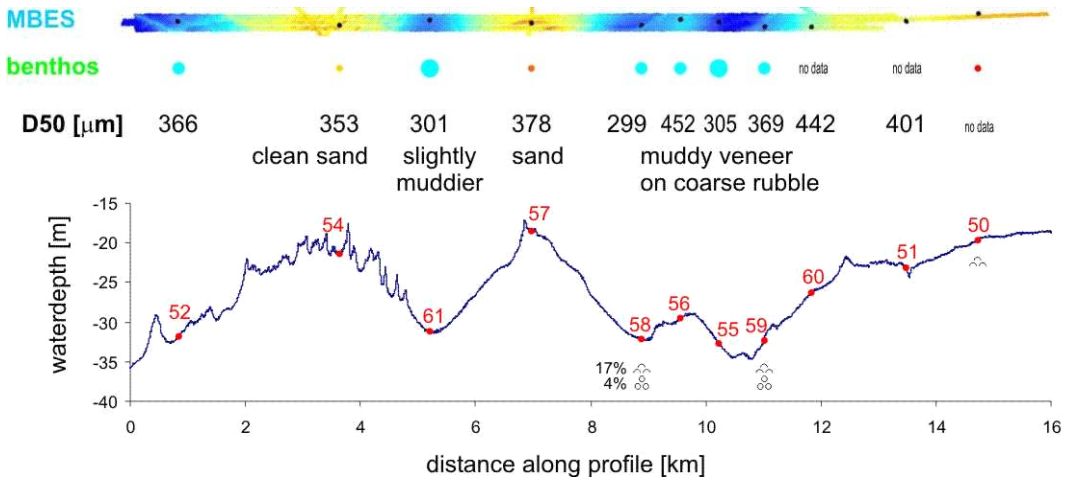


Figure 5: Seabed profile, surface sediment description and benthos community type and density found across tidal ridges in the North Sea. The figure shows (from top to bottom) respectively multibeam data, benthos density and sediment grain size for a total of 11 sample locations denoted by the red numbers. Figure courtesy of Van Dijk et al. (2007), taken from Van Dalfsen and Aarninkhof (2009).

Application of ecological landscaping in mining pits implies the development of the existing habitat into a new habitat, which is not foreseen in current legislation. Therefore, the assessment of post-dredging ecological benefits and their inclusion in evaluation frameworks, will require a mind shift in current policies, permit requirements as well as our approach towards the design and realization of sand mining pits.

Innovative design of borrow pit near Rotterdam

In the framework of the Ecoshape Building with Nature programme (www.ecoshape.nl) a pilot ecological mining pit has been designed to test the feasibility of the concept. The pilot will generate answers to questions such as:

Do the desired enriched habitats (as observed across natural tidal sand banks) indeed develop in landscaped mining pits and if so, on what time scale, which communities will develop over time and how long will these habitats persists, etc. ? These types of questions can only be addressed on the basis of a real-world pilot experiment. Considering the scale of such experiment, this can only be achieved by linking the experiment to a running construction project that involves substantial sand mining.

An opportunity to study the concept of ecological landscaping was offered by the Port of Rotterdam harbor extension (Maasvlakte-2) in the Netherlands consisting of a 1000 ha land reclamation. To realize this over 200 Milion cubic metrs of sand are dredged from a nearby extraction area to a maximum of – 20 m below the existing sea bed. Discussions were held with all stakeholders including the Port of Rotterdam, the consortium of dredging contractors (PUMA) and the authorities (Ministry of Transport, Public Works and Water Management) to explore the possibilities to use this mining area as an experimental testing site. Topics included planning issues (sand balance, timing), dredging operations (feasibility of bed forms), licensing/permits and financial aspects (extra costs for realisation). The experimental location needs to adhere to several important constraints. It must be located along the sides of the mining site and/or the exclusion zone and should remain untouched for a period of at least 5-6 years after construction to allow the monitoring of the geomorphological and ecological development.
Based on these considerations, it was agreed to construct the pilot as a part of the sand mining area for Maasvlakte-2 (Figure 6).

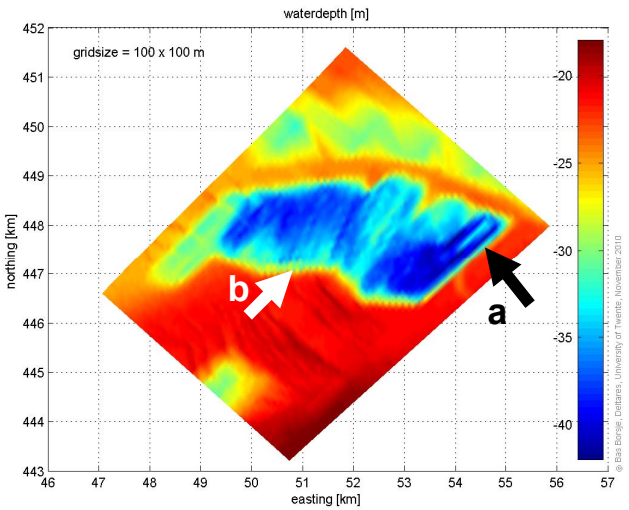


Figure 6. Sand mining area for Rotterdam port extension (Maasvlakte-2) in progress (May 28, 2010). Location 5 km west of the present coastline at a water depth of 20 - 25 m. Extraction depth is 20 m; total excavation volume 220 million cubic meters. The ecological landscaping test sites are indicated by arrows, pointing at a tide-parallel sand ridge (a) and the location of a more natural orientated sand ridge perpendicular to the tide (b) that is currently under construction. (map courtesy PUMA).

During 2010 the first sand ridge has been constructed consisting of a 10 m high, 70 – 100 m wide and 750 m long ridge, parallel to the dominant tidal current. The slopes are between 1:7 and 1:10 (Fig. 7). The slope at the northern end of the test pit is perpendicular to the dominant tide and covers a length of 350 m. The second ridge, perpidicular to the tidal current, is currently under construction.

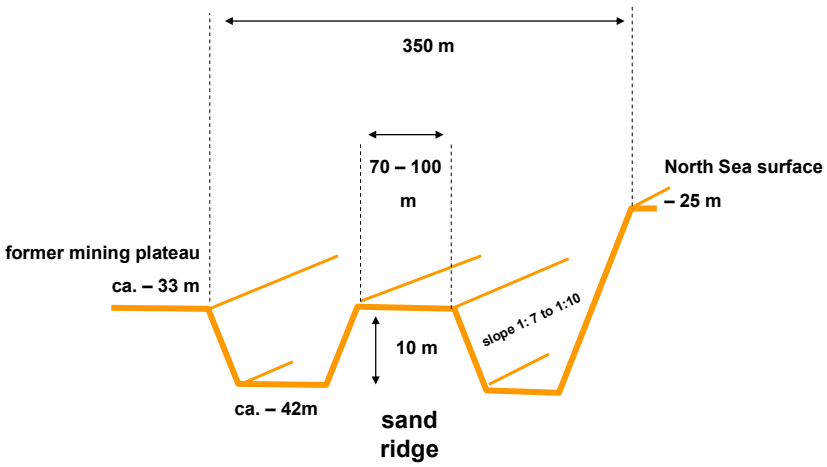


Figure 7. Design of a sand ridge at the ecological landscaping test site.

A monitoring program is in progress both inside the extraction site and in its surroundings. The monitoring activities are carried out as part of the MV2 monitoring program 'Aanleg Maasvlakte 2', under the supervision of Port of Rotterdam. The focus of the monitoring of the landscaping experiment is on the benthic and demersal fish communities, and as well as on the physical development of the sand mining area.

SUMMARY AND CONCLUSIONS

A need for upscaling of sand nourishments to guarantee sustainable conditions for safety against flooding and preservation of coastal functions, combined with the need to enhance an integrated coastal zone management, in the Netherlands has stimulated a number of new developments.
Central theme concerns the question: how can sand nourishments (and related sand mining) optimally serve stakes at different levels? In answering this question, the large-scale requirement for upscaling of nourishments is taken as a starting point. The challenge is to find possible combinations with small scale, short term needs. Adopting Building-with-Nature as a concept to support sustainable coastal development in the Netherlands, has resulted in three pilot projects: two are related to sand nourishments on a mega-scale, one to sand mining.
Both nourishment pilots start from the long term objective to maintain the sand volume in the coastal system. The pilot Sand Engine seeks a combination with medium- and short term needs to provide space for recreation and natural development; the pilot Sandy Sea Dike a combination with short term needs for dike reinforcements to provide safety against flooding and for spatial quality.
The sand mining pilot Ecological Landscaping of Borrow Pits is seeking a combination between the long term demands for nourishment sand with short and medium term ecological needs and requirements. Over time this should result in sand

mining areas in which the ecological functions are enhanced. In turn, this could contribute to the economical potential of mining areas (e.g. fishing or recreation).

Monitoring of the pilots must reveal the effectiveness of the designs. An evaluation of the approach to connect large- and small scales with these pilots, must indicate its wider applicability.

ACKNOWLEDGEMENTS

The work presented in this paper is carried out as part of the Rijkswaterstaat Research Program KPP Beheer en Onderhoud Kust and KPP Deltaprogramma Kust, and of innovation program Building with Nature. The Building with Nature program is funded from several sources, including the Subsidieregeling Innovatieketen Water (SIW, Staatscourant nrs 953 and 17009) sponsored by the Dutch Ministry of Transport, Public Works and Water Management and partner contributions of the participants to the Foundation EcoShape. The program receives co-funding from the European Fund for Regional Development EFRO and the Municipality of Dordrecht.

Contributions to the paper of Pieter Koen Tonnon (Deltares), of Maarten de Groot (Imares) and of Stefan Aarninkhof (Ecoshape) are gratefully acknowledged.

REFERENCES

Aarninkhof, S.G.J., J.A. van Dalfsen, J.P.M. Mulder and D. Rijks (2010). Sustainable development of nourished shorelines; Innovations in project design and realisation*, Proc. PIANC MMX Congress Liverpool UK 2010*, 12p.

Arcadis (2010). Projectnota MER Hondsbossche en Pettemerzeewering, Hoogheemraadschap Hollands Noorderkwartier, Provincie Noord Holland *ARCADIS, Amersfoort (in dutch)*

Deltacommissie (2008). Working together with water; a living land builds for it's future. Findings of the Deltacommissie 2008 *(www.deltacommissie.com)*

De Ronde, J.G. (2008). Toekomstige langjarige suppletiebehoefte.*Deltares report Z4582.24, Delft (in dutch)*

Lubbers, B., J. De Heer, J. Groenendijk, M. Van Bockel, M. Blekemolen, J. Lambeek and R. Steijn (2007). "Evaluatie Derde Kustnota." *Twynstra Gudde & Alkyon, Amersfoort, The Netherlands (in dutch)*

Mulder, J. P.M. and P.K. Tonnon (2010). "Sand Engine": Background and design of a mega-nourishment pilot in the Netherlands, *Proceedings Of The International Conference On Coastal Engineering, No. 32(2010), Shanghai,China. Paper #: management.35. Retrieved from http://journals.tdl.org/ICCE/*

Mulder, J.P.M, S. Hommes and E.M. Horstman (2011). Implementation of coastal erosion management in the Netherlands, O*cean and Coastal Management (accepted)*

NSS (2006). National Spatial Strategy (Nota Ruimte), *Policy Document Ministry of Spatial Planning and Environment , The Hague, The Netherlands*

NWP (2009). Nationaal Water Plan, *Policy Document Ministry of Transport, Public Works and Watermanagement , The Hague, The Netherlands*

Van Dalfsen, J.A. and Aarninkhof, S.G.J. (2009). Building with Nature: Mega nourishments and ecological landscaping of extraction areas. In: *Proc. of EMSAGG Conference 2009, Rome, Italy.*

Van Koningsveld, M. and J.P.M. Mulder (2004). Sustainable Coastal Policy Developments in the Netherlands. A Systematic Approach Revealed. *Journal of Coastal Research,* 20(2), 375-385. ISBN0749-0208

Waterman, R.E. (2008). Integrated Coastal Policy via Building with Nature: Sustainable Coastal Zone Development. *Delft, 500 pp, ISBN 9789080522237*

Vacuum Sewers – A Viable Alternative for Wastewater Collection and Transport in Coastal Areas

Soma Bhadra, P.E.[1] and Denny Moss[2]

[1] CEO, Proteus Consulting, 13738 Stoney Gate Place, San Diego, CA 92128, USA; PH (858) 353-2805; email: soma@consult-proteus.com

[2] Project Design Manager, Airvac, 4217 N. Old U.S. 31, P.O. Box 528, Rochester, IN 46975, USA; PH (800) 247-8229, ext. 229; email: dennym@airvac.com

ABSTRACT

In response to the growing need to protect the fragile and beautiful environment of the Coastal regions there has been increased desire to provide sewer collection systems to areas previously not sewered using less environmentally intrusive construction methods. Gravity sewer systems are the standard for wastewater collection worldwide. Although gravity sewers have been and remain the first choice among design engineers, the topography and constraints encountered in many Coastal locations precludes their use. Some of those constraints include rock at shallow depths, high groundwater table, a saltwater environment, unstable soil and mostly flat topography. The intent of this paper is to show how the use of Vacuum Sewers may help the design engineer overcome these constraints with shallow, narrow trenches and the elimination of infiltration and exfiltration. This technology has proved to be sustainable from both financial and environmental perspectives.

INTRODUCTION

In response to the growing need to protect the fragile and beautiful environment of the Coastal regions there has been increased desire to provide sewer collection systems to areas previously not sewered using less environmentally intrusive construction methods. Gravity sewer systems are the standard for wastewater collection worldwide. Although gravity sewers have been and remain the first choice among design engineers, the topography and constraints encountered in many Coastal locations precludes their use. Some of those constraints include rock at shallow depths, high groundwater table (See Figure 1), a saltwater environment, unstable soil and mostly flat topography. The use of Vacuum Sewers may help the design engineer overcome these constraints with shallow, narrow trenches and the elimination of infiltration and exfiltration. This technology has proved to be sustainable from both financial and environmental perspectives.



Figure 1. Trenching in rock and high groundwater

The following occasions particularly lend themselves to vacuum sewer projects:

- Coastal areas with flat terrain, unfavorable soil conditions (e.g. rocky or swampy grounds) and high groundwater table where trench dewatering may be required trenches. If areas like these are to be served by gravity systems, the cost of installation and maintenance are enormous. Vacuum sewers with small diameter can be laid close to the surface in narrow trenches and save a lot of money in construction.

- Spread-out settlements (also known as ribbon or peripheral settlements) on flat terrain, similar to ranch lots. With sparse population density, the costs of long and deep gravity sewers outweigh the costs for the collection chambers and vacuum stations.

- In seasonal settlements (recreation areas, camping sites etc.) with conventional gravity sewer systems, sedimentation problems can easily occur. This is because regular flushing does not occur through daily waste water transport. The high flow velocities in vacuum sewers prevent such sedimentation problems.

- Environmentally sensitive areas are particularly suited for vacuum sewers as these sewers can pass through water protected areas and through areas with sensitive high ground water tables. Vacuum sewers do not leak as the vacuum does not allow exfiltration.

- Vacuum sewers have gained prominence in old narrow and historical villages where fast, cost-effective, and flexible installation is required. These areas generally have heavy tourism traffic and are culturally sensitive. (See Figure 2)



Figure 2. Installation of vacuum sewer at Key Largo, FL

- Water conservation has also affected aging gravity collection systems where velocity cannot be sustained and leads to solids blocking the pipes. This is not an issue with vacuum system. Also as plastic pipes are used, no solids from disintegrating pipes enter the system.

- There are no manholes in the system and so illegal dumping of wastes into vacuum sewer systems is not possible.

HISTORY AND PREVALENCE

Even though the vacuum sewer concept has been around for almost a century and some vacuum system installations in the US are more than thirty years old, this technology has suffered from some misuse and misapplication in early installations. This technology has now been accepted worldwide as a viable alternative sewer collection system with installations in Europe, Africa, Asia, Australia, and North America. The following standards have been developed specifically for vacuum sewer installations:

1. United Kingdom: BS EN 1091:1997, Vacuum sewerage systems outside buildings, ISBN 0-580-27954-5

2. Germany: DIN EN 1091/DWA-A 116-1 E Special Edition - April 2005 DIN EN 1091 Vacuum Sewerage Systems Outside Buildings and DWA-A 116-1E Special Sewerage Systems Part 1: Vacuum Sewerage Systems Outside Building, ISBN: 978-3-940173-66-9

3. United States of America: Water Environment Federation (WEF) Manual of Practice FD-12, Alternative Sewer Systems

4. Australia: WSA 06-2008 Vacuum Sewerage Code V1.2 Publication no. PC014 and AS 4310 - 2004 (Australian Vacuum Interface Valve Standard)

Vacuum sewer collection systems were patented in the United States in 1888. The first commercial applications of such systems were by the Liljendahl Corporation (now known as Electrolux) of Sweden in 1959. There are several vendors marketing these systems worldwide, the most prominent of them are:

1. Airvac®

2. Qua-Vac B.V.

3. Iseki Vacuum Systems Ltd.

4. Roevac®

While the number of manufacturers is increasing and the design approach is fairly similar. The interface unit configurations vary significantly and are usually proprietary.

WHAT IS A VACUUM SEWER SYSTEM?

A Vacuum Sewer System is and mechanized method of wastewater collection and transport to a central location. Unlike gravity flow, vacuum sewers use differential air pressure to move the sewage. A central source of power to operate vacuum pumps is required to maintain vacuum (negative pressure) on the collection system.

The system is comprised of three main components as shown in Figure 3: a Valve Pit or Interface Unit, the Vacuum Piping Network, and a Vacuum Station. The Valve Pit is usually a sump or collection chamber with a vacuum valve that collects the wastewater from the house (via a gravity line) and discharges the wastewater to the piping network. Wastewater flows through the network in the form of small slugs due to differential pressure (induced vacuum). Uphill transport is achieved using a "saw tooth" profile. Vacuum stations are located at the terminus of the network and collect the wastewater in a vacuum-sealed collection tank. Vacuum pumps draw vacuum from the pipe network and collection tank and maintain a constant level of vacuum. These stations are also equipped with conventional wastewater pumping units to send the collected sewage to a treatment facility.

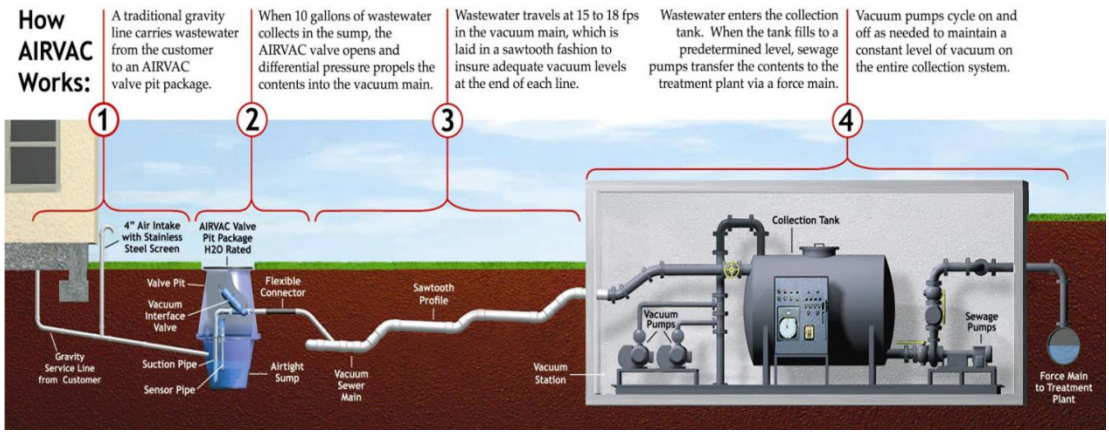


Figure 3. How a vacuum sewer system works

VALVE PIT

A typical residential vacuum sewer service consists of a gravity line from one or more structures to a sump equipped with a vacuum interface valve. The vacuum interface valves regulate the entry of wastewater and air from the valve vault into the collection system piping. A single vacuum vault with interface valve typically serves more than one residence. (See Figure 4)



Figure 4. Valve Pit - Top View

Interface valves that are installed inside the collection chambers work pneumatically. Wastewater flows by gravity into each collection sump. After a certain preset fill level inside the sump is reached (typically 10 gallons), the interface valve will open. The impulse to open the valve is usually transferred by a pneumatically (pneumatic pressure created by fill level) controlled pressure sensor unit. No electricity is needed to open or close the valve. While the valve is open, the resulting differential pressure between atmosphere



Figure 5. Installation of a valve pit

and vacuum becomes the driving force and transports the wastewater towards the vacuum station.

The time that the vacuum valve is open is normally adjusted to twice the time required to discharge wastewater from the sump. This allows air to enter the system behind the wastewater. The proper amount of air is necessary to drive the wastewater in the line to the vacuum station.

As the vacuum system requires atmospheric air to drive the sewage through the valve then piping network there must be a source of atmospheric air. This is accomplished in one of two ways — either with one dedicated air terminal located near the valve pit package, or a gravity line vent on each gravity line service. Up to four homes can be served by one valve pit package. It is not required that each home have its own pit package. (See Figure 5)

A Valve Pit is a polypropylene unit with interface valve, controller, sensor piping, tubing, and sump breather unit all included and can be assembled in the field as shown in Figure 6. It is recommended that the valve be rebuilt every 10 years and the controller every five years and costs approximately $100. The valve pit is polypropylene and is resistant to sewer gases, household cleaners, mold, and other chemicals that can attack some plastics. All metal parts within the valve are stainless steel. These pit packages are generally set on the right of way near the intersection of two property lines so that two or more property owners can access it without easement issues.



Figure 6. Assembled Valve Pit Package

PIPELINE DESIGN



Figure 7. "Steps" in a vacuum sewer pipe

Sewage is transported in small diameter pipes placed at variable grade and deflection underground. Besides the valve pits, no manholes are required for changes in direction or for inspection or connection of branch lines. The high flow rates keep the system free of any blockages or sedimentation. The piping network is usually made up of 4-inch, 6-inch, 8-inch, and 10-inch diameter SDR 21 PVC pipe. These are gasketed pressure pipe rated at 200 psi. Many different pipe manufacturers have been successfully used for vacuum sewer. However, use of a Rieber style gasket is highly recommended because it has proven itself over many years to be very reliable, tough, long-lasting and resistant to sewage and sewer gases. The main sewer line is typically installed in the right-of-way alongside the roadways. The fittings can be either gasketed (Rieber style) or solvent welded Schedule 40 pressure fittings. There are only a few manufacturers that use the Rieber style gasket in their fittings. There are many manufacturers that can supply acceptable solvent welded fittings. Tee fittings and 90-degree elbows are not allowed in the vacuum piping system. Directional changes are made with 45 degree elbows. Branch connections and service connections are made with wye fittings.

The lifts, sometimes called ‘steps’, are made with two 45 degree elbows and a short spool piece between them as shown in Figure 7. The lifts are what allow the system to remain relatively shallow. The piping network has a minimal slope toward the vacuum collection station. Minimum slope on the vacuum piping is 0.2%. As the piping gets to an unacceptably deep level a lift is used to return the pipe to an acceptable depth of burial. Or, lifts can be used to avoid utility pipes or other obstacles. Lifts can also help the sewer ascend small hills and avoid the deep cuts required of a traditional gravity system. A typical profile is shown in Figure 8.

The vacuum system does not require lifts to operate. But lifts cannot be unlimited. There are recommended maximum lifts allowable (static loss) for each flow path from the end of a branch or main line to the vacuum collection station.

The pipes are sized based on expected flow, much as a gravity system would be. However, the minimum pipe size for the vacuum system is 4” for a main or branch line versus 8” for a typical gravity system. Manufacturers have developed typical charts or recommended maximum flows for each pipe size. When that flow is attained the next larger pipe size is used. The wastewater entering travels initially at approximately 15 to 18 ft/second until it comes to a rest as the air and water separate.

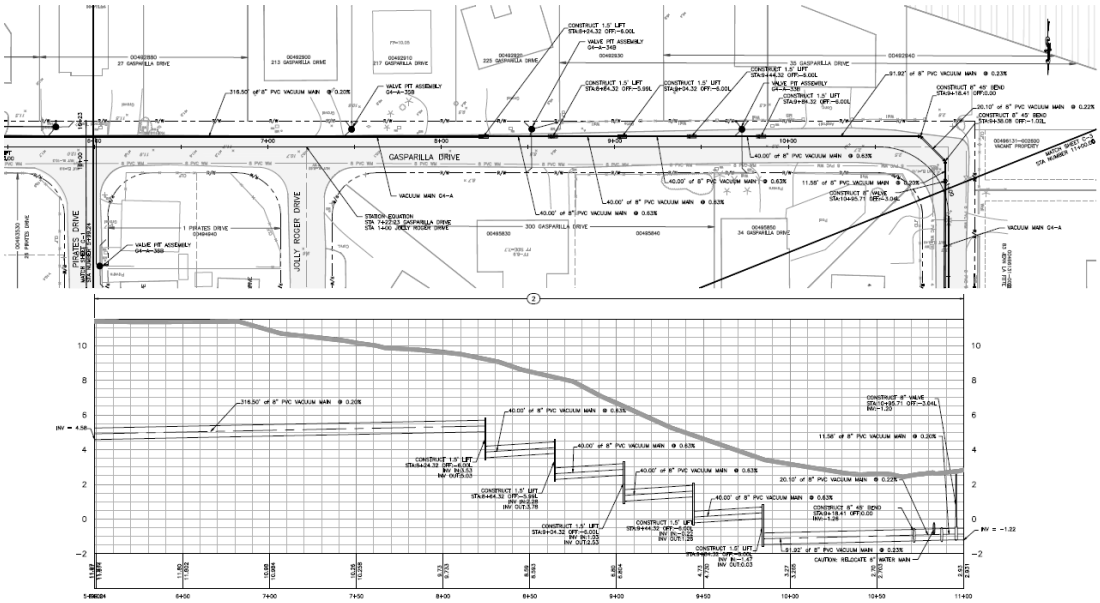


Figure 8. Typical vacuum sewer profile

Another valve cycle moves the sewage further down the line toward the Vacuum Station.

VACUUM STATION

Vacuum stations draw wastewater to the station and pump wastewater to a wastewater treatment plant. Rotary vane vacuum pumps generate an operation pressure of -0.4 to -0.6 bar at the vacuum station, which is also the only element of the vacuum system that must be supplied with electricity. The Collection Tank operates in much the same manner as a wet well, except that it is sealed. As the level rises sewage pumps operate on demand to transfer the sewage to another a lift station or the wastewater plant. The collection tank serves two purposes. It provides a vacuum reservoir to limit the number of vacuum pump starts much like the pressure storage tank of a compressed air system. It also keeps the vacuum pumps from contacting the air/sewage mix being collected into the collection tank. This separation prevents droplets from damaging the vacuum pumps. Vacuum switches on the reservoir tank control operation of the vacuum pumps. (See Figure 9)



Figure 9. Vacuum Pumps and Collection Tank

Sewage pumps can be from any of a number of suppliers. However, since wastewater is being pumped from a tank under vacuum, the NPSH requirements of the sewage pump are critical. The collection tank is generally carbon steel with an

epoxy lining, but the tank can be stainless steel tanks used or fiberglass. Carbon steel tanks are long-lasting with some have been in use for 30+ years showing no sign of deterioration.



Figure 10. Inside a vacuum sewer station

Controls can be simple or complicated. It is common to have PLC controls, but relay logic is also available. Most systems are equipped with a standby Generator. Also common in areas where homes and/or businesses are close by is an odor control system which is usually a very efficient and relatively inexpensive bio-filter odor control system. (See Figure 10)

The Vacuum Station building is generally a garage sized structure with a basement. Common footprint might be 24 ft. x 36 ft. A standard city residential lot is generally sufficient; depending upon how much parking, is required. The basement of the building houses the collection tank and the sewage pumps and accommodates the entry of the vacuum sewer. Manufacturers recommend the vacuum pumps and controls are at ground level, although they can be placed in the basement as well if required.

WHAT IS THE RIGHT APPLICATION?

A successful project not only includes a proper engineering design but also sound procurement approach, permitting, construction, installation, testing, and start-up. Highlighted below are two projects with specific challenges and solutions.

Oak Island, North Carolina

The North Carolina project consisted of the installation of approximately 300,000 feet of 4-inch, 62,000 feet of 6-inch, 33,000 feet of 8-inch, and 26,000 feet of 10-inch PVC collection system piping, nine vacuum collection stations, and approximately 80,000 feet of 8 to 16-inch force mains to serve more than 10,000 residences. Oak Island is a barrier island at the southern-most tip of North Carolina, about 35 miles south of Wilmington. Challenges in this project included high groundwater conditions, flat terrain, high seasonal flow variation, regional cooperative agreements, innovative funding arrangements, and coastal permitting. Several sewer collection system options were evaluated for Oak Island, including gravity collection, vacuum collection, on-site septic tank systems, and septic tank effluent pumping systems. Vacuum collection systems were recommended because of operational advantages over gravity collection systems, no infiltration, and lower initial capital cost.

The vacuum stations were designed to look like three storied beach cottages to blend in with the neighborhood (See Figure 11). The architectural features include vinyl siding, metal hipped roof, false windows, access doors with a "residential" look, and porches with handrails. The vacuum system equipment was located on two levels inside the vacuum station. The bottom "basement" level, located below grade, contained a steel collection tank, two sewage pumps, and a sump pump. The operating floor was on the second level (ground level or just above 100-year flood level). This floor housed the three vacuum pumps and electrical controls. Stairs to the basement level of the vacuum station is located within the building. Six stations of the nine had a third level for use by the Town. Stairs to this level were outside the building. Other onsite equipment included odor control equipment, engine generator, air conditioning, and ventilation system.



Figure 11. Typical Vacuum Sewer Station

Culebra, Puerto Rico

In the Caribbean, a project is currently being installed on the Island of Culebra off the east coast of Puerto Rico. Culebra is a small collection of islands, the main island and 23 smaller islands, approximately 17 miles east of Puerto Rico, and about 12 miles west of the island of St. Thomas in the U.S. Virgin Islands. It is approximately 7 miles long and 3.5 miles wide. Ensenada Honda is the largest harbor on the island. It has been considered the most hurricane secure harbor in the Caribbean. That is why the history of Culebra includes tales of pirates and buried treasure. The capital of Culebra is Dewey.

Culebra is an arid climate. That is, there are no permanent streams or rivers. This is both a blessing and a curse. It is a blessing in that there are no run-offs to pollute the waters of Culebra. However, that means that all fresh water is brought from Puerto Rico via Vieques. Also, the small islands are classified nature reserves and many small reserves exist on the main island. They are protected by the United States Fish and Wildlife Service. Approximately 50,000 sea birds find their way to these sanctuaries each year. In addition, Culebra is one of only two sites in the United States that is a nesting site for the giant sea turtles.



Figure 12. Installation of a valve pit at Culebra

Challenges in this project were environmental protection, extremely tight working space, high Groundwater, and significant rock subsurface conditions (See Figure 12). Only one vacuum station was built in Cubera serving more than 400 residences and businesses.

CONCLUSION

A Vacuum Sewer System enables us to overcome the obstacles of shallow depth, high groundwater table, a saltwater environment, unstable soil and mostly flat topography. A system approach is necessary to ensure an efficient and effective system that is cost competitive with gravity sewers and other alternatives.

The following advantages and limitations should be kept in mind when considering vacuum sewer systems:

Advantages:

- A vacuum sewer system is a closed, pneumatically controlled system with a central vacuum station. Electrical energy is only needed at this central station.
- There are no manholes and no sedimentation occurs in pipelines due to high self-cleansing velocities.
- Investment costs have been shown to be reduced by 50% due to shallow trenching and reduced installation time, small diameter sewer pipes of HDPE, PVC materials.
- A single vacuum pump station is required compared to multiple stations in gravity and low pressure networks. This uses less land, reduces energy costs, and reduces operational costs.
- Due to no infiltration, there is less hydraulic load at treatment plants.
- No leaks, exfiltration and so sewers may be laid in the same trench with other mains, as well as in water protection areas.
- Flexibility in piping routes allows sewer to go over or under obstacles, such as open channels and utilities.
- Aeration of wastewater leads to less development of H2S, and hence reduced danger for workers, customers, as well as corrosion of the pipes may be avoided, no odors.
- Lower cost to maintain in the long term due to shallow trenching and easy identification of problems.

- In combination of vacuum toilets, this sewer system can create concentrated waste streams, which makes it feasible to use different waste water treatment techniques, like anaerobic treatment.

Limitations:

- Vacuum systems are not capable of transporting sewage over very long distances, but can pump long distances from the vacuum station to the next STP or main gravity sewer.

- Vacuum sewer systems are only capable for the collection of wastewater and cannot be applied for collection of storm-water.

- The vacuum lines can only reach up to 3 miles in radius laid in flat area due to restrictions of the system due to head loss.

- These systems should be designed with help of an experienced manufacturer. The concept layouts are usually free of charge.

- External energy is required at a central point for collecting wastewater.

- Odors may exist close to the vacuum station and a biofilter may be necessary.

- Integrity of the pipe joints is paramount and need to be installed by experienced personnel and properly inspected

Sustaining Port Development through Impact Mitigation

Michael Ludwig[1] and Douglas Clarke, PhD[2]

[1] Ocean and Coastal Consultants, a COWI Company, 35 Corporate Drive, Suite 1200, Trumbull, CT 06611; PH (203) 268-5007, FAX (203) 268-8821; email; fmlu@ocean-coastal.com

[2] US Army Corps of Engineers, Engineer Research and Development Center, CEERD-EE-W, 3909 Halls Ferry Road, Vicksburg, Mississippi 39180-6199; PH (601) 634-3770 email: Douglas.G.Clarke@usace.army.mil

ABSTRACT

This paper discusses innovative environmental compensation used in port development. Sustainable development can be complicated by costly regulatory requirements. These requirements stem from the National Environmental Policy (NEPA) and Clean Water Acts (CWA). Federal and state NEPA and CWA versions require identification and evaluation of adverse impacts and methods to avoid, minimize or mitigate them. While some projects find political support helpful in addressing environmental and social conflicts more frequently, designs are used that are environmentally compatible but may limit development. Environmental issues are routinely related to physical attributes that control a site's ecological importance and sensitivity. Taking advantage of local physical attributes to re-nature sites and avoiding maintenance often provides missing but significantly important ecological functions and values with wide ranging benefits. Using natural conditions in designs that create maintenance free habitats that otherwise do not exist, can generate significant benefits. Good projects are environmentally compatible, great ones are beneficial.

INTRODUCTION

There is an innovative evolution occurring in successful environmental compensation measures being used in port development projects. The evolution is being driven by the need to meet the requirement for environmentally compatible coastal development. Sustainable harbor, port and terminal development is increasingly complicated by complex and often times regulatory requirements that include mitigation. These requirements have been evolving since the passage of the National Environmental Policy Act (NEPA) in 1969 and the Clean Water Act (CWA) amendments of 1972. The federal and state versions of NEPA and CWA require evaluation of adverse impacts caused by project then development, identification, and implementation of methods by which they can be avoided, minimized or mitigated. While some port development planners find political support essential in minimizing environmental and social conflicts, it is clear that incorporating designs that are environmentally compatible are necessary to advance a given project, even when this approach may limit further development options. Within the spectrum of perceived environmental concerns, it is routinely the impacts to physical attributes of ecologically important and sensitive habitats that control project acceptability. Taking advantage of physical attributes on-site or in proximity to the adverse impacts has proven to have significant value in mitigating environmental degradation. When naturally

occurring physical attributes can be utilized in project planning and design to create, enhance, or maintain a habitat that might otherwise be lost or damaged, the benefits can be significant. It is desirable that good projects are environmentally compatible but preferred when projects are environmentally beneficial.

The environmental impact issues associated with harbor, port and terminal improvements in tandem with the decreasing availability and escalating costs of waterfront property are challenging port and terminal operators to seek new avenues to advance facility modifications. Many needs for expansion of marine trade infrastructure are constrained by space availability, access, and competing uses. In addition to the finite availability of waterfront property and associated real estate costs, these problems are further complicated by inter-port competition for commerce and the changing nature of transport systems. With the impending completion of the Panama Canal improvements and arrival of newer generations of cargo vessels with their increased draft requirements, restricted port improvement options threaten sustainable commercial development along the entire United States coastline. Without the ability to berth the newest vessels and efficiently handle cargo in a timely manner, terminals and potentially entire ports are likely to suffer economic setbacks if the marine transportation industry relocates to alternative landing sites. Simultaneously, regulatory agencies at all governmental levels are responding to growing scientific evidence of steady declines in the status of their managed resources. Exacerbating the conflicting use pressures is the increasing public pressure for improved access to waterfronts. For example, there is an on-going and growing discussion among planners recognizing a nation-wide need to deepen navigation channels and port and terminal berths beyond the current fifty foot depth. This discussion is occurring at the same time that the movement to revitalize urban living is seeking to include upscale amenities in their offerings. The housing pressure is driving local and regional governments to accommodate these public amenities by "re-capturing" urban waterfront space for recreational use.

The navigation infrastructure of United States harbors and ports has been sustained, historically, by a mixture of dredging and filling. The ratio of the mix was as dependent on the availability of upland real estate at competitive prices as any other criterion. In older ports such as Boston, New York, and Philadelphia, the need for water depth and upland space to accommodate shipping industry growth was achieved over a span of two centuries by filling portions of the harbor and extending piers to access natural water depths necessary for safe shipping. It is said that more fill materials were dumped in New York Harbor than moved to create the Panama Canal. As a result in older ports the shallows, flats and shorelines are greatly reduced and bear little resemblance to their pre-development profiles. Extensive areas of intertidal wetland and shallow subtidal flats were filled or transected by dredged access channels. In the case of the Hudson River Estuary, urbanization and industrialization collectively transformed the natural harbor into a highly modified setting with little resemblance to its pre-development condition (Steinberg et al. 2004). The 1956 sailing of the "Ideal X" and the advent of containerization altered port facility needs forever. Although much of the transformation of the nation's coastal estuaries occurred prior to passage of NEPA in 1969, the continued need for greater channel and berthing depths requires a substantial commitment for capital (new work) and maintenance dredging and dredged material disposal. Similarly, in numerous ports the natural shoreline characteristics have been modified to keep apace of the trend for ever deeper draft vessels with larger cargoes. Today, the shorelines of older ports, even those no longer in service to the cargo industry, consist primarily of bulkheads, seawalls and

relieving platforms with water depths that preclude the occurrence of shallow water, intertidal flats or vegetated wetland shorelines. The real estate needed for these habitats is essentially unavailable. In many instances, even where remnant intertidal flats or wetland habitats persist, altered hydrodynamic and bathymetric conditions, as well as wakes from vessel traffic, do not provide suitable sediment stability to allow sustained growth. It is these intertidal wetland and shallow flat habitats that continue to gradually but inexorably disappear from the seascapes of developed ports. And, this does not include the impacts of rising sea level induced by global climate change.

CURRENT USE OF INOVATIVE MITIGATION

Given the above historical perspective, it is somewhat ironic that early fishermen recognized that many aquatic species had an affinity for "unnatural" structures. Much of the continental shelf and estuarine seafloors are naturally devoid of topographic features that provide substantial vertical relief. The addition of features that change the topography or pattern of water currents has been shown to attract diverse assemblages of aquatic species. Fish, crabs and even some shellfish tend to congregate around structures. In addition to benthic (bottom dwelling) species, numerous species of fish and invertebrates that live between the bottom and the surface (pelagic species) show definite attraction to structures that provide vertical relief. Therefore, it is not surprising that certain fish species have adapted to the unnatural conditions in many harbors by taking advantage of the structures that displaced their natural habitats. In the Port of New York and New Jersey the piers along the Hudson River have created backwater areas with their dense stands of support pilings. The berthing or "interpier" areas between the piers have been shown to afford fish such as striped bass (*Morone saxatilis*) and winter flounder (*Pseudopleuronectes americanus*) suitable habitat for overwintering during the coldest periods of the year (Able et al. 1999). Consequently disruptive activities are closely regulated and monitored to limit adverse impacts on fish during their use of the interpier areas from November until April. One consequence of these regulatory measures is a temporal constraint on construction activities contrary to those typically invoked. Although warmer months are generally associated with peak biological activity, in New York's inner harbor regulatory agencies regularly consider it better to constrain anthropogenic disturbances to warmer months as opposed to jeopardizing the more sensitive assemblages present during colder months. Site-specific conditions further affect decisions regarding protective measures. For example, pile driving activities might be permitted in areas that support primarily benthic rather than pelagic fishery resources.

Regulators routinely seek means to mitigate for impacts or obtain environmental compensation, including public use, from waterfront developers. For instance, New York State requires an alternatives assessment and mitigation for replacement of bulkheads. The State of New Jersey requires that waterfront projects include provision of public access. Massachusetts requires payment for altered or destroyed Essential Fish Habitat not otherwise mitigated. However obvious the need for environmental mitigation might be, in developed harbors the use of conventionally recognized mitigation measures is often constrained by the lack of available or suitable space and funding. Inherently, tradeoffs can be difficult to assess. For example, should a shallow water area be filled to create a vegetated wetland or would it be preferable to excavate an intertidal flat to create shallow water habitats? Similarly, what are appropriate measures for habitat tradeoffs associated with re-grading an existing upland property to create intertidal wetlands? Metrics to

define adequate compensation through out-of-kind habitat replacement have been elusive, but application of new insights into the habitat needs of aquatic resources and methods of providing greater and accessible habitat functions and values are being explored and implemented. Putting these concepts to work has proven a success. A shift in compensatory mitigation away from a primary focus on wetland vegetation to alternative physical habitats that support specific fishery resources has proven far more effective for restoring and/or enhancing native populations in locations where the resources are not intimately associated with tidal wetlands. For example, investigations in Rhode Island have developed habitat alternatives that target juvenile American lobster (Mauseth, et al 2009). Artificial reef construction projects in the Chesapeake Bay and coastal waters of the Gulf of Mexico have been extremely beneficial for species such as cobia (Gulf and Atlantic SMFC 2004; Mark and Szedlmayer (2006)). Restoring displaced or degraded fishery resources back into developed harbors in a manner that allows "peaceful co-existence" of fishery resources and commerce has become the benchmark for successful sustainability of many major harbors in the United States.

The need to move beyond simply creating vegetated wetlands as mitigation is important to the overall port development agenda. While tidal wetlands mitigation measures have their place in ecosystem management and specific waterways, manipulating these vegetated habitats has proven more difficult and expensive than anticipated, with continued debate regarding their limitations in terms of success, maintenance and the need for protracted involvement. Acknowledgment that a return to historical wetland acreages within modern harbors and ports is an impossible goal is a prerequisite step before a path toward optimal development of fishery resource support functions in tandem with inevitable navigation infrastructure development can be pursued. As note above, rising sea level and global climate change have added additional complications to the challenges of creating or enhancing vegetated wetlands. The issues with submerged aquatic vegetation (SAV) are even more extensive.

One solution being implemented is the use of "renaturing", defined herein as designing ecological communities or ecosystems that benefit natural resources and humans. A key assumption underlying this concept is that known environmental losses or habitat components not currently present in a system can be replaced, repaired, and/or created to provide desired habitat attributes. In this approach societal interests and practical constraints bear directly upon which natural characteristics are pursued. Renaturing can target areas of harbors that no longer provide or are unsuitable for water dependent services.

Careful and comprehensive characterization of the physical environment, including local conditions such as wave regimes, current and circulation patterns, along with tidal mixing dynamics can identify opportunities to create and sustain habitats not typically found at a location. This characterization provides a fundamental technical foundation for deploying habitat "units" with hard physical structure. Where appropriate, habitat features can be designed to take advantage of their lower sensitivity or acceptance of condition variability in the hydrology or physical characteristics at a site. These renatured habitats can be used by species on a seasonal or more protracted basis depending on their habitat requirements and motility. For instance, creating oyster habitat in areas where the natural substrate does not provide suitable conditions for recruitment and attachment of larval stages can be overcome by creating elevated surfaces of shell material or other hard attachment surfaces that are routinely washed of accumulating sediment. While natural rock is preferred,

concrete has proven useful to these and other sessile epifaunal (stationary attached organisms) species. As the shellfish mature, they form a food source for predators and refuge for a diverse assemblage of fish and invertebrates, thereby establishing a functional ecological community. Ultimately, the oysters "pave" the structure and it functions as a oyster reef. By creating enhanced conditions for aquatic resources, the overall environmental wellbeing of an area is improved and the human community formerly underserved by existing habitat functions and values benefits.

Creating habitat structure for aquatic resources is a desirable option from many perspectives. Physical structures can be relatively insensitive to minor disturbances in hydrology (e.g., floods or freshets) or storm conditions and can be designed to have very low maintenance needs. For example, in New Jersey, a nearshore artificial reef was constructed to create and enhance shallow water habitat for juvenile stages of several species (Ludwig et al. 2010). The pre-project seascape consisted of a sandy/silt plain, with “structure” limited to scattered small stones. The renaturing mitigation consisted of a series of fabricated modules that rise above the seafloor and provide extensive internal (cryptic) spaces that allow both water movement through the structure and occupation by diverse fish, shellfish and crustacean species. The reef units were specifically designed to remain below the low tide elevation providing a stable, inundated habitat throughout the tidal cycle. The installed habitat was designed, also, to satisfy the site-specific requirements of the native estuarine species community. Aquatic species find shelter within and around the multiple individual reef module components expanding the ecological benefits to the new community, significantly. Within two years of installation, the reef area became populated by the juveniles of the target species, thereby achieving the mitigation objectives. The project has increased overall biological productivity by renaturing an area that lacked the necessary structural attributes. Now it supports the aquatic resources ecological functions and values needs of species that could not use the area..

As ports have consolidated their operations in response to increased goods handling and storage capacity requirements, in many cases urban waterfront infrastructure has been abandoned. The conversion of former marine transport and commercial waterfront infrastructure to non-water-dependent uses has provided opportunities for regulators to to require efforts to restore, recover or increase environmental and public trust resources. Waterfront recapture programs are found throughout the United States. These areas facilitate public awareness and use of unique components of the environment. These re-capture uses contribute to a prioritization of human habitat renaturing opportunities that encourage reoccupation by a public that was displaced by commercial development decades or even centuries ago. Seattle is an example of the rethinking of the waterfront use. Amidst real estate abandoned as relicts of the breakbulk shipping industry and obsolete transportation infrastructure, parcels are being gentrified to supplement open spaces and provide urban parks and recreational “green” spaces. They are currently extending the restoration to aquatic resource restoration Examples of waterfront public areas that serve as vital and vibrant additions to urban settings can be found from Portland, Maine to Seattle. However, efforts to obtain or recover natural resources within these and operating port facility areas can create issues that are likely to complicate regulatory approval even for water-dependent infrastructure. Limited space, security conflicts and public safety issues all create conflicts that influence support for natural resources and make public use problematic. Adding physical and environmental characteristics that are deemed important to environmental resource use and are compatible with maintaining port

infrastructure pose a demanding challenge. Nevertheless, regulatory approvals for port maintenance and modernization projects are increasingly dependent upon minimizing impacts and creating compensation measures for unavoidable impacts to public trust resources. As a result, facility owners and their consultants must work in concert with regulators and other stakeholders knowledgeable and appreciative of the environment at and around a project site, then they are able to offer practical and cost effective solutions.

Perhaps the most important element of "renaturing" an area is an understanding of the existing conditions. In one renaturing project sedimentation was a significant potential issue. A comprehensive wind, wave, current and runoff assessment was undertaken to characterize the physical limitations on creating a structure that would remain functional although sediment deposition might be an issue on the surrounding, natural Bay floor. By aligning the project to take advantage of the prevailing wave regime and local tidal currents, intertidal and shallow subtidal structures were designed and built that provide habitat for intertidal algae (seaweeds) and epifaunal organisms that require relatively clean, hard surfaces. In turn these species attracted forage species and their associated predators. This mix of resources is expected to service both benthic and pelagic species in an area of a harbor that had previously possessed only pile supported piers that had been documented to suffer from shading impacts and overall lower resource use.

Long-term solutions for harbor and port development in estuaries require innovative approaches to habitat mitigation. Similar considerations must be given to offshore opportunities for creating, restoring, or enhancing fishery resource habitat. Although coastal port infrastructure largely lies within estuarine waters, substantial benefits can be gained by inclusion of offshore options. In fact, as spatial constraints for within-harbor boundary mitigation become severe, offshore opportunities remain much less severely constrained in terms of available space. One obvious example involves placement of dredged material derived from inner-harbor channel or berth dredging projects. The concept of using dredged material to achieve fishery habitat functions is not new (Clarke and Kasul 1994). However, broad adoption of this approach has suffered from persistent negative perceptions. Evidence does exist that building topographic features of suitable dredged material can provide viable fishery habitat. For example, investigations at a large stable mound constructed of dredged material in offshore Alabama waters clearly demonstrated that fish assemblages quickly recruited to the mound. These were incidental benefits of mound construction in that it was not designed specifically to provide habitat functions. One finding was that the mound provided a refuge from commercial groundfish trawling activities. Although not uniformly appreciated, the juvenile stages of certain species such as red snapper (*Lutjanus campechanus*) occupied the mound in comparatively high abundances. One conclusion of these investigations (Clarke and Kasul 1994) was that habitat functions and values could be further optimized if they were embedded in the project planning process. The mound had been built with little forethought to enhancing habitat. Mound design features that could be used to maximize fishery resource benefits included location, height, side slope, configuration, volume, and orientation to prevailing water currents. This example demonstrates that the spectrum of mitigation options can and should be expanded.

CONCLUSIONS

In these and other renaturing efforts, underutilized habitats were renatured to create previously limited or unavailable habitats. The benefits are improved or restored resources

displaced by previous or current harbor improvements. Targeting specific resources to receive improvements can have significant value to the overall ecological community. Cost containment is achieved by reuse of structures or local materials routinely available in port development/redevelopment situations. Rock generated by deepening a harbor was reused within the same system reducing costs for all parties involved. In another instance, old concrete piles, available from site improvements, were used to create reef units positioned to maximize habitat functions and values. Even dredged material can be used beneficially if the site characteristics are suitable. Creating self-sustaining and maintenance free projects was achieved by integrating mitigation objectives with site conditions in project design and implementation. To date, projects have successfully targeted finfish, shellfish and crustaceans. These resource enhancements were designed for locations with limited (reduced) existing environmental and public trust resource use or value. These renaturing projects will continue to provide benefits to the environment, the public, and project proponents for the foreseeable future. They accomplish the goals of sustainable port development, project mitigation and public resource needs and availability.

ACKNOWLEDGEMENTS

The aquatic renaturing examples cited in this paper were created through a partnership between Engineers and Biologists. Without that partnership project success would not have been so readily accomplished. As a result, the first author wishes to express his appreciation to Mr. Ryan Prime currently with Skanska, USA and LCDR Stephen Padhi, Civil Engineer Corps, US Navy, Camp Pendleton, CA.

References

Able, K. W., Manderson, J. P., and A. L. Studholme (1999). "Habitat quality for shallow water fishes in an urban estuary: the effects of man-made structures on growth." Marine Ecology Progress Series, 187, 227-235.

Clarke, D. G. and R. Kasul (1994). "Habitat value of offshore dredged material berms for fishery resources." Proceedings of the Second International Conference on Dredging and Dredged Material Placement, American Society of Civil Engineers, Lake Buena Vista, FL, 2, 938-945.

Gulf and Atlantic States Marine Fisheries Commissions 2004. " Guidelines for Marine Artificial Reef Materials." 2nd Edition. Editors R. Lukens and C. Selberg. GSMFC & ASMFC, Wash. D.C. 198 pp.

Ludwig, M., R. Prime, and S. Padhi (2010). "Mitigation site development and third year monitoring of the Constable Hook, New Jersey fishery enhancement project." Ocean and Coastal Consultants, Trumbull, Connecticut.

Mark E. L. and S. T. Szedlmayer (2006). "The influence of habitat complexity on reef fish communities in the Northeastern Gulf of Mexico." Environmental Biology of Fishes. 76:1, 71-80.

Mauseth, G., G. Challenger, J. Catena and J. DeAlteris (2001). "Restoration and compensation of the Rhode Island lobster fishery following the *North Cape* oil spill." Proceedings of the 2001 International oil Spill Conference, Tampa Fl. 755-760.

Steinberg, N., Suszkowski, D., Clark, L., and J. Way (2004). "Health of the Harbor: the First Comprehensive Look at the State of the NY/NJ Harbor Estuary." Hudson River Foundation, www.hudsonriver.org